RHEOLOGICAL PROPERTIES OF LONG-CHAIN BRANCHED CHLORINATED POLY(ISOBUTYLENE-*co*-ISOPRENE)-*graft*-POLYBUTADIENE TERPOLYMERS (CIIR-g-BR)

by

Jerzy (George) Sendorek

A thesis
presented to the University of Waterloo
in fulfillment of the
thesis requirement for the degree of
Doctor of Philosophy
in
Chemical Engineering

Waterloo, Ontario, Canada, 1998

© Jerzy (George) Sendorek, 1998

National Library of Canada
Acquisitions and Bibliographic Services
395 Wellington Street
Ottawa ON K1A 0N4
Canada

Bibliothèque nationale du Canada
Acquisitions et services bibliographiques
395, rue Wellington
Ottawa ON K1A 0N4
Canada

Your file Votre référence

Our file Notre référence

The author has granted a non-exclusive licence allowing the National Library of Canada to reproduce, loan, distribute or sell copies of this thesis in microform, paper or electronic formats.

L'auteur a accordé une licence non exclusive permettant à la Bibliothèque nationale du Canada de reproduire, prêter, distribuer ou vendre des copies de cette thèse sous la forme de microfiche/film, de reproduction sur papier ou sur format électronique.

The author retains ownership of the copyright in this thesis. Neither the thesis nor substantial extracts from it may be printed or otherwise reproduced without the author's permission.

L'auteur conserve la propriété du droit d'auteur qui protège cette thèse. Ni la thèse ni des extraits substantiels de celle-ci ne doivent être imprimés ou autrement reproduits sans son autorisation.

0-612-30643-7

Canada

The University of Waterloo requires the signatures of all persons using or photocopying this thesis. Please sign below, and give address and date.

Abstract

Rheological properties of long-chain branched chlorinated poly(isobutylene-*co*-isoprene)-*graft*-butadiene terpolymers (CIIR-g-BR)

Anionically polymerized "living" polybutadiene (BR) was grafted onto chlorinated poly(isobutylene-*co*-isoprene) (CIIR) to form a series of elastomeric graft copolymers (CIIR-g-BR) of comb-type, long-chain branching structure (LCB) with systematically varying length and number of branches.

A comprehensive program of analytical characterization of the structure and morphology of these materials using SEC/DRI-DV, NMR, FT-IR, DSC, TGA, TEM and other techniques, was designed to determine all relevant structural variables and parameters, as well as to exclude the presence of the potential compositional interferences (gel, residual solvent, unattached branch parent polymer, etc.) for intended correlations between branching structure and rheological properties. The principal branching characteristics of comb-like long-chain branched structures were derived from the stoichiometry of the grafting reaction, confirmed by compositional analysis using a combination of NMR/FT-IR/SEC and supplemented by SEC characterization of the parent linear polymers constituting the backbone (CIIR) and the branch of the graft (BR), respectively.

Linear viscoelastic properties of these materials were determined by a Rheometrics Mechanical Spectrometer (RMS-800) using small amplitude, dynamic (sinusoidal oscillatory) shear. These measurements were supplemented by Rubber Process Analyzer (RPA 2000^{TM}) testing in a comparable range of strain amplitudes, frequencies and temperatures. Stress relaxation experiments, following small amplitude step-strain in shear, complemented the dynamic mechanical measurements.

Non-linear viscoelastic properties in shear were investigated in a series of isothermal strain and frequency sweeps using large strain (up to 800%) oscillations (RPA 2000), and by stress relaxation following a large-amplitude (~75%) step shear strain, using the Dynamic Stress Relaxometer (DSR).

An insight into the morphology of the grafts by means of the TEM and DSC has been compared to the results of the thermo-mechanical analysis (DTMA) in tension, using the Rheometrics Solids Analyzer (RSA-II).

Phenomenological correlation between long-chain branching and rheological parameters was attempted and observed effects of branch length and branching frequency on rheological properties are discussed. Long-chain branching has a profound effect on the behaviour of graft copolymers in the plateau and terminal zones of the viscoelastic spectrum. Systematic changes in the frequency dependence of the dynamic moduli and time dependence of the stress relaxation modulus can be related to the length and the number of branches. On the other hand, modifications in the transition and plateau zones due to grafting are influenced primarily by chemical composition of the graft copolymers. A new method to characterize LCB in elastomers by means of a normalized Cole-Cole plot has been proposed.

Acknowledgments

I would like to thank Dr. Alfred Rudin for his advice and guidance during the earlier stages of my research work, Dr. Charles M. Burns for helpful suggestions and comments, and Dr. John R. Dunn for numerous discussions and suggestions, as well as for the help with the editing of the final versions of this thesis.

Special thanks are extended to Dr. Z. Jack Lobos, my supervisor at Bayer, for suggesting this research topic and his invaluable support, encouragement and patience.

I am indebted to many people in the Rubber Division of Bayer in Sarnia for their help in various areas of the experimental work, in particular, Mr. Bruce Kirby and Mr. Dave Drope for help with the preparation of samples, Drs. William Hopkins, Daniel Ho and Kenneth Watson for help with the characterization of structure and composition of samples and interpretation of data, Mrs. A. King, Mr. B. Martin and Mr. D. Cook for their assistance in rheological measurements and for maintaining equipment in top shape, and Mr. John Van Es for the electron microscope (TEM) photographs.

I would like also to thank my colleague Dr. Kevin Suddaby for introducing me to the GPC system installed in the Chemistry Department Laboratories at the University of Waterloo.

Finally, I would like express my sincere appreciation to the Management of the Technology Department of Bayer (Rubber Division in Sarnia), in particular to Dr. Brian Morris, then Vice President of Research, for his kind permission in the use of laboratory facilities, as well as for financial support.

This work is dedicated to my wife Elizabeth
and to my children Bart, Dorothy and Dominik
for their love, support and understanding

Table of Contents

Abstract		iv
Acknowledgments		v
Dedication		vi
Table of Contents		vii
List of Tables		xiv
List of Illustrations		xviii
Introduction		1
Chapter 1	**Rheological properties of long-chain branched polymers**	4
1.1	Brief overview	4
1.2	Rheological properties of model long-chain branched polymers	8
1.2.1	Regular stars	8
1.2.2	Regular comb-shaped molecules	10
1.3	Randomly branched polymers	10
1.4	Graft copolymers	11
Chapter 2	**Sample preparation**	16
2.1	Brief characteristics of the parent polymers	17
2.1.1	Synthesis, chlorination and purification of the poly (isobutylene-co-isoprene)	20
2.1.2	Polymerization of butadiene	21
2.2	Preliminary grafting experiments	22
2.3	Grafting reaction	24
2.4	Graft purification (extraction of ungrafted parent prepolymers)	28
2.5	Sample stabilization and storage	30

2.6 Specimen preparation for rheological characterization 32
2.6.1 Film casting from solution 33
2.7 Proof of grafting 35
2.8 Additional issues 36
2.8.1 Sample quality 36
2.8.2 Sample integrity, thermo-mechanical stability and effect of aging 37
2.8.3 Homogeneity of sample material 38
2.9 Sample portfolio 39

Chapter 3 Determination of molecular structure: experimental methods 40
3.1 Principal characteristics of molecular architecture of elastomers 40
3.2 Long-chain branching parameters for comb-like structures 41
3.3 Analytical methods suitable for the characterization of LCB structures 47
3.4 Instruments and techniques selected for characterization of structure and composition 54
3.4.1 Size-Exclusion Chromatography (SEC) 55
3.4.2 Nuclear Magnetic Resonance (NMR) Spectroscopy 69
3.4.3 Infra-Red (IR) Spectroscopy 77
3.4.4 Differential Scanning Calorimetry (DSC) 79
3.4.5 Transmission Electron Microscopy (TEM) 82
3.4.6 Thermogravimetric Analysis (TGA) 82
3.4.7 Solubility tests 83
3.4.8 Ion Chromatography (IC) and Wet Chemistry methods 84

Chapter 4 Molecular structure and composition: results 85
4.1 Overview of structural variables, parameters and interferences 85
4.2 Backbone prepolymer (CIIR) characteristics 87

4.2.1 Molecular chain linearity 90
4.2.2 Functionality of branching point 94
4.2.3 Molecular weight distribution 94
4.2.4 Composition/unsaturation 98
4.2.5 Microstructure - compositional heterogeneity 99
4.2.6 Chlorine content and distribution 101
4.3 Branch prepolymer (BR) characteristics 103
4.3.1 Molecular chain linearity 103
4.3.2 Molecular weight distribution 106
4.3.3 Microstructure 114
4.4 Graft composition and structure 117
4.4.1 Graft structure - topology 117
4.4.2 Overall chemical composition 117
4.4.3 Molecular weight distribution 121
4.4.4 Branching number 126
4.4.5 Content of ungrafted prepolymers 130
4.4.6 Molecular characteristics of CIIR/BR blend 131
4.4.7 Content of residual solvent and non-polymeric substances 132
4.4.8 Gel content 135
4.4.9 Random grafting and random coupling assumptions 138
4.5 Special issue: graft morphology and microphase separation 139
4.6 Structure and composition of the grafts - summary 147

Chapter 5 Characterization of rheological properties - experimental methods 150
5.1 Introduction 150
5.1.1 Overview of the rheological characterization program 151
5.1.2 Summary of preliminary rheological characterization 152

5.1.3 Rheological issues 153
5.2 Rheometrics Mechanical Spectrometer - RMS-800 155
5.2.1 Principle of operation 155
5.2.2 Specimen preparation 157
5.2.3 Overview of the experimental program 159
5.2.4 Preliminary experiments 160
5.2.4.1 Time and time/cure sweeps 161
5.2.4.2 Dynamic strain sweep 163
5.2.4.3 Stress relaxation 178
5.2.4.4 Other preliminary issues and tests 180
5.2.5 Test interferences and data validation 185
5.2.6 Test accuracy, precision and sensitivity 186
5.3 Rheometrics Solids Analyzer - RSA-II 195
5.3.1 Principle of operation 195
5.3.2 Specimen preparation 196
5.3.3 Experimental program 197
5.3.4 Preliminary experiments 198
5.3.5 Test interferences and data validation 200
5.3.6 Test accuracy and precision 201
5.4 Rubber Process Analyzer - RPA-2000 203
5.4.1 Principles of operation and data analysis 203
5.4.2 Specimen preparation 207
5.4.3 Experimental program and test conditions 208
5.4.4 Preliminary experiments 212
5.4.5 Instrumental interferences and data validation 212
5.4.6 Test accuracy, precision and sensitivity 214
5.5 Dynamic Stress Relaxometer - DSR 216

5.5.1 Principle of operation 216
5.5.2 Specimen preparation 218
5.5.3 Experimental program and test parameters 219
5.5.4 Preliminary experiments 219
5.5.5 Test interferences and data validation 220
5.5.6 Test precision, sensitivity and accuracy 221
5.6 Special issues and topics 224
5.6.1 Effect of unattached polybutadiene 224
5.6.2 Effect of polymer stabilizer 225

Chapter 6 Linear viscoelastic (LVE) properties of CIIR-g-BR copolymers 226
6.1 Frequency dependence of linear viscoelastic functions 226
6.1.1 Dynamic mechanical moduli, G′(ω) and G″(ω) 227
6.1.2 Viscoelastic parameters and their correlation with LCB structure 241
6.1.3 Frequency dependence of complex viscosity 252
6.1.4 Modified Cole-Cole plots 257
6.2 Frequency-temperature superposition and temperature dependence of linear viscoelastic functions 265
6.2.1 Frequency-temperature superposition and master-curves 267
6.2.2 The issue of thermo-rheological complexity 270
6.2.3 Temperature dependence of the dynamic moduli, G′(T) and G″(T) 275
6.3 Relationship between LCB structure and complex modulus, G* 280
6.4 Time dependence of the stress relaxation modulus - I (10,000s experiment) 286
6.4.1 Normalized stress relaxation modulus, nG(t) 287
6.4.2 Stress relaxation parameters and their correlation with branching structure 299
6.5 Stress relaxation - II (1000s experiment) 305
6.6 Stress relaxation - III (400s experiment) 310

6.6.1. Time dependence of stress relaxation modulus 310
6.6.2 Correlations between branching structure and stress relaxation parameters 317

Chapter 7 Non-linear viscoelastic (NLVE) properties 321
7.1 Strain amplitude dependence of the dynamic moduli, $G_1'(\gamma)$ and $G_1''(\gamma)$ 322
7.2 Frequency and strain amplitude dependence of the viscoelastic functions from a large-amplitude oscillatory shear (LAOS) experiment 329
7.2.1 Non-linear viscoelastic parameters 329
7.2.2 Cole-Cole plot analysis of the dynamic moduli 335
7.2.3 Tangent of the loss angle, $\tan_1 \delta(\gamma, \omega)$ 341
7.2.4 Pipkin diagrams for $G_1'(\gamma, \omega)$ and $G_1''(\gamma, \omega)$ moduli 346
7.3 Effect of large-amplitude oscillatory shear (LAOS) 352
7.4 Non-linear stress relaxation in shear 368
7.4.1 Stress relaxation modulus, G(t) 371
7.4.2 Normalized stress relaxation modulus, nG(t) 379
7.5 Normalized Cole-Cole plot and its interpretation in terms of the LCB parameters 390

Chapter 8 Dynamic thermo-mechanical analysis (DTMA) 407
8.1 Introduction 407
8.2 DTMA of the branch precursor polymer, BR 412
8.3 DTMA of the backbone precursor polymer, CIIR 412
8.4 DTMA spectra of the graft copolymers 413
8.5 DTMA spectra of CIIR-g-BR graft copolymers 415

Chapter 9 Summary and conclusions 420
9.1 Summary 421
9.2 Conclusions 430

9.3 Significance of the work 435

9.4 Recommendations for future work 436

References 438

Appendix I Bibliography: rheological properties of long-chain branched polymers 459

Appendix II Nomenclature, symbols and abbreviations 482

Appendix III Apparent molecular weight distribution of the graft samples 492

Appendix IV Rheological characterization: test conditions and parameters 515

Appendix V Rheological test results - supplementary graphs and tables 521

- Figures 522

- - AFS series 522

- - AFTS series 547

- - A8 (DTMA) series 571

- - Prediction profiles 578

- Tables 599

Appendix VI Interrelations between structural and compositional parameters 615

List of Tables

Table		page
2-1	Comparison of selected physical properties of BR and CIIR rubbers	19
2-2	Summary of preliminary experiments with synthesis of CIIR-g-BR copolymers	23
2-3	Designed long-chain branching parameters and crude graft composition	26
2-4	Grafting efficiency and purification effectiveness	29
2-5	Stabilization and protection of samples	32
3-1	Analytical methods used for characterization of polymer structure, composition and morphology	57
3-2.	Characterization of molecular structure by SEC techniques	60
3-3.	SEC - test configuration and experimental conditions	61
3-4.	M-H-S coefficients	63
3-5.	Assessment of accuracy and test precision of SEC measurements	65
3-6.	Experimental test parameters of the ^{1}H NMR (solution technique)	70
4-1	An overview of methodology used for determination of structure, composition and morphology of CIIR-g-BR graft copolymers	88
4-2	Molecular weight distribution parameters - sample C (backbone prepolymer)	97
4-3	Molecular weight distribution parameters for Bxy samples (branch prepolymers)	113
4-4	Microstructure of branch precursor polybutadiene	115
4-5	Microstructure of BR polymerized using n-BuLi catalyst	116
4-6	Absolute values of refractive indices	117
4-7	Chemical composition of graft copolymers	122
4-8	Parameters of the molecular weight distribution of graft copolymers	124
4-9	Branching parameters	128
4-10	Comparison of molecular weight of branch precursor polymer, before and after grafting	131

Table		page
4-11	Compositional and molecular parameters of CIIR/BR blend and graft G4	132
4-12	TGA examination of short-term thermal stability	134
4-13	Evidence of phase morphology in CIIR-g-BR copolymers	141
4-14	Structure and composition of CIIR-g-BR copolymers - summary	148
5-1	Rheological instruments and test methods	152
5-2	CIIR-g-BR graft copolymers - rheological issues	154
5-3	RMS-800 - overview of the experimental program	160
5-4	Test precision results for RMS-800 dynamic mechanical test	190
5-5	Test precision results for the RMS-800 stress relaxation	191
5-6	Summary of test conditions for temperature sweep (DTMA)	198
5-7	Principal instrumental (RSA-II) interferences for DTMA test in tension	201
5-8	Principal instrumental interferences of the LAOS testing in torsion	213
6-1	MWD and first cross-over point parameters for samples C and B10	230
6-2	Characteristic molecular times estimated from frequency dependence of the dynamic moduli	240
6-3	Linear viscoelastic parameters defined for {FS5dec} frequency sweep test	242
6-4	Correlations coefficients between structural and rheological {FS5dec} parameters	243
6-5	Evaluation of the temperature-frequency shift and comparison of {FTS} master-curves with {FS5dec} isotherms	271
6-6	Coefficients of the WLF and Arrhenius equations	278
6-7	WLF and Arrhenius equation coefficients for CIIR and BR polymers	279
6-8	Definitions of viscoelastic parameters derived from {FSWP1} and FSWP2} experiments	280
6-9	Complex modulus values derived from {FSWP1} and {FSWP2} tests	285
6-10	Principal characteristics of LVE stress relaxation tests (RMS-800)	286
6-11	Definitions of viscoelastic parameters derived from {SR10,000} test	299

Table		page
6-12	Correlation coefficients between structural and rheological {SR10,000} test parameters	300
6-13	Definitions of viscoelastic parameters derived from {SR400} test	318
7-1	Definitions of non-linear viscoelastic parameters from {SSWP2} test	324
7-2	Correlation coefficients between structural and rheological {SSWP2} test parameters	325
7-3	Viscoelastic parameters derived from a large-strain frequency sweep {FSWP3} test	330
7-4	Correlation coefficients between structural and rheological parameters {FSWP3} test	331
7-5	Definitions of the viscoelastic parameters derived from {FSWP3} test	337
7-6	Correlation coefficients between structural and viscoelastic parameters - LAOS {FSWP3} test	338
7-7	Definitions of linear and non-linear viscoelastic parameters - {HSSWP1} test	353
7-8	Correlation coefficients between structural and viscoelastic parameters - {HSSWP1} test	354
7-9	Definitions of non-linear stress relaxation parameters - {TEST2} test	369
7-10	Correlations coefficients between structural/compositional and stress relaxation parameters - {TEST2} test	370
7-11	Classification of LCB structure in CIIR-g-BR copolymers	373
8-1	Definition of the {DTMA} parameters	410
8-2	Pearson product moment correlation coefficients for correlations between structural and {DTMA} parameters	411

(App. I)

A1.	Rheological properties of long-chain branched polymers: references to the selected original experimental contributions	460

Table		page
(App. IV)		
A - part 1	RMS-800 - test conditions and parameters - part 1	516
A - part 2	RMS-800 - test conditions and parameters - part 2	517
B	RSA-II - test conditions and parameters	518
C	RPA 2000 - test configurations	519
D	DSR - test conditions and parameters	520
(App. V)		
A61	Viscoelastic parameters derived from RMS-800 {FS5dec} test - I	599
A62	Viscoelastic parameters derived from RMS-800 {FS5dec} test - II	600
A63	Viscoelastic parameters derived from RMS-800 {FS5dec} test - III	601
A64	Viscoelastic parameters derived from RMS-800 {FS5dec} test - IV	602
A65	Stress relaxation parameters - {SR10,000} experiment	603
A66	Stress relaxation parameters - {SR1000} experiment	604
A67	Stress relaxation parameters - {SR400} experiment	605
A71	Selected rheological parameters from {SSWP2} test	606
A72	Viscoelastic parameters from LAOS - RPA 2000 {FSWP3} test	607
A73	Selected rheological parameters derived from {FSWP3} test	608
A74	Viscoelastic parameters derived from LAOS {HSSWP1} test - I	609
A75	Viscoelastic parameters derived from LAOS {HSSWP1} test - II	610
A76	Viscoelastic parameters derived from LAOS {HSSWP1} test - III	611
A77	Non-linear stress relaxation parameters from {TEST2} test	612
A8a	DTMA parameters - I	613
A8b	DTMA parameters - II	614
(App. VI)		
AppVI	Interrelations between structural and compositional parameters: t-Ratio table	617

List of Illustrations

Figure		page
2-1	Overview of graft sample preparation	18
2-2	Scheme of the grafting reaction	25
2-3	Apparatus for extraction of ungrafted parent polymers	31
3-1	Sampling points for composition and structure characterization	56
3-2	Repeatibility of SEC measurements	67
3-3	Correlation between SEC results obtained by different GPC systems	68
3-4	NMR (200 MHz) spectrum of sample C (backbone prepolymer)	71
3-5	NMR (200 MHz) spectrum of the sample B4q (branch prepolymer of the graft FG8)	72
3-6	NMR (200 MHz) spectrum of the sample FG10	73
3-7	Section of the NMR (500 MHz) spectrum for the sample C	75
3-8	Three forms of polybutadiene microstructure	78
3-9	FT-IR spectrum of sample B4p (branch prepolymer corresponding to FG21)	80
3-10	Definition of the $T_{g,f}$ from DSC scan	81
4-1	M-H-S plots for narrowly polydispersed PMMA	92
4-2	M-H-S plots for narrowly polydispersed PS	92
4-3	M-H-S plots for linear and branched chlorobutyl rubber	93
4-4	SEC(W) traces for sample C	96
4-5	M-H-S plot for Bxy samples - SEC(W)	105
4-6	Examples of M-H-S plot for two commercial "branched" polybutadienes	105
4-7	Normalized SEC(W) traces for sample B9a (FG14)	107
4-8	Normalized SEC(W) traces for sample B4m (FG4)	108
4-9	Normalized SEC(W) traces for sample B4q (FG8)	109

Figure		page
4-10	Normalized SEC(P) trace for sample B5f (FG5)	110
4-11	Normalized SEC(P) trace for sample B6h (FG6)	110
4-12	Normalized SEC(P) trace for sample B3f (FG12)	111
4-13	Normalized SEC(P) trace for sample B4o (FG15)	111
4-14	Correlation between branch length and SEC retention time shift	125
4-15	Algorithm used for calculation of the branching number	127
4-16	Correlation between N_g and N_g^p branching numbers	129
4-17	Molecular weight distribution (SEC/P) - sample M amd its components	133
4-18	TGA scan - sample C	135
4-19	Gel content detection	137
4-20	TEM microphotograph for sample FG18	143
4-21	TEM microphotographs for sample FG5	143
4-22	TEM microphotographs for sample FG19	144
4-23	TEM microphotographs for sample FG1	144
4-24	TGA scan -sample G1	145
4-25	TGA scan -sample G6	145
4-26	Principal branching parameters of CIIR-g-BR graft copolymers	149
5-1	RMS-800 parallel-plate test fixture	156
5-2	RMS-800: isothermal time sweep	162
5-3	RMS-800: isochronous temperature ramp	162
5-4	Definition of the critical strain amplitude, γ_{cr}^{LVE}	165
5-5	RMS-800: isochronous strain sweep, sample G1	167
5-6	RMS-800: isochronous strain sweep, sample G2	167
5-7	RMS-800: isochronous strain sweep, sample G8	168
5-8	RMS-800: isochronous strain sweep, sample G10	168
5-9	RMS-800: isochronous strain sweep, sample G13	169

Figure		page
5-10	RMS-800: isochronous strain sweep, sample G19	169
5-11	RMS-800: isochronous strain sweep, sample C	170
5-12	RMS-800: isochronous strain sweep, sample B10	170
5-13	RMS-800: strain sweep loop experiment	173
5-14	RMS-800: small-large-small strain experiment	175
5-15	RMS-800: anatomy of typical stress relaxation experiment	179
5-16	RMS-800: stress relaxation - effect of strain amplitude	181
5-17	RMS-800: stress relaxation - determination of the LVE limits	182
5-18	RMS-800: sequential stress relaxation experiment	183
5-19	RMS-800: dynamic test precision	192
5-20	RMS-800: stress relaxation - test precision	193
5-21	RMS-800: relation between torque decay and test precision	194
5-22	RSA-II: film/fiber test fixture	196
5-23	RPA 2000: principle of operation and cross-section of test cavity	204
5-24a	RPA 2000: test configuration diagram (I) - small-strain amplitude frequency sweep	209
5-24b	RPA 2000: test configuration diagram (II) - dynamic strain sweep sweep	210
5-24c	RPA 2000: test configuration diagram (II) - and large amplitude oscillatory shear (LAOS) experiment	210
5-24d	RPA 2000: test configuration diagram (III) - large strain-amplitude frequency sweep	211
5-25	RPA 2000 - test precision (a) sample G1, (b) sample G8	215
5-26	Dynamic Stress Relaxameter - principle of operation	217
5-27	DSR - test precision for G(t), c.v.%	222
5-28	DSR - test precision for nG(t), c.v.%	222
5-29	DSR - test precision for G(t), sample G21	223
5-30	DSR - test precision for nG(t), sample G21	223

Figure		page
5-31	Effect of unattached BR content in CIIR-g-BR	225
6-1	Typical dynamic mechanical spectrum for polymers with flexible and linear molecules	228
6-2	Dynamic mechanical spectra for linear molecules - samples C & B10	229
6-3	Dynamic mechanical spectra for samples C & M	231
6-4	Dynamic mechanical spectra for samples M and G4	232
6-5	Dynamic mechanical spectra for samples C and G1	234
6-6	Dynamic mechanical spectra for samples G1 and G7	234
6-7	Dynamic mechanical spectra for samples G5 and G17	235
6-8	Dynamic mechanical spectra for samples G2 and G18	237
6-9	Dynamic mechanical spectra for samples G5 and G21	237
6-10	Dynamic mechanical spectrum for sample G21	239
6-11	Dynamic mechanical spectra for samples G19 and G20	239
6-12	Dynamic mechanical spectra for samples G10 and G22	240
6-13	Composite graph of tan δ - {FS/5dec} test	245
6-14	Tan δ at ω=0.001 rad/s as a function of branch length	247
6-15	Tan δ at ω=0.001 rad/s as a function of branching number	247
6-16	Slope of log G"(ω) at 0.001 rad/s as a function of branch length	250
6-17	Slope of log G"(ω) at 0.001 rad/s as a function of branching number	250
6-18	Slope (G'(ω)/G"^{2}(ω))@0.001 parameter as a function branch length	251
6-19	Complex viscosity curves for representative samples	253
6-20	Frequency dependence of complex viscosity; effect of branch length	255
6-21	Frequency dependence of complex viscosity; effect of branching number	255
6-22	Typical modified Cole-Cole plot - example for sample G17	258
6-23	Modified Cole-Cole contours for linear or weakly-branched molecules	260
6-24	Modified Cole-Cole contours for multi-branched, comb-like structures	261

Figure		page
6-25	Modified Cole-Cole contours for grafts with intermediate branching structures	262
6-26	Modified Cole-Cole contours for grafts with few long branches ("star"-like structures)	263
6-27	Evolution of the modified Cole-Cole contour, a) as a function of branch length, at comparable number of branches b) as a function of branching number, at comparable branch length	264
6-28	Typical normalized Cole-Cole plot - example for sample G17	266
6-29	A series of dynamic moduli isotherms for sample G3	268
6-30	Master-curve of dynamic moduli obtained by shifting a series of isotherms according to t/f-T superposition principle - example for sample G3	269
6-31	Predition profiles for screening between quantified assessment of the agreement between {FTS} and {FS5dec} curves (G' and G") and structural parameters	276
6-32	Prediction profiles for correlations between branching parameters and complex modulus, G*	281
6-33	Frequency dependence of the complex modulus, G* - composite graph	283
6-34	Prediction profiles for correlations between branching content and complex modulus, G*	284
6-35	Stress relaxation of linear parent polymers, their blend and graft (G4)	288
6-36	Stress relaxation - {SR10,000}. Behaviour of weakly-branched structures	290
6-37	Stress relaxation - {SR10,000}. Effect of branch length	291
6-38	Stress relaxation - {SR10,000}. Effect of the number of branches - I	293
6-39	Stress relaxation - {SR10,000}. Effect of the number of branches - II	294
6-40	Stress relaxation - {SR10,000}. Effect of the ungrafted BR content - I	295
6-41	Stress relaxation - {SR10,000}. Effect of the ungrafted BR content - II	296
6-42	Stress relaxation - {SR10,000}. Reproducibility of test results	297
6-43	Composite graph of the normalized stress relaxation modulus, nG(t)	298

Figure		page
6-44	Relationship between INT G(t)dt parameter and branching number	303
6-45	Relationship between slope of nG(t) @ t=10,000s and branching content	303
6-46	Rate of nG(t) decay as a function of specific branching parameters	304
6-47	Correlation between stress relaxation parameters from {SR10,000} and {SR1000} tests	306
6-48	Relation between branch length and nG(t=1000) parameter	307
6-49	Relation between branching number and nG(t=1000) parameter	309
6-50	Stress relaxation - {SR400}. Comparison between samples C, M and G4	311
6-51	Stress relaxation - {SR400}. Effect of branch length - I	312
6-52	Stress relaxation - {SR400}. Effect of branch length - II	313
6-53	Stress relaxation - {SR400}. Effect of number of branches - I	314
6-54	Stress relaxation - {SR400}. Effect of number of branches - II	315
6-55	Stress relaxation - {SR400}. Effect of branching content	316
6-56	Stress relaxation - {SR400}. Summary of observations	317
6-57	Prediction profiles for correlation between compositional and stress relaxation {SR400} parameters	319
7-1	Strain sweep {SSWP2}, sample C	323
7-2	Strain sweep {SSWP2}, sample G19	323
7-3	Effect of branching on the onset of non-linearity in dynamic	327
7-4	Strain sweep {SSWP2}, sample M, T=100°C	327
7-5	Effect of branch length on G_1^* (50%) complex modulus	328
7-6	Effect of branching number on G_1^* (50%) complex modulus	328
7-7	Relationship between length of the branch and in-phase modulus, G_1'(200%/10rad/s)	333
7-8	Relationship between branch length and out-of-phase modulus, G_1'' (200%/10rad/s)	334
7-12	Relationship between branch length and contour length of the modified Cole-Cole plot	340

Figure		page
7-9	Relationship between branching number and out-of-phase modulus, G_l" (200%/10rad/s)	334
7-10	Relationship between branching content and tan_l δ(200%/0.5rad/s)	336
7-11	Relationship between branching content and tan_l δ ratio	336
7-13	Relationship between branching number and contour length of the mC-C plot - chart I for samples with high ungrafted BR content	340
7-14	Relationship between branching number and contour length of the modified Cole-Cole plot - chart II for samples with low ungrafted BR content	341
7-15	Frequency and strain dependence of loss tangent, tan_l δ	343
7-16	Frequency dependence of loss tangent, tan_l δ. Effect of branch length at 200% strain	345
7-17	Frequency dependence of loss tangent, tan_l δ. Effect of branching number at 200% strain	345
7-18	Pipkin diagram of the in-phase dynamic modulus, sample C	348
7-19	Pipkin diagram of the out-of-phase dynamic modulus, sample C	348
7-20	Pipkin diagram of the in-phase dynamic modulus, sample G19	349
7-21	Pipkin diagram of the out-of-phase dynamic modulus, sample G19	349
7-22	Pipkin diagram of the in-phase dynamic modulus, sample G13	350
7-23	Pipkin diagram of the out-of-phase dynamic modulus, sample G13	350
7-24	Pipkin diagram of the in-phase dynamic modulus, sample G6	351
7-25	Pipkin diagram of the out-of-phase dynamic modulus, sample G6	351
7-26	High strain-amplitude experiment, composite plot - storage modulus	358
7-27	High strain-amplitude experiment, composite plot - loss modulus	359
7-28	LAOS experiment, composite plot - I [G"(5%/VI) - (G"(5%/II)]	362
7-29	LAOS experiment, composite plot - II storage modulus, 5%, 200%, 800% strain	364
7-30	LAOS experiment, composite plot - III loss modulus, 5%, 200%, 800% strain	365
7-31	LAOS experiment, composite plot - IV loss tangent,5%, 200%, 800% strain	366
7-32	LAOS experiment, composite plot - V torque, 5%, 200%, 800% strain	367

Figure		page
7-33	Stress relaxation modulus - composite plot	372
7-34	Classification of the main types of the LCB structure in CIIR-g-BR samples	374
7-35	Stress relaxation modulus	375
7-36	Effect of branch length on the stress relaxation modulus at low branching numbers	378
7-37	DSR - evidence of integrity of test results	378
7-38	Normalized stress relaxation modulus, nG(t); composite graph	380
7-39	Normalized stress relaxation modulus - overview of typical relaxational behaviour	381
7-40	Normalized stress relaxation modulus, effect of branch length - I	383
7-41	Normalized stress relaxation modulus, effect of branch length - II	383
7-42	Normalized stress relaxation modulus, effect of branching number - I	384
7-43	Normalized stress relaxation modulus, effect of branching number - II	385
7-44	Normalized stress relaxation modulus, effect of branching number	385
7-45	Normalized stress relaxation modulus, effect of branching parameters at comparable branching content	386
7-46	Relationship between branch length and G(40ms) modulus	388
7-47	Relationship between number of branches and G(40ms) modulus	388
7-48	Relationships between length of the branches and normalized stress relaxation modulus, nG(0.1)	389
7-49	Relationship between number of branches and normalized stress relaxation modulus, nG(0.1)	389
7-50	Normalized Cole-Cole plot - contours for LCB, type A	392
7-51	Normalized Cole-Cole plot - contours for LCB, type B	393
7-52	Normalized Cole-Cole plot - contours for LCB type F	394

Figure		page
7-53	Normalized Cole-Cole plot - contours for LCB type D	395
7-54	Normalized Cole-Cole plot - contours for LCB type E	397
7-55	Normalized Cole-Cole plot - contours for LCB type C	398
7-56	Normalized Cole-Cole plot - Effect of increasing branching content,	399
7-57	Normalized Cole-Cole plot - Effect of branch length	401
7-58	Normalized Cole-Cole plot - Effect of branching frequency	402
7-59	Normalized C-C plot: Effect of branching structure at comparable branching content	403
7-60	Normalized C-C plot: Grafting CIIR-g-BR versus blending CIIR/BR	404
7-61	Normalized C-C plot - effect of LCB structure: final conclusion	406
8-1	Definition of {DTMA} rheological parameters	409
8-2	Summary of changes in the DTMA spectrum induced by grafting	419

(Figures in Appendix III)

MWD/SEC - sample G1		493
MWD/SEC - sample G2		494
MWD/SEC - sample G3		495
MWD/SEC - sample G4		496
MWD/SEC - sample G5		497
MWD/SEC - sample G6		498
MWD/SEC - sample G7		499
MWD/SEC - sample G8		500
MWD/SEC - sample G9		501
MWD/SEC - sample G10		502
MWD/SEC - sample G11		503
MWD/SEC - sample G12		504

Figure		page
MWD/SEC - sample G13		505
MWD/SEC - sample G14		506
MWD/SEC - sample G15		507
MWD/SEC - sample G16		508
MWD/SEC - sample G17		509
MWD/SEC - sample G18		510
MWD/SEC - sample G19		511
MWD/SEC - sample G20		512
MWD/SEC - sample G21		513
MWD/SEC - sample G22		514

(Figures in Appendix V)

AFSC	Dynamic mechanical spectrum - sample C	522
AFSG1	Dynamic mechanical spectrum - sample G1	523
AFSG2	Dynamic mechanical spectrum - sample G2	524
AFSG3	Dynamic mechanical spectrum - sample G3	525
AFSG4	Dynamic mechanical spectrum - sample G4	526
AFSG5	Dynamic mechanical spectrum - sample G5	527
AFSG6	Dynamic mechanical spectrum - sample G6	528
AFSG7	Dynamic mechanical spectrum - sample G7	529
AFSG8	Dynamic mechanical spectrum - sample G8	530
AFSG9	Dynamic mechanical spectrum - sample G9	531
AFSG10	Dynamic mechanical spectrum - sample G10	532
AFSG11	Dynamic mechanical spectrum - sample G11	533
AFSG12	Dynamic mechanical spectrum - sample G12	534
AFSG13	Dynamic mechanical spectrum - sample G13	535

Figure		page
AFSG14	Dynamic mechanical spectrum - sample G14	536
AFSG15	Dynamic mechanical spectrum - sample G15	537
AFSG16	Dynamic mechanical spectrum - sample G16	538
AFSG17	Dynamic mechanical spectrum - sample G17	539
AFSG18	Dynamic mechanical spectrum - sample G18	540
AFSG19	Dynamic mechanical spectrum - sample G19	541
AFSG20	Dynamic mechanical spectrum - sample G20	542
AFSG21	Dynamic mechanical spectrum - sample G21	543
AFSG22	Dynamic mechanical spectrum - sample G22	544
AFSM	Dynamic mechanical spectrum - sample M	545
AFSB10	Dynamic mechanical spectrum - sample B10	546
AFTSC	Master curve - sample C	547
AFTSG1	Master curve - sample G1	548
AFTSG2	Master curve - sample G2	549
AFTSG3	Master curve - sample G3	550
AFTSG4	Master curve - sample G4	551
AFTSG5	Master curve - sample G5	552
AFTSG6	Master curve - sample G6	553
AFTSG7	Master curve - sample G7	554
AFTSG8	Master curve - sample G8	555
AFTSG9	Master curve - sample G9	556
AFTSG10	Master curve - sample G10	557
AFTSG11	Master curve - sample G11	558
AFTSG12	Master curve - sample G12	559
AFTSG13	Master curve - sample G13	560
AFTSG14	Master curve - sample G14	561

Figure		page
AFTSG15	Master curve - sample G15	562
AFTSG16	Master curve - sample G16	563
AFTSG17	Master curve - sample G17	564
AFTSG18	Master curve - sample G18	565
AFTSG19	Master curve - sample G19	566
AFTSG20	Master curve - sample G20	567
AFTSG21	Master curve - sample G21	568
AFTSG22	Master curve - sample G22	569
AFTSM	Master curve - sample M	570

(App. V)

A61	Prediction profiles for correlations between structural (M_p^b, N_g^p) and {FS5dec} viscoelastic parameters - I	578
A62	Prediction profiles for correlations between structural ($w_b,^g$, M_z^G) and {FS5dec} viscoelastic parameters - II	579
A63	Prediction profiles for correlations between structural (w^b, $w_b,^h$) and {FS5dec} viscoelastic parameters - III	580
A64	Prediction profiles for correlations between structural (PDI, vinyl%) and {FS5dec} viscoelastic parameters - IV	581
A65	Prediction profiles for correlations between structural (M_p^b, N_g^p) and stress relaxation {SR10,000} parameters	582
A66	Prediction profiles for correlations between structural ($w_b,^g$, $w^{b,h}$) and stress relaxation {SR10,000} parameters	583
A67	Prediction profiles for correlations between structural (w^b, M_z^G) and stress relaxation {SR10,000} parameters	584
A71(a, b, c, d)	Prediction profiles - M_p^b, N_g^p, $w^{b,g}$, w^b and {SSWP2} parameters	585
A71(e, f, g, h)	Prediction profiles - M_z^G, $w^{b,h}$, PDI, vinyl% and {SSWP2}parameters	586

Figure		page
A72a	Prediction profiles for correlations between structural (M_p^b, N_g^p) and viscoelastic parameters from {FSWP3} experiments	587
A72b	Prediction profiles for correlations between structural ($w^{b,g}$, w^b) and viscoelastic parameters from {FSWP3} experiments	588
A72c	Prediction profiles for correlations between structural ($w^{b,h}$, M_z^G) and viscoelastic parameters from {FSWP3} experiments	589
A72d	Prediction profiles for correlations between structural (PDI, vinyl) and viscoelastic parameters from {FSWP3} experiments	590
A73a	Prediction profiles for correlations between structural (M_p^b, N_g^p) and viscoelastic parameters from {FSWP3} experiments	591
A73b	Prediction profiles for correlations between structural ($w^{b,g}$, w^b) and viscoelastic parameters from {FSWP3} experiments	591
A73c	Prediction profiles for correlations between structural ($w^{b,h}$, M_z^G) and viscoelastic parameters from {FSWP3} experiments	592
A73d	Prediction profiles for correlations between structural (PDI, vinyl%) and viscoelastic parameters from {FSWP3} experiments	592
A74a	Prediction profiles for correlation between structural (M_p^b) and viscoelastic parameters from {HSSWP} experiments	593
A74b	Prediction profiles for correlation between structural (N_g^p) and viscoelastic parameters from {HSSWP} experiments	594
A74c	Prediction profiles for correlation between structural ($w^{b,g}$) and viscoelastic parameters from {HSSWP} experiments	595
A74d	Prediction profiles for correlation between structural (Φ) and viscoelastic parameters from {HSSWP} experiments	596
A75a	Prediction profiles for correlations between structural parameters (M_p^b, N_g^p) and selected stress relaxation parameters from {TEST2} tests	597
A75b	Prediction profiles for correlations between structural parameters ($w^{b,g}$, w^b) and selected stress relaxation parameters from {TEST2} tests	598
A8B10	Dynamic thermo-mechanical spectrum for sample B10	571

Figure		page
A8C	Dynamic thermo-mechanical spectrum for sample C	572
A8G2	Dynamic thermo-mechanical spectrum for sample G2	573
A8G3	Dynamic thermo-mechanical spectrum for sample G3	574
A8G6	Dynamic thermo-mechanical spectrum for sample G6	575
A8G16	Dynamic thermo-mechanical spectrum for sample G16	576
A8G22	Dynamic thermo-mechanical spectrum for sample G22	577
(App. VI)		
AppVIa	Prediction profiles for interrelations between structural and compositional parameters - I	618
AppVIb	Prediction profiles for interrelations between structural and compositional parameters - II	619

Introduction

Long-chain branching (LCB) is one of the principal structural factors influencing the properties of elastomers. Our understanding of the effect that long-chain branching has on the rheological properties of polymers is not yet complete. This is particularly true for non-linear viscoelastic properties and for chemically heterogeneous polymeric systems such as graft copolymers.

Rheological properties are important for processing of polymeric materials. They also can be used as an analytical technique to characterize certain aspects of structure and composition of a polymer. Furthermore, they have potential as a predictive tool for an assessment of the processing performance of a material.

Both precursor polymers used to make graft copolymers for this study, polybutadiene (BR) and chlorobutyl rubber (CIIR), are important commercial elastomers, used in large volumes in the tire making industry. They possess different but complementary properties, which are important for the proper functioning of a modern automobile tire but because these two polymers are immiscible, they cannot be usefully incorporated into the tire tread as a blend. This has numerous technical and economic implications, including the adhesion of the butyl containing innerliner to tire tread, having BR as a main component.

Grafting BR onto CIIR (or vice versa) constitutes one of the possible compatibilization routes but with an additional opportunity to tune-up the copolymer physical properties by appropriate design of its long-chain branching structure. While the chemistry of CIIR-g-BR systems, together with certain physical properties has been investigated in recent years, the rheological properties of CIIR-g-BR copolymers have not. In fact, very little is known about

the rheological properties of graft copolymers regardless of the underlying chemistry, except for studies devoted to thermal transitions in the glassy and transition zones of the viscoelastic spectrum.

Therefore, in order to better understand the relationship between the long-chain branching structure of CIIR-g-BR copolymers and their performance in processing and various applications, it was proposed to carry out systematic studies of rheological properties of these materials. Partial results of this research are the subject of this dissertation.

A series of model graft copolymer samples was prepared using properly modified, patented technology. The chemical and physical composition, as well as molecular structure of these copolymers, was extensively characterized in order to quantify the principal LCB parameters. Special attention was paid to all of those characteristics of the molecular structure and composition, which could interfere with the accuracy of the intended correlations between LCB and rheological parameters. Furthermore, rheological properties of CIIR-g-BR copolymer samples were measured by a variety of techniques, with special emphasis on properties which are dominated by long-time processes, particularly those affected by the presence of long-chain branching. Numerous phenomenological relationships between structure and rheology were then established, with the assistance of appropriate statistical methods.

A brief overview of the rheology of long-chain branched polymers is given in chapter 1. The preparation of the CIIR-g-BR samples is described in the following chapter.
A comprehensive characterization of the structure and composition of these graft copolymers, as well as their backbone and branch precursor polymers by various analytical techniques is described in the next two chapters, namely in chapter 3 (instrumental methods) and in chapter 4 (results). Chapter 5 is devoted to a detailed description of the experimental aspects of rheological characterization. It also contains some preliminary rheological results. The main

results and their interpretation in terms of long-chain branching structure are presented in chapter 6 for linear viscoelastic properties, in chapter 7 for non-linear viscoelastic properties, and in chapter 8 for dynamic thermo-mechanical analysis. The last chapter (9) summarizes the main findings, provides the final conclusions, discusses the significance of this work and presents some ideas for the future work.

Finally, six appendices are attached. The first appendix contains a guided bibliography in the area of rheological properties of long-chain branched polymers. The second appendix contains nomenclature and a list of abbreviations used throughout the thesis. The third appendix includes a collection of MWD/SEC graphs for the entire set of samples. A complete record of the rheological test conditions and parameters is included in Appendix IV, while diagrams and tables with additional data and statistical correlation charts are collected in Appendix V. The correlations which exist among the parameters describing the structure and composition of samples prepared for this project, as well as the implications they might have on the relationship between LCB structure and rheological properties, are discussed in Appendix VI.

Chapter 1

Rheological properties of long-chain branched polymers

1.1 Brief overview

Branching of a macromolecule is one of its primary structural characteristics, as is its length (molecular mass). The type of branching, branch length and branching frequency may have a profound effect on physical properties of the polymer.

In the literature there are many definitions of "short" and "long" branches. In fact, the length of side branches in combs may vary from a methyl group or pendant groups containing a few carbon atoms (ethyl groups in polyethylene, for example) to branch lengths approaching or even exceeding the length of the backbone itself. Indeed, star-shaped structures, frequently made to be used as models of branched polymers, may be regarded as a special class of comb-like molecules, where the backbone length degenerates to nearly zero, while a multi-functional moiety, regardless of its chemical nature, constitutes a single branching point for many branches spreading radially outward. In the context of rheological studies, regular star molecules with up to 270 branches were reported [1].

For the purposes of this work, long branches will be defined as those long enough to detectably influence the particular rheological behaviour under study. For instance, it is well established that short side chains have no noticeable effect on the melt rheology of homopolymers, even if their number per unit length of the backbone (e.g. frequency) is much higher than branching frequency of a typical long-chain branched polymer [2].

On the other hand, thermo-mechanical properties in the glassy zone of viscoelastic behaviour are readily affected by the presence of short branches and the magnitude of the influence depends on the branch size, flexibility and frequency.

Literature reporting original experimental contributions on the rheology of well characterized, long chain branched (LCB) polymers is relatively limited. This is particularly true for chemically heterogeneous branched systems such as graft and star-block copolymers. Hence the rheology of graft copolymers is a largely unexplored area, and there are few references with which to compare results (cf. highlighted areas in Table A1 in Appendix I).

Publications concerned with the effect of long chain branching on rheology can be divided into three groups. The first group deals with samples of commercial materials, where uncontrolled branching is usually a result of the polymerization mechanism. The second group typically describes experimental or developmental materials where branching was induced deliberately by chemical or physical means, in order to modify properties of linear precursors. The third group of papers involves model branched polymers, prepared by special techniques exerting a high degree of control over the structure of the polymer.

For commercial and developmental materials, some information on branching structure is deduced from reaction kinetics and/or characterized by a combination of appropriate analytical techniques. As a result, due to the enormous structural complexity of randomly branched structures and difficulties in separating the influence of other contributing factors (molecular weight, MW, molecular weight distribution, MWD, three-dimensional networks - gels, impurities, etc.) many of these studies can afford only qualitative assessment of the relationship between rheology and LCB. By far, the most frequently investigated commercial polymer has been low density polyethylene (LDPE) [3-13].

For fundamental studies of the relationship between structure and physical/rheological properties, polymeric samples are usually prepared by special techniques yielding highly regular branched structures of known topology and narrow distribution of molecular mass of the branches, arms or backbones [14-15].

As far as long-chain branching parameters are concerned, the structures of certain model polymers such as stars can be completely characterized, while those of combs can be characterized comprehensively enough to allow reliable and quantitative correlation between branching parameters and rheological properties. Many of the published results concern polystyrene [16-22], polybutadiene [23-29] and polyisoprene [30-34]. The research on well characterized, hydrogenated polybutadiene, regarded as a model polymer to study the effect of LCB on melt rheology in LDPE, was also reported [35-37].

Historically, Staudinger and Schulz first suggested, in 1935, the possibility of (long) chain branching in order to explain certain discrepancies between the osmotic and viscometric molecular weights of polystyrenes [38]. Subsequently, in 1937, Flory showed how chain transfer to polymer during radical polymerization can create long-chain branching [39].

Probably the first published work attempting to quantitatively correlate long-chain branching with melt rheological properties was the work of Schaefgen and Flory on branched polyamides [40]. Branching was found to decrease the magnitude of the low shear viscosity, although the effect was not spectacular.

Non-linear structures in commercial polymers are typically generated by some random branching chemistry during the polymerization. Random branching invariably yields a broad distribution of structures, and it becomes difficult to separate the effects of molecular mass distribution width, for instance, from the effects due exclusively to the long chain branching.

Since the 1950s it has become apparent that the quantitative understanding of the effects of branching on rheological behaviour cannot be confidently defined through work on randomly branched structures. This is particularly true if branching is inseparable from the associated changes in the molecular weight distribution, or precedes the formation of three dimensional networks. Developments in controlled polymerization techniques, capable of making polymers of simple and predictable structures, allowed studies of model polymers with more readily measurable branching parameters [14].

Studies based on partial knowledge of chain topology and those which neglect other contributing structural factors (e.g. MW polydispersity) may lead to conclusions, as far as structure-rheological property relationship is concerned, which will be in (apparent) contradiction with other reported data for structurally similar systems. For example, it has been reported that in polyethylene and silicone polymer melts the viscosity decreases with increasing degree of long-chain branching at constant weight-average molecular weight [41], whereas in poly(vinyl acetate) melt viscosity increases under the same circumstances [42]. The reason for this ambivalence appears to lie in a difference in branch length.

In experiments with poly(vinyl acetate) branched by graft polymerization, melt viscosity was lower for the branched polymer than for a linear polymer of comparable molecular weight, provided that the branches were shorter than some critical chain length, Z_e. On the contrary, when the branches were longer than Z_e, the viscosity of branched polymer was higher [42].

Similarly, Kraus and Gruver found that the zero-shear viscosity for tri-chain and tetra-chain star branched polybutadienes was lower than that of the linear polymer with the same molecular weight, but only in the lower molecular weight range. Above certain critical molecular mass the viscosity of the branched polymer increased rapidly with increasing molecular weight and surpassed that of the linear polymer [26]. Similar results were reported by Folt [43].

Most of the comprehensive studies on the rheology of the LCB polymers were done on samples having highly regular, star-branched molecules. Molecular stars of highly uniform structure can be made by "living" anionic polymerization. Branch length can be controlled by

the stoichiometry and conditions of the reaction, while branch point functionality can be varied widely by selection of the appropriate chemistry. While the molecular architecture of stars is relatively easy to control and to characterize, the structure
itself is quite remote from that of many commercially important thermoplastics and elastomers. In fact, it was not until recently that the potential benefit of the incorporation of star-branched molecules into polymeric systems was proven feasible and successful on a commercial scale in elastomers [44-46].

Some effects cannot be studied with stars. Thus regular combs have been prepared and their rheological properties studied in terms of the LCB structure [18-19, 47-48]. Rheological study of well characterized, randomly branched chains, prepared by laborious fractionation of polydisperse samples, was also reported [49].

The introduction of branching can result in thermo-rheologically complex behaviour, in which the normal shift of rheological functions with temperature through time-temperature superposition no longer applies [4, 24, 37, 50]. This is particularly true for heterogeneous polymers such as grafts, star blocks or branched block-copolymers.

1.2 Rheological properties of model long-chain branched polymers

1.2.1 Regular stars

Stars with all arms of equal length represent the topologically simplest structure among branched polymers. For regular stars only two parameters, the number of arms and molecular weight, are necessary to characterize branching structure. Berry and Fox first noted that the viscosity of star molecules below the entanglement threshold molecular weight is similar in magnitude to that of linear chains of the same radius of gyration, $\bar{S}_0$ [51]. A conventional

comparison of branched and linear zero-shear viscosity as a function of the weight-average molecular weight, $\overline{M}_w$, was made for linear and 4-arm and 6-arm polystyrene stars [16]. The branched samples showed considerably lower viscosity than the linear polymer, and the 6-arm star showed lower viscosity than the 4-arm stars. Also the slope of the log η_0 versus log $\overline{M}_w$ curve at higher molecular weights increased progressively with molecular weight.

Similar studies for polyisoprene [30] showed a very similar relation between zero-shear viscosity for three types of polymer structure, namely, linear, four-equal-length-arm and six-equal-length-arm polymers. At low molecular weights the viscosity of both branched polymers were considerably lower than those of linear polymer of the same molecular weight, $\overline{M}_w$. The phenomenon of viscosity increasing exponentially as a function of weight-average molecular weight of the branch, called 'viscosity enhancement', has been observed for other polymers as well [2, 50].

The elastic properties of stars in the melt and in solution show marked deviations from those of linear molecules. The steady-shear recoverable compliance, J_e^o, of polystyrene,

polyisoprene, polybutadiene and poly(α-methyl styrene) as a function of molecular weight has been measured and reported [16, 34, 52-54]. The variation of recoverable compliance with molecular weight is also different for linear and branched polymers. In contrast with the behaviour of nearly monodispersed linear polymers, for which J_e^o becomes constant at $\overline{M}_w$ equal to about 5 times M_e, the value of J_e^o for stars continue to increase with $\overline{M}_w$, in direct proportion to M^b, with reasonable agreement with the prediction of the Rouse model for star molecules [55]. M_e and M^b are the average molecular weight between entanglements, and the molecular weight of the arm, respectively.

1.2.2 Regular comb-shaped molecules

The rheological behaviour of regular, comb-shaped molecules is studied to bridge the gap between the simplest model structures of star-molecules and randomly branched polymers. The simplest type of comb structure reported in the literature is that of H-shaped polystyrenes where each of the five sub-chains are of approximately equal length [56]. As with star-branched polymers, viscosity enhancement is also observed. For the H-shaped structures, the zero-shear compliance increases with molecular weight, as well.

Much less information is available on the rheology of carefully prepared and characterized comb-type polymers. Results for regular combs are not as clear as they are for stars or H-shaped polymers. In contrast with simpler structures, the molecular weight of the branches, the backbone molecular weight, and the number of branch points, as well as their distribution can vary in combs. In addition, the existing literature seems to contain contradictory results regarding the viscosity enhancement and exponential dependence of shear viscosity on branch length [18-19, 57-61].

Recently, relaxation properties of a model structure of 'star-combs', probably the closest known and rheologically characterized approximation of the randomly branched polymers, were reported [61].

1.3 Randomly branched polymers

Studies on rheological properties of randomly branched polymers comprise a substantial portion of the published literature on the subject. This is a reflection of the fact that most of the commercial, branched polymers have randomly distributed branches. Interest in the rheological properties of these materials corresponds to the significance they have for

polymer processing engineering, particularly for performance in forming operations, such as extrusion or moulding [62].

For example, the viscosity enhancement of randomly branched polymers, relative to linear polymers, appears similar to the results on more regularly branched or better characterized systems [4, 63]. Examination of the viscosity as a function of shear rate for polyethylene indicates that the higher the molecular weight, $\overline{M}_w$, and LCB density (typically measured as the number of branches per 1000 CH_2 groups in LDPE), the lower is the melt viscosity and the higher is the critical shear rate at which departure from Newtonian viscosity-shear rate dependence is observed.

A technologically important measure of elastic response in steady shear is the post-extrusion swell ratio. Some reports indicate that the swell ratio increases with branching frequency (#LCB/1000 CH_2) [64-65]. However, when comparisons are made at constant molecular weight, the swell ratio is reported to decrease with branching frequency [4]. It is possible that

this apparent contradiction could be reconciled if *all relevant* details of the molecular structure were known and considered.

1.4 Graft copolymers

As noted earlier, the published work on the rheology of long-chain branched graft copolymers is rather scarce (see Appendix 1).

Some early papers on the subject actually refer to the structures intermediate between branched, dendrite-like and macro-gels as "graft copolymers" [66-67]. The overwhelming structural complexity of these "graft" copolymers - poly(vinyl acetate-g-methyl methacrylate and poly(vinyl chloride-g-methyl methacrylate) - was not quantified and did not allow for a

proper interpretation of results on the solution (osmotic and viscometric) and bulk thermo-mechanical properties of these "grafts".

Rieke and Hart reported the physical and processing properties of (high density) polyethylene-acrylic acid graft copolymers obtained by electron beam irradiation [68]. The mechanical properties of the parent HDPE and those of the graft copolymer were measured in order to determine the effect of the added acrylic acid on the tensile strength, elongation, tensile modulus, impact strength and the dynamic modulus over a broad range of temperatures. It was observed, for instance, that the melt index decreased with increasing amounts of grafted acrylic acid and/or with increasing amounts of radiation, i.e. degree of branching.

In a follow-up paper by the same authors, the melt flow properties were reported for various graft levels [69]. The flow curves obtained by a combination of capillary and rotational

rheometers in the temperature range of 175°C - 250°C were compared with those of the parent HDPE. While the apparent shear viscosity for the graft was somewhat higher, the flow curves were otherwise very similar. The higher viscosity of the graft copolymer was attributed to a small amount of cross-linking caused by irradiation and/or "interactions of the polyacrylic acid branches". The temperature dependence of melt viscosity for the graft copolymer was found to be the same as that for the HDPE. This observation may indicate that there were too few grafted polyacrylic acid branches to measurably alter the activation energy for viscous flow, as was suggested in similar studies for other LCB polymers [70].

Dynamic mechanical properties, in the form of sound velocity and damping factor, as a function of temperature, were measured by an electrostatic resonance method at frequencies in the order of 10 kHz for polystyrene-atactic polybutene and styrene-acrylonitrile/butadiene-acrylonitrile systems [71]. Parent polymers, as well as their blends and grafts at various compositions, were investigated. For blends, the relaxation phenomena characteristic of each

polymer component were located at the same temperature as for the parent polymers. On the other hand, in grafted samples with a sufficiently high degree of branching, the damping peaks were shifted towards lower temperatures.

The viscoelastic properties of purified graft copolymers of poly(ethylene-*co*-propylene)-*graft*-polyvinyl chloride with 72% EP content were reported [72]. Measurements of stress relaxation in tension were carried out over the temperature range from -77°C to 160°C. The relaxation modulus E(t) data suggested that, in addition to the main transition at -57°C, another one occurred at a higher temperature, and was attributed to the microphase separation of the grafts. An attempt to construct a master curve from a series of isothermal stress relaxations, using the time-temperature superposition principle, was not entirely successful, indicating a "thermo-mechanical complexity" of the EP-g-PVC grafts.

Thermo-mechanical properties of homopolymer-free grafts of polyacrylic acid (PAA), polyacrylonitrile (PAN) and polyacrylamide (PAAm) on polypropylene were reported by Pegoraro et al. [73]. The storage and loss moduli in tension were measured over a temperature range broad enough to encompass the viscoelastic α-transition zone of the parent polymers. These transitions for graft polymers appear to be a superposition of those for the parent polymers, that is, all transitions characteristic of the two homopolymers were maintained. The value of storage modulus was usually intermediate between those of the component polymers and the authors concluded that this result was consistent with the existence of a two-phase morphology, evident from electron microscopy analysis.

Synthesis and properties of a new class of thermoplastic elastomers (TPEs) consisting of an elastomeric base with pivalolactone branches was described by Caywood [74]. Mechanical properties of polyacrylate-*graft*-polypivalolactone) were examined. The stress-strain data in tension and in compression showed systematic variations with graft composition. No rheological properties were investigated in melt or solution, although a comprehensive

account of the performance of these graft copolymers in melt processing was given.

A paper by Thamm and Buck details the synthesis, morphology and structure-property relations of graft copolymers of EPDM and polypivalolactone, EPDM-g-PVL [75]. PVL chains with a degree of polymerization varying from 3 to 20 and an average distance between graft sites varying from 3000 to 7700 g/mol were found to crystallize upon cooling. This, in turn, enabled them to form a thermally reversible network, an essential feature of the thermoplastic elastomer. Rheological properties, investigated by means of capillary rheometry, indicated (at low shear rate) an extremely high apparent viscosity of the graft, over one order of magnitude higher than that of the corresponding EPDM. At all temperatures, the melt viscosity of the graft copolymer was more sensitive to shear rate than to the viscosity of the parent polymers. Activation energies for viscous flow (at constant

stress) were several times higher for the grafts than for the EPDM, with specific values depending upon the graft composition. These characteristics of the melt rheology of the graft were, at least partly, explained by phase separation in the melt, the existence of which was confirmed by both electron microscopy and small-angle X-ray scattering. The thermo-mechanical behaviour and selected mechanical properties were discussed also, some of them in the context of the LCB structure of the graft.

More recently, a macromonomer route to produce graft copolymers with crystallising polyester blocks was used to copolymerize butyl acrylate with poly-β-propiolactone macromonomers [76]. Inherent in this technique was an accurate and reliable assessment of the structural details of the comb-shaped copolymer molecules. Unfortunately, their visco-elastic characterization was limited to dynamic thermo-mechanical analysis (DTMA) studied by the low frequency acoustic method over the temperature range of -140°C to 80°C. The correlations between the molecular chain parameters and relaxation transitions, overall degree of crystallinity and the phase separation were discussed.

There has been nothing published on the rheology of well characterized grafts of polybutadiene on butyl rubber.

The literature on the rheological properties of various long-chain branched polymers has been reviewed and is summarized in the form of a bibliography in Appendix I. It contains a more extensive bibliography than the "references" indicated in Chapter 1.

Chapter 2

Sample preparation

A graft copolymer comprises molecules with one or more species of polymer having constitutional or configurational features that differ from those in the main chain, connected to the main chain (backbone) as side chains (branches). Both backbone and branches can be either homopolymeric or copolymeric. For example, CIIR-g-BR graft copolymer represents a chlorinated poly(isobutylene-co-isoprene) backbone with attached polybutadiene branches.

There are many methods suitable for the synthesis of graft copolymers; "grafting onto" and "grafting from" are the best established and most widely used. "Grafting onto" occurs if a backbone polymer chain contains reactive functional groups, which can react with another macromolecular chain which carries reactive functional groups at the chain ends; "grafting from" occurs if active sites are generated along the polymer backbone which are used to initiate the polymerization of a second monomer to form a grafted branch [77].

In order to study structure-property relationships with an acceptable degree of confidence, polymer samples have to be synthesized with a high degree of controlled regularity in structure and of compositional homogeneity throughout the sample. The two preferred techniques for the preparation of model graft copolymers are the macromonomer approach and coupling reactions of pre-formed linear macromolecules [15, 78].

A macromonomer is an oligomer with a polymerizable end group that can copolymerize with various monomers to form comb-type graft copolymers with pendant preformed polymer chains. Macromonomers can be prepared by a variety of polymerization methods. However anionic methods offer the best control of the molecular chain structure. Once a macromonomer has been prepared, living anionic or cationic polymerization methods can be used to copolymerize the macromonomer with the backbone-forming monomer.

In the latter, two-step process, the parent polymers are synthesized first, frequently by anionic polymerization, which allows formation of a linear chain with controlled molecular weight and molecular weight distribution. Subsequently, reactive ends of pre-formed "living" macromolecules can be used for coupling reactions with active sites along the backbone molecule. This type of graft preparation method was used to produce samples for this study.

This chapter briefly describes methods used to prepare the parent polymers (2.1), the grafting reaction (2.3), including some preliminary experiments (2.2) and the graft purification process, designed to extract ungrafted residual prepolymers from the graft mixture (2.4). A description of sample handling in solution (2.5) is followed by discussion of solid specimen preparation by film casting from solution (2.6). Available evidence of successful grafting reaction is listed in section 2.7. Sample quality issues, considered critical for meeting the objectives of this project, received special attention and will be discussed in some detail (2.8).

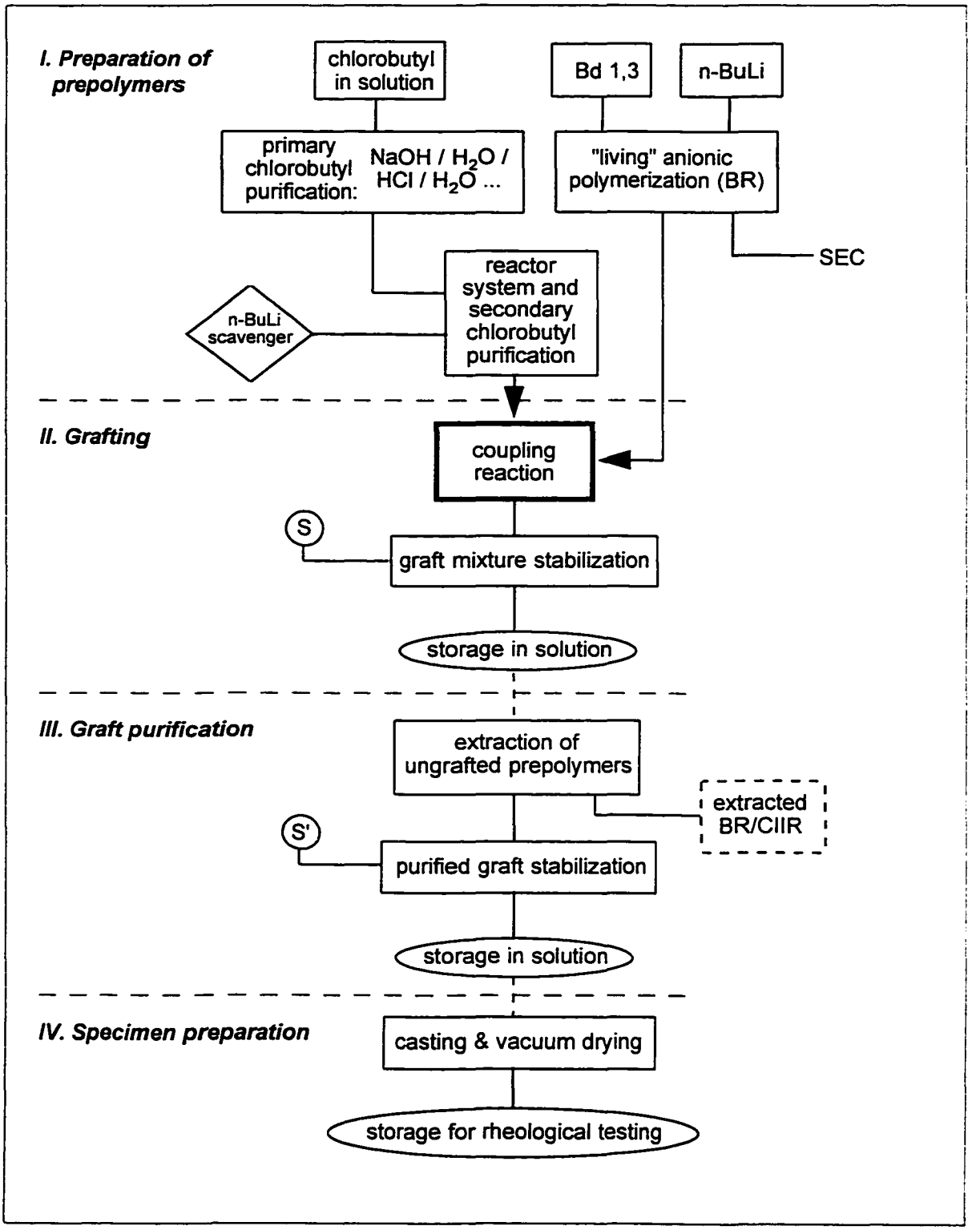
A diagrammatic overview of the method of sample preparation is presented in Fig. 2-1.

2.1 Brief characteristics of the parent polymers

Chlorinated poly(isobutylene-co-isoprene), commonly referred to as chlorobutyl, CIIR and polybutadiene, BR, are important, large volume, commercial elastomers.

High-cis polybutadiene, due to its very low glass transition temperature, can help to improve low-temperature mechanical properties in blends, alloys or grafts. It has excellent abrasion/wear resistance when vulcanized [79].

Figure 2-1. Overview of graft sample preparation.



Butyl rubber (IIR) is a random copolymer of isobutylene with small amounts (~1.5 mol%) of isoprene to supply the elastomeric system with unsaturation (C=C), in order to permit vulcanization by conventional methods. Both IIR and its halogenated derivatives such as CIIR have several outstanding characteristics, including very low gas permeability and high mechanical damping properties.

Together, they possess a unique and complementary combination of performance properties, important in a number of key rubber applications; for example in automotive tire performance. A comparison of properties of these elastomers is given in Table 2-1.

Table 2-1. Comparison of selected physical properties of BR and CIIR rubbers.

Property	BR	CIIR
Gas permeability	fair	excellent
Resilience	excellent	fair
Cut growth resistance	fair	excellent
High temperature resistance	fair	excellent
Ozone resistance	poor	excellent
Weathering	fair	excellent
Abrasion resistance	excellent	good

Rating based on the relative comparison within a group of 14 major commercial thermoset rubbers.

Adapted from: Rubber World, Vol. **184**, No.3, p. 44 (1981)

2.1.1 Synthesis, chlorination and purification of the poly(isobutylene-co-isoprene)

Butyl rubber is made by copolymerizing isobutylene and isoprene during a rapid cationic reaction at a temperature below about -95°C.

The process of chlorination of butyl rubber by reacting it with elemental chlorine, subsequent to polymerization, is designed to improve cure reactivity, which is enhanced by its predominantly allylic halogen structure [80-81] (cf. also Figure 2-2). However, the allylic chlorine atoms attached randomly to the isoprene sites along the essentially polyisobutylene molecular chain can also serve as coupling sites for the BuLi-initiated, "living" polybutadiene molecules with lithium-capped chain ends [82].

A carefully selected batch of a commercial grade of chlorobutyl Polysar CB-1255, dissolved in an inert organic solvent, was kindly supplied by Polysar Rubber Corporation. A *single batch* was secured for the preparation of the *entire set* of graft samples used in this study. This chlorobutyl solution, properly stabilized with a proprietary stabilizing system, was stored in a drum under conditions which prevented change of polymer structure and composition.

Two-stage purification of the chlorobutyl solution was necessary to ensure that any impurities that might have been present in the halogenated butyl rubber would not contribute to the destruction of the "living" alkali metal-terminated molecules during the grafting process.

For the purpose of primary purification, a sample of the CIIR solution was further diluted with cyclohexane and subsequently washed with dilute sodium hydroxide, water, dilute aqueous hydrochloric acid and again water, in that sequence. After neutralization, the solution was centrifuged to remove impurities.

2.1.2 Polymerization of butadiene

The alkyllithium initiated polymerization of butadiene has been proven to be a versatile, powerful and elegant tool for the preparation of model polymers [83]. Using this technique, it has been possible to synthesize linear polymers of narrow molecular weight distribution. However, one of the major drawbacks of the application of this polymerization technique is the need for extremely pure reactants in order to achieve good control of the structural parameters and composition of the synthesized polymers.

Lithium terminated polybutadiene was prepared under anhydrous and anaerobic conditions in a closed one (1) gallon stainless steel reactor. Butadiene dissolved in cyclohexane was charged to the reaction vessel and pre-heated to 50°C, while an appropriate solution of n-butyllithium in cyclohexane was injected. The optimum time of the reaction, kept essentially isothermal at 50°C, was determined experimentally to be in the order of 3 hours. The molecular weight of the BR was controlled by adjusting the concentration of initiator in the butadiene solution, in order to obtain the designed values of BR branch length.

A small aliquot of the solution of the "living" polybutadiene was removed at the end of the reaction and quenched by the addition of an excess of methyl alcohol. Analysis of the molecular weight distribution of the polybutadiene by the SEC method allowed for direct determination of the branch length of the graft copolymer.

Materials used for polybutadiene synthesis were obtained from Phillips Petroleum Co. (polymerization grade 1,3 butadiene and high-purity grade of cyclohexane) and from Lithium Corporation (n-BuLi).

All standard purification procedures were applied as recommended for this type of polymerization [84].

Particular care was exercised over the proper handling of n-BuLi solutions, due to their extreme sensitivity to air, moisture, oxygen and many other substances.

2.2 Preliminary grafting experiments

Due to the unavailability of commercial graft copolymers having a well-defined composition and structure, a set of appropriate samples had to be prepared in quantities necessary for comprehensive rheological characterization.

The method used to prepare these samples was based on procedures described in the patent application [82], and similar to those, reported in related patent literature [85-86]. Details are given in section 2.3.

Due to the necessity to prepare samples of broadly varying branch length and frequency, some experimentation with various reaction conditions and stoichiometric proportions, other than those described by the patents, was attempted and necessary modifications implemented.

Consistently with the scope of this work, only a summary of the preliminary experiments is outlined in Table 2-2.

Table 2-2. Summary of preliminary experiments with synthesis of CIIR-g-BR copolymers.

	Issue	Objective	Results
1	CIIR backbone degradation	simulated grafting reaction with deactivated branch prepolymer under nominal reaction conditions	no change in shape or position of the CIIR MWD as observed by SEC, => no degradation of backbone molecules
2		similar experiments to the above, except with an excess of the n-BuLi initiator only	no change in shape or position of the CIIR MWD as observed by SEC, => no cleavage of backbone molecules
3	Grafting reaction efficiency	optimum reaction time was investigated, assuming values stated in patent literature as guidance	efficiency of grafting reactions was optimized by adjusting reaction times between 2.5 and 4 hours, depending on the MW and concentration and of the BR solution
4	Secondary purification	appropriate level of n-BuLi initiator, used as scavenger, determined experimentally	optimum level of scavenger was found to effectively purify reaction system, while retaining satisfactory concentration of allylic chlorine sites to achieve nominal grafting frequency at all levels
5	Effective level of initiator	length (MW) of the BR branches is determined by initiator concentration. However, calculated values had to be confirmed experimentally, and if necessary, adjusted accordingly	most of targeted values of MW of the BR prepolymer were achieved within +/- 10%
6	Extraction efficiency of ungrafted BR	to optimize a number of extraction cycles	most of the BR was removed after first extraction, 2 to 4 cycles were used depending on BR-branch molecular mass

2.3 Grafting reaction

Immediately before the grafting reaction, it was necessary to treat the reactor, already filled with ready-to-graft chlorobutyl solution, with an excess of n-butyllithium, as determined by preliminary experiments. The n-butyllithium served here as a "scavenger" to further purify the reaction system and improve the grafting efficiency. This process was comparable to in-situ titration of the initiator-consuming impurities present in the filled reaction system [87].

Directly after polymerization in a separate reactor, a known amount of the "living" polybutadiene in solution was combined with a known amount of carefully purified solution of chlorinated butyl rubber. The grafting reaction was carried out in a one-gallon reactor for a specified period of time at 50°C and under vigorous mixing. The reaction was subsequently terminated by the addition of methanol and appropriate stabilizers were added. Concentrated solutions of the crude graft copolymer were stored in one gallon bottles under a nitrogen blanket in a cool dark area, prior to extraction of ungrafted BR prepolymer. Comprehensive details of graft synthesis are given elsewhere [82].

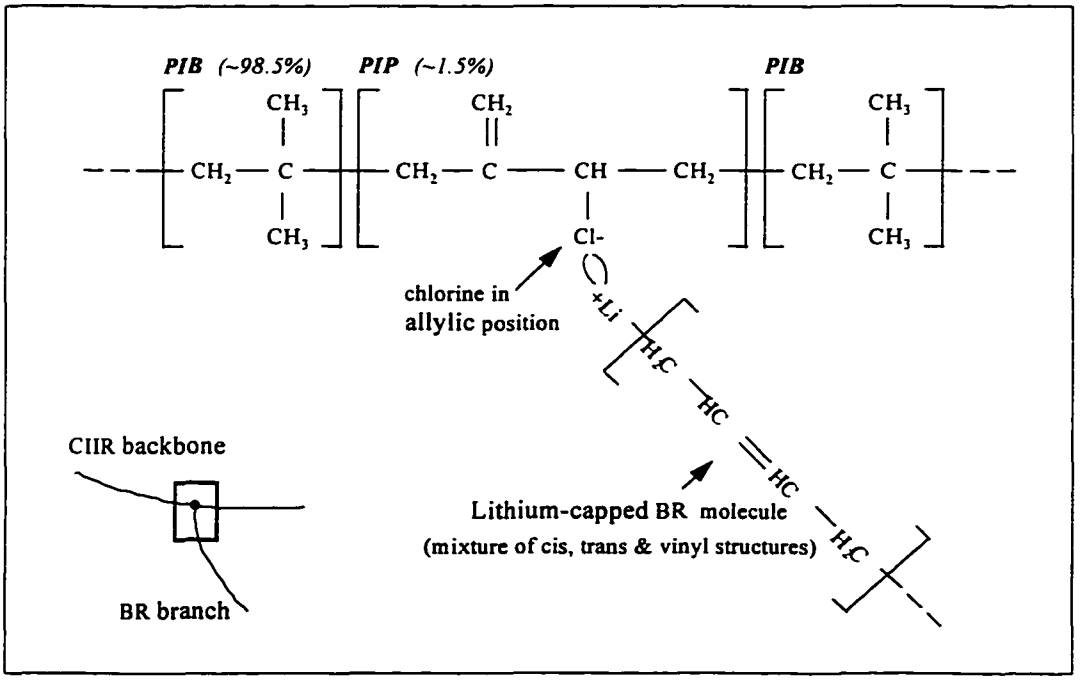
The coupling reaction was capable of producing graft copolymer samples with different numbers of branches per backbone molecule, merely by varying the ratio of the two prepolymers in the grafting reaction mixture. A similar approach was used previously for a series of CIIR-g-PS [80, 88] and (Cl)EPDM-g-PS copolymers [88].

A scheme of the grafting reaction is shown in Figure 2-2. In all samples, the backbone of the graft is always made of CIIR and the branches are made of BR. Table 2-3 contains information about targeted branching parameters and compares nominal (intended) versus actual chemical composition of crude (unextracted) grafts.

Grafting efficiency

It was apparent, from the SEC data that the coupling efficiency was decreasing with increasing length of the BR branch molecules and, to a lesser extent, with the increasing molar ratio of BR to CIIR in the coupling mixture. This observation, consistent with previous experiences with grafting of BR onto CIIR [89], explains lack of samples with long-branches and higher branching frequency (Table 2-3). Overall, 45 batches of graft copolymer mixture were prepared, out of which 22 were accepted for further processing. Selection was based on the evidence of a clean synthesis of 'to-be-grafted' BR parent polymer (lack of "shoulders" or extended "tails" on the MWD) and indication of acceptable coupling efficiency, both obtained by examination of SEC results.

Figure 2-2. Scheme of the grafting reaction.



References: 1) R. Vukov, Proceedings of the Rubber Division, ACS, Houston, Texas, October 25-28, 1983,
2) C.Y. Chu, K.N. Watson, and R. Vukov, Rubber Chem. Technol., 60, 636 (1987)

Table 2-3. Designed long-chain branching parameters and crude graft composition.

Sample code	*Targeted values*			*Non-fractionated graft*	
	Branch length	Branching number	Composition	Sample code	Composition
	M_n, [g/mol]	N_g	BR(wt%)		BR(wt%)
	a	b	c		d
G1	2,500	3	5.4	***CG1***	4.8
G2	5,000	3	10.4	***CG2***	9.9
G3	10,000	3	18.7	***CG3***	17.1
G4	20,000	3	31.5	***CG4***	30.4
G5	40,000	3	48.0	***CG5***	47.1
G6	60,000	3	58.1	***CG6***	53.9
G7	20,000	1	13.3	***CG7***	10.2
G8	20,000	2	24.2	***CG8***	22.2
G9	20,000	6	48.0	***CG9***	47.0
G10	120,000	1	48.0	***CG10***	50.4
G11	60,000	2	48.0	***CG11***	42.9
G12	10,000	12	48.0	***CG12***	43.5
G13	5,000	24	48.0	***CG13***	45.9
G14	80,000	1.5	48.0	***CG14***	50.9
G15	20,000	4	39.3	***CG15***	35.2
G16	10,000	12	48.0	***CG16***	45.2
G17	20,000	3	31.5	***CG17***	28.7
G18	10,000	3	18.7	***CG18***	17.4
G19	2,500	3	5.4	***CG19***	4.2
G20	5,000	24	48.0	***CG20***	44.6
G21	20,000	6	48.0	***CG21***	44.1
G22	120,000	1	48.0	***CG22***	44.6
C	—	0	0.0	***C***	0.0
B10	—	—	100.0	***B10***	100.0
M	—	—	31.5	***M***	29.1
	-by design-	-by design-	-by design-		measured (NMR)

It is believed that the grafting reaction as described is the major reaction and contribution from all other possible side reactions to the grafting efficiency is negligible [89].

The following equations, taken from the literature [90-93], define the *true graft ratio, GR,* (2-1), *grafting efficiency, GE%,* (2-2) and *grafting percentage, GP%,* (2-3),

true graft ratio, GR =

$$\frac{wt.\,fraction \cdot of \cdot branch \cdot polymer \cdot grafted \cdot onto \cdot backbone \cdot polymer}{wt.\,fraction \cdot of \cdot backbone \cdot polymer} = \frac{w^{b.g}}{w^{B}} \qquad (2\text{-}1)$$

grafting efficiency, $GE\%$ =

$$\frac{wt.\,fraction \cdot of \cdot branch \cdot polymer \cdot grafted \cdot onto \cdot backbone \cdot polymer}{wt.\,fraction \cdot of \cdot branch \cdot polymer \cdot (grafted + ungrafted)} \cdot 100\% =$$

$$= \frac{w^{b.g}}{w^{b.g} + w^{b.h}} \cdot 100\% \qquad (2\text{-}2)$$

grafting percentage, $GP\%$ =

$$\frac{wt.\,fraction \cdot of \cdot branch \cdot polymer \cdot grafted \cdot onto \cdot backbone \cdot polymer}{wt.\,fraction \cdot of \cdot pure \cdot graft \cdot copolymer \cdot in \cdot mixture} \cdot 100\% =$$

$$= \frac{w^{b.g}}{w^{G}} \cdot 100\% \qquad (2\text{-}3)$$

The true graft ratio and grafting percentage are different measures of the chemical composition of the graft. The former parameter relates the content of side-chain forming polymer to the content of the backbone polymer, while the latter relates the content of branching prepolymer to the content of the graft copolymer, free of the ungrafted branch prepolymer.

Grafting efficiency describes the success of the grafting reaction by calculating the percentage of branch prepolymer actually attached to the backbone of the graft. Appendix II explains the meaning of abbreviations and symbols used in equations (2-1) to (2-3).

Calculated values of the true graft ratio, grafting efficiency and grafting percentage are included in Table 2-4. In fact, it was more convenient and accurate to calculate grafting efficiency, *GE%*, according to the equation (4-9) for reasons explained in section 4.4.2.

Table 2-4, column "e" contains the results of purification effectiveness, PE%, discussed in more detail in section 2.4.

2.4 Graft purification (extraction of ungrafted parent polymers)

Graft copolymers obtained directly from coupling reactions are seldom pure, that is, free from unreacted homopolymers. Depending on the content of parent polymers and the objective of the studies, graft mixtures usually have to be purified, i.e. graft molecules have to be separated from their mixture with uncoupled parent polymers. Preparative-scale isolation of graft copolymer molecules may be realized by a process of selective extraction or fractional precipitation, if the solubility difference between the parent polymers is sufficiently high. This is not an easy process to carry out successfully (completely), since graft/block copolymers may act as compatibilizers or emulsifiers. This subject received the attention of many researchers from both theoretical and practical points of view [90, 94-98].

As expected, it was found necessary to purify CIIR-g-BR graft copolymers in order to remove uncoupled BR homopolymer. A process of selective solvent extraction was used to eliminate or at least reduce the amount of ungrafted BR as illustrated in Figure 2-3. Rapid stirring and slow, drop-wise precipitant addition to a diluted cyclohexane solution of graft mixture, prevented local precipitation.

The method and parameters of extraction were based on extensive studies carried-out previously [89]. Mixtures of 1,4 dioxane and ethanol, with the solvent composition adjusted

Table 2-4. Branching efficiency and purification effectiveness.

	Grafting parameters			*Purification*	
Sample code	**True graft ratio**	**Grafting efficiency**	**Grafting percentage**	**Number of extractions**	**Purification effectiveness**
	GR	*GE%*	*GP%*		*PE%*
	a	b	c	d	e
	calc. eq. (2-1)	calc. eq. (4-9)	calc. eq. (2-3)	-by design-	calc. eq. (2-4)
CG1	0.046	91.5	4.4	2	>98
CG2	0.088	85.6	8.1	2	79
CG3	0.176	84.5	15.0	2	89
CG4	0.373	88.3	27.1	2	91
CG5	0.637	70.8	38.9	3	59
CG6	0.808	70.2	44.7	3	27
CG7	0.052	32.2	4.9	2	96
CG8	0.235	88.1	19.0	2	89
CG9	0.589	66.0	37.1	2	89
CG10	0.651	13.3	39.4	4	63
CG11	0.601	64.8	37.5	2	77
CG12	0.626	75.1	38.5	2	70
CG13	0.597	75.1	37.4	2	52
CG14	0.582	66.6	36.8	2	55
CG15	0.466	82.5	31.8	2	95
CG16	0.454	54.1	31.2	2	78
CG17	0.278	59.0	21.7	2	97
CG18	0.067	32.2	6.3	2	98
CG19	0.028	46.9	2.7	2	91
CG20	0.692	85.9	40.9	2	79
CG21	0.647	80.5	39.3	2	98
CG22	0.471	21.7	32.0	4	54
C	—	—	—	—	—
B10	—	—	—	—	—
M	—	—	—	—	—

according to BR/CIIR composition, were found to be the most effective for separation of pure CIIR-g-BR grafts. The number of extractions applied for each particular graft depended primarily on the molecular weight and content of the grafted BR and is given in column 'd' in Table 2-4. The products of extraction were analyzed by GPC and NMR and results are discussed in chapter 4. A measure of purification effectiveness after final extraction is expressed as:

purification effectiveness, $PE\,\% =$

$$= \frac{wt.of \cdot ungrafted \cdot branch \cdot polymer \cdot removed \cdot by \cdot extraction}{wt.of \cdot ungrafted \cdot branch \cdot polymer \cdot before \cdot purification} \cdot 100\% =$$

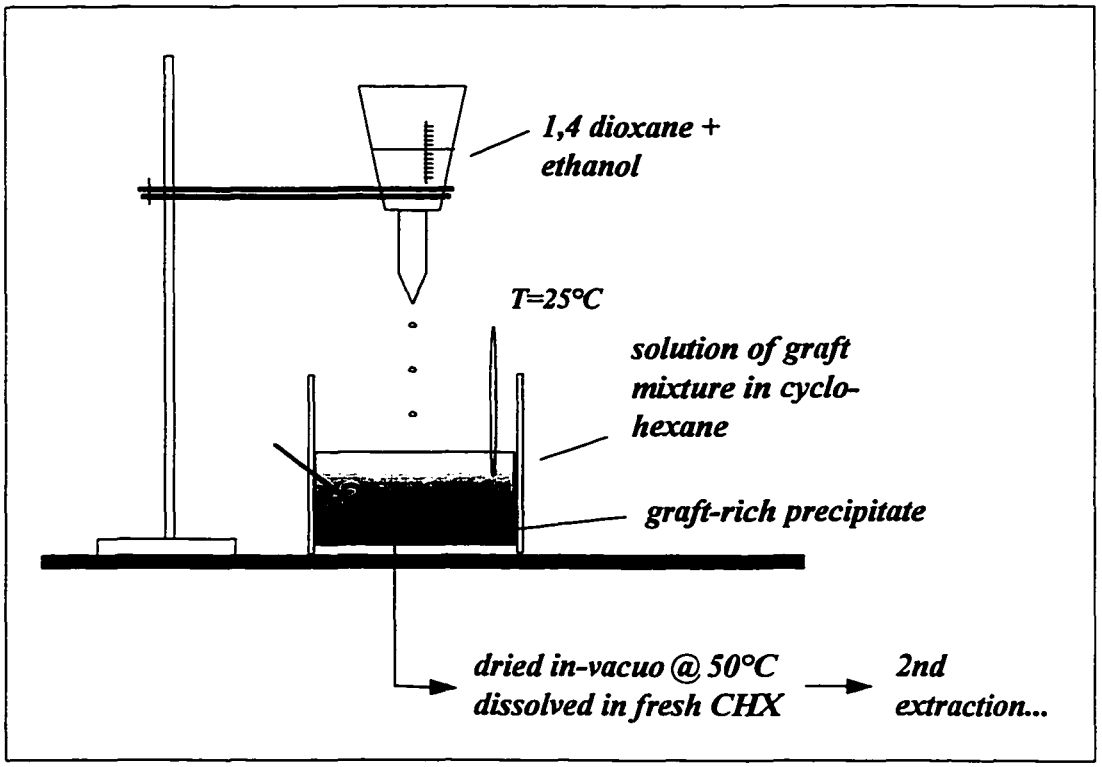
$$= 1 - \frac{A_{hBR}/A_T\,(FG)}{A_{hBR}/A_T\,(CG)} \cdot 100\% \qquad (2\text{-}4)$$

Calculated values of $PE\%$ are included in Table 2-4. Purification was found to be most effective below certain combinations of branch length and unattached branch polymer concentration in a graft mixture. Definition of A_{hBR} and A_T parameters in equation (2-4) can be found in section 4.4.2 in Chapter 4.

2.5 Sample stabilization and storage

Particular care was given to proper handling and storage of samples until the entire analytical and rheological testing program was completed. The products of grafting reactions were immediately protected chemically, stored in solution in dark bottles under a nitrogen blanket and kept for further processing, in dark, cool storage cabinets. A proprietary, four-component stabilizing system [89] including anti-oxidants and calcium stearate ($CaSt_2$), was used.

Figure 2-3. Apparatus for extraction of ungrafted parent polymers.



Reference samples and specimens prepared for analytical characterization were refrigerated and the time between sampling and analysis reduced to minimum.

Representative samples were tested periodically by SEC to detect possible changes in MWD caused by degradation. Within experimental error, no changes in molecular weight, caused by prolonged storage of these materials, were detected. The issue of sample stability and thermo-mechanical degradation, examined by rheometrical methods, will be revisited in

chapter 5. Protective measures to ensure sample material integrity for the life of the project are summarized in Table 2-5.

Table 2-5. Stabilization and protection of samples.

Samples	Solvent	Protective measures
Chlorobutyl	n-hexane	$CaSt_2$, stored in closed drum,
Crude graft mixture	cyclohexane	proprietary, 4-component stabilizing composition (*S*), solution kept in dark bottles under N_2 - blanket, stored in cool and dark area,
Purified graft	cyclohexane	as above but with reduced content of $CaSt_2$ in a stabilizing composition (*S'*),
Solid samples and specimens	not applicable	wrapped in release-paper and/or black foil, refrigerated.

2.6 Specimen preparation for rheological characterization

Measurement of solid-state viscoelastic properties of elastomers requires dry samples, free of residual solvent, moisture or any volatiles or air entrapment.

The RPA-2000 (Rubber Process Analyzer 2000™) and the DSR (Dynamic Stress Relaxometer) readily accept lump test pieces, where neither shape nor exact quantity is critical from the point of view of test result reliability. Such specimens can be readily obtained by evaporating solvent from solution in a hood under controlled air-flow and at the ambient temperature.

On the other hand, testing using the RMS-800 (Rheometrics Mechanical Spectrometer) and the RSA-II (Rheometrics Solids Analyzer) does require test pieces of well defined shape and dimensions. The accuracy and precision of the results depend strongly on the quality of specimens with regard to their shape and dimensional uniformity. Proper preparation of specimens from the materials under study was not straightforward, and required a good deal of experimentation and trial before a satisfactory procedure could be established.

The preparation method for either type of specimen must be designed to approach the development of "thermo-dynamic equilibrium" before complete solidification of the graft material. Consequently, casting from solution requires the use of a solvent which is equally good (i.e. of comparable solubility parameter) for both parent polymers. Reduced evaporation rate is also important to establish "quasi-equilibrium" morphology in solid-state grafts. The related issue of graft copolymer morphology and micro-phase separation is of great importance in studying physical properties of heterogeneous polymeric systems. It will be discussed separately in chapter 4, section 4.5.

2.6.1 Film casting from solution

A bottle of the purified graft solution in cyclohexane was stirred thoroughly and left open overnight to let trapped air leave the solution. This step allowed the homogenization of the solution while minimizing the probability of casting films scarred by imperfections due to entrapped volatiles.

The solvent was evaporated in two stages. First, the solution was poured into shallow trays, made of a release paper, placed under a hood operated with reduced air flow. The resulting reduced evaporation rate helped to obtain smooth films. The solution-filled trays were left for about 48 hours at ambient temperature to allow formation of a dry film of the polymer. Then the trays were transferred to the vacuum oven and dried for at least 24 hour at 40°C to a constant mass.

The absence of solvent in the sample above a level which could interfere with rheological characterization, was additionally confirmed by the time/cure sweep studies on the RMS-800 mechanical spectrometer. Details of this test are reported in chapter 5, section 5.3.4.

For samples designated for the RPA and DSR testing, dry films were separated from the release paper, rolled, weighed, cut into the appropriate size, packed in a black film and stored in freezers for rheological testing.

Specimens for the RMS-800 and RSA-II testing were die-cut from smooth and of uniform-thickness sections of the film. Individual specimens, left on the original release-paper substrate, were protected by an additional layer of non-sticking foil from the top, closed in dark containers and refrigerated.

More specific details of specimen preparation vary depending on the nature of rheological test and will be discussed in appropriate sections of the chapter 5.

Moulding option

Preparation of specimens requiring specific shape and dimensions is usually more difficult from gum elastomers than from thermoplastics or thermoplastic elastomers. The most consistent quality of specimens made from gum elastomers can usually be obtained by vacuum-assisted compression moulding at moulding conditions (temperature, pressure) chosen to suit the polymer.

Unfortunately, the most elaborate procedures capable of preparing good quality specimens for even the most-difficult-to-work-with gum rubbers were not useful for the majority of graft samples, with the exception of a few with the shortest branches, i.e. samples G1, G2 and G19.

As a result, for the sake of consistency, moulding as a technique to prepare specimens was abandoned and specimens for all samples were obtained by casting a film from solution.

A similar process has been described in the literature [99]. The only exceptions were specimens prepared specifically for preliminary experiments investigating the differences in rheological properties of moulded versus cast samples, as reported in section 5.2.4.4.

Casting into release-paper made trays proved to be superior to casting onto glass plates, since it allowed for much easier separation of fragile specimen films from the substrate. It was confirmed by NMR that no appreciable amount of dissolved coating substance (from the release paper) diffused into the specimen material.

The ultimate technique for obtaining near-perfect films by casting from solution is to cast them over mercury [100]. This option was considered but found not feasible due to the large amount of solvent (over 100 liters) to be evaporated.

2.7 Proof of grafting

The most critical question, as far as sample preparation is concerned, is whether the grafting reaction indeed took place, as intended. All available evidence suggests that the grafting actually took place in all cases, as anticipated. The evidence for grafting can be derived from the following considerations:

1. Chemistry of grafting reaction - as discussed in sections 4.2.2 and 4.4.1,

2. Extraction process - by detecting BR present in the insoluble fraction (presumably attached to CIIR backbone by covalent bonds),

3. Structure analysis:
- (a) SEC: (i) shift of the retention time corresponding to the peak of the DRI signal toward shorter times, indicative of increasing hydrodynamic volume of the molecules;

(ii) an increase of the $\overline{M}_z$ (being particularly sensitive to a high-end contributions to the MWD), measured for grafts as compared with $\overline{M}_z$ for reference samples C and M (Table 4-8),

- (b) NMR: disappearance of the peak corresponding to the allylic chlorine in CIIR after the grafting reaction, is indicative of a dramatic decrease in a number of grafting sites,

4. Rheological properties - properties of grafts are significantly different from those obtained on linear polymers (C, B10) or on the blend (M), as documented in chapters 6 and 7.

5. Experience with specimen moulding - most grafts were not moldable (section 2.6.1) and handling behaviour resembled that of lightly cross-linked gum rubbers. Due to the lack of cross-linking, this could not be explained in terms of increased molecular weight of grafts (compared with MW of backbone polymer) and was attributed to the presence of LCB.

2.8 Additional issues

2.8.1 Sample quality

In the course of sample preparation, the following factors were found critical in order to produce homogeneous samples of graft copolymers of designed structure and composition:

- CIIR purification: thorough, multi-step cleaning of the entire reactor system, including reactants and solvents,
- BR synthesis: high-quality reactants, solvents and reactor systems, strict control of initiator concentration,
- Grafting reaction: optimization and strict control of reaction parameters, particularly reaction time and temperature, and equally stringent equipment purity requirements,

- Graft mixture purification: a number of sequential extractions necessary at sufficiently low concentration of the solute (CIIR-g-BR mixture),
- Film casting: homogenization and degassing of solution prior to casting, proper levelling of evaporation trays, reduced evaporation rate and limited amount of solution to be evaporated at any time,
- Specimen forming: gentle handling/storage in non-sticking environment, consistent cutting of discs and dumbbells,

Issues concerned with regularity of structure of graft copolymers are discussed in chapter 4.

2.8.2 Sample integrity: thermo-mechanical stability and effect of aging

For reliable investigations of structure-property relationships, it is essential that the structure and composition of the polymer does not change appreciably during the storage time necessary to complete the physical characterization program. It is equally important that during flow or deformation imposed during rheological testing, the structure of the sample is not being altered, unless this is the objective of the test. For a graft copolymer created by a coupling reaction, where the structure of the graft is derived partly from the MWD of the parent polymers and the stoichiometry of the grafting reaction, necessary verifications will include a check of the integrity of the backbone molecules during the grafting reaction (cf. Table 2-2).

The possibility of degradation of the chlorobutyl backbone during grafting reactions was indicated by various authors [101-102]. Its probability depends on the exact chemistry and conditions of the reaction. No degradation of CIIR molecules was observed, however, for CIIR-g-PS [103], CIIR-g-BR [82, 85], PVC-g-CIIR [104] or SBR-g-PIB [88] copolymeric systems.

The effectiveness of the stabilizing system was examined in a series of preliminary experiments reported in the project proposal. Additionally, sample stability has been periodically monitored throughout the span of the experimental phase of the project. No evidence of any changes in structure or composition was found from periodic checks on selected samples by the GPC, solubility and rheometric tests.

The issue of the thermo-mechanical stability is further discussed in chapter 5.

2.8.3 Homogeneity of sample material

The following precautions and practices were observed in order to ensure the homogeneity of sample material, and therefore, the representativeness of specimens:

1. Thorough mixing of the CIIR solution before sampling for the grafting reaction,
2. No batch blending, i.e. the whole sample was prepared out of the single batch of reactants and out of a single reactor charge,
3. Purification procedures and reaction conditions kept as consistent as possible for all samples,
4. Stirring the solution before casting to avoid possible fractionation due to sedimentation during storage,
5. Specimen preparation and both analytical and rheological test procedures meting or exceeding accepted standards, as far as sample homogenization, randomized specimen selection and multiple experimental determinations were concerned.

2.9 Sample portfolio

The portfolio of samples consisted of 22 graft samples (numbered consecutively from G1 to G22), supplemented by a sample of backbone prepolymer (linear chlorobutyl rubber), sample C, and a sample of anionic BR (sample B10), representative of a branch prepolymer. An additional sample (M), was obtained by blending sample C with a batch of BR, and is compositionally equivalent to graft G4, but does not include the long-chain branched molecules.

Methods used for comprehensive characterization of the structure and composition of these samples by analytical methods are the subject of the following chapter (3) and the results of this characterization are presented in chapter 4.

Chapter 3

Determination of molecular structure: experimental methods

This chapter discusses methods used for determination of structure and composition of graft copolymers. A brief overview of molecular structure of elastomers (Sec. 3.1) is followed by review of branching parameters used to describe LCB structures (Sec. 3.2). Section 3.3 briefly surveys some of the most frequently used analytical techniques applied for estimation of the LCB parameters with particular reference to methods applicable to graft copolymers. Review of instrumental methods actually applied in this work to determine structural characteristics of grafts with a summary of important experimental conditions is the subject of section 3.4. Actual results are presented and discussed in chapter 4, which concludes with a summary of structure of the grafts (Section 4.6) added to consolidate information obtained from various sources and sometimes by different analytical methods.

3.1 Principal characteristics of molecular architecture of elastomers

Perhaps the most striking characteristic of commercial elastomers is their extreme structural complexity due to the potential existence of a variety of topological features (e.g. branching and networks) resulting in compositional and constitutional heterogeneity. This poses a serious challenge for adequate description and complete characterization of elastomeric materials. Any comprehensive program for structure/composition characterization should, in general, consider the following issues [105-106]:

a/ chemical composition, repeat unit distribution, microstructure (tacticity),
b/ compositional and sequence distribution (in copolymers),
c/ molecular weight distribution and its averages,

d/ type and degree of branching,

e/ presence, type and amount of networks (gels and aggregates),

f/ crystallinity (in some elastomers),

g/ morphology/phase separation (in block and graft copolymers)

Also, in the context of structure-property relationships, possible interferences resulting from the presence of oligomers, low MW fluids (solvents, water, etc.), and non-polymeric substances cannot be ignored.

Depending on the objective of the study and nature of the elastomeric sample, some of the above variables may be referred to as ***'variables'*** in structure-property relations, some might be considered as constants or ***'parameters'***, while some others could be regarded as "unwanted" ***'interferences'***. In the latter case, however, their absence or negligible influence on properties under study have to be proved. Otherwise, it is expected that some method of sample purification will be applied, preferably, or the effect of interferences on structure-property relationship will be accounted for.

3.2 Long-chain branching parameters of comb-like structures

The number of long-chain branching parameters necessary to describe completely the structure of branched polymers increases rapidly with increasing complexity of polymer structure, as does the experimental difficulty in determining these parameters. For the simplest branched polymers - regular stars, in principle, only two parameters are necessary to describe the structure: branch length (i.e. molecular weight, MW) and number of arms (branches per star molecule).

For regular homopolymeric combs, several parameters are required for complete description of the branching structure, including parameters describing the number of branches and their length, as well as the backbone length.

LCB parameters of polydispersed, homogeneously branched polymers can be classified into two types [107]:

a/ *overall* LCB parameters, characterizing the state of branching in general by comparison of a selected property (e.g. intrinsic viscosity) of branched and linear polymers,

b/ *structural* LCB parameters, describing specific details of the structure of the branched molecule.

The *overall* LCB parameters include "branching indices", sometimes called "branching degrees" or "shrinking factors" termed g or G and defined as the ratio of a given property of branched and linear macromolecules of the same molecular weight. Commonly used *overall* branching degrees include:

$$G = [\eta]_{br} / [\eta]_{lin}, \tag{3-1}$$

$$g'' = (\bar{S}^2)_{br} / (\bar{S}^2)_{lin}, \tag{3-2a}$$

$$g''' = (\bar{\rho}^2)_{br} / (\bar{\rho}^2)_{lin}, \tag{3-2b}$$

where,

$[\eta]$ - is the intrinsic viscosity,

$\bar{S}^2$ - is the mean-square radius of gyration of the macromolecule,

$\bar{\rho}^2$ - is the mean-square hydrodynamic radius of the macromolecule.

Subscripts 'br' and 'lin' refer to branched and linear molecules, respectively.

These parameters are extensively used in the characterization of branched homopolymers and homogeneously branched copolymers and the relations between them and particular details of certain molecular structures have been theoretically developed and experimentally confirmed [41, 107-111].

Graft copolymers can be considered heterogeneous polymers on three levels,

- chemically, having branches composed of species chemically different from the backbone,
- topologically, having a non-linear, comb-like structure, and
- both backbone and branch molecules having a distribution of molecular weights.

The resulting structure is complex and, practically, cannot be completely characterized by analytical methods without some information being derived from the chemistry of the grafting reaction or without making certain assumptions.

To study the relationship between the LCB structure and polymer properties for graft copolymers (and heterogeneously branched polymers in general) the *overall* LCB parameters are not suitable for the following reasons:

> 1/ no "linear" equivalent of the graft copolymer exists with identical molecular and chemical composition, thus *overall* parameters cannot be defined,
> 2/ *structural* parameters are more descriptive than *overall* LCB parameters, therefore more readily suited for quantitative structure - physical property correlations.

The following are examples of *structural* parameters which can be used to characterize the branching architecture of a comb-type graft copolymer:

a. Chemical composition of those polymers constituting the branches and backbone of the graft copolymer,

b. (Number-) average number of branching points, $\bar{n}^{b}_{n,f}$ of functionality f,

c. Distribution of branch points along the macromolecule backbone,

d. Molecular weight distribution of the backbone molecules and its derivatives, $\bar{M}^{B}_{x}$,

e. Average molecular weight of backbone segments between branching points, $\bar{M}_{x,seg}$,

f. (Number-) average number of branches per backbone molecule, N_g,

g. Molecular weight distribution of branch molecules and its derivatives, $\bar{M}^{b}_{x}$,

h. Branching frequency (or branching density), λ_x,

i. (Number-) average number of chain ends, $\bar{\omega}_n$.

Subscript "x" used in $\bar{M}_x$ and λ_x substitutes for n, w, z, z+1, etc.

Some of the above parameters are interrelated. For example, the following relation holds [112] for branching point functionality, f, the number-average number of branching points, $\bar{n}^{b}_{n,f}$, and the number-average number of chain ends, $\bar{\omega}_n$,

$$\bar{n}^{b}_{n,f} = (\bar{\omega}_n - 2) / (f - 2) \qquad (3\text{-}3)$$

For simple (linear branches and linear backbone) graft copolymers (branch point functionality, $f = 3$) the relation between the number of branching points reduces to a simple and intuitively obvious relation. More importantly, relation (3-3) may be used in many cases to estimate branching frequency through determination of the number of chain ends, carrying functional groups which are detectable by analytical methods like NMR or IR spectrometry.

Branching number, N_g *(sometimes designated in the literature by* b/B or $\overline{B}_n$)

The number-average number of branches per backbone molecule, or simply the branching number, N_g is a branching parameter particularly convenient to describe LCB of graft copolymers. The experimentally convenient form of the equation to calculate N_g depends on the graft synthesis method and experimental techniques available for characterization of the structure of the graft. In cases where number-average molecular mass of the graft, $\overline{M}_n^G$ could be reliably and directly determined (e.g. by osmometry) the following formula has been proposed [90]:

$$N_g = \frac{\overline{M}_n^G \cdot w^{b,g}}{\overline{M}_n^b} \tag{3-4}$$

where:

$\overline{M}_n^G$ - number-average molecular mass of graft copolymer

$\overline{M}_n^b$ - number-average molecular mass of branch polymer

$w^{b,g}$ - weight-fraction of *grafted* portion of the branch prepolymer

Equation (3-4) actually has been used for branching number estimation of CIIR-g-polyindene [102], PEA-g-PS [113], BR-g-αMS [114], PMMA-g-PMMA and PMMA-g-PS [115] graft (co)polymers.

Another equation to estimate the branching number, N_g, has been proposed,

$$N_g = \frac{\overline{M}_n^G - \overline{M}_n^B}{\overline{M}_n^b} \tag{3-5}$$

and was applied to PVC-g-PIB [91], EPDM-g-PS and EPDM-g-αMS [116], CR-g-PIB [117] grafts, as well as more complex bi-graft systems [118].

Combining the above two equations, the following relation (3-6) between the number-average molecular mass of the graft, $\overline{M}_n^G$ and the number-average molecular mass of the backbone polymer, $\overline{M}_n^B$, can be derived [90, 119]

$$\overline{M}_n^G = \frac{\overline{M}_n^B}{1 - w^{b,g}} \tag{3-6}$$

Substituting equation (3-6) into (3-4), N_g can be expressed as,

$$N_g = \frac{\overline{M}_n^B . w^{b,g}}{\overline{M}_n^b (1 - w^{b,g})} \tag{3-7}$$

This form of the equation (3-4) is more convenient for calculation of the N_g for grafts formed by the coupling reaction of preformed ('parent') polymers, because all three independent variables in equation (3-7) can be readily measured [90, 107, 111, 120].

Branching frequency, λ_x

The branching frequency, (or the branching density), λ_x most generally can be defined as the ratio of the x-average number of branching points, $\overline{n}_{x,f}^b$ to the x-average molecular mass of the graft, $\overline{M}_x^G$,

$$\lambda_x = \frac{\overline{n}_{x,f}^b}{\overline{M}_x^G} \tag{3-8}$$

It can be expressed in terms of x-average number of end-points, $\overline{\omega}_x$,

$$\lambda_x = \frac{\overline{\omega}_x - 2}{(f-2)\overline{M}_x^G} \tag{3-9}$$

and for simple grafts (e.g. for $f = 3$ and $N_g = \overline{\omega}_n - 2$) it could be reduced to $\lambda_n = \frac{N_g}{\overline{M}_n^G}$ but is seldom used in the context of structure-property correlations for heterogeneously branched polymers.

It is interesting to note that, for graft copolymers, backbone end-points are not included in the calculation of the average number of branches or branching frequency, resulting in number of branches being equal to the number of branch end-points and equal to the number of branching points. This can be symbolically expressed as

$$\overline{B}_n \ (\text{or } N_g) = \overline{\omega}_n - 2 = \overline{n}^b_{x,f=3}$$

Definitions of important terms and corresponding symbols related to branching terminology in comb-type architectures, including graft copolymers, are included in Appendix II.

3.3 Analytical methods suitable for the characterization of LCB structures

Brief review of analytical methods developed for characterization of LCB

Characterization of LCB polymers requires simultaneous determination of at least two principal aspects of molecular structure: MWD, corrected for branching, and branching parameters. In principle, any combination of two or more techniques measuring the properties of branched polymers having different dependence on branching can be used. As a result, a large variety of techniques has been proposed for characterization of LCB structure in polymers. Systematic reviews of those techniques can be found in [106-107, 121-125].

Some early techniques for the characterization of branched homopolymers (suitable also for homogeneously branched random copolymers) were designed to yield a corrected MWD, supplemented by averaged branching parameter(s) assessed for the whole polymer sample. Examples are the procedures for branching frequency measurements, developed by Drott and Mendelson [126], Kurata et al. [127] and Ram and Miltz [128], using SEC with measurement of the intrinsic viscosity on the whole polymer, or by combining SEC with $\overline{M}_v$ derived from intrinsic viscosity measurements and with $\overline{M}_w$ from static light scattering , both on the whole polymer [106]. The above methods assume that branching frequency is not dependent on MW or the dependence of LCB upon MW follows a simple relationship which can be expressed analytically.

However, as a rule, LCB is heterogeneous in respect to the MWD and complete description of branching would require the knowledge of the LCB distribution as a function of MW. Generally, this is achieved by fractionating (for example by precipitation or preparative chromatographic methods) of polymeric samples, followed by measurement of molecular weight parameters ($\overline{M}_w$, $\overline{M}_n$, etc.) by appropriate methods on the fractions.

More recently, non-preparative fractionation methods with simultaneous (on-line) measurements of appropriate parameters are gaining general acceptance, in particular SEC equipped with a DRI concentration detector supplemented with either dilute solution viscosity (DSV) for continuous eluant viscosity measurements [64, 126, 128-138], or equipped with a light scattering (esp. LALLS) unit [139-144] are particularly useful and were recently critically reviewed from the point of view of their application for branching frequency assessment [122].

Some other methods used for LCB and MWD characterization include:

- quantitative analysis of end-groups or branch-points by spectroscopic methods (particularly high-resolution NMR) under certain conditions and particularly for high branching frequencies [145-147],
- sedimentation velocity profiles with and without SEC to obtain the distribution of branching without fractionation, as well as combination of sedimentation with diffusion [148],
- dynamic viscometric measurements on dilute solutions and stress relaxation combined with intrinsic viscosity measurements [149-151],
- frequency-dependence of dynamic moduli and compliances, or melt steady shear viscosity as a function of shear rate and temperature, [2, 31, 152-153],
- combination of multi-detector SEC (e.g. DRI+DV) plus viscoelastic function(s) - e.g. G′ [154].

The rheological and hybrid methods, combining rheological and physical chemistry techniques, can be very sensitive [106, 155] but require development of appropriate empirical correlations valid only for the polymeric systems in question.

The potential of multi-detector SEC for complete characterization of homogeneous polymers has been outlined [107, 112] and early experimental work involving SEC (DRI) system with on-line DV+LALLS detectors working in tandem, was reported [156].

Methods suitable for characterization of LCB in graft copolymers

Some of the analytical methods established for LCB homopolymers can be used with appropriate modifications for the characterization of heterogenerously branched copolymers (graft copolymers and block star-copolymers). These modifications in procedures must allow

for the effect that the intrinsic chemical heterogeneity of these copolymers may have on physical properties.

The chemical heterogeneity and molecular weight polydispersity of copolymers may be described by chemical composition distribution (CCD) and molecular weight distribution (MWD), or approximated by statistical moments of these functions. Generally, in copolymers (A-polymer-co-B-polymer) their molecular weight distribution can be described by the two-dimensional differential number-distribution function, $N_c = f(M_A, M_B)$. An alternative and more convenient method is to use as independent variables the molecular weight of the copolymer, $M = M_A + M_B$ and its chemical composition, $x = M_A / (M_A + M_B)$. In practice, the following statistical moments of the weight-average distribution function $W(M,x)$ are important:

weight-average chemical composition,
$$\bar{x}_w = \iint_{xM} x \cdot W(M,x)\,dMdx \tag{3-10}$$

weight-average molecular weight,
$$\bar{M}_w = \iint_{xM} M \cdot W(M,x)\,dMdx \tag{3-11}$$

and the parameters of chemical heterogeneity P and Q defined by equations:

$$P = \iint_{xM} (x - x_m)\, M \cdot W(M,x)\,dMdx \tag{3-12}$$

$$Q = \iint_{xM} (x - x_m)^2\, M \cdot W(M,x)\,dMdx \tag{3-13}$$

The parameter P is a measure of the correlation of the distribution of molecular weights and chemical composition, while the parameter Q is a measure of chemical heterogeneity of the copolymer. Similar parameters can be defined for number average distribution function $N(M,x)$. However, most experimental methods for determination of the chemical composition of copolymer give the weight average values [96].

At the present time, work systematically employing an outlined 'universal approach' to both MWD and chemical composition is mostly of a theoretical nature [96, 157] but occasional experimental applications can be found also, for example in work reported by Schroeder [158].

The complete characterization of LCB copolymers remains one of the most difficult and complex issues in polymer science. Chemical and molecular mass heterogeneity is further complicated by the presence of LCB which does not necessarily correlate with the chemical composition distribution. This is the case for simple graft copolymer structures, especially if the presence of ungrafted parent polymer(s) in graft mixture cannot be excluded. At the present time, complete structure elucidation of even the simplest copolymeric structures cannot be achieved by any single analytical technique.

The most promising methods for simultaneous characterization of CCD and MWD of copolymers are based on combination of non-exclusion liquid chromatography (NELC) with size-exclusion chromatography (SEC) [159-160]. While SEC characterizes the MWD of polymers, the CCD is determined by NELC. The NELC might include all techniques of high-performance liquid chromatography (HPLC) except SEC. Specific techniques under NELC classification will include liquid adsorption chromatography (LAC), liquid precipitation chromatography (LPC), normal phase or reversed phase liquid chromatography (NPLC or RPLC, respectively), orthogonal chromatography (OC) and liquid adsorption chromatography at the critical point (LACCP). Many practical implementations of the NELC techniques use gradient elution techniques and application of UV detectors to monitor chemical composition of the effluent. Special techniques were devised for the analysis of copolymers not containing a chromophore, which is required for UV detection [161]. While, theoretically, NELC should be applied first and the functions obtained then subjected to SEC, in practice, SEC is used first and the fractions obtained are then applied to NELC analysis because, typically, more sample can be injected into the SEC than into the NELC system.

The first semi-commercial system (hardware and software) utilizing HPLC+SEC cross-fractionation was described recently [162].

Solvent demixing fractionation was applied for CCD determination in PMMA-g-PDMS grafts [95]. However, this technique cannot be applied generally to determine CCDs, since it is often difficult to find a suitable solvent pair for a given copolymer and the technique is not yet established as a rapid and automated analytical tool. One of the better prospects for a universally used method is the combination of HPLC, based on the absorption mode, with SEC. Indeed, this technique was applied to PMMA-g-PS system for CCD determination [163]. Compositional fractionation of PMMA-g-PDMS grafts by reversed-phase high-performance LC, where copolymer molecules were separated according to their chemical composition, was also reported [164].

Other methods used for determination of both CCD and MWD in copolymers include thin layer chromatography (TLC) [96, 165-167], and Adsorption Column Chromatography (ACC) which was successfully used to separate block copolymers by chemical composition, followed by SEC for MWD [167]. A combination of static light scattering (SLS) with SEC and ^{1}H NMR was also reported [168] for investigation of the CCD and MWD of graft copolymers.

While SEC is generally accepted as a rapid technique for determination of the MWD and derivation of MW average values for linear homopolymers and statistical copolymers, its extension to measure CCD is complicated. The utility of SEC in copolymer analysis is not impaired as long as the limitations of SEC for such an analysis are kept in mind. Copolymers having the same MW but different composition might be different in molecular size, and therefore elute at different retention volumes. On the other hand, fractions eluted at the same elution volume may have different MW and different compositions. For LCB - graft copolymers this ambiguity is compounded by the additional effect of branching on the size

of the molecule, which is in general, independent of MW and chemical composition of the molecule.

Systematic and complete in-situ analysis of graft copolymers constitutes an extraordinarily difficult and complex experimental program. One is faced with handling simultaneously molecular size (MWD), chemical (CCD) and topological (LCB) heterogeneity of the polymer. As a result, *complete* analysis of graft structure, including the estimation of structural branching parameters, without reference to the chemistry of the grafting reaction and without help from characterization of (linear) prepolymers has not yet been reported. However, outlines of such a comprehensive experimental program consistent with satisfactory description of complex structure have been presented [96, 169].

Similarly, it is advantageous to determine the length of the backbone and branches of a graft from prepolymers, whose simpler structure and composition can be more readily elucidated using current methods and analytical procedures [170]. This is possible if grafts are prepared by grafting preformed branch molecules onto active branching sites distributed along the molecules of the backbone precursor polymer.

For grafts synthesized by other methods, a selective oxidative backbone degradation was used for the same purpose [114, 117, 119].

The method used herein provides much higher accuracy and confidence, as well as providing information which frequently cannot be obtained otherwise. This approach was often adopted for characterization of LCB in graft copolymers, for example [90-91, 170], and is applied in this work. Certain assumptions involved with this approach will be discussed in subsequent sections of this chapter.

In addition, the following is postulated: for structure-property characterization complete information about MWD and CCD of the graft may not be necessary, under certain circumstances, in order to arrive at correct and quantitative correlations between branching parameters and the rheological property in question. These circumstances include those aspects of polymer structure/composition which will not interfere with the structure-property relation investigated. For example: one of the fundamental characteristics of a branched polymer is the distribution of branching along the backbone molecule which frequently can be assumed to have random distribution (an assumption supported by reaction kinetics and reactivity ratio calculations).

Furthermore, for this project a single batch of properly homogenized and sampled polymer was used to serve as a backbone prepolymer for all graft samples. Therefore, it is reasonable to assume that the MWD, CCD and branch point distribution of the backbone in all graft samples is identical.

3.4 Instruments and techniques selected for the characterization of molecular structure and composition

Reliable characterization of molecular weight, molecular weight distribution and long-chain branching is of particular importance to this work and was given appropriate attention. Chemical composition, microstructure and their distribution for both parent polymers (BR and CIIR) were examined and are reported in section 4.2 for CIIR and in section 4.3 for BR. The possibility of gel formation during graft synthesis and storage was carefully monitored, due to its potential to alter rheological behaviour. Crystallinity is not an issue for these copolymers and was not investigated experimentally.

In fact, the analytical techniques in this work were employed to meet two additional objectives:

- examination of possible interferences with the principal correlations, and
- monitoring sample integrity throughout the project span.

The choice of analytical methods used was governed by the above mentioned objectives, but was also dependent upon available instrumental resources.

Figure 3-1 is a modified scheme of sample preparation (compare Figure 2-1), supplemented with sampling points for analytical characterization. Table 3-1 lists methods and techniques used for characterization of chemical structure and composition.

3.4.1 Size Exclusion Chromatography (SEC)

Size exclusion chromatography (SEC) is a standard test method for measuring the molecular weight distribution of polymers. A dilute solution of a polymer is injected into a pure solvent stream flowing steadily through a series of columns packed with a porous material. As the solution passes through the column the macromolecules are separated according to their size (hydrodynamic volume) [14]. The largest molecules, which due to their size are likely to be excluded from most of the pores, will have the shortest route to travel along the column bed and as a result will elute from the column(s) first. The smallest molecules, for which the accessible pore volume is largest, will meander a lot more and elute last, while molecules intermediate in size will elute between them, having retention time in certain proportion to their hydrodynamic size.

Figure 3-1. Sampling points for composition and structure characterization.

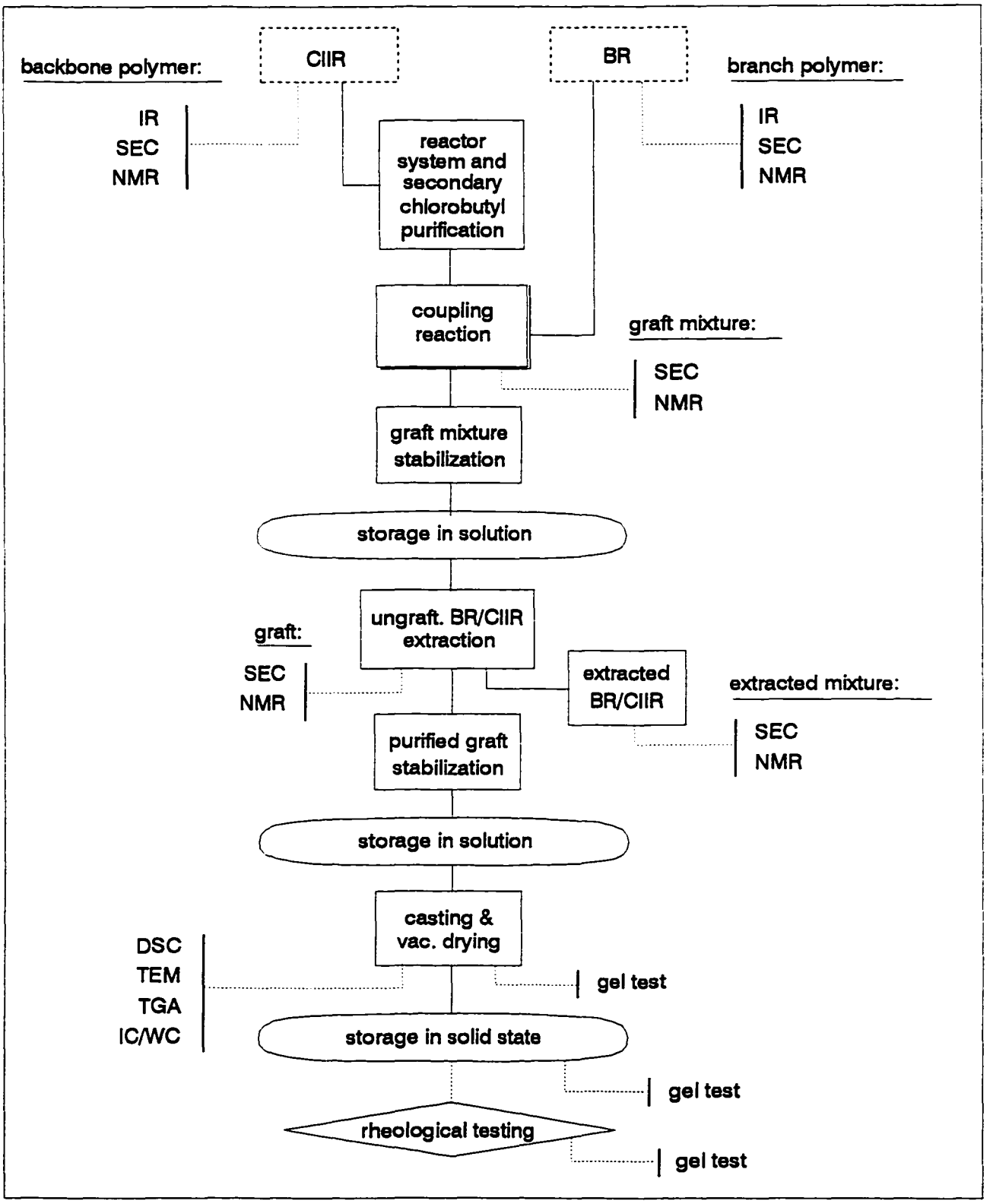


Table 3-1. Analytical methods used for characterization of polymer structure, composition and morphology.

Technique /*	Sample	Issues	Results /**
SEC (3.4.1)	Bxy, B10	MWD (M_x, PDI), linearity, micro-gel	4.3.1, 4.3.2, 4.4.8
	C	MWD (M_x, PDI), linearity	4.2.1, 4.2.3,
	CG	topology, MWD, grafting efficiency, composition	4.4.1, 4.4.2, 4.4.3, chpt. 2, App. III
	FG	MWD, fractionation eff., micro-gel, composition, (LCB)	4.4.2, 4.4.3, 4.4.8, 4.4.4, chpt.2, App. III
	HG	composition	4.4.5
	M	grafting verification (MWD)	4.4.6
NMR (3.4.2)	Bxy, B10	microstructure (1,4 cis+trans / 1,2 vinyl)	4.3.3
	C	unsaturation	4.2.4
	CG	chemical composition	4.4.2
	FG	chemical composition, (LCB)	(4.4.2), 4.4.4
	HG, M	chemical composition	4.4.5-HG, 4.4.6-M
FTIR (3.4.3)	Bxy, B10	microstructure: (1,4-cis / 1,4-trans / 1,2-vinyl)	4.3.3
DSC (3.4.4)	C, B10, G	morphology	4.5
TEM (3.4.5)	G	phase morphology	4.5
TGA (3.4.6)	C	residual solvent / volatiles; thermal stability; residual solids	4.4.7, chpt. 5
Solubility (3.4.7)	C, B10, G, M	macro-gel, degradation	4.4.8, chpt. 2
IC/Wet Chem. (3.4.8)	C	Cl-content (bound & total)	4.2.6

*/ - sections with pertinent experimental details are indicated in parentheses.
**/ - references are made to sections presenting and discussing results.

Sample codes for Table 3-1 (see also Appendix II)

- Bxy - branch precursor polymers (BR) sampled before grafting;
  subscript "x" refers to targeted MW, subscript "y" refers to a batch number,
- B10 - one of the BR samples of similar microstructure to Bxy samples, selected for rheological characterization
- C - backbone precursor polymer (CIIR),
- CG - crude graft samples (mixture of CIIR-g-BR & CIIR/BR),
- FG - purified graft samples (CIIR-g-BR); symbol used in chapters 2, 3, & 4,
- HG - mixture of homopolymers extracted from CG,
- G - identical (structure/composition) to FG, except reserved for samples in solid form; symbol used in chapters 5, 6, 7 & 8.
- M - (pure) blend of two linear CIIR and BR (no graft molecules present).

A concentration detector, typically a differential refractive index (DRI) detector, is used to measure the concentration profile of the eluting solution as a function of elution volume (or retention time at constant elution rate). One way to convert the concentration profile into a molecular mass distribution is to construct a calibration curve in a form of the logarithm of the molecular weight as a function of elution volume. This can be done, for example, by measuring elution volumes of standard polymers of known molecular masses.

Another possibility for conversion of the concentration profile into a molecular mass distribution is through the use of on-line MW-sensitive detectors, making viscometric (DSV) or light scattering (LS) measurements on the eluting solution. SEC separation depends on the size (hydrodynamic volume) of polymer molecules in solution, not the molecular mass. The size of the macromolecules will depend not only on the molecular mass but also on the type of solvent, the type and structure of branching, and on chemical composition in the case of copolymers. As a result, molecules *of the same molecular mass* may have *different sizes*.

This complicates molecular structure characterization using SEC for complex copolymeric and branched molecules, using SEC. It also requires the use of detectors that can measure directly some parameters related to the molecular weight, chemical composition and/or long-chain branching. The potential to use SEC for characterization of other aspects of molecular structure, i.e. in polymers of more complex structure than linear homopolymers, is being explored intensively (cf. literature quoted in section 3.3).

SEC measurements were performed on two different SEC systems, one installed in the Analytical Labs of Polysar Rubber Corp., referred here to as SEC(P), and other located at the University of Waterloo - SEC(W). This arrangement was necessary because samples of branch prepolymers which were synthesized in Polysar Labs had to be characterized immediately after synthesis, in order to promptly examine their quality. Similarly, the grafting reaction and purification efficiency had to be monitored routinely. On the other hand, the principal characterization of molecular structure for graft samples selected for further rheological characterization was scheduled for SEC(W) equipped with dual detectors (DRI+DV), a configuration not available at Polysar. Added confidence, resulting from measurements of critically important structural parameters by two independent SEC systems, was also beneficial. A detailed outline of the SEC characterization program is presented in Table 3-2. The description of samples is identical with that attached to Table 3-1, except that additionally MW standards (polyisobutylene PIB, polybutadiene PBU and polystyrene PS) were used to check the overall integrity of the SEC systems and the algorithms used for calculation of molecular weight averages.

Size exclusion chromatography measurements were performed on a Waters GPC system. The Polysar, SEC(P) instrument was equipped with a Waters 510/590 Dual Piston Pump and a series of 3 Polymer Labs mixed-bed gel columns. The elution concentration was monitored by the Erma 7510/7515A Differential Refractometer. The SEC system used at the University of Waterloo, SEC(W) was a multiple-detection system, equipped for this study with

Differential Refractometer, Model R401 and Viscotek Differential Viscometer, Model 110, connected in parallel.

Table 3-2. Characterization of molecular structure by SEC techniques - program objectives.

Samples	No. of samples	SEC system /*	Test objective
MW standards	3	P & W	system verification / accuracy assessment
C	1	P & W	graft backbone MWD/MW, mol. linearity
B10	1	P	MWD/MW
B	22	P & W	branch MWD/MW, molecular linearity, detection of macro/micro-gel
CG	22	P & W	proof of grafting, coupling efficiency
FG	22	P & W	assessment of fractionation efficiency, nominal graft MWD/MW
HG	8	P	composition of extracted polymers
M	1	P & W	MWD/MW

*/ P - performed at Polysar, W - performed at University of Waterloo.

A series of mixed-bed columns, protected by a guard column was used. Further details of the SEC(W) experimental set-up can be found elsewhere [171]. For both SEC systems, polymer samples were completely dissolved in THF and filtered prior to injection through a 0.45μm SI Teflon membrane filter. In principle, the experimental SEC procedures were similar for both SEC(P) [172] and SEC(W) [173] sessions. Further experimental details and test conditions are included in Table 3-3.

Table 3-3. SEC - test configuration and experimental conditions.

Test parameter	SEC(P)	SEC(W)
Active detectors; - DRI - DV	Erma 7510/7515A ----	Waters R401 DV Viscotek 110
Column configuration	3 mixed-bed PL-gel (Polymer Labs)	3 (30cm long) mixed-bed 1 Jordi+2 PL-gel+1 guard
Beads size, μm	10	10
Eluent temperature, °C	35	30
Solvent	degassed THF, stabilized with BHT	degassed THF (HPLC grade)
Solution concentration, - nominal, mg/mL, - actual, mg/mL	1.0 or 2.0, not calculated	between 0.5 & 2.0, calc. to be known within 1%
Flow rate, mL/min	0.8	1.0
Injection volume, μL	200	100
Scan time, min	45	55 (average)
Sampling rate, points/s	1.00	1.8207
Marker/internal standard	toluene	sulfur

Data analysis and system calibration

SEC(P) - The signal from the DRI detector was monitored by the Waters 840 Data and Chromatography Control Station DEC PRO 350. Average molecular weights and other molecular structure parameters were calculated from

molecular weight distribution. The system was calibrated using the 'universal calibration principle' based on PS Broad MWD Standards - NBS 706 and Waters' Standard Calibration Program. No band-broadening corrections were applied in this work.

SEC(W) - The DRI and DV detectors were linked to a microcomputer through an interface for data acquisition. A multi-detector SEC analysis program GPCMAX, Version D, developed in the Institute for Polymer Research was used [171]. A novel, multi-detector SEC calibration technique developed by Sanayei and Suddaby was implemented, taking into consideration molecular non-uniformity of the calibration standards, in order to correctly calibrate MW-sensitive detectors [14, 174]. Independent calibration curves were established for each detector, thus eliminating the need for lag time estimation in analyses requiring signals from both detectors simultaneously. Calibrations were based on 20 NMWD-PS standards with MW ranging from 680 to 8,000,000 g/mol.

The GPCMAX-D program allows the calculation of average molecular weight based on MWD spectra recorded either from one, two or three detectors (DRI + DV were used in this study). Analysis using the DRI detector signal only, is a conventional SEC analysis based on the Universal Calibration Principle and is valid only for linear and chemically homogeneous polymers.

The 'viscosity distribution', closely related to the MWD, can be obtained from the on-line viscometer signal [171, 175]. The intrinsic viscosity [η] and number-average molecular weight $\overline{M}_n$ can be readily obtained from the viscosity distribution as the zeroth and 1st moment of the viscosity distribution, respectively.

Analysis can be based either on Mark-Houwink-Sakurada (M-H-S) constants {method SEC(W/DVa)} or on the theoretical [η]-MW relationship - {method SEC(W/DVb)}. Multi-detector analysis {method SEC(W/DRI+DV)} - combines intrinsic viscosity from an on-line viscometer (DV) with a concentration detector signal (DRI). Details of those analyses can be found elsewhere [175].

M-H-S Constants

The M-H-S constants adopted for CIIR are similar to those published by the American Standard Corporation for PIB in THF at 30°C [176]. The M-H-S constants of $K=2*10^{-4}$ dL/g and $\alpha=0.67$, were also confirmed as best fit values for the determination of $\overline{M}_w$ for various samples of commercially produced butyl rubber [177]. The M-H-S constants for BR were based on published data for polybutadiene of similar microstructure [178]. Nominal values used for analysis of SEC chromatograms for all graft samples were identical to those used for CIIR. Due to variations in composition and long-chain branching structure of the graft copolymer, the exact values of M-H-S constants would require extensive experimentation. The same set of M-H-S constants, as listed in Table 3-4, was used consistently throughout this project, regardless of the source of data and the algorithm used for calculation of the average molecular weight, $\overline{M}_x$.

Table 3-4. M-H-S constants.

Samples	$K*10^4$ [dL/g]	α [-]
BR (Bxy & B10)	1.3	0.77
CIIR (C), grafts (CG, FG, HG), blend (M)	3.64	0.64

Assessment of the precision and accuracy of $\overline{M}_x$ calculations

The integrity of SEC systems was checked by running control samples with known average or peak MW. Broad MWD polystyrene standards NBS-706*, as well as polybutadiene PBU(240k) and polyisobutylene PBU(240k)** standards were used for that purpose. Accuracy of the average molecular weights could not be assessed experimentally because no absolute method was available to measure directly $\overline{M}_n$ (i.e. by osmometry) or $\overline{M}_w$ (i.e. by light scattering) of the grafts. However, comparisons between reference values of MW standards and those calculated from the MWD may give merit to the various techniques by which whose averages were calculated.

Assessment of the precision of molecular parameters was based on multiple SEC measurements on sample C (the backbone polymer of the graft) and on repeat determinations of some (14) randomly selected graft samples. In the latter case, a pooled (averaged over 14 samples) coefficient of variation (avg. c.v.%) was used as a measure of short term repeatability. MW measurements on some samples were repeated over a period of several months, and no trend (shift) in $\overline{M}_x$ was observed which would be indicative of systematic changes in the MW, for example as a result of polymer degradation. Table 3-5 contains results of SEC measurements on polymer MW standards and estimates of test precision.

* - obtained from National Bureau of Standards (USA)
** - supplied by American Polymer Standards

Table 3-5. Assessment of accuracy and test precision of SEC measurements.

A/ accuracy

Standard sample	MWD parameters	Reference values /*	Results obtained using SEC(...)				
			P(DRI)	W(DRI)	W(DVa)	W(DVb)	W(DRI+DV)
PBU(240k)	$\bar{M}_n$	206,000	114,000	392,000	217,500	298,000	293,000
	$\bar{M}_w$	272,000	233,000	458,000	274,000	408,000	477,000
	M_p **	240,000	266,000	490,000	---	361,000	490,000
PS 706	$\bar{M}_n$	123,000	119,500	---	---	---	---
	$\bar{M}_w$	276,000	269,000	---	---	---	---
PIB(105k)	$\bar{M}_n$	59,200	39,700	58,000	54,400	55,000	70,300
	$\bar{M}_w$	105,300	99,300	118,900	114,700	112,000	124,000

*/ - as reported by standards suppliers

**/ - MW corresponding to maximum concentration in the (SEC)MWD

B/ short-term repeatibility

MWD parameters	Sample "C" / SEC(P)			MWD parameters	Samples "G" / SEC(P)	
	Average	s	CV%			$\overline{CV\%}$ *
$\bar{M}_n$	140,800	4,300	3.0%	$\bar{M}_n$		3.2%
$\bar{M}_w$	457,000	7,800	1.7%	$\bar{M}_w$		1.1%
M_p **	386,000	8,000	2.1%	M_p **	(corresponding to CIIR peak)	0.9%
$\bar{M}_w/\bar{M}_n$	3.25	---	---	M_p **	(corresponding to BR peak)	1.2%
$\bar{M}_z$	874,000	12,000	1.3%	$\bar{M}_z$		2.1%

*/ - averaged coefficient of variation

**/ - MW corresponding to maximum concentration in the (SEC)MWD

Conclusions:

1. Departures from reference $\overline{M}_x$ or M_p values, which are observed for some of the SEC methods used, were substantial (Table 3-5A). However, the results obtained from the SEC(W/DV) detector, using algorithm (a), are in line with the accuracy (5 to 10%) typically reported for SEC measurements. Based on this limited verification, it can be concluded that the SEC(W/DVa) algorithm appears to be the most accurate for the calculation of the MWD momenta ($\overline{M}_x$), while SEC(P/DRI) method gives most reliable values of M_p.

2. The repeatability of SEC(P) measurements was good, particularly for $\overline{M}_w$ and higher MWD momenta, an indicator of both good precision of the instrumental method and sample homogeneity. Figure 3-2 illustrates the repeatability of SEC data on two determinations of a series of Bxy samples on the same SEC system SEC(P) under identical test conditions.

3. Average molecular weights obtained by various methods and reported in Table 3-5 differ considerably but their mutual correlation is quite good (R^2 better than 0.996 in most cases). Examples of such correlations are given in Figure 3-3. Chart I compares M_p , obtained by the SEC(P/DRI) and SEC(W/DRI) methods, and Chart II correlates $\overline{M}_w$, obtained by the SEC(P/DRI) and SEC(W/DVa) methods.

The results of molecular structure characterization using SEC methods are presented in appropriate sections of chapter 4. Specifically, SEC chromatograms and a summary of MW average values in tabular form are in section 4.2.3. for sample C, in section 4.3.2 for samples Bxy and B10, in section 4.4.3 for grafts and in section 4.4.6 for sample M.

Figure 3-2. Repeatability of SEC measurements.

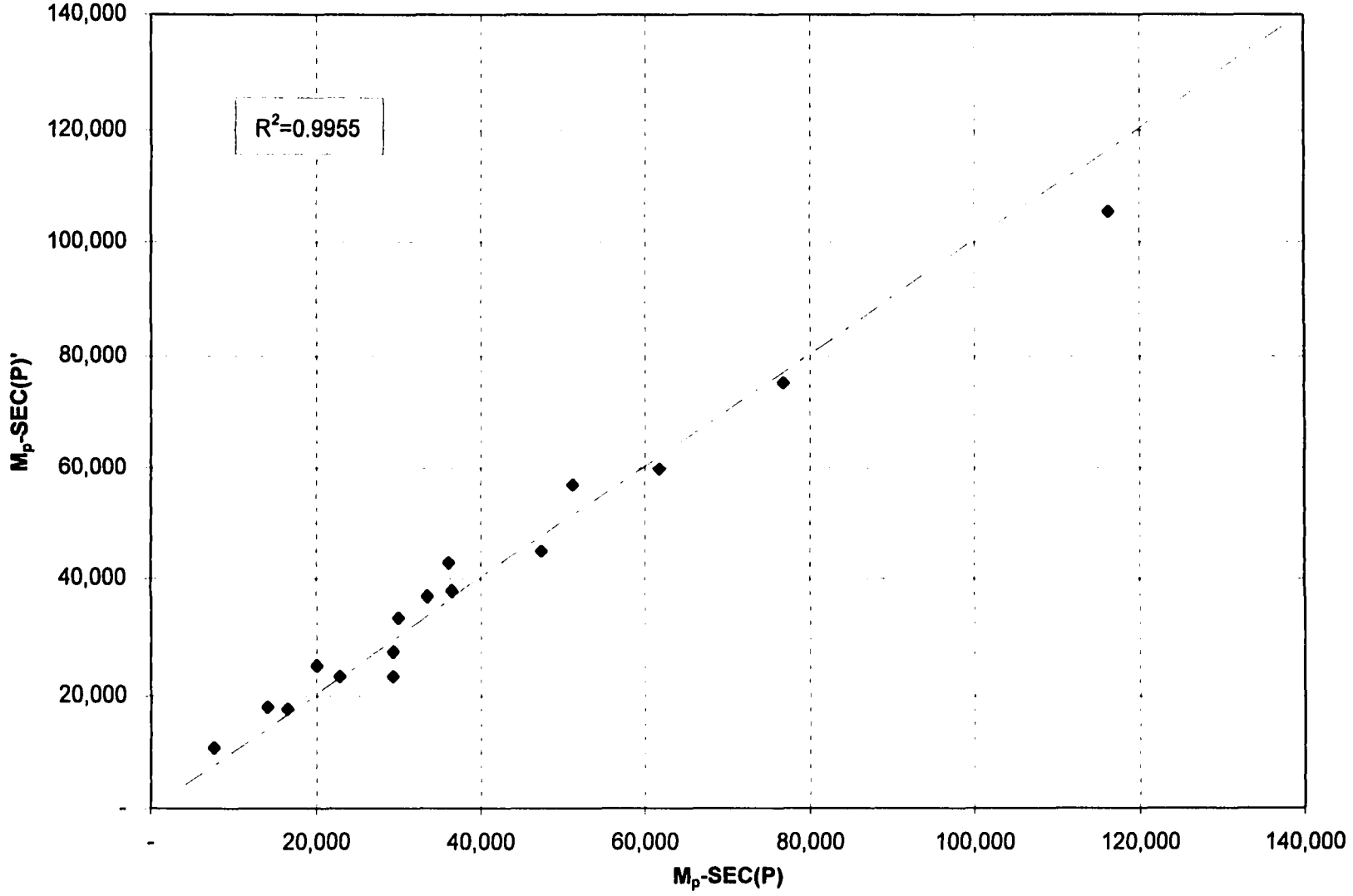
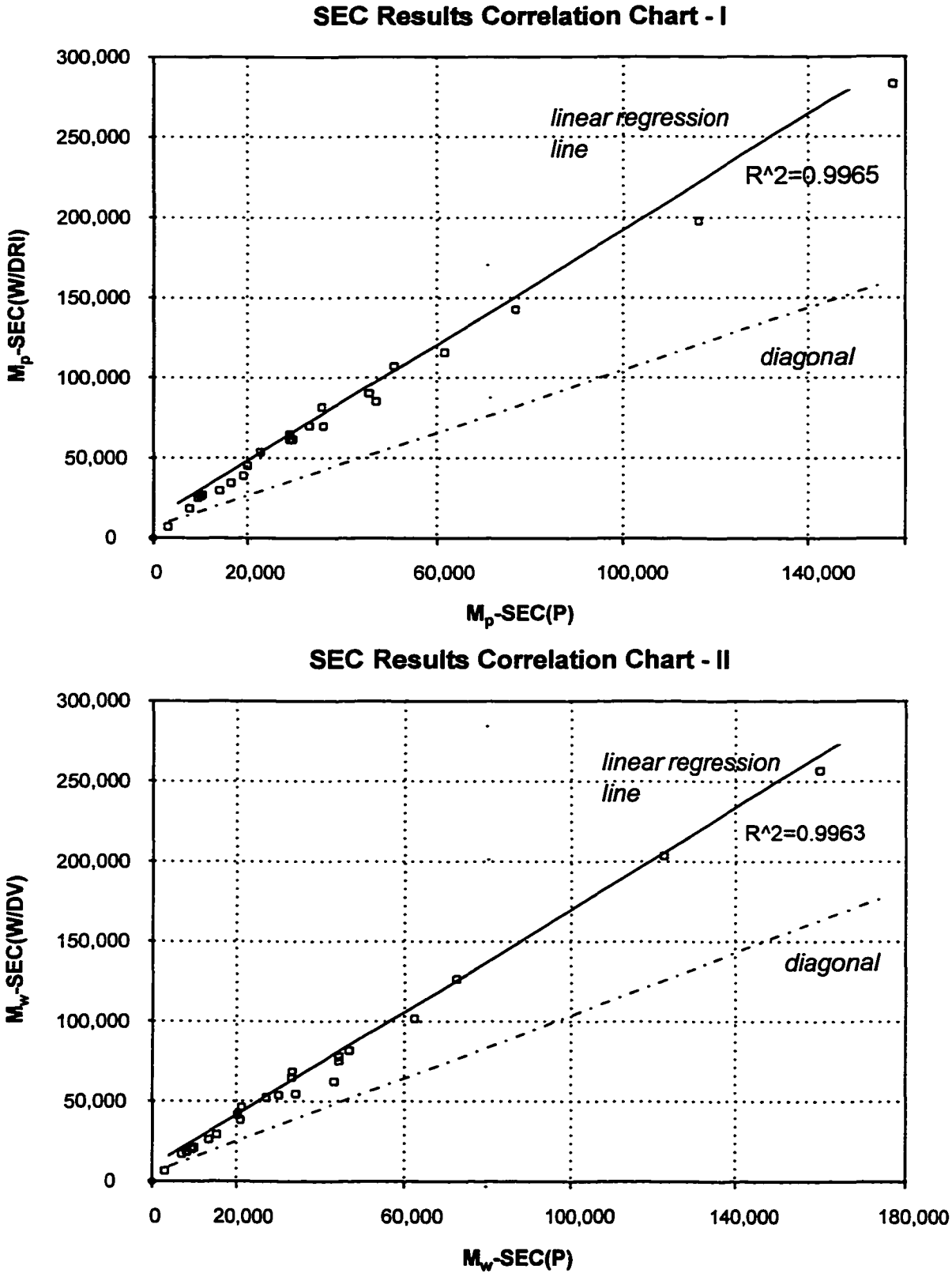


Figure 3-3. Correlation between SEC results obtained by different GPC systems.



3.4.2 Nuclear Magnetic Resonance (NMR) Spectroscopy

Nuclear Magnetic Resonance (NMR) spectroscopy is widely used for the determination of composition and microstructure of polymers [179]. It can provide a considerable amount of detailed information about structure and has the advantage of being an absolute analytical method. NMR spectra are relatively easy for unambiguous interpretation compared with some other spectroscopic methods (e.g. Raman, FTIR or mass spectroscopy). Assignments and discussion of NMR spectra for both precursor polymers (CIIR and BR) are well documented [180-183] and procedures for quantitative analysis of structure and composition exist [184-185].

The solution technique of proton NMR was used for this project to characterize:

1. Microstructure (1,2-BD - 1,4-BD) on the series of Bxy samples, supplemented by similar measurements on series CG, FG and HG samples,
2. Unsaturation (mol% IP) in CIIR (C sample), confirmed by analogous measurements on CG, FG and HG series of samples,
3. Crude graft chemical composition (mol% BR) on the CG series of samples,
4. Purified graft chemical composition on the FG-series of samples,
5. CIIR/BR blend chemical composition (mol% of BR in sample M), and
6. Chemical composition of the homopolymer mixture removed during extraction from crude graft measured on the HG series of samples.

Experimental

NMR specimens were prepared according to the laboratory procedure developed for testing elastomers in $CHCl_3$ solution at room temperature [186]. Measurements were carried out according to procedures established for gum elastomers [187] on a Brucker AC-200 NMR Spectrometer running at 200 MHz. Additional measurements on sample C using a more powerful (in terms of resolution) NMR spectrometer were carried out in order to confirm

some details of the CIIR structure (cf. section 4.2.2). A summary of other important test parameters is assembled in Table 3-6 for both instruments.

Table 3-6. Experimental test parameters of the ^{1}H NMR (solution technique).

Technique	Polysar NMR system	McMaster U. NMR system
Frequency	200 MHz	500 MHz
Probe	5mm dual $^{13}C/^{1}H$	5mm Inverse BB Probe
Sweep width	20 ppm	11 ppm
Relaxation delay time	20s	9s
Pulse width	90° (9.4μs)	90° (6.6μs)
Line broadening factor	0.488	0.3
Number of scans collected	100	120
Spectral width	10 ppm (2000 Hz)	PLOT 8.0 -> -0.5 ppm
Acquisition time	2s	2.96s
Reference chemical shift	TMS	TMS

NMR peaks assignments

A representative ^{1}H NMR spectrum for the backbone prepolymer (sample C), for an example of branch prepolymer (sample B4q corresponding to graft FG8) and for graft sample FG10, are shown in Figures 3-4, 3-5 and 3-6, respectively. Peaks were assigned according to published information [181-182] for CIIR, [184] for BR and were additionally verified [188].

Figure 3-4. NMR (200 MHz) spectrum of sample C (backbone prepolymer).

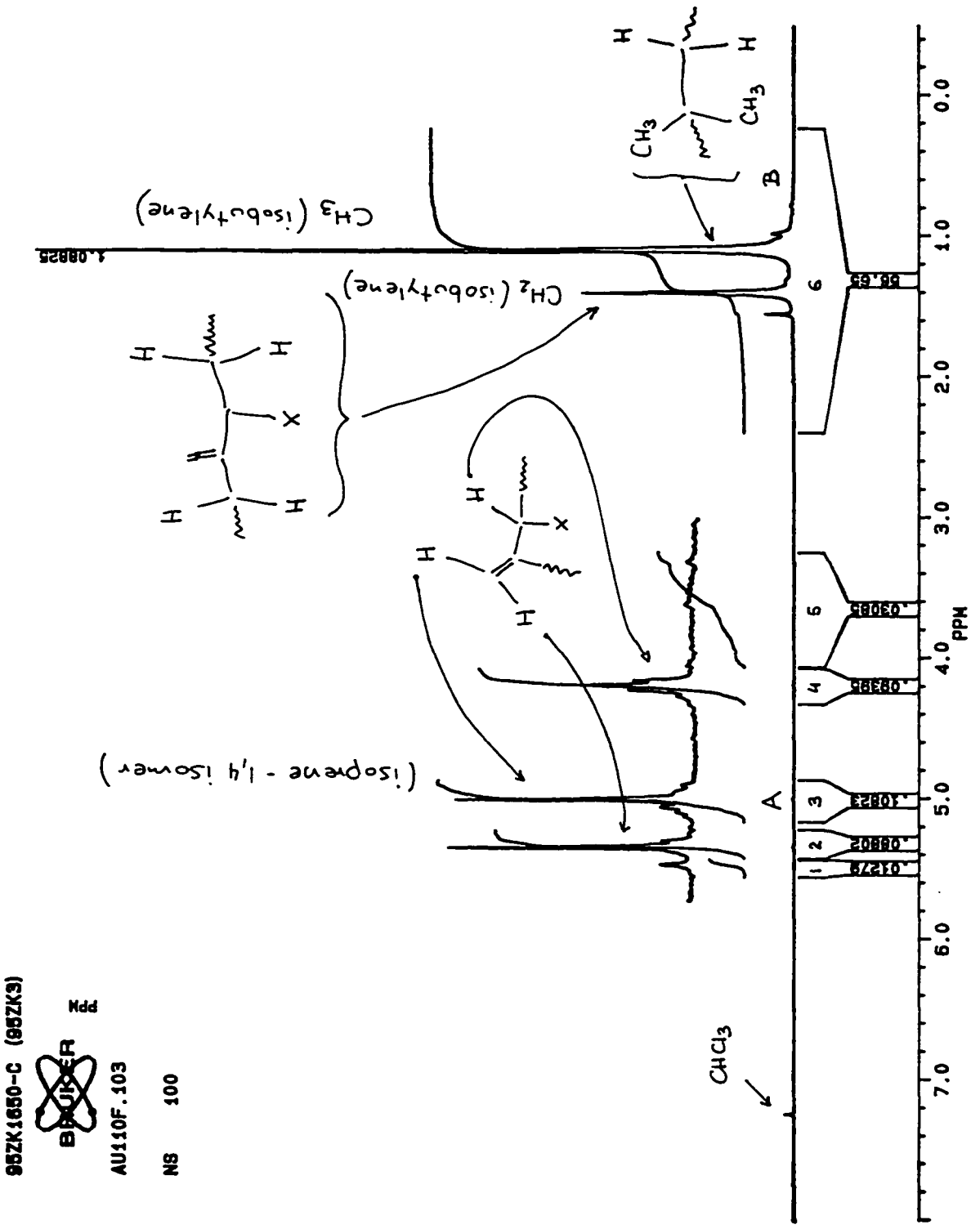


Figure 3-5. **NMR (200 MHz) spectrum of sample B4q (branch prepolymer of the graft sample FG8).**

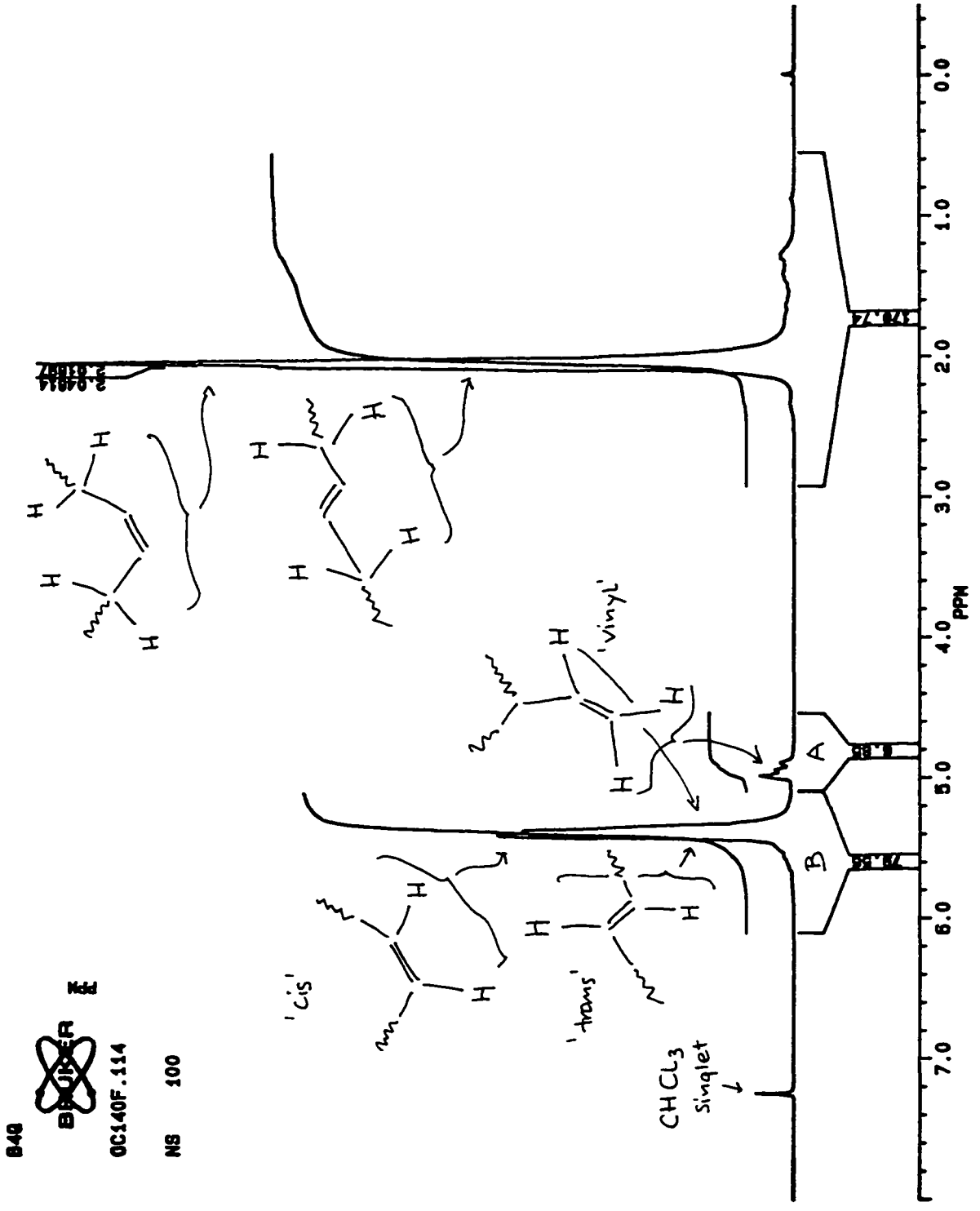
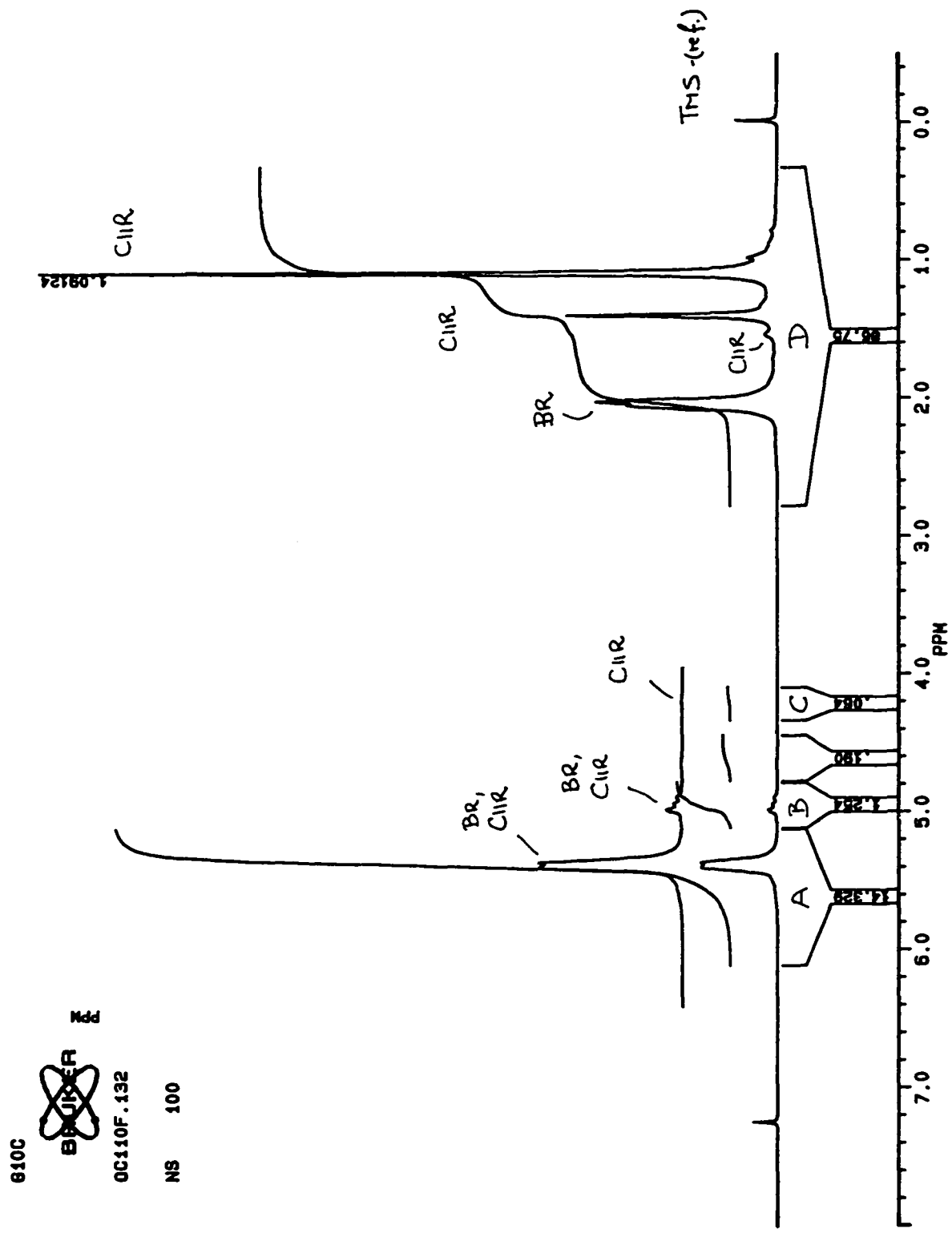


Figure 3-6. NMR (200 MHz) spectrum of sample FG10.



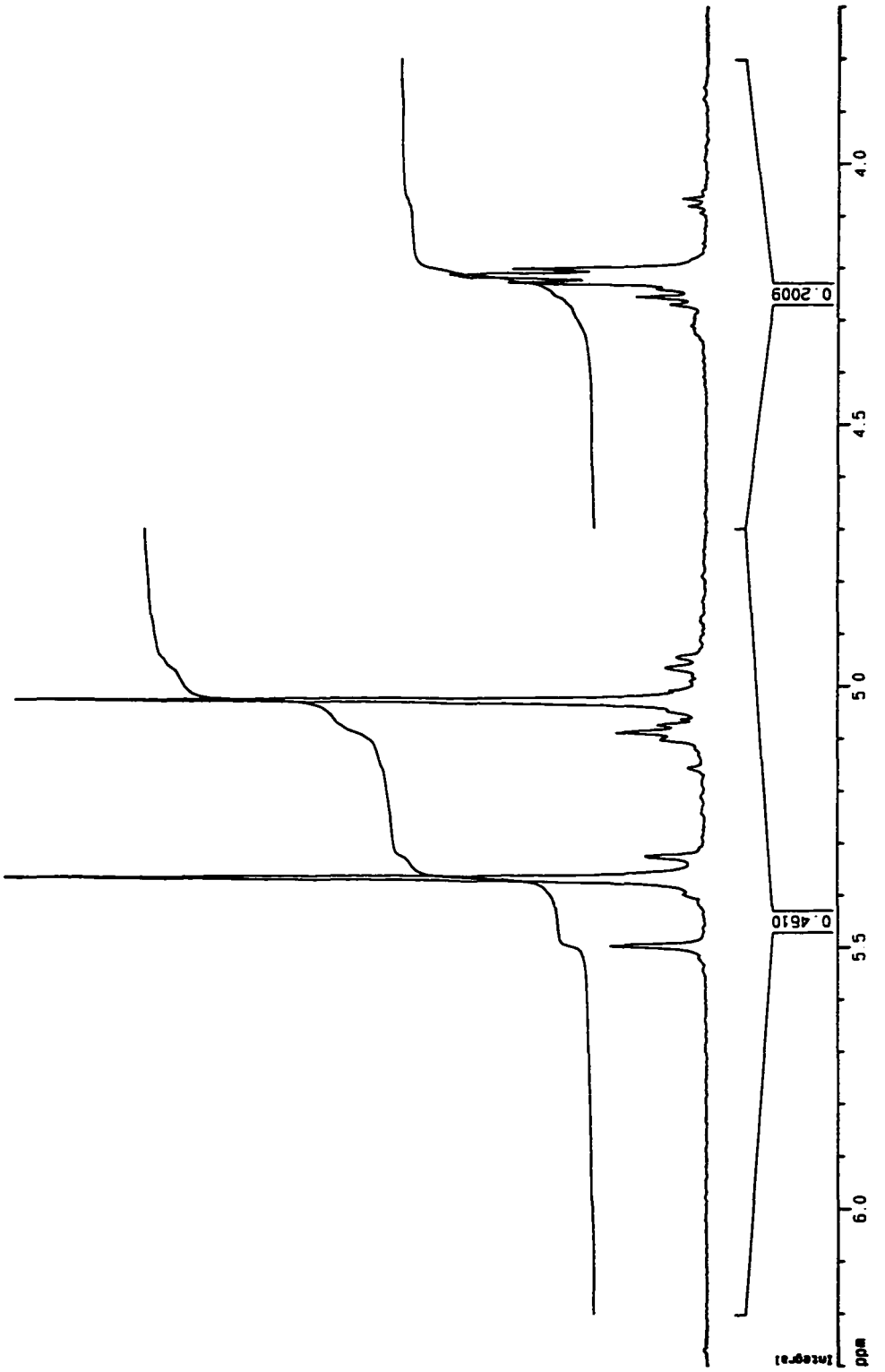
In Figure 3-4, the magnification of a lower-field spectrum of chlorobutyl rubber was included to allow more confident assignment of resonances and precise integration of peaks. The most pronounced peaks at approx. 1.1 and 1.4 ppm are assigned to the methyl and methylene protons, respectively, of the isobutylene (IB) units. The isoprenyl (IP) units have resonances at 1.65 and 1.94 (not visible) and 5.05 ppm. Integrals of those peaks are proportional to a molar IP content in the chlorobutyl batch of about 1.9%. An additional NMR spectrogram for sample C, obtained at 500 MHz, is shown in Figure 3-7. The chemical shift values of ^{1}H NMR resonances were referenced to tetramethylsilane (TMS). Each sample was run at least in duplicate.

Quantitative compositional analysis

The amount of halogen in halobutyl rubber can be determined from the triplet at 4.15 ppm (area "4" in Figure 3-4, or area "C" in Figure 3-6) which comes from the single proton on the carbon also containing the halogen atom. The isobutylene content can be determined from singlets at 1.0 and 1.4 ppm, which are from the methyl and methylene protons, respectively, of isobutylene, with corrections made for presence of the aliphatic peaks of the isoprene moiety.

The microstructural composition of the Bxy samples and the chemical composition of the BR in a graft or blend can be measured from either unsaturation peaks at 4.8 - 5.0 ppm and 5.3 - 5.5 ppm chemical shift zones, or from the aliphatic peak at 2.0 ppm. The two terminal olefinic protons of the vinyl structure show at a chemical shift of about 4.9 ppm, with the remaining vinyl unsaturation peak being under the envelope at 5.3 - 5.5 ppm. This area also contains the unsaturation peaks corresponding to cis-BD and trans-BD. The chemical shifts of olefinic protons of both 1,4-cis and 1,4-trans units appear near 5.4 ppm and these are very difficult to resolve with a frequency lower than approximately 300 MHz [189-190].

Figure 3-7. Section of the NMR (500 MHz) spectrum for sample C.



Three examples of composition calculation from NMR spectra follow. Estimation of molar content of IP in poly(IB-co-IP) random copolymer (butyl rubber) i.e. the unsaturation level, is based on the ability of ^{1}H NMR spectroscopy to distinguish between the vinyl protons of isoprene and the aliphatic protons of isobutylene. Corresponding peaks in NMR spectra can be integrated and unsaturation level calculated.

Example 1

The unsaturation (isoprene mol% content) can be calculated directly from CIIR spectra;

$$\text{mol\% unsat (CIIR)} = \frac{A}{A + \frac{B - 7A}{8}} \; 100\% \qquad (3\text{-}14)$$

where: A - integral of the peak at 5.0 ppm, and B - integral of the peaks at 0.2 -2.4 ppm range, as shown in Figure 3-4.

Example 2

Microstructure of BR was derived directly from Bxy samples using peak integrals:

$$\text{mol\% 1,2 BD} = \frac{\frac{A}{2}}{\frac{A}{2} + \frac{(B - \frac{A}{2})}{2}} \; 100\%, \quad \text{and} \qquad (3\text{-}15)$$

$$\text{mol\% 1,4 BD} = \frac{\frac{B - \frac{A}{2}}{2}}{\frac{\frac{A}{2} + \frac{(B - \frac{A}{2})}{2}}{2}} \; 100\% \qquad (3\text{-}16)$$

where: *A* and *B* peaks assignments are consistent with those in Figure 3-5.

Example 3

To calculate graft composition (BR mol%), microstructural composition of the BR in the graft and backbone prepolymer CIIR unsaturation from NMR spectra of a graft, the following formulas were used [188]:

$$\text{1,4 cis/trans BD} \quad \text{--->} \quad \frac{2A - B + C}{4}, \tag{3-17}$$

$$\text{1,2 vinyl BD} \quad \text{--->} \quad \frac{B - C}{2}, \tag{3-18}$$

$$\text{isoprene} \quad \text{--->} \quad C, \tag{3-19}$$

$$\text{isobutylene} \quad \text{--->} \quad \frac{D - 2A - \frac{B}{2} + \frac{7C}{2}}{8}, \tag{3-20}$$

where peak zone assignments A, B, C and D are as shown in the example Figure 3-6.

Microstructural or chemical composition can be calculated by normalization of appropriate terms. The above or appropriately modified formulas were used to calculate compositions of other samples. Results are discussed in the appropriate sections of chapter 4, namely: microstructure of BR in 4.3.3, microstructure of CIIR in 4.2.5, graft chemical composition in section 4.4.2 for CG and FG samples and in 4.4.5 for HG samples, as well as for the blend (sample M) in section 4.4.6.

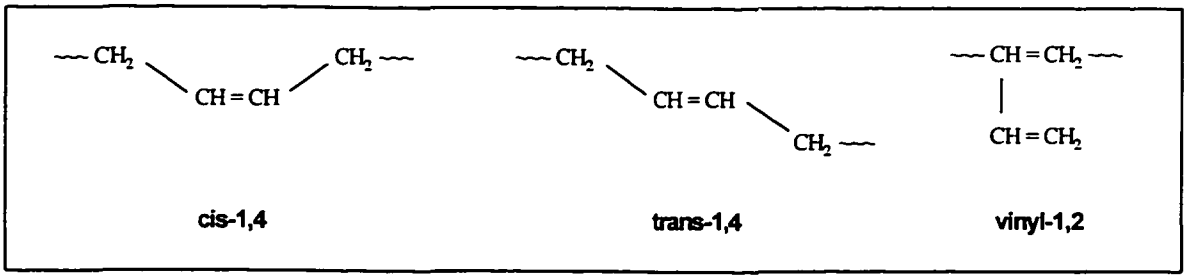
3.4.3 Infra-Red (IR) Spectroscopy

Infra-Red (IR) Spectroscopy is another analytical technique frequently used for quantitative characterization of stereochemical configuration and chain conformations. It is one of the most accessible and quick test methods available for identification and analysis of

microstructure and chemical composition of polymers. IR spectra are obtained by passing infrared radiation through a film made of sample material and recording the amount of radiation energy absorbed as a function of its wavelength. Peaks appearing on the spectrum correspond to specific chemical groups and, under certain circumstances, even particular molecular motions can be detected [191].

IR spectrometry is particularly effective for double-bond determination [192] and this feature of IR is used for this project. Specifically, microstructural analysis of the BR is performed to confirm the isomer ratio, which was initially determined by NMR. In the IR spectrum, polybutadiene shows intense absorptions which are due to wagging vibration of the =CH– group. These bands are characteristic of the content of the 1,4 (cis & trans) and 1,2 (vinyl) linked monomer units. Different isomeric forms of the BR microstructure are shown schematically in Figure 3-8.

Figure 3-8. Three forms of polybutadiene microstructure.



For compositional analysis of isomers in BR, the following bands were selected, [193]:

- for 1,4-trans, the band at 968 cm^{-1}
- for 1,4-cis, the band at 740 cm^{-1}
- for 1,2-vinyl, the band at 914 cm^{-1}

The overlapping of the absorptions at 967 cm^{-1} was judged to be insignificant and not corrected for. Isomeric proportions (1,2-vinyl/1,4-cis/1,4-trans) were calculated according to the procedure established for this type of polybutadiene [194] with the difference in absorbency coefficients accounted for. A Blackman-Harris 3-term function was used to weight the data.

FT-IR spectra were obtained using a Bruker IFS-66 IR Fourier Transform Interferometric Spectrometer. The infrared spectrum was recorded in the region of 1200 - 600 cm^{-1} with 50 scans collected. The zero filling was set to 2 and resolution has been estimated at 4 cm^{-1}. Specimens were prepared by film casting of toluene solutions on a KBr disk.

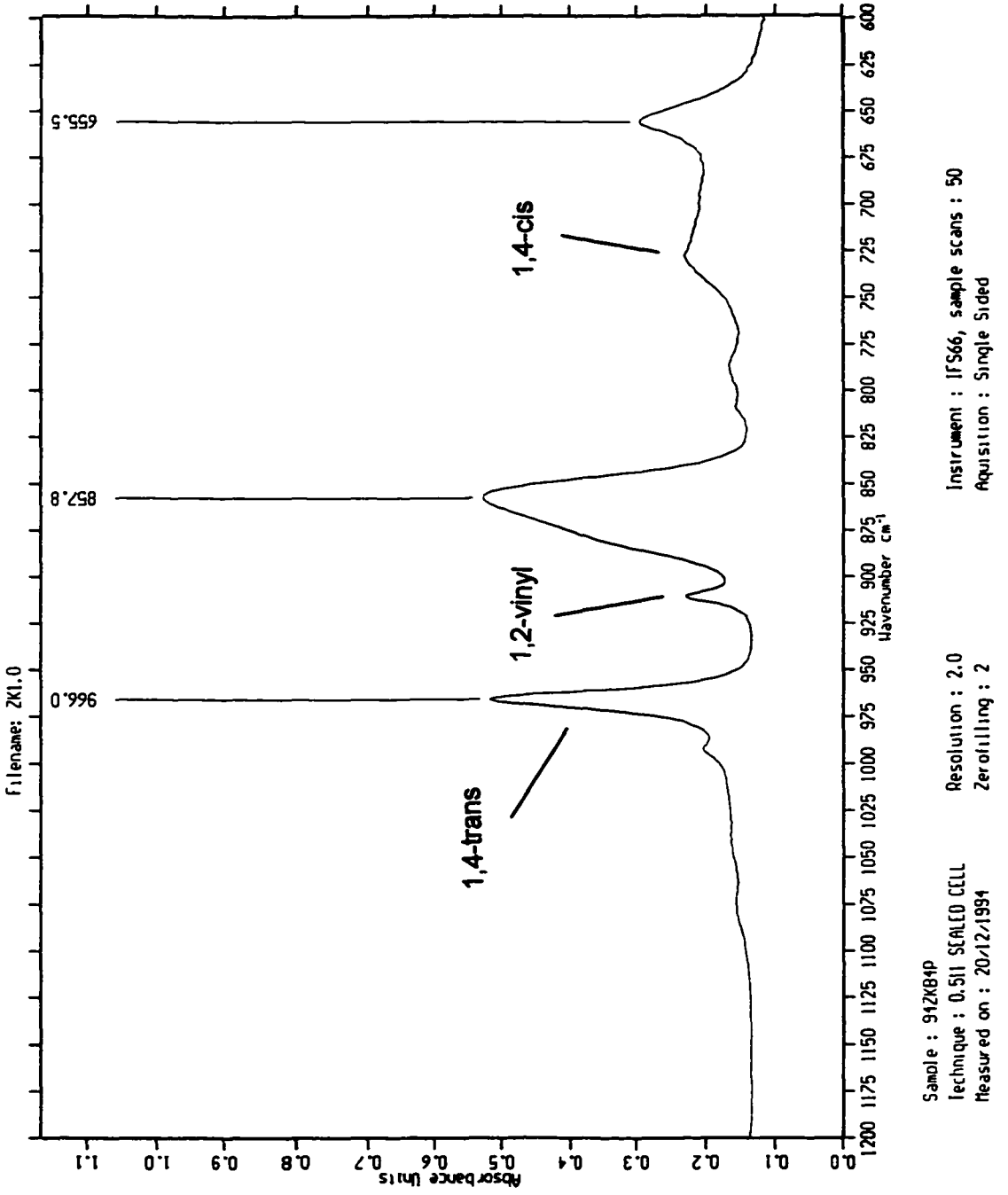
An example of FTIR spectrum is shown in Figure 3-9 for sample B4p, corresponding to graft FG21. Complete numerical results of IR characterization are compared to those obtained by NMR and discussed in section 4.3.3.

3.4.4 Differential Scanning Calorimetry (DSC)

Differential Scanning Calorimetry (DSC) is routinely used to measure thermal characteristics of the material, most typically, transition temperatures and crystallinity [195]. DSC measures the difference in heat flow through the 'sample' and 'reference' cells, as the two are simultaneously heated or cooled at the same rate.

The primary reason for using the DSC in this study was to measure the glass transition point(s) in graft copolymers. The onset of the glass transition, $T_{g,f}$ as defined by DSC, was determined from the heat flow versus temperature traces, by drawing tangents to one of the baselines and the leading edge of the transition (see Figure 3-10). The abscissae corresponding to the point of intersection of the two tangents were interpreted as $T'_{g,f}$ and $T''_{g,f}$. The mid-point between these two temperatures was defined as $T_{g,f}$.

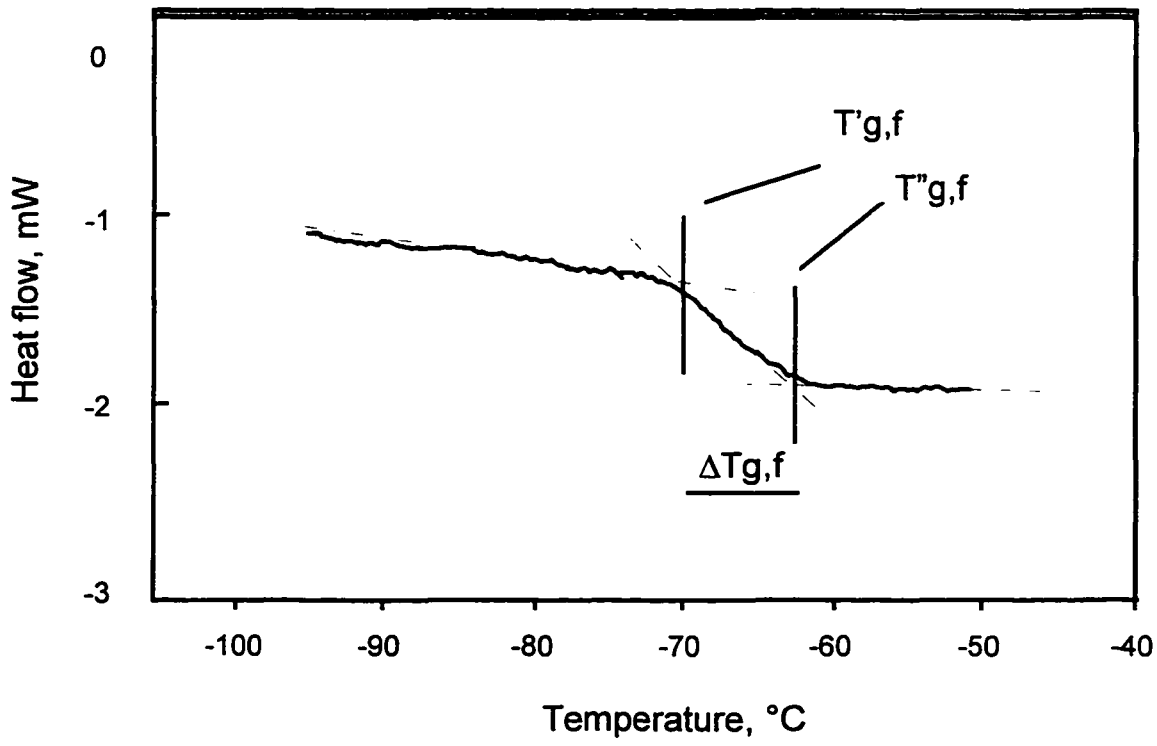
Figure 3-9. FT-IR spectrum of sample B4p (branch prepolymer corresponding to graft sample FG21).



The DSC traces were recorded using a dual cell TA 912 Differential Scanning Calorimeter, equipped with a Thermal Analyst 2200 Data Acquisition/Analysis Module. The instrument was calibrated on the melting temperatures of indium (156.6°C), mercury (-38.9°C) and tin (231.9°C) [196].

All graft samples, precursor polymers and their blend were evaluated by scanning in the range of temperatures between -120°C and 200°C, in triplicate. Samples were heated under nitrogen (N_2) at a rate of 20°C/min. Representative DSC traces are shown in section 4.5 and are discussed in the context of graft phase morphology.

Figure 3-10. Definition of the $T_{g,f}$ from DSC scan.



3.4.5 Transmission Electron Microscopy (TEM)

Microscopy photographs were taken on selected samples using the transmission electron microscope (TEM) Philips EM300 operating at 100 kV. Electron microscopy was performed on thin (about 400Å) films, microtomed with a diamond knife at liquid nitrogen temperatures. The films were exposed to OsO_4 vapour at room temperature in order to achieve contrast between BR and CIIR phases. Evidence of the multi-phase morphology was obtained. However no attempt was made to carry out quantitative analysis of the micrographs. Several pictures, made on samples with various structures and chemical compositions, are included and further discussed in section 4.5.

Microscopic specimens were prepared and micrographs were taken according to techniques developed for gum elastomers [197] and [198], respectively.

3.4.6 Thermo-gravimetric Analysis (TGA)

Thermogravimetric Analysis (TGA) is a suitable method for determination of the content of carbon black and residual fillers in elastomers and rubber compounds. It is also used to obtain information about the nature and approximate content of volatiles like residual solvent or moisture, plasticizers, oils and other similar additives. For small samples, TGA can be considered as a convenient method to impose a well controlled thermal history, in order to investigate the effect of high temperature on polymer stability and determine the upper temperature limit for any given application [172, 199].

A weighed sample of polymer is heated in vacuum or an appropriate atmosphere (air, nitrogen, etc.) following a pre-selected and strictly controlled temperature sweep program [200]. For typical elastomeric unfilled material, most of the volatile components distill off

before the temperature reaches about 200°C, while less volatile, non-polymeric organic substances will leave a solid sample before 300°C. At this point of the heating cycle the loss of mass indicates the approximate amount of non-polymeric, volatile substances. The loss of mass between 300°C and 650° is attributed to the polymeric content of the sample.

Thermogravimetric analysis was accomplished using TA Instruments TGA 951 Analyzer. Weight loss as a function of temperature, in 25 - 800°C range, was measured under vacuum at the heating rate of 20°C/min. Results of the TGA analysis are presented in section 4.4.7 where the content of solvent and non-polymeric substances in samples is discussed.

3.4.7 Solubility tests

Solubility tests are performed routinely to determine the macro-gel content of elastomers. An example is the ASTM Test Method for gel content determination of raw non-oil-extended and non-pigmented gum rubbers [201]. The elastomeric sample is allowed to dissolve for a prescribed amount of time in a suitable solvent. A solution containing the sol, e.g. the soluble portion of the material, is separated from insoluble portion (if any) and allowed to evaporate. The total mass of dried sol is used to determine gel content or alternatively, % solubility of the rubber sample. For the purpose of this project, an appropriate modification of the ASTM Standard Procedure [201], designed to characterize the soluble portion of partially cross-linked butyl polymers, was used [202]. A small but exactly known amount of sample is allowed to dissolve in cyclohexane at room temperature for a period of 48 hours. After subsequent filtration (mesh size 325), a measured portion of filtrate is evaporated to a constant mass. The dry polymer residue is weighed and the percent of soluble portion is calculated. A solubility test was carried out on several sets of samples. Each set included all grafts (FG/G samples), the backbone prepolymer (sample C), and CIIR/BR blend (sample M), as well as sample of branch prepolymer, B10.

The first series of solubility tests was carried out on freshly cast samples, sampled from material designated for rheological testing. Selected control samples, for the second and subsequent series of solubility tests, were kept in identical storage conditions as the bulk of experimental material, and for a period comparable to duration of the rheological characterization sessions (about one year). Sampling points for gel screening are indicated in Figure 3-1 and the results are discussed in section 4.4.8.

In addition to solubility tests, procedures for some analytical tests, such as SEC, include filtration of dissolved samples, thus providing additional screening against gel. Except in rare and isolated cases, all specimens were found to be completely soluble, and therefore free of macro-gel, consistent with filtration evidence.

3.4.8 Ion Chromatography (IC) and Wet Chemistry methods

Knowledge of the molar % of bound chlorine in a backbone molecule can be used for the calculation of the average number of grafting sites and estimation of the *maximum number of possible* grafting points. For that reason, in addition to NMR screening, another supplementary technique to confirm mol% of Cl in CIIR was justified.

Ion Chromatography (IC) offers a quick method for compositional analysis of a variety of materials, including polymers. A Dionex DX-100 Ion Chromatograph was used, according to procedure [203] which was developed specifically to measure Cl (or Br) contents in halogenated butyl rubbers.

The amount of total and bound chlorine content was also measured using standard wet chemistry methods by comparison of the wt% chlorine before and after solvent/non-solvent extraction [204]. Results of both analyses are reported in section 4.2.6.

Chapter 4

Molecular structure and composition: results

The strategy adopted for characterization of graft copolymers takes advantage of the method of preparation of the graft. The principal characteristics of comb-type structures, namely backbone length, branch length and average number of branches were derived from appropriate characteristics of the precursor polymers, prior to the coupling reaction. This approach makes it possible to deduce structural information not easily obtainable from analysis of fully formed grafts and was tried elsewhere for copolymer synthesis by similar 'grafting onto' [170] and by 'macromonomer methods' [205-206].

Section 4.1 defines the terms *variable, parameter* and *interference*. Qualification of a large number of frequently interrelated characteristics of polymer structure, composition and morphology helps to structure properly the analysis of correlations between these and physical properties. Results of structural analysis are discussed in section 4.2 for CIIR (the backbone, precursor polymer for the graft) and in section 4.3 for the Bxy series of branch prepolymers. Sections 4.4 and 4.5 discuss various aspects of graft structure, composition and morphology. A summary of graft structure (4.6) concludes this chapter.

4.1 Overview of structural variables, parameters and interferences

For the sake of clarity, all important structural and compositional factors are grouped into three categories: *variables, parameters and interferences*.

The principal structural *variables,* later referred to as 'variables', are the features of the graft structure which were designed to vary systematically from sample to sample, in order to allow a quantitative study of their effects on rheological behavior. They are: the length of

branch *(V1)* and the number-average number of branches per backbone molecule *(V2)*. Much experimental effort was devoted to accurate measurement of these two structural variables. Accurate and quantitative determination of these variables was a primary objective of structural analysis.

Parameters are all those inherent characteristics of copolymer structure and composition which have the ability to affect rheological behaviour, but which by design were kept constant (or at least approximately constant). Experiments were carried out to estimate their nominal values, or at the very least, to prove that they are invariables as far as the sample portfolio is concerned. Examples of parameters in the above sense are the molecular weight distribution of backbone-forming copolymer, CIIR *(P3)*, and the distribution of branching points along the backbone of the graft *(P5)*. Determination of parameters is a secondary objective of this chapter.

The third category, *interferences*, includes all those features of polymer structure or chemical/physical composition which ideally should be absent in model structures. In reality they are sometimes unavoidable or adventitious by-products of sample synthesis, refining, conditioning or storage. If they cannot be corrected for, removed or minimized, they would typically disqualify sample material from further characterization or would invalidate results obtained. As far as interferences are concerned, characterization is focused on detection of possible interferences and, if present, an estimation of the extent to which they are likely to distort the outcome of intended structure - property correlations. Suspected interferences must either not exist, or have their effect proved to be negligible, or be quantified. Gel, particularly 'macro-gel' *(I4)* is an example of *an interference*, which in the context of long-chain branching studies could complicate analysis beyond a manageable level. Another example , the presence of ungrafted *and* unextractable parent polymers in a graft mixture *(I1)* might be an unavoidable complication. A correction should be included in the structure-property analysis using appropriate statistical methods. Details of possible corrections are

discussed in various sections of this chapter. The tertiary objective of this chapter is to address these issues.

Table 4-1 (in two parts, a & b) lists all identified principal variables, *(V)*, compositional variables dependent on them, *(DV)*, parameters, *(P)*, and interferences, *(I)*. The table is intended to supplement Table 3-1 which specified instrumental methods and analytical characterization techniques used to characterize the structure of CIIR-g-BR copolymers.

Given the present level of established technology available for characterization of the LCB in polymeric systems with MWD, CC and LCB heterogeneities, any additional reliable information about structure and composition can be indispensable. Indeed, as expressed by J. Roovers, "it is most helpful when the type of branching can be derived from a consideration of the synthesis of the polymer" [207]. For a model branched polymer, it is possible to derive the average number of branches from its molecular weight and from that of precursor (parent) polymers. Reliable assessment of the molecular weight distribution of the parent polymers can be made before they are reacted to form a graft, long-chain branched copolymer. This is the methodology adopted in this work.

4.2 Backbone prepolymer (CIIR) characteristics

An opportunity to study structure and composition of the backbone polymer without branches attached to it was fully realized. Structural characteristics of the backbone CIIR copolymer are of interest in this study for two reasons:

1) Foremost, they are the characteristics of the backbone of the graft, which is the same for all the graft copolymers,
2) Secondly, CIIR (sample C) can be regarded as special case of a graft with branches reduced to zero length, serving as a reference for the LCB structure-property studies.

Table 4-1a. An overview of methodology used for determination of structure, composition and morphology of CIIR-g-BR graft copolymers.

V/DV P/I	Structural variable, parameter, interference	how controlled... (synthesis)	how corrected... (modification)	how experimentally measured or detected ...	how corrected or accounted for ...
V1	Average branch length, $\overline{M}_x^b$	Bu-Li concentration	---	from $\overline{M}_x^b$ of branch precursor polymer [SEC]	***two principal variables for LCB structure-rheol. property relationship***
V2	Average number of branches per backbone, N_g	stoichiometry of grafting reaction	---	from adj. graft composition [NMR/SEC] + $\overline{M}_x^b$, $\overline{M}_x^B$ (SEC)	
DV1	Graft chemical composition, w^b	stoichiometry	---	from composition by [NMR/FTIR]	related to graft LCB structure
DV2	Graft total molecular weight , M_x^G	combination of factors (V1+V2+P1)	---	calc. from $\overline{M}_x^B$, $\overline{M}_x^b$, N_g measured $\overline{M}_z^G$ [SEC]	related to graft LCB structure
DV3	Phase morphology	by casting under "thermodynamic equilibrium" cond.	---	[TEM, DSC, DTMA]	no quantitative analysis attempted
P1	Type of branching structure (regular combs)	chemistry (incl. functionality of branch point)	---	linearity of CIIR and BR molecules as confirmed by M-H-S plots [SEC]	---
P2	Average length of backbone	S.T.S.F.A.S.	---	$\overline{M}_x^B$ of backbone precursor polymer [SEC]	---
P3	MWD of backbone molecules	S.T.S.F.A.S.	---	from MWD of backbone precursor polymer [SEC]	---
P4	Microstructure of backbone polymer (CIIR unsaturation)	S.T.S.F.A.S.	---	IP/IB by [NMR] on CIIR	---

S.T.S.F.A.S. - **S**trictly **T**he **S**ame **F**or **A**ll **S**amples (single batch of CIIR being selected for the whole project).

Table 4-1b. An overview of methodology used for determination of structure, composition and morphology of CIIR-g-BR graft copolymers - cont.

V/DV P/I	Structural variable, parameter, interference	how controlled... (synthesis)	how corrected... (modification)	how experimentally measured or detected ...	how corrected or accounted for ...
P5	Distribution of branch points along the backbone	S.T.S.F.A.S.	---	not readily accessible experimentally	random distribution derived from IP/IB reactivity ratio
P6	Distribution of branch points across MWD of the backbone polymer	S.T.S.F.A.S.; (equiv. to distribution of IP units)	---	assessed from studies on similar systems studied by preparative [SEC/NMR]	---
I1	Ungrafted BR content, $w^{b,h}$	depends on $\overline{M}_x^b$, also on N_g and reaction conditions	by extraction of uncoupled BR	by comparison of chem. composition & MWD on crude and purified samples	qualification of results on grafts with high $w^{b,h}$
I2	MWD of the branches	high system purity and strict polymerization conditions	---	from MWD of precursor BR polymer [SEC] + random grafting assumption	samples with broad or irregular/bimodal MWD of the branch rejected
I3	Microstructure of the branch polymer (BR tacticity)	catalyst, solvent, and reaction temperature	---	from compositon of BR by [NMR & FTIR]	---
I4	3-D structures (micro-gel and macro-gel)	stabilizing system added (antioxidants etc.)	---	[SEC] scans (micro-gel); solubility/filtration (macro-gel)	samples with detectable gel would be discarded
I5	Solid residues (stabilizer, impurities)	---	purification and filtration of feedstock	residual sample mass above 450°C [TGA]	very small amount judged to have negligible effect
I6	Residual solvent and moisture (in solid samples)	feedstock purification, reaction conditions	solid sample dried to a constant mass	drop of sample mass in [TGA] scan, up to ~250°C	results on "foamed" samples considered invalid

S.T.S.F.A.S. - **S**trictly **T**he **S**ame **F**or **A**ll **S**amples (single batch of CIIR being selected for the whole project).

4.2.1 Molecular chain linearity

Until recently, butyl rubber and its halogenated modifications were believed to be composed of strictly linear polyisobutylene chains with isoprene units distributed randomly along the molecular chain [208]. Recently it has been suggested that the structure of butyl rubber is somewhat more complicated [209, 210].

The isoprene units have mainly (90-95%) the 1,4-trans configuration [181, 183, 209], but other structures have been identified also, namely 1,2 isoprenyl (IP) enchainment and possibly a small amount of 3,4 configuration [183, 210]. Currently there is no agreement as to the exact nature of the minor isoprenyl structure in butyl rubber. Most recently, the first identification of 3,4 IP addition was reported [209] based on two-dimensional analysis of high-field (500 MHz ^{1}H NMR spectra). This minor structure presumably can result from 1,4 addition, subsequent rearrangement and possible isobutylene (IB) addition to form a branch. The relative concentration of this minor isoprene species capable of forming branch points increases with increasing polymerization temperature.

The amount of 3,4-structures was estimated to be about 0.5% [209]. This number agrees well with our assessment of 3,4-structure content, obtained from 500 MHz ^{1}H NMR [211]. Comparison of the slope of the log η_0 versus log $\overline{M}_w$ for strictly linear polyisobutylene and some polyisobutylene-co-isoprene (butyl) polymers, indicated that a very small amount of long-chain branching may indeed exist in some butyl rubbers [209].

The well established method for LCB detection involves examination of the Mark-Houwink-Sakurada (M-H-S) plot, log [η] vs log M, typically obtained from continuous viscometric measurements on SEC elution fractions [133, 138, 212-213]. A straight line relationship between the log [η] and log molecular weight is frequently interpreted as the evidence of lack of long-chain branching in the structure of a polymeric sample. In fact, it strictly means that

the M-H-S exponent, α is *not* dependent on the molecular weight. This implies that either there is no branching or the branching is uniformly distributed across the MWD, in such a fashion that it is not changing the α-coefficient with changing molecular weight. [214]. The latter is less likely to happen, especially in commercial polymers. Thus it can be inferred that a straight line reflects a lack of branching, at least in detectable amounts.

This method was used to examine whether the CIIR batch used for preparation of grafts indeed contained a small amount of LCB. Figures 4-1 and 4-2 show M-H-S plots for linear, narrowly polydispersed PMMA and PS, respectively. Plots were constructed from intrinsic viscosity, $[\eta]$ data and molecular weight values (weight-average), submitted with SEC standards by the American Polymer Standard Corp., Mento, Ohio. No downward curvature is observed in these M-H-S plots, indicating, within the sensitivity of the method and with the reservation made earlier in this subsection, the lack of any detectable amount of LCB. In Figure 4-3, the sample of linear PIB (a GPC standard polyisobutylene) and CIIR polymer - sample C, share similar characteristics of the M-H-S plot. However, in the case of sample C, a slight curvature of the M-H-S plot is noticeable. The equivalent plot for an experimental butyl of comparable MW in which formation of branching structures was chemically induced, is shown in the same figure. The rather pronounced curvature observed can be confidently related to the presence and non-uniformity of the LCB distribution along the MWD.

Significance for graft structure:

A very small fraction of the chlorobutyl molecules might indeed be branched, and as a result may produce a few graft molecules of a structure more complex than simple, one-level combs. However, their influence on the rheological behaviour in the melt, would probably be negligible, given their very small concentration and the fact that they are reported to be mostly confined to the low end of the molecular weight distribution [209]. Additionally, it

Figure 4-1. M-H-S plots for narrowly polydispersed PMMA.

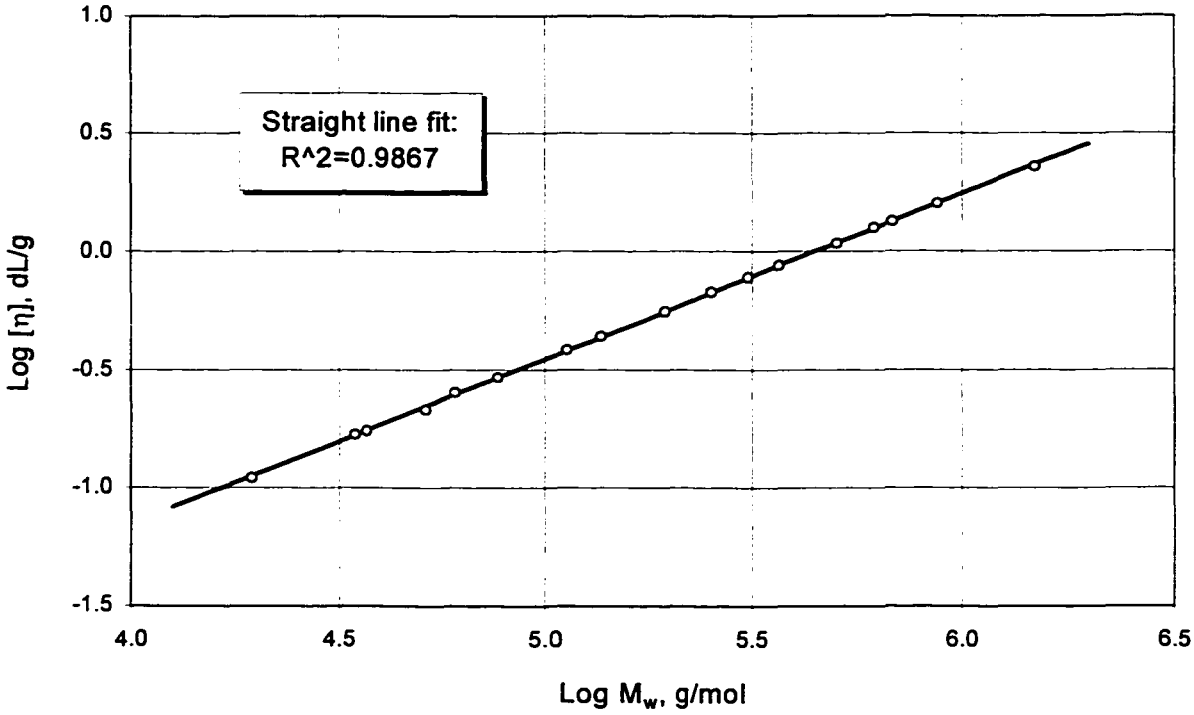


Figure 4-2. M-H-S plots for narrowly polydispersed PS.

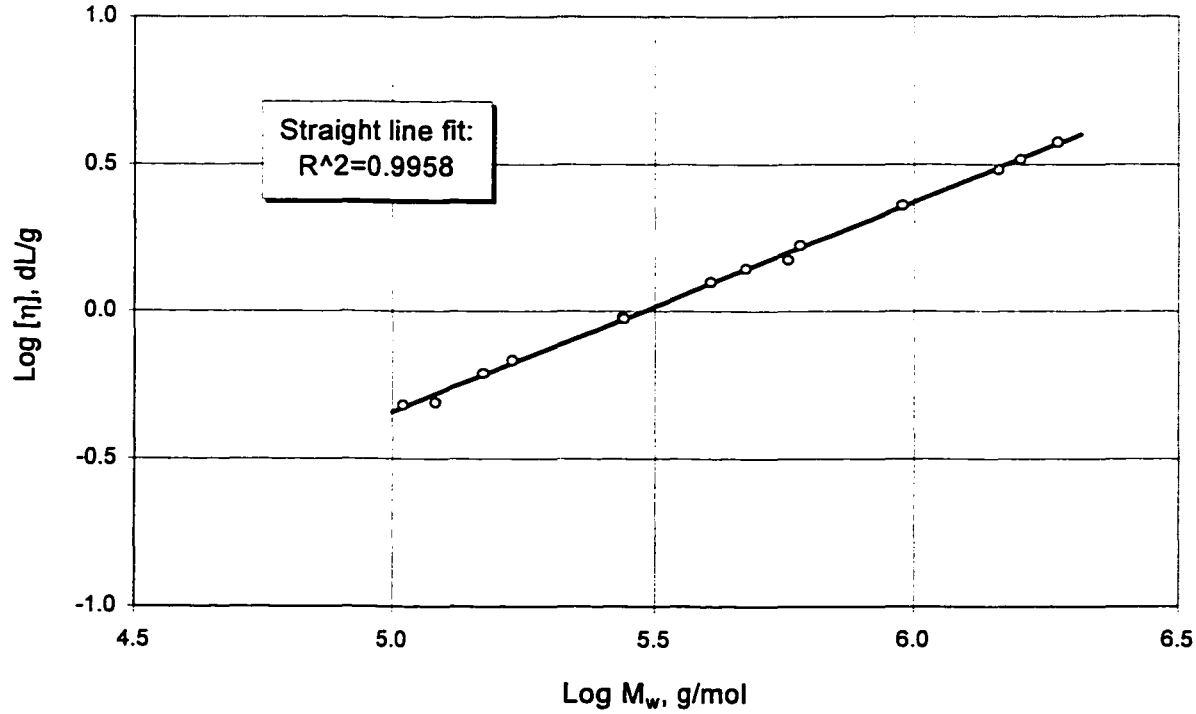
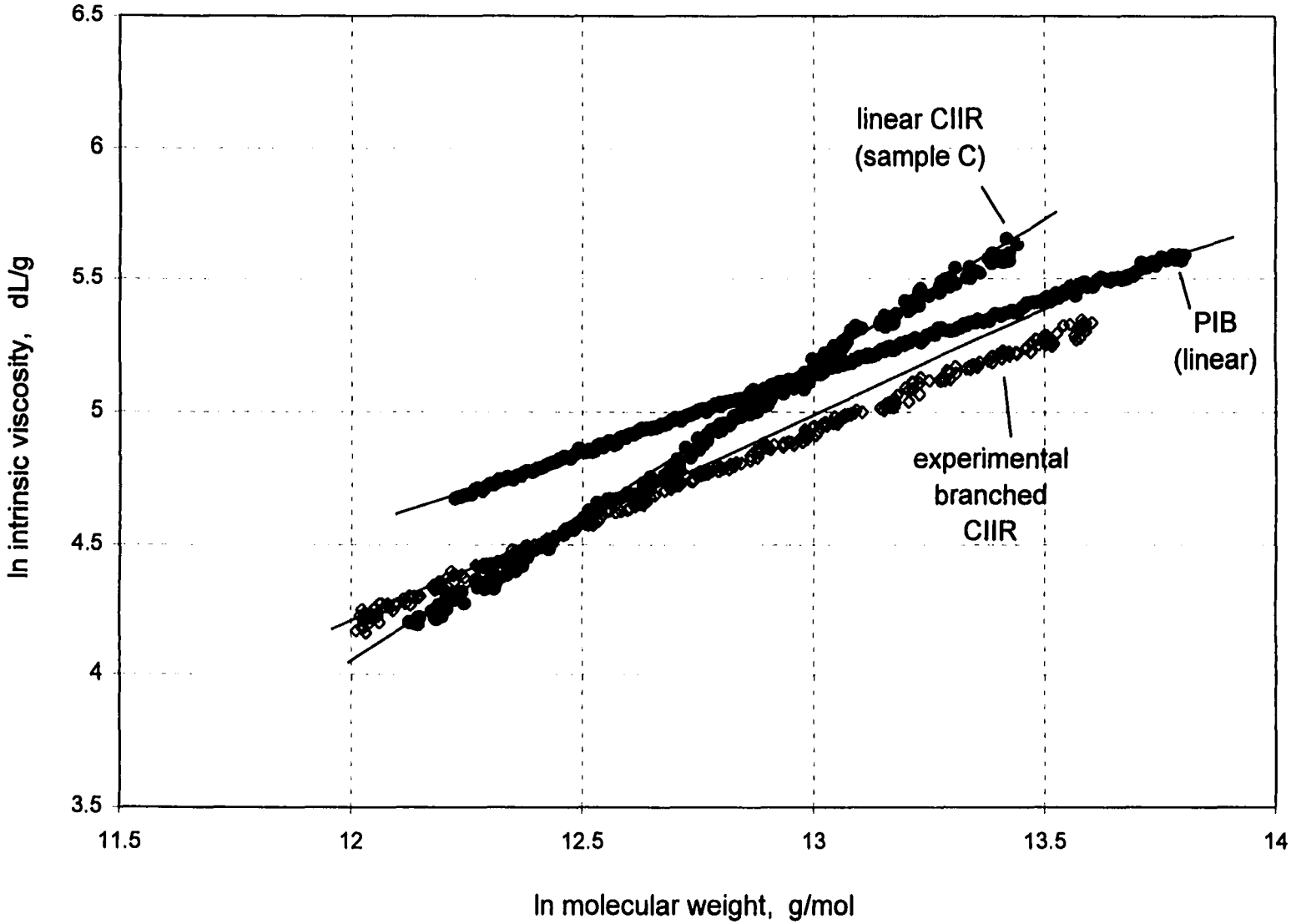


Figure 4-3. M-H-S plot for linear and branched chlorobutyl rubber.



should be emphasized again that, regardless of the nature of small structural irregularities of the backbone molecules, they are statistically identical for all graft samples.

4.2.2 Functionality of branching point

Under normal grafting reaction conditions the only segment of the backbone capable of accepting preformed Li-capped polybutadiene molecules is the isoprene mer with an allylic chlorine ion attached to it [85, 215]. From the nature of 'living' anionic polymerization, Li^+ can be attached to only *one end of the same* BR molecule and only one BR chain can be accepted per branching site. Therefore, from a graft topology point of view, it can be concluded that the nominal branching point functionality, f is three (3), cf. also Figure 2-2.

Significance for graft structure:

The above conclusion, in combination with the results of the preceding section about linearity of the backbone molecule, as well as the analogous conclusion for branch prepolymer molecules, discussed in subsection 4.3.1, support the proposed hypothesis that the bulk of graft molecules consist of simple, comb-type branching structures [85].

4.2.3 Molecular weight distribution

Molecular weight distribution (MWD) of the backbone precursor copolymer was determined by Size Exclusion Chromatography (SEC). Details of the test procedure are described in section 3.4.1. Multiple determinations were carried out during the course of the entire polymerization session (several months) in order to estimate the test (SEC) precision, detect possible changes in molecular weight of the CIIR batch, and compare results obtained using different methods of SEC data calculation.

Twin SEC traces obtained for sample C simultaneously by DRI and DV detectors are shown in Figure 4-4; (a) for DRI and (b) for DV. Secondary peaks visible on the DRI trace above about 30 min retention time are due to sulfur used here as a marker, as well as due to non-polymeric content of the injected solution.

Molecular weight averages, $\overline{M}_n$, $\overline{M}_w$, and $\overline{M}_z$, were calculated and peak molecular weight M_p was estimated from the MWD. Number-average molecular weights, $\overline{M}_n$, in the order of 140,000 g/mol and polydispersity index, PDI of about 3.2 ($PDI \equiv \frac{\overline{M}_w}{\overline{M}_n}$) were found to be typical for this type of elastomer. Some of the results are compared in Table 4-2. For the purpose of numerical peak deconvolution, the shape of the MWD could be most accurately fitted to the *Gamma Peak* Function.

The characteristic "low-end" tail of the MWD is responsible in part for the scatter of calculated molecular weight averages, which is particularly pronounced for $\overline{M}_n$, due to the lack of unequivocal definition of the base line and peak boundaries on the SEC trace.

Backbone degradation - most likely chain scission during processing or due to certain chemical reactions - is a possibility for the CIIR copolymer, and for polyisobutylenes, in general [26, 102, 216]. Consequently, the stability of CIIR under grafting reaction conditions was examined by comparing the MWD of the backbone precursor (sample C) before and after a simulated grafting reaction. The simulated grafting reaction carried out with a deactivated batch of BR, under otherwise identical conditions, led to the creation of pure blend of CIIR and BR, sample M (section 4.4.6). A similar approach has been reported for other grafts (CIIR-g-PS) [80]. However, it does not include the possibility of chain splitting due to the grafting reaction itself. The issue of graft sample stability, i.e. backbone disintegration during storage, sample processing and testing was discussed earlier (chapter 2).

Figure 4-4. SEC(W) traces for sample C.

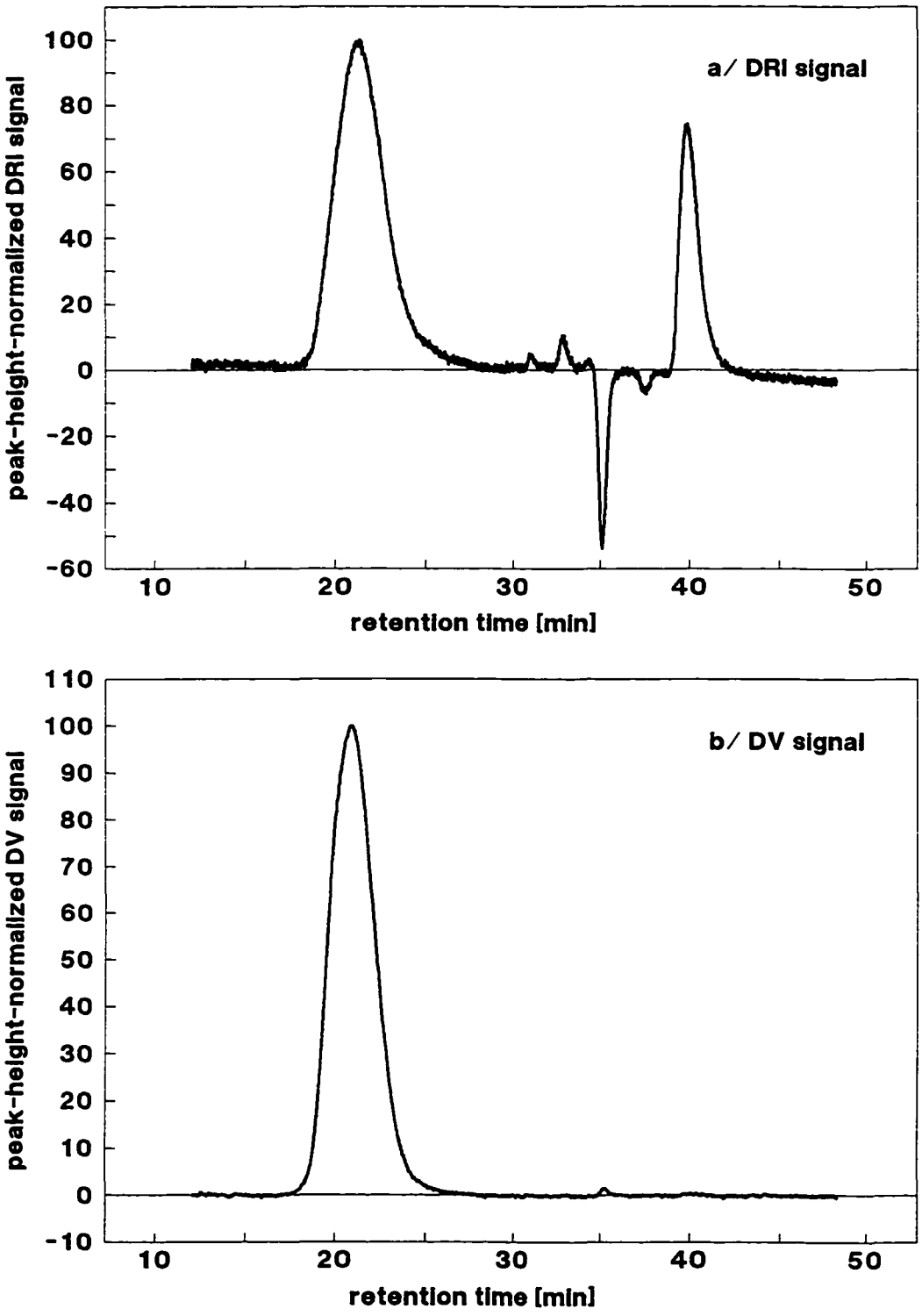


Table 4-2. Molecular weight distribution parameters - sample C (backbone prepolymer).

MOLECULAR WEIGHT DISTRIBUTION PARAMETERS - sample C						
SEC(P)	**specimen**	M_n^B	M_w^B	M_z^B	M_p^B	M_w^B/M_n^B
		a	b	c	d	e
DRI	a	138,800	454,200	864,900	366,800	*3.27*
	b	146,000	469,200	893,800	399,600	*3.21*
	c	137,900	457,300	876,200	372,100	*3.32*
	d	146,600	463,300	877,900	399,600	*3.16*
	e	137,500	449,900	866,000	393,900	*3.27*
	f	137,900	449,900	863,100	372,100	*3.26*
	average	***141,000***	***457,000***	***874,000***	***384,000***	***3.25***
SEC(W)	**specimen**	M_n^B	M_w^B	M_z^B	M_p^B	M_w^B/M_n^B
DRI	a	146,000	433,000	771,000	350,000	*2.97*
	b	175,000	452,000	804,000	394,000	*2.58*
DV-I	a	174,000	379,000	—	—	*2.18*
	b	195,000	412,000	—	—	*2.11*
DV-II	a	180,000	390,000	700,000	330,000	*2.17*
	b	178,000	405,000	720,000	331,000	*2.28*
DV-I & II	***average***	***182,000***	***397,000***	***710,000***	***330,000***	***2.18***

Despite the fact that no separate experiments were carried out to exclude possible backbone molecule disintegration during coupling reaction with a BR chain, close agreement between theoretical and experimental graft molecular weights suggests that no major modification to the integrity of CIIR molecules is taking place. Similarly, a comparison between the MW of extracted (unreacted) homopolymers (samples HG), and those of precursor polymers, support the above conclusion (section 4.4.5).

Significance for graft structure:

It can be assumed then that the MWD and derived molecular weight parameters, $\overline{M}_x$, M_p measured for sample C, i.e. the backbone precursor polymer, do represent the actual MWD and corresponding parameters, $\overline{M}_x^B$ and M_p^b, of the backbone of the graft.

4.2.4 Composition/unsaturation

The molar content of isoprene (IP) in poly(isobutylene-*co*-isoprene), sometimes referred to as 'unsaturation level', was measured by NMR on several specimens of sample C. The average value of 1.9 ± 0.2 mol%, slightly higher than the nominal unsaturation level for this grade of chlorobutyl (1.6 mol%), was subsequently confirmed by additional measurements on a higher resolution NMR spectrometer, which yielded a similar (2.1 mol%) value. This IP content translates into about 55 IP mers per statistical (number-average) butyl molecule of $\overline{M}_n$ = 141,000 g/mol.

Significance for graft structure:

The significance of these measurements lies in the fact that the total unsaturation determines the maximum amount of bound chlorine the copolymer can absorb, which in turn controls the maximum number of available grafting sites per average backbone molecule. Distribution of the isoprene mers both along the backbone and as a function of molecular weight will govern the distribution of branching, and is discussed in the next section.

4.2.5 Microstructure - compositional heterogeneity

For the sake of clarity, the following distinction is made between 'grafting site' and 'grafting point'. A *grafting (or branching) site* is the isoprene unit in the CIIR backbone molecule with potential for accepting Li^+-terminated BR molecules, i.e. an IP mer having allylic chlorine attached to it. A *grafting (or branching) point* is the grafting (or branching) site which has a branch actually connected to it.

a/ Distribution of IP units along the CIIR molecule

While direct experimental verification of CIIR microstructure may be difficult to obtain, the following calculations should suffice. For isobutylene copolymerization with isoprene, in CH_3Cl solvent and with $AlCl_3$ coinitiation at -103°C, the reactivity ratios are $r_1 = 2.5$ and $r_2 = 0.4$ for IB and IP, respectively [217]. This gives $r_1 \cdot r_2 = 1$, i.e. a condition which promotes random structure of a copolymer. In a copolymer, the average sequence length $\overline{m}$, corresponding to polymer M can be estimated from the following formulae [218]:

$$\overline{m}_{M_1} = 1 + r_1 \frac{[M_1]}{[M_2]} \quad \text{and} \quad \overline{m}_{M_2} = 1 + r_2 \frac{[M_2]}{[M_1]}, \qquad \text{(4-1a,b)}$$

where $[M]$ is a molar concentration and r is a reactivity ratio.

Using literature values for isobutylene $[M_1] = 0.985$ and $r_1 = 2.5$, and for isoprene, $[M_2] = 0.015$ and $r_2 = 0.4$, the following average sequence length were calculated: $\overline{m}_{M1} \approx 165$ for IB, and $\overline{m}_{M2} \approx 1.006$ for IP. These results support the well established hypothesis about the solitary nature of IP units, in a predominantly isobutylene, IB-*random*-IP copolymer (sample C).

Significance for graft structure:

In summary, IP mers are isolated (not clustered) and randomly distributed along the CIIR molecule [208]. These results support the conclusion that the spatial distribution of *individual* branches along the backbone molecule will follow the *random* distribution of grafting sites, and hence random distribution of grafting points along the backbone.

b/ Compositional heterogeneity as a function of the molecular weight distribution

The plausible and convenient assumption of chemical homogeneity of CIIR as a function of molecular weight distribution cannot be accepted in the light of recent investigations [219-221]. The content of the IP units in butyl rubber is known not to be uniform as a function of the molecular weight. It could be quantified by either multi-detector SEC [219-220] or by unsaturation measurements on molecular fractions, obtained from preparative size exclusion chromatography. Available results on butyl samples of various origins, indicated that, as a rule, isoprene content steadily increases with increasing MW and more rapidly so at higher molecular weights. Due to the fact that structural/compositional parameters of the backbone polymer are invariant (designated as S.T.S.F.A.S. in Table 4-1), no attempt was made to verify and quantify these results for sample C experimentally.

Under the copolymerization conditions of commercial butyl rubber manufacturing, the reactivity of isoprene is lower than that of isobutylene. Consequently, as copolymerization progresses and molecular weight increase, due to decreasing chain transfer to monomer, the concentration of isoprene in the unreacted monomer mixture increases. This results in the incorporation of a higher number of isoprene mers at the end of the batch reaction, resulting in increased content of IP in the larger macromolecules.

Significance for graft structure:

A non-uniform distribution of IP mers, with greater concentration in larger molecules will cause the high molecular weight tail of the distribution to have a disproportionally higher

number of molecules per graft, and higher impact on those rheological properties which are sensitive to branching. However, again due to the fact that the molecular weight distribution of the backbone copolymer in all grafts is identical, this compositional heterogeneity, while not
determined, should not interfere with conclusions drawn from the effects of other quantified structural variables on the rheological properties.

4.2.6 Chlorine content and distribution

In commercial chlorobutyl, introduction of chlorine to the butyl molecule, at approximately 1:1 molar ratio of chlorine to double bonds, is done primarily to achieve more readily controlled vulcanization or better covulcanization with high unsaturation elastomers [222]. For this project, concerned exclusively with gum rubber (i.e. unfilled and unvulcanized) samples, isoprene units with substituted allylic Cl are providing coupling sites for Li-terminated BR chains, thus allowing the grafting reaction to occur [120, 223].

a/ free Cl content

Most of the chlorine in butyl is forming bonds with unsaturated sites scattered along the poly(IB-co-IP) chains. A certain amount of unreacted, 'free' chlorine usually remains in the bulk of the elastomer. The total chlorine content obtained by Ion Chromatography on a raw chlorobutyl sample (before purification for grafting reaction) selected for this project was 1.34 ± 0.04 wt%.

The batch of chlorinated butyl prepared for grafting 'living' polybutadiene, which is extremely sensitive to 'poisons' including chlorine, had to undergo multiple and very thorough purifications designed to remove residual (free) chlorine completely as well as other impurities. Indeed, no trace of free chlorine could be found in purified CIIR either by Ion Chromatography (IC) or by wet chemical methods. Perhaps an even more stringent indication

of a lack of appreciable amount of unbound chlorine was the high efficiency of the grafting reaction (Table 2-4).

b/ bound chlorine content

The molar composition of bound chlorine was calculated from appropriate peak areas in the 500 MHz ^{1}H NMR spectrum. The 'bound' chlorine content of 1.64 ± 0.04 mol% was in good

agreement with the value obtained by Ion Chromatography (1.5 mol% after conversion from wt%). The wt% (Cl) was recalculated into mol% (Cl), using the following approximate formula:

$$mol\%(Cl) = \frac{wt\%}{wt\% + (100\% - wt\%) \cdot \frac{35.4}{56.6}} \cdot 100\% \qquad (4\text{-}2)$$

where: MW(CIIR) = 56.6 g/mol @CIIR unsaturation = 2.1 mol%, Cl content. = 1.2 mol% and MW(BR) = 35.4 g/mol.

c/ maximum number of branching sites

The bound chlorine content was calculated in order to estimate the number of grafting sites, and thus the maximum branching frequency possible at a given level of CIIR unsaturation. The number-average number of grafting sites per backbone molecule, S_g^n was calculated as follows [114, 117, 215]:

$$S_g^n = \{ \overline{M}_n \text{ / M (CIIR)} \} \cdot \text{IP (mol\%)} \cdot \text{chlorination efficiency} =$$
$$141{,}000 \text{ g/mol} / 56.6 \text{ g/mol} \cdot 2.1\% \cdot 60\% \approx 31 \text{ grafting sites.}$$

Thus, there is a sufficiently high number grafting sites to obtain a sufficiently high number of grafting points (i.e. branches) to satisfy the requirements of this study (column "b" in Table 2-3).

4.3 Branch prepolymer (BR) characteristics

Results of molecular structure characterization of the precursor branch polymers are presented and interpreted in terms of the corresponding branches in the graft. The underlying assumption of non-preferential grafting seems reasonable (cf. section 4.4.9). It implies that the aliquot obtained immediately before grafting accurately represents the characteristics of the BR in the branch.

4.3.1 Molecular chain linearity

The α-exponent in the Mark-Houwink-Sakurada equation, $[\eta] = K \cdot M^{\alpha}$ has been frequently referred to as an indicator of long-chain branching [224-225]. Typically the value of the exponent α decreases with increasing branching. It is generally accepted that branching density is seldom independent of MW, and it usually increases with the MW. Consequently, on a double logarithmic M-H-S plot, a decrease of exponent α with increasing MW results in a decrease of the slope of $[\eta]$ vs MW, resulting in a downward curvature of the plot.

Linearity of the M-H-S plot is frequently, but not always correctly, presented as evidence for the absence of long-chain branching in a polymer (section 4.2.1). Strictly speaking, it should rather be interpreted as evidence that either no branching is present or that branching structure or distribution does not change with MW. A case in point was made by the comparison of linear polystyrene (PS) with model, star-branched polystyrenes samples [226]. The double logarithmic plot $[\eta]$ vs MW was a straight line of the same slope in all cases (i.e. regardless of the number of arms). However, a similar plot for randomly branched PS samples showed curvature, presumably reflecting an increasing degree of branching with the increasing molecular weight. In the case of copolymers, possible compositional heterogeneity may further complicate the interpretation of these plots.

Available literature on long-chain branching in polybutadienes [26, 224-225, 227-230] consistently concludes that the n-butyllithium initiated polybutadienes represent some of the 'most linear' narrow molecular weight distribution polymers known. This is particularly true for BR synthesized by 'living' anionic polymerization, prepared in the laboratory under strictly controlled conditions and made in a reaction system of the highest purity.

Two M-H-S plots of typical Bxy samples (B4j and B4r) are shown in Figure 4-5. Allowing for experimental scatter, the data fit reasonably well to a straight line. These results can be contrasted with analogous plots for two commercial grades of BR, made using a different catalyst. In Figure 4-6 "less-branched" commercial BR sample T-1203 is compared with "more-branched" T-1202 sample.

Significance for graft structure:

The linearity of branch polymer molecules, in connection with the conclusion of section 4.2.1, implies, that the grafted molecule constitutes a simple comb-type structure with linear branches, attached to a linear backbone molecule.

Figure 4-5. M-H-S plot for Bxy samples - SEC(W).

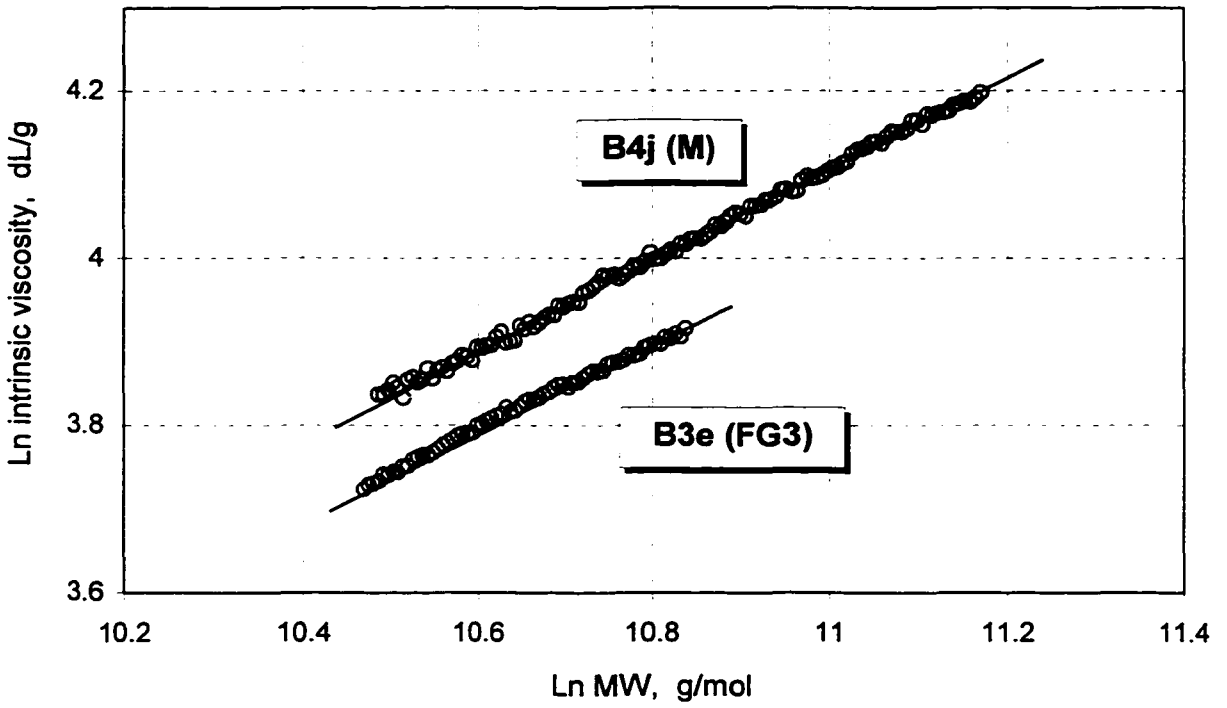
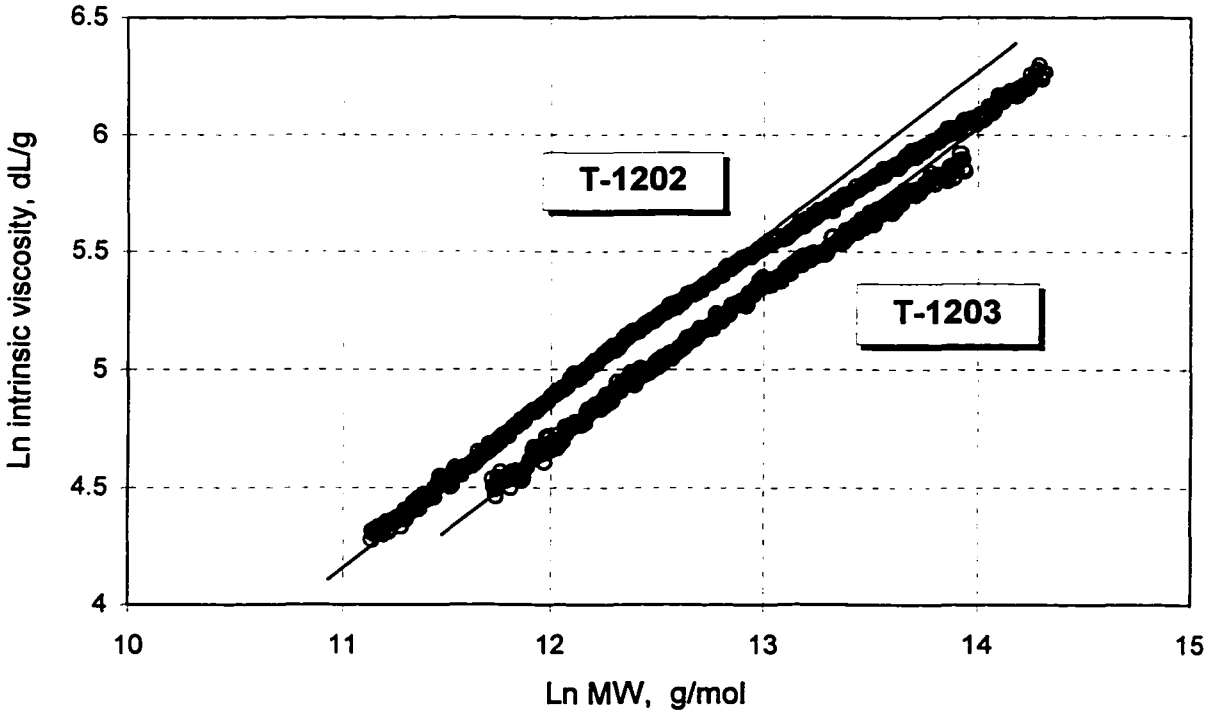


Figure 4-6. Examples of M-H-S plot for two commercial "branched" polybutadienes.



4.3.2 Molecular weight distribution

The molecular weight distribution of Bxy samples was measured on two independent SEC systems, and in some cases in multiple determinations. SEC(W) traces for three representative samples are included in Figures 4-7, 4-8 and 4-9. Both DRI (upper plot) and DV (lower plot) signals are peak-height normalized and plotted over the entire range of relevant retention times. The main peaks between 20 and 30 min retention time are the polymeric peaks corresponding to the polymer under study. The negative DRI scan peak corresponds to the water contained in the sample [173], while the secondary positive DRI peak (not detectable by DV) is due to the marker (sulfur).

DRI traces (SEC/P) of the polymeric section of the chromatogram for four other randomly selected Bxy samples in Figures 4-10, 4-11, 4-12 and 4-13, were area-normalized and smoothed (Savitzky-Goolay) in order to assist in the interpretation of the more complex GPC traces of graft copolymers, as well as the assessment of the grafting efficiency and graft mixture composition.

Statistical moments and other numerical descriptors of the MWD (referred to synonymously as 'MWD parameters') were calculated from the MWD using well known formulas. A summary of MWD parameters for all Bxy samples prepared for grafting, corresponding to graft samples FG1 - FG22 and blend M is included in Table 4-3. Number-average molecular weights of Bxy samples range from 4,300 g/mol to over 100,000 g/mol, the latter figure approaching the molecular mass of the backbone of the graft.

The retention time corresponding to the concentration (DRI-signal) peak maximum is reported as the *peak retention time* (PRT) and M_p is the molecular mass corresponding to the PRT. This can be interpreted as the most probable MW of the branch (Bxy) polymer molecule.

Figure 4-7. Normalized SEC(W) traces for sample B9a (FG14).

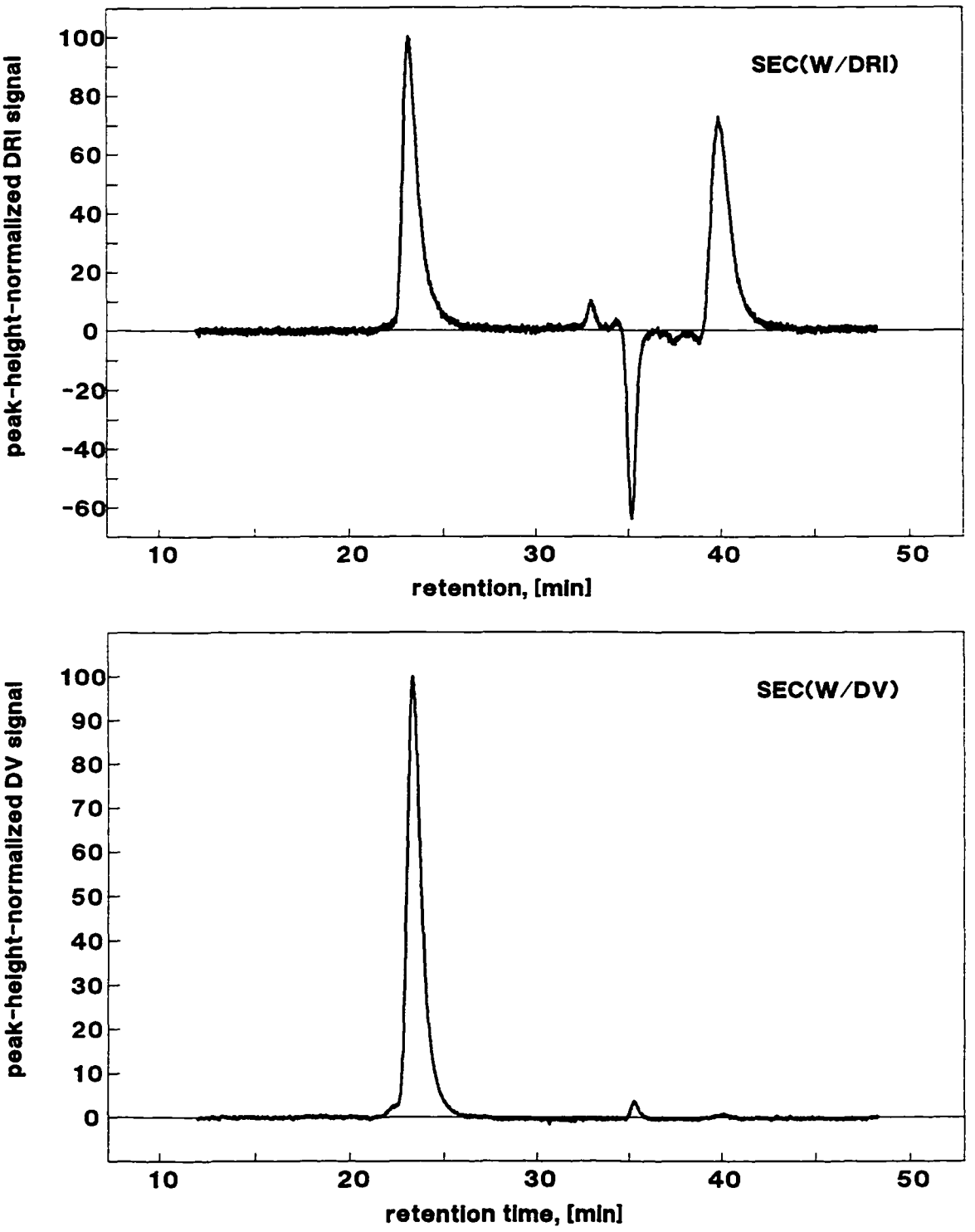


Figure 4-8. Normalized SEC(W) traces for sample B4m (FG4).

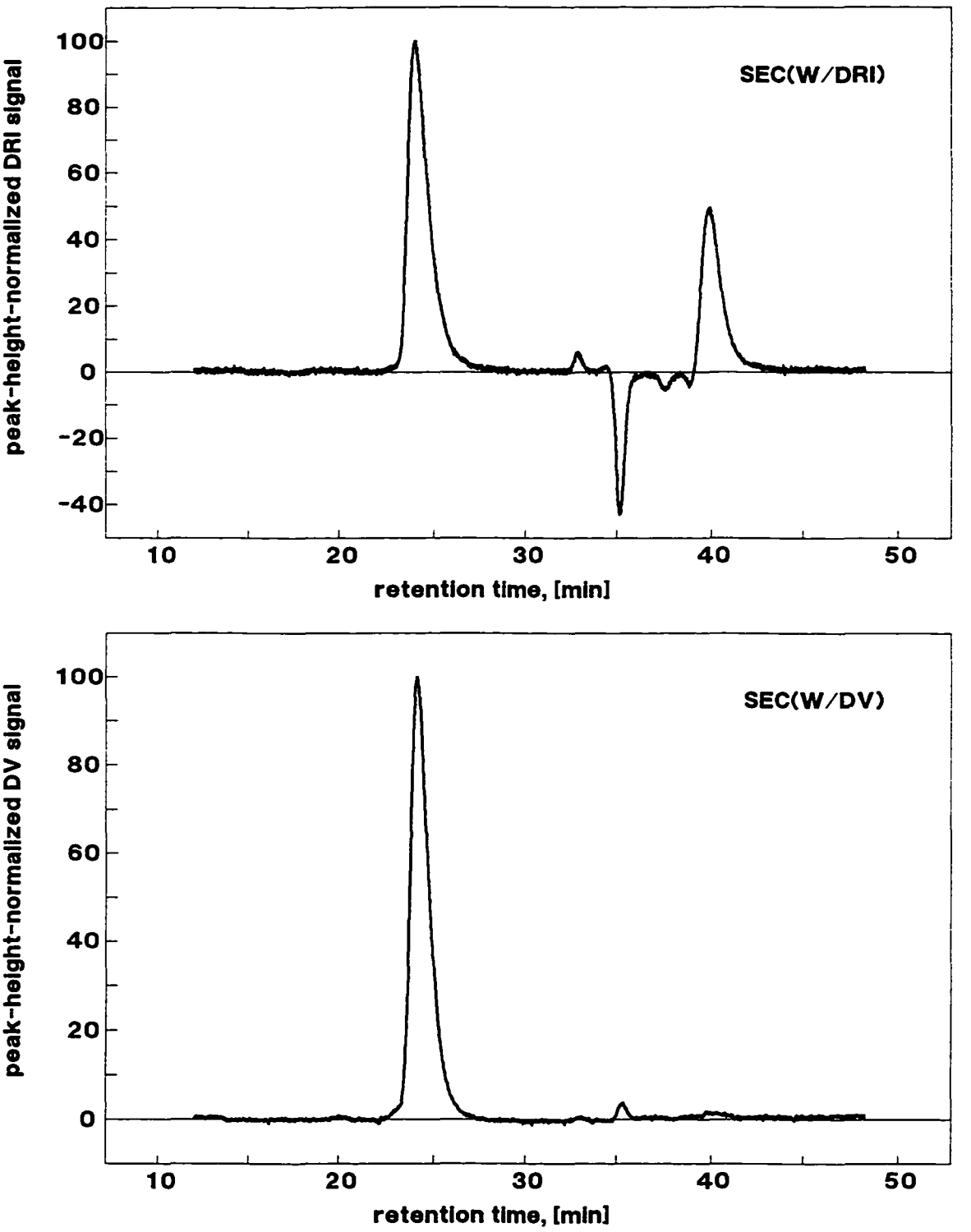


Figure 4-9. Normalized SEC(W) traces for sample B4q (FG8).

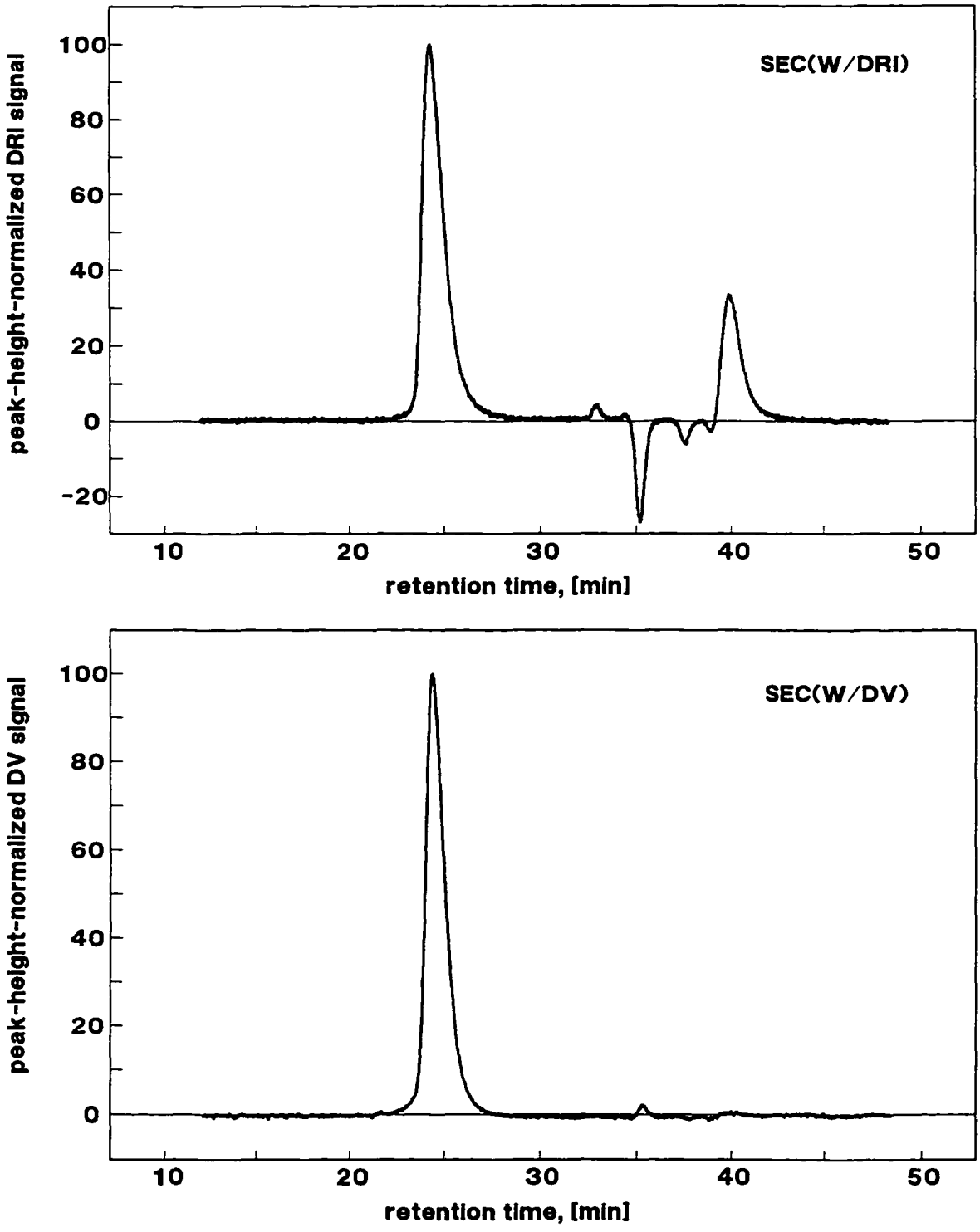


Figure 4-10. Normalized SEC(P) trace for sample B5f (FG5).

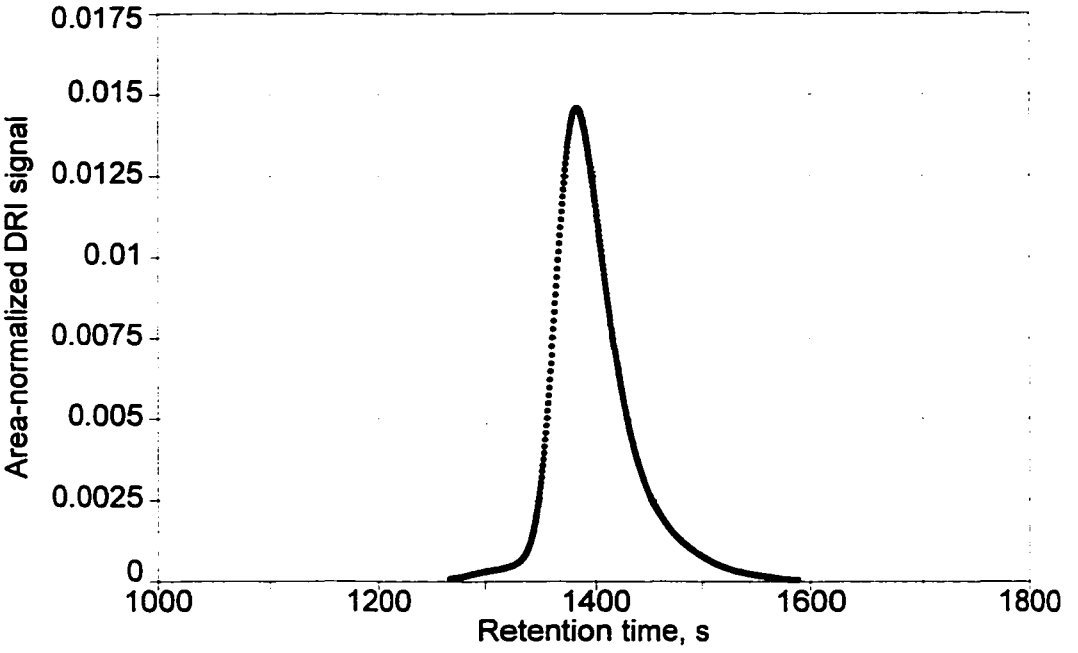


Figure 4-11. Normalized SEC(P) trace for sample B6h (FG6).

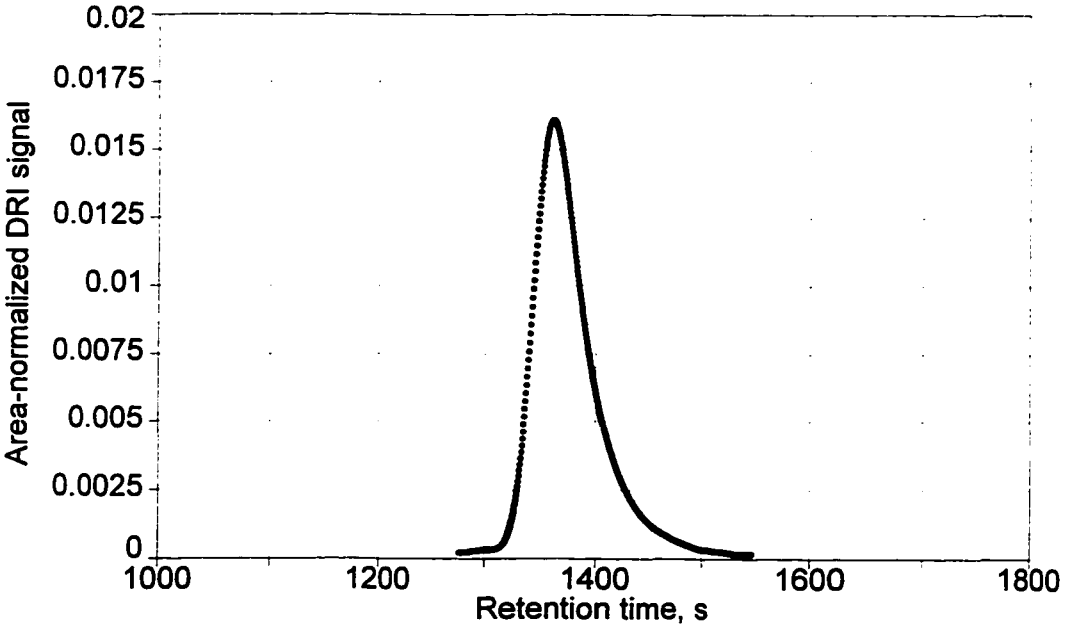


Figure 4-12. Normalized SEC(P) trace for sample B3f (FG12).

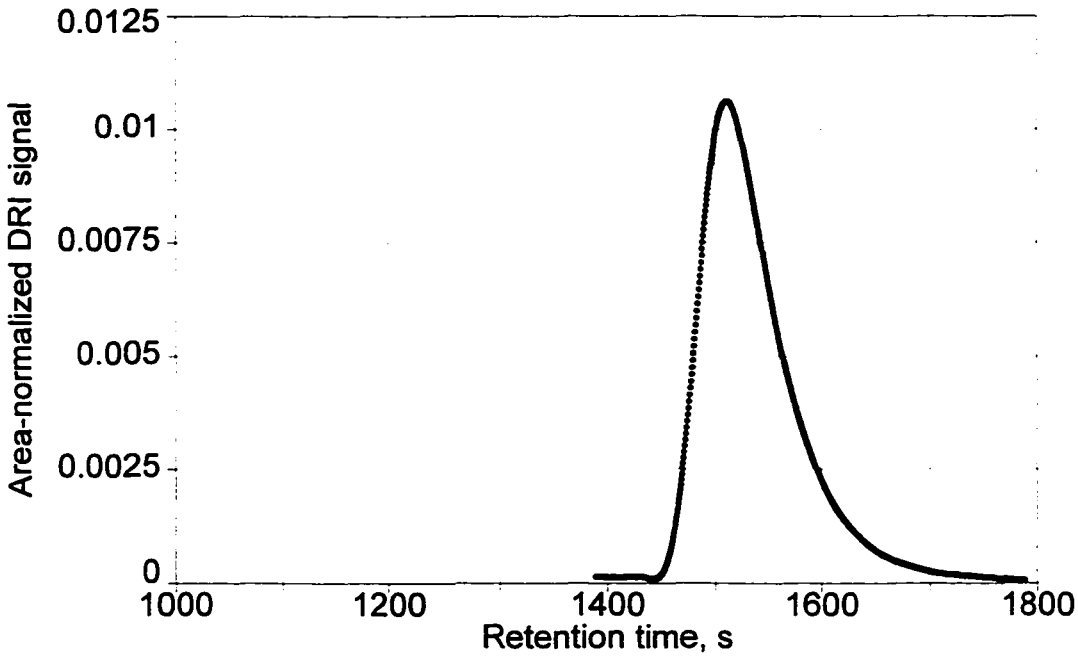
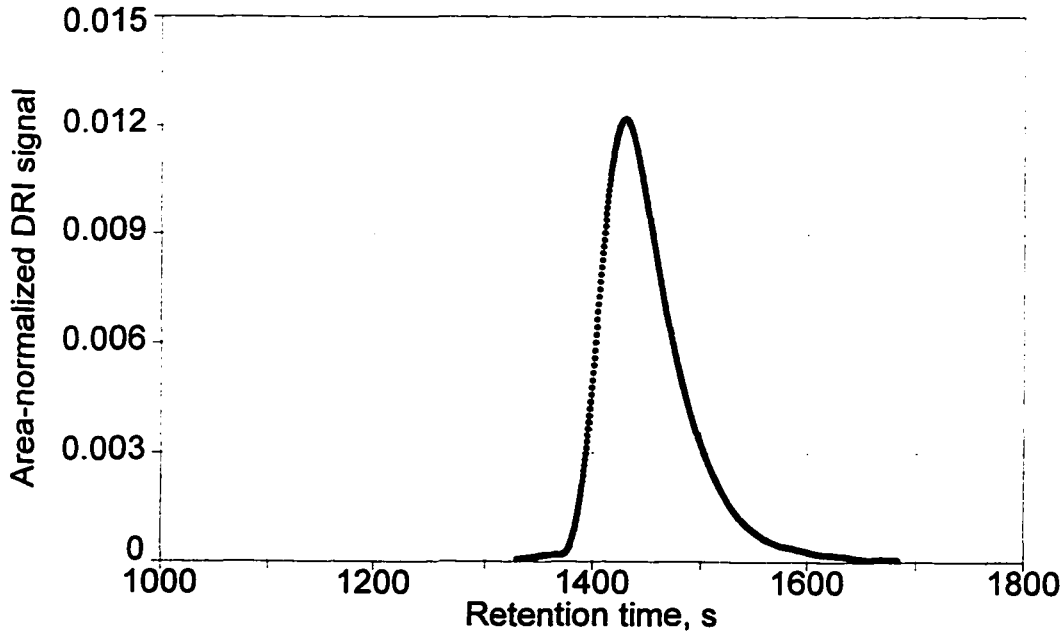


Figure 4-13. Normalized SEC(P) trace for sample B4o (FG15).



In the context of molecular structure - property considerations, the following are the advantages of using M_p , as the measure of the branch length:

a) - not sensitive to subjective assessment of the base-line and peak limits,
b) - not influenced by the effect which the MWD 'tails' might have on the MW average values,
c) - represents the "bulk" of the molecular mass, especially for narrowly polydispersed molecules, and
d) - correlates well with physical property parameters.

The width of the MWD is commonly described by the polydispersity index, PDI, defined as the ratio of the weight-average to the number-average molecular weight, ($\overline{M}_w$ / $\overline{M}_n$). The effect of the PDI on rheological properties can be significant for linear polymers and has been well researched [231-233].

No comparable studies could be found on the effect of polydispersity in comb-type branch homopolymers or graft copolymers. Every effort was made to prepare samples of branch prepolymers with consistent, relatively narrow, polydispersity. For most samples, PDI varies between 1.15 and 1.30 and can be assumed to be have negligible effect on rheology [231]. A few samples with a higher PDI were conditionally included in the portfolio for further studies, on the assumption that they would be scrutinized later for the possible effect of abnormally higher MWD width on studied rheological properties.

Significance for graft structure:

It is assumed that MWD and MWD parameters ($\overline{M}_x$) of the polybutadiene (samples Bxy) accurately represent MWD and $\overline{M}_x$ of branches of the corresponding graft copolymers.

Table 4-3. Molecular weight distribution parameters for Bxy samples (branch prepolymers).

'branch length'		M_n [b]	M_w [b]	M_p [b]	Retention time	M_w [b] / M_n [b]
Sample code	Corresponding graft ID	*SEC(W/DV1)*	*SEC(W/DV1)*	*SEC(P/DRI)*	*SEC(P/DRI)*	*SEC(W/DV1)*
		[g/mol]	[g/mol]	[g/mol]	[min]	[g/mol]
		a	b	c	d	e
B1d	FG1	4,300	4,800	**3,040**	27.9	1.12
B2f	FG2	7,500	10,600	**7,600**	27.7	1.41
B3e	FG3	15,300	17,900	**16,400**	26.9	1.17
B4m	FG4	27,500	31,700	**29,300**	26.3	1.15
B5f	FG5	44,200	53,000	**61,700**	25.3	1.20
B6h	FG6	76,400	85,200	**76,800**	24.8	1.12
B4j	FG7	24,400	28,600	**29,300**	26.4	1.17
B4q	FG8	21,400	25,200	**22,800**	26.4	1.18
B4i	FG9	24,800	32,300	**33,500**	26.1	1.30
B7f	FG10	102,000	130,000	**157,400**	24.0	1.27
B6j	FG11	52,100	61,000	**46,000**	25.2	1.17
B3f	FG12	13,200	15,800	**14,000**	27.0	1.20
B2c	FG13	7,700	10,900	**9,400**	27.5	1.42
B9a	FG14	47,100	54,900	**51,100**	25.3	1.17
B4o	FG15	29,300	48,100	**36,500**	25.8	1.64
B3c	FG16	17,300	22,600	**20,000**	26.5	1.31
B4d	FG17	25,300	34,700	**47,300**	25.6	1.37
B3d	FG18	17,100	23,300	**19,100**	26.5	1.36
B1c	FG19	10,500	12,600	**10,300**	27.4	1.20
B2e	FG20	9,900	11,000	**10,000**	27.5	1.11
B4p	FG21	30,700	36,200	**36,100**	25.6	1.18
B4g	FG22	85,500	110,000	**116,200**	24.2	1.29
B4r	M (blend)	27,500	31,800	29,900	26.0	1.16
B10	—	100,000 /*	140,000 /*	150,000	—	1.40

4.3.3 Microstructure

The microstructure of BR refers to the disposition of the double bonds present in a polymer chain. Three principal types of structures can coexist in polybutadiene: 1,4-cis, 1,4-trans, and 1,2-vinyl. The latter can, in turn, have different tacticities: isotactic, syndiotactic and atactic chain configurations. The microstructural composition (mol% of cis/trans/vinyl) is governed primarily by the type of catalyst system used, but also by synthesis conditions: temperature, solvent, monomer concentration etc. For alkyllithium-initiated polybutadienes, those relations have been well researched [234-235].

The effect of BR microstructure on rheological behaviour has been extensively studied [236-239] and can be particularly pronounced, for large vinyl content variation and for thermo-mechanical properties in the glassy and transition viscoelastic zones. [238-239]. For that reason, the extent to which vinyl content is varying among Bxy samples was examined, to verify that it did not interfere with other correlations between the rheology and polymer structure.

Results of the microstructural composition calculated from the NMR and FT-IR spectra are combined in Table 4-4. At low field (200 MHz) ^{1}H-NMR studies, only 1,2 and 1,4 units can be quantitatively analyzed, because of overlapping of respective resonances. No trends were observed between MW parameters and the vinyl content. This was probably due to a combination of several factors, including limited accuracy of the vinyl content measurements, unavoidable error in $\overline{M}_x$ [1] calculation and relatively weak dependence of the n-BuLi concentration upon vinyl structure content, which in the case of 'living' anionic BR, is also related to MW. Similar studies on BR synthesized under identical conditions showed a small but systematic increase in the vinyl mol% content [235]. A 27-fold increase in n-BuLi

[1] Subscript "x" used in $\overline{M}_x$ can be n, w, z, z+1, etc.

Table 4-4. Microstructure of branch precursor polybutadiene.

Sample code	Corresponding graft ID	NMR Bxy-series, mol%		NMR CG-series, mol%		FTIR Bxy-series, mol%		
		cis/trans	*vinyl*	*cis/trans*	*vinyl*	*cis*	*trans*	*vinyl*
		a	b	c	d	e	f	g
B1d	FG1	-	-	91.7	8.3	-	-	-
B2f	FG2	91.6	8.4	90.3	9.7	-	-	-
B3e	FG3	91.9	8.1	91.5	8.5	-	-	-
B4m	FG4	91.7	8.3	91.7	8.3	-	-	-
B5f	FG5	91.8	8.2	92.1	7.9	-	-	-
B6h	FG6	92.2	7.8	92.0	8.0	-	-	-
B4j	FG7	91.8	8.2	90.6	9.4	-	-	-
B4q	FG8	91.7	8.3	91.3	8.7	-	-	-
B4i	FG9	91.8	8.2	92.1	7.9	-	-	-
B7f	FG10	91.8	8.2	92.2	7.8	-	-	-
B6j	FG11	-	-	92.0	8.0	-	-	-
B3f	FG12	91.5	8.5	92.4	7.6	-	-	-
B2c	FG13	-	-	91.7	8.3	-	-	-
B9a	FG14	92.4	7.6	91.9	8.1	-	-	-
B4o	FG15	-	-	91.4	8.6	35.5	55.4	9.1
B3c	FG16	-	-	92.0	8.0	-	-	-
B4d	FG17	-	-	91.2	8.8	-	-	-
B3d	FG18	-	-	90.0	10.0	-	-	-
B1c	FG19	-	-	92.7	7.3	-	-	-
B2e	FG20	-	-	91.0	9.0	-	-	-
B4p	FG21	-	-	91.6	8.4	34.1	56.5	9.4
B4g	FG22	-	-	91.9	8.1	-	-	-
B4r	M (blend)	-	-	91.0	9.0	-	-	-
B10	-	92.3	7.7	-	-	36.4	54.4	9.2
Average (+/- 2s)		-	**8.1** (0.6)	-	8.4 (1.3)	**35.4**	**54.4**	**9.2**

concentration, comparable with the range of vinyl content variations observed in the series of BRs prepared for this project, increased the vinyl content only from 5.1 mol% to 6.6 mol%.

The average vinyl structure content (mol%) obtained by the NMR and IR methods is, within experimental error, comparable to the results obtained by other researchers working on similar polymeric systems, synthesized using the same catalyst and comparable reaction conditions (Table 4-5).

Significance for graft structure:

It is concluded, based on published results [238-239], that the observed variations of vinyl structure content are negligible from the point of view of their effect on rheological properties, at temperatures well above about -90°C, i.e. the glass transition temperature of polybutadienes having a similar microstructure to that found in samples Bxy.

Similar variability in microstructure was assumed to have a negligible effect on rheology in a similar study concerned with relationship between microstructure of anionically prepared polybutadienes and their linear viscoelastic properties [231]. Many relevant and frequently cited papers tend to ignore the issue of the BR microstructure effect on the rheological properties altogether.

Table 4-5. Microstructure of BR polymerized using n-BuLi catalyst.

FTIR (Br), mol%			Polymerization		Reference
1,4-cis	*1,4-trans*	*1,2-vinyl*	medium	temp.,°C	
38.7	54	7.3	CHX	50	[235]
35	57	8	CHX	30	[83]
36	54	10	—	—	[224]
35	55	10	THF	40	[240]
—	—	8-10	—	—	[85]
43.1	50.1	6.8	CHX	50	[241]
35.4	55.4	9.2	THF	50	this work

4.4 Graft composition and structure

4.4.1 Graft structure - topology

As discussed previously, the structure of the purified graft is predominantly *comb-type*, with linear CIIR backbone and linear BR branches. The following are the main arguments in support of this hypothesis. From the mechanism of "living" anionic polymerization, it is known that BR molecules can be capped by a Li ion on one end only, forming a reactive site for the purpose of an intended grafting reaction with the allylic chlorine ion, located on some of the isoprene units, distributed along the CIIR backbone. Under appropriate conditions, the grafting reaction, attaching a linear branch precursor polymer to a linear backbone precursor polymer is prevailing, leading to a graft copolymer structure of high degree of regularity and essentially free from any "secondary" structures.

4.4.2 Overall chemical composition

Assessment of chemical composition of the polymeric blend or the mixture of graft molecules with linear precursor polymers molecules, can be obtained by estimation of the relative area under deconvoluted SEC/DRI peaks. This procedure requires that relevant peaks are separable with good confidence to allow for an accurate fit of appropriate peak function(s). Additionally, the difference in refractive indices of the component polymers, should be corrected for [242]. Respective values for refractive indices, n_D, for CIIR, n-BuLi BR and THF (SEC carrier) are given in Table 4-6 [243].

Table 4-6. Absolute values of refractive indices.

	CIIR	BR (n-BuLi)	THF
n_D:	1.508	1.516	1.404

In spite of the small difference between refractive indices of CIIR and BR polymers, resulting in only about 2% adjustment to the peak area ratio, the correction was made.

Normalized DRI traces were fitted to a broad spectrum of peak functions used in chromatography, using Jandel's PeakFit™ and TableCurve™ software. The following functions were found to be the best analytical representations for the experimental SEC profiles:

- for sample C: Gamma (4-parameter) Statistical Peak Function,
- for samples Bxy: ADS, (5-parameter Asymmetric Double Sigmoidal Peak Function),
- for (unimodal) samples FG: ADC, (5-parameter Asymmetric Double Cumulative Peak Function).

These functions, with adjustable parameters, were subsequently used for deconvolution of bimodal peaks of CG-samples in order to estimate the A_{hBR}/A_T ratio. A_T is the area under the entire, bi-modal DRI signal and A_{hBR} is the area corresponding to the peak designated as 'BR'. The BR peak - composed primarily of unattached BR molecules - is superimposed on the low MW-tail of the graft MWD. This ratio was used subsequently for calculation of the grafting efficiency, *GE%*. Similarly, FG-samples were analyzed to estimate the unattached BR extraction effectiveness, *PE%*, and the content of the linear BR remaining in a purified graft mixture. Calculations similar to those described elsewhere [244] were used.

Results of those calculations are reported in Table 2-4. Merits of this procedure were examined by using sample M, a blend of sample C and sample B4e. MWD of blend M was deconvoluted into two peaks ("CIIR" and "BR") which were compared to the measured MWD of precursor homopolymers (section 4.4.6 and Figure 4-17).

Graft compositions measured by a combination of the SEC and NMR techniques gave results comparable to nominal stoichiometric proportions (columns "c" and "d" in Table 2-3). However, analytical results were judged to be more reliable and were actually used for subsequent calculations (for example of branching frequency).

The weight fraction of BR in the graft, w^b can be calculated from the molar fraction, m^b using formula:

$$w^b = \frac{1}{1 + (\frac{1}{m^b} - 1) \cdot Y} \tag{4-3a}$$

where: Y = MW(CIIR) / MW(BR) = 1.0425; assuming MW(BR) = 54.1 g/mol and MW(CIIR) ≅ 56.4 g/mol at the actual unsaturation and chlorine level.

The analogous formula for weight fraction of CIIR in the graft, w^B is:

$$w^B = \frac{1}{1 + (\frac{1}{m^B} - 1) \cdot (1 / Y)} \tag{4-3b}$$

Calculation of the grafting efficiency

Grafting efficiency can be determined from SEC/DRI traces if the peak corresponding to ungrafted BR can be confidently separated (and its relative area, A_{hBR} measured), by knowing the composition of CIIR in a crude graft (CG), as measured by NMR.

Assuming that the total area under the normalized DRI peak, A_T, can be represented as,

$$A_T = A_{CIIR} + A_{gBR} + A_{hBR} \tag{4-4}$$

where:

$$A_{CIIR} = w^{B} \cdot \Delta n_{(CIIR)} \cdot K, \quad (4\text{-}5a)$$

$$A_{gBR} = w^{b,g} \cdot \Delta n_{(BR)} \cdot K, \quad (4\text{-}5b)$$

$$A_{hBR} = w^{b,h} \cdot \Delta n_{(BR)} \cdot K \quad (4\text{-}5c)$$

A - denotes the area under the peak, w - is the weight-fraction, K is a certain proportionality factor, and Δn - is the difference of refractive indices, defined as:

$$\Delta n_{(CIIR)} = n_D(CIIR) - n_D(THF) \quad \text{and} \quad \Delta n_{(BR)} = n_D(BR) - n_D(THF)$$

By definition, $w^{B} + w^{b,g} + w^{b,h} = 1$, and for refractive index values (Table 4-6), (4-6)

$$X = \Delta n_{(CIIR)} / \Delta n_{(BR)} = 1.021 \quad (4\text{-}7)$$

From the equation defining the grafting efficiency (2-2), substituting area under the DRI signal curve for weight fraction,

$$GE\% = \frac{A_{gBR}}{A_{hBR} + A_{gBR}} \cdot 100\% \quad (4\text{-}8a)$$

Substituting for A_{gBR} from equation (4-4),

$$GE\% = \frac{A_T - A_{CIIR} - A_{hBR}}{A_T - A_{CIIR}} \cdot 100\% \quad (4\text{-}8b)$$

By substituting equations (4-5a, b, c, 4-6 and 4-7) in equation (4-8b) and following simple transformations, another form of equation (2-2) more convenient for calculation of the grafting frequency directly from experimentally accessible data, can be obtained:

$$GE\% = \frac{1 - w^{B} - [1 + (X - 1)w^{B}](A_{hBR} / A_T)}{1 - w^{B}} \cdot 100\% \quad (4\text{-}9)$$

Results of calculations using the above equation, can be found in Table 2-4.
Compilation of data on chemical composition of samples can be found in Table 4-7.

4.4.3 Molecular weight distribution

The correct shape of the MWD cannot be readily determined for graft copolymers by the GPC equipped with a single, concentration-sensitive detector (like DRI) for the following reasons [245]:

a/ The non-linear (branched) chain configuration of the graft copolymers affects the standard elution volume - MW calibration curve, due to the fact that linear and branched molecules eluting at the same time would have different molecular masses,

b/ The DRI detector responds differently to the backbone chains (CIIR) and branch chains (BR), in proportion to the difference in their refractive indices,

c/ In the general case, the possibility of interchain phase separation in the eluting solution cannot be excluded. If significant, it could disturb the behaviour of the graft copolymer solution and interfere with the separation process [246].

Because of these reservations, the molecular weight distributions of graft samples (FG, CG) reproduced in Appendix III, are labelled as 'apparent' MWD distributions. They were primarily used for estimation of grafting reaction efficiency and effectiveness of graft purification.

Table 4-7. Chemical composition of graft copolymers.

Sample code	BR fraction of the graft				BR content	
	Crude grafts (CG)		Purified grafts (FG)		Grafted	Ungrafted
	molar, m	weight, w	molar, m^b	weight, w^b	$w^{b,g}$, %	$w^{b,h}$, %
	a	b	c	d	e	f
FG1	0.050	0.048	0.047	0.045	4.4	0.1
FG2	0.103	0.099	0.087	0.084	8.1	0.3
FG3	0.177	0.171	0.158	0.153	14.9	0.3
FG4	0.313	0.304	0.282	0.274	27.1	0.3
FG5	0.481	0.471	0.434	0.424	36.7	5.7
FG6	0.549	0.539	0.522	0.512	39.4	11.7
FG7	0.106	0.102	0.054	0.052	4.9	0.3
FG8	0.229	0.222	0.199	0.192	18.9	0.3
FG9	0.480	0.470	0.392	0.382	36.4	1.8
FG10	0.514	0.504	0.502	0.492	33.1	16.1
FG11	0.439	0.429	0.407	0.397	36.3	3.4
FG12	0.445	0.435	0.415	0.405	37.3	3.2
FG13	0.469	0.459	0.418	0.408	35.3	5.5
FG14	0.519	0.509	0.426	0.416	34.0	7.6
FG15	0.362	0.352	0.329	0.320	31.7	0.3
FG16	0.462	0.452	0.353	0.344	29.8	4.6
FG17	0.296	0.287	0.227	0.220	21.7	0.3
FG18	0.180	0.174	0.067	0.064	6.2	0.2
FG19	0.044	0.042	0.030	0.029	2.7	0.2
FG20	0.456	0.446	0.427	0.417	40.4	1.3
FG21	0.451	0.441	0.404	0.394	39.2	0.2
FG22	0.456	0.446	0.439	0.429	26.9	16.0
	NMR	recalc. (4-3a)	NMR	recalc. (4-3a)	calc.(2-2) /*	calc.(4-6)
C	0.000	0.000	*All molar compositions derived from NMR data*			
M	0.300	0.291				
B10	1.000	1.000	*/ Calculated from GE% based on FG composition*			

The statistical moments and other parameters of the MWD of grafts are compiled in Table 4-8, and should be regarded as approximations, because of the above qualifications.They are supplemented by $\overline{M}_n$ and $\overline{M}_w$, calculated for grafts from the molecular weight averages, measured on corresponding parent polymers. Equations used for these calculations are referenced at the bottom of Table 4-8.

A well defined, albeit non-linear, correlation was found between GPC retention time of the grafts and average length of the branch and is shown in Figure 4-14.

It has been observed that addition of branches (of different number and length) to a chemically different backbone, which has the same MWD for all samples, *increases* the size of the graft molecule (its hydrodynamic volume) as indicated by decreasing retention times. The increase in size of the graft molecule appears to depend primarily on branch length, and to be almost independent of the number of branches.

The number-average molecular mass of the graft, $\overline{M}_n^G$, can be calculated, for example, using equation (3-6) from the molecular mass of a backbone, $\overline{M}_n^B$ and the chemical composition of the graft; i.e., the weight content of a branch polymer actually grafted to the backbone, $w^{b,g}$, which is available from analysis of the combined SEC and NMR data.

Similarly, for weight-average molecular mass of the graft the following equation has been suggested [96, 247-248],

$$\overline{M}_w^G = \overline{M}_w^B / w^B + w^{b,g} \cdot \overline{M}_w^b \qquad (4\text{-}10)$$

Table 4-8. Parameters of the molecular weight distribution of graft copolymers.

	Branch	Graft / measured / SEC(W/DV)			Graft / calculated	
Graft ID	M_p^b	Peak retention time		M_z^G	M_n^G /1	M_w^G /2
	[g/mol]	[s]	shift, [s] /*	[g/mol]	[g/mol]	[g/mol]
	a	b	c	d	e	f
FG1	3,040	1,645	25	1,163,000	148,000	471,000
FG2	7,600	1,561	109	1,348,000	154,000	493,000
FG3	16,400	1,505	165	1,428,000	165,000	529,000
FG4	29,300	1,447	223	2,165,000	193,000	624,000
FG5	61,700	1,393	277	1,917,000	211,000	692,000
FG6	76,800	1,373	297	2,590,000	227,000	756,000
FG7	29,300	1,449	221	1,319,000	146,000	466,000
FG8	22,800	1,460	210	1,279,000	175,000	564,000
FG9	33,500	1,437	233	1,677,000	204,000	661,000
FG10	157,400	1,310	360	2,565,000	151,000	491,000
FG11	46,000	1,393	277	2,297,000	195,000	640,000
FG12	14,000	1,516	154	1,774,000	209,000	673,000
FG13	9,400	1,528	142	1,927,000	215,000	691,000
FG14	51,100	1,399	271	1,721,000	213,000	699,000
FG15	36,500	1,436	234	1,821,000	199,000	648,000
FG16	20,000	1,475	195	1,712,000	187,000	602,000
FG17	47,300	1,420	250	1,627,000	170,000	547,000
FG18	19,100	1,491	179	1,304,000	149,000	478,000
FG19	10,300	1,535	135	1,213,000	144,000	459,000
FG20	10,000	1,541	129	1,994,000	229,000	734,000
FG21	36,100	1,426	244	2,323,000	219,000	711,000
FG22	116,200	1,331	339	1,775,000	156,000	509,000
C	—	1,670	0	1,080,000	182,000 /**	397,000 /**
M	29900	—	—	710,000	64,000 /3	328,000 /4

/* - backbone polymer (CIIR) as reference

/** - actually measured/SEC(W/DV) (e.g. not calculated) values

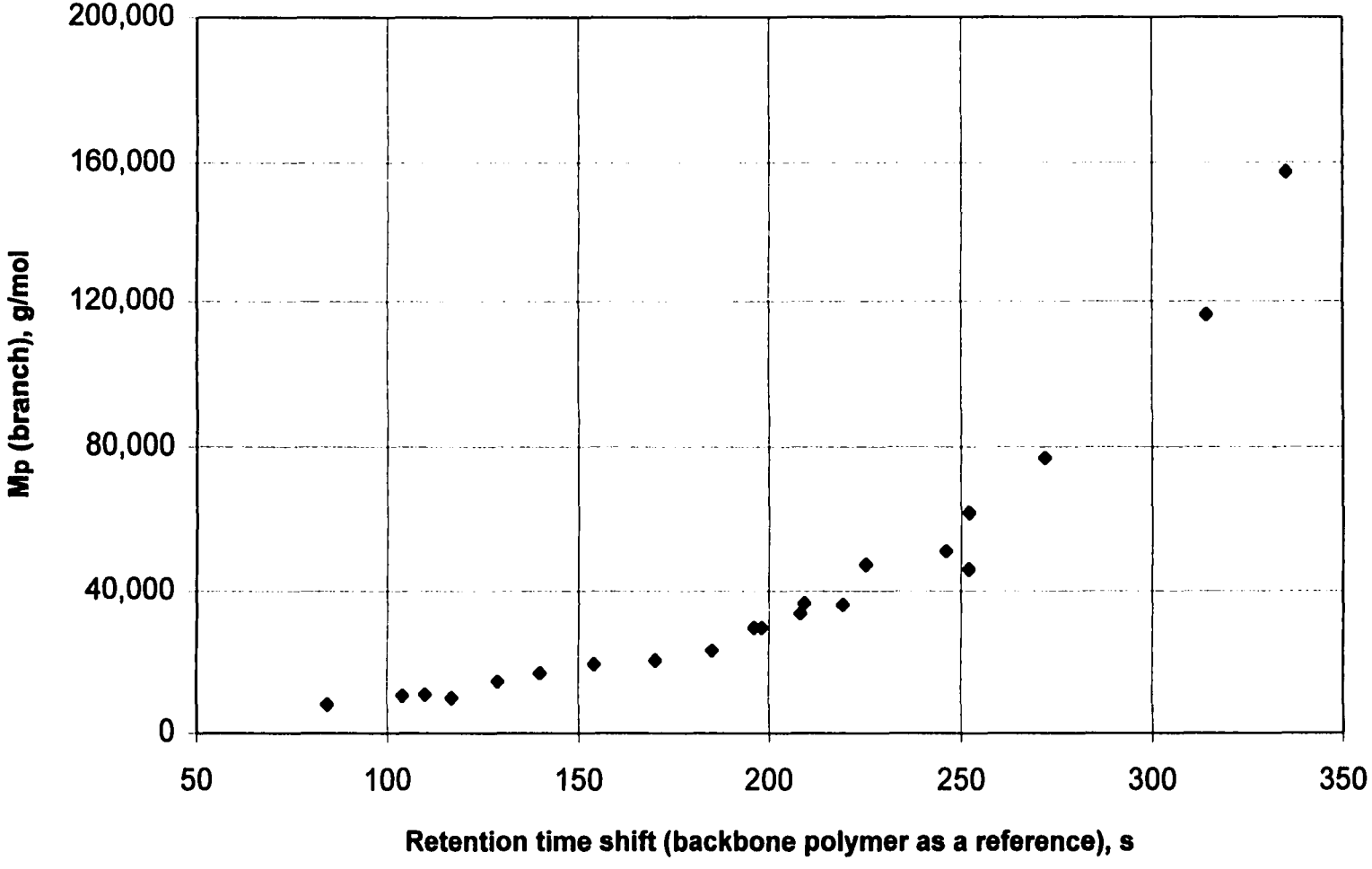
/1 - calculated according to (3-6)

/2 - calculated according to (4-10)

/3 - calculated according to (4-11)

/4 - calculated according to (4-12)

Figure 4-15. Correlation between branch length and SEC retention time shift.



For pure blends of parent polymers (sample M) the following equations were used to calculate molecular weight averages [249]:

$$\overline{M}_n(blend) = 1 / (\sum_i \frac{w_i}{(\overline{M}_n)_i}) \tag{4-11}$$

$$\overline{M}_w(blend) = \sum_i w_i \cdot (\overline{M}_w)_i \tag{4-12}$$

4.4.4 Branching number

The branching number, N_g, defined as the number-average number of branches per backbone molecule, was determined stoichiometrically by combining information from SEC results on the backbone and branch precursor polymers and NMR regarding the chemical composition of the graft. Unless direct experimental measurement of molecular weight of the graft is available, the above approach is the simplest and most reliable method to estimate branching in graft copolymers (heterogeneous systems!). An attempt to estimate branching number/frequency directly from NMR was unsuccessful, due to the large error involved in integration of relevant peaks of very low intensity.

The following assumptions were made:

1. Molecular weights of the backbone ($\overline{M}_x^B$) and branches ($\overline{M}_x^b$) are identical to those of preformed, precursor polymers e.g. non-preferential grafting (with respect to MW) is assumed,
2. No backbone chain scission occurs during the grafting reaction,
3. Both random grafting and random coupling assumptions are valid (section 4.4.9).

Figure 4-15 presents an algorithm used to calculate branching number, N_g, using equation (3-7). The following modification of equation (3-7) has been also employed for calculation of the branching number, N_g^p, based on a peak molecular weight, M_p^b,

$$N_g^p = \frac{\overline{M}_w^B \cdot w^{b,g}}{M_p^b \cdot (1 - w^{b,g})} \qquad (4\text{-}13)$$

where $\overline{M}_n^b$ has been replaced by M_p^b and $\overline{M}_n^B$ by $\overline{M}_w^B$.

Values of the branching numbers (N_g and N_g^p) calculated according to equations (3-7) and (4-13), respectively, are compared in Table 4-9. Branching number based on M_p is, on the average, higher than N_g by a factor of 2.3 but very good correlation betweem them is demonstrated in Figure 4-16. The average standard error for the N_g and N_g^p at 95% conf. level was 0.2.

Figure 4-15. Algorithm used for calculation of the branching number.

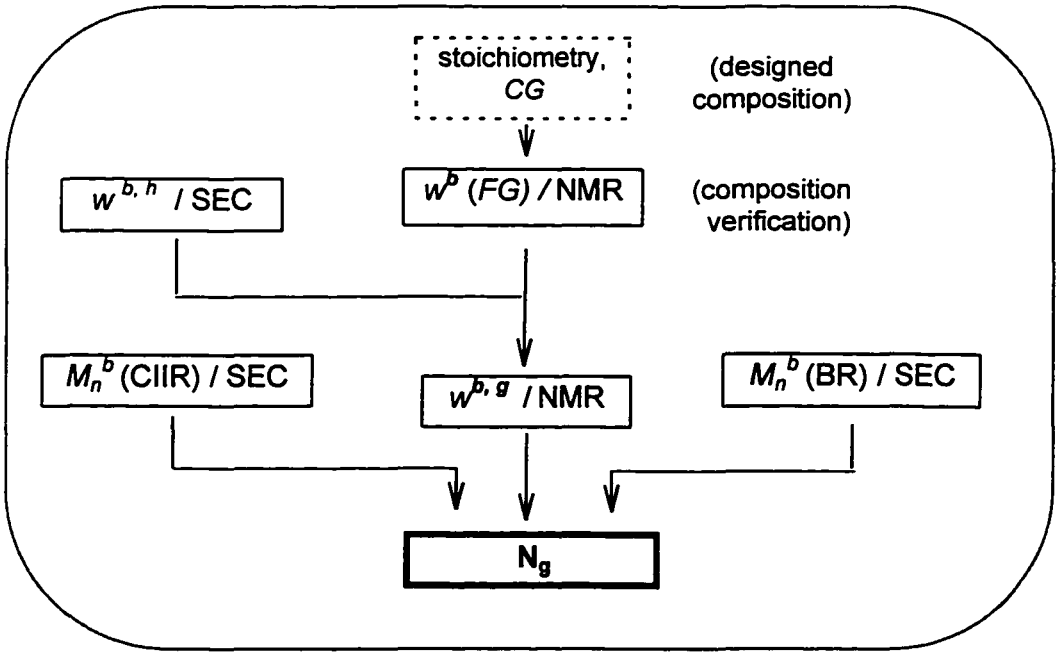
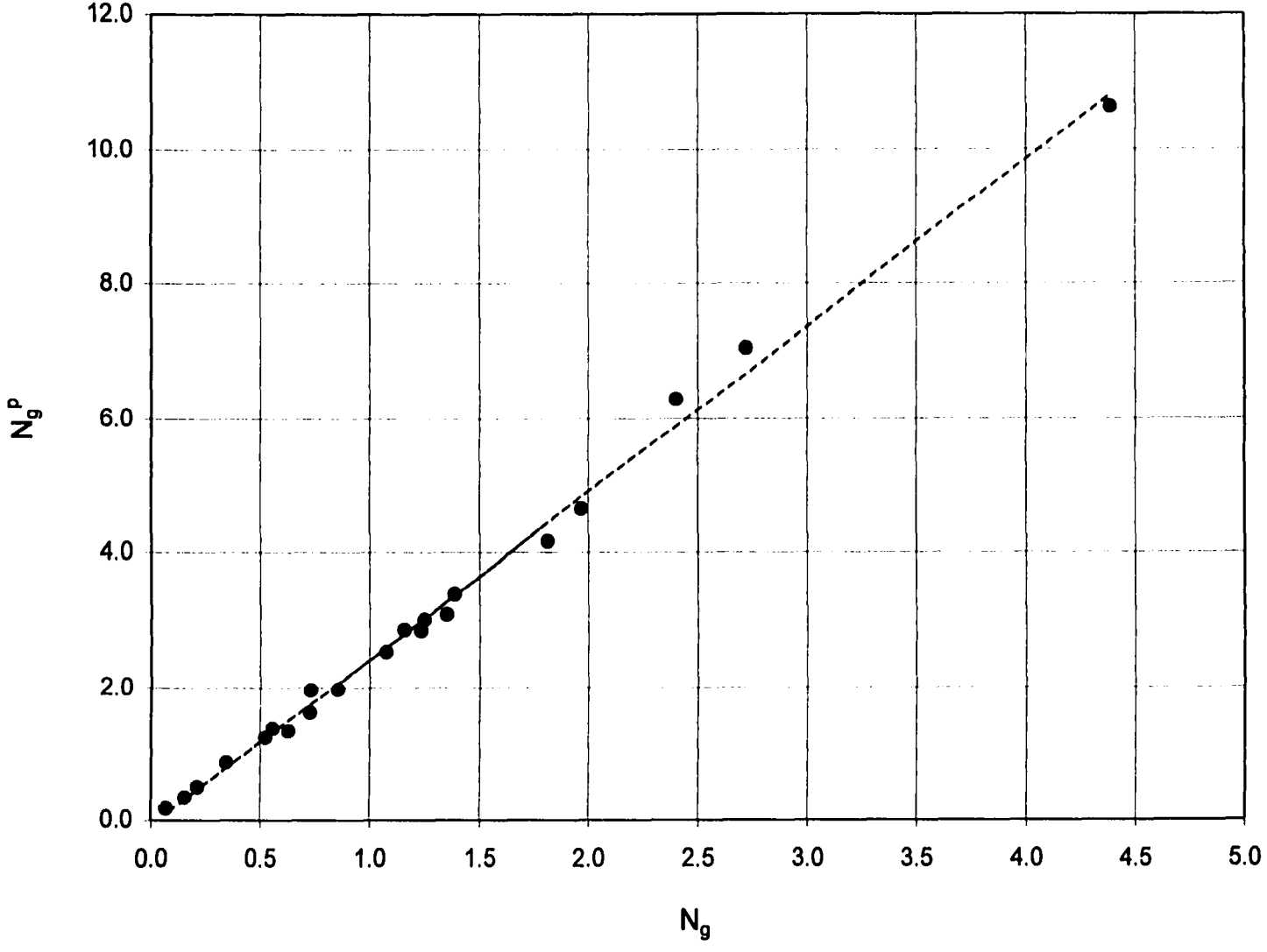


Table 4-9. Branching numbers.

Graft ID	BRANCHING NUMBERS				
	N_g (P/DRI)	N_g (avg)	N_g (W/DV)	N_g^p	N_g^w (W/DV)
	a	b	c	d	e
FG1	2.4	**2.2**	1.8	**6.3**	**3.5**
FG2	1.9	**1.8**	1.8	**4.5**	**2.8**
FG3	1.4	**1.5**	1.5	**3.5**	**2.8**
FG4	1.3	**1.3**	1.3	**3.1**	**2.5**
FG5	0.8	**0.8**	1.0	**1.7**	**1.7**
FG6	0.6	**0.6**	0.6	**1.4**	**1.1**
FG7	0.3	**0.3**	0.3	**0.7**	**0.6**
FG8	1.3	**1.3**	1.3	**3.1**	**2.4**
FG9	1.3	**1.4**	1.7	**3.2**	**2.8**
FG10	0.2	**0.3**	0.4	**0.6**	**0.7**
FG11	0.8	**0.8**	0.8	**2.3**	**1.5**
FG12	2.9	**3.1**	3.2	**7.6**	**5.9**
FG13	5.8	**5.6**	5.4	**11.1**	**8.3**
FG14	0.9	**0.8**	0.9	**2.0**	**1.6**
FG15	1.1	**1.2**	1.3	**2.7**	**1.8**
FG16	2.0	**2.1**	2.2	**4.8**	**3.7**
FG17	0.8	**0.9**	1.2	**1.6**	**1.9**
FG18	0.6	**0.6**	0.6	**1.4**	**1.0**
FG19	0.5	**0.5**	0.5	**1.2**	**0.8**
FG20	4.5	**4.5**	4.4	**11.0**	**8.7**
FG21	1.3	**1.3**	1.4	**3.0**	**2.6**
FG22	0.3	**0.4**	0.4	**0.8**	**0.7**
	eq. (3-7)	avg. /*	eq. (3-7)	eq. (4-13)	modif. eq. (4-13)
(a) & (c) - $N_g = (M_n^b, M_n^B)$, (d) - $N_g^p = (M_p^b, M_w^B)$, (e) - $N_g^w = (M_w^b, M_w^B)$					(M_p^b => M_w^b)
/* - average value, calculation based on sets of M_n^b & M_n^B obtained by three SEC methods; P/DRI, W/DRI & W/DVa					2·s (95%) = 0.2

Figure 4-16. Correlation between N_g and N_g^p branching numbers.



4.4.5 Content of ungrafted prepolymers

As discussed in chapter 2, for most graft architectures, the grafting reaction was less than 100% efficient. In addition, the effectiveness of the fractionation process, designed to remove ungrafted branch polymer was also limited (Table 2-4). This resulted in a dilution of the graft system by precursor polymer molecules to an extent depending on the molecular weight and, to a lesser extent, the stoichiometry of the grafting reaction.

Comparison of the MWD of unpurified and purified grafts can be found in Appendix III.

Table 4-7 in column "f" contains the content (wt%) of the ungrafted, linear polybutadiene. For some graft samples, the content of linear polymer is significant enough to influence its rheological behaviour [23, 99, 250-253]. Therefore, structure-property relations derived from results on samples with appreciable amount of unattached BR will be appropriately qualified. It is not easy to account for those effects quantitatively, as there is only one sample with a given set of branching parameters *and* specific content of the diluant BR, in order to allow for any extrapolations of graft rheological response to that of identical structure but free of linear molecules [254].

Comparison of peak molecular weight corresponding to the "BR" peak on crude graft (CG) SEC chromatogram with that of precursor polymer, as well as comparing $\overline{M}_n$ of precursor polymers with that of HG (extracted polybutadiene) samples (Table 4-10), suggest that an essentially non-selective grafting reaction (with respect to the branch polymer MW) is taking place. This experimental finding supports the first assumption made in the previous section (4.4.4).

Table 4-10. Comparison of molecular weight of branch precursor polymer, before and after grafting.

	M_n (Bxy)	M_n (HG)
G2	8,400	9,400
G3	12,600	16,400
G4	22,300	24,100
G7	20,400	21,900
G17	32,400	30,200
G18	14,200	15,000
G19	7,600	10,100

4.4.6 Molecular characteristics of CIIR/BR blend

The reference CIIR/BR blend (sample M) was obtained by blending in solution two precursor polymers: the backbone CIIR polymer (component A) with *deactivated* BR (component B). Procedures and all reaction conditions were the same as used for graft preparation.

The primary reason to include the CIIR/BR blend in this study, was to contrast its rheological behaviour with its graft copolymer equivalent, at constant chemical composition. The secondary reason was to verify the effectiveness of the extraction process. The latter issue was discussed in section 2.4.

Table 4-11 compares the composition and some molecular parameters of the blend with those of its closest graft equivalent in terms of composition and molecular structure.

Table 4-11. Compositional and molecular parameters of CIIR/BR blend - sample M and graft G4.

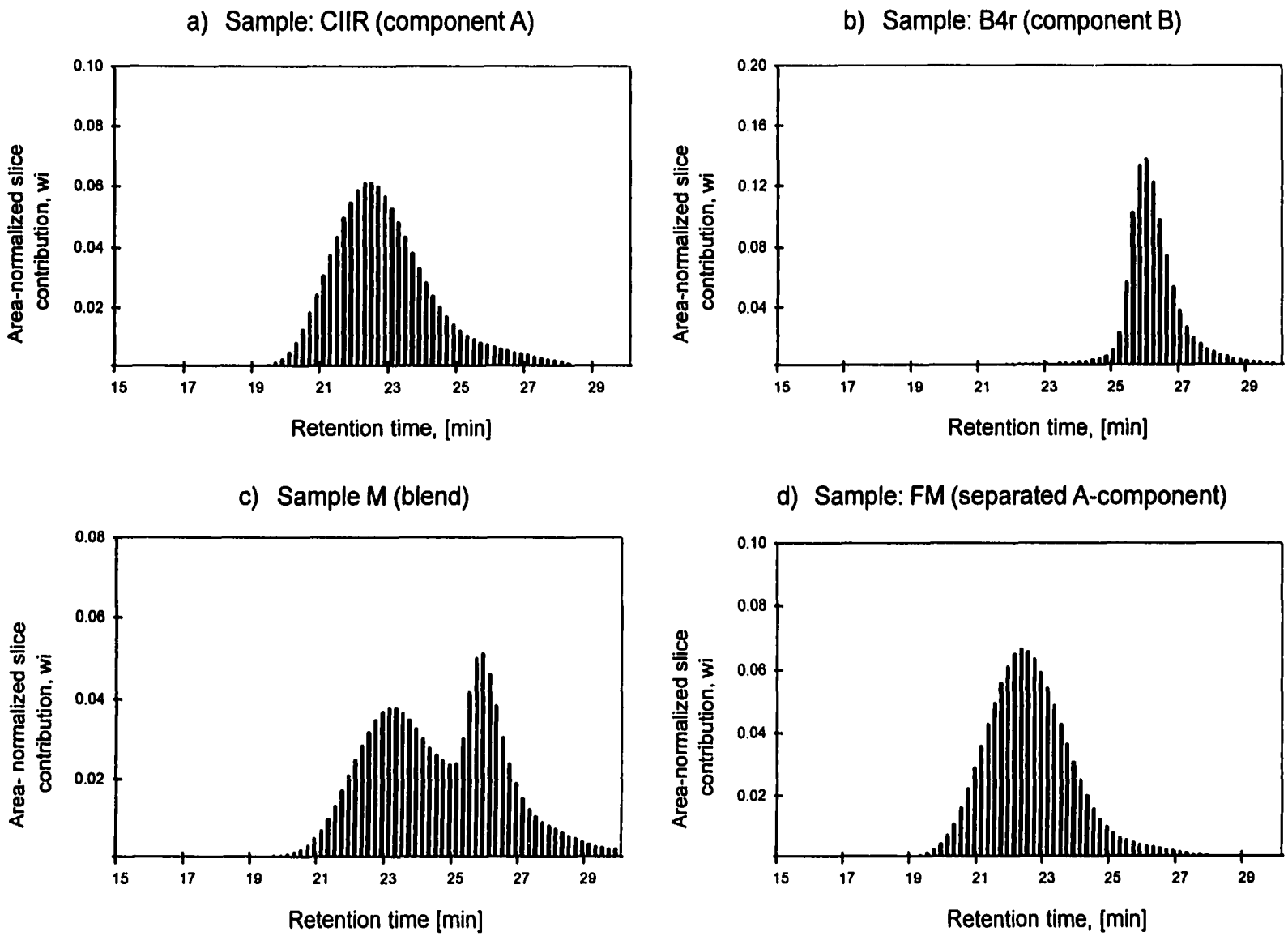
Sample:	M	G4
Polymer type:	blend (A/B)	graft (A-g-B)
MWD modality:	bimodal	unimodal
Chemical composition; BR(wt%):	29.1%	27.4%
Graft's backbone = blend's component A:	CIIR (identical structure and MWD)	
Graft's branch = blend's component B:	anionic n-BuLi initiated BR	
— chemical structure (cis+trans/vinyl):	91.0 / 9.0%	91.7 / 8.3%
— peak molecular weight, Mp:	29,900	29,300

The MWD of the CIIR - component A of the blend (identical to sample C) is shown in Figure 4-17a together with the MWD of the component B in Figure 4-17b. These MWDs are contrasted with chromatograms of the blend M (Figure 4-17c) and that of component A (Figure 4-17d) recovered from the blend by a process identical to the selective solvent extraction used for graft purification. From the similarity of these distributions the lack of backbone degradation or scission can be deduced.

4.4.7 Content of residual solvent and non-polymeric substances

Consistent with the strategy outlined in section 3.4.6, two experiments were carried out using TGA. In the first experiment, a known amount of sample C was heated in the TGA at 125°C in air for 2 hours and then submitted for GPC analysis. Results of this analysis were

Figure 4-17. Molecular weight distribution (SEC/P) - Sample M and its components.



compared with the MWD obtained on virgin material. Neither sample weight loss nor difference in the shape of the MWD curve was detected, as reflected in the MWD parameters shown in Table 4-12.

Table 4-12. TGA examination of short-term thermal stability.

Sample C	virgin sample	heated for 2 hrs @125°C
$\overline{M}_n$	120,800	119,000
$\overline{M}_w$	460,000	447,000
$\overline{M}_z$	1,000,000	1,000,000

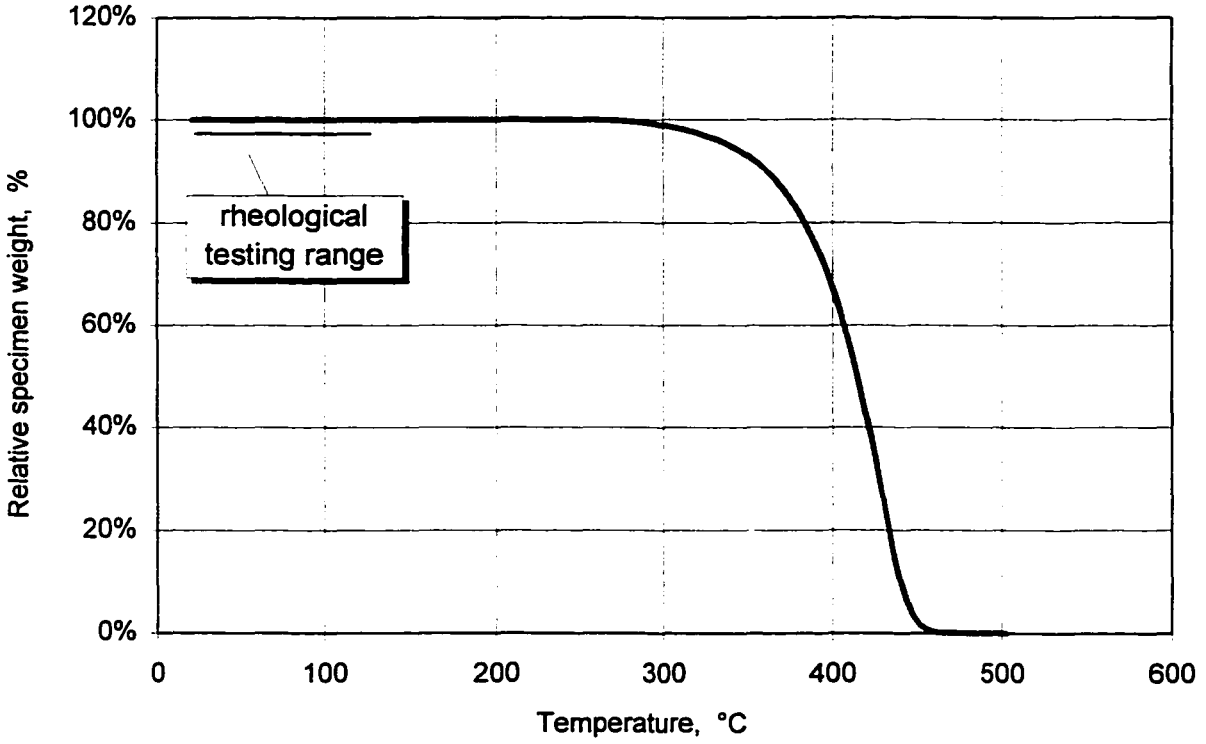
It can be concluded that 125°C is suitable as the upper temperature limit for rheological characterization. This will be further confirmed by appropriate rheological experiments (section 5.2.4.1).

The second experiment involving TGA was carried out in order to assess the content of low MW fluids (residual amounts of solvent and moisture) in a sample. Even small amounts of low MW liquids (frequently volatile at higher temperatures) can substantially alter the rheological response of the polymer. Sample C was selected again, because, being based on butyl rubber, it has extremely low permeability to fluids. Therefore, it is the most likely of all the samples to retain residual solvent or moisture in the body of the sample. A TGA scan between room temperature and 220°C confirmed that no measurable loss of weight occurred, which indicated that there was no release of evaporable liquids from the body of the specimen.

It is evident from the TGA scan (Figure 4-18), that degradation of the sample starts at about 220°C (in vacuum) and becomes quite rapid (in terms of weight loss/°C) above about 290°C

during subsequent heating. From the TGA tests, it can be concluded that the thermal degradation of sample is not an issue at the temperatures used in this study and no detectable amount of solvent nor volatile material can be detected. The amount of non-organic residues was estimated to be about 0.3 wt.%, as indicated by the weight of sample residue at 450°C.

Figure 4-18. TGA scan - sample C.



4.4.8 Gel content

Gel is defined as "chemically connected groups of molecules which possess properties 'significantly different' from those of simple branched structures" [255]. This term relates to a wide variety of frequently complex, 3-dimensional or network structures. The effect of gel on the rheological properties and processing behaviour of elastomers can be significant [256-261].

The potential for macro-gel formation is intrinsic to most rubbers, since unsaturation is built into their structure to facilitate vulcanization. For example, gel can be formed as a result of excessive branching during polymerization or later on in storage or processing, and by various cross-linking reactions [262]. For example, emulsion polymerization almost always produces elastomers with micro-gel of content and particle size which depends on the reaction conditions [263]. Neither regular butyl rubber nor living anionically polymerized polybutadiene, which are both made by solution-based processes, are prone to produce any substantial amount of gel, of any form, provided that the polymerization is properly carried out [82-83, 85, 89].

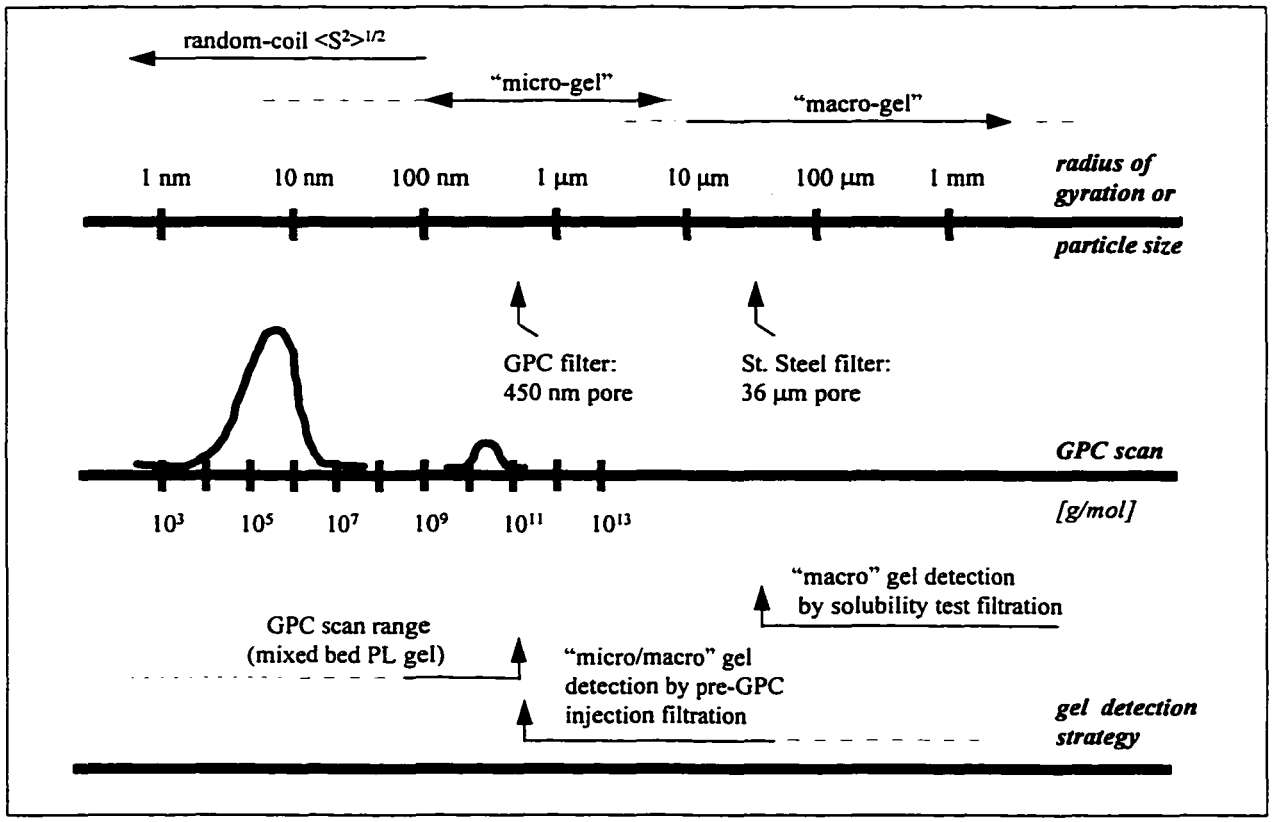
However, due to its serious implications, special attention to the possibility of gel formation during various stages of sample handling is warranted, particularly during mechanical/rheological testing at higher temperatures and high shear rates which introduce the possibility of generating high local thermal gradients, which may accelerate adventitious reactions in otherwise stable material.

A number of methods have been developed to detect and qualitatively characterize various forms of gel in elastomers and plastics [106, 264]. For this work, the strategy adopted for gel screening is similar to that used by other researchers, i.e. [260]. It combines the standard methods of filtration with SEC to screen for a wide size range of gel particules which could form. A standard solubility test method [202], similar to the ASTM D3616-88 Standard Test Procedure, used for characterization of partially cross-linked butyl rubber was adopted.

Application of SEC for the purpose of characterizing micro-gel (particles of the order of 0.5 μm or smaller) is well established [255, 265-267]. It conveniently supplements the filtration method, whose sensitivity depends upon filter size and filtration procedure. Quantitative assessment of solubility by filtration tends to over-estimate the insoluble portion of the

solution due to inclusion of nominally soluble polymer, trapped in the filter for a variety of reasons. Figure 4-19 shows the strategy used for gel detection.

Figure 4-19. Gel content detection.



Based on combined results of :

a) filtration prior to solution injection into the SEC system,

b) solubility tests on samples at various stages of the project, before, during and after rheological experiments, as indicated in Figure 3-1, and,

c) examination of the SEC (DRI & DV) spectra,

it can be confidently concluded that no measurable amount of macro-gel was detected.

4.4.9 Random grafting and random coupling assumptions

In the *random grafting* assumption, all segments of the backbone chain have equal probability of bearing a graft (branch). Random grafting is a common assumption in theoretical derivation of branching parameters from the kinetics of free-radical reactions [247] or purely from the statistics of (random) graft copolymerization [245]. The random grafting hypothesis was one of the assumptions used for derivation of the equations for branching number (3-7 and 4-13). Random allocation of branch points along the backbone molecule and assumption of non-preferential grafting (equal probability of each branch site to accept one active branch molecule regardless of its position along the backbone) implies a random grafting assumption for graft samples prepared for this study.

The *random coupling* assumption assumes that the molecular weight of individual branches in a graft are uncorrelated [268] or, in other words, that each branch molecule has equal chance to graft regardless of its length (MW). Applicability of this hypothesis to copolymers obtained by grafting-onto reaction of pre-formed branch molecules can depend on the molecular weight of the precursor branches mainly for physical reasons (decreasing mobility of molecules in solution with an increasing MW). However, comparison of the molecular weight distribution parameters of Bxy polymers with corresponding samples HG, recovered from the graft mixture CG, indicates only small differences and these could be explained otherwise (cf. section 4.4.5).

This suggests that random coupling statistics is a valid approximation for the copolymer under study. An important implication is that the information about MWD/MW of branches can be reliably based on that from the aliquot obtained from the precursor branch polymer, sample Bxy, collected immediately before the grafting reaction.

4.5 Special issue: graft morphology and microphase separation

Microphase separation may exist in many forms (block, star-block, graft) of copolymers. The A and B blocks of the copolymers tend to separate, forming A- and B-rich regions in order to reduce the number of energetically unfavorable contacts between these blocks.

Graft copolymers are polymeric systems with a multi-phase morphology, prevailing over a broad range of temperatures and chemical composition of the graft. However, in graft copolymers, by contrast with uncompatibilized polymer blends, the phases are joined by covalent bonds, resulting in a limited range of composition-sensitive phase and morphological behaviour. The constraint imposed by the covalent junction of the A and B blocks implies that the A- and B-rich regions remain usually microscopic in size. As a result, structural parameters of the copolymers (MW) may, at least partially, control the microphase morphology [269].

More specifically, phase separation in graft copolymers depends on the length of the individual polymer sequences. Either of the two polymers can form the continuous or matrix phase. Whether a particular phase is continuous or separate (or co-continuous), as well as the details of its morphology, depends on the chemical composition, melting temperature of phases, their density, surface tension and the method/conditions used to obtain the final morphology.

Extensive studies of binary polymeric mixtures demonstrated the importance of the solvent used in preparation of solid experimental samples in respect of morphology [270]. Specifically, for a series of samples solidified from common-solvent solution under the conditions promoting formation of the 'thermodynamic equilibrium morphology' can be achieved [271]. This makes rheological properties dependent on the structure of the graft, e.g. for regular combs, on the number and length of branches.

Indeed, in this project the conditions of sample and specimen preparation were designed to promote achievement of thermodynamic equilibrium by casting thin layers of solvent, using a lower rate of solvent evaporation, long annealing times, lack of post-casting mechanical forming or moulding, etc. (cf. section 2.6 in chapter 2 and sections 5.2.2, 5.3.2, 5.4.2 and 5.5.2 in chapter 5, for further details).

Morphology and microphase separation were not intended to be subject of detailed analysis. Rather, these issues were investigated primarily from the point of view of implications they might have on the structure-property correlations under study. This section is focusing on the *qualitative* determination of what type of morphology (one, two or possibly more phases) has been formed in solid samples, depending on composition and details of the LCB structure of the graft.

The following experimental program was used to probe the phase morphology of the grafts:

1. TEM (transmission electron microscopy) for direct observation of phase separation,
2. DSC (differential scanning calorimetry) over a broad range of temperatures to record endothermic shifts, indicative of glass transition specific to each phase,
3. DTMA (dynamic thermo-mechanical analysis) to monitor tan δ and E″ peaks on a dynamic mechanical spectrum,
4. SEC (size exclusion chromatography) to assess the potential for multi-phase morphology resulting from the presence of unattached BR.

The observations are summarized in Table 4-13. Information obtained by the third technique is discussed more extensively in chapter 8, concerned with the effects of branching structure and chemical composition on the glass transition temperature, T_g.

Table 4-13. Evidence of phase morphology in CIIR-g-BR copolymers.

Graft ID	BR content		TEM	DTMA	DSC	SEC
	w^b, %	$w^{b,h}$, %	two phases	tan δ peaks	endo shifts	DRI peaks
	a	b	c	d	e	f
FG1	4.5	0.1	2	1	1	1
FG2	8.4	0.3	2	1	1	1
FG3	15.3	0.3	— /*	1	1	1
FG4	27.4	0.3	2	(2)	2	1
FG5	42.4	5.7	2	2	2	2
FG6	51.2	11.7	— /*	2	2	2
FG7	5.2	0.3	— /*	1	1	1
FG8	19.2	0.3	— /*	(2)	2	1
FG9	38.2	1.8	— /*	2	2	(2)
FG10	49.2	16.1	— /*	2	2	2
FG11	39.7	3.4	— /*	2	2	(2)
FG12	40.5	3.2	— /*	2	2	(2)
FG13	40.8	5.5	2	2	2	(2)
FG14	41.6	7.6	— /*	2	2	(2)
FG15	32.0	0.3	— /*	(2)	2	1
FG16	34.4	4.6	— /*	2	2	(2)
FG17	22.0	0.3	— /*	(2)	2	1
FG18	6.4	0.2	2	1	1	1
FG19	2.9	0.2	2	1	1	1
FG20	41.7	1.3	— /*	2	2	(2)
FG21	39.4	0.2	— /*	2	2	1
FG22	42.9	16.0	— /*	2	2	2
M	29.1	29.1	— /*	2	2	2

- qualification marked '(...)' in columns "d" and "f" indicates a barely discernible peak

* - no microphotograph available

TEM

Micrographs were obtained for a few samples only and examples are reproduced in Figure 4-20 for graft FG18, in Figure 4-21 for FG5, in Figure 4-22 for FG-19 and in Figure 4-23 for FG1. Despite the poor quality of the micrographs, two distinct phases are clearly visible for *all* screened samples, including those (like FG1 or FG19) in which phase separation is not detected by any other method. Darker spots correspond to the stained BR, dispersed at lower BR content in a continuous CIIR matrix. At least qualitative agreement between chemical composition and the ratio of darker to lighter domains could be observed. However, no quantitative correlation between the domain size from TEM micrographs and branching parameters was attempted.

Analogous observations and conclusions were made for similar graft copolymers of SBR-g-PIB [244] and PS-g-BR [272]. In a follow-up to the first study, Kennedy and coworkers demonstrated, using the same technique, the existence of two distinct phases for SBR content varying in the 17 to 54 wt% range, [273]. Additionally, they attempted to relate size of the domain to branch molecular weight. In another study [274], micro-phase separation was observed for the PS-g-PIB (22-26 wt% PIB) system, with domains of a somewhat diffuse nature (as compared to compositionally equivalent block copolymers). The effect was attributed to the packing difficulties for grafts with random branching spacing along the backbone. By comparison, studies on a well mixed and cured, 70/30 BR/CIIR blend, showed clear evidence of well-defined morphological heterogeneity [275].

DSC

Two-phase morphology of a 2-component mixture of immiscible polymers having sufficiently different glass transition temperatures should be reflected by the presence of two endothermic shifts on the DSC scan. However this was not always the case for CIIR-g-BR samples, as detailed in Table 4-13, column "e". An example of DSC trace for a single endothermic shift is shown for sample FG1 in Figure 4-24 and for a sample with two endothermic shifts (FG6) in Figure 4-25.

Figure 4-20. TEM micrograph for sample FG18.

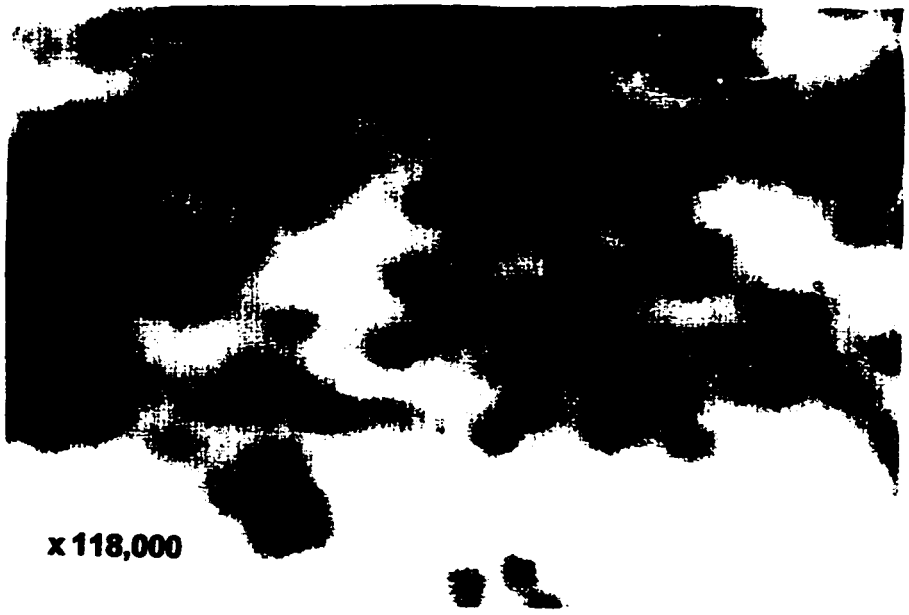


Figure 4-21. TEM micrographs for sample FG5.

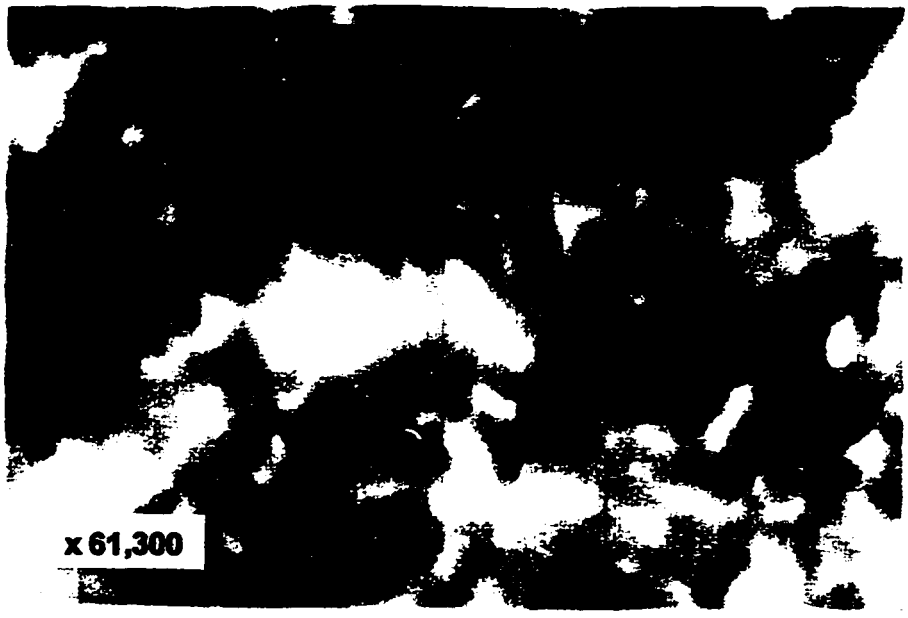


Figure 4-22. TEM micrographs for sample FG19.

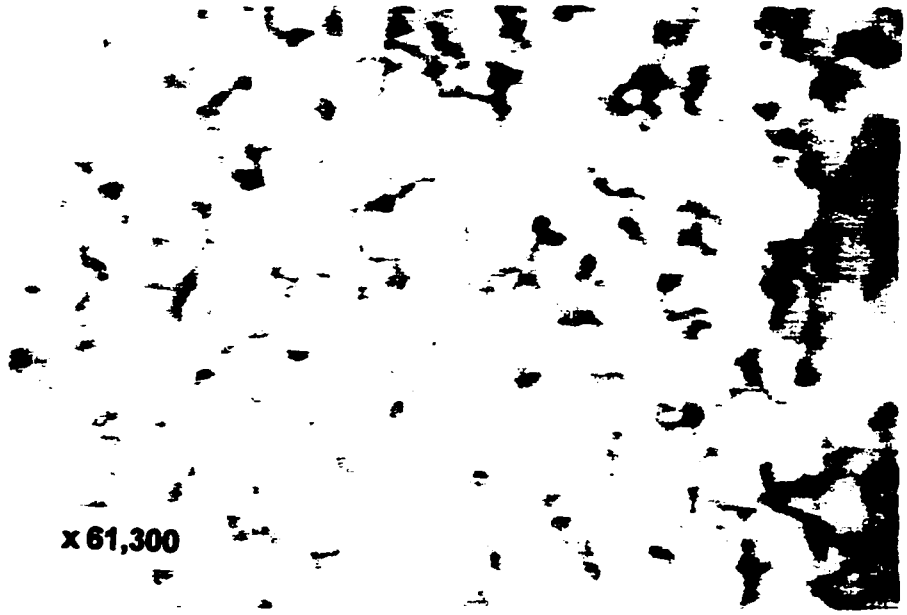


Figure 4-23. TEM micrographs for sample FG1.

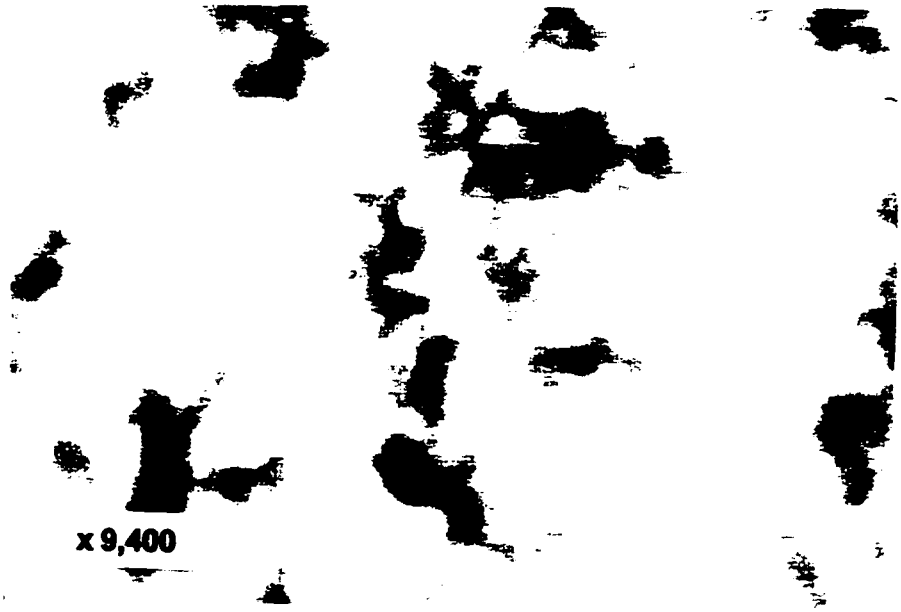


Figure 4-24. DSC scan - sample G1.

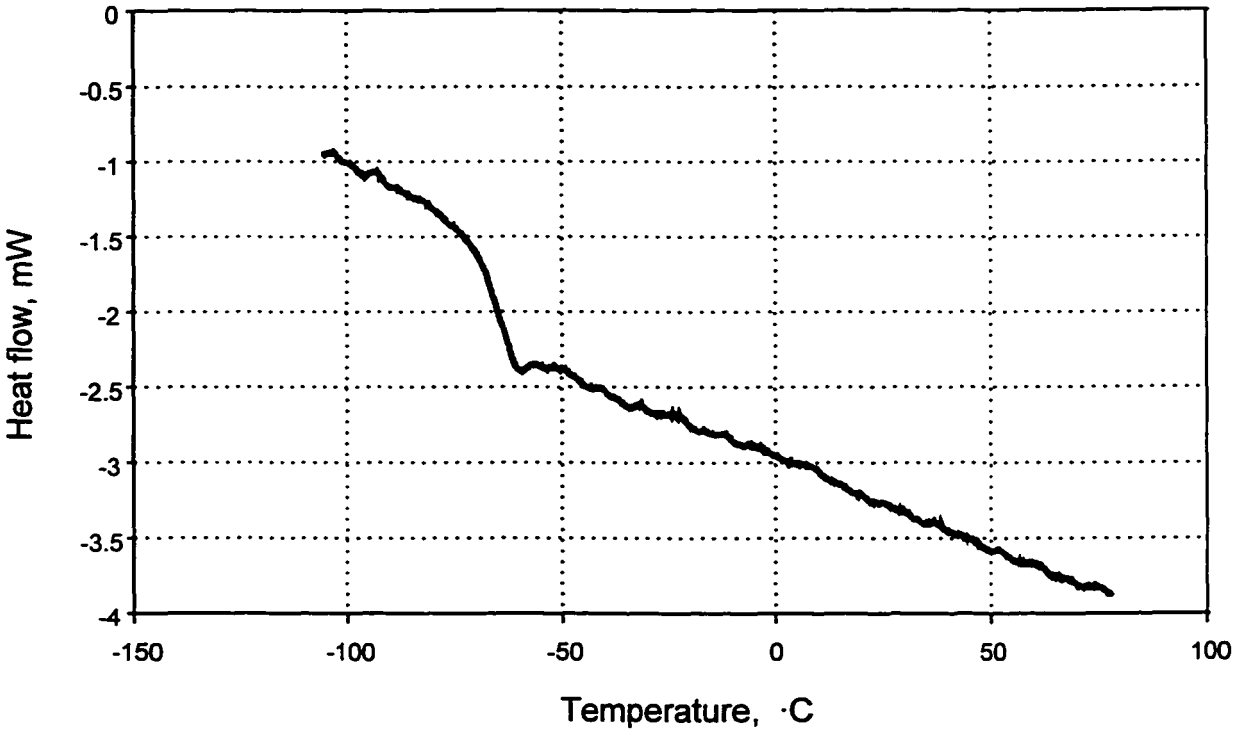
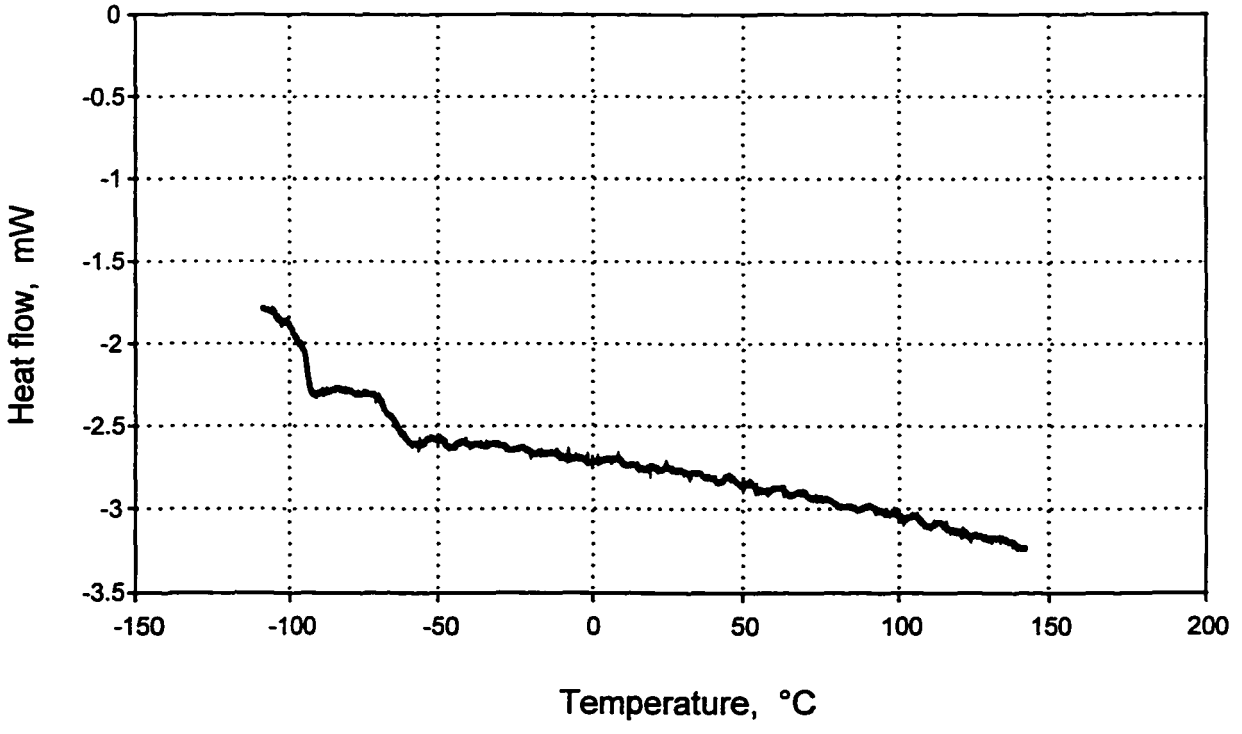


Figure 4-25. DSC scan - sample G6.



DTMA (RSA-II)

Results of the dynamic thermo-mechanical analysis in a form of the temperature dependence of dynamic moduli monitored over a temperature range broad enough to cover glass transitions (α) of both graft's precursor polymers are discussed in detail in chapter 8. Table 4-13 in column "d" contains a summary of evidence of the phase separation, as deduced from the presence of separate tan δ peaks on dynamic spectra.

SEC

For some grafts containing residual amounts of ungrafted polybutadiene, there is a potential for even more complex morphology than in pure grafts. In addition to the BR- and CIIR-rich, graft-bound phase domains, another domain containing exclusively unattached linear BR molecules could possibly exist.

No compelling evidence of this type of morphology can be drawn from available TEM micrographs, however in Figures 4-20 and 4-21 large, very dark spots could well represent pictures of isolated linear BR domains embedded into a regular two-phase morphology of the graft copolymers. Column "f" in Table 4-13, summarizes indirect evidence of this type of morphology obtained from SEC chromatograms.

From comparison of columns (b) and (f) it is clear that the number of DRI peaks observed on the MWD (DRI signal) depends on the content of of ungrafted polybutadiene ($w^{b,h}$). There is no "BR" peak observed at $w^{b,h} < \sim 1\%$, there is a small peak at $w^{b,h}$ in the range 1% to 5% and a pronounced peak at higher contents of ungrafted BR.

The following conclusions regarding the morphology of the CIIR-g-BR grafts can be drawn from experimental results:

1. A multi-phase morphology was detected for *all* graft samples *tested* by TEM, regardless of their composition and branch length and frequency. This include samples (e.g. FG1 or FG18) identified by both DSC and DTMA as having a 'single-phase' morphology. This finding is fully consistent with all reviewed studies on graft copolymers having immiscible parent polymers.
2. Qualitatively, the type of morphology - continuous or discrete - will depend on composition and domain size of the graft and will be governed by certain structural parameters, at least in the equilibrium state, as discussed in literature [276].
3. Due to differences in test method sensitivity and other factors, assessment of the type of phase morphology seems to depend on the test method used. Comparison of columns "d" with "e" in Table 4-13 suggests that, in light of conclusion (1), the DSC is a little more "sensitive" than DTMA as a 'detector' of phase morphology, contrary to what is usually observed.
4. For certain grafts (FG1, FG2, FG3, FG7, FG18, FG19), regardless of the branch length (M_p^b up to 30,000 g/mol), both the DSC and DTMA suggest single-phase morphology,in contrast to direct evidence (TEM). A common characteristic for all those samples is total BR content below 16 wt%.

Finally, it can be concluded that all graft samples in this project have fine two-phase micro-morphology, which is uniquely defined by the composition and structure of the graft.

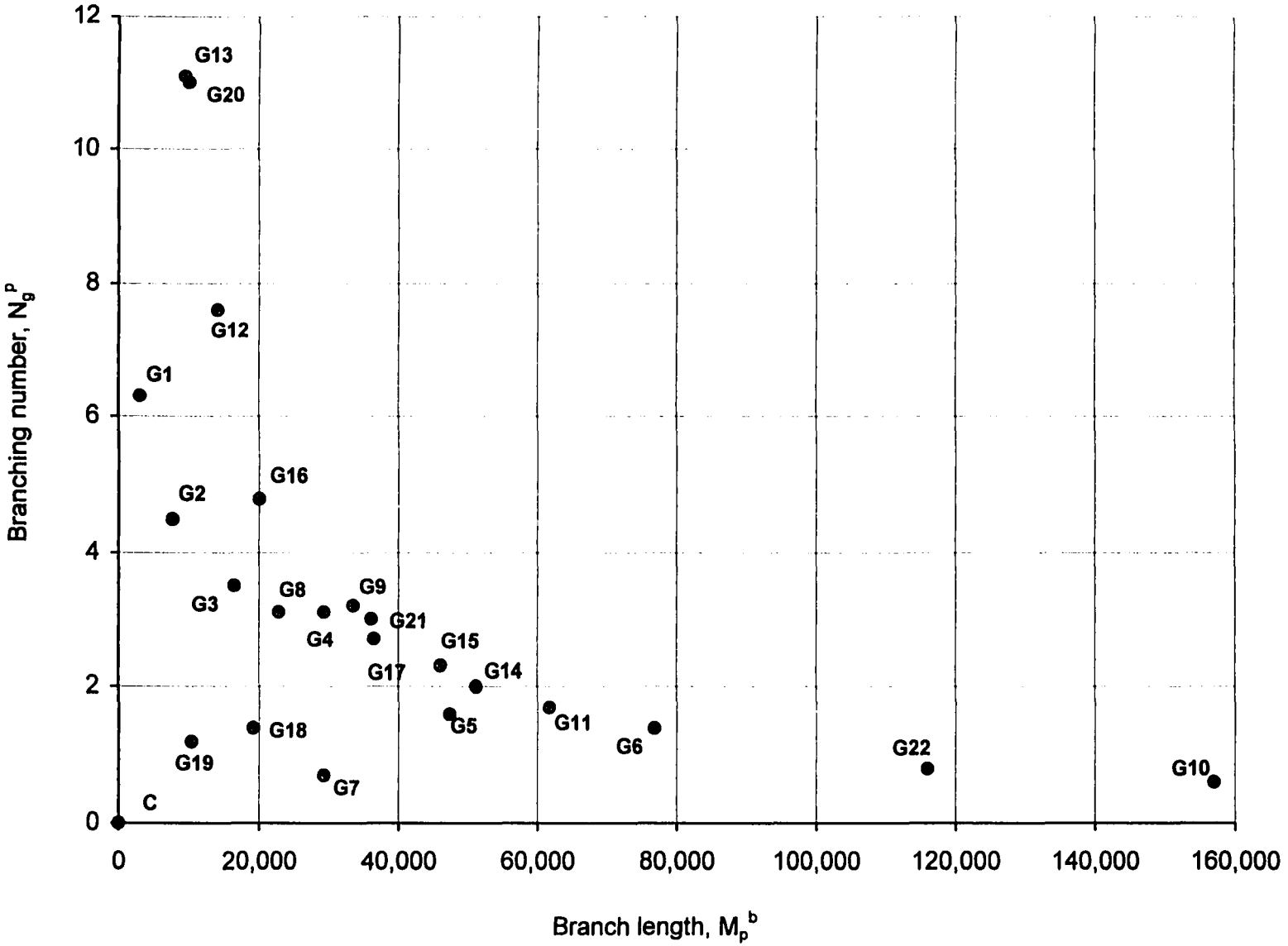
4.6 Structure and composition of the graft samples - summary

A summary of the test methodology and an overview of the analytical techniques was given in Tables 4-1a and 4-1b. Table 4-14 abstracts the main findings regarding the graft structure and composition, with reference to appropriate sections and paragraphs. Mapping of branching parameters, $\overline{M}_w^b$ and N_g, is shown in Figure 4-26, being a grahical representation of the column "b" from Table 4-9 and column "b" from Table 4-3.

Table 4-14. Structure and composition of CIIR-g-BR copolymers - summary.

	Structural parameters		Exper. verification discussed in ...	
	Parameter	***CIIR-g-BR***	***Method(s)***	***Results***
graft	topology	LCB, regular combs	—	4.4.1
	backbone, branch	CIIR, BR	—	—
	number of branches, N_g^p	N_g=0.6-11.1; variable by design	calc.	4.4.4
	branch distribution; (a) ...	randomly along the backbone	calc.	4.4.9
	branch distribution; (b) ...	slightly increasing with MW of backbone	ref.	4.2.6
	solvent content	traceable but negligible	3.4.6	4.4.7
	solids content	negligible, < 0.3 wt%	3.4.6	4.4.7
	grafted BR content	variable (depends on graft structure)	3.4.2	4.4.2
	unattached BR content	variable (depends on branch MW)	3.4.2, 3.4.1	4.4.5
	phase morphology	two-phase, micro-separated	3.4.5, 3.4.4	4.5
	crystallinity	no evidence	3.4.4	4.5
	gel, cross-linking	absent	3.4.7, 3.4.1	4.4.8
backbone (CIIR)	topology	linear molecules	3.4.1, ref.	4.2.1
	MWD/MW	polydisperse (PDI=3.25, M_w=457,000)	3.4.1	4.2.3
	chemical composition	random copolymer; isolated IP units	3.4.2, ref.	4.2.4/5
	isoprene content	1.9 mol%	3.4.2	4.2.4
	"free" Cl content	none (not detectable)	3.4.8	4.2.6
	bound Cl content	1.6 mol%	3.4.8, 3.4.2	4.2.6
	branch site functionality	3	ref.	4.2.2
branch (BR)	topology	linear molecules	ref., 3.4.1	4.3.1
	branch length, M_p^b	variable by design; M_p^b=3,000 - 157,000	3.4.1	4.3.2
	MWD	narrowly polydispersed (PDI=1.11-1.64)	3.4.1	4.3.2
	microstructure (avg.)	cis: 35.4%, trans: 55.4%, vinyl: 9.2%	3.4.3, 3.4.2	4.3.3

Figure 4-26. Principal branching parameters of CIIR-g-BR graft copolymers.



Chapter 5

Characterization of the rheological properties: experimental methods

5.1 Introduction

This chapter describes in detail experimental aspects of the rheological characterization of the graft. The following rheological instruments were used in this study:

- Rheometrics Mechanical Spectrometer, RMS-800, further referred to as 'RMS-800',
- Rheometrics Solids Analyzer, RSA-II, referred to as 'RSA-II',
- Rubber Process Analyzer, RPA 2000™, referred to as 'RPA 2000', and
- Dynamic Stress Relaxometer, DSR, referred to as 'DSR'.

The first two instruments are versatile, general purpose rheometers used extensively to characterize viscoelastic, particularly dynamic mechanical, properties of polymers. The last two (RPA 2000 and DSR) are dedicated instruments designed and used primarily to characterize the properties of gum elastomers, rubber compounds and thermoplastic elastomers.

A separate section of the chapter is devoted to discussion of the experimental test conditions specific to each rheometer. Each section has a similar format and deals with various issues in the following sequence:

5.*.1 - description and principle of rheometer operation,
5.*.2 - details of specimen preparation,
5.*.3 - outline of the experimental program and test procedures,
5.*.4 - preliminary experiments and their results,
5.*.5 - instrumental interferences and data validation, and
5.*.6 - test precision, accuracy and sensitivity.

Results of the rheological characterization of graft copolymers are presented and discussed in:

- chapter 4, section 4.5, in connection with the microphase separation,
- chapter 5, in sections 5.2.4, 5.3.4, 5.4.4, 5.5.4 and 5.6, concerned with various minor issues, in particular with limits of the linear viscoelasticity,
- chapter 6, for the linear viscoelastic (LVE) properties,
- chapter 7, for the non-linear viscoelastic (NLVE) properties, and
- chapter 8, for the dynamic thermo-mechanical (DTMA) properties.

Appendix IV contains a complete report of the test conditions and parameters. Table 9-1 in chapter 9 summarizes results and their interpretation.

5.1.1 Overview of the rheological characterization program

The experimental program has been designed to investigate rheological properties of graft copolymers in both linear and non-linear visco-elastic regimes. CIIR-g-BR copolymers behave as soft, visco-elastic solids (rather than high viscosity elasto-viscous fluids such as thermoplastic melts). Therefore, the selection of rheometers and rheometrical techniques was largely governed by the nature of the samples. For example, rheometrical techniques involving a steady shear could not be used, unless the product of strain rate and test time gave only a very small strain. Dynamic mechanical (oscillatory) and transient deformation - such as stress relaxation following a step shear strain - were found to be the most convenient techniques to study rheological behaviour of these materials. Table 5-1 lists instruments and test methods used in this project.

Table 5-1. Rheological instruments and test methods.

	Deformation	Isothermal dynamic		Isothermal stress relaxation		Dynamic, isochronal (temp. sweep)	Isothermal. dynamic sequential
		LVE	NLVE	LVE	NLVE	LVE	LVE / NLVE
RMS-800	shear	√	√	√	√	√	-
RSA-II	tensile	-	-	-	-	√	-
RPA 2000	shear	√	√	-	-	-	√
DSR	shear	-	-	-	√	-	-

5.1.2 Summary of preliminary rheological characterization

A variety of issues had to be resolved by means of tests referred to as preliminary, before the actual program of rheological characterization could be defined and executed. Screening of various test methods for their suitability for this project was undertaken along with determination of the appropriate temperature range for testing CIIR-g-BR elastomers. The temperature range for the majority of tests was between 25°C and 150°C, with a reference test temperature of 100°C. The lower limit temperature for the thermo-mechanical analysis (DTMA by RSA-II) was dictated by the temperature of the glass transition for polybutadienes with a 1,2-cis structure content of 35%.

Those preliminary tests which were specific to the instrument or test method are discussed separately in appropriate sections (5.*.4) for a given rheometer. Examples of typical preliminary issues include: method development for specimen preparation, test procedure development or modification, including determination of appropriate test parameters, test precision and sensitivity assessment.

Special issues which deserved particular attention, due to their implications for validity of the conclusions for the overall project, will be discussed in section 5.6. of this chapter.

5.1.3 Rheological issues

The rheological issues which will be explored in detail and discussed in the context of branching structure and composition of the CIIR-g-BR copolymers are presented in Table 5-2.

The results of rheological characterization are discussed in detail in chapters 5, 6 and 7 and summarized in Table 9-1 in Chapter 9, following the sequence of Table 5-2.

Rheological nomenclature, including list of rheological parameters defined throughout the thesis, is included in Appendix II, Part Rheology.

Table 5-2. CIIR-g-BR graft copolymers - rheological issues.

1. Viscoelastic properties in the plateau / terminal zone

1.1 LVE

1.1.1 LVE parameters

1.1.2 Frequency-dependence: $G^*(\omega)$, $\tan \delta(\omega)$, $G'(\omega)$, $G''(\omega)$, $\eta^*(\omega)$...

1.1.3 Time-dependence: $G(t)$, $nG(t)$ ...

1.1.4 Temperature-dependence: $G'(T)$, $G''(T)$, ...

1.2 LVE / NVLE

1.2.1 Strain amplitude-dependence $G'(\gamma)$

1.2.2 Strain & frequency-dependence: Pipkin diagrams

1.3 NLVE

1.3.1 NLVE parameters

1.3.2 Frequency-dependence: $G_1'(\gamma', \omega)$, $G_1''(\gamma', \omega)$, nC-C, ...

1.3.3 Time-dependence: $G(\gamma', t)$, $nG(\gamma', t)$

1.3.4 Effect of large-amplitude oscillatory shear (LAOS)

2. Viscoelastic properties in the glassy / transition zone

2.1 LVE (E)

2.1.1 Temperature-dependence: $E'(T)$, $E''(T)$

2.1.2 Temperature-dependence: $\tan \delta(T)$

LVE *- linear viscoelasticity in shear*

NLVE *- non-linear viscoelasticity in shear*

LVE (E) *- linear viscoelasticity in tension*

3. Other issues

3.1 Phase morphology

3.2 LCB - qualitative characterization (mapping): nC-C plots

3.3 LCB - quantitative characterization: rheometrical techniques

5.2 Rheometrics Mechanical Spectrometer, RMS-800

5.2.1 Principle of operation

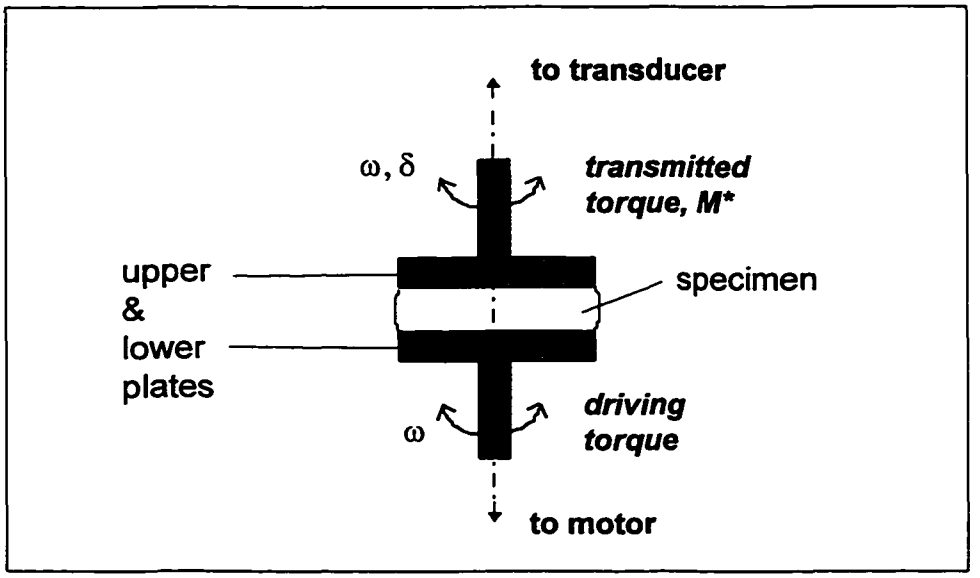
The Rheometrics Mechanical Spectrometer, model RMS-800 is a versatile rotational rheometer designed for characterization of rheological properties of a variety of materials, including polymers. The RMS-800 is a controlled shear-strain instrument with capability to operate in a variety of test modes: steady shear, transient and dynamic (sinusoidal oscillations) within a broad range of test temperatures, strain amplitudes, and frequency ranges [277].

For soft viscoelastic solids (such as the elastomeric graft copolymers of MW in the order of 500 kdaltons or higher) the number of test configurations and test modes is limited due to the instrument's transducer and the driving system limitations, and also because of the nature of the material being tested. Specifically, the potential for instrumental interferences is high and these can take a variety of forms (slippage between specimen and fixture, specimen distortions and fracturing) severely affecting the reliability of measurements. As a result, for these types of materials, the most suitable RMS-800 test methods include limited strain amplitude oscillations in shear (dynamic test modes) and some types of transient tests, for example, stress relaxation, following the application of a step shear strain.

In the most popular and convenient test geometry, namely the parallel-plate configuration (Figure 5-1) a preformed, disk-shaped specimen is sandwiched between two circular flat disk plates, parallel to each other. The bottom plate is driven by a direct-current servo-motor, imposing a precisely executed rotational motion on the specimen while the upper plate is collecting the torque-time profile transmitted through the specimen. In dynamic test modes, the exact amplitude and delay (phase angle, δ) of transmitted torque is measured and used to calculate dynamic moduli (G', G'') and to derive other viscoelastic functions and parameters.

Definitions and brief introduction to the linear viscoelastic functions are given in section 5.4.1. Symbol are listed in Appendix II.

Figure 5-1. RMS-800 parallel-plate test fixture.



For measurements under sufficiently low strain amplitudes (e.g. within the LVE response of tested material) the following calculations are possible following simple relations between measurable quantities (such as torque M*) and dynamic viscoelastic functions [278-279]:

torque, M* + geometric factor ----> G*(ω) ------

relative position of plates ---> phase angle, δ ---

------> G′(ω), G″(ω), tan δ, η*(ω), ...

Analogously, in a stress relaxation experiment, decay of torque resulting from an imposed step-strain deformation of the specimen can be monitored and, under certain assumptions, expressed in the form of stress relaxation modulus, G(t):

torque, M(t) + geometric factor ----> G(t)

The test fixture is contained in an environmental chamber where specimen temperature can be changed and maintained by the influx of inert gas.

Test execution and data acquisition are controlled by the vendor's proprietary software (RHIOS) installed on a dedicated PC.

5.2.2 Specimen preparation

The following distinction was made and is observed throughout this work, regarding the notion of the test sample and test specimen,

- the term 'sample' is referred to a quantity of test material regarded as homogeneous in respect to a set of specific structural and physical properties which make it distinct from other samples,
- a specimen (or test piece) is a portion of the sample having the appropriate weight, and if required, shape and dimensions, required for a given single test or experiment.

All specimens made from a given sample are assumed to be identical in all relevant aspects. Specifically, during multiple determinations of experimental routines a separate specimen is used for each test and a separate specimen is used for each subsequent test. In this context, scatter of results is considered to represent test method precision, unaffected by material inhomogeneity.

Rheological tests, particularly the most sensitive involving only small strains or strain rates, require preparation of homogeneous, isotropic samples and specimens in a fully relaxed state. The specimens should be tested only when it can be assumed that no step in specimen preparation or handling prior to its testing will affect the rheological test output in a fashion which could interfere with data interpretation in terms of structure-property relationships.

Sample preparation by casting concentrated solutions into glass trays to obtain thick, dry films has been described in chapter 2, section 2.6.1.

Specimens for the parallel-plate fixture of the RMS-800 were prepared by plying-up (usually two-fold) strips of polymer film deposited on the release paper substrate. Disks of 30.0 mm in diameter were punched out with their paper coating retained. Subsequently, they were kept under smooth, strictly parallel metal plates of controlled spacing for a few days. The supporting paper was removed immediately before loading a specimen onto the test fixture. Nominal size of the specimens was 25.0 mm in diameter and between 1.25 and 1.5 mm in thickness, as recommended [277]. The recorded thickness of each specimen was the average of several measurements around the circumference and in the middle of the disk. Specimens with non-uniform thickness with individual measurements exceeding 5% (of the average value) or with any visible departures from a nominal disk shape, were rejected.

Further details of specimen preparation are described in section 8.1 of the Polysar Test Procedure [280], resulting from the author's extensive experience in the application of the RMS-800 for testing a wide variety of elastomers.

5.2.3 Overview of the experimental program

The experimental program for the RMS-800 was designed to examine comprehensively the viscoelastic properties of the grafts, primarily in their linear range of viscoelastic behaviour.

Two main techniques, particularly suitable for studying "soft" viscoelastic solids were employed - dynamic (sinusoidal oscillatory in shear) and transient, in the form of stress relaxation, following the step-strain mechanical excitation. The steady state (rotational shear) and controlled-stress experiments, including the creep test, were found not feasible on the RMS-800 for this type of material.

The main experimental program utilized isothermal and non-isothermal frequency sweeps and stress relaxation experiments. Certain test parameters were determined and optimized by preliminary tests: time sweeps (tS), time/cure (tcS), and strain amplitude (SS) sweeps. Preliminary tests will be briefly discussed in the following subsection (5.2.4). Test precision (short term repeatability) was derived from multiple experiments on selected samples, by routines {QFS} and {QSR}, and summarized in subsection 5.2.6. The brackets {...} refer to the test conditions and parameters specific to each test. Complete details of test conditions and parameters are given in Appendix IV.

The dynamic frequency sweep applies a sinusoidal strain of a constant amplitude but with the frequency gradually changing over a pre-selected range. A whole series of measurements is carried out under isothermal conditions at a pre-selected temperature. The dynamic frequency sweep is a convenient method to analyze time-dependent behaviour of a broad range of materials. It is particularly suited for materials under study. Sometimes, a series of isothermal frequency sweeps is executed at progressively higher temperatures on the same specimen, referred to as a frequency/temperature sweep (FTS).

Provided that the thermo-mechanical stability of a sample is not an issue, a temperature-frequency sweep is an effective and more accurate test than a series of isothermal frequency sweeps on individual specimens.

5.2.4 Preliminary experiments

A series of preliminary tests was carried out in order to design the main experimental program. The tests determined the optimum test parameters and conditions, and explored diverse test sequences and options. Table 5-3 contains an overview of the experimental program. Some tests which were conducted on multiple specimens in order to determine the test precision of the two principal test modes, frequency sweep and stress relaxation, are described in section 5.2.6. The results of the main program are the subject of chapter 6 and, those derived from the large-strain amplitude stress relaxation tests, are discussed in chapter 7. A complete listing of test conditions and parameters is included in Table A, Appendix IV.

Table 5-3. RMS-800 - Overview of the experimental program.

	principal objective	
	preliminary tests:	*main study:*
dynamic (oscillatory)	tS & tcS - (thermal stability) SS - (LVE limits) {QFS} - (test precision)	FS & FTS - (frequency dependence) TS - (temperature dependence)
transient (stress relaxation)	{QSR} - (test precision) {PSR} - (LVE limits)	SR@5&10% - small-strain relaxation (relaxational behaviour at LVE limit)

5.2.4.1 Time and time/cure sweeps

Following Rheometrics terminology, 'time sweep' is defined as a type of dynamic mechanical test where all its principal variables (strain amplitude, oscillation frequency and test temperature) are constant during the entire test routine. On the other hand, a 'time/cure sweep' denotes a very flexible test configuration platform which enables design of a sequence of routines, each with its own temperature, strain frequency and amplitude, as well as the duration of the routine.

Two primary objectives of this preliminary study were:

- determination of the limits of thermal stability at the dynamic conditions of rheological testing, and
- fine-tuning of certain test parameters difficult to calculate but necessary for proper design of the frequency and frequency/temperature sweeps.

Several test configurations were explored during preliminary experimentation. Figure 5-2 is an example of time sweep {tS1} results for sample B10, a 100% polybutadiene sample, which, due to the presence of double-bonds, is the most vulnerable to thermal degradation. A perfectly flat response of the dynamic moduli in shear (G', G") indicates lack of any degradation of the material at the applied test temperature and shear conditions, which could be detectable rheologically. The time/cure {tcS1} test as shown in Figure 5-3 is a typical test routine designed to establish the thermal resistance of a material under given shear/flow conditions. The results indicate thermo-mechanical stability of sample C up to 150°C. Each sample was subjected to this screening and 150°C was proven to be a safe upper temperature limit for most rheological tests. Similar time sweeps can be extended to several hours without appreciable change in dynamic moduli at or below the temperature of 130°C. As a result 130°C has been chosen as the maximum test temperature for long-term tests (of the order of a couple of hours or longer).

Figure 5-2. RMS-800: isothermal time sweep.
T=100°C, ω=3 rad/s, γ =2%, sample B10, {tS1}.

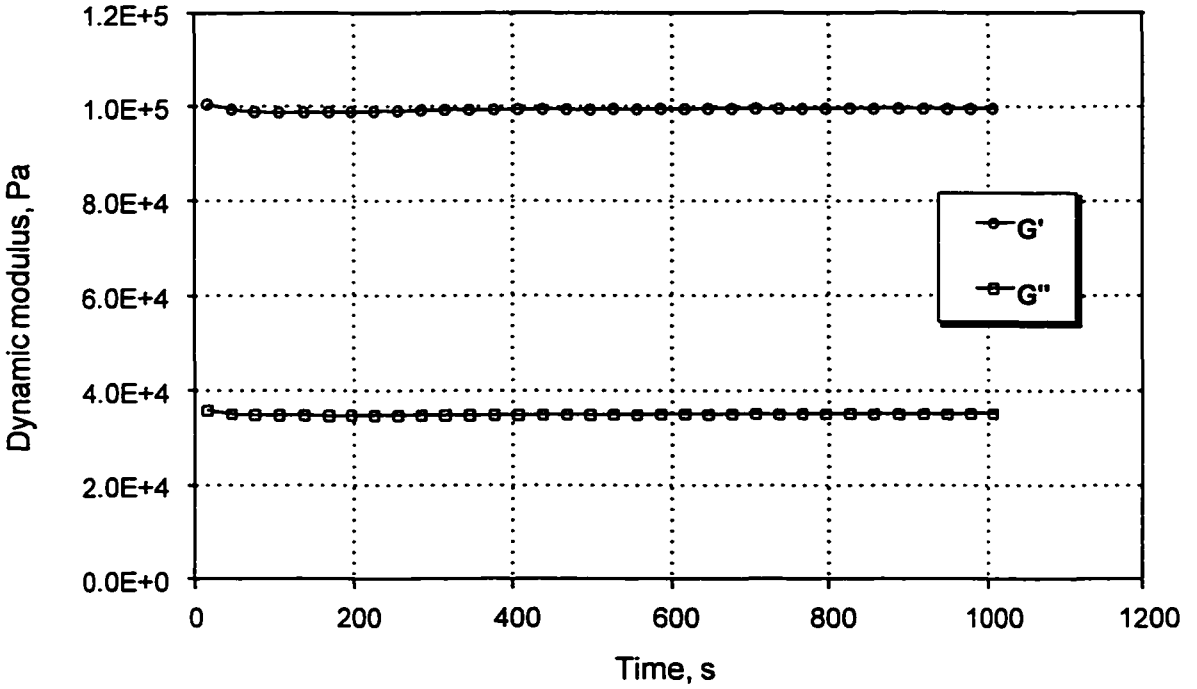
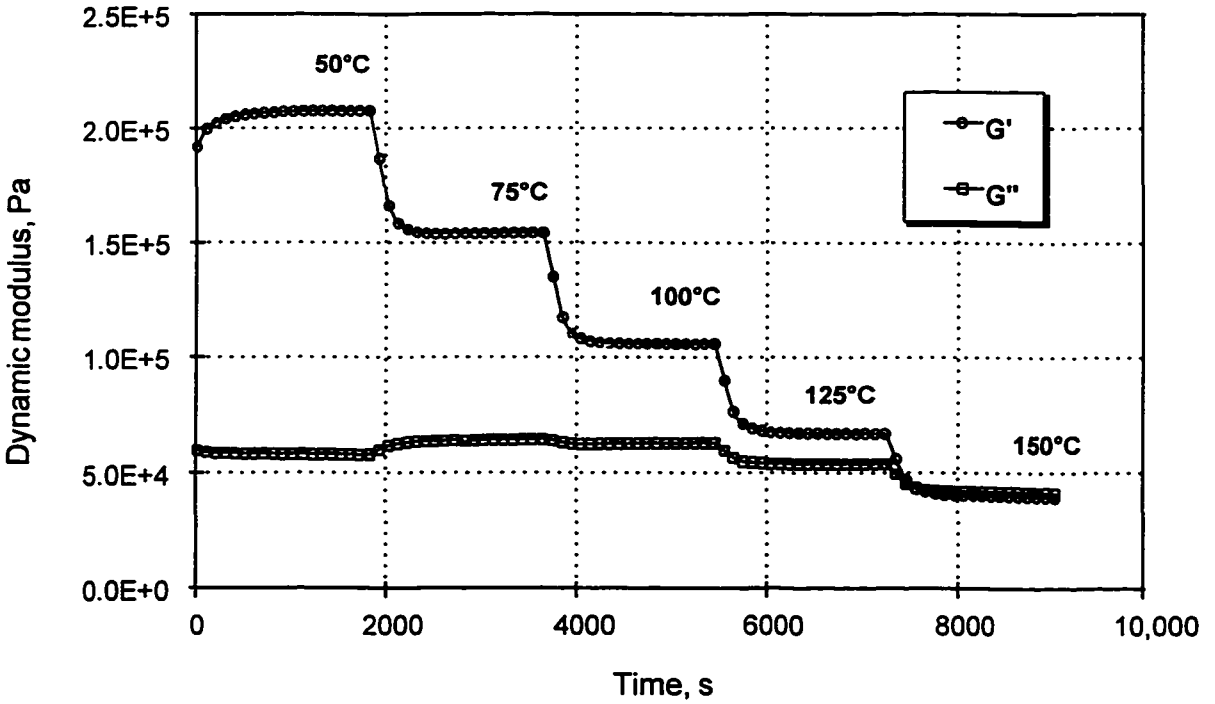


Figure 5-3. RMS-800: isochronous temperature ramp.
T=100°C, ω=1 rad/s, γ =2%, sample C, {tcS1}.



In addition, results of these tests helped to refine some of the test parameters of the frequency and frequency-temperature sweeps for the main part of the study.

Complete and exact test parameters are compiled in Appendix IV.

5.2.4.2 Dynamic strain sweep

Introduction

The strain amplitude-dependence of the dynamic mechanical modulus has been extensively studied for various filled elastomers [281-283] over a wide range of temperatures and frequencies. The exact character of the transition between linear and non-linear viscoelastic behaviour depends on the polymer, the type of filler and filler concentration and distribution. The combined effects of the filler agglomeration and de-sorption/absorption of the hard polymer shell around the filler particle is an important factor to consider in studying this phenomenon [284].

Fewer similar studies exist on unfilled and unvulcanized elastomers, but it has been shown that the strain amplitude has a less dramatic effect on the modulus of gum elastomers [285]. Specifically, the strain amplitude had no significant effect on either the tensile storage modulus, E′ or tensile loss modulus, E″ for pure brominated butyl (BIIR) gum vulcanizates, with the strain amplitude ranging from 0.035% to 2.5%, in tension. The E′ modulus decrease for the same range of the strain amplitude but for BIIR filled with 30%wt carbon black can be of the order of 10-fold [285].

Definition of the dynamic strain sweep test and critical strain amplitude

A 'strain sweep' is an isothermal and isochronal dynamic mechanical experiment during which the strain amplitude is changing systematically (typically increasing) either linearly or logarithmically.

The behaviour of a material is considered to be within the linear viscoelastic (LVE) range, if its viscoelastic functions are strain-amplitude independent. Provided that a) no slip occurs between the specimen and the plates of the fixture, and b) the material is not changing chemically or physically, this implies that the storage modulus (E′ or G′) has constant values during the dynamic strain (amplitude) sweep, carried out at a constant frequency and temperature.

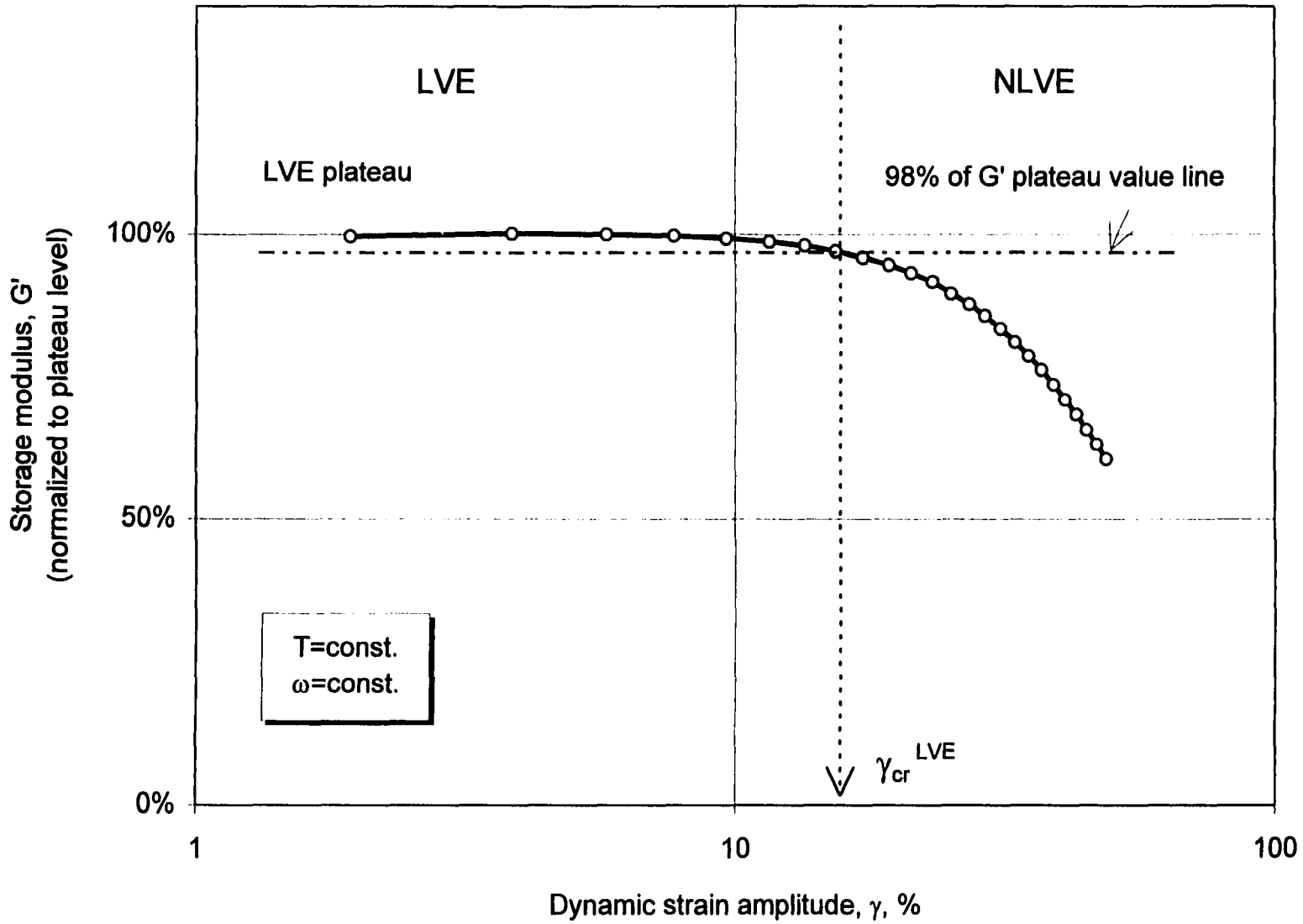
A number of specific definitions for 'critical strain amplitude' have been proposed [286-288] Here it is suggested that the critical strain amplitude, γ_{cr}^{LVE}, be defined as the strain amplitude at which the storage modulus, G′ drops 2% below its value at infinitely small strains. Figure 5-4 illustrates the concept of critical strain amplitude as the borderline between the linear and non-linear viscoelastic behaviour.

The following were the two main objectives of the strain sweep test in this project:

1. As a preliminary test, to predetermine the optimum value of the dynamic strain for other dynamic tests, such as frequency, temperature and frequency/temperature sweeps,
2. To explore possible correlations between some details of the LCB structure and γ_{cr}^{LVE}.

Some observations on the influence of temperature and frequency on the value of the critical strain amplitude were made and compared to similar findings in the literature.

Figure 5-4. Definition of the critical strain amplitude, γ_{cr}^{LVE}.



Experimental details are listed in Appendix IV under the test codes {SS1}, {SS2}, {SS3}, {SS4}, {SS5}, {SS6} and {SS7}. The results and some conclusions are discussed in subsequent sections.

A few representative strain sweep results are included in the following figures:
Figure 5-5 for sample G1, Figure 5-6 for sample G2, Figure 5-7 for sample G8, Figure 5-8 for sample G10, Figure 5-9 for sample G13, Figure 5-10 for sample G19, Figure 5-11 for sample C and in Figure 5-12 for samples B10. This portfolio includes both the extreme (the last two examples) behaviour and a range of curves typical for grafts.

The results presented were obtained for strain sweeps at different temperatures and frequencies as indicated on the graphs, but at the same initial Normal Force (iNF=100G), and using the same set of parallel plates with sand-blasted surface. In all cases the measured strain amplitude was used to plot the diagrams. The strain-amplitude dependence of the dynamic modulus, particularly pronounced for the storage modulus, G′ is the common feature observed in all strain sweep profiles, regardless of sample or test conditions. This strain-amplitude 'thinning' of the storage modulus occurs at strains $\gamma > \gamma_{cr}^{LVE}$, where γ_{cr}^{LVE} depends both on a sample and on certain experimental parameters, which will be discussed later.

Possible causes for the strain-dependence of storage modulus (at constant T and ω)

The drop-off of storage modulus G′ from a plateau defined by the G′ value at very small strains ($\gamma \rightarrow 0$) might be attributed to instrumental artifacts, "genuine" material properties or a combination of both. In the context of transition between linear and non-linear viscoelastic response of a polymer, slippage between specimen and the adjacent surface of a fixture ("specimen slippage") can be considered a primary example of an instrumental artifact.

Figure 5-5. RMS-800 - isochronous strain sweep, {SS2} sample G1, T=30°C, ω=3 rad/s.

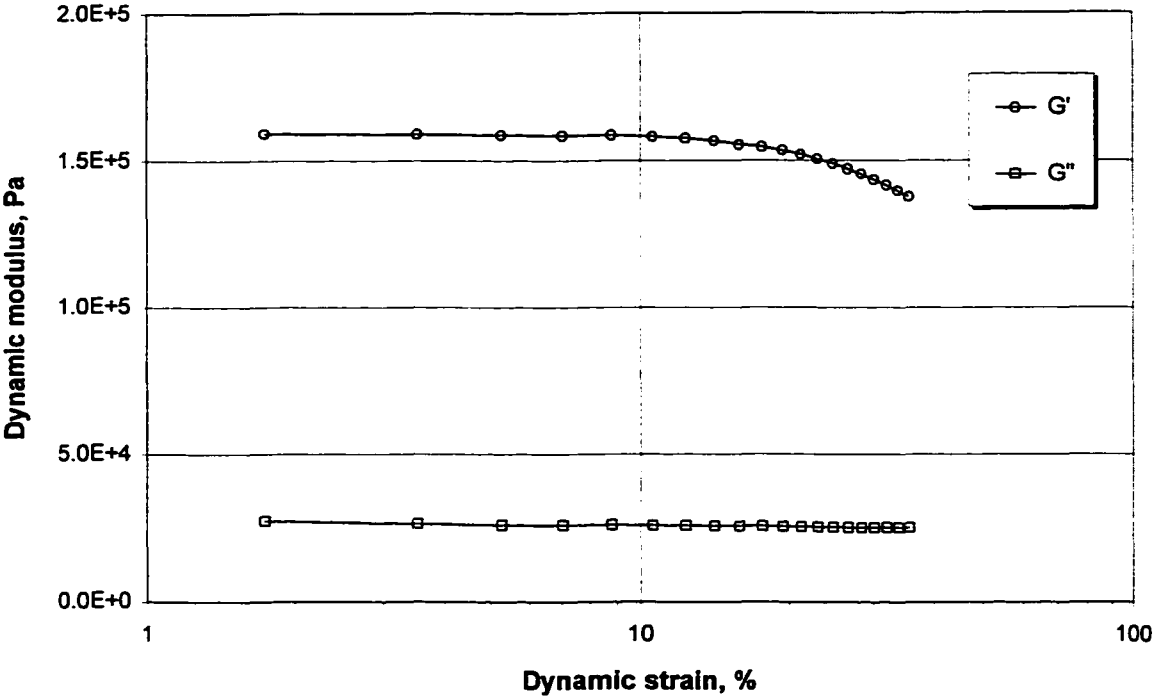


Figure 5-6. RMS-800 - isochronous strain sweep, {SS5} sample G2, T=130°C, ω=3 rad/s.

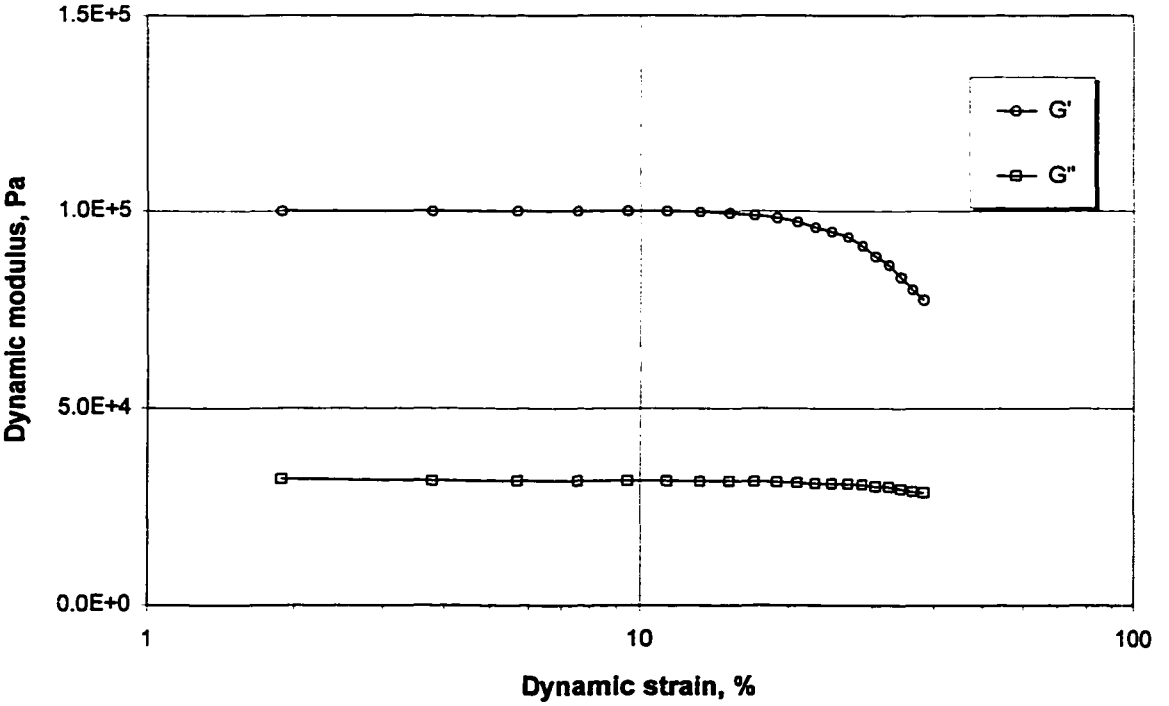


Figure 5-7. RMS-800 - isochronous strain sweep, {SS2} sample G8, T=30°C, ω=3 rad/s.

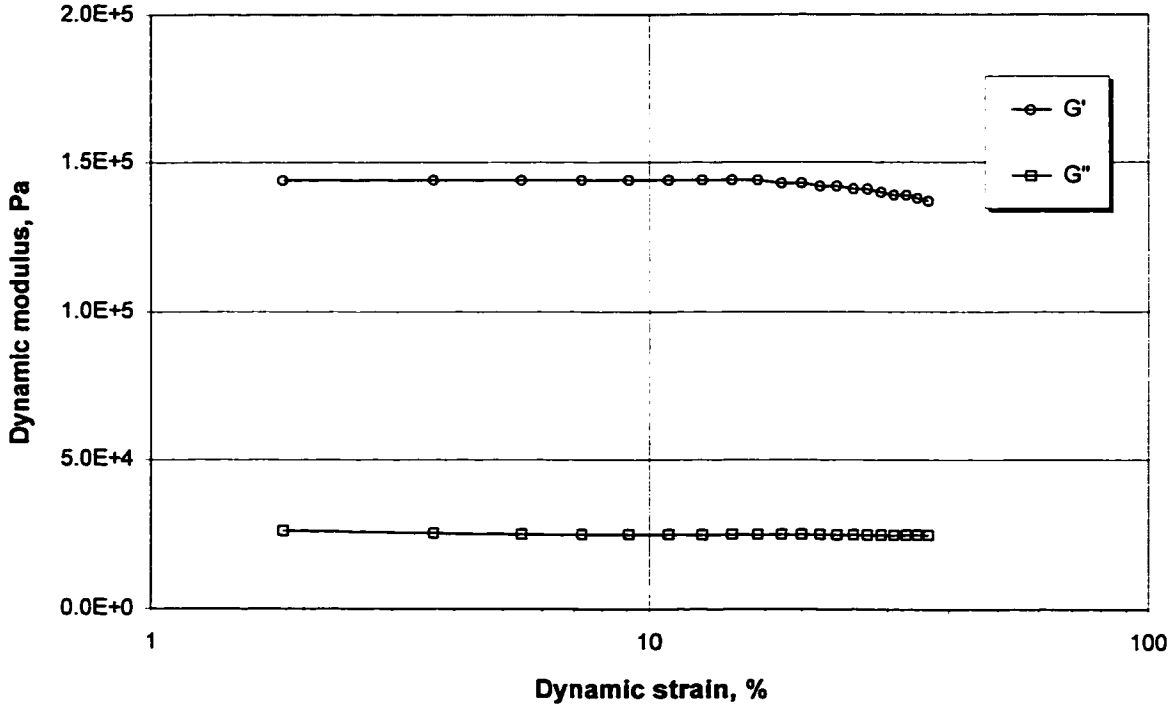


Figure 5-8. RMS-800 - isochronous strain sweep, {SS5} sample G10, T=130°C, ω=3 rad/s.

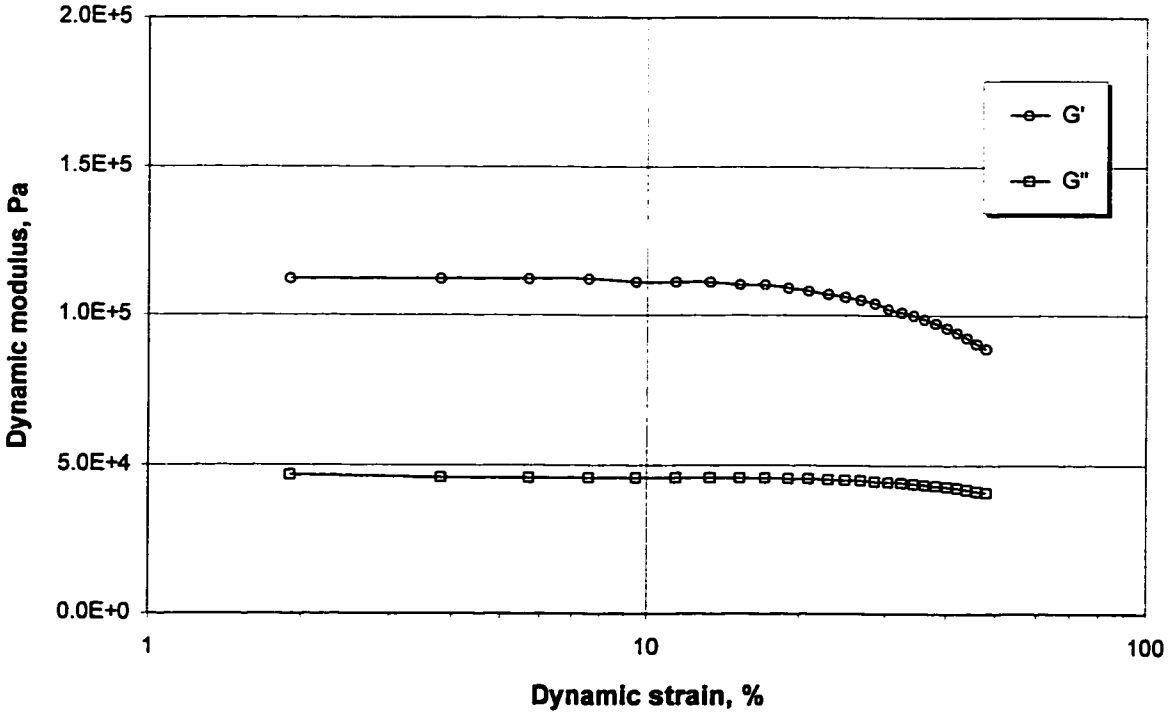


Figure 5-9. RMS-800 - isochronous strain sweep, {SS5} sample G13, T=130°C, ω=3 rad/s.

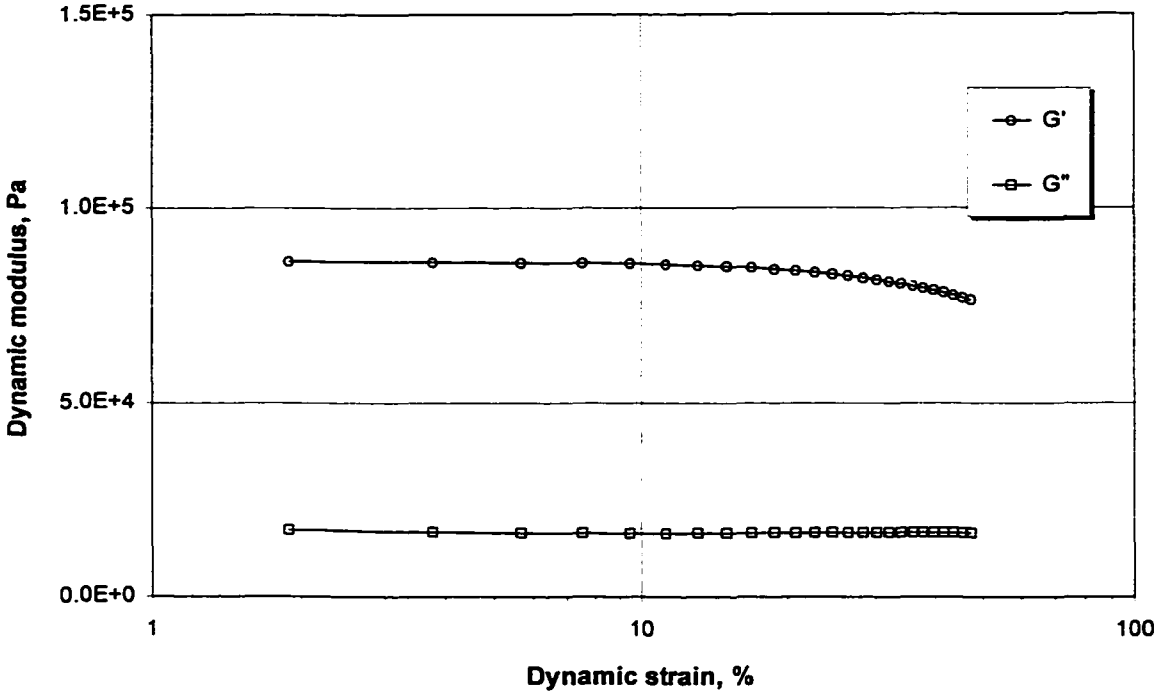


Figure 5-10. RMS-800 - isochronous strain sweep, {SS5} sample G19, T=130°C, ω=3 rad/s.

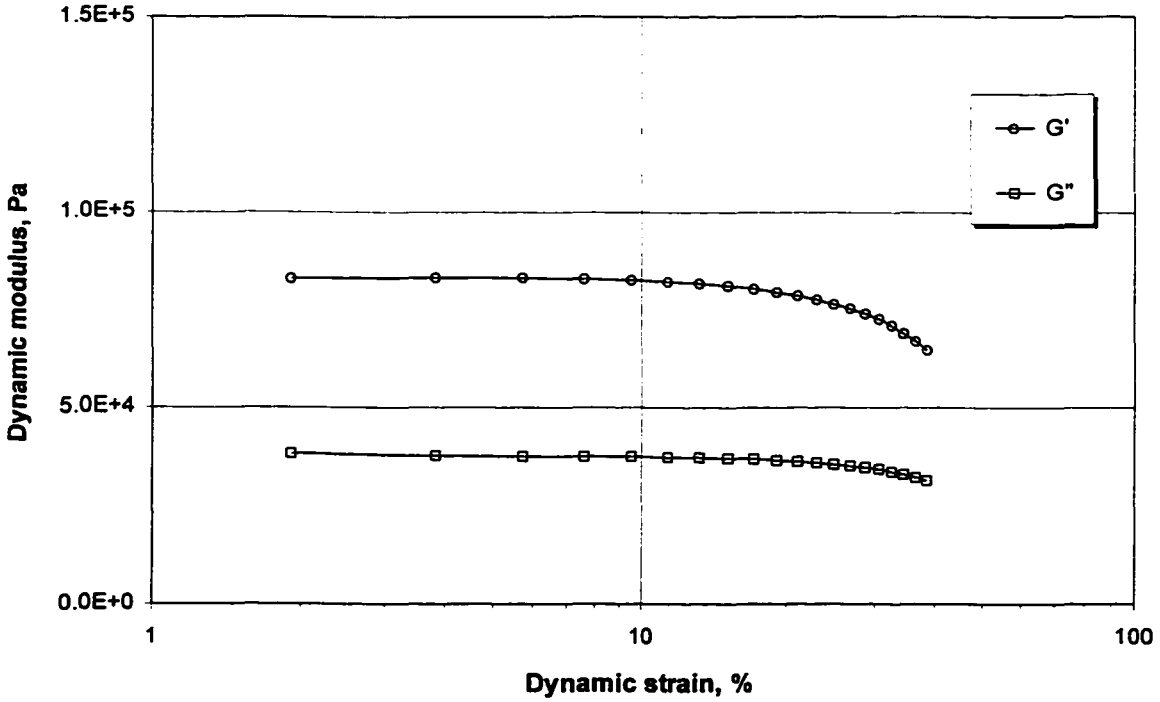


Figure 5-11. RMS-800 - isochronous strain sweep, {SS3} sample C, T=50°C, ω=10 rad/s.

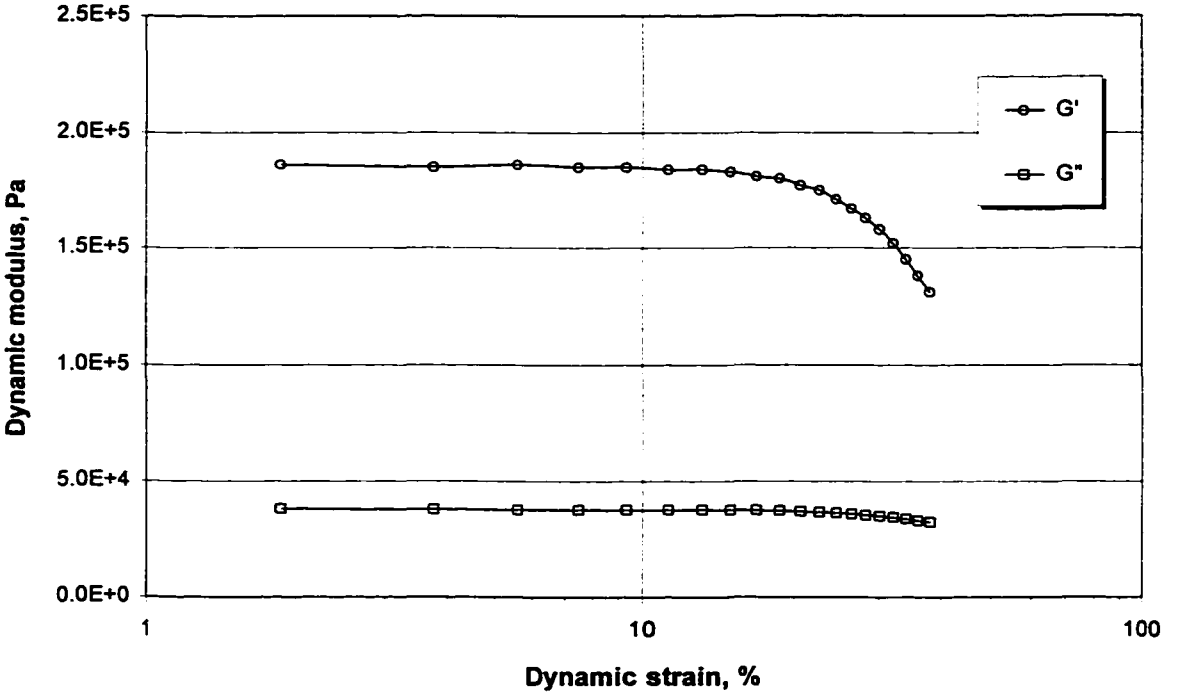
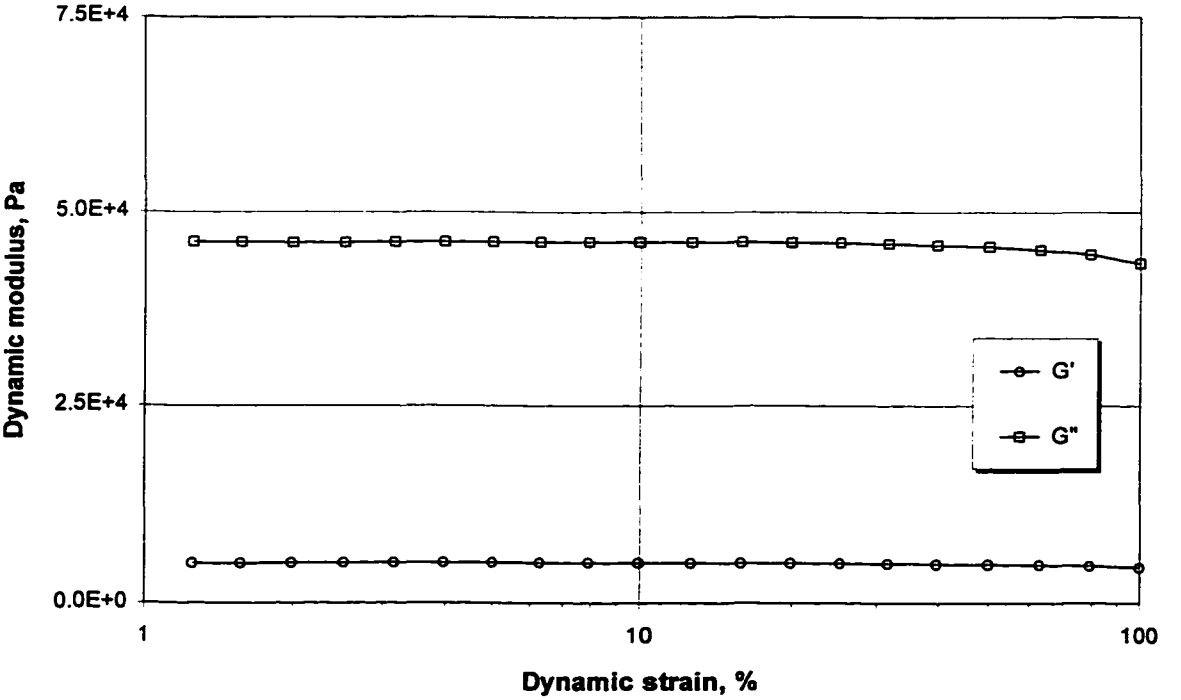


Figure 5-12. RMS-800 - isochronous strain sweep, {SS4} sample B10, T=100°C, ω=3 rad/s.



Advent of "specimen slippage" may cause a gradual decrease of G′ with increasing strain amplitude not readily distinguishable from "softening" of storage modulus due to on-rise of non-linear effects.

Viscous heating

Temperature rise due to the viscous dissipation could lower modulus progressively with increasing strain amplitude. However, both calculation and experiment shows that the viscous heating cannot entirely explain a dramatic drop of modulus with increasing strain amplitude. The calculated modulus drop due to temperature increase would be much smaller than actually observed, even in adiabatic heating conditions, due to the modest temperature increase and small temperature-dependence of the dynamic modulus. This was actually confirmed experimentally for several elastomers [289].

A thin specimen and efficient (nearly isothermal) heating/cooling in the RMS-800 test chamber would cause a further decrease of any contribution to the G′ drop from viscous heating.

Specimen slippage

The possibility of an apparent drop-off in G′ with increasing strain due to specimen slippage is real in a strain sweep test. Experience [290] shows that it depends on instrumental factors, such as elastomer adhesion to the metal, surface texture of the plates and normal force holding the specimen in the fixture.

The magnitude and onset of slippage is difficult to estimate and correct for. The best strategy is to prevent it by elimination, or delay, of the effect by the application of a normal force and by promoting better adhesion between the fixture plates and the specimen.

Comparison between the cross-hatched and flat, but sand-blasted plates, showed an apparent decrease of the γ_{cr}^{LVE} for the former ones. This observation was somewhat surprising and certainly contrary to the intended function of serrated plates, but it was consistent and reproducible for various levels of the Normal Force. A higher initial Normal Force (iNF) leads to a higher γ_{cr}^{LVE}, presumably by improving the adhesion and delaying specimen slippage.

The critical strain amplitude, for identical fixture plates and iNF shows the extreme values for the portfolio of tested samples γ_{cr}^{LVE} = 10.4% for C at 50°C and 44.8% for B10 at 100°C. Grafts have intermediate values of the γ_{cr}^{LVE} . In fact, butyl rubber, such as sample C, is known for its poor adhesion to metal surfaces. On the contrary, polybutadienes, including sample B10, are expected to stick to the fixture plates very well. This might suggest that γ_{cr}^{LVE} could be a function of the graft composition (w^b). However, no correlation was found between the graft composition and γ_{cr}^{LVE} .

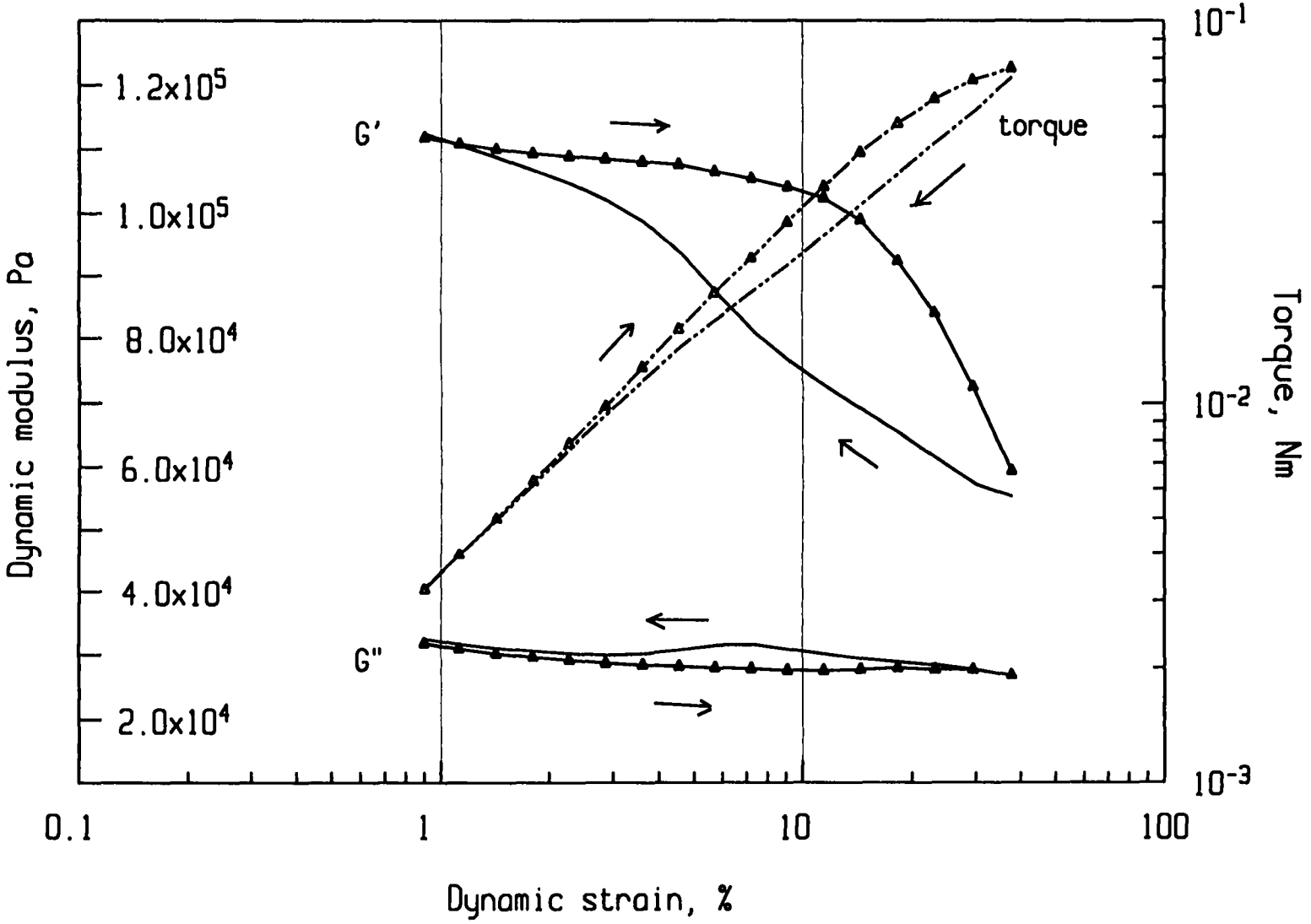
Strain history

It is well known that rheological behaviour is sensitive to the deformation/flow history of a material. This is equally applicable to the strain sweep experiments [289]. Conclusions derived from a limited study helped to improve the test procedure. As a result, each experimental point was based on data taken after an initial period of stabilization, that is after a series of oscillations applied to the specimen exclusively in order to condition it.

The main findings are presented below:

(a) In a dynamic strain sweep loop experiment - a standard (*increasing* strain amplitude) strain sweep, was immediately followed by another strain sweep, applied to the same specimen but with progressively *decreasing* strain amplitude. The observed hysteresis of $G'(\gamma)$ is shown in Figure 5-13. The test configuration is reported in Table A1 of App. IV

Figure 5-13. RMS-800: strain sweep loop experiment.
T=30°C, ω=10 rad/s, sample: G6, {SS6}.



under test code {SS6}. Lines with symbols, corresponding to the experimental points, indicate the first subtest (one with increasing strain amplitudes). A rather dramatic difference between the two consecutive strain sweep subtests was observed, particularly for the storage modulus, G′.

(b) Another 3-subtest, small-large-small strain amplitude experiment {SS7}, is an equally effective demonstration of the shear history influence on the rheological response, as shown in Figure 5-14. Transition from the small (LVE) strain to a larger strain amplitude sinusoidal oscillations reduces storage modulus dramatically, while slightly increasing the loss modulus. However upon restoration of the strain amplitude to its previous level, dynamic moduli did not return to their initial values. The effect of large-amplitude oscillations is particularly pronounced for G′, being not fully reversible. G′ and G″ are both ~10% higher and both are time dependent after reduction of the strain amplitude.

A similar effect can be demonstrated on stress relaxation modulus recovery, as discussed in subsection 5.2.4.3.

Some portion of the storage modulus G′(γ) decrease with increasing strain, often most of it, is related to genuine material properties and marks the transition from the linear to the non-linear viscoelastic (LVE --> NLVE) behaviour.

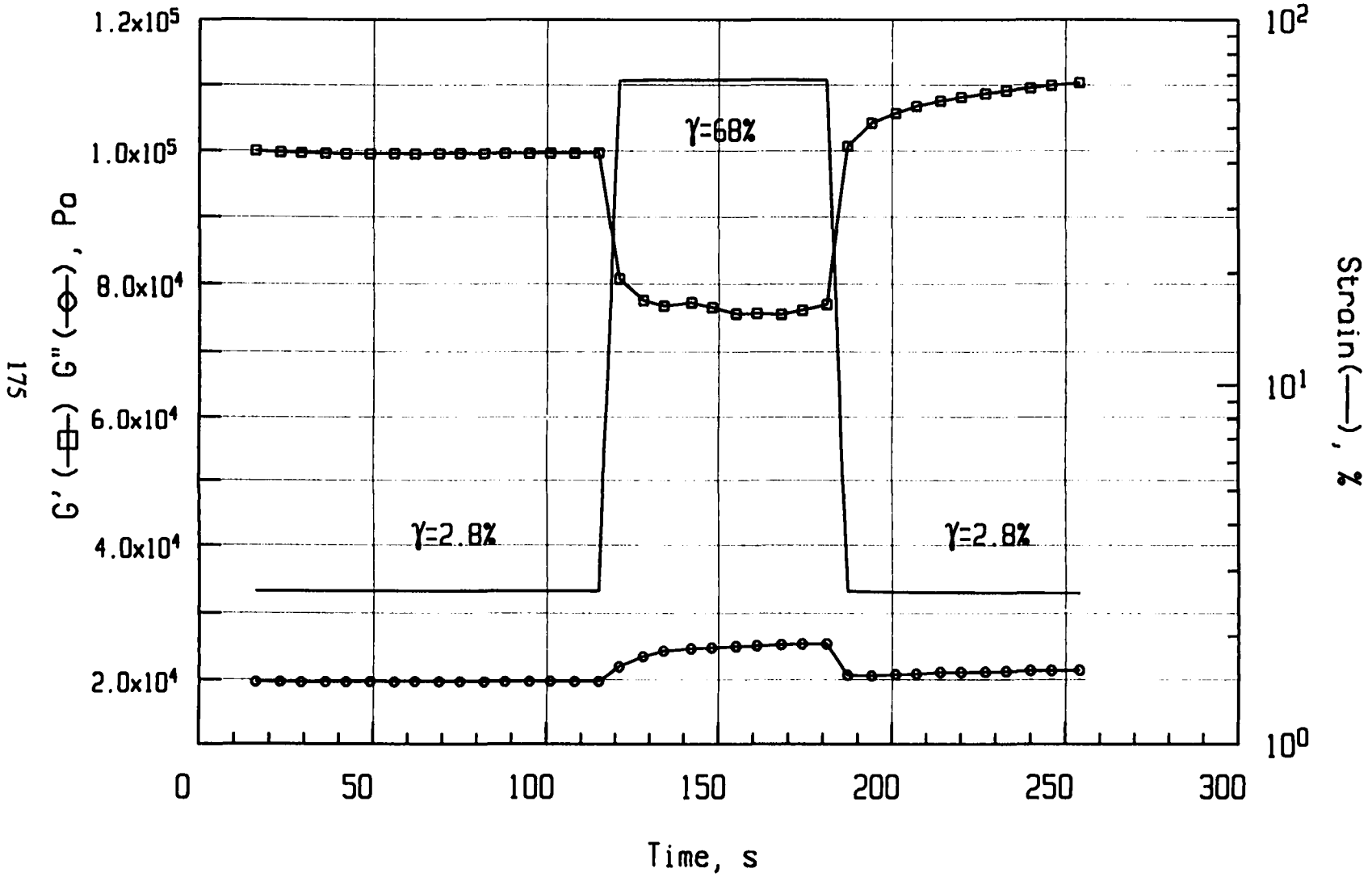
Limits of the LVE behaviour in the context of LCB structure

Based on results obtained, the following qualitative conclusions can be drawn regarding relations between the LCB parameters and the critical strain γ_{cr}^{LVE},

(1) Extending branch length, M^b at comparable branching number, N_g , reduces γ_{cr}^{LVE},

$$\mathbf{M^b \uparrow \ @ \ N_g \approx constant \ \Rightarrow \ \gamma_{cr}^{LVE} \downarrow}$$

Figure 5-14. RMS-800: small-large-small strain experiment.
T=30°C, ω=10 rad/s, sample: C, {SS7}.



(2) Increasing branching number, N_g at comparable branch length, M^b, reduces γ_{cr}^{LVE},

$$\mathbf{N_g \uparrow @ M^b \approx constant \Rightarrow \gamma_{cr}^{LVE} \downarrow}$$

(3) For grafts of comparable composition (e.g. of comparable $M^b \cdot N_g$) decreasing branch length M^b with a corresponding increase of the branching number N_g reduces γ_{cr}^{LVE},

$$\mathbf{(M^b \downarrow \ \& \ N_g \uparrow) \ @ M^b \cdot N_g \approx constant \Rightarrow \gamma_{cr}^{LVE} \downarrow}$$

and,
$$\mathbf{(M^b \uparrow \ \& \ N_g \downarrow) \ @ M^b \cdot N_g \approx constant \Rightarrow \gamma_{cr}^{LVE} \uparrow}$$

(4) Consistent with observations (3) and (4) the effect of branching frequency seems to be prevailing over the length of the branch, as far as the effect of LCB architecture on the LVE limits is concerned.

The above conclusions were derived from a series of strain sweep experiments at 30°C, ω=3 rad/s, using flat fixture plates and applying iNF of 100G. No comparable results for comb-type branched (co)polymers could be found in the literature.

Limits of the LVE behaviour - effects of the temperature and frequency

In terms of the temperature and frequency effects on γ_{cr}^{LVE}, the following observations can be made:

- effect of temperature

1) Within the 25°C - 130°C range, only a small effect of the temperature on the γ_{cr}^{LVE} could be noticed. An increase in temperature slightly increases the γ_{cr}^{LVE},

$$\mathbf{T \uparrow @ \omega \approx constant \Rightarrow \gamma_{cr}^{LVE} \uparrow}$$

This is consistent with both findings reported in the literature [289] and as well as similar relations for the non-branched polymers [290].

- effect of oscillation frequency

2) The γ_{cr}^{LVE} gradually decreases with increasing frequency of oscillation. The effect appears to be stronger for elastomers with a lower branching number or with shorter branches, which is consistent with similar reported observations [289]. Frequency-dependence of the critical shear strain for the polystyrene-star-(polyisoprene)$_2$ and PS-star-PI-star-PBd graft co/terpolymers was investigated also by Floudas and coworkers [291]. They also found that increasing frequency ω decreases γ_{cr}^{LVE}. This effect of LVE reduction by increasing oscillation frequency can be expressed as:

$$\omega \uparrow \ @ \ \mathbf{T = constant} \Rightarrow \gamma_{cr}^{LVE} \downarrow$$

Practical implications of the γ_{cr}^{LVE} assessment

Regardless of the true origin or causes of the storage modulus "strain thinning" , the apparent value of the critical strain γ_{cr}^{LVE} will serve as an upper limit of the dynamic strain amplitude for all linear dynamic tests. Based on strain sweep test results for various combinations of other relevant test parameters (including frequency and temperature) and for all samples, the nominal value of dynamic strain has been established at 5%. This single strain amplitude commonly applied to all samples, is sufficiently below the lowest γ_{cr}^{LVE} observed, while large enough to secure a strong transducer signal.

Note on strain sweep test precision

Test precision of the γ_{cr}^{LVE} measurements was assessed from multiple determinations of {SS2} and {SS4} test configurations. As an example, at the intermediate frequency (ω=3 rad/s) the average coefficient of variation, c.v.% was 6.8%. This level of test precision may contribute to the difficulties in deriving a quantitative relationship between the structural parameters and γ_{cr}^{LVE}.

5.2.4.3 Stress relaxation

There were two objectives for using stress relaxation, following a sudden step-strain in shear, as a part of the preliminary testing.

1. To verify that the imposed strain amplitude is within the LVE limits, and
2. To confirm the feasibility of designed property parameters, given instrument capabilities.

This involves at least three important issues:

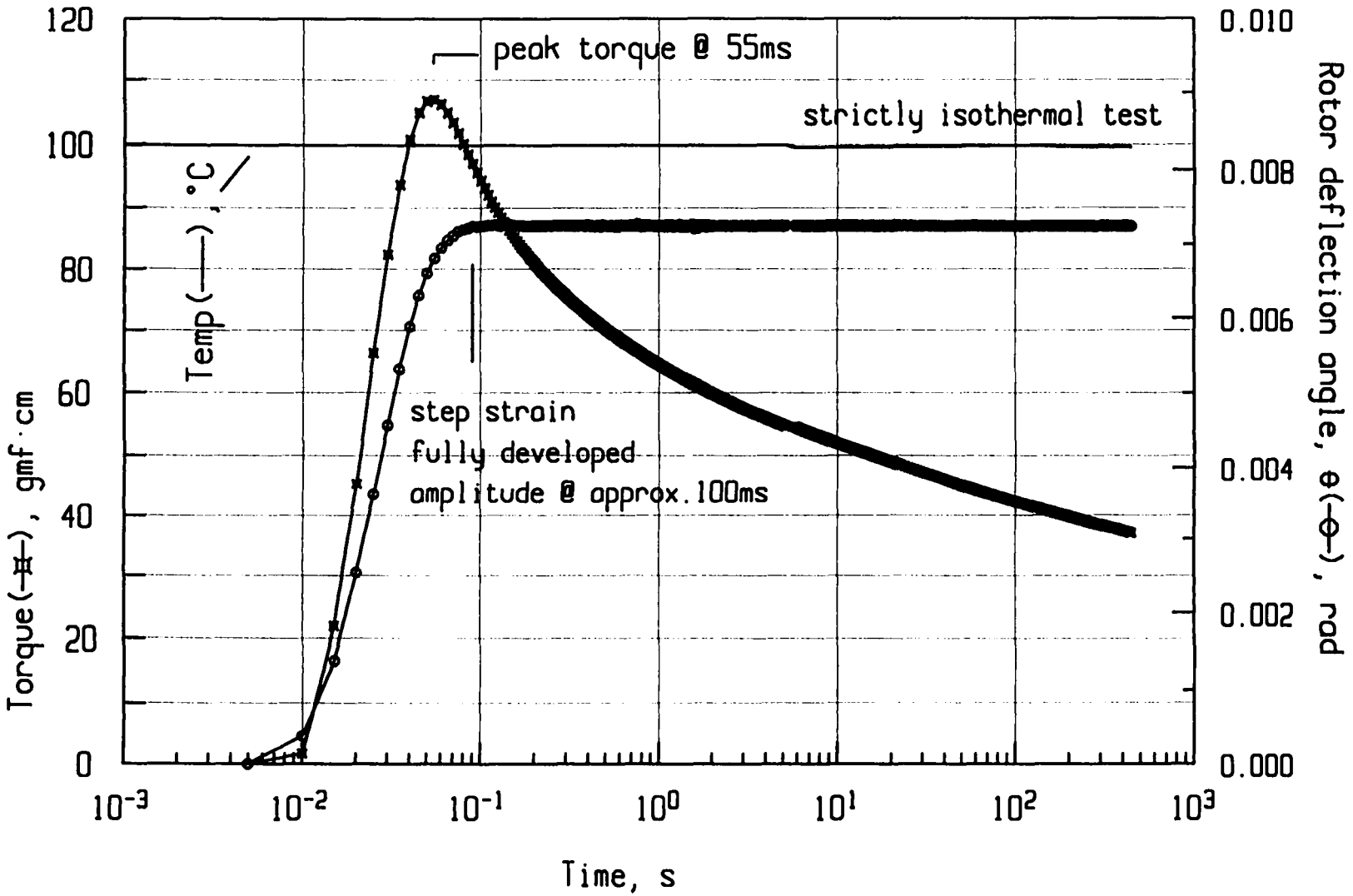
a) whether the stress level induced by the strain application is well within the capabilities of both the driving system (actuator) and the transducer,

b) whether the actual strain amplitude is closely (>90%) approximating the nominal (demanded) strain amplitude, given the finite compliance of the instrument, and

c) whether the stress relaxation monitoring time is appropriate to prevent interpretation of the torque level being below the accepted level, in terms of material properties.

The typical torque decay related to the stress relaxation experiment is shown in Figure 5-15. Due to instrument inertia, it takes nearly 100 ms for the rotor to deflect fully to a position corresponding to the commanded strain (i.e. 10%). By this time, the torque profile has passed its peak (at about 55 to 60 ms) and is on a strong decay curve. It is reasonable to assume that the lower limit for the stress relaxation monitoring using the RMS-800 is 100 ms. The G(t) at 100 ms will be used as the reference value for the normalization of the stress relaxation modulus.

Figure 5-15. RMS-800: anatomy of typical stress relaxation experiment.
T=100°C, γ=5%, sample: G9, {SR400@5%}.



The results of preliminary tests helped to establish the final stress relaxation test program. Particular attention was given to determination of suitable strain amplitude. Figure 5-16 shows the effect of strain amplitude on the relaxation modulus, G(t).

A series of consecutive stress relaxations {PSR}, at progressively increasing strain amplitudes, demonstrated that the upper limit of linear viscoelasticity is between 25% and 35%. This value compares well with γ_{cr}^{LVE} = 27.5% obtained for the same sample by a dynamic strain sweep. Stress relaxation activated by a very low amplitude torsional displacement corresponding to 3% and 5%, gave 'noisy' relaxation profiles, which at longer relaxation times tend to "bend upward", clearly an instrumental artifact.

Figure 5-17 illustrates the process of estimation of the limiting strain amplitude. Data from the same experiment {PSR} were used.

The effect of strain history on the results of the stress relaxation test is demonstrated by means of a simple test {SSR}, the results of which are shown in Figure 5-18. A series of consecutive step-shear-strains, each followed by the 1000 s relaxation period, were applied *on the same specimen.* The first stress relaxation curve differs appreciably from the second and subsequent curves. This result is interpreted as evidence of a virgin (never before deformed) sample sensitivity to strain history. This effect has been confirmed for other samples and will be investigated more thoroughly in chapter 7.

5.2.4.4 Other preliminary issues and tests

In addition to tests discussed in previous subsections, the following issues were addressed, as a part of the preliminary experimental sessions. The conclusions helped to refine both the

Figure 5-16. RMS-800 stress relaxation: effect of strain amplitude.

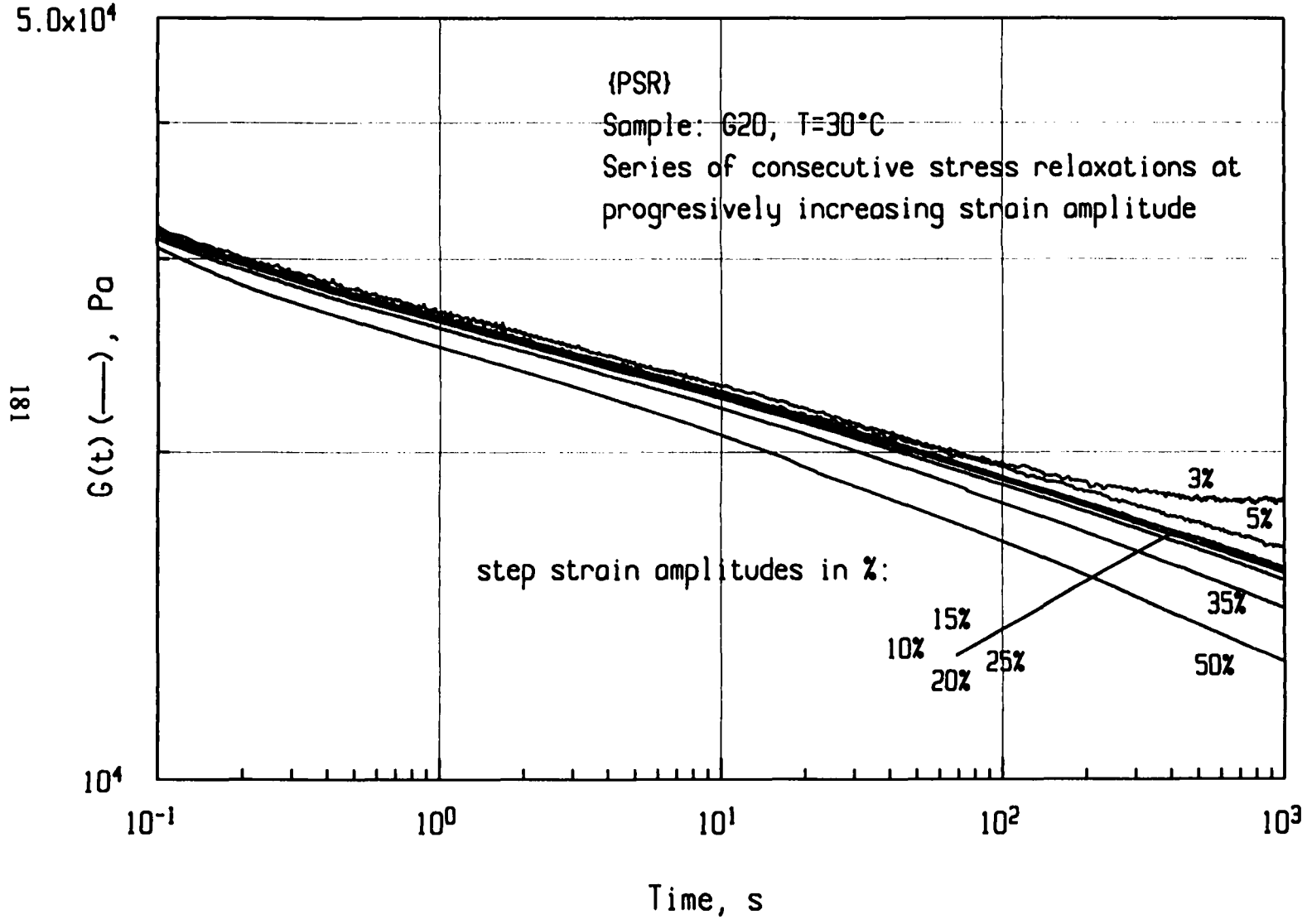


Figure 5-17. RMS-800 - stress relaxation: determination of the LVE limits. T=30°C, sample G20, {PSR}.

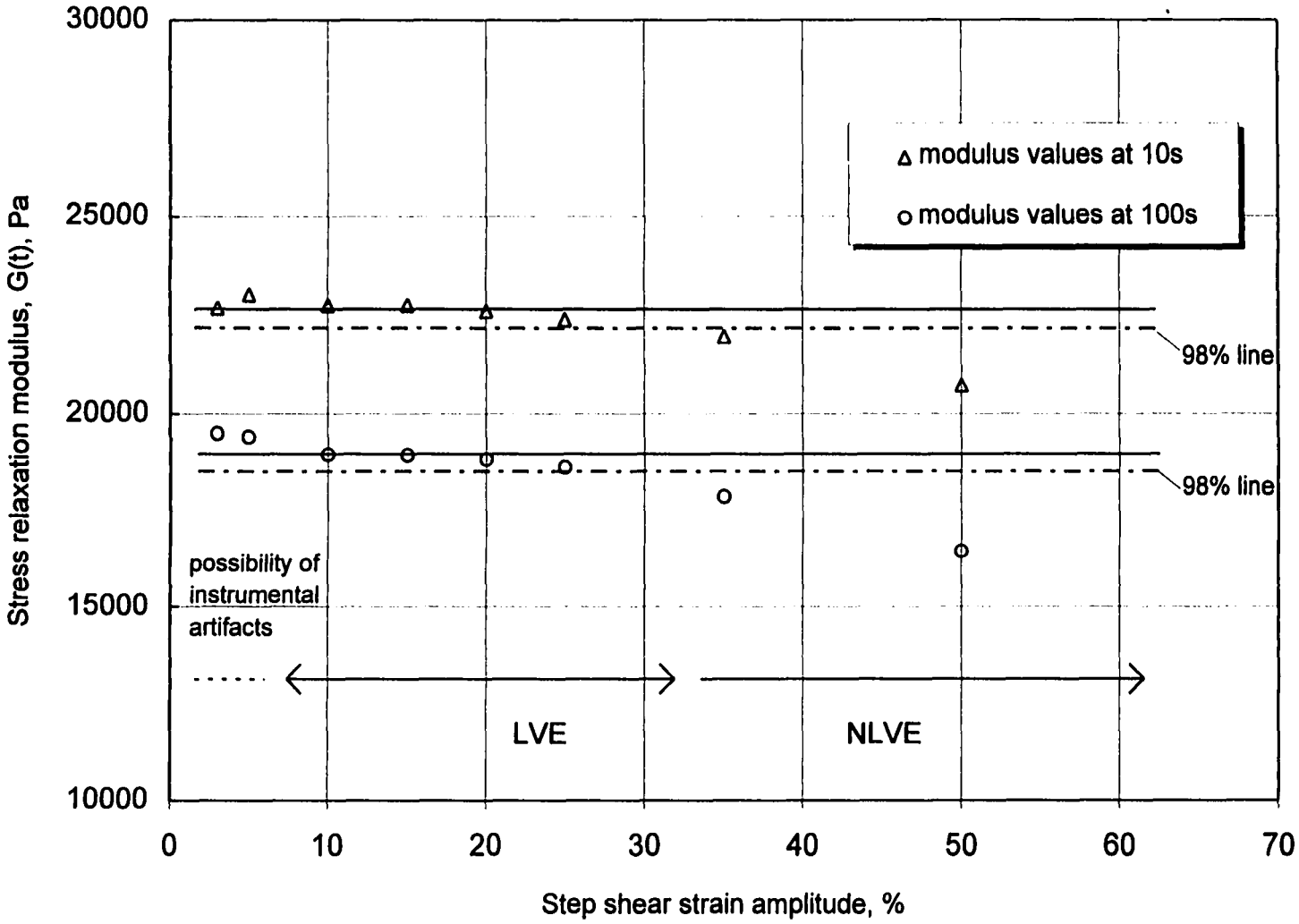
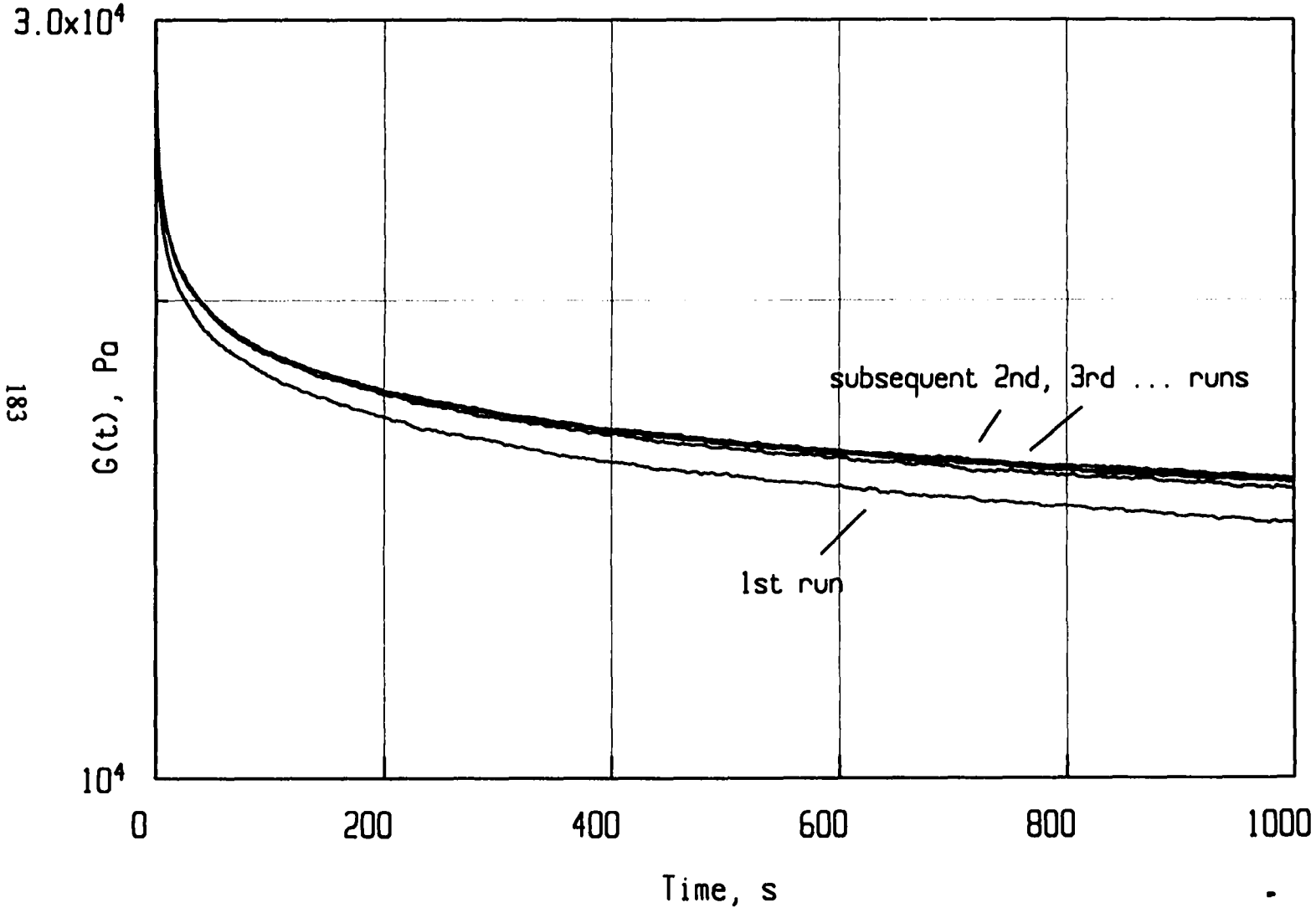


Figure 5-18. RMS-800: sequential stress relaxation experiment.
T=30°C, γ =10 %, sample: G20, {SSR}.



program and test conditions for the main experimental program, as well as helping in the interpretation of test results.

1. *Casting versus moulding of test specimens*

The CIIR (sample C) , BR (sample B10) and some graft samples with shorter branches could be moulded to give specimens suitable for rheological testing. These were compared with specimens identical in size which were cast from a solution. A marginal difference in modulus was found, but no difference in terms of the modulus-frequency dependence.
Moulded specimens provided slightly better test precision than cast specimens. However, because most of the grafts were not mouldable under conditions which would not have a possible impact on their viscoelastic properties, only the cast specimens were used.

2. *Effect of post-mounting specimen preparation*

Specimens were cut as 30.0 mm diameter thin disks. It was found to be beneficial for test precision to leave the outstanding ring intact as opposed to trimming it manually in order to match the diameter (25.0 mm) of the plate of the fixture.

3. *Effect of specimen thickness and of folding-up several layers of film*

No significant effect has been observed. (A change in the average value of γ_{cr}^{LVE} due to any given variation in the experimental set-up, exceeding a double standard deviation, i.e. 2σ of the γ_{cr}^{LVE} value obtained from multiple determinations at the identical experimental conditions, would be considered significant).

4. *Effect of the initial normal force (iNF) imposed by the fixture plates on a specimen*

Positive (compressive) normal (perpendicular to the specimen face) force is necessary to secure adhesion between plates and specimen, thereby satisfying a principal prerequisite of a

reliable dynamic test. Nonetheless, shear moduli were shown to be affected by this force and its consistent application at the beginning of the test and a strict timing of the test sequence was essential.

5. *Effect of fixture plate surface*

During preliminary measurements, smooth, sand-blasted surfaces of the plates contacting the specimen were found to give more consistent results than grooved or cross-hatched plates and subsequently were used exclusively.

5.2.5 Test interferences and data validation

Due to the potential for experimental interferences, a systematic and consistent scrutiny of raw experimental data, along with careful monitoring of the experiment, is an essential element of a reliable rheological characterization.

Test and result validation items address all critical aspects of the experiment which have a high potential to affect data negatively, as proven by past experience, and are very specific to the instrument, test method and procedure used, as well as the type of materials characterized.

A properly maintained and up-to-date calibration was a prerequisite of any experiment.

(a) examination of the specimen before and during loading onto the fixture,
(b) observation of the test, the specimen during the test and the instrument for warning signals,
(c) examination of raw experimental data to verify validity of the test,
(d) examination of tested specimen,
(e) check of control samples run in series with the test samples.

The following are a few examples of the "check-points" applicable to the dynamic mechanical testing in torsion, using a parallel-plate fixture installed on the RMS-800:

(a) an acceptable specimen in terms of its shape, dimensions and lack of visible inclusions (i.e. air bubbles),
(b) monitoring of the 'Normal Force indicator' for correct gap adjustments due to thermal expansion/contraction of the specimen during heating/cooling,
(c) torque for each experimental point to be valid within transducer specifications (2 - 2000 g·cm),
(d) actual imposed strain amplitude within 80% of its commanded value,
(e) lack of any sudden shifts in data curves or scattered experimental points,
(f) tested specimen free of any distortions, foaming and signs of degradation, etc.

Important test validation items specific to stress relaxation tests are:

1. constant spacing between plates and fully isothermal conditions during the entire relaxation time,
2. torque profile during a step strain application, not indicative of transducer overload, or specimen slippage.

Only data which passed these examinations are presumed to be free of large or systematic errors and would be further analyzed and interpreted.

5.2.6 Test accuracy, precision and sensitivity

Proper attention paid to the accuracy and precision of rheological measurements increases their reliability. However, until recently [292-293] this issue was seldom explicitly treated in the context of rheological characterization of materials and even now little attention is being paid to these issues in the rheological literature.

Accuracy

The accuracy of measurement is defined as "the closeness of agreement between a test result and the accepted reference value", if referred to a single experimental result. For a series of test measurements, the average value is to be compared with a reference value and the term 'trueness' is recommended. [294]

Due to the lack of suitable standards for dynamic mechanical testing, assessment of the accuracy with which viscoelastic properties are measured is impossible. However, an indirect method using Cannon viscosity standards (PDMS) for the RMS-800 operated at a steady shear and at a low shear rates has been conducted and showed discrepancy between reference values and measured within 5% [295]. Practice shows that a strict adherence to the detailed test procedures on a periodically calibrated and well maintained instrument, gives consistent results on control samples. This is frequently accepted as a substitute for a check using standards. For the purpose of comparative studies, emphasis on the elimination of potential causes of systematic errors (bias) rather than an estimation of their magnitude appears to be an appropriate strategy.

Precision

Precision can be defined as: "the closeness of agreement between two or more independent tests obtained under stipulated conditions" [296]. Stipulated test conditions consistent with the character of this research mean: "conditions where independent test results are obtained with the same method on identical test items in the same laboratory by the same operator, using the same equipment within a short interval of time" [296]. These conditions are sometimes referred to as 'short-term repeatability' conditions.

This is an issue of great importance to any structure-property studies because it refers to the statistical significance of the difference between any two measurements (or means of two series of measurements). In the case where inhomogeneity of a material under study may contribute to the scatter of experimental data (and thus to decrease the test precision), no substitute for multiple determinations exists in order to estimate the test precision properly. This would imply that any nominal test precision derived from previous tests conducted under identical conditions but carried-out on different materials may not be applicable.

Two series of experiments were conducted for the assessment of the RMS-800 test precision; one for the frequency sweep, configuration {QFS}, and another one for the stress relaxation, configuration {QSR}. Both tests were carried out using randomized sampling. No suspected outliers were identified and the data were validated according to a common procedure outlined previously. The number of replicates varied between 6 and 8 per sample and has been carried out on all samples ({QFS}) or on a few randomly selected samples ({QSR} test).

Sensitivity

The notion of 'sensitivity' can be useful to identify those characteristics (further referred to as rheological parameters) of rheological properties which are most sensitive to the LCB parameters of molecular architecture [297-298].

For n determinations of a parameter X, for each of m samples, sensitivity, SE, of a *given rheological parameter X,* is defined as the ratio of the standard deviation $S(\bar{x})$ of the average values $\bar{x}_j$, to the geometric average $\bar{s}_x$ of the standard deviations s_j of the same parameter.

$$SE = S(\bar{x}) / \bar{s}_x \text{ , where} \qquad (5 - 1)$$

$$S(\bar{x}) = \sqrt{\frac{\sum_{j}^{m} (\bar{x}_j - \tilde{x})^2}{m-1}} \qquad (5-2)$$

$$\bar{s}_x = \sqrt{\frac{\sum_{j}^{m} s_j^2}{m}} \qquad (5-3)$$

$$s_j = \sqrt{\frac{\sum_{i}^{n} (x_{ij} - \bar{x}_j)^2}{n-1}} \qquad (5-4)$$

x_{ij} - value of the i-th measurement (of a given parameter, X) for the j-th sample,
$\bar{x}_j$ - average value of n-determinations for the j-th sample,
s_j - standard deviation of n measurements for the j-th sample,
$\bar{s}_x$ - geometric average of the standard deviations of all (m) samples
$\tilde{x}$ - (arithmetic) average value of all (n·m) measurements of the parameter *X*.

Alternatively, the difference between the largest and the smallest measured value can be used in place of the standard deviation in all above formulae.

It is intuitively clear that the higher the test method sensitivity (i.e. *SE* number), the better is its ability to differenciate between samples in terms of the relevant rheological property and the underlying differences in molecular structure or composition. In fact, the *SE* has been calculated for a number of parameters which can be defined for a given rheological function and only those with the high *SE* values were selected for further quantitative correlation with the LCB parameters. A $SE > 1$ is necessary to render any value of a test method for the purpose of structure - property relationship, and practically $SE > 4$ is desired, depending on the test method precision.

In the context of dynamic testing, examples of rheological parameters include: the cross-over modulus, G_c (ω_c) = G'(ω=ω_c) = G"(ω=ω_c), the plateau modulus, G_N^0 , the slope of the loss modulus in the terminal zone, or the zero shear viscosity, η_0.

Precision -{QFS} test results

Results of the {QFS} routine are summarized in Table 5-4. Reported values are averaged over the 0.1 - 100 rad/s frequency range and the whole population of samples.

Table 5-4. Test precision results for RMS-800 dynamic mechanical test.

TEST	Function	Avg. c.v.%
{QFS}	storage modulus, G'	5.0
-"-	loss modulus, G"	6.0
-"-	tan δ	1.5

Specific values of the c.v.% depend on oscillation frequency and also may vary considerably from sample to sample. Typically, precision of dynamic moduli for strain-controlled rheometers increases with the frequency and this is in agreement with other published results [293]. For the purpose of quantitative correlations between selected rheological and structural (LCB) parameters, sample and frequency specific values of the standard error (based on c.v.%) will be used.

On average, precision results obtained for grafts are slightly worse than whose obtained on control samples (PDMS and IIR), for which c.v.% was 3 - 4 %, for either G' or G", and about 1% for the tan δ [295]. Those differences can be partly attributed to greater irregularities in

the shape of cast specimens, as opposed to the molded standards. Difficulties in retaining a consistent level of the normal force (iNF) on the much more resilient grafts might also be a factor. Figure 5-19 shows the results of a typical {QFS} test, with all experimental points shown as symbols (short dashes). The continuous lines represent the average and interpolated values.

Precision - {QSR} test results

Results of this study are summarized in Table 5-5. The average c.v.% values obtained on all tested samples are quoted.

Table 5-5. Test precision results for the RMS-800 stress relaxation.

Time, s	Avg. c.v.%, G(t)	Avg. c.v.%, nG(t)
1	2.0	1.1
10	2.7	1.5
100	4.1	2.3
1000	11.8	6.7

Analogously to dynamic data, specific values of the c.v.% vary from sample to sample, but variations are small enough, particularly for normalized stress relaxation modulus, nG(t), to permit adoption of the average c.v.% as representative for all samples. The c.v.% of the G(t) steadily increases as a function of the relaxation time. Figure 5-20 illustrates this dependence for sample C, taken as an example.

Furthermore, the stress relaxation modulus at the longer relaxation times can be dramatically affected by errors associated with a very low torque signal. Figure 5-21 illustrates a dramatic decrease of the test precision at the relaxation times long enough for the torque to fall below a certain threshold level (data from experiment {SR1}).

Sample C at 100°C was selected as an extreme (worst) case, where data from a test designed to last 1000 s had to be truncated above approx. 150 s, in order to meet pre-set test precision criteria. The normalized stress relaxation modulus, such as nG(t), was found to be consistently more precise then any absolute stress relaxation function derived from the same experiment.

Figure 5-19. RMS-800: dynamic test precision.
T=100°C, sample G16, γ=10%, Stat.: 6x, {QFS}.

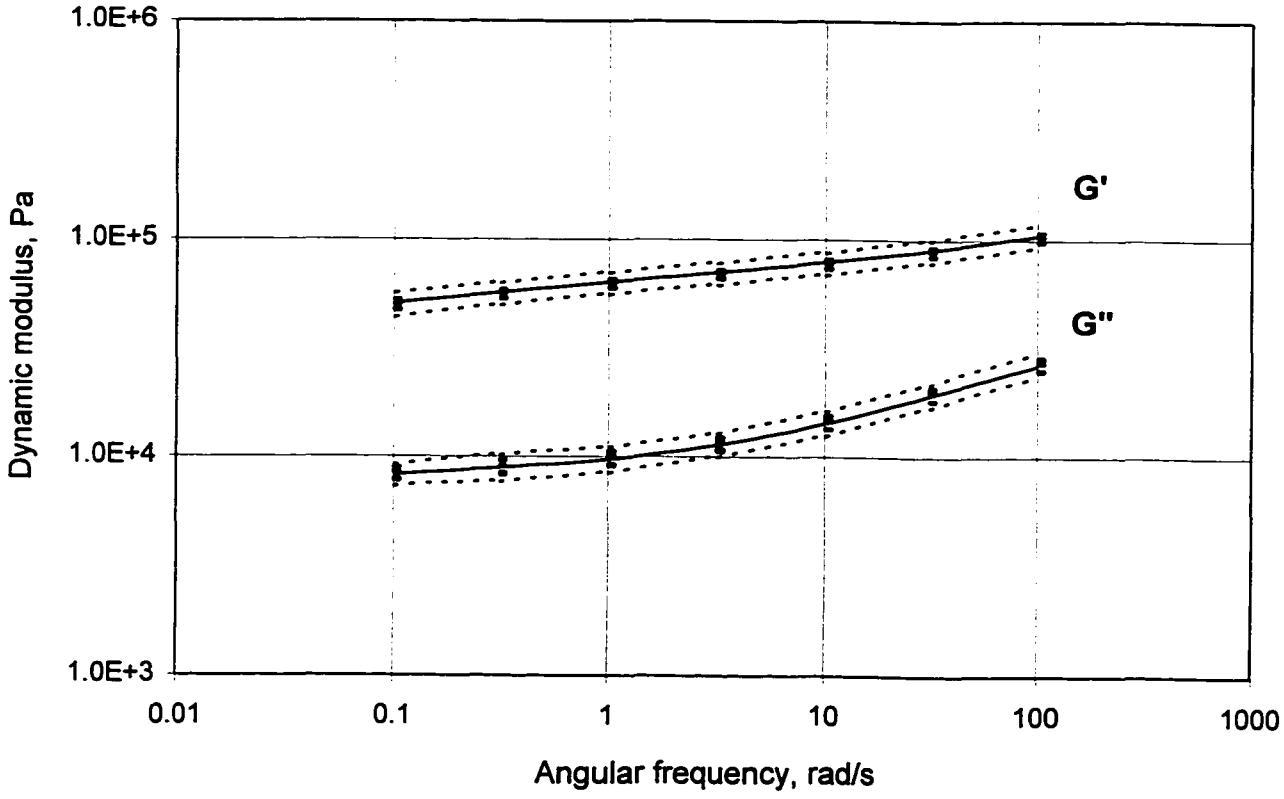


Figure 5-20. RMS-800: stress relaxation - test precision.
T=30°C, γ =5 %, sample: C, 6 determinations/sample,{QSR}.

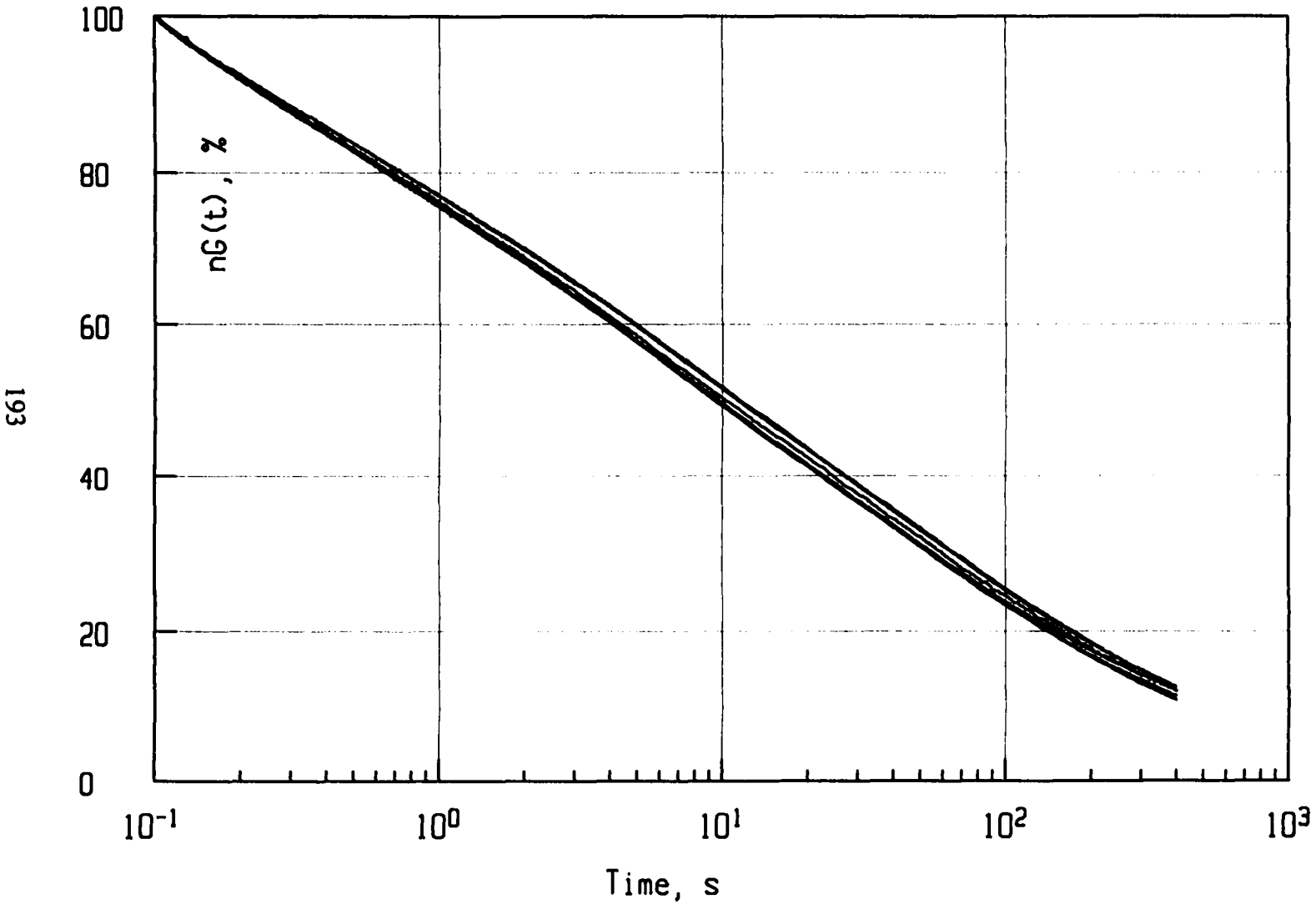
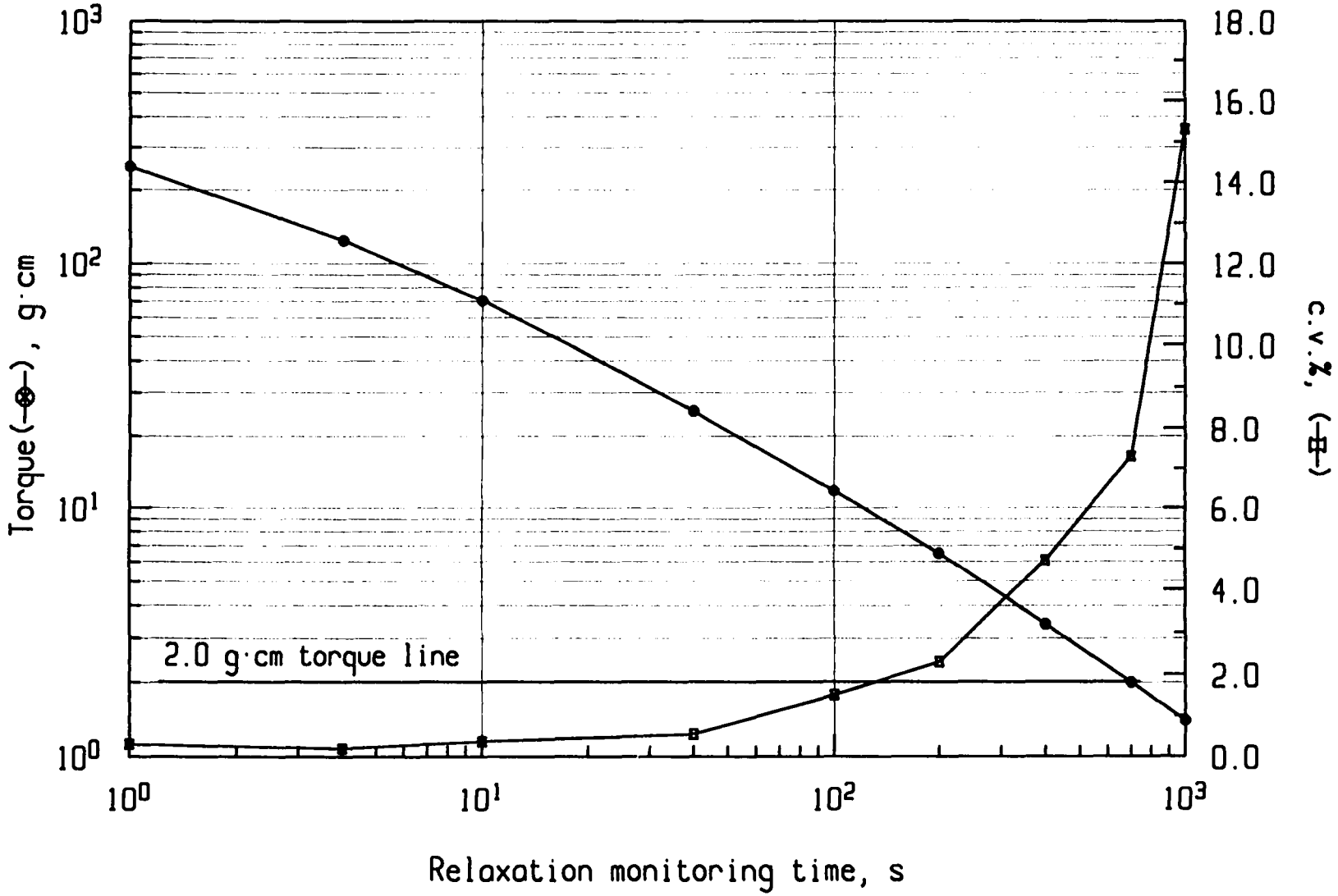


Figure 5-21. RMS-800: relation between torque decay and test precision.
G(t)/G(t=0.1s), T=100°C, γ =10 %, sample: C.



5.3 Rheometrics Solids Analyzer, RSA-II

5.3.1 Principle of operation

Rheometrics Solids Analyzer, model RSA-II is another example of a versatile, strain-controlled mechanical spectrometer, designed for evaluation of the viscoelastic properties of a wide range of materials, particularly those having a solid form at the test temperature. Similarly to the RMS-800 spectrometer the main test station consists of three main components: actuator, transducer and environmental chamber. The whole system is controlled by a dedicated PC unit, which synchronizes the operation of the various components and processes experimental data received from the test station [299].

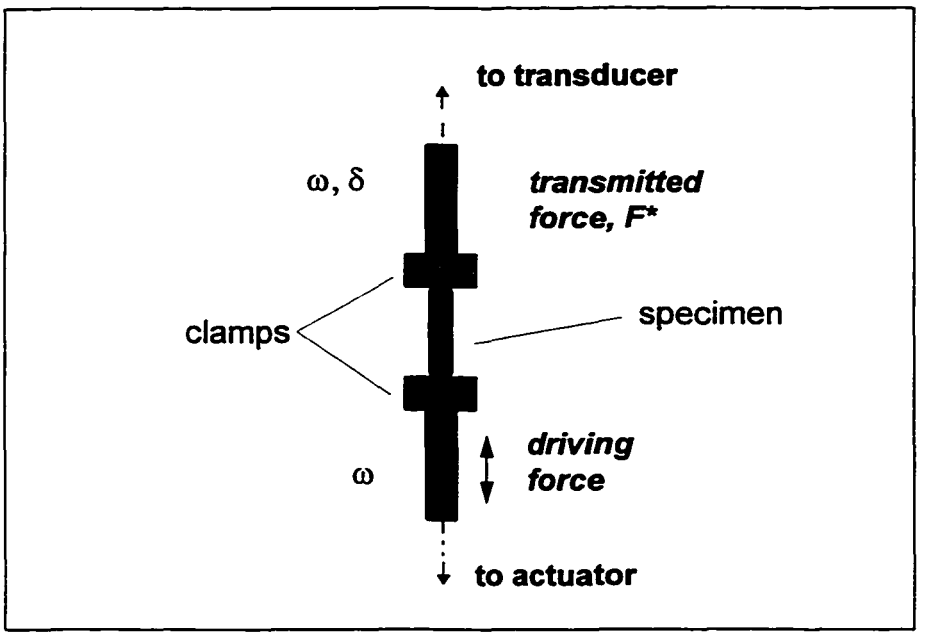
Each of the test fixtures available for the RSA-II is designed to transform linear motion of the actuator into well defined deformation of the specimen. Depending on the type of fixture, deformation can be applied in one of the following ways: tension, shear, compression and 3-point or dual-cantilever bending. The film/fiber fixture proved to be particularly suitable for testing elastomers and rubber vulcanizates over a broad range temperatures and was selected to be used in this project (Figure 5-22).

Available test modes include oscillatory, transient and steady state.

Both the RMS-800 and RSA-II share the same methodology, software (RHIOS & RHECURVE) and terminology. As a result, much of the comment included in previous sections devoted to the RMS-800 would be applicable here, and usually will not be repeated.

In this project, only the temperature dependence of some of the linear viscoelastic functions in tension (E′, E″, tan δ) was examined.

Figure 5-22. RSA-II film/fiber test fixture.



In this configuration, the actuator applies a small amplitude oscillatory tensile strain, which is superimposed on appropriate 'static' tensile strain (so-called 'pre-tension') necessary to avoid buckling of the thin specimen during each compressive phase of the sinusoidal oscillations. A transducer measures specimen response - magnitude and phase angle of the transmitted force - which combined with the dimensions of the specimen yields storage (E′) and loss (E″) moduli of the material and their derivatives (tan δ, complex viscosity, etc.).

5.3.2 Specimen preparation

Specimen preparation for RSA-II (film/fiber fixture) is similar in many respects to that described for the RMS in subsection 5.2.2. The main differences are:

a) specimens were cut in the exact shape and dimensions required directly from a dry polymer film (without plying them up),

b) specimens were in the form of rectangular strips, 4.0 mm wide, approximately 30 mm long (nominal length) and of uniform thickness, usually in the range of 0.7 to 1.0 mm. The thickness of each specimen was measured at several equally spaced points along the length, by a constant-force gauge (± 0.01 mm). The average value was accepted as the thickness of specimen, provided that the difference between extreme readings was less than 5% of the specimen average. The exact distance between clamps was taken as the actual specimen length - typically in the order of 23.0 mm. Any changes in specimen dimensions during a test, due to a thermal expansion or shrinkage, were automatically corrected for. Every precaution was taken not to stretch a tiny specimen during its preparation and loading.

5.3.3 Experimental program

The experimental program for the RSA-II spectrometer was of one type: the temperature sweep during which temperature was programmed to increase within a range and the frequency of oscillations was kept constant while the strain amplitude was allowed to vary within the LVE limit to accommodate for the rapidly changing modulus of the tested material. All test parameters, after being fine-tuned during preliminary trials, were kept the same for all samples. A summary of test conditions is given in Table 5-6, while a complete set of test parameters {DTMA}, is included in Table B, Appendix IV.

The temperature range was dictated by the principal objective of this study to fully encompass the transitions corresponding to either component of the graft copolymer.

Table 5-6. Summary of test conditions for temperature sweep (DTMA).

Test parameter	Nominal value	Units
Temperature range:	-100 to +20 /*	°C
Oscillation frequency:	70	rad/s
Temperature increments, DT:	2	°C
Initial dynamic strain:	0.5	%
Automatic adjustment of dynamic strain	active	—
Automatic adjustment of static pre-tension	active	—

/* - for some samples the temperature range had to be modified, see Table B, App. IV for details.

5.3.4 Preliminary experiments

Dynamic thermo-mechanical analysis (DTMA) is a rheometrical technique in which dynamic moduli and damping properties (tan δ) are measured as a function of temperature under isochronal, oscillatory strains or stresses. From the experimental point of view, this is one of the more complex and difficult test routines, particularly if carried out in tension and over a wide temperature range.

Selection of the appropriate test parameters may require additional, preliminary experimentation, particularly for testing of a new type of material.

Preliminary tests, on a few representative samples, included:

(a) - a series of single-point dynamic measurements (constant γ, ω, and T) performed at the extreme test temperatures in order to establish the best combination of strain amplitude and frequency of oscillation for the whole range of temperatures,

(b) - a few 'static strain' sweeps (simple, limited strain tensile test experiment), to define a suitable "pre-tension" imposed on a specimen prior to the cycle of dynamic strains, in order to avoid specimen buckling yet carry out the entire sweep within the capability of a single force transducer,

(c) - temperature *ramps* (similar to temperature *sweeps* except with temperature changing not step-wise but continuously) were necessary to fine-tune some of the test parameters.

1. To optimize the schedule for the 'autostrain' and 'autotension' adjustments, necessary to accommodate specimen thermal expansion and rapidly decreasing force-signal due to the 1000-fold modulus decrease between glassy and rubbery zones,

2. to set-up the optimum heating rate to avoid excessive heat degradation of the sample material while maintaining negligible thermal lag,

3. to properly allocate temperature increments, particularly for the transition zone, in order to obtain a good definition of tan δ and E" peaks.

Previous experience in testing elastomers in similar circumstances, the vendor's recommendations [299] and existing standard test conditions developed for gum elastomers [300] were the starting point for these experiments.

Conclusions drawn from these preliminary tests allowed uniform test parameters to be defined for all DTMA scans, reported in Table B, Appendix IV.

5.3.5 Test interferences and data validation

Continuous attention paid to specimen quality and condition prior to, during and after the test, a strict adherence to the test procedure, and monitoring of test execution, are essential components of reliable characterization of material properties. Validation of test results against common instrumental interferences is a prerequisite for analysis of results.

Measurement of dynamic moduli over a broad range of temperature during a single experimental run involves measurement of stresses which can vary by a factor of a thousand. This factor is comparable to a dynamic range of a force-rebalance transducer of the RSA-II unit, making the selection of the parameters a tight fit and basically an iterative process.
The significant thermal expansion coefficient of polymeric materials complicates specimen loading and necessitates appropriate corrections. Particular potential for instrumental interferences exists for such a test sequence during which a specimen is loaded at room temperature, subsequently cooled down to the initial test temperature, and then heated progressively up to a temperature high enough on the rubbery plateau to confidently capture the α transition.

The list of all potential interferences for DTMA test in tension can be extensive. A shorter list of the most relevant interferences is given in Table 5-7.

Table 5-7. Principal instrumental (RSA-II) interferences for DTMA test in tension.

Interference	Validation "check-point"
Force signal beyond transducer range	upper limit: monitoring "out-of-range" transducer indicator, lower limit: dyn. force always > 2G-force
Specimen buckling	monitoring "auto-strain" limit indicator; dynamic force always < static force for the entire temperature range; auto-strain allowance not exceeded (DL<4.0 mm)
Specimen slippage or icing	examination of G', G" (T) curves for any translations or abnormalities
Malfunctioning ("hunting") of temperature controller	examination of data for uneven distribution of experimental points
Inaccurate temperature readings	RTD and thermocouple calibration; setting heating rate sufficiently low to minimize thermal lag
Implicit strain-dependence of moduli	verification that actual dynamic strain amplitude is indeed within LVE range at any given temperature

5.3.6 Test accuracy and precision

The principles and definitions described in subsection 5.2.6. are equally applicable to the RSA-II and the other two instruments.

The nominal accuracy of temperature measurements for the RSA-II is ± 0.5°C and temperature reading resolution is 0.1°C [299]. Temperature sensors and controllers were calibrated and a proper heating schedule was implemented as described in the previous section.

The standard error associated with measurements of temperature corresponding to tan δ (T) or G″ (T) peaks has been estimated, by multiple measurements on the same samples, to be about 2°C. This result is consistent with our previous assessments [301].

For the DTMA analysis, an accurate assessment of the absolute values of moduli is considered to be of secondary importance.

5.4 Rubber Process Analyzer, RPA-2000

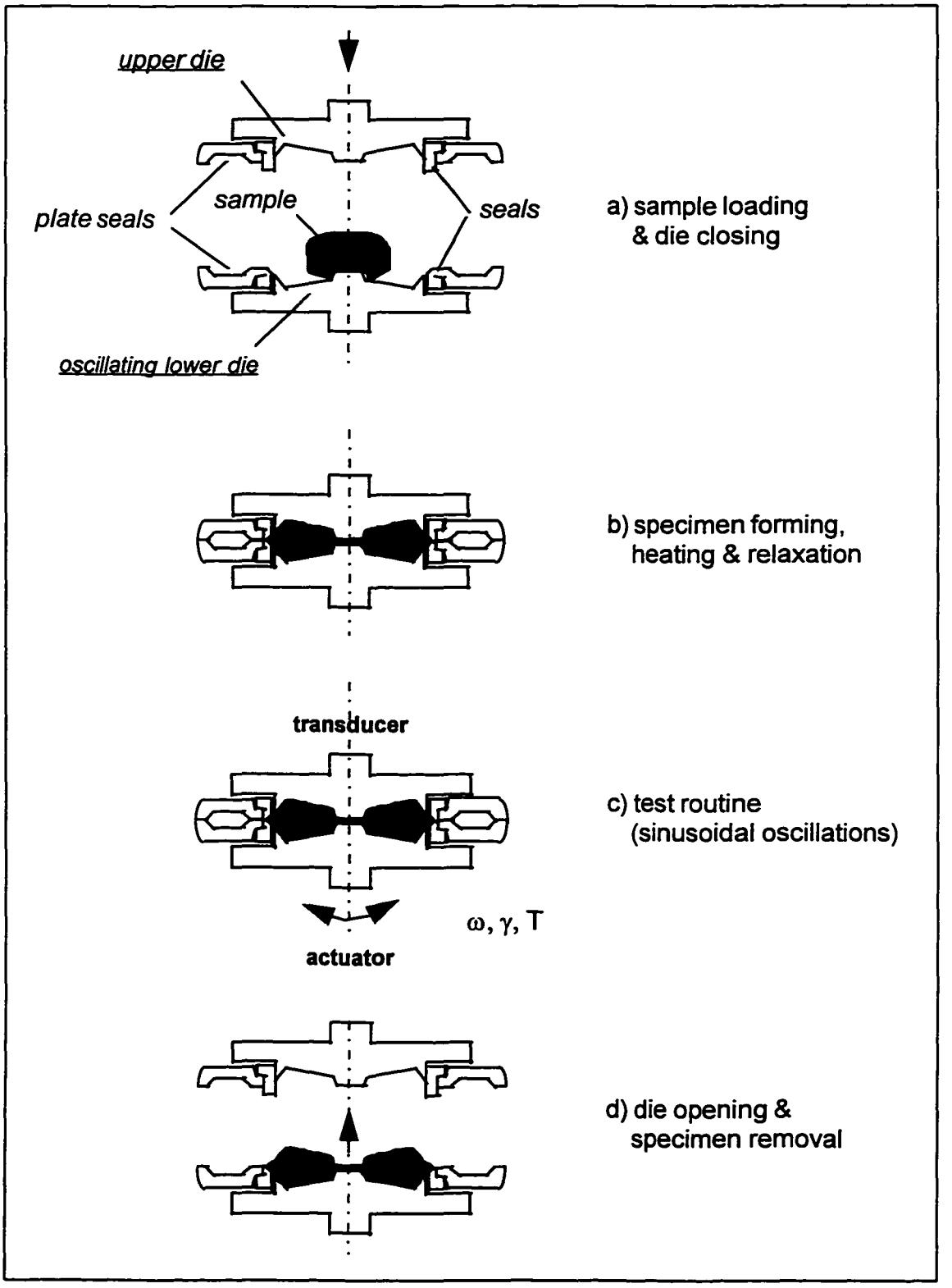
5.4.1 Principle of operation and data analysis

The Rubber Process Analyzer RPA 2000™ is a dynamic thermo-mechanical spectrometer specifically designed for testing polymeric materials in rubbery and terminal viscoelastic zones [302]. The sealed and pressurized test chamber of the instrument allows for the application of sinusoidal oscillations over a large range of frequencies, strain amplitudes and temperatures. The RPA 2000 design allows for a confident exploration of both linear and non-linear viscoelastic behaviour of unfilled gum elastomers [303].

The test cavity has a bi-conical shape to maximize radial uniformity of strain. A cross-sectional view of the test chamber and the principle of the RPA 2000 operation are shown in Figure 5-23. A mechanical actuator (driven by a stepper motor) is driving lower platen while a torque transducer attached to the upper platen measures the torque transmitted through the sample [304-305].

Computerized test sequence control and data acquisition allow for a variety of rheological experiments to be consistently executed and analyzed. Most rheological experiments consist of a sequence of a few simple routines or subtests. Principal subtests include an isothermal frequency sweep at constant strain amplitude and a strain sweep at constant frequency. Other subtests (at a constant frequency and strain) are the temperature and time sweeps, typically used to examine temperature-dependence of the dynamic moduli and thermo-mechanical stability of the material [306-307].

Figure 5-23. RPA 2000 - Principle of operation and cross-section of test cavity.



Linear viscoelastic (LVE) functions [ε]

In linear viscoelastic deformation, stress σ is proportional to strain γ. For oscillatory shear deformation of an angular frequency ω the shear strain is described by,

$$\gamma(t) = \gamma_0 \cdot \sin(\omega \cdot t) \qquad \text{where } \gamma_0 \text{ is the shear strain amplitude}$$

For a sufficiently small strain amplitude ($\gamma_0 << 1$ for polymer melts), the shear stress response $\sigma(t)$ to an oscillatory strain is also sinusoidal,

$$\sigma(t) = \sigma_0 \cdot \cos(\omega \cdot t + \delta) \qquad \text{where } \delta(\omega) \text{ is a mechanical loss angle,}$$
$$\text{and the amplitude ratio } \sigma_0 / \gamma_0 \equiv G^*(\omega)$$

$G^*(\omega)$ is a complex number and depends, at constant temperature, only on frequency.

It is customary to express the complex modulus, $G^*(\omega)$ in terms of a pair of numbers, called the dynamic moduli. The storage modulus G' and loss modulus G'' can be expressed as the product of the absolute value of the complex modulus $|G^*(\omega)|$ and one of the trigonometric functions:

$$G'(\omega) = |G^*(\omega)| \cdot \cos\delta \quad \text{and} \quad G''(\omega) = |G^*(\omega)| \cdot \sin\delta,$$

The other frequently used LVE functions include: $\tan\delta \equiv G''/G'$, complex viscosity $\eta^*(\omega) = G^*/\omega$, dynamic viscosity $\eta'(\omega)$ and out-of-phase component of complex viscosity $\eta''(\omega)$, as well as the complex, storage, and loss compliances, $J^*(\omega)$, $J'(\omega)$ and $J''(\omega)$, respectively.

[ε] Note: in this (5.4.1) section, a distinction is made between an implicitly time-dependent sinusoidal strain $\gamma(t)$ and a strain amplitude γ_0. In all other part of this work, symbol γ is used to designated the amplitude of the oscillatory strain, in dynamic experiments or step strain amplitude in stress relaxation experiments.

Non -linear viscoelastic (NLVE) functions

Large amplitude oscillatory shear (LAOS), particularly its most popular sinusoidal form, is a convenient method for studying the non-linear viscoelasticity of polymers for the following reasons [308]:

- sinusoidal mechanical oscillations are relatively easy to generate accurately,
- the strain-amplitude and the time (or frequency) scale can be varied independently,
- interpretation of results and error analysis (content of higher harmonics) are relatively straightforward.

The significance of the LAOS testing lies in at least two areas:

- interpretation of material behaviour in processing operations, which involve large amplitudes and rates of deformation/flow, therefore are predominantly non-linear,
- testing of the validity of the constitutive equations for which large-strain oscillatory shear is considered particularly discriminating [309].

For sinusoidal deformation at strain amplitudes above a certain critical value, $\gamma_0 > \gamma_{cr}^{LVE}$, both the complex modulus $G^*(\omega, \gamma_0)$ and the phase delay $\delta(\omega, \gamma_0)$ will also be strain-amplitude dependent. As a result, the stress response will not be exactly sinusoidal anymore. Consequently, rheological functions such as $|G^*|$ and $\tan\delta$ are not meaningful for non-linear viscoelastic behaviour. A few cycles after starting the oscillatory test, shear stress (or strain, depending on the type of test) becomes a standing wave, containing higher harmonics with amplitudes $\sigma_i(\omega, \gamma_0)$ and phases $\delta_i(\omega, \gamma_0)$, depending upon both the frequency and strain amplitude ('i' denotes the i^{-th} harmonic).

A periodical stress function can be described by a Fourier series of odd harmonics,

$$G(t) = \sum_{n=1,odd}^{N} \sigma_n \sin(n \cdot \omega \cdot t + \delta_n),$$

where σ_n is the shear stress amplitude and δ_n is the phase angle of the n-th harmonic. Under isothermal test conditions, σ_n and δ_n will depend on both frequency and strain amplitude. Although the traditional functions $G'(\omega)$ and $G''(\omega)$ do not have meaning for non-linear oscilatory deformations, analogous functions can be defined, one for each harmonic. The modulus for the n-th harmonic is $G_n = \sigma_n / \gamma_0$, and by analogy, the in-phase and out-of-phase modulus of the n-th harmonic are: $G_n' = G_n \cdot \cos(\delta_n)$ and $G_n'' = G_n \cdot \sin(\delta_n)$, respectively. Thus, by transforming the experimental signal into a series of harmonics and ignoring higher terms, a good approximation of the non-sinusoidal response can be achieved.

This approximate method of non-linear stress response analysis, based on a Fast Fourier Transform Algorithm, has been adopted for the data analysis in the RPA 2000 analyzer [310].

5.4.2 Specimen preparation

The RPA 2000 does not require specimens to have any particular shape. However, specimen shaping resulting in spheroidal or circular shape might improve test precision [311]. Depending on the specific gravity of the material, about 4 to 6 grams is required to fill the test cavity (4.5 cm^3), allowing for a controlled overflow. All samples used in this project had comparable density, and 5 ± 0.2 g for each specimen was consistently used.

5.4.3 Experimental program and test conditions

For this project the RPA 2000 analyzer has been used with the following objectives:

1. To characterize viscoelastic properties in the LVE range and compare results to those obtained by the RMS-800,
2. To investigate the transition from the LVE to NLVE behaviour, and primarily,
3. To explore non-linear viscoelastic behaviour through a variety of large-strain amplitude experiments.

The RPA 2000 characterization program, taking advantage of the unique capabilities of the instrument, focused on the investigation of non-linear viscoelastic properties. All tests were carried out under isothermal conditions at 100°C. The exact test conditions and parameters are listed in Table C, Appendix IV.

The following is a brief description of test configurations, accompanied by diagrams in Figures 5-24a to 5-24d.

a) *Low strain amplitude frequency sweep* - {FSWP1} & {FSWP2} consist of two tests in sequence, (Figure 5-24a)

(I) - time sweep, common to all RPA test configurations at the standard strain $\gamma = 2\%$ and frequency $\omega = 1$ rad/s, designed as a consistency check, followed by,

(II) - frequency sweep at $\gamma = 5\% = \text{const.}$ and covering a range of frequencies (0.2 - 200 rad/s).

This test was designed to measure the viscoelastic behaviour of the grafts in the LVE range and is, in principle, comparable to the RMS-800 frequency sweep {FS/3d@100}.

b) *Dynamic strain sweep* - {SSWP2} consists of two tests in sequence, (Figure 5-24b)

(I) - control time sweep, identical to the one described above, followed by,

(II) - strain sweep at constant frequency ω = 10 rad/s.

This test was designed to investigate the transition from LVE to NLVE behaviour and is comparable to a series of RMS-800 strain sweeps, namely {SS2} and {SS3}.

c) *Large strain amplitude experiment* - {HSSWP1} consists of a sequence of tests, applying high amplitude strains, $\gamma >> \gamma_{cr}^{LVE}$, separated by probing time sweeps with γ = 5% and ω = 1 rad/s, (Figure 5-24c). This test configuration has been designed to explore the effects of a high strain deformation on branched molecular structures.

d) *Large strain amplitude frequency sweep* - {FSWP3} is a sequence of three frequency sweeps, each with a constant (within each zone) but progressively higher strain amplitude. Figure 5-24d illustrates details of this test, designed as an extension of the {FSWP1} and {FSWP2} tests toward higher strain deformations. It should probe NLVE behaviour in terms of its frequency and strain dependence.

Figure 5-24a. The RPA 2000 test configuration - diagram (I).

a) Low strain-amplitude frequency sweep - {FSWP1} & {FSWP2}

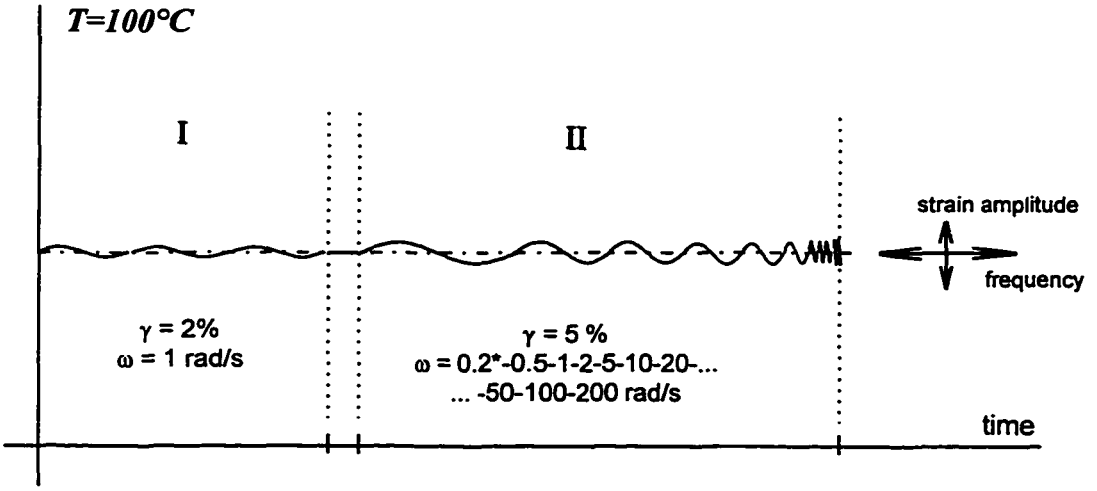
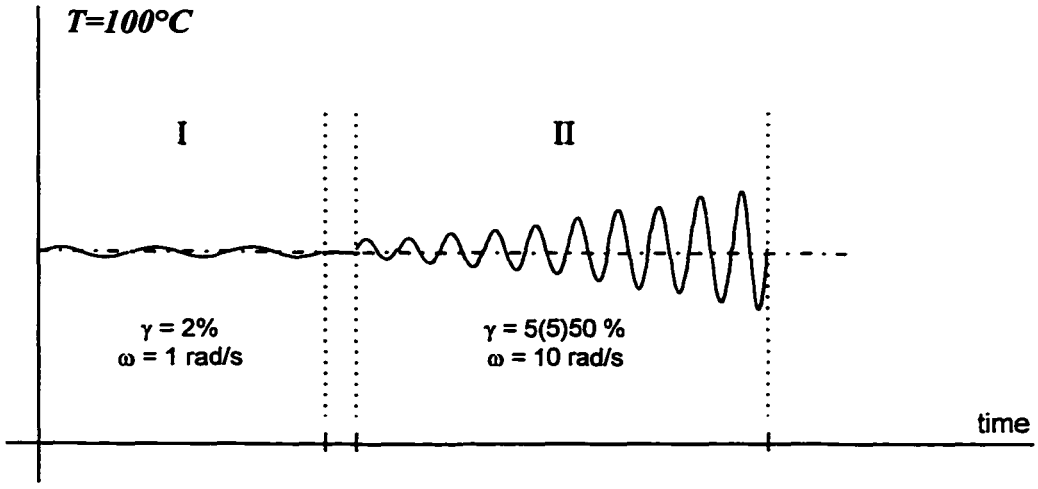


Figure 5-24 b&c. The RPA 2000 test configurations - diagram (II).

b) Dynamic strain sweep - {SSWP2}



c) Large amplitude oscillatory shear experiment - {HSSWP1}

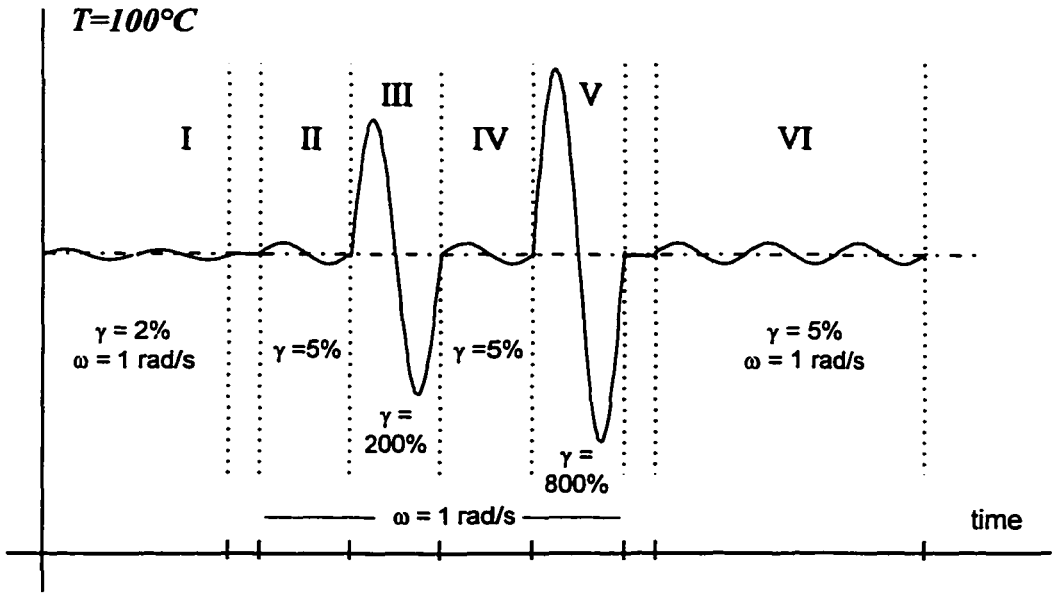
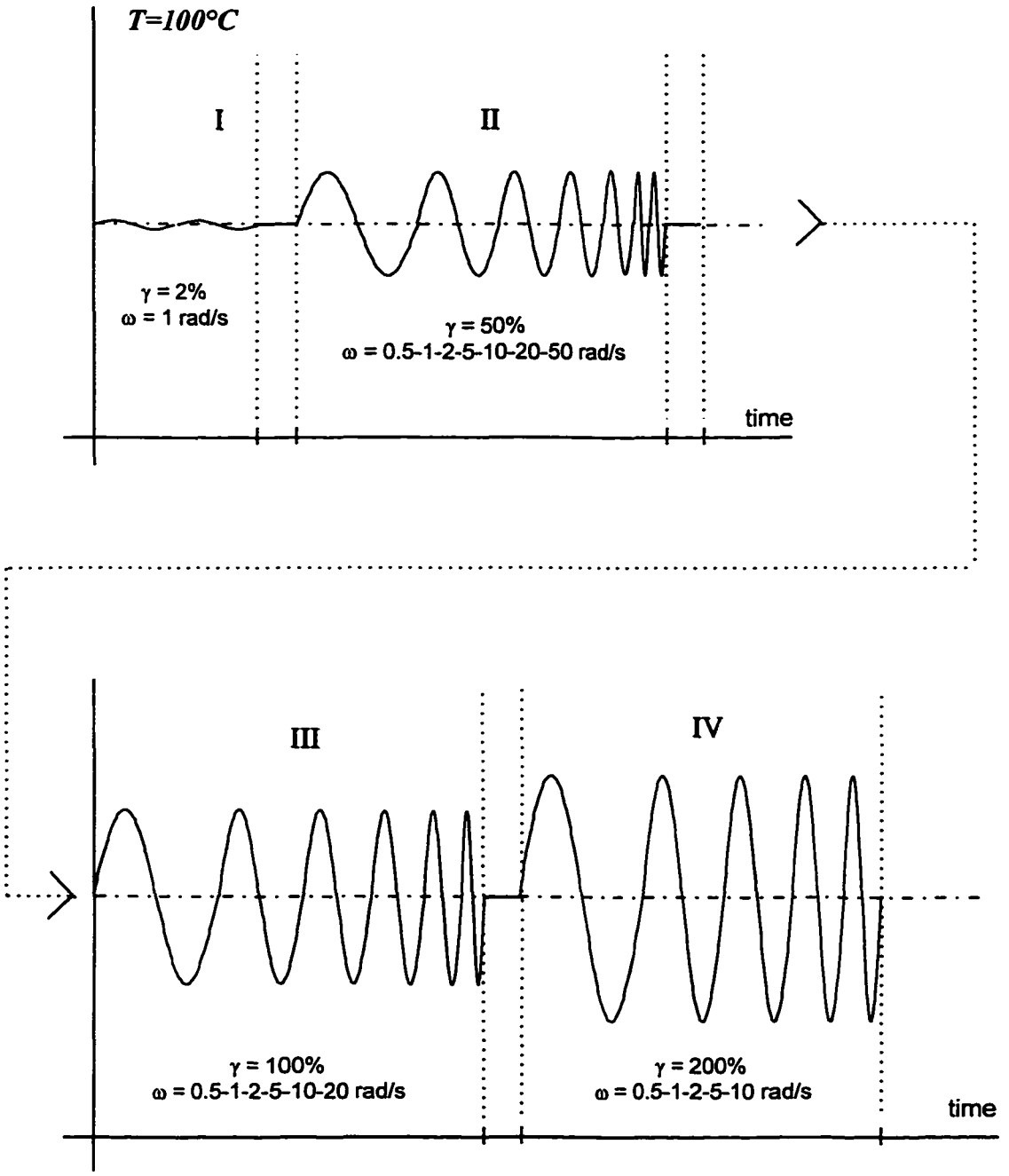


Figure 5-24d. The RPA 2000 test configurations - diagram (III).

d) Large strain amplitude frequency sweep - {FSWP3}



5.4.4 Preliminary experiments

The objective of preliminary testing was to explore different test configurations available on the RPA 2000 analyzer, as well as to confirm that the selected test conditions were equally suited for all samples. All preliminary tests were isothermal and test conditions for these tests, being similar to those adopted for the main experimental program, are not reported.

5.4.5 Instrumental interferences and data validation

The RPA 2000 analyzer is a very robust and dependable instrument. CIIR-g-BR graft copolymers fitted well into the operational range of the transducer and actuator.

However, certain aspects of experimentation with the RPA 2000 may require special attention. Due to test cavity design - fixed volume without compensation for specimen (thermal or chemically induced) shrinkage - there is a possibility for the loss of adhesion between specimen surface and test cavity wall. This can result in erroneous readings and misinterpretation of a measured torque. No provision is available for monitoring the shrinkage-induced changes in specimen size, for example by measuring during the test the 'in-cavity' pressure or the normal force.

Testing at very high strain amplitudes, corresponding to up to ±90° angular deflection, increases potential for specimen slippage. Specimen slippage is difficult to detect, particularly if it gradually increases with increasing magnitude of dynamic strain. An apparent decrease of the storage modulus due to slippage would interfere with quantitative assessment of non-Newtonian behaviour of the material. The RPA 2000 rheometer provides positive pressure in the test cavity (typically in the order of 100 bars) to delay or decrease the effect. In addition, the part of the platens in direct contact with the sample is grooved, which

further prohibits or delays the advent of specimen slippage during large amplitude oscillations in shear. Nevertheless, results of tests at strain amplitudes in excess of 50% to 100% require particular scrutiny [312].

An unevenly or only partially filled test cavity, due to insufficient specimen size or off-centering of the specimen, may result in erroneous measurements. Examination of each individual specimen immediately after the test for its geometric integrity, shape and lack of voids or porosity is also part of the validation procedure.

The experimental aspects of the LAOS testing are reviewed in Table 5-8 against the test conditions specific to the RPA 2000 analyzer.

Table 5-8. Principal instrumental interferences of the LAOS testing in torsion.

Possible interference	Comments: CIIR-g-BR by the RPA 2000
Viscous heating	- given the small value of the ($\gamma \cdot \omega$) product and the small temperature-dependence (at ~100°C) of tested samples this effect is negligible
Effect of inertia	- negligible (low Reynolds number flow)
Loss of adhesion ('no-slip' boundary conditions)	- grooved chamber surface + positive pressure + very good adhesion of a sample to metal, reduce greatly the possibility for appreciable slippage
Outflow due to centripetal acceleration	- none, due to the sealed test chamber design
Edge effects due to shear-induced normal stresses	- assumed negligible (for reasons as given above)
Radial non-uniformity of the flow field	- strain amplitude is (approximately) radially uniform due to specimen's 'inverted double-cone' shape

5.4.6 Test accuracy, precision and sensitivity

In order to estimate test precision (short-term repeatability) of the RPA 2000 measurements, two series of tests {QFSWP} and {QSSWS} were performed on a few selected samples. The {QFSWP} routine was identical to {FSWP2}, except that the first two frequencies, ω_1 and ω_2 were omitted from the test routine and the test was run in multiple determinations. Similarly, the {QSSWS} routine was a clone of the {SSWP2) sequence, run in the multiple determinations per sample.

Results of a series of 6 to 8 runs per sample are summarized below. The coefficient of variation (c.v.%) is plotted in Figure 5-25a as a function of angular frequency, and in Figure 5-25b as a function of strain amplitude. The data presented are typical for all other samples used for the RPA 2000 test precision assessment and these results are assumed to be representative for the whole project.

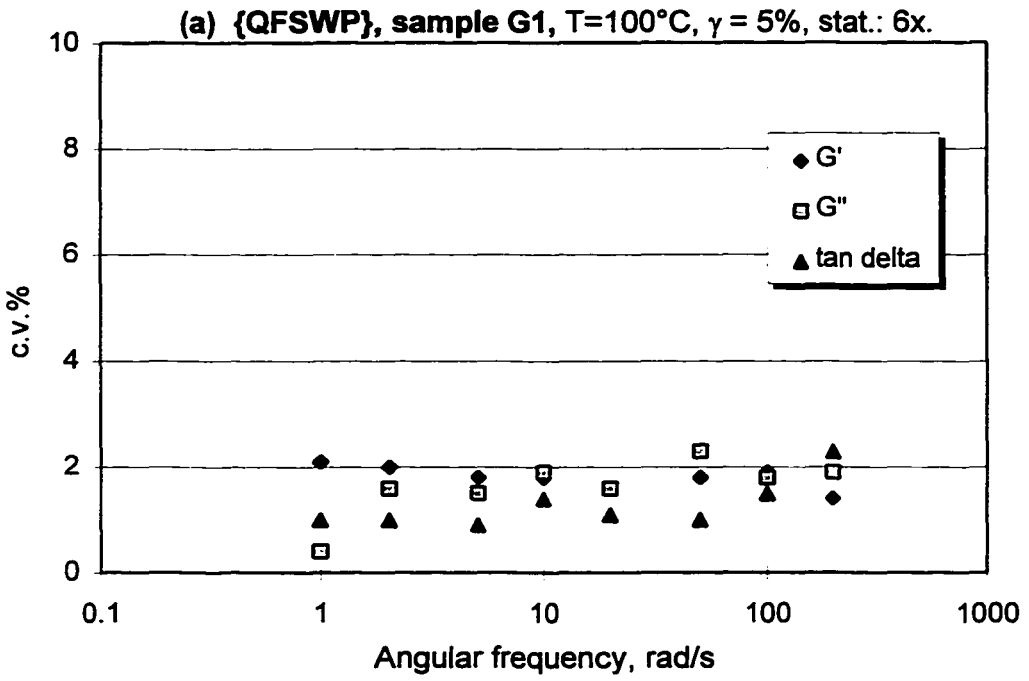
Conclusions:

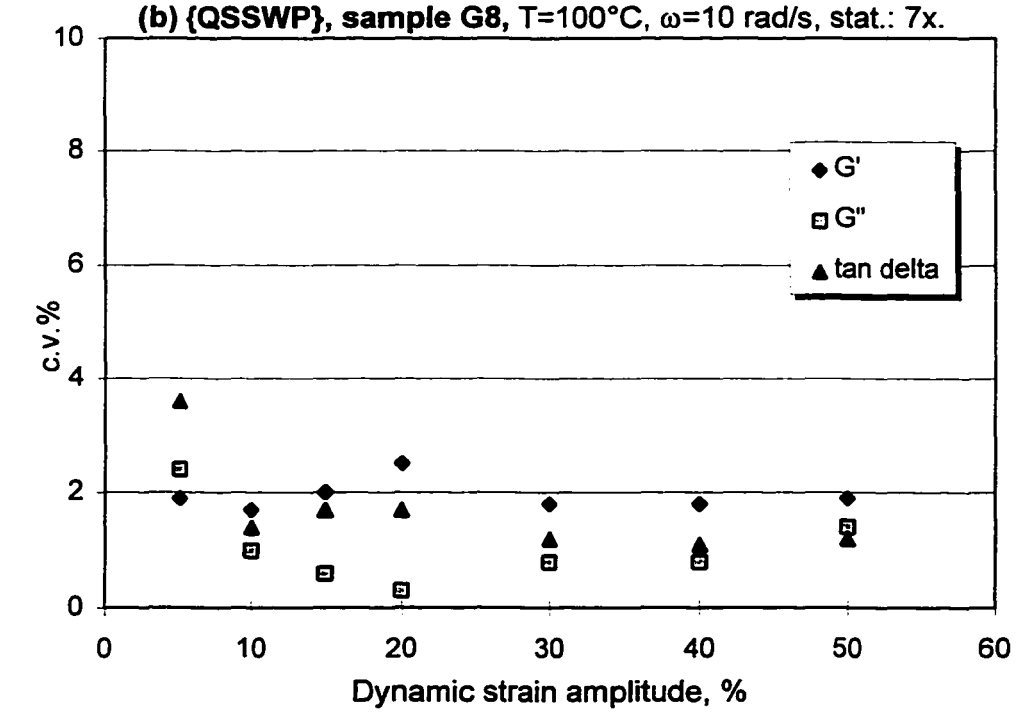
Based on these results, c.v.% of 2% is assumed as a representative figure for test precision of all viscoelastic functions, measured within the 5% to 50% dynamic strain range.

Torque measurement resolution (± 0.1 in·lb) may limit test precision for experimental points obtained at a low value of the product of strain amplitude and frequency, ($\gamma \cdot \omega$).

The above results are comparable to those reported by Burhin [313]. Short term repeatibility determined from five replicates gave a coefficient of deviation of about 2%, using a standard SBR compound tested at 1.4 Hz, 7% strain and at 177°C.

Figure 5-25. RPA 2000 - test precision.





5.5 DSR

5.5.1 Principle of operation

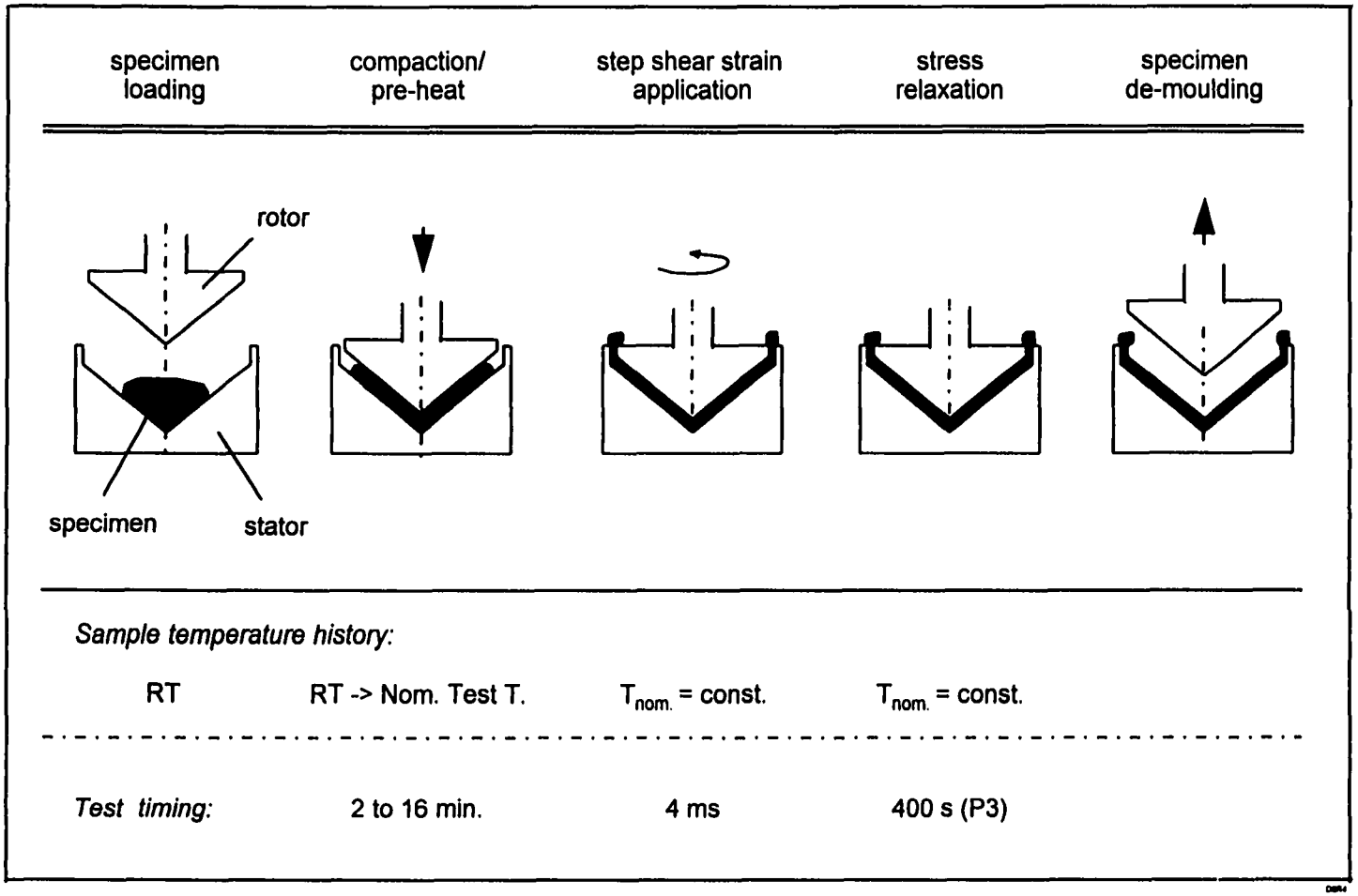
The Dynamic Stress Relaxometer, DSR, is another example of a specialized rheometer designed to characterize stress relaxation of elastomers and their compounds. Figure 5-26 summarizes the principle of DSR operation. A semi-closed test chamber is formed by a stator with conically-shaped cavity and a matching, movable rotor. The cavity of the stator and specimen-facing surface of the rotor are grooved to prevent slippage during application of the step-strain deformation, which involves a very fast (4 ms) angular deflection.

The DSR transducer measures stress relaxation following a well-defined step-strain in shear by monitoring torque decay over a period of up to 400 s. Due to the radial profile of the specimen imparted by cavity design, the radial profile of the strain is not uniform (i.e. it increases toward the edge of a specimen). The strain amplitude is also large (up to 102% in the case of 2° angular deflection angle and 0.1" stator-rotor gap) in comparison with the typical upper limit of LVE behaviour.

Strain distribution inherent in the DSR test geometry and derivation of the form factors required for conversion of a decaying torque into the time-dependent shear stress relaxation modulus, G(t) has been described elsewhere [314] and empirically verified on materials of accurately known modulus [315].

The DSR software uses an algorithm based on the Yagii-Maekawa approximation [316] to transform the shear stress modulus from a time domain into a frequency-dependent dynamic moduli and its derivative viscoelastic functions: $G'(\omega)$, $G''(\omega)$, $\eta^*(\omega)$ and $\tan \delta(\omega)$.

Figure 5-26. Dynamic Stress Relaxometer - principle of operation.



Qualification

Strictly speaking, DSR is considered to be an indexer (not a rheometer) due to the fact that it does not correct for strain non-uniformity being of magnitude large enough to enter into a non-linear response for most polymeric materials. Application of the necessary analytical correction, while possible, is not practical because it would require the knowledge of certain material parameters which are time consuming to obtain. Consequently, the DSR-derived stress relaxation modulus G(t), should be regarded as a time-dependent material parameter, rather than the strain-dependent relaxation modulus G(t, γ), obtainable from cone-plate rotational rheometers. Notwithstanding the above reservations, comparison of DSR results to those obtained with cone-plate equipped RMS-800 showed good agreement and excellent correlation for many elastomers [314, 317-318]. However, the results obtained from the DSR must be qualified when compared with those from the cone-plate rheometer (e.g. having homogeneous strain distribution).

All DSR results reported in this work were obtained under identical test conditions and parameters (details are in Appendix IV, Table D) and are considered to be valid for comparative studies.

5.5.2 Specimen preparation

The DSR is designed to accept a lump of material and the shape of the specimen is usually not critical, provided that the test cavity is filled properly and specimen overflow does not bridge the stator and the rotor. In this project, spheroidally-shaped specimens, pre-warmed (at 75°C) and having consistent weight of (18 ± 0.5) g were used. It was found that these conditions tend to improve test precision [319].

5.5.3 Experimental program and test parameters

All tests were carried out at 100°C and complete test conditions and parameters are detailed in Appendix IV, Table D under the test code {TEST1} for some preliminary work, and {TEST2} for the main project work and test precision assessment.

The number of determinations was limited for some samples by the availability of sample, but typically, tests were repeated 3 to 6 or more times per sample, using a new specimen for each test run. The standard test procedure [320] was used with minor modifications stipulated by results of preliminary tests, reflecting much longer relaxation times for grafts, as discussed in the previous subsection.

5.5.4 Preliminary experiments

The initial set of test conditions and parameters was taken from a standard test procedure developed by the author for commercial gum elastomers [320-321]. Some issues had to be revisited specifically for this project to reflect certain differences between grafts and regular gum rubbers and were the subject of preliminary tests on representative graft samples. As a result, the following changes were made to the procedure and test parameters:

1) The time period between loading of the specimen and start of the experiment, called test pre-heat time (PHT), had to be extended and specimens pre-warmed prior to placing them into the test chamber, in order to minimize the effect of specimen compaction, by closing the rotor into the stator cavity, on the results of the relaxation experiment.

2) Platen closing speed was halved for the same reason.

3) Optimum combination of the gap between the rotor and stator, which defines specimen thickness, and the angle of deflection was selected using the sensitivity as criterion, as discussed in subsection 5.2.6.

4) Optimum sample size was also confirmed experimentally.

A series of multiple determinations on a few selected samples allowed for calculation of the coefficient of variation as a test precision indicator and these results are discussed in subsection 5.5.6.

5.5.5 Test interferences and data validation

All tests and raw experimental data had to meet the following criteria before they could be further analyzed and interpreted:

a. A fully developed collar, made of test material overflowing out of the stator but not touching the rotor, to assure that the specimen attained a nominal shape and dimensions,
b. Rotor-stator distance confirmed at the nominal pre-set value, to maintain the nominal thickness of the specimen,
c. Pressure of the compressed air activating the pneumatic actuator above 80 psi, to minimize system compliance and to maintain a nominal (< 4 ms) deflection time,
d. A peak torque value within a nominal operating range of 2.0 to 400 in·lb,
e. Relaxation time at nG(t)=13.6% confirmed to be much shorter than pre-heat-time for reasons discussed in subsection 5.5.3 (for nG(t) definition see subsection 5.5.6).

5.5.6 Test precision, sensitivity and accuracy

Short-term repeatability was established by a series of multiple measurements on 3 to 6 specimens for each graft sample and compared to the analogous measurements on selected samples, repeated 8 to 12 times. Results of both series were comparable. Test precision, defined as the coefficient of variation, c.v.%, decreases with a relaxation time. Typical results are shown in Figures 5-27 and 5-28, for the stress relaxation modulus, G(t), and the normalized stress relaxation modulus, nG(t), respectively. Typical stress relaxation curves with standard error windows, indicated by dashed lines, are shown for the same sample in Figures 5-29 and 5-30, for G(t) and nG(t) functions, respectively.

For all DSR test results, nG(t) is defined as (5 - 5):

$$nG(t) \equiv G(t) / G(t=40ms) \qquad (5 - 5)$$

Standard error, ε, was calculated (5 - 6) as the product of standard deviation, s, and the t-factor from the Student-t distribution, taken at the 95% confidence level. The following error model was used with the offset error, ε^0, set to zero.

$$\varepsilon = s \cdot t + \varepsilon^0 \qquad (5 - 6)$$

Sensitivity analysis was carried out, in the same fashion as previously described, to select the most meaningful rheological parameters for a quantitative interpretation of stress relaxation results in terms of the branching structure.

The accuracy was not determined directly due to the lack of a suitable standard. However, every effort was made, including instrument calibration, to ensure reliability of the data.

Figure 5-27. DSR: test precision for G(t).

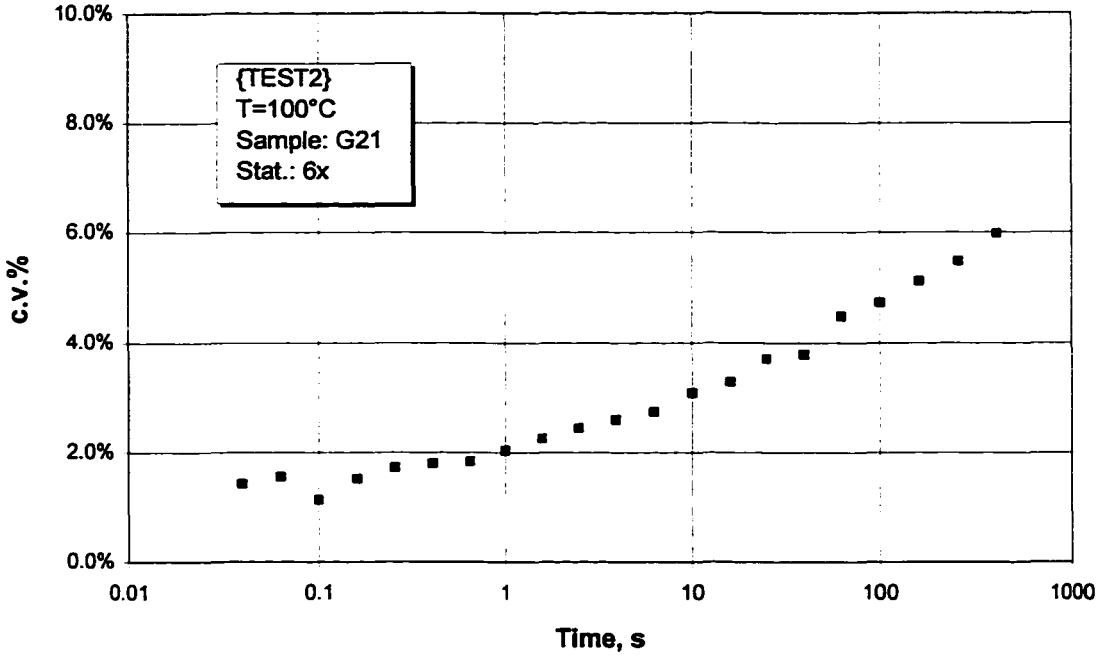


Figure 5-28. DSR: test precision for nG(t).

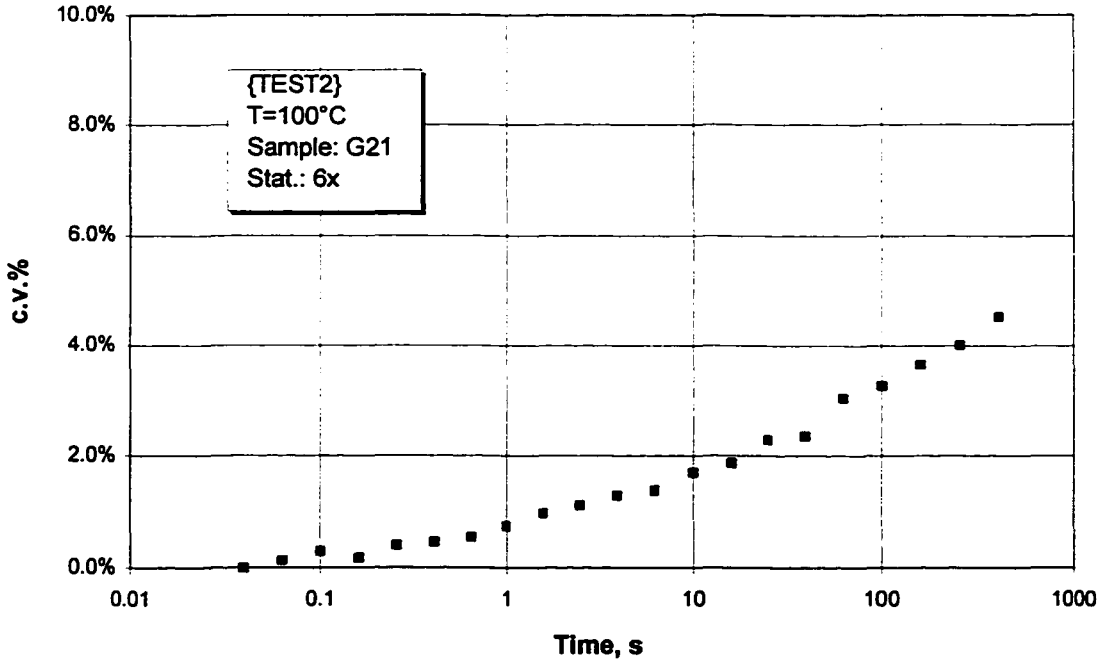


Figure 5-29. DSR test precision,
T=100°C, sample: G21, stat.: 6x, {TEST2}.

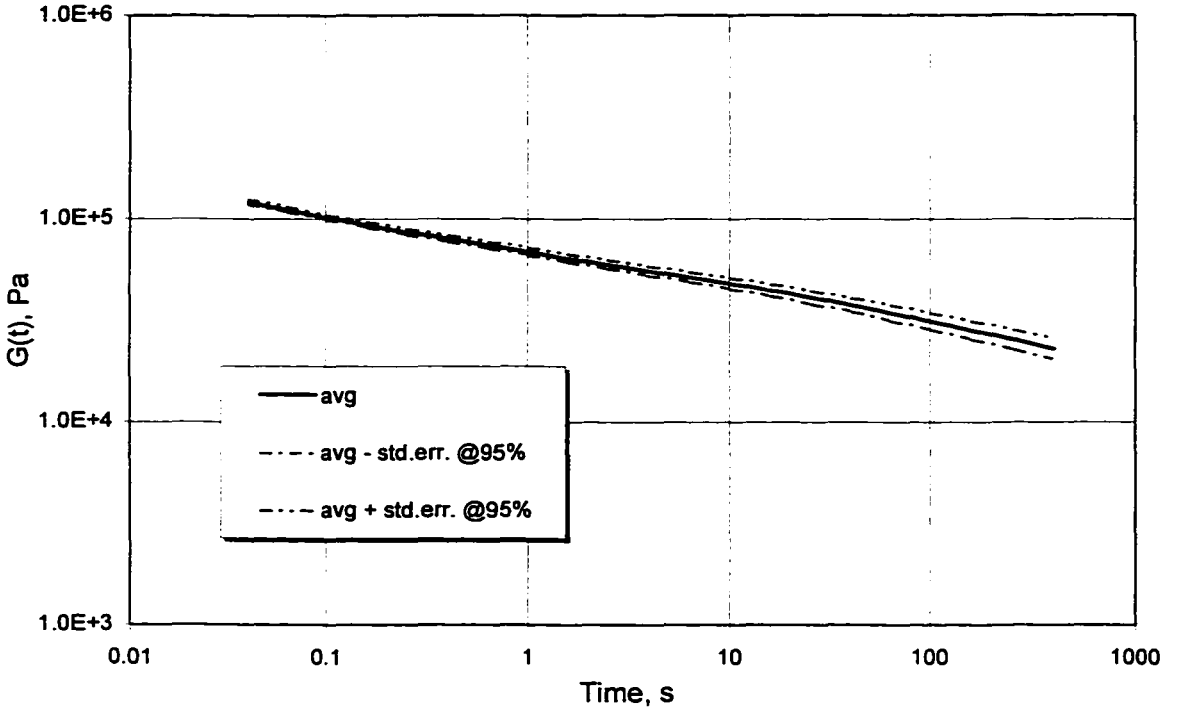
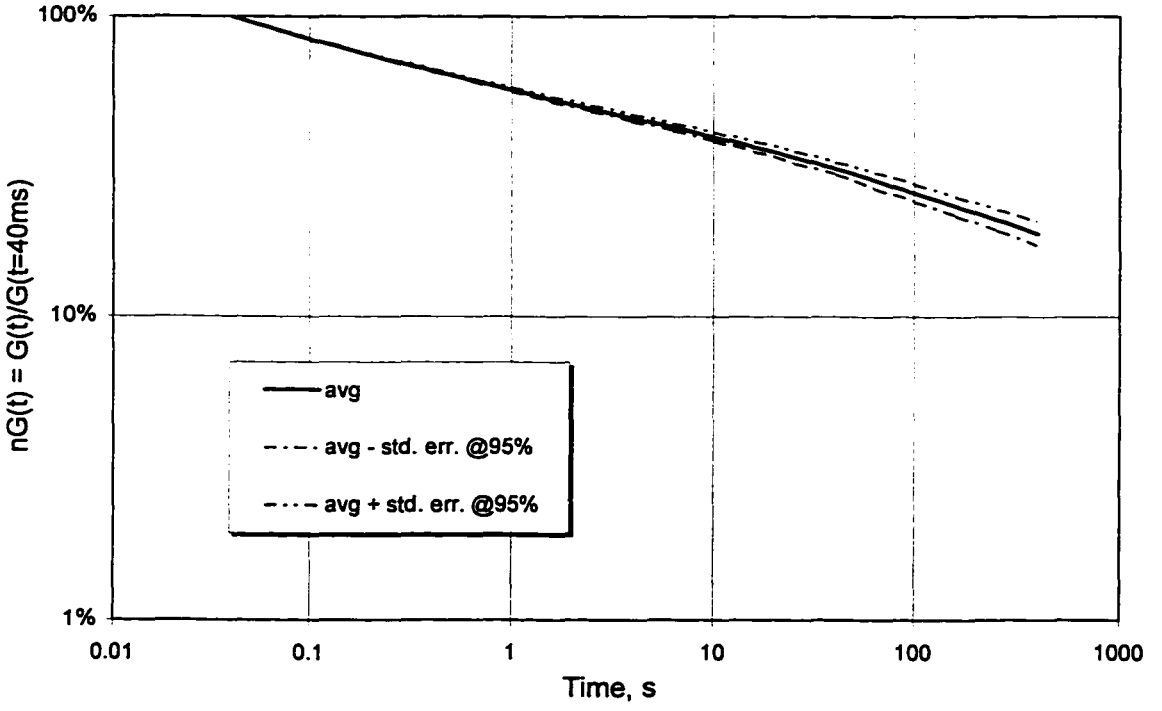


Figure 5-30. DSR - Test precision,
T=100°C, sample G21, stat.: 6x, {TEST2}.



5.6 Special issues and topics

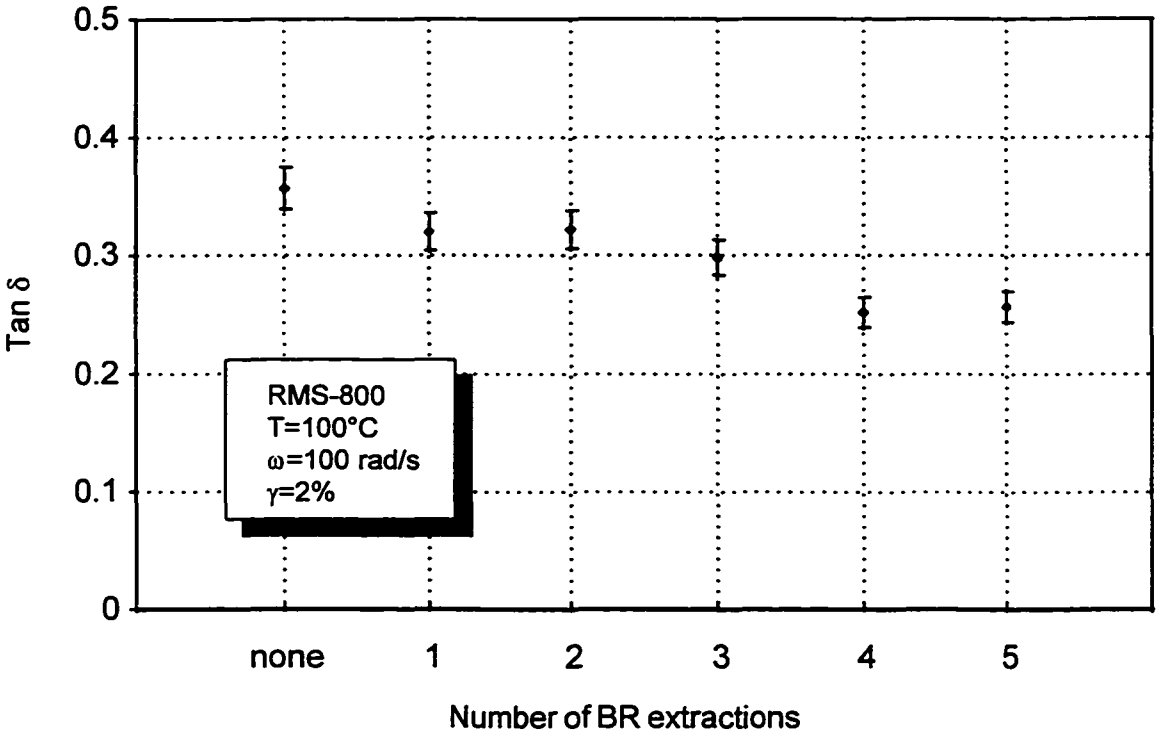
5.6.1 Effect of unattached polybutadiene

In some grafts, the content of ungrafted, linear polybutadiene (BR) can be substantial (see Table 2-5). This is best evidenced by the GPC chromatograms (App. III) and its potential effect cannot be ignored when interpreting rheological data.

Large differences between molecular characteristics of the branched, high molecular weight graft copolymers and linear, low molecular weight BR, result in proportional differences in rheological properties [23, 50, 251]. Consequently, in a mixture of graft molecules diluted by a minor component of the unattached polybutadiene (hBR), the effect of the latter on the rheological behaviour of the graft-hBR mixture can be noticeable. For example, linear low MW BR will decrease the modulus and increase tan δ, an effect particularly pronounced in high frequency dynamic tests. Figure 5-31 illustrates the effect of a decreasing content of unattached BR due to subsequent extractions.

Fortunately, these effects are specific and may not interfere with the interpretation of rheological behaviour of the graft. For example, the time-dependence and frequency-dependence of viscoelastic functions are distinctly different for long-chain branched molecules (including grafts) when compared with much shorter, linear molecules of the attendant BR diluent. This issue will be revisited during discussion of rheological results in chapters 6, 7, and 8.

Figure 5-31. Effect of unattached BR content in the CIIR-g-BR.



5.6.2 Effect of polymer stabilizer

A standard concentration of the stabilizing system present in graft copolymers did not have a measurable effect on rheological properties. This conclusion was based on results of a series of dynamic mechanical tests (RMS-800) on samples containing various amounts of stabilizing composition, including samples with a standard content and with no stabilizer at all.

Chapter 6

Linear viscoelastic (LVE) properties of CIIR-g-BR copolymers

This chapter describes the linear viscoelastic properties of graft copolymers, based on results obtained from RMS-800 and RPA-2000 experiments. Emphasis has been put on interpretation of these results in terms of the LCB structure. Rheological properties of grafts were compared to those of the backbone and branch precursor polymers, as well as contrasted with those of their blend.

To better understand how specific details of the comb-type branching architecture of graft copolymers affect their rheology, two principal rheometrical techniques were employed: dynamic frequency sweeps (sections 6.1-6.3) and isothermal stress relaxation experiments following (small amplitude) step-strain (sections 6.4-6.6).

Experimental aspects of rheological characterization, including a review of preliminary test results, were discussed in chapter 5. Tabulated test results, results of statistical analysis and certain additional graphs are included in Appendix V, in support of the conclusions discussed in this chapter.

Few results could be compared to analogous results for other graft copolymers, due to the scarcity of published reports of comparable scope.

6.1 Frequency dependence of linear viscoelastic functions

A series of sinusoidal oscillations at constant strain amplitude but with systematically increasing frequency, further referred to as 'frequency sweeps', constitutes the most direct experimental method to characterize frequency-dependence of viscoelastic functions, including the dynamic moduli: the storage modulus, G', and the loss modulus, G".

Isothermal frequency sweeps were carried out on the RMS-800 mechanical spectrometer over five (5) decades of angular frequency (0.001-100 rad/s) at 30°C. Appropriate dynamic strain amplitude (5%) was selected to retain deformations within the LVE range for all samples, yet to obtain the strongest possible torque signal for the best test precision. Details of the {FS5dec} test conditions are reported in Appendix IV, Table A, Part 2.

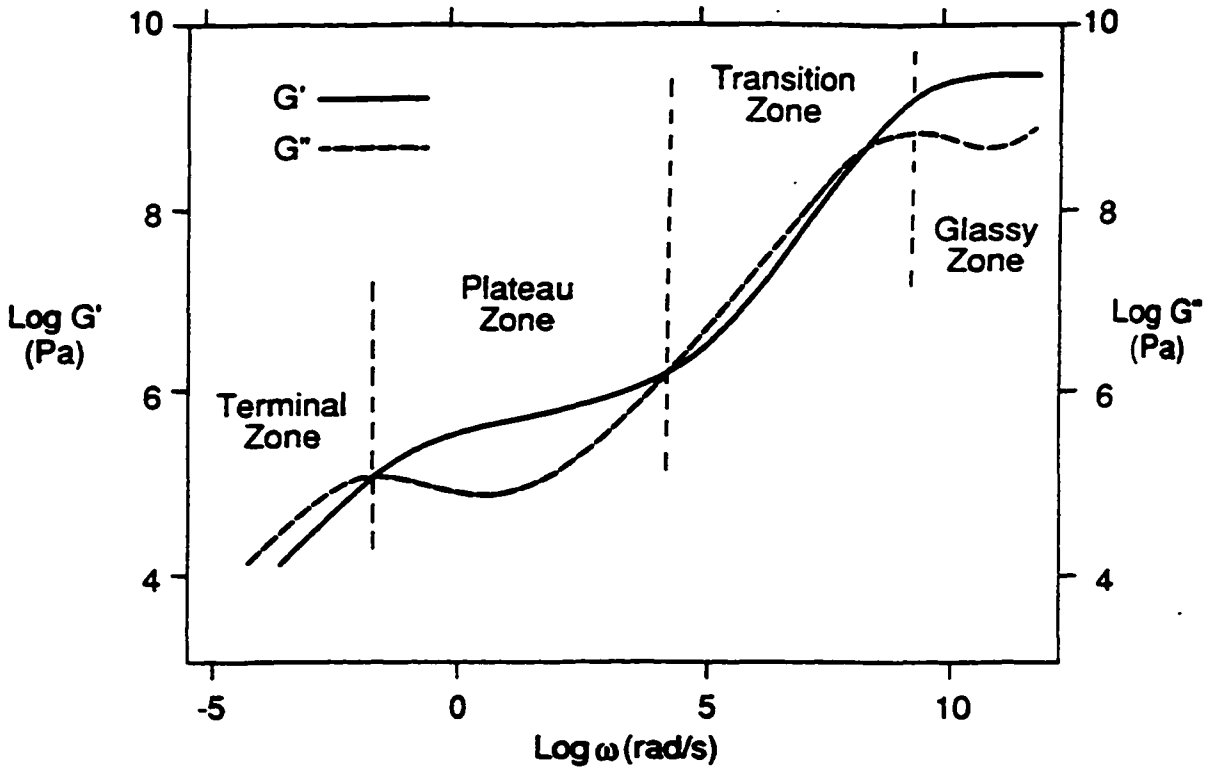
A complete set of double-logarithmic plots of dynamic moduli and tan δ, as a function of the angular frequency (log ω), is included in Appendix V, section 6.1.

In addition to the {FS5dec} test, two additional series of frequency sweeps were completed over the same frequency range (0.1 - 100 rad/s) and with identical dynamic strain amplitude (5%) but at the different temperatures, 30° and 100°C. Their experimental details are also included in Appendix IV, Table A, Part 2 under test codes {FS3d@30} and {FS3d@100}, respectively. While some of the test parameters, including test temperature, were different than those for {FS5dec} test, they were designed to measure material properties within the linear viscoelastic range. Results obtained from these tests consistently and fully support the conclusions discussed further in this section. Details however are not being reported. Results of other tests within the LVE range but performed on the RPA 2000, {FSWP1} and {FSWP2}, will be discussed in section 6.3.

6.1.1 Dynamic mechanical moduli, G'(ω) and G"(ω)

Scanning the dynamic properties of the material even over 5 decades of frequency enables access to a relatively narrow section of the whole viscoelastic spectrum of practical relevance (Figure 6-1).

Figure 6-1. Typical dynamic mechanical spectrum for polymers with flexible and linear molecules [322].

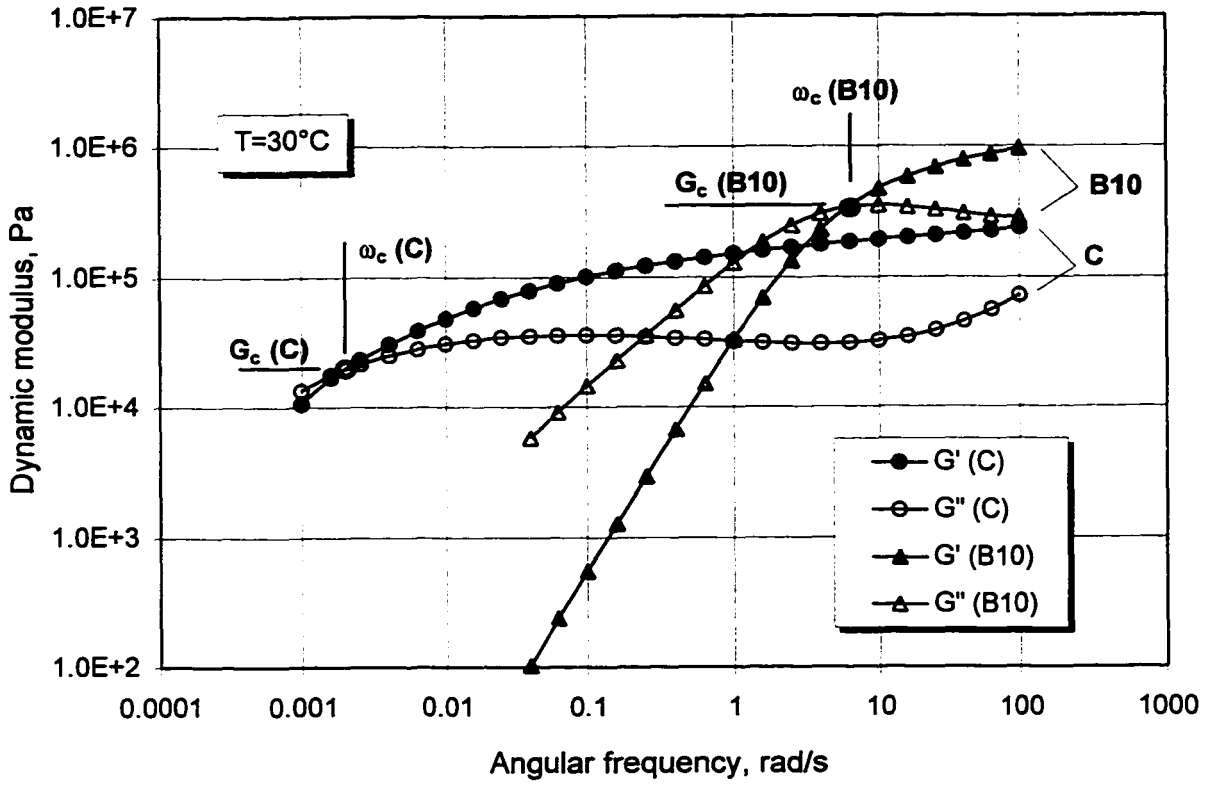


Dynamic spectra of linear precursor polymers

Dynamic spectra for samples C and B10, precursor polymers for backbone and branch, respectively, are characteristic for linear elastomers with molecular weight typical of commercial elastomer grades and are shown in Figure 6-2.

For sample C, the accessible section of the visco-elastic spectrum at 30°C includes a major section of the plateau zone and the area immediately below the first cross-over point. The first (G'/G") cross-over point is defined as the point ($x = \omega_c$, $y = G_c$) on the G', G"- ω plane, where $G'(\omega_c) = G"(\omega_c) = G_c$. The G_c is called cross-over modulus and ω_c - the cross-over frequency. The rubbery plateau for sample C is well defined and spans over five decades of frequency, from 0.0018 rad/s to approximately 600 rad/s.

Figure 6-2. Dynamic mechanical spectra for linear molecules - samples C & B10.



For sample B10, the first cross-over point has a higher cross-over modulus and a much higher cross-over frequency. As a result, a substantial portion of the terminal zone, as well as the low frequency section of the plateau is contained within the experimental range of frequencies. In the terminal zone, the shape (straight line) and slopes of the straight-line portion of either log G′ versus log ω and log G″ versus log ω curves are comparable with those reported in the literature for (high-cis) polybutadienes [27, 251].

The cross-over parameters (ω_c, G_c) of the first cross-over point for uncompounded, uncross-linked elastomers were shown to relate to the $\overline{M}_w$ and to the molecular weight distribution [322]. According to this study, based on correlation of the first cross-over point data with molecular parameters for a series of butyl samples of various $\overline{M}_w$ / PDI combinations, the cross-over frequency, ω_c is inversely proportional to the $\overline{M}_w$, while increasing values of G_c correlate to decreasing values of PDI, as summarized below,

$$\omega_c \sim 1 / \overline{M}_w$$

$$G_c \sim 1 / \text{PDI}$$

Indeed, these empirical observations can be confirmed for samples C and B10, as shown in Table 6-1.

Table 6-1. MWD and first cross-over point parameters for samples C and B10

	M_w, dalton /*	PDI /*	ω_c, rad/s	G_c, Pa
C	457,000	3.25	$1.8 \cdot 10^{-3}$	$2.2 \cdot 10^{4}$
B10	140,000	1.40	6.2	$3.4 \cdot 10^{5}$

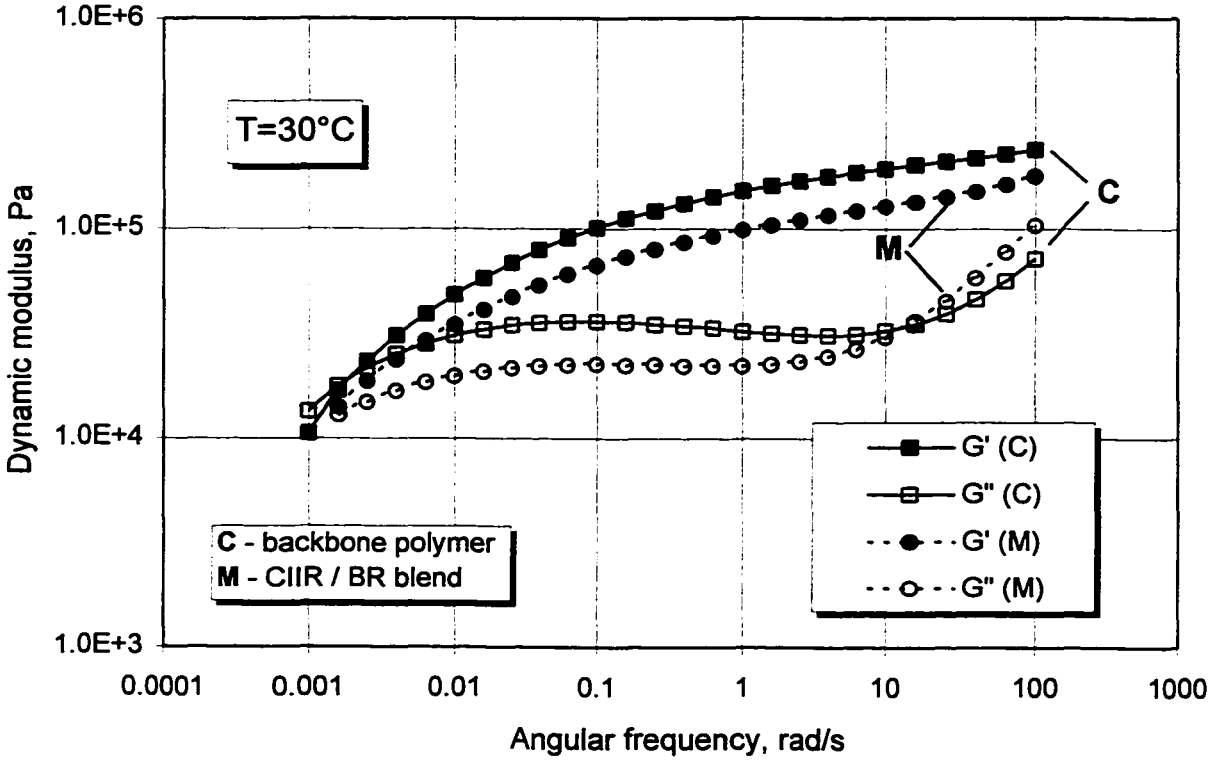
/* - calculated from MWD measured by SEC

Backbone precursor polymer compared with its blend with a branch precursor polymer

Blending the backbone precursor with a significant (30 wt%) amount of linear BR ($\overline{M}_w$ = ~30,000) resulted in only slight modification of the dynamic spectrum (Figure 6-3). The shape of the spectrum is virtually unchanged and the first cross-over frequency (within experimental error) is comparable. The addition of the low $\overline{M}_w$ component (BR) results in a softer blend (both G′ & G″ are lower). The rubbery plateau for sample M is noticeably narrower, accompanied by the shift of the second cross-over point toward lower frequencies.

This observation is important for proper interpretation of the results for samples (especially G10, G22 and G6) for which the residual content of unattached BR is significant (>15%), and might contribute to the overall rheological behaviour of the graft, "diluted" by low $\overline{M}_w$ iinear polymer. This effect can be particularly strong at higher frequencies. Table 4-2 in chapter 4 contains molecular characteristics of sample C and Table 4-11 for sample M.

Figure 6-3. Dynamic mechanical spectra for samples C & M.

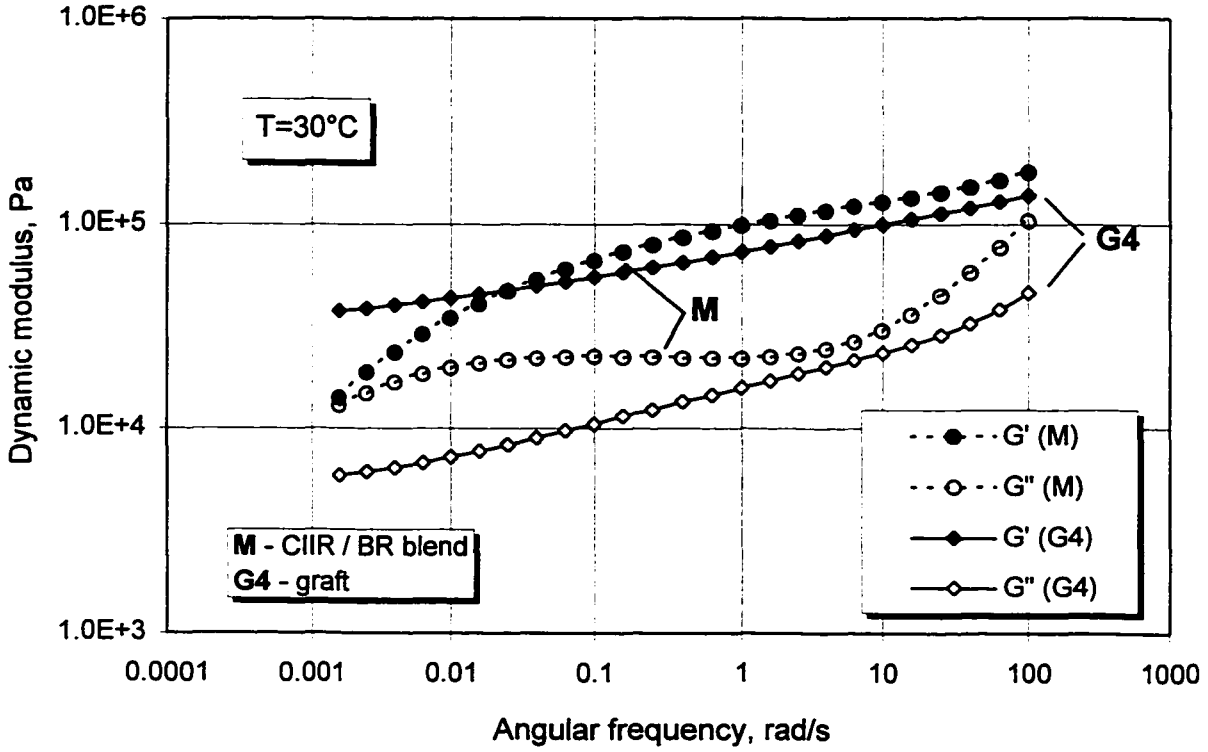


Blend M compared with its structurally and compositionally equivalent graft, G4

A much more spectacular difference in the frequency-dependence of dynamic moduli is observed by comparison of samples M and G4, whose spectra are shown in Figure 6-4. Sample G4 is a graft of very similar chemical composition to that of a blend M (Table 4-11). Component 'C' of the blend is structurally (MWD) identical to the backbone of the graft. the MWD of the component 'B' of the blend is identical to the MWD of the branches in sample G4. However, directly as a result of grafting, the shape of either modulus (within 0.001-100 rad/s range) differs significantly.

The frequency dependence of the dynamic moduli at the transition from the plateau to the terminal zone, as observed for sample G4, is typical for polymers with a 'well developed' branching structure, i.e., graft molecules with a significant number of sufficiently long branches.

Figure 6-4. Dynamic mechanical spectra for samples M & G4.



This markedly different viscoelastic behaviour can be confidently assigned to the existence of the long-chain branching structure (comb-type).

Summarizing observations on the dynamic spectra for all samples, specific features found in the viscoelastic spectrum for LCB elastomers as compared to the linear polymers include:

(a) lack of the first cross-over point within a readily observable range of frequencies, and lack of a clear distinction between the plateau and terminal zones,

(b) much smaller slope of both dynamic moduli at low ω, corresponding to the terminal zone for linear molecules of comparable MW,

(c) higher slope of dynamic moduli (particularly G″) in the plateau zone,

(d) frequency-dependence of both moduli on a double-log plot consists of virtually straight lines of comparable slope, with storage modulus G′ dominating consistently over loss modulus G″.

These observations confirm those reported elsewhere [57, 61] for other comb-branched polymers.

For linear polymers, a rubbery plateau zone, positioned between the transition and terminal zones of the viscoelastic behaviour, is characterized by domination of the storage modulus G′ over loss modulus G″ (Figure 6-1). For the majority of branched polymers, the plateau zone appears to be extended to the lowest experimentally accessible frequencies with no indication of an imminent cross-over point.

The plateau zone is commonly associated with molecular entanglements [232]. Modification of the plateau zone and its significant extension towards much lower frequencies, suggest the existence of additional mechanisms in molecular reptation in which branches are playing a major role.

Effect of branch length, M^b

To investigate more closely the nature of changes in the viscoelastic spectrum (G′(ω), G″(ω)) caused by branch length, results for a series of grafts with progressively increasing branch length were compared in Figures 6-5 to 6-7. Figure 6-5 contrasts the viscoelastic spectrum of the linear backbone polymer (sample C) with that of a graft with very short branches, sample G1 (M_p^b=3,000). Figure 6-6 compares spectra of sample G1 with G7 (M_p^b=10,300) while Figure 6-7 includes dynamic spectra of samples with even longer branches, G17 (M_p^b=47,300) and G5 (M_p^b=61,700). A systematic change of the shape and mutual correspondence between G′(ω) and G″(ω) curves is readily observed as branch length increases. It appears, as if the lower limit of the rubbery plateau (e.g., the first cross-over point) is rapidly pushed toward lower frequencies with increasing branch length. The most striking feature in these graphs

Figure 6-5. Dynamic mechanical spectra for samples C & G1.

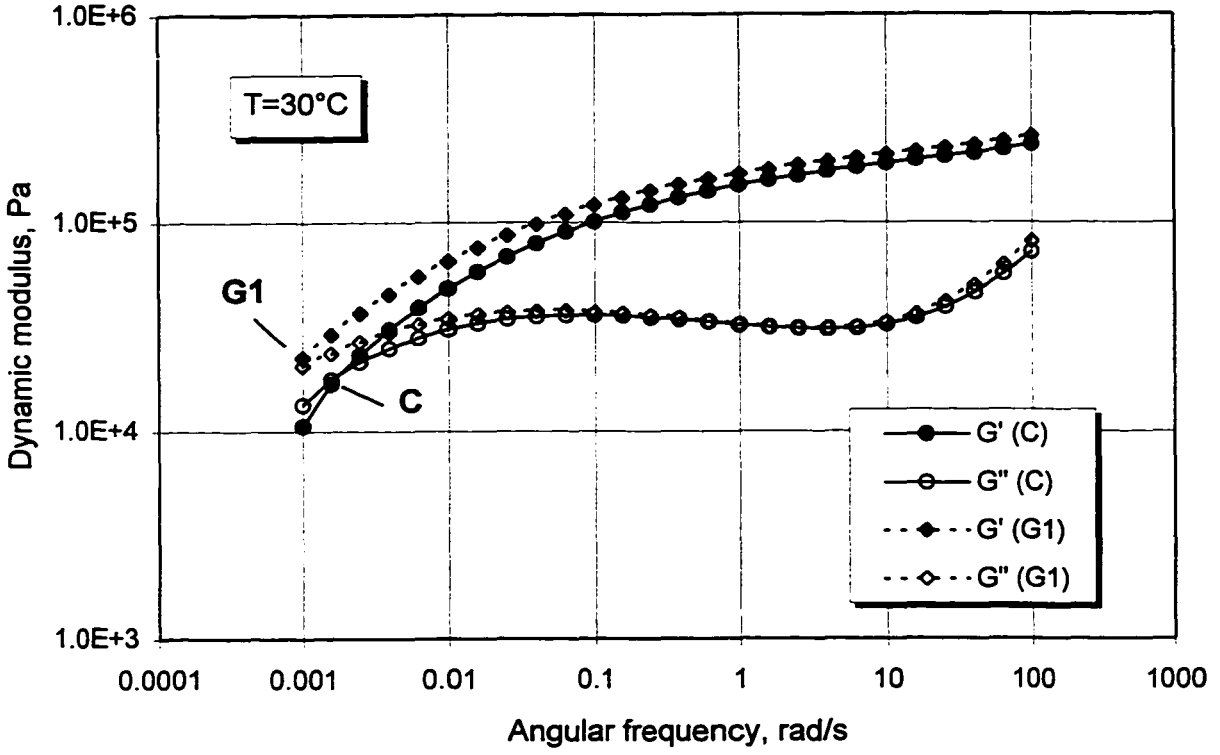


Figure 6-6. Dynamic mechanical spectra for samples G1 & G7.

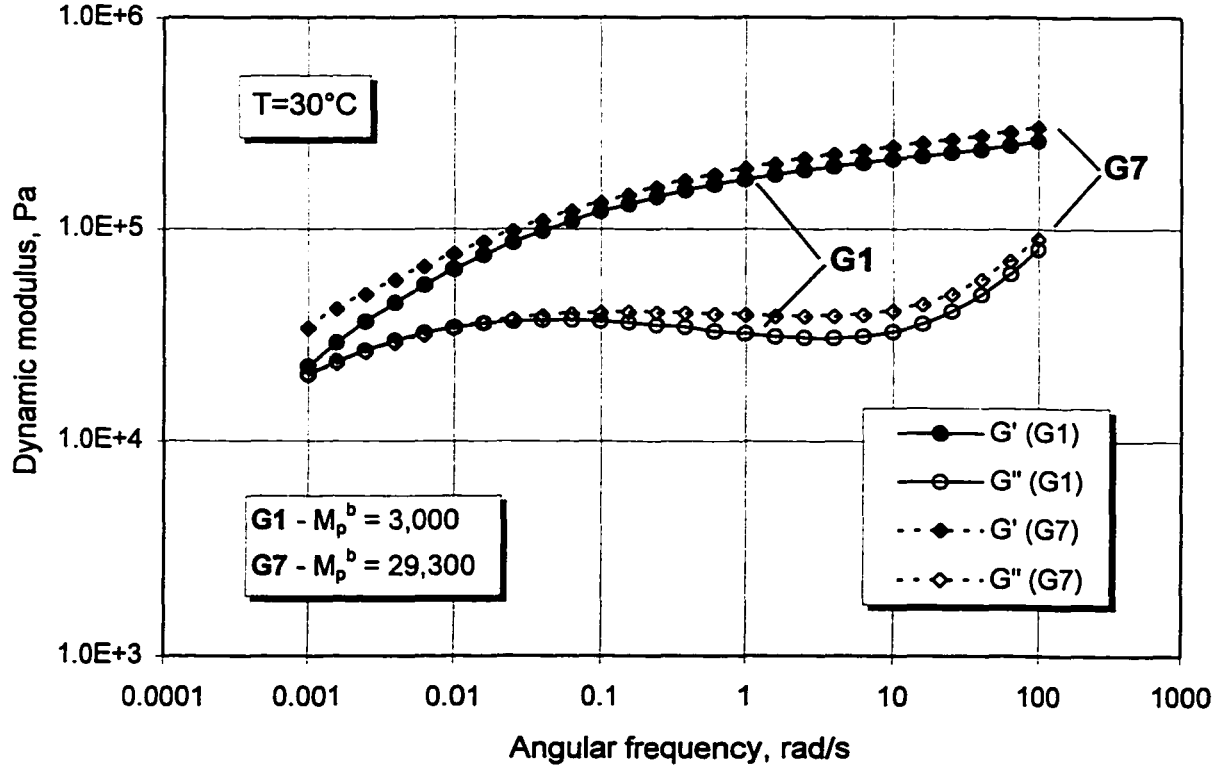
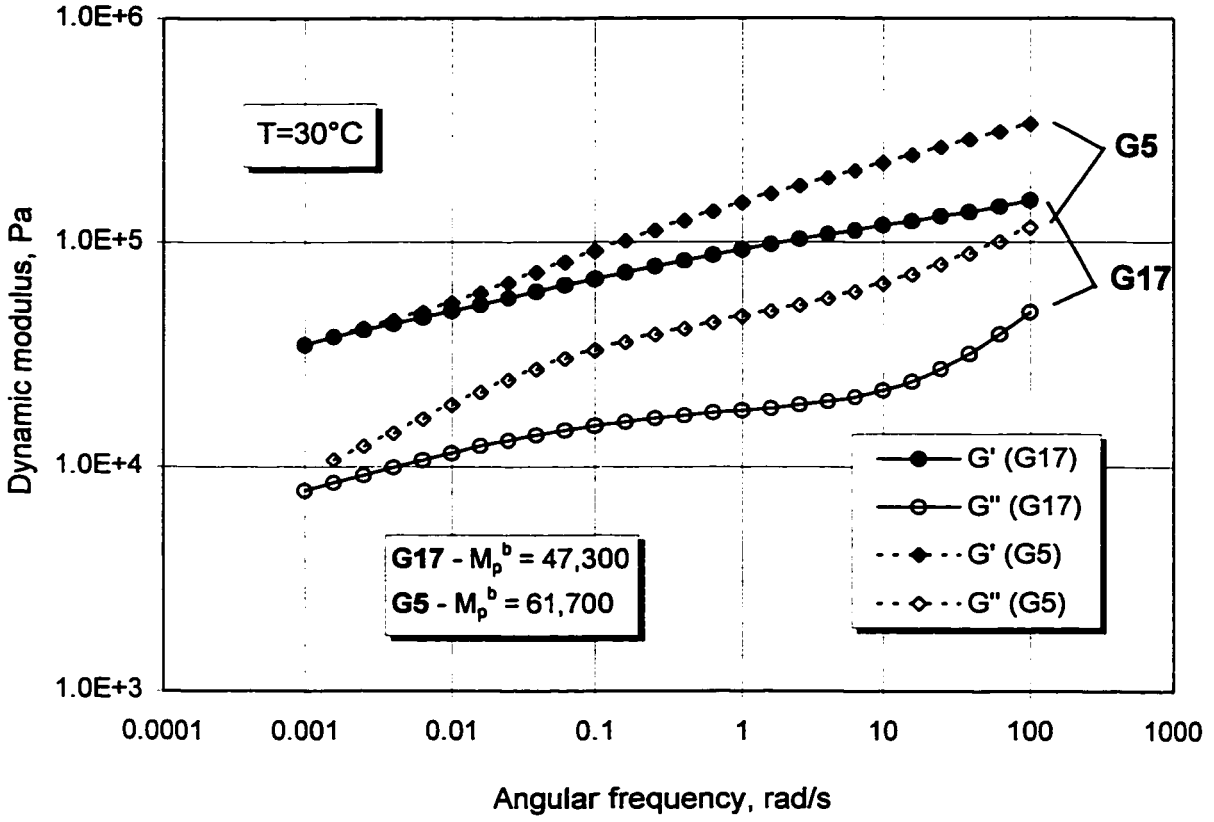


Figure 6-7. Dynamic mechanical spectra for samples G5 & G17.



is the "opening" of the G'- G" envelope toward lower frequencies occurring for the most branched (high $M^b \cdot N_g$) grafts. This extreme behaviour resembles that of lightly cross-linked, unfilled elastomers.

Effect of branching content, $w^{b,g}$

For samples with under-developed branching, that is for $w^{b,g}$ <10%, the dynamic modulus curves converge with decreasing oscillation frequency, regardless of the value of specific branching parameters (M^b, N_g), as exemplified in Figure 6-6 for samples G7 and G1. In Figure 6-8, dynamic mechanical spectra for samples G2 and G18 are compared in support of the above observation.

At and above a certain (critical) combination of branch length and number of branches ($M_p^{\,b} \cdot N_g^{\,p} \sim w^{b,g} \approx 10\%$), the G'(ω) and G"(ω) profiles run parallel to each other as frequency decreases. Sample G17 (in Figure 6-7) is a representative sample of such an intermediate behaviour. For grafts with both long branches and substantial branching frequency, for example in samples G5, G21 in Figure 6-9, (also cf. spectra for samples G14 and G11 in Figures AFSG11 and AFSG14, in Appendix V), dynamic spectra actually diverge with diminishing oscillation frequency (ω->0).

For these samples, the first cross-over probably does not exist. Likewise, there is no range of frequencies for which G" > G', constituting for a linear polymer a terminal (flow) zone of the viscoelastic behaviour. To prove this experimentally, the range of mechanical oscillation frequencies for the isothermal frequency sweep would have to be extended for many decades below 0.001 rad/s, with a single measurement in the order of weeks or months. The alternative approach of extending the frequency range through frequency/temperature superposition offers certain limited possibilities and will be discussed in the next section of this chapter.

Comparable transition in mutual correspondence between storage and loss modulus has been reported for polyacrylate elastomers [323].

Modification of the rubbery plateau by branching frequency and branch length

1. Divergence of the dynamic moduli at the lowest frequencies is related to the presence of two plateaus in the G"(ω) response. The primary plateau, presumably due to backbone entanglements, is located in a frequency range comparable to that of linear molecules of the same length. The secondary plateau, positioned always at lower frequencies, can be related to the "interference" of branching in the disentaglement process of the backbone molecules.

Figure 6-8. Dynamic mechanical spectra for G2 & G18.

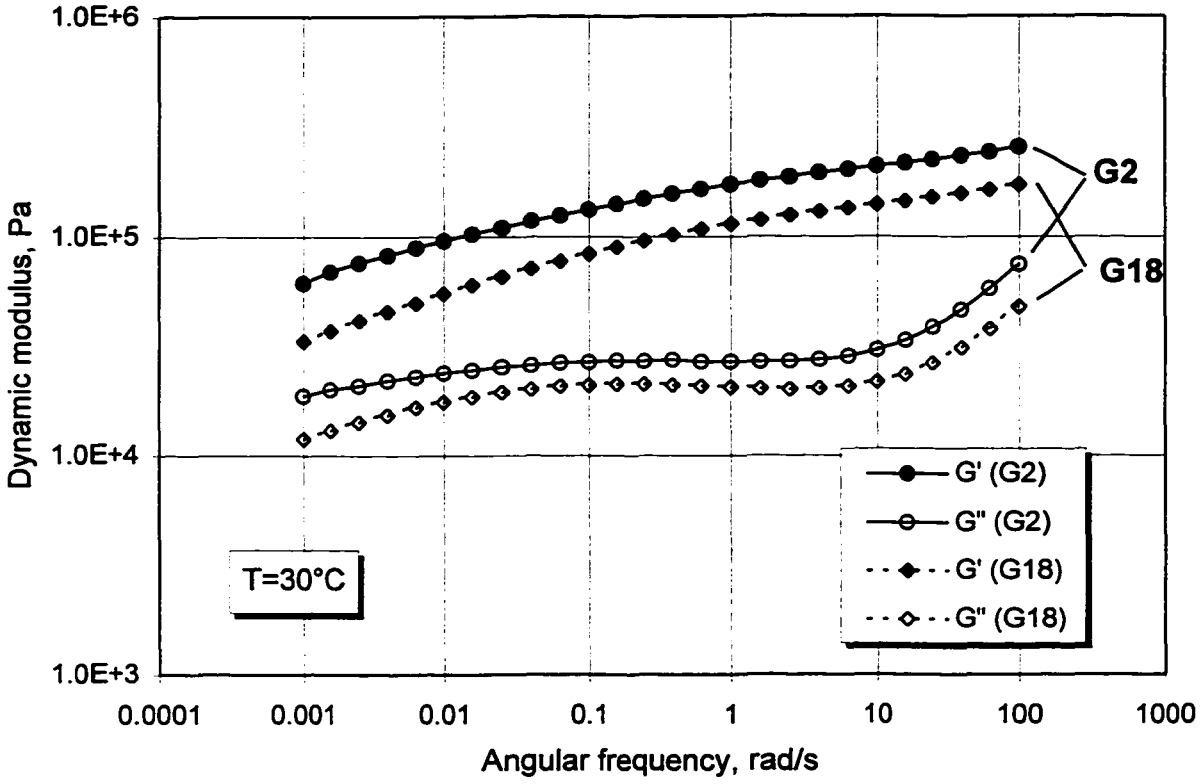
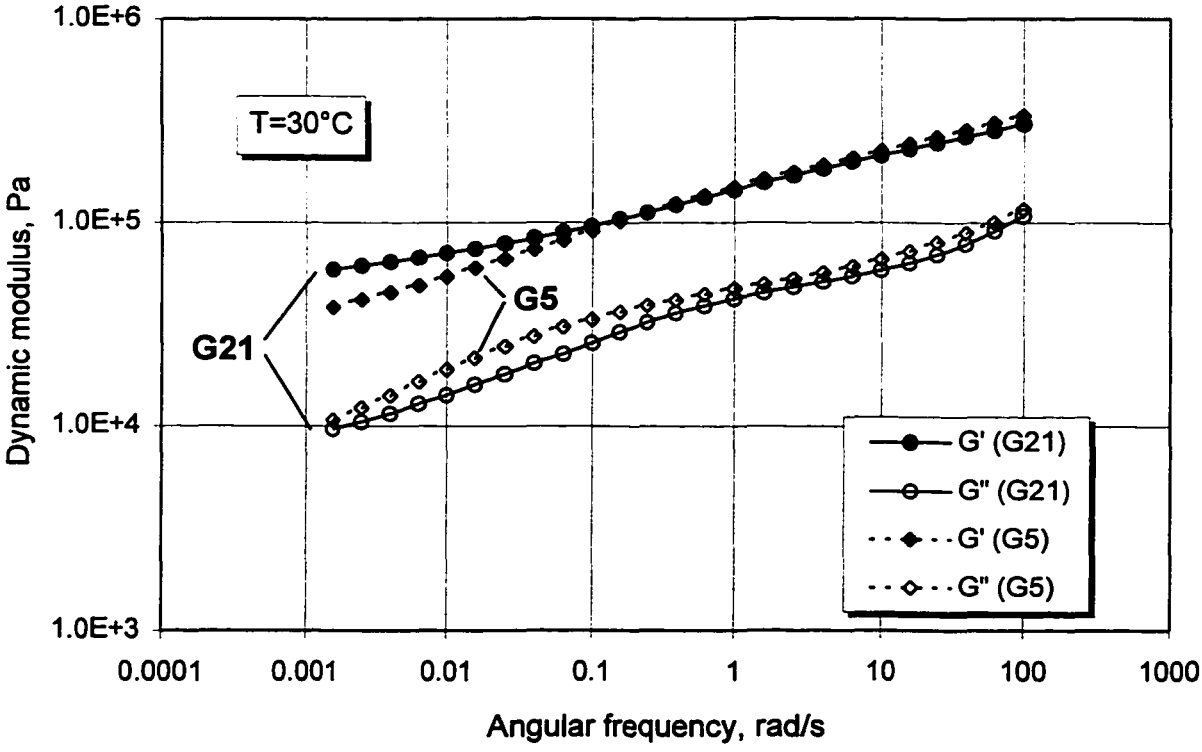


Figure 6-9. Dynamic mechanical spectra for G5 & G21.



2. For grafts with intermediate branch length, in the order of 30,000-50,000, combined with an appreciable number of branches, N_g^p = 2.0-3.3 (samples G5, G9, G14, G15 or G21), the loss modulus G″ has two shallow valleys. The first, at higher frequencies, roughly corresponding to the entanglement plateau, and the second, less distinct and extending toward frequencies well below 0.001 rad/s, on the tan δ(ω) plot, also provides a convenient means of monitoring effects due to branching - cf. Figure 6-10.

A similar observation of a second plateau in dynamic moduli was made by Nakajima and Parkey for "multiple-branched molecules" [324].

For grafts with shorter branches (10,000-20,000) and a high branching frequency, N_g>5, the contribution of branching to the shape of the plateau largely superimposes on the entanglement plateau due to backbones, enlarging its width and particularly its depth. Separation of the G′(ω) - G″(ω) curves increases, which is equivalent to reduction of tan δ due to the presence of short but numerous branches. Comparison between samples G19 and G20 in Figure 6-11 should provide good illustration for this observation. Both grafts have similar M_p^b but different branching number (N_g^p =1.2 for G19 and N_g^p =11.0 for G20). Other examples include samples G13, G20, G16 and G12 - cf. Figures AFSG13, AFSG20, AFSG16 and AFSG12 in Appendix V.

For even longer branches, such as in samples G10, G22 (Figure 6-12), their impact on G″(ω) or tan δ (ω) in the form of a secondary plateau is not observable within 0.001-100 rad/s frequency range. This is probably due to extremely slow molecular disentanglement caused by the presence of long side chains - cf. Figure AFSG10 or AFSG22 in Appendix V.

If the abscissa of the tan δ (ω) minimum could be adopted as a measure of the time-scale associated with the disentanglement process, the characteristic times can be estimated as presented in Table 6-2.

Figure 6-10. Dynamic mechanical spectrum for sample G21.

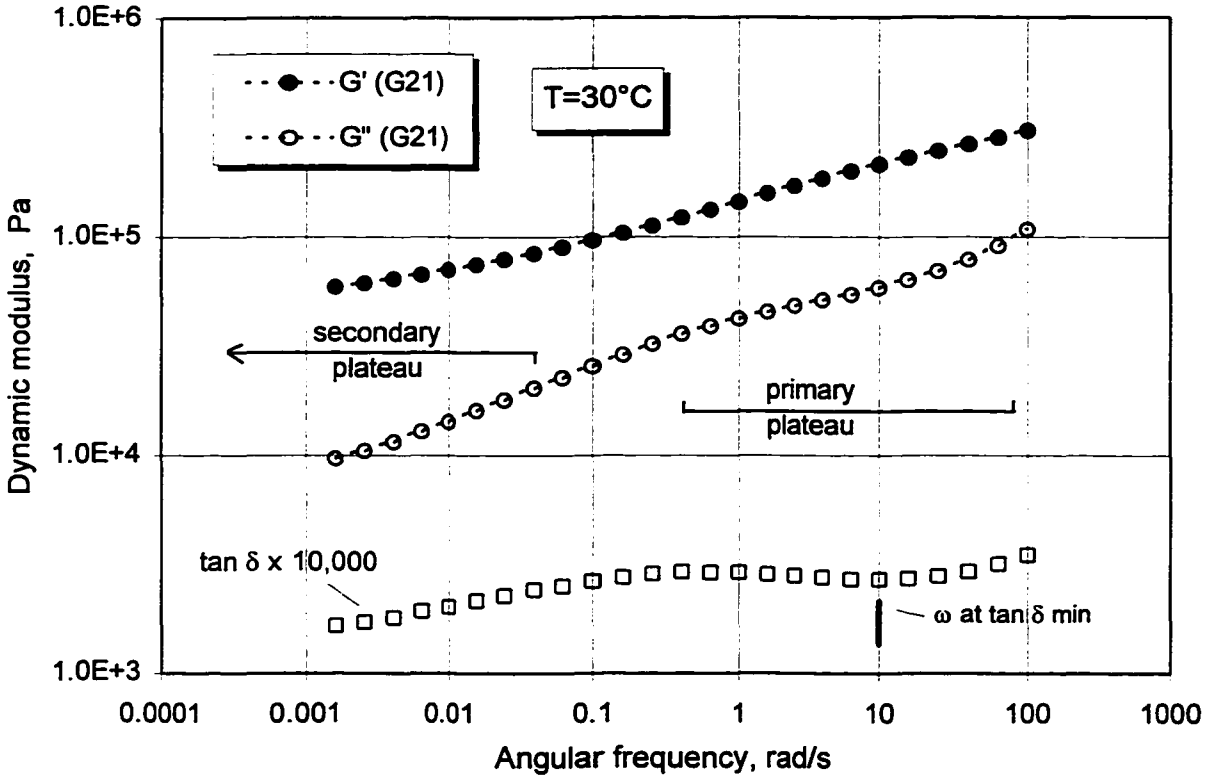


Figure 6-11. Dynamic mechanical spectra for samples G19 & G20.

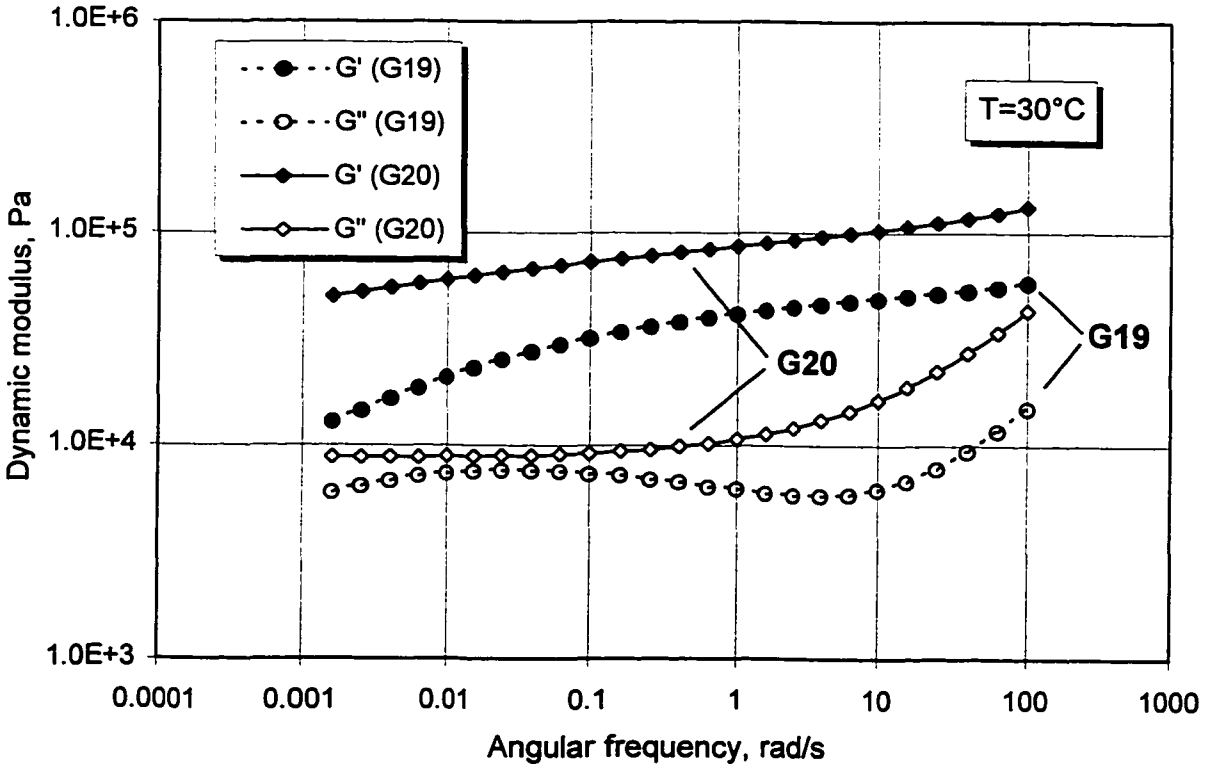


Figure 6-12. Dynamic mechanical spectra for samples G10 & G22.

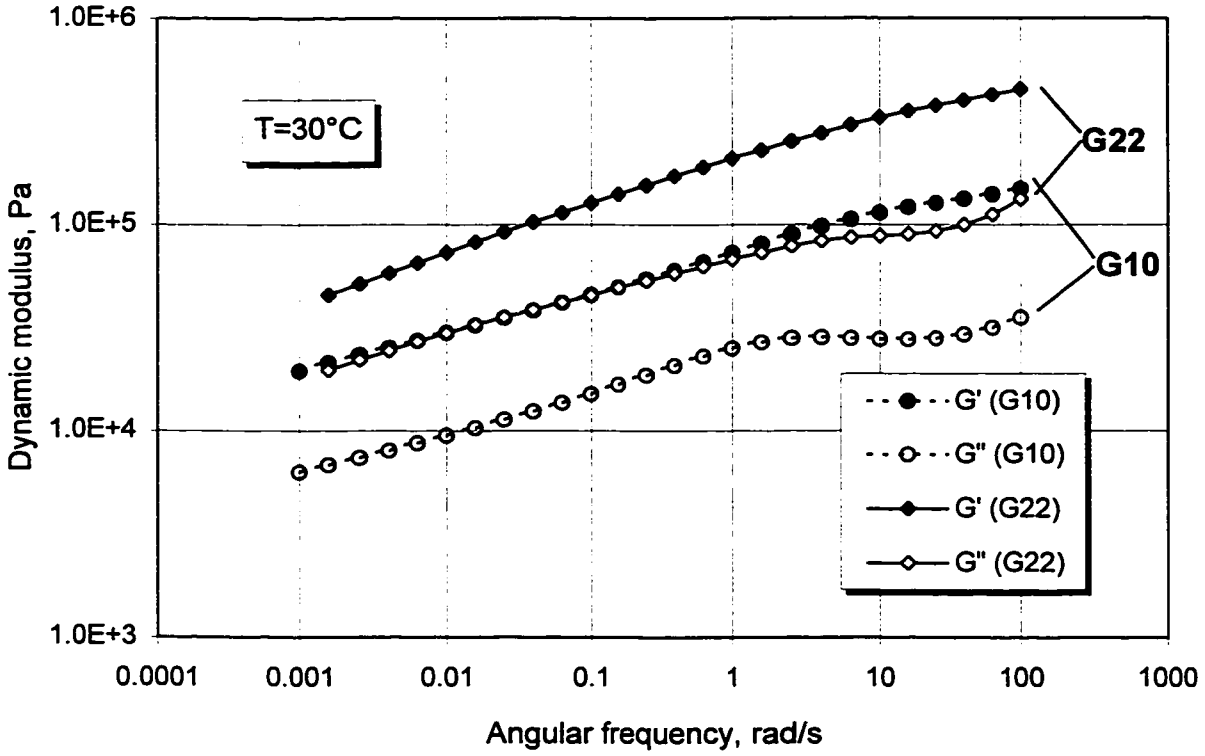


Table 6-2. Characteristic molecular times estimated from frequency dependence of the dynamic moduli.

Sample	Characteristic time	estimated from G"(ω)...
B10	$\tau \approx 0.01$s	... primary plateau
C	$\tau \approx 0.25$s	... minimum of primary plateau
G2 (M_p^b = 7,600)	$\tau \approx 1$s	... minimum of primary plateau
G15 (M_p^b = 36,000)	$\tau \approx 1000$s	... minimum of secondary plateau
G10 (M_p^b = 150,000)	$\tau >> 1000$s	... minimum of secondary plateau

6.1.2 Viscoelastic parameters and their correlation with LCB structure

Rheological parameters which are used to characterize viscoelastic behaviour in the terminal zone and are frequently discussed in the literature in the context of branching structure are: 'zero-shear' viscosity, η_0 (6-1), elasticity coefficient A_G (6-2), and steady-state recoverable compliance, J_e^o (6-3) [325-326],

$$\eta_0 = \lim_{\omega \to 0} (G''/\omega) \tag{6-1}$$

$$A_G = \lim_{\omega \to 0} (G'/\omega^2) \tag{6-2}$$

$$J_e^o = 1/\eta_0^2 \lim_{\omega \to 0} (G'/\omega^2) \tag{6-3}$$

Calculation of these parameters was not possible for the majority of samples examined in this project (B10 being the only exception) due to lack of a 'well-defined' terminal zone, within an experimentally accessible portion of the viscoelastic spectrum.

The principal viscoelastic parameter describing the (rubbery) plateau region is a plateau modulus, G_N^0. It is defined by equation (6-4):

$$G_N^0 = 2/\pi \int_{-\infty}^{+\infty} G''(\omega)\, d(\ln\omega) \tag{6-4}$$

where integration is taking place over the entire range of the independent variable, angular frequency, ω.

The plateau modulus, G_N^0 is indicative of distance between entanglements and can be successfully calculated only if the $G''(\omega)$ peak is well defined within an experimentally accessible range of frequencies. This is usually the case for narrowly-dispersed, flexible and linear molecules [27]. Unfortunately, for all CIIR-g-BR grafts, either the $G''(\omega)$ peak

was poorly defined or the frequency range (0.001 - 100 rad/s) was too narrow to allow for the calculation of the G_N^0 with acceptable accuracy.

Nevertheless, direct readings of the loss modulus, taken in the middle of the rubbery plateau or, in the absence of a well-defined plateau, at the inflection point of the G"(ω) curve, are listed in column "f" in Table A61, Appendix V.

Several other viscoelastic parameters were also defined and calculated, with the intention of correlating them with branching structure. Definitions of those parameters are given below in Table 6-3 and their values are compiled in Tables A61, A62, A63, and A64, in Appendix V. A comprehensive collection of other viscoelastic data from {FS5dec} tests can be found in those Tables as well.

Table 6-3. Linear viscoelastic parameters defined for {FS5dec} frequency sweep.

abbreviation	definition
tan δ(0.001)	- tan δ (=G"/G') at ω=0.001 rad/s
tan δ(0.1)	- tan δ at ω=0.1 rad/s
slope (G'/G"^{2}) @0.001	- slope of (G'/G"^{2}), plotted as a function of log ω, calculated at ω=0.001 rad/s
slope G"(0.001)	- slope of the loss modulus, log G"(log ω) at ω=0.001 rad/s
G"(plateau)	- approximate plateau (or inflection) value of the loss modulus, G" (or G" at 1 rad/s, in the absence of a well defined plateau/inflection point)
n(0.001)	- Power Law Index, for complex viscosity (log η*) plotted as a function of log ω, at ω=0.001 rad/s
n(0.001-100)	- Power Law Index, for complex viscosity (log η*) plotted as a function of log ω, averaged over ω=0.001-100 rad/s range

Screening for correlations between structural/compositional and selected rheological parameters were carried out using JMP® software, as described in Appendix VI.

Prediction profiles for a few chosen parameters are included in Figures A61, A62, A63, A64, in Appendix V. Table 6-4 summarizes results of this screening.

Table 6-4. Correlations coefficients (t-Ratio) between structural/compositional and rheological {FS5dec} parameters.

	RMS {FS5dec}	M_p^b	N_g^p	$w^{b,g}$	$w^{b,h}$	w^b	PDI	vinyl	M_z^G
1	**tan δ(0.001)**	0	0	**-2.89**	0	-	-	0	-2.65
2	**tan δ(0.1)**	+3.83	**-4.15**	0	+2.93	0	-	0	0
3	**slope G"(0.001)**	+	**-3.39**	0	+	0	-	0	0
4/*	**slope (G'/G"^{2})@0.001**	**-9.82**	+	-3.41	-	-3.42	0	0	-3.36
5	**G"(plateau)**	**+2.63**	-	0	+	0	0	0	0
6	**n(0.001)**	0	-	**-2.73**	0	-	-	0	-
7	**n(0.001-100)**	**+4.38**	-3.68	+	+3.40	+	0	-	+

Number indicate the t-Ratio for a statistically significant correlation, that is when |t-Ratio| value is above 2.50 (corresponding to 95% conf. interval).
'-' - negative, statistically not significant correlation (|t-Ratio| values below 2.50)
'+' - positive, statistically not significant correlation (|t-Ratio| values below 2.50)
'0' - week or no correlation (|t-Ratio| values below 1.00)
/* - samples G6, G10 and G22 were excluded from screening for correlations (see text)

Tan δ(0.001)

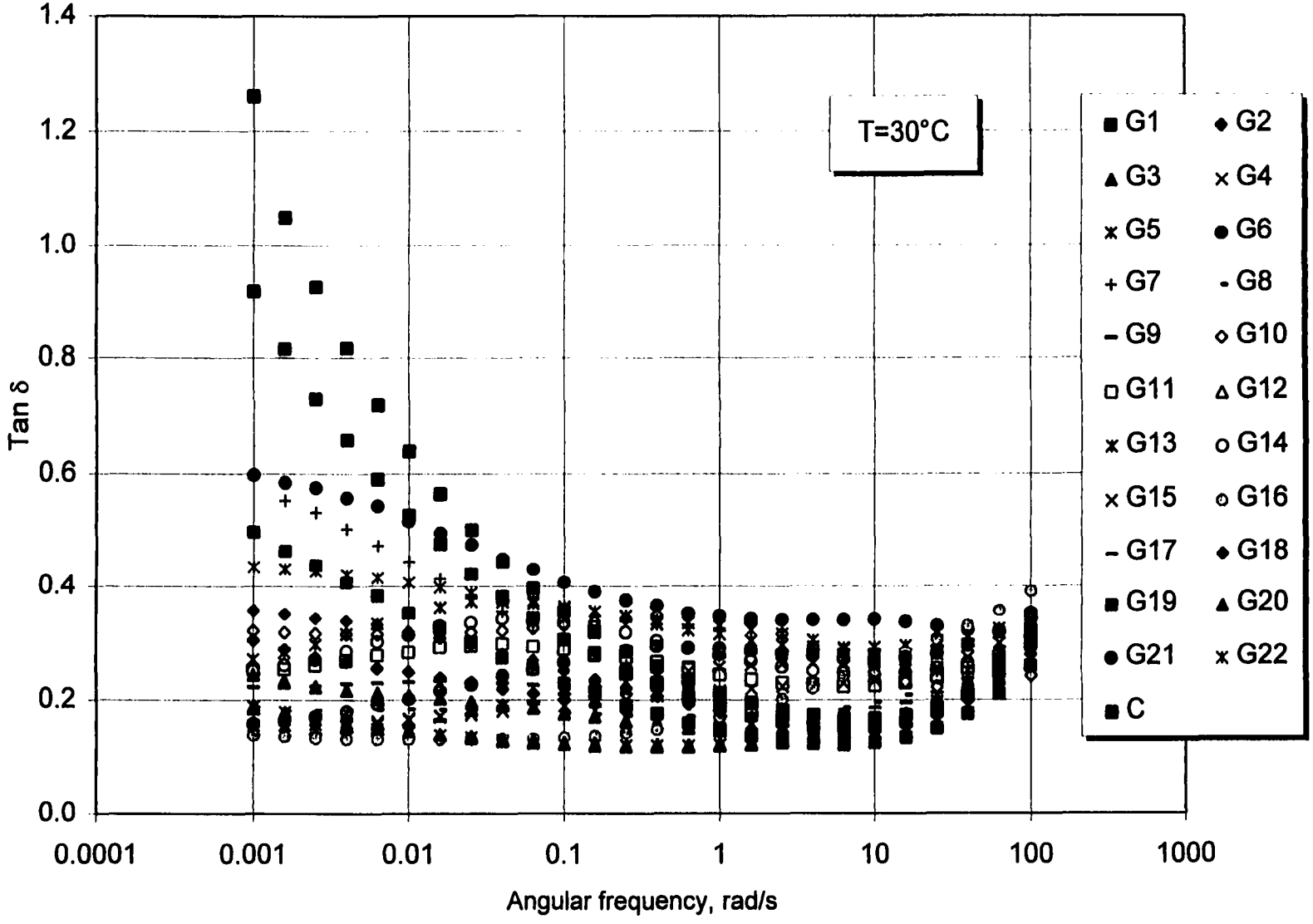
One of the viscoelastic functions which shows the greatest range of variation for whole population of graft samples is the tangent of the loss angle, tan δ. Differences in tan δ(ω) between linear and branched molecules are most prominent at low frequencies. A composite plot of tan δ versus log ω illustrates this point well in Figure 6-13.

This can be explained as follows: due to differences in relaxation times corresponding to the backbone-backbone disentanglement of linear polymers and those resulting from backbone-branch, branch-backbone and branch-branch disentanglements of comb-type polymers [61], it is reasonable to expect that tan δ at 0.001 rad/s will depend to a greater extent on details of branching architecture than tan δ at any other frequency within the range.

Screening for correlation analysis, based on the entire portfolio of samples, suggests that there is no correlation between **tan δ(0.001)** and two specific branching parameters, M_b^p or N_g^p, Table 6-4, row "1". However, an increased branching content, as measured by $w^{b,g}$ parameter, causes **tan δ(0.001)** to decrease. This is equivalent to a graft copolymer behaving more like an "elastic" body, when subjected to mechanical oscillations at very low frequencies. No other structural or compositional effect on **tan δ(0.001)** was identified by screening analysis, except for M_z^G, which is believed to be a result of strong interrelation between $w^{b,g}$ and M_z^G parameters.

However, direct x-y analysis of the relationship between **tan δ(0.001)** and both specific branching parameters reveals an interesting relationships, provided that samples are compared at comparable values of the complementary parameter. The plot of **tan δ(0.001)** as a function of branch length (M_p^b), compared at similar branching number, N_g^p, is shown in Figure 6-14. Branching presence significantly reduces **tan δ(0.001)**, even for samples with very short, G1 (M_p^b =3000) or very few branches, G7 (N_g^p=0.7). **Tan δ(0.001)** for sample C, a linear polymer with comparable molecular weight, is shown there for reference. Further extension of either branch length or number reduces **tan δ(0.001)** even more. However, increasing branch length beyond a certain critical branching degree, estimated to be in order of $w^{b,g}$ = 10%, had little effect on **tan δ(0.001)** as evidenced by the flat lines of **tan δ(0.001)** plotted against M_p^b in Figure 6-14.

Figure 6-13. Composite graph of tan δ - {FS/5dec} test.



Dependence of **tan δ(0.001)** upon branch length is weak regardless of the branching number. More pronounced reduction in **tan δ(0.001)** can be achieved by increasing the number of the branches. Effectiveness of the number of branches in reducing **tan δ(0.001)** value, depends on their length (M_p^b) as is evident from Figure 6-15. The longer the branches, the stronger is the dependence of **tan δ(0.001)** upon N_g^p. Saturation of the **tan δ(0.001)** dependence upon N_g^p is observed at higher N_g^p values, as evidenced by the logarithmic character of the tan δ - N_g^p relation. Even fractional branching numbers (e.g. $N_g^p < 1$) have a significant impact on **tan δ (0.001)**, and this effect is particularly strong for longer branches.

Tan δ(0.1)

With increasing frequency, dependence of tan δ(ω) upon graft LCB structure is becoming more complicated and the influence of the residual ungrafted BR ($w^{b,h}$) on tan δ(ω) is becoming significant. As an example, **tan δ(0.1)** was correlated with structural parameters and results of this screening are shown in Table 6-4 - row "2".

Slope of the loss modulus G" at 0.001 rad/s, ***slope G"(0.001)***

Preliminary screening for correlations suggested that the slope of the loss modulus, G"(ω) at ω=0.001 rad/s, could depend on the branching number, N_g^p. An increase in N_g^p causes a decrease in a slope of the loss modulus. No other (statistically significant) correlations were found for this parameter (Table 6-4 - row "3").

Plots of the **slopeG"(0.001)** as a function of branch length and branching number, are shown in Figure 6-16 and Figure 6-17, respectively.

Figure 6-14. Tan δ at ω=0.001 rad/s as a function of branch length.

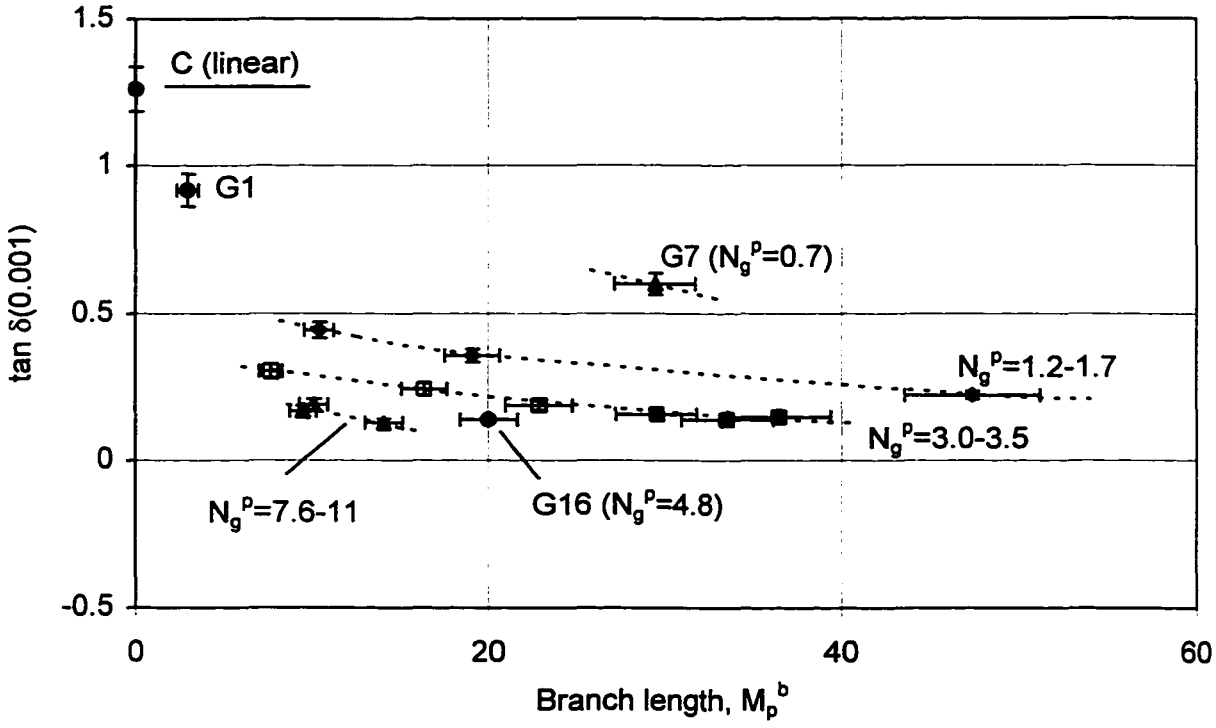
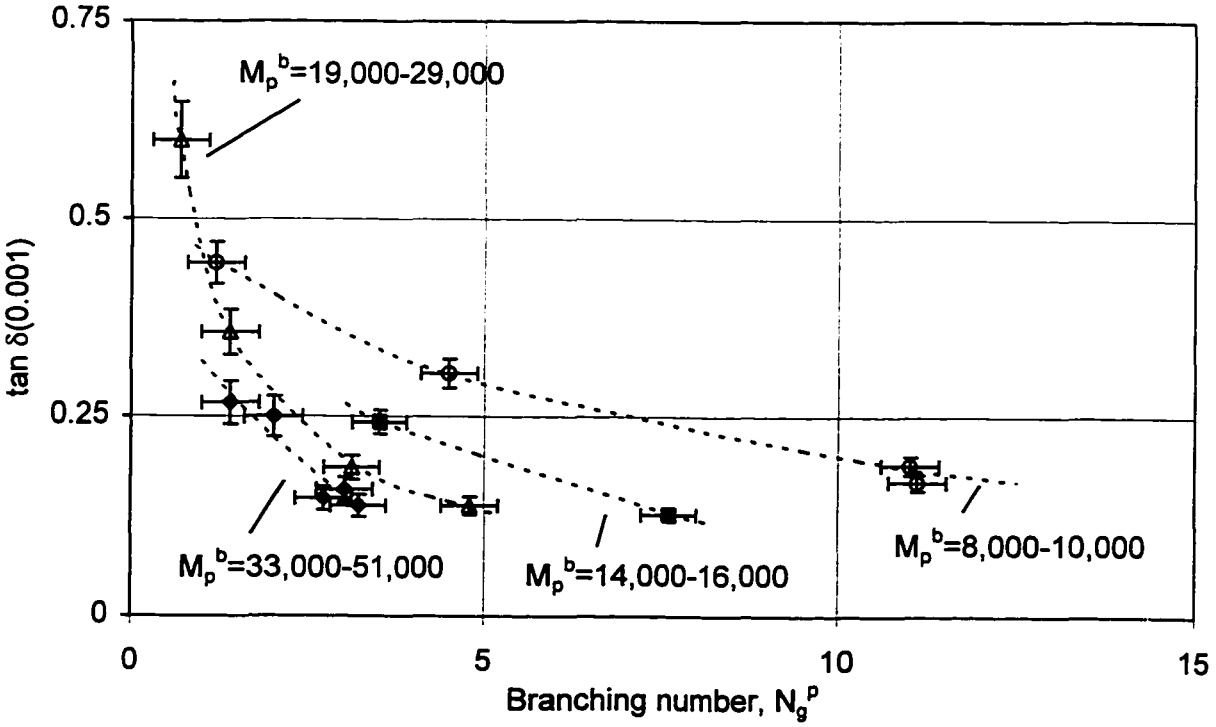


Figure 6-15. Tan δ at ω=0.001 rad/s as a function of branching number.



The following observations were made:

(a) for backbone precursor polymer, sample C

The slope of the log G″(ω) at ω=0.001 rad/s for sample C (+0.517) is different from that reported for flexible, linear polymers in the terminal zone, namely +1.0, [21, 27, 37] and predicted theoretically from the Rouse model [232]. This difference is due to the fact that at ω = 0.001 rad/s, the slope of the loss modulus log G″(ω) has not reached its constant value (see, for example, Figure 6-3). Examination of the analogous curve for lower MW, flexible molecules of the sample B10, provides a supporting argument. Dynamic moduli curves for sample B10 within the same range of frequencies are well advanced into the terminal zone and their slope assumes the terminal proportionalities of $G' \sim \omega^2$ and $G'' \sim \omega$, in agreement with accepted values [232].

(b) *effect of branch length*

The change of the slope **G″(0.001)** as a function of branch length provides dramatic evidence for the impact of side-chain entanglements on viscoelastic behaviour of the graft (Figure 6-16). Introduction of very short branches into linear molecules initially causes a dramatic reduction in slope of the G″(ω) at 0.001 rad/s with increasing length of the branches.

At the branch length corresponding to M_p^b of about 10,000 g/mol, change in the direction of the slope is observed. Slope of the G″ at ω=0.001 rad/s starts increasing, as the length of the branch increases. The relation between the **Slope G″(0.001)** and M_p^b, at $M_p^b > 10{,}000$, fits well a power function in the form $y=a+b\cdot\sqrt{x}$, where y stands for the **Slope G″(0.001)**, x for M_p^b and 'a' and 'b' are fit constants. This functional dependence suggests a certain saturation of the **slope G″(0.001)** function at sufficiently long branches.

(c) *Effect of number of branches*

The parameter **slope G"(0.001)** is exponentially decaying with increasing number of branches, reaching virtually zero at the value of N_g^p about 6 (Figure 6-17).

The considerable scatter in Figures 6-16 and 6-17 is due to the influence of the second principal factor, that is N_g^p for the **slope G"(0.001)** - M_p^b relation, and M_p^b for the **slope G"(0.001)** - N_g^p relationship.

G"(plateau)

Despite the considerable experimental error associated with measurement of the absolute values of dynamic moduli by the RMS-800 using parallel-plate geometry for highly elastic materials, an attempt was made to correlate plateau value of G"(ω) with branching parameters. Indeed, screening for correlations revealed proportional dependence of the plateau modulus upon the branch length (Table 6-4) although the correlation is barely statistically significant.

Slope (G'/G"^{2}) @0.001

J.D. Ferry and coworkers [327-328] noticed that a reduced intrinsic steady-state compliance $j^0_{e,R} = \lim_{\omega->0} [G']_R/[G"]_R^2$, (where $[G']_R$ and $[G"]_R^2$ are intrinsic storage and loss modulus, respectively) is a sensitive indicator of the branching in randomly branched molecules.

Following Ferry's idea, a related viscoelastic parameter proposed by the author, the slope of the $G'(\omega)/G"^2(\omega)$ function, plotted against log ω and calculated at ω = 0.001 rad/s, indeed shows a high degree of sensitivity upon branching, particularly in relation to the length of the branch. Slope of the $G'(\omega)/(G"(\omega))^2$ function calculated at 0.001 rad/s is plotted as a function of the branch length, M_p^b in Figure 6-18.

Figure 6-16. Slope of log G"(ω) at 0.001 rad/s as a function of branch length.

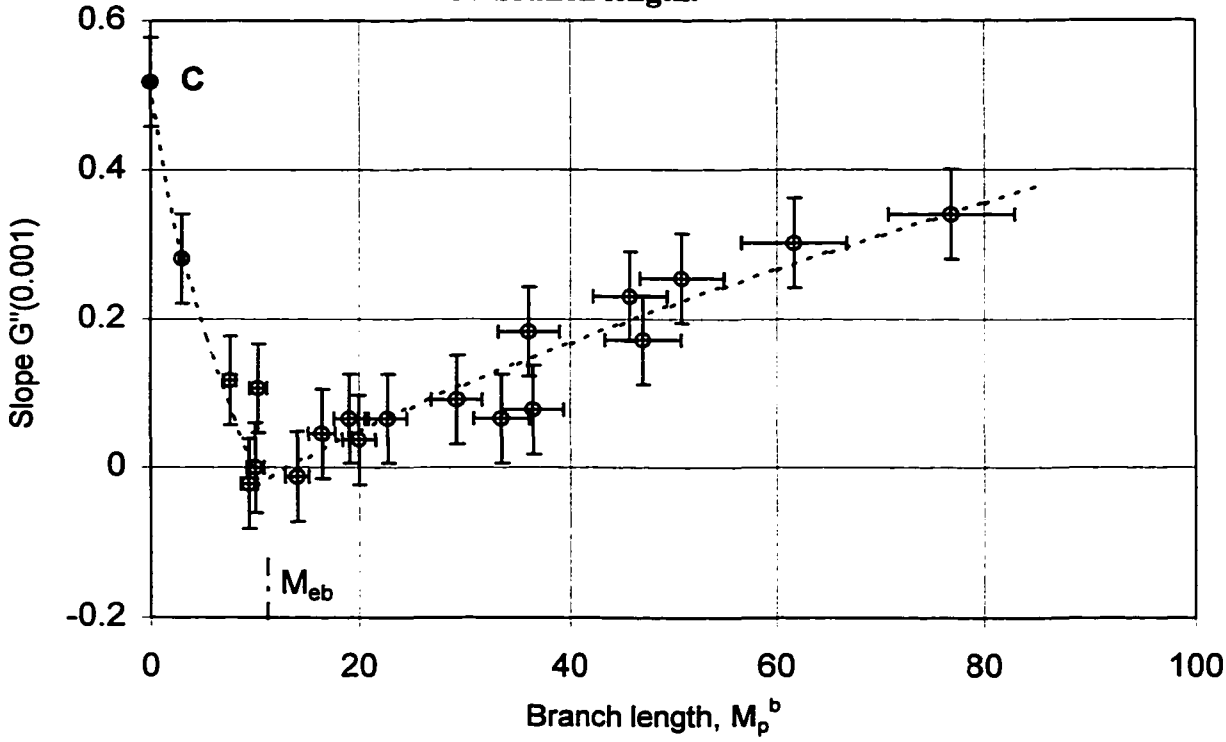
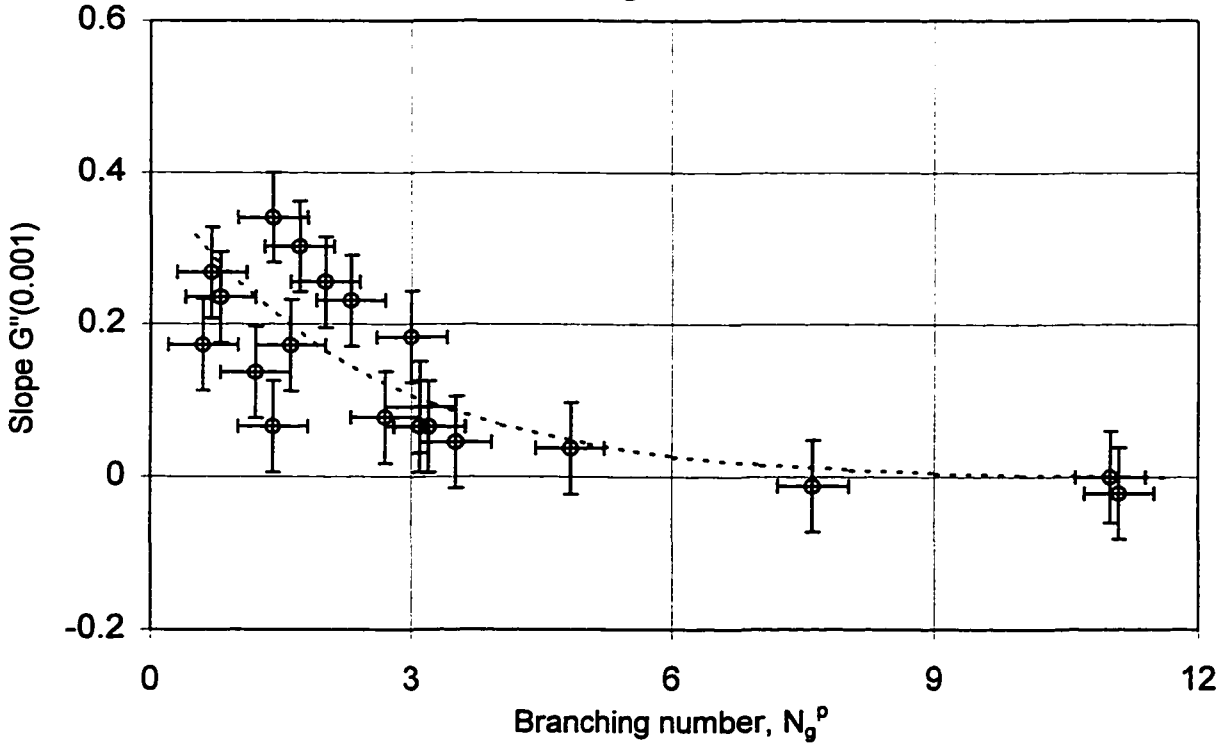


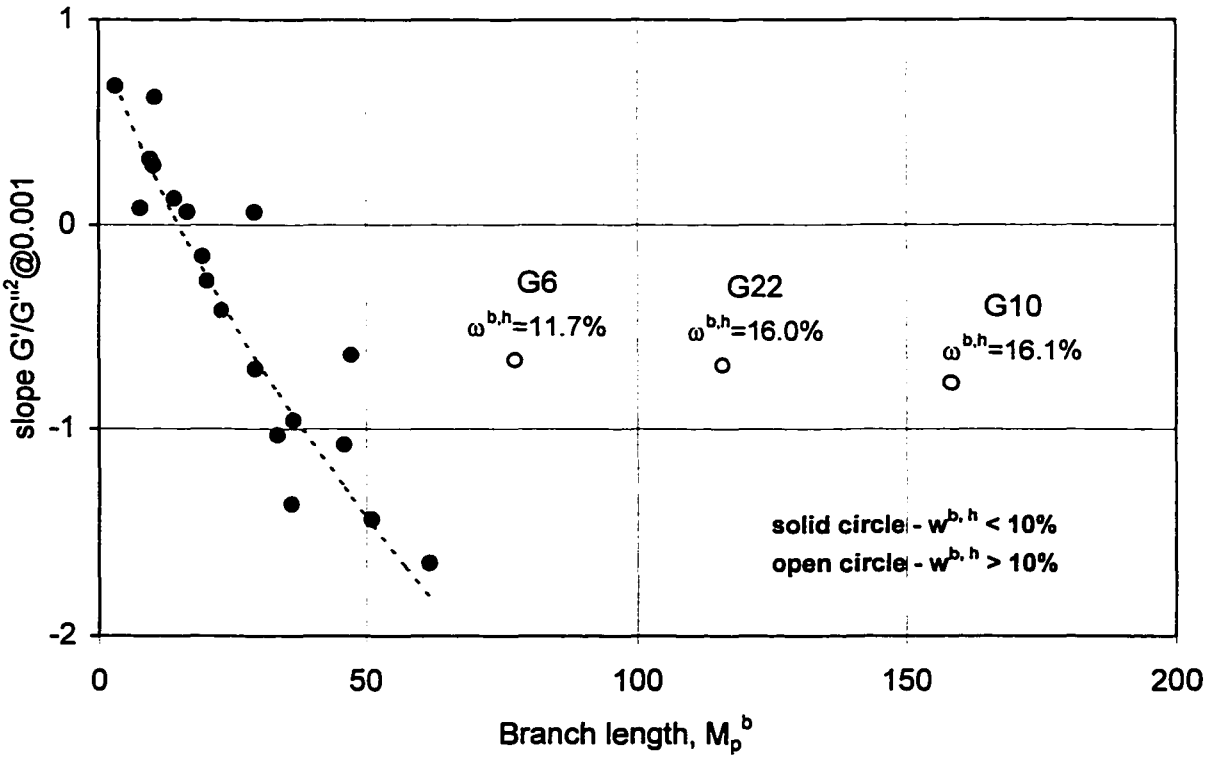
Figure 6-17. Slope of log G"(ω) at 0.001 rad/s as a function of branching number.



A strong correlation between the branch length and **slope (G'/G''^2)@0.001** parameter, is observed. Those samples and only those, marked in Figure 6-18 with open circles, which do not fit the trend line well, distinguish themselves by a high content of ungrafted linear molecules ($w^{b,h}$ > 10%). This suggests that the proposed parameter is also sensitive to the content of linear molecules in a matrix of branched molecules. This might limit potential application of this parameter as a tool for the characterization of the LCB in commercial polymers.

Discussion of the two remaining parameters, defined in Table 6-3, **n(0.001)** and **n(0.001-100)**, is postponed to the next section of this chapter.

Figure 6-18. Slope (G'/G''^2)@0.001 parameter as a function branch length.



6.1.3 Frequency-dependence of complex viscosity

Complex viscosity, $\eta^*(\omega)$ is related to the complex modulus, $G^*(\omega)$, according to equation (6-5),

$$\eta^*(\omega) = G^*(\omega) / i \cdot \omega \qquad (6\text{-}5)$$

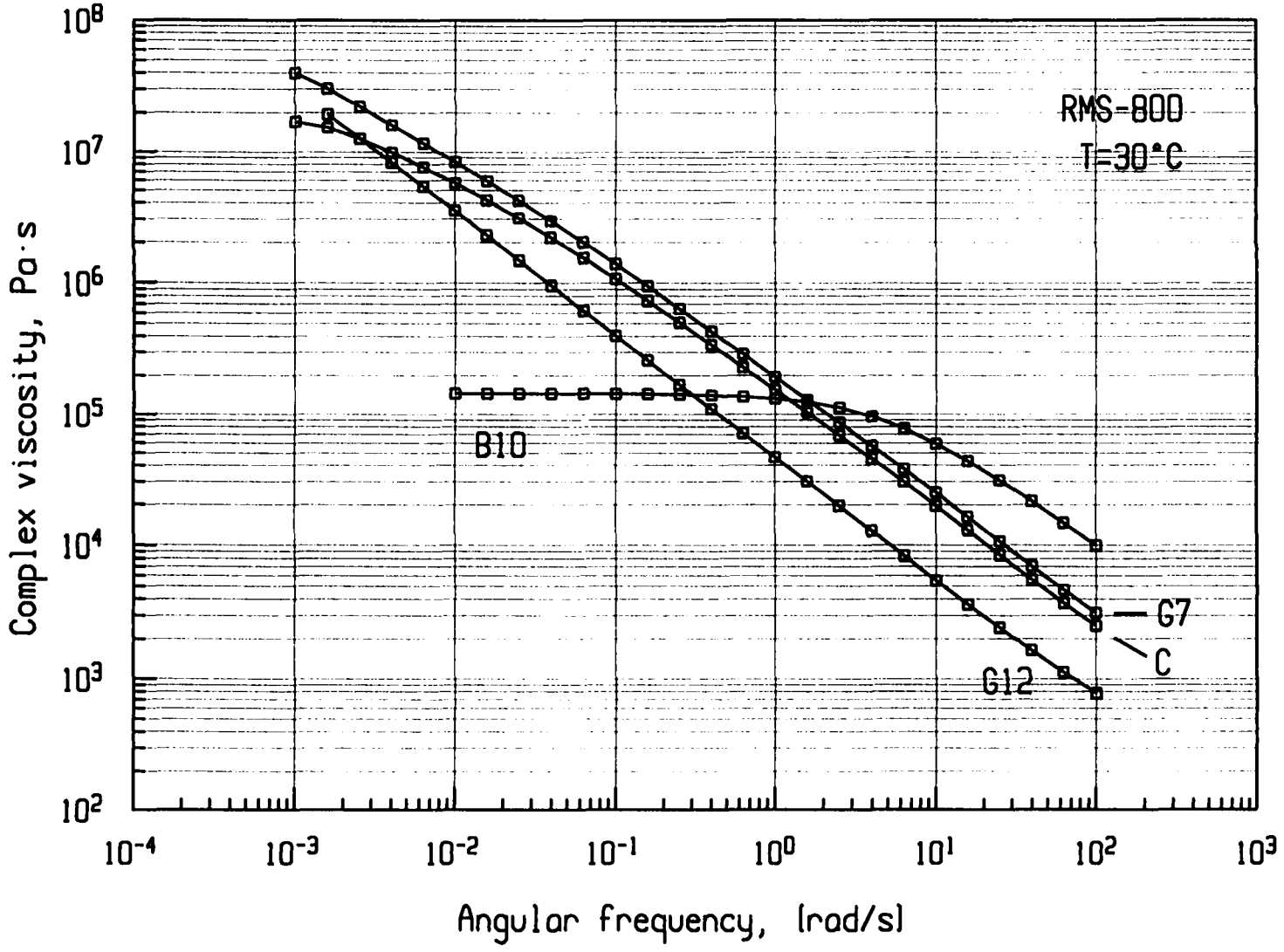
The absolute value of the complex viscosity, $|\eta^*(\omega)| = \text{sqrt}\,[(\eta')^2 + (\eta'')^2]$ and further referred to simply as η^*, is plotted as a function of angular frequency, ω, in Figure 6-19, for a few representative samples. For grafts regardless of their grafting architecture, the shape (frequency-dependence) of the η^* shows only small differences. Sample G12 has the η^* function typical for most grafts. It constitutes a nearly perfect straight line on a double-logarithmic ($\log \eta^*$- $\log \omega$) graph, and therefore it fits the Power Law model equation very well (6-6),

$$\eta^* = K' \cdot \omega^{n-1} \qquad (6\text{-}6)$$

One of the rheological parameters which is most frequently investigated in the context of the structure-property relashionship, is the 'zero-shear' viscosity, η_0 [17, 27, 47, 57, 63].
The η_0 is defined as a limiting value of the steady-shear (or complex viscosity) at the diminishing rates of shear (or ω->0 for η^*). Direct experimental measurement of the η_0 was possible only for sample B10 (e.g. a low MW, narrowly-polydispersed polybutadiene, representative of a branch prepolymer), as evident from Figure 6-19. In fact, for graft samples with well-developed branching (G12 is a good example) no indication of the (first) Newtonian plateau exists within the 0.001-100 rad/s frequency range.

However, for some samples, particularly those with a low branching content like G7, there is evidence of change in the slope of $\log \eta^*$- $\log \omega$ at the lowest frequencies (Figure 6-19). This "leveling-off" of the slope of $\log \eta^*$ - $\log \omega$ is even more pronounced for sample C, for

Figure 6-19. Complex viscosity curves for representative samples.



which the critical frequency, ω_c (frequency marking the transition from a Newtonian to a shear/frequency-thinning zone), could be estimated to be about 0.001 rad/s. The value of the same parameter for sample B10 was estimated to be 6-7 rad/s. Either value corresponds very well to the corresponding first cross-over frequency, reported in Table 6-1, section 6.1.1. Similar changes in the slope of log η^* - log ω curve at low frequencies were reported for many polymers [2, 232, 323].

Attempts to fit the complex viscosity to a model (Ellis or Carreau), which could give an estimate of η_0, gave no reliable results, due to the very poor definition of the Newtonian plateau in the experimental data. As a result, no correlations could be made for graft copolymers (CIIR-g-BR) between zero-shear viscosity, η_0, and details of the LCB structure.

In certain instances, the Power Law index, n (equation 6-6) can be used as a measure of frequency-dependence of the complex viscosity, η^*. Index n, is related to the slope of the log η^*- log ω line by the simple relation (6-7),

$$n = 1 + \text{slope of the } (\log \eta^* - \log \omega) \text{ plot} \qquad (6\text{-}7)$$

Due to the fact that the slope of the log η^*- log ω plot is always negative and never less than -1, the lower value of the Power Law index is, the more frequency-sensitive is the complex viscosity.

Power Law Index values, n were either calculated at ω=0.001 rad/s or averaged over the entire spectrum of frequency, 0.001 - 100 rad/s. Values are tabulated in Table A61, Appendix V. Both parameters were screened for correlation with structural parameters. Results of this screening in the form of prediction profiles are included in Figures A61, A62, A63 and A64, Appendix V, and correlation coefficients are summarized in Table 6-4 in section 6.1.2.

Figure 6-20. Frequency-dependence of complex viscosity; effect of branch length.

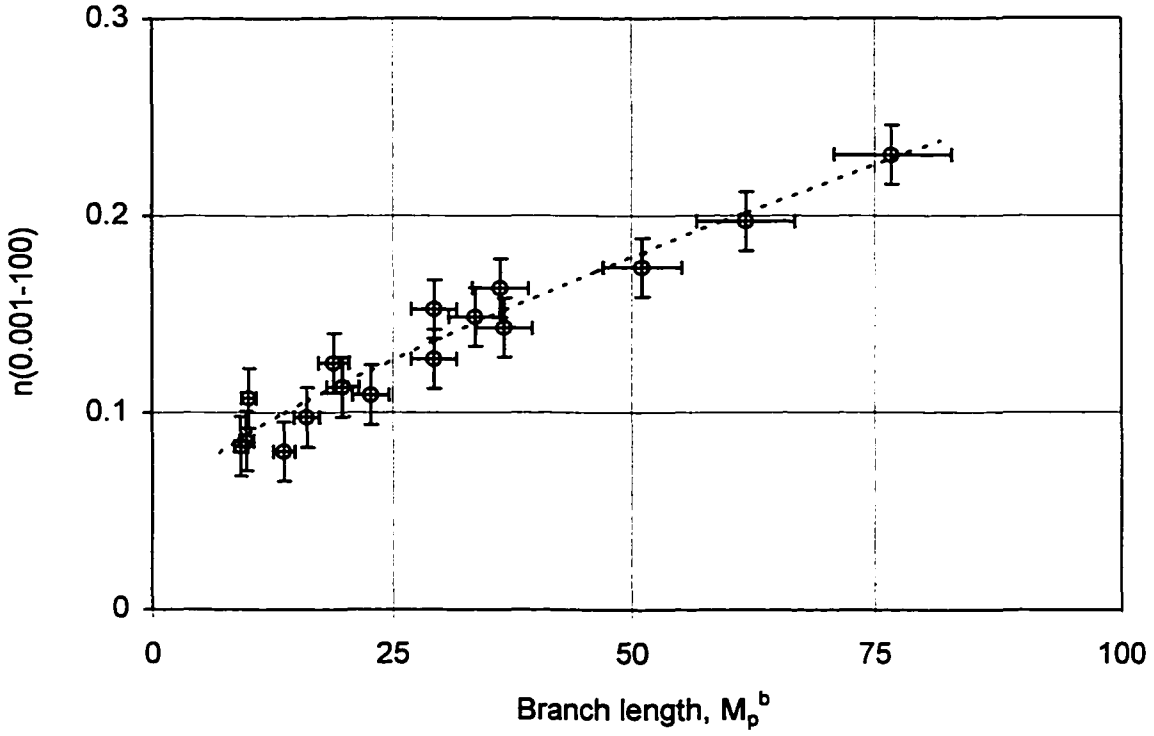
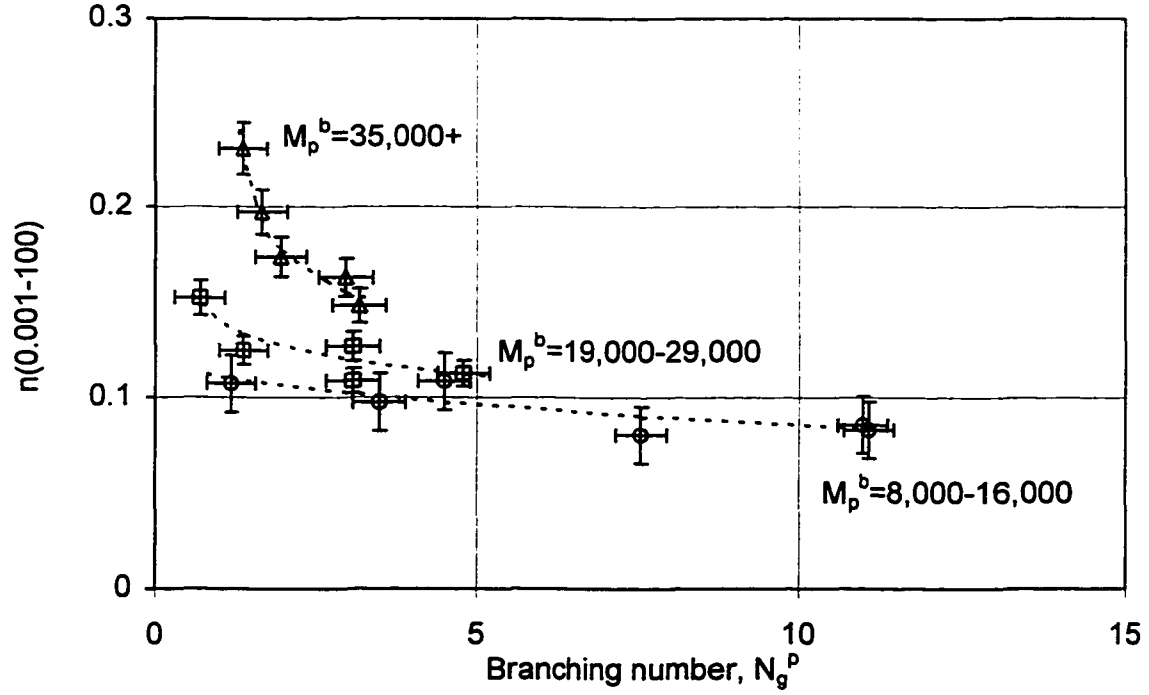


Figure 6-21. Frequency-dependence of complex viscosity; effect of branching number.



*Parameter **n(0.001)***

Parameter **n(0.001)** seems to be a good indicator of the branching content $w^{b,g}$. Screening analysis for correlations provides no evidence for any other structural or compositional parameter, having statistically significant influence on **n(0.001)** - Table 6-4.

*Parameter **n(0.001-100)***

Power Law index, averaged over the 0.001-100 rad/s, **n(0.001-100)**, is becoming more sensitive to specific LCB parameters than to $w^{b,g}$. For the majority of graft architectures (possibly excluding samples with extreme values of N_g^p) increasing length of the branch decreases the frequency-dependence of η^*, as seen in Figure 6-20. This is equivalent to saying that the longer the branches attached to the backbone of the graft are, the higher the **n(0.001-100)** values. The nearly proportional relation between branch length and **n(0.001-100)** parameter, does not require qualification of the branching structure according to their branching number. Grafts with longer branches approximate the behaviour of linear polymers, as far as frequency-dependence of the complex viscosity is concerned.

The effect of the branching number N_g on the **n(0.001-100)** parameter is just the opposite. The slope of $\log \eta^*$- $\log \omega$ curve increases with number of branches and effect of N_g is stronger for grafts with longer branches and at lower branching number ($N_g^p < 2.0$) - Figure 6-21. As a result, the frequency dependence of complex viscosity is highest for grafts with shorter but numerous (N_g^p ~10 or more) branches. Consequently, **n(0.001-100)** increases, i.e. grafts became less rate-dependent as branches are becoming longer and fewer of them are attached to the backbone.

The values of the **n(0.001-100)** for "star-like" structures, samples G10 and G22 are 0.177 and 0.198, respectively, and are very similar or identical with **n(0.001-100)** for sample C (0.198). This result is in agreement with relevant data published for branched polymers [329-330].

The upper limit of the Power Law Index for shear-thinning fluids equals to unity (1.0) and this is the case for Newtonian fluids. For the majority of graft samples, **n(0.001-100)** falls to below 0.20, or even below 0.10 for some multi-branched grafts (samples G12, G13 and G20), a very low value by comparison with many gum elastomers or thermoplastic melts.

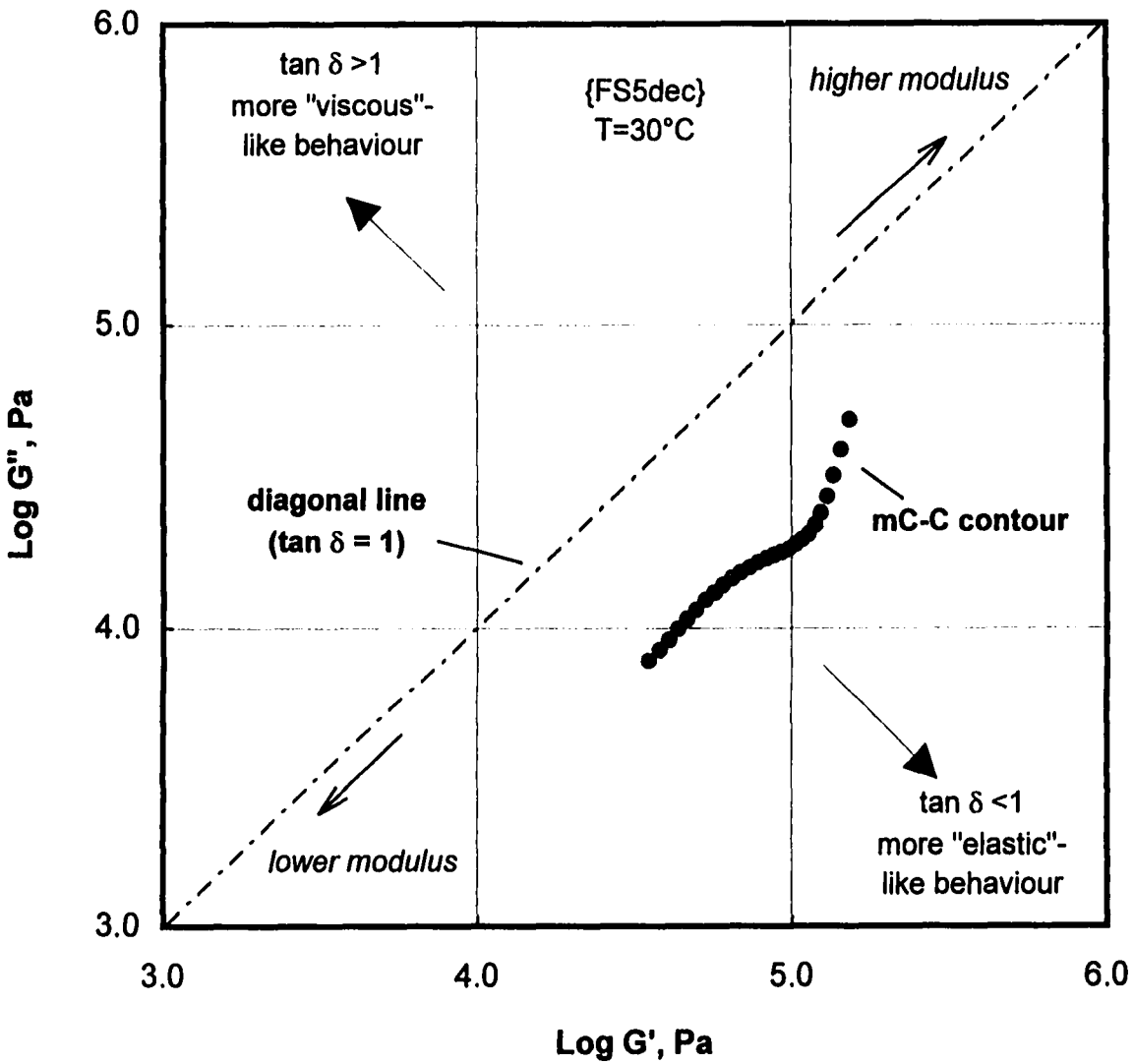
6.1.4 Modified Cole-Cole plots

The Cole-Cole plot offers an alternative way to explore frequency-dependence of dynamic viscoelastic functions, by explicitly illustrating the mutual correspondence of both dynamic moduli, G′ and G″ [256, 259, 331]. A *modified* Cole-Cole plot (mC-C plot) is a special case of the Cole-Cole plot, in which log G″(ω) is plotted against log G′(ω). The position and the shape of the modified Cole-Cole contour has been related to the structure and composition of elastomers. In particular, mC-C plots were used to define and quantify long-chain branching [256-257, 259, 323, 331-334]. A typical mC-C plot for long-chain branched structures together with basic interpretation, is shown in Figure 6-22.

The shape of the mC-C contour has been shown for homogeneous polymers to be essentially independent of molecular weight [256, 335] and for thermo-rheologically simple materials, also independent of temperature [336]. On the other hand, the contour of the mC-C plot has been found to be particularly sensitive to branching architecture and the MWD, as well as being able to assume certain characteristic shapes, depending on the type and details of the branching structure [256-257, 259, 323, 331].

For series of CIIR-g-BR graft copolymers, mC-C plots were prepared from the dynamic moduli {FS5dec} data. Examination of mC-C contours with relation to known details of the branching structure, allows for the following observations regarding the shape of mC-C contours.

Figure 6-22. Typical modified Cole-Cole plot - example for sample G17.



"OK"-shaped contours in Figure 6-23 for sample C, G18 and G19, are typical for either linear molecules or molecules with few, short branches which modify the rheological behaviour (at temperatures well above T_g) only slightly. Short branches might, for example, shorten the length of the contour, while preserving its shape.

For grafts with shorter but numerous branches (say $N_g^p > 5$), the contour assumes a "hockey-stick"-like shape (Figure 6-24), while for a graft having an intermediate number and length of branches ($M_p^b \sim 30{,}000$, $N_g^p \sim 3.0$), it assumes a "worm"-like shape with two inflection points (Figure 6-25). Comparison of the mC-C plots with corresponding dynamic spectra (Figures AFSG5, AFSG8, AFSG9 or AFSG4 in Appendix V, reveals, that these inflection points correspond to the double "plateaus" found in log G″ - log ω or tan δ - log ω curves.

Another class of long-chain branched polymers with a branching number about unity or less but with branches of comparable length to that of the backbone ("star"-like), tend to have long and "stretched" mC-C contours (Figure 6-26).

The value and possible applications of the mC-C plots lie in their ability to map different branching structures, to facilitate the characterization of branching in unknown samples, as well as to monitor changes of polymer structure in a manufacturing environment.

Gradual evolution of the mC-C contour can be readily observed in a series of samples in Figure 6-27. Contour changes due to systematic increase of the branch length at the comparable N_g^p are shown in column (a) and changes induced by increasing branching number, at the comparable M_p^b, in column (b).

Figure 6-23. Modified Cole - Cole contours for linear or weakly-branched molecules.

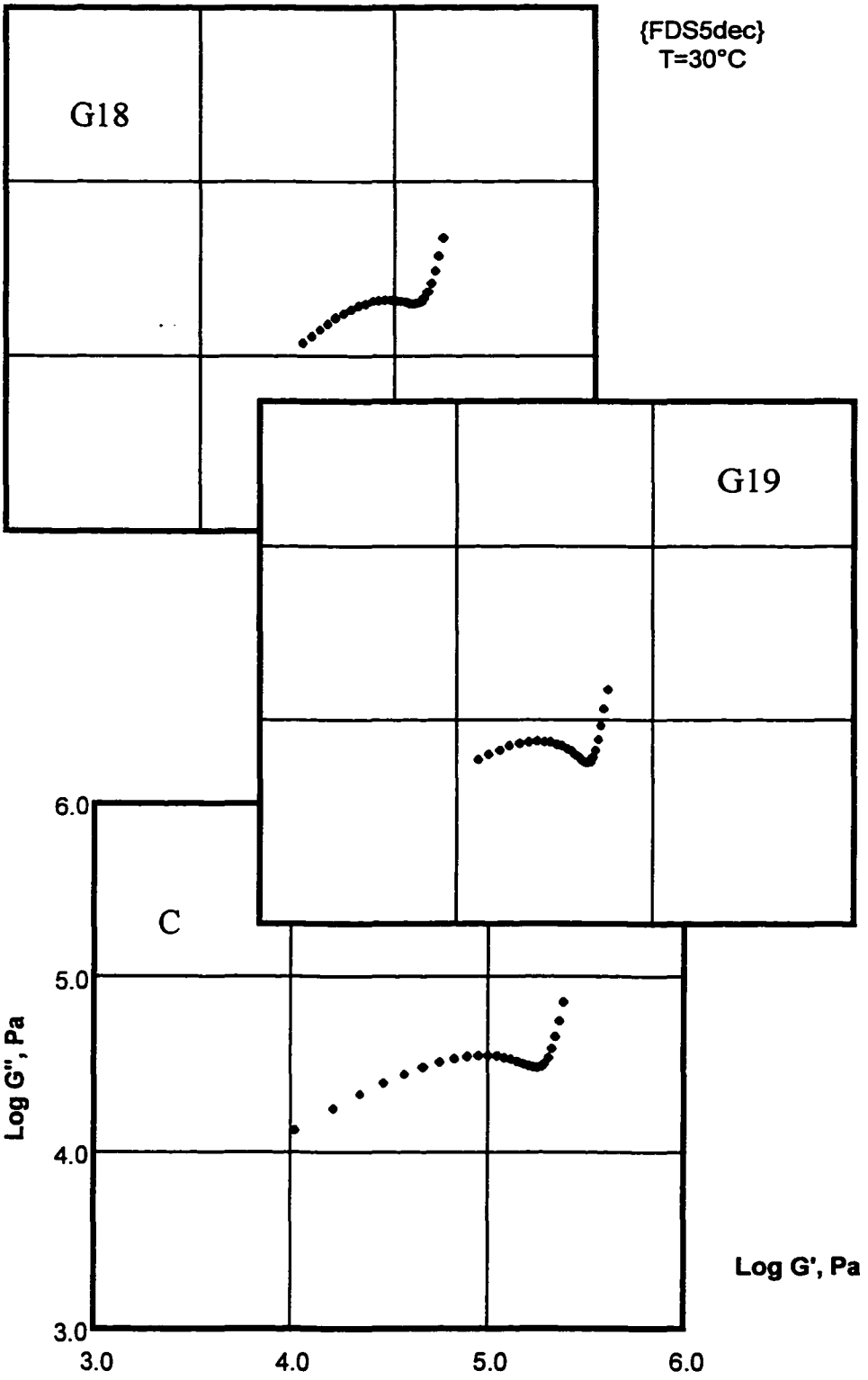


Figure 6-24. Modified Cole - Cole contours for multi-branched, comb-like structures ($N_g^p > 5$).

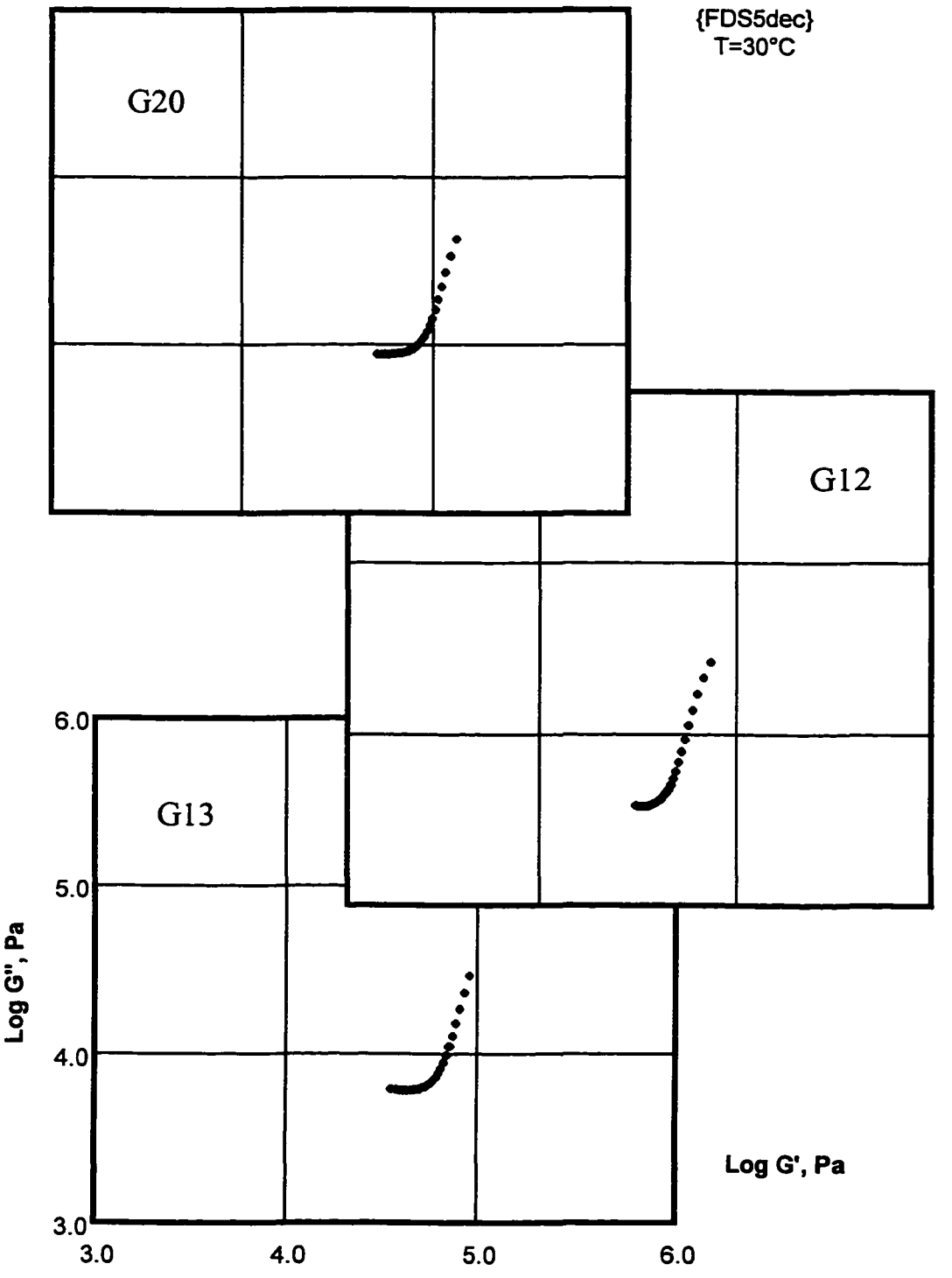


Figure 6-25. Modified Cole - Cole contours for grafts with intermediate branching structures ($M_p^b \sim 30{,}000$, $N_g^p \sim 3.0$).

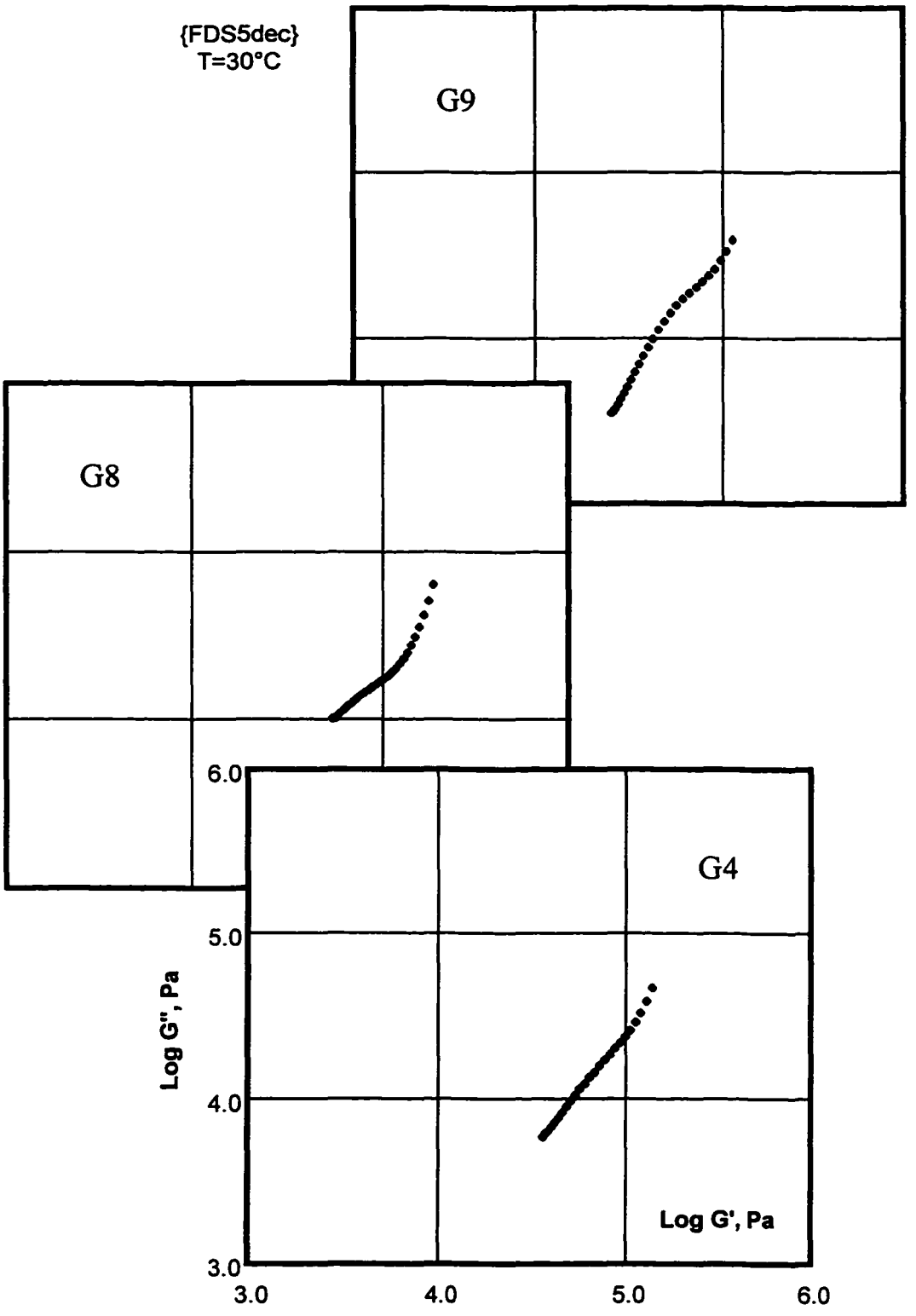


Figure 6-26. Modified Cole - Cole contours for grafts with few long branches ("star"-like structures).

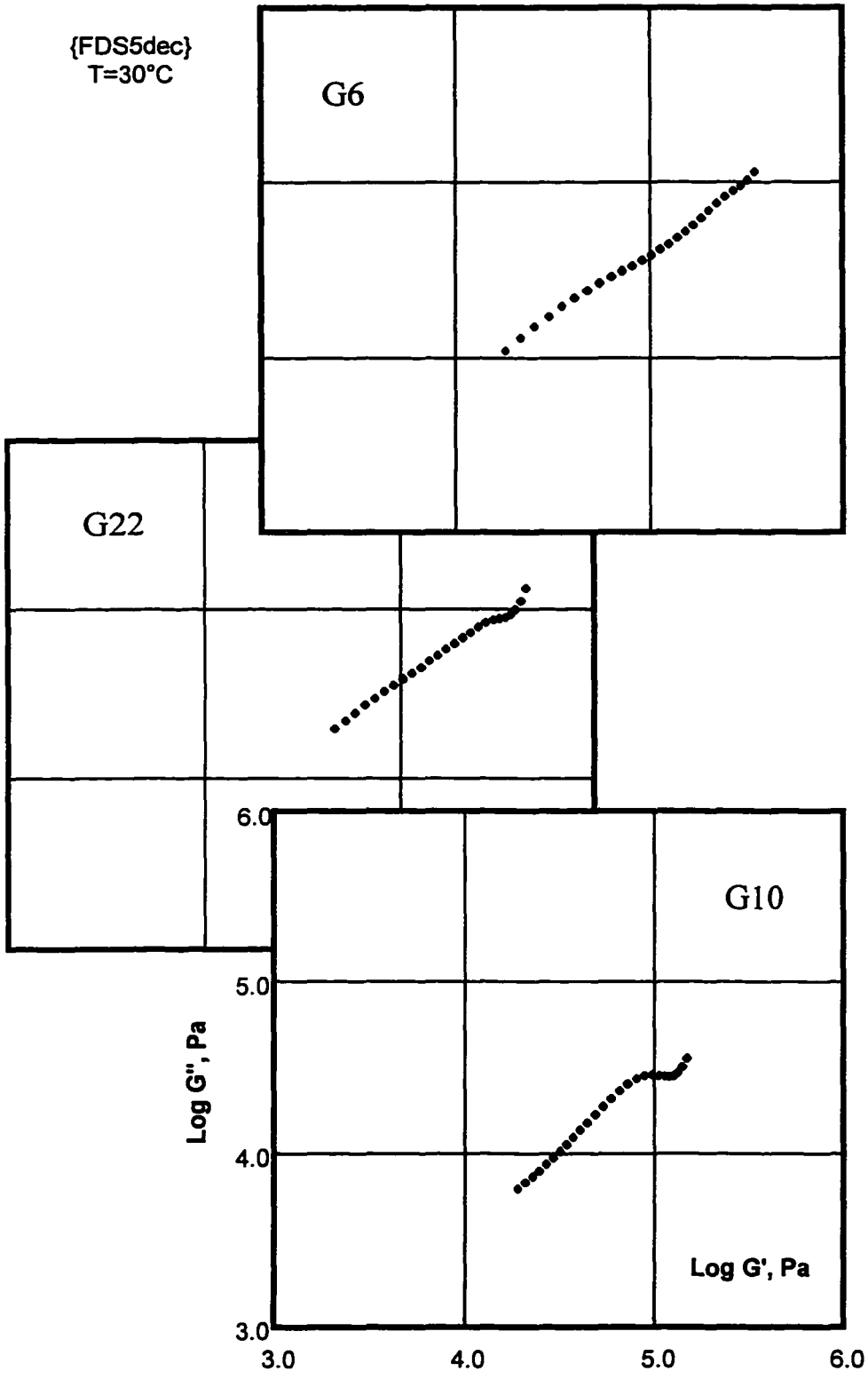
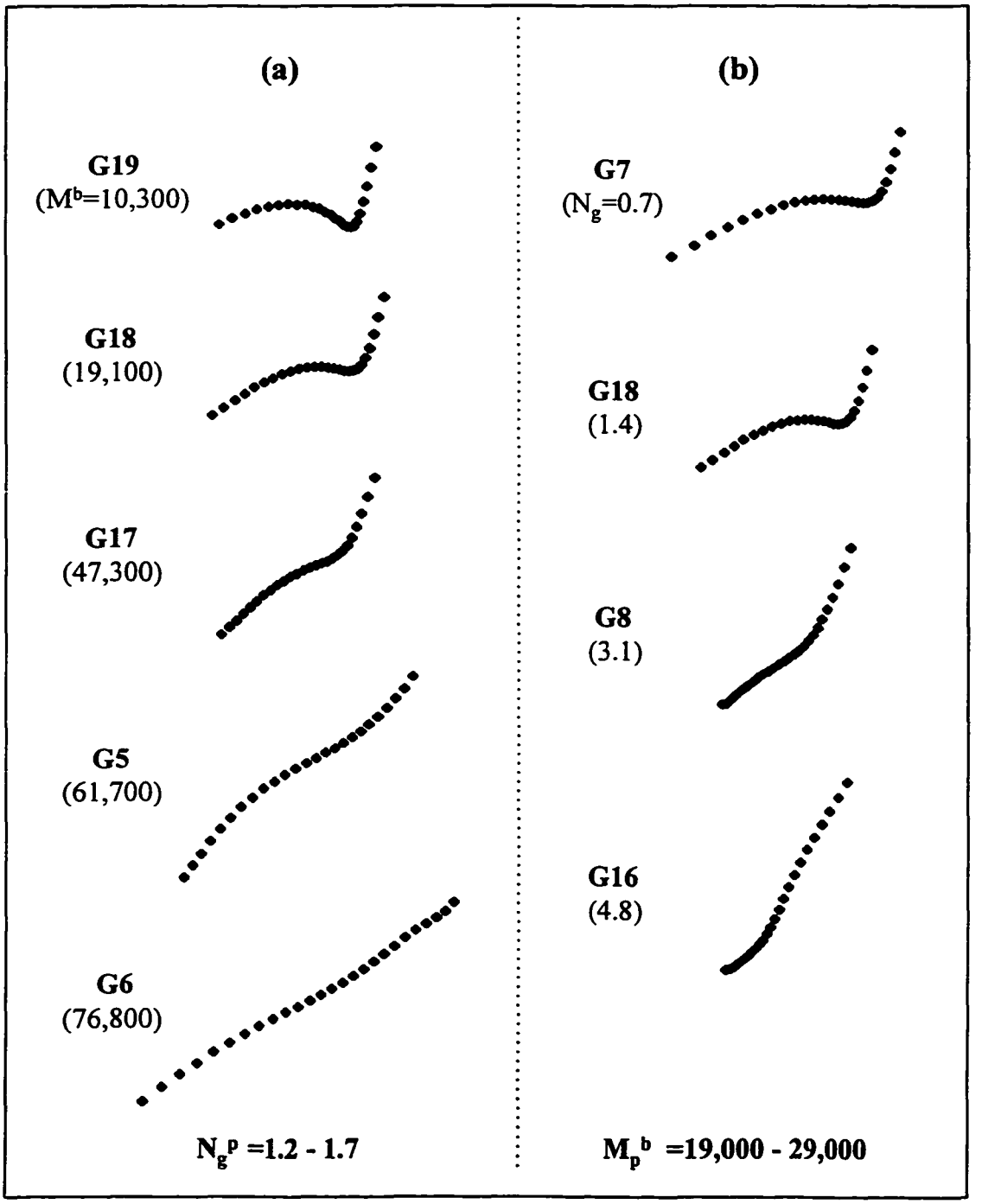


Figure 6-27. Evolution of modified Cole - Cole contour;
a) as a function of branch length, at comparable branching number,
b) as a function of branching number, at comparable branch length.



Another form of the Cole-Cole plot, named by the author a "normalized" Cole-Cole plot (nC-C), was found to be an even more effective tool for mapping LCB structures. An example of an nC-C plot derived from a set of data identical to those used to construct the mC-C plot in Figure 6-22, is shown in Figure 6-28. This approach to characterization of the long-chain branching from the dynamic mechanical data, will be discussed in Chapter 7, section 7.5.

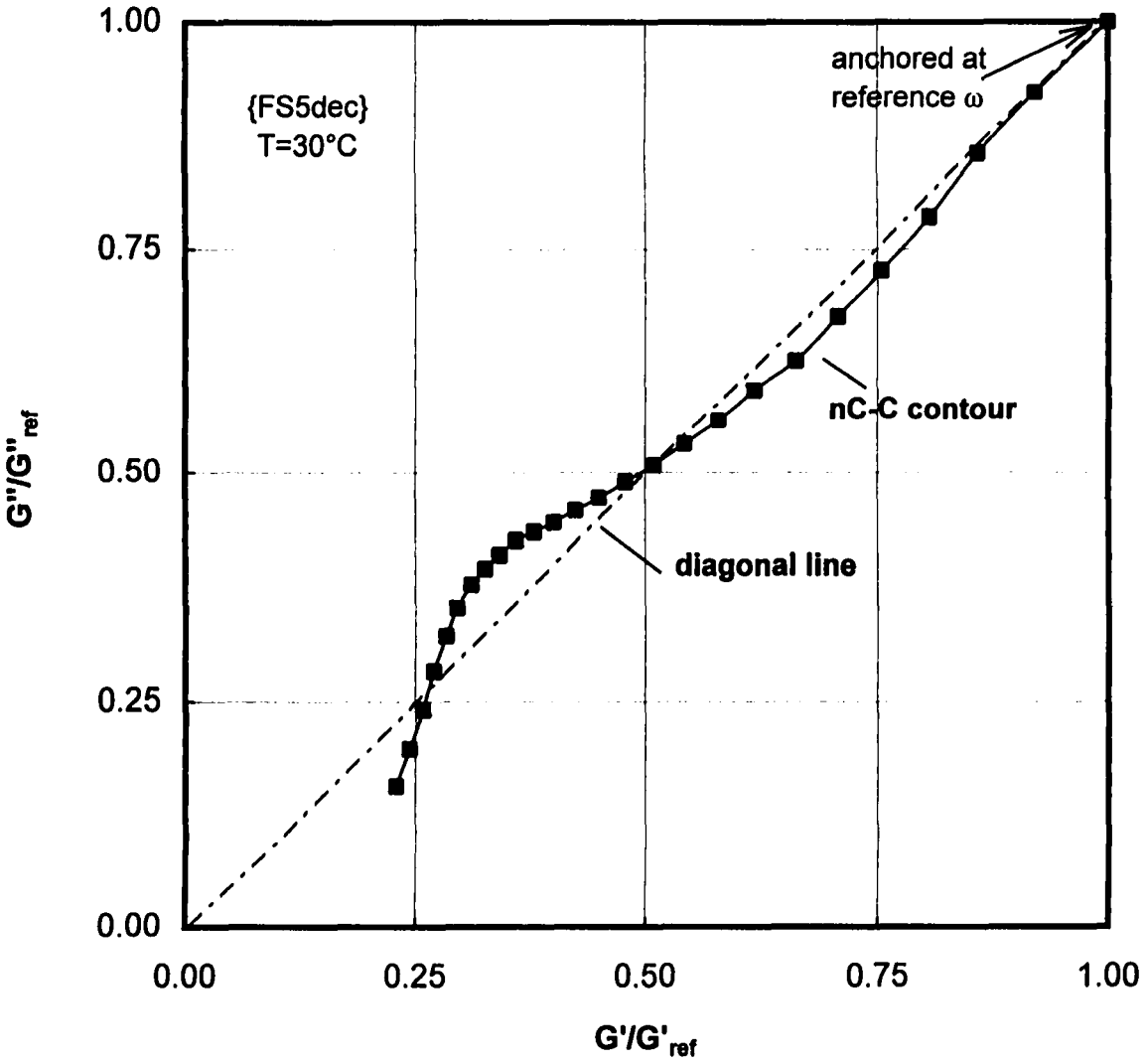
6.2 Frequency-temperature superposition and temperature dependence of linear viscoelastic functions

Rheological measurements carried out using the RMS-800, test configuration {FTS}, were designed to examine simultaneously both temperature and frequency dependence of the linear viscoelastic functions. Experiments consisted of a series of isothermal frequency sweeps, carried out over the same frequency range and on the same specimen, at progressively increasing temperatures; 30, 55, 80, 105 and 130°C. Complete test conditions, listed in Appendix IV, Table A, Part 2, were designed to allow for a comparison between isothermal (30°C) {FS5dec} test results and the "master-curves" reduced from {FTS} data, at the reference temperature of 30°C.

The complete collection of the master-curves (Figures AFTS***), regardless of the success of the shift procedure, is included in Appendix V.

The ability of frequency-temperature (f/T) shift to determine the behaviour of a material beyond an experimentally convenient or accessible frequency range is one of the major benefits of this technique. This shift technique can also be applied in order to obtain a measure of temperature dependence of viscoelastic functions. Finally, under certain assumptions, from a successful (or otherwise) superposition of data, thermo-rheological simplicity (or complexity) can be inferred.

Figure 6-28. Typical normalized Cole - Cole plot - example for sample G17.



6.2.1 Frequency-temperature superposition and master-curves

A series of frequency sweep isotherms were shifted and transformed into a single "master-curve", at the reference temperature of 30°C, using Rheometrics RHECALC® software [337]. The RHECALC® program uses several algorithms for data transformation, all based on the time/frequency-temperature (t/f-T) superposition principle [338]. Both horizontal and vertical shifts and a few shift algorithms were employed. Identical shifting procedure was applied consistently to all samples. In particular, no "manual re-shift" was attempted, in order to possibly improve the quality of the transformation in some cases. Average values from several shifts are reported. Horizontal shift parameters $a_T(T)$ were calculated and fitted to both WLF (6-8) and Arrhenius (6-9) equations,

$$\log a_T = -c_1 (T-T_0) / (c_2 + T-T_0) \tag{6-8}$$

where, a_T - horizontal shift factor
c_1, c_2 - WLF constants
T - temperature, K
T_0 - reference temperature, K

$$a_T = K \cdot \exp [E_a / RT] \tag{6-9}$$

where, a_T - horizontal shift factor
K - proportionality factor
E_a - activation energy, J/mol
T - temperature, K
R - gas constant, J/mol·K

Figure 6-29 shows a family of G'(ω) and G"(ω) isotherms for sample G3, as an example. Figure 6-30 presents a master-curve generated from these isotherms by a combination horizontal and vertical t/f-T shifts. Both graphs use the same scale for convenient comparison of data. In some cases, transformation allowed more than double the frequency range available for the interpretation of the G'(ω) and G"(ω) curves.

Figure 6-29. A series of dynamic moduli isotherms for sample G3.

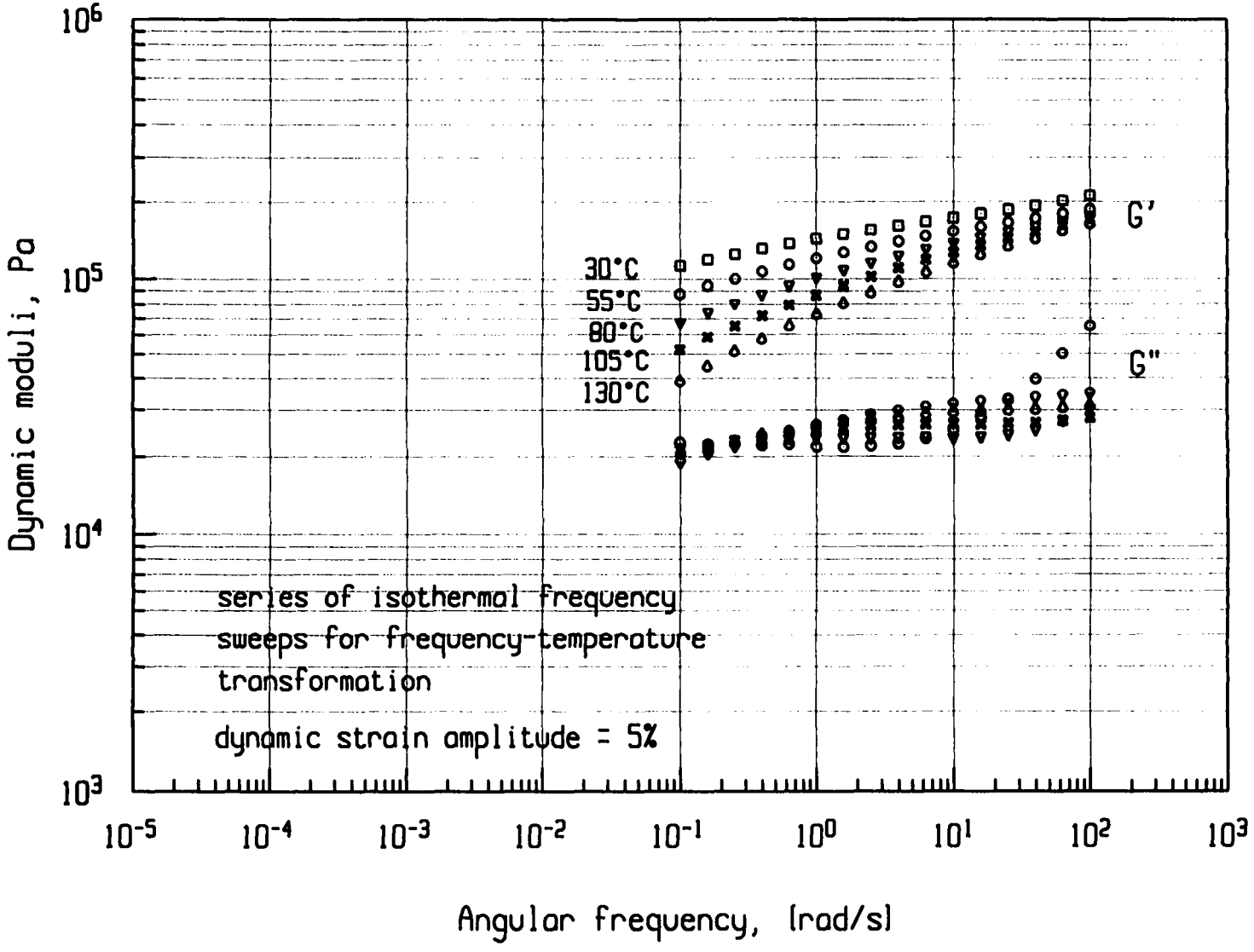
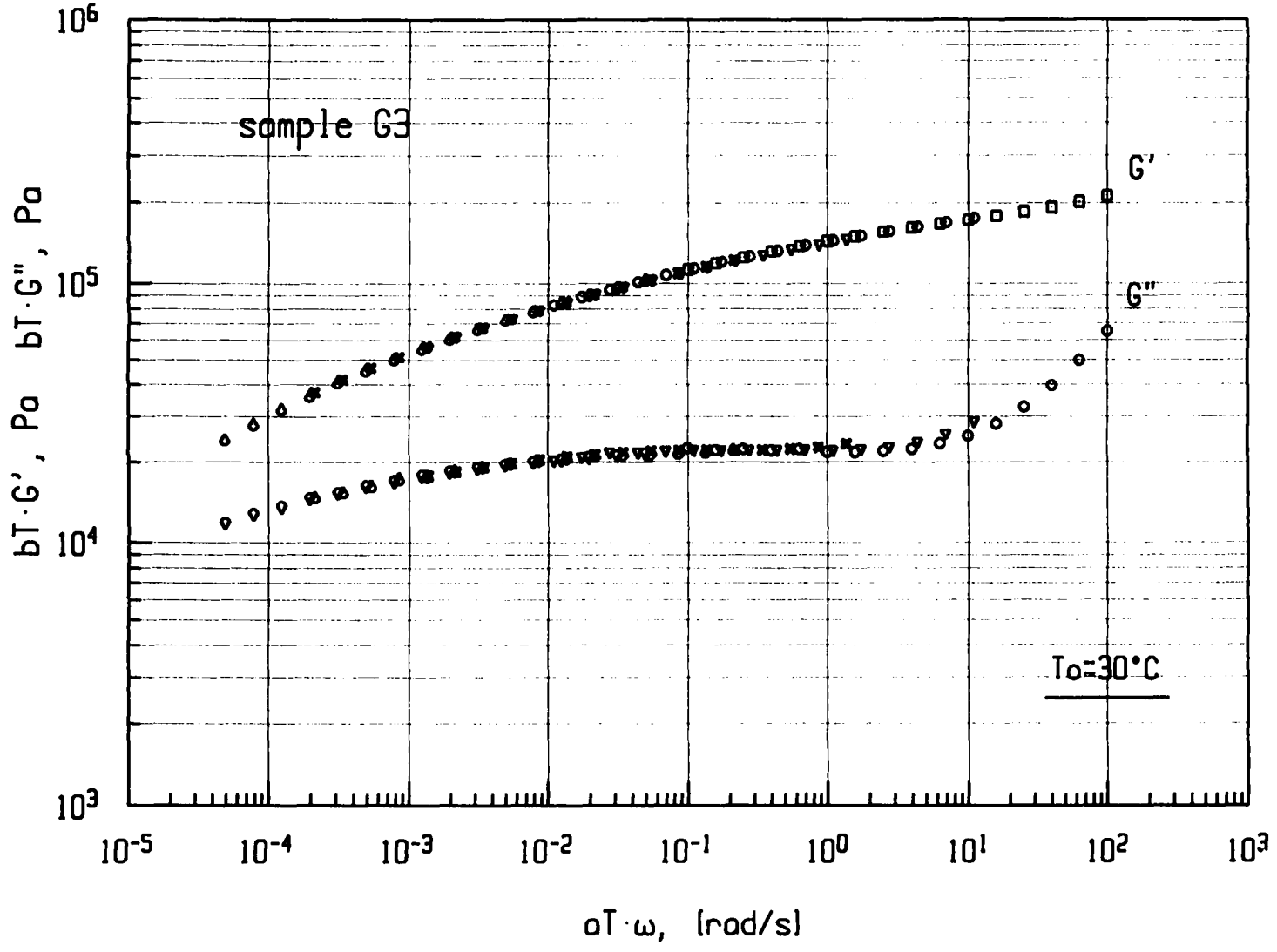


Figure 6-30. Master-curve of dynamic moduli obtained by shifting a series of isotherms according to t/f-T superposition principle, sample G3.



In order to assess whether the t/f-T shift was successful, the following criteria were used [339-340]:

(a) - subjective visual assessment of the master curves, a very good shift would consist of nearly perfect overlay of individual isotherms, thus forming a virtually single curve, spanning an appropriately larger range of frequencies than each isotherm would separately.

(b) - degree to which {FTS}master-curve matches an applicable portion of the {FS5dec} isotherm obtained by a single frequency sweep at the reference temperature, and carried out over 5 decades of frequency,

(c) - fit of the plot log a_T - log $(T-T_0)$ to either WLF or Arrhenius equation; assessment based on the value of the correlation coefficient, r^2,

(d) - positive and within a "reasonable range" value of the WLF equation coefficients

(e) - comparable values of $a_T(T)$ shift parameter (and resulting WLF or Arrhenius fit coefficients) obtained for all viscoelastic functions.

Assessment of the t-T shifts based on the above criteria is included in Table 6-5.

For those samples for which a plot of the a_T versus T was either erratic, or attempted fits to WLF and Arrhenius equations gave negative values of the parameters, or WLF coefficients differred significantly, depending on details of the shift algorithm, the f/T shift was judged not successful. In all these cases, fit coefficients are not reported in Table 6-5.

6.2.2 The issue of thermo-rheological complexity

The issue of thermo-rheological simplicity/complexity has important theoretical and practical implications and it is closely related to the nature of the temperature dependence of the relaxation processes of a polymer.

Table 6-5. Evaluation of the temperature-frequency shift and comparison of {FTS} master-curves with {FS5dec} isotherms.

Graft ID	Comparative rating of the shift quality	Agreement between {FS5dec} and {FTS} master-curves	Smooth plot: log a_T versus temperature	Positive values for c_1 & c_2 (WLF)	Comparable shift parameters obtained for G' & G" and J' & J"
	a	b	d	c	e
G1	++	***	y	y	y
G2	+	***	y	y	y
G3	+	***	y	y	y
G4	-	**	y	y	y
G5	++	***	y	y	y
G6	+	*	y	y	y
G7	+	**	y	y	y
G8	no data	no data	no data	no data	no data
G9	o	**	y	y	y
G10	- -	**	no	f.n.a.	f.n.a.
G11	+	***	y	y	y
G12	o	*	y	y	y
G13	- -	o	no	f.n.a.	f.n.a.
G14	++	**	y	y	y
G15	-	**	y	y	y
G16	-	*	y	y	y
G17	- -	*	no	f.n.a.	f.n.a.
G18	o	***	y	y	y
G19	+	**	y	y	y
G20	- -	*	no	f.n.a.	f.n.a.
G21	-	**	no	f.n.a.	f.n.a.
G22	-	**	no	f.n.a.	f.n.a.
C	+ (ref.)	*** (ref.)	y	y	y
M	worst	*	y	y	y

f.n.a. - fit not attempted due to data scatter in a_T (T) plot.

rating:

++	***	very good
+	**	good
o	*	fair
-	o	poor
- -		not acceptable

There is considerable ambiguity and confusion in the literature regarding the issue of thermo-rheological complexity, particularly in reference to materials of more complex structure (including LCB) or those chemically heterogeneous.

Polymer behaviour is termed as "thermo-rheologically simple", if for a given range of temperatures and a specified range of frequency, simple shift along the frequency axis provides satisfactory superposition of the viscoelastic functions (i.e. dynamic moduli), obtained at different temperatures. Simple shift is synonymous here with a single $a_T(T)$ function, being applicable to the whole range of temperatures and frequencies under study.

For long-chain branched polymers, this issue has not yet been definitely settled in the literature. For example, the following long-chain branched polymers were classified as thermo-rheologically simple polymers: 4-arm star-branched polybutadienes [27], polystyrene (PS) combs, regardless of the length and number of branches [19, 57], 4- and 6-arm PS stars [16] and star-branched polyisoprenes [24, 32, 341]. A similar conclusion was reached, based on success of the f/T shift, in a number of independent studies for butyl rubber (randomly branched elastomer, as well as its blends of the star-like with linear molecules) [45]. Similarly, a star-branched, hydrogenated polybutadiene [24] was identified as thermo-rheologically simple polymer.

On the other hand, the same elastomer, hydrogenated polybutadiene, of only slightly different structural parameters, was considered by other researchers as thermo-rheologically complex polymer [37, 50]. Other polymers for which time-temperature superposition failed, include a star-branched, hydrogenated polyisoprene [24, 341], branched polyisoprene [342], as well as randomly branched low density polyethylene LDPE, [4, 343].

There are at least two factors contributing to this ambiguity:

- inconsistency and ambivalence in applying the criterion of what indeed constitutes a thermo-rheologically simple material, and,
- a lack of clear specification (i.e. temperature and frequency ranges, for dynamic experiments) for which superposition of the dynamic moduli was examined and appraised.

For graft copolymers, due to the combined effects of chemical heterogeneity and long-chain branching, this issue is becoming even more complicated. Different temperature dependence of both chemical components of the graft had to be accounted for, and the effect of the interphase may necessitate a correction for the a_T shift factor, in addition to the vertical shift, b_T, for successful superposition,

$$b_T = T / T_0 \cdot \rho_0 / \rho \qquad \text{where } \rho \text{ is the density of a polymer}$$

Successful t/f-T transformations, leading to "acceptable" master-curves, were reported for a number of block and graft copolymers [344]. However, for multi-phase materials the empirical shifting procedure, even one based on a single and unmodified a_T (T) shift factor superposition, does not necessarily lead to a master-curve, which would permit "valid" conclusions about the thermo-rheological simplicity of the copolymer [345].

Appropriate factorization of the a_T shift factor may lead to master-curves satisfactory enough for exploration of frequency-dependence of viscoelastic functions into a frequency range not otherwise experimentally accessible, but the very need for a_T modification would indicate the material behaviour to be thermo-rheologically complex. [344].

As a rule, graft copolymers are thermo-rheologically complex materials by the nature of their chemical heterogeneity, strictly, due to the different thermo-rheological properties of their

constituents. However, depending on details of LCB, they might in some cases permit a successful shift based of the time/frequency superposition principle and yield acceptably smooth "master-curves".

I. Taking sample C, a chlorinated poly(isobutylene-co-isoprene) copolymer, universally regarded as a thermo-rheologically simple copolymer [45, 338], as a reference, equally good or even smoother master-curves were generated for a few graft architectures, including those with long branches. Superposition results for samples G5 and G14 could serve as examples - Figures AFTSG5 and AFTSG14 in Appendix V. Samples with extreme values of specific branching parameters, with either very long branches (samples G10 or G22) or with relatively many branches (samples G13, G20 or G16) tend to give poor master-curves. The least successful shift was for a blend M. This suggests that the "less-controllable" phase morphology of the blend may be a factor.

It is also possible, that master curves reflect the capabilities of the shifting algorithm to handle certain types of isotherms better than others.

II. Probably, a more credible criteria for assessment of the t/f-T shift would be how well the master-curves are reproducing the shape of the dynamic moduli, obtained by a frequency sweep at the reference temperature and over a comparable frequency range. (Assuming an absence of time-related, adventitious phenomena like degradation etc.).

Results of this comparison are surprisingly good. Even for samples which gave diffused and only partially overlapping G′ and G″ master-curves, it was possible to correctly predict the frequency-dependence of the dynamic moduli through transformation. This observation might be construed as the most definitive evidence in support of the applicability of time-temperature superposition technique for potentially thermo-rheologically complex materials [335, 345].

From the comparison between {FS5dec} and {FTS} derived master-curves, it can be concluded that the grafts of the highest branching number (N_g) or with a high branching content ($w^{b,g}$), showed the poorest agreement (Table 6-5, col."b")

Furthermore, there is a statistically significant correlation between the degree to which {FTS} master-curves match {FS5dec} isotherms, and either of the $N_g^{\ p}$ or $w^{b,g}$ parameters. This means, that an increase in the number of branches or a branching content, will decrease the ability of the f/T shift to create master-curves matching {FS5dec} isotherms, considered here as reference. Incidentally, no such correlation is observed for either $M_p^{\ b}$ or $w^{b,h}$ (see prediction profiles in Figure 6-31).

These conclusions should be treated as tentative, as they are based on a few measurements per sample. A more comprehensive study would be required to verify these conclusions with confidence.

6.2.3 Temperature dependence of the dynamic moduli, G'(T) and G"(T)

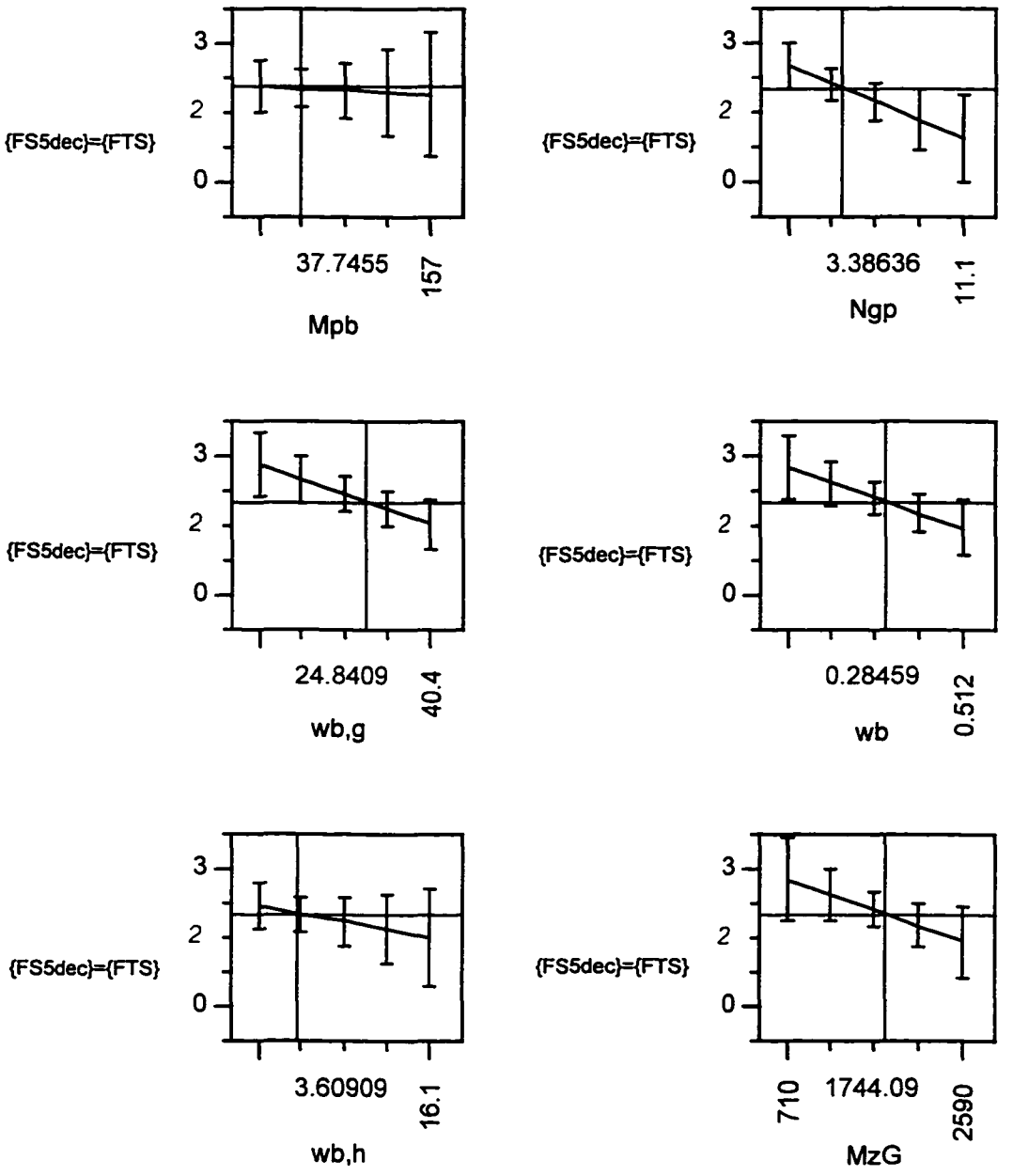
Temperature dependence of rheological properties can be described in terms of specific material constants, such as the activation energy, E_a, (equation 6-9) or constants, c_1 and c_2, from WLF (equation 6-8).

Alternatively, and more generally, the shift factor, a_T [338] which itself is a function of temperature, can be used,

$$\omega\ (T) = a_T(T) \cdot \omega\ (T_0) \qquad (6\text{-}10)$$

where, ω denotes the angular fequency.

Figure 6-31. Predition profiles for screening between quantified assessment of the agreement between {FTS} and {FS5dec} curves (G′ and G″) and structural parameters.



A review of the available literature concerned with temperature dependence of the rheological properties of branched polymers indicates that this subject is still open to discussion [342, 346]. Most of the reported evidence indicates that the presence of branches increases, sometimes substantially, the activation energy of branched polymers. Numerous examples are reported for randomly branched polymers [6, 63, 347-348] and for narrowly distributed, star-branched polymers [27, 37, 50].

On the other hand, several reports present data which show no difference in the flow activation energy, E_a (or other equivalent measures of temperature dependence of viscoelastic properties) between linear and branched polymers [346], narrowly polydispersed polyisoprene (PI) and hydrogenated polybutadiene stars [29, 32]. Several analyses attempted to relate an enhancement in activation energy to the number and length of branches in polydispersed systems, for example [6, 63, 347, 349].

Relatively few reports discuss this issue for well-characterized, model LCB polymers, particularly for combs [18-19] and graft copolymers [69]. For stars, little or no enhancement in temperature dependence was attributed to the arms being too short to produce measurable effects [24, 27]. In fact, it is known [37, 350] that increased temperature dependence of branched molecules is a function of the molecular weight of the arms, or more specifically, the number of entanglements per long-chain branch. As an example, a study for hydrogenated polybutadiene was reported [37]. For HDPE-g-Acrylic acid graft copolymer, an identical activation energy for viscous flow for the backbone parent polymer (HDPE) and the graft was attributed to an insufficient number of polyacrylic acid branches [69].

The horizontal shift factor, a_T has been fitted to both Arrhenius and WLF equations. Material parameters, together with the fit assessment (r^2) are given in Table 6-6, for those cases where the fit was satisfactory (r^2>0.9000). Overall, the Arrhenius equation was found to fit the experimental data slightly better than the WLF equation. This well known fact is a standard recommendation for the usage of these equations for this temperature range [351].

Table 6-6. Coefficients of WLF and Arrhenius equations.

Graft ID	WFL			Arrhenius	
	c_1	c_2	r^2	E_a (ω=const.)	r^2
	[-]	[K]	[-]	[kcal/mol]	[-]
	a	b	c	d	e
G1	7.8	191	*0.9996*	63.7	*0.9966*
G2	-	-	-	77.9	*0.9995*
G3	-	-	-	100.3	*0.9959*
G4	2.1	56	*0.9106*	38.7	*0.9509*
G5	6.6	195	*0.9959*	53.8	*0.9969*
G6	7.6	164	*0.9963*	69.2	*0.9937*
G7	7.9	215	*0.9667*	59.3	*0.9965*
*G8 /**	—	—	—	—	—
G9	3.3	185	*0.9972*	30.6	*0.9970*
G10	-	-	-	-	-
G11	8.7	263	*0.9968*	61.1	*0.9995*
G12	1.72	70	*0.9201*	23.8	*0.9110*
G13	-	-	-	-	-
G14	5.2	156	*0.9924*	54.0	*0.9915*
G15	-	-	-	-	-
G16	1.8	78	*0.9956*	23.4	*0.9481*
G17	-	-	-	-	-
G18	13.0	326	*0.9953*	74.3	*0.9999*
G19	12.1	319	*0.9659*	68.9	*0.9994*
G20	-	-	-	-	-
G21	-	-	-	-	-
G22	-	-	-	-	-
C	8.3	211	*0.9983*	57.1	*0.9977*
M	5.1	178	*0.9928*	50.0	*0.9954*

/* - No valid results collected for sample G8.
"-" - WLF or Arrhenius coefficients values were fitted but with correlation coefficient $r^2 < 0.900$, therefore not shown, see footnote in Table 6-5.

Indeed, the lower end of the {FTS} temperature range, which is the reference temperature (30°C) for the t/T shift, is about 100°C above the T_g for CIIR (backbone prepolymer) and over 120°C above the T_g for BR (branch prepolymer).

Literature values for the activation energy, E_a, as well as the WLF constants (c_1 and c_2) are compared with values calculated from data obtained in this study in Table 6-7. Excellent agreement was obtained for sample C. For polybutadienes of comparable microstructure, typical values of the E_a, c_1, and c_2 coefficients are much lower.

For some grafts, these coefficients are still lower which suggest that the branching may play some role here, particularly since the lowest coefficients are for the samples with the highest branching number (Table 6-6). However, the screening for correlations between temperature-dependence coefficients and the structural parameters, gave no results at acceptable confidence levels.

The results obtained suggest that the BR content, w^b (not directly $w^{b,g}$) might be a prevailing factor in determining the temperature dependence of CIIR-g-BR graft copolymers, due to the very low values of E_a or c_1, c_2 coefficients for polybutadiene. Due to large differences between those coefficients, any other possible effect (for example, increased temperature dependence due to the existence of branching) might be easily overwhelmed.

Table 6-7. Arrhenius and WLF equation coefficients for CIIR and BR.

	Arrhenius			WLF				
	E_a, [kcal/mol·K]			c_1 [-]		c_2 [K]		
polymer/ sample	this study	litera-ture	[ref.]	this study	litera-ture	this study	litera-ture	[ref.]
CIIR / C	57.1	57.4	[45]	8.3	8.61	211	200.4	[352]
BR / Bxx	---	7.5 - 8.5	[346]	---	3.64	---	186.5	[353]

Further studies, preferably using a dynamic temperature sweep configuration for direct assessment of the effect of temperature on the dynamic moduli, are recommended to confirm these preliminary results and help to explain why certain graft architectures result in abnormally low temperature dependence coefficients.

6.3 Relationship between LCB structure and complex modulus

This section presents some of the results of the two series of tests, {FSWP1} and {FSWP2}, carried out using the RPA 2000 at the constant strain amplitude of 5% and temperature of 100°C. Experimental test conditions were described in Chapter 5 and the complete details are included in Appendix IV, Table C.

Screening for correlations

Definition of the rheological parameters used for correlations between rheological and structural parameters are listed in Table 6-8.

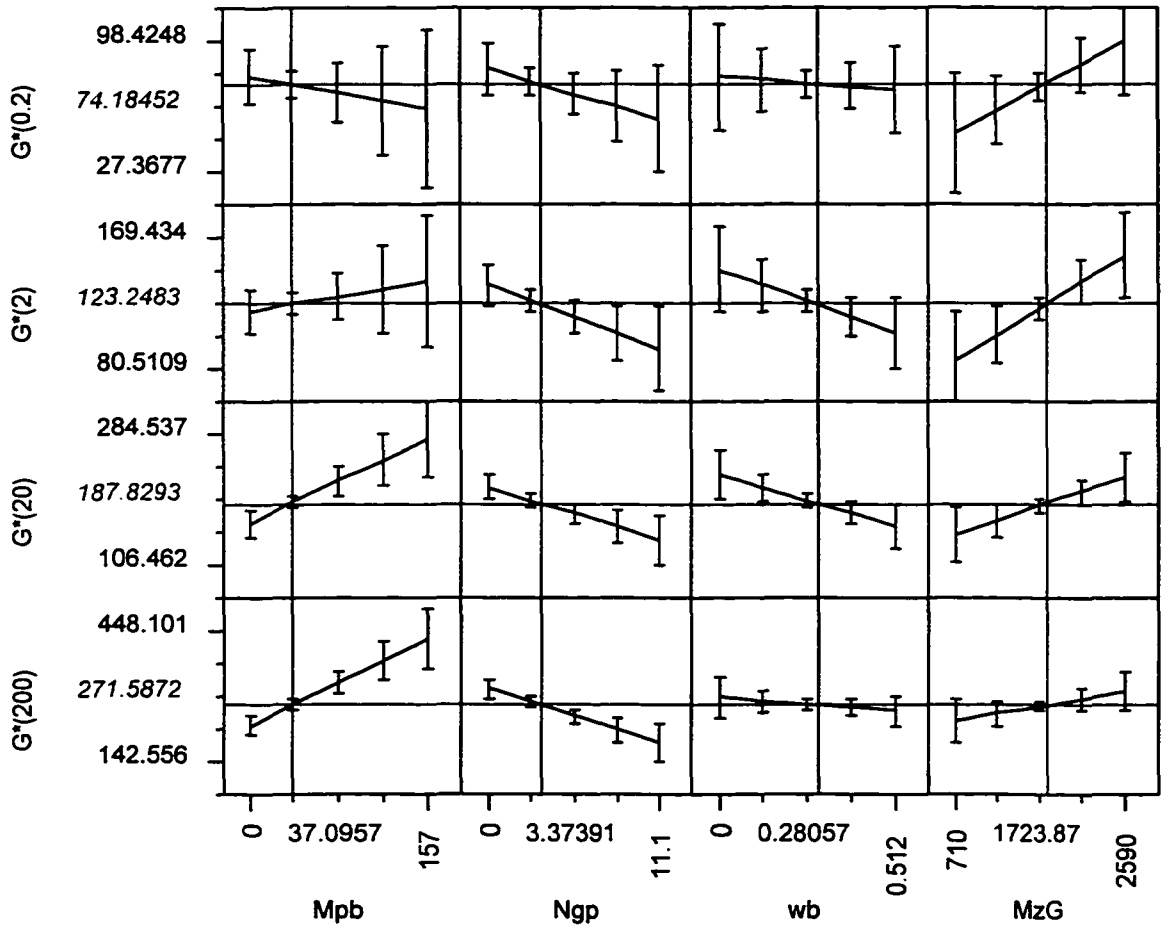
Table 6-8. Definition of viscoelastic parameters derived from {FSWP1} and FSWP2} experiments.

abbreviation.	definition
G* (0.2)	- absolute value of the complex modulus G* at ω=0.2 rad/s & γ=5%
G* (2)	- absolute value of the complex modulus G* at ω=2 rad/s & γ=5%
G* (20)	- absolute value of the complex modulus G* at ω=20 rad/s & γ=5%
G* (200)	- absolute value of the complex modulus G* at ω=200 rad/s & γ=5%

Screening for correlations was carried out using JMP® software as described in Appendix VI. Viscoelastic parameters for the entire set of the 22 graft samples were used for the screening analysis. The most relevant prediction traces are included in Figure 6-32.

Results obtained using {FSWP1} and {FSWP2} test routines are similar to analogous results obtained by the RMS-800, under comparable test conditions.

Figure 6-32. Prediction profiles for correlations between branching parameters and complex modulus, G^*.



However, as explained in Chapter 5, for the highly viscous and elastic materials, RPA 2000 is capable of measuring the dynamic properties with superior accuracy and precision [354]. This would permit the analysis of the LCB effect on the absolute values of the moduli or complex viscosity, in addition to verification of the strain, frequency and the temperature

dependence. In this section, only results of the complex modulus, $G^*(\omega)$ measured at a few selected frequencies are presented and discussed.

Figure 6-33 shows a composite graph of the complex modulus, G^*, plotted as a function of the angular frequency.

For each sample, the complex modulus increases steadily with frequency. The difference between samples of various graft architectures becomes more pronounced with increasing frequency. Taking sample C as a reference, branching tends to increase modulus (up to over 100% at ω=200 rad/s in the extreme case for sample G10). Only the grafts with numerous and relatively short side chains (samples G12, G20, G13, for example) are exceptions to this rule, having flat frequency-dependence of the complex modulus.

For the majority of the grafts, the complex modulus $G^*(\omega)$ curves band within a relatively narrow range. Consequently, differences in the branching parameters impart only a minor effect on the modulus. Samples with the highest G^* in the range of 10 to 200 rad/s, are those with the longest branches (samples G10, G22, G6) as shown in Figure 6-33. Therefore, it is concluded that the increase of the length of the branch increases the rigidity of the graft. This conclusion is consistent with the screening analysis results in Figure 6-32.

Analysis of correlations for the complex modulus, G^* reveals its significant (at $\omega \geq 10$ rad/s) dependence upon branch length and negative correlation with the branching number, while no dependence on chemical composition of the graft, w^b. In either case, M_p^b or N_g^p, correlation is stronger at higher oscillation frequencies. As a result of the mutually canceling effect of M_p^b and N_g^p, it is possible to build a series of increasingly more branched structures with modulus being virtually independent of the branching content, $w^{b,g}$. Results of the screening analysis for the $w^{b,g}$ in Figure 6-34 and data in Table 6-9 confirm this observation.

Figure 6-33. Frequency dependence of the complex modulus, G*. Composite graph.

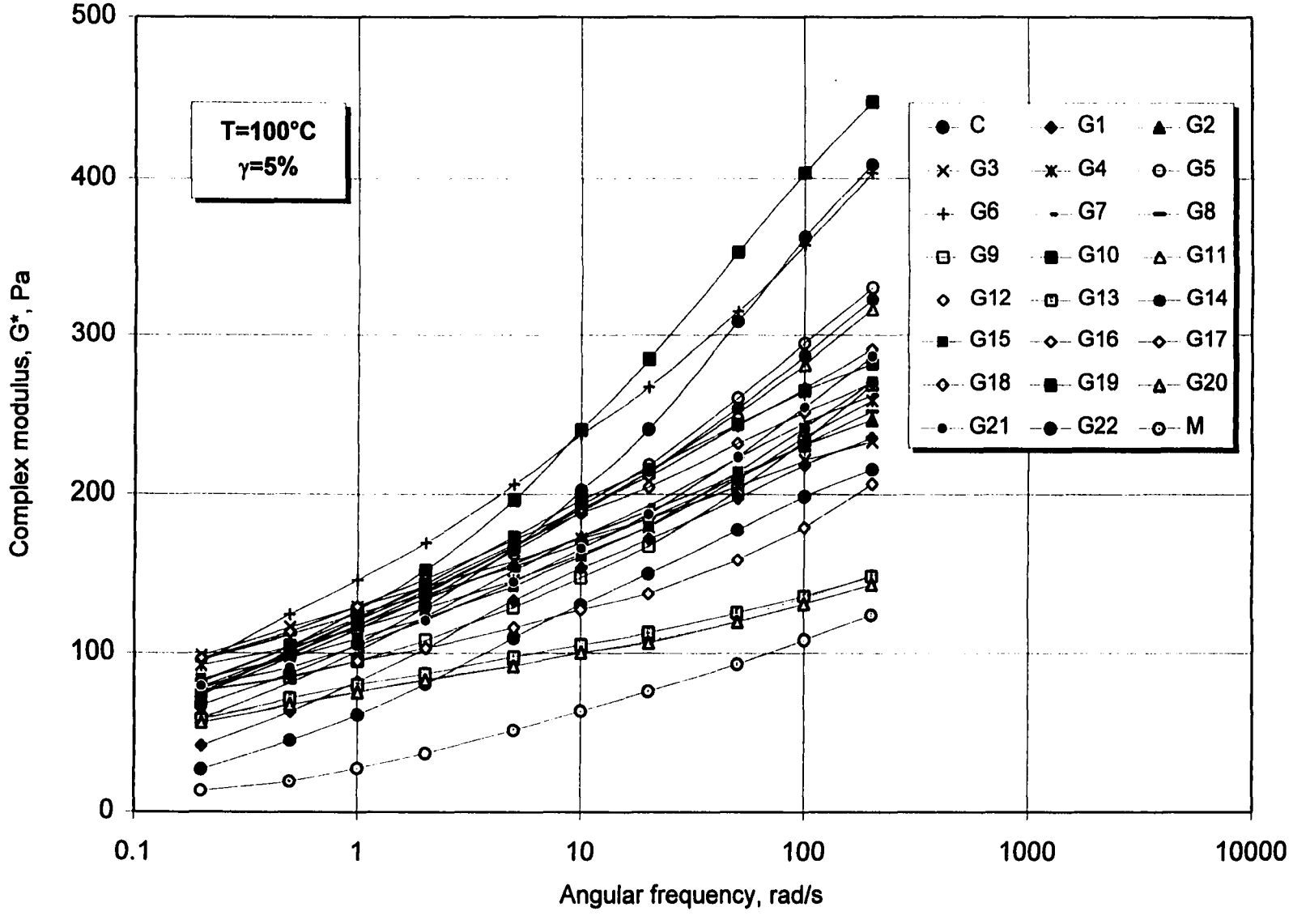
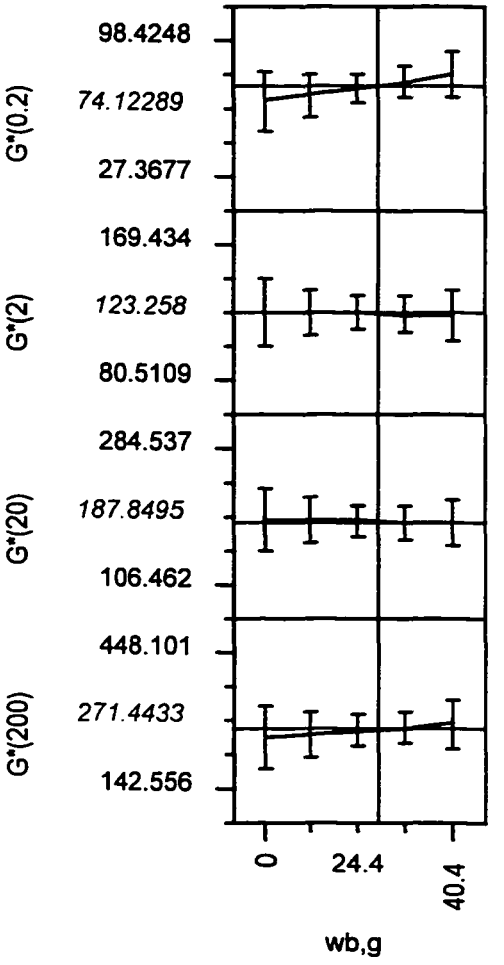


Figure 6-34. Prediction profiles for correlations between overal branching content, $w^{b,g}$ and complex modulus, G^*.



Additionally, as per screening analysis, it appears that regardless of the oscillation frequency, there is no correlation between molecular weight of the graft (M_z^G) and complex modulus, G*. Results of the G* for various M_p^p and N_g^p configurations included in Table 6-9 further illustrate the effect of the LCB on the complex modulus.

Grafting a few long branches onto a linear backbone polymer doubles the value of the complex modulus with reference to the backbone prepolymer (sample C), while presence of

many shorter branches reduces the value of G* by about 25%. Branching structures with intermediate values of specific branching parameters (M^b, N_g) result in median values of the complex modulus. No statistically significant correlation between chemical composition of the graft and G* was found, despite a large differences in modulus between prepolymers (sample C and for example, sample B10).

Table 6-9. Complex modulus values from {FSWP1} and {FSWP2} tests, T=100°C, ω=200 rad/s, γ=5%.

Sample	M_p^b (daltons)	N_g^p	G* (kPa)	Comments
G6	76,400	1.4	404	few long branches - high G* values
G10	157,000	0.6	448	
G22	116,000	0.8	409	
G12	14.0	7.6	149	many short branches - low G* values
G13	9,400	11.1	148	
G20	10,000	11.0	143	
G8	22,800	3.1	262	intermediate branching structures resulting in similar values of the complex modulus, G*
G9	33,500	3.2	268	
G15	36,500	2.7	270	
G18	19,100	1.4	270	
C	—	—	216	(reference)

6.4 Time dependence of the stress relaxation modulus - I

Stress relaxation, following a step-strain application is another type of rheometrical test which is often used to investigate the viscoelastic properties of polymers. It involves a fast application of a well-defined strain and subsequent monitoring of the decaying stress, over a period of time, usually under isothermal conditions.

This section discusses the results of the first of a series of stress relaxation experiments, {SR10,000} carried out at 30°C and following a 10% step-strain in shear. The stress relaxation was monitored over a period of 10,000s. The summary of the main characteristics of this and the other two stress relaxation experiments is enclosed in Table 6-10.

Table 6-10. Principal characteristics of the LVE stress relaxation tests (RMS-800).

Test code	Monitoring time, s	Temperature, °C	Strain amplitude, %	Results discussed in section...
{SR 10,000}	10,000	30	10	**6.4**
{SR 1000}	1000	30	10	**6.5**
{SR 400}	400	100	15	**6.6**

The experimental conditions and parameters for these test were presented in Chapter 5 and are summarized in in Table IV, Part 2, Appendix IV. A non-linear (amplitude-dependent) stress relaxation test, involving large strain amplitudes, will be discussed in chapter 7.

6.4.1 Normalized stress relaxation modulus, nG(t)

Time dependence of the stress relaxation modulus, G(t) can be conveniently represented by the normalization of the G(t), that is by dividing all G(t) values by a certain (specific or arbitrary) number. In this study, for all three stress relaxation experiments on the RMS-800, the absolute value of the relaxation modulus at 100 ms was taken as a reference value (see section 5.2.4.3 in chapter 5). As a result, the normalized stress relaxation modulus, nG(t) is defined by equation 6-11,

$$nG(t) = G(t)/G(t=100ms) \qquad (6\text{-}11)$$

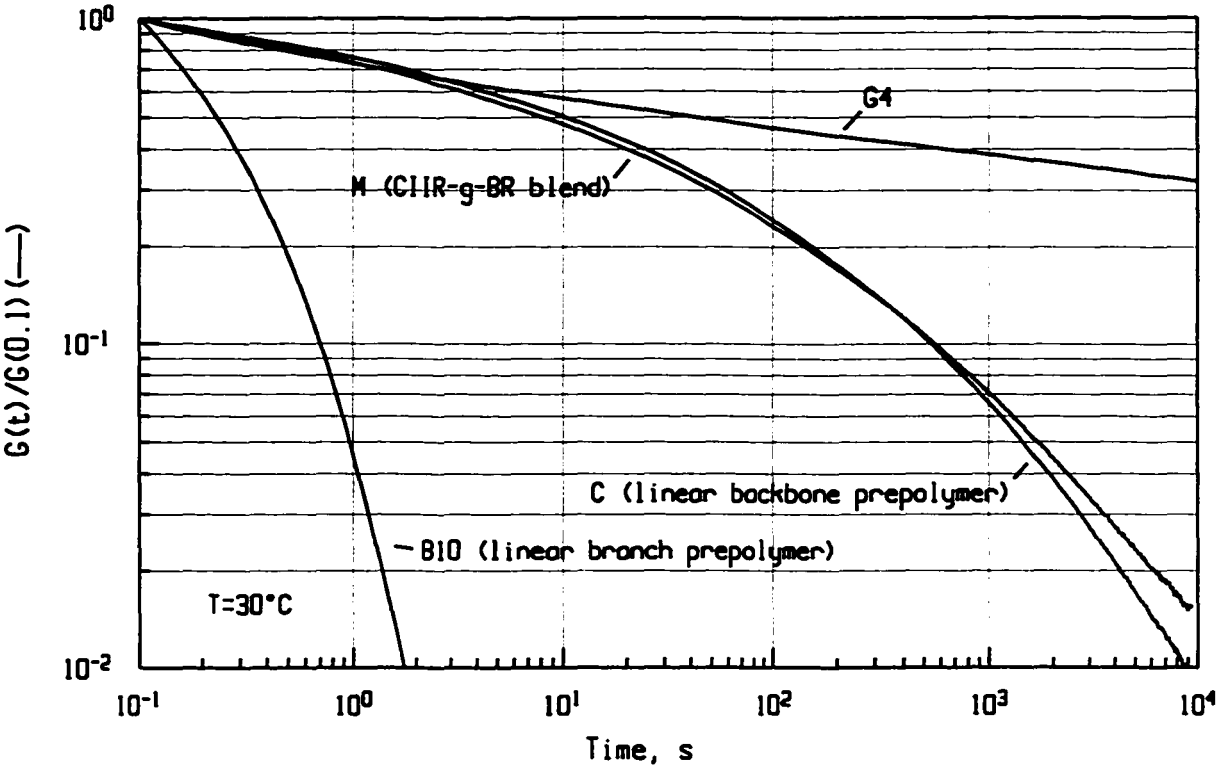
A normalized stress relaxation modulus permits a straightforward assessment of time-dependence of the moduli, without possible interference from the limited accuracy of moduli measurements.

The following are the observations on the influence of LCB on stress relaxation:

Stress relaxation of linear polymers

Topology of the molecular chain can have a significant impact on the molecular relaxation process, resulting in dramatically different stress relaxation curves. Figure 6-35 compares the nG(t) profiles for linear polymers (samples B10 & C), blend M and compositionally (w^b) equivalent graft copolymer, sample G4. Relaxation profiles for B10 and C samples are characteristic of those of polymers containing linear molecules. However, a striking difference in relaxation behaviour between these two chemically different polymers exists, in part due to the differences in the M_w and MWD, B10 (BR, M_w=100,000, PDI=1.41) and C (CIIR, M_w=400,000, PDI=4.24), but primarily due to the differences in molecular "mobility" between BR and CIIR.

Figure 6-35. Stress relaxation linear parent polymers, their blend (CIIR/BR) and CIIR-g-BR graft (sample G4) - {SR10,000}.



Stress relaxation of the backbone prepolymer(C) and its blend (M) with branch prepolymer

Samples C and M make an interesting comparison of the differences between relaxation of the linear, polydispersed polymer and its blend with polybutadiene of lower MW (Figure 6-3).

Their nG(t) curves cross-over, with blend M relaxing slightly faster during the first several hundred seconds. This is presumably due to the significant content (w^b) of the very mobile polybutadiene molecules (M_p^b of 30,000). For long term relaxation (in the order of a thousands second and longer) the analogous curve for the blend relaxes a little a more slowly. This effect is attributed to the existence of phase morphology, which exists due to the incompatible nature of the CIIR and BR (co)polymers [269].

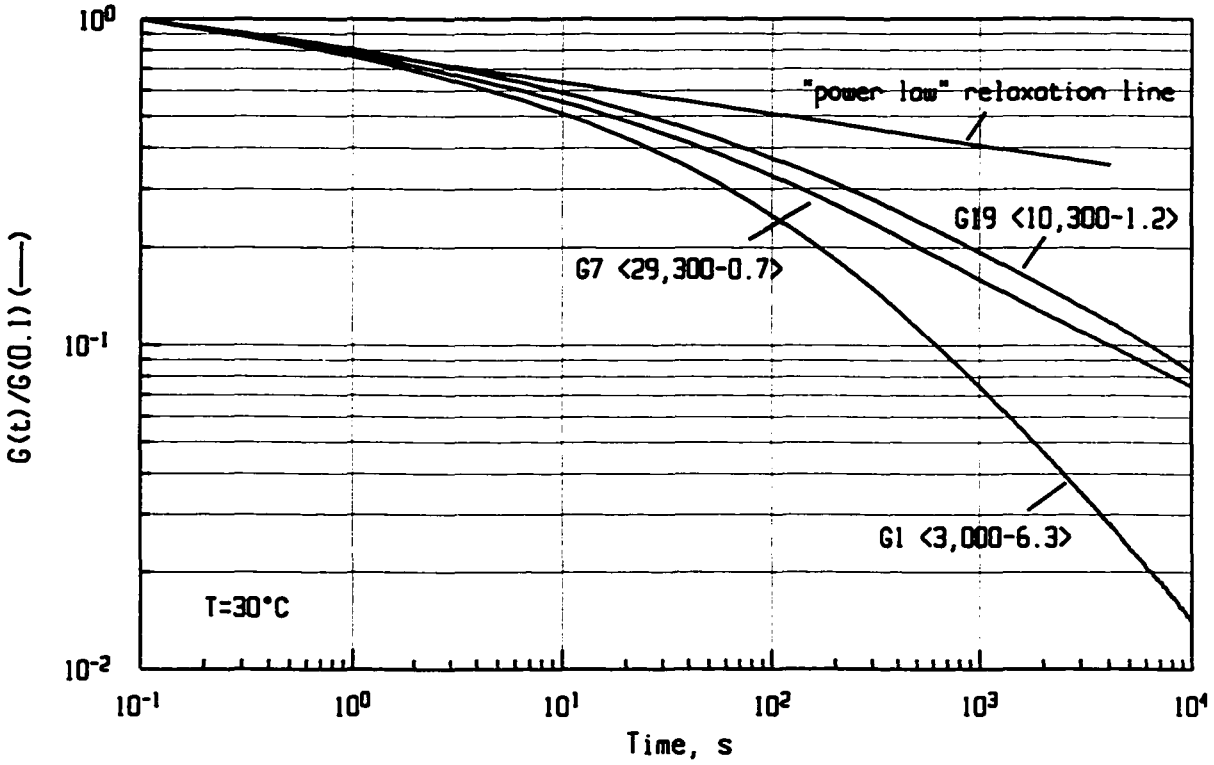
Comparison between blend and graft of comparable composition and structural characteristics

As indicated previously, samples M and G4 have many common structural characteristics; identical overall chemical composition w^b, identical microstructure and molecular weight distribution for the CIIR, and very similar for the BR. The only relevant difference between them is molecular topology; sample M (CIIR/BR) is composed of linear molecules of bimodal MW, while sample G4 (CIIR-g-BR) has a comb-like LCB structure of the graft copolymer. Resulting differences in the time dependence of the normalized relaxation modulus are spectacular (Figure 6-35) and the difference is even more dramatic when compared on the basis of the absolute relaxation modulus, G(t). This result is the most demonstrable example of the effect which long chain branching has on the time dependence of the stress relaxation modulus. By comparison to backbone prepolymer (sample C) the nG(t) curve for sample G4 is raised and the difference in the nG(t) profiles is increasing with time. Qualitatively, the relaxation behaviour of the LCB graft copolymer in the terminal viscoelastic zone is intermediate between that of the linear polymer and the fully cross-linked (unfilled) elastomer.

Relaxation of weakly branched LCB structures

Relaxation profiles for most of the graft structures, particularly for those of the linear polymers, decline monotonically and the rate of relaxation can be much faster than "power law". In Figure 6-36 this observation is illustrated by contrasting the nG(t) curves for grafts with weakly developed branching (samples G1, G7 and G19; all with $w^{b,g} < 5\%$) with the "power law' line representing, on a double-log graph, exactly "power law" relaxation. The normalized relaxation curves follow nearly identical paths in the first decade (that is for relaxation times up to 1 second), then gradually diverge with time. Samples G7 and G19, while both having about one branch per statistical backbone, resulting in a virtually 3-arm, heterogeneous star-like molecule, differ in branch length quite substantially. The branch length of sample G7 is about 3 times longer than that of sample G19. This results in the

Figure 6-36. Stress relaxation - {SR10,000}. Behaviour of weakly-branched structures.

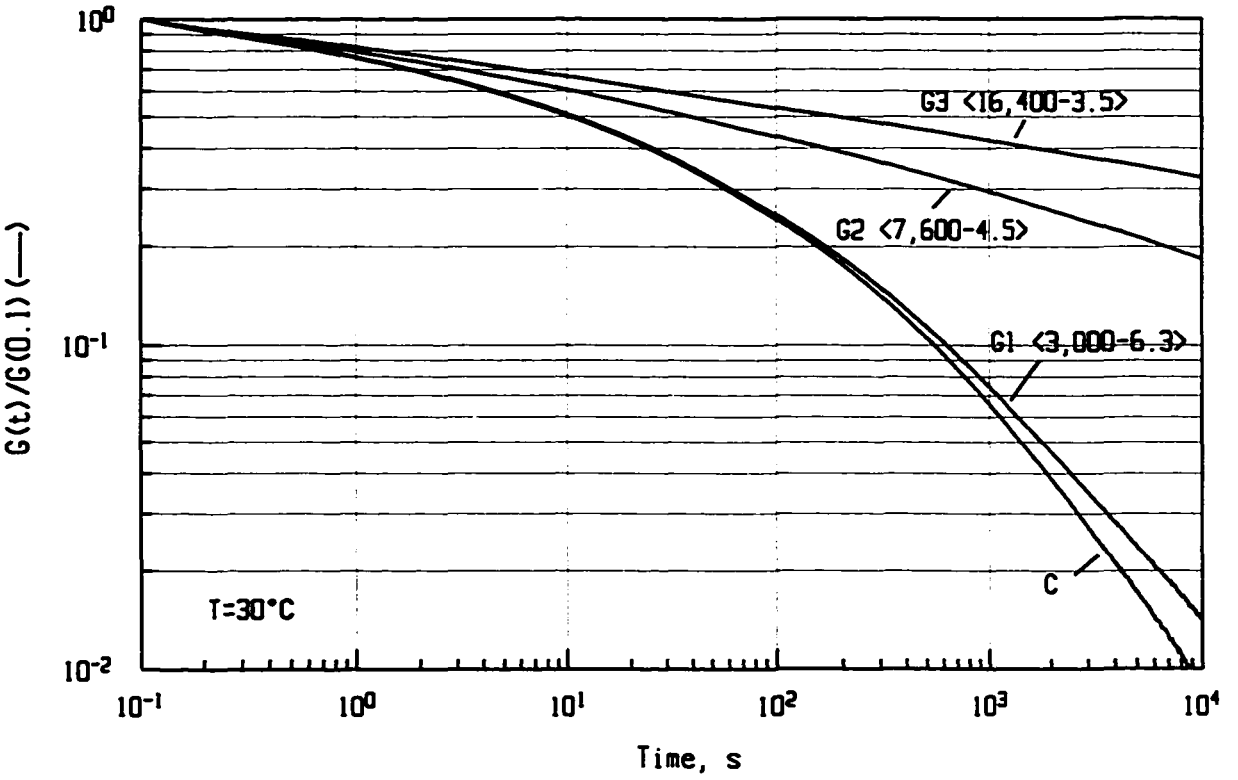


relaxation slowing down somewhat for the longest observation times, especially those in order of 10^3 - 10^4 seconds, as it is apparent from the "convergence" of the G7 and G19 stress relaxation curves.

Effect of branch length

The stress relaxation profiles (nG(t)) for several grafts with branches becoming progressively longer are shown in Figure 6-37. It is apparent that the presence of very short branches (sample G1, M_p^b >>1.5 M_e) modifies the relaxation behaviour of the graft in the terminal zone only slightly. Further increase in the branch length causes a major difference in the relaxation behaviour of the LCB molecules. The suppression of relaxation of the graft

Figure 6-37. Stress relaxation - {SR10,000}. Effect of branch length.



molecules due to branching is very significant, as demonstrated by the difference in nG(t) for samples G1 and G2. The critical branch length for such a quantum increase in relaxation times can only be roughly estimated to be between 1.5 and 4, in terms of the molecular weight between entanglements, M_e. The M_e for polybutadienes of comparable microstructural composition is 1,900 g/mol [341, 355].

A proportional increase in the branch length (between samples G2 and G3) results in a decrease of the relaxation rate but the difference is not as big.

Effect of branching number

Examination of the effect which the branching number has on the stress relaxation for grafts with comparable branch length ($M_p^b \approx 10{,}000$), reveals a different nature of the structural

dependence of the relaxation process. Increased branch length and number both greatly extend the relaxation times by suppressing relaxation of the molecules due to long branches. However, the relaxation time is prolonged proportionally to the branching number, as seen in Figure 6-38. An identical conclusion can be reached by comparison of the relaxation curves for another set of grafts, of comparable but higher branch length (20,000) in Figure 6-39.

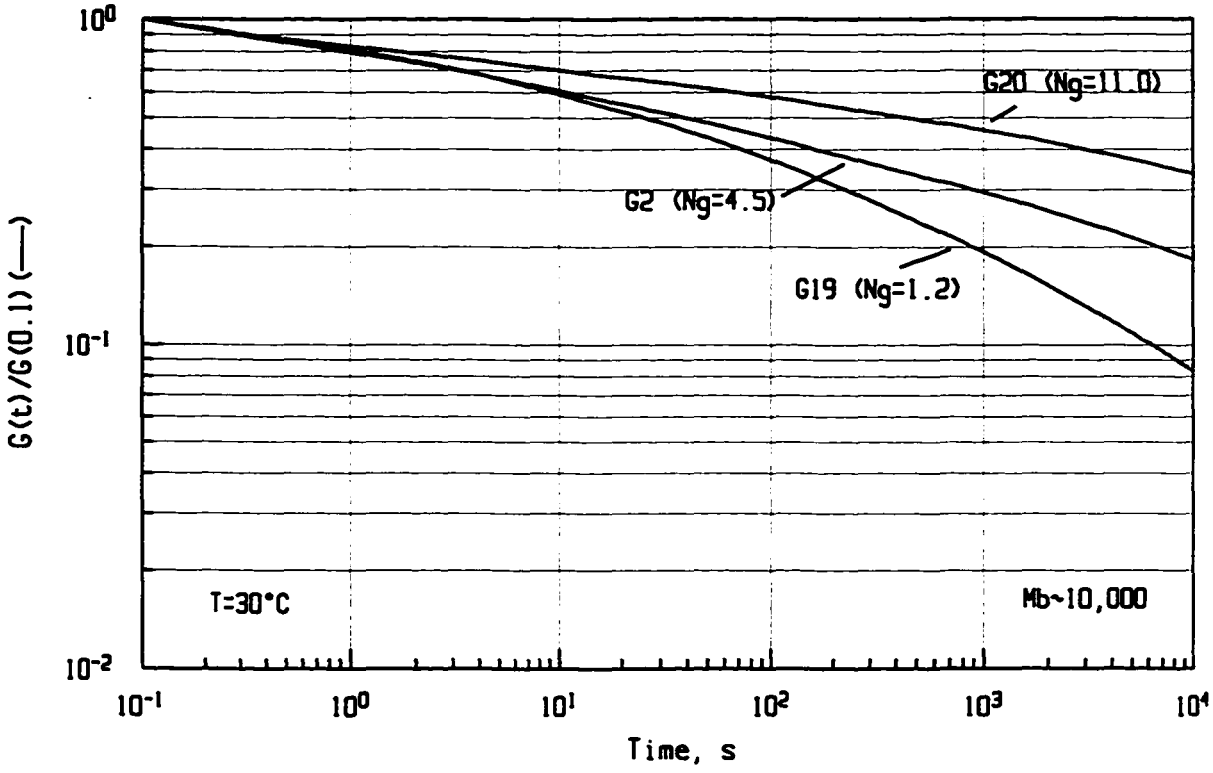
Curvature of the nG(t) curve, observed in Figure 6-39 for sample G16 at the shortest relaxation times, is believed to be a result of a relatively high content of low molecular weight of the ungrafted branch precursor molecules. Their content for sample G16 is $w^{b,h} = 4.6\%$ as compared with $w^{b,h}$ of about 0.3% or less for the other two samples. Comparison of 2-arm star-branched polybutadiene with linear molecules, all of comparable molecular weight, indicated that the number of arms is the most effective branching parameter to suppress molecular relaxation [23, 99].

Effect of the presence of linear molecules in a graft mixture

The presence of a noticeable amount of the residual branch precursor polymer (>2%), which has similar MWD to that of the branches, is reflected in the slope and the shape of the nG(t) function at short times (less than 10s). Comparison of the nG(t) for the grafts G14 and G17 in Figure 6-40 illustrates this relation. Both grafts have comparable branch length and frequency, resulting in the identical shape and the slope of the nG(t) curves at longer observation times (>>100s) where relaxation mechanisms due to branching become dominant.

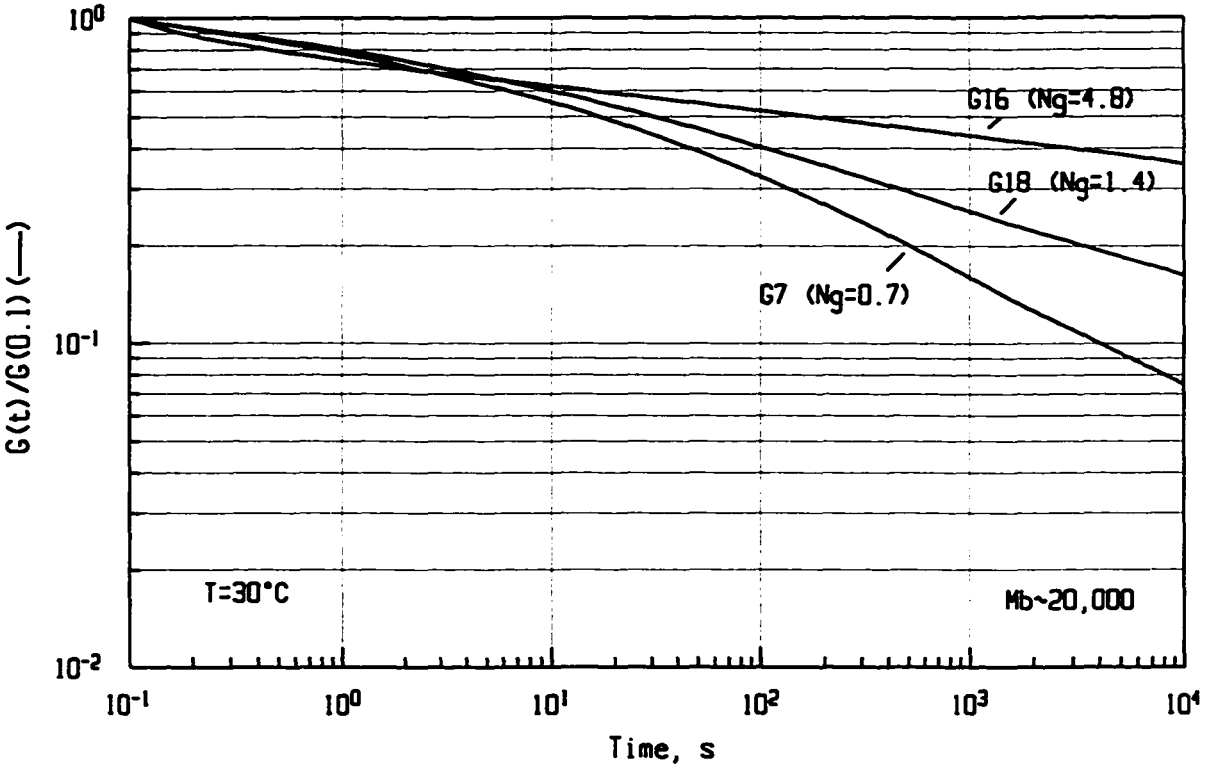
It appears, that even the slightly longer branches of the G14 are responsible for postponement of the "branching plateau" toward somewhat longer times. However, the major slope difference in nG(t) at shorter times can confidently be related to the large content of ungrafted BR in sample G14 ($w^{b,h} = 7.6\%$). In fact, the initial slope of the relaxation curve will depend not only on the content of the linear molecules in a graft mixture $w^{b,h}$, but also

Figure 6-38. Stress relaxation - {SR10,000}. Effect of number of branches - I.



upon their length (MW), which is assumed to be identical to that for branches. This point is best illustrated in Figure 6-41, for samples G10 and G22, where the amount ($w^{b,h}$=16%) of ungrafted polybutadiene is identical but samples differ considerably in their molecular weight (M_p^b). Unlike in the previous graph, little change in the nG(t) slope is observed. This fact is difficult to interpret unequivocally from the limited experimental evidence, but it is possible that the lack of visible flattening in the observable portion of the nG(t) curve is also due to the very low N_g^p number (0.6 - 0.8). It is also possible that relaxation is dominated by branching at much longer times than those experimentally accessible during these experiments.

Figure 6-39. Stress relaxation - {SR10,000}. Effect of number of branches - II.



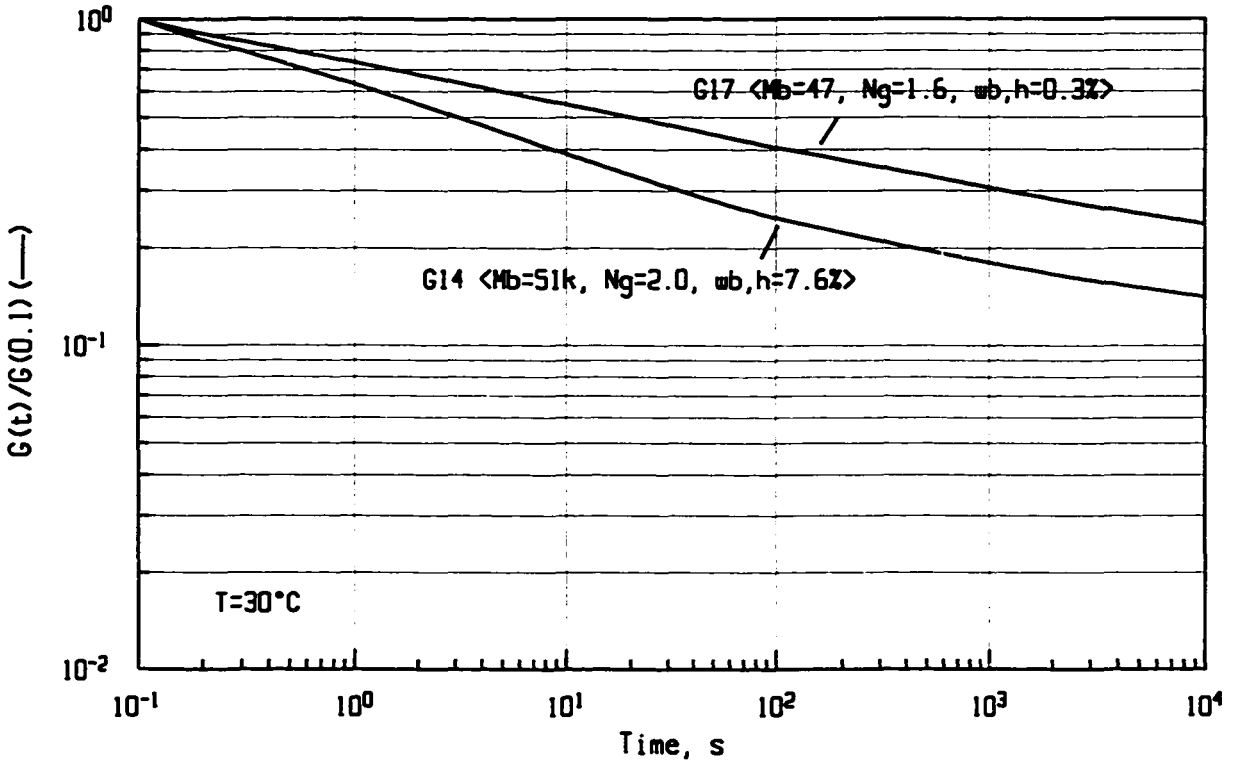
Verification of the integrity of test results

The accuracy and precision of the stress relaxation results as well as the integrity of structural characterization can be verified by comparison of the nG(t) profiles between samples of nearly identical or very similar branching parameters (M_p^b and N_g^p). Two pairs of samples were selected which met these two criteria:

(a) samples G15 (36,500 / 2.7) and G21 (36,100 / 3.0), and
(b) samples G13 (9,400 / 11.1) and G20 (10,000 / 11.0).

In Figure 6-42 the stress relaxation profiles of these two pairs superimpose very well, which is consistent with the similarity of their branching structure. The excellent reproducibility of stress relaxation data on two separate sets of "twin" samples, suggests that the two specific branching parameters (M^b, N_g) used to describe the comb-type,

Figure 6-40. Stress relaxation - {SR10,000}. Effect of the ungrafted BR content - I.

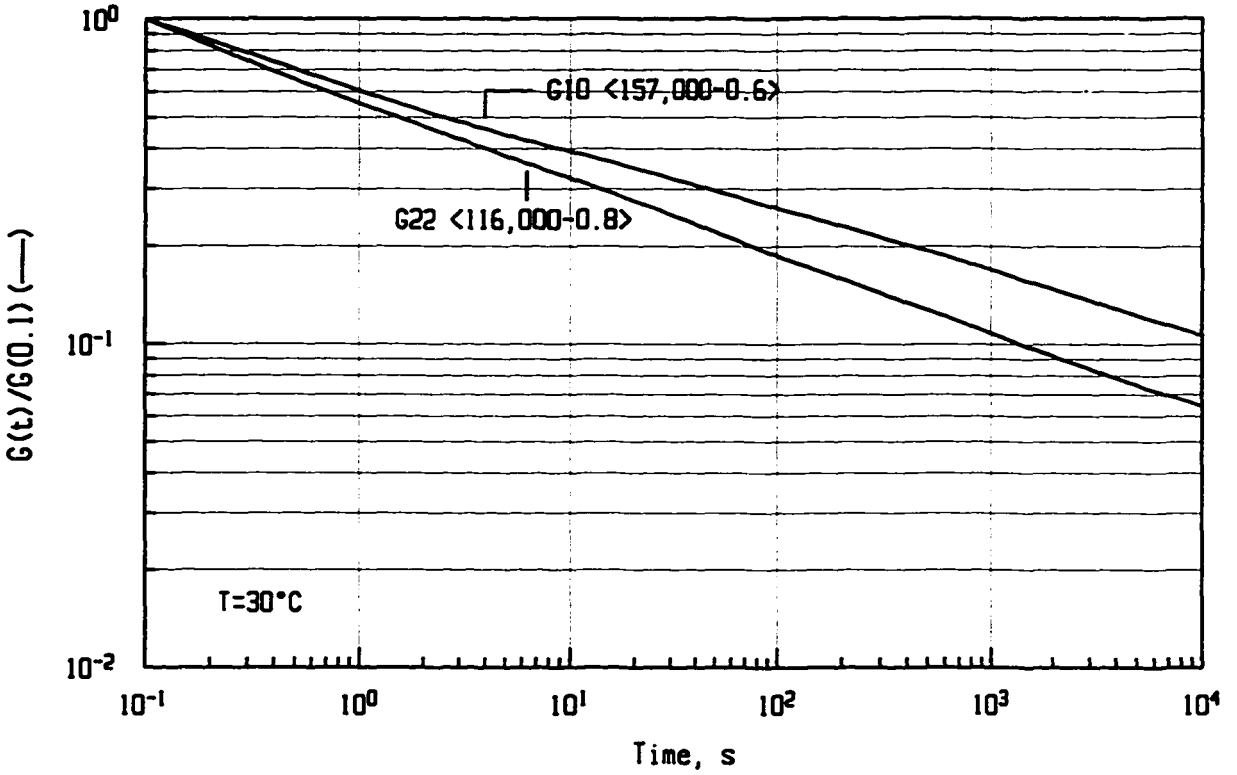


structure of the graft copolymers, constitute a sufficiently complete description of the LCB structure for interpretation of the rheological behaviour of these copolymers.

Overview and summary

Figure 6-43 is a composite graph of the nG(t) function and is designed to represent the range of relaxational behaviour for all LCB structures in this study. Samples G22 and G12 constitute the envelope of the relaxational behaviour. Sample G12 combines an appreciable branch length with a high branching number of 7.6. In the case of the sample G22, even its long branches (M_p^b =116,000) are not effective in the suppression of the relaxation due to the very low number of branches attached (N_g^p=0.8)to the backbone and the high content of unattached BR molecules ($w^{b,h}$=16%). The behaviour of almost all graft samples (G1 being a

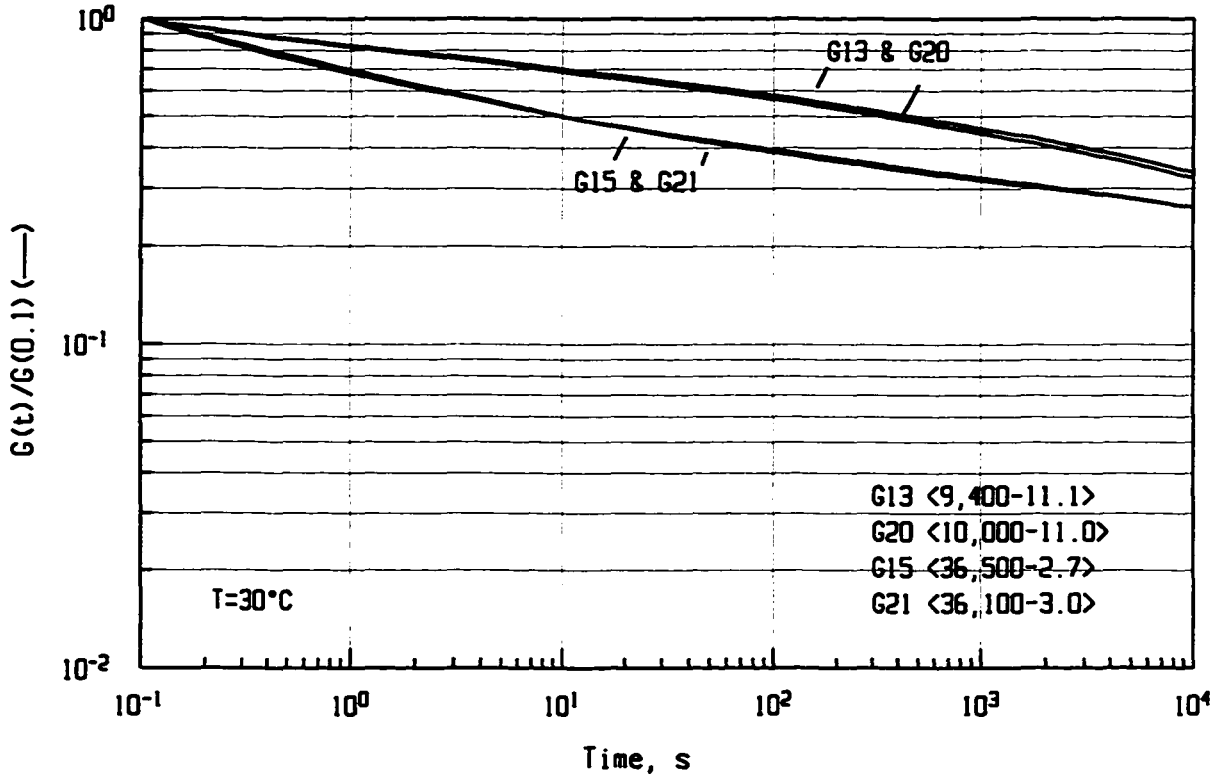
Figure 6-41. Stress relaxation - {SR10,000}. Effect of the ungrafted BR content - II.



notable exception) will fall within this envelope. Relaxational behavior of sample G1 is entirely different due to very short side chains and even the substantial branching number (N_g^p = 6.3) combined with an absence of a detectable amount of linear molecules, cannot prevent a very fast decay of the stress relaxation modulus nG(t) at long enough times.

Comparatively, the shape of these curves is different; convex for samples with many, shorter branches and concave for much longer and with fewer branches but still significant in number. These characteristics could be qualitatively interpreted in term of specific branching parameters. A lower nG(t) slope at lower to intermediate relaxation monitoring times, resulting in higher modulus values, appears to be due to a high branching number, N_g. The slope of the nG(t) curve at the highest times, 10^3 seconds and beyond, and therefore

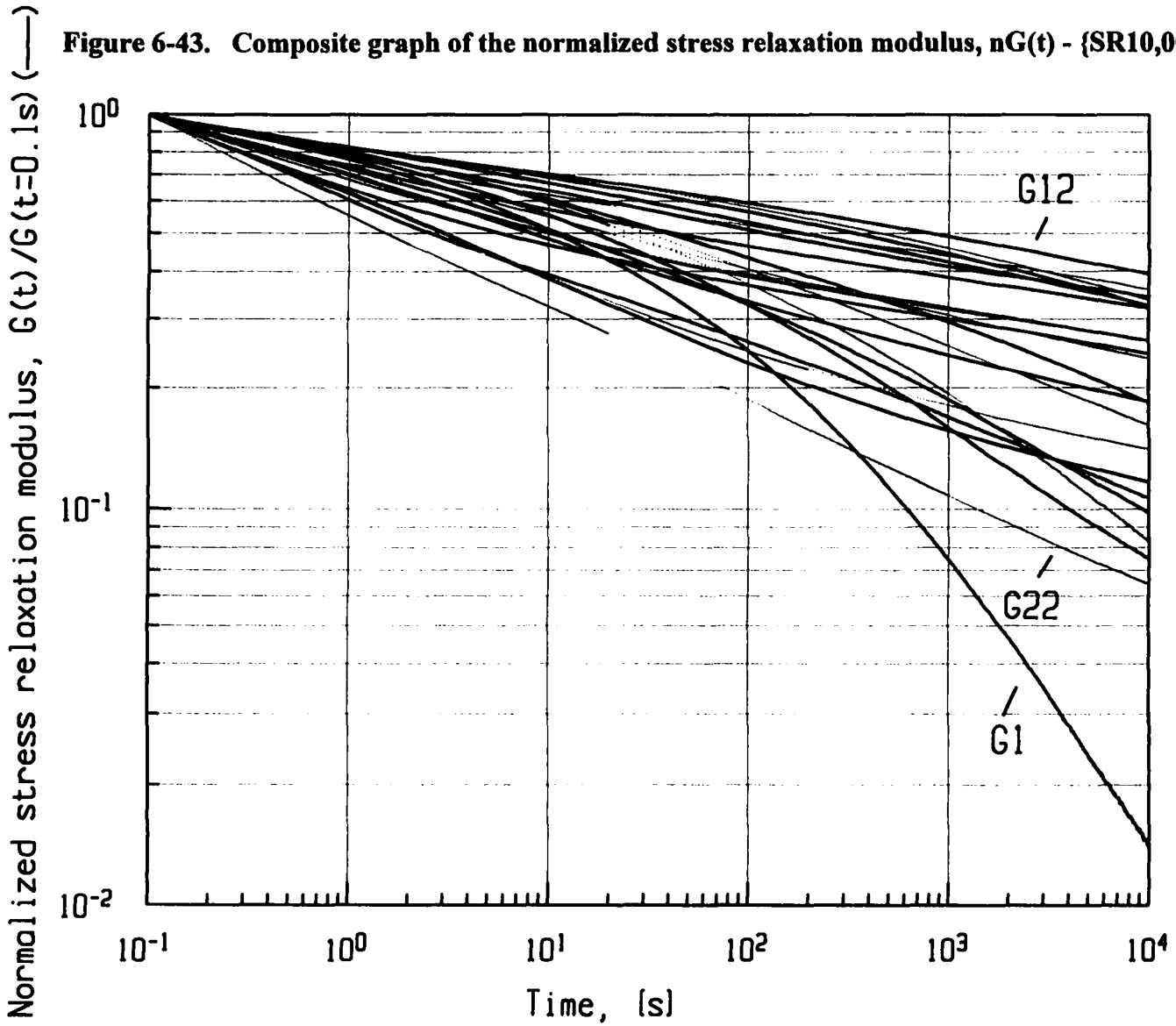
Figure 6-42. Stress relaxation - {SR10,000}. Reproducibility of test results.



eventually nG(t) at very long relaxation monitoring times (>>10^4 seconds) will depend on the length of the branches. Comb-like molecules with very long branches require a very long time for rearrangement imposed by an application of a sudden stress, which cannot be realized by molecular reptation only.

Branched polymers exhibit a much broader relaxation spectrum than linear polymers with narrowly polydispersed molecules and much longer relaxation times in the terminal zone. These differences are attributed to the suppression of chain reptation by long branches [23, 356] or from processes other than reptation, such as tube renewal [357-358].

Figure 6-43. Composite graph of the normalized stress relaxation modulus, nG(t) - {SR10,000}.



6.4.2 Stress relaxation parameters and their correlation with branching structure

Stress relaxation parameters are defined in Table 6-11 and their values are reported in Table A66, Appendix V. Results of the screening for correlations between LCB and stress relaxation parameters are in Table 6-12 and the prediction profiles are in Figures A65, A66 and A67, Appendix V.

Table 6-11. Definitions of viscoelastic parameters derived from {SR10,000} test.

abbreviation.	definition
nG(t=1)	- normalized (eq.6-5) stress relaxation modulus at 1s
nG(t=10)	- normalized stress relaxation modulus at 10s
nG(t=100)	- normalized stress relaxation modulus at 100s
nG(t=1000)	- normalized stress relaxation modulus at 1000s
nG(t=10,000)	- normalized stress relaxation modulus at 10,000s
|slope@t=0.1|	- (absolute value of the) slope of the log nG-log t curve at 0.1s
|slope@t=40|	- (absolute value of the) slope of the log nG-log t curve at 40s
|slope@t=10,000|	- (absolute value of the) slope of the log nG-log t curve at 10,000s
INT G(t)dt	- time integral of the G(t) within 0.1-10,000 s range

Normalized stress relaxation parameters nG(t) at long times, for example **nG(t=1000)** or **nG(t=10,000),** are influenced primarily by the branching number, N_g^p.

Correlations N_g^p // **nG(t=...)** [1] are strongest around t=100s. Interestingly, there is no indication of a systematic (and statistically significant) correlation between either branch length or content of branching.

[1] - nG(t=...) stands for any of defined nG(t) parameters

Table 6-12. Correlation coefficients (t-Ratio) between structural/compositional and selected rheological {SR10,000} parameters.

RMS {SR10,000}	M_p^b */*	N_g^p	$w^{b,g}$	$w^{b,h}$	w^b	M_z^G	PDI	vinyl
nG(t=1)	-2.90	+2.68	-	-3.97	-3.01	-	0	0
nG(t=10)	-	+3.87	0	-3.18	-	-	0	0
nG(t=100)	0	+4.51	0	-	0	0	0	0
nG(t=1000)	0	+3.98	+	-	+	+	0	0
nG(t=10,000)	+	+3.26	+	-	+	+	0	0
|slope@t=0.1|	+3.30	-	+2.83	+3.95	+3.73	+	0	0
|slope@t=40|	-	-	-3.09	0	-	-	0	0
|slope@t=10,000|	-2.60	0	-2.75	0	-3.25	-3.11	0	0
INT G(t)dt	0	+3.57	+	-	+	+	0	0

*/ - screening on reduced number of samples (no grafts included with a high $w^{b,h}$ > 0.3% content)

Explanation:
Numbers indicate the t-Ratio for a statistically significant correlation, that is when the |t-Ratio| value is above 2.50 (corresponding to 95% conf. interval).
'-' - negative, statistically not significant correlation (|t-Ratio| values below 2.50)
'+' - positive, statistically not significant correlation (|t-Ratio| values below 2.50)
'0' - weak or no correlation (|t-Ratio| values below 1.00)

Correlation between the branch length and any of the parameters depends on the relaxation monitoring time, t. It can be confidently concluded that the apparent negative correlation M_p^b // **nG(t=1)** is an effect of the strong M_p^b // $w^{b,h}$ interrelation, especially given the relative value of the t-Ratio for both correlations (e.g. higher for **nG(t=1)** // $w^{b,h}$). In fact, the sign of correlations between M_p^b and nG(t=...) changes from negative into positive at longer times. The diminishing influence of the $w^{b,h}$ content is also observed.

nG(t=...) parameter at short times are affected very significantly by the content of short, linear BR molecules (i.e. t-Ratio of -3.97 for $w^{b,h}$ // **nG(t=1)**). This is in agreement with previous observations about the inference $w^{b,h}$ has on the shape of the nG(t) at short times.

From the shape analysis of the nG(t) function reported in the previous section, the slope of the nG(t) curve at the lowest recorded relaxation times appears to be related to the content of the ungrafted branch prepolymer, $w^{b,h}$. Correlation analysis confirms this observation (t-Ratio = - 3.97 for M_p^b-$w^{b,h}$ pair). (t-Ratio of +3.95 for $w^{b,h}$ // **|slope@0.1|** pair. However, as judged by screening analysis, the slope of the nG(t) relates to the graft structure and its chemical composition in a quite complicated manner. In addition to the influence of $w^{b,h}$ (strongest), chemical composition (w^b) is also a contributing factor.

The relation between structural parameters and the **|slope@t=10,000|** is even more complex. It is intuitively obvious and in agreement with previous observations that increasing branch length and branching content (or even M_z^G) will decrease the slope of the nG(t) at very long times. The role of graft chemical composition, the very high correlation coefficient for **|slope@t=10,000|** // w^b, is not easy to explain.

The area under the relaxation curve, **INT G(t)dt**, calculated over the whole range of monitored relaxation times 0.1-10,000s, correlates significantly only with the branching number, N_g^p. For that reason this parameter could be considered as a potential indicator of the branching frequency in the long-chain branched copolymers.

Similarly, the normalized stress relaxation modulus at long relaxation times (>1000s) appears to be particularly sensitive to N_g^p and possibly suitable as a method to characterize branching frequency in elastomers by rheometrical methods.

INT G(t)dt - N_g^p relation

In Figure 6-44 **INT G(t)dt** is plotted versus branching number, N_g^p. The area under the log G - log t, within t=0.1-10,000s range, which is proportional to the **INT G(t)dt**, increases with the branching number. Substantial scatter in Figure 6-44 is caused, in addition to experimental error, by a few minor factors such as M_p^p, w^b and $w^{b,g}$. Proportionality between **INT G(t)dt** and N_g^p is maintained up to a value of N_g^p of about 3, then the curve reaches a plateau.

|Slope@t=10,000| - $w^{b,g}$ relation

The absolute value of the slope of the log nG(t)-log t curve at 10,000s decreases exponentially with $w^{b,g}$ up to ~20%. and then reaches a plateau. The higher content of branching, results in the flatter G(t) curves, which is equivalent to the smaller slope of the nG(t) function, as shown in Figure 6-45.

An attempt to classify, the rate of the nG(t) decay (slope of the log nG(t) - log t plot), based on the LCB architecture of the grafts, is shown in Figure 6-46. For grafts with very short or very few branches the rate of decay is much faster than exponential, as is the case for samples C, G1, G7 and G19, (Figure 6-43), resulting in convex shapes of the log nG - log t plots. On the other hand, the shape of the log nG-log t curve for samples with the highest degree of branching, $w^{b,g} > 36\%$, is concave. This is a result of the initial slope of the curve decreasing with time. Two intermediate shapes of the log nG - log t curves are derived unambiguously from boundary relaxational behaviour which corresponds to a strictly exponential decay of the normalized stress relaxation modulus (straight line on a double logarithmic plot of nG(t) versus time).

Figure 6-44. Relation between INT G(t)dt parameter and branching number, N_g.

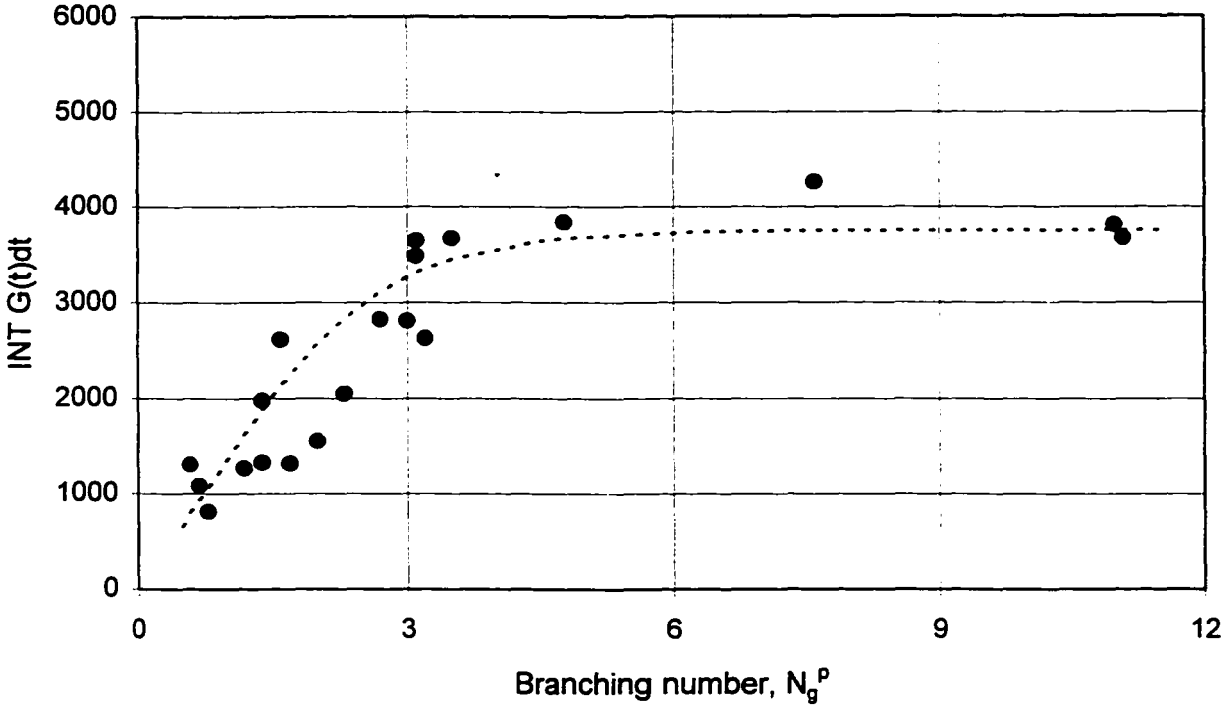


Figure 6-45. Relation between slope of the nG(t) at t=10,000s and branching content, $w^{b,g}$.

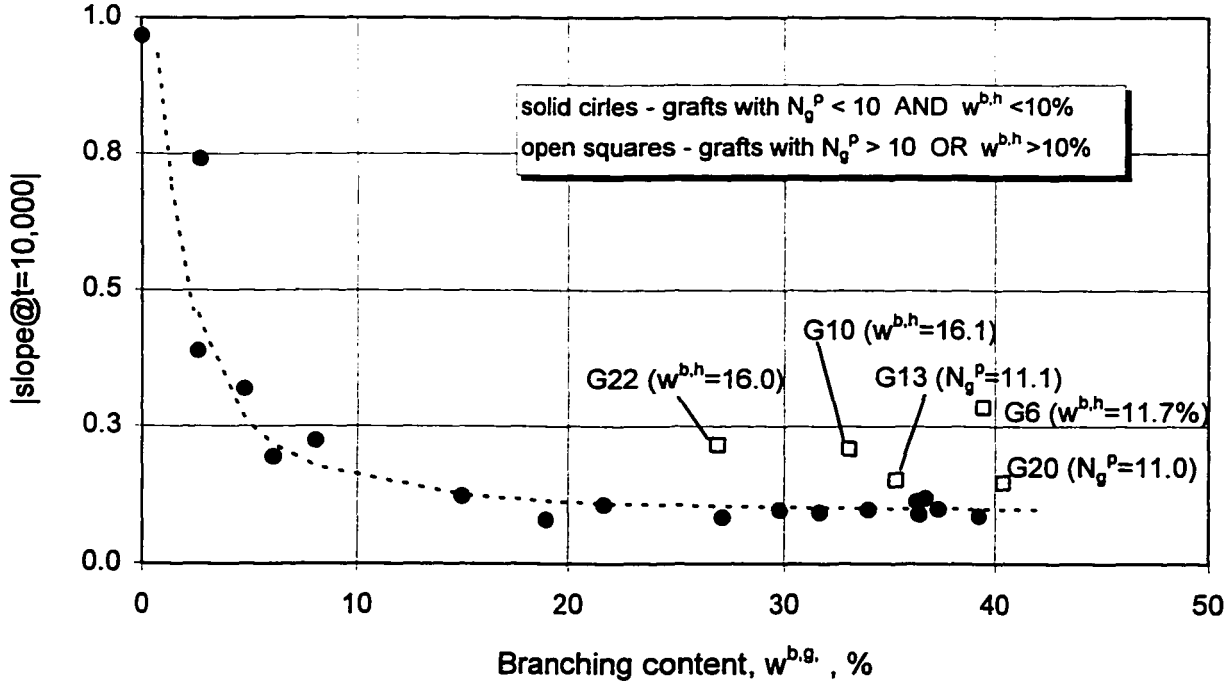
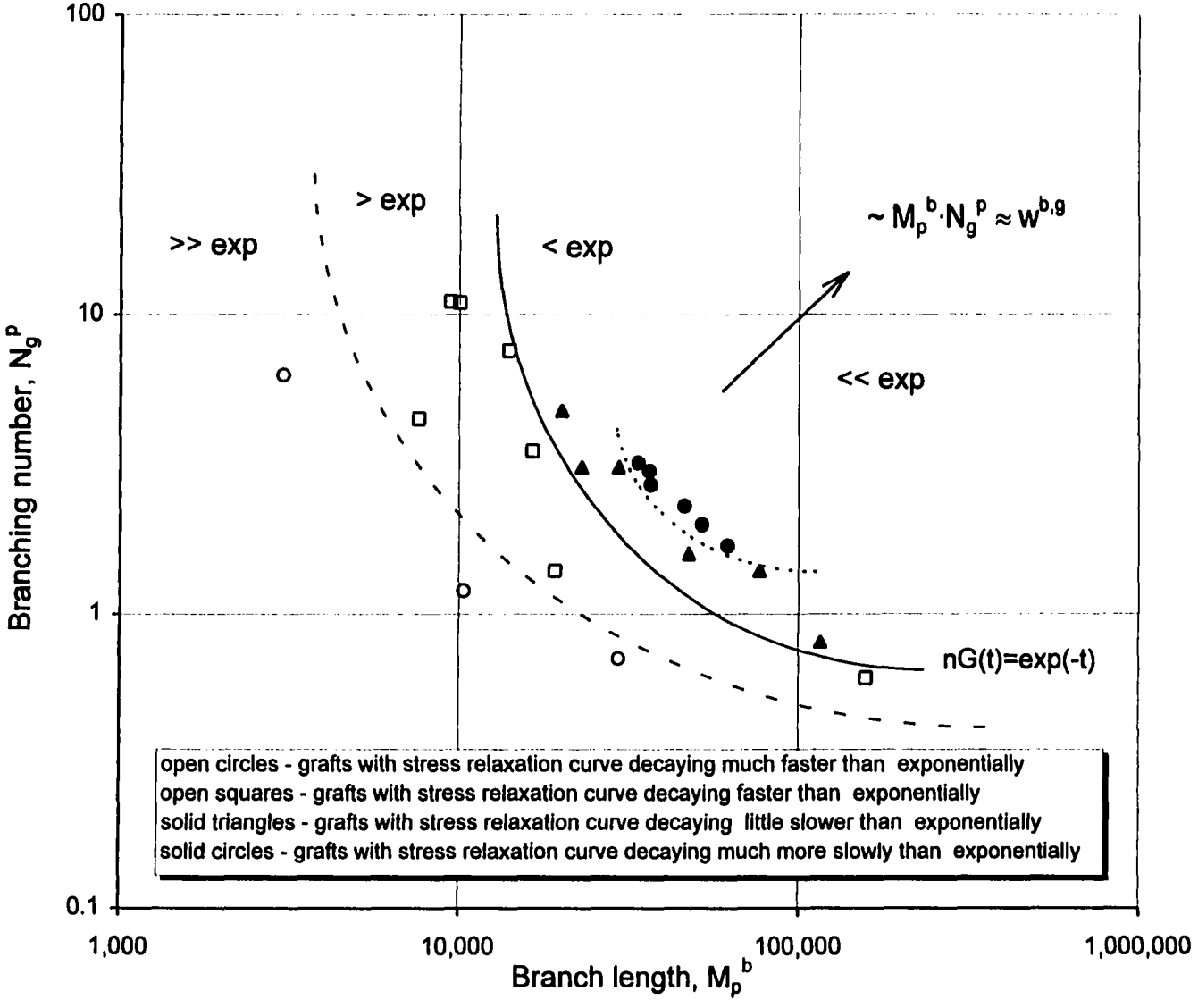


Figure 6-46. Rate of nG(t) decay as a function of the specific branching parameters - {SR10,000}.



6.5 Stress relaxation - II

Test conditions for a series of {SR1000} experiments were identical to those for the (SR10,000} test, except for a shorter (10-fold) relaxation monitoring time. The test was carried out primarily for statistical reasons, to verify {SR10,000} test results.

A very good correlation between corresponding relaxation curves was obtained, as shown in Figure 6-47. The values of selected parameters derived from normalized stress relaxation modulus data are listed in Table A66, in Appendix V.

To augment the analysis reported in the previous section of this chapter, the effects of branch length and branching number on the stress relaxation, are discussed.

*Effect of branch length on **nG(t=1000)***

The effect of branch length at comparable values of $N_g^p \approx 3$ (see footnote [1]) is examined for the **nG(t=1000)** parameter, representing a value of the normalized stress relaxation modulus at 1000s after step shear strain was imposed. It is readily observed from Figure 6-48 that up to a certain critical branch length (~10,000), the **nG(t=1000)** increases rapidly with the branch length, and then remains virtually independent of the branch length.

Only 3 samples could be found with comparable values of N_g^p and $w^{b,h}$ while yet having an appreciable branching level ($N_g^p = 3.0$ - or more) and with different M_p^b (marked with solid diamonds in Figure 6-48).

[1] In fact, very short branched samples (G1, G2) are also included for comparison (marked by open diamonds). Their branching number is higher ($N_g^p > 3.0$) and their content of $w^{b,h}$ is negligible ($w^{b,h} < 0.3$), and therefore their position below the plateau can only be explained as due to presence of short branches.

Figure 6-47. Correlation between stress relaxation parameters from {SR10,000} and {SR1000} test series.

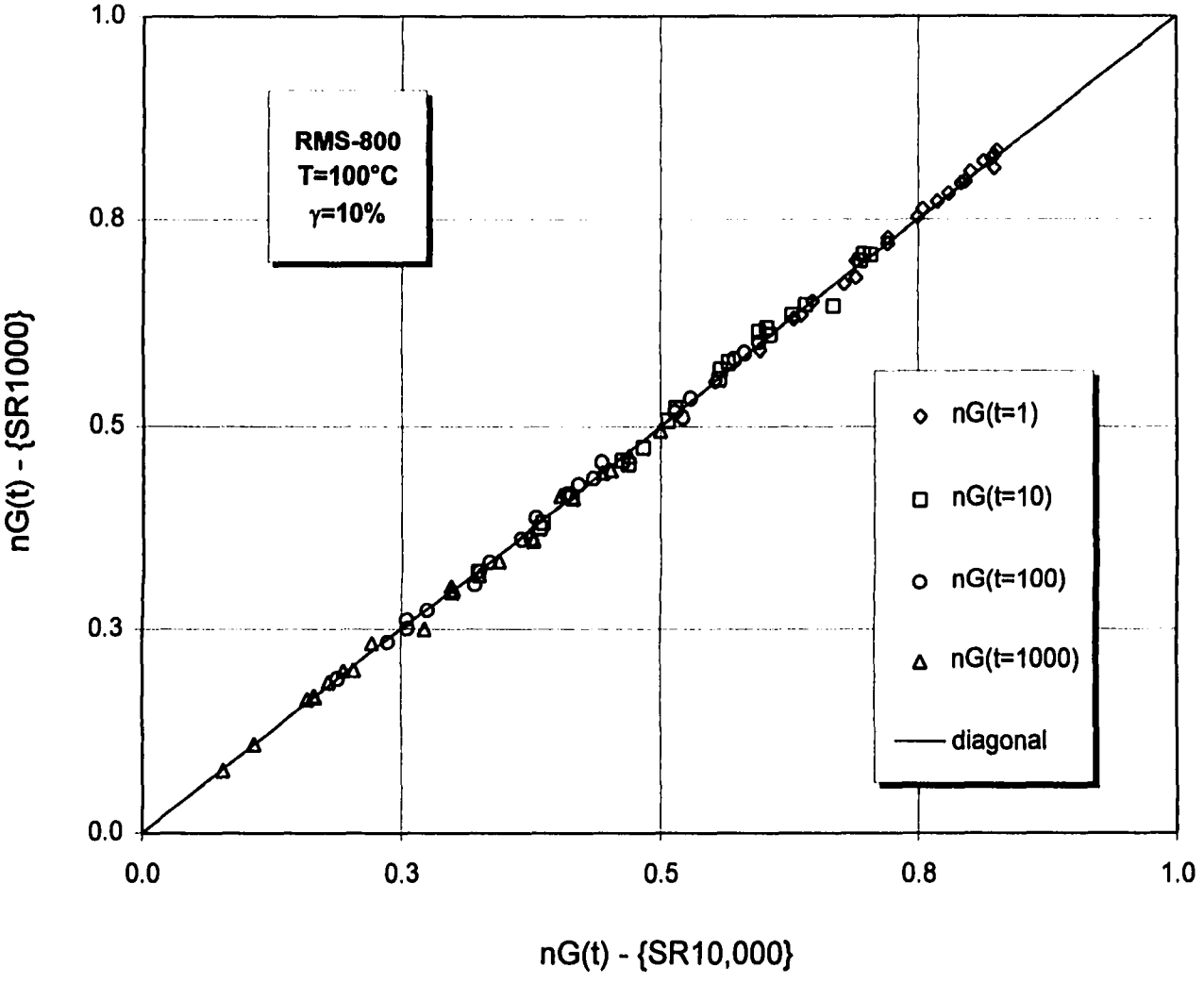
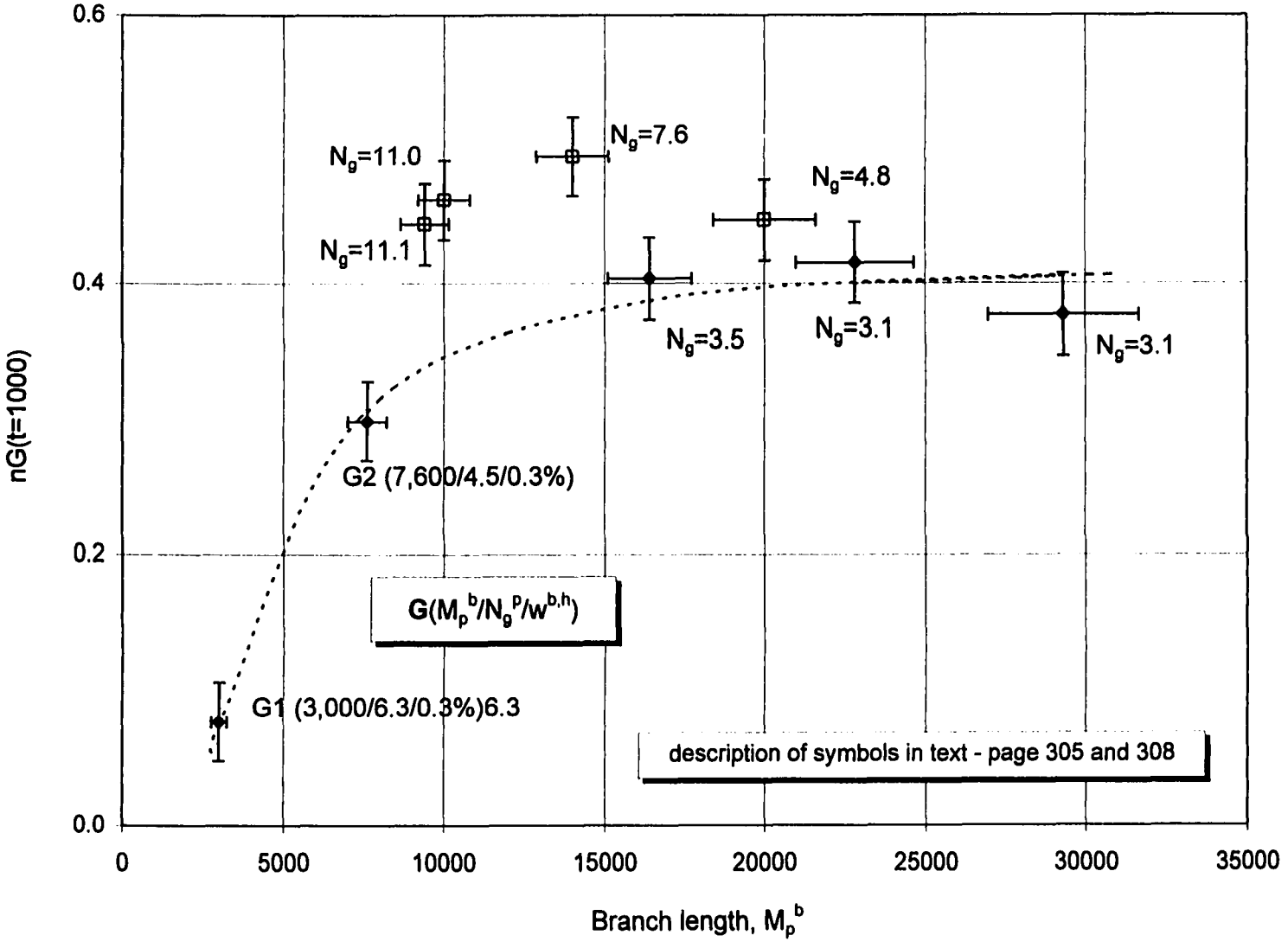


Figure 6-48. Relation between branch length and nG(t=1000) parameter.



The number of branches can also contribute to the increase in the value of nG(t). Thus, the actual value of nG(t) is a superposition of both effects. In Figure 6-48 samples with a high N_g^p are marked by open squares. In order to demonstrate the effect of branch length on **nG(t=1000)** with allowance for N_g^p as a contributing factor, samples with a high content of ungrafted BR ($w^{b,h}$ more than 0.3 %) were not included in this comparison.

*Effect of branching number on **nG(t=1000)***

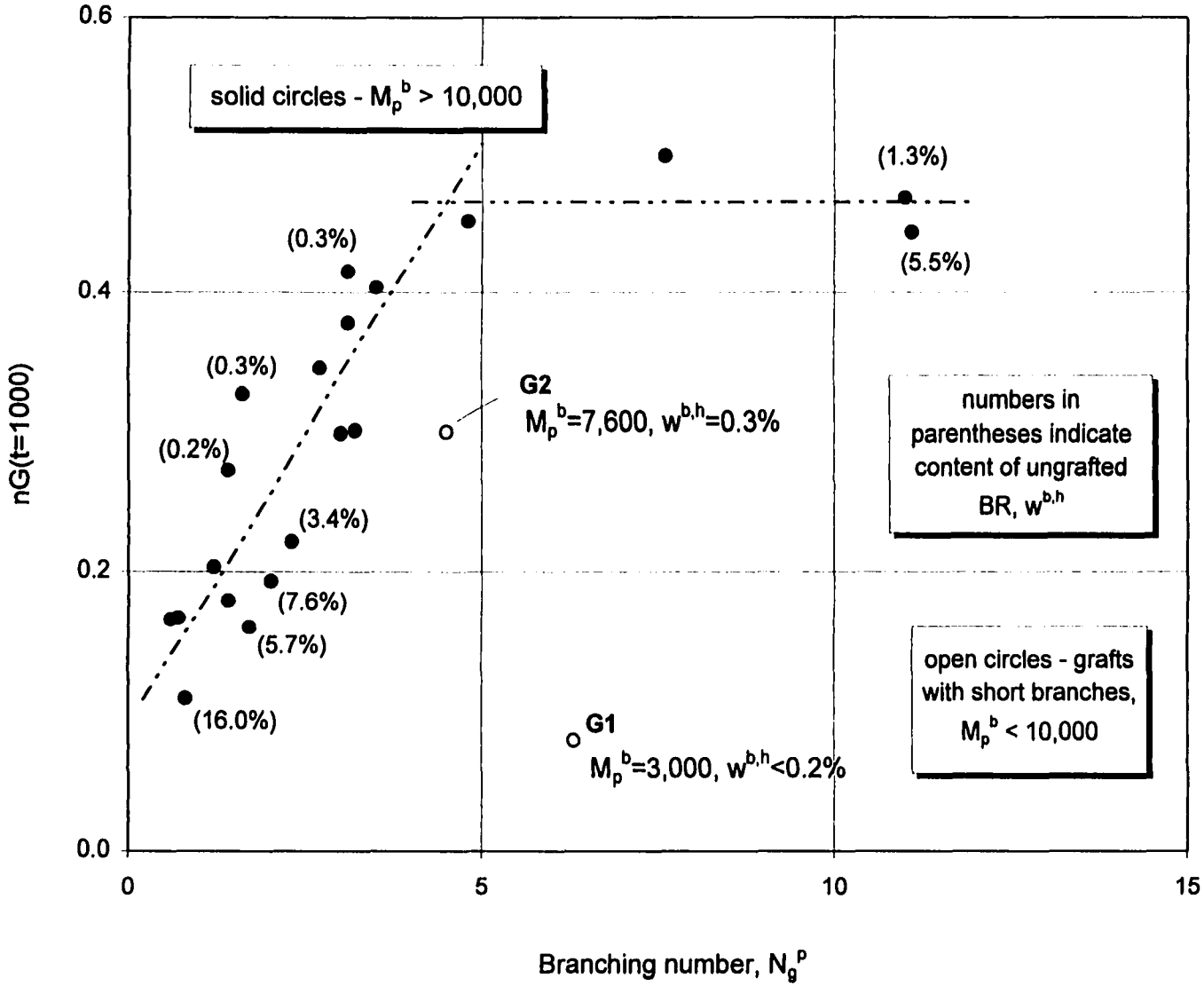
A plot of **nG(t=1000)** versus N_g^p permits further analysis of the manner in which the number of long-chain branches controls stress relaxation. In Figure 6-49 solid circles are assigned to samples with M_p^b greater than 10,000 which belong to the plateau region of the plot in the previous Figure 6-48. Open circles indicate samples which, due to very short branches, do not fit the trend (G1, G2).

Increasing the branching number will systematically increase the value of **nG(t=1000)** until N_g^p has value of 4.0-4.5. For branches above a certain length (~10,000 g/mol) and branching number, a further increase in either branching parameter does not alter **nG(t=1000)** appreciably.

The presence of ungrafted, linear molecules, reduces nG(t) quite significantly. The effect appears to be particularly strong for grafts with fewer branches. The degree of **nG(t=1000)** reduction due to a high $w^{b,h}$ content can be observed by the vertical spacing between the points of comparable abscissa (N_g^p) - samples G1 and G2 in Figure 6-49.

The observation that all samples with M_p^b higher or equal to about 10,000, fit reasonably well one of the two lines in Figure 6-49, indicates that the branching number (N_g^p) is primarily responsible for the **nG(t=1000)** parameter, provided that the branches are sufficiently long.

Figure 6-49. Relation between branching number and nG(t=1000) parameter.



6.6 Stress relaxation - III

A third series of stress relaxation experiments was carried out at 100°C and over 400s. The higher test temperature thanused for two stress relaxation experiments previously discussed (30°C), helped to explore polymer behaviour deeper into the terminal zone of the viscoelastic spectrum.

6.6.1. Time dependence of stress relaxation modulus

The time dependence of the normalized stress relaxation modulus, $nG(t) \equiv G(t)/G(0.1)$ at 100°C is discussed below as a comment to a series of graphs in Figures 6-50 to 6-52.

Comparison between samples C, M and G4

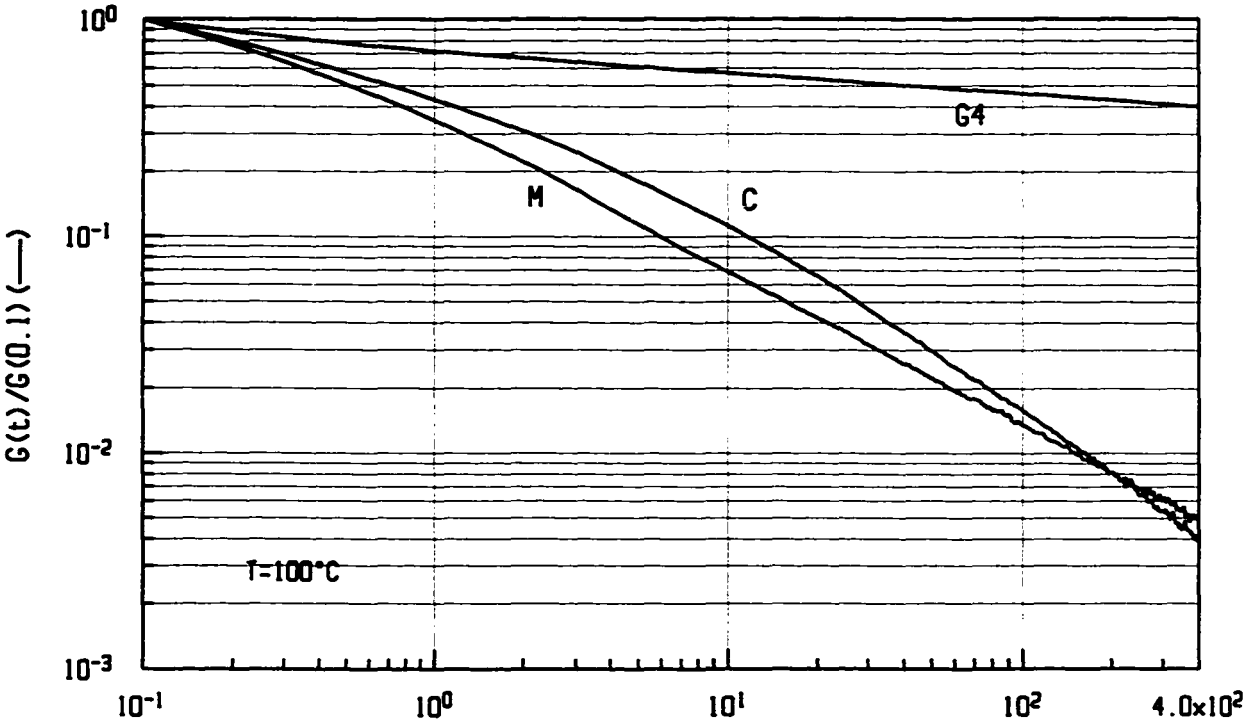
In Figure 6-50 the stress relaxation for the backbone polymer (sample C) is compared to that for blend M, in which the CIIR component is identical to sample C, while the BR structure (MW, MWD, microstructure) and its overall content (w^b) are very similar to those of the branches in graft G4 and to the graft G4. The corresponding graph, based on data from the {SR10,000} test at 30°C, is shown in Figure 6-35. Comparing the relaxation curves at the two temperatures and making allowance for the different scales used in these graphs, the following observations can be made:

(a) - relaxation of graft G4 is scarcely affected by the 70°C temperature difference,

(b) - to the contrary, the relaxation of both linear polymer C and the blend M is greatly accelerated by increased temperature of the samples. For example, the relative value of modulus retained after the 100s relaxation time is 1.6% (Table A67, column 'c' in Appendix V) as compared with 23.8% at 30°C (Table A65, column 'c', Appendix V),

(c) - the mutual relationship between the cross-over of the nG(t) curves for samples C and M, observed at 30°C, is preserved, if not even more temperature-accentuated,

Figure 6-50. Stress relaxation - {SR400}. Comparison between samples C, M and G4.



particularly within 1-100s range. This can be explained by the much increased mobility of the short, flexible and linear BR molecules, present in the blend M,

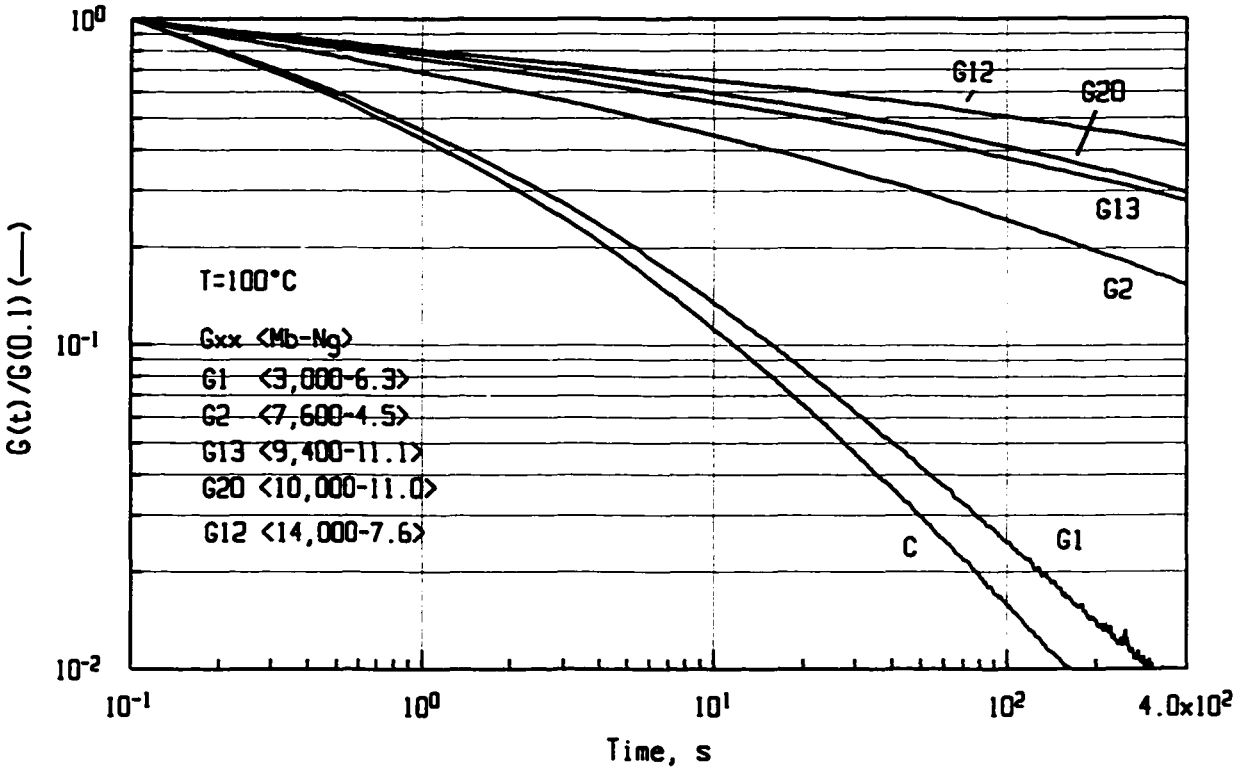
(d) - it is interesting to notice that the cross-over of the nG(t) curves for samples C and M, occurs at a shorter relaxation time, about 200s at 100°C, versus 350s at 30°C,

(e) - the incorporation of long-chain branches (G4, M_p^b=29,300, N_g^p=3.1) results in a 100-fold reduction of the relaxation modulus after 400s at 100°C.
Alternatively, the modulus relaxes to 40% of the value it had in 0.1s after the application of step-strain, during approximately the first 1s for sample C and 400s for graft G4.

Effect of branch length

An increase of the branch length at a sufficiently high N_g^p will systematically elevate the entire nG(t) curve as shown in Figure 6-51.

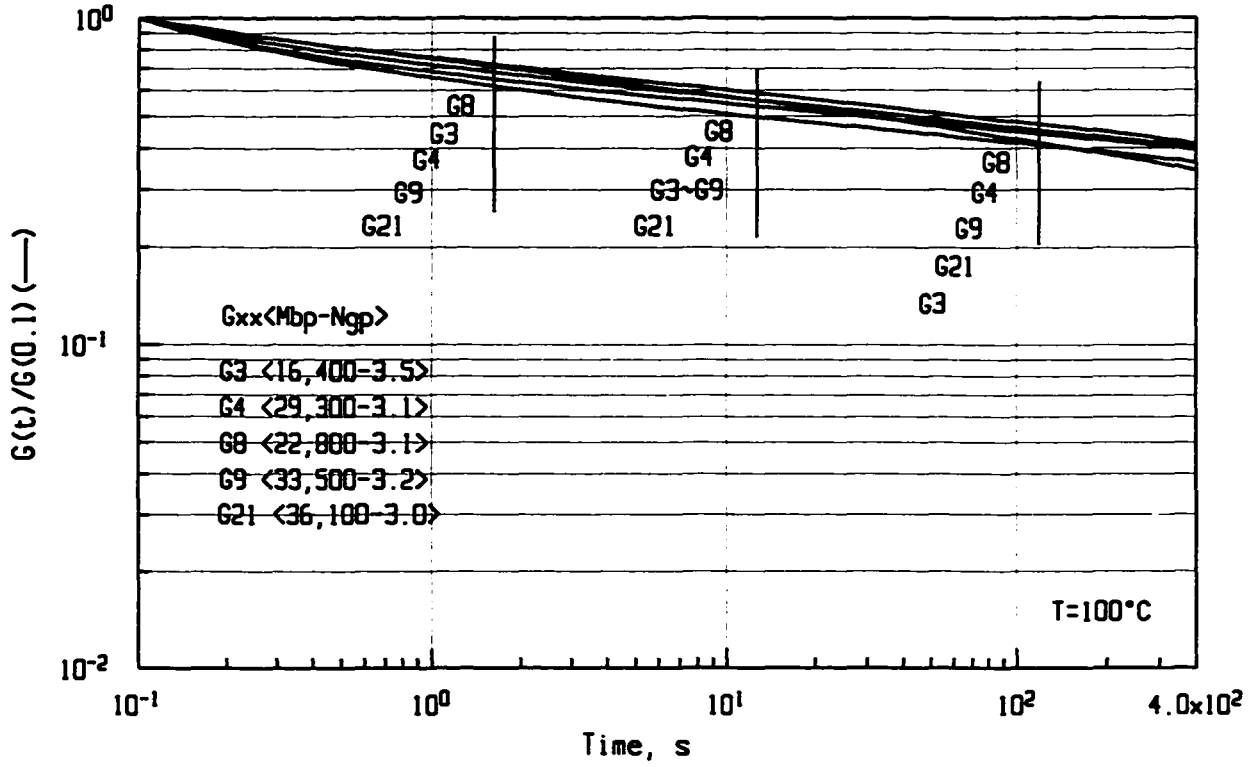
Figure 6-51. Stress relaxation - {SR400}. Effect of branch length - I.



Separation of the nG(t) curves is increasingly more pronounced at longer relaxation monitoring times. This is particularly evident for samples G1 and G2, suggesting an additional important mechanism of molecular relaxation developing when the length of the branch is sufficiently long.

The confirmation of results discussed in connection with data in Figure 6-48, can be found in Figure 6-52. The nG(t) curves for five graft samples with branch lengths ranging from 16,400 to 36,100 but similar N_g^p (3.0 to 3.5), are compared. The effects of even considerable branch length extension (more than two-fold) on the nG(t) were minor, corresponding to the plateau observed in the **nG(t=1000)** - M_p^b plot in Figure 6-48.

Figure 6-52. Stress relaxation - {SR400}. Effect of branch length - II.



Effect of branching number

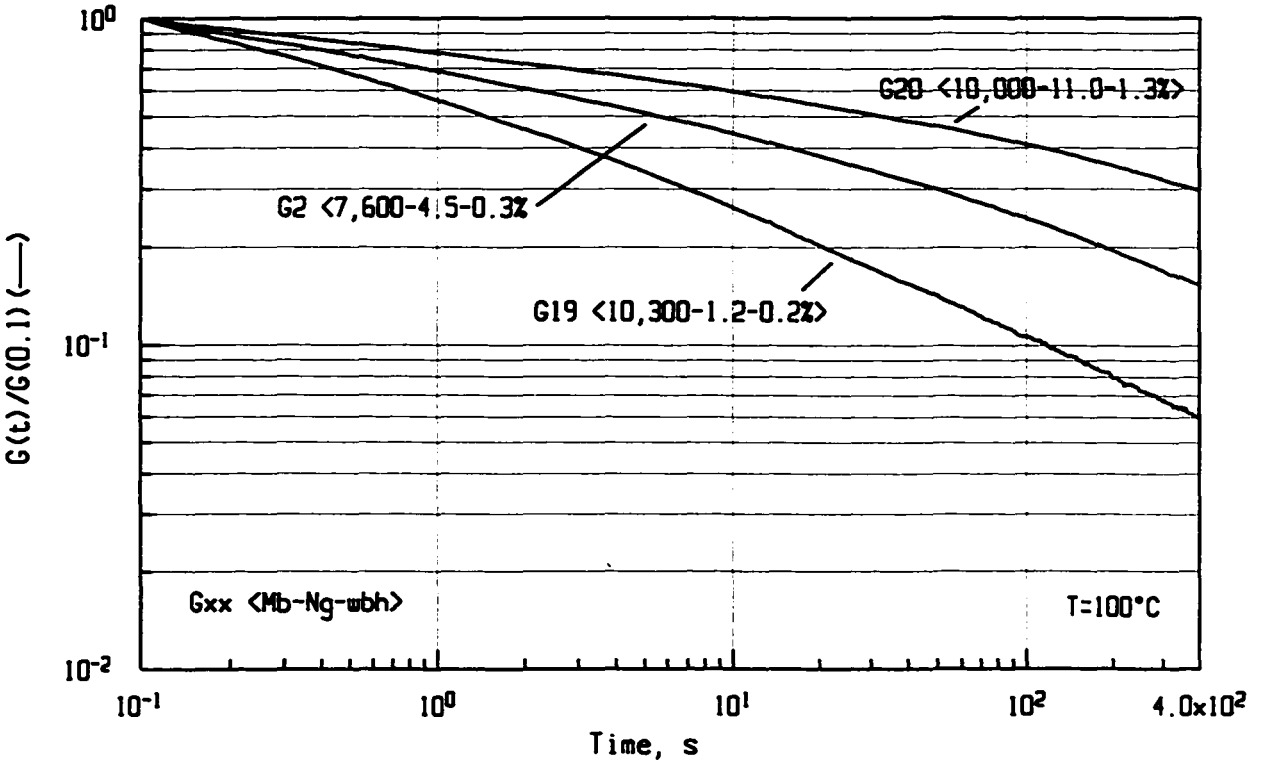
The influence of branching on stress relaxation can be most explicitly demonstrated by a direct comparison of the nG(t) curves for grafts having branches of a similar length.

In Figure 6-53 the effect increasing branching number has on the nG(t), at a branch length of the order of 10,000, is clearly demonstrated. Another comparison for several grafts with M_p^b in a range between 19,100 - 29,300 and a progressively increasing N_g^p gave similar results (Figure 6-54).

Effect of ungrafted BR

Sample G16 was purposefully included in the comparison to demonstrate the role of ungrafted, residual BR, which has the opposite effect on nG(t) than branching number.

Figure 6-53. Stress relaxation - {SR400}. Effect of number of branches - I.

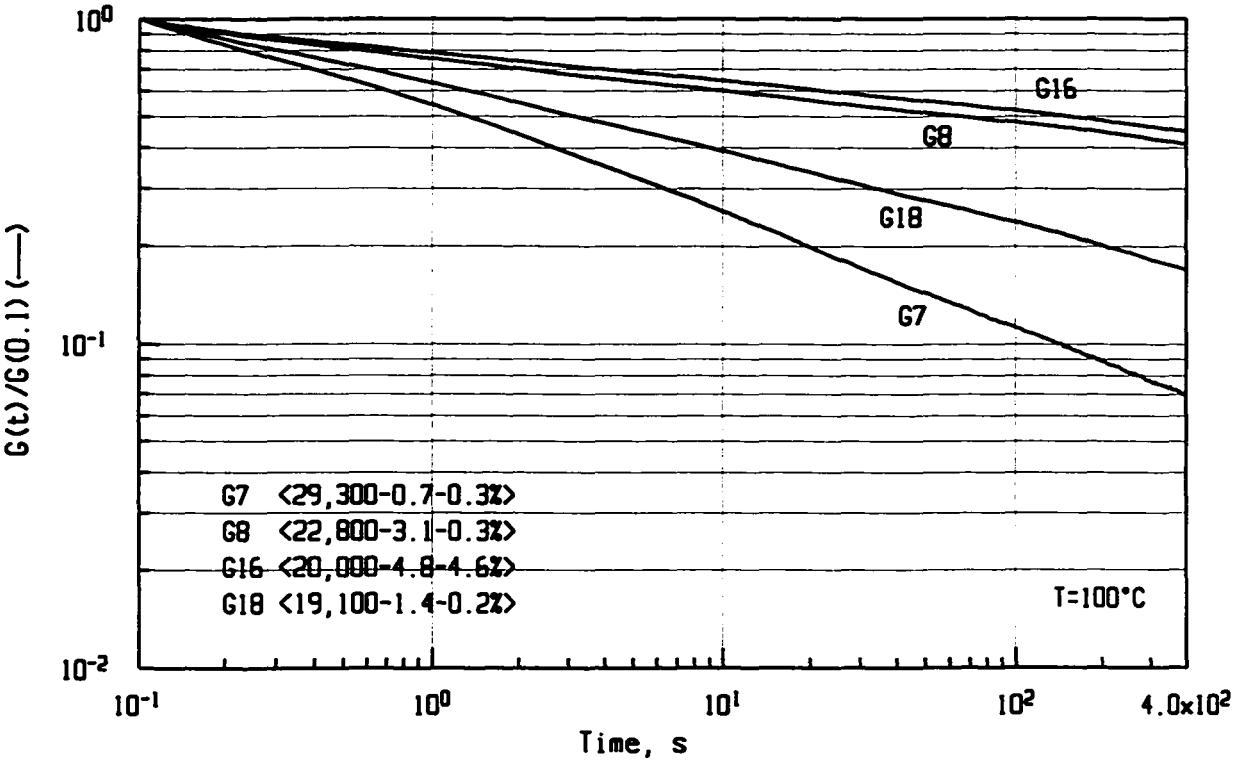


Ignoring the presence of even small amounts of low molecular weight, linear molecules in a graft mixture may lead to the wrong conclusions. In fact, an increase in branching number of over 50% (from 3.1 to 4.8) has been nearly offset by the effect of the presence of 4.6% of low MW (20,000) polybutadiene as can be seen by comparing nG(t) for samples G16 and G8 in Figure 6-54. This issue will be again revisited in the next section of this chapter (6.6.2).

Effect of branching content

There is ample evidence that the presence of the long chain branching is slowing down relaxation processes. Within certain limits, as discussed previously, this process will be in proportion to both specific parameters, M_p^b and N_g^p. Consequently, the stress relaxation curve will be "elevated" at the prolonged times, in proportion to the increasing branching content, $w^{b,g}$, which in turn is proportional to the product of M_p^b and N_g^p.

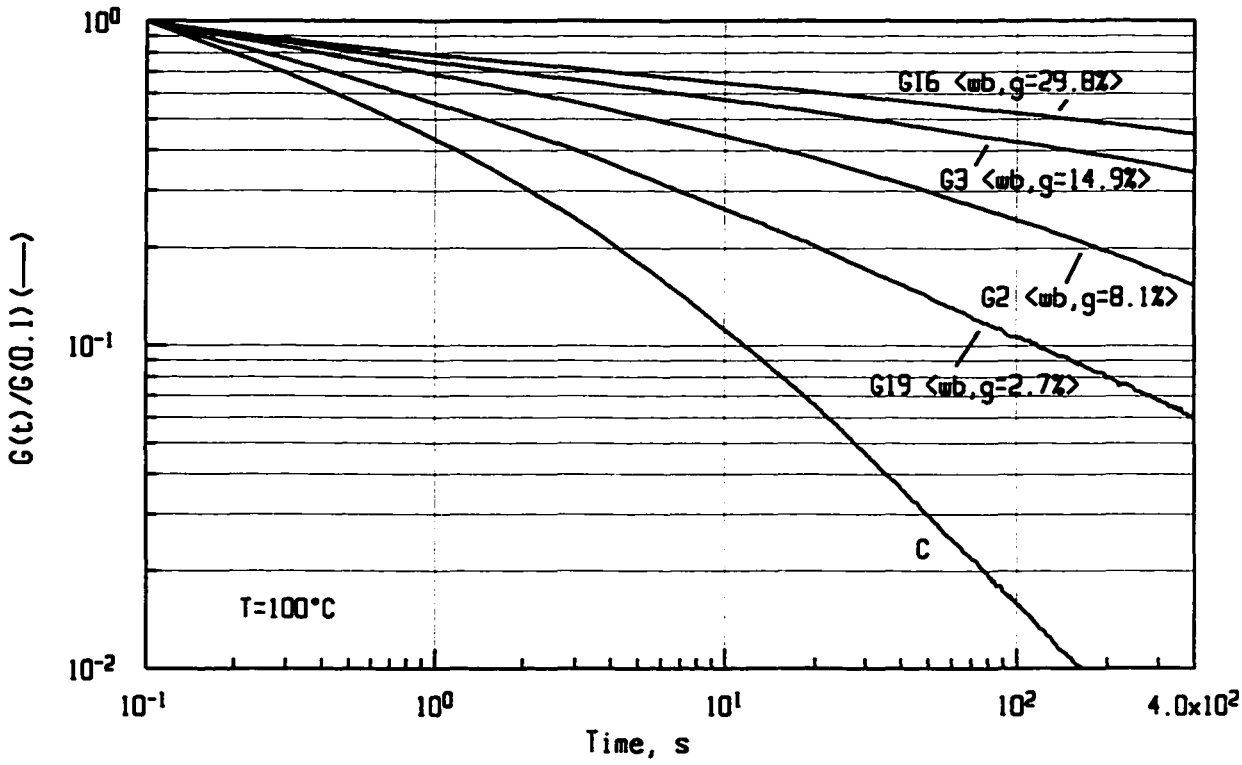
Figure 6-54. Stress relaxation - {SR400}. Effect of number of branches - II.



The relation between the branching content and stress relaxation is demonstrated in Figure 6-55. A certain "saturation" effect is observed for the nG(t) curves, as they approach the limiting values for the normalized stress relaxation function (nG(t)≡1) of a perfectly elastic body. For example, sample G16 has both specific branching parameters, M_p^b and N_g^p 20,000 and 4.8, respectively, above their respective critical values (M_p^b > ~10,000 and N_g^p > ~4.5) - compare also Figures 6-48 and 6-49.

Consequently, the nG(t) curve corresponding to the sample G16 represent asymptotic behaviour for the class of graft copolymers under study.

Figure 6-55. Stress relaxation - {SR400}. Effect of branching content.

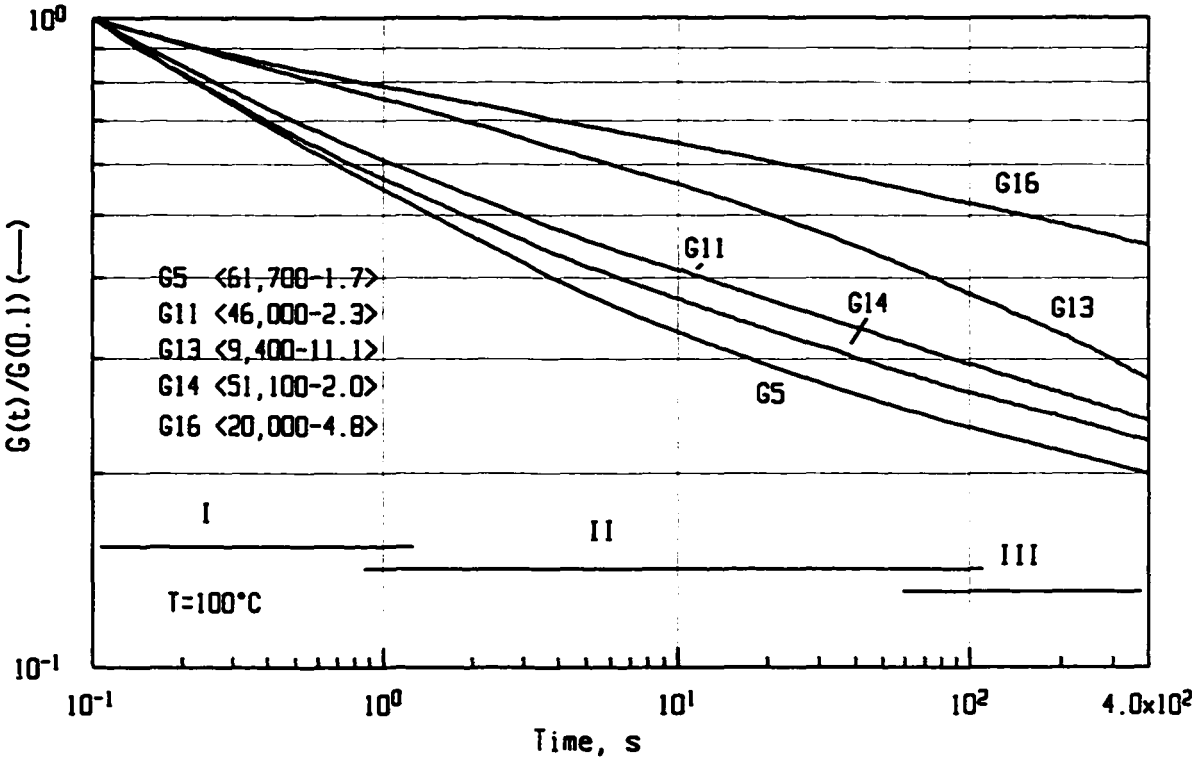


Summary

For LCB structures with sufficiently long branches (for example, samples G5, G11, G14 or G16), the slope of the nG(t) at short times (zone I in Figure 6-56) and corresponding values of nG(t) at intermediate times (zone II) depend upon the branching number.

However, if the branch is not long enough (for example, G13), even with a high number of branches, the relaxations tend to "accelerate", particularly at longer relaxation monitoring times (zone III, Figure 6-56).

Figure 6-56. Stress relaxation - {SR400}. Summary of observations.



6.6.2 Correlations between branching structure and stress relaxation parameters

Screening for the correlations which might exist between the structural and stress relaxation parameters gave similar results to those reported in section 6.4 and 6.5 for related experiments. Therefore, for the {SR400} test, the correlation summary is not included. The viscoelastic parameters defined in Table 6-13, are listed in Table A67, Appendix V.

Table 6-13. Definition of viscoelastic parameters derived from {SR400} tests.

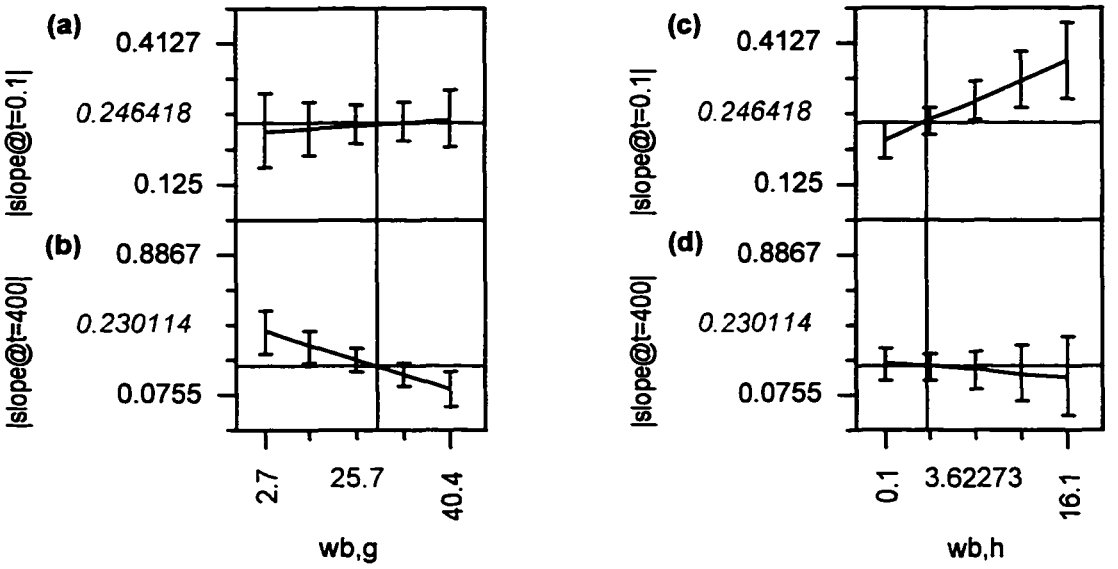
abbreviation.	definition
nG(t=1)	normalized (eq.6-5) stress relaxation modulus at 1s
nG(t=10)	normalized stress relaxation modulus at 10s
nG(t=100)	normalized (eq.6-5) stress relaxation modulus at 100s
nG(t=400)	normalized (eq.6-5) stress relaxation modulus at 400s
|slope@t=0.1|	(absolute value of the) slope of the log nG-log t curve at 0.1s
|slope@t=400|	(absolute value of the) slope of the log nG-log t curve at 400s

The prediction profiles in Figure 6-57, are included only for $w^{b,g}$ and $w^{b,h}$ parameters to illustrate the two following observations:

1. The prediction profile (profile "b" in the Figure 6-57) suggests a possibility of the dependence of the slope of the log nG-log t curve at 400s upon the branching content, $w^{b,g}$. This decrease in the slope of the nG(t) with increasing level of branching, at the long observation times, has been previously shown for the relaxation at lower temperatures (30°C) through a direct comparison between $w^{b,g}$ and **|slope@t=10,000|** parameters in Figure 6-45. It is worth noting that the slope of the stress relaxation curve at very short times (profile 'a', Figure 6-57) does not correlate with branching content.

2. The presence of ungrafted linear BR will influence not only the **nG(t=...)** but also the slope of the nG(t). The effect is significant at the short relaxation monitoring times, as seen from prediction profiles 'c' and 'd' in Figure 6-57.

Figure 6-57. Prediction profiles for correlation between compositional ($w^{b,g}$, $w^{b,h}$) and stress relaxation {SR400} parameters.



Summary

Based on analysis of results from all relaxation experiments, the shape of the normalized relaxation modulus appears to be influenced by three structural parameters: branch length, M^b, number of branches, N_g, and content, if any, of ungrafted branch precursor polymer, $w^{b,h}$. The overall slope of the nG(t) curve, in particular values of the normalized G(t) is governed by the branching number. The higher is the N_g, the flatter and higher is nG(t) curve.

There is no evidence of a direct dependence of CCD, graft molecular weight and interferences (PDI of MWD of branches, vinyl content of BR made branches) on stress relaxation behaviour as judged from an absence of correlations of these parameters with the viscoelastic parameters.

The tail of the relaxation curve is affected by the length of the branches. For example, for shorter branches it is steeply declining, for branch length above a certain intermediate length,

no decline is observed. For some combination of N_g and M^b, the tail of nG(t) is even leveling-off. To the contrary, shape of the nG(t) at low t<1s is much affected by the presence and MW of the residual linear BR.

Absence of linear BR ($w^{b,h}$<0.5%), results in a linear nG(t) curve at very short times. However, a pronounced "downward curvature" is observed in most cases where $w^{b,h}$ is high and M_p^b is 20,000. Due to normalization of the nG(t) function at 0.1s, it is likely that a large portion of the "contribution" from the short (M_p^b<< 20,000) linear branches has taken place prior to 0.1s (compare relaxation of sample B10, M_w=100,000 at 30°C, in Figure 6-40).

Chapter 7
Non-linear viscoelastic (NLVE) properties

This chapter describes the non-linear viscoelastic properties of graft copolymers, based on results obtained from RPA-2000 and DSR experiments. Emphasis has been put on the interpretation of these results in terms of the LCB structure. Rheological properties of grafts were compared to those of the backbone and branch precursor polymers, and CIIR/BR blend.

Following the pattern established in Chapter 6, screening analysis for correlations between branching and viscoelastic parameters was confirmed and extended by interpretation of the viscoelastic functions and parameters in terms of the details of the long-chain branching structure.

The principal rheometric techniques employed were: large-amplitude oscillatory shear in strain and frequency sweep (sections 7.1-7.3) and isothermal stress relaxation experiments following (large amplitude) step-shear strain (sections 7.4-7.5).

Experimental aspects of rheological characterization, including review of preliminary test results were discussed in chapter 5. Tabulated test results, results of statistical analysis and certain additional graphs are included in Appendix V.

No comparable results on the non-linear viscoelastic properties of graft copolymers could be found in the literature.

7.1 Strain-amplitude dependence of the dynamic moduli, $G_1'(\gamma)$ and $G_1''(\gamma)$

Isothermal strain sweeps at a constant frequency and temperature {SWP2} by means of the RPA 2000 were used to examine the effect of branching structure and graft composition on the onset of non-linear behaviour in oscillatory shear. This test is comparable, in principle, to a series of tests {SS1} to {SS7}, carried out using the RMS-800, the results of which were reported in Chapter 5, section 5.2.4.2.

Strain dependence of the dynamic moduli

Figure 7-1 shows a plot of the 'in-phase torque', S′ versus dynamic strain amplitude at 100°C and 10 rad/s, for sample C. The upper, "inclined" row of experimental points represents the torque measurements at progressively increasing strain amplitude, while the lower, horizontal row consists of measurements obtained at the low (2%, LVE) strain. The bottom, low-strain line in Figure 7-1 serves as a control, to verify test integrity from the instrumental point of view, as well as to help detect potential thixotropic effects. Departure from the linearity of the upper line can be considered as qualitative indication of the material's non-linearity (in a rheological sense).

An alternative method for assessment of the degree of non-linearity was adopted. Instead of calculating the strain at which storage modulus drops a certain percentage below its plateau value (at small amplitude strains), the difference between storage modulus G_1' at 50% and at 2% dynamic strain was calculated. The two methods are compared in Figure 7-2, except that 95% (instead 98%) threshold level was chosen for illustration purpose. which also contains an example of the strain sweep plot in the form of the first harmonic of the storage modulus G_1' versus dynamic strain amplitude. All measurements were carried out at the constant temperature (100°C) and frequency (10 rad/s). Strain sweep profiles for all grafts were found to be quite similar.

Figure 7-1. Strain sweep {SSWP2}, sample C.

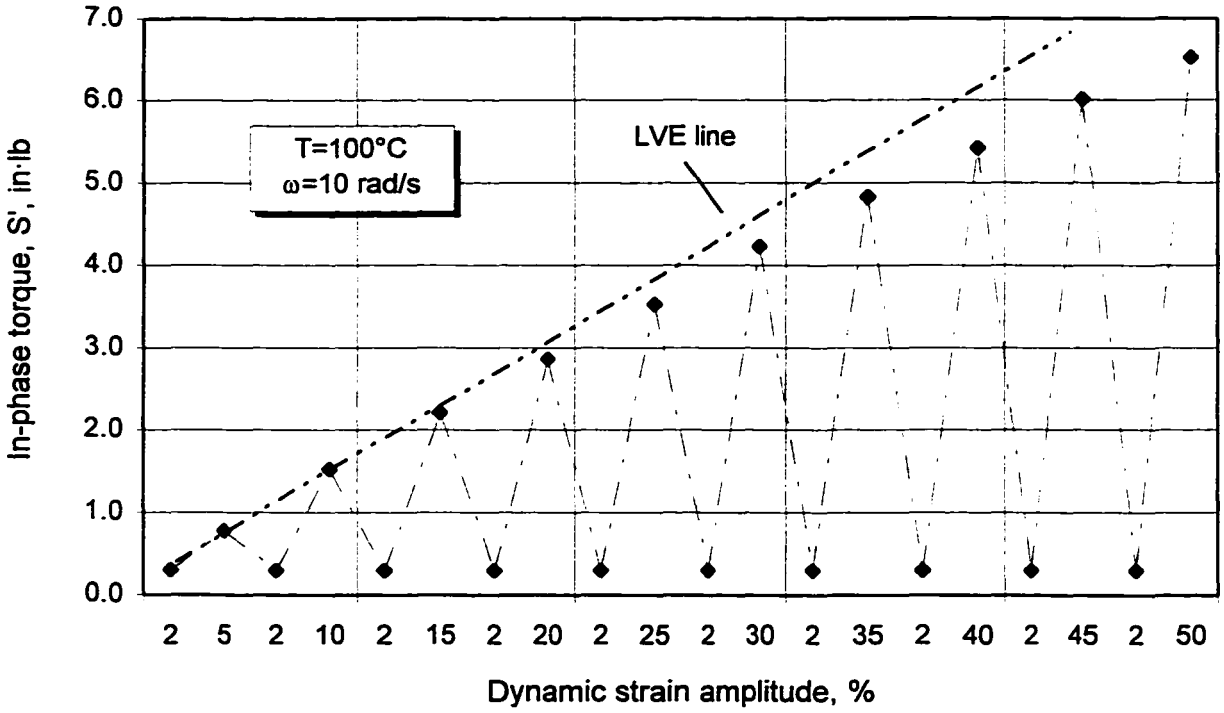
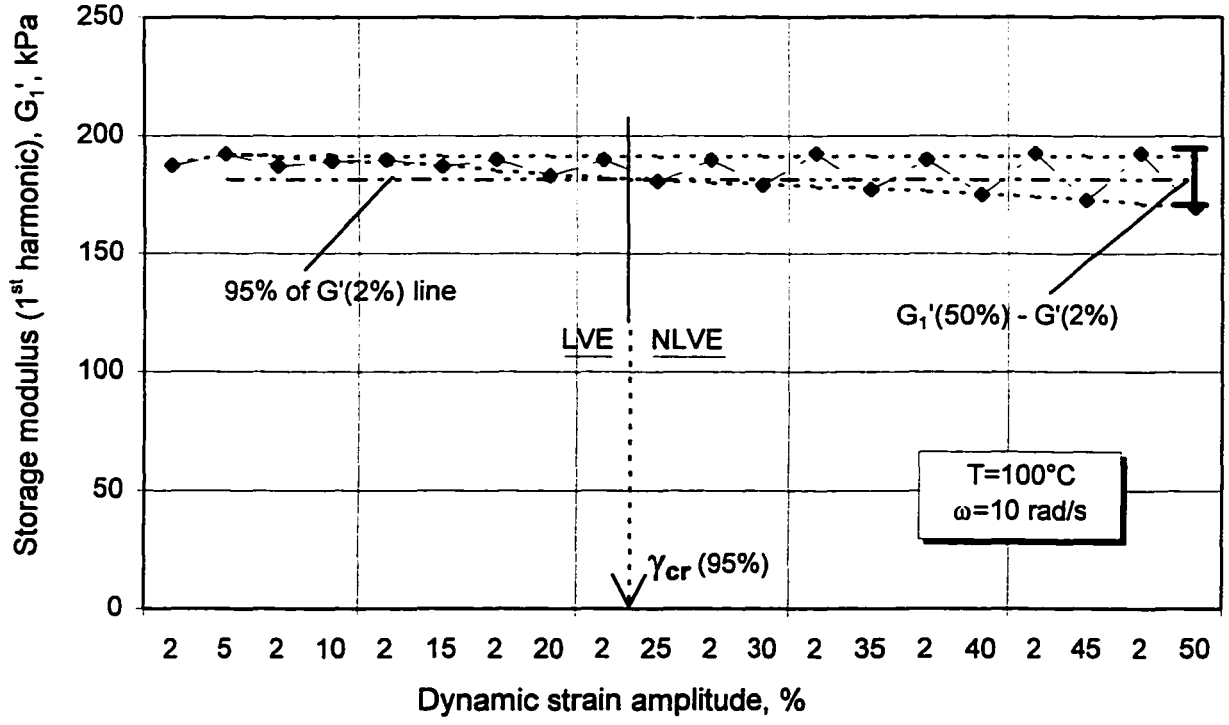


Figure 7-2. Strain sweep {SSWP2}, sample G19.



Rheological parameters defined for the {SSWP2} test are listed in Table 7-1.

Partial {SSWP2} test results are included in Table A71, in Appendix V. The values of the parameter **G'(2%)-G_1'(50%)** are supplemented by the 1st harmonic of the dynamic moduli, complex modulus, $\tan_1 \delta$, as well as the 'in-phase' and 'out-of-phase' torque data, all measured at 50% strain amplitude.

Table 7-1. Definitions of the non-linear viscoelastic parameters; {SSWP2} test.

abbreviation	definition
S'(50%)	- 'in-phase' component of the torque, measured during isothermal oscillations at the frequency of 10 rad/s and 50% dynamic strain,
S"(50%)	- 'out-of-phase' component of the torque, measured during isothermal oscillations at the frequency of 10 rad/s and 50% dynamic strain,
G_1'(50%)	- first harmonic of the storage modulus at 50% dynamic strain and 10 rad/s oscillation frequency,
G_1"(50%)	- first harmonic of the loss modulus at 50% dynamic strain and 10 rad/s oscillation frequency,
G_1*(50%)	- first harmonic of the complex modulus at 50% dynamic strain and 10 rad/s oscillation frequency,
G'(2%)-G_1'(50%)	- difference between storage moduli at 50% and 2% dynamic strain amplitude (at 10 rad/s)
$\tan_1 \delta$(50%)	= G_1"(50%) / G_1'(50%)

Prediction traces for correlations between non-linear viscoelastic and structural parameters are included in Figures A71a through A71h, Appendix V. Table 7-2 contains a summary of correlations in the form of correlation coefficients (t-ratio).

The onset of a non-linear response in the oscillatory shear, characterized by the **G'(2%)-G_1'(50%)** parameter, depends on the branch length, overall molecular weight of the graft and branching number. However, the effect is not large and even for the strongest correlation such as N_g^p // **G'(2%)-G_1'(50%)**, only a rather weak trend is discernible (Figure 7-3).

Increase the number of branches will decrease the difference **G'(2%)-G_1'(50%)**. This corresponds to an increase in γ_{cr}^{LVE}, which in turn can be interpreted as the postponement of the onset of the non-linear viscoelastic response of a polymer.

Table 7-2. Correlation coefficients (t-Ratio) between structural and rheological {SSWP2} parameters.

RPA 2000 {SSWP2}	M_p^b	N_g^p	$w^{b,g}$	w^b	$w^{b,h}$	M_z^G	PDI	vinyl
G_1'(2%)-G_1'(50%)	+2.67	-3.63	+	0	0	+2.54	-	0
G_1'(50%)	+3.50	-8.71	-	0	+	0	0	0
G_1"(50%)	+6.04	-6.22	0	0	+3.75	+	0	-
G_1*(50%)	+3.99	-8.85	-	0	+	0	0	0
$tan_1 \delta$ (50%)	+4.55	-3.84	0	+	+3.19	+	0	-

Explanation:
Number indicates t-Ratio for a statistically significant correlation, that is when |t-Ratio| is above 2.50 (corresponding to 95% conf. interval), '0' - weak or no correlation (|t-Ratio| values < 1.00)
'-' - negative, statistically not significant correlation (t-Ratio values negative & below 2.50)
'+' - positive, statistically not significant correlation (t-Ratio values positive & below 2.50)

The above results confirm the conclusions based on more comprehensive experiments reported in Chapter 5.

Entirely different behavior in strain sweep behaviour was observed for sample M (CIIR/BR blend). While the drop-off of the $G_1'(\gamma)$ function is comparable to that of some of the grafts, steadily declining modulus of the small amplitude portion can be attributed to thixotropic effects associated with a fragile/unstable morphology of the CIIR/BR blend (Figure 7-4).

Dynamic moduli and tan$_1\delta$ at 50% strain

The relation between specific branching parameters and dynamic moduli at intermediate (50%) strain amplitude is similar to that established for the low strain data but correlations are much stronger (cf. Figure 6-33 in Chapter 6).

The most general conclusion which can be drawn from the correlation table (Table 7-2) is that the dynamic moduli tend to increase rapidly with increasing branch length, while they decrease with increasing branching number, at a rate that depends on the type of a viscoelastic parameter. The independence of the dynamic moduli at intermediate strain amplitudes (up to 50%) of chemical composition of the graft is shown in Figure A71d, and from M_z^G in Figure A71e, both in Appendix V (cf. also Table 7-2).

There is no evidence for influence of the interferences (PDI, vinyl%) on large-strain dynamic moduli - Figures A71g and A71h in Appendix V. However, some dependence of the loss modulus, (and to lesser extent G_1^* and tan$_1$ δ) upon the content of ungrafted BR, can be seen.

The relationship between two specific branching parameters and the complex modulus, parameter $\mathbf{G_1^*(50\%)}$, is shown in explicit form (x-y) in Figure 7-5 and Figure 7-6. The only samples which do not fit the trend line in Figure 7-5 are those with a less developed branching structure, e.g. with $w^{b,g} < 10\%$ which are marked with open circles. These conclusions are consistent with results of the data analysis from a small amplitude oscillatory shear, discussed in section 6.3.

Figure 7-3. Effect of branching on the onset of non-linearity in dynamic test - {SSWP2}.

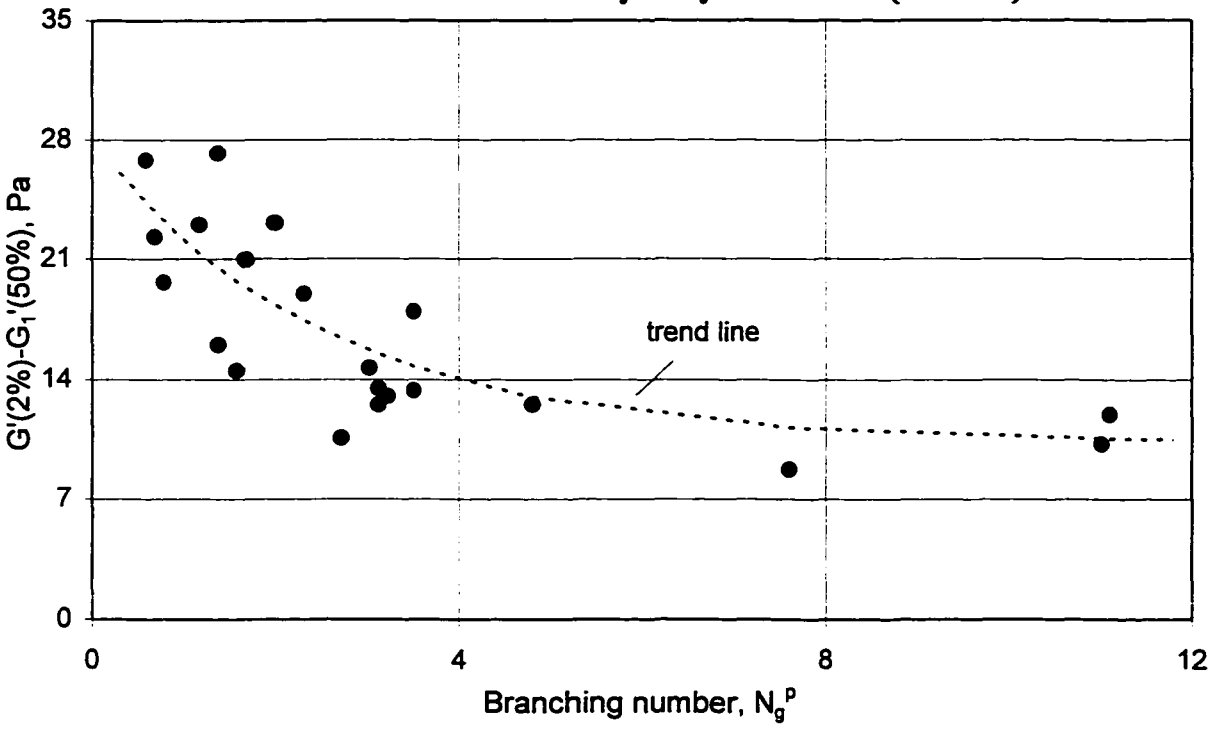


Figure 7-4. Strain sweep {SSWP2}, sample M, T=100°C.

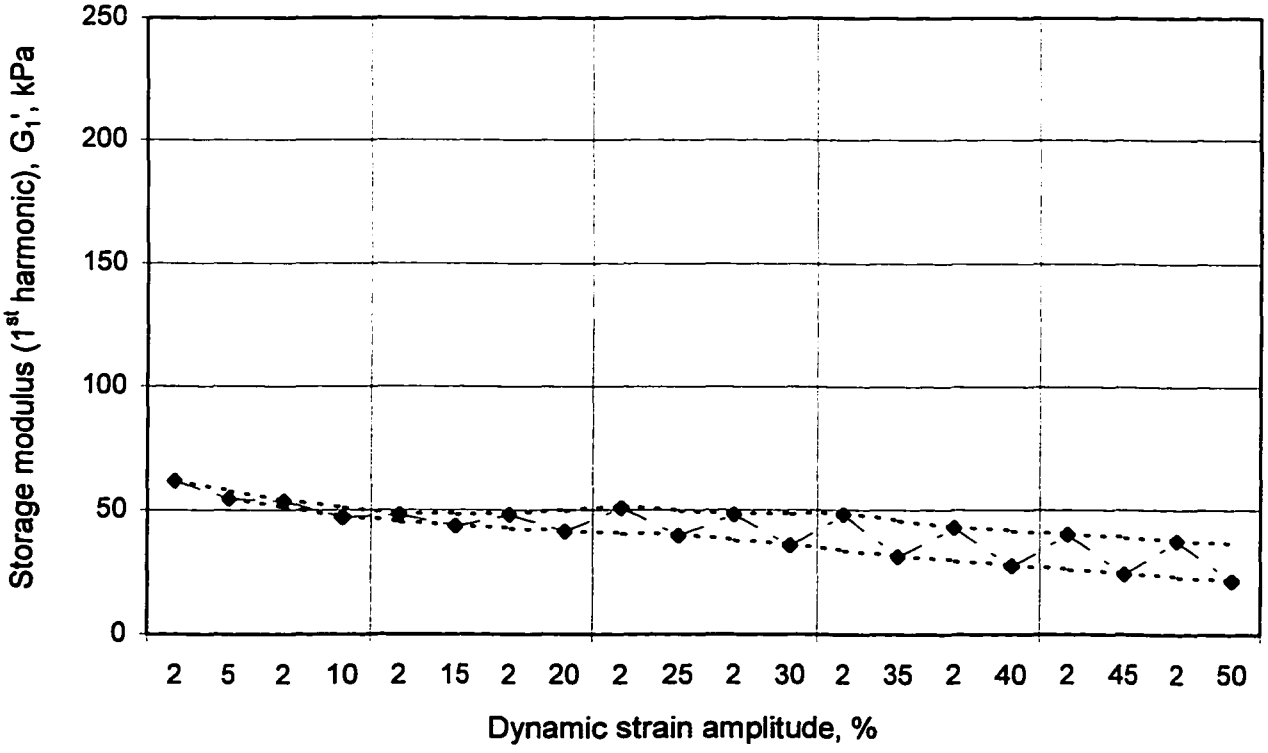


Figure 7-5. Effect of branch length on G_1^* (50%) modulus.

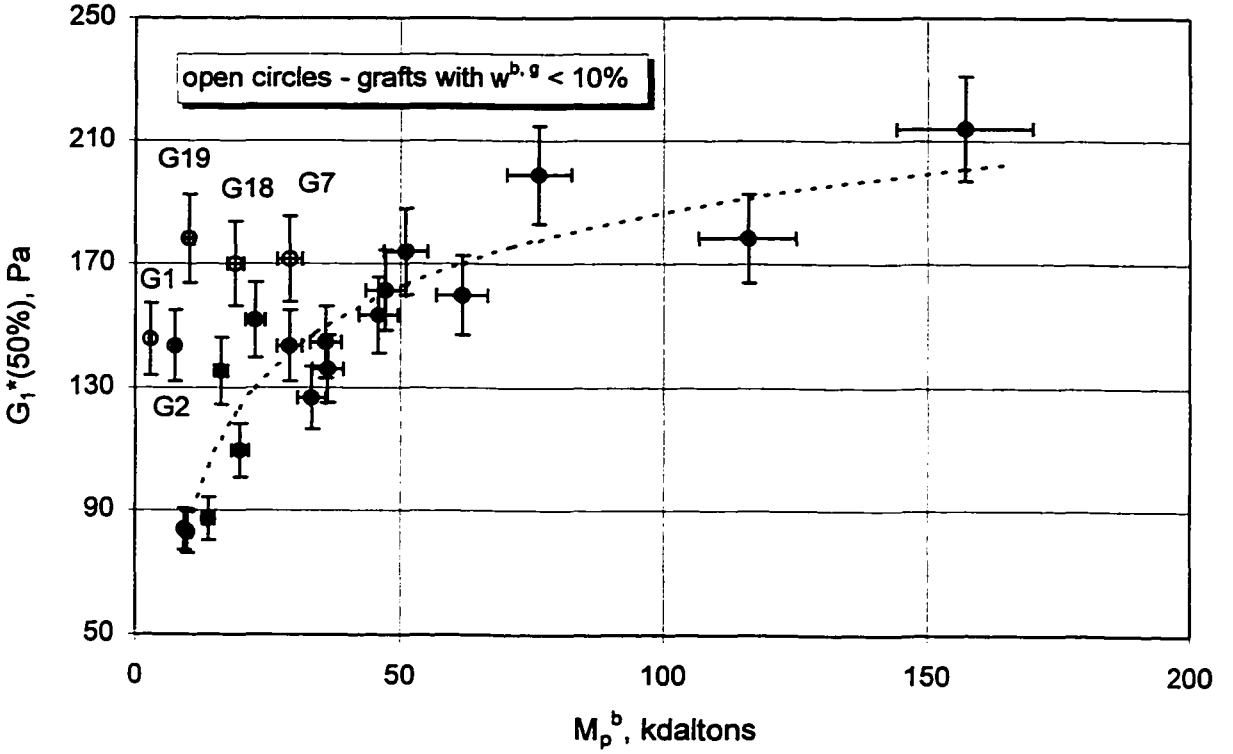
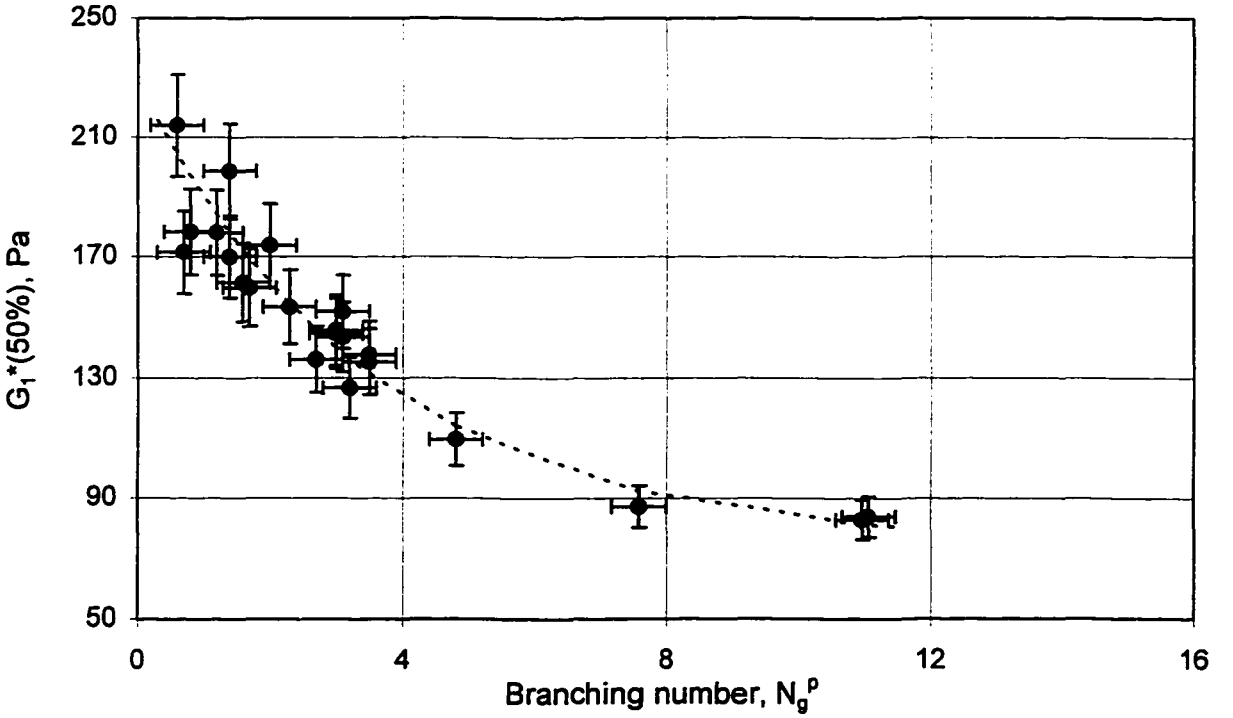


Figure 7-6. Effect of branching number on G_1^* (50%) modulus.



7.2 Frequency and strain-amplitude dependence of the viscoelastic functions from a large-amplitude oscillatory shear (LAOS) experiment

Another series of dynamic experiments was designed and carried out on the RPA 2000 in order to investigate certain aspects of the non-linear viscoelastic behaviour of the LCB graft copolymers. Test conditions and instrumental details of the experiments were described in chapter 5, section 5.4 and summarized in Appendix IV, Table C, under the test code {FSWP3}.

Some of the results of these tests are reported and discussed in the following four subsections.

7.2.1 Non-linear viscoelastic parameters

Preliminary analysis of results from a series of isothermal, large-strain amplitude (up to 200%) oscillatory shear experiments, carried out at several frequencies, indicated that the main findings can be illustrated by presentation of a relation between LCB parameters and certain representative viscoelastic parameters. These parameters are defined in Table 7-3. Their numerical values are listed in Table A72, Appendix V.

Screening for correlations

To search effectively for possible relationships that may exist between branching structure and rheological properties, the same statistical technique as described in Appendix VI, was used throughout this chapter. Complete prediction profiles are included in Figures A72 a, b, c and d, Appendix V. The t-Ratios, which can be considered as a measure of the correlation strength, are listed in Table 7-4. The t-ratio numbers shown in bold face mark the most significant correlations, explored further in a direct (x-y) comparison.

Table 7-3. Viscoelastic parameters (G_1', G_1'' and $\tan_1 \delta$) derived from a large strain frequency sweep - {FSWP3} test.

abbreviation	definition
G_1' (200%/0.5rad/s)	- 1st harmonic of the storage modulus at 200% dynamic strain and 0.5 rad/s oscillation frequency
G_1' (200%/10rad/s)	- 1st harmonic of the storage modulus at 200% dynamic strain and 10 rad/s oscillation frequency
G_1'' (200%/0.5rad/s)	- 1st harmonic of the loss modulus at 200% dynamic strain and 0.5 rad/s oscillation frequency
G_1'' (200%/10rad/s)	- 1st harmonic of the loss modulus at 200% dynamic strain and 10 rad/s oscillation frequency
$\tan_1 \delta$ (200%/0.5rad/s)	= G_1'' (200% / 0.5 rad/s) / G_1' (200% / 0.5 rad/s)
$\tan_1 \delta$ (200%/10rad/s)	= G_1'' (200% / 10 rad/s) / G_1' (200% / 10 rad/s)
$\tan_1 \delta$ ratio	= tan δ (200% & 0.5 rad/s) / tan δ (5% & 200 rad/s)

The main observations resulting from comparison of data in (Table A72) and certain hints suggested by screening analysis (Table 7-4), can be summarized as follows:

1. Dynamic moduli (1st harmonic at 200% strain) appear to be strongly affected by specific branching parameters (M_p^b, N_g^p) at higher oscillation frequencies (10 rad/s or more). In the case of loss modulus, **G_1'' (200%/10rad/s)** some contributions to modulus from the residual BR are possible (as indicated by t-Ratio = +3.19 for $w^{b,h}$ // G_1''(200%/10 rad/s) correlation, Table 7-4.

2. Loss tangent ($\tan_1 \delta$) seems to be related to the overall branching content, $w^{b,g}$ rather than to the number or length of the branches. However, the significance of these correlations is marginal (t-Ratio = -2.61 for **$\tan_1 \delta$(200%/0.5 rad/s)**). The ratio of $\tan_1 \delta$ obtained at large

strain/low frequency to $\tan_1 \delta$ at small strain/high frequency, defined as the **$\tan_1 \delta$ ratio**, was identified as a particularly potent indicator of the branching content, $w^{b,g}$. A relatively high degree of correlation between w^b and **$\tan_1 \delta$ ratio** and M_z^G and **$\tan_1 \delta$ ratio** is very likely the result of a strong interrelation between these structural parameters and $w^{b,g}$ (cf. Appendix VI).

Table 7-4. Correlation coefficients (t-Ratio) between structural and rheological {FSWP3} parameters.

RPA {FSWP3}	M_p^b	N_g^p	$w^{b,g}$	w^b	$w^{b,h}$	M_z^G	PDI	vinyl
G_1' (200%/0.5rad/s)	+	-	0	0	-	+	<	<
G_1' (200%/10rad/s)	+3.81	**-6.40**	0	0	+	+	<	<
G_1'' (200%/0.5rad/s)	+2.72	-5.75	-	-	+	0	<	<
G_1'' (200%/10rad/s)	**+5.09**	**-6.31**	0	0	+3.19	+	<	<
$\tan_1 \delta$ (200%/0.5rad/s)	+	-	**-2.61**	-	+	-	<	<
$\tan_1 \delta$ (200%/10rad/s)	+	-	-	0	+	0	<	<
$\tan_1 \delta$ ratio	0	-	**-6.51**	-4.43	0	-3.33	<	<

Explanation:
Numbers indicate the t-Ratio for a statistically significant correlation, that is when |t-Ratio| value is above 2.50 (corresponding to 95% conf. interval).
'-' - negative, statistically not significant correlation (|t-Ratio| values below 2.50)
'+' - positive, statistically not significant correlation (|t-Ratio| values below 2.50)
'0' - weak or no correlation (|t-Ratio| < 1)
'<' - no statistically significant correlations detected (for "PDI" and "vinyl" columns only)

3. A statistically significant correlation observed for the **G"(200%/10rad/s)** // $w^{b,h}$ pair is interpreted as a result of interrelation between $w^{b,h}$ and M_p^b. Similarly, correlations between $\tan_1 \delta$ ratio - w^b and $\tan_1 \delta$ ratio - M_z^G, are the result of interrelations between $w^{b,g}$ and w^b, and $w^{b,g}$ and M_z^G, respectively (see Appendix VI).

Relations between LAOS viscoelastic parameters and LCB structure

Direct comparison of results collected in Table A72, Appendix V, reveals large differences for all defined viscoelastic parameters, between the backbone precursor polymer (sample C), blend M and a family of long-chain branched grafts (samples G1 to G22).

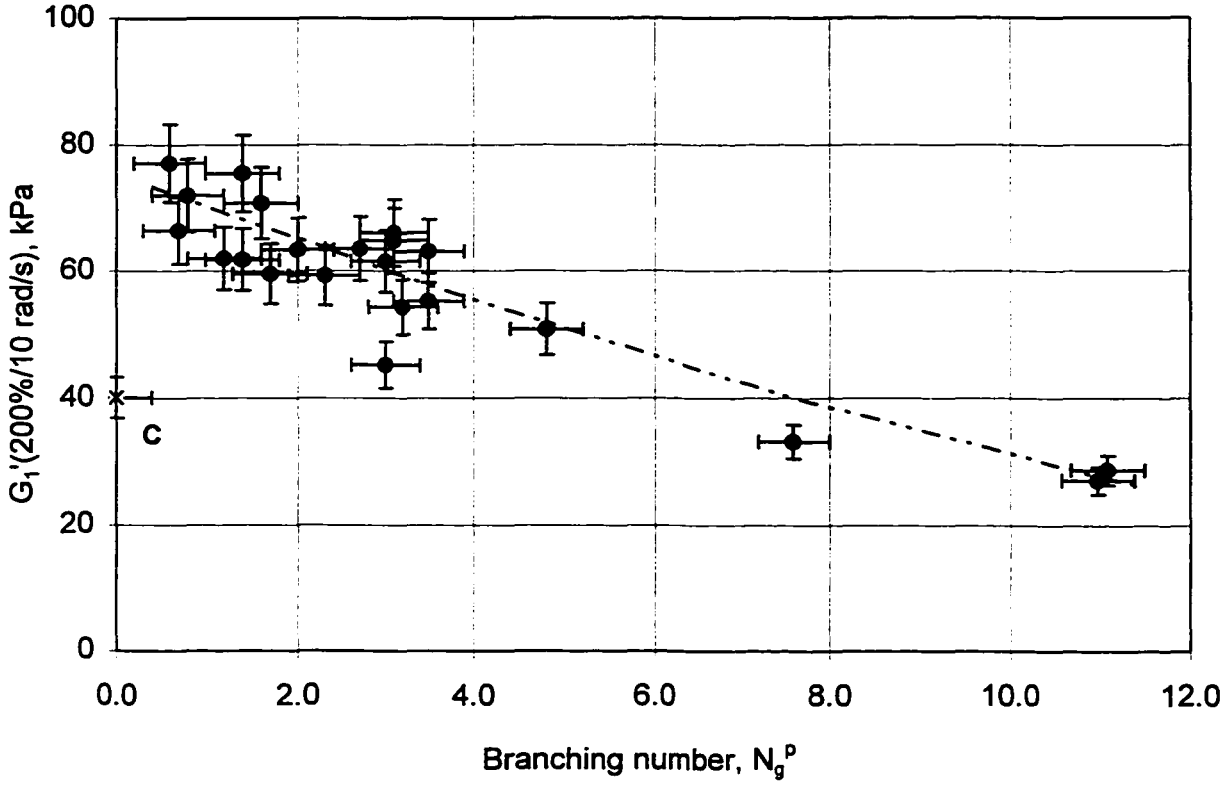
The first harmonic of the storage modulus, measured at 200% strain and frequency of 0.5 rad/s, $\mathbf{G_1'(200\%/0.5rad/s)}$ is consistently higher for all grafts (19.9 to 47.9 kPa range) when compared with sample C (14.8 kPa) but dramatically lower for sample M (0.67 kPa). The higher oscillation frequency (10 rad/s at the same strain) increases modulus but the effect is much less pronounced for long-chain branched copolymers than for samples C or M. Still within various grafts, dependence on frequency is lower for grafts with higher branching numbers. In fact, at higher oscillation frequencies, for grafts with N_g^p value of 7.6 or higher, their modulus is lower than for linear backbone precursor polymer (sample C) - cf. also Figure 7-7. This is in agreement with published data on plateau modulus values of branched polymers with reference to the comparable (MW) linear systems [16, 57].

The loss angle δ (and its tangent) is lower for the long-chain branched polymers, regardless of the details of their LCB architecture or oscillation frequency (cf. also Figure 7-10). However, for $\tan_1 \delta$, differences are more pronounced at lower frequencies. Blending backbone precursor polymer with BR of M_p = ~30,000, a median value for branch polymer, results in a much softer and more "viscous" material than sample C.

Effect of branching number on in-phase modulus, $G_1'(200\%/10rad/s)$

Increasing the number of branches attached to the backbone of the graft tends to lower the storage modulus $\mathbf{G_1'(200\%/10rad/s)}$, even below that for the backbone precursor polymer. This effect is shown explicitly in Figure 7-7. Considerable scatter is due to the unaccounted effect of the branch length.

Figure 7-7. Relationship between branching number and in- phase modulus, G_1' (200%/10rad/s).



Effect of branch length on out-of-phase modulus, G_1''(200%/10rad/s)

The effect of branch length on the out-of-phase modulus **G_1''(200%/10rad/s)** is shown in Figure 7-8. This asymptotic relation indicates that the increase of the branch length will steadily increase the out-of-phase modulus, regardless of the exact value of the branching number, as long as branching structure is sufficiently developed. Graft samples with branching content $w^{b,g}$ below approximately 10% are marked with open circles in Figure 7-8 and do not fit the trend line.

Effect of branching number on out-of-phase modulus, G"(200%/10rad/s)

The plot of **G"(200%/10rad/s)** versus branching number N_g^p in Figure 7-9, indicates a monotonic decrease of modulus with increasing number of branches, but the curve shape is different from that for the in-phase modulus, suggesting a different functional relationship for

Figure 7-8. Relationship between branch length and out-of-phase modulus, G_1"(200%/10rad/s).

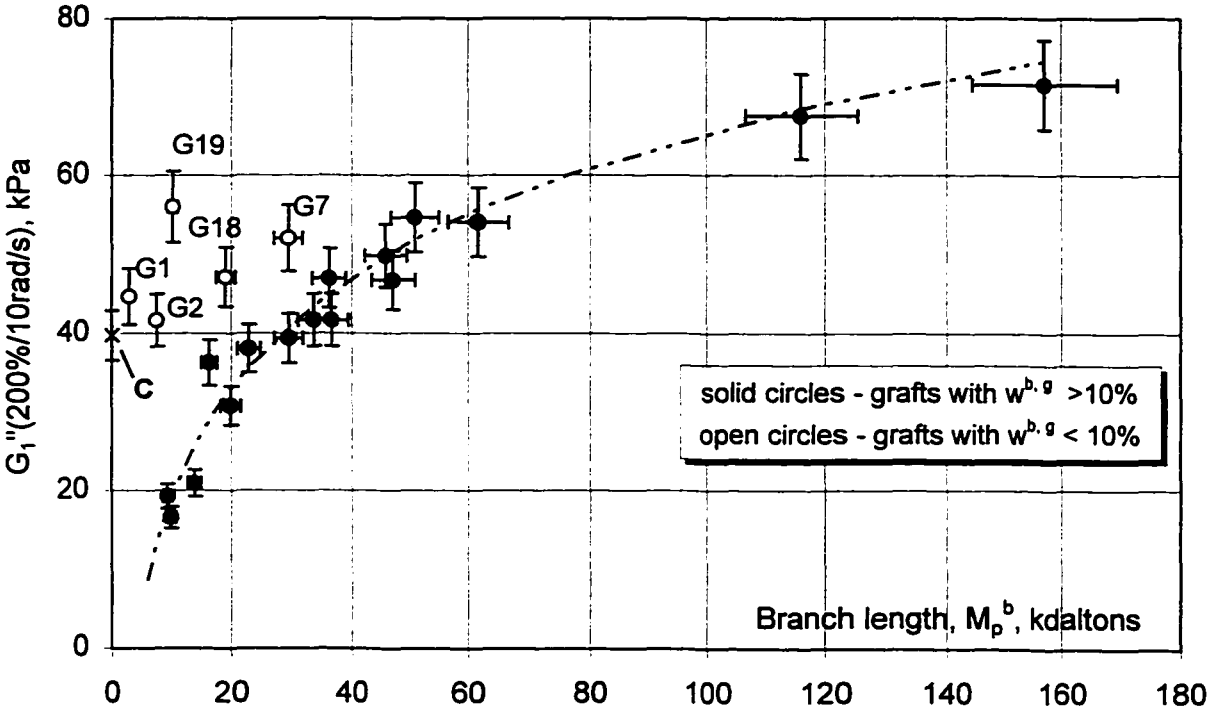
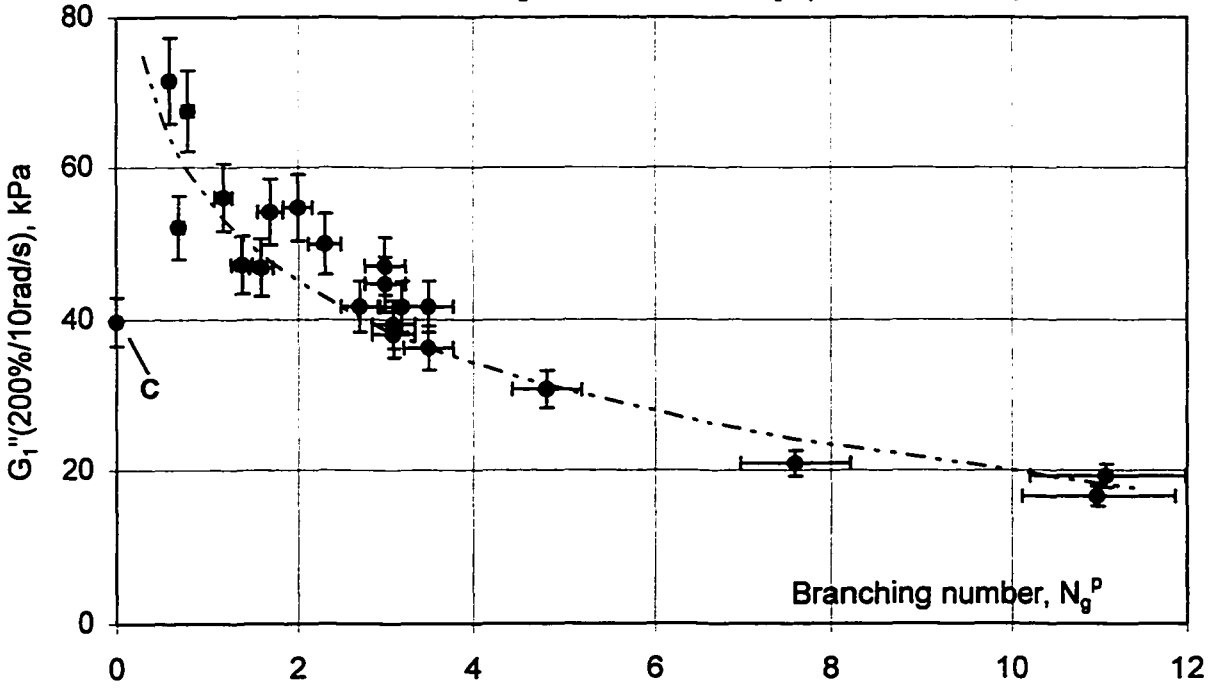


Figure 7-9. Relationship between branching number and out-of-phase modulus, G_1"(200%/10rad/s).



N_g^P // **G"(200%/10rad/s)** than for N_g^P // **G'(200%/10rad/s)** - Figures 7-7 and 7-9.

Effect of branching content on loss tangent, ***tan$_1$ δ(200%/0.5%)***

Screening analysis suggests that **tan$_1$ δ(200%/0.5%)** correlates particularly well with overall branching content but it might also be sensitive to the presence of linear molecules of the ungrafted branches in a graft mixture. In Figure 7-10, **tan$_1$ δ(200%/0.5%)** is plotted against $w^{b,g}$. For "pure" grafts ($w^{b,h}$ < 0.3%, indicated by solid circles), **tan$_1$ δ(200%/0.5%)** is exponentially decreasing with increasing branching content up to about 20% and then virtually does not change. Addition of short molecules predictably [50, 99] increases $\tan_1 \delta$ roughly in proportion to the $w^{b,h}$ content of the graft, as shown in Figure 7-10. Grafts with $w^{b,h}$ > 0.3% are identified by open circles. The numbers attached to some symbols correspond to $w^{b,h}$.

A similar plot (Figure 7-11) for **tan$_1$ δ ratio** may offer some potential for the characterization of the long-chain branching content, over a considerable range of branching content (up to 40% or more). Unfortunately, this technique might not be able to identify and specify the content of unattached molecules without the help of another rheological parameter or an additional method of analytical characterization (i.e. SEC).

7.2.2 Cole-Cole plot analysis of the dynamic moduli

Cole-Cole plot formalism has been introduced in section 6.1.4 of the Chapter 6 and used there as a tool to investigate the frequency-dependence of the linear dynamic moduli, G'(ω) and G"(ω). One of the most interesting applications of the Cole-Cole plots is the identification of various topologies of the long-chain branching in polymers including

Figure 7-10. Relationship between branching content and $\tan_1 \delta$(200%/0.5rad/s).

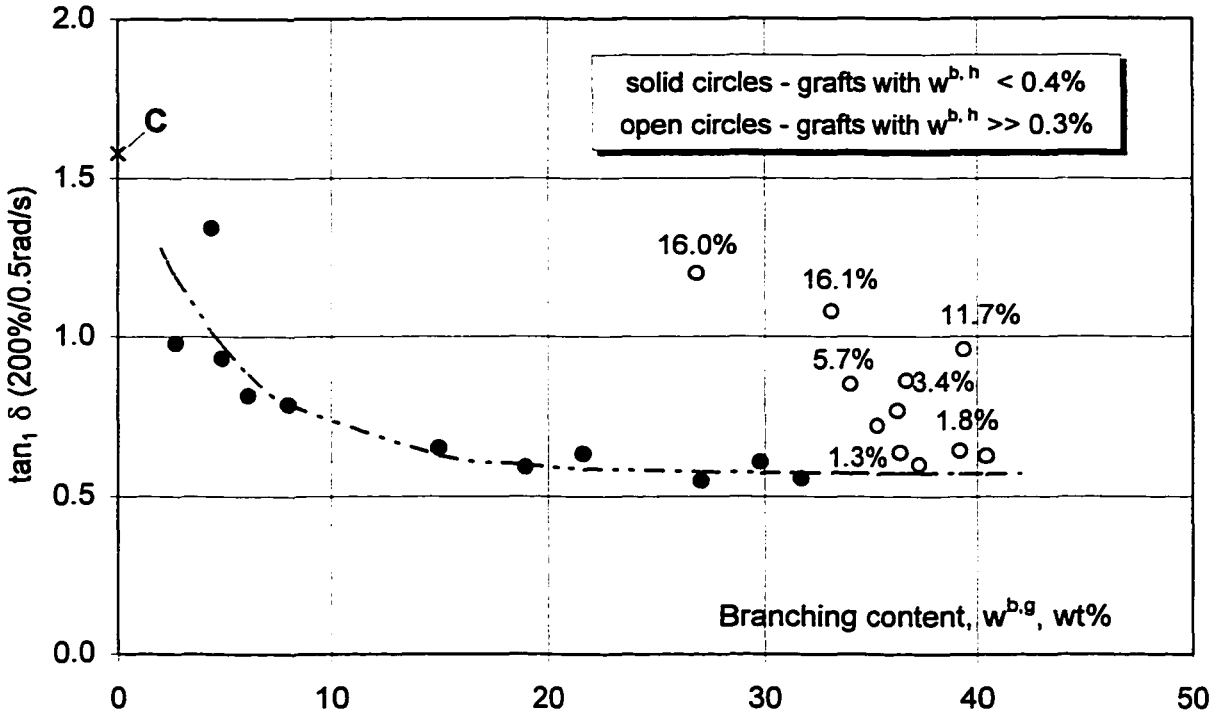
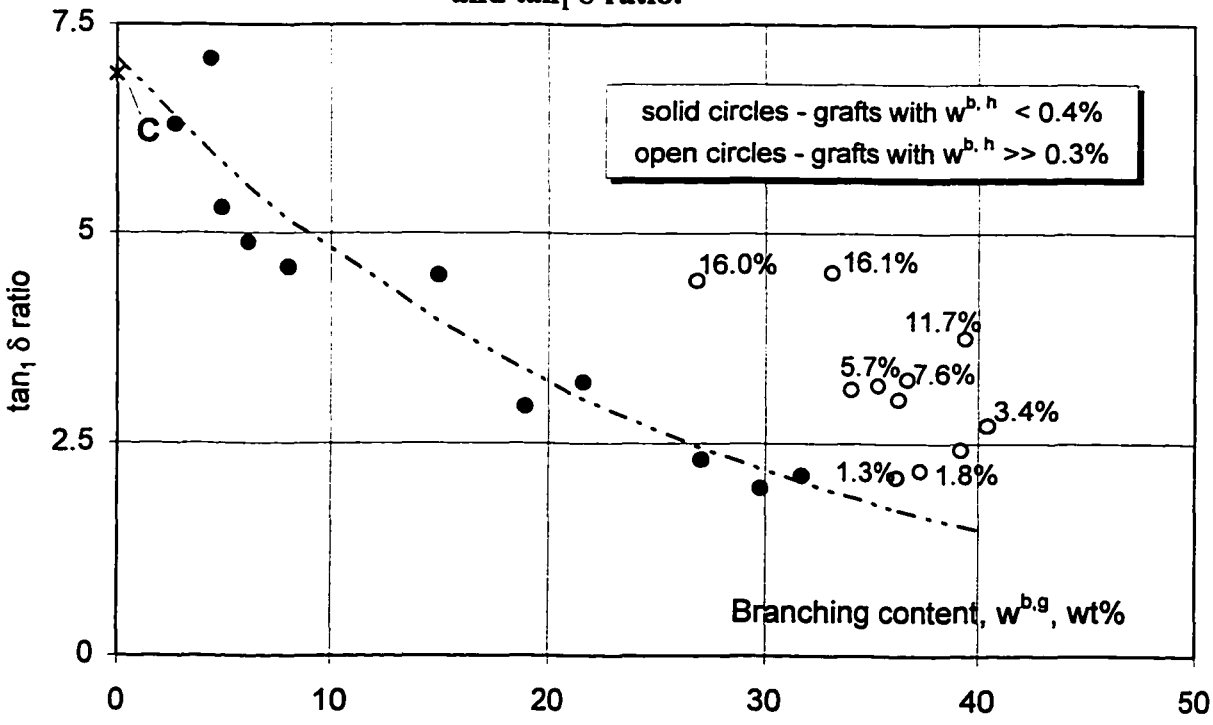


Figure 7-11. Relationship between branching content and $\tan_1 \delta$ ratio.



commercial elastomers [359]. An example of the interpretation of the normalized Cole-Cole contours, obtained from non-linear dynamic mechanical data, in terms of the LCB structure will be discussed in detail in section 7.5 of this chapter.

This section presents an attempt to relate certain quantifiable features (i.e. parameters) of both modified and normalized Cole-Cole contours with the LCB structure of graft copolymers. This analysis follows the previously used pattern starting with screening for possible correlations to identify the most significant and then exploring selected structure-property relations directly between chosen structural and rheological parameters. All data presented here are derivatives of the {FSWP3} test results and relevant references to test conditions and other experimental details were given at the beginning of section 7.2.

Viscoelastic parameters are defined in Table 7-5 and listed in Table A73, App. V. The length of the Cole-Cole contour can be interpreted as a measure of the frequency-dependence of isothermal dynamic moduli, within a specified frequency range (0.5 - 10 rad/s) and at a given strain amplitude (200%) in the case discussed below.

Table 7-5. Definition of viscoelastic parameters derived from {FSWP3} test data.

abbreviation	definition
mC-C p.c.l.	- contour length of the modified Cole-Cole plot (log G_1'- log G_1''), γ=200%, ω=0.5-10 rad/s
nC-C p.c.l.	- contour length of the normalized Cole-Cole plot ($G_1'(\omega)/G_1'(\omega_{ref})$ - $(G_1''(\omega)/G_1''(\omega_{ref})$, γ=200%, ω=0.5-10 rad/s
nC-C quad.	- the location of the nC-C contour, relative to the diagonal of the plot. '+1' = above diagonal in the first quadrant, '-1' = below diagonal in the first quadrant

Screening for correlations

Screening analysis between the parameters defined above and the standard eight structural parameters gave prediction profiles reproduced in Figures A73a, A73b, A73c and A73d, Appendix V. A summary of correlations in the form of the t-Ratio table is given in Table 7-6.

Table 7-6. Correlation coefficients (t-Ratio) between structural and viscoelastic parameters derived from LAOS {FSWP3} test.

RPA {FSWP3}	M_p^b	N_g^p	$w^{b,g}$	w^b	$w^{b,h}$	M_z^G	PDI	vinyl
mC-C p.c.l.	+7.71	-5.49	0	+	+4.48	+	0	-
nC-C p.c.l.	+4.37	-3.04	0	+	+3.69	+	0	-
nC-C quad.	0	0	-2.57	-	0	-	0	0

Explanation:
The number indicates the t-Ratio for a statistically significant correlation, e.g. |t-Ratio| value is above 2.50 (corresponding to 95% confidence interval).
'-' - negative, statistically not significant correlation (|t-Ratio| values below 2.50)
'+' - positive, statistically not significant correlation (|t-Ratio| values below 2.50)
'0' - weak or no correlation

The length of the mC-C contour is proportional to the modulus change during the isothermal frequency sweep. It represents a certain aspect of the frequency dependence of the dynamic moduli.

The length of the Cole-Cole contour depends on the length of the branch (most significantly), the number of branches and the content of ungrafted, linear BR ($w^{b,h}$). The dependence is consistent for both modified and normalized C-C plots, but correlations are stronger for the modified Cole-Cole plot. Weaker but singular correlations were detected between the position of the normalized Cole-Cole contour on a nC-C plot (**nCC quad**) and branching content, $w^{b,g}$.

Contour length of the mC-C plot

The relationship between rheological properties and those details of graft LCB structure suggested by the prediction profiles can be verified by plotting a structural versus rheological parameter.

The plot of the contour length of the modified Cole-Cole plot (**mC-C p.c.l.**) versus branch length, M_p^b, is shown in Figure 7-12. For all grafts with well developed branching structure ($w^{b,g} > 10\%$), relation between **mC-C p.c.l.** and branch length follow an exponential relation reasonably closely. The other two parameters influencing contour length, namely N_g^p and $w^{b,h}$ contribute to data scatter in this plot. For a multi-dimensional correlation, such as **mC-C p.c.l.** - M_p^b, N_g^p, $w^{b,h}$, the ability to plot a single curve without qualification with regard to other parameters, indicates a strong domination of a given parameter (M_p^b in this example) over all others, the given physical property in question. This is consistent with a higher correlation factor (t-Ratio) for M_p^b (see Table 7-6).

A relationship between **mC-C p.c.l.** and branching number, N_g^p can be directly shown only when other relevant factors are kept approximately constant. In Figure 7-13, the contour length of the mC-C plot corresponding to samples with $w^{b,h}$ over 0.3% and M_p^b above 33,000, is shown to decrease exponentially with the branching number. A similar plot (Figure 7-14) for samples with a negligible value of $w^{b,h}$ (0.4%) appears to be linear and reveals a slight downward trend. Direct comparison of **mC-C p.c.l.** for samples G19 and G20 of very similar M_p^b and $w^{b,h}$ parameters but N_g^p of 1.2 and 11.0, respectively, shows 4.4 - fold decrease in the parameter value due to the increased number of branches (Table A73, Appendix V).

Conclusions based on the last two graphs indicate that both branching number and $w^{b,h}$ (in addition to M_p^b) influence the length of the mC-C contour.

Figure 7-12. Relation between branch length and contour length of the modified Cole-Cole plot.

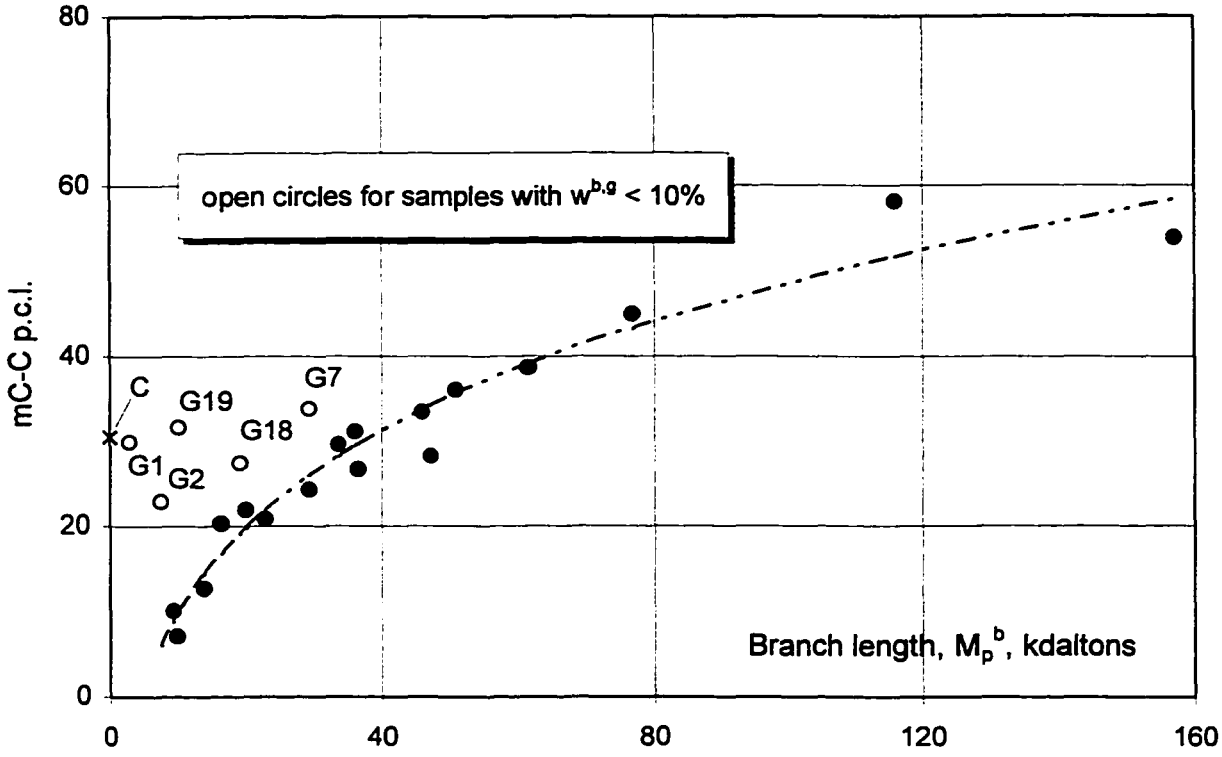


Figure 7-13. Relation between branching number and contour length of the mC-C plot - chart I for samples with $w^{b,h}$ > 0.3%.

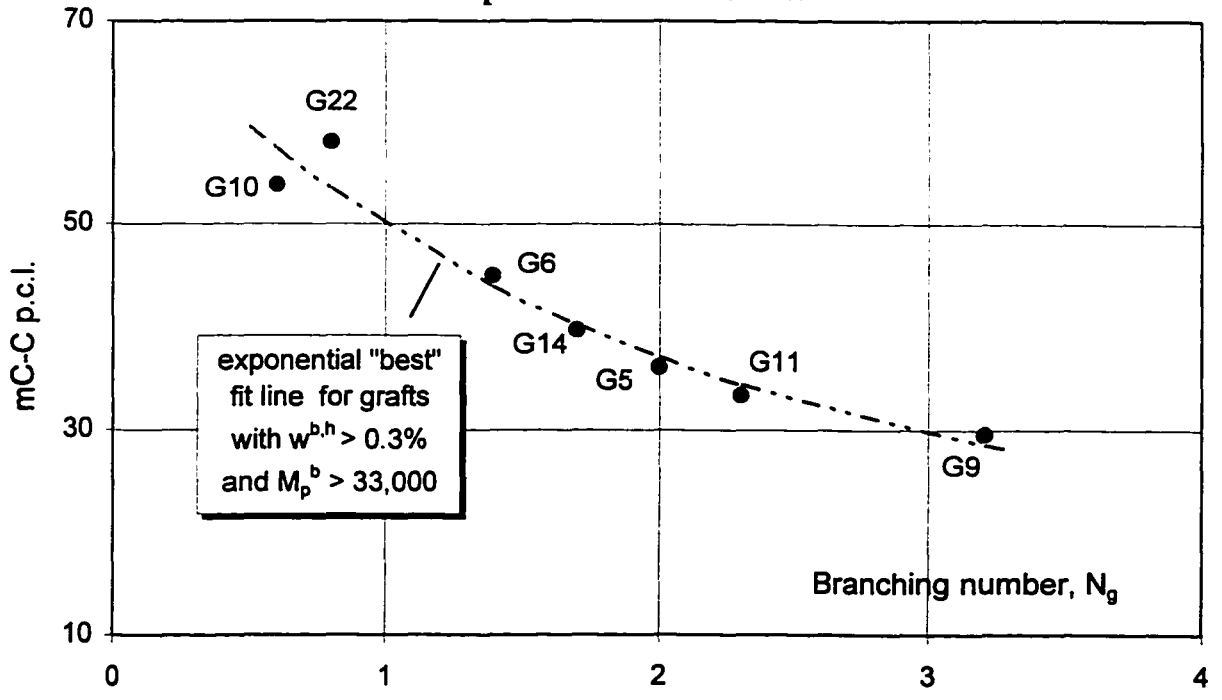
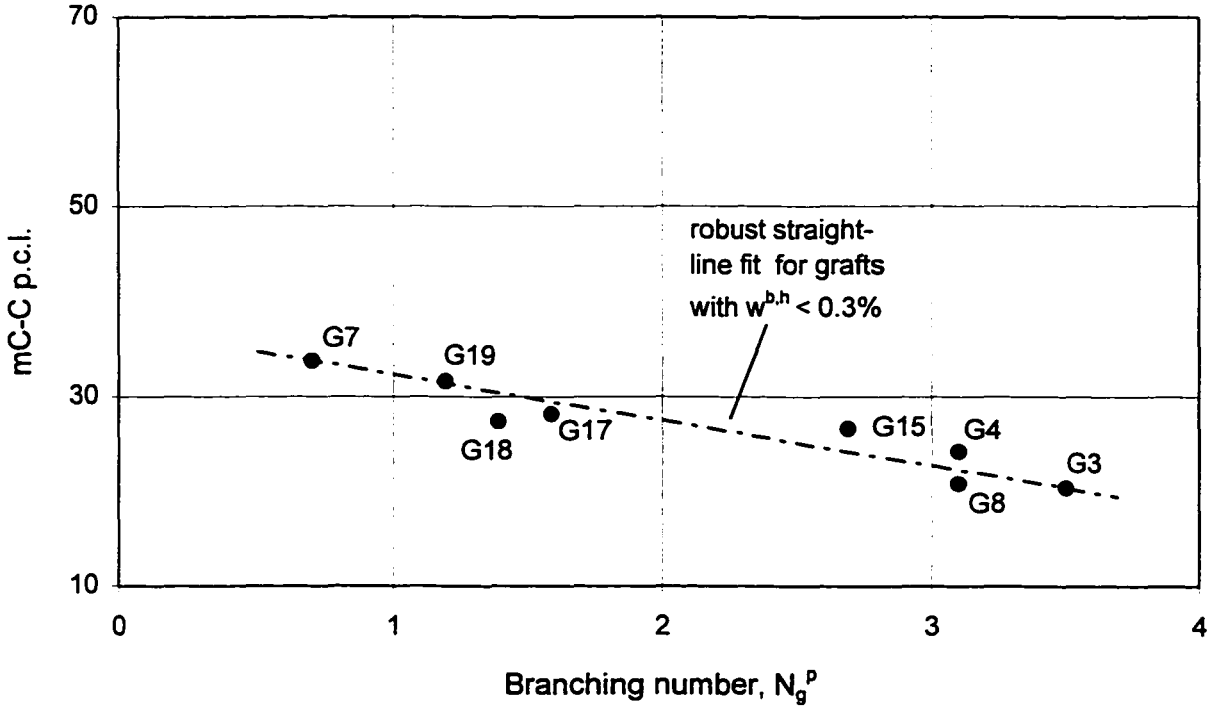


Figure 7-14. Relation between branching number and contour length of the modified Cole-Cole plot - chart II for samples with $w^{b,h} < 0.4\%$.



7.2.3 Tangent of the loss angle, $\tan_1 \delta(\gamma, \omega)$

The tangent of the loss angle, tan δ, is an important viscoelastic function describing the relative importance of in-phase and out-of-phase components of the complex modulus.

Tan δ, in addition to being a temperature-sensitive property, can also vary with frequency and strain-amplitude. The frequency and strain dependence of the first harmonic of tan δ, $\tan_1 \delta(\gamma, \omega)$, with particular reference to its behaviour at large strains (NLVE), is the subject of this section.

Comparison between linear, blend and graft polymers

$Tan_l\ \delta(\gamma, \omega)$ results obtained from a series of four isothermal frequency sweeps, each at progressively higher dynamic strain amplitude, γ=5, 50, 100 and 200%, are plotted in Figure 7-15 for samples C, M and G4.

1. Significant differences are observed in $tan_l\ \delta(\gamma, \omega)$ for sample C, blend M and graft G4. Decreasing values of loss angle tangent with increasing frequency, as observed for sample C, are typical for linear polymers under the conditions (T, ω and γ ranges) of the LVE experiment. This experiment confirms that the tan $\delta(\omega)$ relation established for small strain amplitude extends toward much higher strain amplitudes, at least for sample C and grafts.

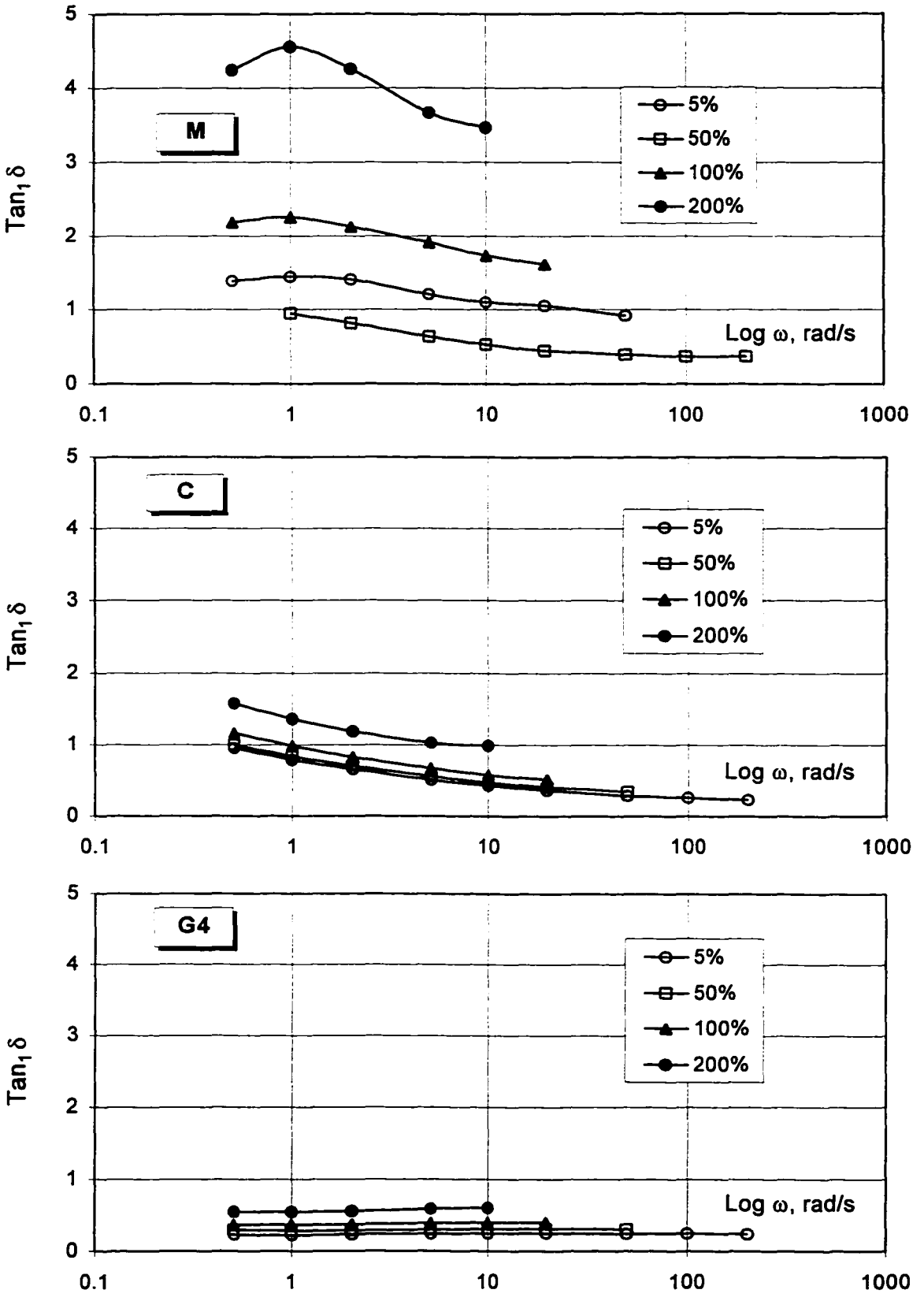
2. For grafts with well-developed branching, $w^{b,g}$ >10%, sample G4 ($w^{b,g}$ =27.1%) being a typical example, the $tan_l\ \delta(\omega)$ response is almost flat with respect to frequency, at all strains, and assumes very low values. Such behaviour qualifies the CIIR-g-BR graft copolymers to be considered as soft, visco-elastic solids, at least up to a temperature of 100°C. Their rheological behaviour has obvious implications for the selection of suitable experimental methods for characterization, as well as on a commercial processing of these materials.

Increasing strain amplitude only slightly elevates $tan_l\ \delta(\gamma, \omega)$ curves, with the effect only being appreciable at the highest amplitudes.

3. Large differences in spacing (expressing strain-dependence) and the shape of $tan_l\ \delta$ -log ω curves (related to ω-dependence) are observed, for sample M.

The relatively high level of the strain-amplitude sensitivity of $tan_l\ \delta$ for blend M, as compared with grafts or sample C, could be explained by sensitivity of the phase morphology of the blend to flow and deformation, particularly that involving large strains and strain rates

Figure 7-15. Frequency and strain dependence of $tan_1 \delta$.



[360]. Since the phase morphology of the grafts, is controlled partially by the size of the average length of backbone segments between branching points and the length of their branches rigidly attached to their backbones by strong covalent bonds, the grafts are far less vulnerable to imposed sinusoidal oscillations.

This would make branched structures much less responsive to changes in both strain amplitude and frequency of oscillations, precisely what is observed in Figure 7-15.

4. Overall, strain and frequency dependence of $\tan_l \delta$ for a graft with well-developed, comb-type LCB structures is not spectacular, with relatively minor differences in $\tan_l \delta(\gamma, \omega)$ with large differences in branching architecture.

Effect of branch length, at comparable number of branches

Changes in $\tan_l \delta(\gamma = 200\%, \omega)$ with increasing branch length are shown are Figure 7-16 for a series of grafts with comparable N_g^p values. Systematic increase in branch length is associated with simultaneous change in the slope and the shape of the $\tan_l \delta(\omega)$ spectra. As branch length increases, the $\tan_l \delta(\omega)$ decreases, initially rapidly, then it eventually becomes independent of branch length at M_p^b about 20,000.

Effect of branching number at comparable length of the branch

Similar changes in shape for $\tan_l \delta(\gamma = 200\%, \omega)$ are observed for analogous ($N_g^p = 0$ to 11.0) changes in the branching number, as shown in Figure 7-17.

Figure 7-16. Frequency dependence of tan_1 δ. Effect of branch length @ 200% strain.

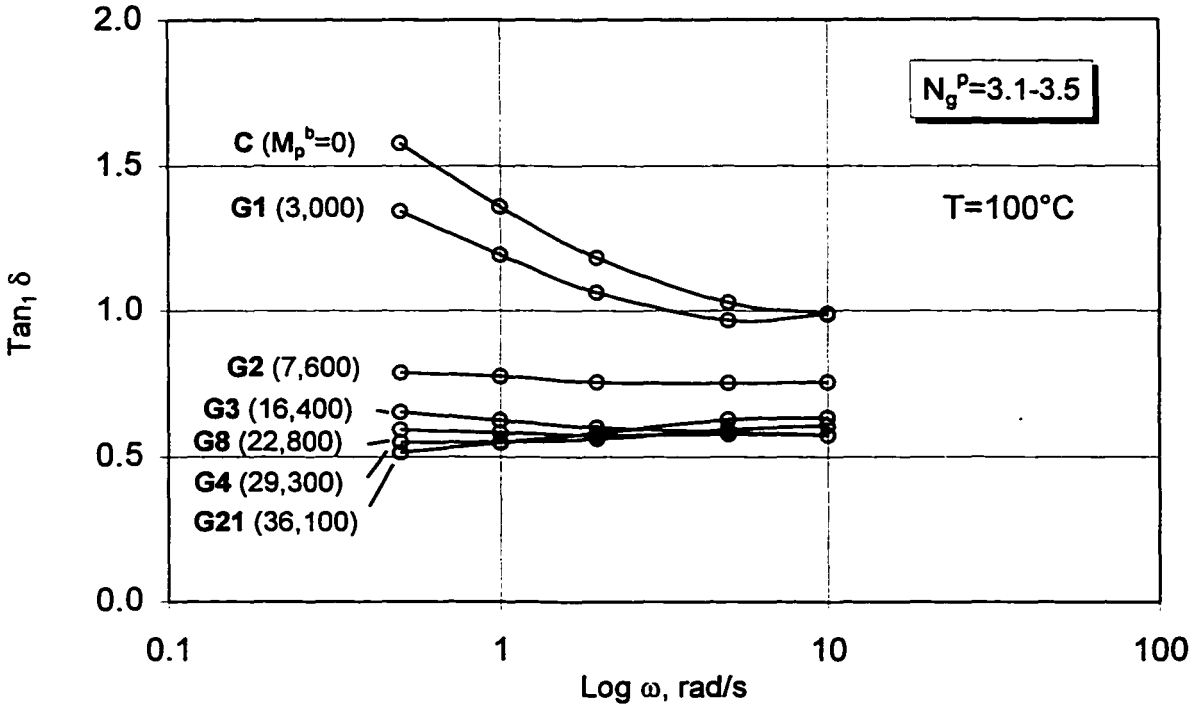
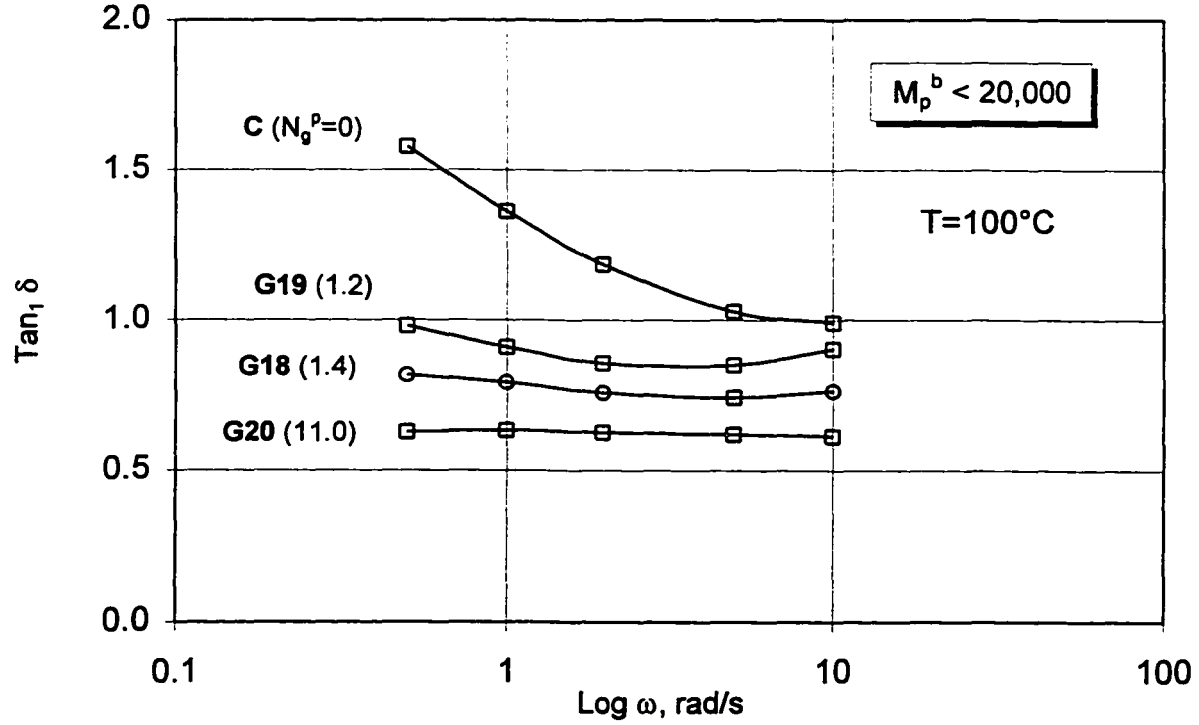


Figure 7-17. Frequency dependence of tan_1 δ. Effect of branching number @ 200% strain.



7.2.4 Pipkin diagrams for $G_1'(\gamma, \omega)$ and $G_1''(\gamma, \omega)$ moduli

A convenient way to display simultaneously the strain amplitude (x) and the frequency (y) dependence of the isothermal viscoelastic function (z) is by using a 3-dimensional plot z=F(x,y), referred to in the literature as the Pipkin diagram [361].

Figures 7-18 to 7-25 contrast the behaviour of linear polymer (sample C) with graft copolymers of various branching architectures present in samples G19, G13 and G6. Figures 7-18, 7-20, 7-22 and 7-24 compare Pipkin diagrams of the 1st harmonic of the in-phase modulus, $G_1'(\gamma, \omega)$ and in Figures 7-19, 7-21, 7-23 and 7-25 diagrams of the 1st harmonic of the out-of-phase modulus, $G_1''(\gamma, \omega)$. Axis scales are individualized for each diagram to emphasize the shape of the $G'_1(\gamma, \omega)$ and $G''_1(\gamma, \omega)$ functions. The modulus and strain amplitude scales are linear and the frequency scale is logarithmic.

Examination of the Pipkin diagrams for representative samples C, G6, G13 and G19, allows for some general observations. The "elastic" nature of these graft copolymers, even at the elevated temperature of 100°C, is immediately apparent. Out-of-phase moduli are several times smaller than $G_1'(\gamma, \omega)$, resulting in fractional (< 1.0) values of $\tan_1 \delta$ (cf. section 7.2.3). Similarly, the absolute values of the complex moduli, $|G^*(\gamma, \omega)|$ will be dominated, both in terms of the values, as well as of their strain- and frequency dependence, by the in-phase component of the modulus.

On the other hand, $G''_1(\gamma, \omega)$ shows greater sensitivity to branching structure than the in-phase or the complex modulus. For all grafts, regardless of the details of the branching structure, the strain and frequency dependence can be characterized as follows:

- G_1' increases exponentially with an increasing frequency at a constant strain; the increase is greater for lower strain amplitudes,

- G_l' decreases with an increasing strain amplitude at a constant frequency; the decrease is quasi-linear at the low frequencies but is becoming much stronger (exponential) with increasing frequency.

The details, slope and functional relations of the dynamic moduli , $G_l'(\gamma, \omega)$ and $G_l''(\gamma, \omega)$ will depend upon structural details, but always large strain amplitudes and low oscillation frequencies will result in the lowest values of complex, in-phase, and in the majority of cases, out-of-phase moduli. In the opposite case, the oscillations at low strain amplitudes and the highest frequencies will result in the highest values of in-phase and, in most cases, complex moduli. Out-of-phase modulus, particularly its functional dependence $G_l''(\gamma, \omega)$, cannot be generalized and it remains the most LCB-sensitive and discriminative dynamic viscoelastic function.

For linear molecules the $G_l''(\omega)$ function at low strains (~5%) follows a partial parabola as seen in Figure 7-19 for sample C. Addition of a small amount of shorter branches results in a more fully defined parabolic shape of the $G_l''(\omega)$ function, as seen for sample G19 (10,300/1.2) in Figure 7-21 . For a graft with long branches (sample G6), the shape of the out-of-phase modulus is nearly linear (Figure 7-23), while for the comb-like structures with many short side chains (for example, sample G13) it is exponential (Figure 7-25).

As a final comment, it should be noted that for the characterization of the LCB, the application of a high strain amplitude (at least up to 200%, that is well into the NLVE range for the CIIR-g-BR grafts), does <u>not</u> provide any new insight, as compared to low-strain (LVE) techniques. However, application of higher strains, results in improved sensitivity of the measurements.

Figure 7-18. Pipkin diagram of the in-phase modulus, RPA 2000, {FSWP3}, T=100°C, sample C.

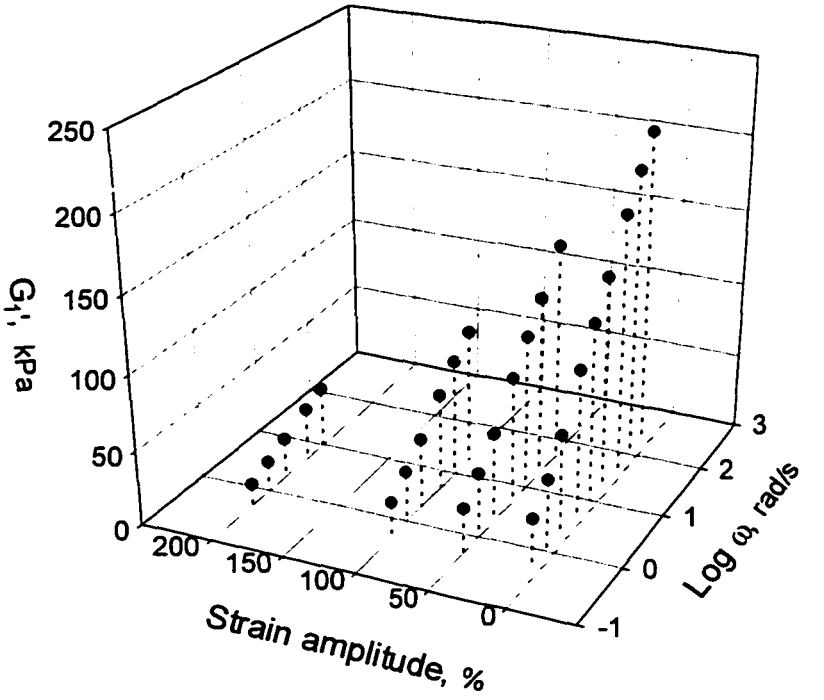


Figure 7-19. Pipkin diagram of the out-of-phase modulus, RPA 2000, {FSWP3}, T=100°C, sample C.

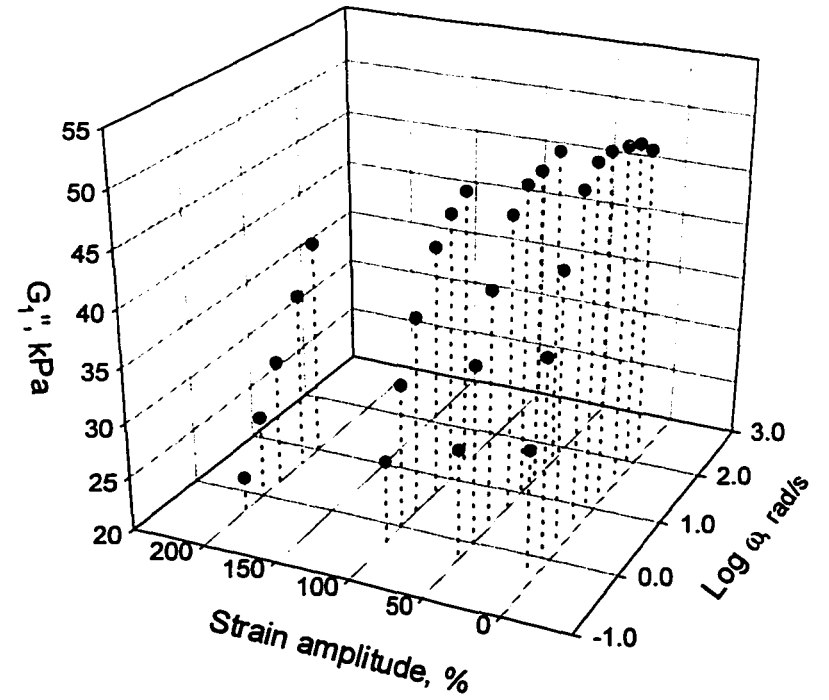


Figure 7-20. Pipkin diagram of the in-phase modulus, RPA 2000, {FSWP3}, T=100°C, sample G19.

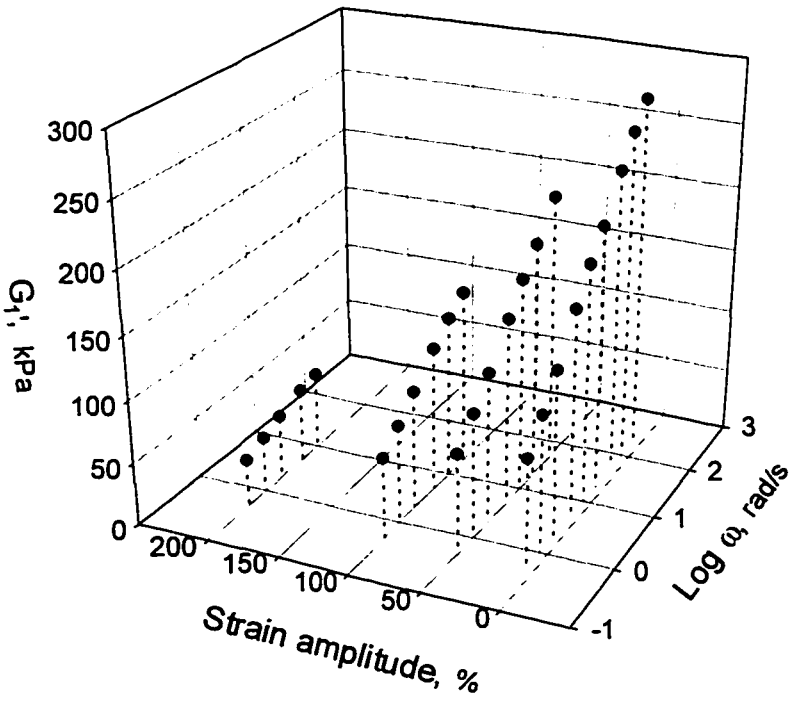


Figure 7-21. Pipkin diagram of the out-of-phase modulus, RPA 2000, {FSWP3}, T=100°C, sample G19.

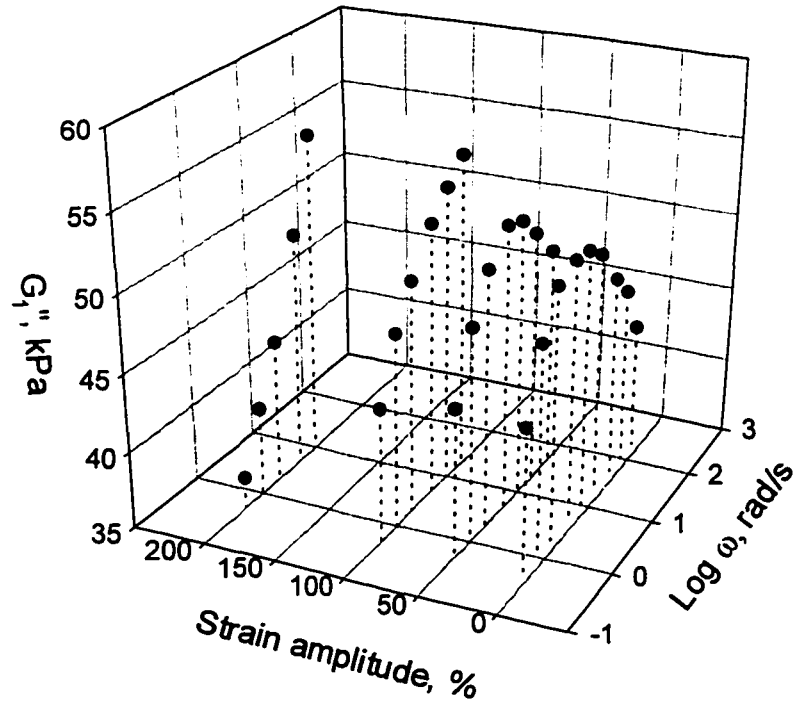


Figure 7-22. Pipkin diagram of the in-phase modulus, RPA 2000, {FSWP3}, T=100°C, sample G13.

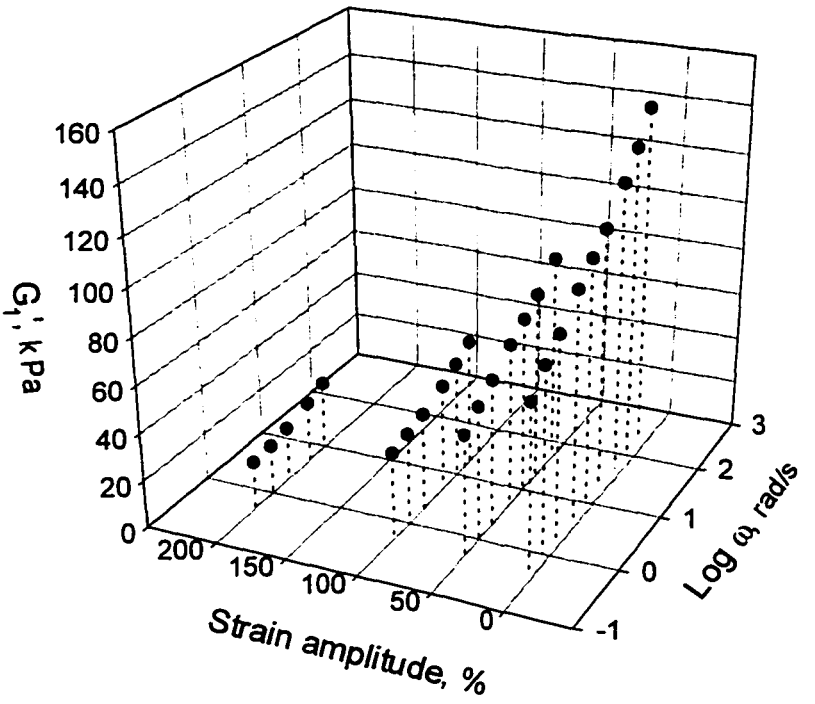


Figure 7-23. Pipkin diagram of the our-of-phase modulus, RPA 2000, {FSWP3}, T=100°C, sample G13.

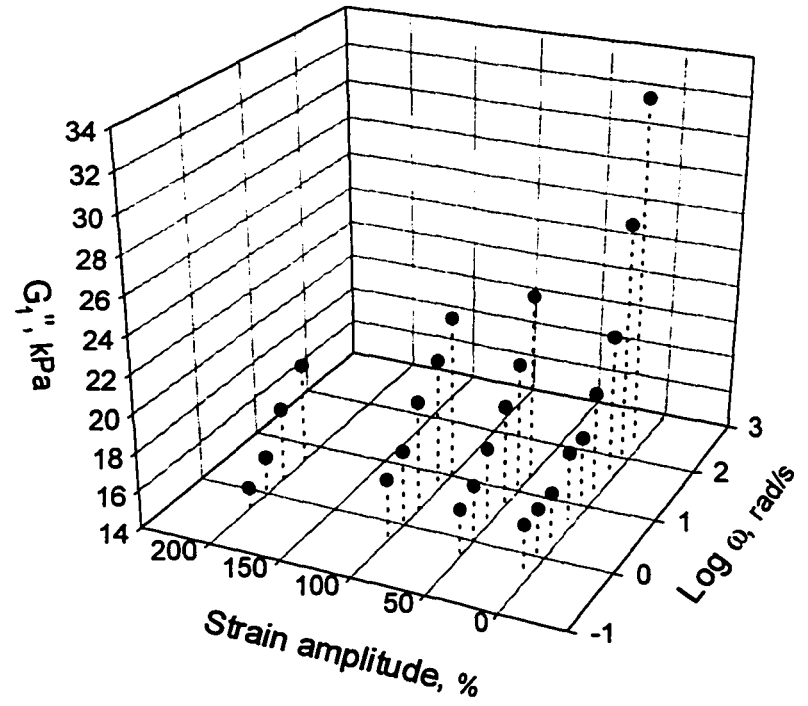


Figure 7-24. Pipkin diagram of the in-phase modulus, RPA 2000, {FSWP3}, T=100°C, sample G6.

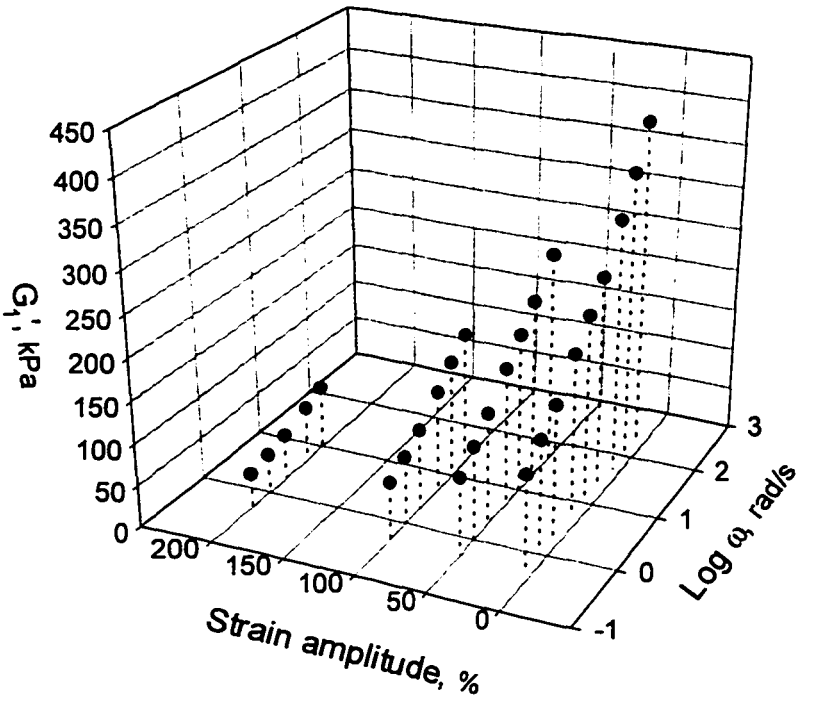
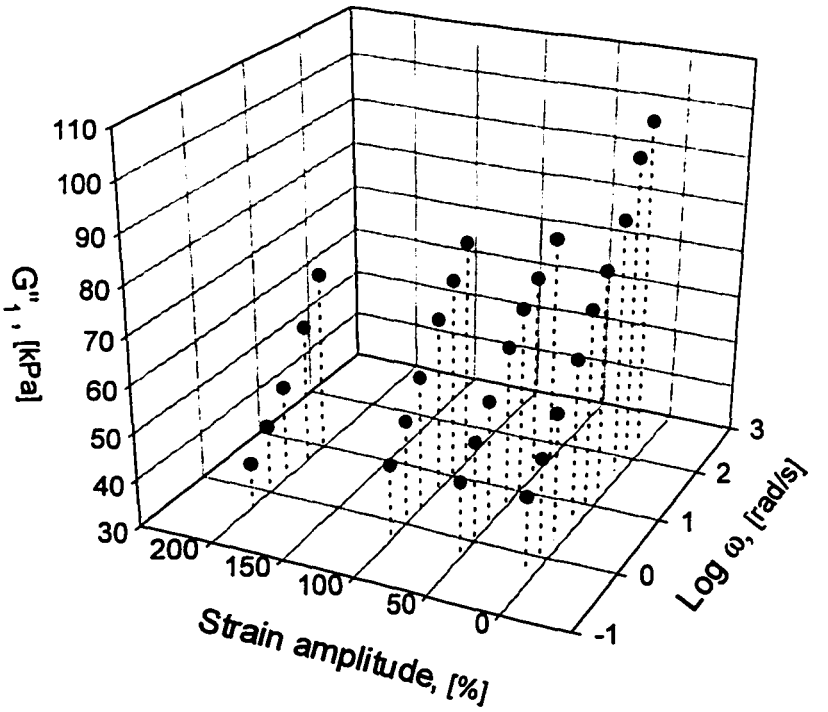


Figure 7-25. Pipkin diagram of the out-of-phase modulus, RPA 2000, {FSWP3}, T=100°C, sample G6.



7.3. Effect of large-amplitude oscillatory shear (LAOS)

To investigate the effect of large strain-amplitude oscillatory shear (LAOS) on the viscoelastic properties of the grafts, a series of time-controlled, alternate, small and large strain amplitude dynamic time sweeps were applied. Small amplitude (5%), 'probing' oscillatory shear before and after (200% strain) and again following 800% strain shear. In order to accomplish these objectives, a sequence of small and large strain amplitude oscillatory sweeps, referred to as steps or subroutines, was performed, according to test routine {HSSWP1}. Test details were reported in Chapter 5, section 5.4.3. Figure 5-24c provides details of the test routine. It is interesting to notice that both strain amplitudes are well above the limit of LVE for the majority of grafts (42% or less), as determined by the sequential strain sweep (section 7.1).

Small strain time sweeps (at constant T, γ, ω and sweep duration) were designed to probe the viscoelastic response of the material. They were applied in steps II, IV and VI (see diagram in Figure 5-24c), first, in step II, before imposing a large strain (200%) deformation, then immediately after, in step IV, and finally (in step VI), after subjecting the sample to a very large (800%) oscillatory strain.

A constant oscillation frequency maintained throughout 6-step routine, was set deliberately low at 1 rad/s in order to minimize the heat generated internally due to large strain shear. Specimen temperature, with allowance for a viscous heating, was closely controlled and directly monitored. Intermittent increase of the specimen temperature above the nominal test temperature of 100°C was found to be small and could be related to the complex modulus of the polymer.

Tabulated test results are collected in Table A74, A75 and A76, which are included in Appendix V. Definitions of the viscoelastic parameters pertinent to this experiment are the subject of Table 7-7.

Table 7-7. Definitions of linear and non-linear viscoelastic parameters derived from {HSSWP1} test.

abbreviation	definition
G'(5%/(II)) **G'(5%/(IV))** **G'(5%/(VI))**	- steady-state value of the storage modulus at 5% dynamic strain and 1 rad/s frequency, in step II, step IV or step VI, respectively,
G"(5%/(II)) **G"(5%/(IV))** **G"(5%/(VI))**	- steady-state value of the loss modulus at 5% dynamic strain and 1 rad/s frequency, in step II, step IV or step VI, respectively,
tan δ (5%(II)) **tan δ (5%(IV))** **tan δ (5%(VI))**	- steady-state value of the tangent of the phase angle, δ at 5% dynamic strain and 1 rad/s frequency, in step II, step IV or step VI, respectively,
G_1'(200%) **G_1'(800%)**	- 1st harmonic of the in-phase component of the modulus at 1 rad/s frequency and dynamic strain of 200% and 800%, respectively,
G_1"(200%) **G_1"(800%)**	- 1st harmonic of the out-of-phase component of the modulus at 1 rad/s frequency and dynamic strain of 200% and 800%, respectively,
tan_1 δ (200%) **tan_1 δ (800%)**	- tangent of phase angle, δ at 1 rad/s frequency and 200% and 800% dynamic strain, respectively,
G*(5%/(II)) **G*(5%/(VI))**	- steady-state (absolute) value of the complex modulus at 5% dynamic strain and 1 rad/s frequency, in step II and step VI, respectively,
G_1*(200%) **G_1*(800%)**	- 1st harmonic of the (absolute value of the) complex modulus at 1 rad/s frequency and dynamic strain of 200% and 800%, respectively,
S_1'(200%) **S_1'(800%)**	- 1st harmonic of the in-phase component of the torque at 1 rad/s frequency and dynamic strain of 200% and 800%, respectively,
S_1"(200%) **S_1"(800%)**	- 1st harmonic of the out-of-phase component of the torque at 1 rad/s frequency and dynamic strain of 200% and 800%, respectively,
S_1 (5%) **S_1 (200%)** **S_1 (800%)**	- 1st harmonic of the torque at 1 rad/s frequency and dynamic strain of 5%, 200% and 800%, respectively.

Table 7-8 contain a table with correlation coefficients. Prediction profiles can be found in Figures A74a, A74b, A74c and A74d, in Appendix V.

Table 7-8. Correlation coefficients (t-Ratio) between structural and viscoelastic parameters - {HSSWP1} test.

RPA 2000 {HSSWP1}	ω=1 rad/s	M_p^b	N_g^p	$w^{b,g}$	Φ	w^b	$w^{b,h}$	M_z^G	PDI	vinyl
G'(5%/II)	I	+	-	0	-3.70	0	+	+	0	0
G"(5%/II)	II	+2.79	-4.67	-	-5.62	0	+	0	0	0
G*(5%/II)	III	+2.57	-3.16	0	-4.78	+	+	+	0	0
G'(5%/IV)	IV	+	-	0	-3.79	0	0	+	0	0
G"(5%/IV)	V	+3.22	-4.93	0	-5.79	0	+	0	0	0
G'(5%/VI)	VI	+	-2.81	0	-3.58	0	0	+	0	0
G"(5%/VI)	VII	+	-6.68	0	-8.76	0	0	0	0	0
G_1'(200%)	VIII	+	-2.67	0	-3.85	0	0	0	0	0
G_1"(200%)	IX	+4.00	-6.13	-	-7.25	0	+	0	0	0
G_1*(200%)	X	+2.58	-4.99	0	-7.23	0	0	0	0	0
G_1'(800%)	XI	+	-	+3.16	-	+2.98	+	+3.34	0	0
G_1"(800%)	XII	+2.95	-5.13	0	-5.42	0	+	+	0	0
G_1*(800%)	XIII	+2.96	-4.60	0	-4.74	+	+	+	0	0
tan δ (5%/II)	XIV	0	-2.55	-3.17	-3.34	-	0	-	-	0
tan δ (5%/IV)	XV	+	-2.78	-2.65	-3.32	-	+	-	-	0
tan δ (5%/VI)	XVI	+	-4.10	-3.23	-5.98	-	0	-	0	0
tan_1 δ (200%)	XVII	+	-2.68	-	-2.81	0	+	0	-	-
tan_1 δ (800%)	XVIII	0	-3.04	-6.77	-5.19	-4.91	0	-3.72	0	0

$\Phi \equiv (M_p^b / M_e) \cdot (N_g)^2$

Explanation:
The numbers indicate the t-Ratio for a statistically significant correlation, that is when the |t-Ratio| value is above 2.50 (corresponding to 95% conf. interval), '0' - weak or no correlation
'-' - negative, statistically not significant correlation (|t-Ratio| values below 2.50)
'+' - positive, statistically not significant correlation (|t-Ratio| values below 2.50)

The standard set of eight (8) structural and compositional parameters was supplemented by a dimensionless parameter Φ, derived from the two principal branching parameters, $M_p^{\,b}$ and $N_g^{\,p}$, and defined by equation (7-1),

$$\Phi = (M_p^{\,b} / M_e) \cdot (N_g^{\,p})^2 \qquad (7\text{-}1)$$

where M_e is the average molecular weight between entanglements of the (BR) branch prepolymer.

The typical value of M_e reported in the literature for polybutadienes of comparable microstructure to those used in this study is 1,900 g/mol [362, 341, 355]. This value was adopted for numerical calculation of the Φ parameter. It was shown (in Table 7-8) that branching parameter Φ correlates very well with a number of viscoelastic parameters, derived from LAOS experiments.

Upon examination of the correlation coefficients, the following general observations are made:

- storage modulus G' at 5% strain, and to some extent G_1' (200%), does not relate well to parameters which describe the details of the branching structure. This observation is consistent with the applicable conclusion in subsection 7.2.4, derived from a different set of experiments,

- the similarity of correlation factors for the corresponding pairs of the G″(...) and G*(...) moduli, indicates that no new insight into the relationship between the LCB structure and viscoelasticity (either LVE or NLVE) would be gained by studying the effect of both factors (comparing rows II vs. III, IX vs X and XII vs. XIII, in Table 7-8). Therefore, the loss modulus (or out-of-phase component of the complex modulus, in the case of non-linear dynamic moduli) is a preferable choice, due to consistently higher coefficients of correlation,

- parameter Φ has the highest correlation coefficients with almost every viscoelastic parameter listed in Table 7-8, except correlations in rows XI and XVIII. However, as an empirical parameter, its physical meaning is less straightforward than for specific branching parameters (M_p^b, N_g^p) or branching content, defined by $w^{b,g}$,

- qualitatively, and as a rule, branching length and branching number have opposite effects on most of the viscoelastic parameters, and this finding is consistent with all previous screening analyses,

- parameter **G_1 '(800%)** stands out, as far as its dependence upon structural parameters is concerned. It is primarily related to the total molecular weight of the graft, M_z^G.

A. Effect of shear deformation history and its interpretation in terms of branching structure

Two sets of linear viscoelastic parameters, suitable to quantify this behaviour are: the first being **G'(5%/IV), G″(5%/IV)** and **tan δ(5%/IV),** to probe the effect of the 200% shear (corresponding to step III in Figure 5-24c) , and the second being **G '(5%/VI), G ″(5%/VI)** and **tan δ(5%/VI)**, following step V (800% strain shear). **G '(5%/II), G ″(5%/II)** and **tan δ(5%/II)** were used as a reference. They were calculated from data obtained from the step II of the {HSSWP1} test. A series of alternate low/high strain subroutines was preceded by a small amplitude (2%) oscillation, consistently used in all RPA 2000 experiments, in order to

allow for thermal homogenization of the specimen, and to serve as a check for test consistency.

Figures 7-26 and 7-27 present composite results for the storage and loss moduli, respectively, measured in the step II, IV and VI of the experiment.

In general, the effect of shear history depends on details of the branching structure. More specific observations are summarized below.

*Storage modulus; parameters **G'(5%/II), G'(5%/IV), G'(5%/VI)***

1. The large strain (200%) oscillations, step III, leave no or hardly any discernible effect on the majority of samples, as judged by comparison of the storage modulus G', before and after the time-controlled, large amplitude (200%) oscillatory shear - Figure 7-26.

2. Application of oscillatory shear involving even larger strain amplitudes (800%) introduced a substantial "hardening" of the storage modulus (up to 75%, in the case of sample G14, col. "c" and "e" in Table A74, part I). The effect is most pronounced for samples with fewer but longer branches (i.e. samples G14, G5, G6, G21). For linear polymer (sample C) the effect is much smaller (about 30% increase) than for most grafts. An exception are grafts with many (N_g^p = 7.6 to 11.1) short branches, where the effect is even smaller, of the order of 5 - 8%, as for example for samples G12, G13 and G20.

These observations suggest a definitive role of the branch length in the "strain-hardening" effect, induced by the strain amplitude of oscillatory shearing. The average backbone length is constant for all grafts and only the number and length of branches might contribute to the phenomenon. Also, from the screening analysis there is no evidence for the chemical composition playing any role here (compare Table 7-8, rows I, IV and VI).

Figure 7-26. High-strain-amplitude experiment, {HSSWP1}
RPA 2000, T=100°C, ω=1 rad/s, γ=5%.

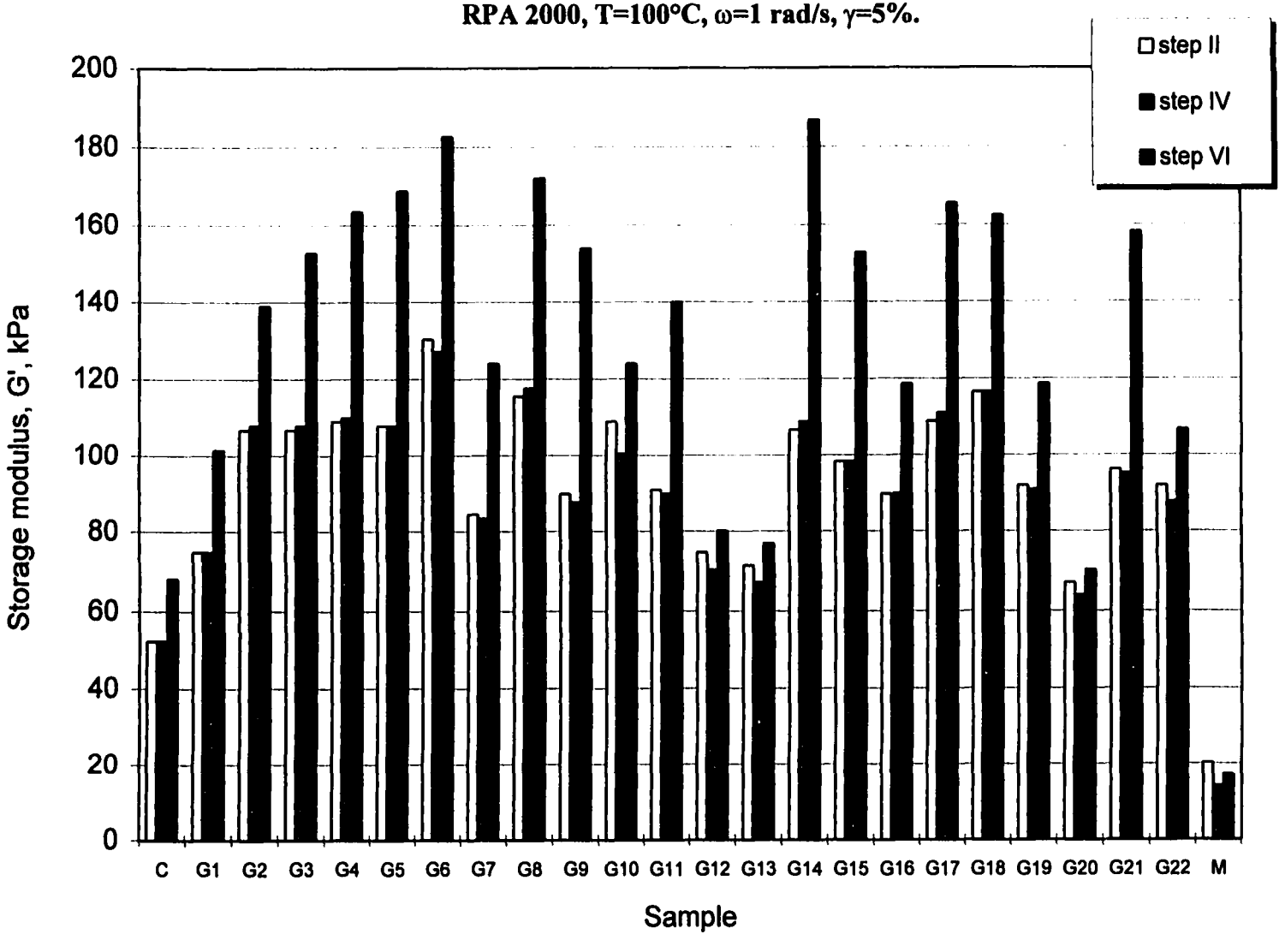
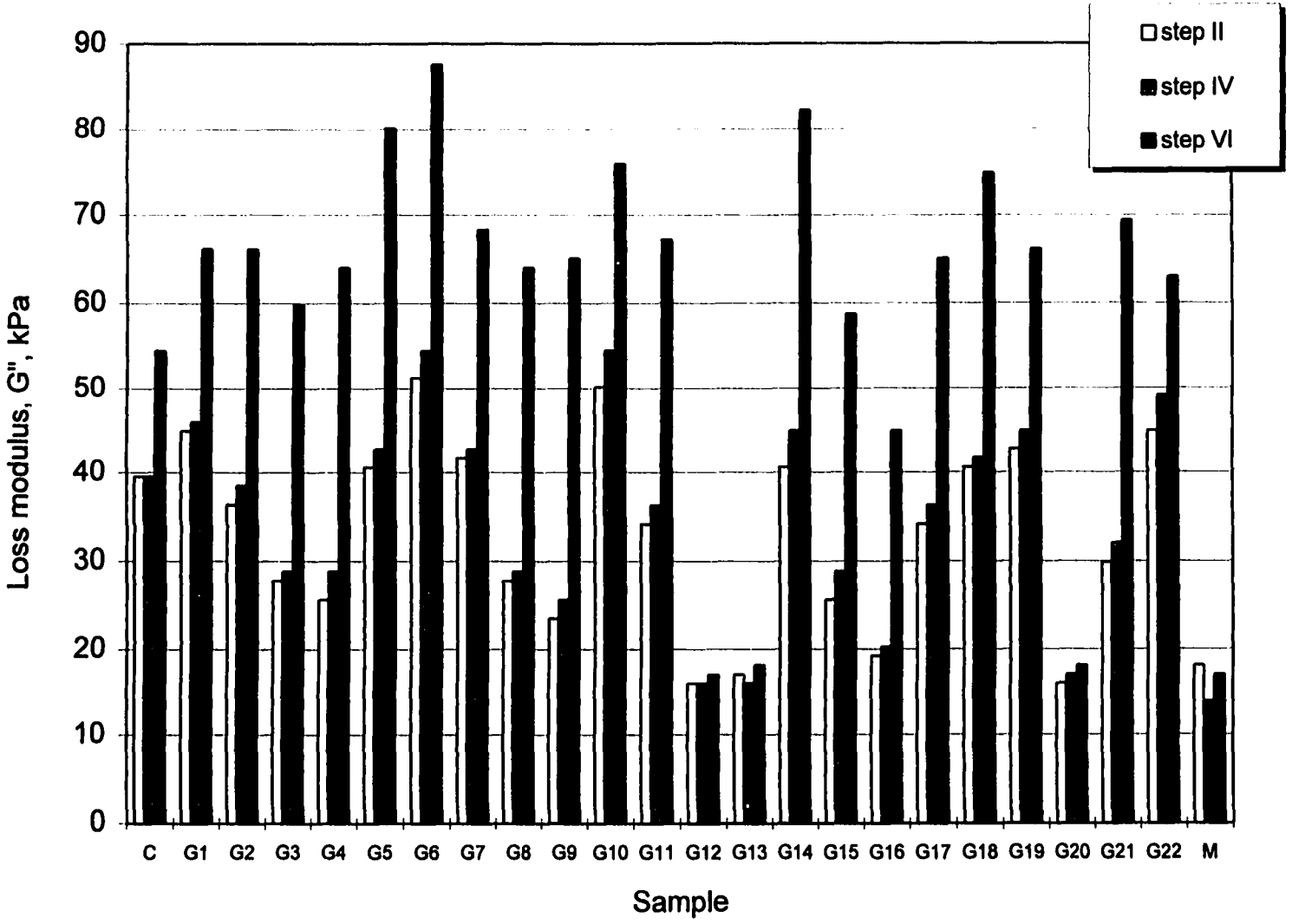


Figure 7-27. High-strain-amplitude experiment, {HSSWP1}
RPA 2000, T=100°C, ω=1 rad/s, γ=5%.



Loss modulus, G"; parameters ***G"(5%/II), G"(5%/IV), G"(5%/VI)***

All the above observations are equally applicable to loss modulus with the differences being even more dramatic (Figure 7-27). Differences between the **G"(5%/VI)** and **G"(5%/II)** parameters could be more conveniently examined when compared directly as in Figure 7-28. For blend M slight but measurable softening of either moduli is taking place upon shearing. This is qualitatively consistent with similar behaviour reported for incompatible blends in a molten state [363].

Screening analysis indicated a strong, negative correlation between loss modulus, measured directly after high-strain shearing, **G"(5%/VI)** and branching number. An even stronger correlation exists when branching parameter, Φ is used (as can be seen in row VII in Table 7-8).

The effect of shearing is best illustrated by considering the difference between **G"(5%/VI)** and **G"(5%/II)** parameters in Figure 7-28. The type of branching structure that stands out is one with numerous branches (samples G13, G20, G12), undergoing no shear modification as defined by the **G"(5%/VI)** and **G"(5%/II)** difference. On the other hand, intermediate branching structures, which combine longer branches (~30,000) with appreciable branching number (~3), were shown to be the most sensitive to shear history.

Judging from the results of the large-amplitude oscillatory shear experiment, introduction of long-chain branching into the molecular structure of the linear elastomer, will increase the polymer sensitivity to previous shear history, except for graft molecules with numerous (N_g^p > 5) short branches (Figure 7-28). This conclusion is in agreement with previously published results [11, 364-367].

B. Linear viscoelastic parameters (at 5% strain) - revisited

Linear viscoelastic parameters, namely **G'(5%/II), G" (5%/II), G*(5%/II)** and **tan δ(5%/II),** measured in the step II of the {HSSWP1} experiment, that is before subjecting specimen to a series of large-strain deformations, allow for additional confirmation of the results obtained during dedicated small-strain dynamic experiments.

Numerical values can be found in Table A74 (col.a, b), Table A75 (col. k) and Table A76 (col. p), with graphical presentation in Figure 7-26 (for G') and Figure 7-27 (for G") and the outcome of their correlations with LCB structure and composition included in Table 7-8, rows: I, II, III and XIV. Conclusions from the analysis of these data fully confirm those previously reported and need not be detailed here.

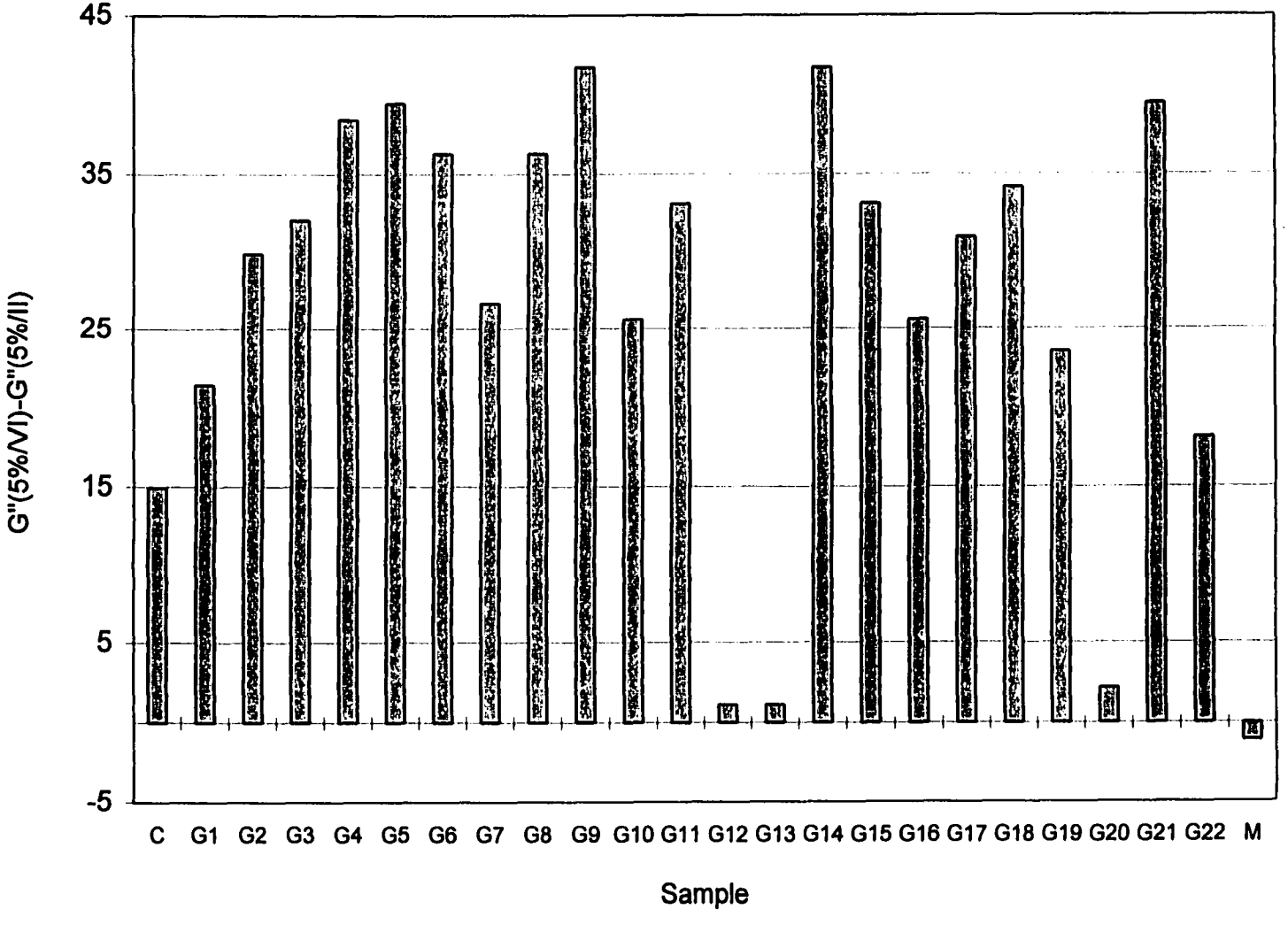
C. Non-linear viscoelastic parameters at 200% strain - revisited

Analogous comparison between viscoelastic parameters obtained at 200% and 1 rad/s, during the 3rd step of the {HSSWP} test and corresponding data from {FSWP3} large amplitude frequency sweep, also gave comparable results.

D. Non-linear viscoelastic parameters at 800% strain

Direct graphical comparison of the dynamic moduli at 5%, 200% and 800% strains in Figure 7-29 for storage/in-phase modulus, and in Figure 7-30 for loss/out-of-phase modulus, clearly show that branched molecules follow the same pattern as linear molecules or blends do. In all cases, an increased strain of the sinusoidal oscillation will lower both dynamic components of the modulus, but much more significantly so for storage modulus. This will result in increased $\tan_1 \delta$ for tests carried out at higher strains, as shown in Figure 7-31. $\text{Tan}_1 \delta$ values are consistently lower for grafts, when compared to $\tan_1 \delta$ for sample C, yet differences among graft structures are relatively small and the pattern is amazingly consistent, regardless of strain amplitude.

Figure 7-28. LAOS experiment {HSSWP1}, effect of large-amplitude (800%) oscillatory shear. RPA 2000, T=100°C, ω=1 rad/s.



From the point of view of correlations between viscoelastic parameters and those describing the branching structure, an advantage for using large-strain (in shear) dynamic tests over their linear counterparts is primarily in better definition of the relationship which exists between viscoelastic properties and the underlying molecular structure, reflected by higher correlation coefficients. (comparing for example, row I with VIII, row II with IX and III with X, in Table 7-8).

On the other hand, parameters defined for the highest strain (800%), those describing the "elastic" aspect of the viscoelastic behaviour, namely $\mathbf{G_1'(800\%)}$ and $\mathbf{\tan_1 \delta(800\%)}$ show different "affinity" as far as structural parameters are concerned. $\mathbf{G_1'(800\%)}$ seems to be most sensitive to the overall MW of the graft and $\mathbf{\tan_1 \delta(800\%)}$ is correlating well with the overall branching content, $w^{b,g}$ (and also with Φ).

In the plateau and terminal zones of the viscoelastic spectrum, the viscous component (S_1'', G_1'') will dominate the response of the material when using large strains (comparing the height of the solid black bars in Figure 7-29 and Figure 7-30). For deformations at small strain amplitudes, on the other hand, an elastic response will be predominant, as reflected by decreasing values of $\tan_1 \delta$, as the amplitude of the oscillations becomes smaller (800%-200%-5%) - Figure 7-31.

E. Final comments on the experimental aspects of the large-strain dynamic measurements.
Dynamic tests using larger strain amplitudes, in principle, will produce higher torque signals, which, in absence of experimental artifacts (i.e. wall slippage, viscous heating, etc.) will result in improved sensitivity of the measurements. This point is dramatically demonstrated in Figure 7-32, where large differences in measured torque values, presumably related to differences in branching structure, will translate into a much better resolution of the test [1], if used to characterize molecular structure of a polymer.

[1] assuming that the test precision is not a function of the transducer signal, within a nominal range of the torque transducer

Figure 7-29. LAOS experiment, {HSSWP1}
RPA 2000, T=100°C, ω=1 rad/s.

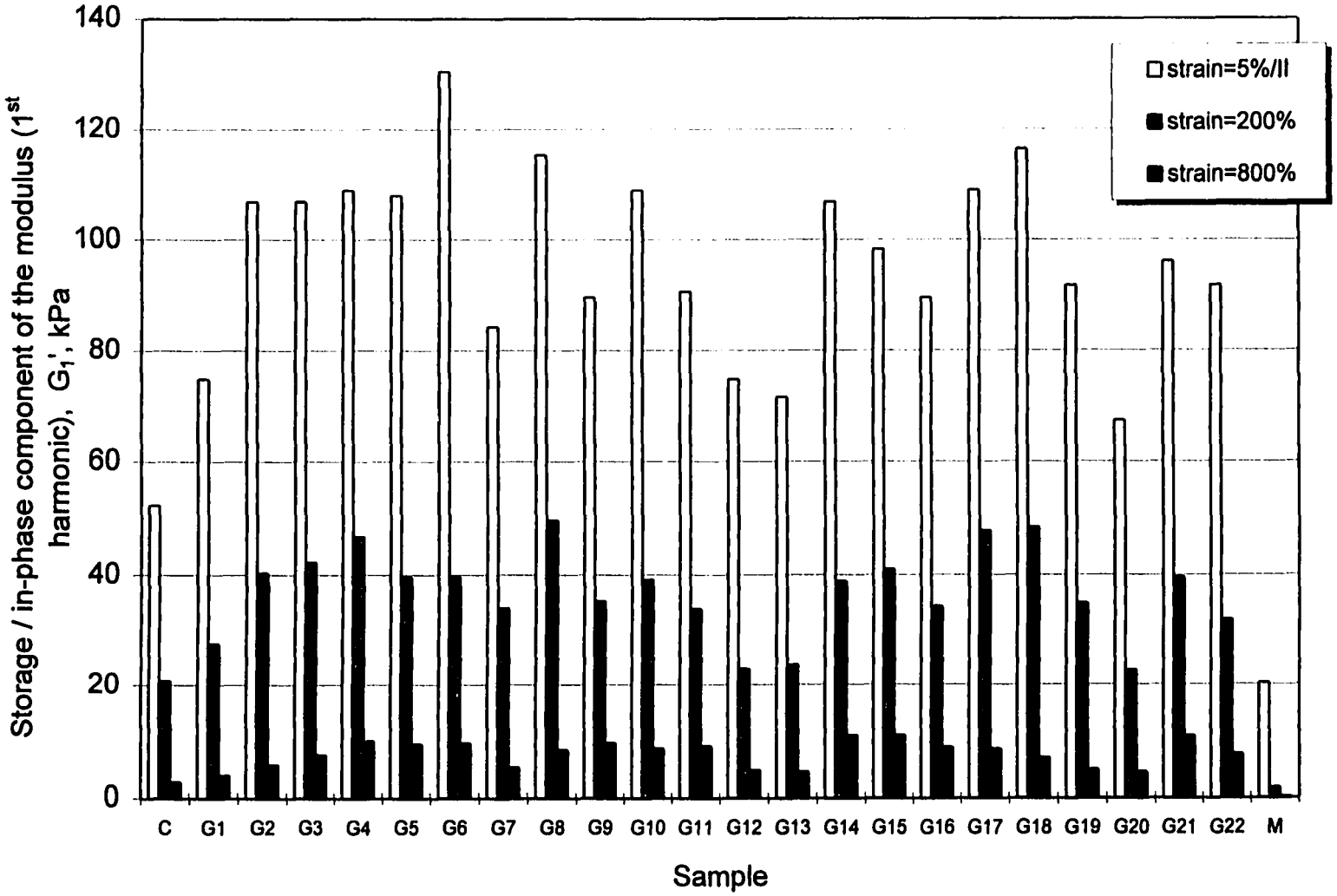


Figure 7-30. LAOS experiment, {HSSWP1}
RPA 2000, T=100°C, ω=1 rad/s.

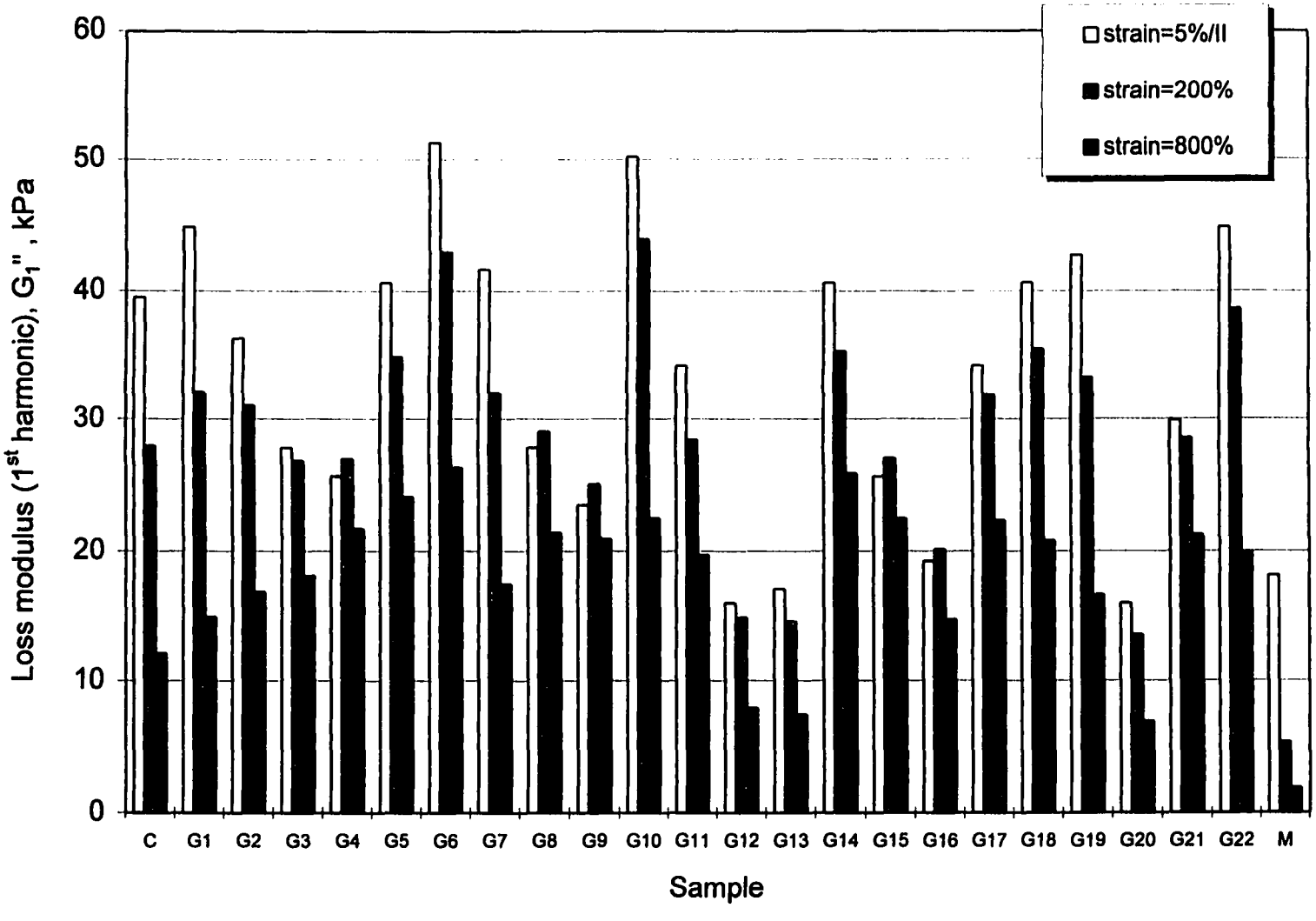


Figure 7-31. LAOS experiment, {HSSWP1}
RPA 2000, T=100°C, ω=1 rad/s.

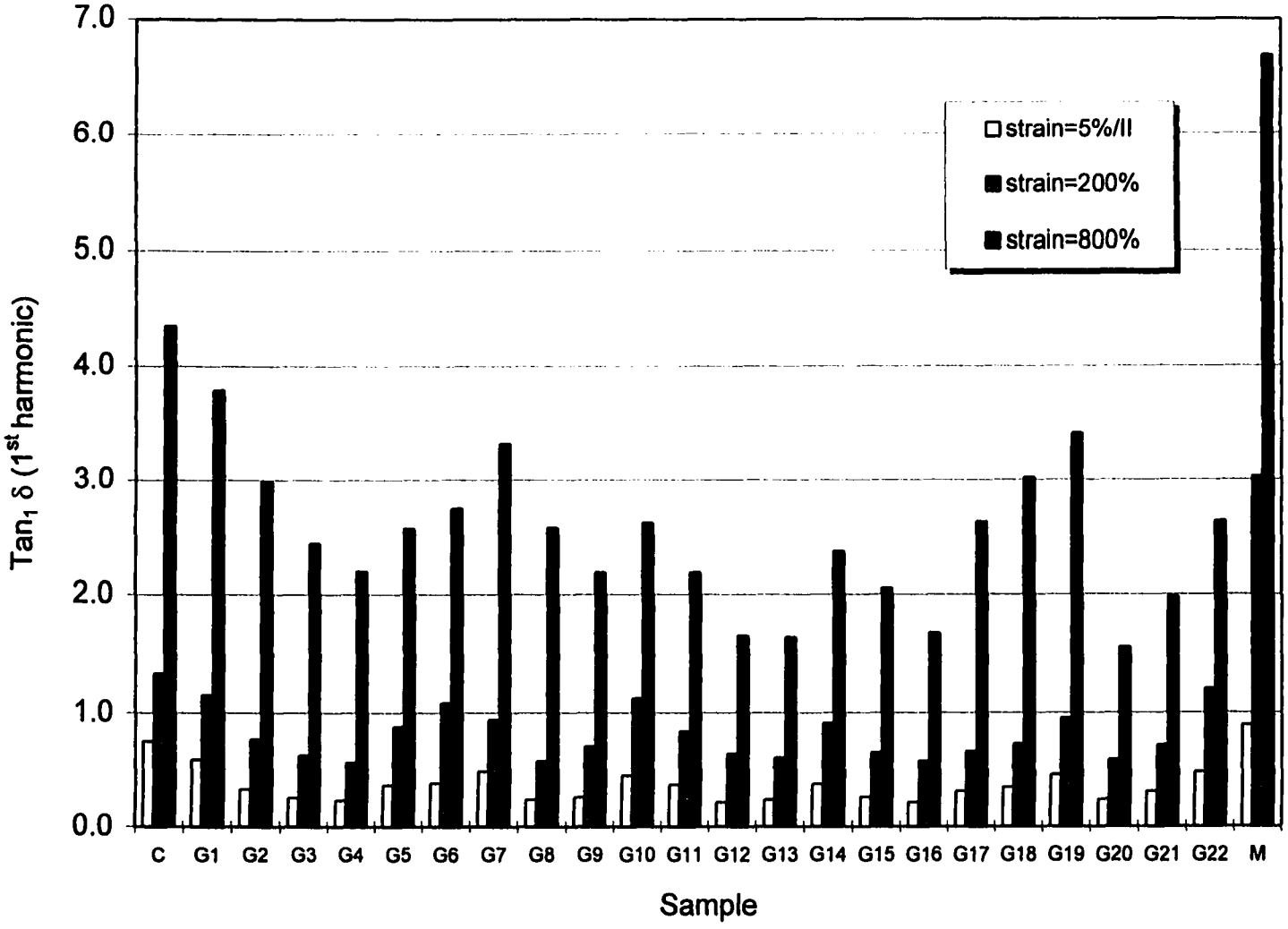
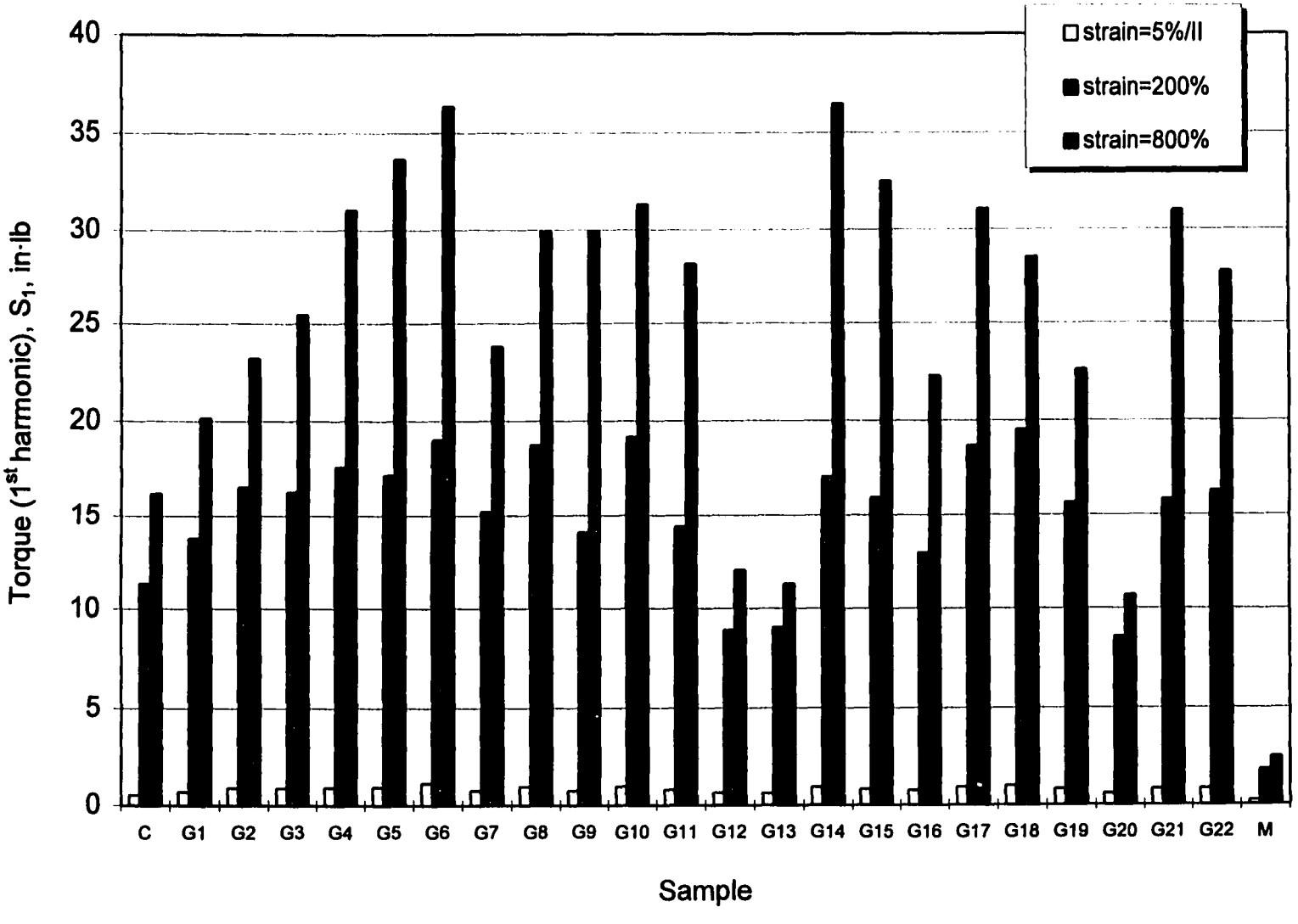


Figure 7-32. LAOS experiment, {HSSWP1}
RPA 2000, T=100°C, ω=1 rad/s



7.4 Non-linear stress relaxation in shear

The results of the non-linear stress relaxation experiments, carried out using the DSR and their interpretation in terms of branching structure are the subject of this section. Complete test conditions and experimental details of the {TEST2} test configuration, were reported in Chapter 5, section 5.5 and are summarized in Appendix IV, Table D.

For preliminary investigations of the possible correlations between the structural and rheological parameters, the stress relaxation modulus, G(t) and its derivative, the normalized stress relaxation modulus, nG(t), were quantified in the form of various rheological parameters.

Normalized stress relaxation modulus, nG(t), is defined as the ratio between value of the G(t) at any time within the relaxation monitoring period, and the G(t) at 40 ms. This definition is similar to that given by equation (6-11) except for a different reference time.

Stress relaxation parameters and screening for correlations

A large number of parameters could be defined for stress relaxation experiments to characterize every possible aspect of the stress relaxation behaviour of the material. In practice, however, many of them are strongly interrelated. Table 7-9 defines only parameters used in this study. Table A77, Appendix V includes the value of G(40ms) and nG(t') parameters. However, values of the modulus G(t') can be readily calculated using the relation which defines the nG(t') parameters, namely, $G(t') = G(40ms) \cdot nG(t')$.

Screening for correlations between structural parameters, including interferences and selected rheological parameters was carried out as usual. Prediction profiles are included in Appendix V Figure A75a for M_p^b and N_g^p, and in Figure A75b for $w^{b,g}$ and w^b.

Table 7-9. Definitions of non-linear stress relaxation parameters derived from {TEST2} test.

abbreviation	definition
G(40ms)	- stress relaxation modulus measured 40ms after application of a sudden step-shear strain
G(1)	- stress relaxation modulus, measured 1.0 s after application of a sudden step-shear strain
nG(0.1)	- normalized (G(t)/G(t=40ms)) stress relaxation modulus, measured 0.1 s after application of a sudden step-shear strain
nG(1)	- normalized (G(t)/G(t=40ms)) stress relaxation modulus, measured 1 s after application of a sudden step-shear strain
nG(10)	- normalized (G(t)/G(t=40ms)) stress relaxation modulus, measured 10 s after application of a sudden step-shear strain
nG(100)	- normalized (G(t)/G(t=40ms)) stress relaxation modulus, measured 100 s after application of a sudden step-shear strain
nG(400)	- normalized (G(t)/G(t=40ms)) stress relaxation modulus, measured 400 s after application of a sudden step-shear strain

Correlation coefficients in Table 7-10 serve as a guide to discover where the meaningful structure-property correlations exist and which are worth exploring. Detailed analysis follows in the form of x-y plots.

From the examination of the correlation coefficients, based on a full portfolio of graft samples, several conclusions can be made to facilitate interpretation of the stress relaxation curves.

a. The modulus recorded at 40 ms after the application of a step shear strain is related quite strongly to both M^b and N_g. This relation is consistent with results previously reported on dynamic moduli. Correlation with $w^{b,h}$ is weaker and proved to be a result of a strong interrelation between $M_p{}^b$ and $w^{b,h}$.

Table 7-10. Correlations coefficients (t-Ratio) between structural and stress relaxation {TEST2} parameters.

DSR {TEST2}	M_p^b	N_g^p	$w^{b,g}$	w^b	$w^{b,h}$	M_z^G	PDI	vinyl
G(40ms)	+4.24	-5.76	-	0	+2.91	0	0	0
nG(0.1)	-6.74	+5.06	0	0	-3.68	-	0	0
nG(1)	-4.15	+5.48	+	0	-2.71	0	0	0
nG(10)	-2.83	+4.07	+	0	-	0	0	0
nG(100)	-	+2.58	+	0	-	0	0	0
nG(400)	-	+	+	+	-	0	0	0

'0' - |t-Ratio| values below 1.00; '+' or '-' - positive or negative correlation, respectively, with |t-Ratio| values below 2.50, e.g. corresponding to 95% conf. interval.

b. The rate of modulus decay, expressed as the normalized G(t) and taken at various intervals, is also strongly dependent, albeit in a different manner, upon branch length and frequency.

c. Negative t-Ratio values for correlation between the nG(t) and M^b would suggest that increasing branch length speeds up the relaxation process, while an increased number of branches has the opposite effect. While the second effect is intuitively obvious and explainable by the concept of molecular entanglements, the former finding remains puzzling and requires scrutiny.

d. Chemical composition, w^b, molecular weight of the graft, M_z^G and branching content, $w^{b,g}$ do not correlate with either of the stress relaxation parameters defined in Table 7-9.

e. No effect from structural interferences (PDI or vinyl content of branches) was observed.

7.4.1 Stress relaxation modulus, G(t)

Interpretation of G(t) profiles in terms of branching structure

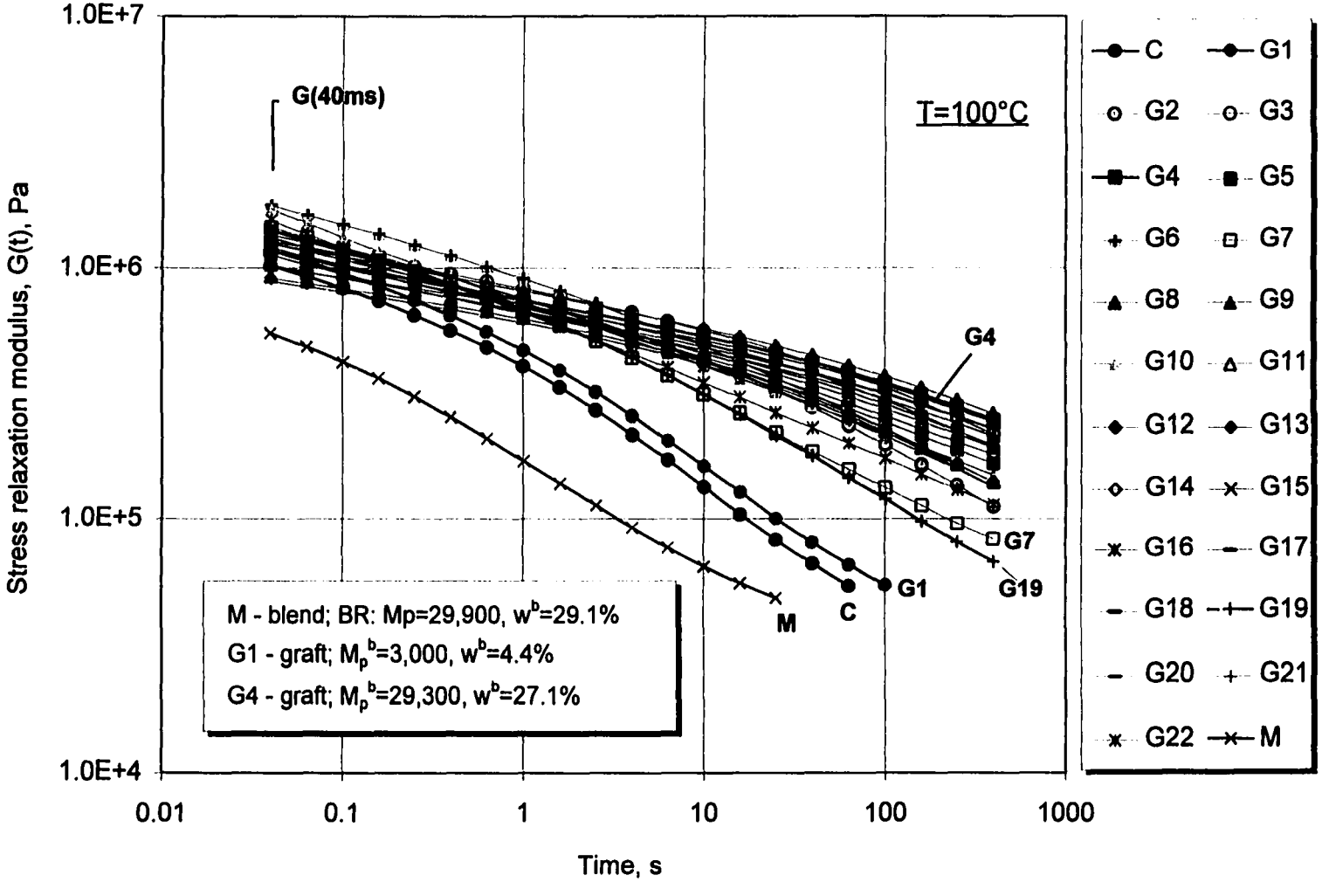
A comparison the time dependence of the non-linear stress relaxation modulus, G(t) for all samples, is shown in Figure 7-33. A composite graph was prepared in order to indicate the range of relaxation behaviour observed for the entire portfolio of branching architectures. The stress relaxation curves for sample C, blend M, and a graft sample (G4), structurally and compositionally equivalent to blend M, as well as sample G1 (a graft with very short branches), are highlighted by thick continuous lines.

The function G(t) for sample C is characteristic of linear elastomers of molecular weights, typical for commercial elastomer grades. The time dependence of relaxation modulus for sample G1, is very similar to that of sample C. The only difference which can indicate the existence of short branches, is the modulus increase of about 20%.

Blending of a precursor backbone polymer with a branch polymer of relatively low MW (but ten times higher than the branches in graft G1), reduces relaxation modulus very significantly, by a factor of 2.1. Change in a shape of the G(t) curve is also noticeable.

The stress relaxation function, G(t), for most grafts, in spite of substantial differences in branching structure, is confined to a relatively narrow band. A possible exception could be made for linear or weakly-branched molecules, such as samples G19 or G7. The difference between stress relaxation modulus of linear and long-chain branched molecules increases systematically with relaxation time. A direct comparison between the G(t) modulus for blend M and graft G4, having nearly identical compositional and structural parameters, provides the best evidence of the role the long-chain branching can play in slowing down the relaxation process.

Figure 7-33. Stress relaxation modulus - composite plot; DSR {TEST2}.



The entire spectrum of graft architectures can be categorized into several types, each having a distinct combination of branch length and branching number (Table 7-11). For grafts with branches longer than a certain minimum length, the following types of branching structures can be distinguished, with a representative sample given for each type.

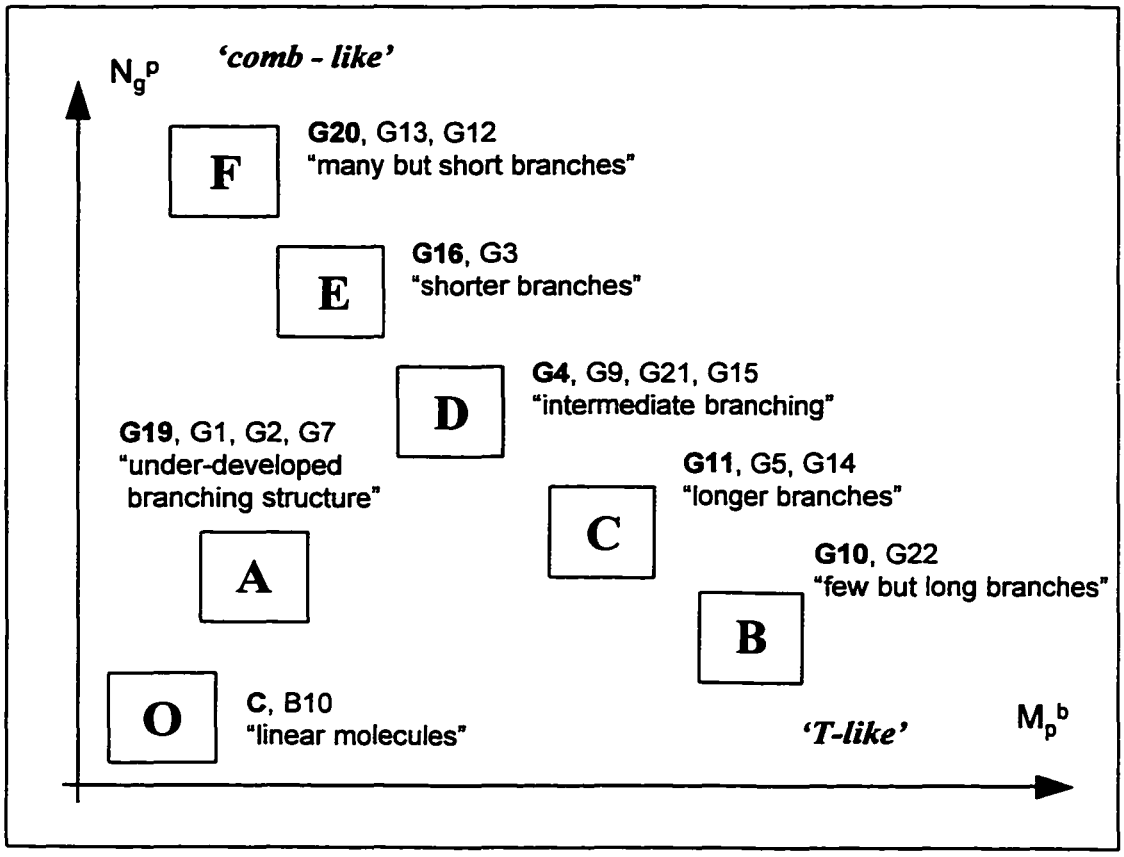
Table 7-11. Classification of LCB structure in CIIR-g-BR copolymers.

type of branching structure	description	example (M_p^b / N_g^p)
- type A -	grafts with 'few & short' branches,	**G19** (10,300 / 1.2)
- type B -	grafts with 'few but long' branches,	**G10** (157,000 / 0.6)
- type C -	grafts with 'longer' branches,	**G11** (46,000 / 2.3)
- type D -	grafts with 'intermediate' branching structure,	**G4** (29,300 / 3.1)
- type E -	grafts with 'shorter' branches,	**G16** (2 0,000 / 4.8)
- type F -	grafts with 'many but short' branches,	**G20** (10,000 / 11.0)

Figure 7-34 illustrates this classification which allows for a qualitative but quick analysis of trends in the rheological behaviour of graft copolymers, in terms of branching structure.

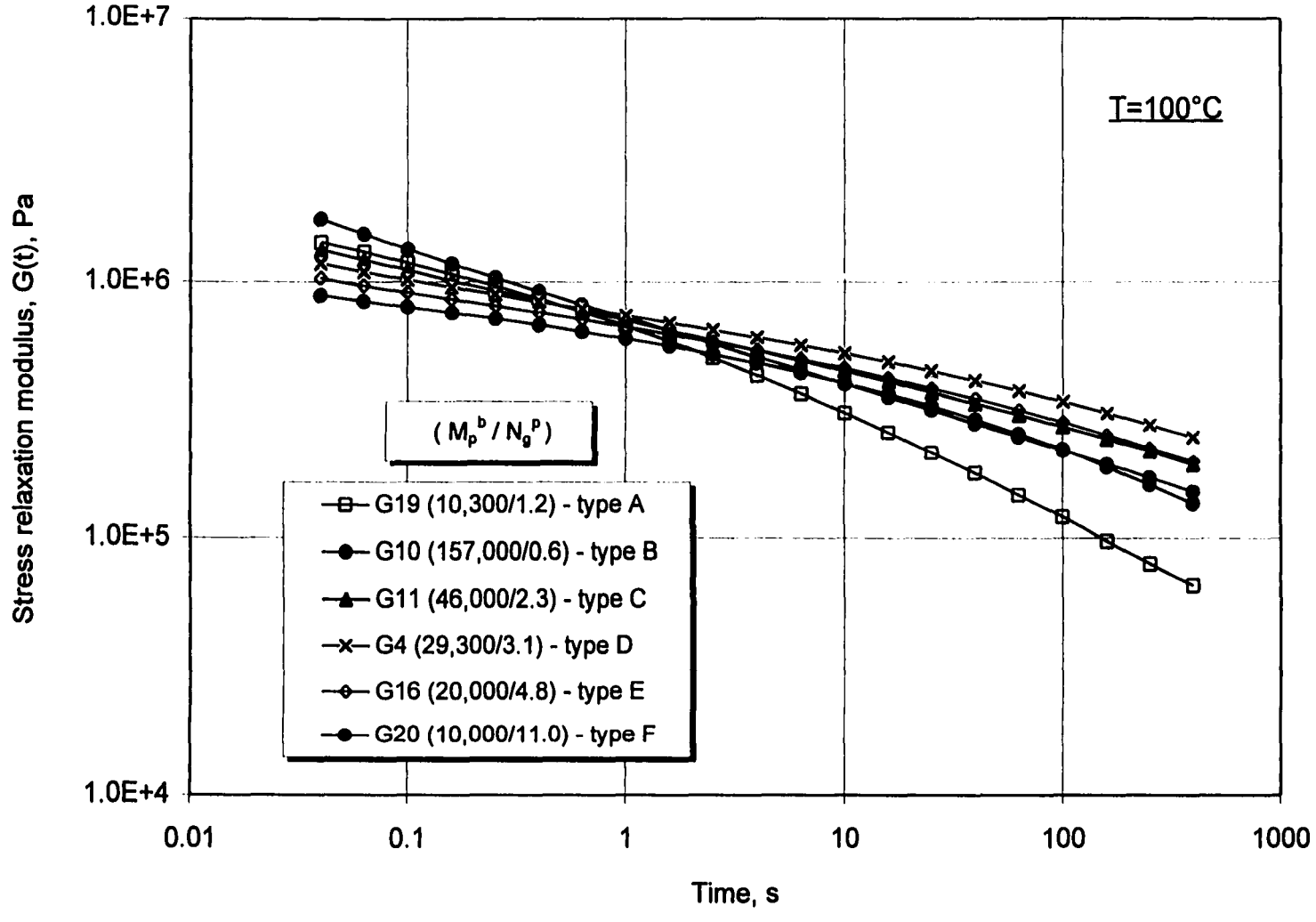
The stress relaxation function, G(t) for representative samples is shown in Figure 7-35. By comparison with the previous graph, it is clear that their behavior covers all extremes, as well as intermediate stress relaxation characteristics. At short relaxation times, 0.1s or less, modulus G(t) decreases in the exact sequence as branching number is increasing. The slope of the relaxation curves tends to increase at somewhat longer times, in the order of 1 second, with the exception of the sample with very long branches (sample G10), for which the time at which "accelerated" relaxation is noticeable, is presumably beyond the maximum relaxation monitoring time of the experiment (400s).

Figure 7-34. Classification of the main types of LCB structure in CIIR-g-BR samples.



Analysis of the relationship between the characteristic time when this occurs, the slope of the relaxation curve at 400s and the branching parameters suggests a strong role of the branch length in shaping the G(t) curve at longer relaxation times. A pair of samples G11 and G16, having "complementary" branching parameters (in Table 7-11), makes for an interesting comparison (Figure 7-35).

Figure 7-35. Stress relaxation modulus - DSR {TEST2}, T=100°C.



Initially, the modulus corresponding to sample G11 is higher and the G(t) has a higher slope than that for sample G16. This is consistent with sample G11 having fewer branches. This configuration leads to the cross-over of G(t) curves, which actually occurs within the first few seconds of the relaxation process. As relaxation progresses, the function describing this process, G(t), decreases more slowly for sample G11, due to longer branches being increasingly more effective in slowing down relaxation at longer times (even if relatively few of them exist). This leads to the imminent second cross-over of the relaxation curves, which for samples G11 and G16 is just beyond the test monitoring time at test temperature - Figure 7-35.

Analogous behavior is observed for samples G20 and G10. Moduli and slope differences at low relaxation times are even more pronounced, in line with more dramatic differences in specific branching parameters (M_p^b, N_g^p) and the second cross-over occurs at ~100s, due to larger difference in branch length between samples G10 and G20, as compared with the previous case.

Samples G19 and G20 have branches of the same length but branching numbers which are almost at the opposite ends of the range. Again, relaxation at short observation times follows a pattern as described previously but the slope of G(t) at the longest (monitored) times is comparable for both samples, which is consistent with identical length of the branches, considered as a controlling factor.

In the long term, grafts with intermediate branching parameters (for example in sample G4) relax slowest, while branched structures with few, short branches (sample G19) relax fastest. These observations are intuitively obvious and fully consistent with the linear stress relaxation results, reported in sections 6.4 to 6.6 of the chapter 6.

A direct comparison between branch length and stress relaxation modulus, G(t), at comparable branching number, is shown in Figure 7-36. While initial relaxation modulus is comparable for all samples, its value at longer observation times becomes increasingly more dependent upon branch length. It increases with branch length when compared at constant branching number.

More detailed correlations between stress relaxation parameters and LCB will be discussed in the next section, devoted to the normalized stress relaxation modulus, nG(t).

Note on integrity of test results

Stress relaxation modulus G(t), can be conveniently used to demonstrate the integrity of {TEST2} test configuration. This was achieved by comparing the results for two pairs of samples (G15 & G21, and G13 & G20), each sample nominally different but within a given pair, incidentally having both specific branching parameters nearly identical. Agreement between corresponding results, shown in Figure 7-37, are judged to be very good. Slight vertical translation of the G(t) curves observed for samples G15 and G21 could be partially due to small difference in branching number.

In fact, such a close agreement of the rheological data, confirmed also in other tests, reflects positively on the reliability of characterization of the structural parameters, as well.
(Data presented in Figure 7-37 were the average values from several test runs per sample).

Figure 7-36. Effect of branch length on the stress relaxation modulus at low branching numbers - DSR {TEST2}.

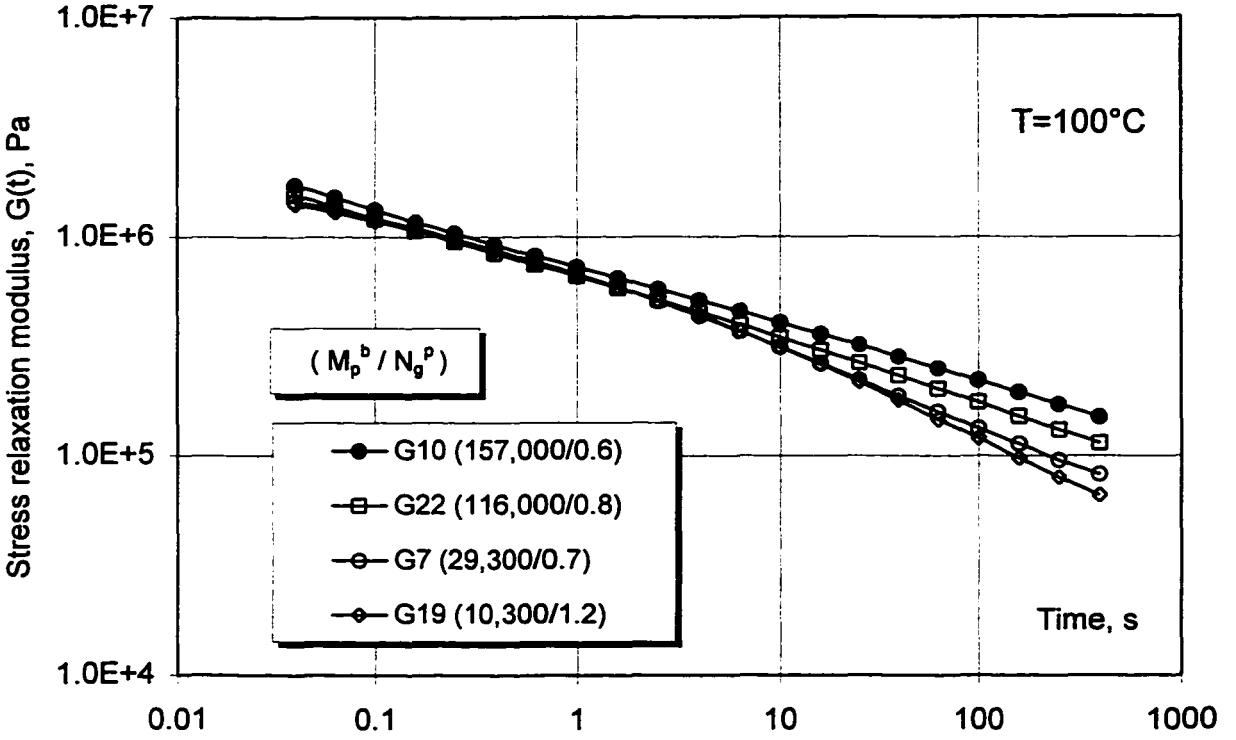
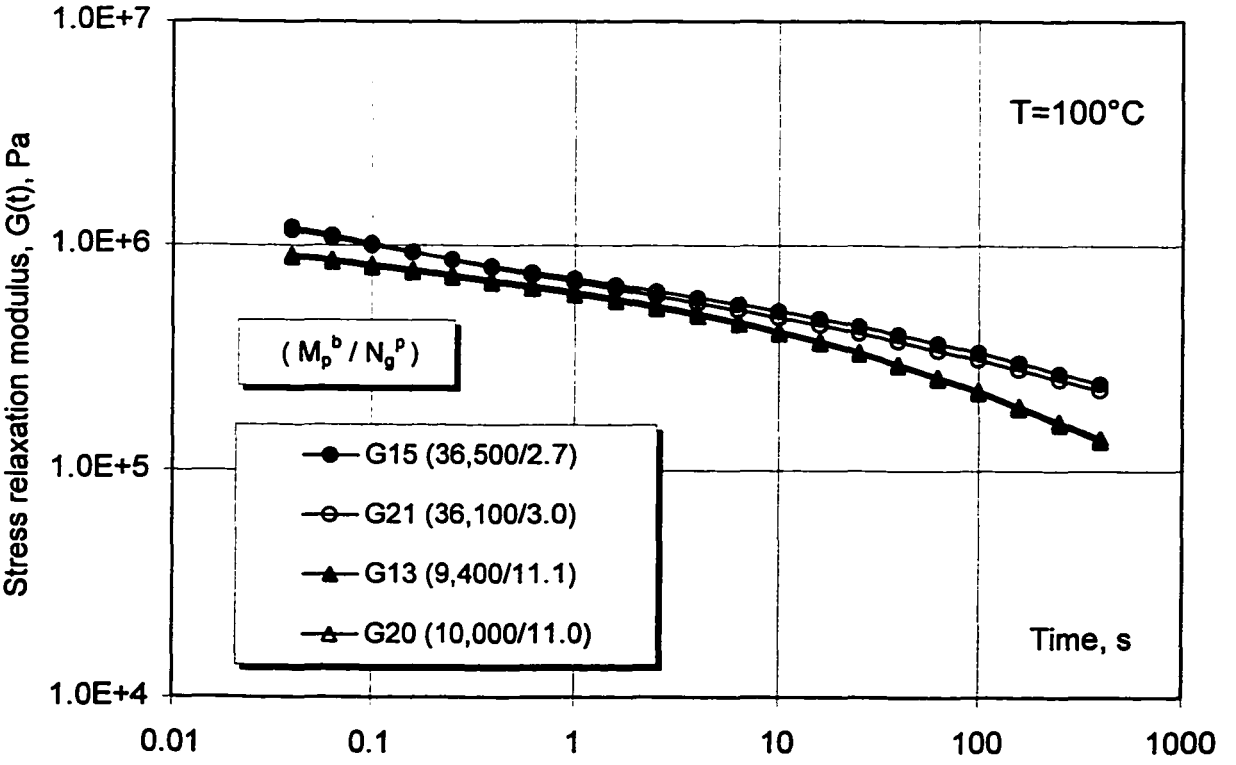


Figure 7-37. DSR {TEST2} - evidence of test results integrity.



7.4.2 Normalized stress relaxation modulus, nG(t)

Interpretation of nG(t) profiles in terms of branching structure

The normalized stress relaxation modulus, nG(t) introduced in section 6.4.1. and defined at the beginning of this section, is a direct derivative of the G(t) function. It can be used to directly characterize *the rate* of stress relaxation, that is to monitor the stress relaxation process irrespective of absolute values of the stress relaxation modulus. An additional benefit of using nG(t) is an improvement in precision and accuracy of data, achieved by a reduction (due to data normalization) of the systematic errors during the measurement of the absolute values of the stress relaxation modulus.

A composite, semi-logarithmic plot of the nG(t), normalized at 40ms after the application of the 'instantaneous' (~4ms) step shear strain, is shown in Figure 7-38. Relaxational behaviour of the samples M (CIIR/BR blend) and G12 (14,000/7.6) - highlighted by a continuous lines - in Figure 7-38 - serve as an envelope for the behaviour of the family of grafts under study. The upper boundary defined by the nG(t) corresponding to sample G12 is only marginally exceeded, at the longest relaxation times, by nG(t) profiles for LCB structures with M_p^b/N_g^p combinations which emphasize the longer branches, for example samples G15(36,500/2.7), G17(47,300/1.6) or G22(116,000/0.8). This confirms an earlier observation that the disentanglement processes involving very long branches, starts to dominate the relaxation process at sufficiently long times.

Fig.7-39 presents an overview of the relaxational behaviour for typical LCB structures, using the normalized stress relaxation function, nG(t). This plot is analogous to that in Figure 7-39, with coordinated graph symbols and the same description regarding the branching structure. Presentation of relaxational data in a form of the normalized stress relaxation modulus seems to emphasize their time-dependence better.

Figure 7-38. Normalized stress relaxation modulus, nG(t); lin-log composite graph - DSR {TEST2}.

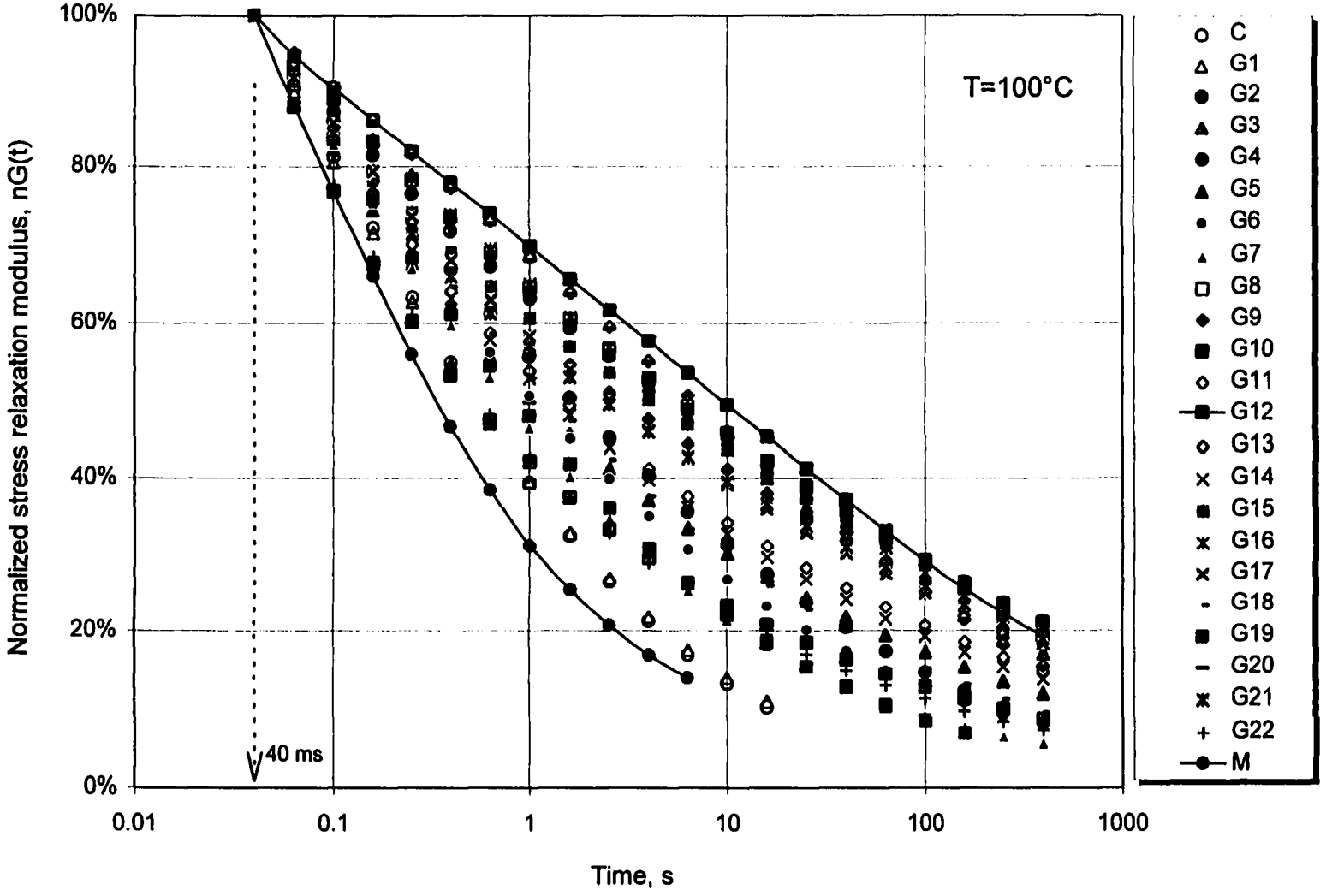
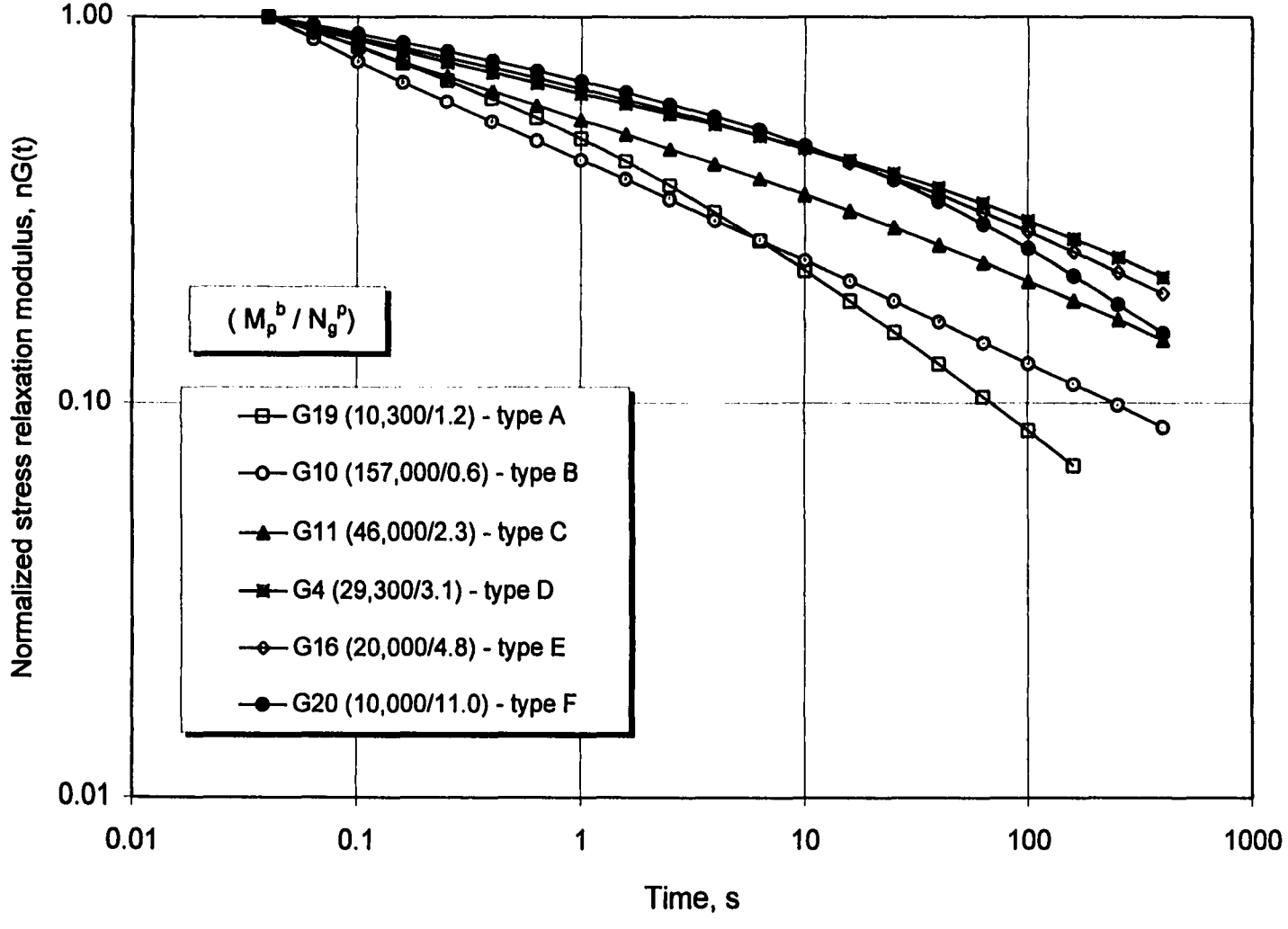


Figure 7-39. Normalized stress relaxation modulus, DSR {TEST2}; Overview of typical relaxational behaviour.



It can be readily inferred from the nG(t) profiles for samples representing the main types of branching structure, that the number of branches "control" the initial (t = ~ 0.1 to 10s) slope of the nG(t) curves and, consequently, their position within the 0.1-10s period (or equivalently, the values of the relevant parameter, for example **nG(1)**). The slope of the nG(t) curves at longer relaxation monitoring times (in order of 100-400 s in this experiment) depends primarily on the length of the branch. The position of the "tail" of the nG(t) curve will be determined in fact by a superposition of contributions from both specific branching parameters.

Effect of branch length

Figure 7-40 illustrates the effect of branch length on nG(t) at a high branching number, N_g^p of 4.5 or above. Generally, progressively increasing branch length is causing nG(t) curves to flatten. The relation between branch length and stress relaxation modulus (normalized or not) is not proportional. Addition of very short branches to linear molecules will not modify their relaxation behaviour significantly, especially regarding time dependence, as can be seen by comparing nG(t) for sample G1(3,000/6.3) and for sample C in Figure 7-40.

Once the average length of the branches exceeds a certain minimum value, its effect on the time dependence of the nG(t) will change rather dramatically - cf. sample G1 versus G2 (7,600/4.5). Further increases of the branch length (even with an associated increase in N_g, which qualitatively will cause a similar effect) are not as "effective" in modification of the relaxation time profiles and "saturation" in the nG(t) - M_p^b plot of the dependence upon the branch length is observed.

Similar relations between branch length and the nG(t) is shown in Figure 7-41 for three samples having similar branching number (N_g^p in the range of 1.2 - 1.6). This additional result allows for some generalization of the M_p^b - nG(t) relationship over a full range of branching frequency.

Figure 7-40. Normalized stress relaxation modulus, DSR {TEST2}; Effect of branch length - I.

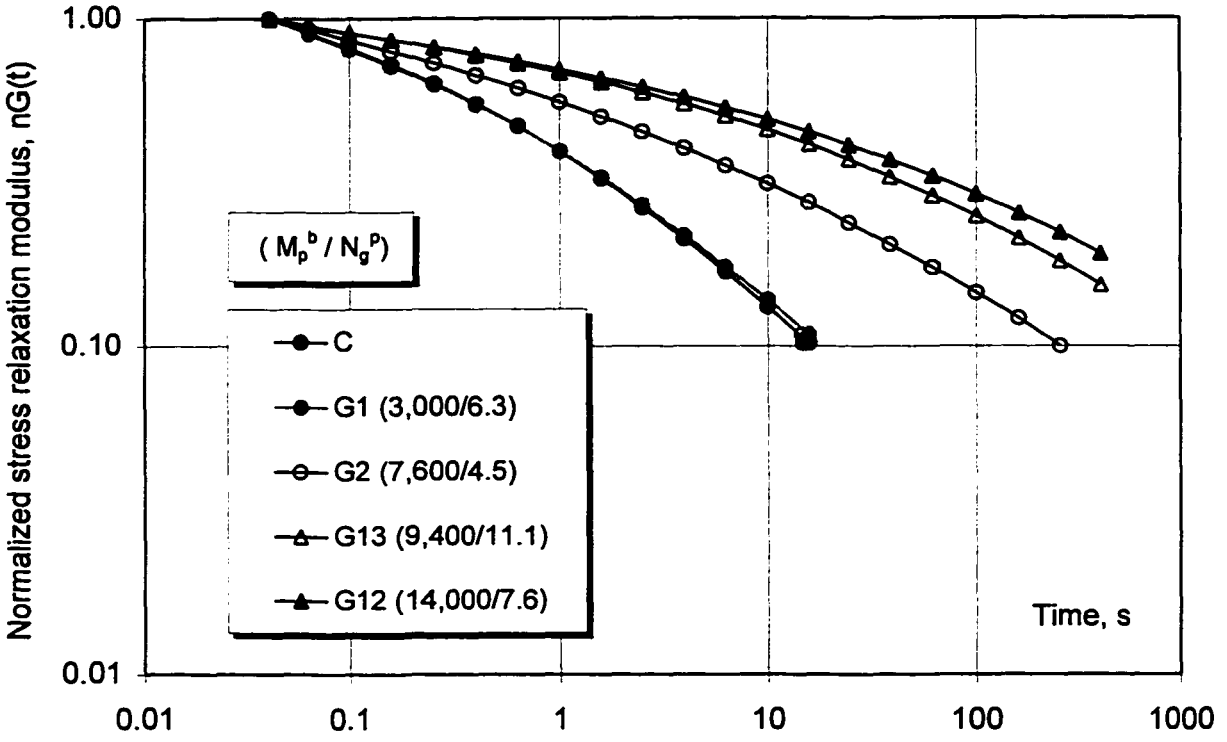
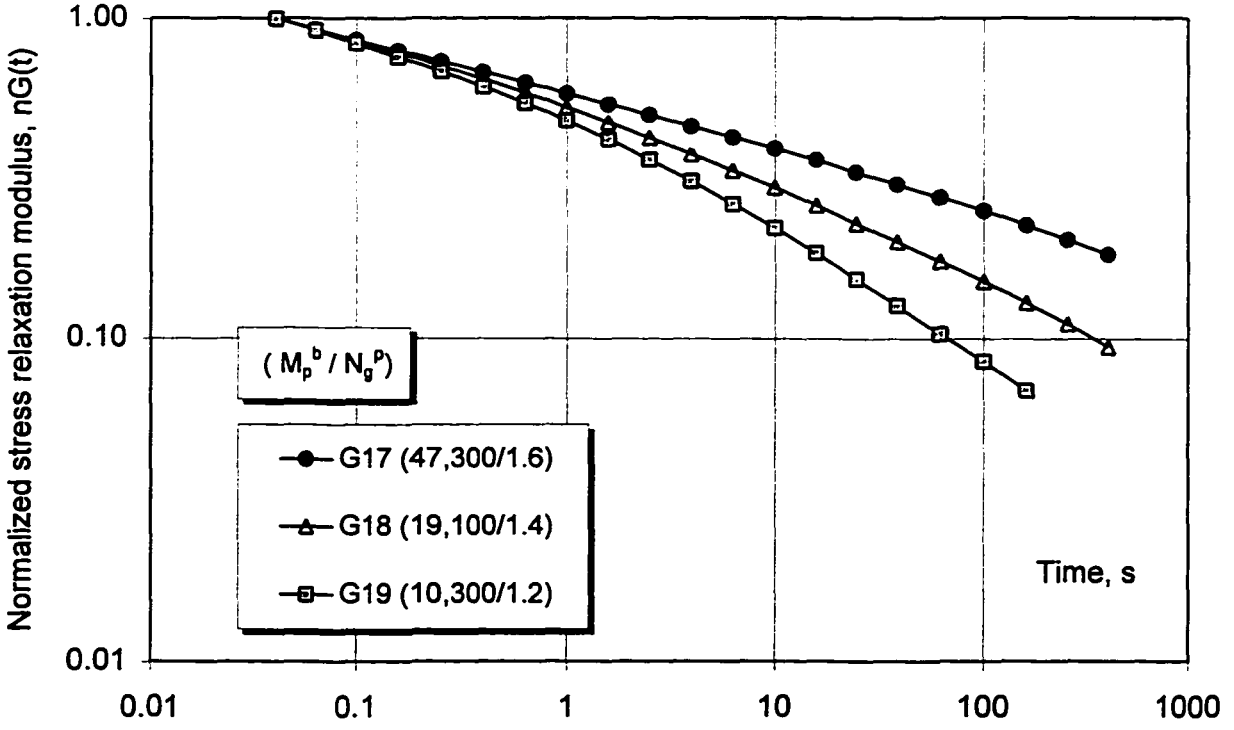


Figure 7-41. Normalized stress relaxation modulus, DSR {TEST2}; Effect of branch length - II.



Effect of branching number

The average number of branches per backbone of the graft has a qualitatively similar effect on nG(t) functions to that exerted by length of the branches. The influence which the branching number has on the nG(t) function for a series of grafts with short branches of comparable length, is illustrated in Figure 7-42. Subsequent figures (Figure 7-43 and Figure 7-44), illustrate further the influence of the N_g on the normalized stress relaxation curves for grafts with longer branches.

The plot in Figure 7-45 was constructed in order to illustrate an important point: it is the specific branching parameters, not overall branching content, $w^{b,g}$, which in this and many other cases, influence the rheological behaviour of comb-type branched polymers. The samples selected for comparison display a broad range of branch length and branching number combinations but have one common characteristic: very similar branching content

Figure 7-42. Normalized stress relaxation modulus, {TEST2}; Effect of branching number - I.

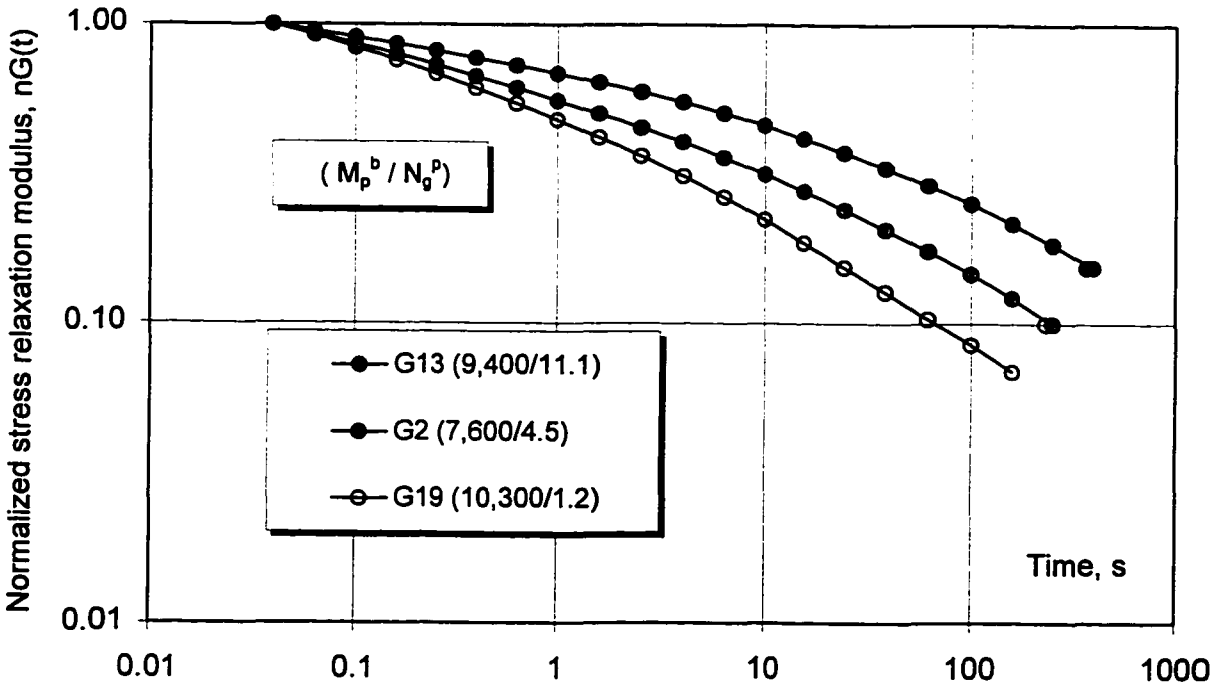


Figure 7-43. Normalized stress relaxation modulus, {TEST2}; Effect of branching number - II.

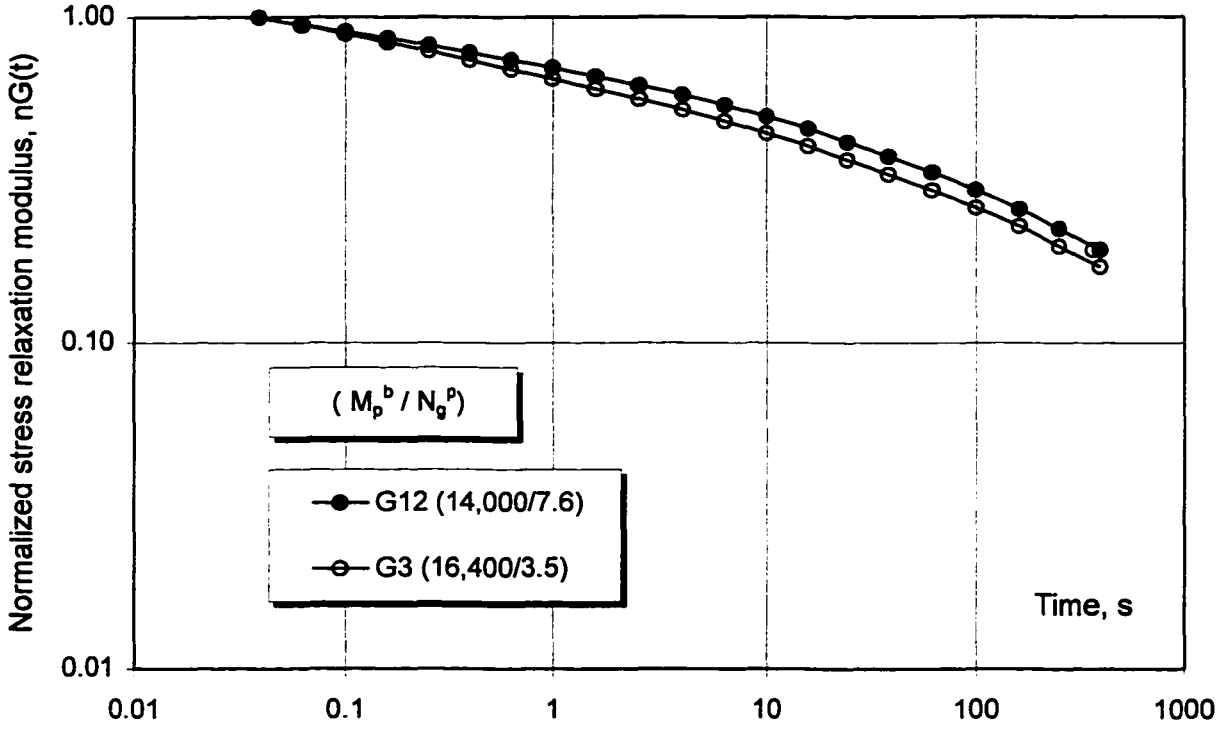


Figure 7-44. Normalized stress relaxation modulus, {TEST2}; Effect of branching number - III.

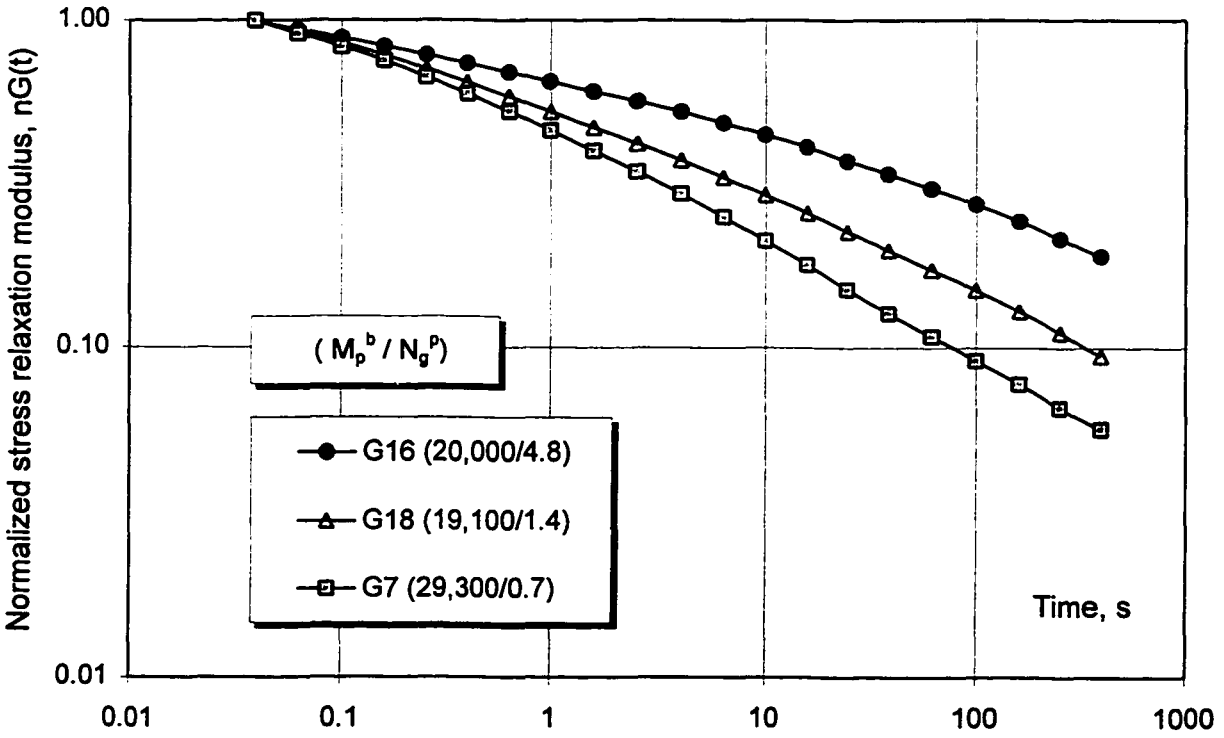
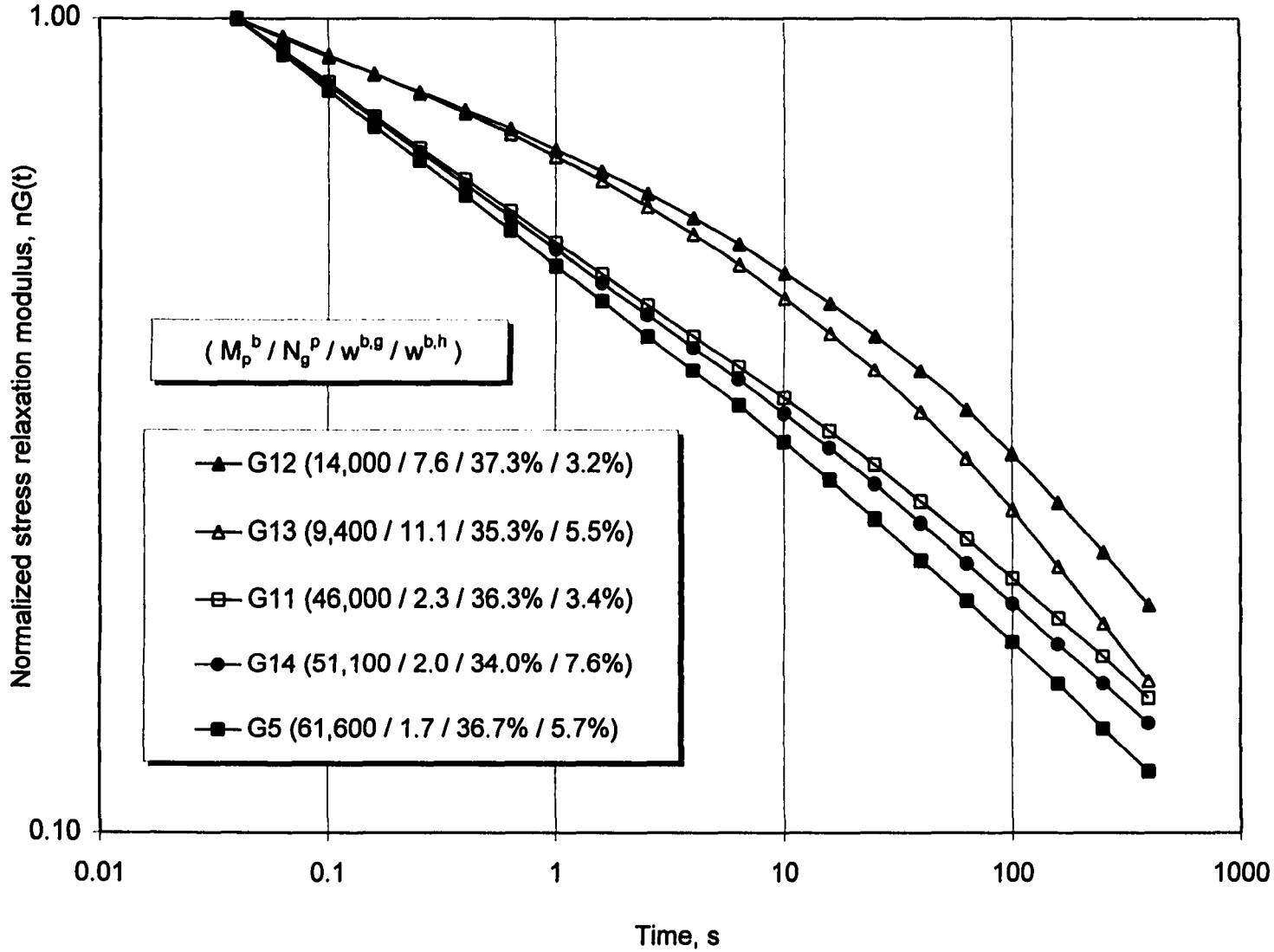


Figure 7-45. Normalized stress relaxation modulus; DSR {TEST2}; Effect of branching parameters at comparable branching content.



($w^{b,g}$ = 34.0-37.3%). Also, the content of the ungrafted polybutadiene, $w^{b,h}$, is comparable. However, significant differences in nG(t) modulus are observed, in spite of the similarity in branching content and chemical composition, among graft samples in Figure 7-45.

*Relations between branching and selected (**G(40ms)** and **G(0.1)**) relaxation parameters*

The relationship between branching structure and stress relaxation can be verified and quantified by plotting corresponding parameters directly.

The graph of the **G(40ms)**, plotted as a function of the branch length, M_p^b, is shown in Figure 7-46. For samples with the $w^{b,g} > 15\%$, a well defined relationship exists between **G(40ms)** and the branch length. This result quantitatively confirms the similar relation observed in Figure 7-36, both predicted by the screening analysis for correlation. Similarly, by plotting **G(40ms)** against branching number, as shown in Figure 7-47, a definite trend can be identified.

It can be concluded, based on the above analysis and the corresponding prediction profiles, that parameter **G(40ms)**, representing instantaneous modulus after a sudden application of large-amplitude shear strain, increases with branch length and decreases exponentially with the number of branches.

Normalized stress relaxation modulus at t=0.1s, e.g. **nG(0.1)** can be used as a measure of the average slope of the nG(t) for 40-100ms range. Parameter **nG(0.1)** decreases (corresponding to the nG(t) slope increase) exponentially with increasing branch length (Figure 7-48). Similarly to the **G(40ms)** - M_p^b relationship discussed earlier, samples with $w^{b,g} < 10\%$ do not fit this relation.

When **nG(0.1)** is plotted against branching number, it increases logarithmically and reaches a certain plateau (Figure 7-49). Sample G2 and more so sample G1 do not fit the trend probably due to insufficient length of their branches, as argued earlier.

Figure 7-46. Relationship between branch length and G(40ms) modulus.

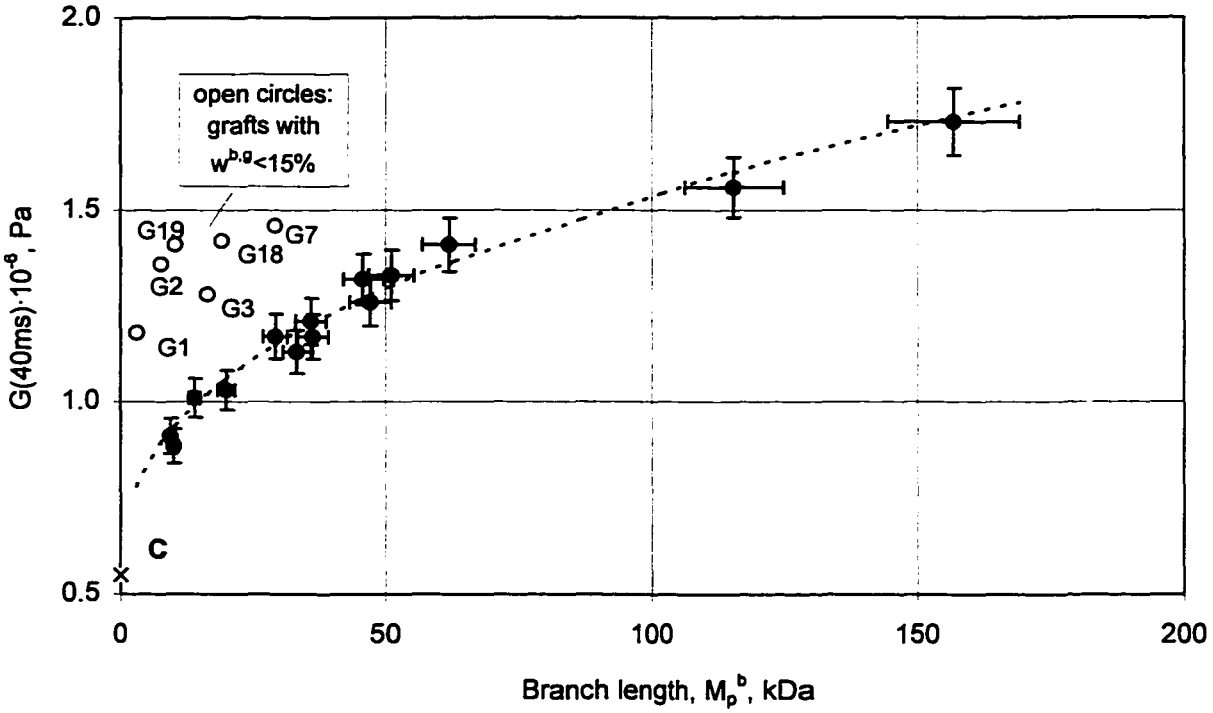


Figure 7-47. Relationship between number of branches and G(40ms) modulus.

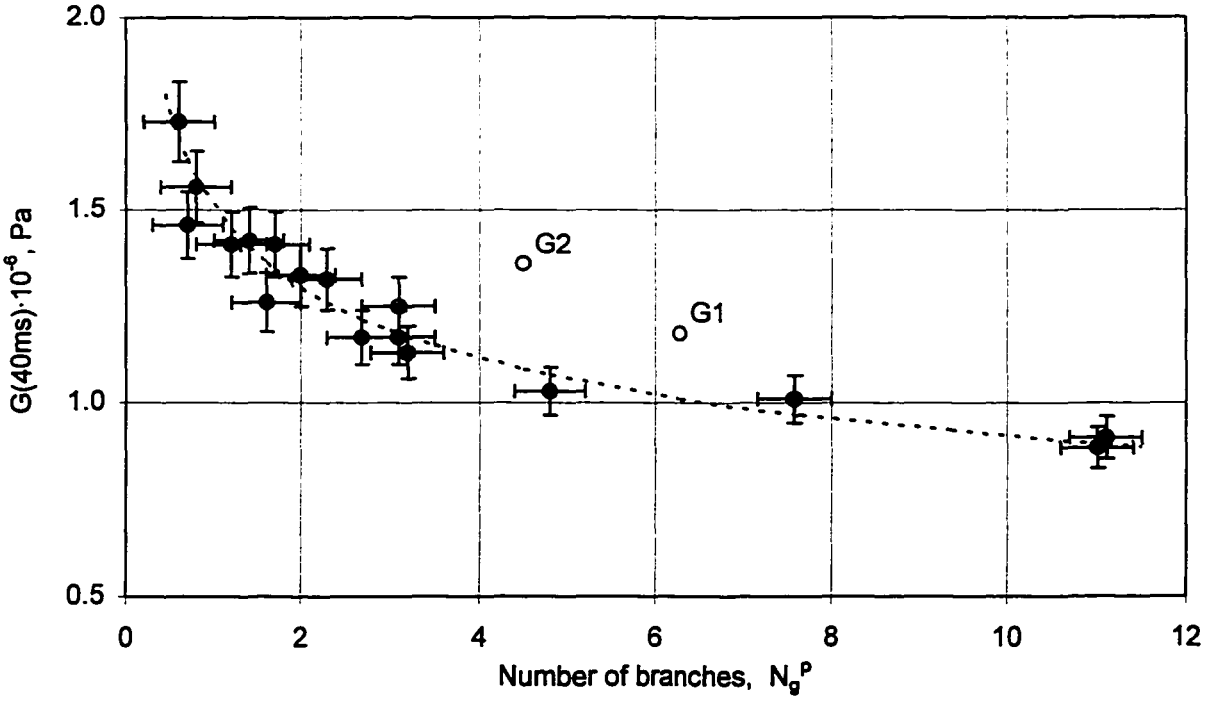


Figure 7-48. Relationships between length of the branches and normalized stress relaxation modulus, nG(0.1).

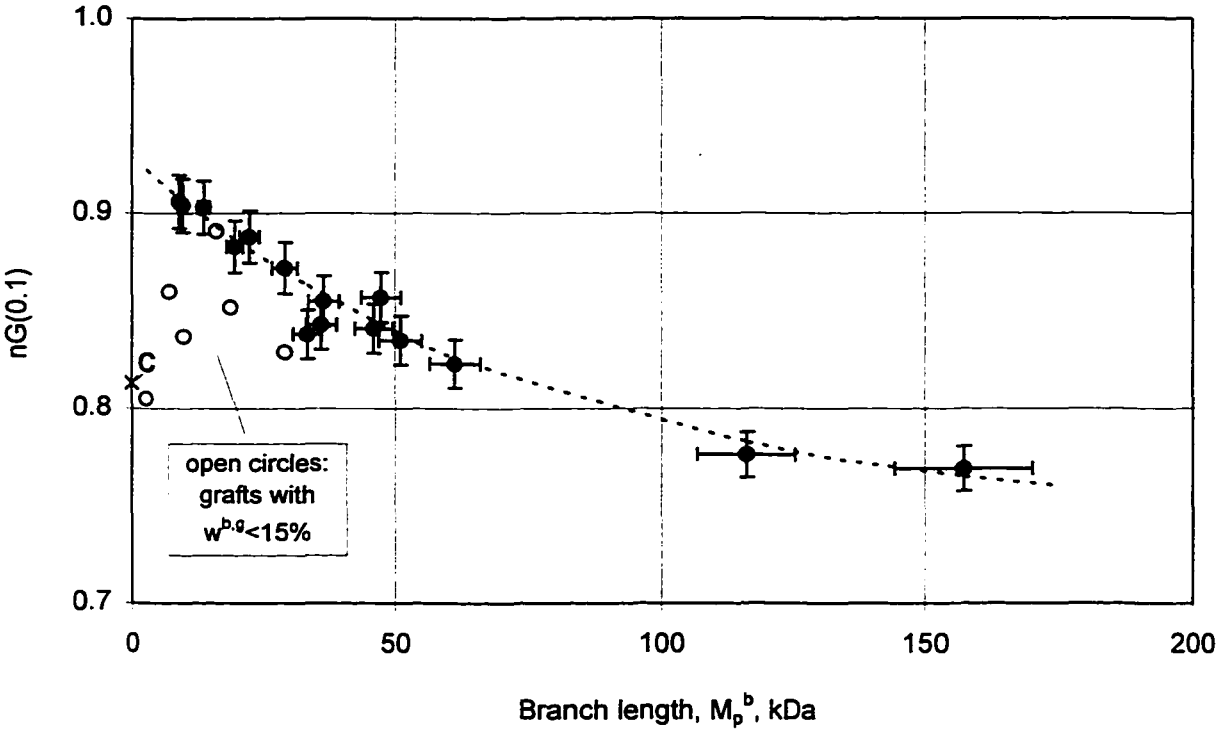
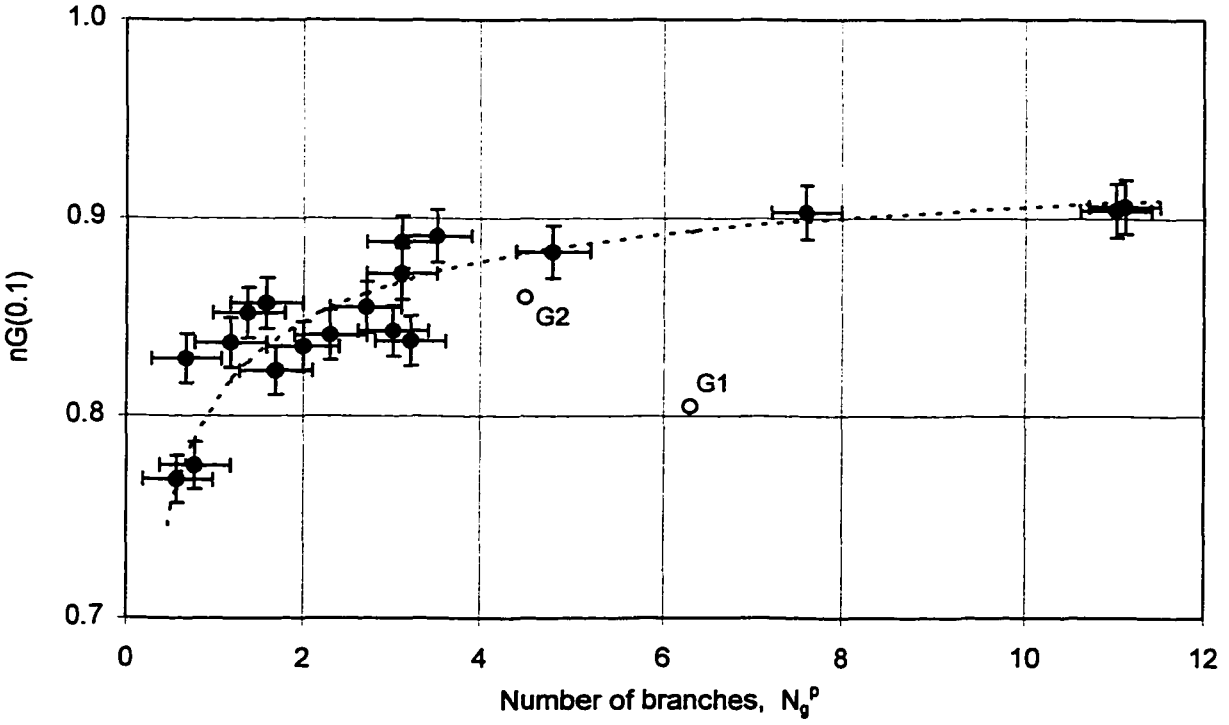


Figure 7-49. Relationship between number of branches and normalized stress relaxation modulus, nG(0.1).



7.5 Normalized Cole-Cole plot and its interpretation in terms of the LCB parameters

The concept of the normalized Cole-Cole plot (nC-C) has been introduced in section 6.1.4 of the Chapter 6.

Normalized Cole-Cole plots were found useful for characterization of long-chain branching, and particularly, for the identification of the type of branching structure present in commercial elastomers [368].

A normalized Cole-Cole plot is composed of the $G''(\omega)/G''(\omega_{ref})$ versus $G'(\omega)/G'(\omega_{ref})$ curve, referred to later as a contour of the nCC plot, and a diagonal line which the locus of points satisfying the $G''(\omega)/G''(\omega_{ref}) = G'(\omega)/G'(\omega_{ref})$ condition. All nC-C plots discussed in this section are based on data obtained during isothermal, non-linear stress relaxation, which were transformed into a dynamic domain (frequency dependent) using the "Yagii-Maekawa" transformation, described in more detail in section 5.5.1 of the chapter 5.

In terms of physical significance, the nC-C contours depict the mutual frequency-dependence of the independently normalized dynamic moduli, measured at constant temperature and compared within a strictly defined frequency range.

Stress relaxation was monitored over a (40ms-400s) interval, corresponding to the frequency range of 5 to 0.005 rad/s. The highest frequency in the range was selected as the reference frequency (ω_{ref}) for normalization purposes. By definition, nC-C contour always starts at the point (x=1, y=1), upper right corner of the nC-C square and the contour progresses along a certain path, usually toward the origin of the system of coordinates. The normalization of the moduli, necessary to create the nC-C plot, decreases the influence of the MW and MWD on the contour in the modified C-C plots, while increasing its sensitivity to the type of LCB structure.

Overview of nC-C contours

Distinct shapes and orientation of nC-C contours appear to be unambiguously related to their LCB branching structure. The following first six figures, Figure 7-50 to Figure 7-55, illustrate how the various shapes of nC-C contours reflect different types of branching architectures, related to certain combinations of the specific branching parameters, M^b and N_g.

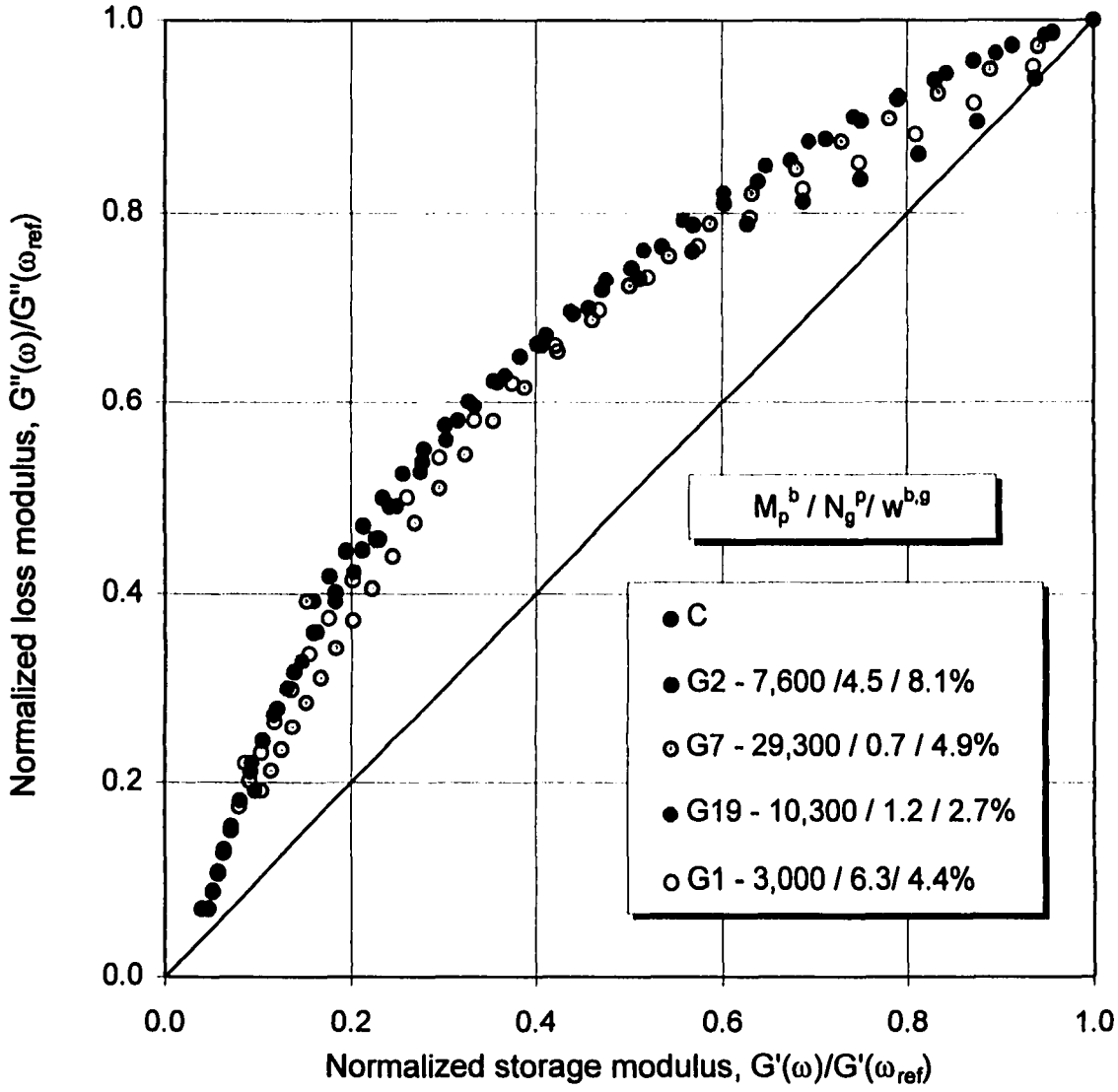
For polymers made of linear molecules (like sample C) or grafts with branching content below a certain limit ($w^{b,g}$ about 10% or less), the shape of the nC-C contour has a convex (crescent-like) shape as shown in Figure 7-50. This category includes grafts either with very short branches (sample G1), a few short branches (sample G19), or very few branches of intermediate length (sample G7).

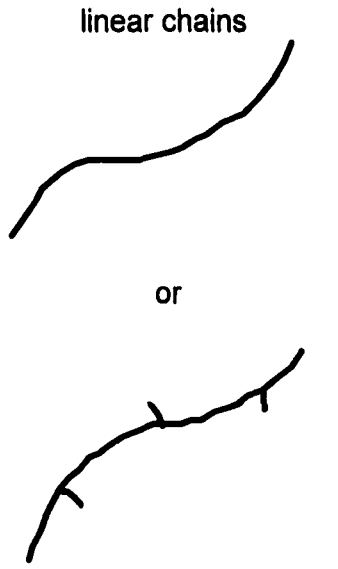
The nC-C contour for samples with few but very long branches, resembling star-like molecules, are shown in Figure 7-51. Contours are stretched along a diagonal, reflecting a very similar frequency dependence of either dynamic modulus over the experimentally examined frequency range.

Samples with short (yet above $M_p^b \sim 8{,}000$) but numerous branches ($N_g^p > 5$) produce nC-C contours with an inflection point which are positioned at the top of the diagram. The nC-C contours for samples G12, G13 and G20, which all meet the above specifications, are shown in Figure 7-52.

For graft samples in which the long-chain branching structure is well developed and balanced, that is they contain branches which have intermediate branching length (~30,000) and branching number (~3.0), the corresponding nC-C contours for representative samples (G4, G9, G15, G21) possess a characteristic "ice-hockey" stick shape, crossing the diagonal from below at a certain angle, as shown in Figure 7-53.

Figure 7-50. Normalized Cole-Cole plot - contours for LCB, type A {TEST2}, T=100°C

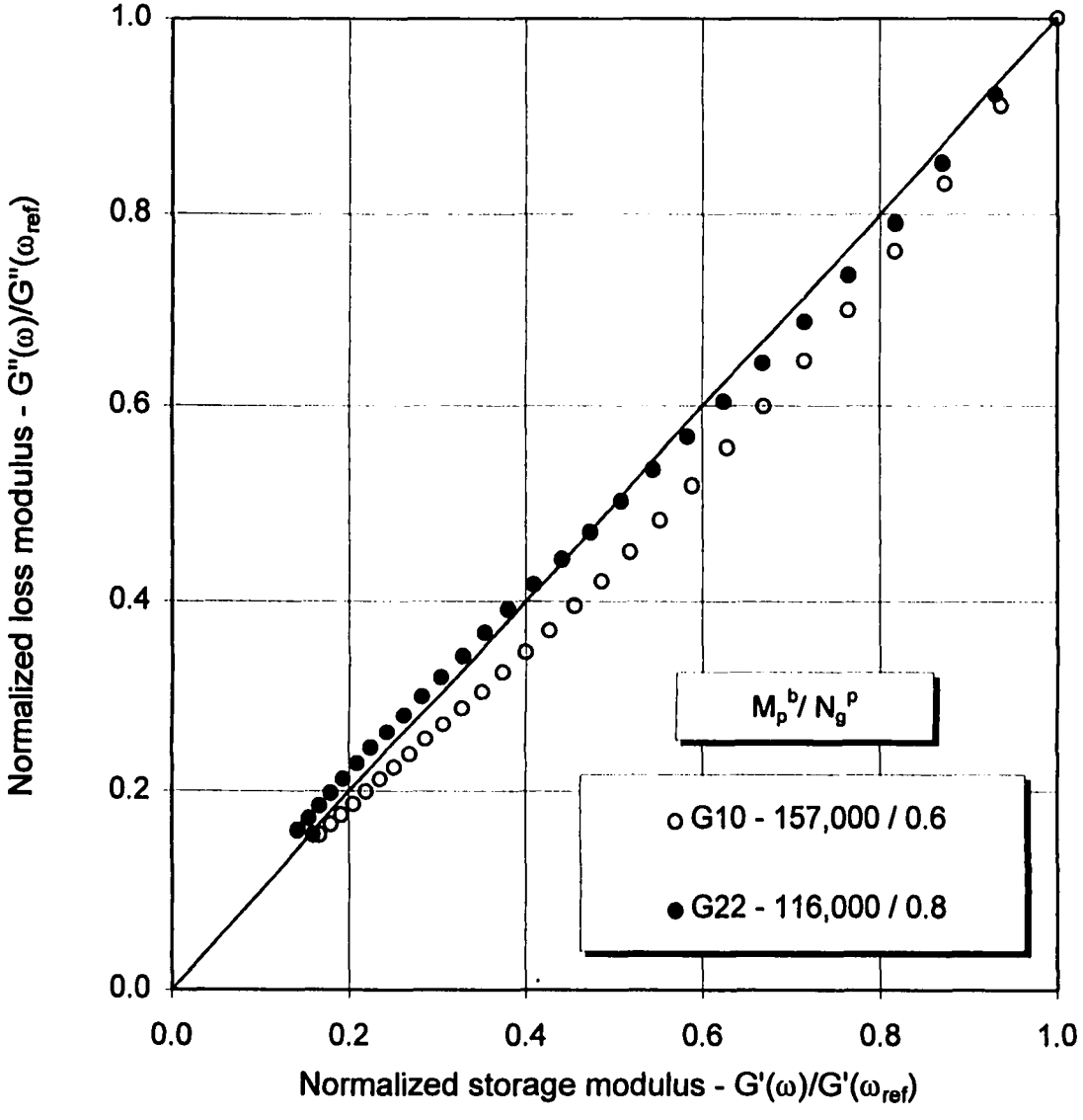


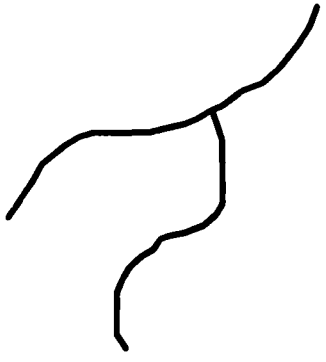


branched, with very short (M_p^b < 12,000) or very few (N_g^p < 1) branches

$w^{b,g}$ < 10%

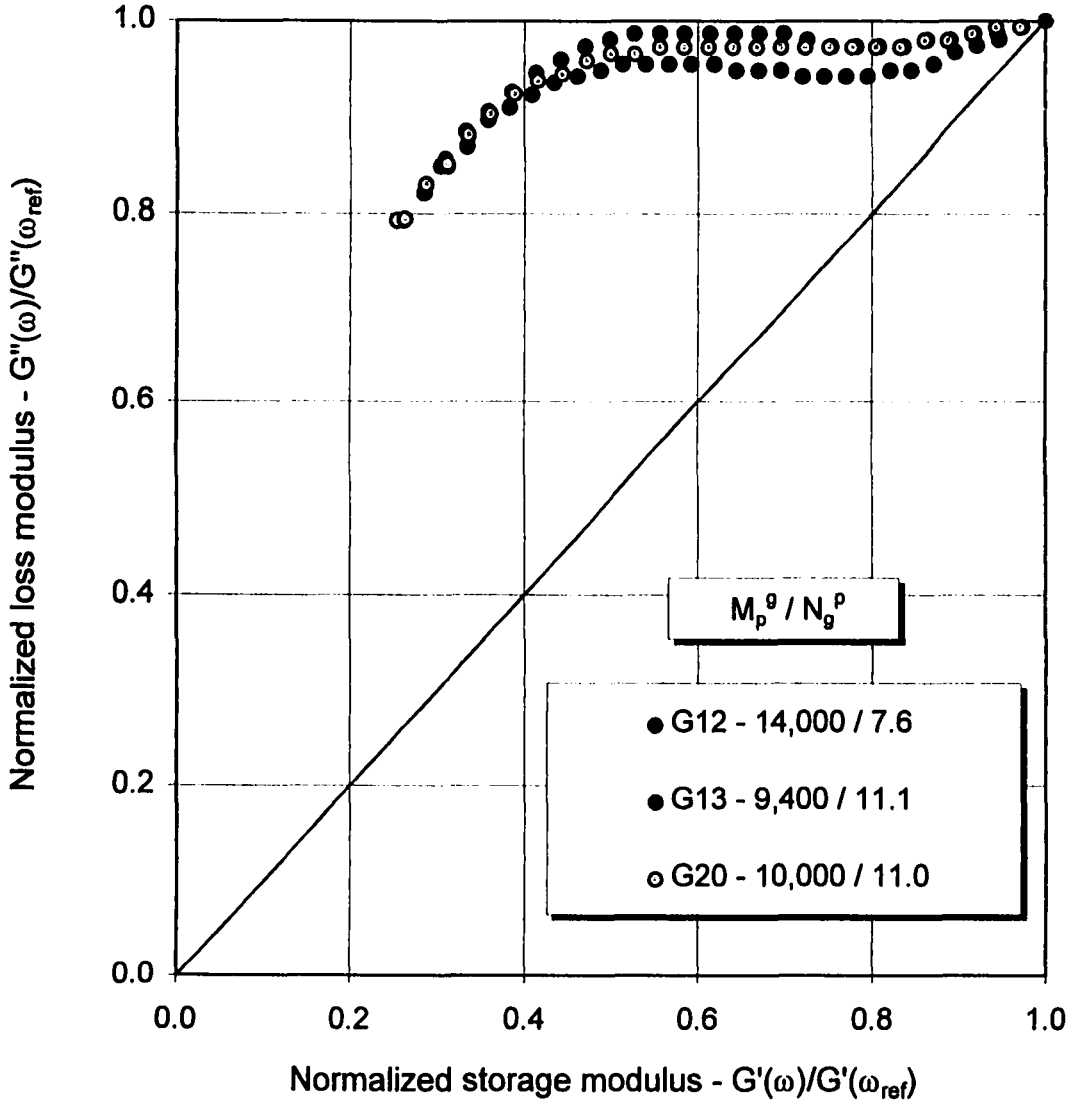
Figure 7-51. Normalized Cole-Cole plot - contours for LCB, type B {TEST2}, T=100°C

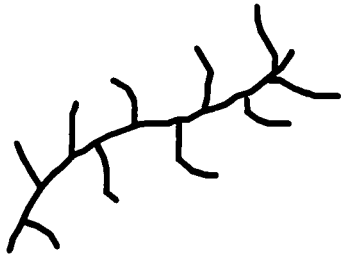




branched with a few ($N_g^p < 1.0$) but long branches ($Mp^b > 100,000$)

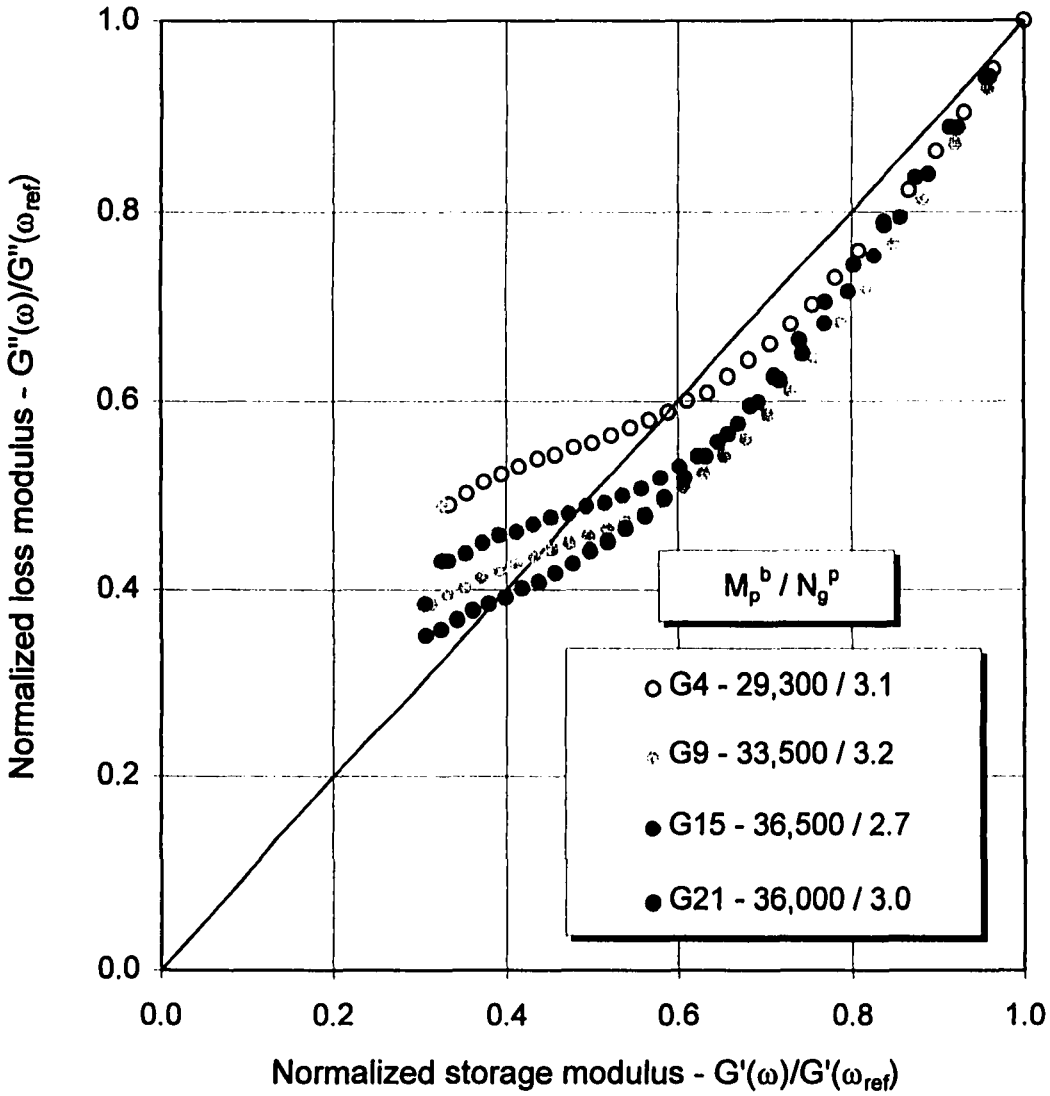
Figure 7-52. Normalized Cole-Cole plot - contours for LCB type F {TEST2}, T=100°C

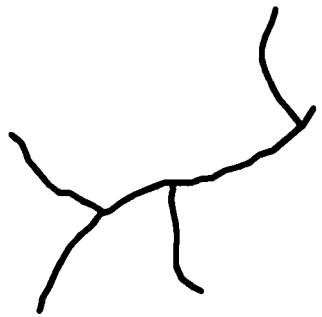




branched with numerous ($N_g > 4$) shorter branches ($9{,}000 < M_b < 15{,}000$)

Figure 7-53. Normalized Cole-Cole plot - contours for LCB type D {TEST2}, T=100°C





branched with a combination of a few (N_g^p= 2 - 4) medium length branches (M_p^b = 25,000-40,000)

Two other types of nC-C contour can be identified and related to the branching structure. One is typical for grafts with higher than average branching number (N_g^p=3.1-4.8) but shorter (in M_p^b 16,400-22,800 range) branches - type "E" LCB structure - is shown in Figure 7-54. The second -type "C" is characteristic for grafts with below average branching number (N_g^p =1.6-2.3) but longer branches (M_p^b = 46,000-51,000) and are shown in Figure 7-55.

The apparent ability of nC-C plots to map different types of branching, a task far more challenging than merely relating "branching content" to rheological behaviour, might allow them to be used as a convenient tool to characterize long-chain branching in polymers. In fact, initial studies carried out on several series of commercial elastomers revealed that the distinct shapes of nC-C plot contours can be assigned to different generic types of rubbers [368].

Cole-Cole plots can also be used to follow a systematic variation in a branching structure. Three examples are given below.

Progressively increasing branching content ($w^{b,g}$), realized primarily by increasing the length of branches, is shown in Figure 7-56, to affect the contour length initially, and subsequently also its shape.

In a first stage, (for $w^{b,g}$ up to approx. 10%), the nC-C contour retains its crescent shape but is becoming shorter with increasing $w^{b,g}$, as can be seen comparing the contour shape for the sequence of samples C, G19, and G2, in Figure 7-56. In the second stage, following a further increase in branching content, the shape of nCC contour begins changing and its position moves closer to a diagonal (samples G3, G8). In the final stage, occurring at $w^{b,g}$ of about 20% and above, it straightens and starts "creeping" along the diagonal (samples G17, G5).

Figure 7-54. Normalized Cole-Cole plot - contours for LCB type E {TEST2}, T=100°C

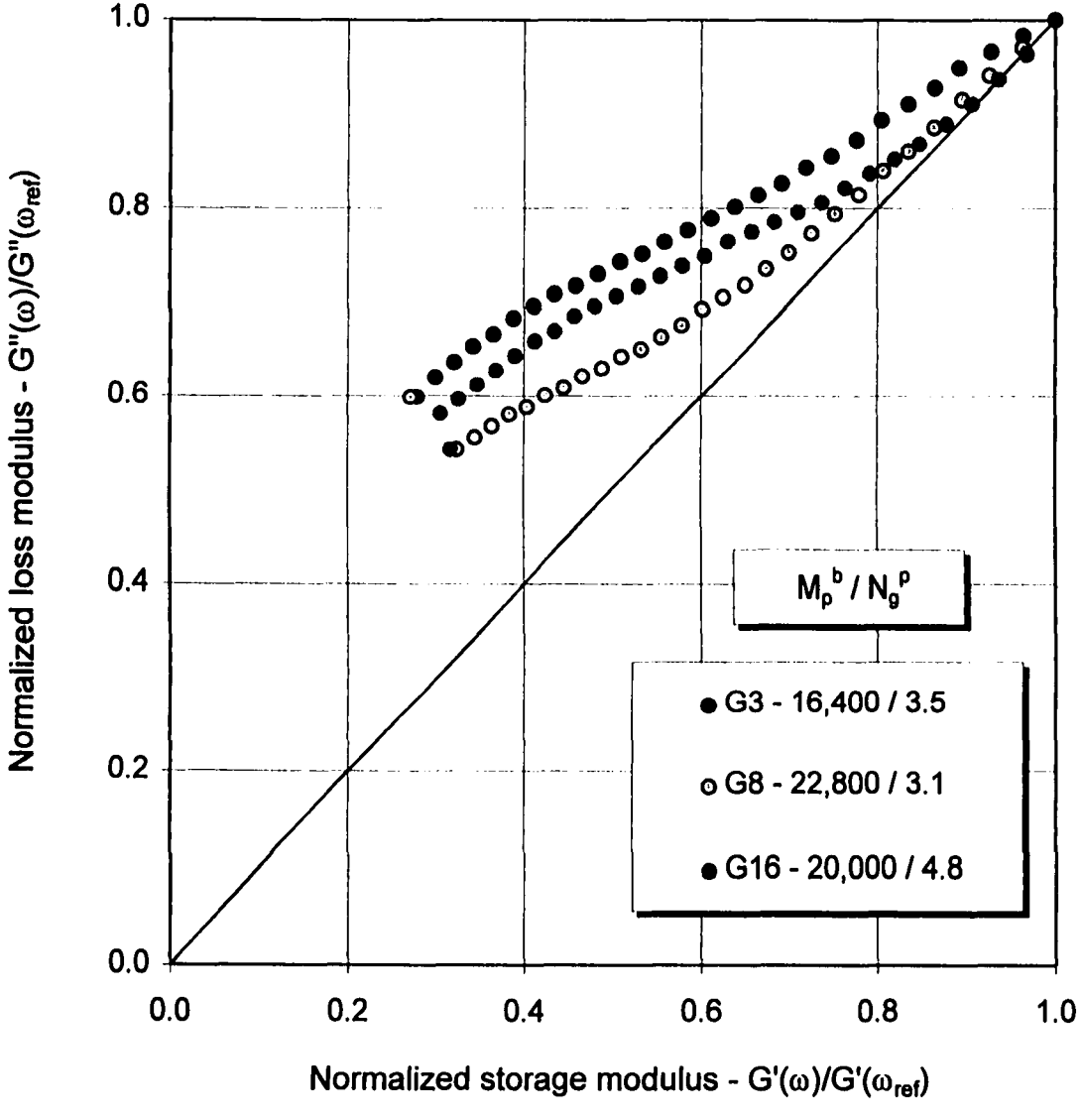


Figure 7-55. Normalized Cole-Cole plot - contours for LCB type C {TEST2}, T=100°C

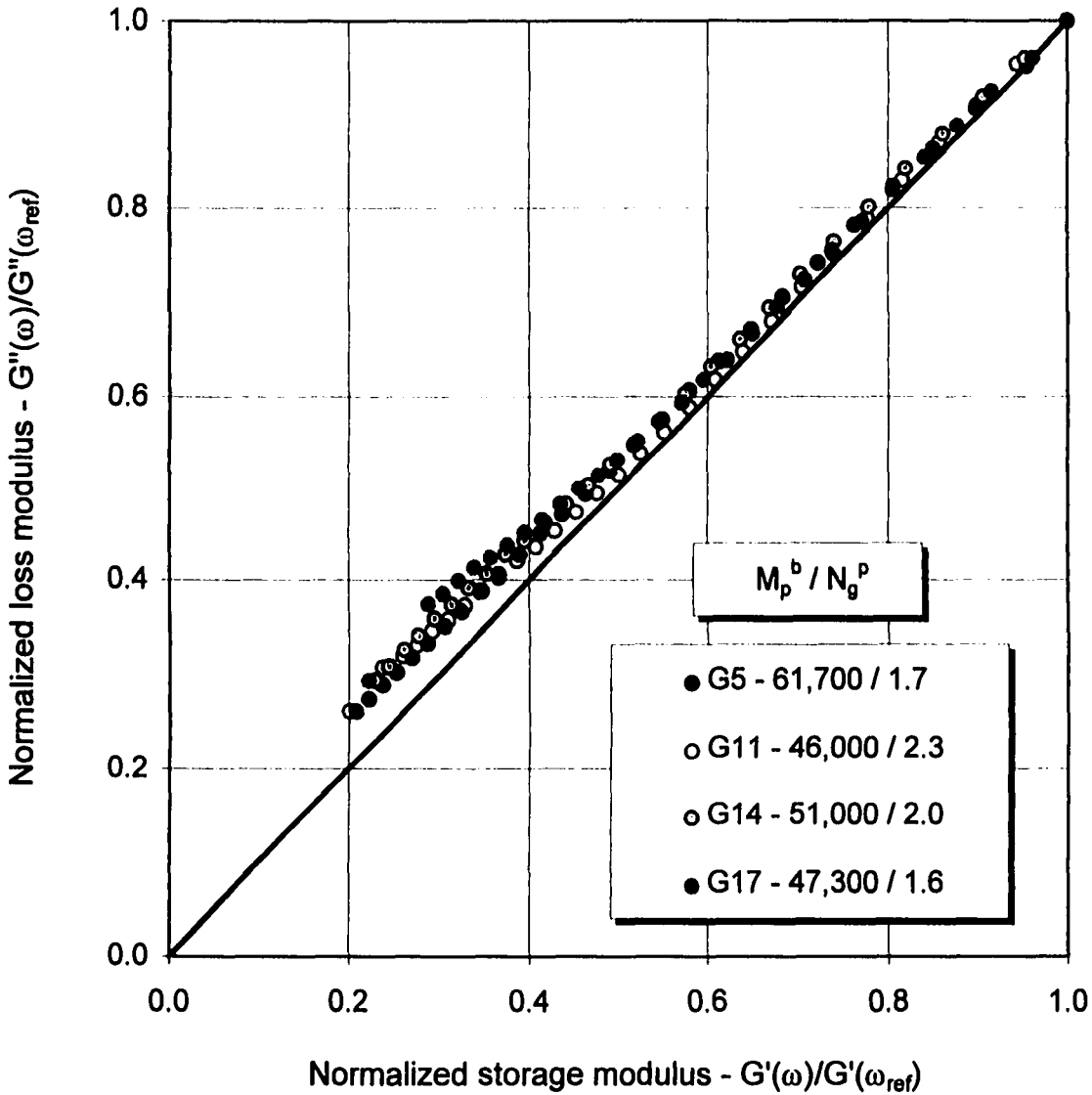
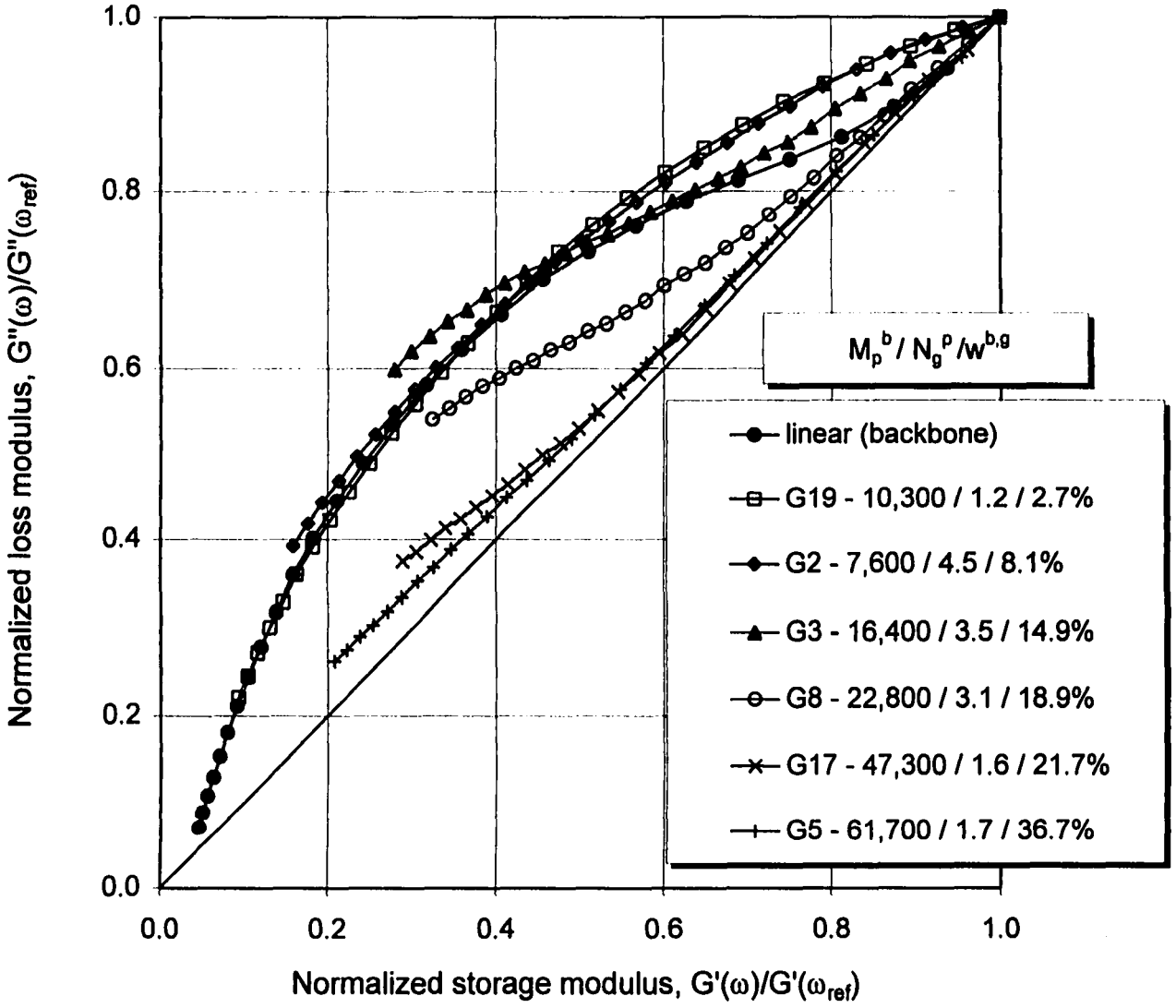


Figure 7-56. Normalized Cole-Cole plot - Effect of increasing branching content, {TEST2}, T=100°C



Another example of systematic change in the nC-C contour with increasing branch length at a comparable branching number, N_g^p = 0.6-1.2, is shown in Figure 7-57. The length of the contour is independent of the branch length. The shape of the contour is changing from convex (G19, G7) to concave (G22, G10).

For a series of grafts having branch length within the 10,000-22,800 range and an increase of the branching number, the nC-C contour elevates above the path established for a linear molecule, and it changes its shape toward that characteristic for samples with a high number of branches (Figure 7-58).

While the branching content ($w^{b,g}$) and chemical composition (w^b) for the series of grafts based on a common backbone are related to both M_p^b and N_g^p, the observed characteristics of the nC-C contour depend on specific branching parameters rather than the chemical composition of the grafts. Figure 7-59 compares 3 grafts, namely G5, G13 and G9, all having nearly identical content of branches ($w^{b,g}$). However, their viscoelastic properties, as reflected by the nC-C plot, are very different, as a result of their dramatically different long-chain branching structure.

A characteristic difference between the rheological properties of a graft copolymer and the equivalent, in terms of its chemical composition and MWD, blend was demonstrated previously. Further proof is seen by comparing the nC-C for the blend M with that of the two grafts, G4 and G15, in Figure 7-60. Again, the nC-C contours (of blend versus grafts) are very different, both in terms of their shape and length. In fact, merely blending CIIR with BR does not affect the shape of the nC-C contour appreciably, as compared with that of sample C.

Figure 7-57. Normalized Cole-Cole plot - Effect of branch length (N_g^p = 0.6 - 1.2)

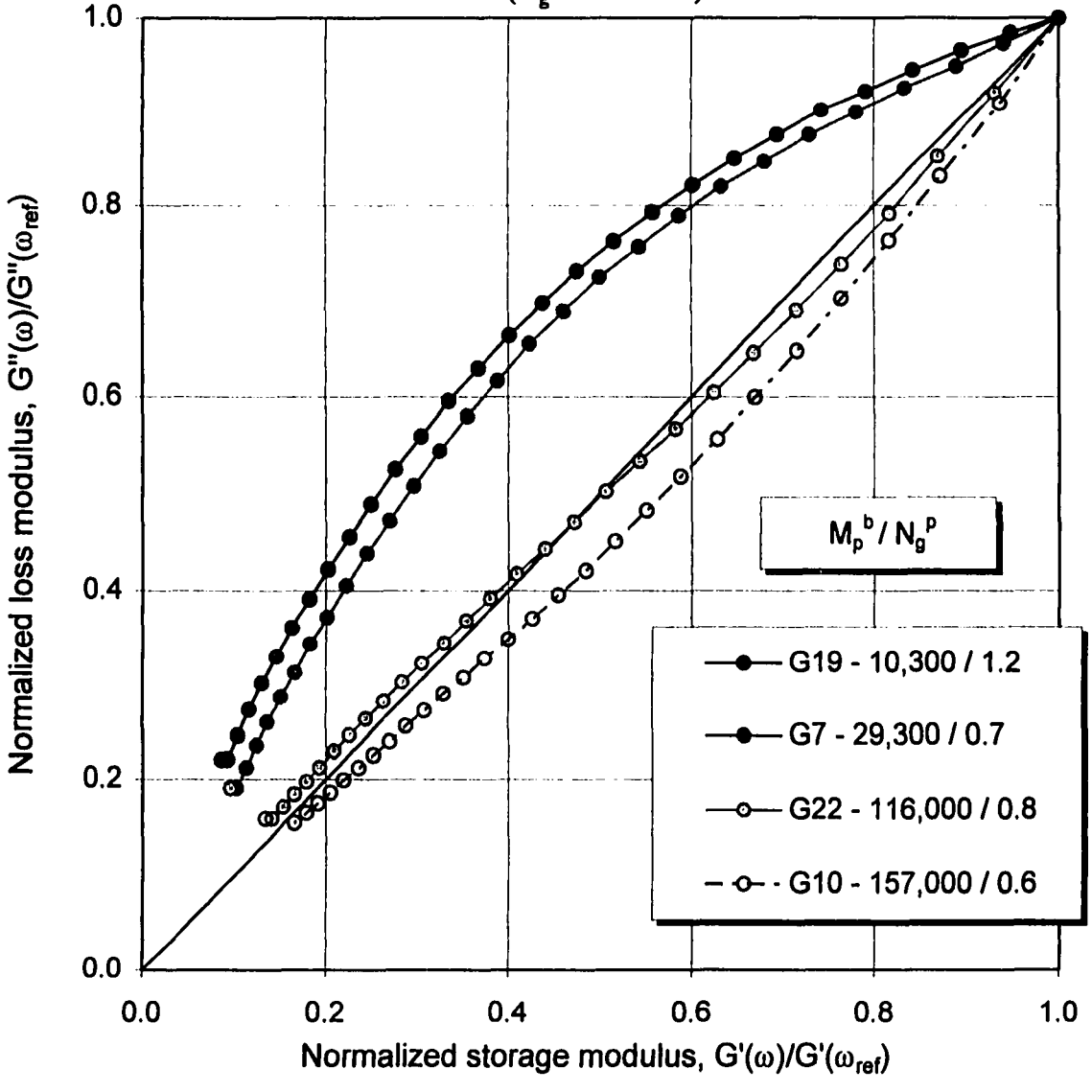


Figure 7-58. Normalized Cole-Cole plot - Effect of branching number (M_p^b = 10,000 - 22,000)

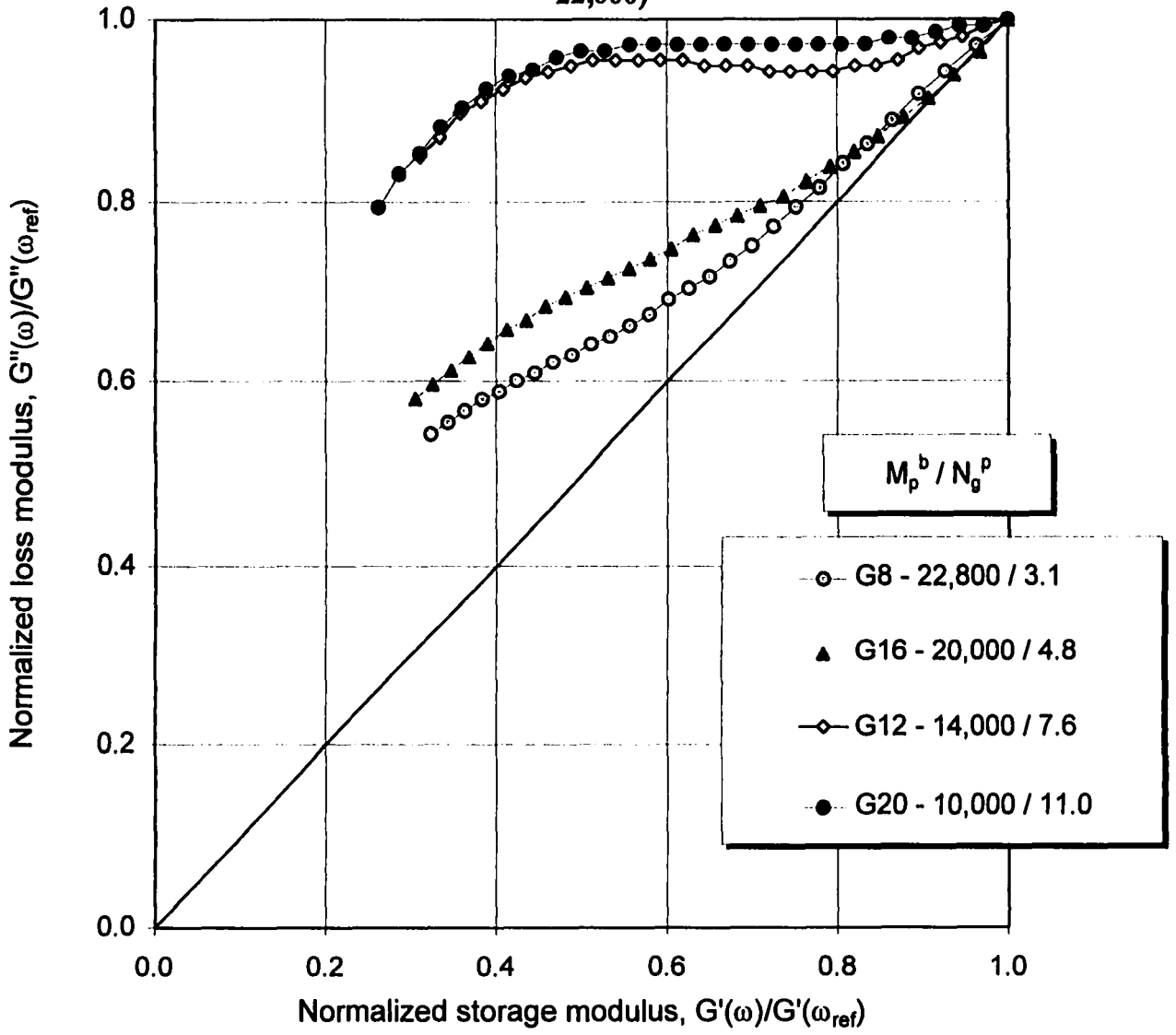
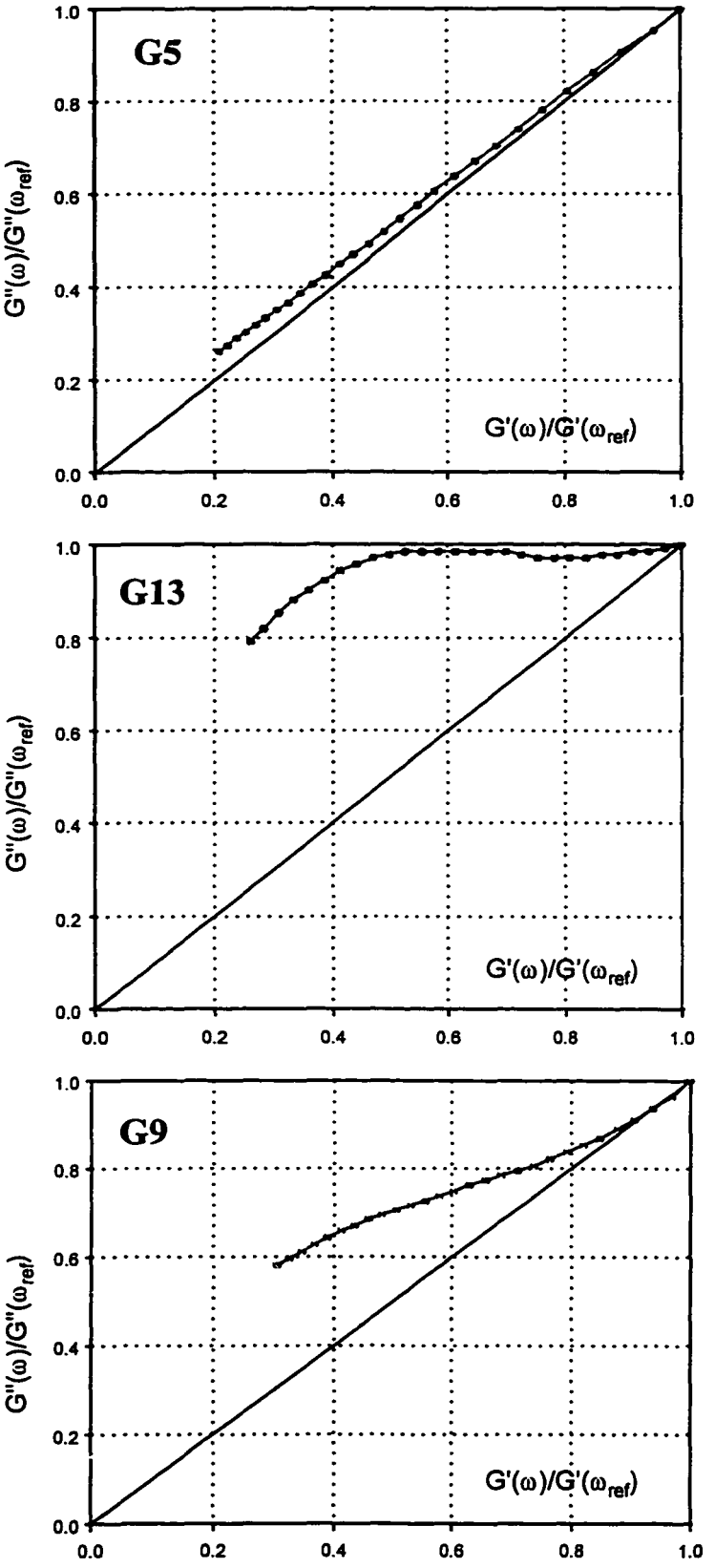


Figure 7-59. NC-C plot: Effect of branching structure at comparable branching content.

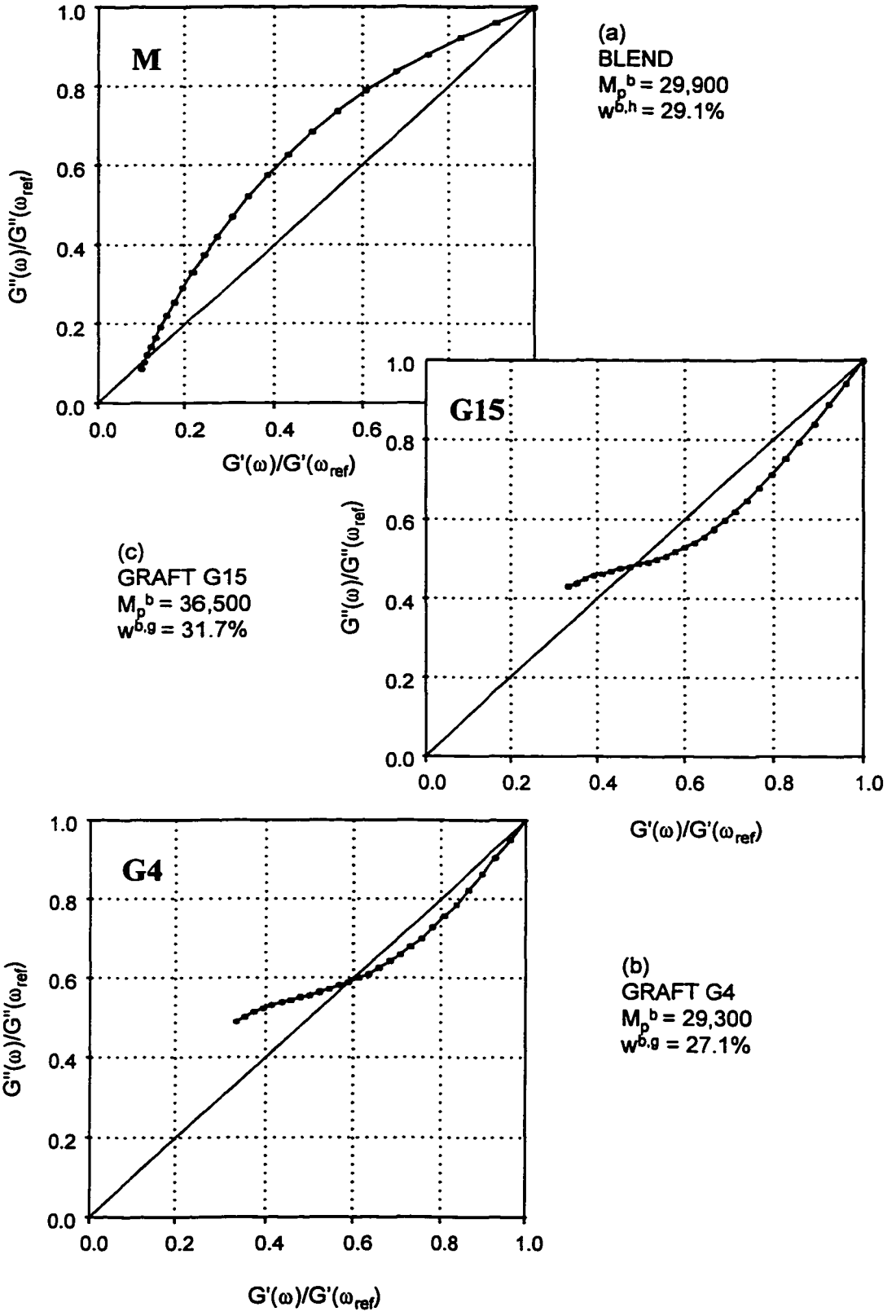


$w^{b,g}$ = 36.7%
N_g^p = 1.7
M_p^b = 61,700

$w^{b,g}$ = 35.3%
N_g^p = 11.1
M_p^b = 9,400

$w^{b,g}$ = 36.4%
N_g^p = 3.2
M_p^b = 33,500

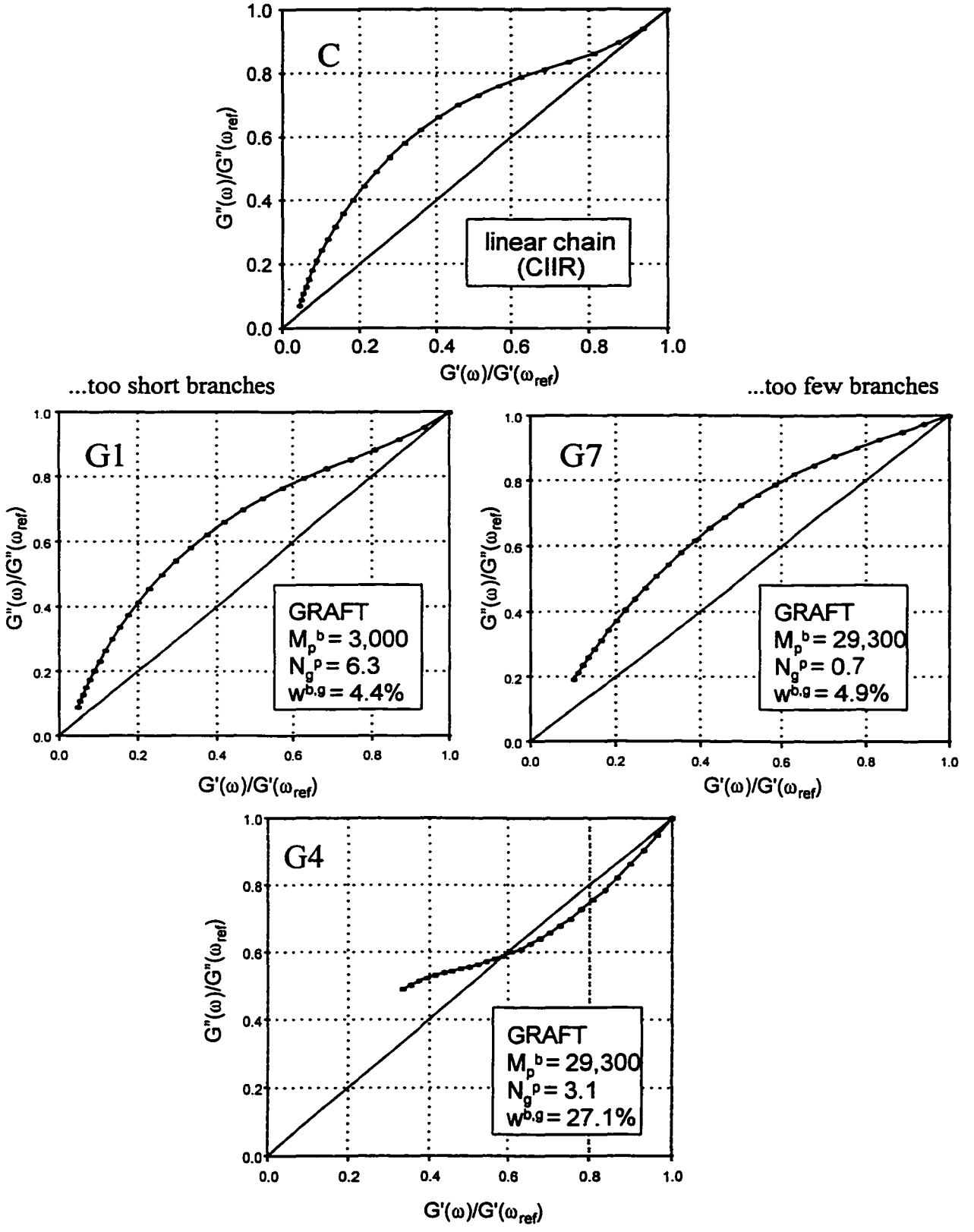
Figure 7-60. NC-C plot: Grafting CIIR-g-BR versus blending CIIR/BR.



As a final comment, for the branching structure to have an appreciable effect on the nC-C contour, and therefore on the underlying rheological properties, a certain combination of branch length and number of branches is necessary. When branch length is below a minimum value, e.g. $M_p^b = 3{,}000$ for sample G1- graph (b) in Figure 7-61, even a considerable number of them ($N_g^p = 6.3$) will not alter the nC-C contour shape. Similarly, too few branches, ($N_g^p = 0.7$), even of considerable length, ($M_p^b = 29{,}300$) as is the case for sample G7 - graph (c), will not modify the shape of the nC-C plots which remain essentially unchanged, compared to sample C (graphs (b) and (c) with (a) in Figure 7-61).

However, a high enough combination of the branch length and branching number results in a dramatically different shape of the normalized Cole-Cole contour, a result of substantially different rheological properties of graft copolymers, compared to their linear parent polymers.

Figure 7-61. NC-C plot - effect of LCB structure: final conclusion.



Chapter 8

Dynamic thermo-mechanical analysis (DTMA)

8.1 Introduction

The glass-transition temperature (T_g) is one of the most important properties of polymeric materials. It marks the transition from a glassy state to the viscoelastic plateau, and therefore determines the nature of the polymer at a given temperature. Thus it indirectly defines the temperature range suitable for processing and applications of the material.

The objective of experiments reported in this chapter was to determine how the long-chain branching and chemical composition of graft copolymers influence the dynamic moduli and loss tangent in the transition zone of the viscoelastic behaviour. Reference to the transitions observed for both precursor polymers, CIIR and BR, was made also.

Note on the difference between the glass-transition temperature, T_g and the temperature corresponding to α-transition in the DTMA spectrum

The glass-transition temperature is defined as the temperature at which a volumetric thermal expansion coefficient undergoes a step change at the heating and cooling rate of 1°C/min [369-370]. This is the least ambiguous and the most established definition of the T_g.

None of the parameters obtained through DTMA, including parameters most frequently compared in the literature to the T_g, namely a temperature corresponding to the E″ peak maximum or an inflection point on the low-temperature side of the tan δ peak, should be regarded as synonymous with the glass-transition temperature, T_g [371-372].

Consequently, in this work reference is made to the temperatures of the E″ or tan δ peaks, as the α-transition temperatures, which are the DTMA equivalents to the dilatometric definition of the T_g.

Among various methods used to measure transitions in polymeric materials, the dynamic thermo-mechanical methods became one of the most popular, due to their good sensitivity and resolution, as well as availability of reliable and automated instruments [373]. A typical experimental DTMA configuration include a temperature sweep with oscillation of a constant frequency and at small strain amplitudes, which are continually adjusted to stay within the LVE range of the material response. The strain amplitude adjustment is usually necessary to keep the signal (force or torque) within the capabilities of a transducer, which has to track the modulus changing over 3 decades of magnitude across the transition zone.

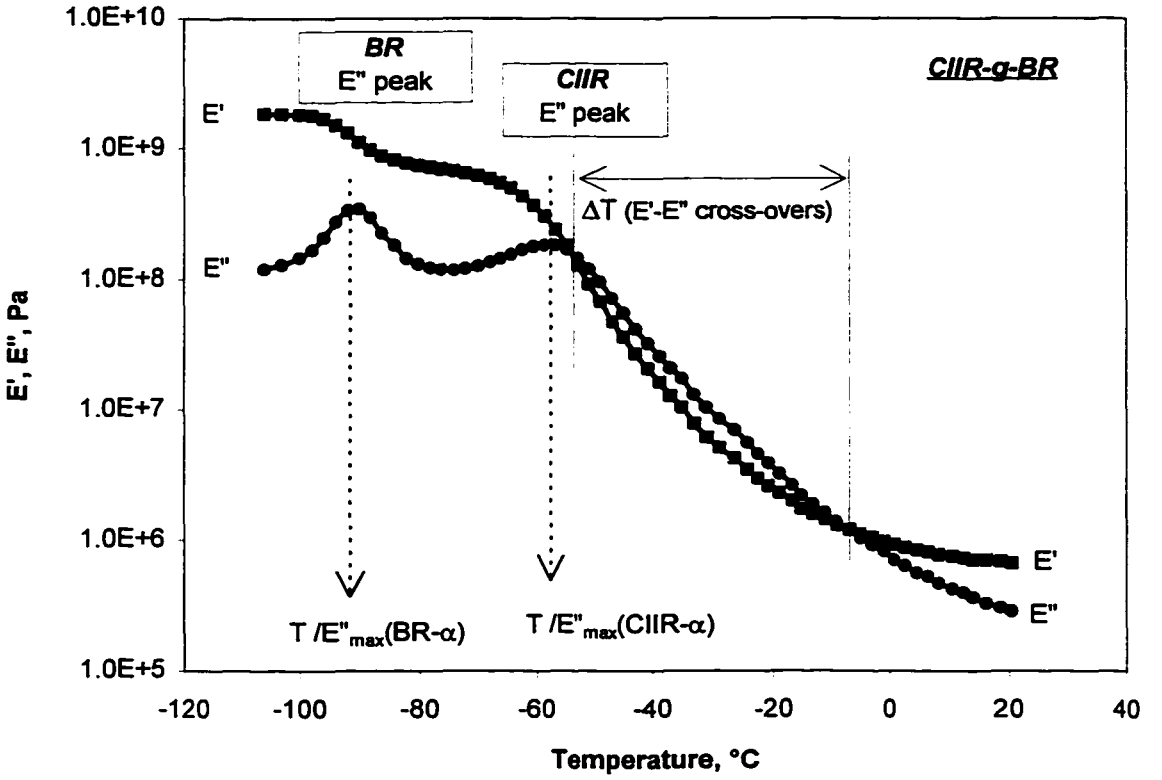
In this project the RSA-II was used to apply the small strain-amplitude oscillations in tension, over a temperature range wide enough to capture the entire transition zone, corresponding to both parent polymers, CIIR and BR.

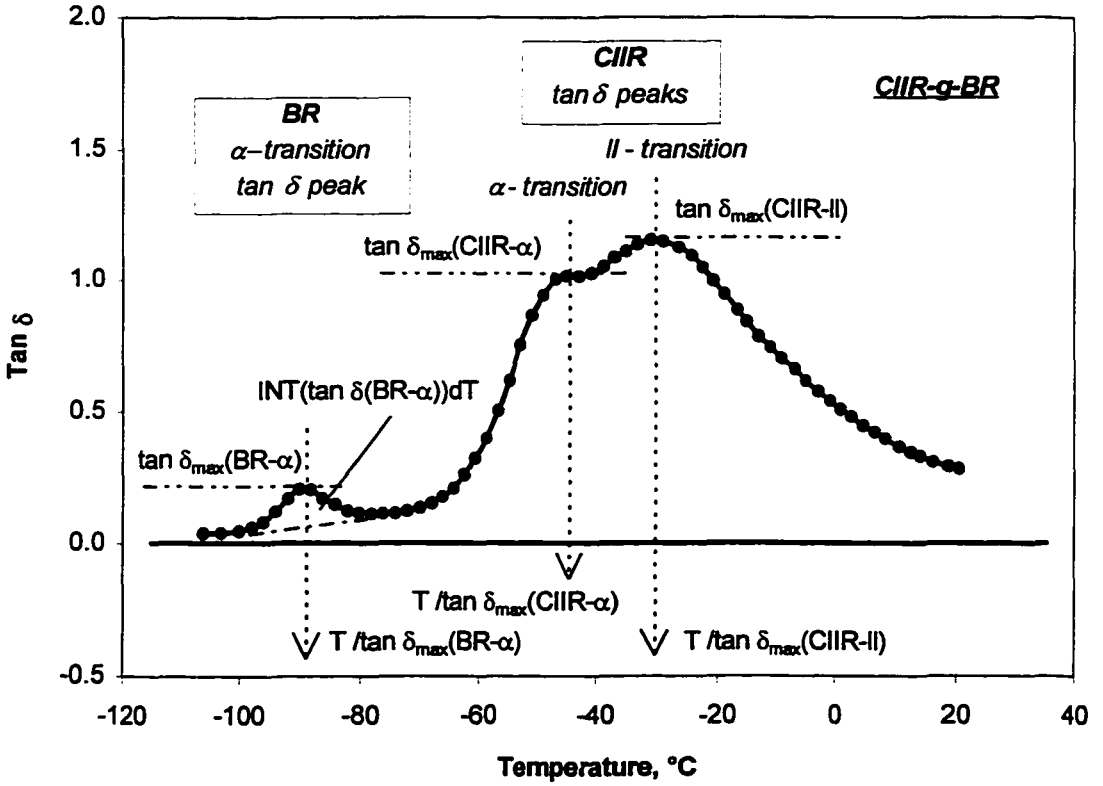
Experimental aspects of the DTMA experiments were described in Chapter 5, section 5.3, and test conditions are detailed in Appendix IV, Table B. DTMA temperature scans were collected for all samples, at least in duplicate, including those for parent polymers. Only representative DTMA spectra are included in Appendix V, for parent polymers, samples C and B10 in Figures A8C and A8B10 respectively, as well as for grafts: G2, G3, G6, G16 and G22 in Figures A8G2, A8G3, A8G6, A8G16 and A8G22 respectively.

A typical DTMA spectrum for the CIIR-g-BR copolymers is shown in Figure 8-1.
The main transitions observed in the spectrum were identified as: the α-transition for the BR (see section 8.2) and α and ll transitions for the CIIR (section 8.3). No higher order transitions (β, γ, ...) could be identified within the range of temperatures examined.

The E″ or tan δ peaks corresponding to these transitions are the main features of the transition zone of the viscoelastic behaviour of the graft copolymers studied. For the purpose of studying the structure-property relationship, they can be conveniently parametrized in terms

Figure 8-1. Definition of {DTMA} rheological parameters.





of the E″ and tan δ peak position (abscissa) and the ordinate of the peak apex, as well as the width and the area of under the peak.

Definition of the DTMA parameters, which describe the main characteristics of the DTMA spectrum, are given in Table 8-1 and in Figure 8-1. Their values were determined analytically from the E″(T) and tan δ(T) profiles and are included in Tables A8a and A8b, in Appendix V, section 8.

Table 8-1. Definition of the {DTMA} parameters.

(a)	**T /E"$_{max}$ (BR-α)**	- temperature corresponding to maximum of the E"(T) peak (BR α-transition)
(b)	**T /tan$_{max}$ δ (BR-α)**	- temperature corresponding to maximum of the tan δ peak (BR α-transition)
(c)	**tan$_{max}$ δ (BR-α)**	- maximum value of the tan δ, corresponding to BR α-transition
(d)	**T /E"$_{max}$ (CIIR-α)**	- temperature corresponding to maximum of the E"(T) peak (CIIR α-transition)
(e)	**T /tan$_{max}$ δ (CIIR-α)**	- approximate temperature corresponding to the maximum tan δ (CIIR α-transition)
(f)	**tan$_{max}$ δ (CIIR-α)**	- maximum value of the tan δ peak corresponding to the CIIR α-transition
(g)	**T /tan$_{max}$ δ (CIIR-II)**	- temperature corresponding to the maximum of the tan δ peak (CIIR II-transition)
(h)	**tan$_{max}$ δ (CIIR-II)**	- maximum value of the tan δ at the peak corresponding to CIIR II-transition
(i)	**INT(tan δ (BR-α)) dT**	- temperature integral of the tan δ, corresponding to BR α-transition, integrated over the temperature range of -100°C to - 80°C
(j)	**ΔT (E'-E" cross-over)**	- difference between temperatures corresponding to the E'-E" cross-over points; a measure of the width of the tan δ (CIIR-α+II) damping peaks

Small but systematic differences exist between the position and height of the E″(T) and tan δ(T) peaks among various LCB architectures of the grafts. A standard screening procedure was applied to discover meaningful correlations between structural (LCB) and DTMA parameters. A correlation matrix with the Pearson r_{xy} coefficients[1] is included in Table 8-2.

Table 8-2. Pearson product moment correlation coefficients for correlations between structural/compositional and {DTMA} parameters.

Correlation matrix (Pearson)		Branch length	Number of branches	Branching content	Graft MW	Graft chem. composition	Interferences		
		M_p^b	N_g^p	$w^{b,g}$	M_z^G	w^b	$w^{b,h}$	PDI	vinyl
		1	2	3	4	5	6	7	8
T /E"$_{max}$ (BR-α)	a	-	0	-	-	0.7977	0	0	0
T /tan$_{max}$ δ (BR-α)	b	0	+	0	0	0	0	0	0
tan$_{max}$ δ (BR-α)	c	+	0	+	+	0.8581	0.8631	0	0
T /E"$_{max}$ (CIIR-α)	d	0	-0.8126	-	0	0	0	0	0
T /tan$_{max}$ δ (CIIR-α)	e	0	0	0	0	0	0	0	0
tan$_{max}$ δ (CIIR-α)	f	-	0.8148	0	0	0	-	0	+
T /tan$_{max}$ δ (CIIR-II)	g	-	0	-	-	-0.7987	0	0	0
tan$_{max}$ δ (CIIR-II)	h	-0.7462	0	-	-	-0.7950	-	0	0
INT(tan δ(BR-α))dT	i	0.7946	0	0	+	0.7784	0.8599	0	0
DT(E'- E" cross-over)	j	-	+	0	0	0	0	0	0

zero indicates that $|r_{xy}| < 0.5000$

"-" indicates: $-0.7500 < |r_{xy}| < -0.5000$

"+" indicates: $0.5000 < |r_{xy}| < 0.7500$

r_{xy} value given for $|r_{xy}| > 0.7500$

[1] Pearson product moment coefficient, r_{xy}, is a dimensionless index that ranges from -1.0 to 1.0 inclusive, and reflects the extent of a linear relationship between the two data sets [JMP Manual, V3.1, 1995, p. 317].

8.2 DTMA of the branch precursor polymer, BR

For the BR, both E″ and tan δ peaks corresponding to the α-transition, have a typical (unimodal) shape, as shown in Figure A8B10 in Appendix V, section 8.

The abscissa of the E″ peak maximum, the **T /E″$_{max}$ (BR-α)** parameter, was reported as one of the temperatures in a DTMA spectrum best approximating glass-transition temperature, T_g [374]. In addition to the influence made by microstructure of the BR, particularly its vinyl content, the position and the shape of the E″ and tan δ peaks will depend on the method and exact test conditions of the measurements. For example, in the case of the dynamic mechanical test, the oscillation frequency will, and the heating/cooling rate might, affect the **T /E″$_{max}$ (BR-α)** values [375].

The temperature **T/E″$_{max}$ (BR-α)** obtained in this study for pure polybutadiene (sample B10), -92.9°C, is as close to the values reported in the literature, for polybutadienes of similar microstructure, as those values are among themselves [224, 376-378].

8.3 DTMA of the backbone precursor polymer, CIIR

The tan δ peak for CIIR in the transition zone has a unique bi-modal shape, similar to those reported for IIR (butyl rubber) and other PIB-derived elastomers. In fact, this "double-peak" is a superposition of the two tan δ peaks stretching between -70°C and about 20°C [152, 352, 373, 379-383]. Its breadth is caused by a molecular mobility being impaired by the large intermolecular friction due to steric hindrance coming from methyl groups, which is effective over a broad temperature range, extending well into positive temperatures on the Celsius scale [379, 381].

A low-temperature peak corresponds to the α-transition (Figure A8C in Appendix V, section 8) [352, 382, 384], while a more pronounced peak on the tan δ(T) profile has been termed by Sanders and Ferry [380] as a 'slow relaxation process' or a 'liquid-liquid' transition by Boyer [383]. The molecular origin of ll-transition peak is still not clear [379], although several explanations were offered [380, 383].

Temperatures corresponding to the $\tan_{max}$ δ (CIIR-α) and $\tan_{max}$ δ (CIIR-ll), approximately -42°C and -28.3°C, respectively, agree well with the published data of Boyer [381].

8.4 DTMA spectra of the graft copolymers

Regular graft copolymers are chemically heterogeneous and have a long-chain branched, comb-like structure. Each of these two characteristics has its own implication for the DTMA spectrum.

Grafts copolymers as chemically heterogeneous polymeric systems

Typically, graft copolymers will have two α-transitions, one corresponding to a branch precursor polymer, and another one to a backbone precursor polymer [385-386]. It was found in a many cases, that both these transitions are shifted toward lower temperatures in grafts, as compared with a position of corresponding peaks in the homopolymers [68, 71, 387]. Other combinations of peak shift directions were reported also, for example [67, 388], as well as no shift at all of the loss tangent peak [91]. The graft copolymers with a single DTMA tan δ peak were described also [389], as well as a few copolymeric systems in which, depending on the exact molecular structure and composition, either one or two α-transitions could be seen [390].

To study specifically the effects of the chemical composition on DTMA transitions, without possible interference from the LCB, a blend or linear block-copolymer would usually be used.

Grafts as long-chain branched polymers

Likewise, the effect of the long-chain branching on the glass-transition (and corresponding α-transition) is best studied with long-chain branched homopolymers, thus without a possibility of interference from a chemical heterogeneity.

Bulk properties of polymers which depend on a local conformation of the macromolecules, for example the glass-transition temperature, are not usually strongly affected by the presence of the LCB.

The T_g value for the comb-type branched polymer is frequently similar to that of the linear homologue. However, when the ratio of chain ends to M_n^b becomes high, the T_g of the branched polymer with comparable M_n^b, shifts toward lower temperatures [391-393].

The effect is not as strong as in stars of comparable number of arms, due to the fact that in comb-type polymer, the number of branches matches the number of branch-points, which are known to have the opposite effect on T_g [109].

The difference between T_g for linear polymers and that of chemically equivalent comb-like molecules will always result from the balance between the effects of end groups (lowering T_g), branch points (increasing T_g) and the sensitivity of the glass-transition temperature to the effect of either.

It is highly probable that, for graft copolymers, effects of the chemical composition and LCB on the DTMA spectrum will superimpose.

8.5 DTMA spectra of CIIR-g-BR graft copolymers

A. Loss modulus E"(T) peaks corresponding to the α-transition for the BR and CIIR

1. E"(BR-α) peak position - Table A8a, col.(a), Table 8-2, row (a)

Shift of the E"(BR-α) peak (upon grafting) toward higher temperatures is small but consistent. The **T /E"$_{max}$ (BR-α)** is -92.3°C for sample B10 and within the -87.9 to 91.0°C for grafts. Temperature shift of the E"(BR-α) peak is most significant upon the overall BR content (w^b). No statistically significant correlation between specific branching parameters and the magnitude of the shift could be identified. This observation can be summarized as follows:

$$w^b \uparrow \Rightarrow \mathbf{T\ /E''_{max}\ (BR\text{-}\alpha)} \uparrow$$

2. E"(CIIR-α) peak position - Table A8a, col.(d), Table 8-2, row (d)

As compared with the value of **T /E"$_{max}$ (CIIR-α)** for sample C (-58.4°C) grafting of the BR-branches can shift the E"(CIIR-α) peak position toward lower temperatures, up to 8°C in the case of grafts with the highest number of branches. The magnitude of shift is strongly dependent upon branching number, N_g and the shift direction suggests a dominating role of the sidechain-ends.

$$N_g \uparrow \Rightarrow \mathbf{T\ /E''_{max}\ (CIIR\text{-}\alpha)} \downarrow$$

B Loss tangent peaks, tan δ(T) - corresponding to α-transition for BR, and α and ll transitions for CIIR

1. Tan δ (BR-α) peak position - Table A8a, col.(b), Table 8-2, row(b)

Tan δ(BR-α) peak is consistently positioned at lower temperatures for grafts than it is for sample B10 (-85.6°C) (**T /tan$_{max}$ δ(BR-α)** is between -87.4°C and -90.7°C for grafts).

This peak is drifting in the opposite direction than the corresponding E″(BR-α) peak, which can be partially explained as being influenced by a step-change in the E′(T) modulus, occurring within a comparable temperature range.

2. *Tan δ (CIIR-α+ll) peak position*

a) CIIR-α transition - Table A8a, col. (e), Table 8-2, row (e)

No correlation between structure/composition of the graft and the position of the tan δ (CIIR-α) peak is observed. Significant spread of the **T /tan$_{max}$ δ (CIIR-α)** for various grafts, -47.2 to -41.0°C, with -42.6°C for sample C can be explained by a relatively high degree of uncertainty in a determination of the apex abscissa of the poorly defined tan δ (CIIR-α) peak.

b) CIIR-ll transition - Table A8b, col. (g), Table 8-2, row (g)

The position of the tan δ (CIIR-ll) peak can be confidently related to the chemical composition of the graft. Increasing the overall content of the BR tend to decrease the **T /tan$_{max}$ δ(CIIR-ll)** of the grafts,

$$w^b \uparrow \Rightarrow \mathbf{T /tan_{max}\ \delta(CIIR\text{-}ll)} \downarrow$$

3. *Tan δ (BR-α) peak height and size - Table A8a, col.(c), Table 8-2, row(c) - peak height, and Table A8b, col.(i) and Table 8-2, row (I) - peak area*

The height of the tan δ (BR-α) peak appears to be strongly controlled by the content of the ungrafted BR, $w^{b,h}$. Judging by a positive correlation between $w^{b,h}$ and **tan$_{max}$ δ (BR-α)**, the slightly weaker correlation which exists between w^b and **tan$_{max}$ δ (BR-α)** can assumed to be due to interrelation between the w^b and $w^{b,h}$ structural parameters. In fact, the effect of

increasing w^b associated with the increased branching content, $w^{b,g}$, would have an opposite effect on the **tan$_{max}$ δ (BR-α)** parameter than that caused by an increased dilution of the graft by linear and short BR branches, therefore,

$$w^{b,h} \uparrow \Rightarrow \mathbf{tan_{max}\ \delta(BR\text{-}\alpha)} \uparrow \text{ and}$$

$$w^{b} \uparrow \Rightarrow \mathbf{tan_{max}\ \delta(BR\text{-}\alpha)} \uparrow$$

The size of the tan δ (BR-α) peak - represented by the value of the **INT(tan δ(BR-α))dT** parameter, is also in proportion to the $w^{b,h}$. A strong correlation between the $M_p{}^b$ and peak area, suggested by a screening analysis (Table 8-2, row (i), col. (1)), is believed to be merely a result of a strong interrelation between $M_p{}^b$ and $w^{b,h}$ parameters (see Appendix VI),

$$w^{b,h} \uparrow \Rightarrow \mathbf{INT(E'\text{-}E''\ cross\text{-}over)\ \delta(BR\text{-}\alpha)} \uparrow \text{ and}$$

$$w^{b} \uparrow \Rightarrow \mathbf{INT(E'\text{-}E''\ cross\text{-}over)\ \delta(BR\text{-}\alpha)} \uparrow$$

4. Tan δ(CIIR-ll) peak height - Table A8b, col. (h), Table 8-2, row (h)

The height of the tan δ(CIIR-ll) peak appears to be inversely proportional to the BR content and this fact remains difficult to interpret,

$$w^{b} \uparrow \Rightarrow \mathbf{tan_{max}\ \delta(CIIR\text{-}ll)} \downarrow$$

5. Tan δ(CIIR-α) peak height - Table A8b, col. (f), Table 8-2, row (f)

The height of the tan δ (CIIR-α) peak is strongly dependent upon specific branching parameters, particularly N_g. $\mathbf{Tan_{max}\ \delta\ (CIIR\text{-}\alpha)}$ value can be modified either way, as compared with that of a pure CIIR, by designing a specific set of branching parameters. Observed relations can be summarized as follows,

$N_g \uparrow \Rightarrow \mathbf{tan_{max}\ \delta(CIIR\text{-}\alpha)} \uparrow$, and to lesser extent, $M^b \uparrow \Rightarrow \mathbf{tan_{max}\ \delta(CIIR\text{-}\alpha)} \downarrow$

Therefore, the highest value of $\mathbf{tan_{max}\ \delta\ (CIIR\text{-}\alpha)}$ would be expected for grafts with many short branches.

6. Width of the tan δ(CIIR-α+ll) double-peak - Table A8b, col. (j), Table 8-2, row (j)

The number of branches tends to broaden the tan δ (CIIR-α+ll) peak, while the length of the branch appears to have an opposite effect. While neither correlation was found to be statistically significant, this observation is consistent with a the one the preceding section.

Additional observations can be summarized as follows:

(a) The effect of the chemical composition, (w^b, $w^{b,h}$) on the DTMA spectra, prevails over those which could be directly traced to the branching structure (M^b, N_g),

(b) Polydispersity and the vinyl content of the branch precursor polymer has no measurable effect on the viscoelastic properties of the grafts in the transition zone,

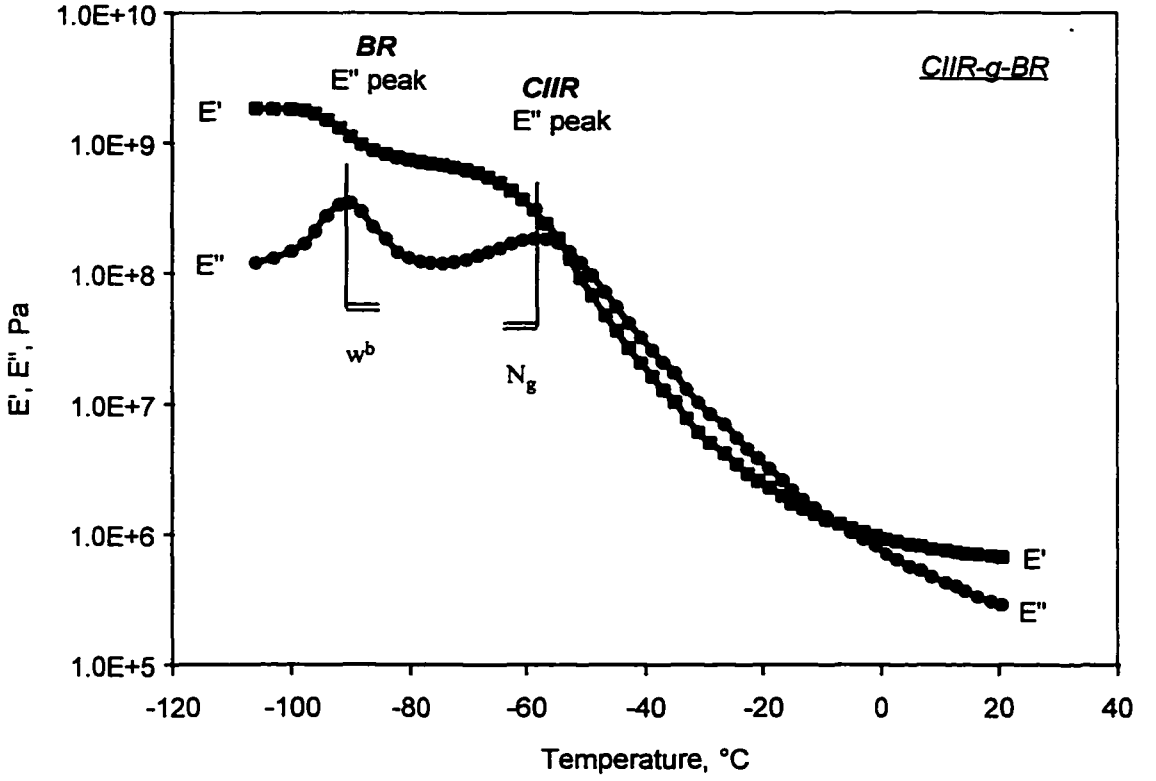
(c) Similarly, neither the overall branching content ($w^{b,g}$) nor the molecular weight of the graft (M_z^G) were shown to have a statistically significant effect on the DTMA spectrum, in the temperature range between -100°C and +20°C,

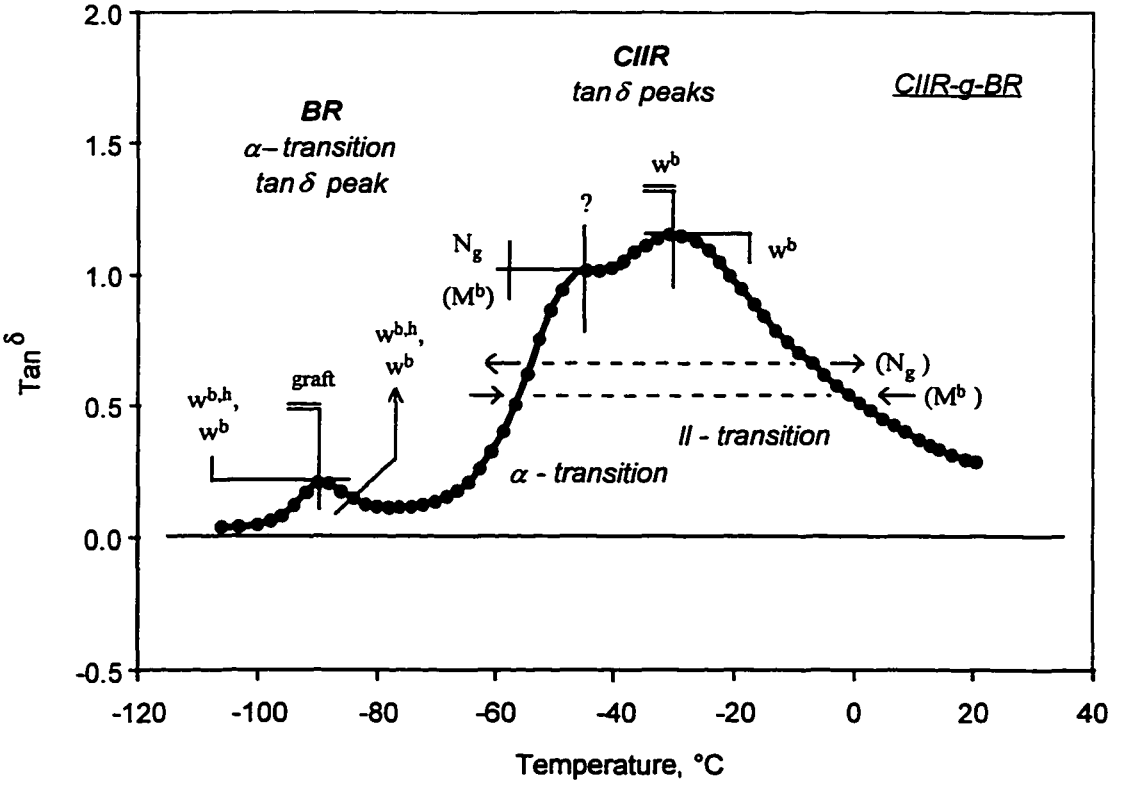
(d) The number of branches primarily influences the parameters of the α–transition corresponding to CIIR,

(e) The ll-transition in the CIIR tan δ spectrum appears to be controlled mostly by the chemical composition of the graft, w^b.

Figure 8-2 summarizes the main conclusions regarding the relationship between branching parameters and chemical composition of the graft and selected features of the DTMA spectrum of the CIIR-g-BR graft copolymers.

Figure 8-2. Summary of changes in the DTMA spectrum induced by grafting.





Chapter 9

Summary and conclusions

9.1 Summary

A systematic study of the relationship between long-chain branching structure and rheological properties of well characterized CIIR-g-BR graft copolymers has been performed.

A series of graft copolymer samples having regular, comb-like structure was prepared. Their structure and composition were comprehensively characterized, with particular attention paid to the principal branching parameters, length of the branch and the average number of branches per backbone molecule. A backbone prepolymer (CIIR) and typical branch prepolymer (BR), as well as their blend were added to the sample portfolio, as reference materials.

Results of the comprehensive rheological characterization program were reduced to material parameters (numbers), in order to permit quantitative correlation analysis with the long-chain branching parameters.

The most significant findings are summarized in Tables 9-1a, b, c, d, e, f and g, listed in the sequence of rheological topics categorized in Table 5-2, chapter 5. For each topic discussed in Tables 9-1, a reference is given to the relevant section(s) of the thesis.

The more general observations derived from these results are presented in section 9.2 in the form of conclusions. The significance of this work is outlined in the subsequent section, (9.3) while some suggestions for a possible future work in this area are included in subsection 9.4, concluding this chapter.

Table 9-1a. Summary of results - I.

#	Issue	Experimental	Main result / significant relationship / observation	Text ref.	Table 5-2 ref.
1	complex modulus, G* (LVE)	T=100°C, γ=5%, ω=0.2 rad/s	• no statistically significant correlation between branching parameters (M^b, N_g, $w^{b,g}$) and G* at low ω	6.3	1.1.1
		T=100°C, γ=5%, ω=1 rad/s	• barely statistically significant correlations (as shown immediately below)		
		T=100°C, γ=5%, ω=200 rad/s	• M^b ↑ => G* ↑ • N_g ↑ => G* ↓ • G* ≠ f (w^b, $w^{b,g}$, M_z^G); G* is not related to neither w^b nor $w^{b,g}$ nor M_z^G	6.3 7.3	
2	storage modulus, G'	T=100°C, γ=5%, ω=1 rad/s	• grafting => G' ↑ at any (M^b, N_g) combination, up to 2.5x with reference to sample C, • blending => G' ↓ (2.5x for sample M, as compared to sample C)	7.3	
3	loss modulus, G"	T=100°C, γ=5%, ω=0.2, 1 & 200 rad/s	• all above conclusions for G* are applicable here as well	Table A73a	
4	plateau modulus, G"(plateau)	T=30°C, γ=5%, (ω=0.001-100rad/s)	• M^b ↑ => G"(plateau) ↑	6.1.2	
5	loss tangent, tan δ	T=30°C, γ=5%, ω=0.001 rad/s	• $w^{b,g}$ ↑ => tan δ ↓ ' grafting reduces tan δ, most significantly at lower ω, • M^b ↑ at N_g=const. => tan δ ↓ • N_g ↑ at M^b=const. => tan δ ↓	6.1.2 Fig.6-9	
		T=100°C, γ=5%, ω=1 rad/s	• $w^{b,g}$ ↑ => tan δ ↓; grafting reduces tan δ;	7.3	
6	frequency - dependence of the complex modulus, G*(ω)	T=100°C, γ=5% (ω=0.001-100rad/s)	• monotonically increase with ω for all grafts, - weakest ω-dependence for graft with multiple short branches - strongest ω-dependence for graft with few long branches	6.3 Fig. 6-29	1.1.2

Table 9-1b. Summary of results - II.

#	Issue	Experimental	Main result / significant relationship / observation	Text ref.	Table 5-2 ref.
7	frequency - dependence of the dynamic moduli, G'(ω) and G"(ω) (LVE)	T=100°C, γ=5% (ω=0.001-100rad/s)	graft/linear polymers as compared with linear polymers: • show no cross-over point and lack of clear transition point between plateau and terminal zones; G' over G" consistently, • have much smaller ω-dependence, slope G(ω) for both G' and G" at the lowest ω, • slope of G'(ω) and particularly G"(ω) in the ω-range corresponding to plateau zone, is higher for grafts than for linear molecules, • existence of the second plateau due to branching; position (ω-scale) appears to be related to M^b and its depth to a N_g	6.1.1 7.2.4	1.1.2
8	frequency - dependence of dynamic moduli, **slope G'/G"^{2} (0.001)**		• M_p^b ↑ => **slope G'/G"^{2}** ↓ , for $w^{b,h}$ <10%	6.1.2	
9	frequency - dependence of the dynamic moduli, **slope G"(0.001)**		• M_p^b ↑ => **slope G"(0.001)** ↓ ; (for $M_p^b < M_e^b$, M_e^b= 10,000-11,000) • M_p^b ↑ => **slope G"(0.001)** ↑ ; (for $M_p^b > M_{eb}$) • N_g^p ↑ => **slope G"(0.001)** ↓ ; plateau at N_g^p > 8-10		
10	frequency - dependence of the dynamic moduli, mC-C plot		• each type of graft copolymer LCB structure can be identified by specific shape of the mC-C plot contour; systematic variations in either of specific branching parameter will induce regular changes in mC-C contour shape	6.1.4	
11	frequency - dependence of the loss tangent, tan δ (ω)	T=30°C, γ=5%, (ω=0.001-0.1rad/s)	• ω-dependence for grafts is generally lower than for linear polymers; dependence of the tan δ upon branching structure and composition of the graft depends upon frequency, • it relates best to $w^{b,g}$ at ω=0.001 rad/s • M^b and N_g at ω=0.1 rad/s, with possible contributions from $w^{b,h}$	6.1.2 7.2.3 Fig.6-9 Fig7-17	

Table 9-1c. Summary of results - III.

#	Issue	Experimental	Main result / significant relationship / observation	Text ref.	Table 5-2 ref.
12	frequency-dependence of the complex viscosity, **n(0.001-100)**	T=30°C, γ=5%, (ω=0.001-100rad/s)	• η(ω) fits very well Power Law Model for well-developed branching structure, • M^b ↑ => **n(0.001-100)** ↑, at $w^{b,g}$ < 10% • N_g ↑ => **n(0.001-100)** ↓, at $w^{b,g}$ < 10% • $w^{b,g}$ => **n(0.001-100)** ↓, at $w^{b,g}$ > 10%	6.1.3	1.1.2
13	time-temperature superposition	γ=5%, (ω=0.001-100rad/s), (T=30(25)130°C)	• f/T shift quality: - deteriorates with $w^{b,g}$ ↑, M^b ↑ or N_g ↑, • correspondence between master curves and corresponding isotherms as ref. - is surprisingly good but decreasing in accuracy with $w^{b,g}$ ↑ or N_g ↑, • fit to Arrhenius/WLF equations: - generally successful with exception for a few grafts with either very long branches, M^b or with highest frequency, N_g	6.2.1	1.1.3
14	thermo-rheological complexity	T=30-130°C	• CIIR-g-BR copolymers are considered thermo-rheologically complex materials based on the chemical heterogeneity and immiscibility of the parent polymers, • success of t/f-T shift is a necessary but not sufficient condition for thermo-rheological simplicity	6.2.2	1.1.4
15	temperature-dependence of dynamic moduli, G'(T), G"(T) or c_1, c_2, E_a	T=30-130°C	• obtained results are not conclusive; superposition of effects from chemical composition and LCB has on the coefficients representing the temperature-dependence of viscoelastic functions is apparent, with the former prevailing. No systematic relations between c_1, c_2 or E_a coefficients and LCB parameters could be derived with acceptable statistical confidence	6.2.3	1.1.5
16	time-dependence of the stress relaxation modulus, nG(t)	T=30°C, γ=10%, (t=0.1-up to 10000s)	branching significantly slows down stress relaxation process: • N_g ↑ => nG(t') ↑ at any t' within the tested range • $w^{b,h}$ ↑ => nG(t') ↓ at shorter relaxation times, t<100s • presence of unattached, low MW branch precursor molecules "speeds-up" relaxation at shorter times, details depending upon M^b and $w^{b,h}$	6.4 6.5	1.1.3
		T=100°C, γ=5%, (t=0.1-400s)		6.6	
		T=30°C, γ=10% (t=0.1-10,000s)		6.4.1 6.4.2	

Table 9-1d. Summary of results - IV.

#	Issue	Experimental	Main result / significant relationship / observation	Text ref.	Table 5-2 ref.
17	... **|slope nG(t)|**	T=30°C, γ=10%, (t=0.1-10,000s)	• average slope of the nG(t), depends on the number of structural and compositional variables; **|slope nG(t)|** = f(M^b, N_g, $w^{b,g}$, $w^{b,h}$, w^b), with relative contribution from individual factors depending on the relaxation time	6.4.2	
		T=100°C, γ=5%, (t=0.1-400s)		6.6	
18	... **INT G(t) dt**	T=30°C, γ=10%, (t=0.1-1000s)	• N_g ↑ => **INT G(t)dt** ↑ (plateau at N_g > 6-7) • average rate of decay = f($w^{b,g}$)	6.5 Fig. 6-42	
19	... G(t) and nG(t) curves	T=30°C, γ=10%, (t=0.1-10,000s)	• overall rate of relaxation appears to be controlled primarily by the number of branches N_g, while delay in onset of significant decay of the relaxation curve depends on length of the branches (M^b)	6.4	1.1.3
		T=100°C, γ=5%, (t=0.1-400s)		6.6	
20	... **nG(t=1000)**	T=100°C, γ=5%, t=0.1-400s	• M^b ↑ => **nG(t=1000)** ↑; (plateau at M_p^b < ~10,000) • N_g ↑ => **nG(t=1000)** ↑; (plateau at N_g > ~4.5)		
21	... nG(t)		• $w^{b,g}$ ↑ => nG(t) ↑		
22	strain-dependence of the storage modulus, γ_{cr}^{LVE}	c.f. text and App. IV, Table A, for details	• M^b ↑ => γ_{cr}^{LVE} ↓ at N_g =const. • N_g ↑ => γ_{cr}^{LVE} ↓ at M^b =const. • (M^b ↓ & N_g ↑) at ($M^b \cdot N_g$) = const. => γ_{cr}^{LVE} ↓ • T ↑ => γ_{cr}^{LVE} ↑ at ω =const. • ω ↑ => γ_{cr}^{LVE} ↓ at T =const.	5.2.4.2	1.2.1
23	strain-dependence of the dynamic modulus, G'(γ)	T=100°C, (γ=50 - 200%), ω=1rad/s	• • γ ↑ => G' ↓ at ω, T=const. (weak dependence)	7.2.4	

Table 9-1e. Summary of results - V.

#	Issue	Experimental	Main result / significant relationship / observation	Text ref.	Table 5-2 ref.
24	strain-dependence of the loss tangent, tan δ(γ)	T=100°C, (γ=50 - 200%), ω=1rad/s	• grafting => $\tan_1 \delta(\gamma, \omega)$ ↓ • γ ↑ => tan δ ↑ at ω, T=const. (weak dependence) • flat ω-dependence for grafts	7.2.3	1.2.1
25	strain-dependence of the storage modulus, **G'(2%) - G_1'(50%)**	T=100°C, ω=10rad/s	• N_g^p ↑ => (**G'(2%) - G_1'(50%)**) ↓ (to a plateau)	7.1	
26	strain-dependence of stress relaxation modulus, G(t, γ)	T=30°C (γ= 3-50%) (t=0.1-1000)	• values of the γ_{cr}^{LVE} obtained during variable-strain amplitude stress relaxation experiments are comparable to those obtained by dynamic strain sweep	5.2.4.3	1.2.2
27	complex modulus, G_1^* (NLVE)	T=100°C, γ=50%, ω=10rad/s	• M^b ↑ => G_1^* ↑ ($w^{b,g}$ > 10%) • N_g ↑ => G_1^* ↓	7.1	1.3.1
28	complex modulus, G_1^* (NLVE)	T=100°C, γ =200 and γ =800%, ω=1rad/s	• M^b ↑ => G_1^* ↑ ($w^{b,g}$ > 10%) • N_g ↑ => G_1^* ↓	7.3	
29	stress relaxation modulus, **G(40ms), G(1)**	T=100°C, γ'=75%	• M^b ↑ => G(t') ↑ for $w^{b,g}$ > 15%, t'=40ms - 1s • N_g ↑ => G(t') ↓ for M_p^b > 7,600, t'=40ms - 1s	7.4	
30	dynamic moduli, G_1', G_1'' (NLVE)	T=100°C, γ=50%, ω=10rad/s T=100°C, γ=200 and 800%, ω=0.5 and 10 rad/s	• G_1': M^b ↑ => G_1' ↑ and N_g ↑ => G_1' ↓ • G_1'': M^b ↑ => G_1'' ↑ ($w^{b,g}$ > 15%) and N_g ↑ => G_1'' ↓ • $w^{b,h}$ might modify G_1'', especially at high ω	7.1 7.2.1 7.3	

Table 9-1f. Summary of results - VI.

#	Issue	Experimental	Main result / significant relationship / observation	Text ref.	Table 5-2 ref.
31	loss tangent, $\tan_1 \delta$ (NLVE)	T=100°C, γ=50%, ω=10 rad/s	• $M^b \uparrow$ => $\tan_1 \delta \uparrow$ • $N_g \uparrow$ => $\tan_1 \delta \downarrow$ • $w^{g,h}$ has been identified as a possible interference at higher ω	7.1	1.3.1
		T=100°C, γ=200%, ω=0.5rad/s	• $w^{b,g} \uparrow$ => $\tan_1 \delta \downarrow$ (to a plateau)	7.2.1	
		T=100°C, γ=800%, ω=1rad/s		7.3	
32	**$\tan_1 \delta$ ratio** (def. Tab.7-3)	T=100°C, γ=200%, ω=0.5rad/s	• $w^{b,g} \uparrow$ => **$\tan_1 \delta$ ratio** $\downarrow$ for $w^{b,h} < 0.4\%$	7.2.1	
33	frequency - dependence of dynamic moduli $G_1'(\gamma, \omega)$, $G_1''(\gamma, \omega)$ (NLVE)	T=100°C, γ=50-200%, ω=0.5-200rad/s, depending upon γ value	• $G_1'(\gamma, \omega) > G_1''(\gamma, \omega)$ for any γ & ω combination within the range • $G_1''(\gamma, \omega)$ is more sensitive to details of LCB structure than $G_1'(\gamma, \omega)$ is • $G_1''(\gamma, \omega)$ at low strain amplitudes (LVE) better correlates with branching parameters, while applications of higher strains improves test sensitivity	7.2.4	1.3.2
34	frequency - dependence of the loss tangent, $\tan_1 \delta(\gamma, \omega)$ (NLVE)	T=100°C, γ=50, 100, 200%, ω=0.5-200 rad/s, depending upon γ value	• grafting will lower $\tan_1 \delta(\gamma, \omega)$ as compared with backbone prepolymer (C) • both strain and ω-dependence for $\tan_1 \delta(\gamma, \omega)$ is much lower for grafts • $M^b \uparrow$ => $\tan_1 \delta(\gamma, \omega) \downarrow$ and $\tan_1 \delta(\gamma, \omega)$ is less ω-dependent • $N_g \uparrow$ => $\tan_1 \delta(\gamma, \omega) \downarrow$ • first two statements would be are just opposite for a blend (sample M)	7.2.3	1.3.2
35	frequency - dependence of dynamic moduli **mC-C p.c.l.**		• in general, **mC-C p.c.l.** = $f(M^b, N_g, w^{b,h})$ • $M^b \uparrow$ => **mC-C p.c.l.** $\uparrow$ • $N_g \uparrow$ => **mC-C p.c.l.** $\downarrow$ at $w^{b,g} < 10\%$ (plateau at $w^{b,g} > 10\%$)	7.2.2	

Table 9-1g. Summary of results - VII.

#	Issue	Experimental	Main result / significant relationship / observation	Text ref.	Table 5-2 ref.
36	effect of LAOS (large-amplitude oscillatory shear) **G'(5%/VI)**, **G"(5%/VI)**, **tan δ (5%/VI)**	LAOS: γ = 200%, ω=1rad/s; probing oscillations: γ=5%, ω=1rad/s	• no LAOS effect on **G'(5%/VI)** observed • only small effect on **G"(5%/VI)** and **tan δ (5%/VI)**	7.3 Fig. 7-28 Fig. 7-29	1.3.3
			• significant increase of dynamic moduli (particularly G") observed • marginal effect observed for grafts with high N_g and low M^b • highest effect for branching structure with intermediate M^b, N_g but high $w^{b,g}$	7.3 Fig. 7-30	
37	large-strain stress relaxation, G(γ', t) (NLVE)	T=100°C, γ_{eff}=~75%, t>~1s, t<400s	• grafting slows down G(t) resulting in flatter G(t) response, effect increasingly more significant with increasing relaxation times (within 400s range) • most effective in retaining implied stress is branching structure having certain combination of M^b & N_g • $M^b \uparrow$ => G(γ', t) $\uparrow$ at $w^{b,g}$ > 15% • $N_g \uparrow$ => G(γ', t) $\downarrow$ at $M_p{}^b$ >7,600	7.4.1	1.3.4
38	large-strain stress relaxation, **nG(t=0.1)** (NLVE)	T=100°C, γ_{eff}=~75%	• $M^b \uparrow$ => **nG(0.1)** $\downarrow$ • $N_g \uparrow$ => **nG(0.1)** $\uparrow$ @ $M_p{}^b$ >5,000 • $w^{g,h}$ is a factor for nG(t) for t < 10s	7.4.2	
39	temperature-dependence of dynamic moduli E'(T), E"(T)	T=-80 to +40°C γ =2% (adj.) ω =70rad/s	• $w^b \uparrow$ => **T /E"$_{max}$ (BR-α)** $\uparrow$ i.e. E"/(BR-α) peak drifts toward higher temperatures with increasing BR content • $N_g \uparrow$ => **T /E"$_{max}$ (CIIR-α)** $\downarrow$ i.e. E"/(CIIR-α) peak shifts toward lower temperatures with increasing branching frequency	8.5 Fig. 8-2	2.1.1

Table 9-1h. Summary of results - VIII.

#	Issue	Experimental	Main result / significant relationship / observation	Text ref.	Table 5-2 ref.
40	temperature-dependence of loss tangent, tan δ(T)	T=-80 to +40°C γ =2% (adj.) ω =70rad/s	<u>BR-tan δ peak</u>: • grafting => T /tan_{max} δ(BR-α) ↓ i.e. tan δ (BR-α) peak drifts toward lower temperatures upon grafting • $w^{b,h}$ ↑, $w^{b,g}$ ↑ or w^b ↑ => tan_{max} δ(BR-α) ↑ • $w^{b,h}$ ↑, $w^{b,g}$ ↑ or w^b ↑ => INT tan δ(BR-α) ↑ i.e. height and the area of the E" /(BR-α) peak increases with BR composition ($w^{b,h}$, w^b) <u>CIIR-II tan δ peak</u>: • w^b ↑ => T /tan_{max} δ (CIIR-II) ↓ • w^b ↑ => tan_{max} δ (CIIR-II) ↓ <u>CIIR-α tan δ peak</u>: • Mb ↑ => tanmax d (CIIR-a) ↓ • Ng ↑ => tanmax d (CIIR-a) ↑ <u>CIIR (α+II) peak</u>: • M^b ↑ narrows and N_g ↓ widens the double-peak	8.5 Fig.8-2	2.1.2
41	phase morphology	TEM at RT DSC (-120 to +200°C) SEC (30°C, in solution) DTMA (-80 to +40°C)	• 2-phase micro-morphology (CIIR - continuous phase, BR - discrete) exists as per combined TEM/DSC/DTMA evidence, • domain size appears to depend primarily on the chemical composition of the graft, • grafts with small w^b and/or short branches result in major continuous phase (CIIR) and minor isolated domains (BR), for samples with high w^b content, evidence of two co-continuous phases exists (TEM), • TEM was confirmed as the most reliable tool for morphology studies and could be used as a benchmark to assess the sensitivity of other analytical tools, which can be rated as: TEM > DSC > DTMA >> SEC	4.5	3.1

Table 9-1i. Summary of results - IX.

#	Issue	Experimental	Main result / significant relationship / observation	Text ref.	Table 5-2 ref.
42	mapping LCB structure (qualitative characterization of the branching structure), isothermal nC-C plot mC-C plot	isotherms (T=100°C) obtained within the same frequency range (ω=0.005-5 rad/s)	• shape and position of the nC-C and mC-C contour can be related to: a) type of branching structure (star, comb, etc.) b) M^p at N_g =const. c) N_g at M^p =const. d) certain M^b and N_g combination • for nC-C plot, its contour shape is invariant of graft's: 1) explicit chemical composition, w^b, 2) overall molecular weight, M_z^G 3) common structural interferences, PDI and vinyl wt% Effect of ungrafted branch precursor polymer, $w^{b,h}$, if detectable, is limited to the section of the nC-C contour adjacent to its origin.	7.5	3.2
43	characterization of LCB by rheometrical techniques (solid-state)	A few unequivocal * relations between branching parameters and rheological properties were identified as listed below. Those relations can evolve into a calibration curve, potential solid-state (e.g. non-solution) rheometrical techniques for characterization of the LCB in comb-type branching structures, including regular graft copolymers.			
		length of the branch, M^b	a) **slope [G'/G"^{2}]** at 0.001rad/s b) **n(0.001-100)** - from $\eta^*(\omega)$ data	6.1.2 6.1.3	3.3
		branching number, N_g	a) **slope G"(0.001)** b) **G'$_1$(50%)** or **G$_1$*(50%)**	6.1.2 7.1	
		branching content, $w^{b,g}$	a) **n(0.001)** - from $\eta^*(\omega)$ data b) **tan δ ratio**	6.1.3 7.2.1	

*/ 1) the structural parameter (either M^b or N_g or $w^{b,g}$) being the single dominating and statistically significant factor influencing a given rheological parameter with a relationship strong enough to yield acceptable precision in the branching parameter estimation, S=f(R).

2) there is a monotonic relation between a pair of structural and rheological parameters, holding over a relevant range of independent variable (no minimum, maximum or plateau in the S=f(R) relationship, where S and R are a given structural and rheological parameter, respectively.

9.2 Conclusions

1.

The presence of long-chain branching in graft copolymers has a pronounced effect on their rheological properties in the plateau, and particularly in the terminal zone of viscoelastic behaviour. On the other hand, no explicit relationship exists between the chemical composition of the copolymer (w^b) and rheological parameters in these zones. Consequently, many aspects of graft rheological behaviour in these viscoelastic zones resemble those of homopolymeric combs of comparable LCB structure.

To the contrary, the principal features of viscoelastic response in the transition from the glassy to rubbery zones, i.e. the position and height of the transition DTMA (E″(T) and tan d(T)) peaks are controlled primarily by chemical composition of the graft, with LCB related influence being of secondary magnitude only.

2.

It is essential for the proper understanding of the quantitative relationship between LCB structure and rheological properties to consider both principal branching parameters which describe the structure of regular polymeric combs, namely, branch length (M^b) and the (average) number of branches per backbone of the graft molecule, N_g^p. An overall measure of the branching present in a polymeric system, such as overall content of branches, $w^{b,g}$ will relate closely to only a few rheological parameters and is frequently not a sufficient description of the LCB structure from the structure-property relationship point of view.

In most cases, the molecular structure - viscoelastic properties relationship due to branching is monotonic; that is, it steadily increases or decreases within a given range of the LCB parameter, frequently reaching certain plateau or saturation at a sufficiently high value of a specific branching parameter.

Generally, the effect of branch length tends to be of a "step-wise" character, while branching frequency has a more gradual influence on many of the rheological parameters.

Short branches result in only minor or no modification of the rheological behaviour. The effect of branches was found significant only if their length was above a certain critical value, corresponding to about 7,800 - 10,000 g/mol for CIIR-g-BR, which is 4 to 5 times the molecular weight between entanglements, M_e , for BR of comparable microstructure. However, in many cases, an extension of the branch length even significantly above the critical value resulted in only marginal modification of the property in question.

Additionally, a certain critical level of branching, as quantified by $w^{b,g}$, is necessary for branching to have a measurable effect on the rheological properties. It is estimated that for CIIR-g-BR copolymer, the value of this parameter is 10-15%, depending on specific rheological parameters and the branching number.

3. *Frequency dependence of dynamic moduli*

The influence of LCB on frequency dependence is profound, particularly in the terminal zone. Unlike for parent polymers of comparable molecular weight, no cross-over of dynamic moduli is observed above 0.001 rad/s at 100°C for the majority of grafts. Branching tend to elevate both $G'(\omega)$ and $G''(\omega)$ curves and but the effect is particularly pronounced for storage modulus in a terminal zone. The depth of resulting $G'(\omega)$ - $G''(\omega)$ separation depends on the number of branches (N_g), while the position of the corresponding tan δ valley can be related to the length of the branches (M^b). The longer the branches, the lower is the characteristic frequency identified with the presence of branching, which in turn, is related to a delay of the disentanglement process due to branches. For certain combinations of branch length and branching number, in addition to the entanglement plateau (backbone), a second "branching"

plateau is observed, shifted toward much lower frequencies, with shift magnitude being in a certain relation to a branch length.

4. *Stress relaxation*

The shape of the stress relaxation modulus appears to be influenced by three structural parameters: the length of the branches (M^b), the number of branches (N_g) and the content (as well as its average MW ~ M^b) of the ungrafted portion of the branch prepolymer ($w^{b,h}$). While the effect of $w^{b,h}$ is observable only at short relaxation times (< 100s), the slope of both G(t) and nG(t) curves is primarily influenced by the branching number. The higher the branching number the flatter is the stress relaxation curve. The influence of branch length is similar to that observed in dynamic experiments. It relates to the time at which the effect of branches on relaxation process of the graft molecules starts to dominate.

However, the normalized relaxation modulus nG(t') at t' > 100s was found to correlate well with the overall branching content, $w^{b,g}$.

5. *Frequency dependence of complex viscosity*

Frequency dependence of complex viscosity, $\eta^*(\omega)$, fits very well to the Power Law relation. The slope of the log η^* - log ω line relates to branching content, $w^{b,g}$ at $w^{b,g}$ >10%. At lower branching content ($w^{b,g}$ <10%) shear-thinning more closely correlates with specific branching parameters (M^b, N_g).

6. *Grafting versus blending*

Dramatic differences were observed in rheological properties between a graft sample (G4) and a blend of precursor polymers (sample M), equivalent in terms of chemical composition and structure. These differences can only be attributed to the presence of long-chain branching. The differences observed are particularly pronounced for large-strain shear experiments.

7. *Effect of the overall molecular weight of the graft, M_z^G*

For the spectrum of rheological properties examined, no explicit relationship between the overall molecular weight of the graft (M_z^G) and any of the rheological parameters analyzed,

could be found. Weak but statistically significant correlations indicated by screening analysis could be interpreted as resulting from the interrelation which exists among structural parameters of comb-type topology based on a common backbone.

8. *Effect of ungrafted branch precursor polymer, $w^{b,h}$*

Dilution of the graft molecules by linear and low molecular weight molecules originating from residual content of the ungrafted branch prepolymer may, under certain circumstances, give observable effects, thus becoming an interference to the relationship between the LCB structure and rheological properties. The effect, which is experimentally observable if the content of these molecules exceeds 8-10% ($w^{b,h}$), is usually distinguishable from that caused by long branches. It is only observed in experiments involving higher frequencies, shorter relaxation monitoring times and small strain amplitudes.

9. *Effect of other monitored structural/compositional interferences (PDI, vinyl%)*

Neither the polydispersity of the MWD of branches (PDI) nor a small variation of their microstructural composition (specifically vinyl content) had any statistically significant effect on the investigated rheological properties of the CIIR-g-BR.

10. *Effect of the thermo-mechanical history*

The effect of previous shear history of the polymeric sample cannot be ignored in reliable measurements of rheological properties. This is particularly the case for complex polymeric materials, including graft copolymers. The effect of large-amplitude oscillatory shear (LAOS) on small-strain (probing) measurements immediately following it was significant. LAOS resulted in an increase of the values of dynamic moduli, particularly of loss modulus,

G″. The increase was particularly high for grafts with intermediate branching parameters, that is, for those with the highest overall branching content, $w^{b,g}$.

11. *Small-strain (LVE) versus large-strain amplitude (NLVE) dynamic measurements*

Results obtained from large-amplitude dynamic tests in shear did not provide any significant additional insight into the nature of the LCB-rheology relationship. Loss modulus, G″ measured at low strain amplitudes (LVE) provided better correlation with specific branching parameters than its large-strain counterpart, while large-strain dynamic experiments (NLVE) resulted in improved test sensitivity due to stronger signal-to-noise ratio.

12. *DTM analysis of transitions in the glass/transition zones*

For all grafts, regardless of their structure and chemical composition, two separate DTMA E″ and tan δ peaks were observed, corresponding to both parent prepolymers, CIIR and BR. Their position, height and the size, were influenced primarily by the chemical composition of the graft copolymer, and to a lesser extent, by LCB structure of the graft. A summary of findings is included in Figure 8-2.

13. *Phase morphology*

Two phase micro-morphology was observed for the graft copolymers as identified by TEM, and confirmed by DSC and DTMA. No quantitative relationship between structure and composition of the copolymers could yet be obtained. Further details are provided in Table 9-1h, item #41.

14. *Normalized Cole-Cole plots*

The normalized Cole-Cole plot has the potential for identification of the type of long-chain branching in elastomers. Follow-up studies carried out on a wide variety of elastomers confirmed its value for efficient mapping of branching structures in commercial elastomers (Table 9-1i).

15. *Techniques for characterization of LCB*

Suggestions of a few new methods to characterize LCB by solid state (non-solution) rheometrical methods are given in Table 9-1i, item # 43. While they appear to be suitable for quantitative estimation of the branching parameters for comb-type molecules, their application to more complex branched (co)polymers should be verified.

9.3 Originality and significance of the work

This work is believed to constitute an original contribution on the premise that to the best knowledge of the author and as of the day of completion of this work (December 18, 1997):

- no work was published on the rheological properties of CIIR-g-BR graft copolymers,
- no publication reporting the non-linear viscoelastic properties of well-characterized graft copolymers (and few concerned with chemically homogeneous combs) could be found,
- the concept of the normalized Cole-Cole plot was derived during the analysis of data and offers significant improvement over a modified Cole-Cole plot, as a characterization tool for mapping different branching structures present in elastomers, including commercial grades.

The significance of this study can be summarized in the following statements:

(a) it offers explicit directions for designing molecular structure (LCB) in order to achieve a desired set of properties giving improved performance in processing and applications,

(b) it provides a foundation for test methods to qualitatively and quantitatively characterize LCB in elastomers (polymers),

(c) it contributes to fundamental understanding of structure (LCB) - property (rheological) relationship for CIIR-g-BR systems, which might be generalized to graft copolymers, and extended to heterogeneous, comb-type long-chained polymeric systems.

In 1971, Pannell [47] commented in one of the most frequently cited papers, published during the last 30 years concerned with the rheological properties of long-chain branched polymers: "few systematic studies of the effect of varying the branch length and branching frequency on the properties of branched polymer have been published". As far as graft copolymers and rheological properties are concerned, this is still true, with the possible exception of (D)TMA studies in the glassy and transition zones of the linear viscoelastic behaviour.

9.4 Recommendations for future work

Our understanding of the relationship between details of the molecular structure and basic aspects of rheological behaviour is still fragmentary for long-chain branched polymers, with the possible exception of regular, star-like molecules. Much effort will still be required, particularly for more complex polymeric systems such as graft copolymers, to obtain comprehensive and quantitative knowledge of the rheological properties in terms of their long-chain branching structure.

Two-tier research on the rheological properties of the LCB polymers should be continued. One approach involves model polymeric systems obtained by methods which enable a high level of control over the molecular structure and composition of the polymer (macromonomeric, controlled grafting, etc.). Those studies are usually accompanied by a comprehensive analytical characterization program, which contributes to high accuracy with which the LCB structure is known. This in turn permits a confident interpretation of the rheological properties in terms of LCB parameters.

Parallel efforts should continue on commercial branched polymers or systems derived from linear precursors by partial cross-linking by chemical or radio-isotopic means. The resulting

LCB structures are beyond rigorous description and little, if any, structural characterization has been achieved with highly complex LCB structures. As a result, only phenomenological branching parameters (i.e. concentration of the branching agent or dose of radiation) can be related to rheological properties. Complete and quantitative description of the structure-property relationships, comparable to that for model but much simpler LCB structures, might be unattainable for branched, commercial thermoplastics and elastomers.

Any studies which would bridge the large gap existing between these two approaches, for example by studying carefully prepared and well-characterized polymeric systems of progressively more complex branching structures (that is beyond stars and regular combs) would contribute to a better understanding of the structure-property relationship for polymers of commercial importance.

As far as this project is concerned, follow-up work which could be suggested, includes:

- further rheological characterization, including techniques known to be sensitive to LCB, namely creep and recovery experiments, both in shear and tension, and extensional rheometry, particularly high-strain/strain rate techniques,

- rheological characterization of grafts containing a narrowly-polydispersed backbone precursor polymer or a series of backbone molecules of different molecular weight at a range of branch length and frequency,

- similar research programs for other regular graft copolymers; results would allow for subsequent generalization of findings,

- correlation of properly quantified behaviour in a melt/solid processing with rheological properties which could permit better understanding of the relationship between structure (MWD, LCB, gel, etc.) and polymer performance in processing.

References

[1] J. Roovers, *J. Non-Cryst. Solids* **131-133**, 793 (1991)

[2] W.W. Graessley, *Accts. of Chemical Research* **10**, 332 (1977)

[3] F.P. La Mantia, A. Valenza and D. Acierno, *Polym. Eng. Sci.* **28**, 90 (1988)

[4] R.A. Mendelson, W.A. Bowles, and F.L. Finger, *J. Polym. Sci.* A-2, **8**, 105 (1970)

[5] A. Ghijsels, J.J.S. Ente, and J. Raadsen, *Intern. Polym. Process.* **7**, 44 (1992)

[6] M.S. Jacovic, D. Pollock , and R.S. Porter, *J. Appl. Polym. Sci.* 23, 517 (1979)

[7] D. Acierno, F.P. La Mantia, D. Romanini, and A. Savadori, *Rheol. Acta* **24**, 566 (1985)

[8] B.H. Bersted, *J. Appl. Polym. Sci.* **26,** 1001 (1981)

[9] H. Muenstedt and H.M. Laun, *Rheol. Acta* **20**, 211 (1981)

[10] S. Pedersen and A. Ram, *Polym. Eng. Sci.* **18,** 990 (1978)

[11] M. Rokudai and T. Fujiki, *J. Appl. Polym. Sci.*, **26,** 1343 (1981)

[12] D. Romanini, A. Savadori, and G. Gianotti, *Polymer* **21**, 1092 (1980)

[13] J.L. White and H. Yamane, *Pure & Appl. Chem.* **59**, 193 (1987)

[14] A. Rudin, The Elements of Polymer Science and Engineering, Academic Press, San Diego, 1982

[15] R.P. Quirk, *Rubber Chem. Technol.* **57**, 557 (1984)

[16] W.W. Graessley and J. Roovers, *Macromolecules* **12**, 959 (1979)

[17] T. Masuda, Y. Ohta, T. Yamauchi, and S. Onogi, *Polymer J.* **16**, 273 (1984)

[18] T. Fujimoto, H. Kajiura, M. Hirose, and M. Nagasawa, *Polymer J.* **3**, 181 (1972)

[19] T. Fujimoto, H. Narukawa, and M. Nagasawa, *Macromolecules* **3**, 57 (1970)

[20] T. Masuda, Y. Ohta, and S. Onogi, in Current Topics in Polymer Science - Vol. II, Hanser Publishers, R.M. Ottenbrite, L.A. Utracki, S. Inoue, Eds., 1987, p. 140

[21] T. Masuda, Y. Ohta, and S. Onogi, *Macromolecules* **4**, 763 (1971)

[22] S. Onogi and E. Kamei, *J. Appl. Polym. Sci.* **33**, 49 (1978)

[23] C.A. Berglund, C.J. Carriere, and J.D. Ferry, *J. Rheol.* **25**, 251 (1981)

[24] J.M. Carella, J.T. Gotro and W.W. Graessley, *Macromolecules* **19**, 659 (1986)

[25] N. Hadjichristidis and J. Roovers, *Polymer* **26**, 1087 (1985)

[26] G. Kraus and J.T. Gruver, *J. Polym. Sci.* Part A **3**, 105 (1965)

[27] W.E. Rochefort, G.G. Smith, H. Rachapudy, V.R. Raju, and W.W. Graessley, *J. Polym. Sci. Polym. Phys. Ed.* **17**, 1197 (1979)

[28] J. Roovers, *Macromolecules* **24**, 5895 (1991)

[29] P.M. Toporowski and J. Roovers, *J. Polym. Sci. Polym. Chem. Ed.* **24**, 3009 (1986)

[30] W.W. Graessley, T. Masuda, J. Roovers, and N. Hadjichristidis, *Macromolecules* **9**, 127 (1976)

[31] L.J. Fetters, A.D. Kiss, D.S. Pearson, G.F. Quack, and F.J. Vitus, *Macromolecules* **26**, 647 (1993)

[32] D.S. Pearson, S.J. Mueller, L.J. Fetters, and N. Hadjichristidis, *Polym. Prep.* **23**, 21 (1983) and *J. Polym. Sci. Polym. Phys.* **21**, 2287 (1983)

[33] D.S. Pearson and E. Helfand, *Macromolecules* **17**, 888 (1984)

[34] J. Roovers, *Polymer* **22,** 1603 (1981)

[35] V.S. Au-Yeung, C.W. Macosko, and V.R. Raju, *J. Rheol.* **25**, 445 (1981)

[36] R.L. Arnett and C.P. Thomas, *J. Phys. Chem.* **84**, 649 (1980)

[37] V.R. Raju, H. Rachapudy and W.W. Graessley, *J. Polym. Sci. Polym. Phys. Ed.* **17**, 1223 (1979)

[38] H. Staudinger and G.V. Schulz, *Ber. Dtch. Chem. Ges.* **68**, 2320 (1935)

[39] P.J. Flory, *J. Am. Chem. Soc.* **59**, 241 (1937)

[40] J.R. Schaefgen and P.J. Flory, *J. Amer. Chem. Soc.* **70**, 2709 (1948)

[41] N.G. Kumar, *J. Polym. Sci. Macromol. Revs.* **15**, 255 (1980)

[42] V.C. Long, G.C. Berry and L.M. Hobbs, *Polymer* **5**, 517 (1964)

[43] V.L. Folt, *Rubber Chem. Technol.* **42**, 1294 (1969)

[44] L. Gursky, J.V..Fusco, I. Duvdevani, and T. Takeda, *Kautschuk + Gummi Kunststoffe* **43**, 692 (1990)

[45] P.R. Soskey, I. Duvdevani, H.C. Wang and T.E. Richards, ACS Rubber Div. Meeting, Detroit, paper #54, 1989

[46] E.N. Martinez, J.E. Vazquez, and E. Bernal, ACS Rubber Div. Meeting, Mexico City, 1989

[47] J. Pannell, *Polymer* **12**, 558 (1971)

[48] J. Pannell, *Polymer* **13**, 2 (1972)

[49] T. Masuda, Y. Nakagawa, Y. Ohta, and S. Onogi, *Polymer J.* **3**, 92 (1972)

[50] W.W. Graessley and V.R.Raju, *J. Polym. Sci. Polym. Symp.* **71**, 77 (1984)

[51] G.C. Berry and T.G. Fox, *Adv. Polymer Sci.* **5**, 261 (1968)

[52] Y. Isono, T. Fujimoto, H. Kajiura, and M. Nagasawa, *Polym. J.* **12**, 369 (1980)

[53] L.A. Utracki and J.E.L. Roovers, *Macromolecules* **6**, 373 (1973)

[54] Y. Isono, T. Fujimoto, H. Inagaki, M. Shishido, and M. Nagasawa, *Polym. J.* **12**, 131 (1980)

[55] J.S. Ham, *J. Chem. Phys.* **26**, 625 (1957)

[56] J. Roovers, *Macromolecules* **17**, 1196 (1984)

[57] J. Roovers and W.W.Graessley, *Macromolecules* **14,** 766 (1981)

[58] I. Noda, T. Horikawa, T. Kato, T. Fujimoto, and M. Nagasawa, *Macromolecules* **3,** 795 (1970)

[59] Z. Dobkowski, *Eur. Polym. J.* **17,** 1131 (1981)

[60] T.A. Yurasova, T.C.B. McLeish and A.N. Semenov, Macromolecules, **27,** 7205 (1994)

[61] J. Roovers and P.M. Toporowski, *Macromolecules* **20,** 2300 (1987)

[62] W.W. Graessley and J.S. Prentice, *J. Polym. Sci.* A-2 **6,** 1887 (1968)

[63] B.H. Bersted, J.D. Slee, and C.A. Richter, *J. Appl. Polym. Sci.* **30,** 3751 (1985)

[64] L. Wild, R. Ranganath, and D.C. Knobeloch, *Polym. Eng. Sci.* **16,** 811 (1976)

[65] L.A. Hamielec and J.Vlachopoulos, *J. Appl. Polym. Sci.* **28,** 2389 (1983)

[66] G. Smets et M. Claesen, *J. Polym. Sci.* **8,** 289 (1952)

[67] J.A. Blanchette and L.E. Nielsen, *J. Polym. Sci.* **20,** 317 (1956)

[68] J.K. Rieke and G.M. Hart, *J. Polym. Sci.* C **1,** 117 (1963)

[69] J.K. Rieke, G.M. Hart, and F.L. Saunders, *J. Polym. Sci.* C **4,** 589 (1963)

[70] L.H. Tung, *J. Polym. Sci.* **46,** 409 (1960)

[71] B.M. Baccaredda, E. Butta and V. Frosini, *J. Polym. Sci.* C **4,** 605 (1963)

[72] J. Bares and M. Pregoraro, *J. Polym. Sci.* A-2 **9,** 1287 (1971)

[73] M. Pegoraro, L. Szilagyi, and A. Penati, *Rheol. Acta* **13,** 49 (1974)

[74] S.W. Caywood, *Rubber Chem. Technol.* **50,** 127 (1977)

[75] R.C. Thamm and W.H. Buck, *Polym Sci. Polym. Chem. Ed.* **16,** 539 (1978)

[76] Yu. Shibanov, G.N. Arkhipovich and S. Sosnowski, *Intern. Polym. Sci. Technol.*, **20,** T/73 (1993)

[77] J.P. Kennedy, *J. Appl. Polym. Sci. Appl. Polym. Symp.* **30**, 1 (1977)

[78] K. Nakamae, M. Tanaka and S. Li, *Intern. Polym. Sci. Technol.* **20**, T/52 (1993)

[79] Ullman's Encyclopedia of Industrial Chemistry, Vol. **A23**, VCH Publishers, Weinheim, 1993, section 3.1.2

[80] J.P. Kennedy and J.J.Charles, *J. Appl. Polym. Sci. Appl. Polym. Symp.* **30**, 119 (1977)

[81] F.P. Baldwin, I.J. Gardner, A. Malatesta, and J.E. Rae, ACS Rubber Div. Meeting, New Orleans, LA, 1975

[82] C.H. Ho, and W. Hopkins, European Patent Application 92107529.7 (1992)

[83] M. Morton and L.F. Fetters, *Rubber Chem. Technol.* **48**, 359 (1975)

[84] J.Odar - Polysar Polymerization Handbook (unpublished)

[85] G. Jalics and R.G. Bauer, European Patent Application 90630239.3 (1990)

[86] B.W. Brooks and K.M. Riches, British Patent 1,097,997 (1968)

[87] V.M. Monroy, G. Guevara, I. Leon, A. Correa, and R. Herrera, *Rubber Chem. Technol.* **66**, 588 (1993)

[88] Y. Minoura, H. Hironaka, T. Kasabo and Y. Ueno, *J. Polym. Sci.* A-1 **6**, 2773 (1968)

[89] C.H. Ho, private communication

[90] Y. Ikada, *Adv. Polym. Sci.* **29**, 47 (1984)

[91] J.P. Kennedy and D.L. Davidson, *J. Appl. Polym. Sci. Appl. Polym. Symp.* **30**, 13 (1977)

[92] T. Kotaka, *Makromol. Chem.* **177**, 159 (1976)

[93] N.-J. Huang and D.C. Sundberg, *Polymer* **35**, 5693 (1994)

[94] P. Dreyfuss and J.P. Kennedy, *J. Appl. Polym. Sci. Appl. Polym. Symp.* **30**, 165 (1977)

[95] J. Stejskal, D. Strakova, P. Kratochvil, S.D. Smith and J.E. McGrath, *Macromolecules* **22**, 861 (1989)

[96] H. Inagaki and T. Tanaka, in Developments in Polymer Characterization - 3, J.V. Dawkins, Ed., Applied Science Publ., London, 1981, p. 1

[97] D.J. Lohse, S. Datta, and E.N. Kresge, *Macromolecules* **24**, 561 (1991)

[98] G.E. Molau, in Characterization of Macromolecular Structure, D. McIntyre, Ed., National Academy of Sciences, Washington, DC, 1968, p. 245

[99] H-C. Kan, J.D. Ferry, and L.J. Fetters, *Macromolecules* **13**, 1571 (1980)

[100] M. Reiney, *J. Res. Natl. Bur. Standards* **51**, 155 (1953)

[101] J.P. Kennedy, *J. Macromol. Sci.- Chem.* **A4**, 8, 1759 (1970)

[102] P. Sigwalt, A. Polton, and M. Miskovic, *J. Polym. Sci. Symp.* **56**, 13 (1976)

[103] J.P. Kennedy, J.J. Charles, and D.L. Davidson, in Recent Advances in Polymer Blends, Grafts and Blocks, L.H. Sperling, Ed., Plenum, New York, 1974, p. 157

[104] J.P. Kennedy and D.L. Davidson, *J. Polym. Sci. Polym. Chem. Ed.* **14**, 153 (1976)

[105] E. Schroeder, G. Mueller, and K-F. Arndt, Polymer Characterization, Hanser Publ., Munich, 1989

[106] G. Ver Strate and D.J. Lohse, Chapter 3 in Science and Technology of Rubber, 2nd Ed., J.E. Mark, B. Erman and F.R. Eirich, Eds., Academic Press, San Diego, 1994

[107] Z. Dobkowski, in Applied Polymer Analysis and Characterization - Vol. 1, J. Mitchell, Jr, Ed., Hanser Publ., New York, 1997

[108] P.A. Small, *Adv. Polym. Sci.* **18**, 1 (1975)

[109] S. Bywater, *Adv. Polym. Sci.* **30**, 89 (1979)

[110] W. Burchard, *Adv. Polym. Sci.* **48**, 1 (1983)

[111] T. Kotaka, *Makromol. Chem.* **177**, 159 (1976)

[112] Z. Dobkowski, *J. Appl. Polym. Sci.* **28**, 3105 (1983)

[113] M. Rabeony, D.G. Peiffer, W.D. Dozier, and M.Y. Lin, *Macromolecules* **26**, 3676 (1993)

[114] R.J. Ambrose and J.J. Newell, *J. Polym. Sci.* **17**, 2129 (1979)

[115] H-Q. Xie, X-D. Wu, and J-S. Guo, *J. Appl. Polym. Sci.* **45**, 1079 (1994)

[116] A. Gadkari and M. F. Farona, *Polymer Bull.* **17**, 299 (1987)

[117] L.P. Kennedy and D.K. Metzler, *J. Appl. Polym. Sci. Appl. Polym. Symp.* **30**, 141 (1977)

[118] J.P. Kennedy and A. Vidal, *J. Polym. Sci. Polym. Chem. Ed.* **13** (8) 1765 (1975)

[119] J.P. Kennedy, S.S. Plamthottam, and B. Ivan, *J. Macromol. Sci.- Chem.* **A17**, 637 (1982)

[120] J.P. Kennedy and S. C. Guhaniyogi, *J. Makromol. Sci. - Chem.* **A18**, 103 (1982)

[121] E. Schroeder, G. Mueller, and K-F. Arndt, Polymer Characterization, Hanser Publ., Munich, 1989, section 3.6

[122] A. Rudin, "Measurements of Long-Chain Branch Frequency in Synthetic Polymers", Ch. 3 in Modern Methods of Polymer Characterization, H.G. Barth and J.W. Mays, Eds., J. Wiley & Sons, New York, 1991

[123] Th.G. Scholte, in Development in Polymer Characterization - 4 , J.V. Dawkins, Ed. Elsevier, New York, 1986

[124] J. Mays and N. Hadjichristidis, in Modern Methods of Polymer Characterization, Chemical Analysis, Vol. **113**, H.G. Barth and J.W. Mays, Eds., J. Wiley & Sons, NewYork, 1991

[125] W. Burchard, *Adv. Polym. Sci.* **48**, 1 (1983)

[126] E.E. Drott and R.A. Mendelson, *J. Polym. Sci.* A-2, **8**, 1361 (1970)

[127] M. Kurata, M. Abe, M. Iwama, and M. Matsushima, *Polymer J.* **6**, 729 (1972)

[128] A. Ram and J. Miltz, *J. Appl. Polym. Sci.* **15**, 2639 (1971)

[129] D. Constantin, *Europ. Polym. J.* **13**, 907 (1977)

[130] M.M. Coleman and R.E. Fuller, *J. Macromol. Sci.-Phys.* **B11**, 419 (1975)

[131] P. Cheung, R. Lew, S.T. Balke, and T.H. Mourey, *J. Appl. Polym. Sci.* **47**, 1701 (1993)

[132] Z. Dobkowski and J. Brzezinski, *Eur. Polym. J.* **17**, 537 (1981)

[133] H. Kraemer-Lucas, J.Ramthun, and H.W. Lucas, *Makromol. Chem. Macromol. Symp.* **61**, 284 (1992)

[134] G. Kraus and C.J. Stacy, *J. Polym. Sci. Symp.* No. **43**, 329 (1973)

[135] F.M. Mirabella and L.Wild, ACS Polymeric Materials: Science and Engineering Division, Vol. **59**, 7 (1988)

[136] S. Pang and A. Rudin, *J. Appl. Polym. Sci.* **46**, 763 (1992)

[137] W.S. Park and W.W. Graessley, *J. Polym. Sci. Polym. Phys. Ed.* **15**, 85 (1977)

[138] A. Servotte and R. De Bruille, *Makromol. Chem.* **176**, 203 (1975)

[139] A. Rudin and V. Grinshpun, *J. Liq. Chromatogr.* **7**, 1809 (1984)

[140] T. Kato, A.Itsubo, Y.Yamamoto, T. Fujimoto, and M. Nagasawa, *Polymer J.* **7**, 123 (1975)

[141] T. Kato, A. Kanda, A. Takahashi, I. Noda, S. Maki, and M. Nagasawa, *Polymer J.* **11**, 575 (1979)

[142] D.E. Axelson and W.C. Knapp, *J. Appl. Polym. Sci.* **25**, 119 (1980)

[143] S. Shiga and Y.Sato, *Rubber Chem.Technol.* **60**, 1 (1987)

[144] Th.G. Scholte and N.L.J.Meijerink, *Brit. Polym. J.* **9**, 133 (1977)

[145] F.A. Bovey, *Macromolecules* **9**, 76 (1976)

[146] G.N. Foster, *Polym. Prepr.* **20**, 463 (1979)

[147] J.C. Randall, *ACS Symp. Ser.* **142**, 93 (1980)

[148] H. Matsuda, I.Yamada, and S. Kuroiwa, *Polymer J.* **8**, 415 (1976)

[149] Y. Mitsuda, J.L. Schrag, and J. D. Ferry, *J. Appl. Polym. Sci.* **18**, 193 (1974)

[150] Y. Mitsuda, J.L. Schrag, and J. D. Ferry, *Polymer J.* **4**, 668 (1973)

[151] K. Osaki, J.L. Schrag, and J. D. Ferry, *J. Appl. Polym. Sci.* **11**, 549 (1973)

[152] J.D. Ferry, Viscoelastic Properties of Polymers, 3rd Ed., J. Wiley & Sons, New York, 1980, p. 385

[153] H.C. Booij, *Kautschuk + Gummi. Kunstoffe* **44**, 128 (1991)

[154] E. Kraemer-Lucas, private communication

[155] T. Usami, Ch.13 in Handbook of Polymer Science and Technology - Vol. I, N. Cheremisinoff, Ed., Dekker, New York, 1988

[156] S. Pang, J. Pronovost, and A. Rudin, *Polym. Mater. Sci. Eng.* **58**, 474 (1988)

[157] J. Stejskal and P. Kratochvil, *Polymer J.* **14**, 603 (1982)

[158] E. Schroeder, *Plaste u. Kautschuk* **20**, 241 (1973)

[159] S. Mori, in Size Exclusion Chromatography, B.J. Hunt and S.R. Holding, Eds., Blackie, 1989

[160] G. Gloeckner, *J. Appl. Polym. Sci. Appl. Polym. Symp.* **51**, 45 (1992)

[161] S. Mori, *J. Chromatogr.* **542**, 375 (1991)

[162] P. Kiz, R.-P. Krueger, H. Much, and G. Schulz, ACS Proceedings, Div. Polym. Mat. Sci. and Eng. Vol. **69**, 114 (1993)

[163] S. Tanaka, M. Uno, S. Teramachi, *Polymer* **36**, 2225 (1995)

[164] T. Kawai, M. Akashima, S. Teramachi, *Polymer* **36**, 285 (1995)

[165] S. Teramachi, A. Hasegawa, and S. Hasegawa, *Polymer J.* **13**, 319 (1981)

[166] P. Stejskal, P. Kratochvil, *Macromolecules* **11**, 1097 (1978)

[167] T. Tanaka, M. Omoto, N. Donkai, and H. Inagaki, *J. Macromol. Sci.- Phys.* **B17**, 211 (1980)

[168] A. Kikushi and T. Nose, *Polymer* **36**, 2781 (1995)

[169] J. Vorlicek and P. Kratochvil, *J. Polym. Sci. Polym. Phys. Ed.* **11**, 1251 (1973)

[170] S.de Vos, M., Moeller, K. Vissler and P.F. Mijnlieff, *Polymer* **35**, 2644 (1994)

[171] K.G. Suddaby, Ph.D. Thesis, University of Waterloo, 1994

[172] Polysar Analytical Lab Procedure LP# 01-08-437

[173] R.A. Sanayei and K.G. Suddaby, private communication

[174] K.G. Suddaby, R.A. Sanayei, K.F. O'Driscoll, and A. Rudin, *Makromol. Chem.* **194**, 1965 (1993)

[175] R.A. Sanayei, K.G. Suddaby and A. Rudin, *Makromol. Chem.* **194**, 1953 (1993)

[176] American Standard Corp., Mentor, OH

[177] J.E. Puskas and R.Hutchinson, "GPC Calibration for the Molecular Weight Measurement of Butyl Rubbers", Polysar Technical Report ERDD, TR.133.92 #1

[178] ASTM Standard Test Method D3593-86

[179] J.L.Koenig, Spectroscopy of Polymers, ACS, Washington, DC, 1992

[180] H.N. Cheng, *J. Appl. Polym. Sci. Appl. Polym. Symp.* **51**, 21 (1992)

[181] C.Y. Chu and R.Vukov, *Macromolecules* **18**, 1423 (1985)

[182] C.Y. Chu, K.N.Watson, and R.Vukov, *Rubber Chem.Technol.* **60**, 636 (1987)

[183] D.M. Cheng, I.J.Gardner, H.C.Wang, C.B.Frederick, and A.H.Dekmezian, *Rubber Chem. Technol.* **63**, 265 (1990)

[184] J.A. Frankland, H.G.M. Edwards, A.F. Johnson, I.R. Lewis and S. Poshyachinda, "Critical Assessment of Vibrational and NMR Spectroscopic Techniques for the Microstructure Determination of Polybutadienes" (unpublished report)

[185] Polysar Analytical Lab Procedure LP#01-08-369 (92)

[186] Polysar Analytical Lab Procedure LP#01-08-376 (92)

[187] Polysar Analytical Lab Procedure LP#01-08-375 (92)

[188] K. Watson, private communication

[189] S. Poshyachinda, H.G.M. Edwards, and A.F. Johnson, Polymer **32**, 338 (1991)

[190] H.J. Harwood, *Rubber Chem. Technol.* **55**, 769 (1982)

[191] T.R. Crompton, Analysis of Polymers - An Introduction, Pergamon Press, New York, 1989, p. 90

[192] J.L. Binder, *J. Polym. Sci. A*, **1**, 47 (1963)

[193] E. Schroeder, G. Mueller, and K-F. Arndt, Polymer Characterization, Hanser Publ., Munich, 1989, p. 215

[194] Polysar Analytical Lab Procedure LP#01-08-464 (93)

[195] Calorimetry and Thermal Analysis of Polymers, Ed. by V.B.F. Mathot, Hanser Publ., Munich, 1994, chapter 5

[196] Polysar Analytical Lab Procedure LP# 01-08-429 (93)

[197] Polysar Analytical Lab Procedure LP# 01-08-385

[198] Polysar Analytical Lab Procedure LP# 01-08-392

[199] Calorimetry and Thermal Analysis of Polymers, Ed. by V.B.F. Mathot, Hanser Publ., Munich, 1994, p. 64

[200] H.H. Willard, L.L. Merritt, Jr., J.A. Dean, and F.A. Settle, Jr., Instrumental Methods of Analysis, 7th Ed., Wadsworth Publishers, Belmont, CA, 1988

[201] ASTM Standard Test Method, D3616-88

[202] Polysar Analytical Lab Procedure LP#01-08-118 (48-hrs method)

[203] Polysar Analytical Lab Procedure WC-20

[204] Polysar Analytical Lab Procedure WC-2

[205] S.C. deVos and M. Moeller, *Makromol. Chem. Macromol. Symp.* **75**, 223 (1993)

[206] Y. Frere, Y. Guilbert, and Ph. Gramain, *New Polym. Mater.* **3**, (3) 175 (1992)

[207] J. Roovers, in: "Encyclopedia of Polymer Science and Engineering", Vol. **2**, J.I. Kroschwitz, Ed., J. Wiley & Sons, N.Y., 1985, p. 483

[208] I. Kuntz, K.D. Rose, *J. Polym. Sci. Part A Polym. Chem.* **27**, 107 (1989)

[209] J.L. White, T.D. Shaffer, C.F. Ruff, and J.P. Cross, *Macromolecules* **28**, 3290 (1995)

[210] J.E. Puskas and C. Wilds, *Rubber Chem. Technol.* **67**, 329 (1994)

[211] J.J. Sendorek and W. Hopkins, unpublished study

[212] J.R. Francis, Ph.D. Thesis, U. of Massachusetts, 1980

[213] M.R. Ambler, *J. Appl. Polym. Sci.* **21**, 1655 (1977)

[214] J.L. Leblanc, *Plast. Rubber Proc. Appl.* **1**, 187 (1981)

[215] W. Hopkins, private communication

[216] D. Padliya, private communication

[217] M.P. Stevens, Polymer Chemistry, 2nd Ed., Oxford U. Press, 1990, p. 248

[218] H.R. Allcock and F.W. Lampe, Contemporary Polymer Chemistry, Prentice Hall, 2nd Ed., 1990, p. 312

[219] G. Kaszas, J.E. Puskas, and J.P. Kennedy, *Macromolecules* **25**, 1771, 1775 (1992)

[220] G. Kaszas, Polysar Technical Report: TR 93-022

[221] A. Koski, private communication

[222] M. Morton, Anionic Polymerization: Principles and Practice, Academic Press, New York, 1982, p. 297

[223] F.P. Baldwin, I.J. Gardiner, A. Malatesta, and J.E. Rae, ACS Rubber Div. Meeting Proceedings, New Orleans, 1975

[224] W.S. Bahary, D.I. Sapper, and J.H. Lane, *Rubber Chem. Technol.* **40**, 1529 (1967)

[225] G. Kraus and J. Gruver, *J. Polym. Sci.* **A-2**, 797 (1964)

[226] J.W. Mays and N. Hadjichristidis, *J. Appl. Polym. Sci. Appl. Polym. Symp.* **51**, 55 (1992)

[227] H.L. Hsieh, *Rubber Chem. Technol.* **39**, 491 (1966)

[228] H.L. Hsieh, *J. Polym. Sci.* **A3**, 153, 163, 173, 191 (1965)

[229] J. Carella, Ph.D. Thesis, Northwestern University, 1983

[230] S. Bywater, *Adv. Polym. Sci.* **4**, 66 (1965)

[231] J. Roovers, *Polymer J.* **18**, 153 (1986)

[232] W.W. Graessley, "Viscoelasticity and Flow in Polymer Melts and Concentrated Solutions", Ch. 3 in Physical Properties of Polymers, 2nd Ed., ACS, Washington, DC, 1993

[233] M.J. Struglinski, Ph.D. Thesis, Northwestern University, 1984

[234] C.A. Uraneck, *J. Polym. Sci.* Part A-1 **9**, 2273 (1971)

[235] H.L. Hsieh, *J. Polym. Sci.* A **3**, 181 (1965)

[236] Y.G. Yanovsky, G.V.Vinogradov and L.I.Ivanova, *Chem. Eng. Commun.*, **32**, 219 (1985)

[237] G.V. Vinogradov., A. Ya. Malkin, and V.G. Kulichikhin, *J. Polym. Sci.* A-2 **8**, 333 (1970)

[238] J. Carella, Ph.D. Thesis, Northwestern University, 1983

[239] J.M. Carella, W.W. Graessley, and L.J. Fetters, *Macromolecules* **17**, 2775 (1984)

[240] A. Barlow, L. Wild, and T. Roberts, *J. Chromatogr.* **55**, 155 (1971)

[241] R.H. Valentine, J.D. Ferry, T. Homma, and K. Ninomiya, *J. Polym. Sci.* A-2 **6**, 479 (1968)

[242] Zs. Fodor, A. Fodor, and J.P. Kennedy, *Polym. Bull.* **29**, 689 (1992)

[243] Polymer Handbook, 3rd Ed., J. Brandrup and E.H. Immergut, Eds., J. Wiley & Sons, New York, 1989, p. VI/657 and VI/658

[244] J. Oziomek and J.P.Kennedy, *J. Appl. Polym. Sci. Appl. Polym. Symp.* **30**, 91 (1977)

[245] L.H. Tung and R.M. Wiley, *J. Polym. Sci. Polym. Phys. Ed.* **11**, 1413 (1973)

[246] H. Ohnuma, T. Kotaka, and H. Inagaki, *Polymer J.* **1**, 716 (1970)

[247] T. Kotaka, *Makromol. Chem.*, **177**, 159 (1976)

[248] J. Vorlicek and P. Kratochvil, *J. Polym. Sci. Polym. Phys. Ed.* **11**, 1251 (1973)

[249] A. Rudin, The Elements of Polymer Science and Engineering, Academic Press, San Diego, 1982, p. 70

[250] J. Roovers, *Macromolecules* **20**, 148 (1987)

[251] M.J. Struglinski, W.W. Graessley, and L.J. Fetters, *Macromolecules* **21**, 783 (1988)

[252] J.E. Guillet, R.L. Combs, D.F. Slonaker, D.A.Weemes, and H.W. Coover, Jr., *J. Appl. Polym. Sci.* **8**, 757 (1965)

[253] J.E. Guillet, R.L. Combs, D.F. Slonaker, D.A. Weemes, and H.W. Coover, Jr., *J. Appl. Polym. Sci.* **9**, 767 (1965)

[254] Prof. T. Duever, University of Waterloo, private communication

[255] G. Ver Strate and D.J. Lohse, Science and Technology of Rubber, 2nd Ed., J.E. Mark, B. Erman and F.R. Eirich, Eds., Academic Press, San Diego, 1994, p.140

[256] N. Nakajima, J.J. Scobbo, Jr., and E.R. Harrell, *Rubber Chem.Technol.* **60**, 742 (1987)

[257] N. Nakajima and E.R. Harrell, *Rubber Chem.Technol.* **53**, 14 (1980)

[258] N. Nakajima and E.R. Harrell, *Rubber Chem.Technol.* **59**, 305 (1986)

[259] N. Nakajima and E.R. Harrell, "Viscoelastic Characterization of Long-Chain Branching and Gel in Elastomers", in Encyclopedia of Fluid Mechanics, Vol. 9, Gulf Publ., 1990, chapter 16

[260] N. Nakajima, *J. Appl. Polym. Sci. Applied Polym. Symp.* **50**, 79 (1992)

[261] N. Nakajima and E.A. Collins, *J. Rheol.* **22**, 547 (1978)

[262] J.P. Kennedy and E.G.M. Tornquist, Polymer Chemistry of Synthetic Elastomers, Interscience Publishers, New York, 1968

[263] W.O.Baker, *Rubber Chem. Technol.* **22**, 935 (1949)

[264] S. Lee, *TRIP* **1**, 303 (1993)

[265] B.J.R. Scholtens and T.L. Welzen, *Makromol. Chem.* **182**, 269 (1981)

[266] V.F. Gaylor, H.L. James, and J.P. Herdering, *J.Polym.Sci.* **13**, 1575 (1975)

[267] T. Hjertberg, L.-I. Kulin, and E. Soervik, *Polymer Testing* **3**, 267 (1983)

[268] H. Inagaki and T Tanaka, "Separation and Molecular Characterization of Copolymers", Developments in Polymers Characterization - 3, J.V. Dawkins, Ed., Applied Science, 1981, p. 15

[269] L. Bohn, *Rubber Chem. Technol.* **41**, 495 (1968)

[270] A. Rudin, The Elements of Polymer Science and Engineering, Academic Press, San Diego, 1982, chapter 12

[271] A. Rudin and H.P. Schreiber, *Polym. Eng. Sci.* **23**, 422 (1983)

[272] D.C. Evans, M.H. George, and J.A. Barrie, *Polymer* **16**, 690, (1975)

[273] J.P. Kennedy and J..M. Delvaux, *Adv. Polym. Sci.* **38**, 141 (1981)

[274] C. Price, R. Singleton, and D. Woods, *Polymer* **15**, 117 (1974)

[275] R.F. Bauer and E.A. Dudley, *Rubber Chem. Technol.* **50**, 35 (1977)

[276] D.B. Alward, D.J.Kinning, E.L. Thomas, and L.J. Fetters, *Macromolecules* **19**, 215 (1986)

[277] RMS-800 - Owner's Manual & related materials, Rheometrics Inc., 1992

[278] R.W. Whorlow, Rheological Techniques, 2nd Ed., Ellis Horwood, London, 1992, chapter 6

[279] K. Walters, Rheometry, Chapman and Hall, London, 1975, chapter 6

[280] Polysar Test Procedure, LP# 01-02-266

[281] A.R Payne and R.E. Whittaker, *Rubber Chem. Technol.* **44**, 440 (1971)

[282] A.I. Medalia, *Rubber Chem. Technol.* **51**, 437 (1978)

[283] J.D. Ulmer, *Rubber Chem. Technol.* **69**, 15 (1996)

[284] N.K. Dutta and D.K. Tripathy, *Kautschuk + Gummi. Kunststoffe* **42**, 665 (1989)

[285] A.K. Sircar and T.G. Lamond, *Rubber Chem. Technol.* **48**, 79 (1975)

[286] L.G. Nielsen and R.L. Landel, Mechanical Properties of Polymers and Composites, 2nd Ed., Marcel Dekker, New York, 1994, p. 155

[287] B. Maxwell and C. Guimon, *J. Appl. Polym. Sci.* **6**, 83 (1962)

[288] M.N. Rahaman and J. Scanlan, *Polymer* **22**, 673 (1981)

[289] G.E. Warnaka and H.T. Miller, *Rubber Chem. Technol.* **39**, 1421, 1428 (1966)

[290] J. Sendorek - unpublished results

[291] G.Floudas, N. Hadjichristidis, H. Iatrou, T. Pakula, and E.W. Fisker, *Macromolecules* **27**, 7735 (1994)

[292] W.J. Tchir and P.C. Saucier, ANTEC '91 Proceedings, page 2321

[293] S. S. Bafna, *Polym. Sci. Eng.*, **36**, 90 (1996)

[294] ISO 3534-1 1993, point 3.11

[295] H. Tang, unpublished reports and private communication

[296] ISO 3534-1 1993, point 3.14

[297] J. Mandel and R.D. Stiehler, *J. Res. Nat. Bur. Stand.* **53**, 155 (1954)

[298] R. Koopmann, unpublished BAYER AG Technical Report, 1995

[299] Rheometrics Solids Analyzer, RSA-II - User's Manual, Rheometrics Inc., 1990

[300] H. Tang, Polysar Technical Report, 1988 and J. Sendorek unpublished data (1990-1994)

[301] J. Sendorek and H. Tang, unpublished results and reports (1988-1992)

[302] RPA 2000 - Product Brochure, Alpha Technologies Inc., Akron, Ohio

[303] H. Pawlowski, R. Barker, and D. King, BR&PI 25th Intern. Conference, Leuven, 1994

[304] H. Pawlowski and J. Dick, *Rubber World* June 1992, page 37

[305] H. Pawlowski and J. Dick, ACS Rubber Div. Meeting, Louisville, 1992, paper #70

[306] H. Pawlowski and J. Dick, Presentation to the Akron Rubber Group, Akron 1992

[307] H. Pawlowski and J. Dick, *Rubber & Plastics News*, January 1997

[308] A.J. Giacomin and J.M. Dealy, "Large Amplitude Oscillatory Shear", Chpt. 4 in Techniques in Rheological Measurements, A.A. Colyer, Ed. , Chapman & Hall, London 1993

[309] M.J. Reimer and J.M. Dealy, *J. Rheol.* **40**, 167 (1996)

[310] J.S. Dick and H. Pawlowski, ACS Rubber Div. Meeting, Chicago, Ill., 1994, paper #5

[311] H. Pawlowski, private communication

[312] M.D. Graham, *J. Rheol.* **39**, 697 (1995)

[313] H.G. Burhin, Monsanto Technical Centre, Louvain-La-Neuve, Belgium, unpublished report, 1992

[314] E.R. Harrell, J.P. Porter, and N. Nakajima, *Rubber Chem. Technol.* **64**, 254 (1991)

[315] E.R. Harrell, J.P. Porter, and N. Nakajima, ACS Rubber Div..Meeting, Detroit, October 1989, paper #76

[316] K. Yagii and E. Maekawa, *Nippon Gomu Kyokashi* **40**, 46 (1967)

[317] D. Hasman, G.F. Goodrich, unpublished presentation to the ASTM Committee and private comunication

[318] J. J. Sendorek, unpublished reports, 1993 - 1994

[319] J. J. Sendorek, unpublished reports, 1994

[320] Bayer Rubber Div. Test Procedure # LP 01-02-268, 1995

[321] J.J. Sendorek, unpublished work

[322] Z.J. Lobos, H. Tang, *Rubber Chem. Technol.* **62**, 623 (1989)

[323] N. Nakajima, R.A. Miller, and E.R. Harrel, *Intern. Polymer Processing* **2**, 88 (1987)

[324] N. Nakajima and J.P. Parkey, Paper presented at the 69th Annual Meeting of The Society of Rheology, Columbus, OH, October 1997

[325] J.D. Ferry, Viscoelastic Properties of Polymers, 3rd Ed., J. Wiley & Sons, New York, 1980, p. 379

[326] S.Onogi, T. Masuda, and K. Kitagawa, *Macromolecules* **3**, 109 (1970)

[327] J.D. Ferry, Viscoelastic Properties of Polymers, 3rd Ed., J. Wiley & Sons, New York, 1980, p. 203

[328] Y. Mitsuda, J.L. Schrag, and J.D. Ferry, *J. Appl. Polym. Sci.* **18**, 193 (1974)

[329] A.V. Tobolsky, *J. Chem. Phys.* **42**, 723 (1965)

[330] G. Akovali, *J. Polym. Sci.* Part A-2, **5**, 875 (1967)

[331] N. Nakajima, and E.R. Harrell, "Modified Cole-Cole Plot as a Tool for Rheological Analysis of Polymers" in Current Topics in Polymer Science - Vol. II, R.M. Ottenbridge, L.A. Utracki, S. Inoue, Eds., Hanser Publ., Munich, 1987

[332] E.R. Harrell and N. Nakajima, *J. Appl. Polym. Sci.* **29**, 995 (1984)

[333] N. El Kissi, J.M. Piau, P. Attane, and G. Turrel, *Rheol. Acta* **32**, 293 (1993)

[334] B.H. Bersted, "Effect of Long Chain Branching on Polymer Rheology", in Encyclopedia of Fluid Mechanics, Vol.7, Gulf Publ., 1988, p. 635

[335] C.D. Han and J.K. Kim, *Polymer* **34**, 2533 (1993)

[336] C.D. Han and M.S. Jhou, *J. Appl. Polym. Sci.* **32**, 3809 (1986)

[337] RHECALC - User's guide, Rev. C, February 1994

[338] J.D. Ferry, Viscoelastic Properties of Polymers, 3rd Ed., J. Wiley & Sons, New York, 1980, chapter 11

[339] Rheometrics Inc., Application Newsletter, 1988

[340] M. Van Gurp and J. Palmen, *Rheology Bulletin* **67**, No. 1, Jan. 1998

[341] J.T. Gotro and W.W. Graessley, *Macromolecules* **17**, 2767 (1984)

[342] C.A. Bero and C.M. Roland, *Macromolecules* **29**, 1562 (1996)

[343] A. Santamaria, *Mat. Chem. Phys.* **12,** 1 (1985)

[344] L.A. Utracki, Polymer Alloys and Blends, Hanser Publ., New York, 1989, p. 234

[345] D.G. Fesko and N.W. Tschoegl, *J. Polym. Sci.* **C35**, 51 (1971)

[346] A. Munari, G. Pezzin, and F. Pilati, *Rheol. Acta* **29**, 469 (1990)

[347] L. Boghetich and R.F. Kratz, *Trans. Soc. Rheol.* **9**, 255 (1965)

[348] W.W. Graessley and E.S.Shinbach, *J. Polym. Sci. Polym. Phys. Ed.* **12**, 2047 (1974)

[349] R.A. Mendelson, *Trans. Soc. Rheol.* **9**, 53 (1965)

[350] W.W. Graessley, *Macromolecules* **15,** 1164 (1982)

[351] J.D. Ferry, Viscoelastic Properties of Polymers, 3rd Ed., J. Wiley & Sons, New York, 1980, p. 276

[352] E.R. Fitzgerald, L.D. Grandine, and J.D. Ferry, *J.Appl.Phys.* **24**, 650 (1953)

[353] J.D. Ferry, Viscoelastic Properties of Polymers, 3rd Ed., J. Wiley & Sons, New York, 1980, p. 277

[354] J.J. Sendorek, unpublished data and reports

[355] J.D. Ferry, Viscoelastic Properties of Polymers, 3rd Ed., J. Wiley & Sons, New York, 1980, p. 374

[356] M. Doi and N.Y. Kuzuu, *J. Polym. Sci. Polym. Lett. Ed.* **18,** 775 (1980)

[357] W.W. Graessley, *J. Polym. Sci. Phys. Ed.* **27**, 18 (1980)

[358] P-G. DeGennes, Scaling Concepts in Polymer Physics, Cornell University Press, Ithaca, 1979, p. 230

[359] J.J. Sendorek, unpublished data, 1995-1997

[360] L.A. Utracki, Polymer Alloys and Blends, Hanser Publishing, New York, 1989, p. 229

[361] M.J. Reimers and J.M. Dealy, *J. Rheol.* **40**, 167 (1996)

[362] R.G. Mancke, R.A. Dickie, and J.D. Ferry, *J. Polym. Sci.* A-2, **6**, 1783 (1968)

[363] L.A. Utracki, Polymer Alloys and Blends, Hanser Publishing, New York, 1989, p. 194

[364] T. Fujiki, *J. App. Polym. Sci.* **15**, 47 (1971)

[365] B. Maxwell and A. Breckwoldt, *J. Rheol.* **25**, 55 (1981)

[366] M. Rokudai, S. Mihara, and T. Fujiki, *J. Appl. Polym. Sci.* **23,** 3289 (1979)

[367] M. Rokudai and T. Fujiki, *J. Appl. Polym. Sci* , **23,** 3295 (1979)

[368] J.J. Sendorek, unpublished reports

[369] L.E. Nielsen and R.F. Landel, Mechanical Properties of Polymers and Composites, 2nd Ed., M. Dekker, New York, 1994, page 16

[370] J.D. Ferry, Viscoelastic Properties of Polymers, 3rd Ed., J. Wiley % Sons, New York, 1980, page 36

[371] J.D. Ferry, Viscoelastic Properties of Polymers, 3rd Ed., J. Wiley & Sons, New York, 1980, page 285

[372] L.E. Nielsen and R.F. Landel, Mechanical Properties of Polymers and Composites, 2nd Ed., M. Dekker, New York, 1994, page 17

[373] R.F. Boyer, *J. Polym. Sci.* C **14**, 3 (1966)

[374] L.E. Nielsen and R.F. Landel, Mechanical Properties of Polymers and Composites, 2nd Ed., M. Dekker, New York, 1994, chpt. 1

[375] J. Heijboer, *Br. Polym. J.*, **1**, 3 (1969)

[376] E. Maekawa, R.G. Mancke, and J.D. Ferry, *J. Phys. Chem.* **69**, 2811 (1965)

[377] Ullman's Encyclopedia of Industrial Chemistry, Vol. A23, VCH Publishers, Weinheim, 1993, p. 274

[378] J.D. Ferry, Viscoelastic Properties of Polymers, 3rd Ed., J. Wiley & Sons, New York, 1980, page 324

[379] F-S. Liao, Au-C. Su, and T-C. J. Hsu, *Polymer* **35**, 2579 (1994)

[380] J.F. Sanders and J.D. Ferry, *Macromolecules* **7**, 681 (1975)

[381] R.F. Boyer, *J. Appl. Polym. Sci.* **32**, 4075 (1986)

[382] S.E. Keinath and R.F. Boyer, *J. Appl. Polym. Sci.* **28**, 2105 (1983)

[383] R.F. Boyer, in "Order in the Amorphous State of Polymers", S.E. Keinath, R.L. Miler and J.K. Rieke, Eds., Plenum Publ., New York, 1987, p. 135

[384] R.F. Boyer, *Macromolecules* **14**, 376 (1981)

[385] V.A. Kargin, *J. Polym. Sci.* C, **4**, 1601 (1963)

[386] A.J. Braettaerd and G.W. Tregear, Graft Copolymers, J. Wiley, New York 1967,

[387] C.E. Locke and D.R. Paul, *J. Appl. Polym. Sci.* **17**, 2597 (1973)

[388] I.A. Tumanova, O.B. Semenov and Yu.G. Yamanovsky, *Intern. J. Polymeric Mater.* **8**, 225 (1980)

[389] J.P. Kennedy and M. Nakao, *J.Appl. Polym. Sci. Appl. Polym. Symp.* **30**, 7 (1977)

[390] D.J. Lohse, S. Datta, and E.N. Kresge, *Macromolecules* **24**, 561 (1991)

[391] J. Roovers and P. Toporowski, *J. Appl. Polym. Sci.* **18**, 1685 (1974)

[392] F. Rietsch, D. Daveloose, and D. Froelich, *Polymer* **17**, 859 (1976)

[393] C. Kow, M. Morton, and L.J. Fetters, *Polymer* **17**, 245 (1976)

Appendix I

Bibliography: rheological properties of long-chain branched polymers

Important references to the literature on rheological properties of the long-chain branched polymers were grouped according to two principal criteria: type of branching topology (by rows) and type of the rheological experiment (by columns).

First six rows (A, B, C, Ds, Dr, & E) are concerned with "homogeneous" long-chain branched structures. They could be either homopolymers or copolymers sharing one common characteristics: all their structural elements; (backbone, branches, arms etc.) are built of molecules of identical chemical composition, microstructure, secondary branching etc. Heterogeneous polymers of certain structural regularity include graft copolymers (G) and star-blocks (F). Blends of branched polymers with chemically different linear matrices and some other more complex structures (H) complete the collection of references to published research on rheological properties of solid polymers. A few selected papers on branched systems in solution are also listed (Ss, Sc, Sr).

Types of rheological experiments (and coterminous rheological properties) are grouped in three main categories: linear (I-V) and non-linear (VI-IX) viscoelastic properties, and some other tests (X). References discussing linear viscoelastic properties are for convenience, divided according to the four main viscoelastic zones; glassy (I), transition (II) and plateau/terminal. The latter category, due to the number of references is subsequently subdivided according to the type of experiments used: dynamic (III) (almost always sinusoidal oscillatory), transient (IV) (such as stress relaxation or creep/recovery experiments) and steady shear or extension (V). The term 'limiting' refers to rheological parameters such as zero-shear viscosity or recoverable compliance. No reports on the non-linear viscoelastic properties of LCB polymer referring specifically to the transition zone could be found. Large strain amplitude/rate tests below the glass transition point are frequently considered as 'mechanical' tests and references some to some papers are given in column X.

Areas in Table A1 highlighted by bold frames correspond directly to the type of branched samples and testing methodology used in this work. No published studies on the non-linear viscoelastic properties of graft copolymers are known to the author. Most of the literature concerned with rheological properties of grafts report results of dynamic thermo-mechanical studies, particularly the effects of graft composition, morphology and, in a few cases, details of branch structure on the position and magnitude of tan δ (or loss modulus) peaks.

The main thrust of this literature search was to find references on model or highly regular structures relevant to this work. It should not be considered as complete.

Table A1. Rheological properties of long-chain branched polymers: references to selected original experimental contributions.

			LINEAR VISCO-ELASTIC				NonLINEAR VISCO-ELASTIC				Other types of flow /deformation
			glassy & transition	plateau & terminal: dynamic	plateau & terminal: transient	plateau & terminal: steady or limiting	shear: dynamic	shear: transient	shear: steady	extension: tensile bi-axial planar	
			I/II	*III*	*IV*	*V*	*VI*	*VII*	*VIII*	*IX*	*X*
CHEMICALLY HOMOGENEOUS	Regular stars	*A*	A1 - 6	A7 - 28	A26 A29 - 30	A10 - 27 A29 A31 - 42		A40	A3 A27 A41 - 44	A10 A45	A46
	Regular combs	*B*	B1 - 2	A39 B3	A36 B4				A39 B5		B5 - 6
	Other regular structures	*C*		B3 C1		B3 C1					
	Star/linear Comb/linear blend	*Ds*	A5	A15 A25 D1 - 4	A30 D5	A15 A25 D1			D6		
	Random/ linear blend	*Dr*		D10				D8	D7 - 12	D7 D13 - 14	D8 D15
	Randomly branched structures	*E*	E1 - 3	D10 G19 E4 - 29	E11 - 12 E30 - 32	A7 D12 E9 - 12 E22 - 23 E33 - 48	E45	E4 E30 E45 E49 - 52	D10 - 12 D15 E10 - 13 E17, 30 E26 - 28 E33 - 36 E40 - 42 E45 - 47 E49 E53 - 95	D13 - 14 E6 - 7 E21,28,30 E34,45,52 E59 - 60 E64 E71 - 73 E88 - 89 E92 E96 - 104	B6, D15 E10, 17 E23, 27 E42, 50 E65 - 68 E89, 91 E105 - 116
CHEM. HETEROGENEOUS	Star-blocks/*	*F*	F1 - 2/* A4/*	*A30* *G37 - 38*	*G23* *G25*	*G38*			E55, G6 G13, 22 G39 - 41	A30 G14	E106 G42 - 43
	Grafts	*G*	*G1 - 36*								
	Randomly branched & blends	*H*	G16	H1	H1			H2 - 3			H2
IN CONCENTRATED SOLUTIONS	Stars in solutions	*Ss*		A15, 21 A27 S1 - 6	S7	A15,27,40 S2 - 5 S8 - 13		A22, 40 S3, 7	A27, G38 S3, 8, 11 S14 - 15		
	Combs/ grafts in solutions	*Sc*				A21, 39 S9, 16			A39 S17		
	Random structures in solutions	*Sr*		S18 - 20		S18 - 20 S21			S21		

References for bibliography

A1 Gorda, K.R. and D.G. Peiffer,
"Star-Shaped Condensation Polymers: Synthesis, Characterization, and Blend Properties",
J. Appl. Polym. Sci., **50**, 1977 (1993)

A2 Kow, C., M.Morton, and L.J.Fetters,
"Glass Transition Behaviour of Polyisoprene: The Influence of Molecular Weight, Terminal Hydroxy Groups, Microstructure, and Chain Branching",
Rubber Chem.Technol., **55**, 245 (1982)

A3 Wyman, D.P., L.J.Elyash, and W.J.Frazer,
"Comparison of Some Mechanical Properties of Linear and Tetrachain Branched "Monodisperse" Polystyrenes",
J. Polym. Sci., A **3**, 681 (1965)

A4 Roovers, J.E.L. and P.M. Toporowski,
"The Glass Transition Temperature of Star-Shaped Polystyrenes"
J.Appl.Polym.Sci., **18**, 1685 (1974)

A5 Rietsch F., D. Daveloose and D. Froelich,
"Glass Transition Temperature of Ideal Polymeric Network",
Polymer, **17**, 859 (1976)

A6 Takeichi, T. and J.K. Sille,
"Star and Linear Oligomers Containing Reactive End Caps: Preparation and Thermal Properties",
Macromolecules, **19**, 2093 (1986)

A7 Berger, T., D.A. McIntyre, and E. Hager,
"Effect of Entanglement on a High Molecular Weight Graft Elastomer",
ACS Rubber Div. Meeting, Denver, Colorado, May 1993

A8 Pearson, D.S. and E.Helfand,
"Visco-Elastic Properties of Star-Shaped Polymers",
Macromolecules, **17**, 888 (1984)

A9 Ohta, Y., T. Masuda, and S. Onogi,
"Viscosity and Steady-State Compliance of Multi-Branched Star Polystyrenes",
Polym. J., **18**, 337 (1986)

A10 Au-Yeung, V.S., C.W.Macosko, and V.R.Raju,
"Extensional Flow of Linear and Star-Branched Hydrogenated Polybutadiene with Narrow Molecular Weight Distribution",
J. Rheol., **25**, 445 (1981)

A11 Masuda T., Y.Ohta, T.Yamauchi, and S.Onogi,
"Characterization and Rheological Properties of Multi-Branched Star Polystyrenes",
Polymer J., **16**, 273 (1984)

A12 Hadjichristidis N. and J. Roovers,
"Linear Viscoelastic Properties of Mixtures of 3- and 4-Arm Polybutadiene Stars",
Polymer, **26**, 1087 (1985)

A13 Graessley, W.W. and J.Roovers,
"Melt Rheology of Four-Arm and Six-Arm Star Polystyrenes",
Macromolecules, **12**, 959 (1979)

A14 Carella, J.M., J.T.Gotro and W.W.Graessley,
"Thermorheological Effects of Long-Chain Branching in Entangled Polymer Melts",
Macromolecules, **19**, 659 (1986)

A15 Graessley, W.W. and V.R.Raju,
"Some Rheological Properties of Solutions and Blends of Hydrogenated Polybutadiene",
J. Polym. Sci.: Polym. Symp., **71**, 77 (1984)

A16 Roovers, J.,
"Melt Rheology of Highly Branched Polymers",
J. Non-Cryst. Solids, **131-133**, 793 (1991)

A17 Roovers, J.,
"Properties of the Plateau Zone of Star-Branched Polybutadienes and Polystyrenes",
Polymer, **26**, 1091 (1985)

A18 Raju, V.R., H.Rachapudy and W.W.Graessley,
"Properties of Amorphous and Crystallizable Hydrocarbon Polymers. IV. Melt Rheology of Linear and Star-Branched Hydrogenated Polybutadiene"
J. Polym. Sci. Polym. Phys. Ed., **17**, 1223 (1979)

A19 Roovers, J.,
"Viscoelastic Properties of 32-Arm Star Polubutadienes",
Macromolecules, **24**, 5895 (1991)

A20 Rochefort, W.E., G.G. Smith, H.Rachapudy, V.R. Raju, and W.W.Graessley,
"Properties of Amorphous and Crystallizable Hydrocarbon Polymers. II. Rheology of Linear and Star-Branched Polybutadiene",
J. Polym. Sci. Polym. Phys. Ed., **17**, 1197 (1979)

A21 Raju, V.R., E.V.Menezes, G.Marin, W.W.Graessley, and L.J.Fetters,
"Concentration and Molecular Weight Dependence of Viscoselastic Properties in Linear and Star Polymers",
Macromolecules **14**, 1668 (1981)

A22 Fetters, L.J., A.D.Kiss, D.S. Pearson, G.F.Quack, and F.J. Vitus,
"Rheological Behaviour of Star-Shaped Polymers"
Macromolecules, **26**, 647 (1993)

A23 Masuda, T., Y. Ohta, and S. Onogi,
"Viscoelastic Properties of Multi-Branched Polystyrenes",
in: Current Topics in Polymer Science - Vol. II.
R.M.. Ottenbrite, L.A. Utracki, S. Inoue, Eds. (1988)

A24 Masuda, T., Y.Ohta, and S. Onogi,
"Rheological Properties of Anionic Polystyrenes. III. Characterization and Rheological Properties of Four-Branch Polystyrenes",
Macromolecules, **4**, 763 (1971)

A25 Masuda, T., Y. Ohta, M. Kitamura, Y. Saito, K. Sato, ans S. Onogi,
"Rheological Properties of Anionic Polystyrenes. 7. Viscoelastic Properties of Six-Branched Star Polystyrenes and Their Concentrated Solutions",
Macromolecules, **14**, 354 (1981)

A26 Pearson, D.S., S.J. Mueller, L.J. Fetters, and N. Hadjichristidis,
"Comparison of the Rheological Properties of Linear and Star-Branched Polyisoprenes in Shear and Elongational Flows",
Polym. Prep., **23**, 21 (1983) & J. Polym. Sci.: Polym. Phys., **21**, 2287 (1983)

A27 Yasuda, K., R.C.Armstrong, and R.E.Cohen,
"Shear Flow Properties of Concentrated Solutios of Linear and Star Branched Polystyrenes",
Rheol. Acta, **20**, 163 (1981)

A28 Quack, G. and L.J. Fetters,
"Dilute Solution Properties and Rheology of Star Shaped Polymers",
Polym. Prep., **18**, 558 (1977)

A29 Isono, Y., T. Fujimoto, H. Inagaki, M. Shishido, and M. Nagasawa,
"Viscoelastic Properties of Branched Polymers. I. At the Undiluted State",
Polym. J., **12**, 131 (1980)

A30 Kan, H-C., J.D. Ferry, and L.J. Fetters,
"Rubber Networks Containing Unattached Macromolecules. 5. Stress Relaxation in Styrene-Butadiene-Styrene Block Copolymers with Unattached Linear and Star Polybutadienes",
Macromolecules, **13**, 1571 (1980)

A31 Arnett, R.L. and C.P. Thomas,
"Zero-Shear Viscosity of Some Ethyl Branched Paraffinic Model Polymers",
J. Phys. Chem., **84**, 649 (1980)

A32 Ajroldi, G., G.Pezzin, and G.Palma,
"Influence of Branching on Melt Viscosity of Polydisperse Polymers",
Rheol. Acta., **10**, 418 (1971)

A33 Bauer, B.J., N.Hadjichristidis, G. Quack, J. Vitous and L. Fetters,
"The Synthesis and Characterization of Model 8- and 12-arm Star-Shaped Polyisoprenes",
Polym. Prep., **20**, 126 (1979)

A34 Fetters, L.J.,
"The Synthetic Capacity of Anionic Polymerization Systems",
Polym. Prep., **23**, vii (1982)

A35 Bartels,C.R., B.Crist, Jr., L.J. Fetters, and W.W. Graessley,
"Self-diffusion in Branched Polymer Melts",
Macromolecules, **19**, 785 (1986)

A36 Fujimoto, T., H.Narukawa, and M.Nagasawa,
"Viscoelastic Properties of Comb-Shaped Polystyrene",
Macromolecules, **3**, 57 (1970)

A37 Pannell J.,
"Polystyrene of Known Structure: Part 3. Polymers with Long-Chain Branching",
Polymer, **13**, 2 (1972)

A38 Roovers J.,
"The Steady State Shear Compliance of Regular Star Polymers",
Polymer, **22**, 1603 (1981)

A39 Roovers, J. and W.W.Graessley,
"Melt Rheology of Some Model Comb Polystyrenes",
Macromolecules **14**, 766 (1981)

A40 Vrentas, C.M. and W.W.Graessley,
"Study of Shear Stress Relaxation in Well-Characterized Polymer Liquids",
J. Rheol., **26**, 359 (1982)

A41 Kraus, G. and Gruver, J.T.,
"Rheological Properties of Multichain Polybutadienes",
J. Polym. Sci., Part A, **3**, 105 (1965)

A42 Yoshida, H., H. Shohi, and Y. Mikami,
"Viscoelastic Properties of Star Poly(vinyl ether)",
Jap. J. Rheol. (abstract only available)

A43 Kraus, G. and J.T. Gruver,
"Effect of Diluents on the Melt Viscosity of Branched Polybutadienes",
J. Polym. Sci., A2, **8**, 305 (1970)

A44 Leblanc, J.L.,
"Rheological Properties of a Star-Shaped Butadiene-Styrene Block Copolymer",
Rheol. Acta, **15**, 654 (1976)

A45 Onogi, S. and E.Kamei,
"Extensional and Fractural Properties of Star Polystyrenes at Elevated Temperatures",
J. Appl. Polym. Sci., **33**, 49 (1978)

A46 Johnson, B.L., H.E. Adams, F.C. Weissert, and K. Farhart,
"Linear and Branched Polybutadienes",
Intern. Rubber Conf., p29, (1967) Brighton, U.K.

B1 Dobkowski, Z.,
"General Approach to Polymer Properties Dependent on Molecular Characteristics",
Eur. Polym. J., **17**, 1131 (1981)

B2 Roovers, J.,
"Synthesis and Dilute Solution Characterization of Comb Polymers",
Polymer, **20**, 843 (1979)

B3 Roovers, J. and P.M.Toporowski,
"Relaxation by Constraint Release in Combs and Star-Combs",
Macromolecules, **20**, 2300 (1987)

B4 Fujimoto, T., H.Kajiura, M.Hirose, and M.Nagasawa,
"Viscoelastic Properties of Comb-Shaped Polystyrenes Having Parent Polymers of Different Molecular Weights",
Polymer J., **3**, 181 (1972)

B5 Toggenburger, R., S. Newman, and Q.A. Trementozzi,
"Melt Flow and Strength of Branched Styrene Copolymers",
J. Appl. Polym. Sci., **11**, 103 (1967)

B6 Long V.C., G.C.Berry, L.M.Hobbs,
"Solution and Bulk Properties of Branched Polyvinyl Acetates, Part IV - Melt Viscosity",
Polymer, **5**, 517 (1964)

C1 Roovers, J.,
"Melt Rheology of H-Shaped Polystyrenes",
Macromolecules **17**, 1196 (1984)

D1 Struglinski, M.J., W.W. Graessley, and L.J. Fetters,
"Effect of Polydispersity on the Linear Viscoelastic Properties of Entangled Polymers.
3. Experimental Observations on Binary Mixtures of Linear and Star Polybutadienes",
Macromolecules, **21**, 783 (1988)

D2 Watanabe, H., H. Yoshida, and T. Kotaka,
"Entanglement in Blends of Monodisperse Star and Linear Polystyrenes. 1. Dilute Blends",
Macromolecules, **21**, 2175 (1988

D3 Monroy, V.M., J.L. Contreras, E.N. Martinez, and O. Robles-Vasquez,
"A Rheological and Structural Study of High-Styrene Content Solution SBR's",
ACS Rubber Div. Meeting, Detroit, 1989

D4 Roovers, J.,
"Tube Renewal in the Relaxation of 4-Arm Star Polybutadiene in Linear Polybutadienes",
Macromolecules, **20**, 148 (1987)

D5 Berglund, C.A., C.J.Carriere, and J.D.Ferry,
"Relaxation of Linear Polybutadiene in a Star-Branched Environment",
J. Rheol., **25**, 251 (1981)

D6 Ghijsels, A. and H.J.M.A.Mieras,
"Melt Flow Behaviour as a Tool for the Determination of the Extend of Long-Chain Branching in Polymers",
J. Polym. Sci.: Polym. Phys. Ed., **11**, 1849 (1973)

D7 Valenza, A., F.P. LaMantia and D. Acierno,
The Rheological Behaviour of HDPE/LDPE Blends. V. Isothermal Elongation at Constant Stretchning Rate",
J. Rheol., **30**, 1085 (1986)

D8 Duvdevani, I., L.Gursky, and I.J.Gardner,
"Star Branched Butyl - A Novel Butyl Rubber for Improved Processability. II Properties and Applications",
ACS, Rubber Div. Meeting, May 9-12, 1989, paper No.22

D9 Bersted, B.H.,
"Prediction of Rheological Behaviour of Branched Polyethylene from Molecular Structure",
J. Appl. Polym. Sci., **26**, 1001 (1981)

D10 Jacovic, M.S., D.Pollock , and R.S.Porter,
"A Rheological Study of Long Branching in Polyethylene by Blending",
J. Appl. Polym. Sci., **23**, 517 (1979)

D11 Busse, W.F. and R. Longworth,
"Effect of Molecular Weight Distribution and Branching on the Viscosity of Polyethylene Melts",
J. Polym. Sci., **58**, 49 (1962)

D12 Santamaria, A. and J.L. White,
"Rheological Properties, Shrinkage and Melt Spinning Instability of Blends of Linear Polyolefins with LDPE"
J. Appl. Polym. Sci., **31**, 209 (1986)

D13 Valenza, A., F.P.La Mantia and D.Acierno,
"Influence of Molecular Parameters on the Elongational Behaviour of Different Polyethylenes and Their Blends",
Progress and Trends in Rheology II, 365 (1988)

D14 Attalla, G. and D. Romanini,
"Influence of Molecular Structure on the Extensional Behaviour of Polyethylene Melts",
Rheol. Acta, **22**, 471 (1983)

D15 Minoshima, W. and J.L. White,
"Instability Phenomena in Tubular Film, Cast Film and Melt Spinning of Rheologically Characterized High Density, Low Density and Linear Low Density Polyethylenes",
Polymer Engineering Center Report #32, University of Akron, 1985

E1 Tumanova, I.A., O.B. Semenov and Yu. G. Yamanovsky,
"Evaluation of Branching in Polyvinyltrimethylsilane on the Basis of Analysis of Temperature Dependence of Mechanical Losses",
Intern. J. Polymeric Mater., **8**, 225 (1980)

E2 Kline, D.E., J.A. Sauer, and A.E. Woodward,
"Effect of Branching on Dynamic Mechanical Properties of Polyethylene",
J. Polym. Sci., **22**, 455, (1956)

E3 Dobkowski, Z.,
"Influence of Molecular Weight Distribution and Long Chain Branching on the Glass Transition Temperature of Polycarbonate",
Eur. Polym. J., **18**, 563 (1982)

E4 Nakajima, N. and E.R. Harrell,
"Test of Strain-Time Correspondence Principle with Gel-Containing Elastomers",
Rubber Chem.Technol., **59**, 305 (1986)

E5 Nakajima, N. and E.R. Harrell, P.R. Kumler, D.A. Seil, and A.H. Jorgensen,
"From Polymerization to Product: The Effect of Molecular Structure on the Properties of Butadiene-Acrylonitrile Copolymers Elastomer",
Adv.Polym.Technol., **4**, 267 (1984)

E6 Nakajima, N.,
"Quantitative Characterization of Gels in Elastomers Through Temperature Dependence and Strain Dependence of Deformational Behaviour",
J. Appl. Polym. Sci.: Applied Polym. Symp., **50**, 79 (1992)

E7 Nakajima, N., R.A. Miller, and E.R. Harrel,
"Mill Processability, Rheology and Structure Differences of Polyacrylate Elastomers",
Intern. Polymer Processing, **2**, 88 (1987)

E8 Bersted, B.H., J.D. Slee, and C.A. Richter,
"On the Effects of Very Low Levels of Long-Chain Branching on the Rheological Behaviour in Polyethylene",
J. Appl. Polym. Sci., **30**, 3751 (1985)

E9 Chartoff, R.P. and B. Maxwell,
"Viscoelastic Properties of Branched Polyethylene Melts",
J. Polym. Sci., A-2, **8**, 455 (1970)

E10 Beardsley, K.P. and R.W. Tomlison,
"Processing of EPDM Polymers as Related to Structure and Rheology",
Rubber Chem. Technol., **63**, 540 (1990)

E11 El Kissi, N., J.M.Piau, P.Attane, and G.Turrel,
"Shear Rheometry of PDMS Master Curves and Testing of Gleissle and Yamamoto Relations",
Theoretical and Applied Rheology, Proc. XI Int. Congr. on Rheology, Brussels, Belgium, 1992, p. 907

E12 El Kissi, N., J.M.Piau, P.Attane, and G.Turrel,
"Shear Rheometry of PDMS Master Curves and Testing of Gleissle and Yamamoto Relations",
Rheol. Acta, **32**, 293 (1993)

B-14 Bersted, B.H., J.D. Slee, and C.A. Richter,
"On the Effects of Very Low Levels of Long-Chain Branching on the Rheological Behaviour in Polyethylene",
J. Appl. Polym. Sci., **30**, 3751 (1985)

E13 Onogi, S., T. Masuda and T. Ibaragi,
"Rheological Properties of Polymethyl Methacrylate and Polyvinyl Acetate in the Molten State",
Koll. Zeit. u. Zeit. f. Polymere, **222**, 110 (1968)

E14 Harrell, E.R. and N.Nakajima,
"Modified Cole-Cole Plot Based on Viscoelastic Properties for Characterizing Molecular Architecture of Elastomers",
J. Appl. Polym. Sci., **29**, 995 (1984)

E15 Harrell E.R. and N. Nakajima,
"Viscoelastic Properties as a Means of Characterizing Molecular Architecture of Elastomers",
Polym. Prep., **23**, 69 (1982)

E16 Hughes, J.K.,
"Analysis of Long Chain Branching in High Density Polyethylene",
ANTEC p 306 (1983)

E17 Starck , P. and J. J. Lindberg,
"Influence of Long-Chain Branching on the Rheological Properties of Low Density Poly(ethylene)",
Angew. Makromol. Chem., **75**, 1 (1979)

E18 Tuminello, W.H., W.H.Buck, and D.L.Kerbow,
"Rheological Molecular Weight Distribution Determinations of Ethylene/Tetrafluoroethylene Copolymers: Implications for Long-Long-Chain Branching",
Macromolecules, **26**, 499 (1993)

E19 Tuminello, W.H., W.H.Buck, and D.L.Kerbow,
"Rheological Molecular Weight Distribution Determinations of Ethylene/Tetrafluoroethylene Copolymers: Implications for Long-Chain Branching",
Theoretical and Applied Rheology, Eds. P.Moldenaers and R. Keunings, Proc. XIth Int. Congr. on Rheology, Brussels, 1992

E20 White, W.H., J.C.Randall, and C.H.Leigh,
"On the Contribution of Long Chain Branching to Polyethylene Melt Rheology",
Chem. Eng. Commun., **24**, 139 (1983)

E21 Nakajima, N., J.J.Scobbo, Jr., and E.R.Harrell,
"Viscoelastic Characterization of Long Branching and Gel in Elastomers by Comparison of Large and Small Deformational Behaviour",
Rubber Chem.Technol., **60**, 742 (1987)

E22 Valentine, R.H., J.D. Ferry, T. Homma, and K. Ninomiya,
"Viscoelastic Properties of Polybutadienes - Linear and Lightly Crosslinked Near the Gel Point",
J. Polym. Sci., A-2, **6**, 479 (1968)

E23 Beardsley, K.P. and C.C. Ho,
"Rheological Properties as Related to Structure from EPDM Polymers",
J. Elast. Plast., **16**, 20 (1984)

E24 Harrell, E.R.,
"The Effect of Branching on the Rheological Properties of EPCAR 305 (EPCAR 405) <EPM>",
B.F.Goodrich Technical Report: SR-381-78-18

E25 Martinez, E.N., J.E. Vazquez, and E. Bernal,
"Improvement in Processability of Polybutadiene for Tire Applications",
ACS Rubber Div. - Meeting, Mexico City, 1989

E26 Wild, L., R.Ranganath, and D.C.Knobeloch,
"Influence of Long-Chain Branching on the Viscoelastic Properties of Low-Density Polyethylenes",
Polym. Eng. Sci., **16**, 811 (1976)

E27 Nakajima, N., E.R. Harrell and E.A. Collins,
"Viscoelastic Characterization of Ethylene-Propylene-Diene Terpolymer Elastomers",
Rubber Chem. Technol., **50**, 99 (1977)

E28 Leblans, P.J.R. and C.Bastiaansen,
"Shear Modification of Low-Density Polyethylene: Its Origin and Its Effect on the Basic Rheological Fuctions of the Melt",
Macromolecules, **22**, 3312 (1989)

E29 Labaig, J.J., Ph. Monge and J. Bednarick,
"Steady Flow and Dynamic Viscoelastic Properties of Branched Polyethylene",
Polymer, **14**, 384 (1973)

E30 Samurkas, T, R.G. Larson, and J.M.Dealy,
"Strong Extensional and Shear Flows of a Branched Polyethylene",
J. Rheol., **33**, 559 (1989)

E31 Hansen, M.G., and J.B. Jansma,
"A Rheological Study of Branching in Polycarbonate by Blending",
Polym. Prep., **20**, 157 (1979)

E32 Bubeck , R.A. and H.M. Baker,
"The Influence of Branch Length on the Deformation and Microstructure of Polyethylene",
Polymer, **23**, 1680 (1982)

E33 Dobkowski, Z.,
"Influence of Polydispersity and Long-Chain Branching on the Melt Viscosity of Polycarbonate",
Eur. Polym. J., **18**, 1051 (1982)

E34 Constantin, D.,
"Linear Low Density Polyethylene Melt Rheology: Extensibility and Extrusion Defects",
Polym. Eng. Sci., **24**, 268 (1984)

E35 Miltz, J.and A.Ram,
"Flow Behaviour of Well Characterized Polyethylene Melts",
Polym. Eng. Sci., **13**, 273 (1973)

E36 Ram, A.,
"Viscoelastic Parameters of Characterized Branched Polyethylenes",
Polym. Eng. Sci. **17**, 793 (1977)

E37 Schreiber H.P. and E.G.Bagley,
"The Newtonian Melt Viscosity of Polyethylene: An Index of Long-Chain Branching",
J. Polym. Sci., **58**, 29 (1962)

E38 Peticolas, W.L.,
"Viscoelastic Properties of Branched Whole Polymers. II. Regularities in the Solution Viscosity, Melt Viscosity, and Molecular Weight",
J. Polym. Sci., **58**, 1405 (1962)

E39 White, J.L., G. Shida, and G.A. Tirpak,
"Branching and Flow Activation Energy of Conventional High Pressure Process Polyethylene",
J. Polym. Sci., **B3**, 1089 (1965)

E40 Wang, K.J. and L.J. Lee,
"Rheological and Extrusion Behaviour of Dispersed Multiphase Polymeric Systems",
J. Appl. Polym. Sci., **33**, 431 (1987)

E41 Graessley, W.W. and E.S.Shinbach,
"Flow Properties of Branched Polydisperse Polymers",
J. Polym. Sci., Polym. Phys. Ed., **12**, 2047 (1974)

E42 Ghijsels, A., J.J.S. Ente, and J. Raadsen
"Melt Strength Behaviour of PE Blends",
Intern. Polym. Process., **7**, 44 (1992)

E43 Valles, E.M., C.W. Macosko,
"Structure and Viscosity of Poly(dimethylsiloxanes) with Random Branches",
Macromolecules, **12**, 521 (1979)

E44 Lokati, G. and L.Gargani,
"Detection of Branching in Polyethylene Systems by Rheological Measurements",
Proc. of the Congress on Rheology, Goetheborg, Sweden, 1976, p.530

E45 Laun, H.M.,
"Prediction of Elastic Strains of Polymer Melts in Shear and Elongation",
J. Rheol., **30**, 459 (1986)

E46 Munari, A., F.Pilati, and G.Pezzin,
A Study on the Melt Viscosity of Linear and Branched Poly(butyleneterephtalate)",
Rheol. Acta, **23**, 14 (1984)

E47 Mendelson, R.A., W.A.Bowles, and F.L.Finger,
"Effect of Molecular Structure on Polyethylene Melt Rheology. II. Low Shear Behaviour",
J. Polym. Sci., A-2, **8**, 105 (1970)

E48 Shroff, R.N. and M. Shida,
"Effect of Long-Chain Branching on the Relation between Steady Flow and Dynamic Viscosity of Polyethylene Melts",
J. Polym. Sci., A-2, **8**, 1917 (1970)

E49 Kraus, G. and J.T.Gruver,
"Rheological Properties of cis-Polybutadiene",
J. Appl. Polym. Sci., **9**, 739 (1965)

E50 Morris, D.L.,
"The Effect of EPDM Molecular Parameters on Stress Relaxation",
B.F.Goodrich Report: SR-381-72-#108

E51 Osaki, K., S.Kimura, and M.Kurata,
"Stress Relaxation of a Branched Polybutadiene in Double-Step Shear Deformations",
J. Rheol., **29**, 533 (1985)

E52 Wagner, M.H.,
"Analysis of Time-Dependent Non-Linear Stress-Growth Data for Shear and Elongational Flow of a Low-Density Branched Polyethylene Melt",
Rheol. Acta, **15**, 136 (1976)

E53 Acierno, D., F.P. La Mantia, D. Romanini, and A.Savadori,
"An Experimental Investigation of the Shear Behaviour of Polyethylenes with Different Structures",
Rheol. Acta, **24**, 566 (1985)

E54 Boghetich, L. and R.F.Kratz,
"The Effect of Branching on the Melt Rheology of Polyethylene",
Trans. Soc. Rheol., **9**, 255 (1965)

E55 Blyler, L.L., Jr.,
"Some Aspects of the Relationship between Molecular Structure and Flow Behaviour of Polymer Melts",
Rubber Chem. Technol., **42**, 823 (1969)

E56 Bontinck, W.J.
"Correlation between Rheological Properties of Polyolefin Melts and Solutions and Their Molecular Structure",
Rheol. Acta, **8**, 328 (1969)

E57 Combs, R.L., D.F. Slonaker, and H.W. Coover, Jr.,
"Effects of Molecular Weight Distribution and Branching on Rheological Parameters of Polyolefin Melts",
SPE Trans., 104, (1967)

E58 Charlesby, A.,
"Viscosity Measurements in Branched Silicones",
J. Polym. Sci., **17**, 379 (1955)

E59 Chohan, R.K.,
"Shear and Elongational Flow of Some Branched Polyethylenes",
J. Appl. Polym. Sci., **54**, 487 (1994)

E60 Dobkowski, Z.,
"The Linear Master Dependence for Polymer Melts in the Non-Newtonian Range",
Polymer Bull., **19**, 165 (1988)

E61 Daane, J.H., F.C. Schilling, and L.L. Blyler, Jr.,
"Effect of Branches on the Flow Activation Energy and Melt Elasticity of Polyethylene",
SPE Trans., **35**, 282 (1977)

E62 Fujiki, T.,
"Concept of Secondary Heterogeneous Structure of Long-Chain Branched Polyethylene",
J. Appl. Polym. Sci., **15**, 47 (1971)

E63 Graessley, W.W. and J.S.Prentice,
"Viscosity and Normal Stresses in Branched Polydisperse Polymers",
J. Polym. Sci., A-2, **6**, 1887 (1968)

E64 Furumiya, A., Y. Akana, Y. Ushida, T. Masuda and A. Nakajima,
"Relationship between Molecular Characteristics and Physical Properties of Linear Low Density Polyethylenes",
Pure & Appl. Chem., **57**, 823 (1985)

E65 Guillet, J.E., R.L. Combs, D.F.Slonaker, D.A.Weemes, and H.W.Coover, Jr.,
"Effect of Molecular Weight Distribution and Branching on Rheological Parameters of Polyethylene Melts. Part I. Unfractionated Polymers",
J. Appl. Polym. Sci., **8**, 757 (1965)

E66 Folt, V.L.,
"The Effect of Mechanical Degradation on Rheological Properties of Elastomers",
Rubber Chem. Technol., **42**, 1294 (1969)

E67 Guillet, J.E., R.L. Combs, D.F.Slonaker, D.A.Weemes, and H.W.Coover, Jr.,
"Effect of Molecular Weight Distribution and Branching on Rheological Parameters of Polyethylene Melts. Part II. Fractions and Blends",
J. Appl. Polym. Sci., **9**, 767 (1965)

E68 Ghijsels, J.J.S., M. Ente and J. Raadsen,
"Melt Strength Behaviour of PE and its Relation to Bubble Stability in Film Blowing",
Intern. Polymer Processing, **5**, 284 (1990)

E69 Hanson, D.E.,
"Shear Modification of Polyethylene",
Polym. Eng. Sci., **9**, 405 (1969)

E70 Hamielec, L.A. and J.Vlachopoulos,
"Influence of Long-Chain Branching on Extrudate Swell of Low-Density Polyethylene",
J. Appl. Polym. Sci., **28**, 2389 (1983)

E71 Huang, D.C. and R.N.Schroff,
"Converging Flow of Polymer Melts",
J. Rheol., **25**, 605 (1981)

E72 Laun, H.M. and H.Schuch,
"Transient Elongational Viscosities and Drawability of Polymer Melts",
J. Rheol., **33**, 119 (1989)

E73 LaMancia, F.P., and D. Acierno,
"Influence of the Molecular Structure on the Melt Strength and Extensibility of Polyethylenes",
Polym. Eng. Sci., **25**, 279 (1985)

E74 Munari, A., G.Pezzin, and F.Pilati,
"Linear and Branched Poly(butyleneisophtalate): Activation Energy for Melt Flow",
Rheol. Acta, **29**, 469 (1990)

E75 Mendelson, R.A.,
"Effect of Molecular Structure on Polyethylene Melt Rheology. III. Effects of Long-Chain Branching and Temperature on Melt Elasticity in Shear",
J. Appl. Polym. Sci., **17**, 797 (1973)

E76 Mendelson, R.A., W.A.Bowles, and F.L.Finger,
"Effect of Molecular Structure on Polyethylene Melt Rheology. II. Shear-Dependent Viscosity",
J. Polym. Sci., A-2, **8**, 127 (1970)

E77 Manaresi, P., P. Parrini, G.L. Semeghini and E. de Fornasari,
"Branched Poly(ethylene terephtalate) Correlations between Viscosimetric Properties and Polymerization Parameters",
Polymer, **17**, 595 (1976)

E78 Munari, A., F. Pilati and G. Pezzin,
"Melt Viscosity of Linear and Branched Poly(butyleneisophtalate)",
Rheol. Acta, **27**, 145 (1988)

E79 Munari, A., G. Pezzin, F. Pilati and P.Manaresi,
"Rheological Characterization of Highly Branched Poly(ethyleneterephtalate)",
Rheol. Acta, **28**, 25 (1989)

E80 Manaresi P., A. Munari, F. Pilati, G.C. Alphonso, S. Russo and M.L. Sartirana,
"Synthesis and Characterization of Highly Branched Poly(ethylene terephtalate)",
Polymer, **27**, 955 (1986)

E81 Mendelson, R.A.,
"Flow Properties of Polyethylene Melts",
Polym. Eng. Sci., **9**, 350 (1969)

E82 Ondas, M. and E. Spirk,
"Structural and Rheological Investigation of Low Density Polyethylenes",
Angew. Makromol. Chem., **204**, 37 (1993)

E83 Pedersen, S. and A.Ram,
"Prediction od Rheological Properties of Well-Characterized Branched Polyethylenes from the Distribution of Molecular Weight and Long-Chain Branches",
Polym. Eng. Sci., **18**, 990 (1978)

E84 Rokudai, M.,
"Influence of Shearing History on the Rheological Properties and Processability of Branched Polymers. V. Effect of Molecular Structural Parameters on Die Swell of Low-Density Polyethylenes",
J. Appl. Polym. Sci., **26**, 1427 (1981)

E85 Prichard, J.H. and K.F.Wissbrun,
"Reversible Melt Flow Rate Increase of Branched Acetal Polymers",
J. Appl. Polym. Sci., **13**, 233 (1969)

E86 Pearson D.S. and V.R. Raju,
"Configurational and Viscoelastic Properties of Branched Polymers",
Macromolecules, **15**, 294 (1982)

E87 Porter, R.S., J.P.Knox, and J.F.Johnson,
"On the Flow and Activation Energy of Branched Polyethylene Melts",
Trans. Soc. Rheol., **12**, 409 (1968)

E88 Piau, J.M., N.El Kissi and B.Tremblay,
"Low Reynolds Number Flow Visualization of Linear and Branched Silicones Upstream of Orifice Dies",
J.Non-Newtonian Fl.Mech., **30**, 197 (1988)

E89 Romanini, D., A. Savadori, and G. Gianotti,
"Long Chain Branching in Low Density Polyethylene: 2. Rheological Behaviour of the Polymers",
Polymer, **21**, 1092 (1980)

E90 Schaefgen J.R. and P.J.Flory,
"Synthesis of Multichain Polymers and Investigation of their Viscosities",
J. Amer. Chem. Soc., **70**, 2709 (1948)

E91 Teh, J.W., A.Rudin, and H. Schreiber,
"Shear Modification of Low Density Polyethylene",
J. Appl. Polym. Sci., **30**, 1345 (1985)

E92 Yamane, H.Y. and J.L.White,
"Rheological Investigation of Molecularly Characterized Commercial High Density, Low Density and Linear Low Density Polyethylene Melts",
J. Soc. Rheol. Jap., **15**, 87 (1987)

E93 Vinogradov, G.V., A. Ya. Malkin, and V.G. Kulichikhin,
"Microstructure and Rheological Properties of Polybutadienes",
J. Polym. Sci., A-2, **8**, 333 (1970)

E94 Pinaud, F.,
"Effect of Molecular Parameters on the Viscoelastic Properties of Polymer Melts",
J. Non-Newtonian Fluid Mech., **23**, 137 (1987)

E95 Porter, R.S. and J.F. Johnson,
"Temperature Dependence of Polymer Viscosity. The Influence of Shear Rate and Stress",
J. Polym. Sci., **C15**, 365 (1966)

E96 Fuller, K.N.G. and W.S. Fulton,
"The Influence of Molecular Weight Distribution and Branching on the Rexation Behaviour of Uncrosslinked Natural Rubber",
Polymer, **31**, 609 (1990)

E97 Schroff, R.N., L.V.Cancio, and M.Shida,
"Extensional Flow of Polymer Melts",
Trans. Soc.Rheol., **21**, 429 (1977)

E98 Wagner, M.H.,
"Analysis of Stress-Growth Data for Simple Extension of a Low-Density Branched Polyethylene Melt",
Rheol. Acta, **15**, 133 (1976)

E99 White, J.L.,
"Experimental Studies of Elongational Flow od Polymer Melts",
J. Appl. Polym. Sci., **33**, 31 (1978)

E100 La Mantia, F.P., A. Valenza and D. Acierno,
"Elongational Behaviour of Low Density and Linear Low Density Polyethylenes",
Polym. Eng. Sci., **28**, 90 (1988)

E101 Muenstedt, H.,
"The Influence of Various Deformation Histories on Elongational Properties of LDPE",
Colloid & Polymer Sci., **259**, 966 (1981)

E102 Muenstedt, H. and H.M.Laun,
"Elongational Properties and Molecular Structure of Polyethylene Melts",
Rheol. Acta, **20**, 211 (1981)

E103 Soskey, P.R. and H.H.Winter,
"Equibiaxial Extension of Two Polymer Melts: Polystyrene and LDPE",
J. Rheol., **29**, 493 (1985)

E104 Yuan-ze, X.,
"Characterization of Polymer Chains Structure by Means of Entry Flow of Melts",
Proc. Xth Intern. Congress on Rheology, Sydney, 1988

E105 Booij, H.C.,
"Long-Chain Branching and Viscoelasticity of Ethylene-Propylene-Diene Elastomers",
Kautschuk + Gummi.Kunstoffe, **44**, 128 (1991)

E106 Ford R.W.,
"Physical Properties of Some Ethylene Polymers",
J. Appl. Polym. Sci., **9**, 2879 (1965)

E107 Maxwell, B. and A.Breckwoldt,
"Controlled Shear Modification of Low-Density Polyethylene",
J. Rheol., **25**, 55 (1981)

E108 Moore, L.D.,
"Relations among Melt Viscosity, Solution Viscosity, Molecular Weight and Long-Chain Branching in Polyethylene",
J. Polym. Sci., **36**, 155 (1959)

E109 Rokudai, M., S.Mihara, and T.Fujiki,
"Influence of Shearing History on the Rheological Properties and Processability of Branched Polymers. II. Optical Properties of Low-Density Polyethylene Blown Films",
J. Appl. Polym. Sci., **23**, 3289 (1979)

E110 Rokudai, M. and T.Fujiki,
"Influence of Shearing History on the Rheological Properties and Processability of Branched Polymers. III. An Amorphous Long-Chain Branched Polymer",
J. Appl. Polym. Sci., **23**, 3295 (1979)

E111 Rokudai M.,
"Influence of Shearing History on the Rheological Properties and Processability of Branched Polymers",
J. Appl. Polym. Sci., **23**, 463 (1979)

E112 Ritzau, G., A. Ram, and L. Izrailov,
"Effect of Shear Modification on the Rheological Behaviour of Two Low-Density Polyethylene (LDPE) Grades",
Polym. Eng. Sci., **29**, 214 (1989)

E113 Roovers, J., L-L. Zhou, P.M. Toporowski, M. van der Zwan, H. Iatrou and N. Hadjichristidis,
"Regular Star Polymers with 64 and 128 Arms. Models for Polymeric Micelles",
Macromolecules **26**, 4324 (1993)

E114 Sperati, C.A., W.A. Franta, and H.W. Starkweather,
"The Molecular Structure of Polyethylene. V. The Effect of Chain Branching and Molecular Weight on Physical Properties", .
J. Am. Chem. Soc., **75**, 6127 (1953)

E115 White, J.L. and H. Yamane,
"A Collaborative Study of the Stability of Extrusion, Melt Spinning and Tubular Film Extrusion of Some High-, Low- and Linear-Low Density Polyethylene Samples",
Pure & Appl. Chem., **59**, 193 (1987)

E116 Zoller, P.,
"The Pressure-Volume-Temperature Properties of Three Well-Characterized Low-Density Polyethylenes",
J. Appl. Polym. Sci., **23**, 1051 (1979)

F1 Clark, R.J. and C.S. Henkee,
"Poly)ether Amide) Triblock and Star Block Copolymers",
Macromol. Symp., 91, 27 (1995)

F2 Alward D.B., D.J.Kinning, E.L. Thomas, and L.J. Fetters,
"Effect of Arm Number and Arm Molecular Weight on the Solid-State Morphology of Poly(styrene-isoprene) Star Block Copolymers",
Macromolecules, **19**, 215 (1986)

G1 Kennedy, J. P. and A. Vidal,
"Block and Graft Copolymers by Selective Cationic Initiation. IV. Physical Properties of Bigraft Copolymers",
J. Polym. Sci., Polym. Chem., **13**, 2269 (1975)

G2 Kennedy, J.P.,
"Synthesis, Characterization, and Properties of Block and Bigraft Copolymers",
J. Polym. Sci., Polym. Chem., **13**, 2213 (1975)

G3 Kennedy, J.P. and M. Nakao,
"Poly(vinyl Chloride-g-Styrene): Synthesis, Characterization, and Physical Properties",
J. Macromol. Sci. - Chem., **A12**, 197 (1978)

G4 Kargin, V.A,
"Solid-state Properties of Graft Copolymers"
J. Polym. Sci., C, **4**, 1601 (1963)

G5 Kennedy, J.P. and M.Nakao,
"Synthesis, Characterization and Physical Properties of Poly(vinyl Chloride-g-Styrene)",
J. Appl. Polym. Sci.: Appl. Polym. Symp., **30**, 73 (1977)

G6 Rieke, J.K. and G.M. Hart,
"Properties of Polyethylene-Acrylic Acid Graft Copolymers"
J. Polym. Sci., C, **1**, 117 (1963)

G7 Rimmerand, S. and M.H. George,
"Dynamic Mechanical Thermal Analysis of Some Well Defined Poly(e-caprolactone)-g-poly(methyl methacrylate)-co-polyurethanes",
Polymer, **35**, 5782 (1994)

G8 Shinohara, Y.,
"Dynamic Mechanical Properties of Graft Copolymers of Nylon",
J. Appl. Polym. Sci., **1**, 251 (1959)

G9 Shibanov, Yu., G.N. Arkhipovich and S. Sosnowski,
"New Graft Copolymer with a Crystallizing Polyester Block",
Intern. Polym. Sci. Technol., **20**, T/73 (1993)

G10 Smith, S.D., J.M. DeSimone, H.Huang, G. York, D.W. Dwight, G.L.Wilkes, and J.E.McGrath,
"Synthesis and Characterization of Poly(methyl methacrylate)-g-poly(dimethylsiloxane) Copolymers.
1. Bulk and Surface Characterization",
Macromolecules, **25**, 2575 (1992)

G11 Sakurada, I., Y. Ikada and F. Horii,
"True and Apparent Graft",
Makromol. Chem., **139**, 171 (1970)

G12 Bohn, L.,
"Incompatibility and Phase Separation in Solid Polymer Mixtures and Graft and Block Copolymers",
Rubber Chem. Technol., **41**, 495 (1968)

G13 Thamm, R.C.and W.H. Buck,
"Polypivalolactone Graft on EPDM",
J. Polym Sci.: Polym. Chem. Ed., **16**, 539 (1978)

G14 Takahashi, T., Y. Takagi, K. Minagawa, K. Iwakura, and K. Koyama,
"Anomalous Temperature in the Elongational Viscosity of Ethylene Based Graft Copolymers Melts",
Polymer, **35**, 4472 (1994)

G15 Lohse, D.J., S.Datta, and E.N.Kresge,
"Graft Copolymers Compatibilizers for Blends of Polypropylene and Ethylene-Propylene Copolymers",
Macromolecules, **24**, 561 (1991)

G16 Locke, C.E. and D.R. Paul,
"Graft Copolymer Modification of Polyethylene-Polystyrene Blends. I. Graft Preparation and Characterization",
J. Appl. Polym. Sci., **17**, 2597 (1973)

G17 Vidal, A. and J.P. Kennedy,
"Block and Graft Copolymers by Selective Cationic Initiation. V. Compatibilization of EPDM and Polyisobutylene in a Bigraft Copolymer",
J. Polym. Sci., Polym. Lett., **14**, 489 (1976)

G18 Liang, Z. and H.L. Williams,
"Interfacing Polypropylene/Poly(BPA carbonate) Blend Phases with Graft Copolymers: Thermal and Dynamic Mechanical Analyses",
J. Appl. Polym. Sci., **43**, 379 (1991)

G19 Lebel ,P. and C. Job,
"Etude Rheologique de Copolymeres Greffes a Base de Polychlorure de Vinyle et de Copolymere Styrolene-Anhydride Maleique",
J. Polym. Sci., C, **4**, 649 (1963)

G20 Lucas, E.F. and R.S. Porter,
"Thermal Analyses of Graft Copolymers of Poly(Methyl Methacrylate) Main Chain with Poly(Propylene Oxide-B-Ethylene Oxide) Graft Chain",
J. Appl. Polym. Sci., **49**, 1211 (1993)

G21 Sung, P-H. and W-G. Wu,
"Graft Copolymer Networks of Polyurehthane and Epoxy Structures - I. Dynamic Mechanical Properties",
Eur. Polym. J., **30**, 905 (1994)

G22 Rieke, J.K., G.M.Hart, and F.L.Saunders,
"Graft Copolymers of Polyethylene and Acrylic Acid",
J. Polym. Sci., C **4**, 589 (1963)

G24 Cameron, C.G. and M.S. Chisholm,
"Polymerization of PDMS Macromers: 2. Glass Transition Temperatures of Macromer/Styrene Copolymers",
Polymer, 27, 437 (1986)

G25 Bares, J. and M. Pregoraro,
"Properties of Ethylene-Propylene-Vinyl Chloride Graft Copolymers. II. Viscoelasticity and Composition of Graft Copolymer and Composite",
J. Polym. Sci., A-2, **9**, 1287 (1971)

G26 Pegoraro, M, L.Szilagyi, and A.Penati,
"Mechanical-Dynamic Properties of Some Polymers Grafted on Polypropylene",
Rheol. Acta, **13**, 49 (1974)

G27 Pendle, T.D.,
"Properties and Aplications of Block and Graft Copolymers of Natural Rubber",
in: Block and Graft Copolymerization .

G28 Blanchette, J.A. and L.E. Nielsen,
"Characterization of Graft Copolymers",
J. Polym. Sci., **20**, 317 (1956)

G29 Roha, M., W.-T. wang, H.J. Harwood and A. Sebenik,
"'Living' Free Radical Graft Copolymers. I. Preparation and Properties",
Macromol. Symp., **91**, 81 (1995)

G30 Matzner, M, D.L. Schober and J.E. McGrath,
"Polystyrene-Nylon 6 Graft Copolymer",
Eur. Polymer J., **9**, 469 (1973)

G31 Kennedy, J.P. and R.R. Smith,
"The Synthesis, Characterization and Physical Properties of EPDM-g-PS Thermoplastic Elastomers",
in "Recent Advances in Polymer Blends, Grafts and Blocks", H. Sperling, Ed., Plenum, New.York., p. 303 (1974)

G32 Oziomek, J. and J.P.Kennedy,
"SBR-g-Polyisobutylene. I. Synthesis and Characterization",
J. Appl. Polym. Sci.: Appl. Polym. Symp., **30**, 91 (1977)

G33 Baccaredda, M., E.Butta and V.Frosini,
"Dynamic Mechanical Properties of Some Graft Copolymers",
J. Polym. Sci., C **4**, 605 (1963)

G34 Pegoraro, M, L.Szilagyi, and A.Penati,
"Mechanical-Dynamic Properties of Some Polymers Grafted on Polypropylene",
Rheol. Acta, **13**, 49 (1974)

G35 Datta, S. and D.J. Lohse,
"Graft Copolymer Compatibilizers for Blends of Isotactic Polypropylene and Ethene-Propene Copolymers.
2. Functional Polymers Approach",
Macromolecules, **26**, 2064 (1993)

G36 Falk, J.C., R.J. Schlott, and D.F. Hoeg,
"Anionic Graft Copolymer. I. Vinylaromatic Graft on Polydienes",
J. Macromol. Sci.-Chem., **A7**, 1647 (1973)

G37 Monfort, J.P., J.Lebez, G.Marin, and Ph.Monge,
"Viscoelastic Properties of Copolymers: Relations with Structure",

G38 Verney, V., E.Koerper, and A. Michel,
"Melt Rheology as a Powerful Tool to Follow Chemical Reactions in a Polyolefin Mastrix",
Makromol. Chem., Makromol. Symp., **25**, 187 (1989)

G39 Bates, T.W.,
"The Melt Viscosity of Branched Polydispersed Polymers",
Europ. Polym. J., **8**, 19 (1972)

G40 Henderson, A.M. and A. Rudin,
Extrusion Behaviour of Starch Graft Copolymers: Starch-g-Polystyrene and Starch-g-poly(methyl Acrylate)",
Angew. Macromol. Chem., **194**, 23 (1992)

G41 Scholskey, K.M., E.B. Orler, K.J. Bixler and R.W. Stackman,
"Thermal and Rheological Properties of Acrylic Polymers Possessing Crystallizable Polyester Side Chains",
Makromol. Chem. Macromol. Symp., **42/43**, 219 (1991)

G42 Caywood, S.W.,
"Block and Graft Copolymers of Polypivalolactone: Poly(acrylate-g-pivalolactone)",
Rubber Chem. Technol., **50**, 127 (1977)

G43 Zhang, X., L. Wang, and B. Qian,
"Influnce of Crosslinking Density of Poly(butyl-acrylate) Backbone on Processibility of Poly(vinyl-chloride) Grafted onto Poly(butylacrylate)",
Angew. Makromol. Chem., **209**, 1 (1993)

H1 Soskey, P.R., I.Duvdevani, H.C.Wang and T.E.Richards,
"Star-Branched Butyl - A Novel Butyl Rubber for Improved Processability. III Polymer Rheology",
ACS Rubber Div. Meeting, Detroit, paper #54, (1989)

H2 Gursky, L., J.V.Fusco, I.Duvdevani, and T.Takeda,
"Star-Branched Butyl - A Novel Butyl Rubber for Improved Processability.
Part IV. Compounding and Vulcanization Lattitude",
Kautschuk + Gummi.Kunststoffe, **43**, 692 (1990)

H3 Friedersdorf, C.B. and I. Duvdevani,
"The Application of Mooney Relaxation to Quality Control of Elastomers", ACS Rubber Div. Meeting, Chicago, 1994

S1 Hadjichristidis, N. and J.E.L. Roovers,
"Synthesis and Solution Properties of Linear, Four-Branched, and Six-Branched Star Polyisoprenes",
J. Polym. Sci.; Polym. Phys. Ed., **12**, 2521 (1974)

S2 Masuda, T., Y. Ohta, M. Kitamura, M. Minamide, K. Kato, and S. Onogi,
"Concentration Dependence of Viscoelastic Properties of a Mixture of Three- and Four-Branched Star Polystyrenes",
Polym. J., **13**, 869 (1981)

S3 Menezes, E.V., and W.W. Greassley,
"Nonlinear Rheological Behaviour of Polymer Systems for Several Shear-Flow Histories",
J. Polym. Sci., Polym. Phys. Ed., **20**, 1817 (1982)

S4 Ohta, Y., Y. Saito, T. Masuda and S. Onogi,
"Concentration Dependence of Viscoelastic Properties of Concentrated Solutions of Six-Branched Polystyrenes",
Macromolecules, **14**, 1128 (1981)

S5 Ohta, Y., M. Kitamura, T. Masida, and S. Onogi,
"Viscoelastic Properties of Concentrated Solutions of Mixtures of Three- and Four-Branched Star Polystyrenes",
Polymer J., **13**, 859 (1981)

S6 Toporowski P.M. and J.Roovers,
"Synthesis and Properties of Eighteen-Arm Polybutadienes",
J. Polym. Sci., Polym. Chem. Ed., **24**, 3009 (1986)

S7 Osaki, K., E.Takatori, M.Kurata, H.Watanabe, H.Yoshida, and T.Kotaka,
"Viscoelastic Properties of Solution of Star-Branched Polystyrene",
Macromolecules, **23**, 4392 (1990)

S8 Graessley, W.W., T.Masuda, J.Roovers, and N.Hadjichristidis, "Rheological Properties of Linear and Branched Polyisoprene",
Macromolecules, **9**, 127 (1976)

S9 Isono, Y., T. Fujimoto, H. Kajiura, and M. Nagasawa,
"Viscoelastic Properties of Branched Polymers. II. In Concentrated Solutions",
Polym. J., **12**, 369 (1980)

S10 Kajiura, H., Y. Ushiyama, T. Fujimoto, and M. Nagasawa,
"Viscoelastic Properties of Star-Shaped Polymers in Concentrated Solutions",
Macromolecules, **11**, 894 (1978)

S11 Ramachandran, S. and E.B. Christiansen,
"The Dependence of Viscoelastic Flow Functions on Polymer Structure for Linear and Branched Polystyrene and Polybutadiene",
AIChE J., **31**, 1621 (1985)

S12 Utracki, L.A. and J.E.L. Roovers,
"Viscosity and Normal Stresses of Linear and Star Branched Polystyrene Solutions. I. Application of Corresponding States Principle to Zero-Shear Viscosities",
Macromolecules, **6**, 366 (1973)

S13 Utracki, L.A. and J.E.L. Roovers,
"Viscosity and Normal Stresses of Linear and Star Branched Polystyrene Solutions. II. Shear-Dependent Properties",
Macromolecules, **6**, 373 (1973)

S14 Lee, C-S., J.J.Magda, K.L.DeVries, and J.W.Mays,
"Measurements of the Second Normal Stress Difference for Star Polymers with Highly Entangled Branches",
Macromolecules, **25**, 4744 (1992)

S15 Ramachandran, S., H.W.Gao and E.B.Christiansen,
"Dependence of Viscoelastic Flow Functions on Molecular Structure for Linear and Branched Polymers",
Macromolecules **18**, 695 (1985)

S16 Ito, K., Y. Tomi, and S.Kawaguchi,
"Poly(ethylene Oxide) Macronomers. 10. Characterization and Solution Properties of the Regular Comb Polymers with Polystyrene Main Chains and Poly(ethylene Oxide) Side Chains",
Macromolecules, **25**, 1534 (1992)

S17 de Vos, S, M., Moeller, K. Vissler and P.F. Mijnlieff,
"Synthesis and Determination of Poly(acrylamide)-g-poly(ethylene) Oxide-co-Propylene Oxide)",
Polymer, **35**, 2644 (1994)

S18 Masuda, T., Y. Ohta, and S. Onogi,
"Rheological Properties of Randomly Branched Polystyrenes",
Polym. Prep., **23**, 40 (1982)

S19 Masuda, T. Y.Nakagawa, Y.Ohta, and S.Onogi,
"Viscoelastic Properties of Concentrated Solutions of Randomly Branched Polystyrenes",
Polymer J., **3**, 92 (1972)

S20 Masuda, T., Y.Ohta, and S.Onogi,
"Rheological Properties of Randomly Branched Polystyrenes with Different Molecular Weights between Branch Points",
Macromolecules, **19**, 2524 (1986)

S21 Onogi, S., S. Kimura, T. kato, T. Masuda and N. Miynaga,
"Effect of Molecular Weight and Concentration of Flow Properties of Concentrated Polymer Solutions",
J. Polym. Sci., **C15**, 381 (1966)

Appendix II

Nomenclature, symbols and abbreviations

Part A - Structure and chemical composition

Nomenclature, and particularly symbols, used for classification and description of structure/composition of branched polymers are not fully standardized. The following definitions, associated symbols and abbreviations are fairly common in the literature concerned with LCB copolymers and were adopted for consistent use in this thesis.
Some examples of usage are also included (section 2 and 3).

Section 1 - superscripts and subscripts

The following superscript and subscript notation standards were adopted:

Superscripts (with N_g as an exception)

"B" - corresponds to backbone prepolymer or backbone of the graft molecule, CIIR,
"b" - corresponds to branch prepolymer or branch of the graft molecule, BR,
"g" - corresponds to grafted portion of branch polymer molecules, gBR,
"h " - corresponds to the ungrafted ("free") branch polymer molecules, hBR,
"G" - corresponds to graft copolymer, CIIR-g-BR.

Subscripts

"n" - corresponds to the number-average,
"w" - corresponds to the weight-average,
"z" - corresponds to the z-average,
"v" - corresponds to the viscosity average,
"x" - general symbol to denote any of the average values; e.g. n, w, z, in M_n, M_w, M_z, respectively,
"f" - functionality of the branching point,
"p" - corresponds to the 'peak' value; see section 3.

Section 2 - composition

W - total weight [in grams] of the sample (copolymer)
W^B - weight of a backbone polymer, (CIIR)
W^b - weight of a branch polymer, (BR)
$W^{b,g}$ - weight of a branch polymer *grafted* onto backbone,

$W^{b,h}$ - weight of a branch polymer *not grafted* onto backbone, (free BR polymer)
W^{G} - weight of a pure graft copolymer in a graft mixture, (CIIR-g-BR)

Note: From the point of view of the analysis of relationship between polymer structure and corresponding property, the backbone (linear) molecules could be regarded as a special type of graft molecules with branches degenerated to the zero length.

The following relations hold:

$$W = W^{B} + W^{b} = W^{B} + W^{b,g} + W^{b,h} = W^{G} + W^{b,h}$$

Weight (mass) fractions can be defined by:

w^{b} - weight (mass) fraction of a branch polymer, (BR); $w^{b} = W^{b} / W$

w^{B} - weight (mass) fraction of a backbone polymer, (CIIR); $w^{B} = W^{B} / W$

Analogously, weight percent fractions can be defined,

$$w^{b}\,(\%) = w^{b} \cdot 100\% \quad \text{and} \quad w^{B}\,(\%) = w^{B} \cdot 100\%$$

By definition, $w^{b} + w^{B} = 1$ and $w^{b}\,(\%) + w^{B}\,(\%) = 100\%$.

Similarly,
$w^{b,g}$ - weight fraction of a branch polymer *grafted* onto backbone,
$w^{b,h}$ - weight fraction of a branch polymer *not grafted* onto backbone,
w^{G} - weight fraction of a pure graft copolymer in a graft mixture,

By definition, $w^{G} + w^{b,h} = 1$ or $w^{G}\,(\%) + w^{b,h}\,(\%) = 100\%$.

Weight fraction of grafted branch polymer w^{b} is, in general case, composed of the weight fraction of grafted branch polymer, $w^{b,g}$ and the weight fraction of ungrafted branch polymers, $w^{b,h}$. Thus, $w^{b,g} + w^{b,h} = w^{b}$.

$w^{b,g}$ - is referred to as "branching content" in chapters 6, 7 and 8,
w^{b} - is referred to as "chemical composition of the graft" in chapters 6, 7 and 8,

The most frequently calculated measures of grafting reaction efficiency are:

- *grafting efficiency*, in %, defined as: $GE\% = (w^{b,g} / w^{b}) \cdot 100\%$

- *grafting percentage*, in %, defined as: $GP\% = (w^{b,g} / w^{G}) \cdot 100\% = w^{b,g} / (w^{B} + w^{b,g}) \cdot 100\%$

- *true graft ratio*, defined as: $GR = (w^{b,g} / w^{B})$

- ungrafted branch polymer content, in %, defined as:

$$HPC = (W^{b,h} / W) \cdot 100\% = w^{b,h} \cdot 100\%$$

Section 3 - structure

Average molecular masses (examples):

$\overline{M}_x^b$ - x-average molecular mass of branch polymer,

$\overline{M}_n^{b,g}$ - number-average molecular mass of branch polymer actually grafted on,

$\overline{M}_z^B$ - z-average molecular mass of backbone polymer,

$\overline{M}_w^G$ - weight-average molecular mass of graft copolymer,

$M_p^{b,h}$ - 'peak' molecular mass of ungrafted branch polymer; molecular mass of molecular having the highest concentration across the MWD, i.e. corresponding to the peak value on the concentration (DRI) detector signal.

Branching parameters:

$\overline{\omega}_x$ - x-average number of end-points (including both backbone and branch molecules),

$\overline{B}_x$ - x-average number of branches per backbone molecule

N_g - number-average number of branches; special case of $x \equiv n$ ($\overline{B}_x = \overline{B}_n$), sometimes referred to in the literature as "b/B" e.g. average number of branches per backbone molecule),

$\overline{n}_{x,f}^b$ - x-average number of branching points of functionality *f*,

$\overline{\lambda}_x$ - x-average branching frequency (branching density).

S_g^n - number-average number of grafting sites (*potential* grafting points or branches) per backbone molecule

M_e - average molecular weight between entanglements

$[\eta]$ - intrinsic viscosity

n_D - refractive index, Δn - difference of refractive indices

Please note that the term 'molecular mass' (MM) and 'molecular weight' (MW) are used in this work interchangeably wherever there is no possibility of confusion.

Section 4 - abbreviations

LCB - Long Chain Branching
MW(D) - Molecular Weight (Distribution)
DRI - Differential Refractive Index
DSV - Dilute Solution Viscometry
DV - Differential Viscometer
LALLS - Low Angle Laser Light Scattering
SEC - Size Exclusion Chromatography

SEC(P) - *corresponds to experiments and analysis carried out in Polysar Labs,*
SEC(W) - *corresponds to experiments and analysis carried out in Chemistry Department Laboratories (University of Waterloo)*

GPC - Gel Permeation Chromatography
CCD - Chemical Composition Distribution
CIIR - Chlorinated Isobutylene-co-Isoprene Rubber
BR - Butadiene Rubber
PDI - Polydispersity Index (= M_w / M_n)
(FT)IR - (Fourier Transform) Infra-Red (spectroscopy)
IV - Intrinsic Viscosity, $[\eta]$

sample codes:

C - graft's backbone precursor polymer (CIIR),
B(xy) - graft's branch precursor polymer (BR); (if included) 'x' refers to the type and 'y' to the sequential number of synthesis,
B10 - B sample with microstructure identical all B samples, made as a reference comparison with grafts,
M - blend of CIIR and BR, made as a reference blend for comparison with grafts,
CG - crude graft (mixture of graft and homopolymers) - term used in chapters 2 & 3 only,
FG - purified graft samples, notation used in chapters 2 and 3 only,
HG - (unreacted) homopolymers extracted from crude graft mixture (CG),
G - purified graft sample in solid form - notation used primarily in chapters 4 to 8, (chemically and compositionally equivalent to FG)

Part B - Most frequently used rheological symbols

(a) rheological functions and independent variables

t - τιμε

T - temperature

T_0 - reference temperature

T_g - glass transition temperature

γ - shear strain

ω - (angular) frequency

δ - phase angle

$\tan \delta (\omega)$ - loss tangent

$G'(\omega)$ - storage modulus (in shear), E' (in tension)

$G''(\omega)$ - loss modulus (in shear), E'' (in tension)

$G^*(\omega)$ - complex modulus, $G^*(\gamma, \omega)$ - strain-amplitude dependent (non-linear) complex modulus,

$\eta^*(\omega)$ - complex viscosity

G_N^0 - plateau modulus

G(t) - shear stress relaxation modulus

nG(t) - normalized stress relaxation modulus

γ_{cr}^{LVE} - critical strain amplitude (borderline between linear and non-linear viscoelastic behaviour)

G_c - cross-over modulus, $G'(\omega=\omega_c) = G''(\omega=\omega_c)$

ω_c - cross-over (angular) frequency

n - Power Law index, (equation 6-6)

a_T - horizontal shift factor for time-temperature superposition

b_T - vertical shift factor for time-temperature superposition

G_1' - 1st harmonic of the in-phase modulus, G_n' - n^{th} harmonic of the in-phase modulus,

G_1'' - 1st harmonic of the out-of-phase modulus, G_n'' - n^{th} harmonic of the out-of-phase modulus

$G(t, \gamma)$ - strain-dependent relaxation modulus

c_1, c_2 - WLF equation constants

$\Phi = (M_p^b / M_e) \cdot (N_g^p)^2$, Me - average molecular weight between entanglements of the (BR) branch prepolymer

(b) rheological parameters - defined and specific to this work (in alphabetical order)

G(40ms) - stress relaxation modulus measured 40ms after application of a sudden step-shear strain

G(1) - stress relaxation modulus, measured 1.0 s after application of a sudden step-shear strain

G'(5%/(II)) - steady-state value of the storage modulus at 5% dynamic strain and 1 rad/s frequency, in step II

G'(5%/(IV)) - steady-state value of the storage modulus at 5% dynamic strain and 1 rad/s frequency, in step IV

G'(5%/(VI)) - steady-state value of the storage modulus at 5% dynamic strain and 1 rad/s frequency, in step VI

G"(plateau) - plateau (or inflection) value of the loss modulus, G" (or G" at 1 rad/s in the absence of well defined plateau/inflection point)

G"(5%/(II)) - steady-state value of the loss modulus at 5% dynamic strain and 1 rad/s frequency, in step II

G"(5%/(IV)) - steady-state value of the loss modulus at 5% dynamic strain and 1 rad/s frequency, in step IV

G"(5%/(VI)) - steady-state value of the loss modulus at 5% dynamic strain and 1 rad/s frequency, in step VI

G*(0.2) - absolute value of the complex modulus G* at ω=0.2 rad/s & γ=5%

G*(2) - absolute value of the complex modulus G* at ω=2 rad/s & γ=5%

G*(20) - absolute value of the complex modulus G* at ω=20 rad/s & γ=5%

G*(200) - absolute value of the complex modulus G* at ω=200 rad/s & γ=5%

G*(5%/(II)) - steady-state (absolute) value of the complex modulus at 5% dynamic strain and 1 rad/s frequency, in step II

G*(5%/(VI) - steady-state (absolute) value of the complex modulus at 5% dynamic strain and 1 rad/s frequency, in step VI

G'(2%)-G_1'(50%) - difference between storage moduli at 50% and 2% dynamic strain amplitude (at 10 rad/s)

G_1'(50%) - First harmonic of the storage modulus at 50% dynamic strain and 10 rad/s oscillation frequency,

G_1'(200%) - 1st harmonic of the in-phase component of the modulus at 1 rad/s frequency and dynamic strain of 200%

G_1'(200%/0.5rad/s) - 1st harmonic of the storage modulus at 200% dynamic strain and 0.5 rad/s oscillation frequency

G_1'(200%/10rad/s) - 1st harmonic of the storage modulus at 200% dynamic strain and 10 rad/s oscillation frequency

G_1'(800%) - 1st harmonic of the in-phase component of the modulus at 1 rad/s frequency and dynamic strain of 800%

G_1''(50%) - First harmonic of the loss modulus at 50% dynamic strain and 10 rad/s oscillation frequency

G_1''(200%) - 1st harmonic of the out-of-phase component of the modulus at 1 rad/s frequency and dynamic strain of 200%

G_1''(200%/0.5rad/s) - 1st harmonic of the loss modulus at 200% dynamic strain and 0.5 rad/s oscillation frequency

G_1''(200%/10rad/s) - 1st harmonic of the loss modulus at 200% dynamic strain and 10 rad/s oscillation frequency

G_1''(800%) - 1st harmonic of the out-of-phase component of the modulus at 1 rad/s frequency and dynamic strain of 800%

G_1^*(50%) - First harmonic of the complex modulus at 50% dynamic strain and 10 rad/s oscillation frequency,

G_1^*(200%) - 1st harmonic of the (absolute value of the) complex modulus at 1 rad/s frequency and dynamic strain of 200%

G_1^*(800%) - 1st harmonic of the (absolute value of the) complex modulus at 1 rad/s frequency and dynamic strain of 800%

INT G(t)dt - time integral of the G(t) within 0.1-10,000 s range

INT(tan δ (BR-α)) dT - temperature integral of the tan δ, corresponding to BR α-transition, integrated over the temperature range of -100°C to - 80°C

mC-C p.c.l. - contour length of the modified Cole-Cole plot (log G_1'- log G_1''), γ=200%, ω=0.5 -10rad/s

n(0.001) - Power Law Index, for complex viscosity (log η^*) plotted as a function of log ω, calculated at ω=0.001 rad/s

n(0.001-100) - Power Law Index, for complex viscosity (log η^*) plotted as a function of log ω, averaged over ω=0.001-100 rad/s range

nC-C p.c.l. - contour length of the normalized Cole-Cole plot ($G_1'(\omega)/G_1'(\omega_{ref})$ - $G_1''(\omega)/G_1''(\omega_{ref})$, γ=200%, ω=0.5-10rad/s

nC-C quad. - the location of the nCC contour, relative to the diagonal of the plot. '+1' = above diagonal in the first quadrant, '-1' = below diagonal in the first quadrant

nG(0.1) - normalized (G(t)/G(t=40ms)) stress relaxation modulus, measured 0.1 s after application of a sudden step-shear strain

nG(1) - normalized (G(t)/G(t=40ms)) stress relaxation modulus, measured 1 s after application of a sudden step-shear strain

nG(10) - normalized (G(t)/G(t=40ms)) stress relaxation modulus, measured 10 s after application of a sudden step-shear strain

nG(100) - normalized (G(t)/G(t=40ms)) stress relaxation modulus, measured 100 s after application of a sudden step-shear strain

nG(400) - normalized (G(t)/G(t=40ms)) stress relaxation modulus, measured 400 s after application of a sudden step-shear strain

nG(t=1) - normalized (eq.6-5) stress relaxation modulus at 1s

nG(t=10) - normalized stress relaxation modulus at 10s

nG(t=100) - normalized stress relaxation modulus at 100s

nG(t=400) - normalized (eq.6-5) stress relaxation modulus at 400s

nG(t=1000) - normalized stress relaxation modulus at 1000s

nG(t=10,000) - normalized stress relaxation modulus at 10,000s

S' (50%) - 'In-phase' component of the torque, measured during isothermal oscillations at the frequency of 10 rad/s and 50% dynamic strain,

S″ (50%) - 'Out-of-phase' component of the torque, measured during isothermal oscillations at the frequency of 10 rad/s and 50% dynamic strain,

S_1 (5%) - 1st harmonic of the torque at 1 rad/s frequency and dynamic strain of 5%,

S_1 (200%) - 1st harmonic of the torque at 1 rad/s frequency and dynamic strain of 200%,

S_1 (800%) - 1st harmonic of the torque at 1 rad/s frequency and dynamic strain of 800%

S_1'(200%) - 1st harmonic of the in-phase component of the torque at 1 rad/s frequency and dynamic strain of 200%

S_1'(800%) - 1st harmonic of the in-phase component of the torque at 1 rad/s frequency and dynamic strain of 800%

S_1''(200%) - 1st harmonic of the out-of-phase component of the torque at 1 rad/s frequency and dynamic strain of 200%

S_1''(800%) - 1st harmonic of the out-of-phase component of the torque at 1 rad/s frequency and dynamic strain of 800%

slope (G'/G''^2) @0.001 - slope of the (G'/G''^2), plotted as a function of log ω, calculated at ω=0.001rad/s

slope G″ (0.001) - slope of the loss modulus, log G″(log ω) at ω=0.001 rad/s

|slope@t=0.1| - (absolute value of the) slope of the log nG-log t curve at 0.1s

|slope@t=40| - (absolute value of the) slope of the log nG-log t curve at 40s

|slope@t=400| - absolute value of the) slope of the log nG-log t curve at 400s

|slope@t=10,000| - (absolute value of the) slope of the log nG-log t curve at 10,000s

T /E''_{max} (BR-α) - temperature corresponding to maximum of the E"(T) peak (BR α-transition)

T /E''_{max} (CIIR-α) - temperature corresponding to maximum of the E"(T) peak (CIIR α-transition)

T /$\tan_{max}$ δ (BR-α) - temperature corresponding to maximum of the tan δ peak (BR α-transition)

T /$\tan_{max}$ δ (CIIR-ll) - temperature corresponding to the maximum of the tan δ peak (CIIR ll-transition)

T /$\tan_{max}$ δ (CIIR-α) - approximate temperature corresponding to the maximum tan δ (CIIR α-transition)

tan δ (0.001) - tan δ (=G″/G′) at ω=0.001 rad/s

tan δ (0.1) - tan δ at ω=0.1 rad/s

tan δ (5%(II)) - steady-state value of the tangent of the phase angle, δ at 5% dynamic strain and 1 rad/s frequency, in step II

tan δ (5%(IV)) - steady-state value of the tangent of the phase angle, δ at 5% dynamic strain and 1 rad/s frequency, in step IV

tan δ (5%(VI)) - steady-state value of the tangent of the phase angle, δ at 5% dynamic strain and 1 rad/s frequency, in step VI

$\tan_1$ δ ratio - = tan δ (200% & 0.5 rad/s) / tan δ (5% & 200 rad/s)

$\tan_1$ δ(50%) - = G_1″(50%) / G_1′(50%)

$\tan_1$ δ (200%) - tangent of phase angle, δ at 1 rad/s frequency and 200% dynamic strain

$\tan_1$ δ (200%/0.5rad/s) - = G_1″ (200% / 0.5 rad/s) / G_1′ (200% / 0.5 rad/s)

$\tan_1$ δ (200%/10rad/s) - = G_1″ (200% / 10 rad/s) / G_1′ (200% / 10 rad/s)

$\tan_1$ δ (800%) - tangent of phase angle, δ at 1 rad/s frequency and 800% dynamic strain

$\tan_{max}$ δ (BR-α) - maximum value of the tan δ, corresponding to BR α-transition

$\tan_{max}$ δ (CIIR-ll) - maximum value of the tan δ at the peak corresponding to CIIR ll-transition

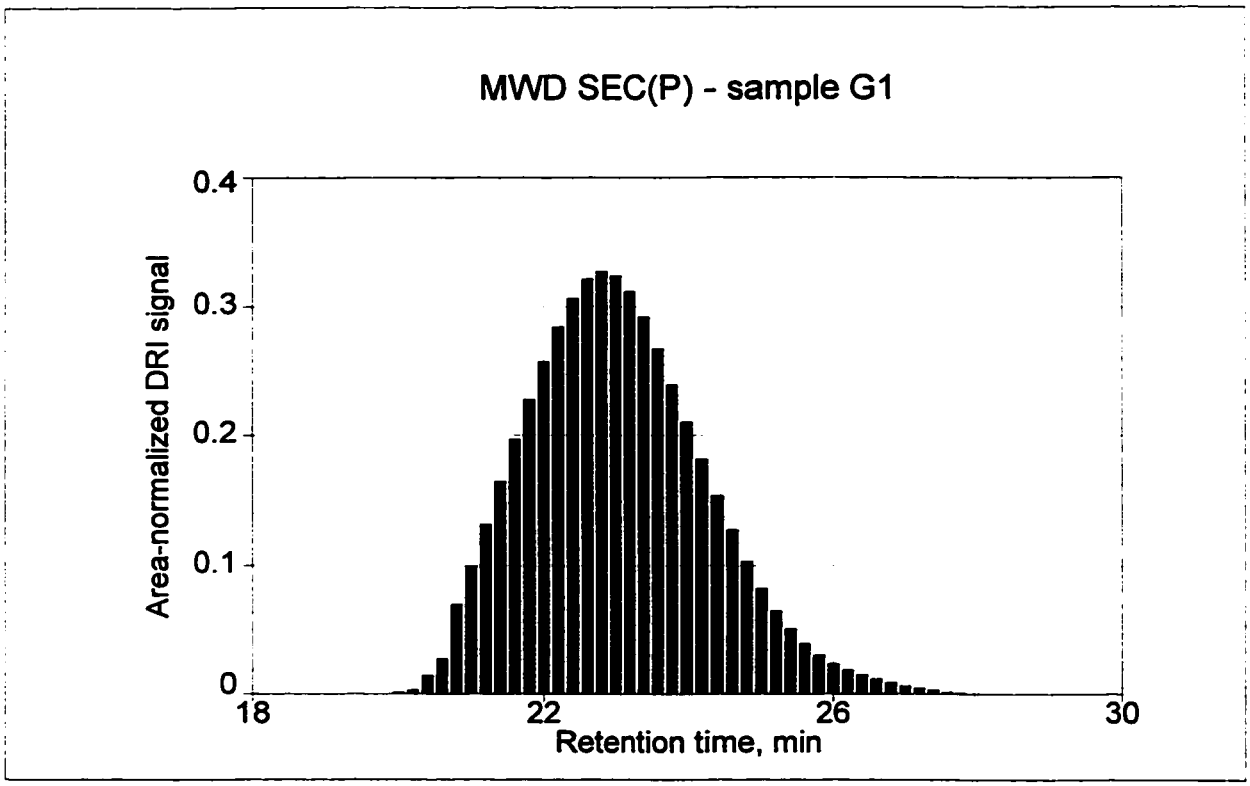
$\tan_{max}$ δ (CIIR-α) - maximum value of the tan δ peak corresponding to the CIIR α-transition

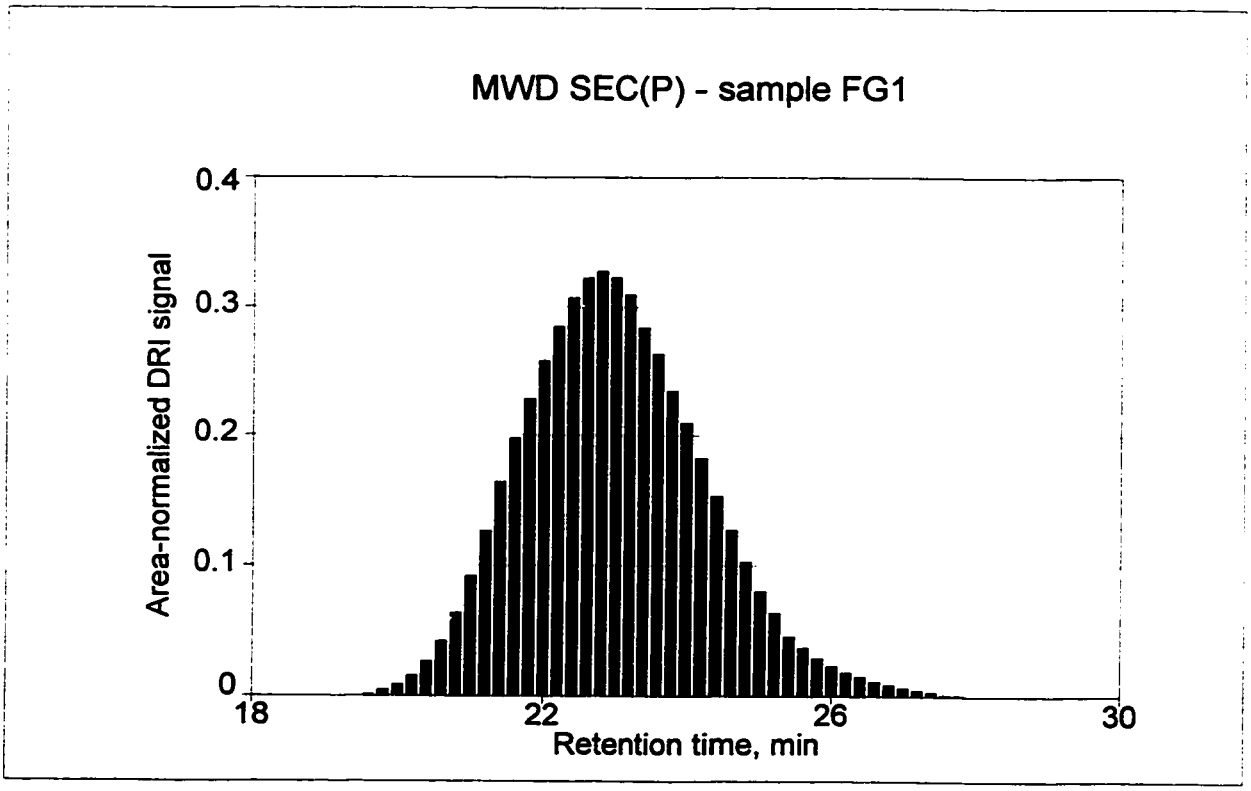
ΔT (E'-E" cross-over) - difference between temperatures corresponding to the E'-E" cross-over points; a measure of the width of the tan δ (CIIR-α+ll) damping peaks

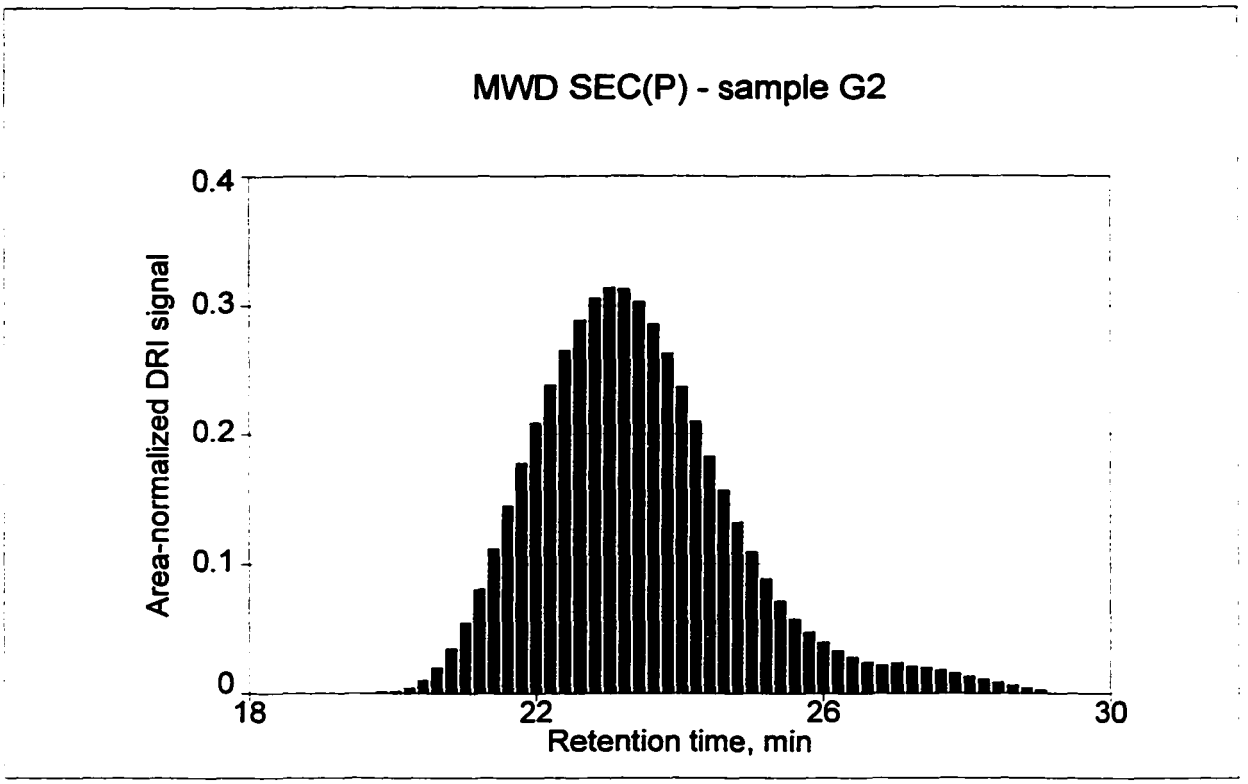
Appendix III

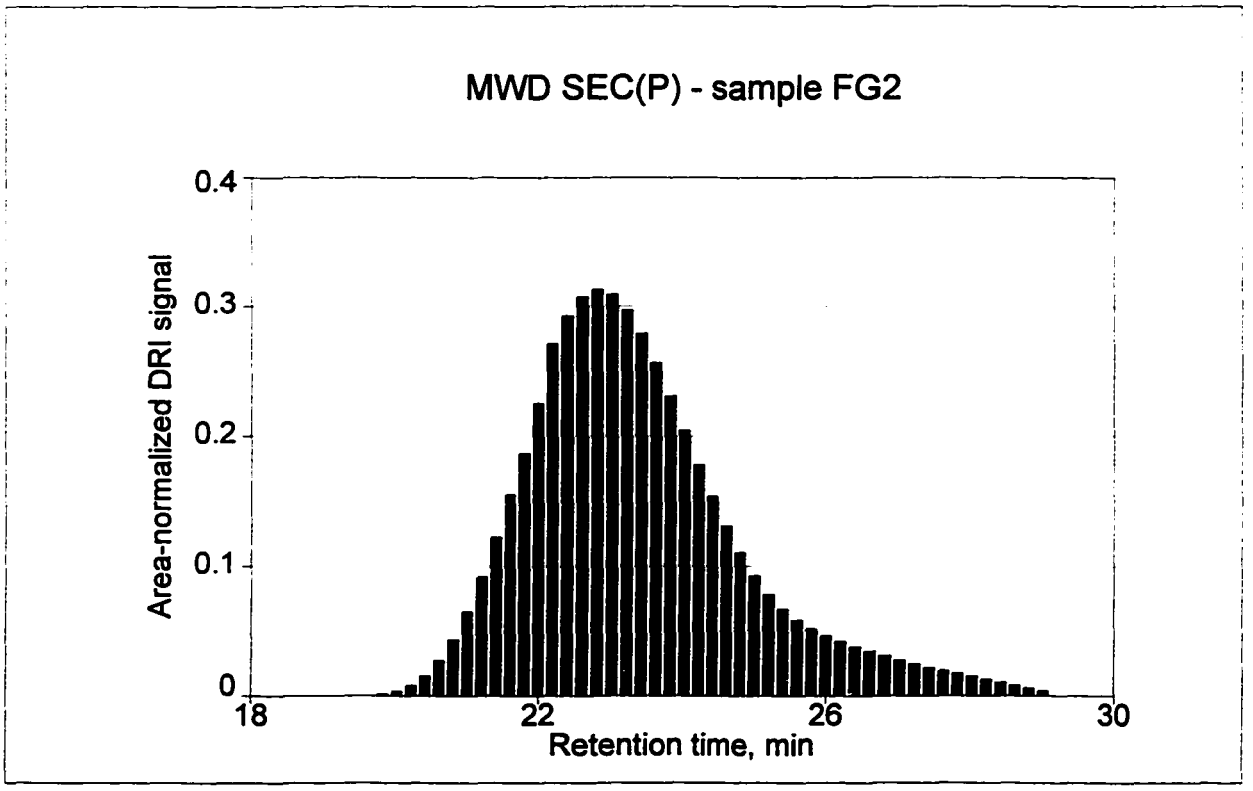
Apparent Molecular Weight Distributions of the Graft Samples

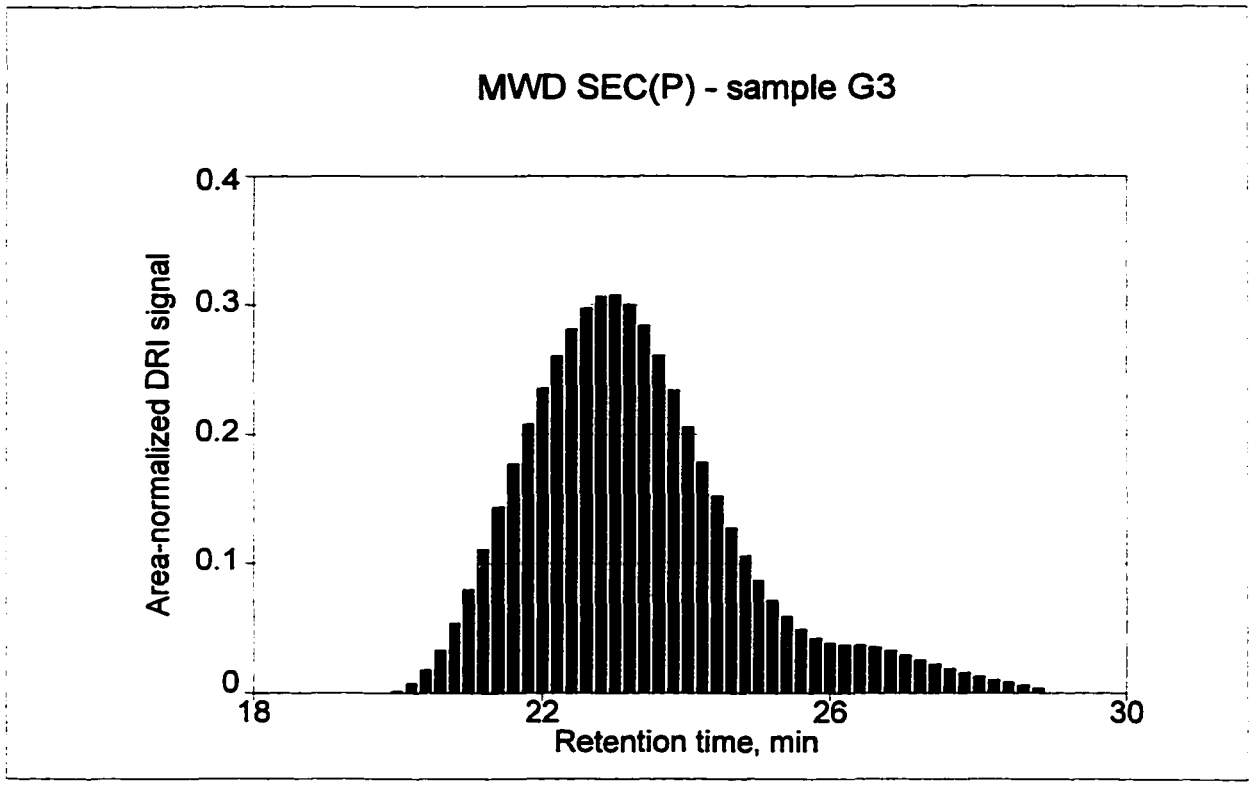
This appendix contain MWD profiles in a form of the area-normalized DRI signal (proportional to polymer concentration) as a function of retention time, related to the logarithm of the molecular weight. Each page is devoted to a single, with top diagram corresponding to the MWD of the crude graft sample (CG), while bottom diagram to its purified (fractionated) correspondent (samples FG). For additional comment refer to subsection 4.4.3.

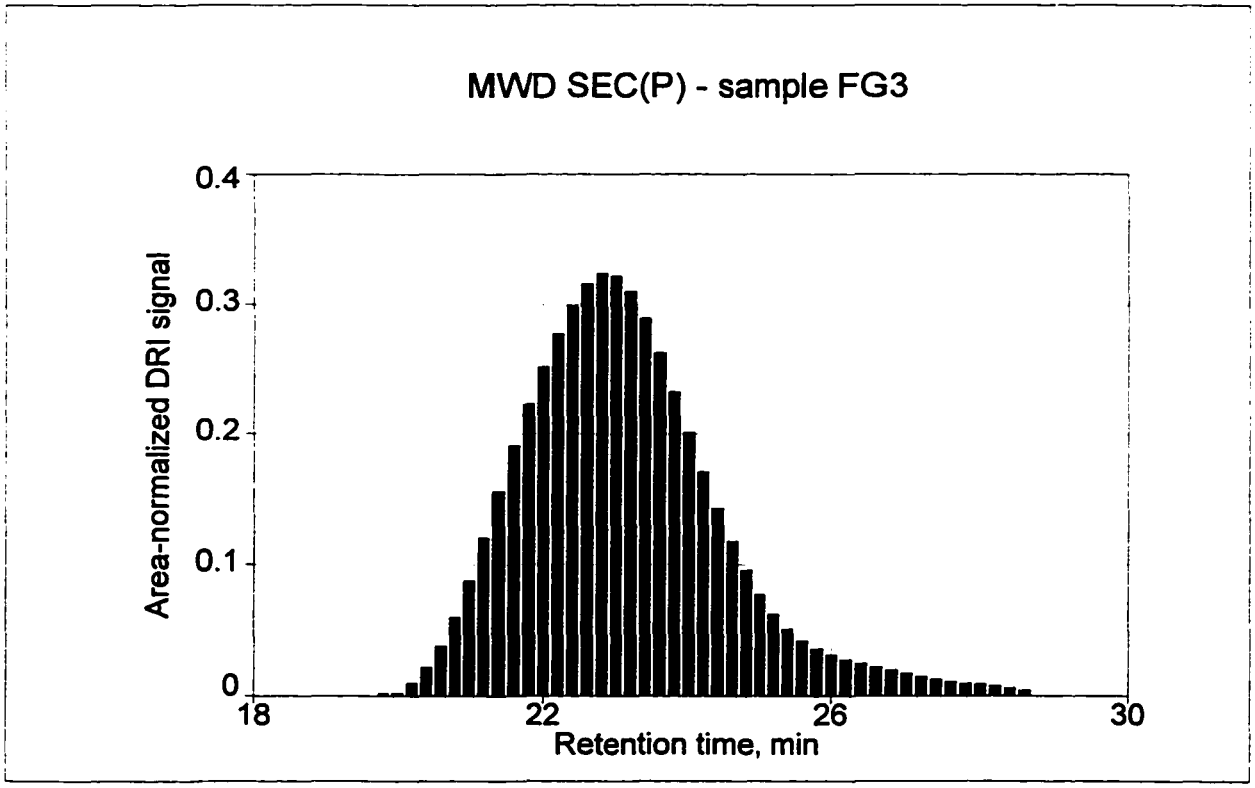

MWD SEC(P) - sample G1
Area-normalized DRI signal
0.4
0.3
0.2
0.1
0
18
22
26
30
Retention time, min

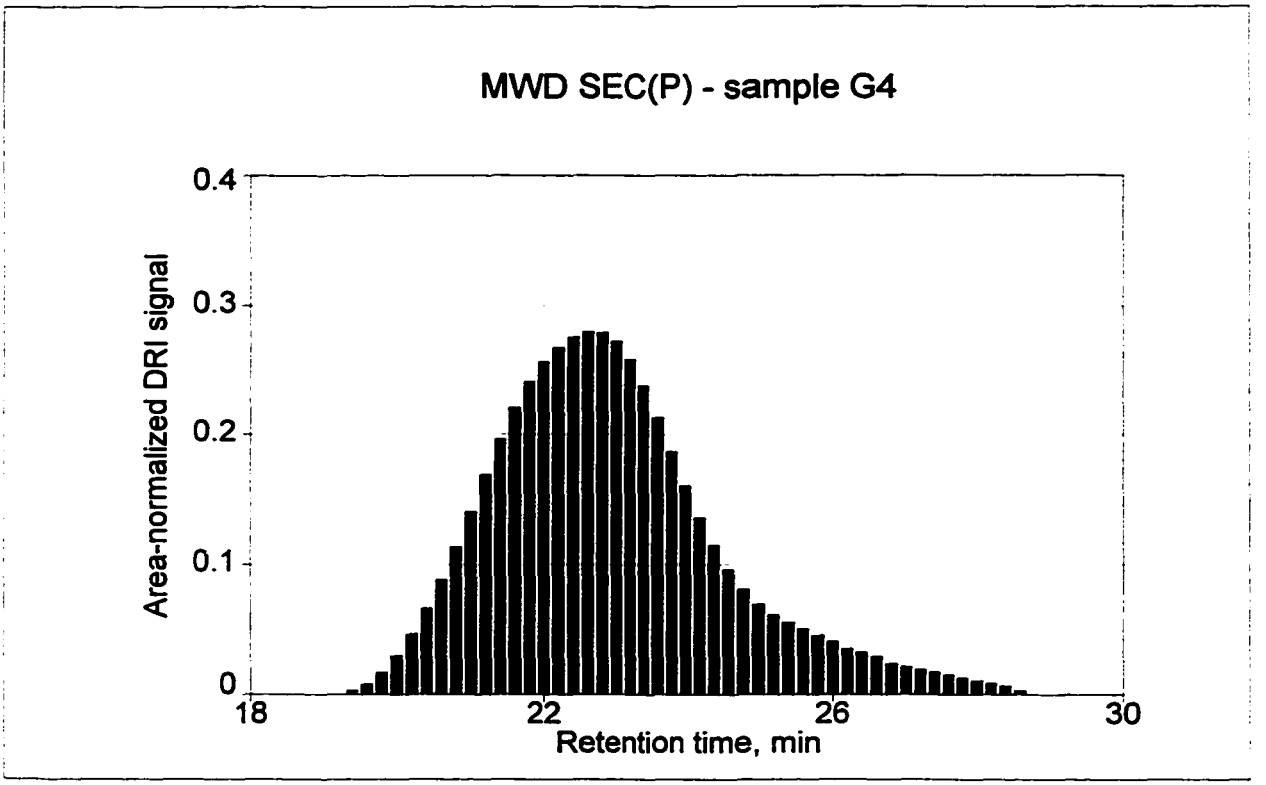

MWD SEC(P) - sample FG1
Area-normalized DRI signal
0.4
0.3
0.2
0.1
0
18
22
26
30
Retention time, min

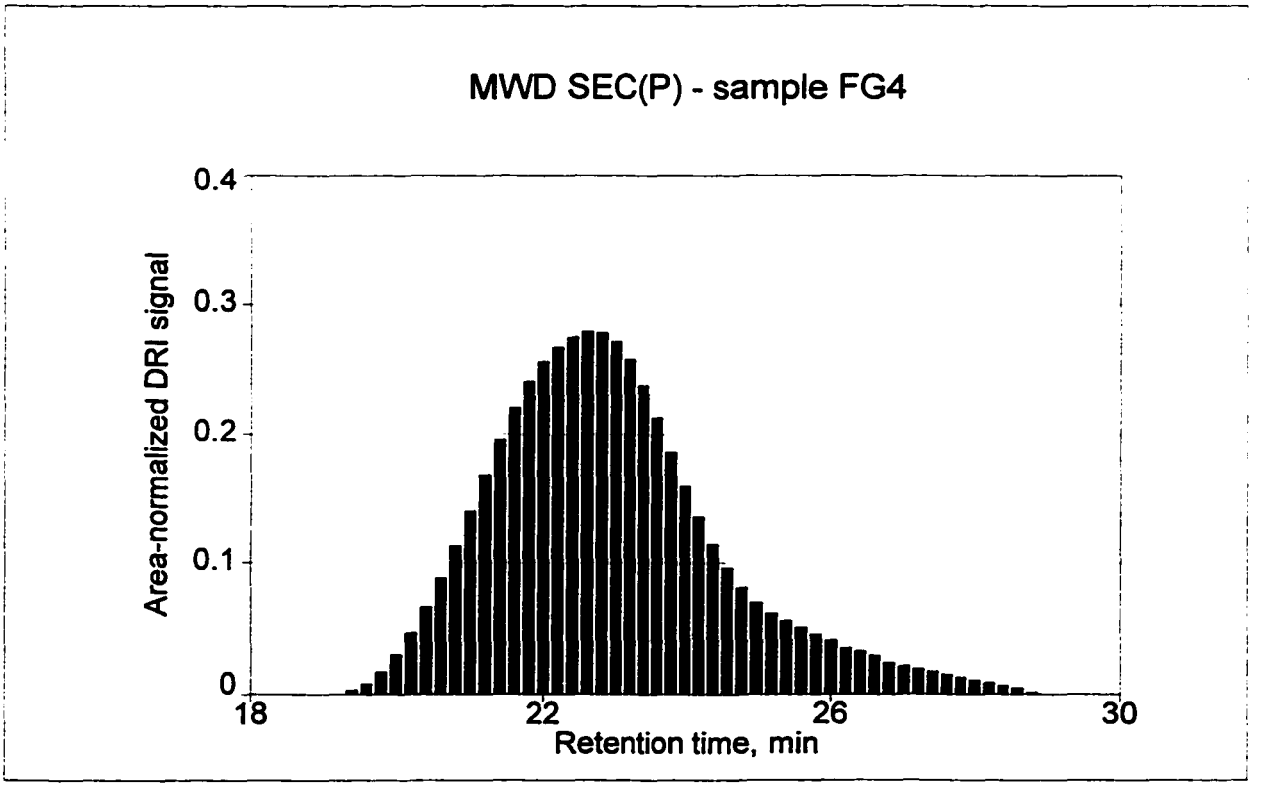

MWD SEC(P) - sample G2
Area-normalized DRI signal
0.4
0.3
0.2
0.1
0
18
22
26
30
Retention time, min

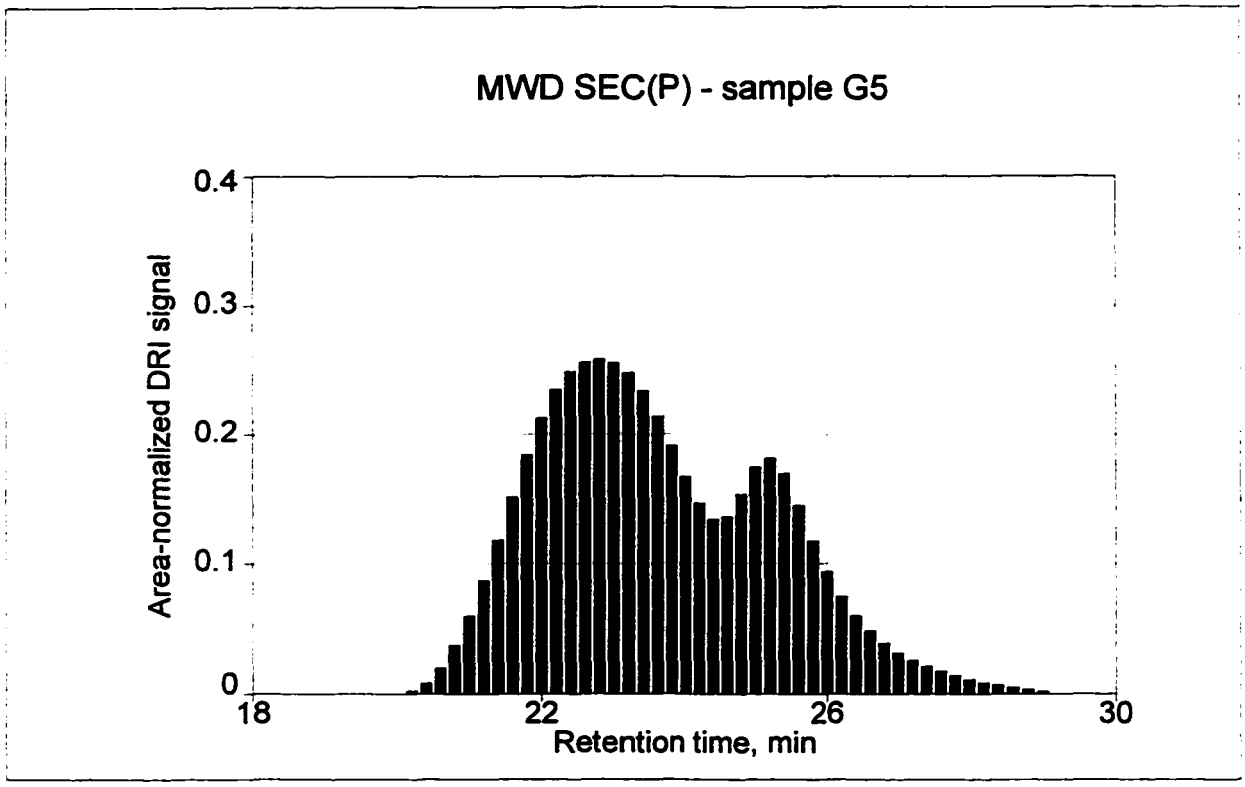

MWD SEC(P) - sample FG2
Area-normalized DRI signal
0.4
0.3
0.2
0.1
0
18
22
26
30
Retention time, min

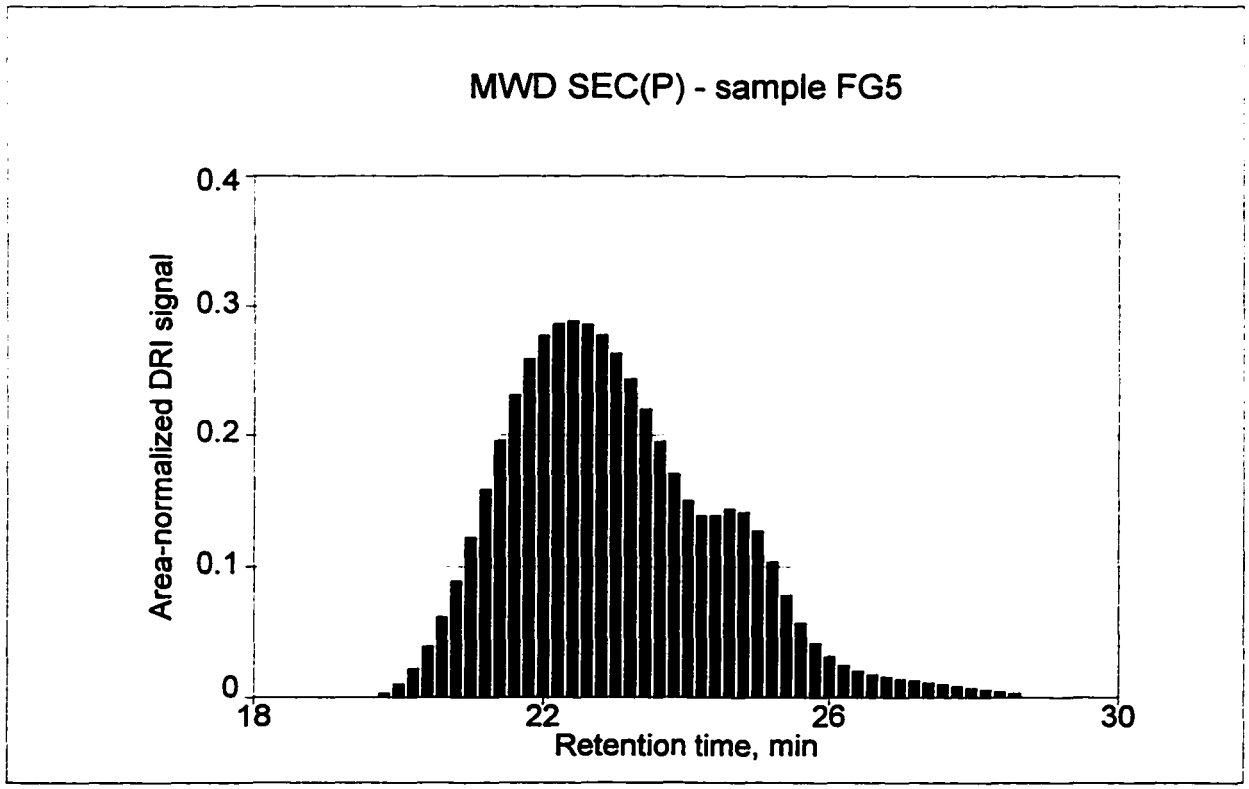

MWD SEC(P) - sample G3
Area-normalized DRI signal
0.4
0.3
0.2
0.1
0
18
22
26
30
Retention time, min

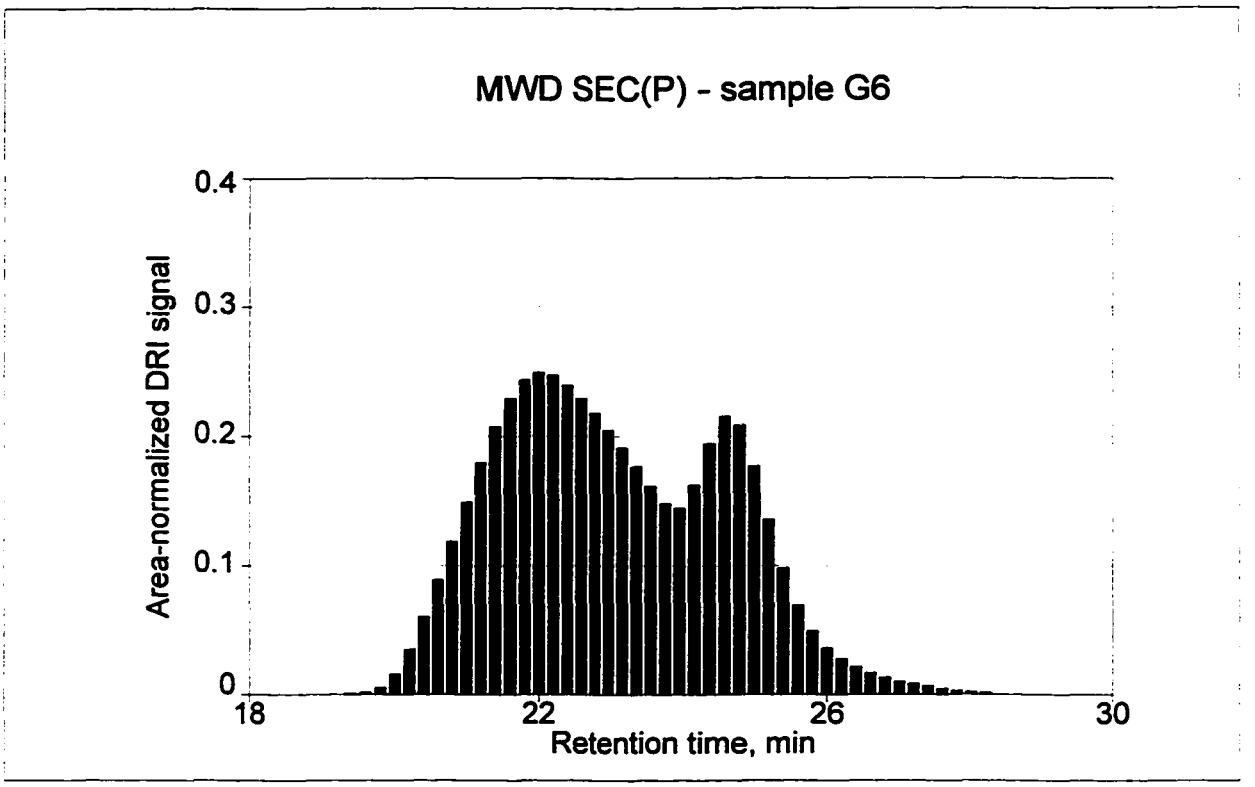

MWD SEC(P) - sample FG3
Area-normalized DRI signal
0.4
0.3
0.2
0.1
0
18
22
26
30
Retention time, min

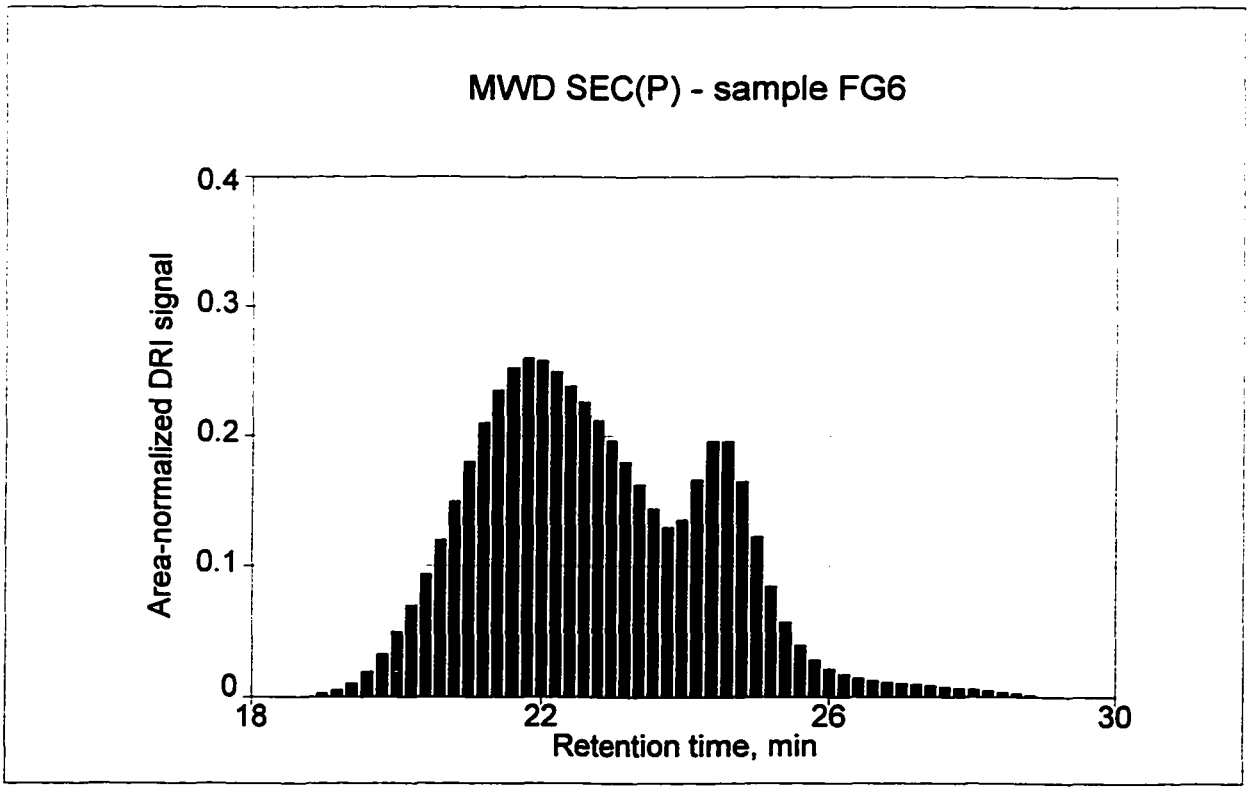

MWD SEC(P) - sample G4
Area-normalized DRI signal
0.4
0.3
0.2
0.1
0
18
22
26
30
Retention time, min

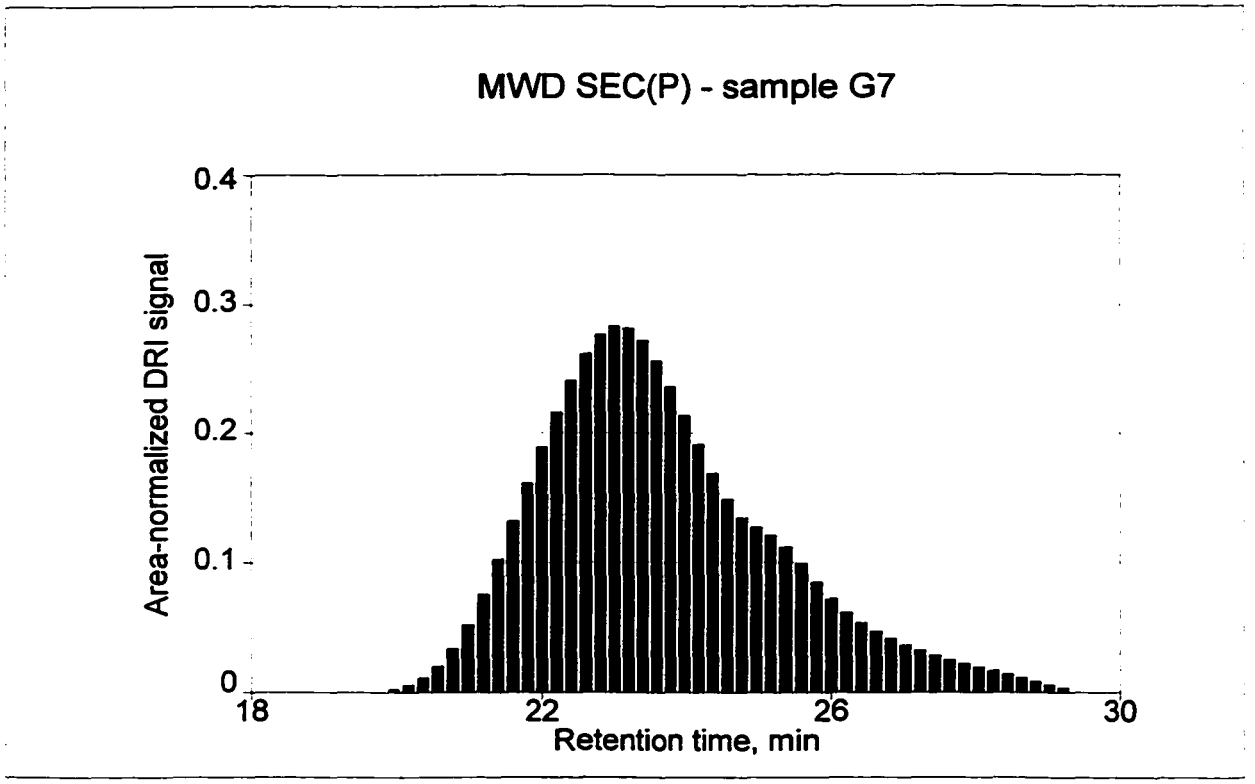

MWD SEC(P) - sample FG4
Area-normalized DRI signal
0.4
0.3
0.2
0.1
0
18
22
26
30
Retention time, min

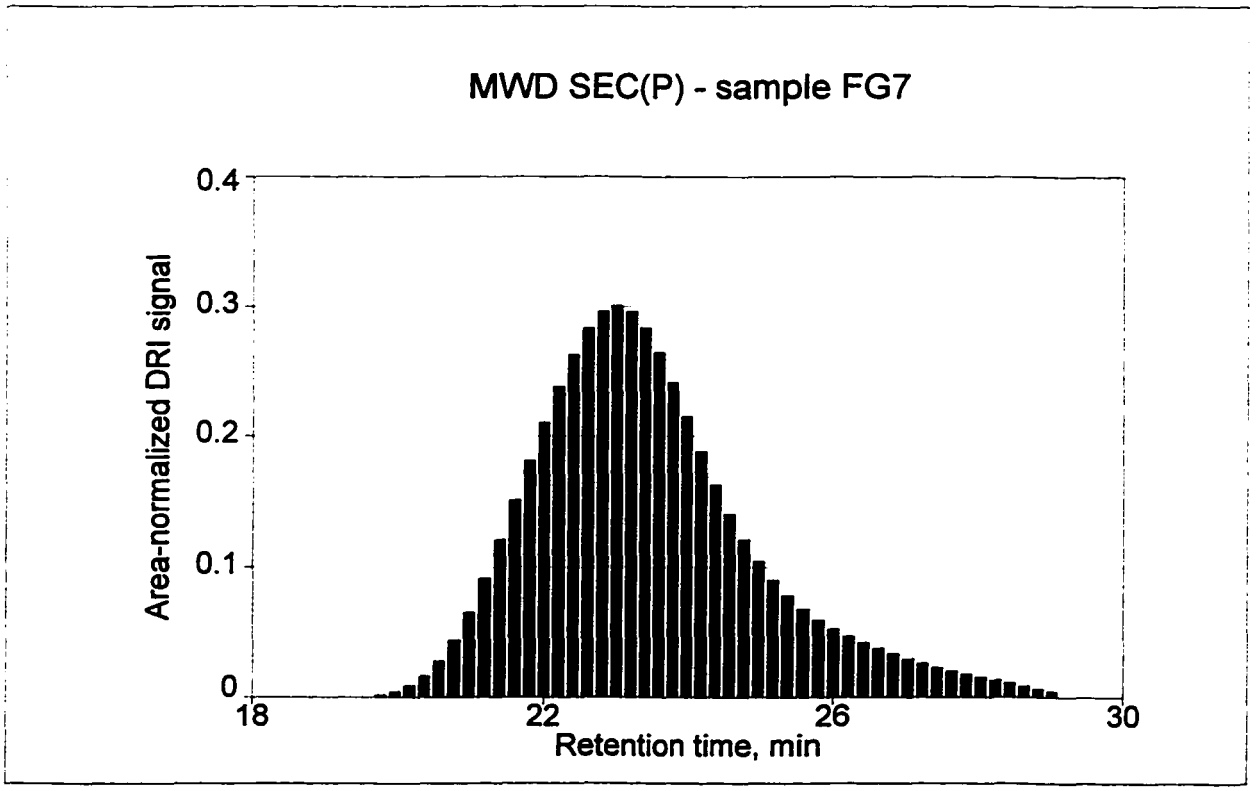

MWD SEC(P) - sample G5
Area-normalized DRI signal
0.4
0.3
0.2
0.1
0
18
22
26
30
Retention time, min

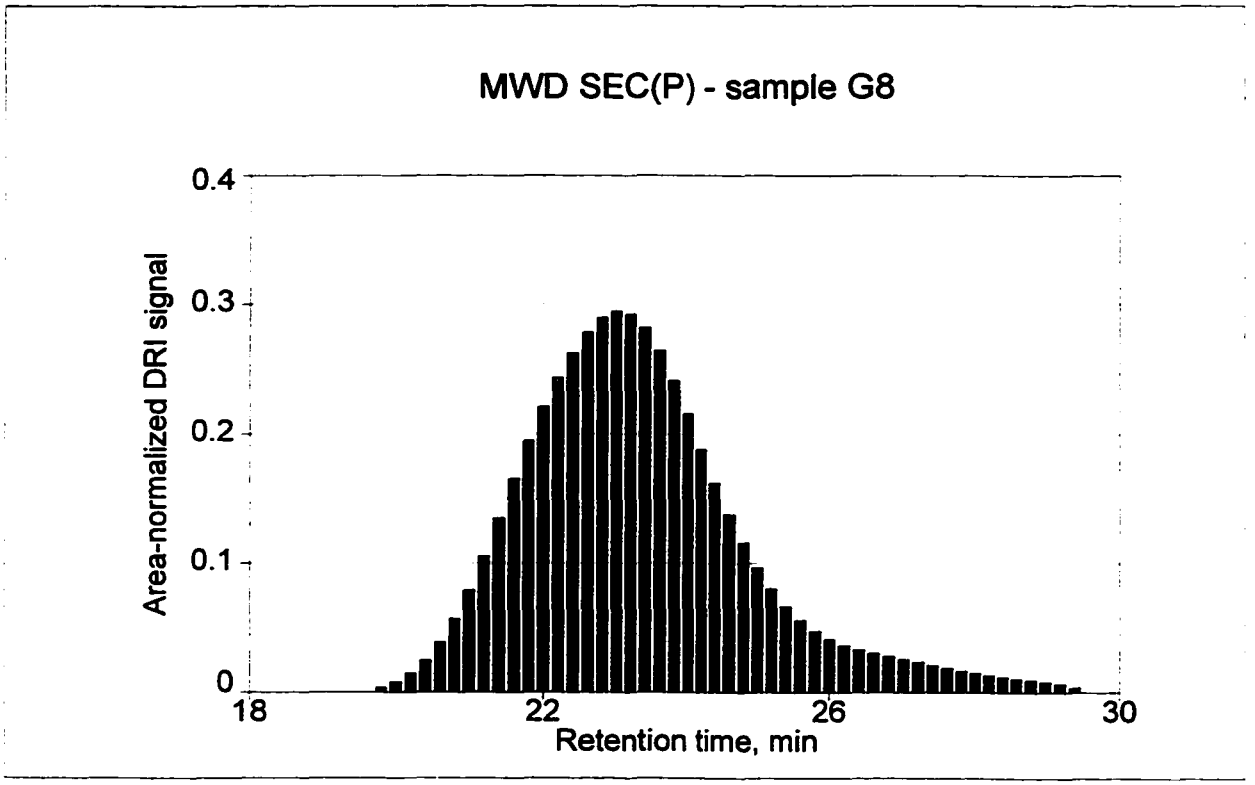

MWD SEC(P) - sample FG5
Area-normalized DRI signal
0.4
0.3
0.2
0.1
0
18
22
26
30
Retention time, min

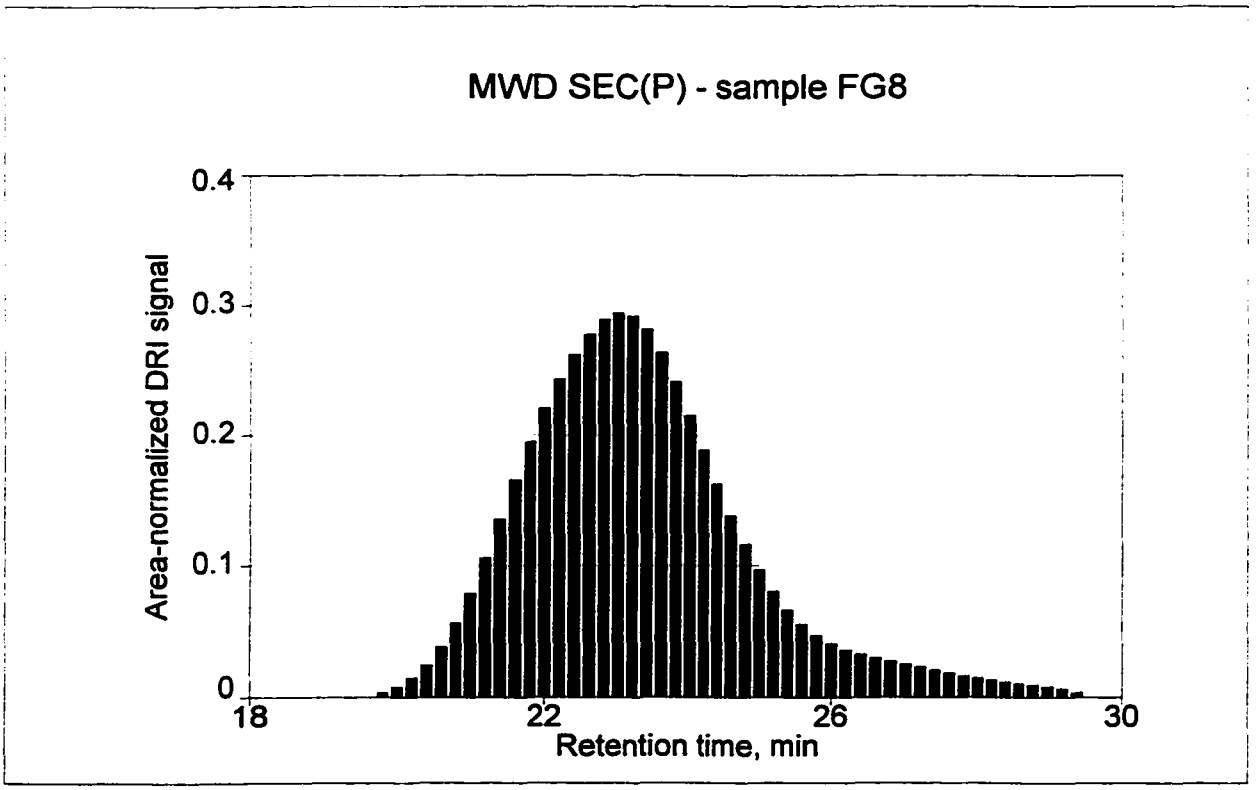

MWD SEC(P) - sample G6
Area-normalized DRI signal
0.4
0.3
0.2
0.1
0
18
22
26
30
Retention time, min

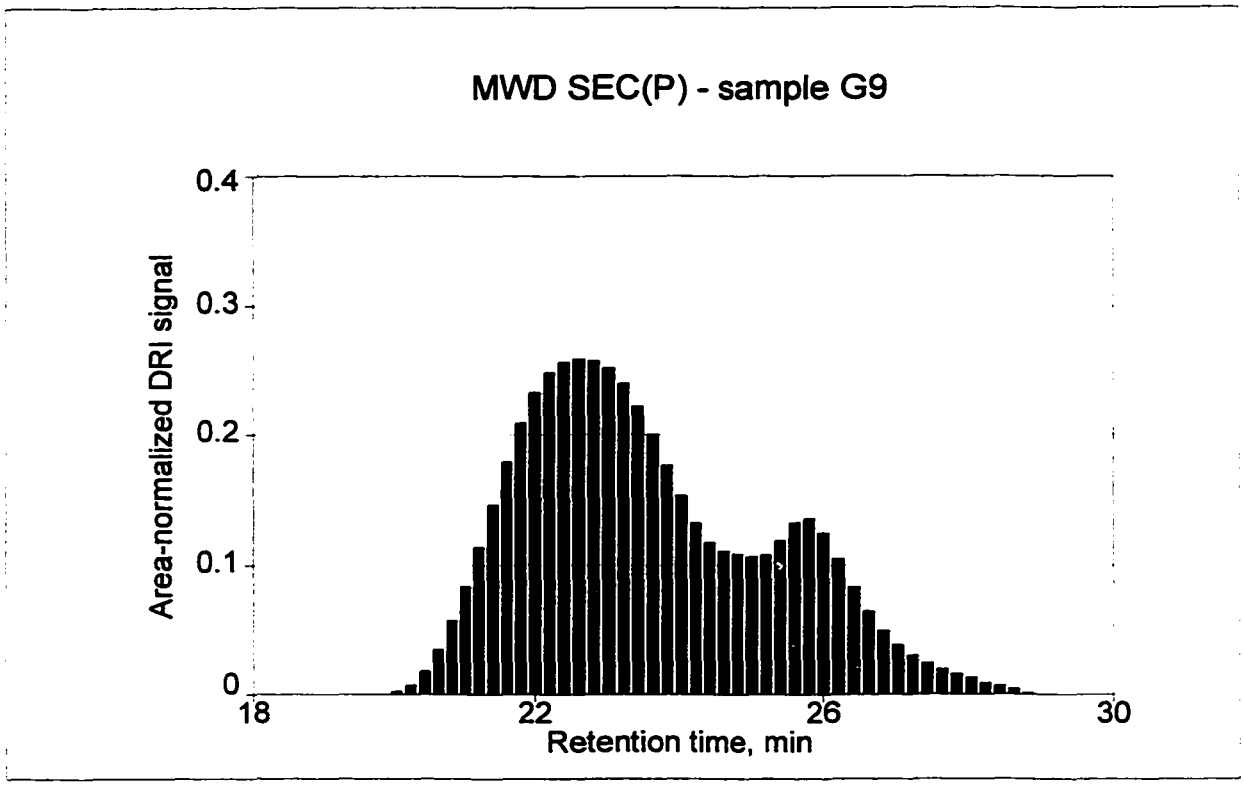

MWD SEC(P) - sample FG6
Area-normalized DRI signal
0.4
0.3
0.2
0.1
0
18
22
26
30
Retention time, min

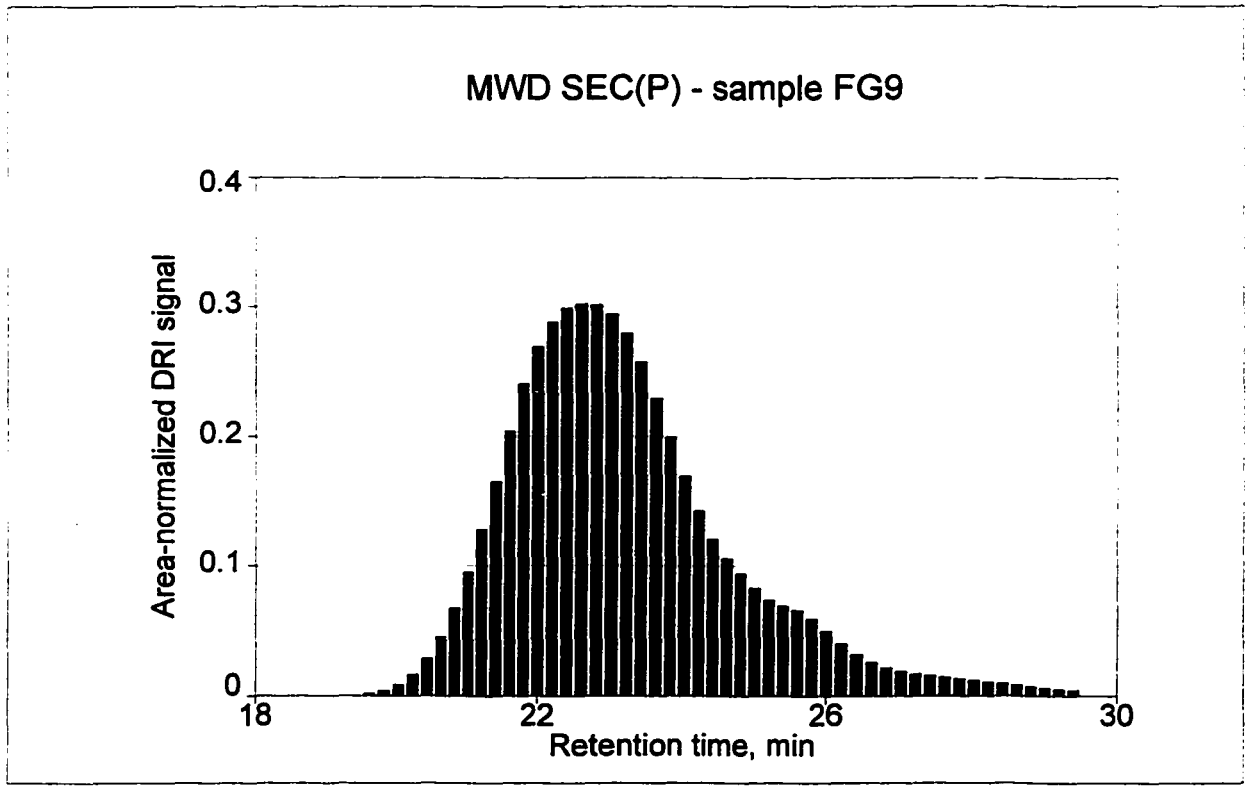

MWD SEC(P) - sample G7
Area-normalized DRI signal
0.4
0.3
0.2
0.1
0
18
22
26
30
Retention time, min

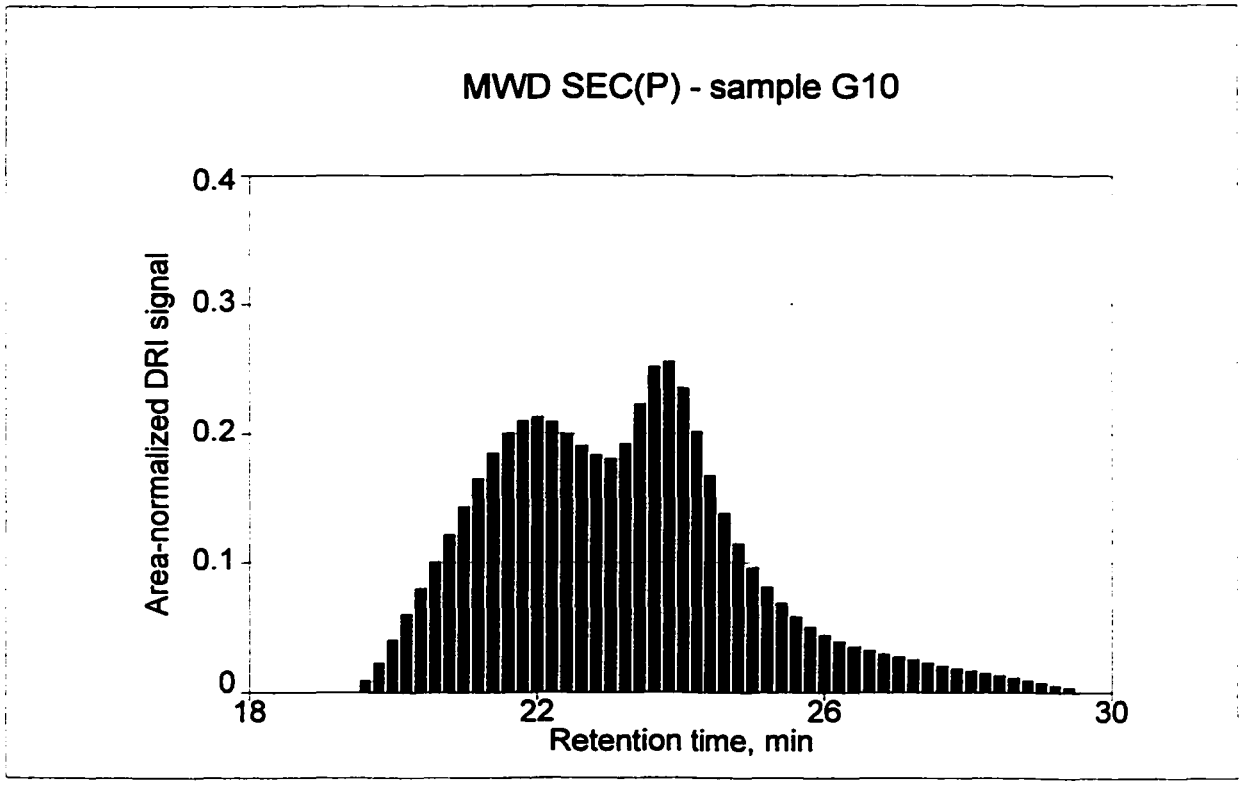

MWD SEC(P) - sample FG7
Area-normalized DRI signal
0.4
0.3
0.2
0.1
0
18
22
26
30
Retention time, min

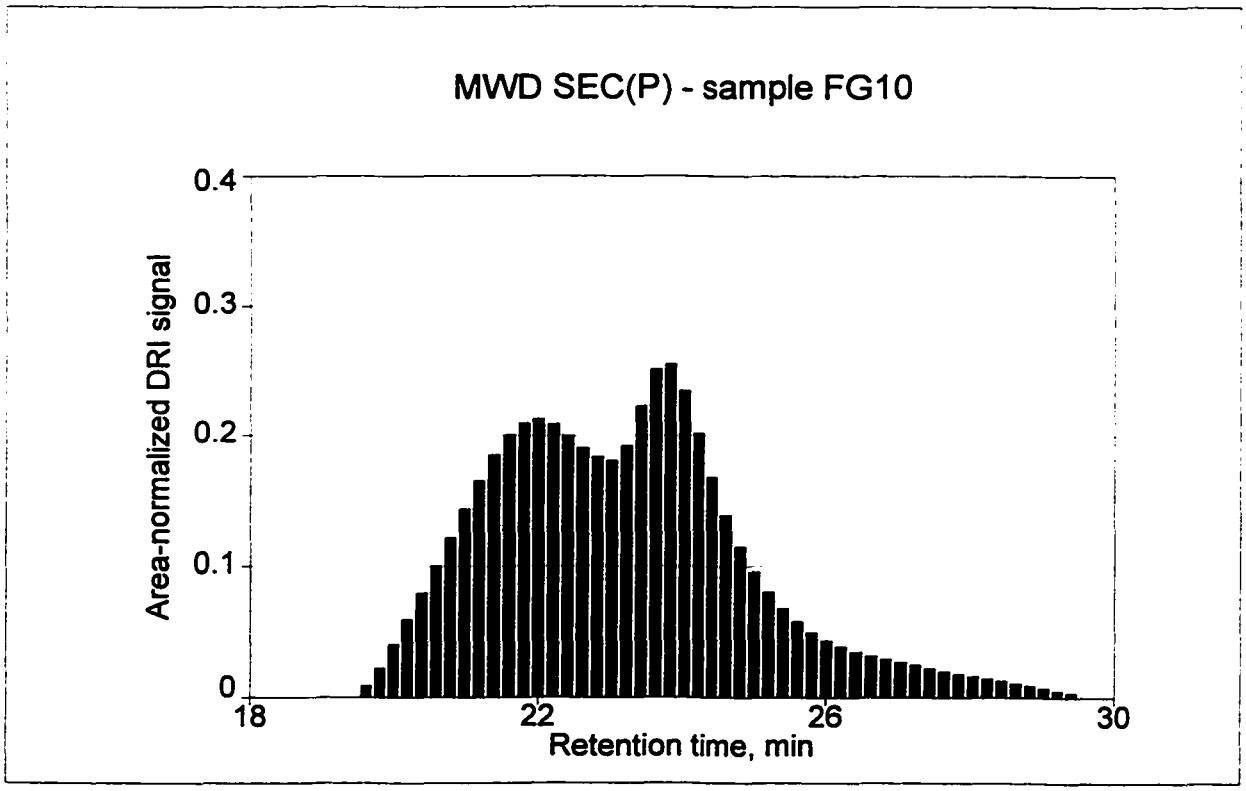

MWD SEC(P) - sample G8
Area-normalized DRI signal
0.4
0.3
0.2
0.1
0
18
22
26
30
Retention time, min

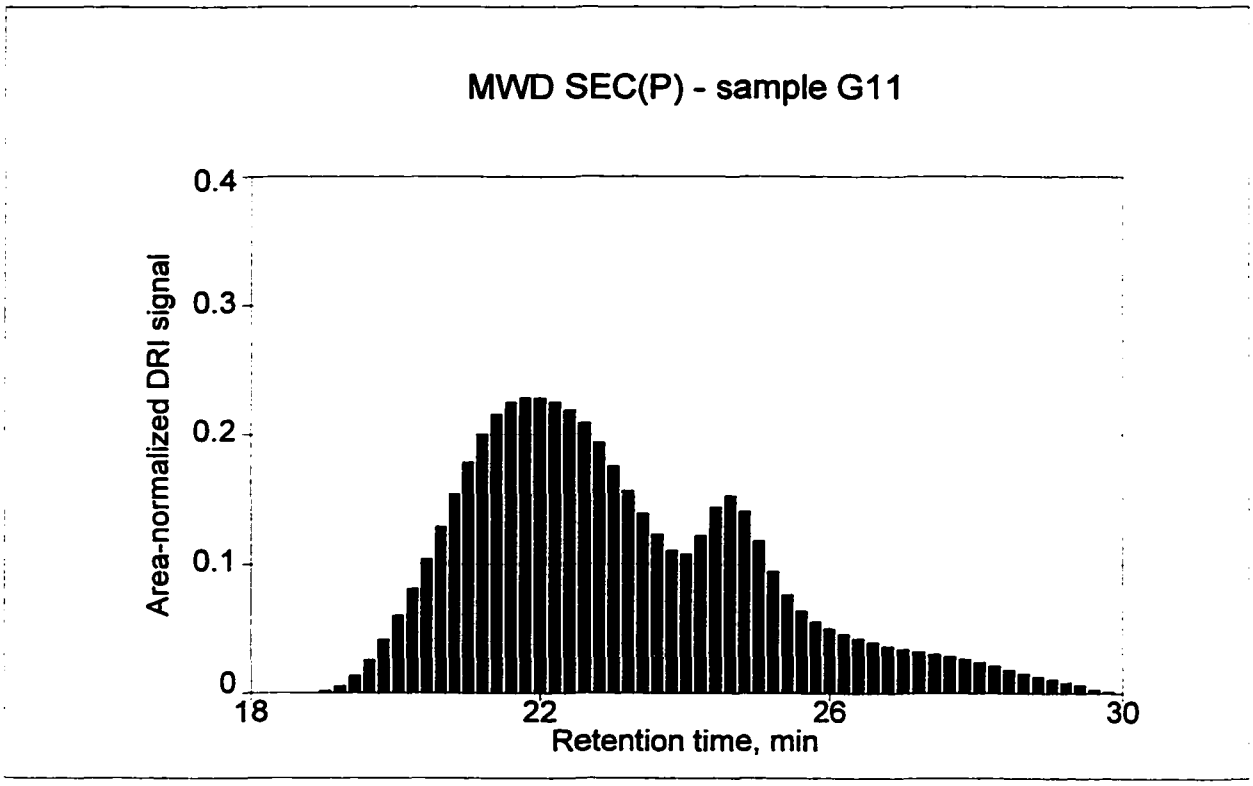

MWD SEC(P) - sample FG8
Area-normalized DRI signal
0.4
0.3
0.2
0.1
0
18
22
26
30
Retention time, min

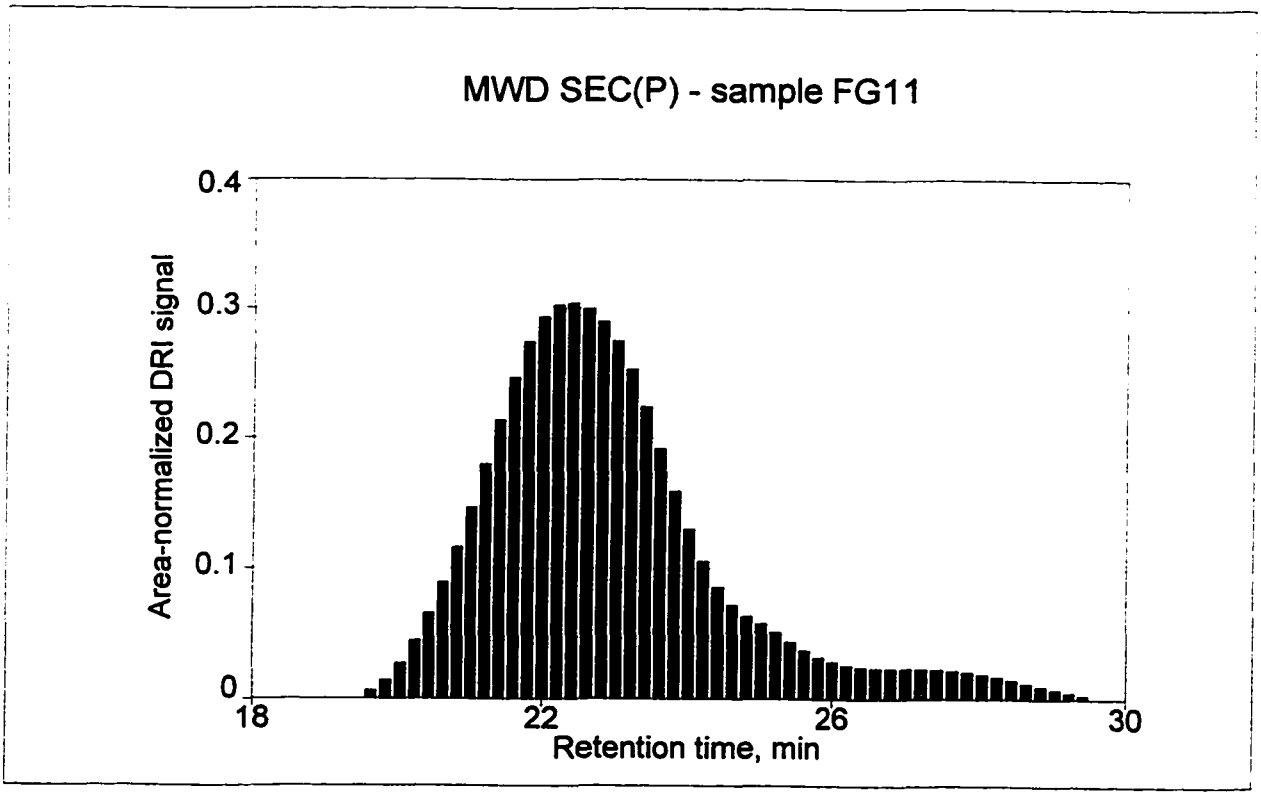

MWD SEC(P) - sample G9
Area-normalized DRI signal
0.4
0.3
0.2
0.1
0
18
22
26
30
Retention time, min

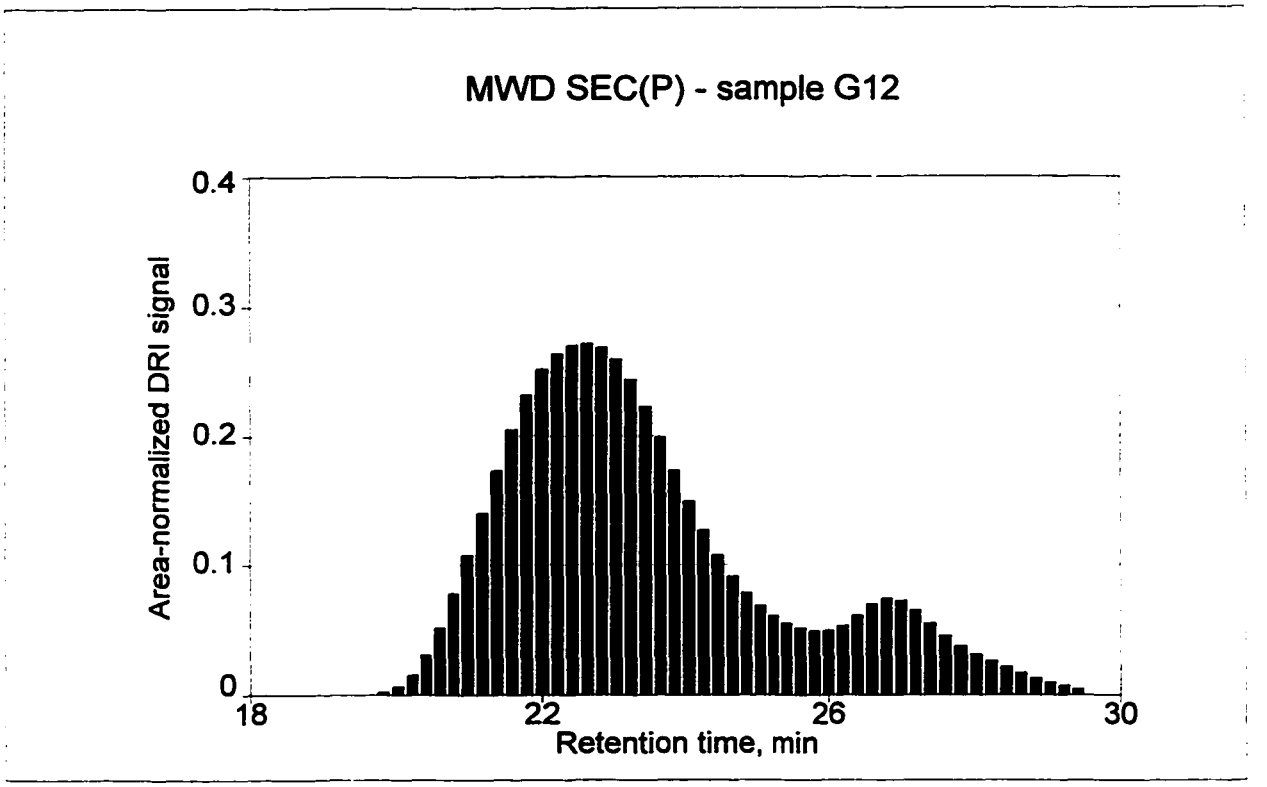

MWD SEC(P) - sample FG9
Area-normalized DRI signal
0.4
0.3
0.2
0.1
0
18
22
26
30
Retention time, min

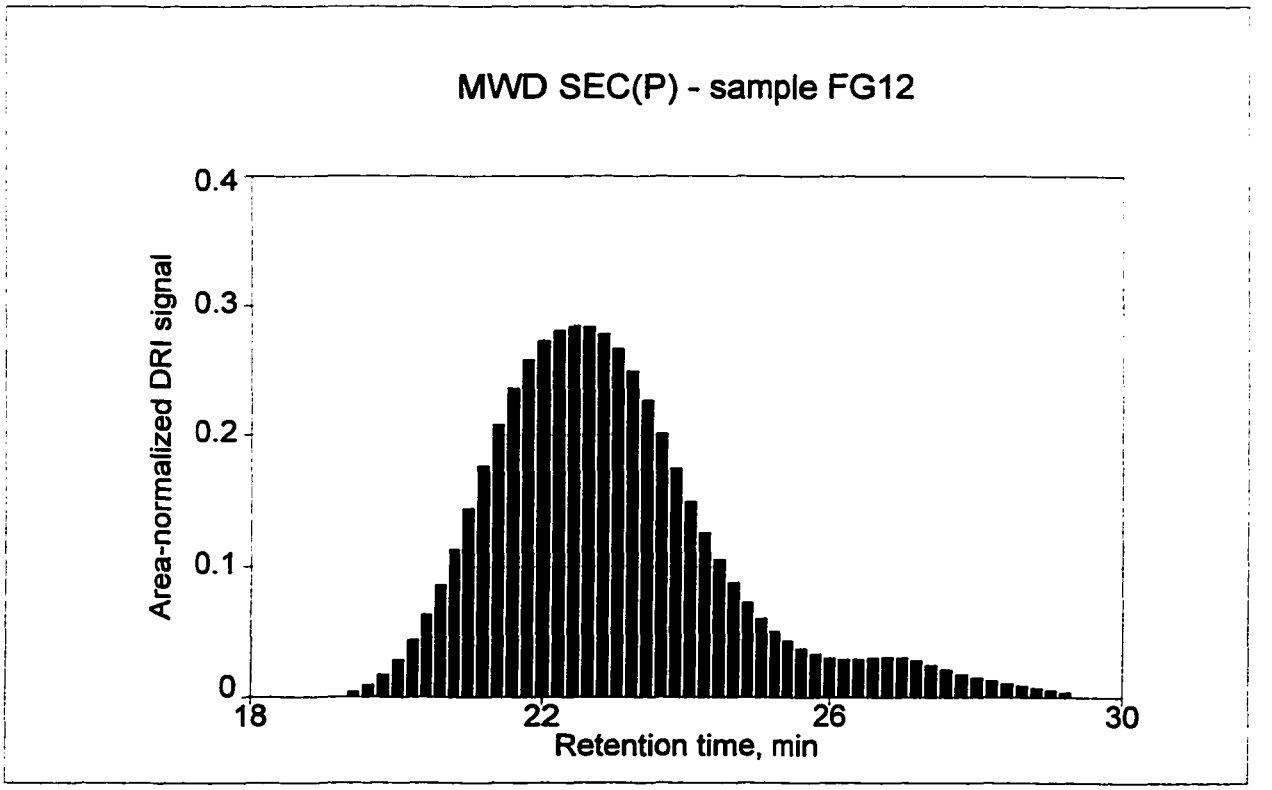

MWD SEC(P) - sample G10
Area-normalized DRI signal
0.4
0.3
0.2
0.1
0
18
22
26
30
Retention time, min

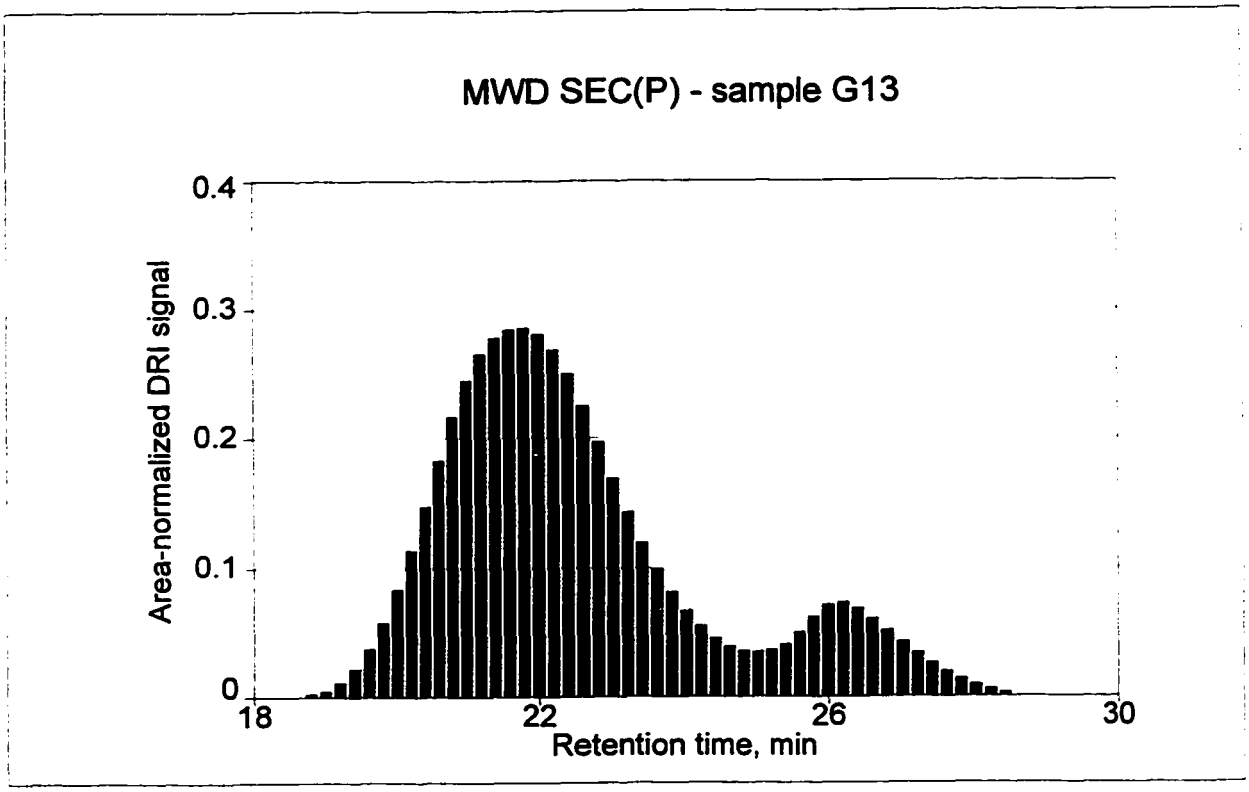

MWD SEC(P) - sample FG10
Area-normalized DRI signal
0.4
0.3
0.2
0.1
0
18
22
26
30
Retention time, min

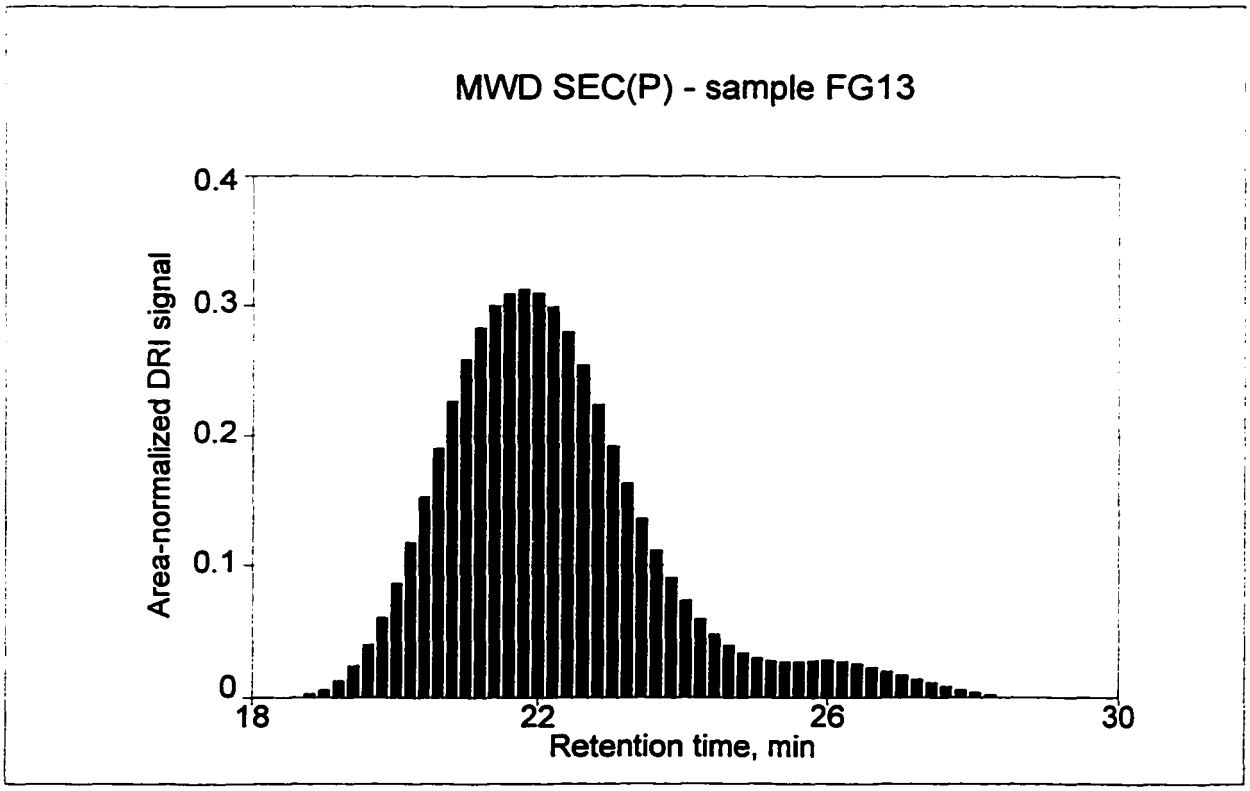

MWD SEC(P) - sample G11
Area-normalized DRI signal
0.4
0.3
0.2
0.1
0
18
22
26
30
Retention time, min

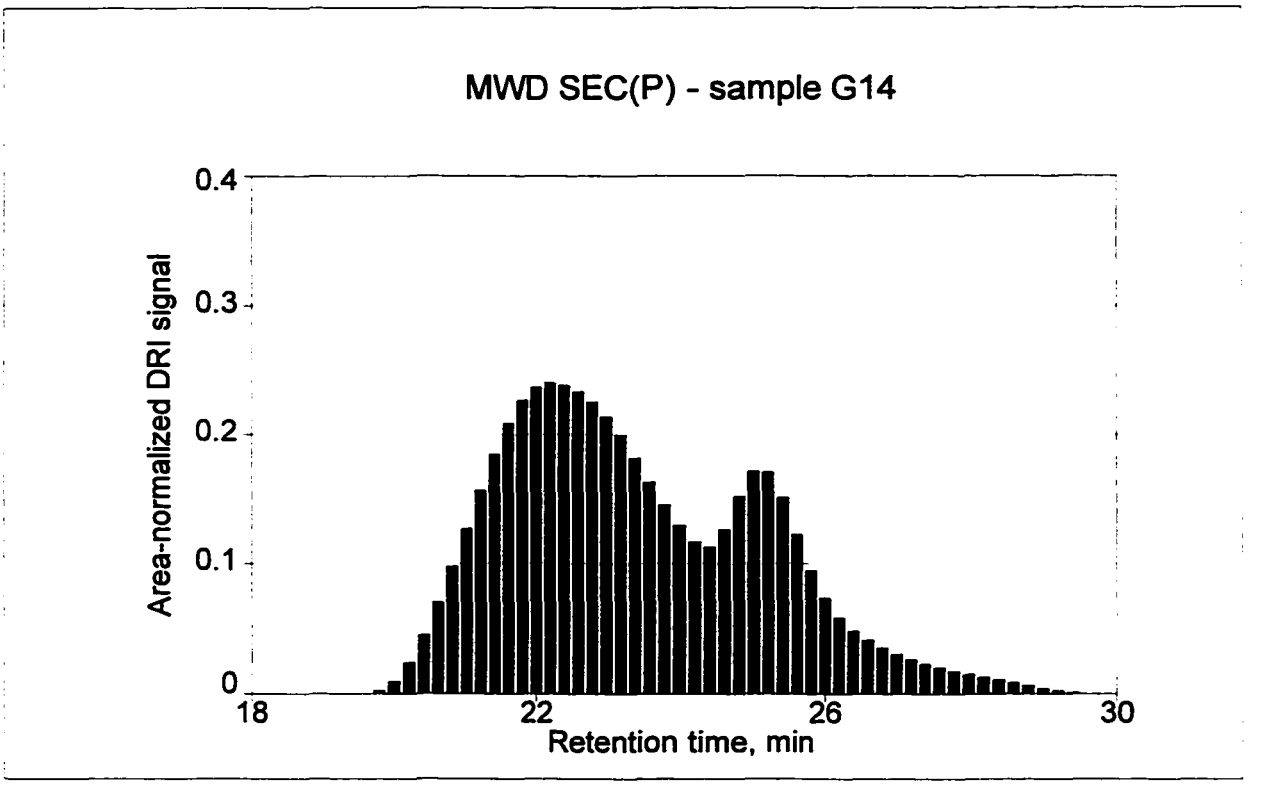

MWD SEC(P) - sample FG11
Area-normalized DRI signal
0.4
0.3
0.2
0.1
0
18
22
26
30
Retention time, min

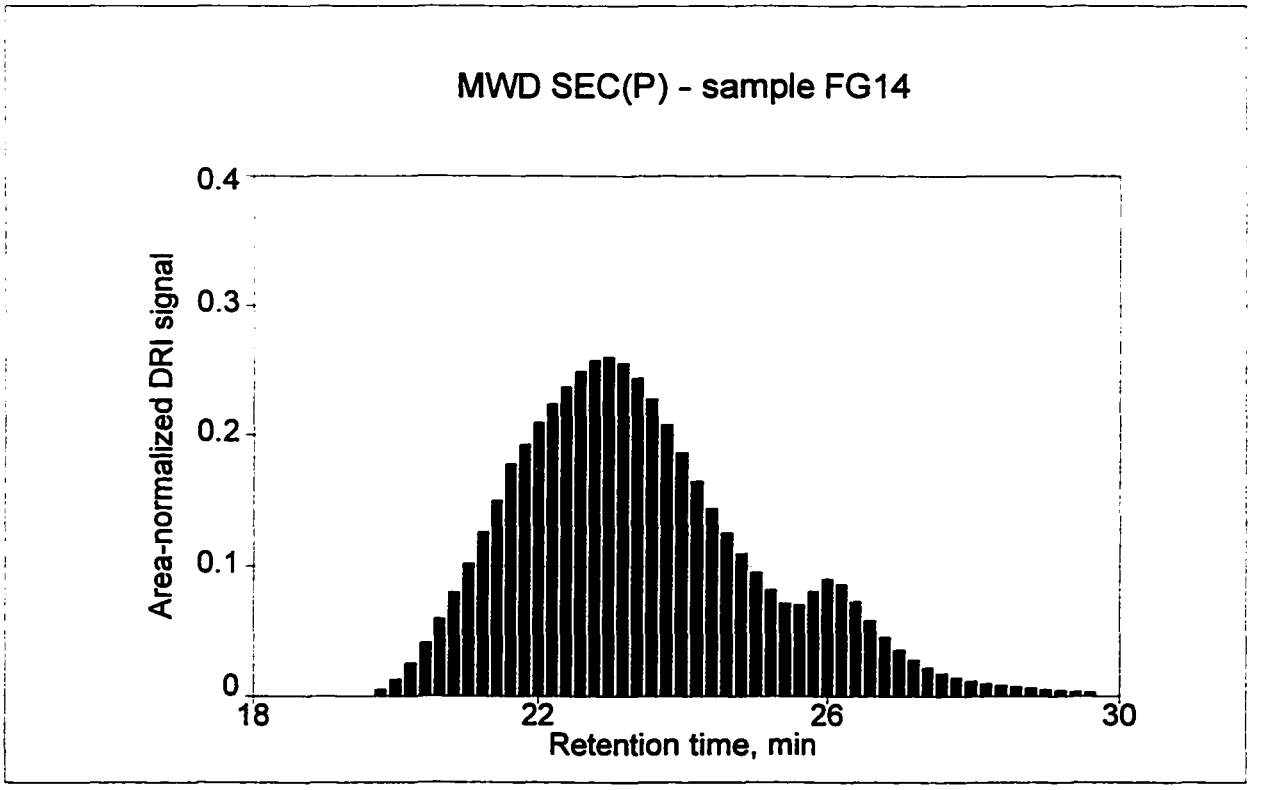

MWD SEC(P) - sample G12
Area-normalized DRI signal
0.4
0.3
0.2
0.1
0
18
22
26
30
Retention time, min

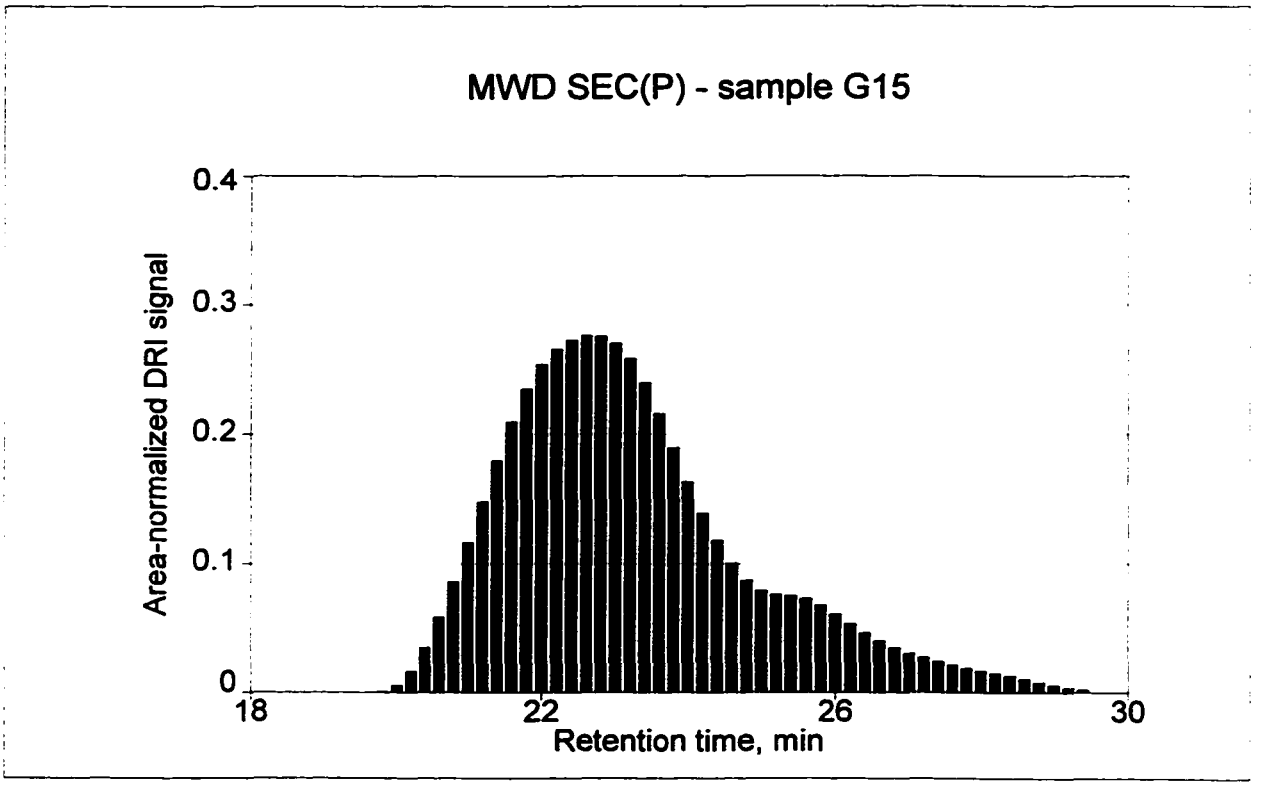

MWD SEC(P) - sample FG12
Area-normalized DRI signal
0.4
0.3
0.2
0.1
0
18
22
26
30
Retention time, min

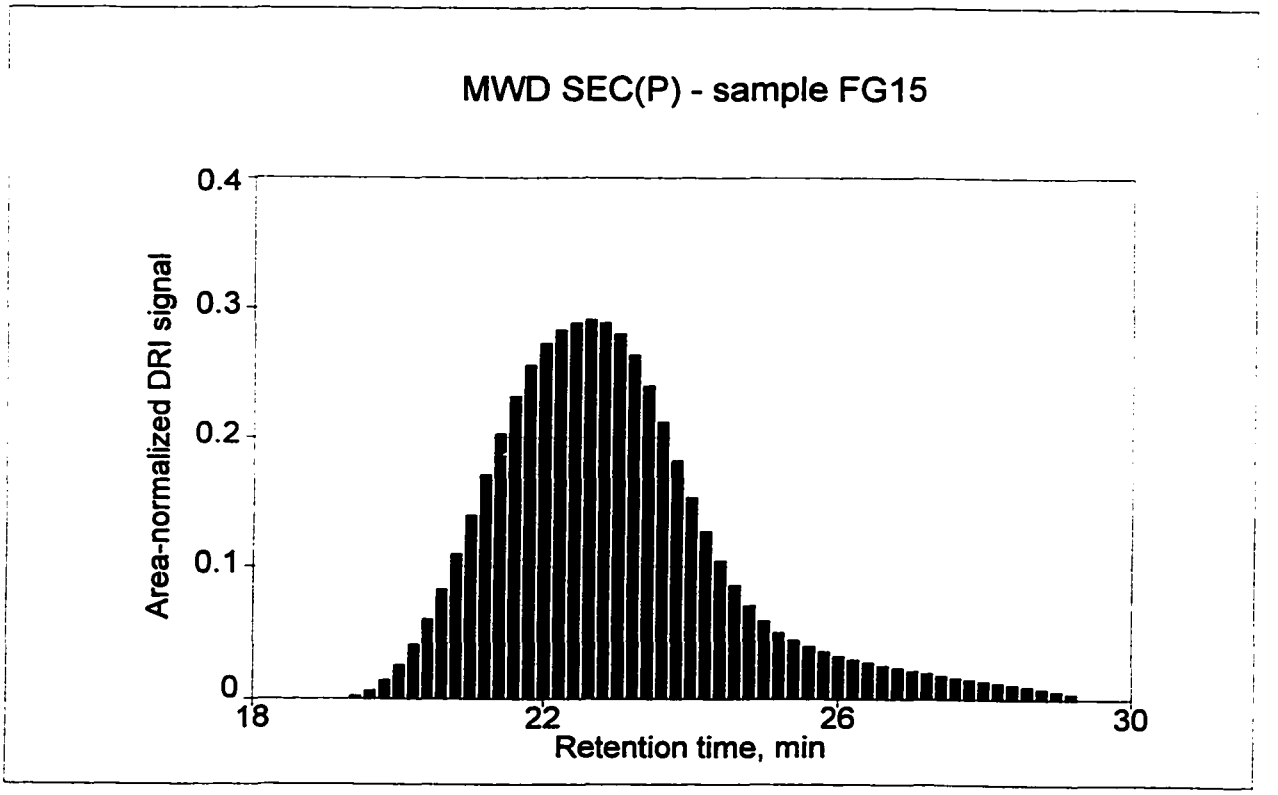

MWD SEC(P) - sample G13
Area-normalized DRI signal
0.4
0.3
0.2
0.1
0
18
22
26
30
Retention time, min

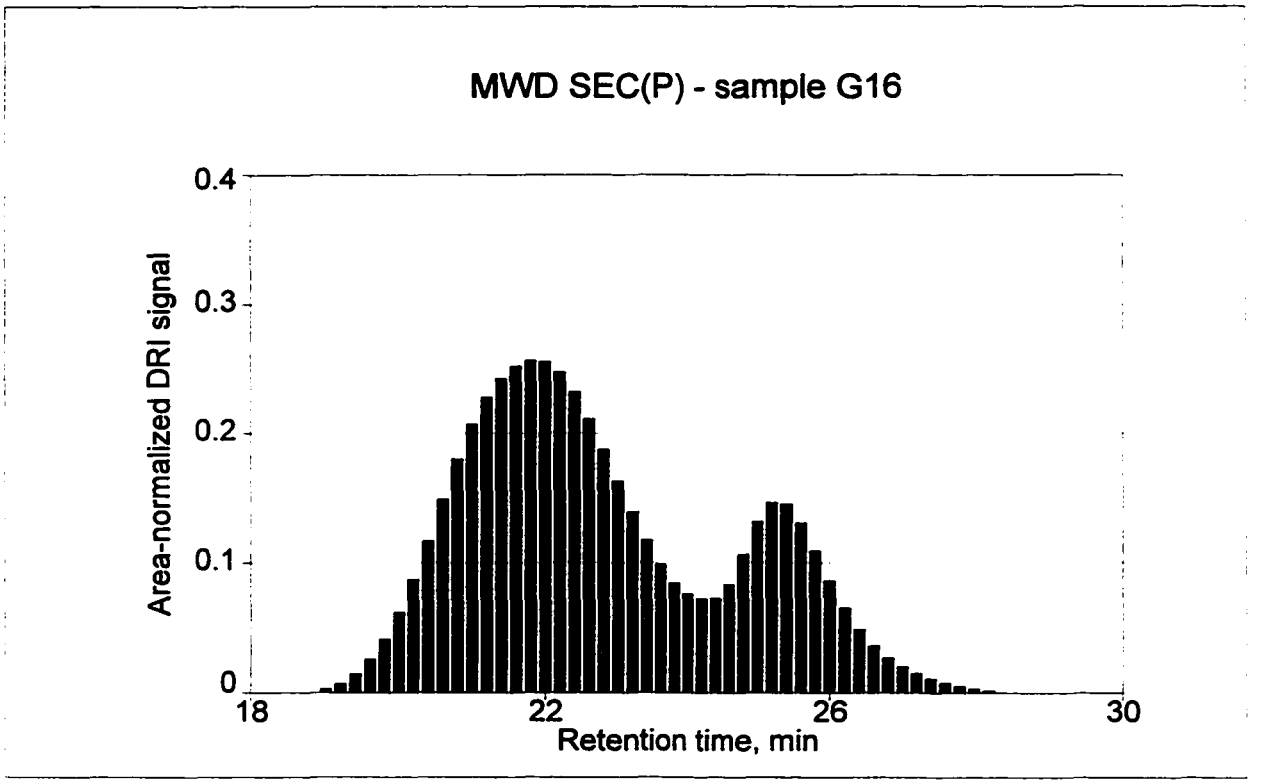

MWD SEC(P) - sample FG13
Area-normalized DRI signal
0.4
0.3
0.2
0.1
0
18
22
26
30
Retention time, min

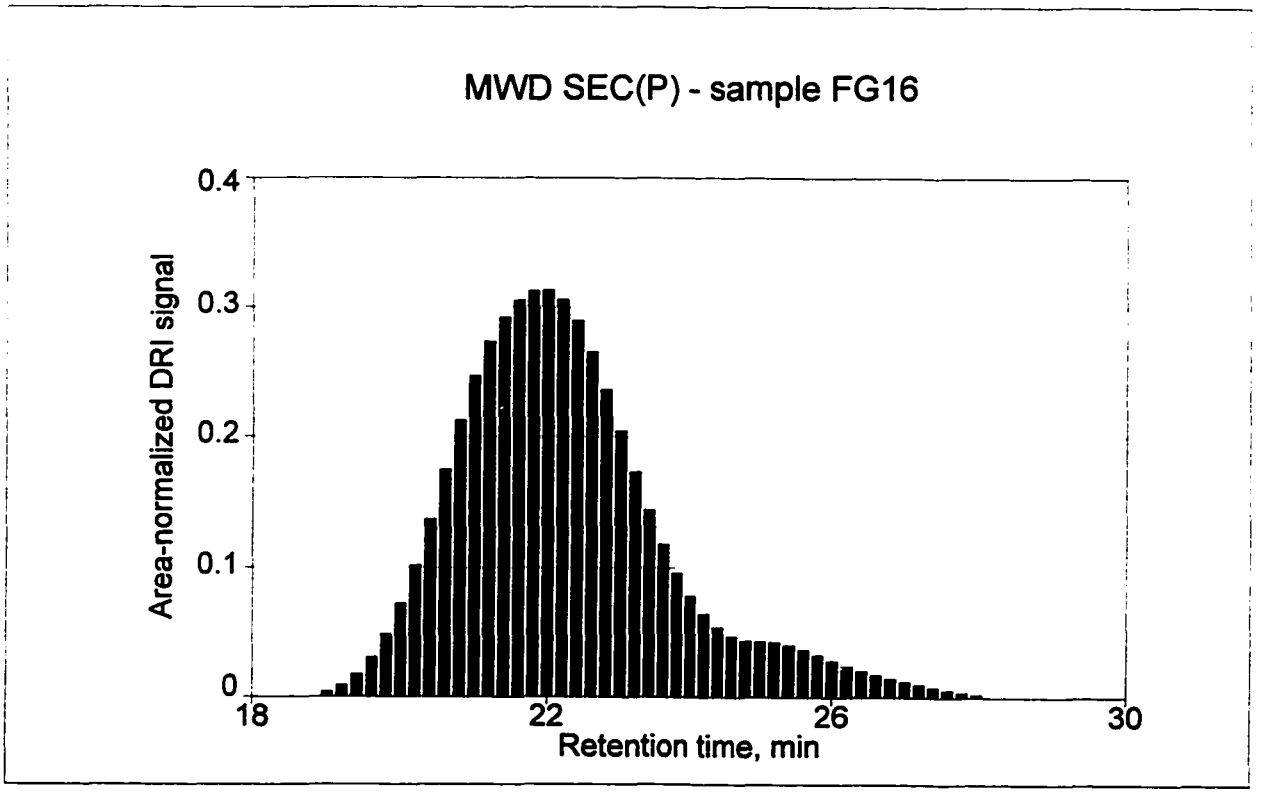

MWD SEC(P) - sample G14
Area-normalized DRI signal
0.4
0.3
0.2
0.1
0
18
22
26
30
Retention time, min

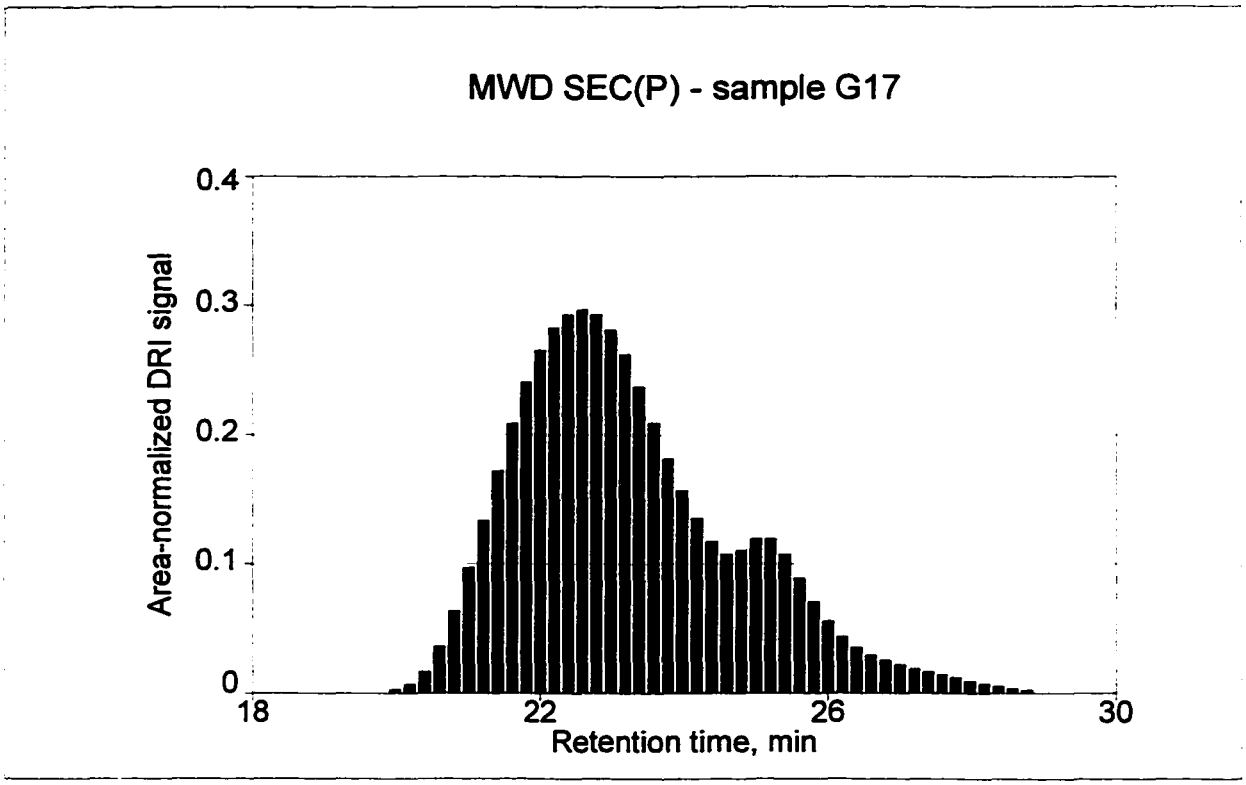

MWD SEC(P) - sample FG14
Area-normalized DRI signal
0.4
0.3
0.2
0.1
0
18
22
26
30
Retention time, min

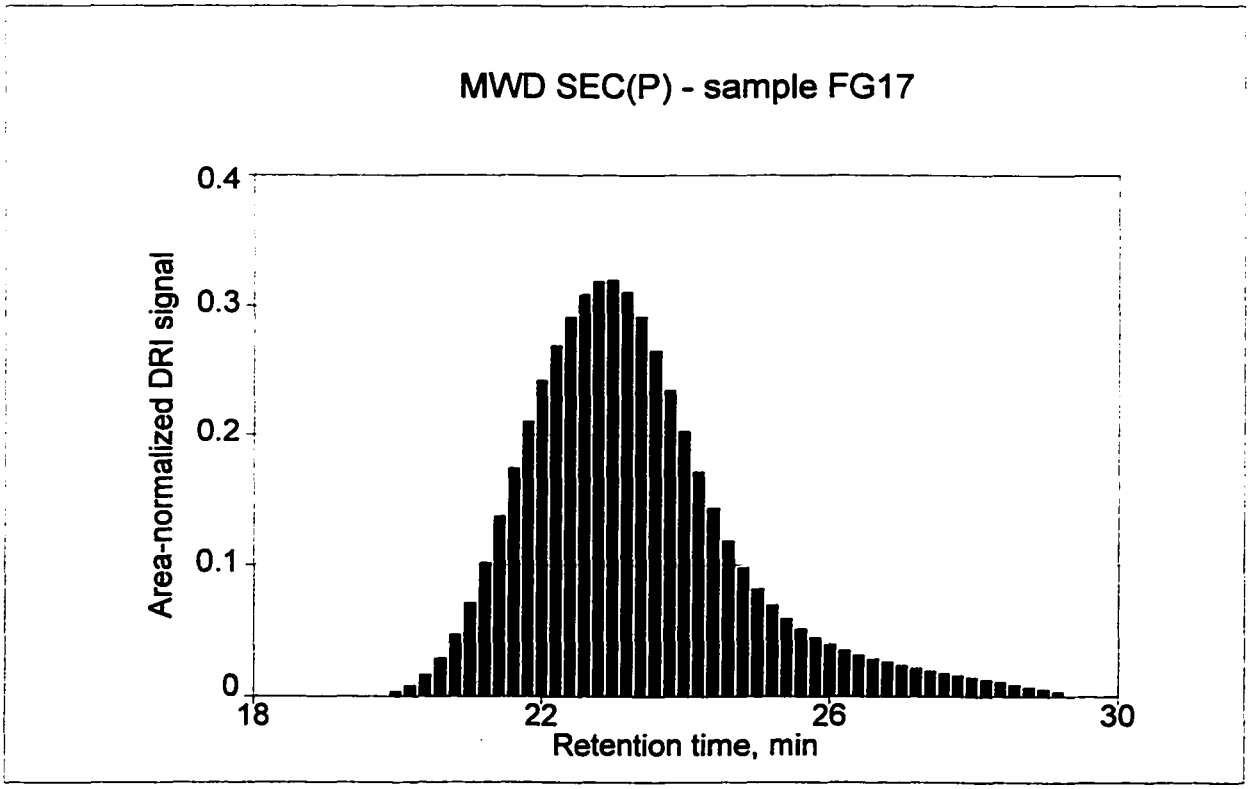

MWD SEC(P) - sample G15
Area-normalized DRI signal
0.4
0.3
0.2
0.1
0
18
22
26
30
Retention time, min

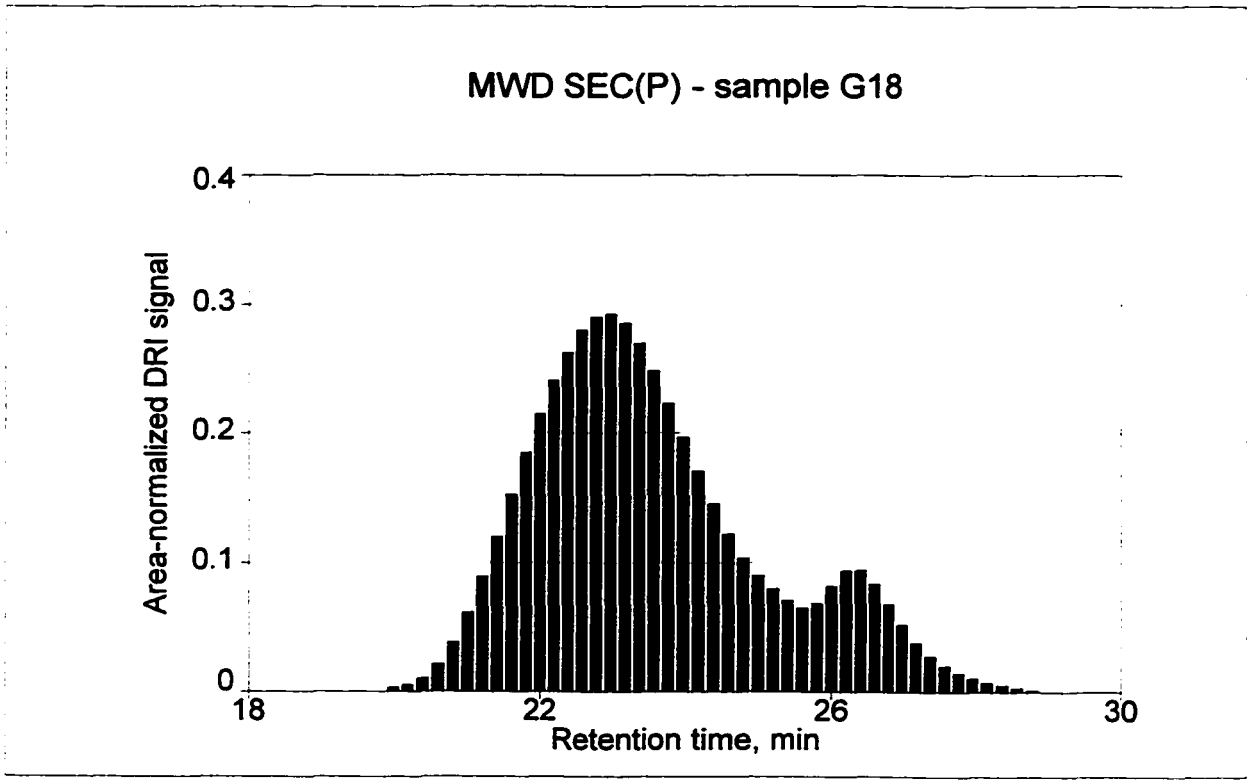

MWD SEC(P) - sample FG15
Area-normalized DRI signal
0.4
0.3
0.2
0.1
0
18
22
26
30
Retention time, min

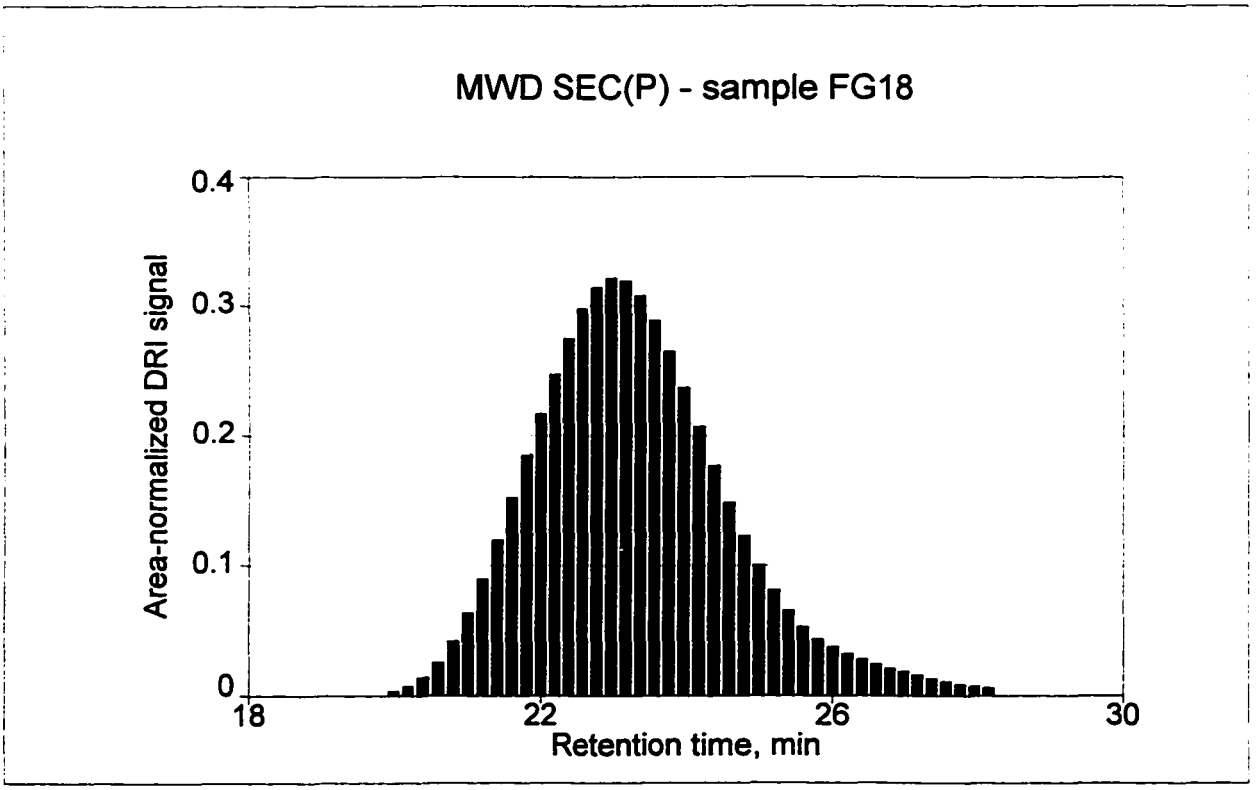

MWD SEC(P) - sample G16
Area-normalized DRI signal
0.4
0.3
0.2
0.1
0
18
22
26
30
Retention time, min

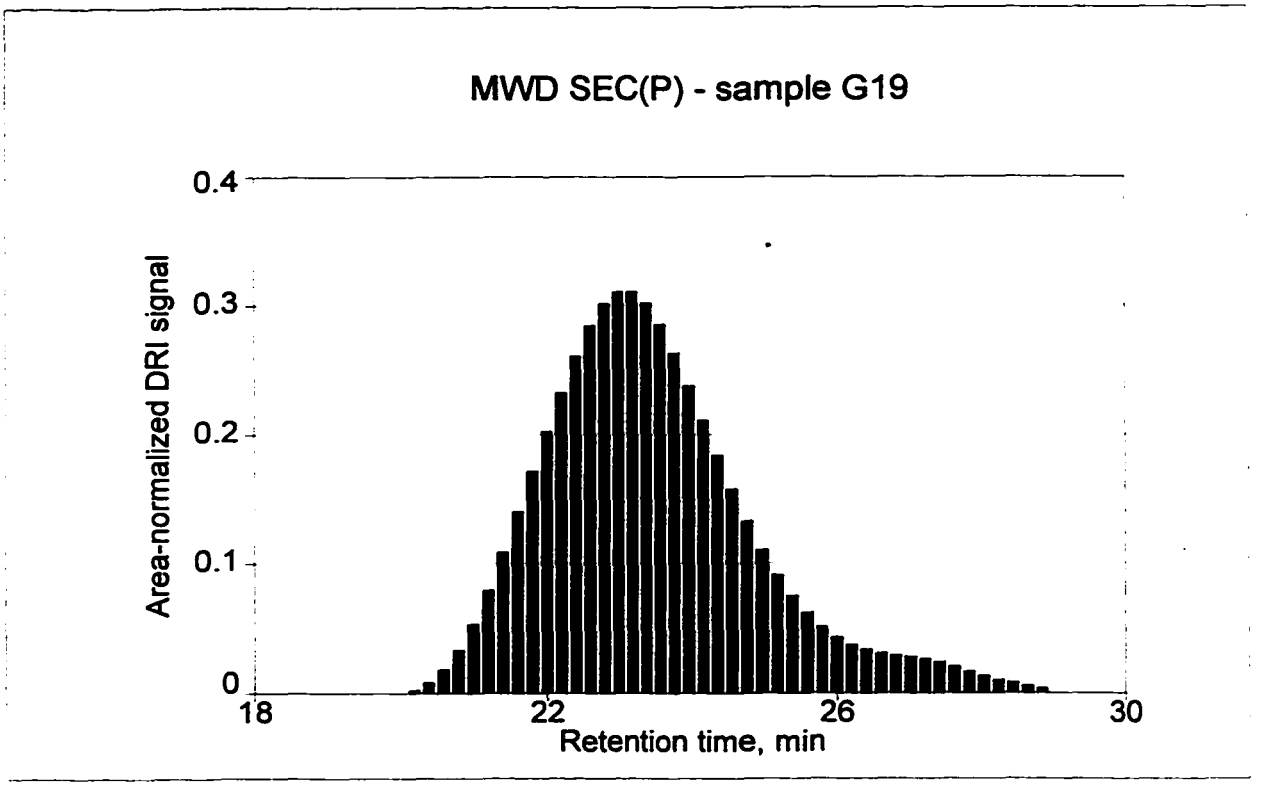

MWD SEC(P) - sample FG16
Area-normalized DRI signal
0.4
0.3
0.2
0.1
0
18
22
26
30
Retention time, min

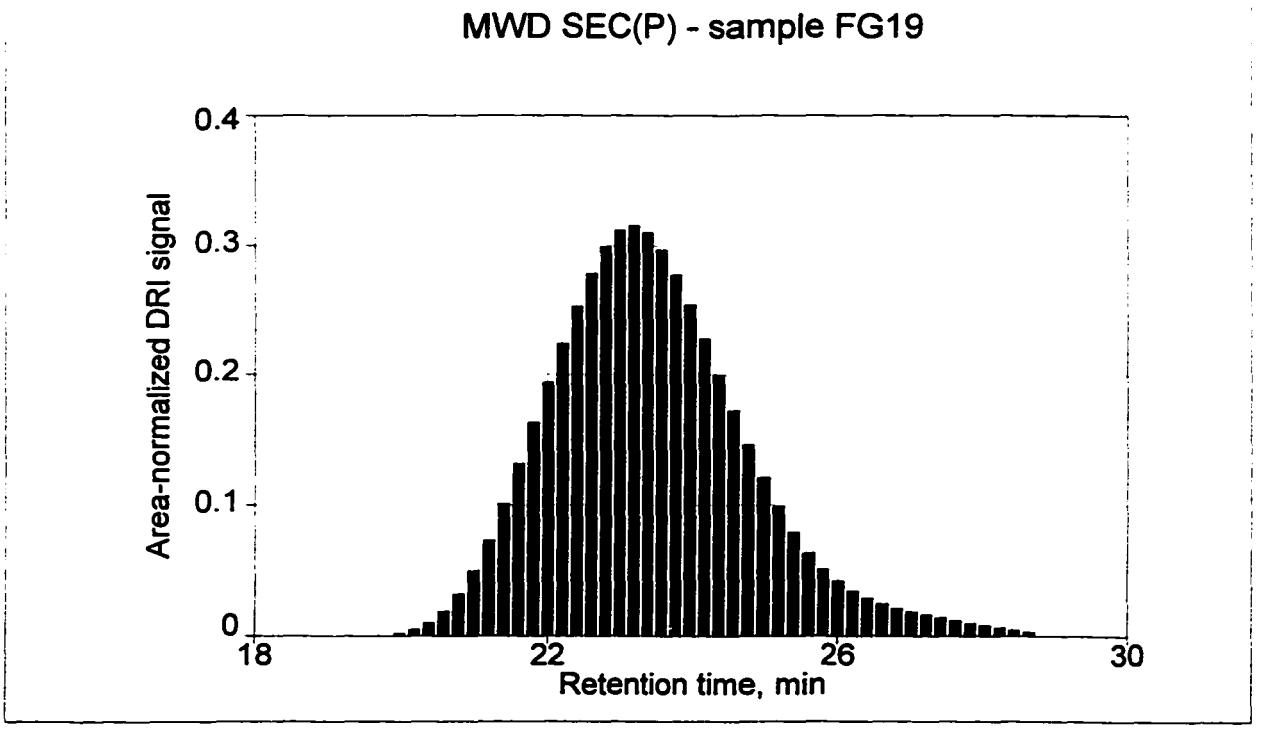

MWD SEC(P) - sample G17
Area-normalized DRI signal
0.4
0.3
0.2
0.1
0
18
22
26
30
Retention time, min

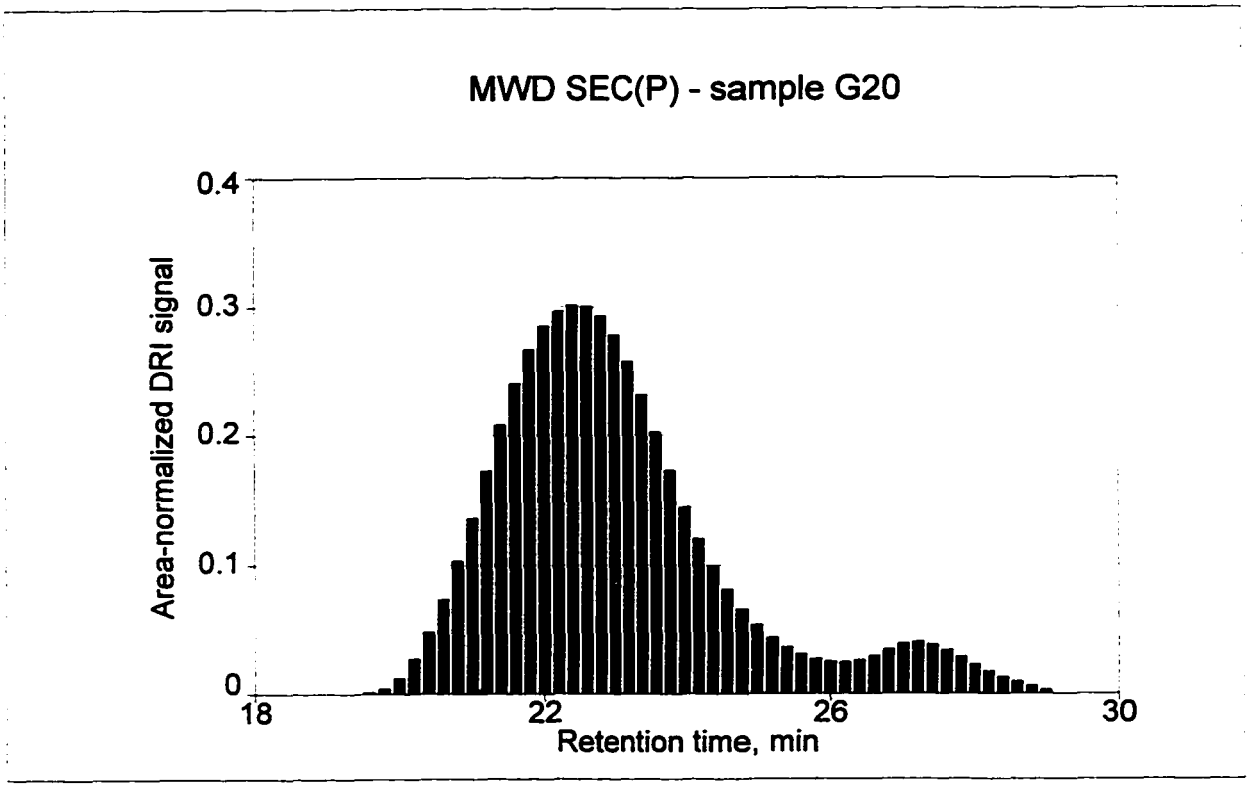

MWD SEC(P) - sample FG17
Area-normalized DRI signal
0.4
0.3
0.2
0.1
0
18
22
26
30
Retention time, min

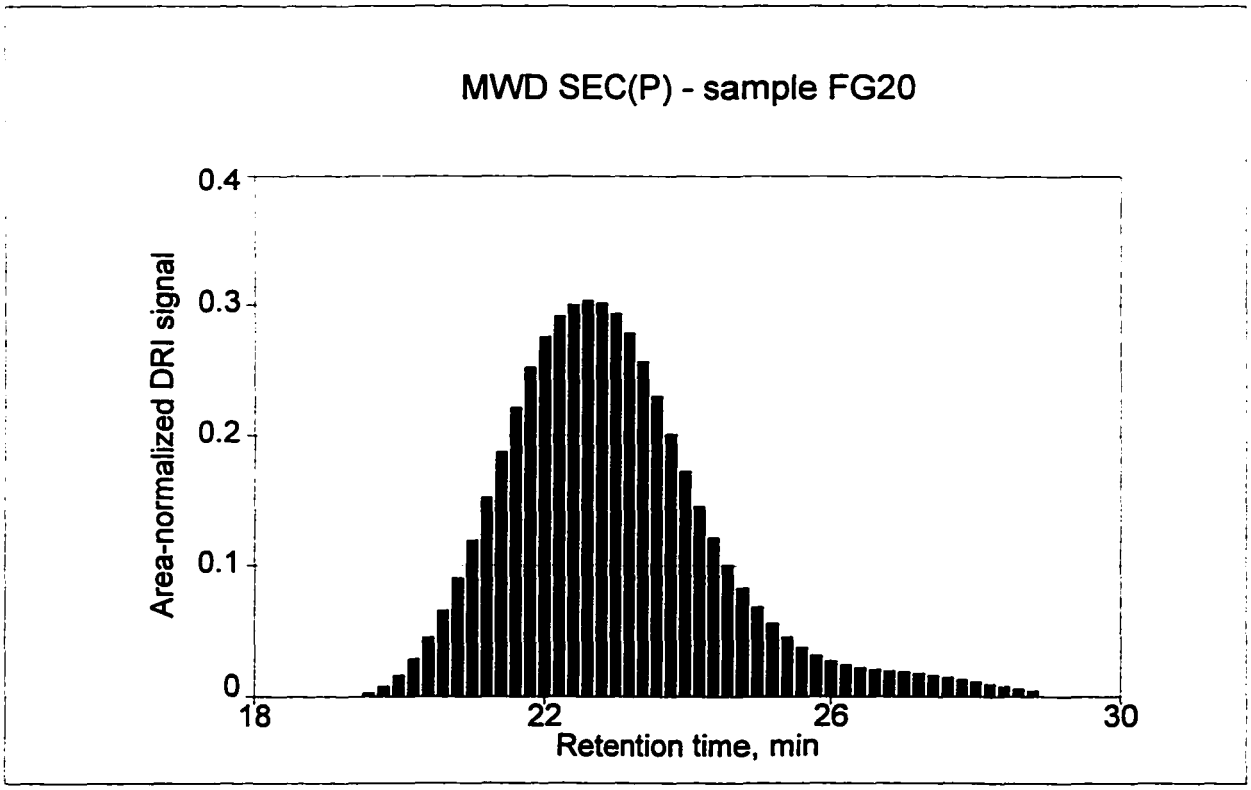

MWD SEC(P) - sample G18
Area-normalized DRI signal
0.4
0.3
0.2
0.1
0
18
22
26
30
Retention time, min

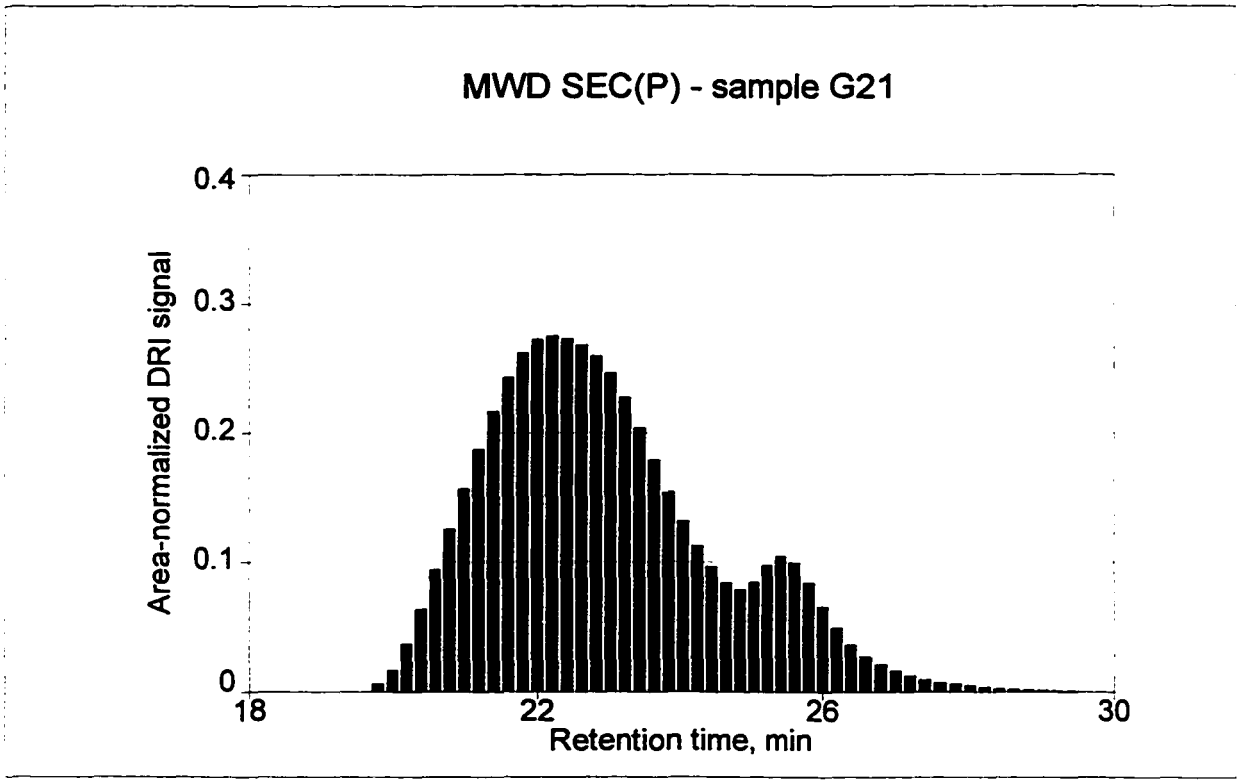

MWD SEC(P) - sample FG18
Area-normalized DRI signal
0.4
0.3
0.2
0.1
0
18
22
26
30
Retention time, min

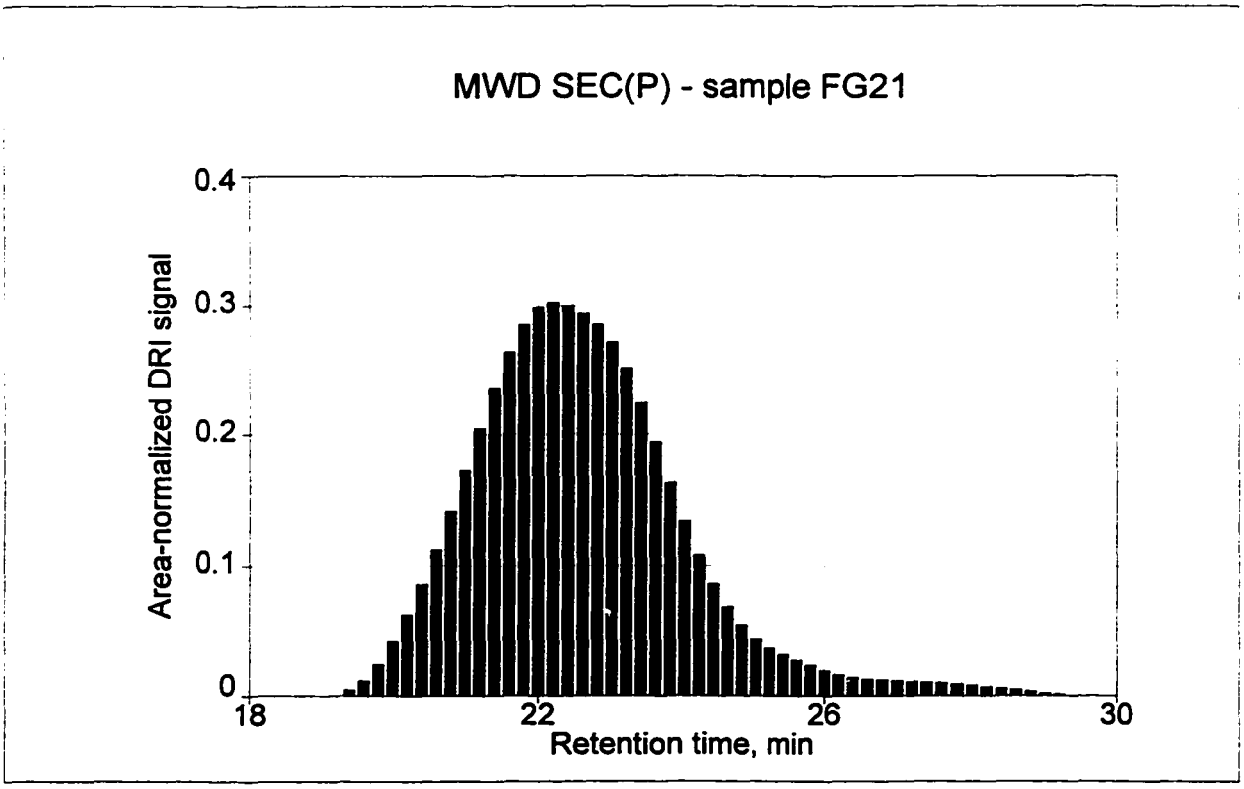

MWD SEC(P) - sample G19
Area-normalized DRI signal
0.4
0.3
0.2
0.1
0
18
22
26
30
Retention time, min

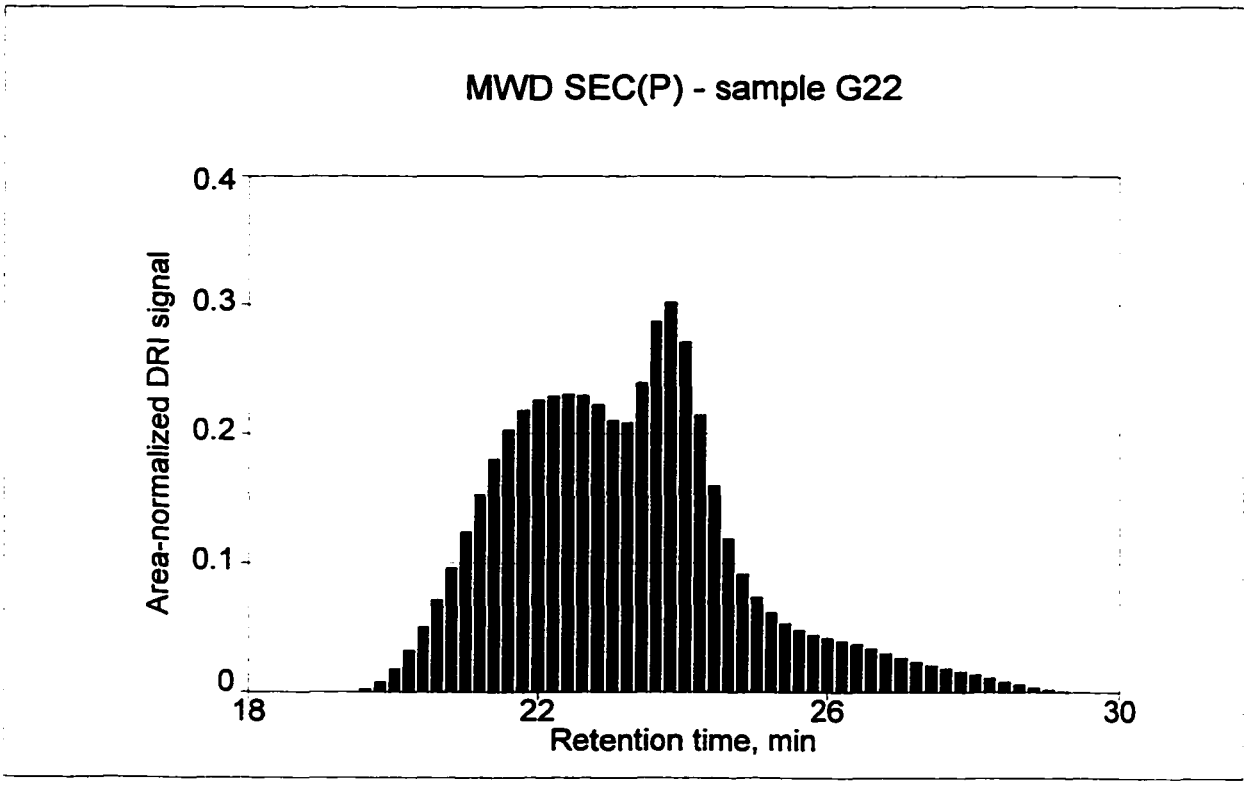

MWD SEC(P) - sample FG19
Area-normalized DRI signal
0.4
0.3
0.2
0.1
0
18
22
26
30
Retention time, min

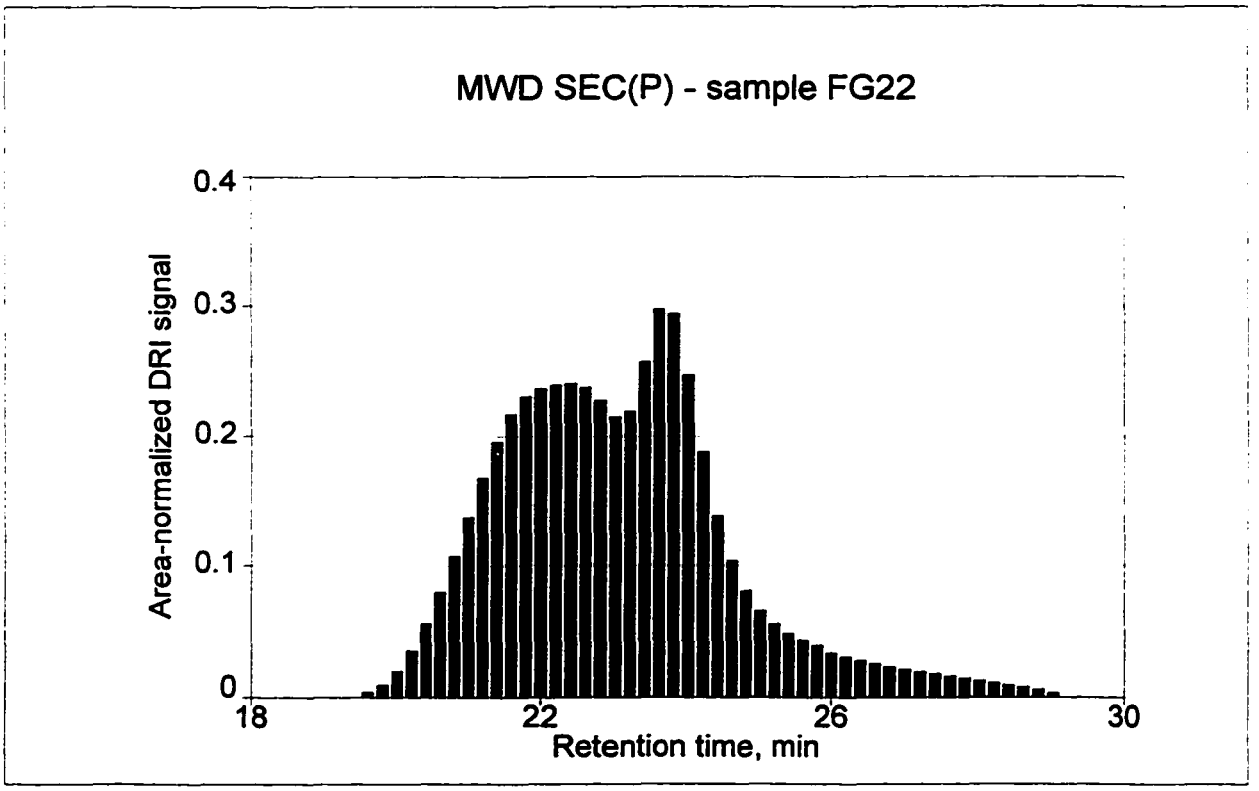

MWD SEC(P) - sample G20
Area-normalized DRI signal
0.4
0.3
0.2
0.1
0
18
22
26
30
Retention time, min


MWD SEC(P) - sample FG20
Area-normalized DRI signal
0.4
0.3
0.2
0.1
0
18
22
26
30
Retention time, min


MWD SEC(P) - sample G21
Area-normalized DRI signal
0.4
0.3
0.2
0.1
0
18
22
26
30
Retention time, min


MWD SEC(P) - sample FG21
Area-normalized DRI signal
0.4
0.3
0.2
0.1
0
18
22
26
30
Retention time, min


MWD SEC(P) - sample G22
Area-normalized DRI signal
0.4
0.3
0.2
0.1
0
18
22
26
30
Retention time, min


MWD SEC(P) - sample FG22
Area-normalized DRI signal
0.4
0.3
0.2
0.1
0
18
22
26
30
Retention time, min

Appendix IV

Rheological characterization: test conditions and parameters

Table A. RMS-800 - Test conditions and parameters - part 1.

Test code	Temperature °C	Dyn.strain [nom.] %	Frequency rad/s	Other relevant test parameters	Test statistics	Samples tested
{tS1}	100, (75), (130)	2	3	delay before test=60s, reads.=60s/point, correl.delay=0.1 cycles, sweep time=1000s, 1 cycle correl.=yes, AutoTension=ON : const. force, iNF=100G, AutoStrain=OFF.	1	selected
{tcS1}	50-/25/-150	2	1	delay before test=10s, reads.=100s/point, correl.delay=0 cycles, sweep time=1800s/zone, 1 cycle correl.=yes, AutoTension=ON: const. force, iNF=100G, AutoStrain=OFF.	1	selected
{tcS2}	75-/25/-125 (150)	5	3	delay before test=10s, reads.=20s/point, correl.delay=0.2 cycles, sweep time=1800s/zone, 1 cycle correl.=no, AutoTension=ON : const. force, iNF=100G, AutoStrain=OFF.	1	all
{tcS3}	75-/25/-125	2	10	delay before test=10s, reads.=50s/point, correl.delay=0 cycles, sweep time=1800s/zone, 1 cycle correl.=yes, AutoTension=OFF, iNF=100G, auto-strain=OFF.	1	selected
{SS1}	25	(Lin) 2-/2/-40; (-50), (-100)	0.1, 3, 100	iNF=100G, plate surface=flat, delay before test=100s, correl. delay=0 cycles, 1 cycle correl.=no, AutoTension=OFF.	1	selected
{SS2}	30	(Lin) 2-/2/-40; (-50), (-100)	0.1, 3, 10, 100	iNF=100 & 500G, plate surface=flat & grooved, delay before test=100s, correl. delay=0 cycles, 1 cycle correl.=no, AutoTension=OFF.	1, (4)	all
{SS3}	50 & 70	(Lin) 2-/2/-40	0.3, 1, 3, 10, 30, 100	iNF=100G, plate surface=flat, delay before test=100s, correl. delay=0 cycles, 1 cycle correl.=no, AutoTension=OFF.	1	selected
{SS4}	100 & 125	(Log) 2-/2/-40	1, 3, 5.	iNF=100G, plate surface=flat, delay before test=100s, correl. delay=0 cycles, 1 cycle correl.=no, AutoTension=OFF.	1, (4)	selected
{SS5}	130	(Lin) 2-/2/-40, (-50,-100)	3	iNF=100G, plate surface=flat, delay before test=100s, correl. delay=0 cycles, 1 cycle correl.=no, AutoTension=OFF.	1, (2)	all
{SS6}	30	(Log) 1-40,40-1	10	iNF=100G, plate surface=flat, delay before test=100s, correl. delay=0 cycles, 1 cycle correl.=no, AutoTension=OFF.	1	selected, (G6)
{SS7}	30	(discreet) 3, 75, 3	10	iNF=100G, plate surface=flat, delay before test=100s, correl. delay=0 cycles, 1 cycle correl.=no, AutoTension=OFF, zone timing shown in Fig. 5-14.	1	selected, (C)

Table A. RMS-800 - Test conditions and parameters - part 2.

	Temperature	Dyn.strain	Frequency	Other relevant test	Test	Samples
Test code	°C	[nom.] %	rad/s	parameters	statistics	tested
{QFS}	30, (100)	5, (10)	0.1-100	delay before test=110s, LOG=1p/dec, correl.delay=0.1 cycles, 1 cycle correl.=no, AutoTension=OFF, iNF=100G, AutoStrain=OFF.	6+	all, (G16)
{FS3d@30}	30	5	0.1-100	delay before test=10+120s, LOG=5p/dec, correl.delay=0.1 cycles, 1 cycle correl.=no, AutoTension=OFF, iNF=100G, AutoStrain=OFF.	1	all
{FS3d@100}	100	5	0.1-100	delay before test=100+120s, LOG=5p/dec, correl.delay=0.1 cycles, 1 cycle correl.=no, AutoTension=OFF, iNF=100G, AutoStrain=OFF.	1, (2)	all
{FS5dec}	30	5	0.001-100	delay before test=10+120s, LOG=5p/dec, correl.delay=0.1 cycles, 1 cycle correl.=no, AutoTension=OFF, iNF=100G, AutoStrain=OFF.	1, (2)	all
{FTS}	30-/25/-130	5	0.1-100	soak time=200s, delay before test=10+120s, LOG=5p/dec, correl.delay=0.2 cycles, 1 cycle correl.=no, AutoTension=ON, iNF=100G, AutoStrain=OFF.	1, (2)	all
	Temperature	Step strain	Rel. time	Other relevant test	Test	Samples
	°C	[nom.] %	s	parameters	statistics	tested
{QSR}	30	5	0.1-400	delay before test=100+100s, Autotension=OFF, zone timing=(2/18/380)	6-8	selected
{PSR}	30	3 to 50	0.1-1000	delay before test=100+10s, Autotension=OFF, zone timing=(2/18/80/900)	1	several, (G20)
{SSR}	30	10	0.1-1000	delay before test=100+10s, Autotension=OFF, zone timing=(2/18/80/900), single sps.	1	several, (G20)
{SR1}	100	10	1-1000	delay before test=100+10s, Autotension=OFF, zone timing=(2/18/80/900)	1	(C)
{SR400}	100	15	0.1-400	delay before test=100+100s, Autotension=OFF, zone timing=(2/18/380)	1, (2)	all
{SR1000}	30, (25)	10	0.1-1000	delay before test=100+10s, Autotension=OFF, zone timing=(2/18/80/900)	1, (2-6)	all
{SR10,000}	30	10	0.1-10,000	delay before test=100+10s, Autotension=OFF, zone timing=(2/18/980/9000)	1, (2)	all

Table B. RSA-II - Test conditions and parameters.

{DTMA} test parameter	Nominal value	Units
Test fixture:	film / fiber	-
Deformation:	in tension	-
Test mode:	isochronal temperature sweep	-
Temperature range:	-100 to +20 (grafts + M) -120 to - 40 (B10) -100 to +40 (C)	°C
Temperature increments (DT):	+ 2	°C
Frequency:	70	rad/s
Soak time before measurement:	60	s
Delay before test:	100	s
Correlation delay:	2	cycles
1 cycle correlation:	no	-
AutoStrain (dynamic) adjustment:	active	-
- max. dynamic strain allowed:	2	%
- increase dyn. strain if dynamic force drops below:	2.5	G
- decrease dyn. strain if dynamic force goes above:	900	G
- change current strain, if prompted, by:	20	%
AutoTension (static) adjustment:	active	-
- mode:	static force (pre-tension) tracking dynamic force	-
- intial static force:	100	G
- lower limit of static force adj.:	6	G
- static force to exceed dynamic force by:	25	%

Table C. RPA 2000 - Test configurations.

(a)	(b)	(c)	(d)
{SSWP2}	**{HSSWP1}**	**{FSWP1}** **{FSWP2}**	**{FSWP3}**
T=100°C subtest 1 γ = 2% ω = 1 rad/s t = 3 min subtest 2 ω = 10 rad/s γ_1 = 2% γ_2= 5% γ_3 = 2% γ_4= 10% γ_5= 2% γ_6= 15% γ_7= 2% γ_8= 20% γ_9 = 2% γ_{10}= 25% γ_{11}= 2% γ_{12}= 30% γ_{13}= 2% γ_{14}= 35% γ_{15}= 2% γ_{16}= 40% γ_{17}= 2% γ_{18}= 45% γ_{19}= 2% γ_{20}= 50%	**T=100°C** subtest 1 γ = 2% ω = 1 rad/s t = 3 min subtest 2 ω = 1 rad/s γ_1 = 5% γ_2 = 200% γ_3 = 5% γ_4 = 800% subtest 3 γ = 5% ω = 1 rad/s t = 2 min	**T=100°C** subtest 1 γ = 2% ω = 1 rad/s t = 3 min subtest 2 γ = 5% ω_1 = 0.2 rad/s /* ω_2 = 0.5 rad/s ω_3 = 1 rad/s ω_4 = 2 rad/s ω_5 = 5 rad/s ω_6 = 10 rad/s ω_7 = 20 rad/s ω_8 = 50 rad/s ω_9 = 100 rad/s ω_{10} = 200 rad/s --- *) - FSWP1 only	**T=100°C** subtest 1 γ = 2% ω = 1 rad/s t = 3 min subtest 2 γ = 50% ω_1 = 0.5 rad/s ω_2 = 1 rad/s ω_3 = 2 rad/s ω_4 = 5 rad/s ω_5 = 10 rad/s ω_6 = 20 rad/s ω_7 = 50 rad/s subtest 3 γ = 100% ω_1 = 0.5 rad/s ω_2 = 1 rad/s ω_3 = 2 rad/s ω_4 = 5 rad/s ω_5 = 10 rad/s ω_6 = 20 rad/s subtest 4 γ = 200% ω_1 = 0.5 rad/s ω_2 = 1 rad/s ω_3 = 2 rad/s ω_4 = 5 rad/s ω_5 = 10 rad/s

Table D. DSR - Test conditions and parameters.

	{TEST1}	{TEST2}
Objective:	preliminary work	main program + test precision
DSR test program:	P3	
Test temperature:	100°C	
Specimen weight:	18.0±0.1g	
Specimen shape:	spheroidal	
Relaxation time monitored: (by default)	0.04 - 400 s	
Step-strain application time: (by default)	4 ms	
Angular rotor deflection:	1°	2°
Stator-rotor gap: (= avg. specimen thickness)	2.54 mm (0.1 in)	
Rotor closing speed:	slowest (~3mm/s)	
Test statistics (# of determ./sample)	2 -17, depending on test & sample availability	
Sample strain history: (during specimen loading)	compression moulding; complex but fairly reproducible	
Specimen pre-heat time (PHT):	15 min	
Specimen pre-warm time (PWT):	30 min (in vacuum-oven) @ 65°C	
Step-strain amplitude range:	35 to 51%	69 to 101%
Test procedure:	Polysar LP# 01-02-268	

DSR3

Appendix V

Rheological test results - supplementary graphs and tables

Figure AFSC. Dynamic mechanical spectrum - sample C.

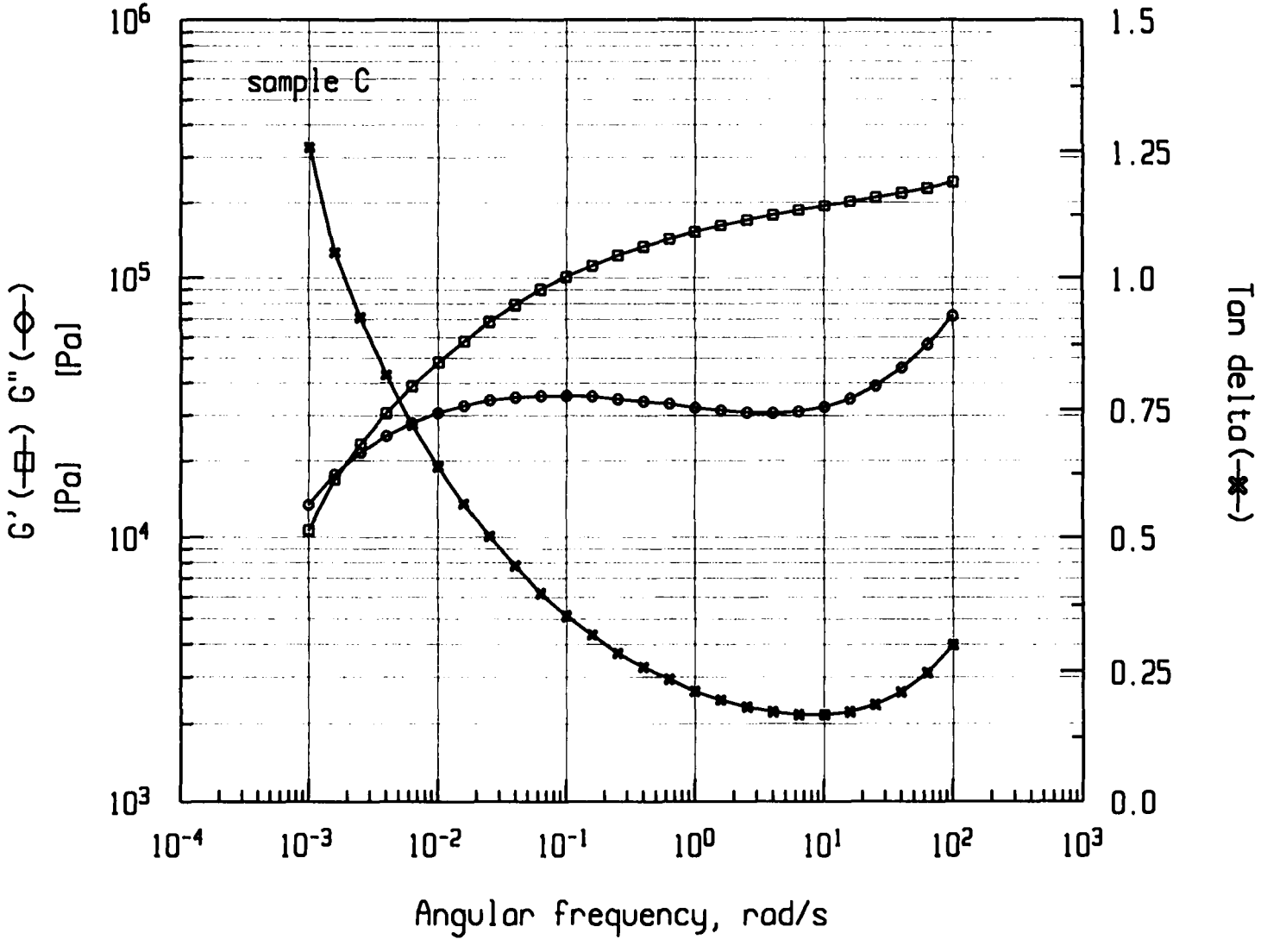


Figure AFSG1. Dynamic mechanical spectrum - sample G1.

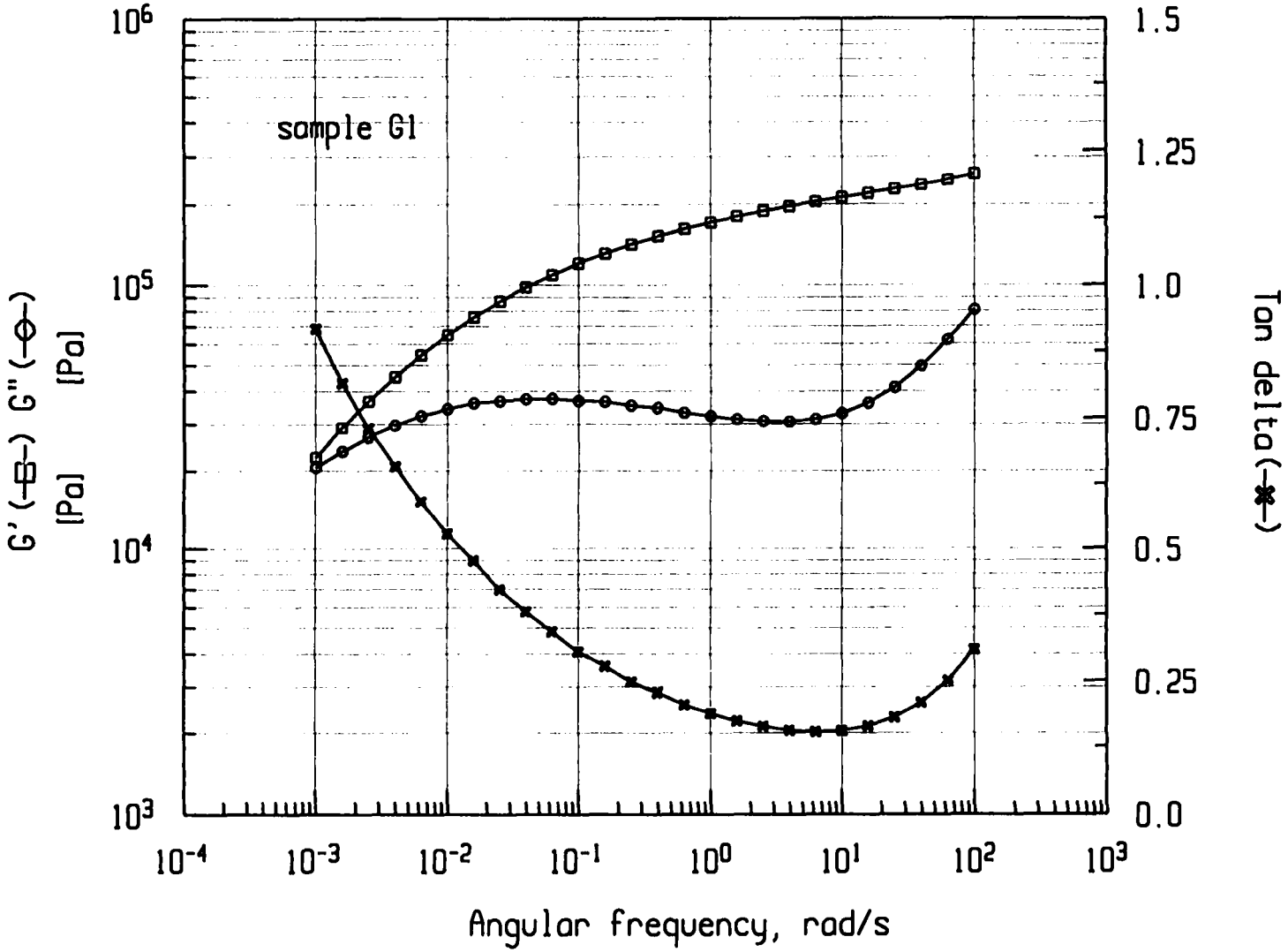


Figure AFSG2. Dynamic mechanical spectrum - sample G2.

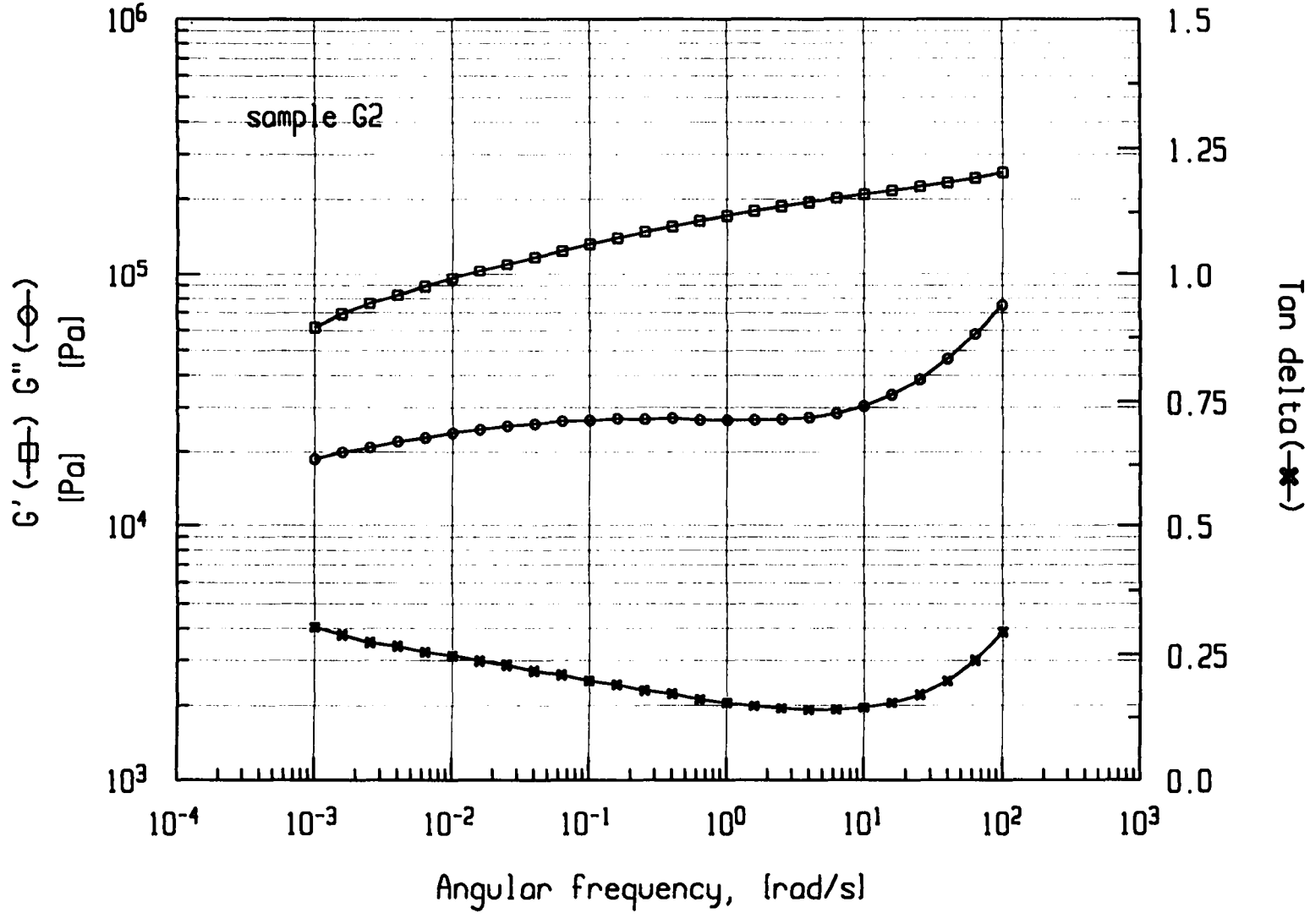


Figure AFSG3. Dynamic mechanical spectrum - sample G3.

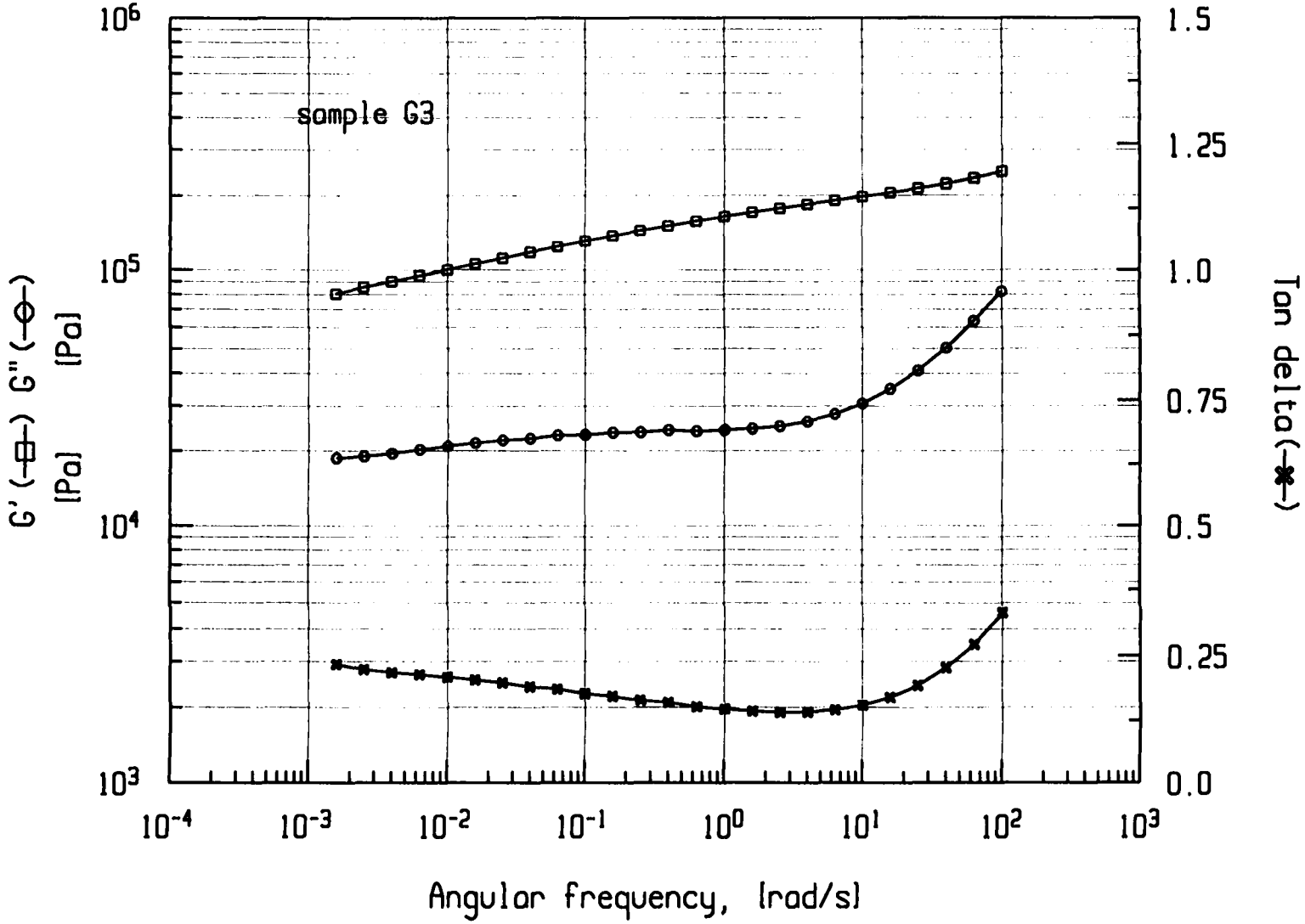


Figure AFSG4. Dynamic mechanical spectrum - sample G4.

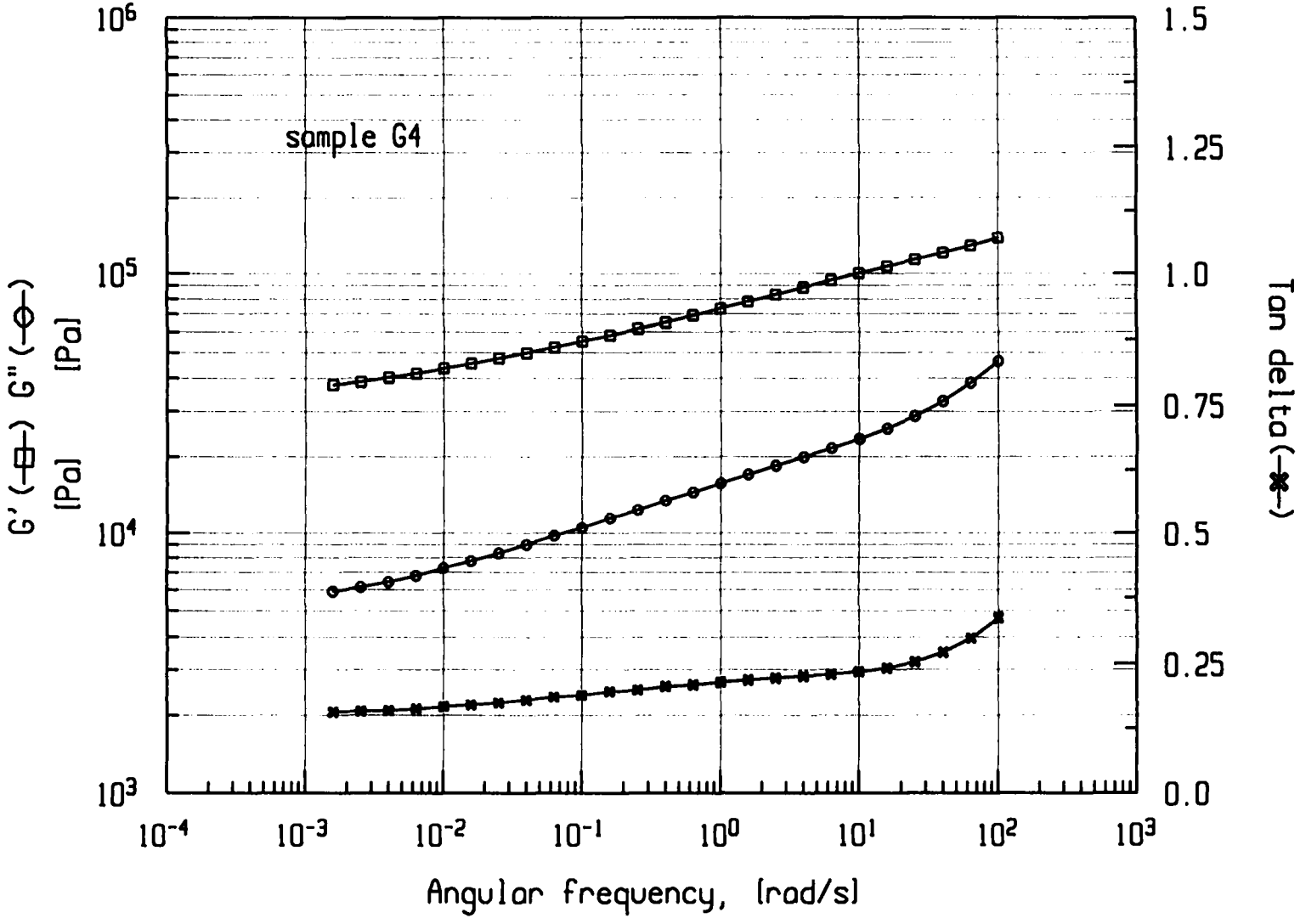


Figure AFSG5. Dynamic mechanical spectrum - sample G5.

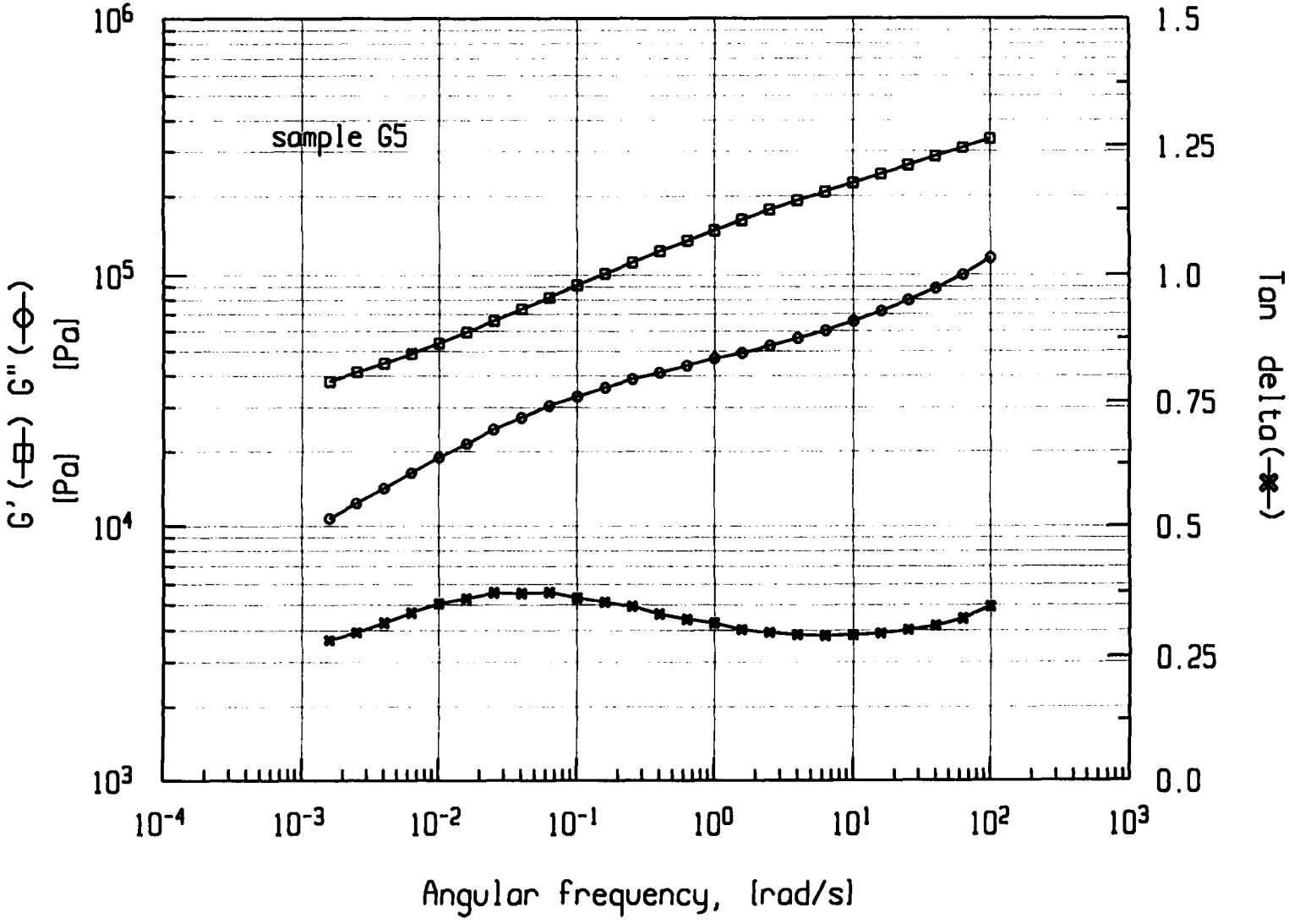


Figure AFSG6. Dynamic mechanical spectrum - sample G6.

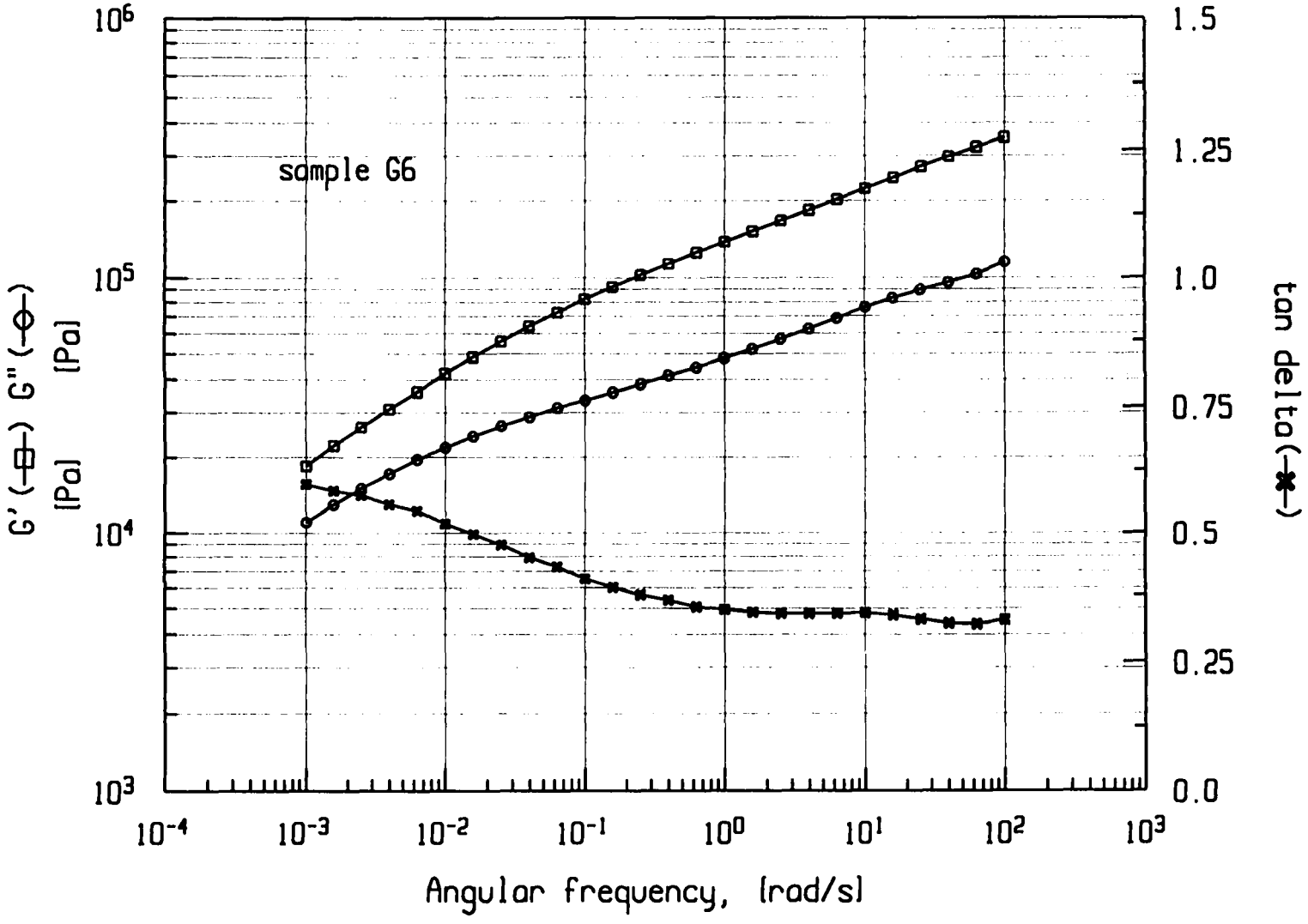


Figure AFSG7. Dynamic mechanical spectrum - sample G7.

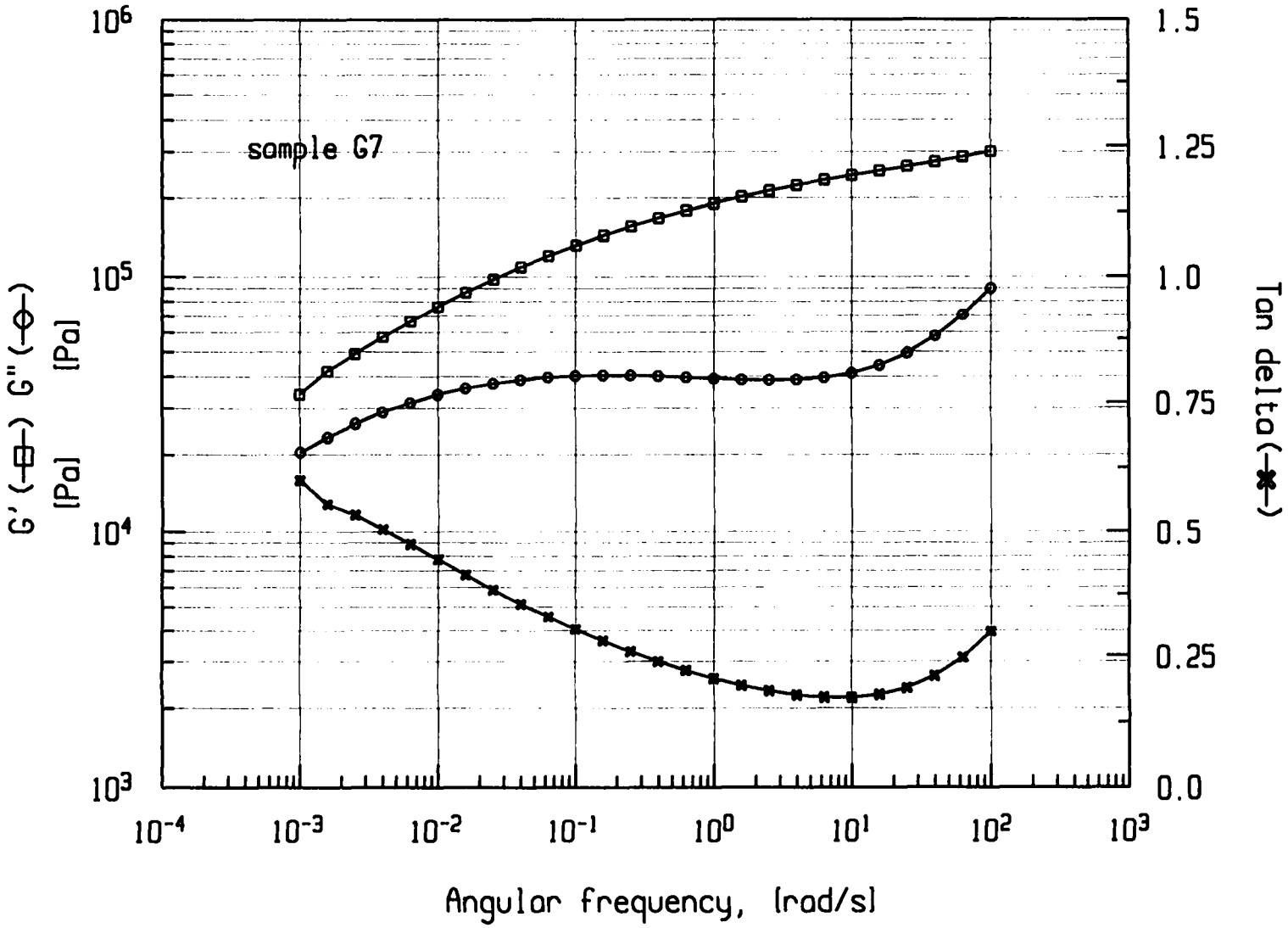


Figure AFSG8. Dynamic mechanical spectrum - sample G8.

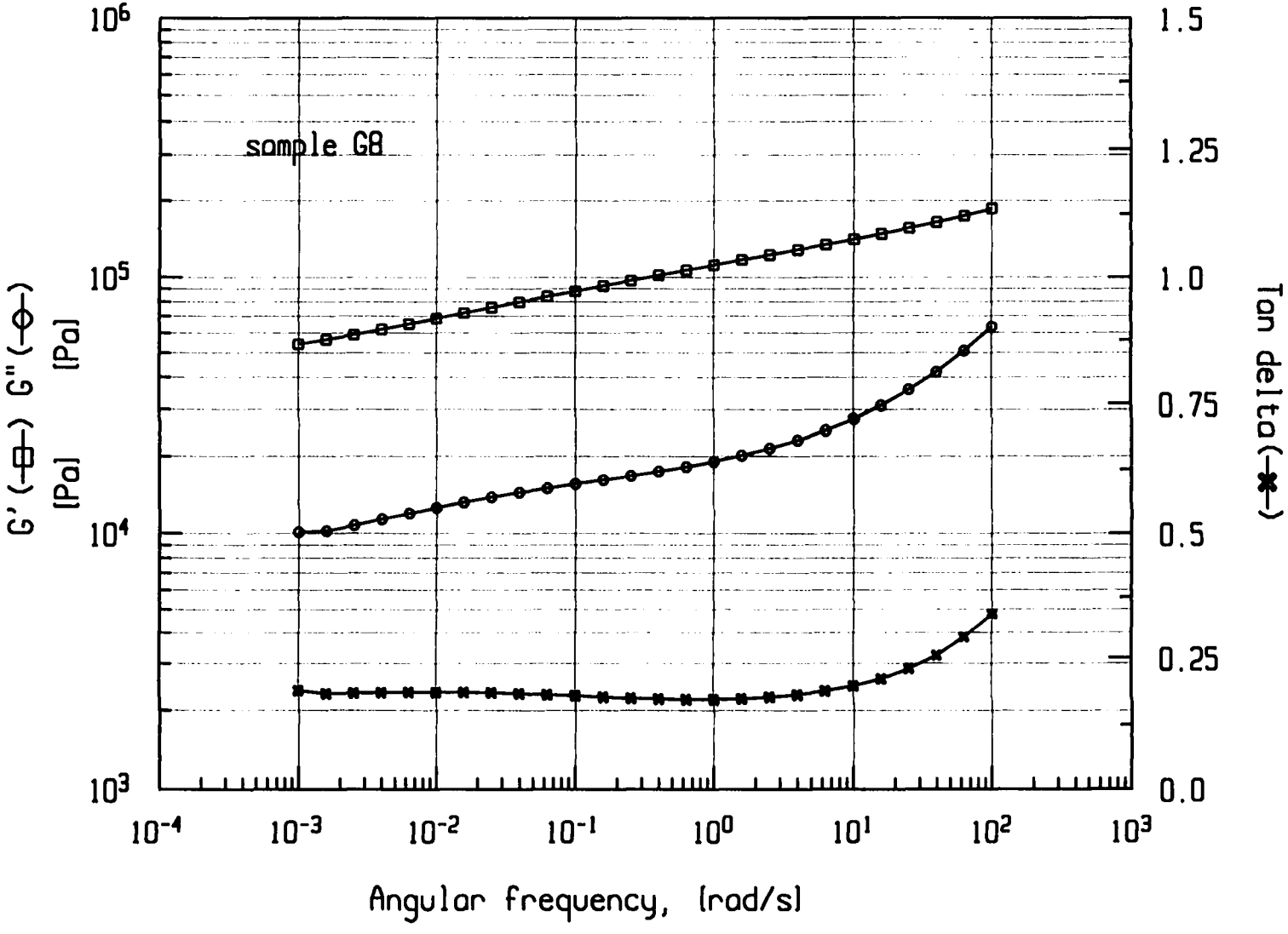


Figure AFSG9. Dynamic mechanical spectrum - sample G9.

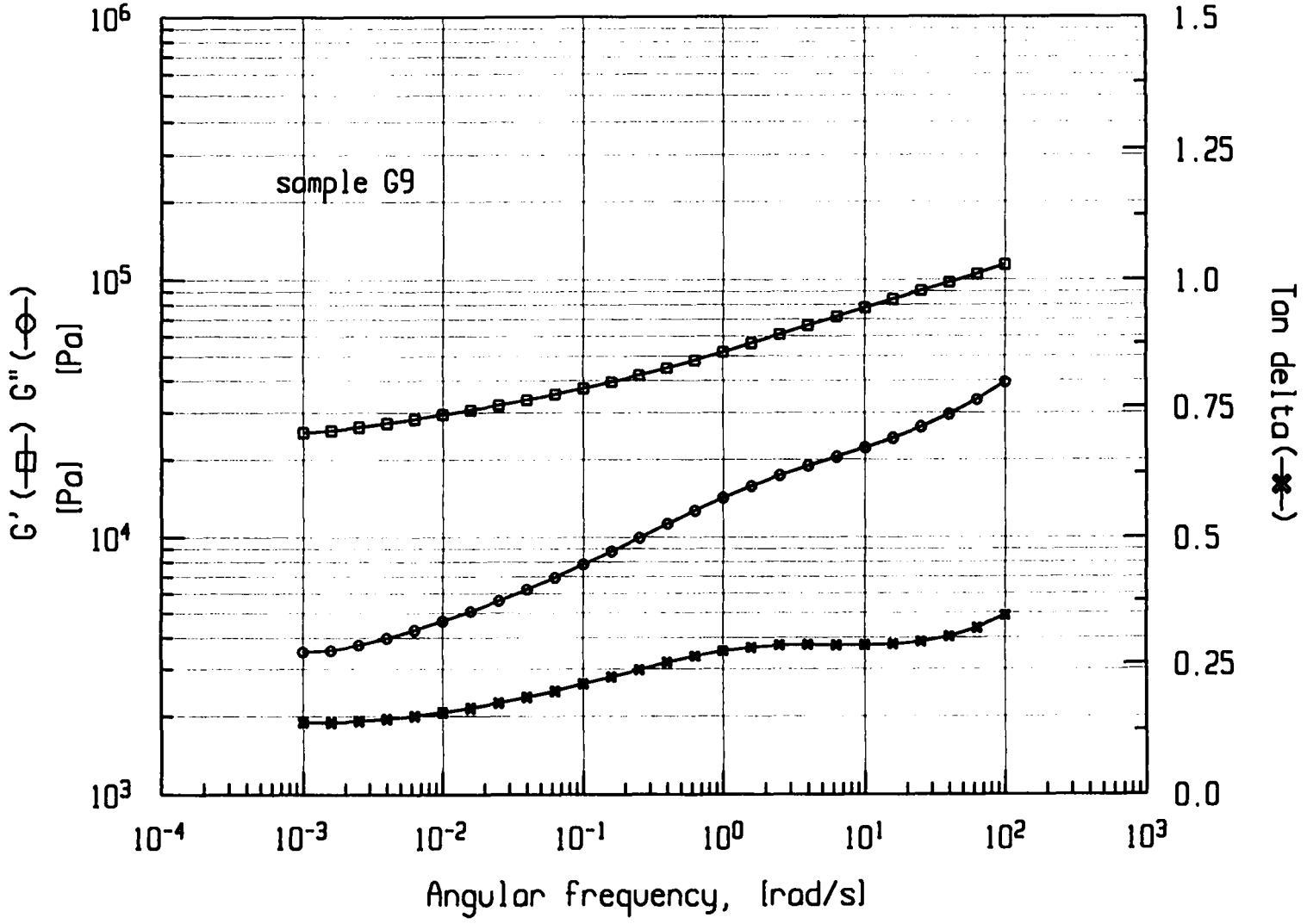


Figure AFSG10. Dynamic mechanical spectrum - sample G10.

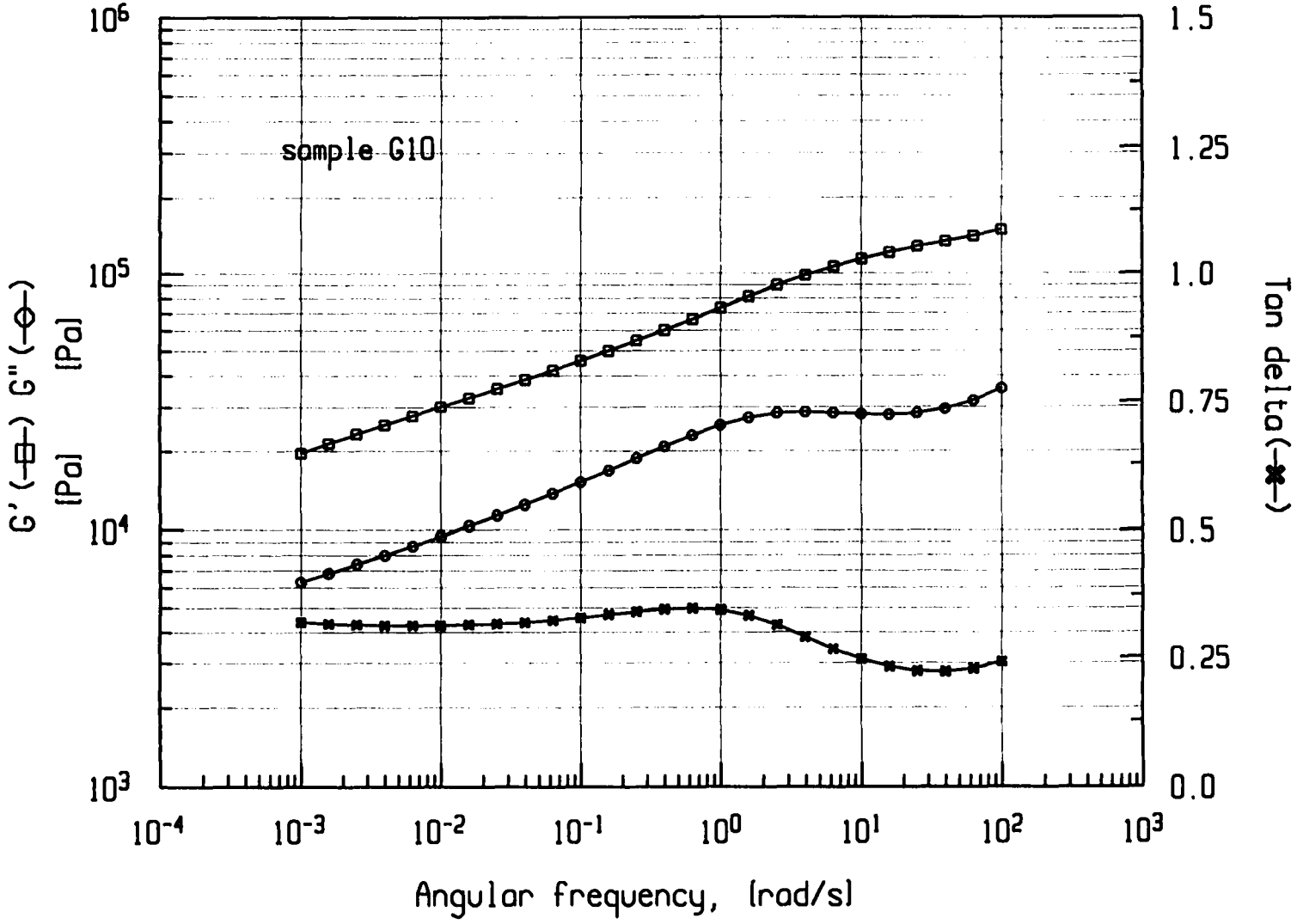


Figure AFSG11. Dynamic mechanical spectrum - sample G11.

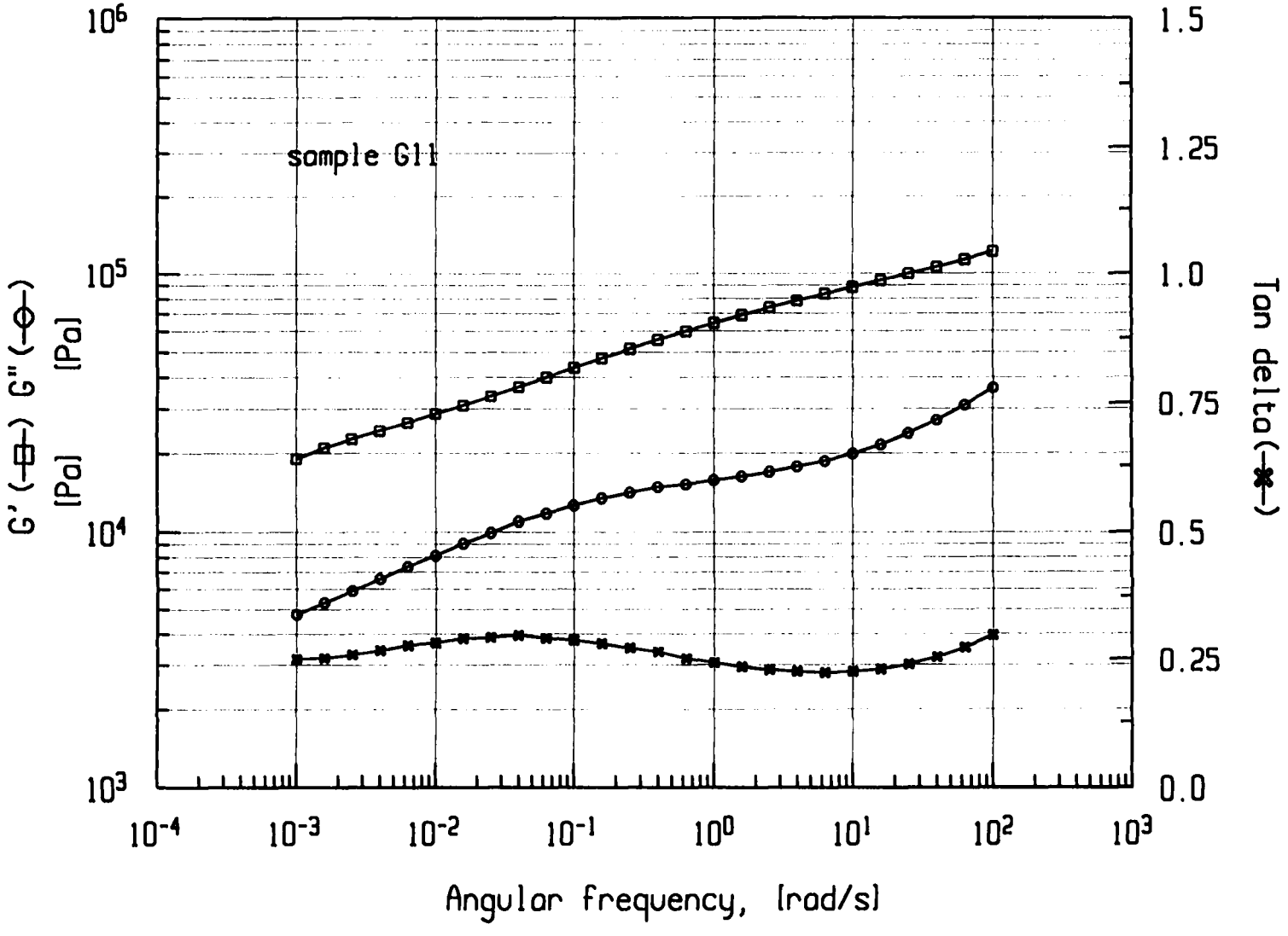


Figure AFSG12. Dynamic mechanical spectrum - sample G12.

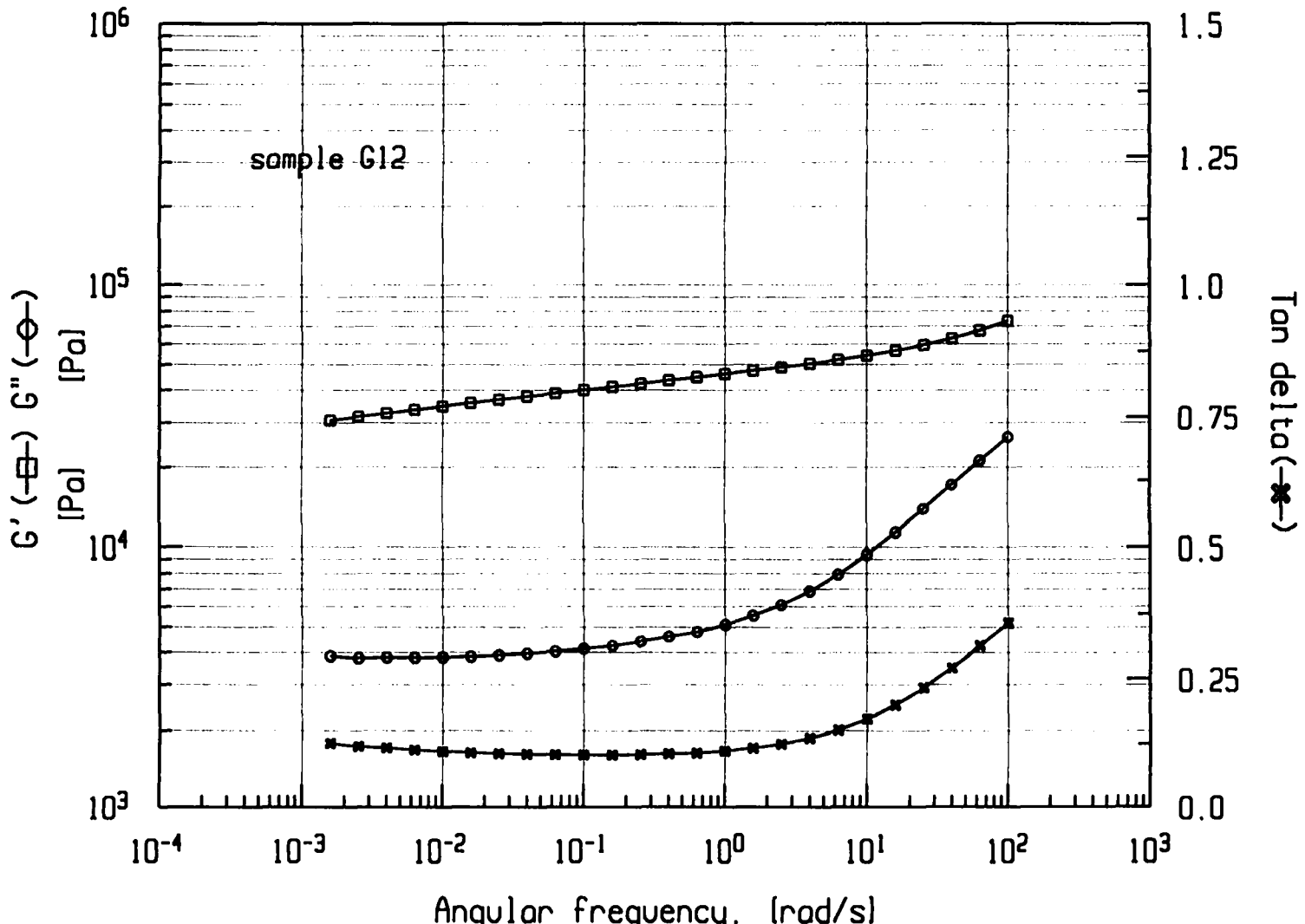


Figure AFSG13. Dynamic mechanical spectrum - sample G13.

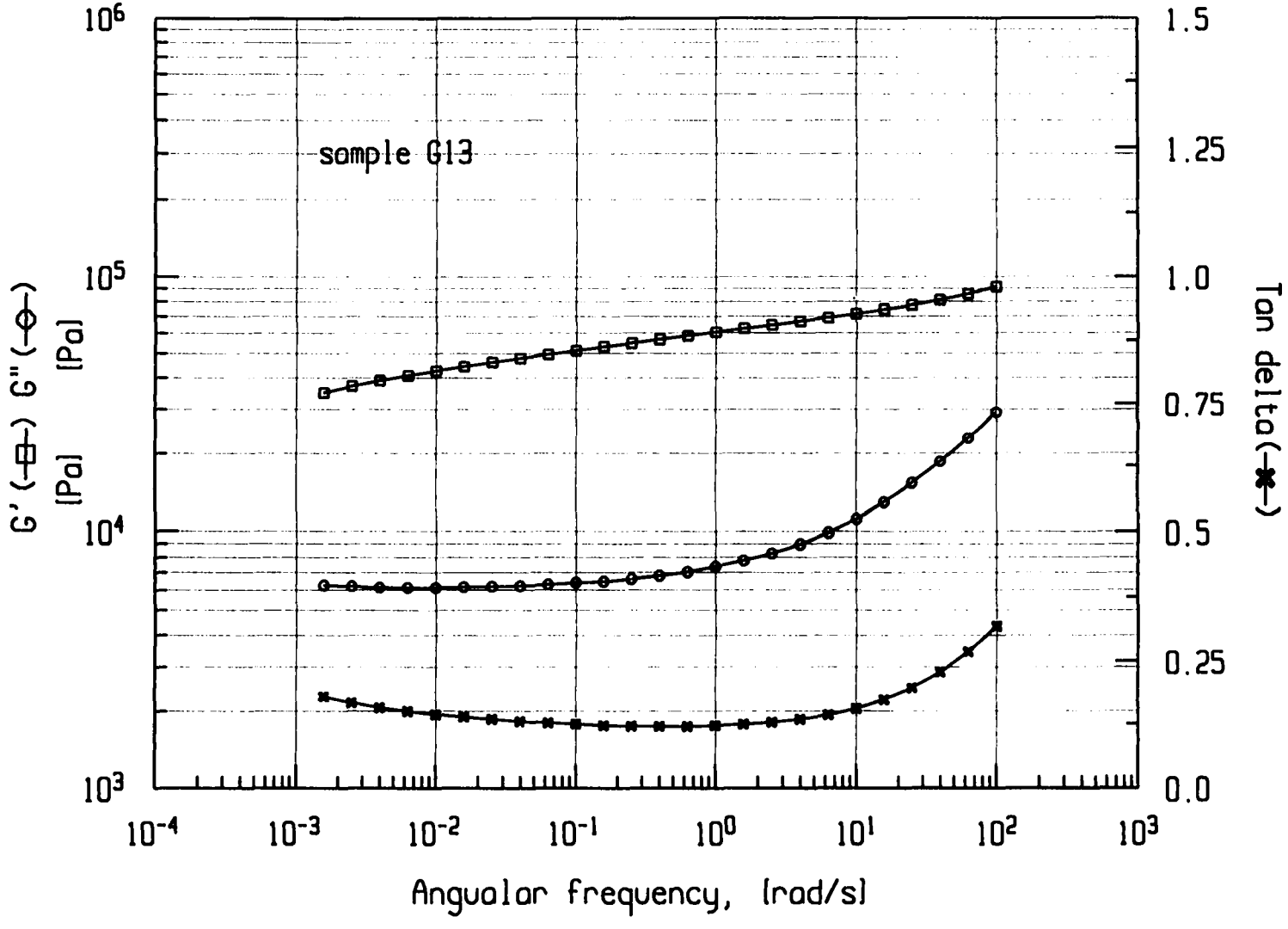


Figure AFSG14. Dynamic mechanical spectrum - sample G14.

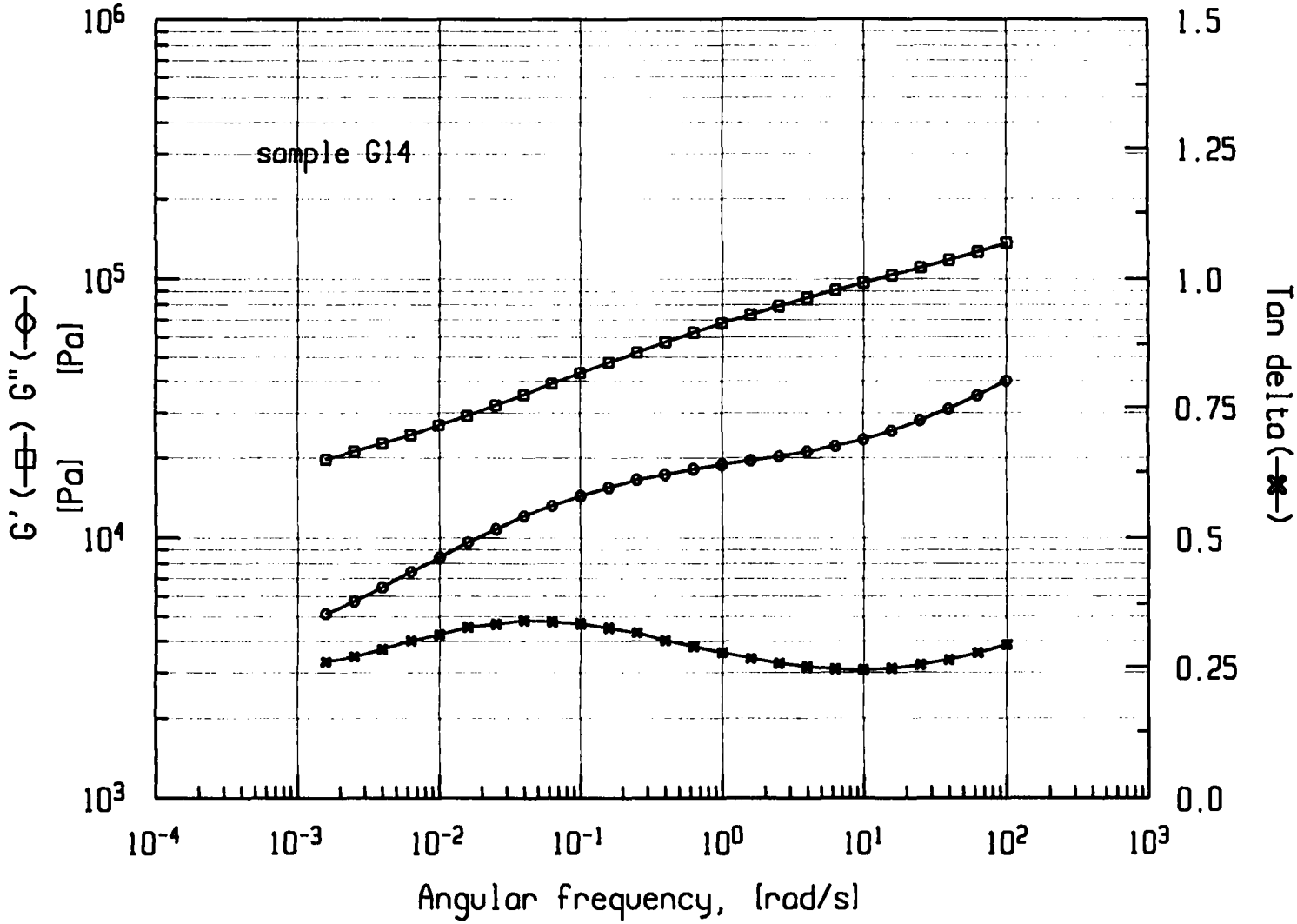


Figure AFSG15. Dynamic mechanical spectrum - sample G15.

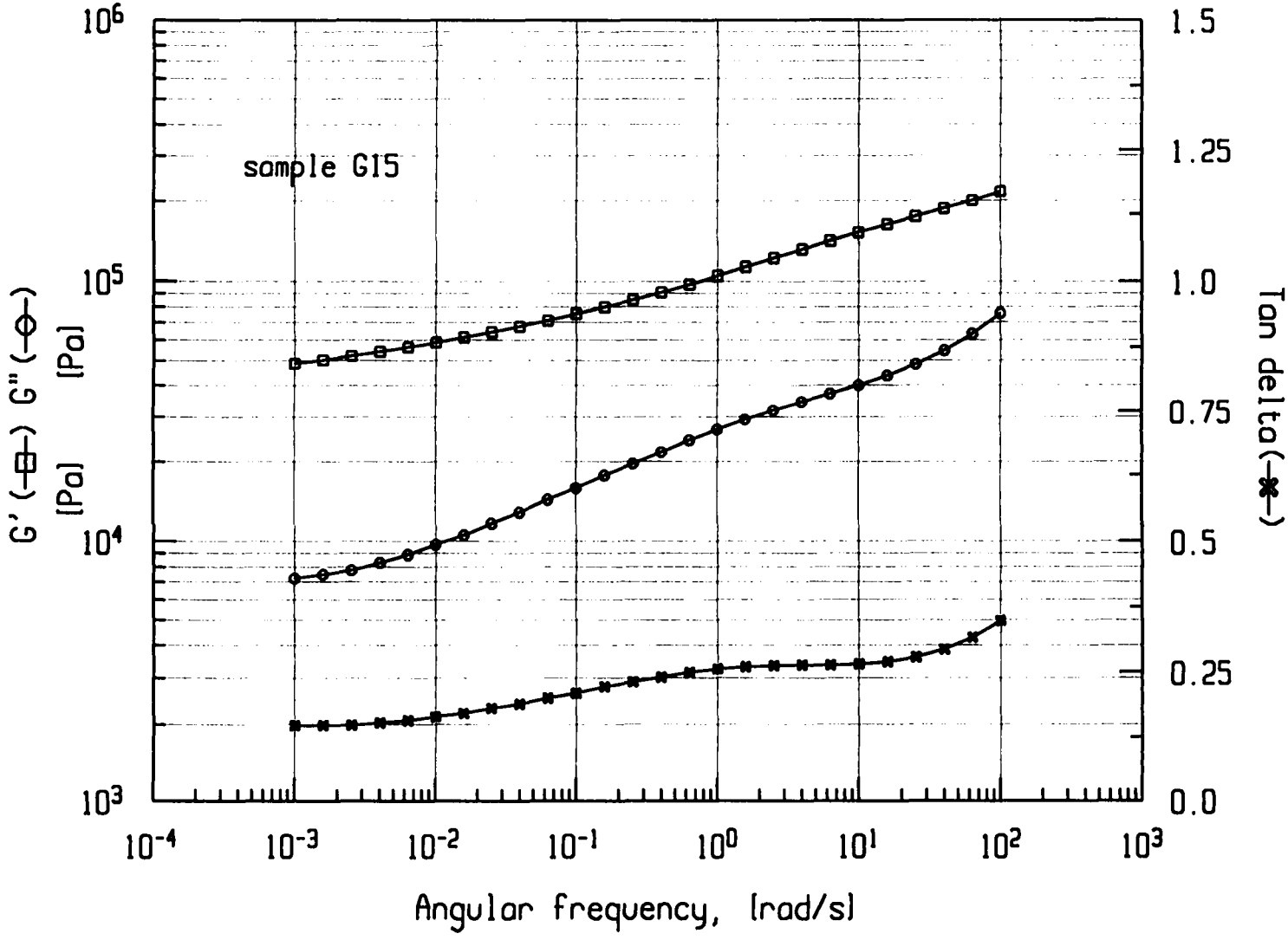


Figure AFSG16. Dynamic mechanical spectrum - sample G16.

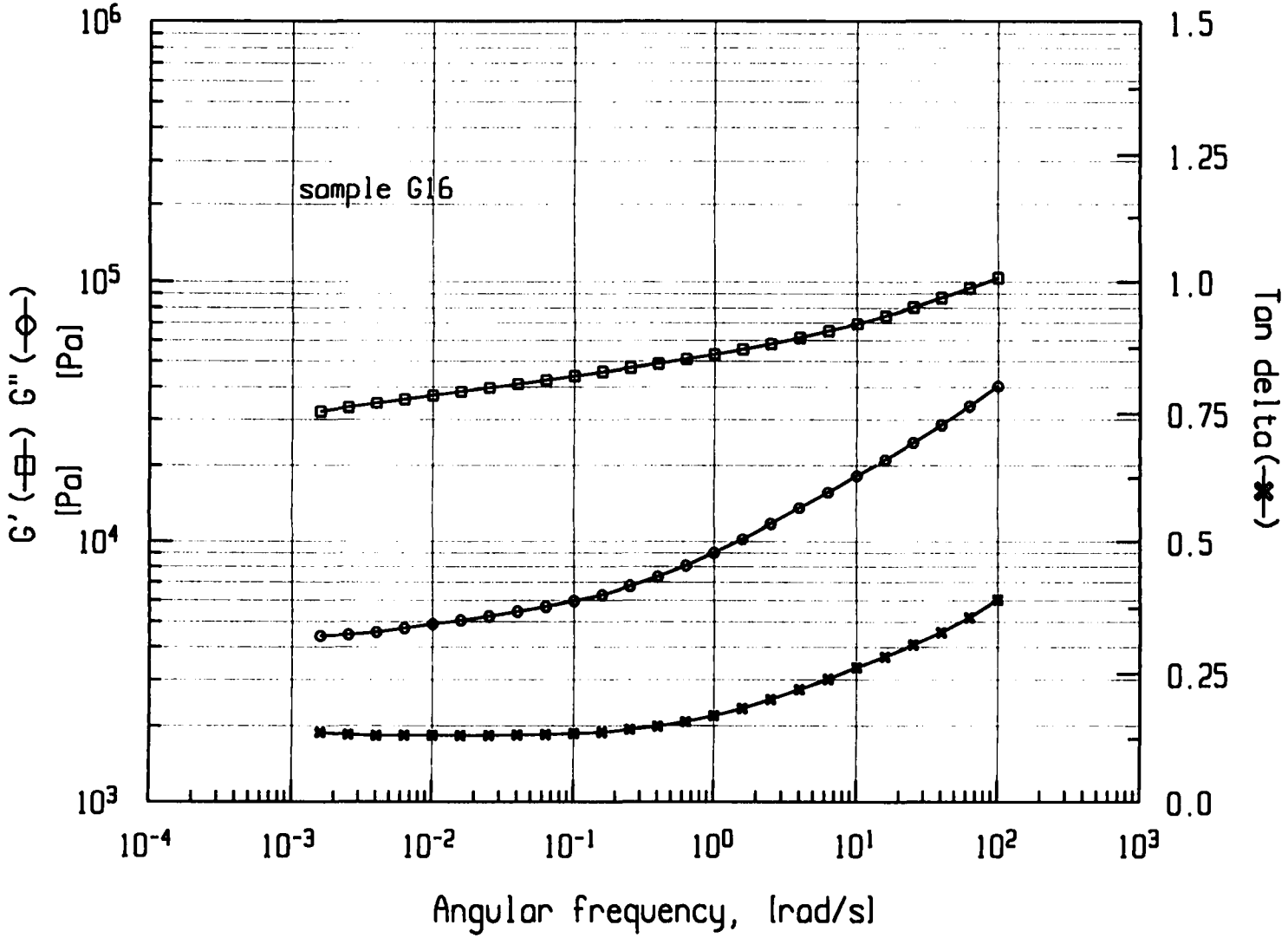


Figure AFSG17. Dynamic mechanical spectrum - sample G17.

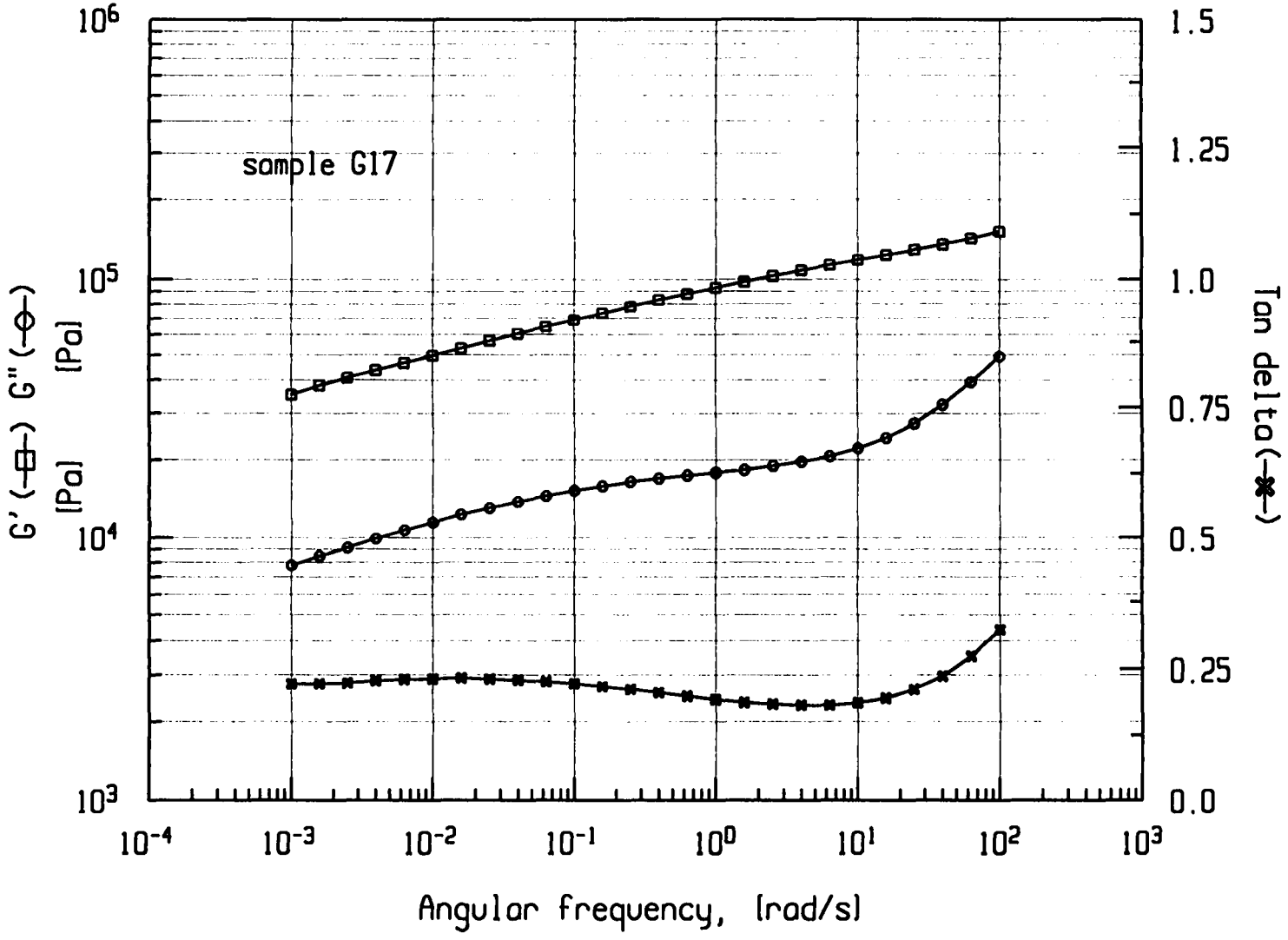


Figure AFSG18. Dynamic mechanical spectrum - sample G18.

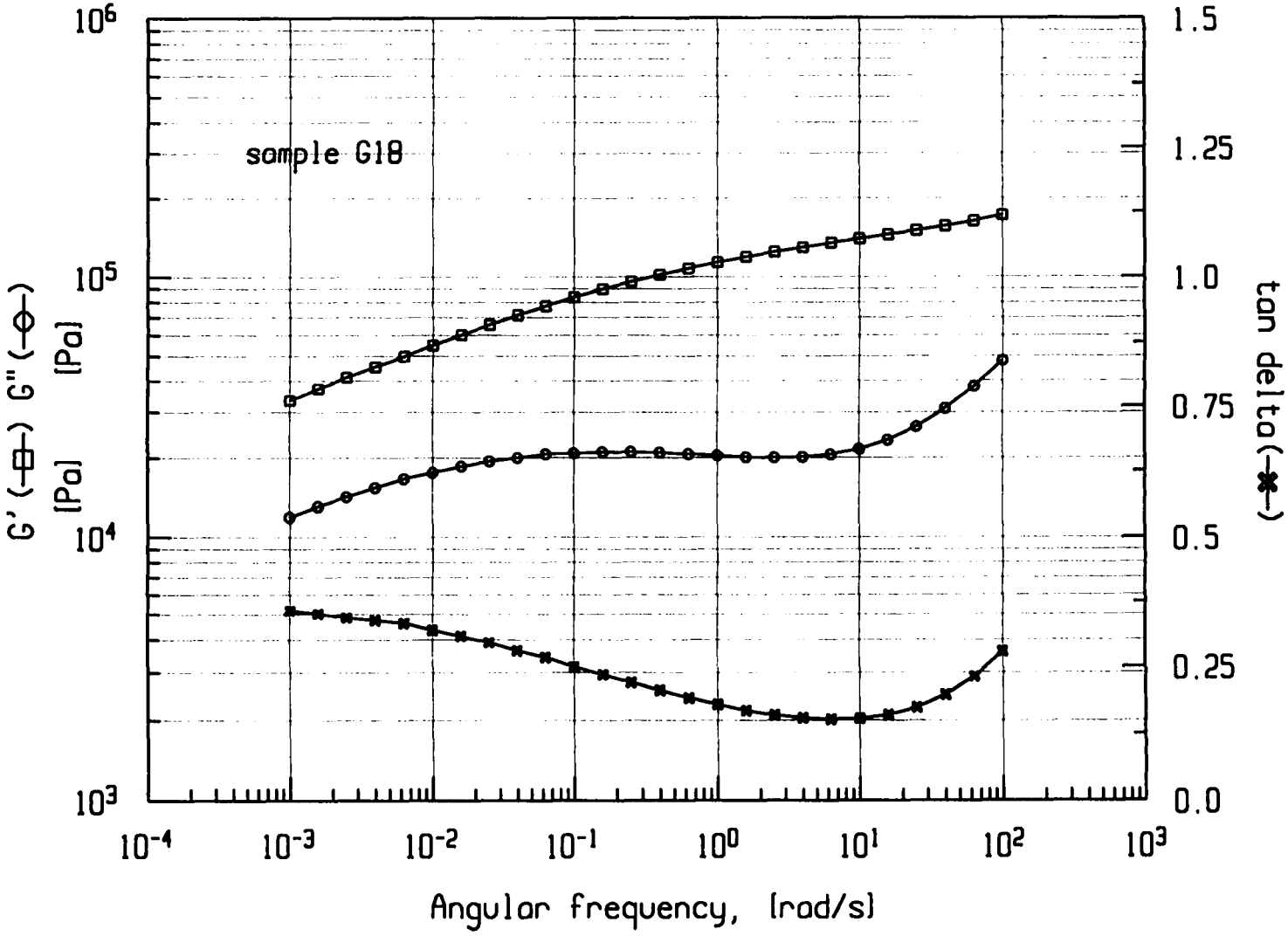


Figure AFSG19. Dynamic mechanical spectrum - sample G19.

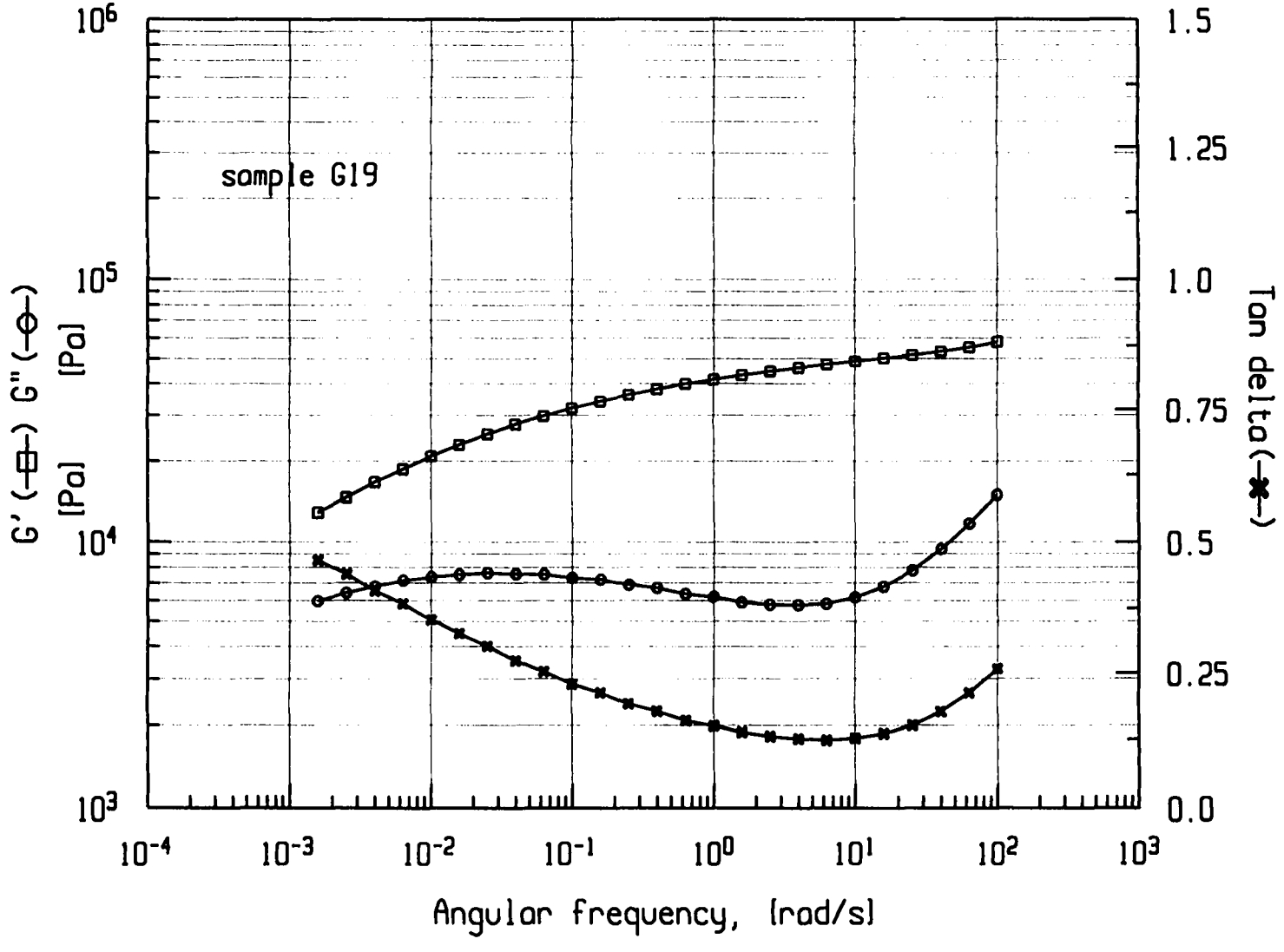


Figure AFSG20. Dynamic mechanical spectrum - sample G20.

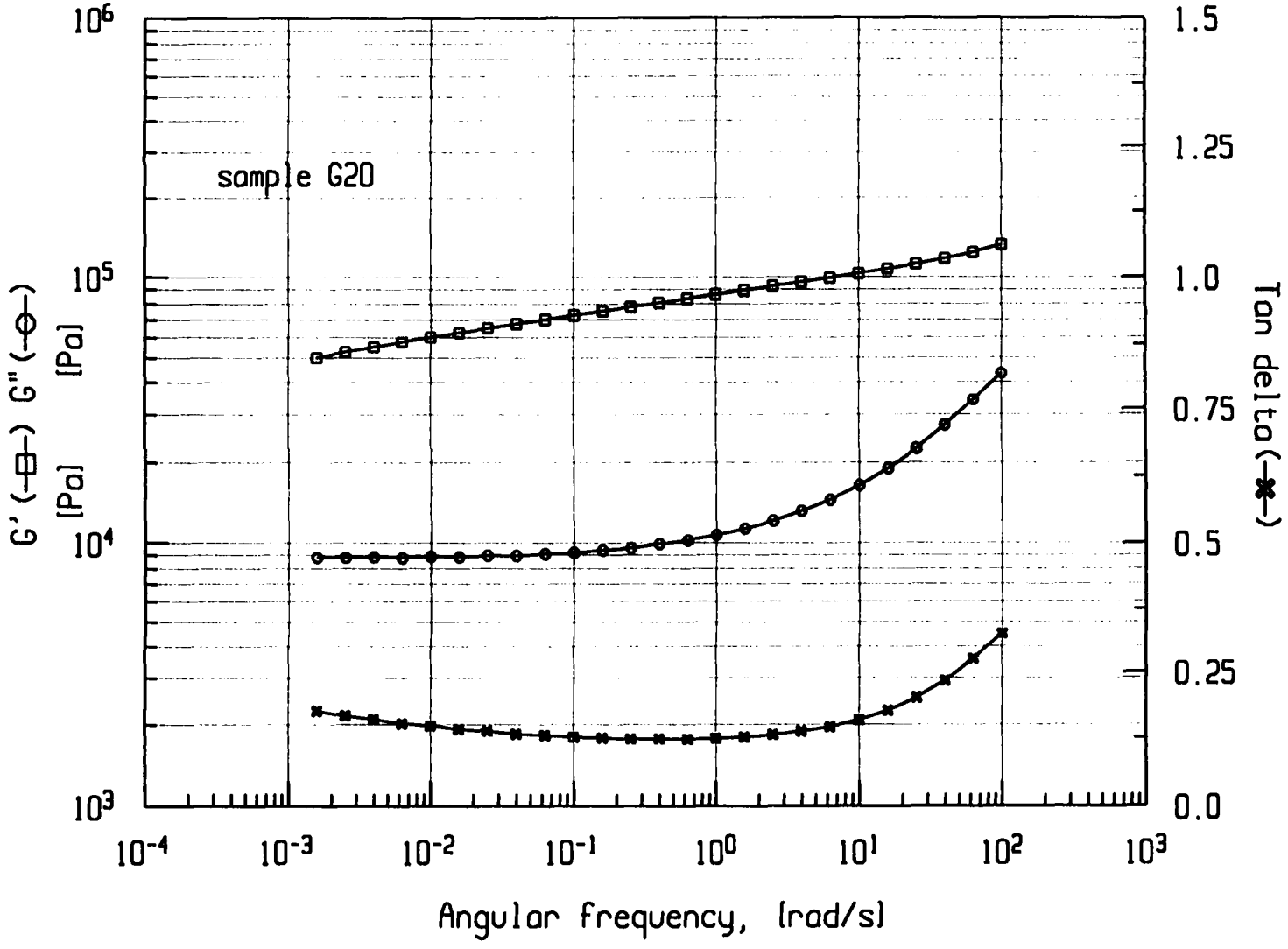


Figure AFSG21. Dynamic mechanical spectrum - sample G21.

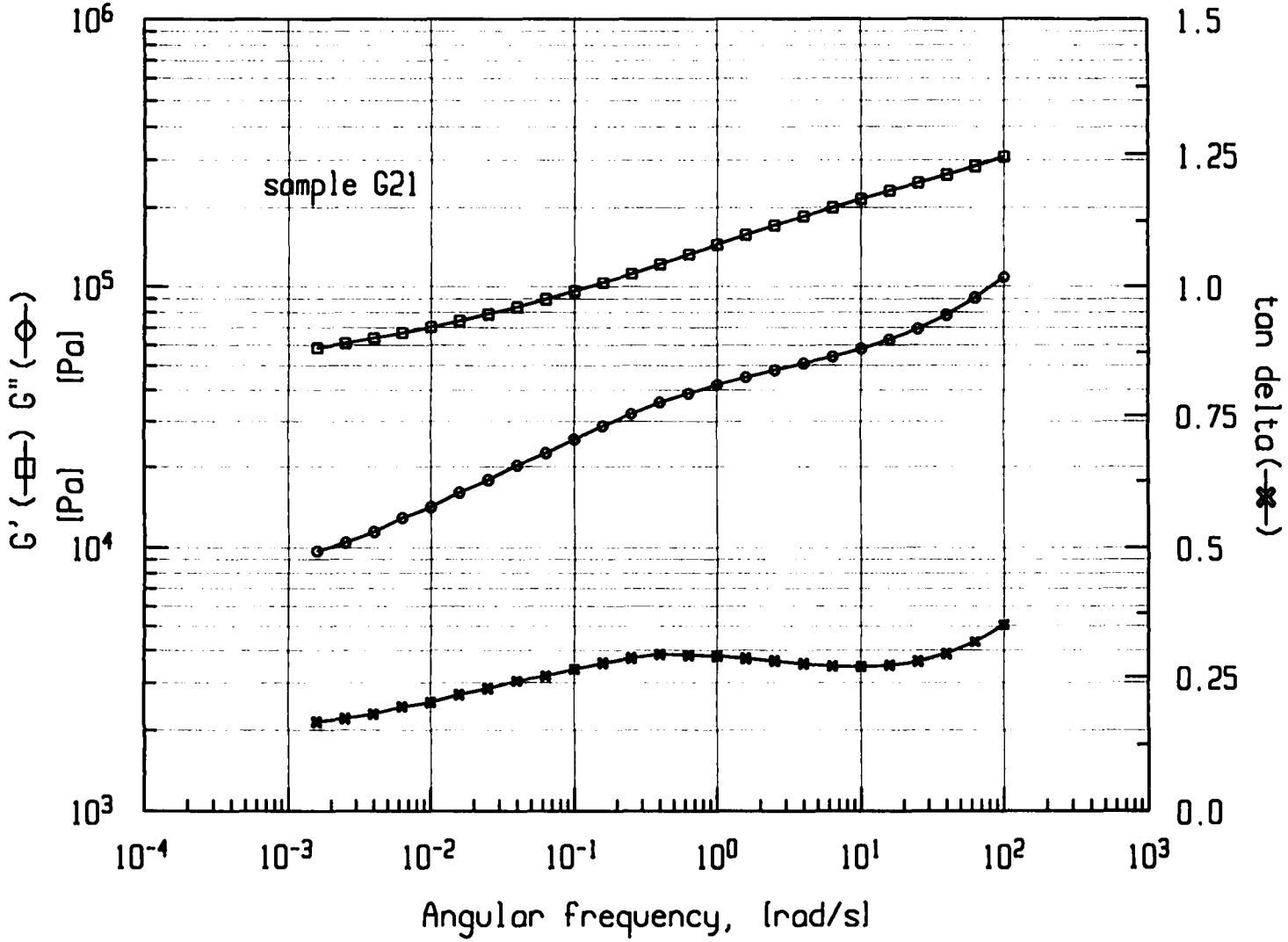


Figure AFSG22. Dynamic mechanical spectrum - sample G22.

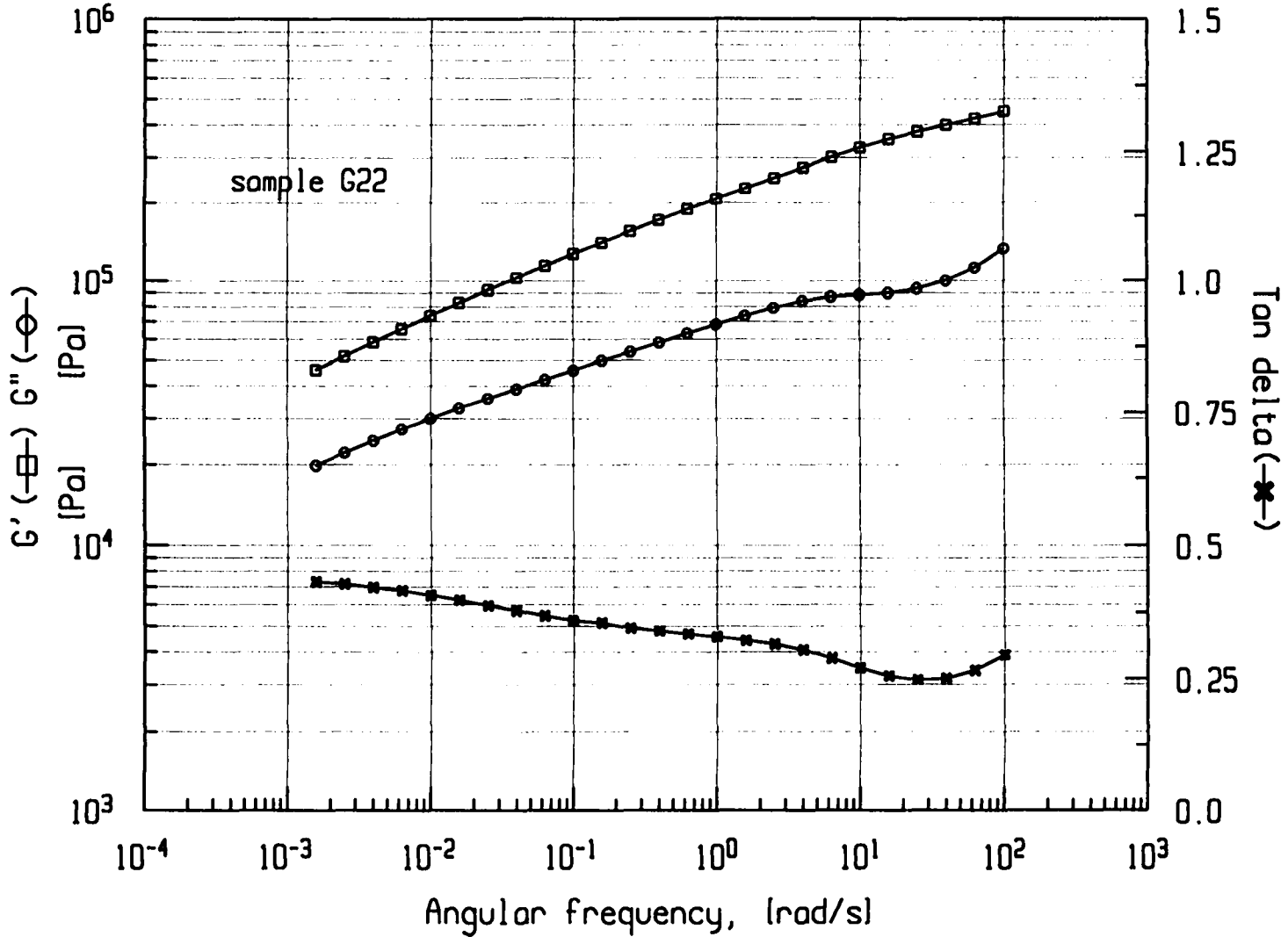


Figure AFSM. Dynamic mechanical spectrum - sample M.

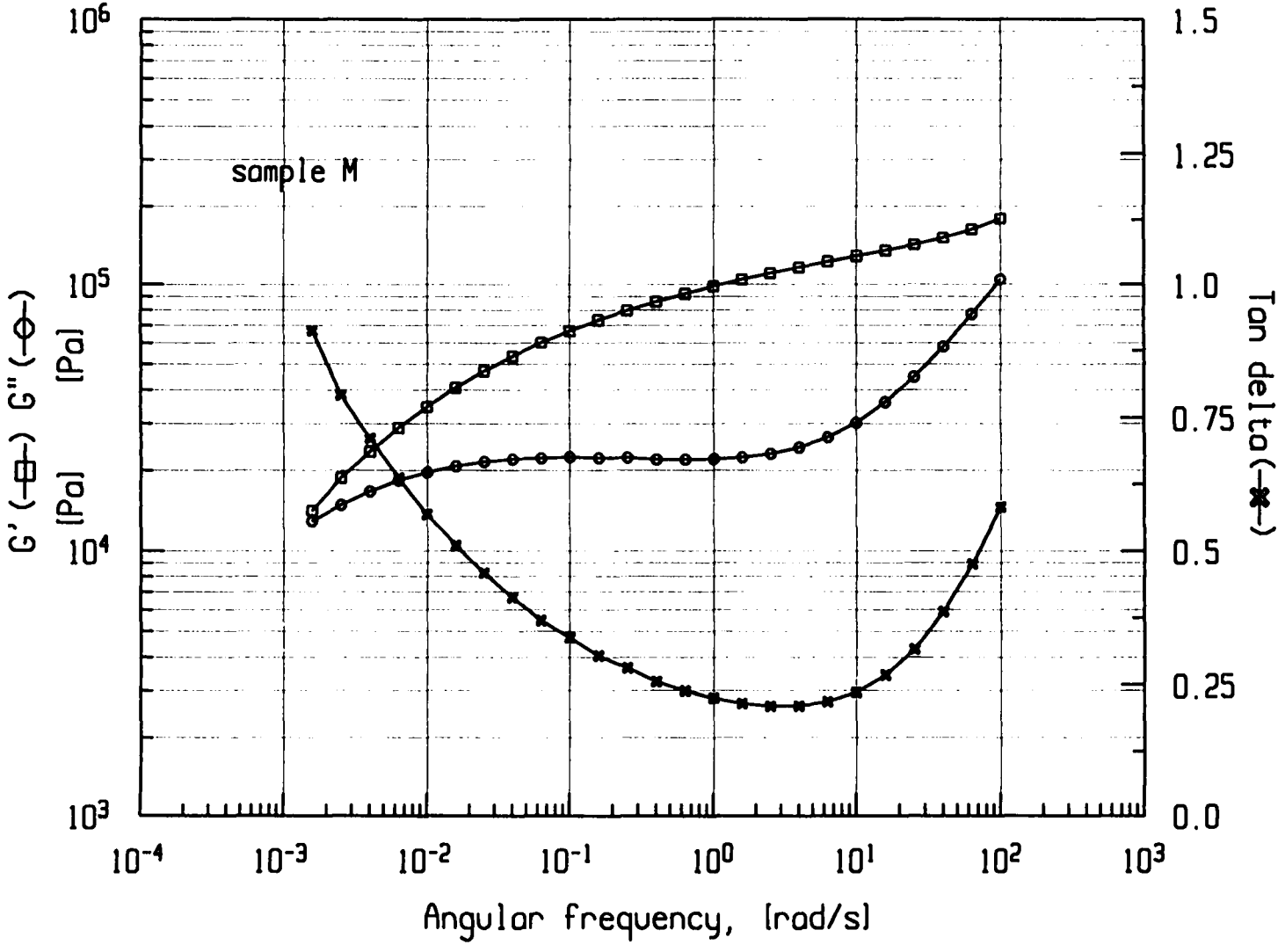


Figure AFSB10. Dynamic mechanical spectrum - sample B10.

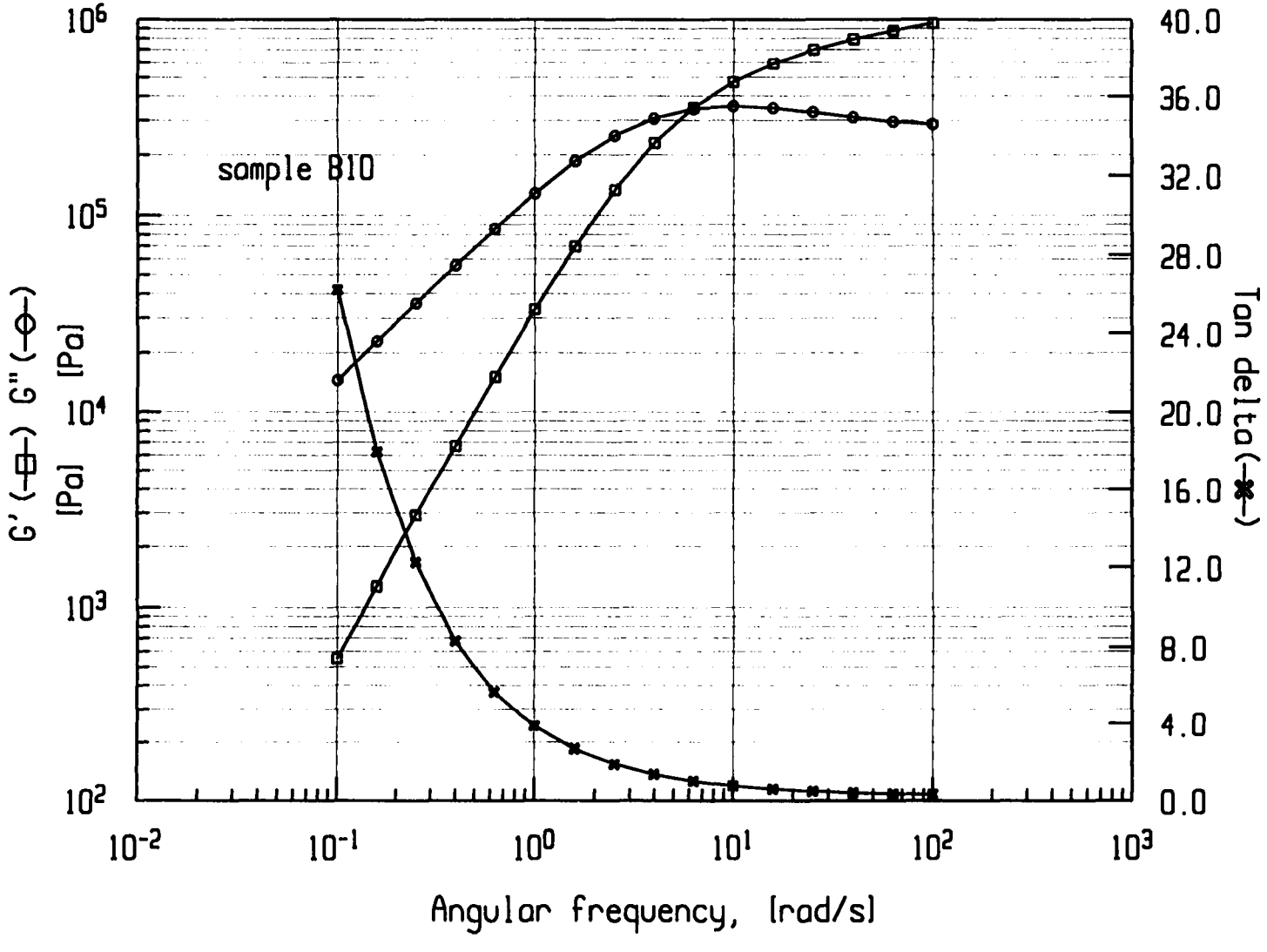


Figure AFTSC. Master curve - sample C.

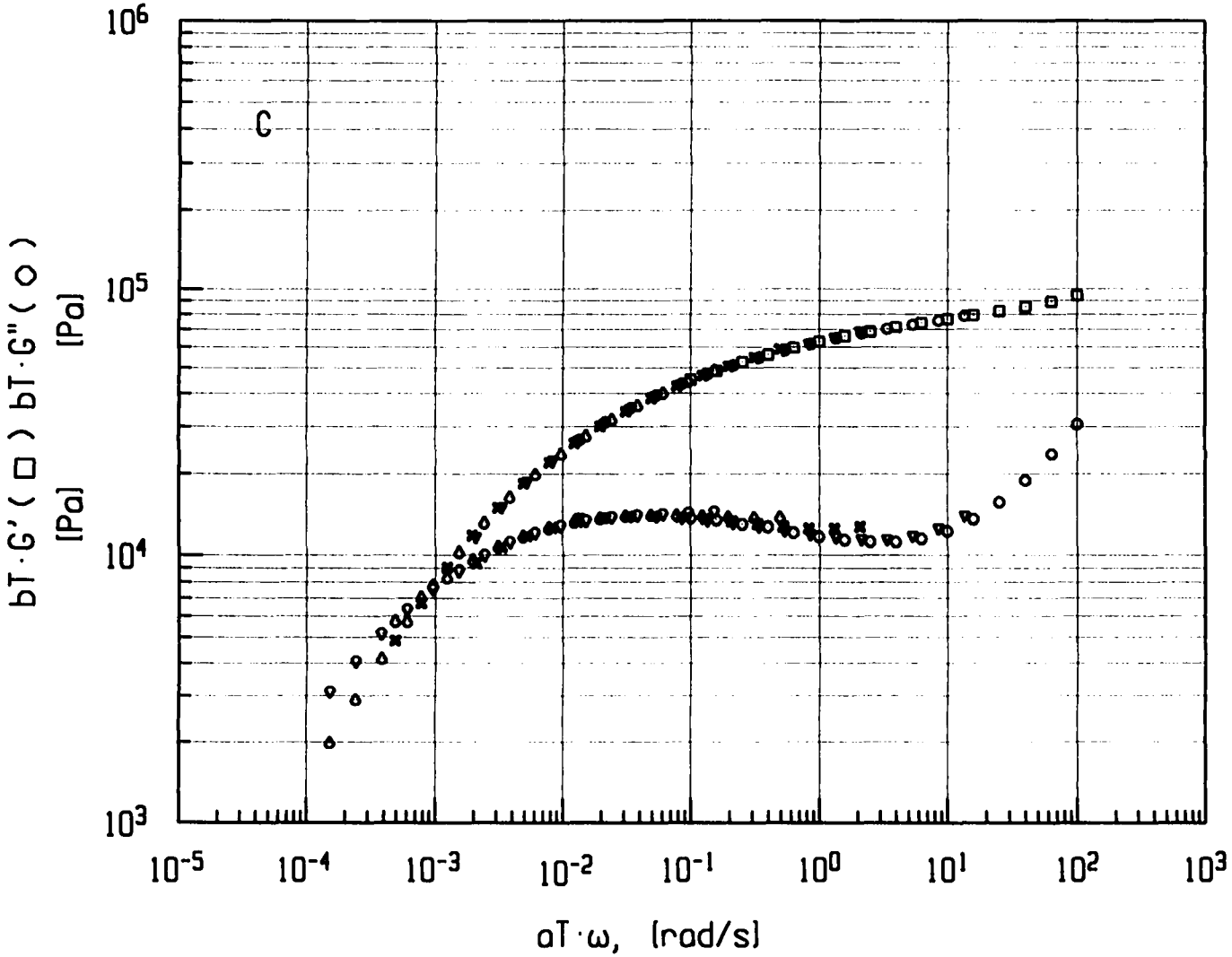


Figure AFTSG1. Master curve - sample G1.

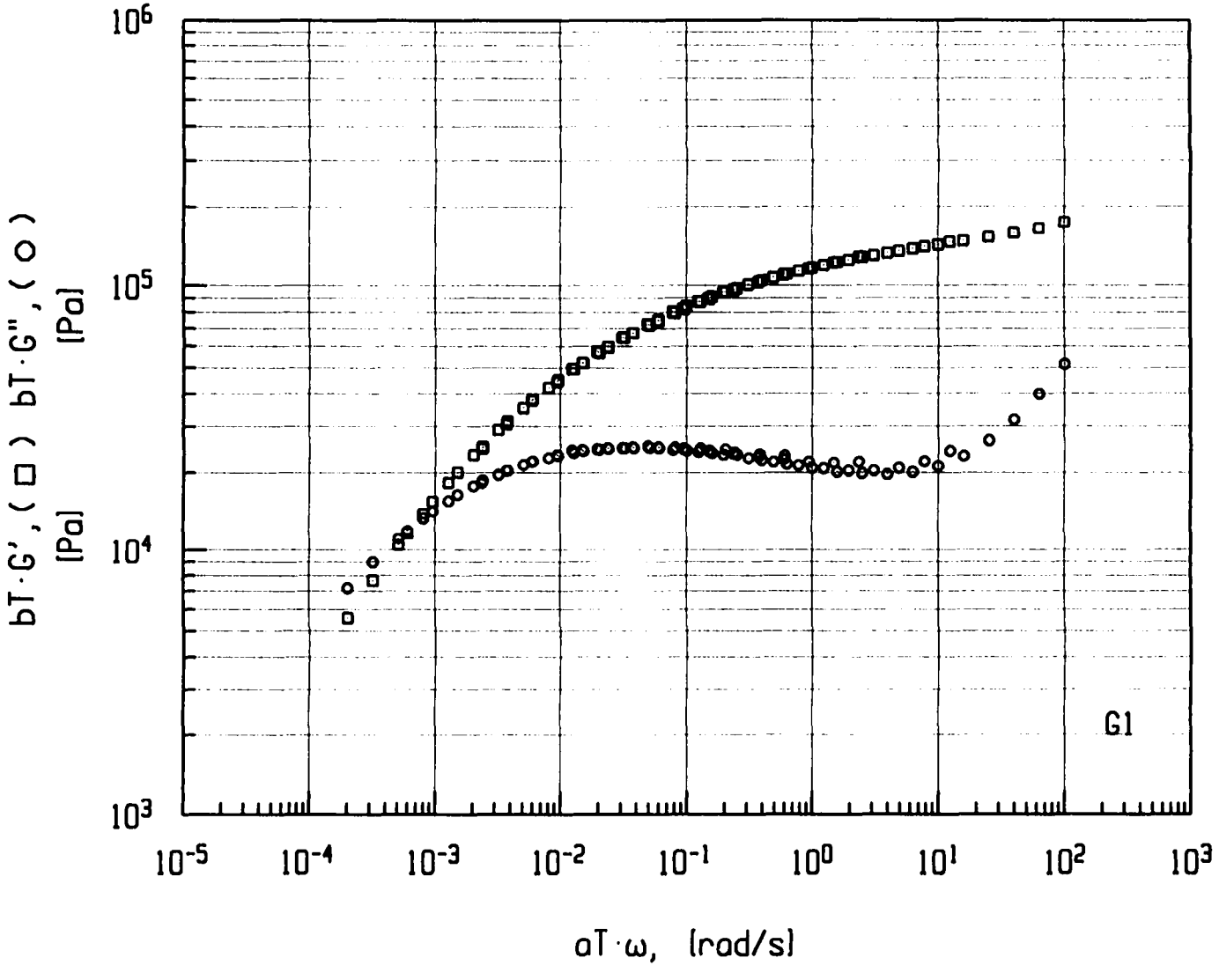


Figure AFTSG2. Master curve - sample G2.

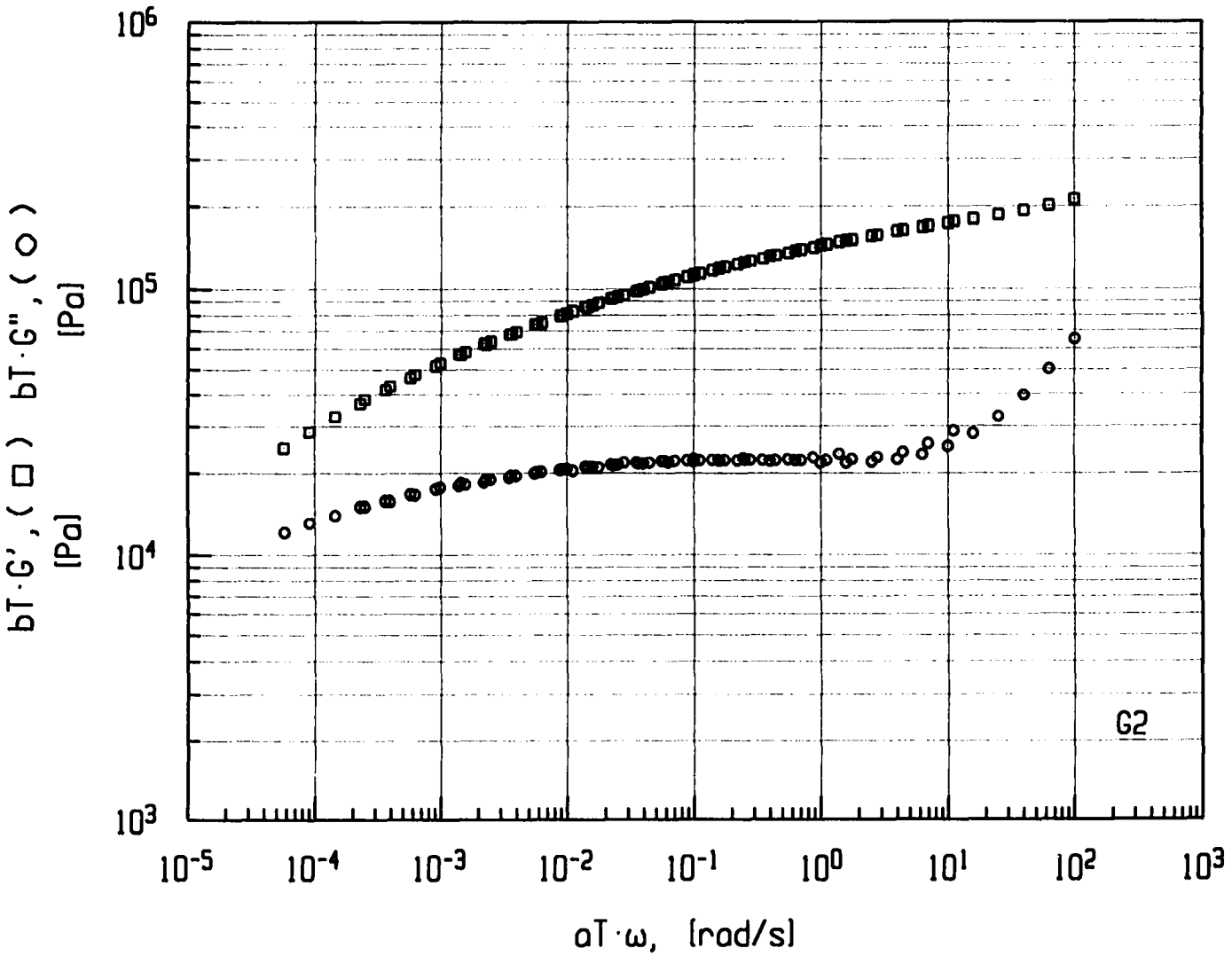


Figure AFTSG3. Master curve - sample G3.

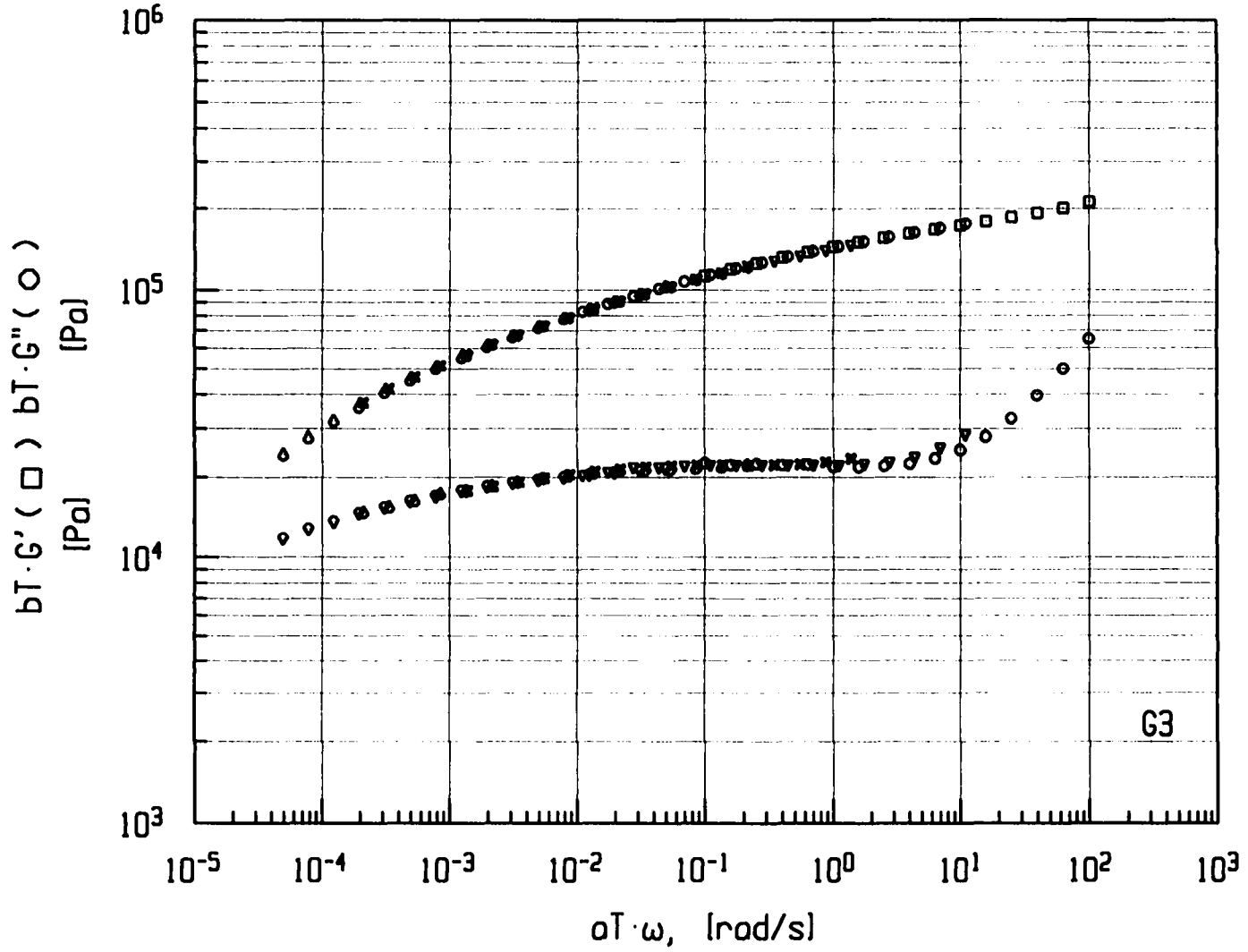


Figure AFTSG4. Master curve - sample G4.

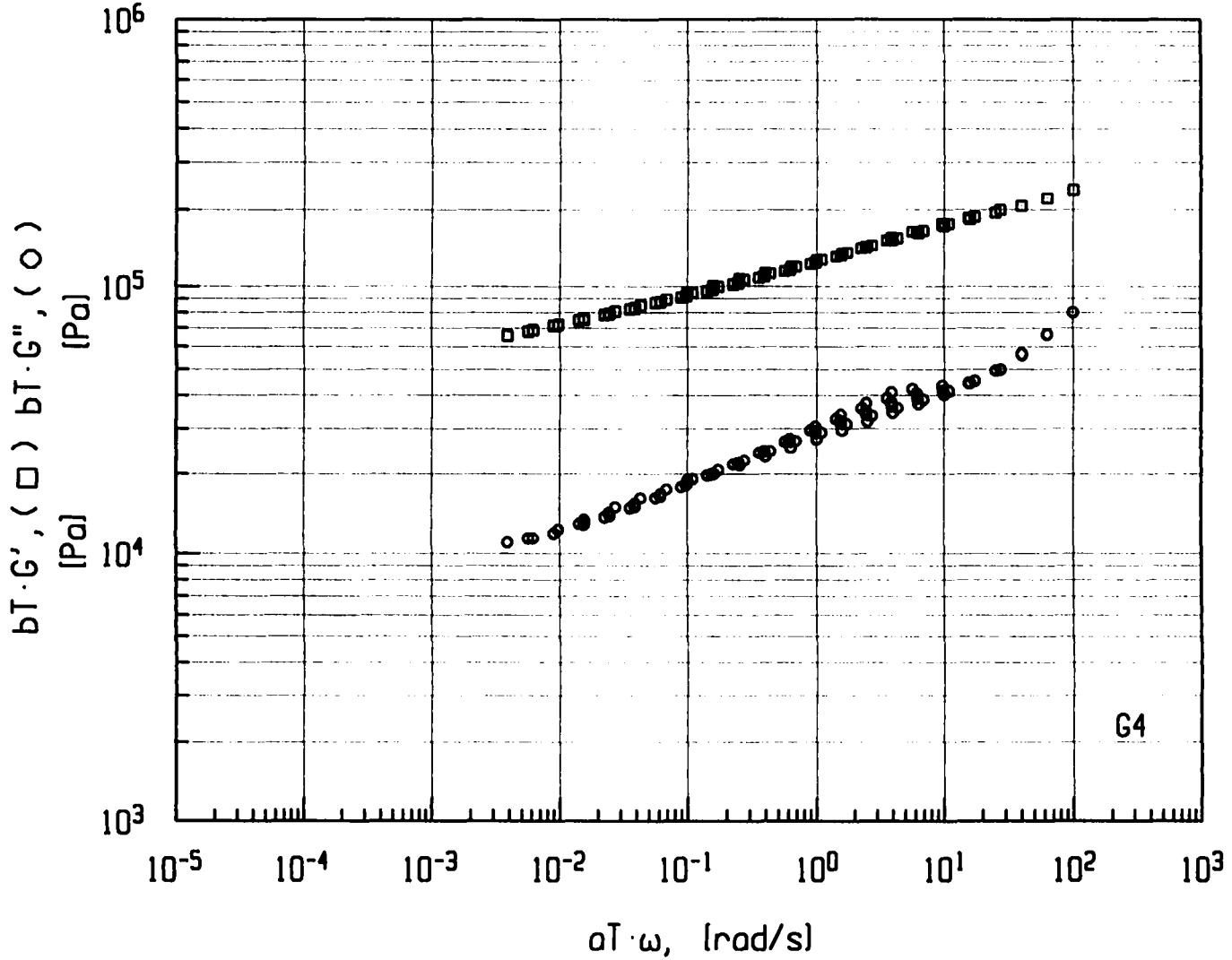


Figure AFTSG5. Master curve - sample G5.

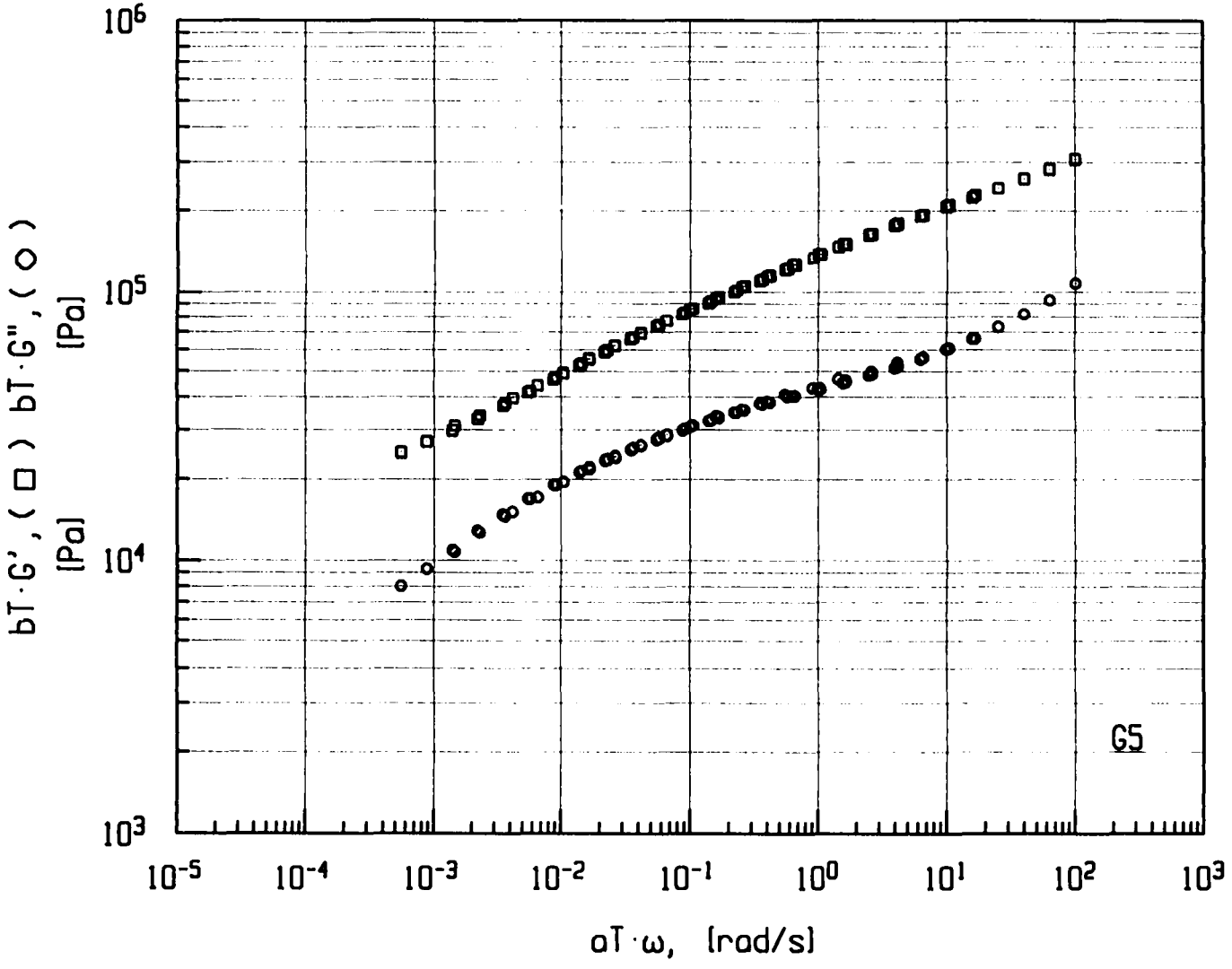


Figure AFTSG6. Master curve - sample G6.

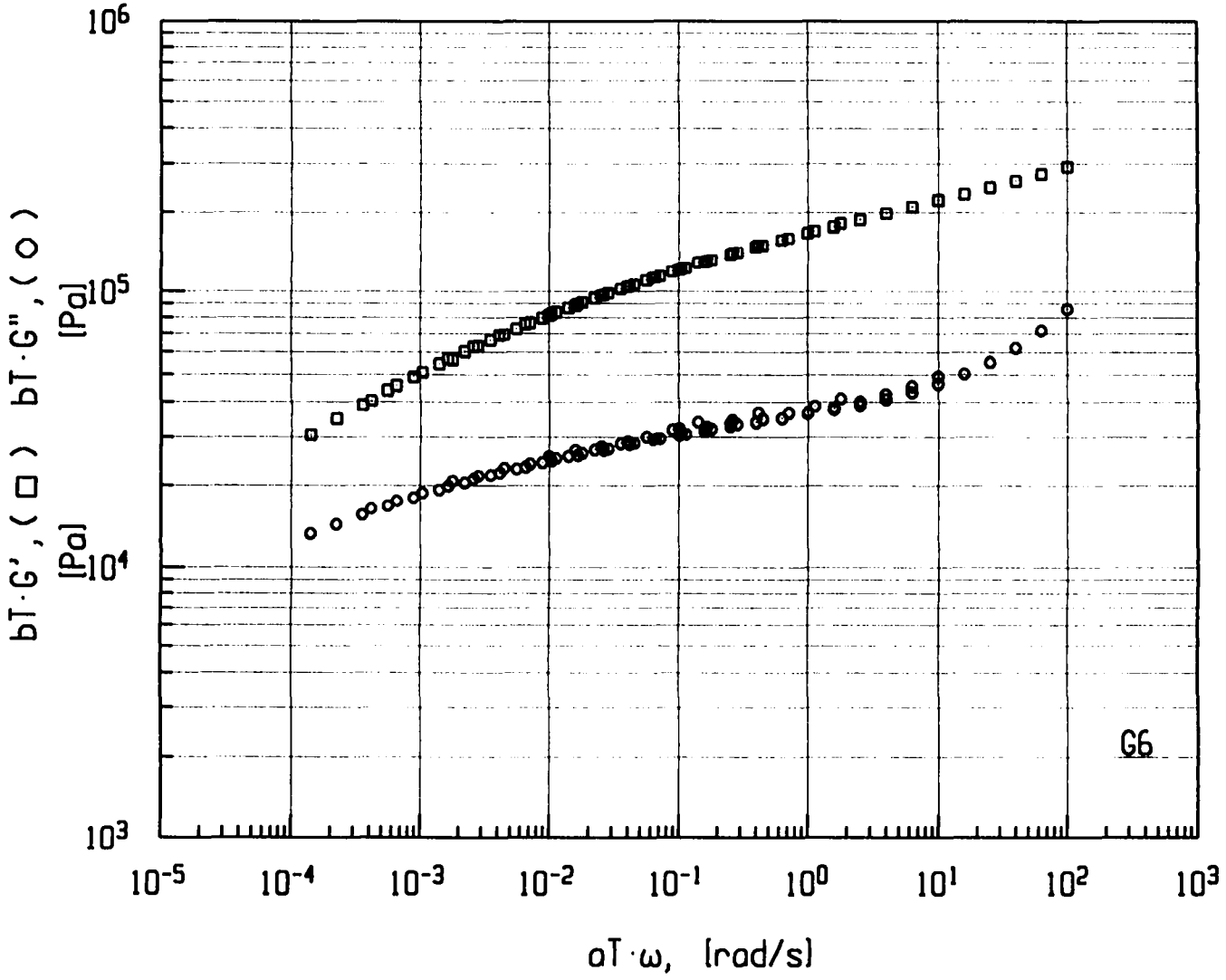


Figure AFTSG7. Master curve - sample G7.

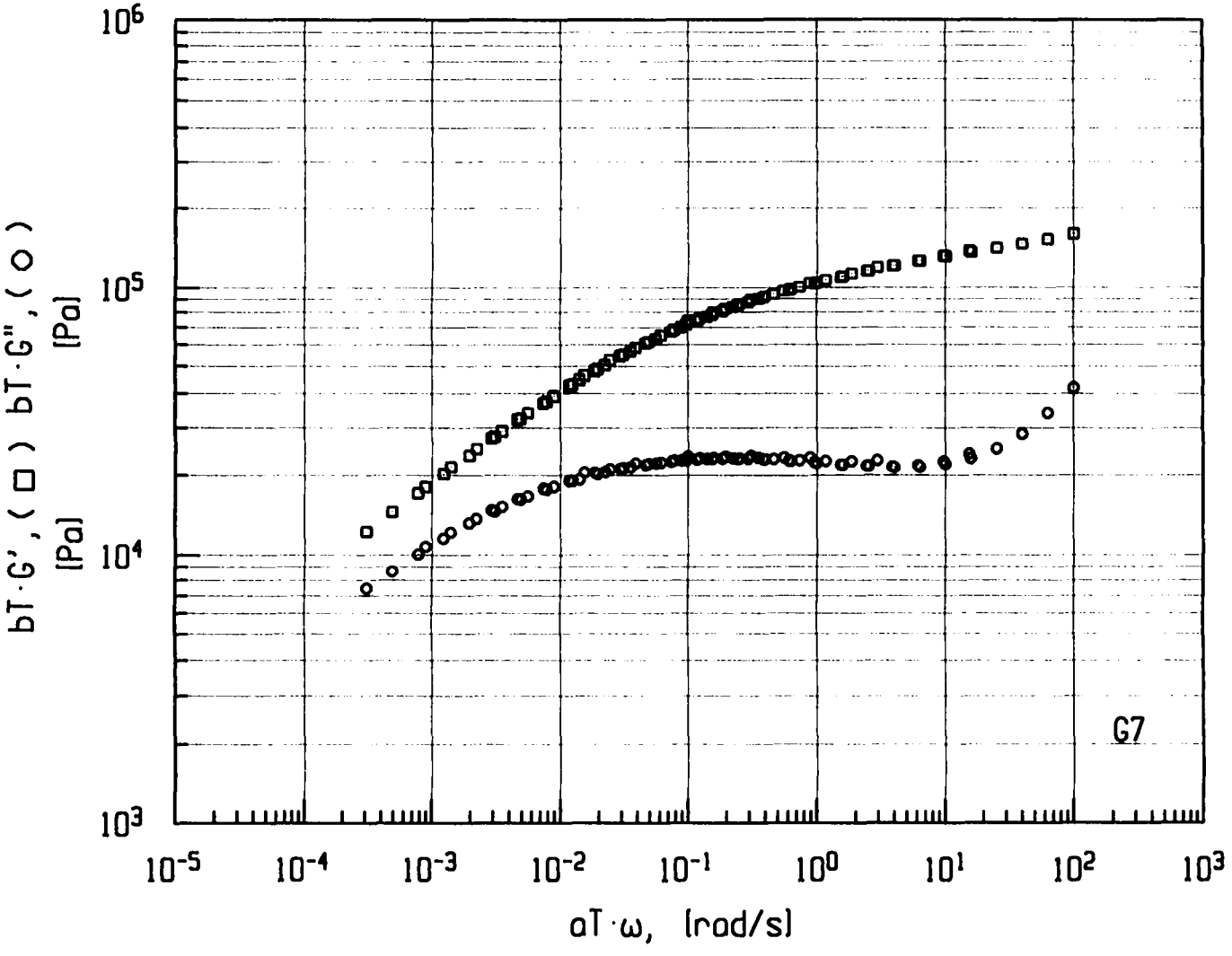


Figure AFTSG8. Master curve - sample G8.

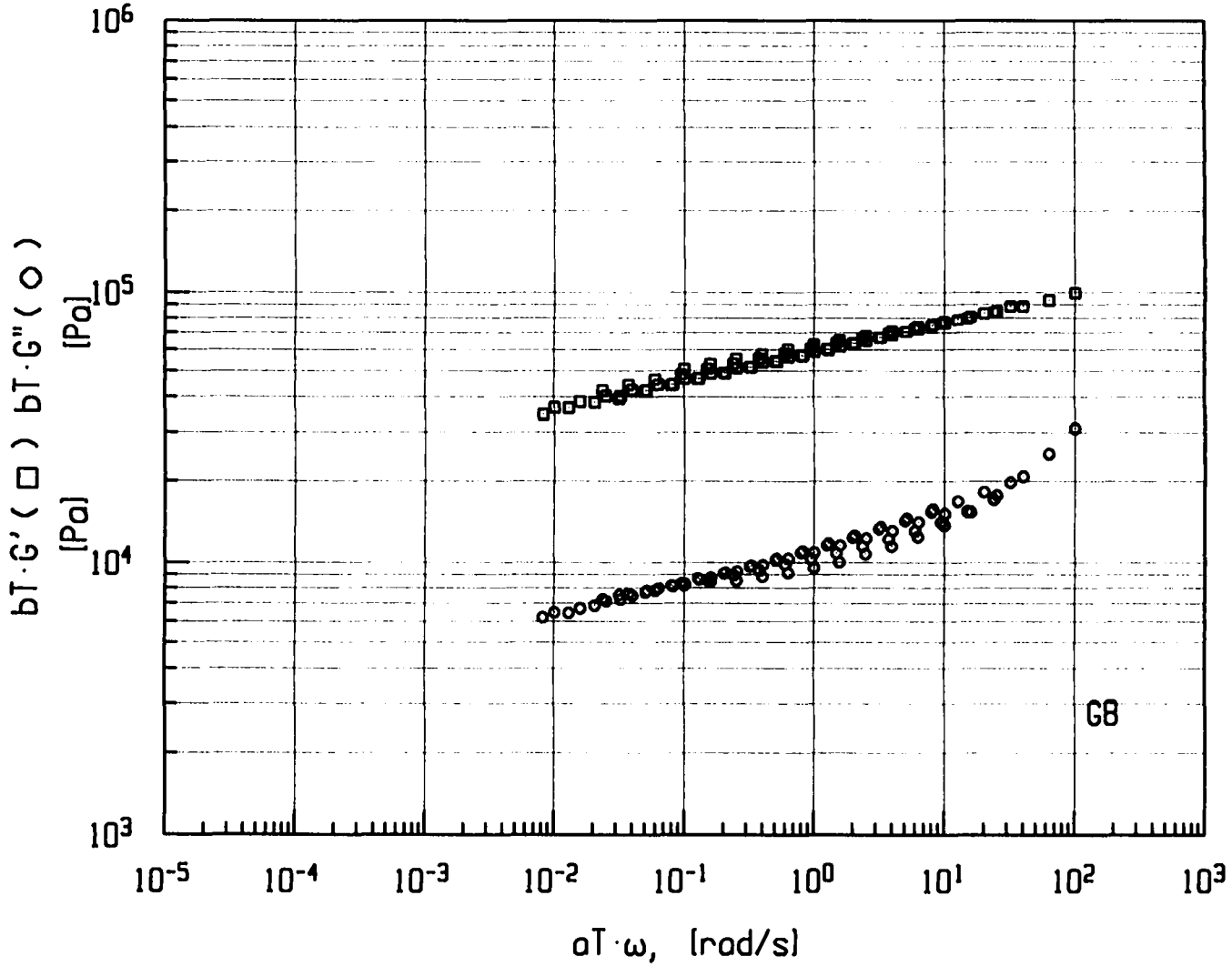


Figure AFTSG9. Master curve - sample G9.

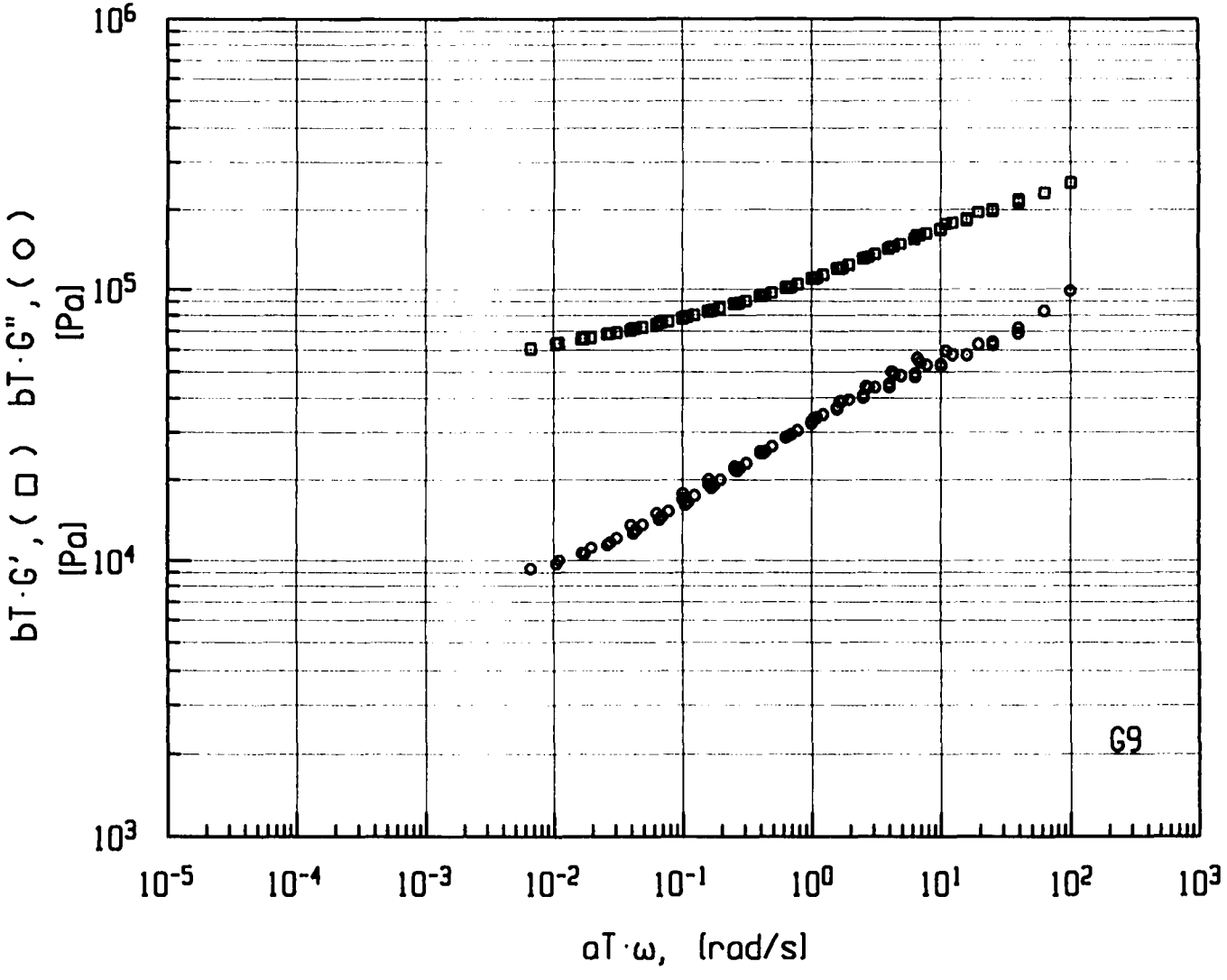


Figure AFTSG10. Master curve - sample G10.

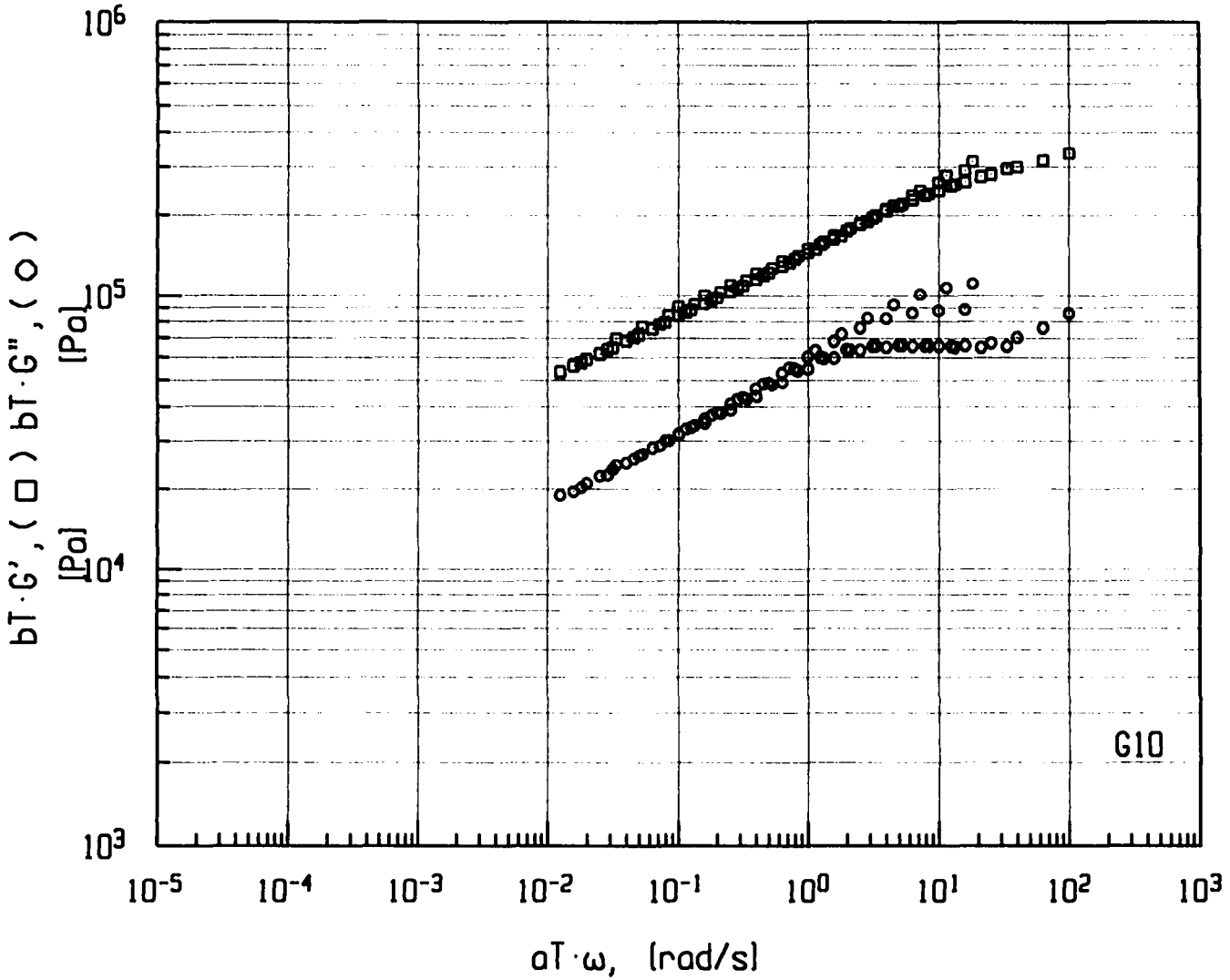


Figure AFTSG11. Master curve - sample G11.

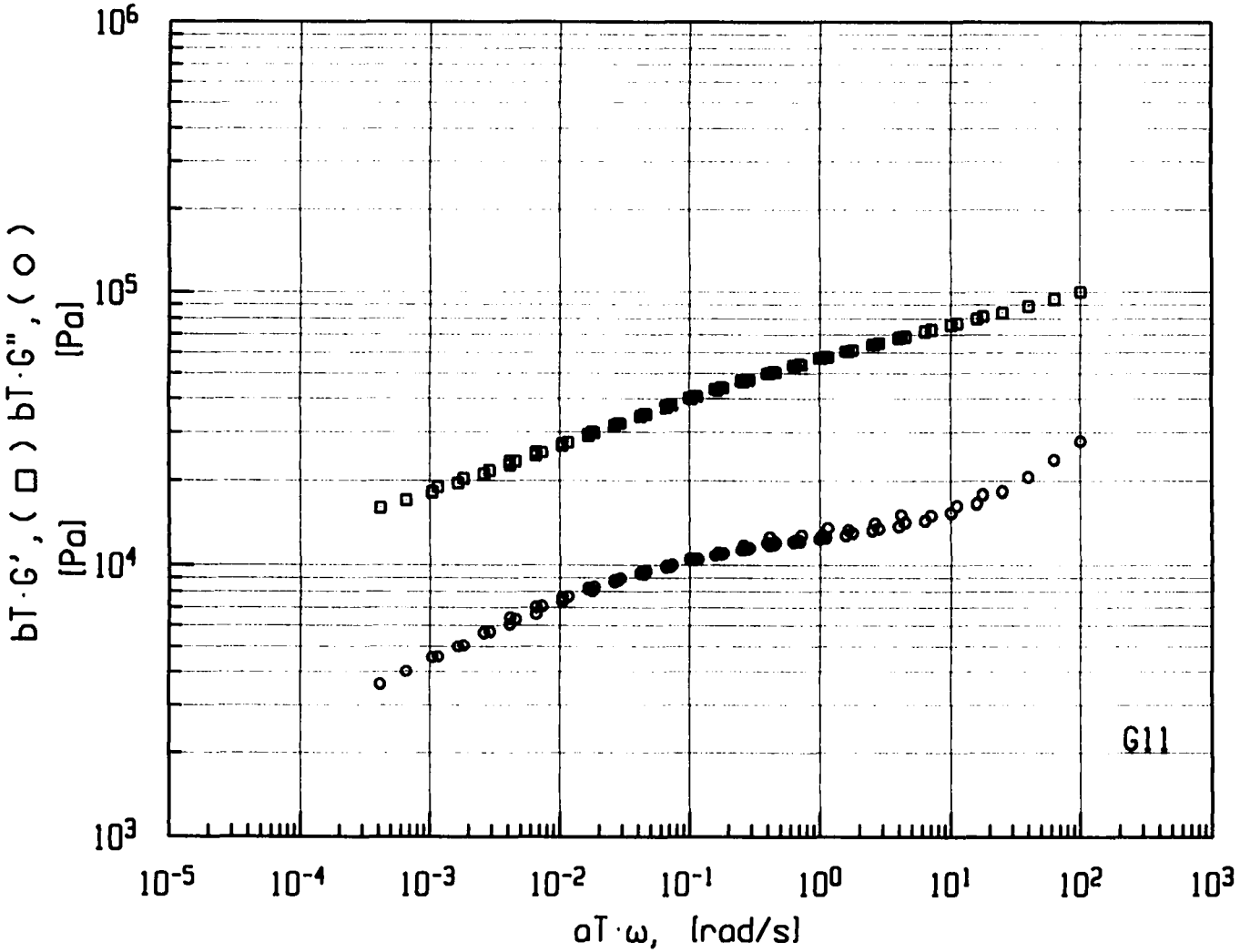


Figure AFTSG12. Master curve - sample G12.

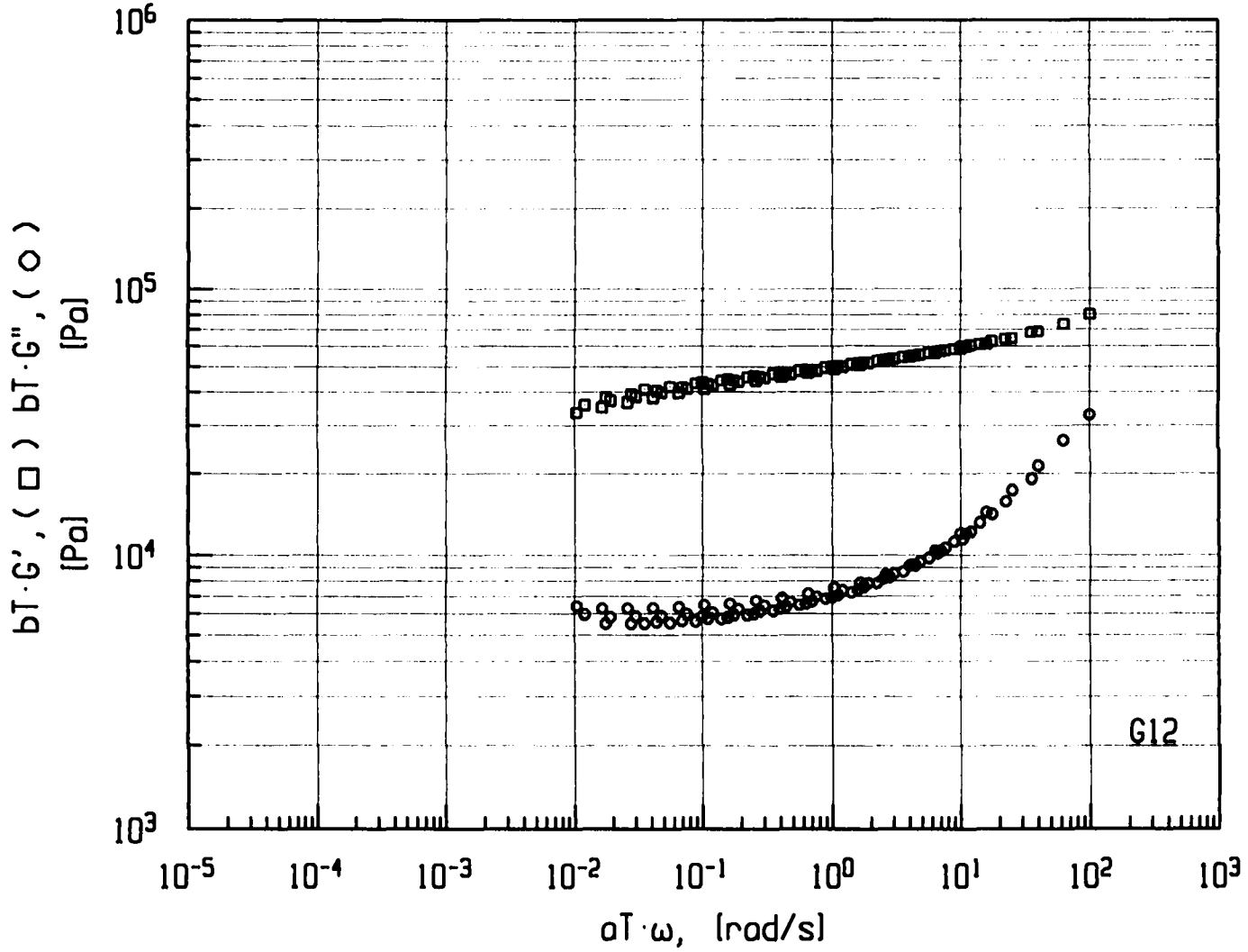


Figure AFTSG13. Master curve - sample G13.

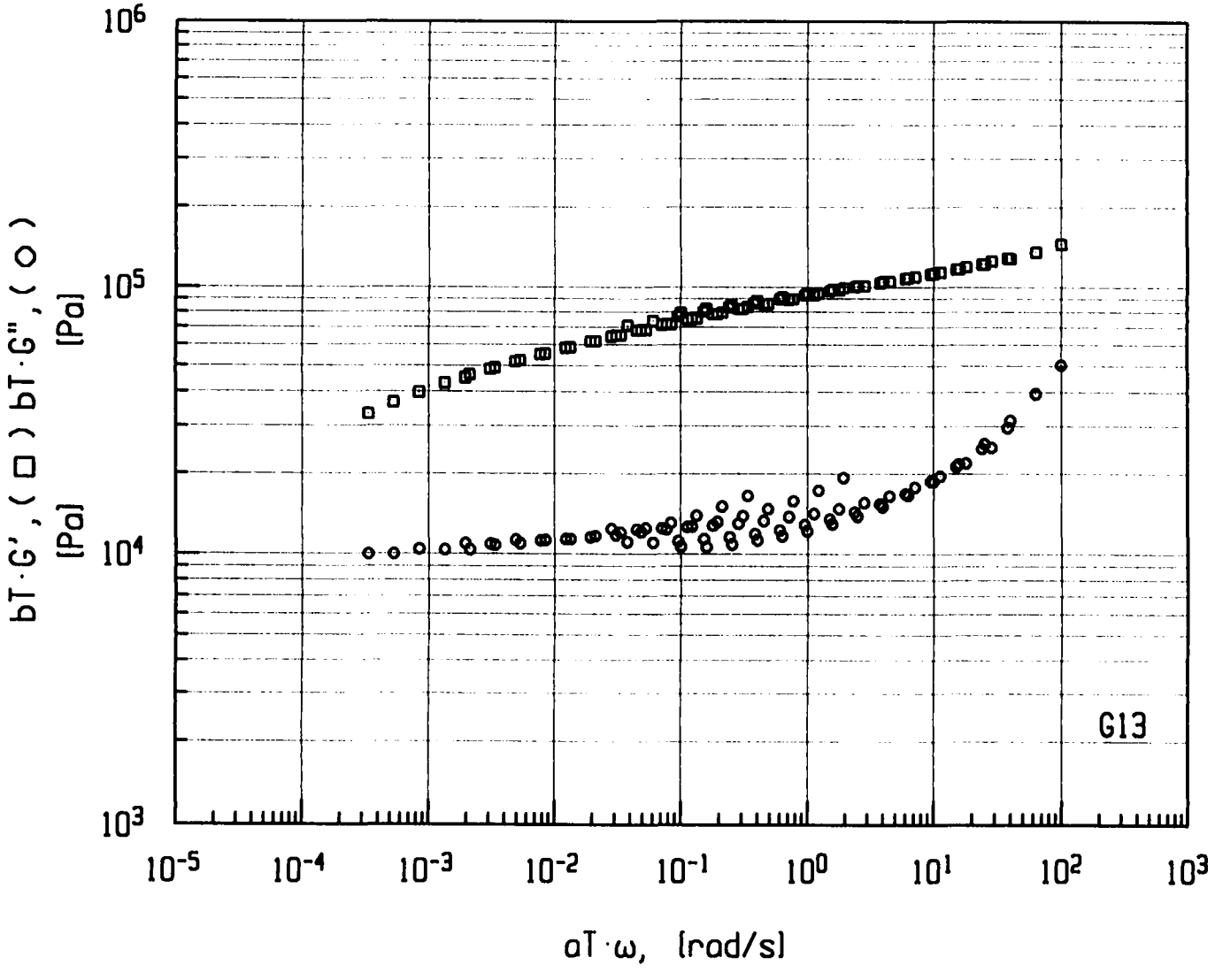


Figure AFTSG14. Master curve - sample G14.

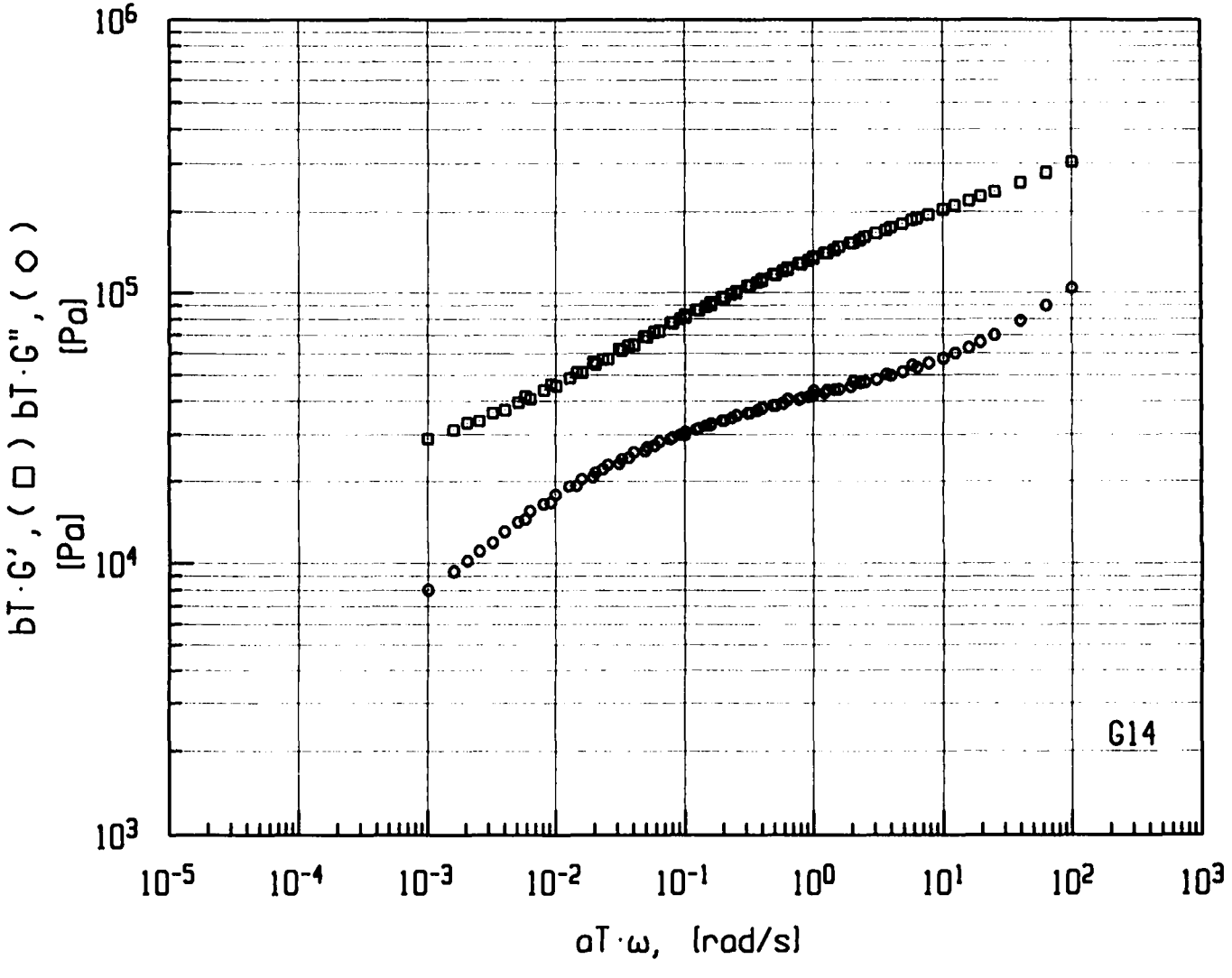


Figure AFTSG15. Master curve - sample G15.

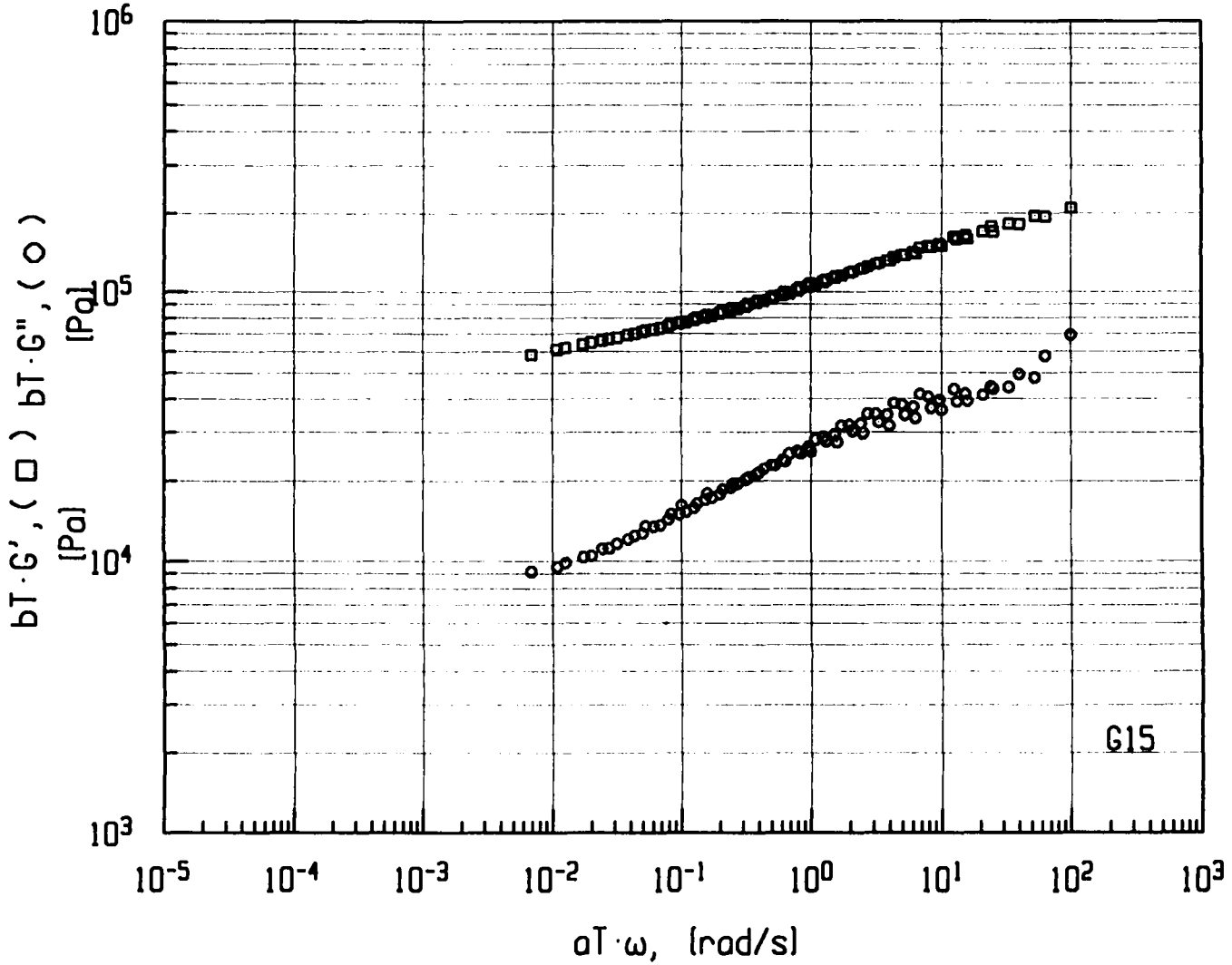


Figure AFTSG16. Master curve - sample G16.

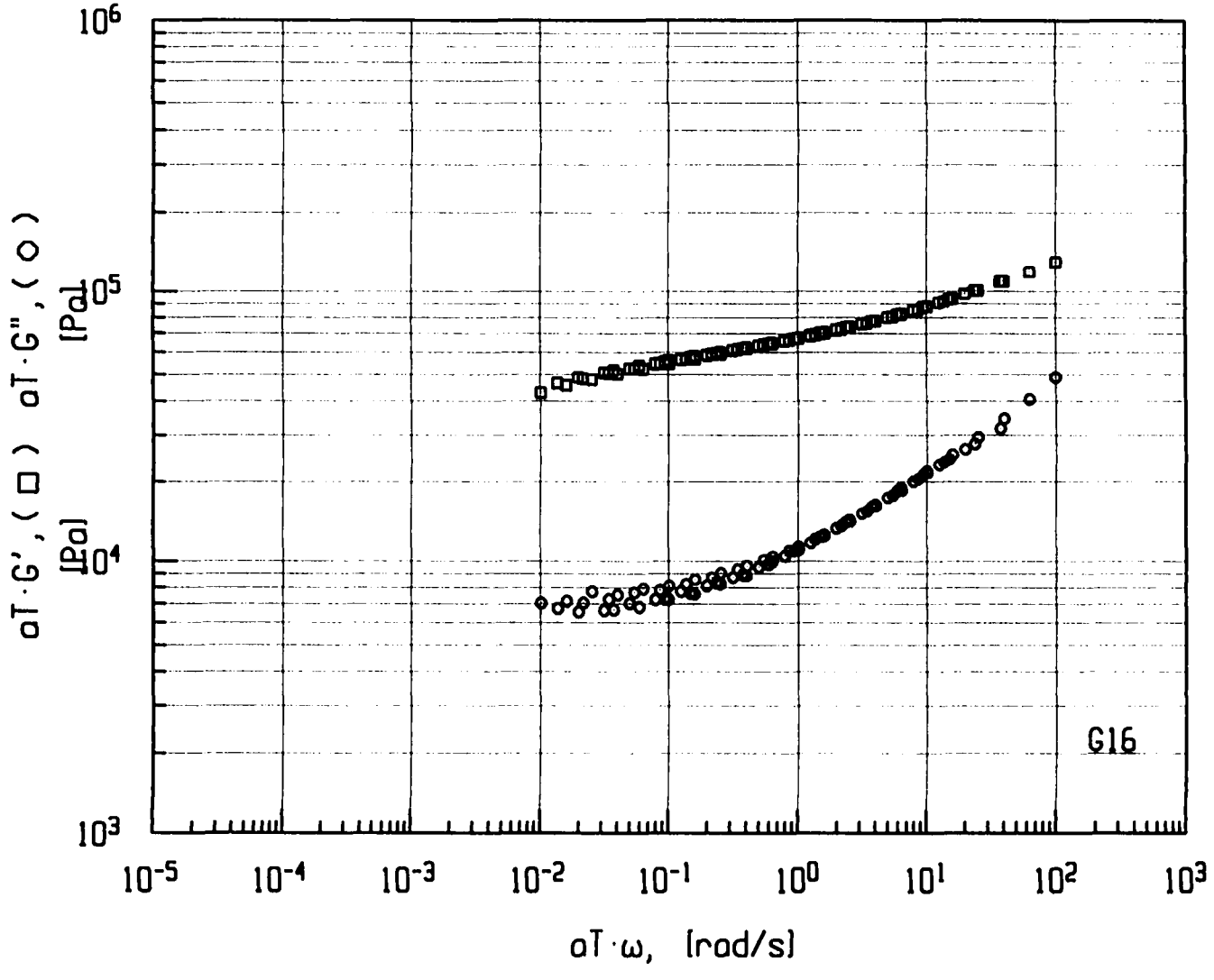


Figure AFTSG17. Master curve - sample G17.

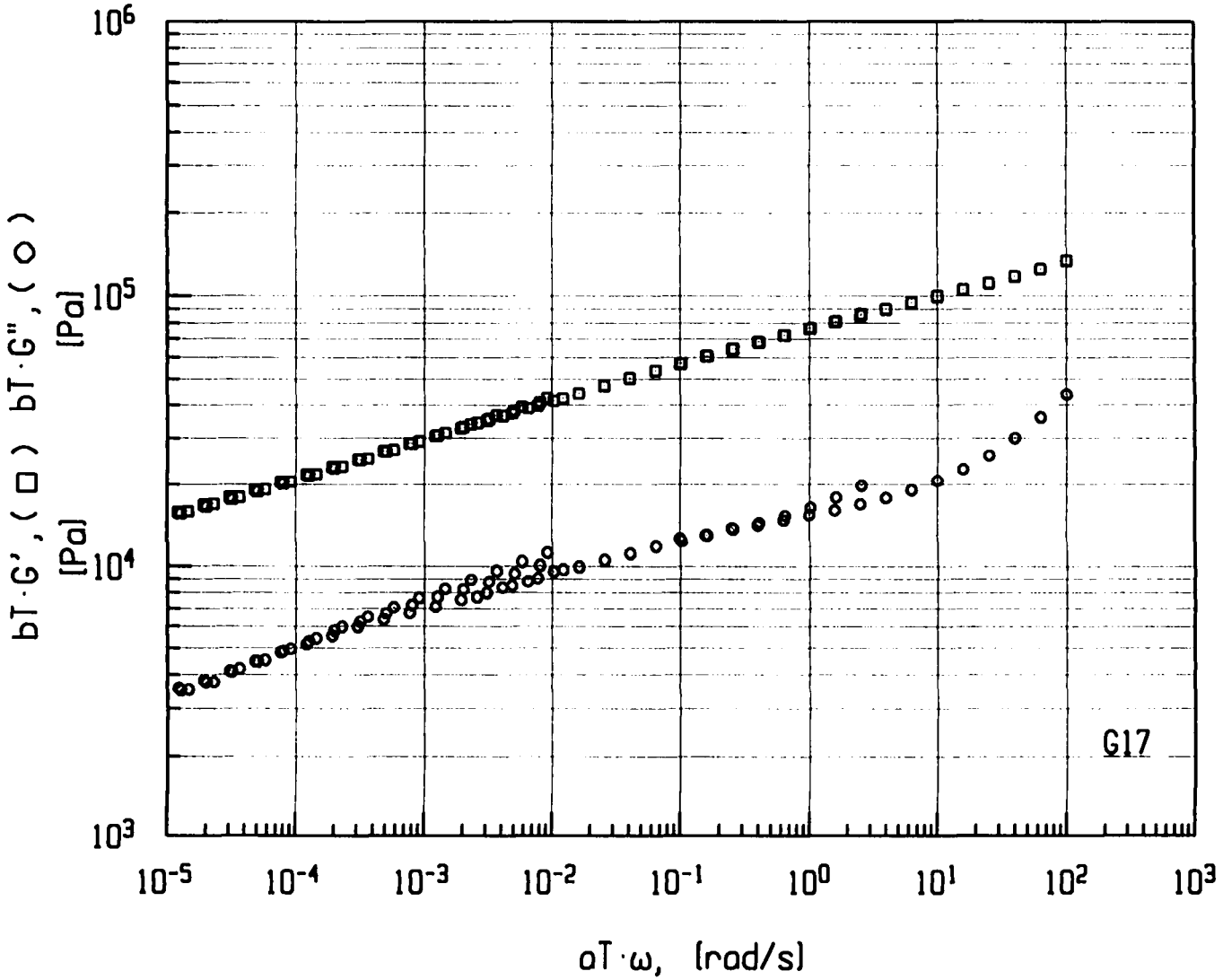
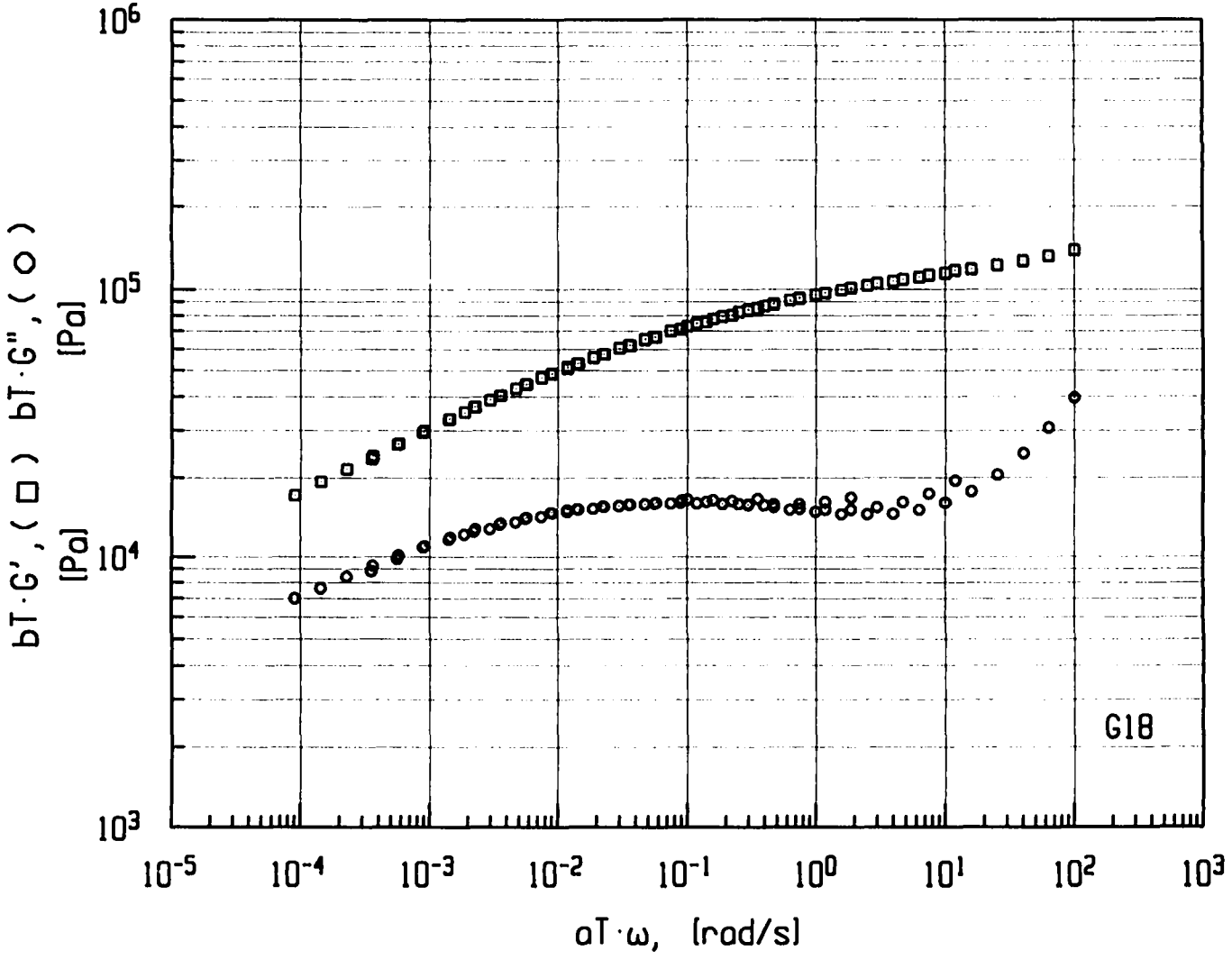


Figure AFTSG18. Master curve - sample G18.



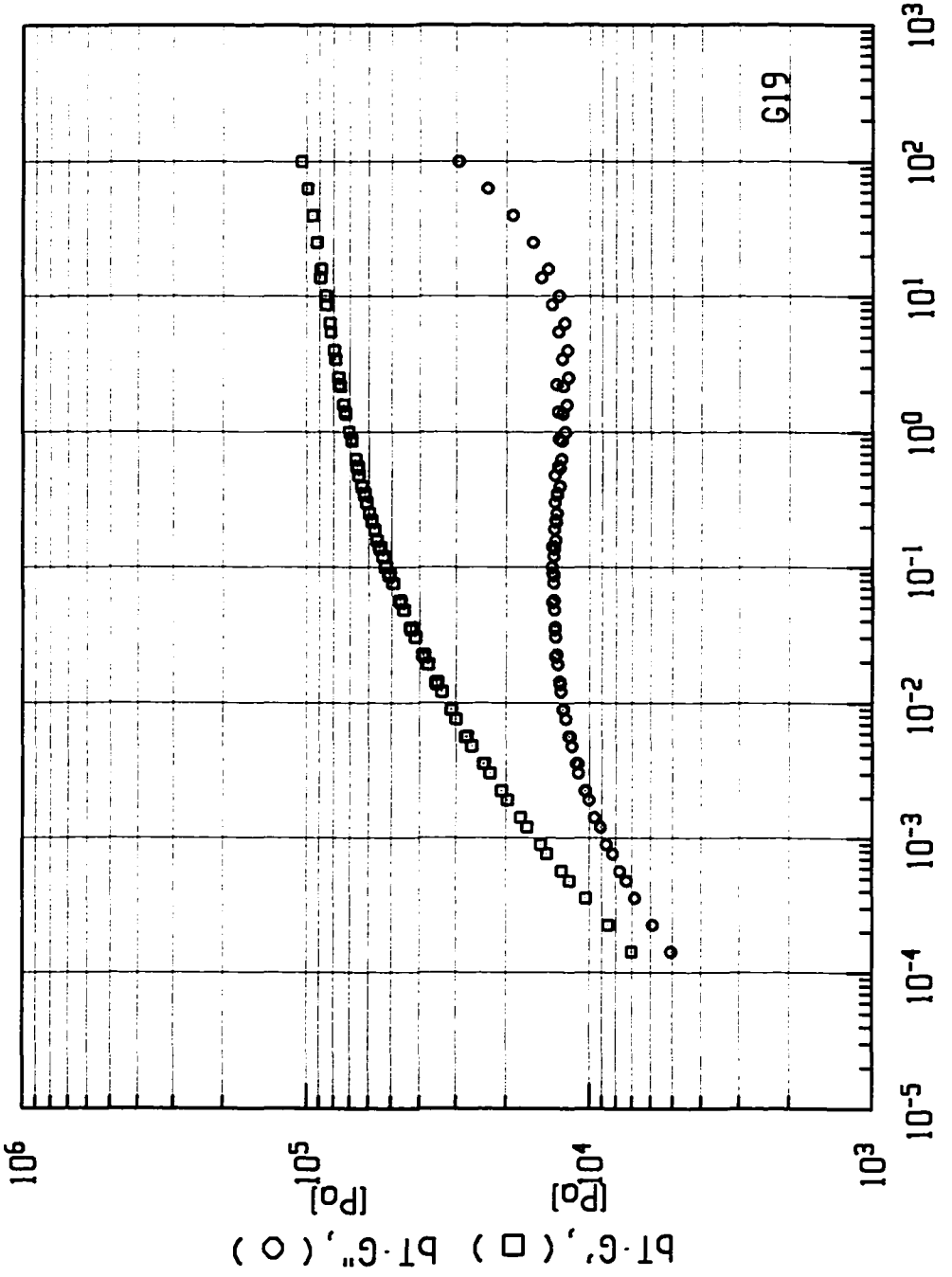


Figure AFTSG19. Master curve - sample G19.

Figure AFTSG20. Master curve - sample G20.

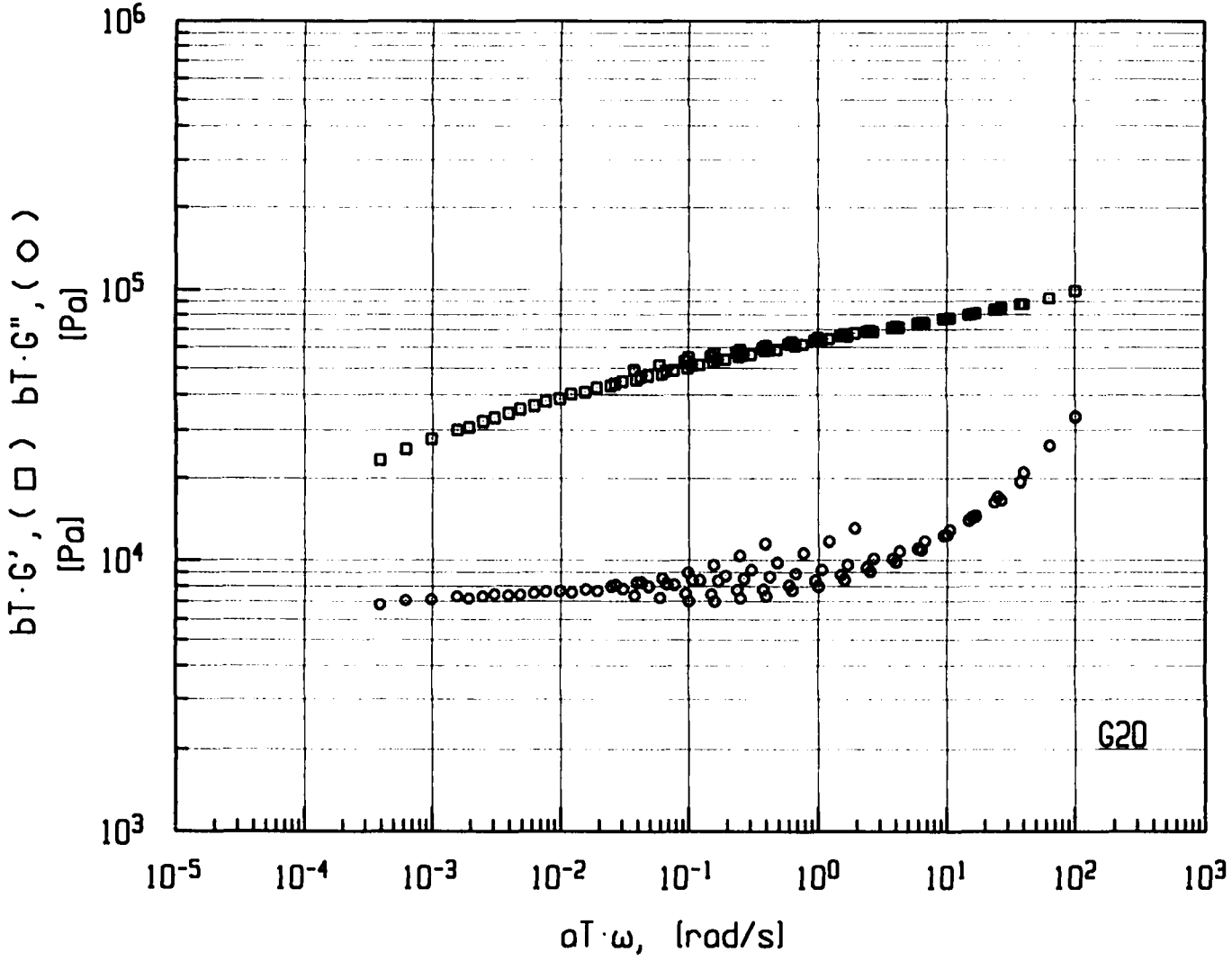


Figure AFTSG21. Master curve - sample G21.

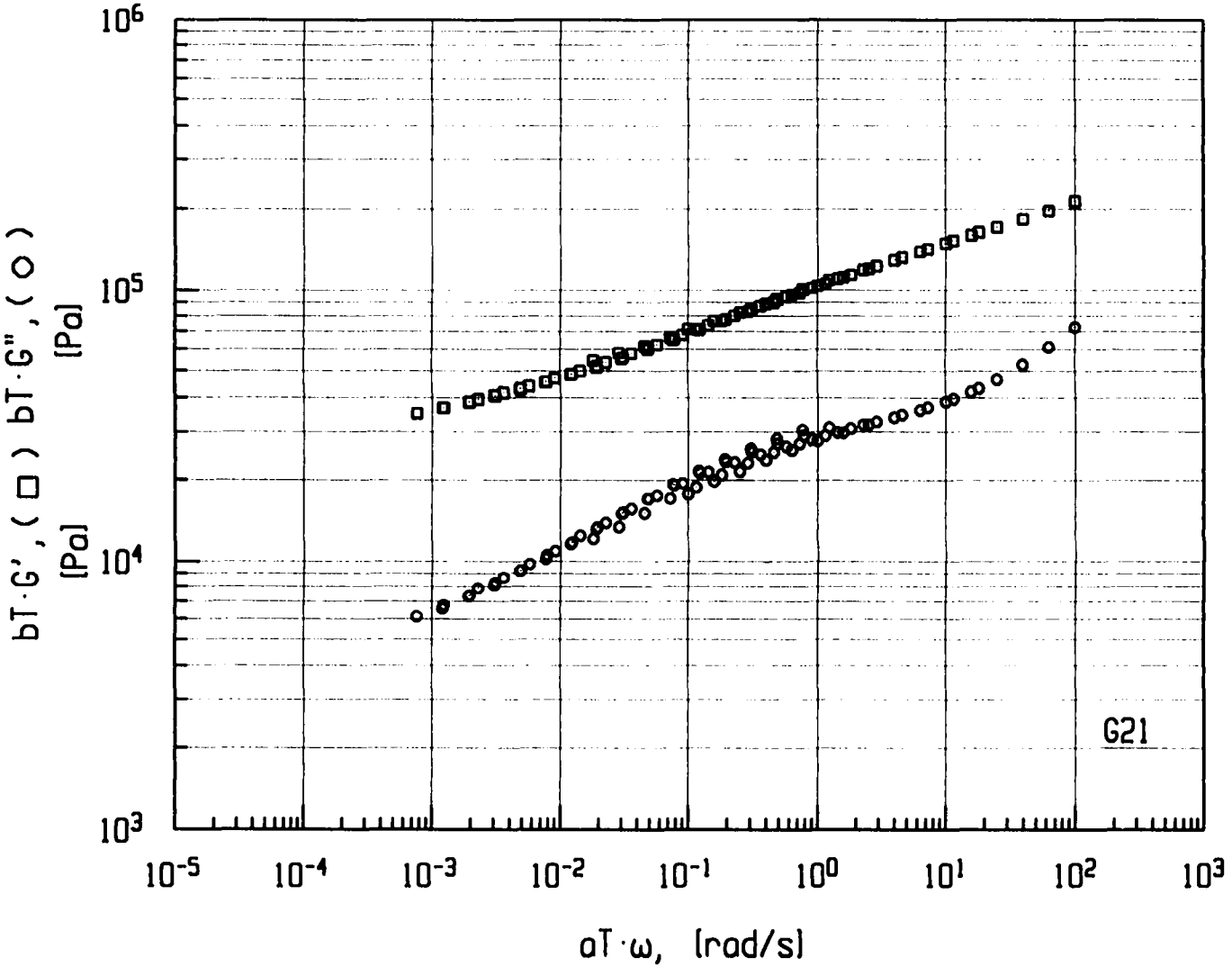
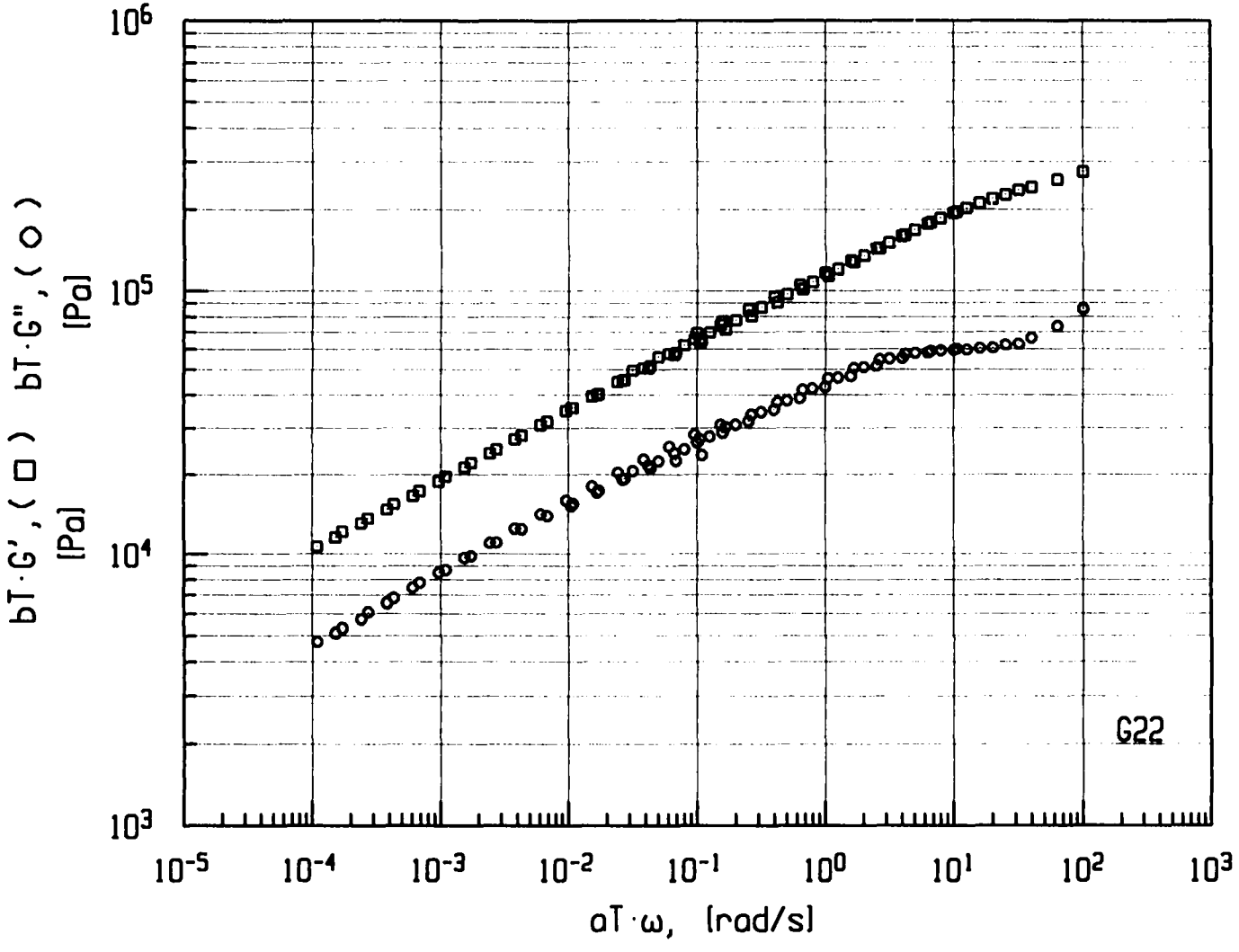


Figure AFTSG22. Master curve - sample G22.



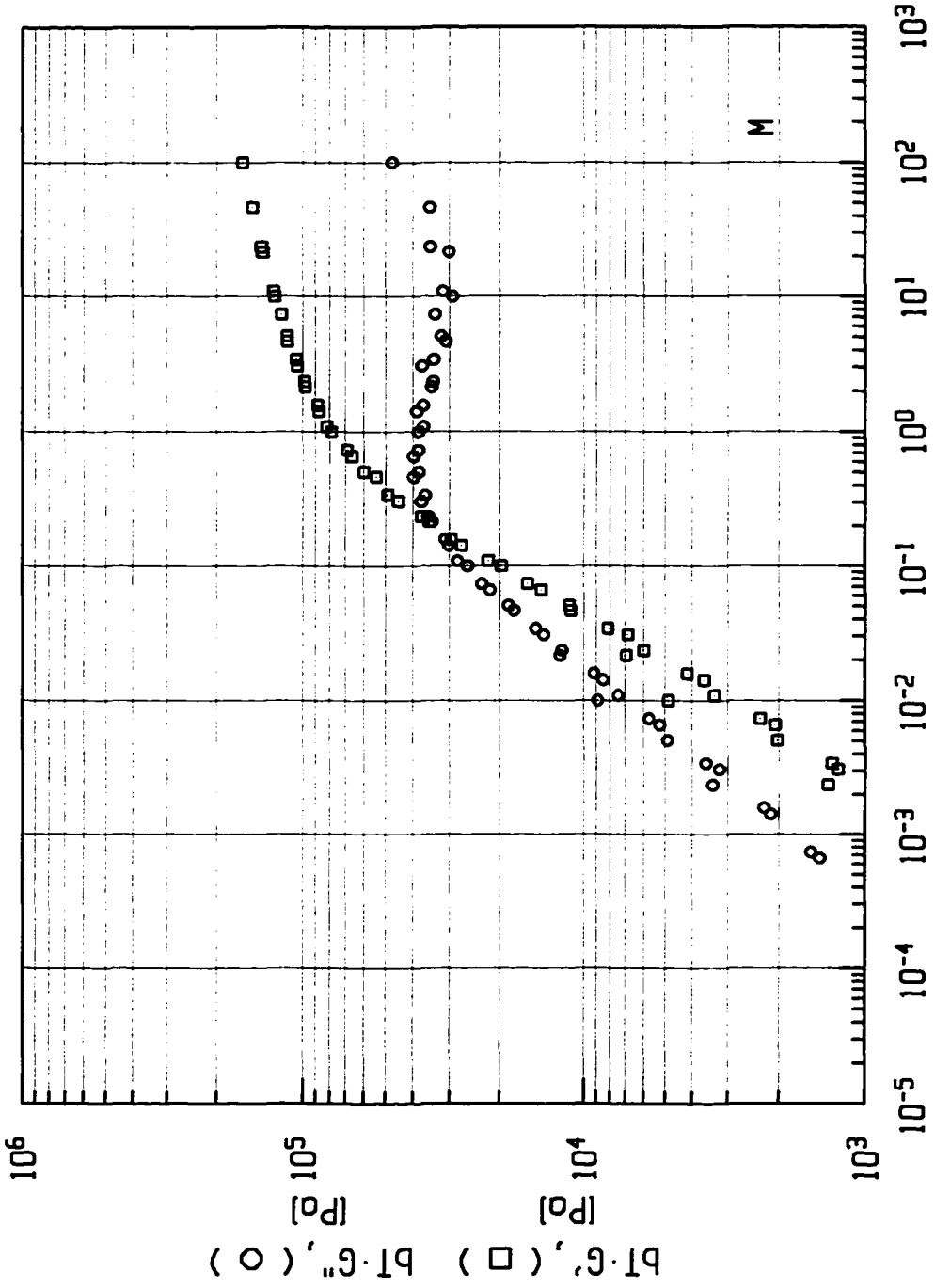


Figure AFTSM. Master curve - sample M.

Figure A8B10. Dynamic thermo-mechanical spectrum for sample B10 - {DTMA}.

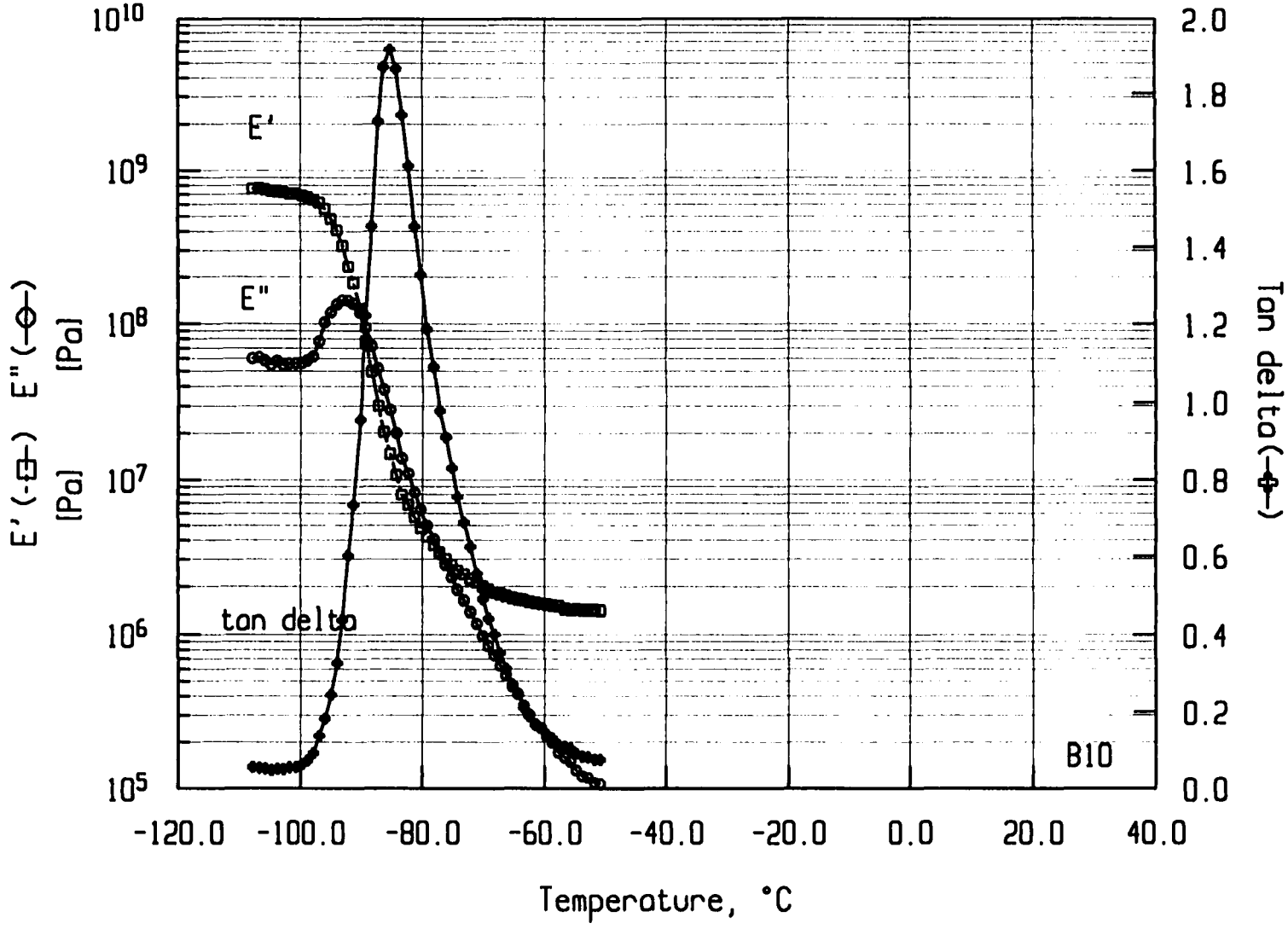


Figure A8C. Dynamic thermo-mechanical spectrum for sample C - {DTMA}.

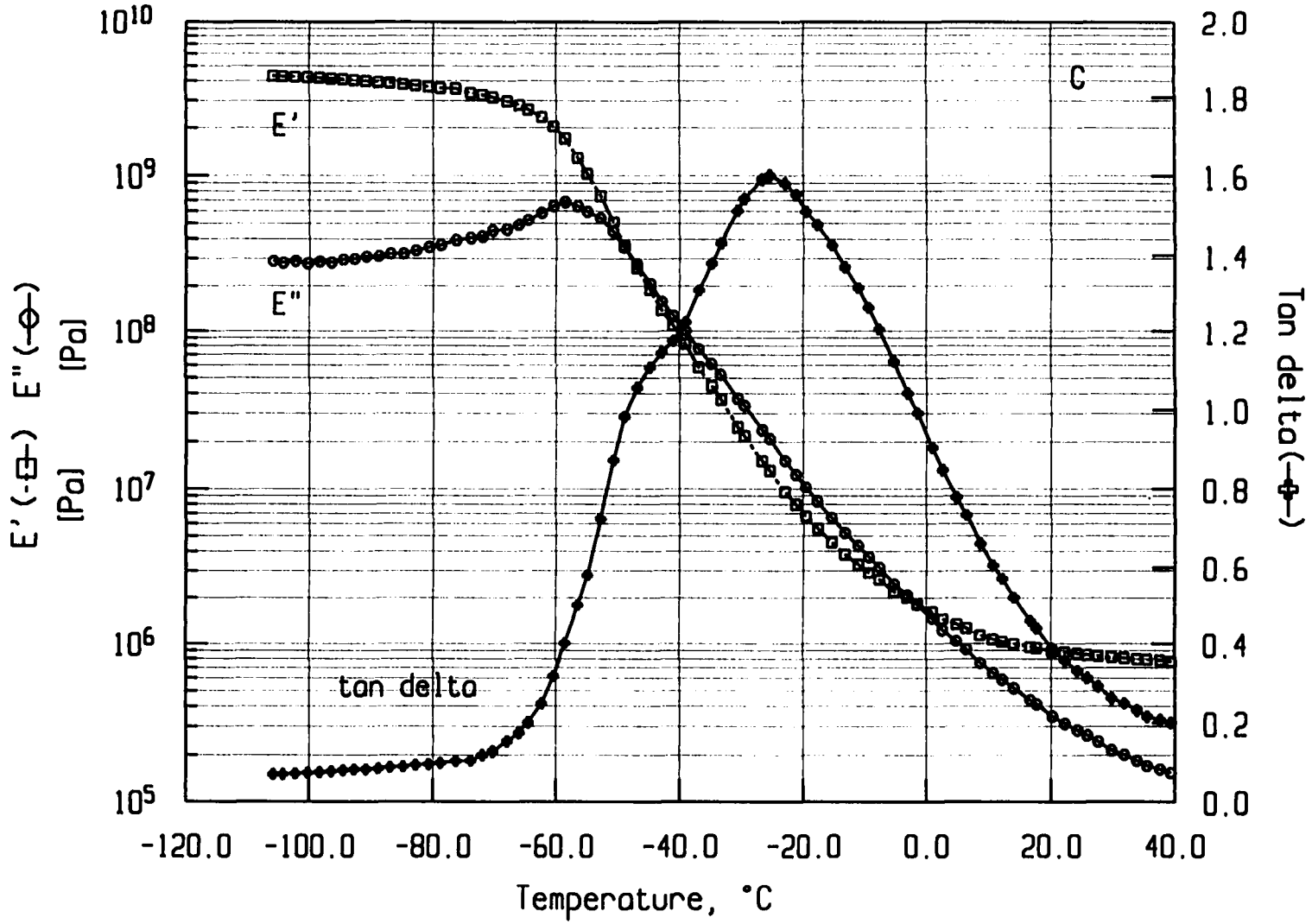


Figure A8G2. Dynamic thermo-mechanical spectrum for sample G2 - {DTMA}.

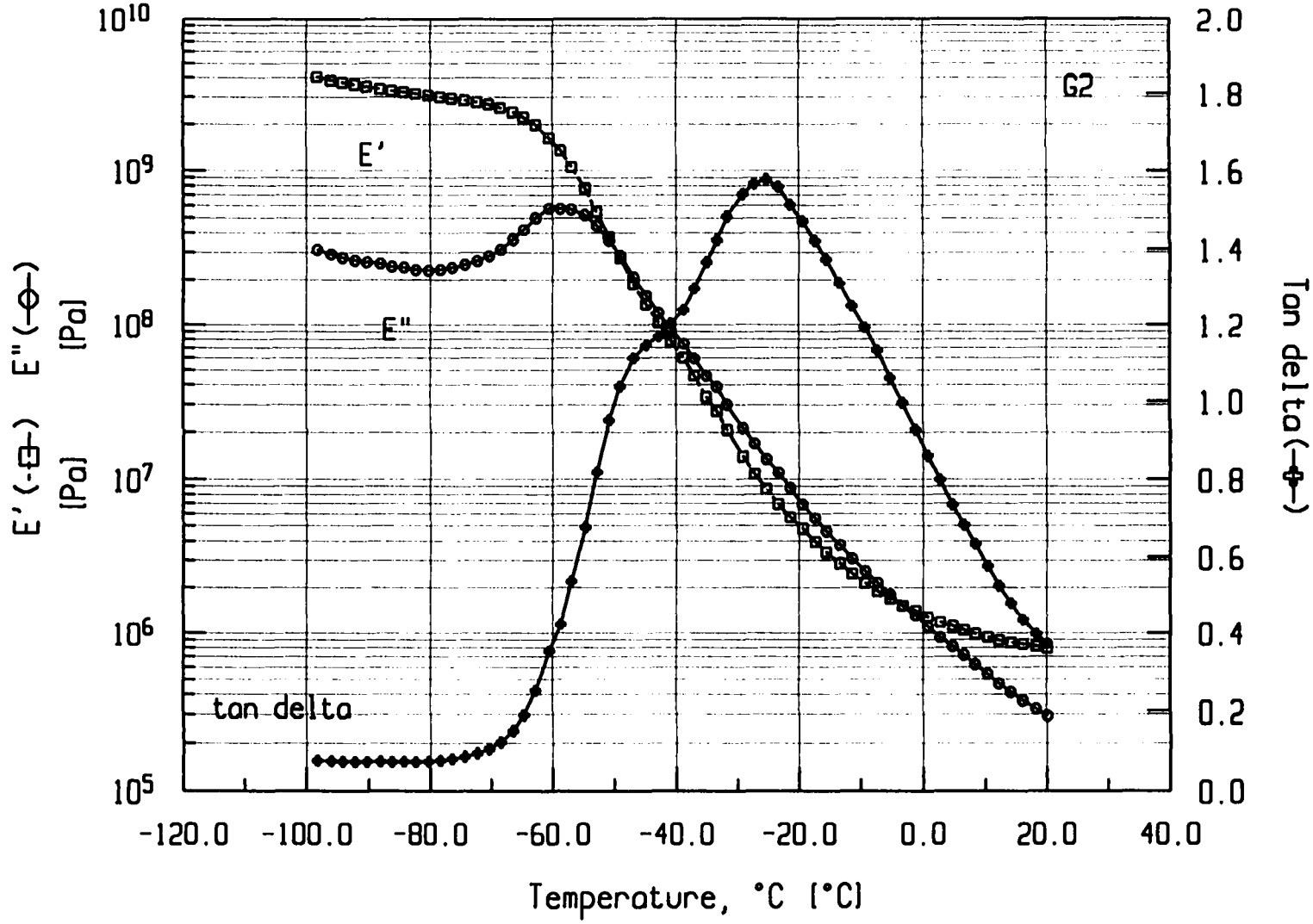


Figure A8G3. Dynamic thermo-mechanical spectrum for sample G3 - {DTMA}.

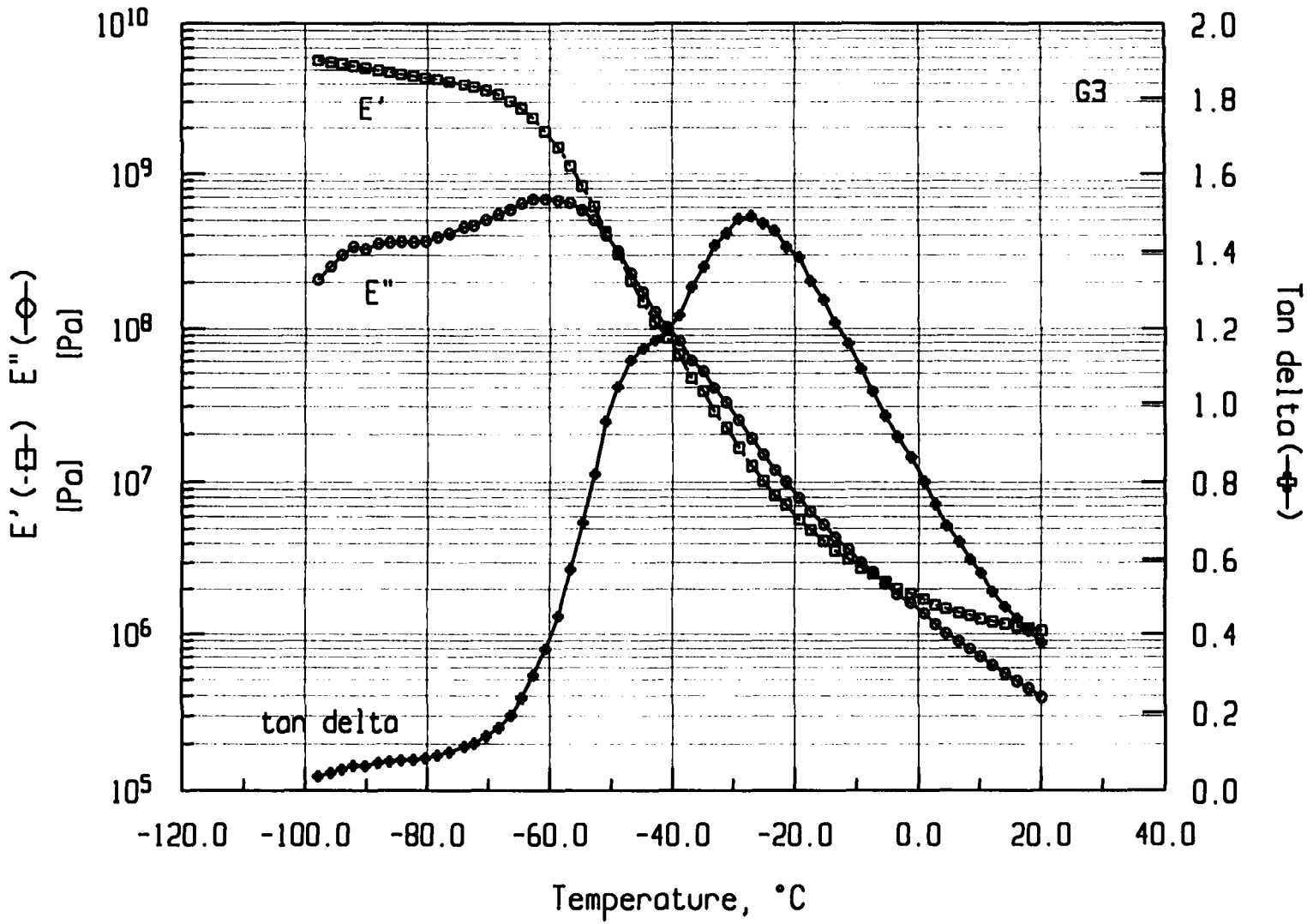


Figure A8G6. Dynamic thermo-mechanical spectrum for sample G6 - {DTMA}.

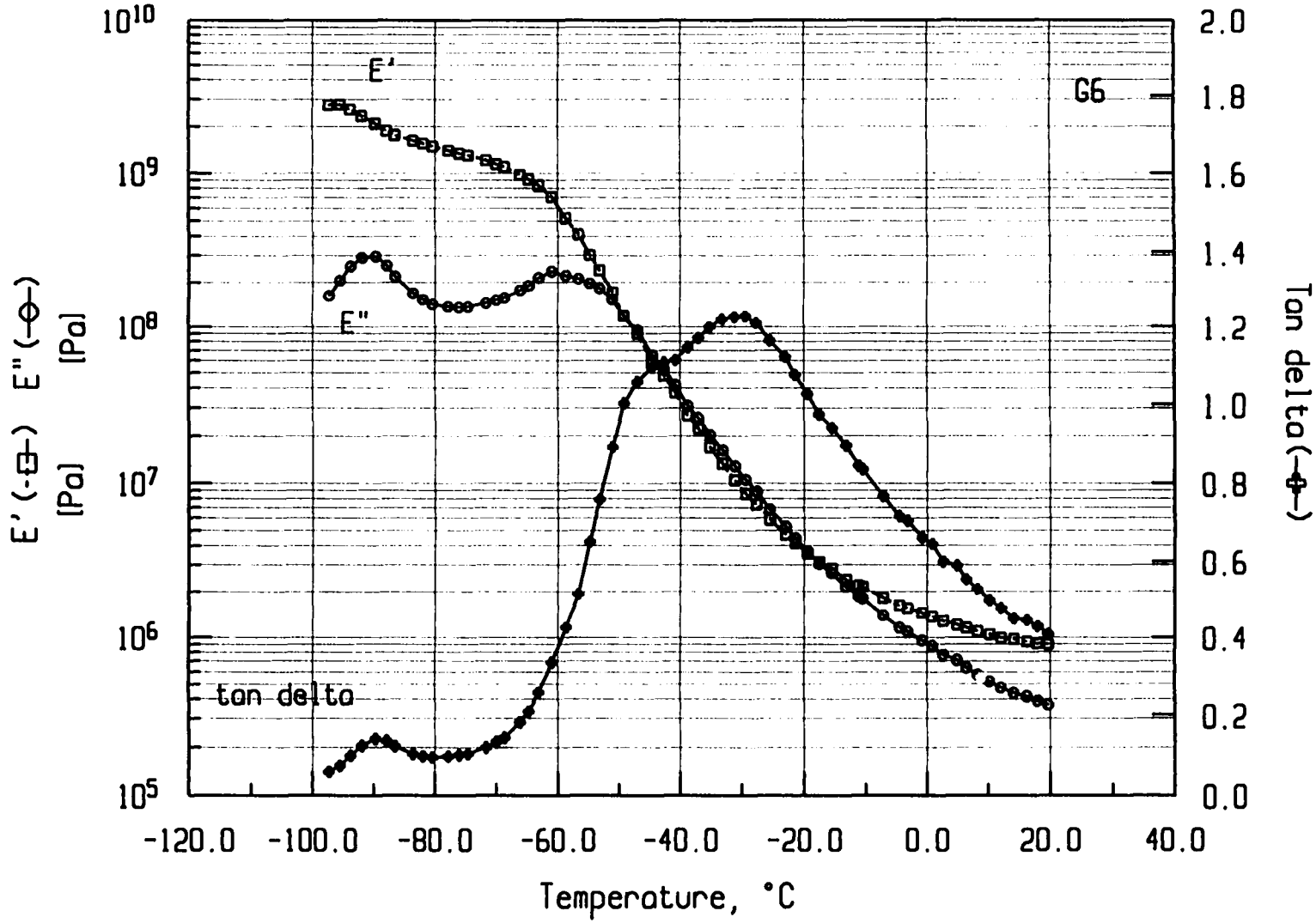


Figure A8G16. Dynamic thermo-mechanical spectrum for sample G16 - {DTMA}.

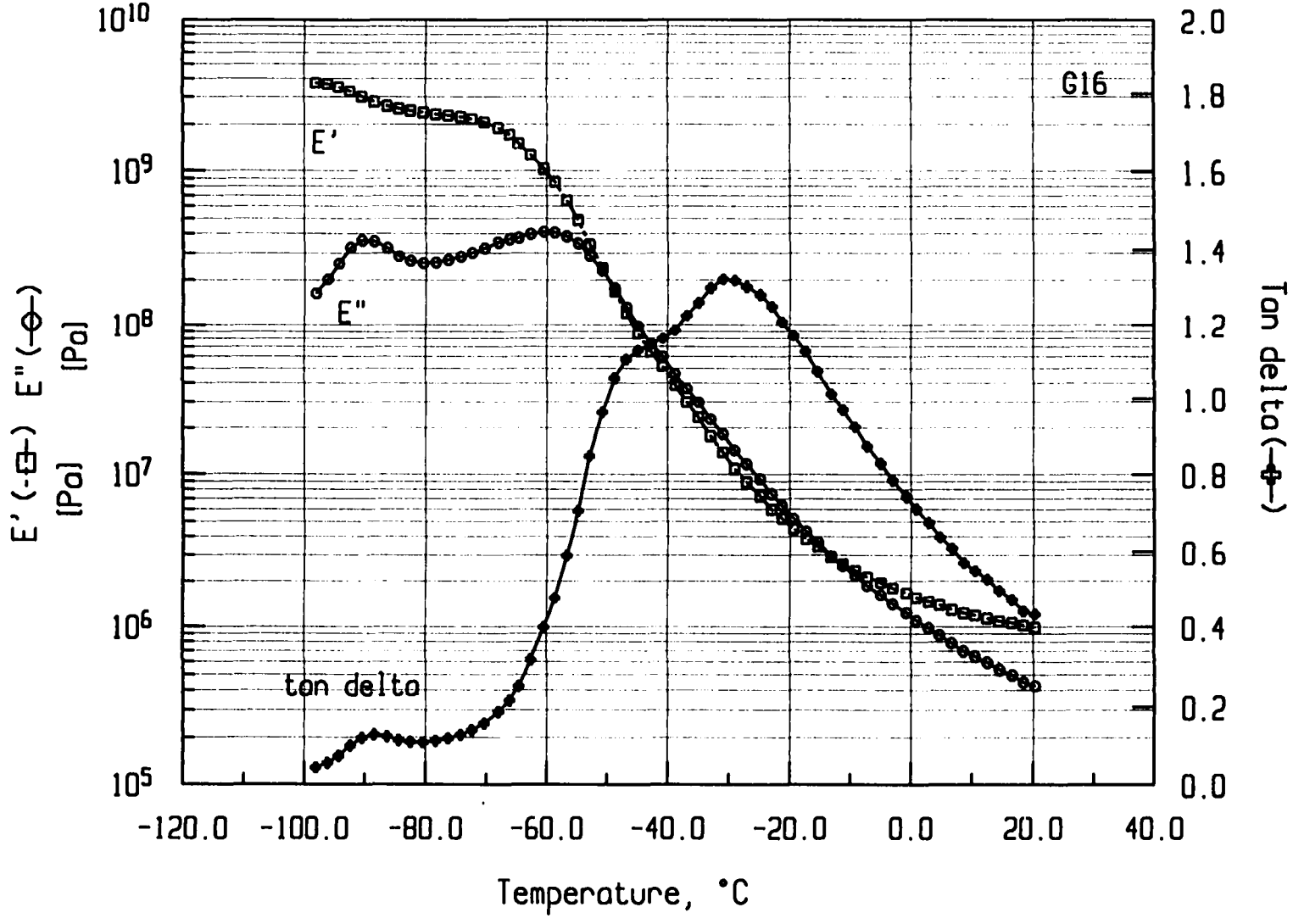


Figure A8G22. Dynamic thermo-mechanical spectrum for sample G22 - {DTMA}.

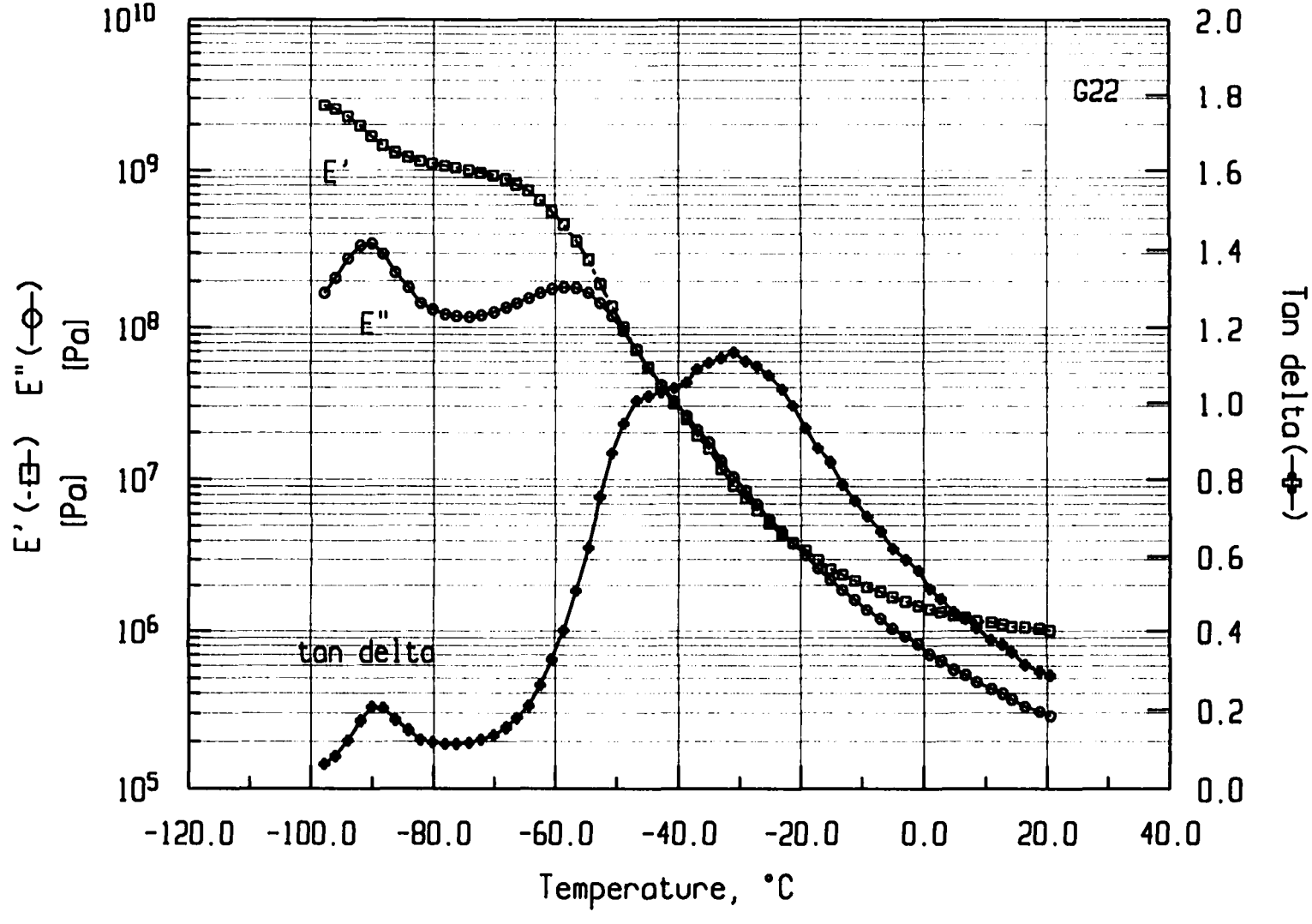


Figure A61. Prediction profiles for correlations between structural (M_p^b, N_g^p) and {FS5dec} viscoelastic parameters - I.

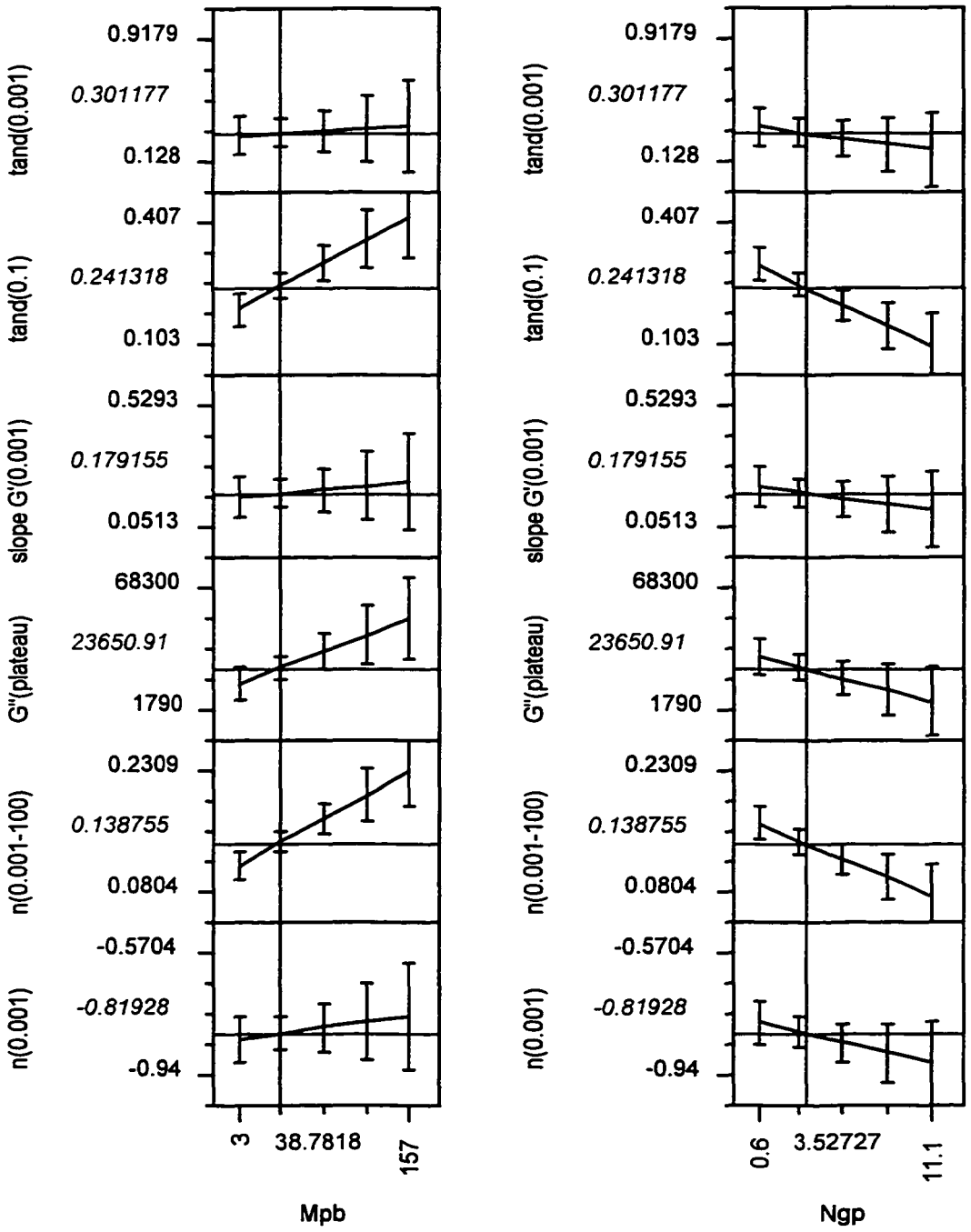


Figure A62. Prediction profiles for correlations between structural ($w^{b,g}$, M_z^G) and {FS5dec} viscoelastic parameters - II.

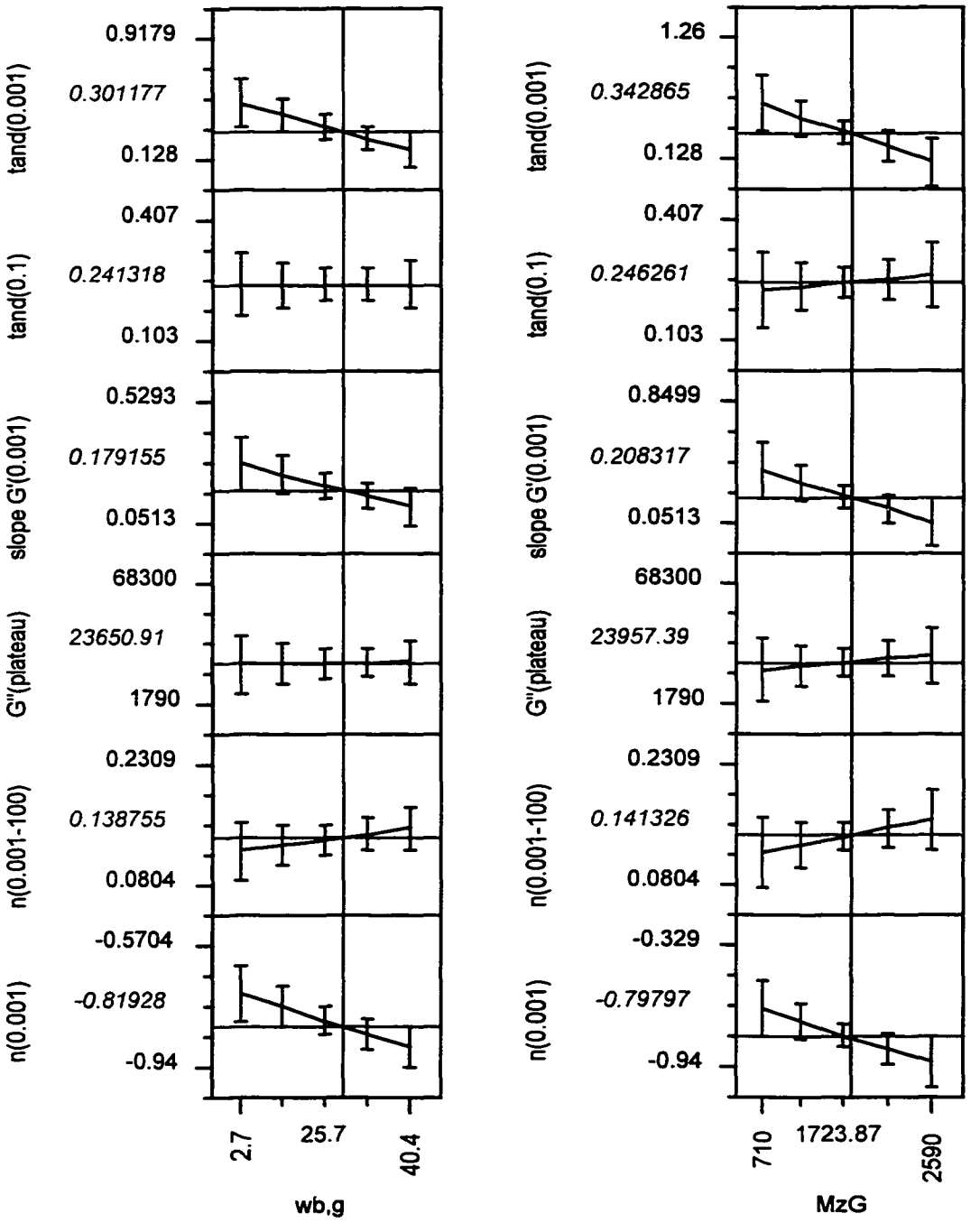


Figure A63. Prediction profiles for correlations between structural (w^b, $w^{b,h}$) and {FS5dec} viscoelastic parameters - III.

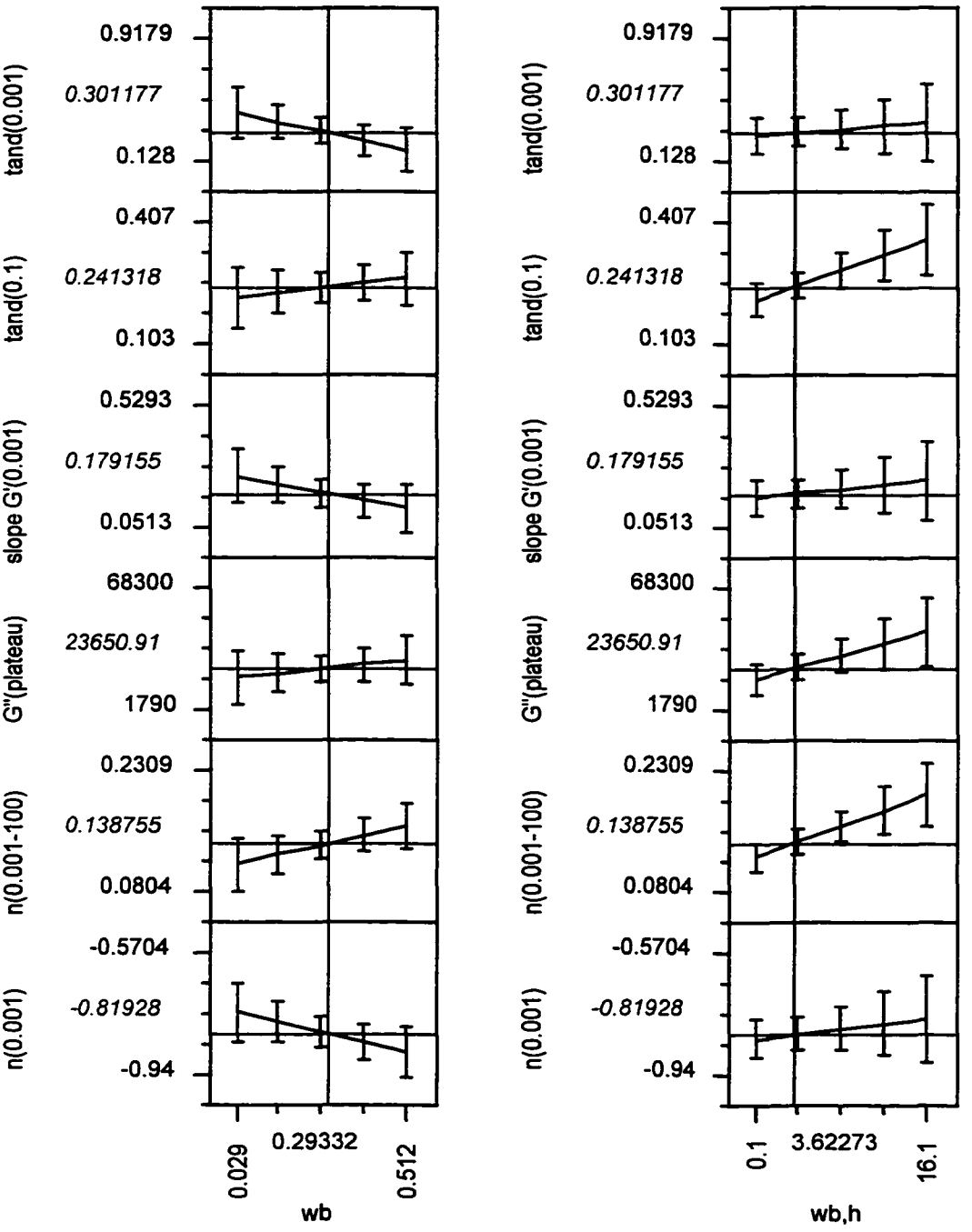


Figure A64. Prediction profiles for correlations between structural (PDI, vinyl%) and {FS5dec} viscoelastic parameters - IV.

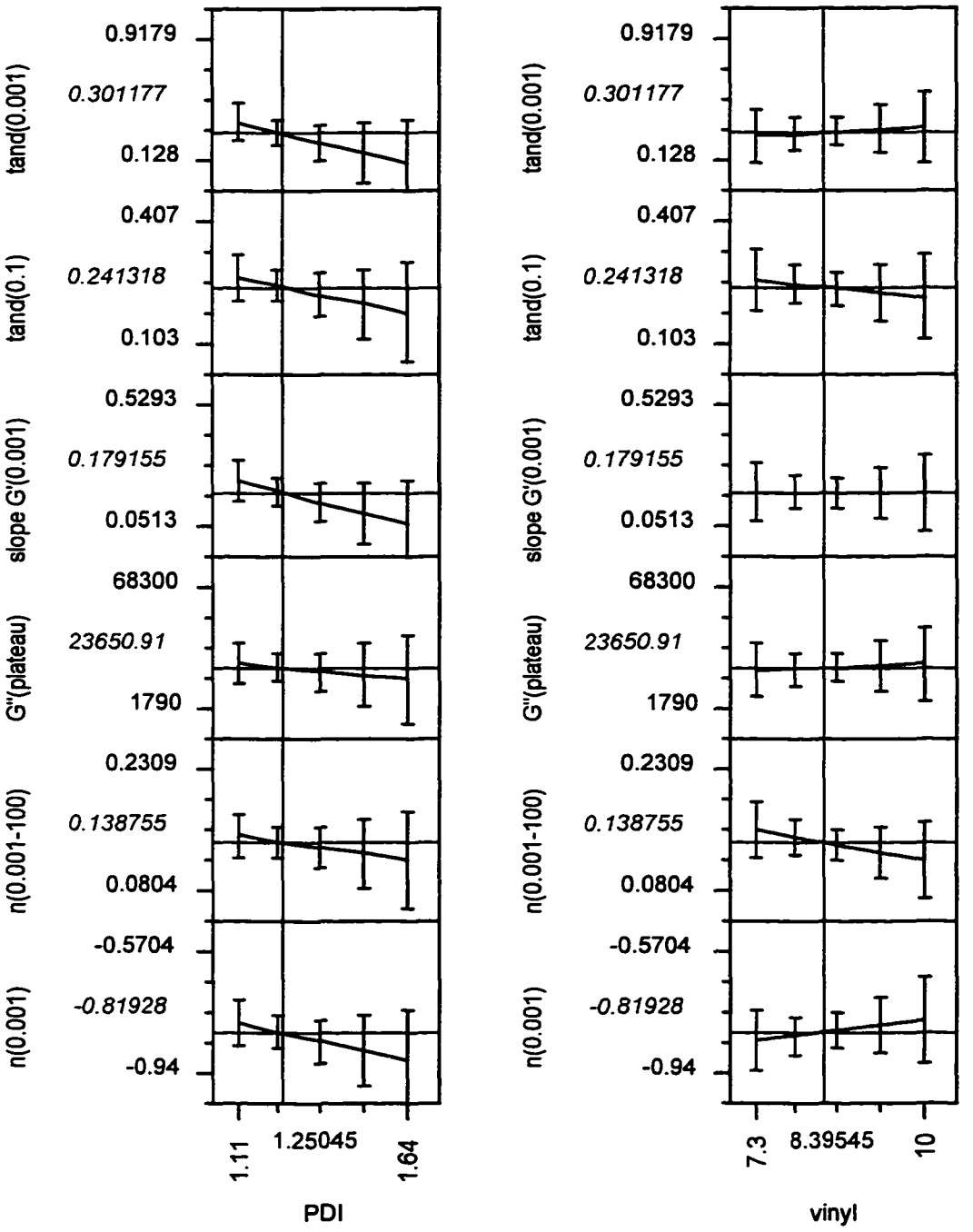


Figure A65. Prediction profiles for correlations between structural (M_p^b, N_g^p) and stress relaxation {SR10,000} parameters.

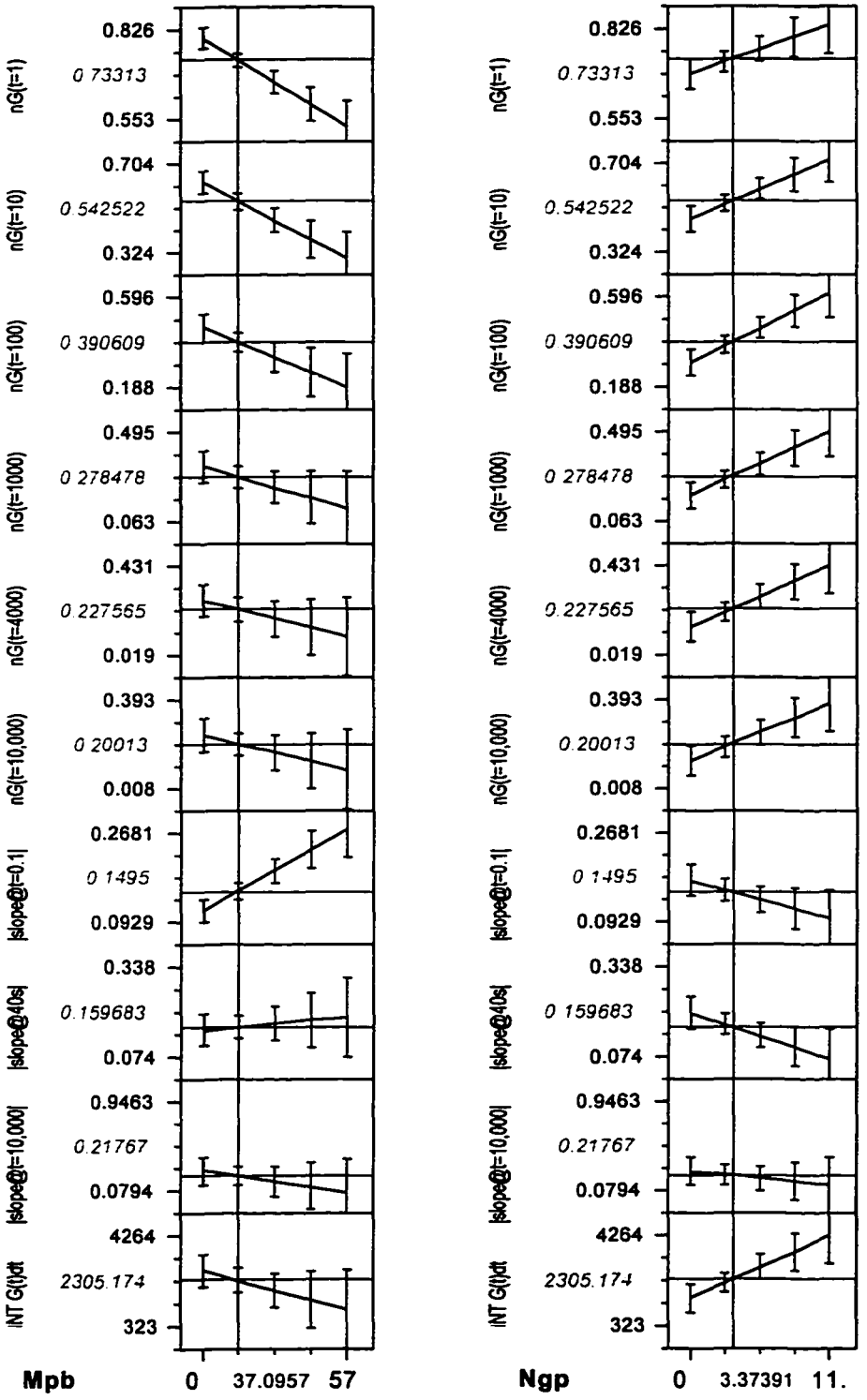


Figure A66. Prediction profiles for correlations between structural ($w^{b,g}$, $w^{b,h}$) and stress relaxation {SR10,000} parameters.

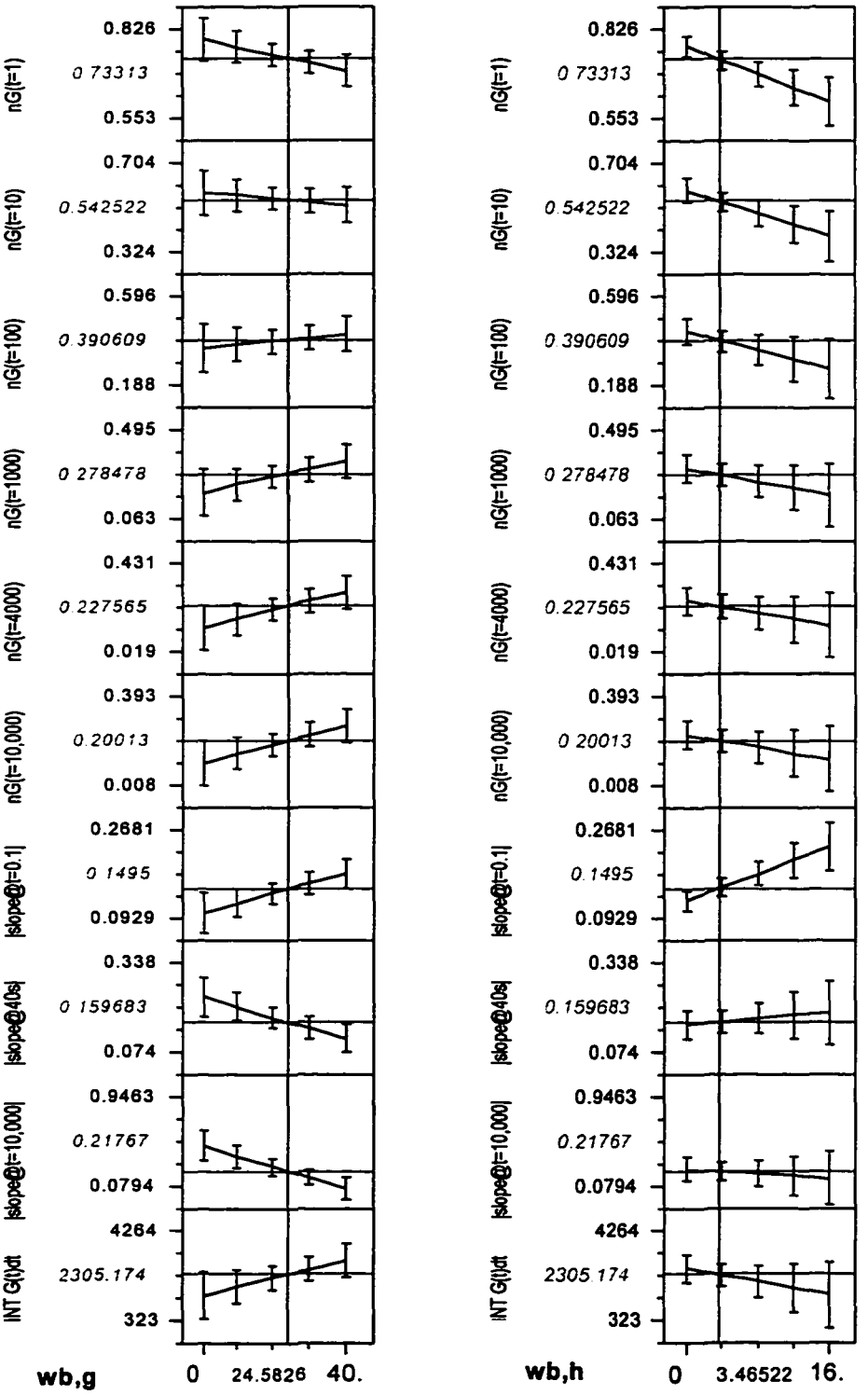


Figure A67. Prediction profiles for correlations between structural (w^b, M_z^G) and stress relaxation {SR10,000} parameters.

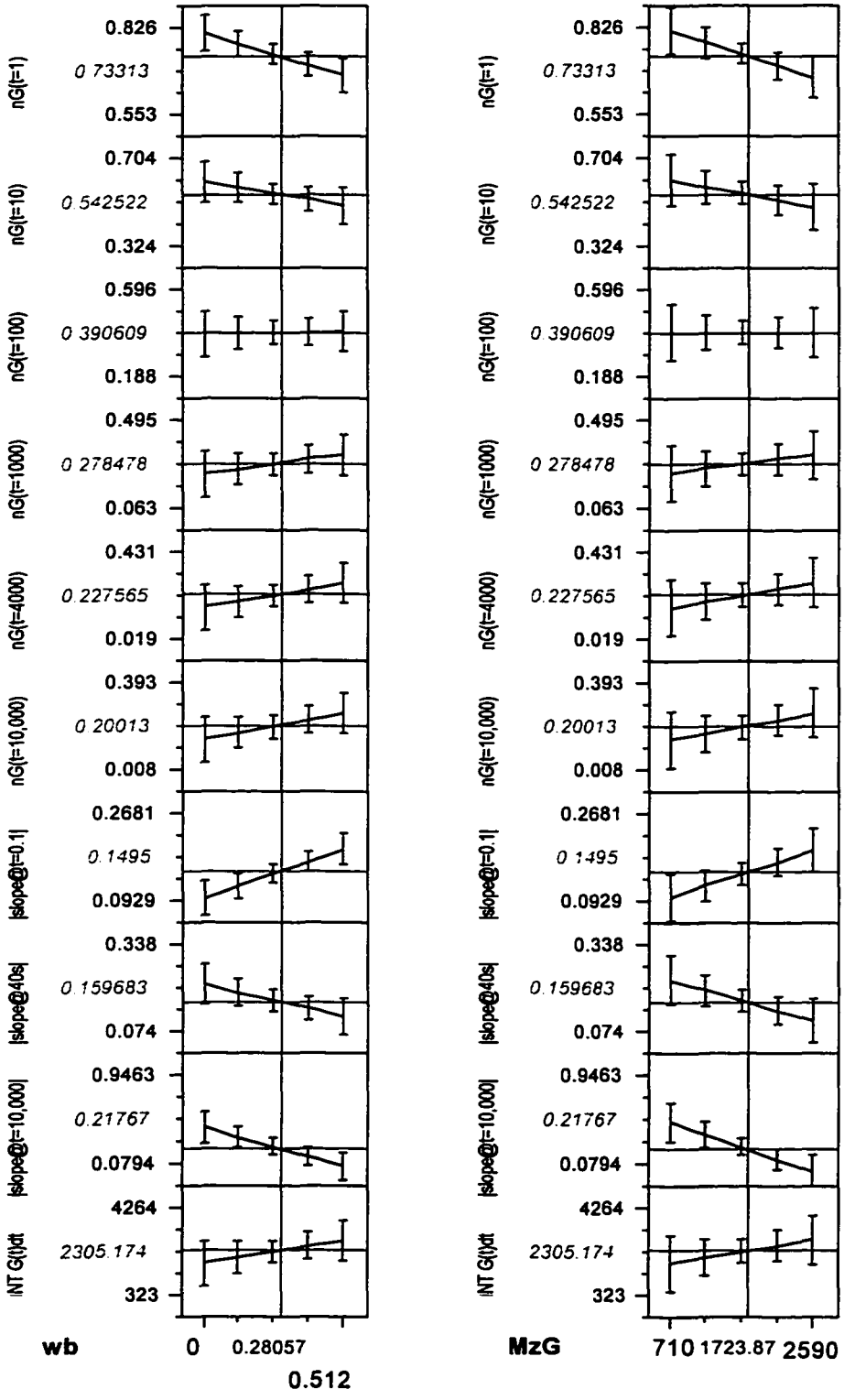


Figure A71a,b,c,d. **Prediction profiles - M_p^b, N_g^p, $w^{b,g}$, w^b and {SSWP2} parameters.**

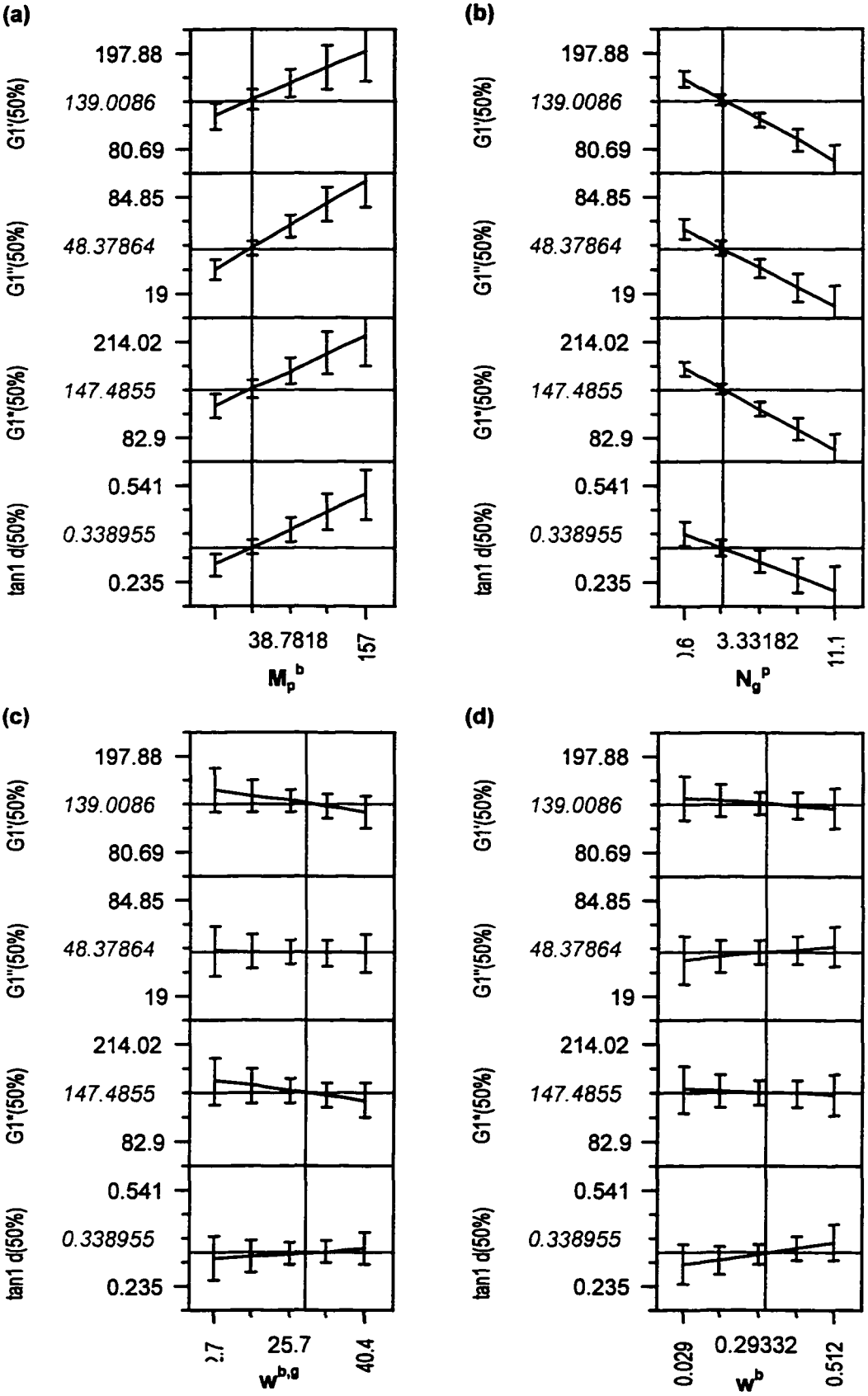


Figure A71e,f,g,h. **Prediction profiles - M_z^G, $w^{b,h}$, PDI, vinyl% & {SSWP2} parameters.**

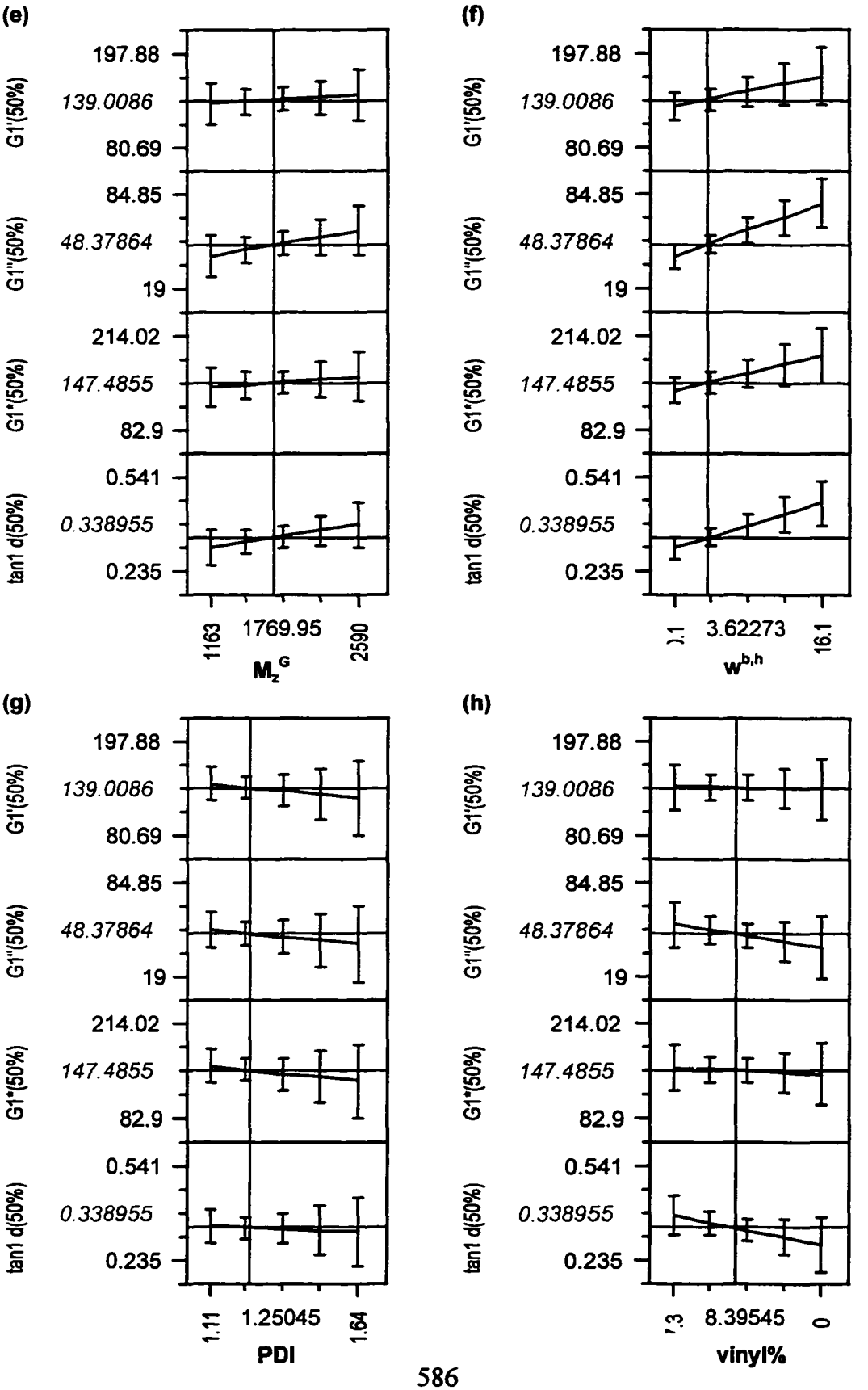


Figure A72a. Prediction profiles for correlations between structural parameters (M_p^b, N_g^p) and viscoelastic parameters from {FSWP3} experiments.

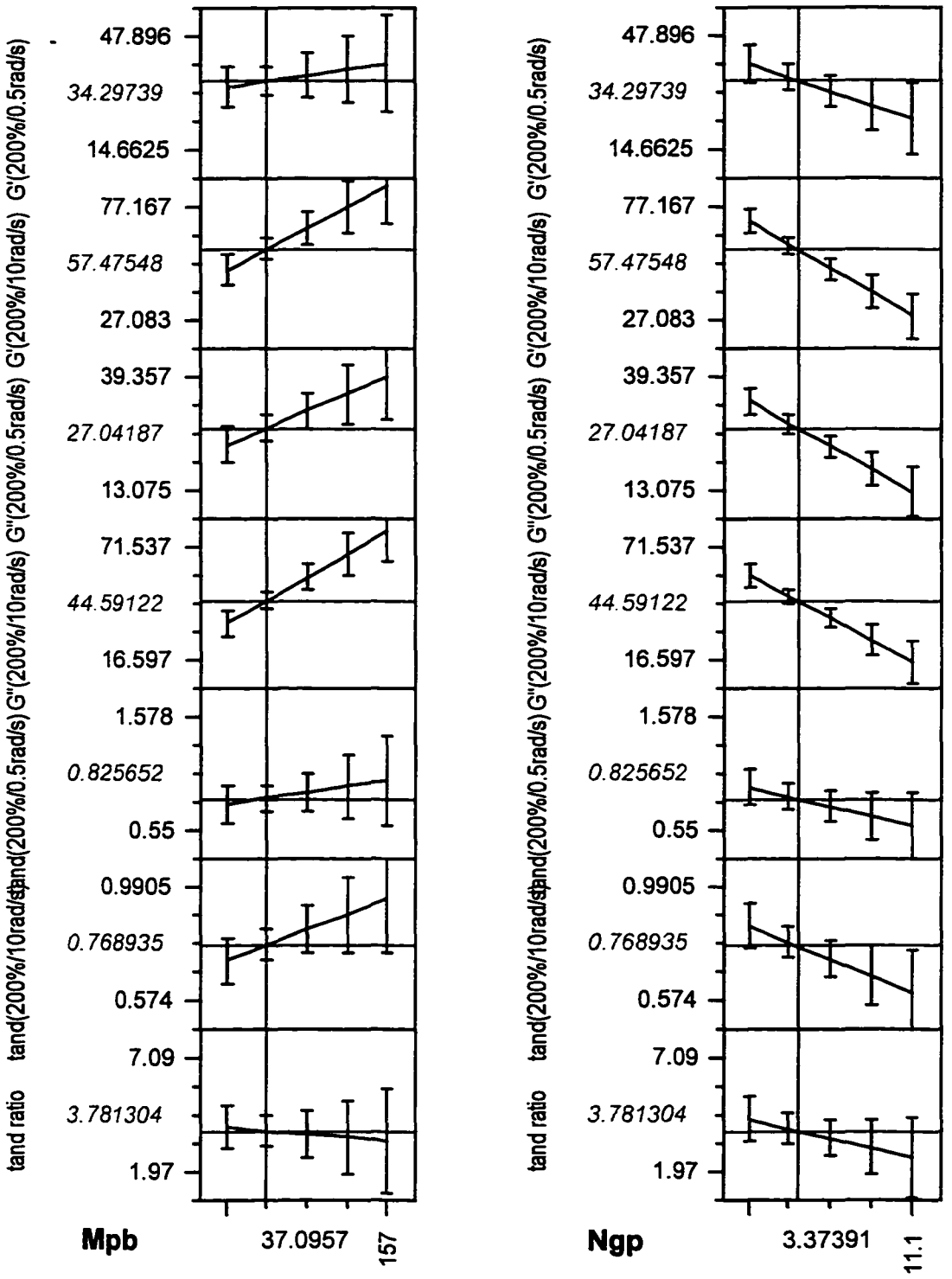


Figure A72b. Prediction profiles for correlations between structural parameters ($w^{b,g}$, w^{b}) and viscoelastic parameters from {FSWP3} experiments.

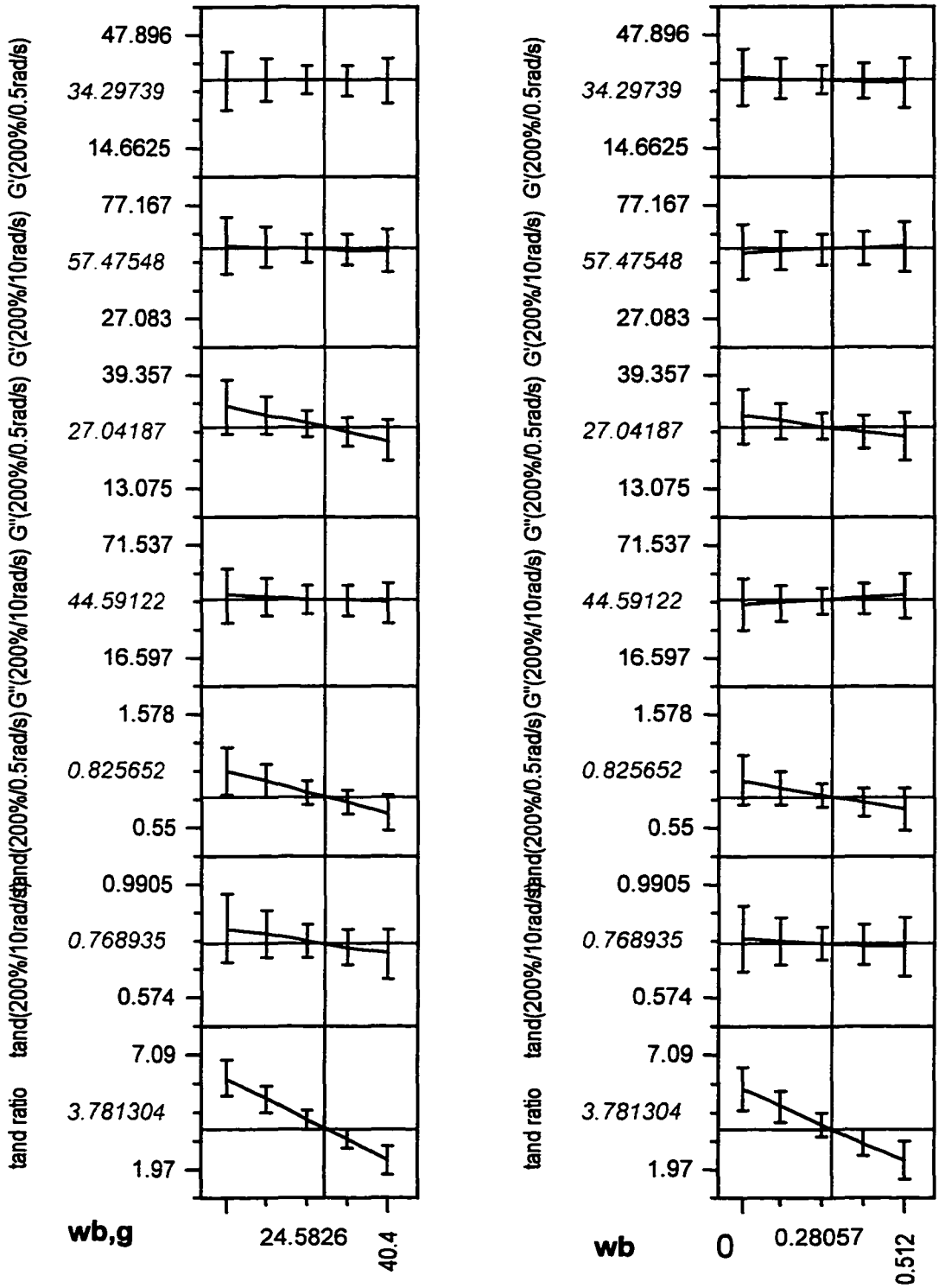


Figure A72c. Prediction profiles for correlations between structural parameters ($w^{b,h}$, M_z^G) and viscoelastic parameters from {FSWP3} experiments.

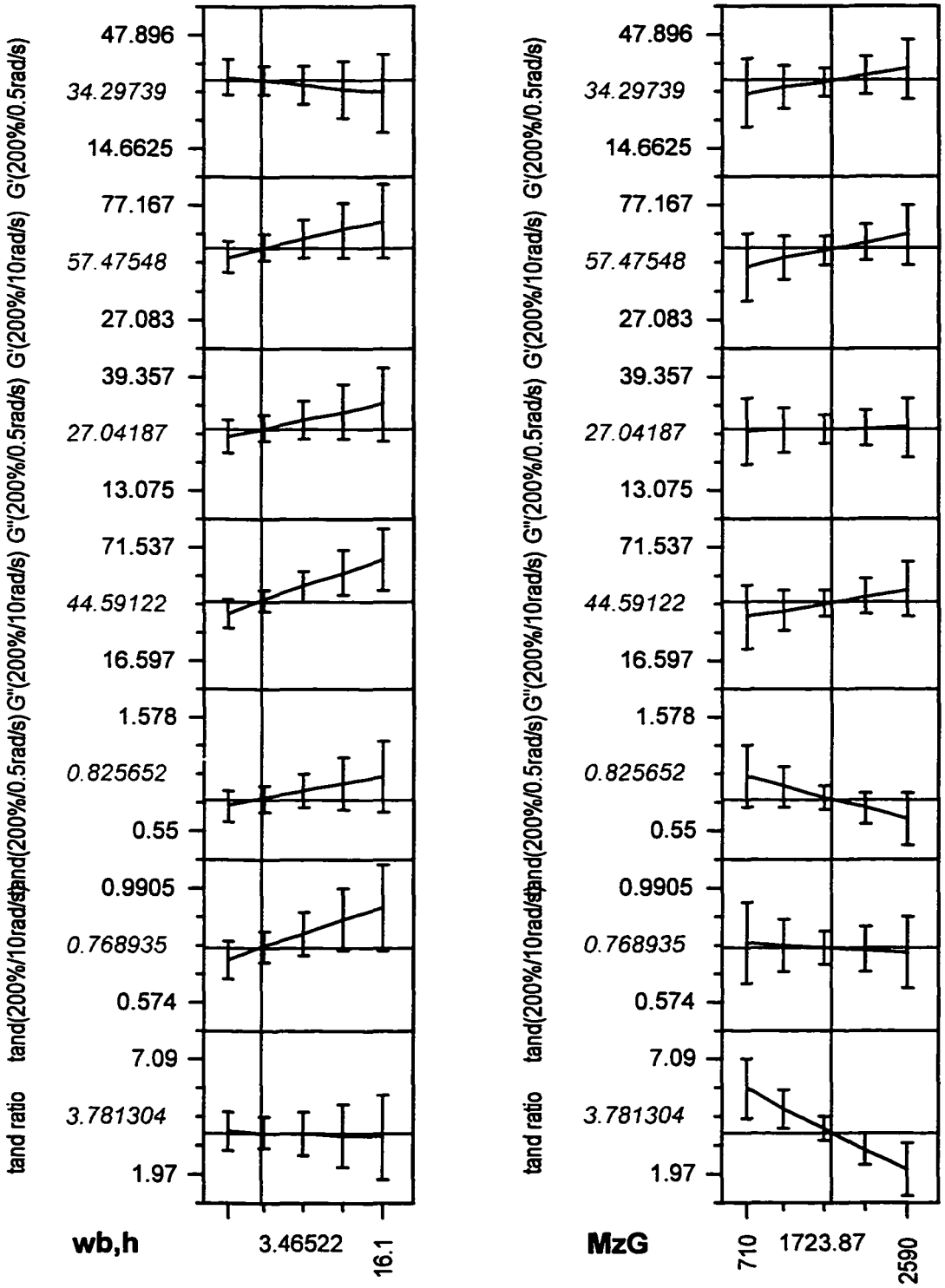


Figure A72d. Prediction profiles for correlations between structural parameters (PDI, vinyl) and viscoelastic parameters from {FSWP3} experiments.

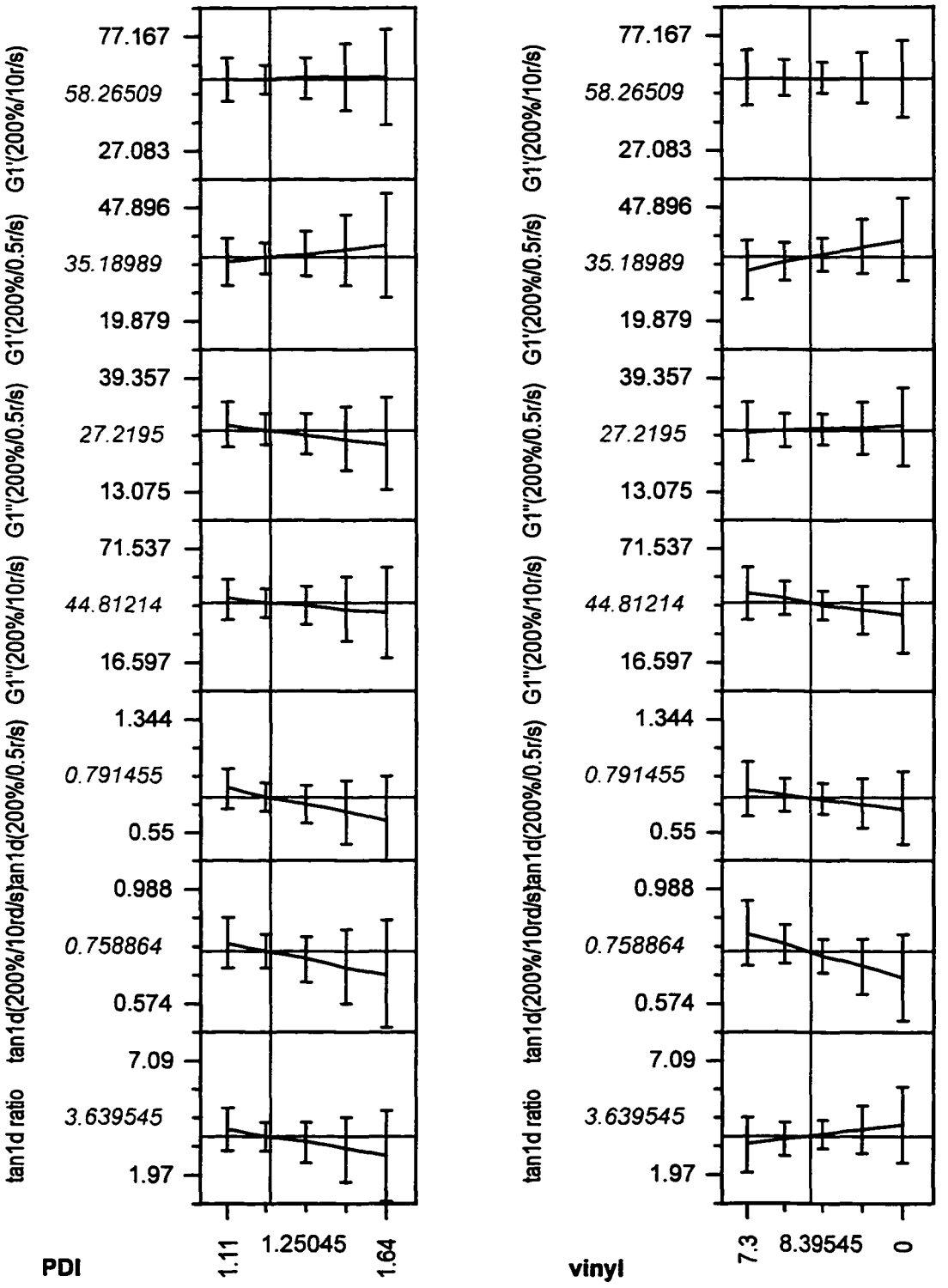


Figure A73a Prediction profiles for correlations between structural parameters (M_p^b, N_g^p) and viscoelastic parameters from {FSWP3} experiments.

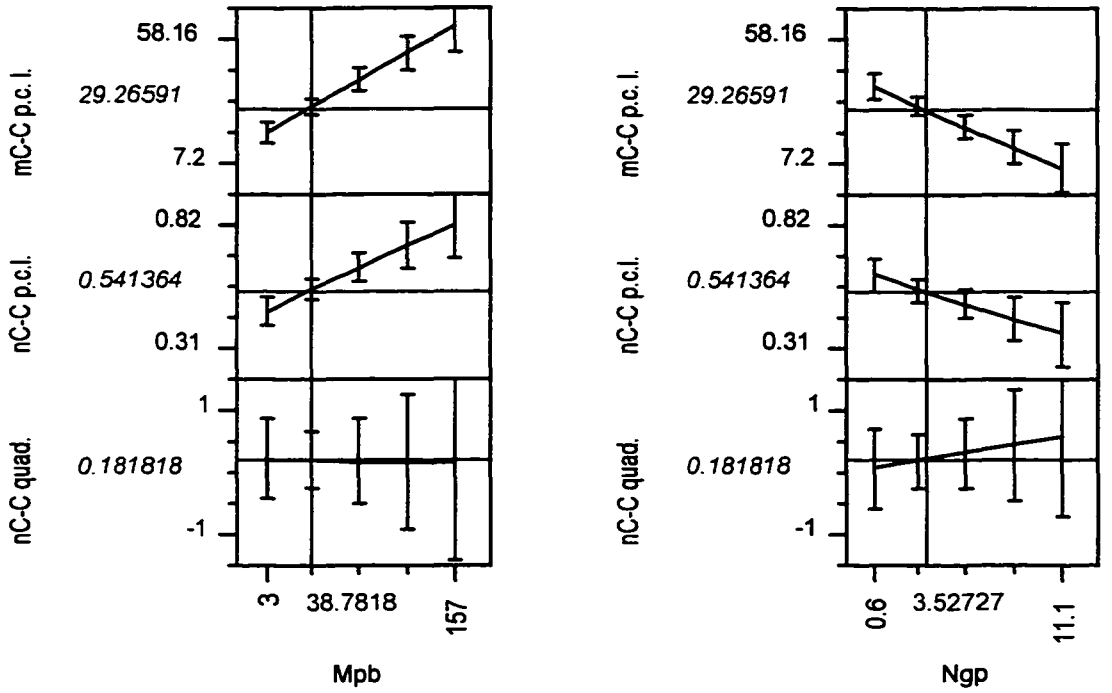


Figure A73b. Prediction profiles for correlations between structural parameters ($w^{b,g}$, w^b) and viscoelastic parameters from {FSWP3} experiments.

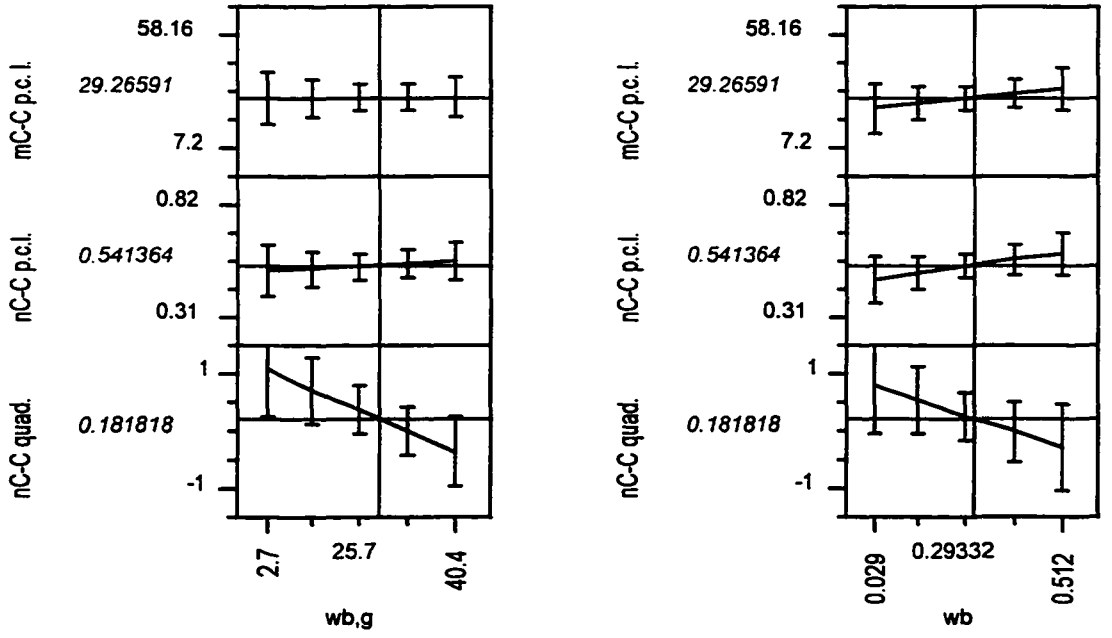


Figure A73c. Prediction profiles for correlations between structural parameters ($w^{b,h}$, M_z^G) and viscoelastic parameters from {FSWP3}experiments.

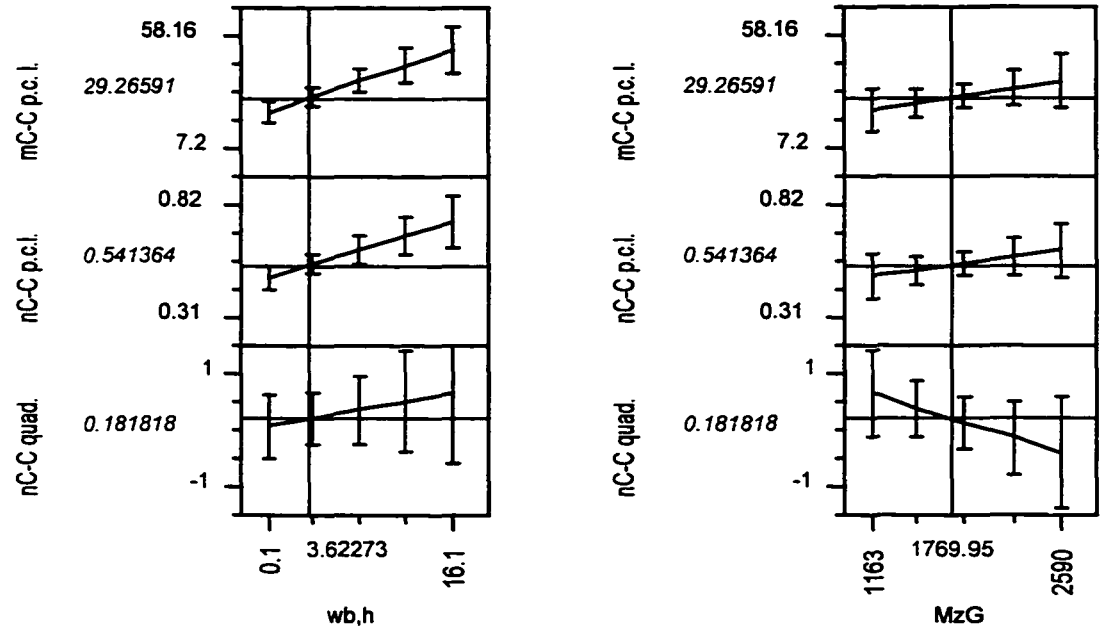


Figure A73d. Prediction profiles for correlations between structural parameters (PDI, vinyl) and viscoelastic parameters from {FSWP3}experiments.

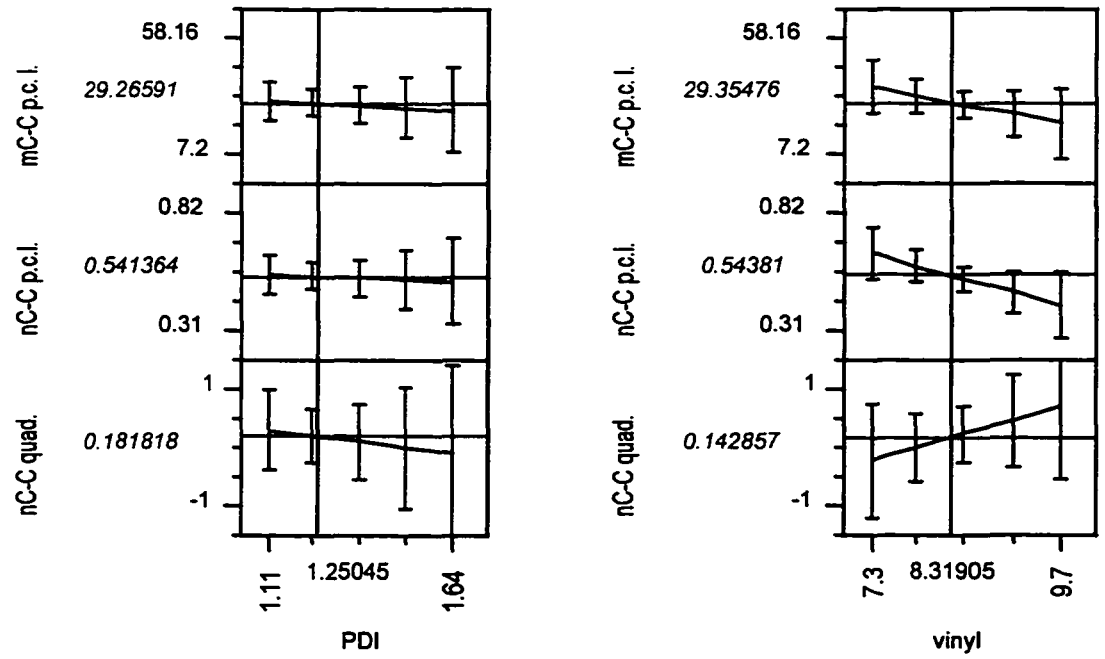


Figure A74a. Prediction profiles for correlation between structural parameter (M_p^b) and viscoelastic parameters from {HSSWP} experiments.

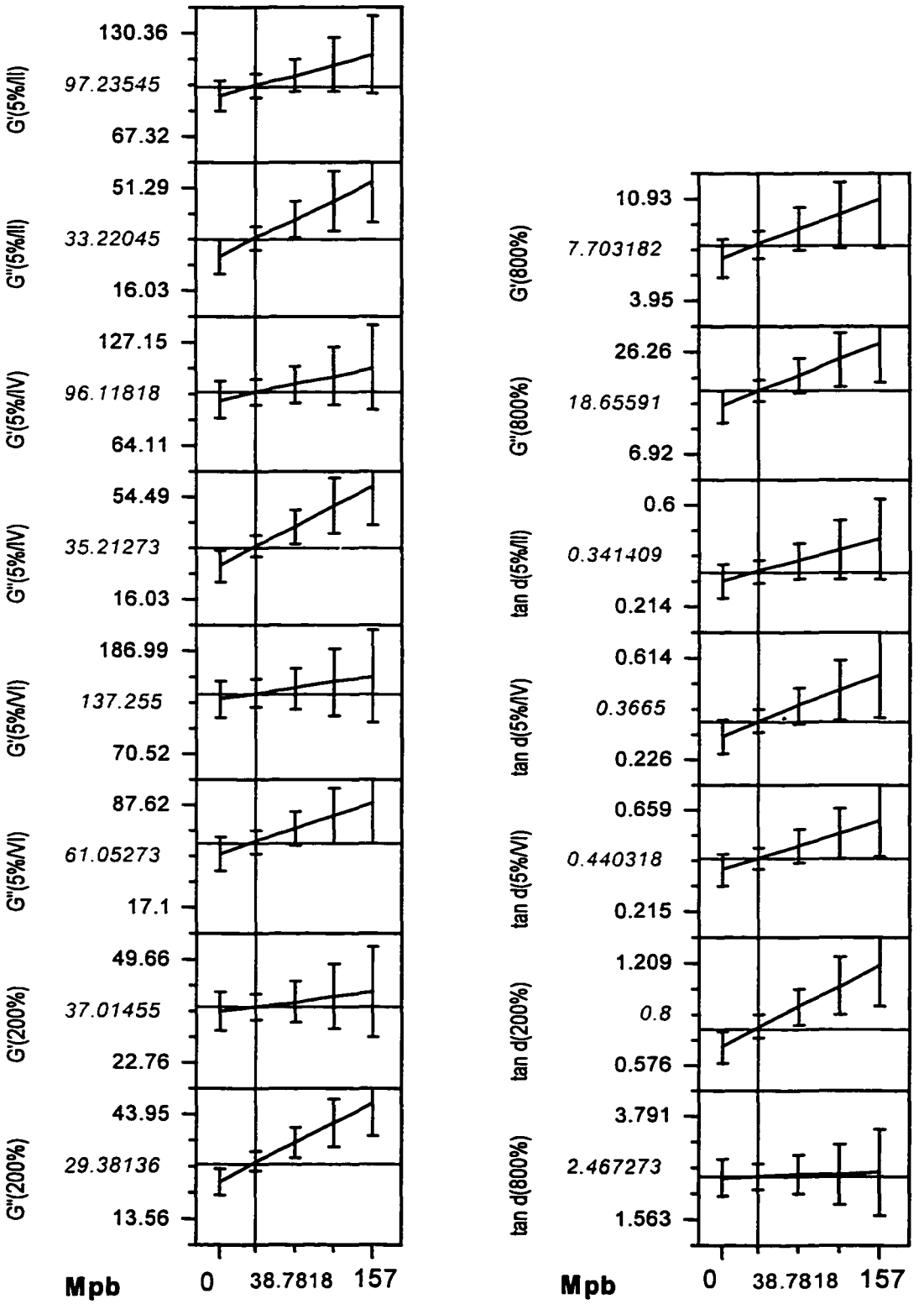


Figure A74b. Prediction profiles for correlation between structural parameter (N_g^p) and viscoelastic parameters from {HSSWP} experiments.

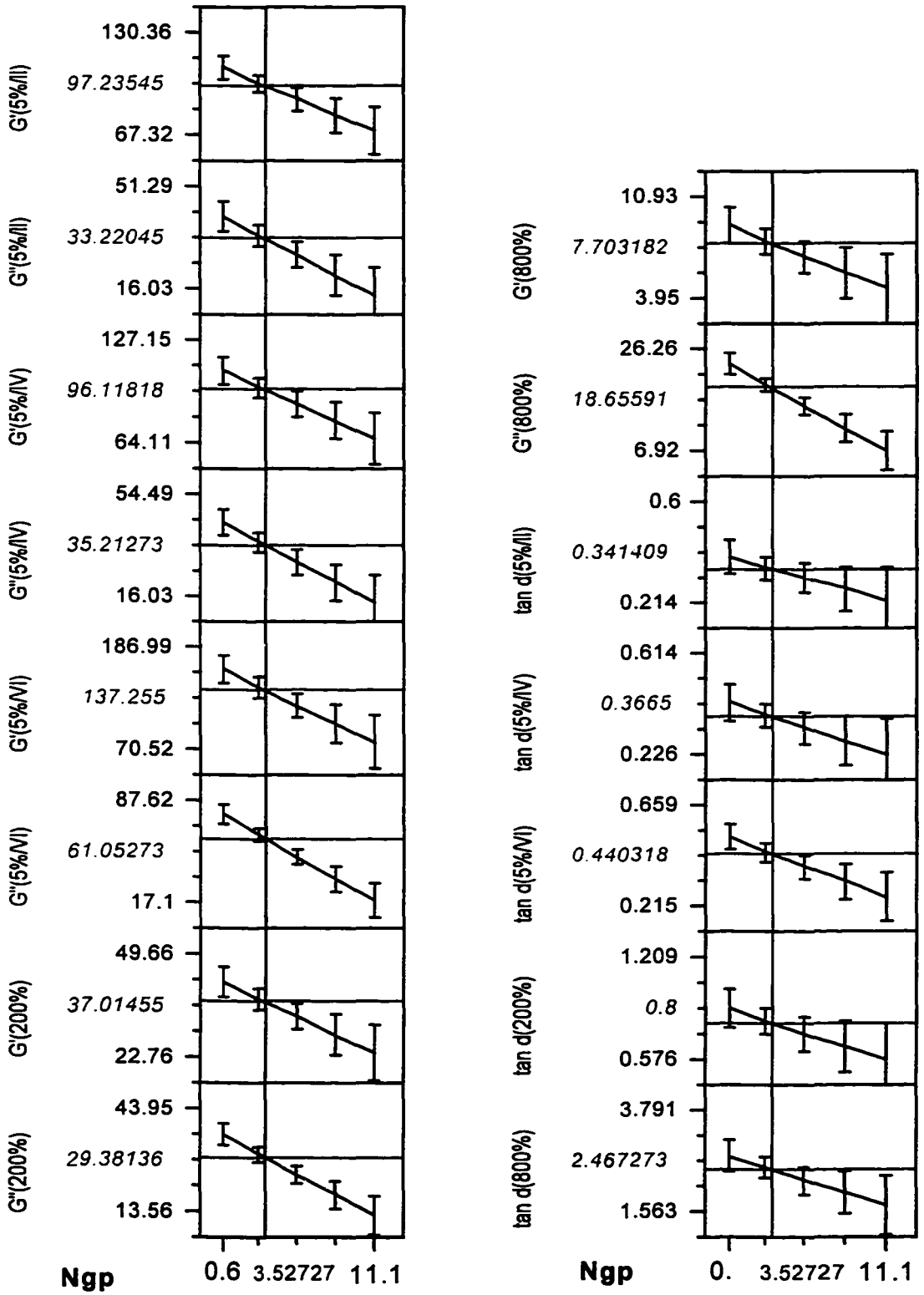


Figure A74c. Prediction profiles for correlation between structural parameter ($w^{b,g}$) and viscoelastic parameters from {HSSWP} experiments.

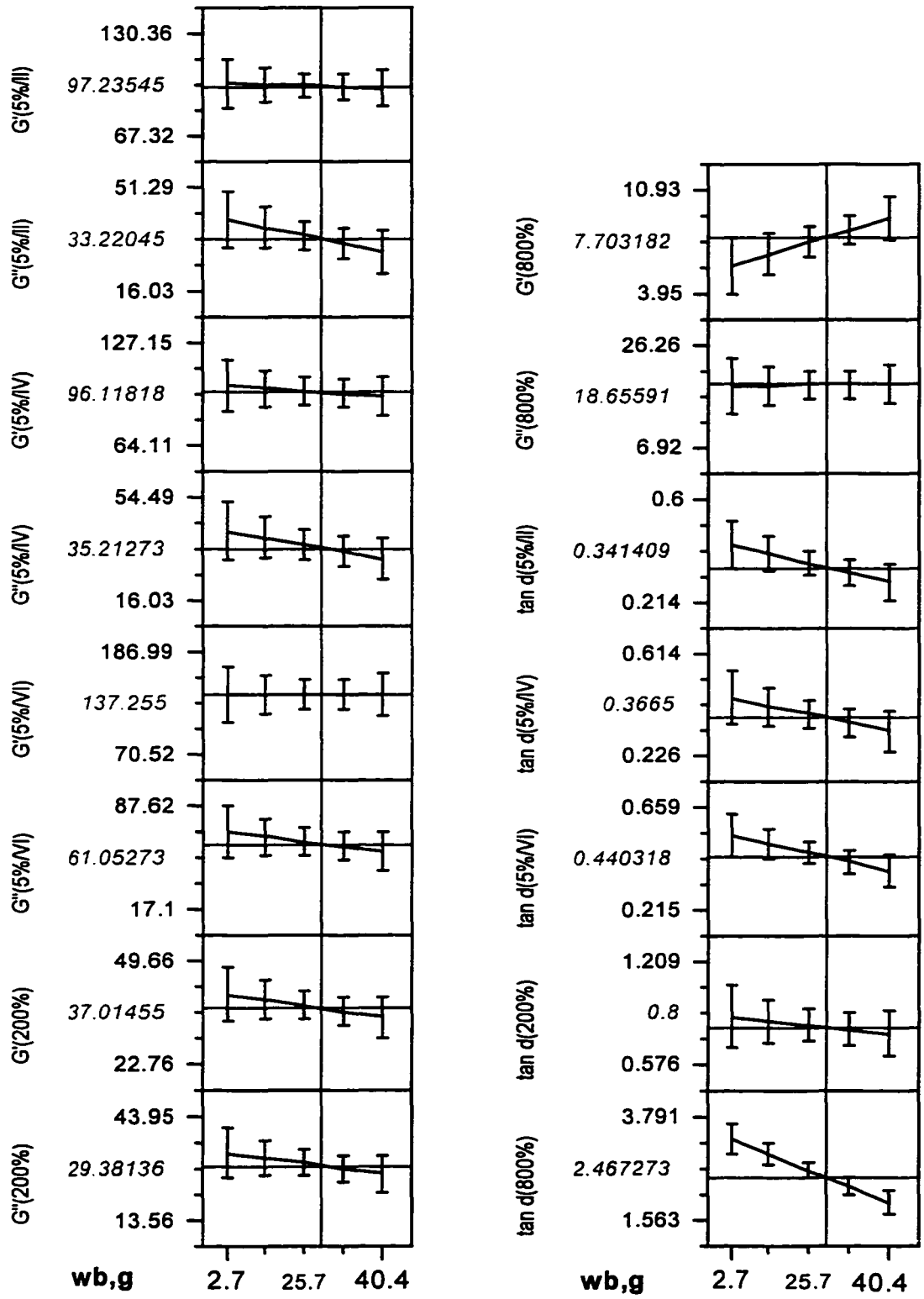


Figure A74d. Prediction profiles for correlation between structural parameter (Φ) and viscoelastic parameters from {HSSWP} experiments.

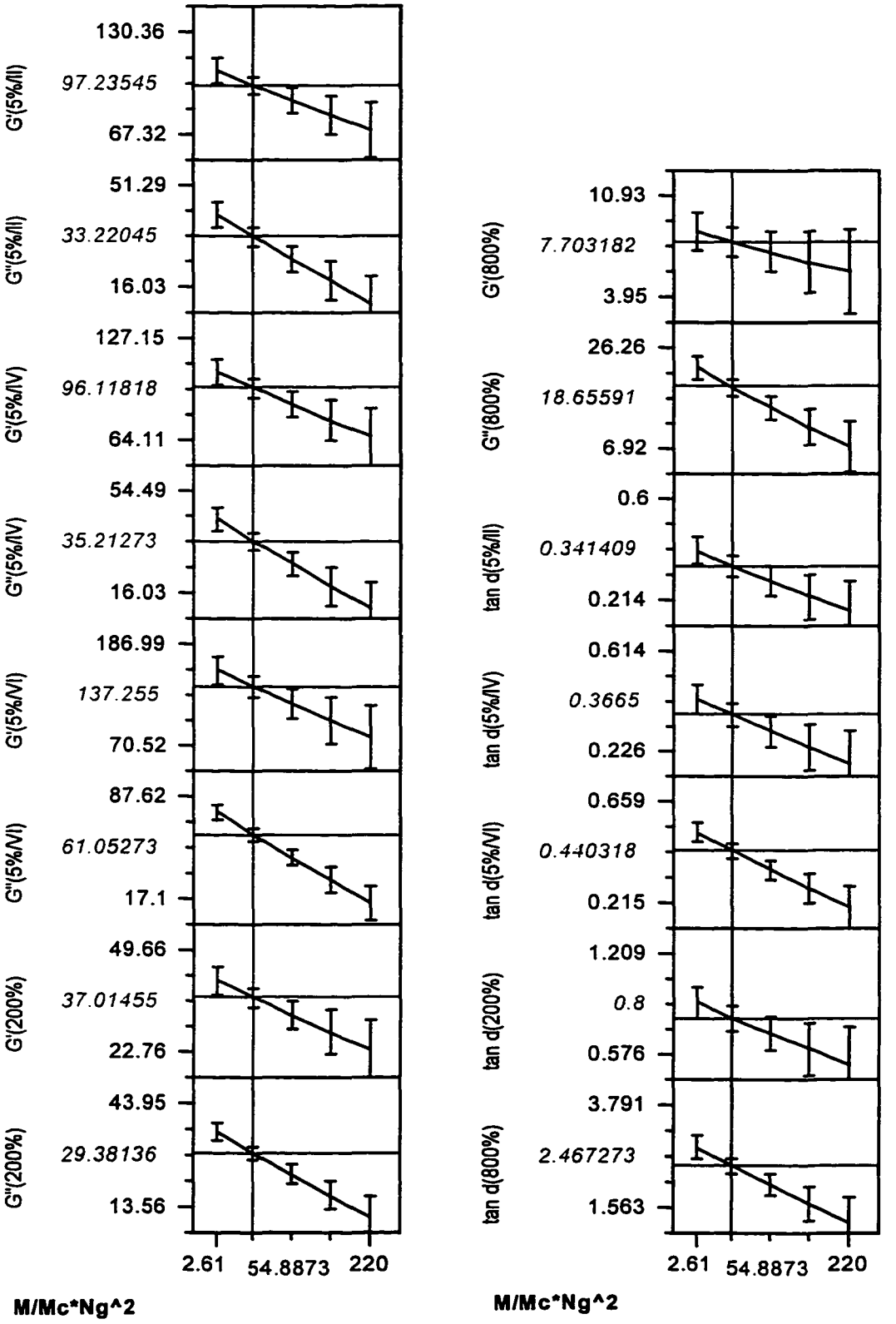


Figure A75a. Prediction profiles for correlations between structural parameters (M_p^b, N_g^p) and selected stress relaxation parameters from {TEST2} tests.

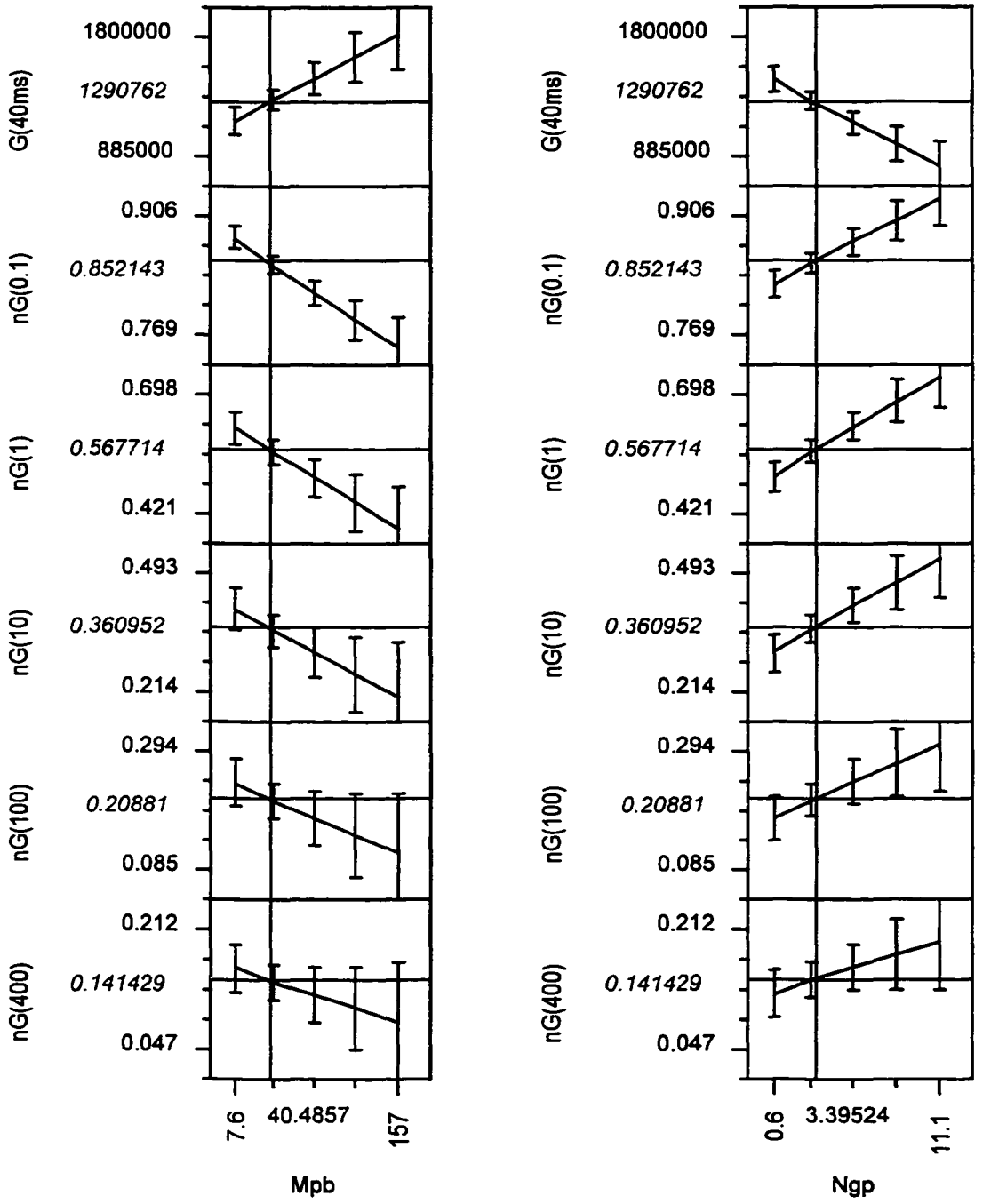


Figure A75b. Prediction profiles for correlations between structural parameters ($w^{b,g}$, w^{b}) and selected stress relaxation parameters from {TEST2} tests.

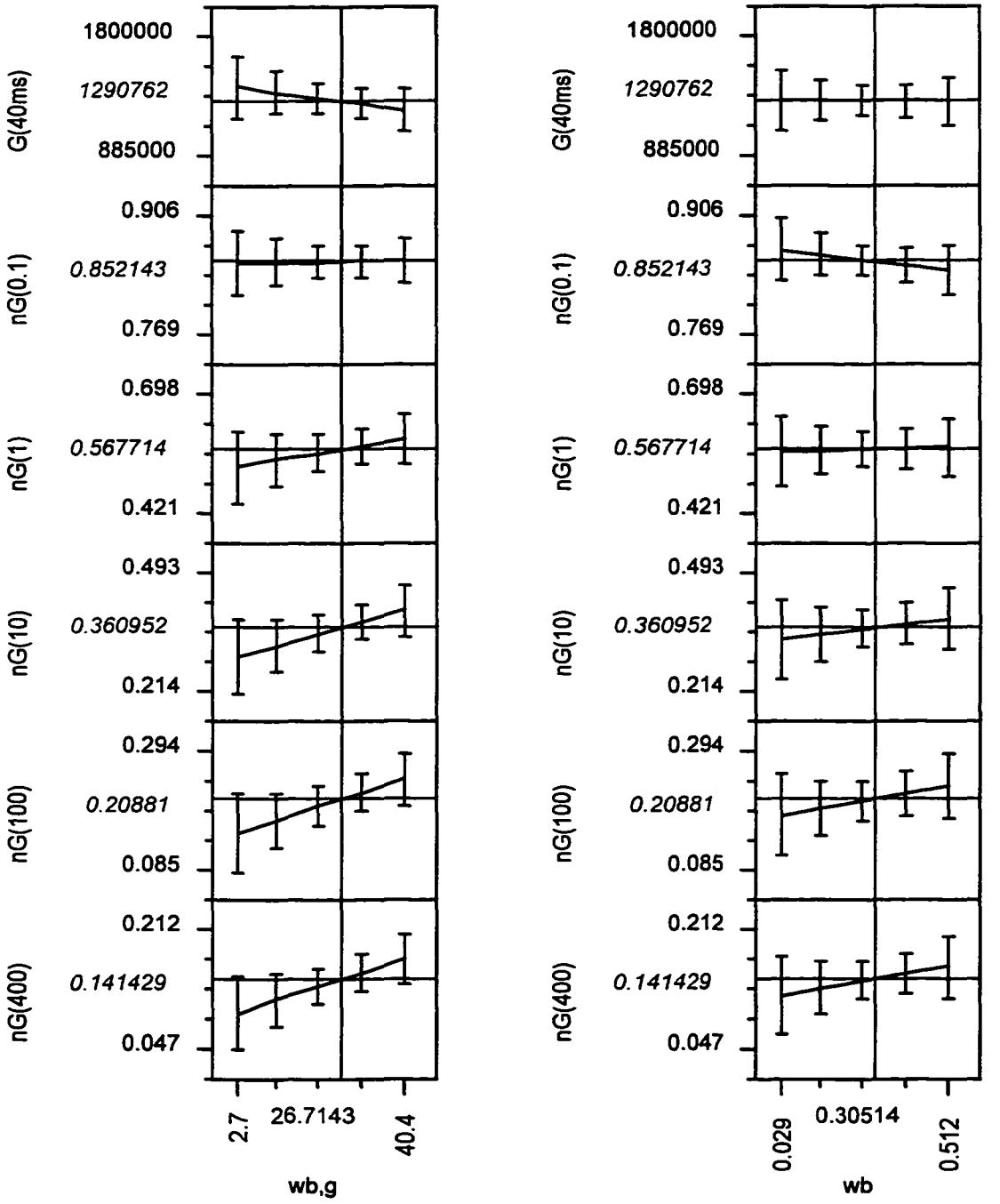


Table A61. Viscoelastic parameters derived from RMS-800 {FS5dec} test - I.

RMA-800 {FS5dec} T=30°C	tan δ(0.1)	n(0.001)	slope(G'/G"^{2})@ 0.001	n(0.001-100)	slope G"(0.001)	G" (plateau)
sample	a	b	c	d	e	f
G1	0.305	0.430	0.675	0.154 (*)	0.281	3.07E+04
G2	0.200	0.223	0.082	0.109	0.117	2.68E+04
G3	0.177	0.119	0.318	0.098	0.045	2.41E+04
G4	0.189	0.072	0.289	0.127	0.091	1.58E+04
G5	0.363	0.189	0.621	0.197	0.302	4.69E+04
G6	0.407	0.371	0.127	0.231	0.341	4.81E+04
G7	0.304	0.366	0.065	0.1522 (*)	0.268	3.88E+04
G8	0.177	0.093	-0.151	0.109	0.066	1.91E+04
G9	0.210	0.060	-0.271	0.148	0.065	1.42E+04
G10	0.330	0.189	-0.417	0.177	0.172	2.53E+04
G11	0.288	0.196	0.063	0.157	0.231	1.57E+04
G12	0.103	0.069	-0.703	0.080	-0.012	5.10E+03
G13	0.125	0.117	-1.03	0.083	-0.022	7.40E+03
G14	0.335	0.163	-1.364	0.174	0.255	1.89E+04
G15	0.210	0.074	-0.958	0.143	0.078	2.67E+04
G16	0.135	0.080	-1.076	0.113	0.037	9.03E+03
G17	0.222	0.228	-0.634	0.123	0.172	1.79E+03
G18	0.250	0.228	-1.439	0.125	0.066	1.91E+04
G19	0.228	0.257	-1.648	0.107	0.137	5.80E+03
G20	0.126	0.099	-0.66	0.086	0.000	1.07E+04
G21	0.265	0.096	-0.685	0.163	0.183	4.20E+04
G22	0.360	0.258	-0.771	0.198	0.235	6.83E+04
C	0.355	0.671	—	0.1979 (*)	0.517	3.07E+04
B10	26.200	0.999	—	—	—	—
M	0.338	0.430	—	0.1755 (*)	0.282	2.20E+04

/* - poor Power Law fit
Refer to Table 6-3 for definition of parameters

Table A62. Viscoelastic parameters derived from RMS-800 {FS5dec} test - II.

RMA-800 {FS5dec} T=30°C	Storage modulus, G', Pa					
sample	ω=0.001 rad/	ω=0.01 rad/s	ω=0.1 rad/s	ω=1 rad/s	ω=10 rad/s	ω=100 rad/s
	a	b	c	d	e	f
G1	2.25E+04	6.48E+04	1.21E+05	1.71E+05	2.13E+05	2.61E+05
G2	6.16E+04	9.61E+04	1.33E+05	1.73E+05	2.09E+05	2.55E+05
G3	7.50E+04	1.00E+05	1.31E+05	1.64E+05	1.98E+05	2.48E+05
G4	3.66E+04	4.35E+04	5.53E+04	7.34E+04	1.00E+05	1.38E+05
G5	3.45E+04	5.37E+04	9.12E+04	1.49E+05	2.25E+05	3.36E+05
G6	1.85E+04	4.21E+04	8.21E+04	1.39E+05	2.23E+05	3.51E+05
G7	3.40E+04	7.62E+04	1.32E+05	1.91E+05	2.43E+05	3.01E+05
G8	5.41E+04	6.85E+04	8.81E+04	1.12E+05	1.41E+05	1.86E+05
G9	2.52E+04	2.95E+04	3.72E+04	5.19E+04	7.76E+04	1.14E+05
G10	1.96E+04	3.01E+04	4.58E+04	7.32E+04	1.14E+05	1.48E+05
G11	1.90E+04	2.86E+04	4.36E+04	6.44E+04	8.84E+04	1.22E+05
G12	2.96E+04	3.47E+04	4.00E+04	4.61E+04	5.41E+04	7.34E+04
G13	3.28E+04	4.26E+04	5.13E+04	6.05E+04	7.16E+04	9.15E+04
G14	1.82E+04	2.68E+04	4.31E+04	6.78E+04	9.68E+04	1.36E+05
G15	4.87E+04	5.87E+04	7.53E+04	1.04E+05	1.51E+05	2.17E+05
G16	3.08E+04	3.71E+04	4.41E+04	5.31E+04	6.94E+04	1.03E+05
G17	3.51E+04	4.96E+04	6.89E+04	9.28E+04	1.19E+05	1.53E+05
G18	3.33E+04	5.50E+04	8.35E+04	1.14E+05	1.40E+05	1.72E+05
G19	1.12E+04	2.09E+04	3.20E+04	4.15E+04	4.88E+04	5.81E+04
G20	4.74E+04	6.00E+04	7.28E+04	8.63E+04	1.03E+05	1.33E+05
G21	5.61E+04	7.04E+04	9.61E+04	1.45E+05	2.15E+05	3.08E+05
G22	4.00E+04	7.37E+04	1.27E+05	2.08E+05	3.28E+05	4.50E+05
C	1.06E+04	4.81E+04	1.01E+05	1.52E+05	1.94E+05	2.40E+05
B10	---	0.00E+00	5.53E+02	3.32E+04	4.73E+05	9.57E+05
M	1.02E+04	3.46E+04	6.65E+04	9.83E+04	1.28E+05	1.79E+05

Table A63. Viscoelastic parameters derived from RMS-800 {FS5dec} test - III.

RMA-800 {FS5dec} T=30°C	tanδ						η* slope
sample	ω=0.001 rad/s	ω=0.01 rad/s	ω=0.1 rad/s	ω=1 rad/s	ω=10 rad/s	ω=100 rad/s	ω=0.001
	a	b	c	d	e	f	g
G1	0.9179	0.5277	0.3050	0.1879	0.1548	0.3091	-0.5704
G2	0.3040	0.2480	0.2000	0.1550	0.1450	0.2940	-0.7774
G3	0.2430	0.2080	0.1770	0.1470	0.1550	0.3310	-0.8812
G4	0.1560	0.1670	0.1890	0.2150	0.2340	0.3360	-0.9280
G5	0.2670	0.3520	0.3630	0.3150	0.2920	0.3460	-0.8106
G6	0.5980	0.5180	0.4070	0.3470	0.3410	0.3280	-0.6293
G7	0.6000	0.4450	0.3040	0.2060	0.1690	0.2990	-0.6340
G8	0.1870	0.1840	0.1770	0.1710	0.1960	0.3400	-0.9070
G9	0.1390	0.1570	0.2100	0.2740	0.2860	0.3440	-0.9400
G10	0.3210	0.3150	0.3300	0.3460	0.2460	0.2410	-0.8115
G11	0.2510	0.2830	0.2880	0.2430	0.2250	0.2980	-0.8036
G12	0.1280	0.1100	0.1030	0.1110	0.1730	0.3570	-0.9313
G13	0.1690	0.1440	0.1250	0.1220	0.1550	0.3180	-0.8830
G14	0.2500	0.3140	0.3350	0.2780	0.2440	0.2940	-0.8371
G15	0.1480	0.1650	0.2100	0.2560	0.2650	0.3480	-0.9265
G16	0.1390	0.1320	0.1350	0.1700	0.2620	0.3900	-0.9199
G17	0.2220	0.2310	0.2220	0.1930	0.1860	0.3220	-0.7718
G18	0.3570	0.3190	0.2500	0.1800	0.1540	0.2780	-0.7718
G19	0.4440	0.3530	0.2280	0.1500	0.1270	0.2580	-0.7428
G20	0.1900	0.1480	0.1260	0.1240	0.1590	0.3260	-0.9013
G21	0.1590	0.2020	0.2650	0.2900	0.2700	0.3520	-0.9036
G22	0.4360	0.4070	0.3600	0.3290	0.2700	0.2950	-0.7421
C	1.2600	0.6390	0.3550	0.2120	0.1670	0.3000	-0.3290
B10	—	0.0100	26.2000	3.8800	0.7490	0.2990	-0.0013
M	1.0000	0.5680	0.3380	0.2240	0.2360	0.5820	-0.5696

Table A64. Viscoelastic parameters derived from RMS-800 {FS5dec} test - IV.

RMA-800 {FS5dec} T=30°C	G"		G*		slope of G' @ω=0.001	slope of G" @ω=0.001	G" at plateau or inflection or 1 rad/s
sample	ω=0.1 rad/s	ω=100 rad/s	ω=0.1 rad/s	ω=100 rad/s			
	a	b	c	d	e	f	g
G1	3.68E+04	8.07E+04	3.05E+04	1.26E+05	0.5293	0.2812	3.07E+04
G2	2.67E+04	7.50E+04	1.36E+05	2.66E+05	0.2314	0.1169	2.68E+04
G3	2.31E+04	8.21E+04	1.33E+05	2.61E+05	0.1226	0.0452	2.41E+04
G4	1.05E+04	4.64E+04	5.63E+04	1.46E+05	0.0716	0.0909	1.58E+04
G5	3.31E+04	1.16E+05	9.70E+04	3.56E+05	0.1794	0.3021	4.69E+04
G6	3.34E+04	1.15E+05	8.86E+04	3.70E+05	0.3810	0.3406	4.81E+04
G7	4.02E+04	8.99E+04	1.38E+05	3.14E+05	0.3975	0.2675	3.88E+04
G8	1.56E+04	6.35E+04	8.94E+04	1.97E+05	0.0939	0.0657	1.91E+04
G9	7.82E+03	3.92E+04	3.81E+04	1.21E+05	0.0513	0.0653	1.42E+04
G10	1.51E+04	3.56E+04	4.82E+04	1.52E+05	0.1901	0.1724	2.53E+04
G11	1.26E+04	3.62E+04	4.53E+04	1.27E+05	0.1942	0.2307	1.57E+04
G12	4.13E+03	2.62E+04	4.03E+04	7.80E+04	0.0700	-0.0120	5.10E+03
G13	6.41E+03	2.91E+04	5.17E+04	9.60E+04	0.1210	-0.0215	7.40E+03
G14	1.44E+04	4.01E+04	4.54E+04	1.42E+05	0.1561	0.2550	1.89E+04
G15	1.58E+04	7.55E+04	7.69E+04	2.30E+05	0.0734	0.0775	2.67E+04
G16	5.97E+03	4.03E+04	4.45E+04	1.11E+05	0.0809	0.0372	9.03E+03
G17	1.53E+04	4.92E+04	7.06E+04	1.60E+05	0.1639	0.1719	1.79E+03
G18	2.09E+04	4.79E+04	8.60E+04	1.79E+05	0.0939	0.0657	1.91E+04
G19	7.31E+03	1.50E+04	3.28E+04	6.00E+04	0.2800	0.1366	5.80E+03
G20	9.18E+03	4.33E+04	7.33E+04	1.39E+05	0.1040	0.0000	1.07E+04
G21	2.55E+04	1.08E+05	9.94E+04	3.27E+05	0.0938	0.1829	4.20E+04
G22	1.27E+05	4.50E+05	1.35E+05	4.69E+05	0.2621	0.2350	6.83E+04
C	3.58E+04	7.21E+04	1.07E+05	2.51E+05	0.8499	0.5173	3.07E+04
B10	1.45E+04	2.86E+05	1.45E+04	9.99E+05	—	—	—
M	2.25E+04	1.04E+05	7.02E+04	2.07E+05	0.5537	0.2819	2.20E+04

Table A65. Stress relaxation parameters - {SR10,000} experiment.

T=30°C	nG(t=1)	nG(t=10)	nG(t=100)	nG(t=1000)	nG(t=10,000)	|slope@ t=10,000|	INT G(t)dt
Sample ID	[-]	[-]	[-]	[-]	[-]	[arb]	[arb]
	a	b	c	d	e	f	g
G1	0.7680	0.5150	0.2550	0.0760	0.0140	0.7409	392
G2	0.7950	0.6070	0.4350	0.2970	0.1830	0.2235	2310
G3	0.8230	0.6680	0.5210	0.4160	0.3240	0.1216	3673
G4	0.7200	0.5580	0.4430	0.3620	0.3200	0.0839	3483
G5	0.6300	0.3870	0.2370	0.1630	0.1170	0.1188	1318
G6	0.7200	0.5070	0.3250	0.1840	0.0980	0.2849	1329
G7	0.7790	0.5570	0.3350	0.1660	0.0700	0.3187	1085
G8	0.7910	0.6410	0.5140	0.4130	0.3420	0.0794	3647
G9	0.6370	0.4630	0.3660	0.3000	0.2450	0.0898	2627
G10	0.5970	0.3840	0.2560	0.1670	0.1060	0.2085	1310
G11	0.6900	0.4690	0.3210	0.2320	0.1840	0.1128	2051
G12	0.8210	0.7040	0.5960	0.4950	0.3930	0.0994	4264
G13	0.8230	0.6940	0.5720	0.4440	0.3230	0.1519	3676
G14	0.6480	0.4140	0.2750	0.1980	0.1330	0.0979	1552
G15	0.6900	0.5150	0.4090	0.3370	0.2630	0.0930	2828
G16	0.7490	0.6280	0.5290	0.4470	0.3580	0.0968	3847
G17	0.7540	0.5660	0.4210	0.3190	0.2380	0.1066	2616
G18	0.8000	0.5960	0.4110	0.2500	0.1480	0.1940	1980
G19	0.8130	0.6040	0.3800	0.1990	0.0830	0.3889	1270
G20	0.8260	0.6970	0.5820	0.4640	0.3240	0.1468	3811
G21	0.6790	0.4830	0.3750	0.3050	0.2640	0.0862	2811
G22	0.5530	0.3240	0.1880	0.1080	0.0650	0.2158	816
C	0.7560	0.4970	0.2380	0.0630	0.0080	0.9463	323
B10	0.0450	—	—	—	—	—	—
M	0.7400	0.4840	0.2390	0.0770	0.0160	0.7123	366

Table A66. Stress relaxation parameters - {SR1000} experiment.				
T=30°C	nG(t=1)	nG(t=10)	nG(t=100)	nG(t=1000)
Sample	[-]	[-]	[-]	[-]
ID	a	b	c	d
G1	0.7714	0.5215	0.2613	0.0777
G2	0.7952	0.6075	0.4366	0.2993
G3	0.8114	0.6425	0.5107	0.4037
G4	0.7267	0.5669	0.4569	0.3773
G5	0.6269	0.3828	0.2331	0.1591
G6	0.7202	0.5066	0.3238	0.1791
G7	0.7811	0.5557	0.3353	0.1664
G8	0.7934	0.6443	0.5171	0.4156
G9	0.6313	0.4586	0.3633	0.3005
G10	0.5898	0.3767	0.2504	0.1652
G11	0.6778	0.4543	0.3071	0.2216
G12	0.8236	0.7067	0.5989	0.4995
G13	0.8271	0.6994	0.5790	---
G14	0.6485	0.4142	0.2736	0.1935
G15	0.6990	0.5223	0.4170	0.3439
G16	0.7524	0.6317	0.5336	0.4520
G17	0.7626	0.5753	0.4297	0.3252
G18	0.8074	0.6114	0.4181	0.2724
G19	0.8196	0.6157	0.3891	0.2036
G20	0.8325	0.7074	0.5867	0.4693
G21	0.6703	0.4744	0.3634	0.2983
G22	0.5531	0.3242	0.1883	0.1073

Table A67. Viscoelastic parameters - {SR400} stress relaxation experiment.

T=100°C	nG(t=1)	nG(t=10)	nG(t=100)	nG(t=400)	|slope@t=0.1|	|slope@t=400|
Sample	[-]	[-]	[-]	[-]	[arb]	[arb]
ID	a	b	c	d	e	f
G1	0.464	0.140	0.026	0.009	0.3035	0.8867
G2	0.687	0.443	0.246	0.155	0.1723	0.3057
G3	0.749	0.576	0.430	0.348	0.1574	0.1410
G4	0.717	0.570	0.459	0.399	0.2217	0.1124
G5	0.547	0.330	0.236	0.200	0.3084	0.1200
G6	0.577	0.326	0.152	0.100	0.3234	0.2620
G7	0.540	0.255	0.115	0.072	0.2648	0.4276
G8	0.745	0.586	0.462	0.394	0.1694	0.1412
G9	0.685	0.548	0.452	0.401	0.2743	0.0913
G10	0.556	0.355	0.231	0.176	0.3914	0.1952
G11	0.608	0.411	0.295	0.242	0.2731	0.1161
G12	0.803	0.650	0.506	0.413	0.1250	0.1092
G13	0.754	0.559	0.379	0.280	0.1542	0.2402
G14	0.569	0.371	0.267	0.225	0.3190	0.1340
G15	0.694	0.549	0.446	0.389	0.2546	0.0755
G16	0.788	0.647	0.524	0.453	0.1575	0.1186
G17	0.666	0.484	0.367	0.314	0.2380	0.1437
G18	0.630	0.384	0.231	0.166	0.2123	0.2977
G19	0.558	0.263	0.106	0.060	0.2547	0.4652
G20	0.782	0.595	0.410	0.297	0.1399	0.2403
G21	0.656	0.508	0.414	0.381	0.2936	0.1654
G22	0.494	0.268	0.150	0.107	0.4127	0.2735
C	0.431	0.113	0.016	0.004	0.3345	1.3121
B10	—	—	—	—	—	—
M	0.346	0.068	0.013	0.050	0.3898	0.1167

Table A71. Selected rheological parameters from {SSWP2} test.

Sample ID	S' (50%)	S" (50%)	G_1' (50%)	G_1" (50%)	G_1* (50%)	$\tan_1 \delta$ (50%)	G_1'(50%) - G'(2%)
	[in·lb]	[in·lb]	[kPa]	[kPa]	[kPa]	[-]	[kPa]
	a	b	c	d	e	f	g
G1	11.05	4.29	135.76	52.78	145.66	0.389	24.75
G2	10.73	3.24	131.87	39.76	137.73	0.302	17.94
G3	10.66	2.75	131.07	33.83	135.37	0.258	13.38
G4	11.16	3.41	137.26	41.95	143.53	0.306	12.54
G5	12.00	5.00	147.56	61.48	159.85	0.417	20.97
G6	14.97	6.08	184.11	74.71	198.69	0.406	27.22
G7	13.20	4.51	162.29	55.45	171.50	0.342	22.29
G8	11.96	3.11	147.02	38.21	151.90	0.260	13.48
G9	9.60	3.74	118.05	46.00	126.70	0.390	13.03
G10	16.09	6.63	197.88	81.54	214.02	0.412	26.82
G11	11.62	4.57	142.86	56.14	153.50	0.396	18.98
G12	6.90	1.64	84.85	20.17	87.22	0.238	8.77
G13	6.64	1.57	81.65	19.32	83.90	0.237	11.98
G14	13.25	4.95	162.82	60.78	173.80	0.373	23.10
G15	10.45	3.64	128.50	44.72	136.06	0.348	10.60
G16	8.55	2.51	105.13	30.85	109.56	0.293	12.57
G17	12.52	3.95	154.01	48.56	161.49	0.315	14.52
G18	13.27	3.9	163.19	47.92	170.08	0.294	16.04
G19	13.79	4.44	169.60	54.54	178.15	0.322	23.00
G20	6.56	1.54	80.69	19.00	82.90	0.235	10.26
G21	10.99	4.21	135.12	51.77	144.70	0.383	14.68
G22	12.76	6.9	156.90	84.85	178.37	0.541	19.65
C	6.52	3.63	80.16	44.61	91.73	0.557	13.47
M	1.74	1.81	21.45	22.20	30.87	1.035	—
						RPA2000 {SSWP2} T=100°C ω=10 rad/s γ=50%	

Table A72. Viscoelastic parameters from LAOS - RPA 2000 {FSWP3} test.

Graft ID	G_1'		G_1''		$\tan_1 \delta$		$\tan_1 \delta$ ratio
	γ=200%		γ=200%		γ=200%		(*)
	ω=0.5 rad/s	ω=10 rad/s	ω=0.5 rad/s	ω=10 rad/s	ω=0.5 rad/s	ω=10 rad/s	
	[kPa]	[kPa]	[kPa]	[kPa]	[-]	[-]	[-]
	a	b	c	d	e	f	g
G1	20.81	45.20	27.96	44.67	1.344	0.988	7.09
G2	36.40	55.23	28.66	41.68	0.787	0.755	4.60
G3	44.21	63.16	28.84	36.26	0.652	0.574	4.50
G4	45.41	64.87	24.98	39.36	0.550	0.607	2.31
G5	31.75	59.58	27.40	54.11	0.863	0.908	3.27
G6	40.99	75.49	39.36	68.20	0.960	0.903	3.76
G7	37.60	66.44	35.06	52.06	0.933	0.784	5.30
G8	47.76	66.12	28.28	38.05	0.592	0.575	2.94
G9	33.06	54.27	21.08	41.68	0.638	0.768	2.10
G10	35.09	77.17	37.89	71.54	1.080	0.927	4.54
G11	35.06	59.29	26.95	49.87	0.769	0.841	3.03
G12	22.76	33.18	13.68	20.93	0.601	0.631	2.18
G13	19.88	28.74	14.38	19.27	0.723	0.670	3.20
G14	36.34	63.40	30.95	54.67	0.852	0.862	3.15
G15	43.44	63.56	24.20	41.68	0.557	0.656	2.12
G16	32.05	50.78	19.51	30.77	0.609	0.606	1.97
G17	47.90	70.82	30.37	46.78	0.634	0.661	3.23
G18	39.22	61.82	32.02	47.15	0.816	0.763	4.89
G19	37.84	62.04	37.06	56.03	0.980	0.903	6.30
G20	20.81	27.08	13.08	16.60	0.628	0.613	2.72
G21	39.30	61.56	25.32	46.99	0.644	0.763	2.43
G22	26.50	72.04	31.81	67.53	1.200	0.937	4.44
C	14.66	40.10	23.13	39.73	1.578	0.991	6.90
M	0.67	3.10	2.83	10.73	4.240	3.466	11.46
B10	—	—	—	—	—	—	—

(*) - tan δ ratio = $\tan_1 \delta$ (200% & 0.5 rad/s) / tan δ (5% & 200 rad/s)

Table A73. Selected rheological parameters derived from {FSWP3} test.

Sample ID	C-C plot	nC-C plot	
	mC-C p.c.l.	nC-C p.c.l.	nC-C quad.
	a	b	c
G1	29.88	0.67	1
G2	22.93	0.46	1
G3	20.36	0.36	1
G4	24.25	0.47	-1
G5	38.68	0.68	-1
G6	44.99	0.62	1
G7	33.79	0.55	1
G8	20.82	0.38	1
G9	29.59	0.63	-1
G10	53.94	0.72	1
G11	33.41	0.62	-1
G12	12.76	0.47	-1
G13	10.14	0.40	1
G14	36.06	0.61	-1
G15	26.67	0.53	-1
G16	21.86	0.52	1
G17	28.20	0.48	-1
G18	27.40	0.49	1
G19	31.65	0.53	1
G20	7.20	0.31	1
G21	31.11	0.59	-1
G22	58.16	0.82	1
C	30.45	0.76	1
M	8.27	1.08	—
B10	—	—	—
			RPA 2000 {FSWP3} T=100°C ω-range γ=200%

Table A74. Viscoelastic parameters derived from LAOS {HSSWP1} test - I.

Sample ID	G'(5%/II)	G"(5%/II)	G'(5%/IV)	G"(5%/IV)	G'(5%/VI)	G"(%5/VI)	G_1'(200%)	G_1"(200%)
	γ=5%(II)		γ=5%(IV)		γ=5%(VI)		γ=200%	
	[kPa]	[kPa]	[kPa]	[kPa]	[kPa]	[kPa]	[kPa]	[kPa]
	a	b	c	d	e	f	g	h
G1	74.80	44.88	74.80	45.95	101.51	66.25	27.67	32.07
G2	106.85	36.33	107.92	38.47	138.91	66.25	40.32	31.06
G3	106.85	27.78	107.92	28.85	152.80	59.84	42.24	26.82
G4	108.99	25.64	110.06	28.85	163.48	64.11	46.78	26.95
G5	107.92	40.60	107.92	42.74	168.82	80.14	39.57	34.88
G6	130.36	51.29	127.15	54.49	182.72	87.62	39.60	42.96
G7	84.41	41.67	83.34	42.74	123.95	68.39	34.05	32.02
G8	115.40	27.78	117.54	28.85	172.03	64.11	49.66	29.06
G9	89.76	23.51	87.62	25.64	153.87	65.18	35.25	25.08
G10	108.99	50.22	100.44	54.49	123.95	75.86	39.14	43.95
G11	90.82	34.19	89.76	36.33	139.97	67.32	33.89	28.42
G12	74.80	16.03	70.52	16.03	80.14	17.10	23.03	14.89
G13	71.59	17.10	67.32	16.03	76.93	18.17	23.77	14.57
G14	106.85	40.60	108.99	44.88	186.99	82.28	38.82	35.30
G15	98.30	25.64	98.30	28.85	152.80	58.77	40.96	26.98
G16	89.76	19.23	89.76	20.30	118.60	44.88	34.31	20.12
G17	108.99	34.19	111.12	36.33	165.62	65.18	47.76	31.89
G18	116.47	40.60	116.47	41.67	162.41	74.80	48.40	35.46
G19	91.89	42.74	90.82	44.88	118.60	66.25	34.88	33.22
G20	67.32	16.03	64.11	17.10	70.52	18.17	22.76	13.56
G21	96.17	29.92	95.10	32.06	158.14	69.45	39.52	28.52
G22	91.89	44.88	87.62	49.15	106.85	63.04	31.94	38.61
C	52.36	39.54	52.36	39.54	68.39	54.49	20.84	27.94
M	20.30	18.17	13.89	13.89	17.10	17.10	1.76	5.34
B10	—	—	—	—	—	—	—	—

RPA2000
{HSSWP}
ω=1 rad/s
T=100°C

Table A75. Viscoelastic parameters derived from LAOS {HSSWP1} test - II.

Sample ID	G_1'(800%)	G_1''(800%)	tanδ(5%/II)	tanδ(5%/IV)	tanδ(5%/VI)	$tan_1\delta$(200%)	$tan_1\delta$(800%)
	γ=800%		γ=5%(II)	γ=5%(IV)	γ=5%(VI)	γ=200%	γ=800%
	[kPa]	[kPa]	[-]	[-]	[-]	[-]	[-]
	i	j	k	l	m	n	o
G1	3.95	14.97	0.60	0.61	0.66	1.16	3.79
G2	5.66	16.90	0.34	0.36	0.48	0.77	2.98
G3	7.42	18.10	0.26	0.27	0.40	0.64	2.44
G4	9.89	21.71	0.24	0.26	0.39	0.58	2.20
G5	9.37	24.13	0.38	0.40	0.47	0.88	2.57
G6	9.56	26.26	0.39	0.43	0.48	1.09	2.75
G7	5.26	17.50	0.49	0.51	0.55	0.94	3.33
G8	8.31	21.43	0.24	0.25	0.37	0.59	2.58
G9	9.58	20.93	0.26	0.29	0.42	0.71	2.19
G10	8.58	22.49	0.46	0.54	0.61	1.12	2.62
G11	9.01	19.70	0.38	0.41	0.48	0.84	2.19
G12	4.78	7.92	0.21	0.23	0.22	0.65	1.66
G13	4.52	7.42	0.24	0.24	0.24	0.61	1.64
G14	10.90	25.83	0.38	0.41	0.44	0.91	2.37
G15	10.93	22.48	0.26	0.29	0.39	0.66	2.06
G16	8.75	14.74	0.21	0.23	0.38	0.59	1.68
G17	8.49	22.34	0.31	0.33	0.39	0.67	2.63
G18	6.89	20.82	0.35	0.36	0.46	0.73	3.02
G19	4.88	16.66	0.47	0.49	0.56	0.95	3.41
G20	4.43	6.92	0.24	0.27	0.26	0.60	1.56
G21	10.75	21.25	0.31	0.34	0.44	0.72	1.98
G22	7.56	19.93	0.49	0.56	0.59	1.21	2.64
C	2.79	12.13	0.76	0.76	0.79	1.34	4.35
M	—	1.87	0.90	1.00	1.00	3.03	—
B10	—	—	—	—	—	—	—

RPA2000
{HSSWP}
ω=1 rad/s
T=100°C

Table A76. Viscoelastic parameters derived from LAOS {HSSWP1} test - III.

Graft ID	G*(5%/II)	G*(5%/VI)	G_1*(200%)	G_1*(800%)	S_1'(200%)	S_1"(200%)	S_1'(800%)	S_1"(800%)
	γ=5%		γ=200%	γ=800%	γ=200%		γ=800%	
	[kPa]	[kPa]	[kPa]	[kPa]	[in·lb]	[in·lb]	[in·lb]	[in·lb]
	p	q	r	s	t	u	v	w
G1	87.23	121.22	42.36	15.48	9.00	10.43	5.14	19.48
G2	112.86	153.90	50.89	17.82	13.11	10.10	7.37	21.99
G3	110.40	164.10	50.03	19.57	13.74	8.72	9.66	23.56
G4	111.97	175.60	53.98	23.86	15.22	8.77	12.87	28.25
G5	115.31	186.88	52.75	25.88	12.87	11.34	12.19	31.39
G6	140.09	202.64	58.42	27.95	12.88	13.97	12.44	34.17
G7	94.14	141.56	46.74	18.28	11.08	10.42	6.85	22.78
G8	118.70	183.59	57.53	22.99	16.15	9.45	10.81	27.89
G9	92.78	167.11	43.26	23.02	11.47	8.16	12.46	27.24
G10	120.00	145.32	58.85	24.07	12.73	14.30	11.16	29.27
G11	97.05	155.32	44.23	21.66	11.02	9.24	11.73	25.63
G12	76.49	81.94	27.42	9.26	7.49	4.84	6.22	10.31
G13	73.60	79.05	27.88	8.68	7.73	4.74	5.88	9.65
G14	114.30	204.29	52.47	28.04	12.63	11.48	14.18	33.62
G15	101.59	163.71	49.04	25.00	13.32	8.78	14.23	29.25
G16	91.79	126.81	39.78	17.14	11.16	6.54	11.39	19.17
G17	114.23	177.98	57.43	23.90	15.54	10.37	11.05	29.07
G18	123.34	178.81	60.00	21.93	15.74	11.54	8.97	27.09
G19	101.35	135.85	48.16	17.36	11.34	10.81	6.35	21.68
G20	69.20	72.82	26.49	8.22	7.40	4.41	5.76	9.01
G21	100.71	172.72	48.74	23.81	12.85	9.28	13.98	27.65
G22	102.26	124.06	50.11	21.32	10.39	12.56	9.83	25.93
C	65.61	87.44	34.85	12.44	6.78	9.09	3.63	15.78
M	—	—	—	—	—	—	—	—
B10	—	—	—	—	—	—	—	—

RPA2000
{HSSWP}
ω=1 rad/s
T=100°C

Table A77. Non-linear stress relaxation parameter from {TEST2} tests.

Sample ID	G(40ms)	nG(0.1)	nG(1)	nG(10)	nG(100)	nG(400)
	[kPa]	[-]	[-]	[-]	[-]	[-]
	a	b	c	d	e	f
G1	1.180E+06	0.805	0.395	0.138	0.045	/[1]
G2	1.360E+06	0.860	0.556	0.314	0.146	0.082
G3	1.280E+06	0.891	0.646	0.438	0.258	0.170
G4	1.170E+06	0.872	0.632	0.452	0.294	0.212
G5	1.410E+06	0.823	0.503	0.302	0.172	0.118
G6	1.800E+06	0.833	0.505	0.268	0.127	0.078
G7	1.460E+06	0.829	0.463	0.214	0.091	0.057
G8	1.250E+06	0.888	0.646	0.456	0.294	0.210
G9	1.130E+06	0.838	0.583	0.411	0.264	0.189
G10	1.730E+06	0.769	0.421	0.234	0.127	0.087
G11	1.320E+06	0.841	0.537	0.342	0.207	0.146
G12	1.010E+06	0.903	0.698	0.493	0.292	0.192
G13	9.110E+05	0.906	0.685	0.459	0.250	0.154
G14	1.330E+06	0.835	0.527	0.328	0.192	0.136
G15	1.170E+06	0.855	0.607	0.436	0.287	0.209
G16	1.030E+06	0.883	0.650	0.450	0.277	0.192
G17	1.260E+06	0.857	0.583	0.391	0.250	0.183
G18	1.420E+06	0.852	0.527	0.295	0.151	0.094
G19	1.410E+06	0.837	0.479	0.221	0.085	0.047
G20	8.850E+05	0.904	0.681	0.459	0.251	0.153
G21	1.210E+06	0.843	0.569	0.395	0.258	0.188
G22	1.560E+06	0.776	0.424	0.222	0.112	0.073
C	5.460E+05	0.813	0.394	0.131	—	/[1]
M	—	0.767	0.313	0.116	/[1]	—
B10	—	—	—	—	—	—

/[1] - Corresponding torque measured below nominal range for the transducer and reading was rejected.

DSR {TEST2} T=100°C

Table A8a. {DTMA} parameters - I.

sample	T/E''_{max}(BR-α)	$T/\tan_{max}\delta$ (BR-α)	$\tan_{max}\delta$ (BR-α)	T/E''_{max}(CIIR-α)	$T/\tan_{max}\delta$ (CIIR-α)
	[°C]	[°C]	[-]	[°C]	[°C]
	a	b	c	d	e
G1	p.n.d.	p.n.d.	p.n.d.	-63.7	-45.1
G2	p.n.d.	p.n.d.	p.n.d.	-60.5	-42.6
G3	-88.4	p.n.d.	p.n.d.	-60.8	-43.0
G4	-90.8	-90.7	0.084	-62.5	n.m.
G5	-91.0	-89.5	0.193	-58.8	-44.7
G6	-90.3	-87.8	0.239	-60.6	-44.1
G7	p.n.d.	p.n.d.	p.n.d.	-59.0	-41.0
G8	-88.6	-88.2	0.059	-57.5	-42.5
G9	-90.6	-89.3	0.141	-61.2	-42.6
G10	-90.8	-89.1	0.252	-58.6	-44.3
G11	-90.9	-89.9	0.136	-60.4	-45.0
G12	-90.0	-87.8	0.156	-63.3	-44.8
G13	-89.7	-87.7	0.163	-63.1	-44.7
G14	-89.9	-89.2	0.212	-61.1	-44.7
G15	-90.6	-89.7	0.097	-61.5	-45.1
G16	-89.8	-88.1	0.128	-60.1	-44.8
G17	-89.7	-89.4	0.086	-58.4	-44.9
G18	*-90.0*	p.n.d.	p.n.d.	-60.3	-45.1
G19	-87.9	-87.5	0.068	-58.1	-45.2
G20	-89.6	-87.4	0.148	-65.2	-47.2
G21	-90.0	-89.1	0.142	-59.3	-44.8
G22	-90.6	-89.3	0.211	-59.7	-44.8
C	n/a	n/a	n/a	-58.4	-42.6
B10	-92.9	-85.6	2.039	n/a	n/a
M	-91.3	-89.8	0.097	-55.5	-42.7
avg *(1)(3)*	-90.0	-88.8	0.148	-60.6	-44.3
s (2)	0.36	0.61	0.038	1.25	0.44
min *(3)*	-91.0	-90.7	0.059	-65.2	-47.2
max *(3)*	-87.9	-87.4	0.252	-57.5	-41.0
range *(3)*	3.1	3.3	0.193	7.8	6.2
SE *(4)*	8.6	5.4	5.1	6.2	14.1

(1) - used for statistical purposes only (may not have physical meaning)

(2) - pooled standard deviation from multiple determinations on selected samples

(3) - calculated for grafts only

(4) - df. SE = range / s *(4) - df. SE = range / s*

n/a - not applicable; p.n.d. - peak not distinguishable; n.m. - parameter not measurable

Table A8b. {DTMA} parameters - II.

sample	tan_{max} δ (CIIR-α)	T /tan_{max} δ (CIIR-II)	tan_{max} δ (CIIR-II)	INT(tan δ (BR-α)dT	ΔT (E'-E" cross-overs)
	[-]	[°C]	[-]	[arb]	[°C]
	f	g	h	i	j
G1	1.239	-27.4	1.581	p.n.d.	46.1
G2	1.168	-27.3	1.513	p.n.d.	49.5
G3	1.173	-27.7	1.510	0.04	47.8
G4	n.m.	-28.3	1.399	0.21	48.8
G5	1.037	-33.1	1.113	0.68	43.0
G6	0.974	-30.6	1.258	1.31	50.8
G7	1.158	-24.7	1.534	p.n.d.	51.5
G8	1.129	-27.1	1.344	0.15	50.7
G9	1.106	-29.8	1.230	0.55	51.9
G10	0.967	-36.2	1.030	1.31	46.6
G11	1.065	-30.2	1.248	0.36	48.0
G12	1.170	-29.3	1.324	0.50	53.4
G13	1.202	-32.2	1.333	0.31	54.4
G14	1.095	-34.0	1.151	1.03	43.6
G15	1.144	-32.4	1.356	0.36	47.6
G16	1.128	-30.3	1.324	0.43	50.4
G17	1.123	-29.5	1.422	0.23	50.0
G18	1.147	-27.7	1.586	p.n.d.	49.3
G19	0.989	-24.0	1.545	0.00	48.3
G20	1.208	-33.5	1.306	0.44	52.8
G21	1.078	-31.6	1.248	0.57	48.9
G22	1.018	-31.2	1.136	1.00	44.4
C	1.143	-28.3	1.591	n/a	50.0
B10	n/a	n/a	n/a	n/a	n/a
M	1.097	-23.7	1.545	0.17	53.1
avg *(1)(3)*	1.110	-29.9	1.340	0.53	49.0
s (2)	0.049	1.36	0.098	0.269	2.72
min *(3)*	0.967	-36.2	1.030	0.00	43.0
max *(3)*	1.239	-24.0	1.586	1.31	54.4
range *(3)*	0.272	12.2	0.556	1.31	11.4
SE *(4)*	5.6	8.9	5.7	4.9	4.2

(1) - used for statistical purposes only (may not have physical meaning)
(2) - pooled standard deviation from multiple determinations
(3) - calculated for grafts only
n/a - not applicable; p.n.d. - peak not distinguishable;
n.m. - parameter not measurable

Appendix VI

Interrelations between structural and compositional parameters

Parameters quantifying the principal features of the branching structure; M_p^b, N_g and $w^{b,g}$, chemical composition; w^b and $w^{b,h}$, as well as parameters characterizing some of the potential interferences such as *PDI* and vinyl (wt%) content, were screened for correlations, further referred to as "interrelations". Understanding of these interrelations, which might exist between any given pair of structural or compositional parameters is very important for proper interpretation of the relationship between structure and composition and parameters representing rheological properties of the grafts.

JMP® is an experimental design & statistical analysis software developed by The SAS Institute Inc. and it offers a platform for screening correlations among many variables having relatively few observations. The JMP prediction profiler displays simultaneously prediction profiles (Figures AppVIa and AppVIb) for all combinations of relevant parameters.

A summary of the correlations expressed by t-Ratio[1] values is given in Table AppVI. Several detected interrelations are interpreted below, based on prediction profiles and corresponding t-Ratios.

(a) *Interrelation* $M_p^b // N_g^p$

For combs, in principle, branch length is not related to the number of branches attached to a backbone. For the portfolio of samples under study, an apparent correlation (t-Ratio: -2.83) was found between parameters N_g^p and M_p^b. This is due to highly preferential combinations of branching parameters which was caused by experimental difficulties in preparing grafts

[1] - t-Ratio is defined as the ratio of the parameter estimate (i.e. coefficients of the linear model) to its standard error.

with certain branching characteristics. For example, it was impossible to produce samples having simultaneously a high branching number and long branches. Most of graft samples have either short branches or low branching number, with only a few having intermediate values of both specific branching parameters. However, no samples with long branches and, simultaneously high or even an appreciable number of branches could be produced, due to low and rapidly decreasing grafting efficiency and purification effectiveness. This statistical condition, analogous to non-randomized sampling, is reflected in the prediction profile by negative slope of the trace and large error bars (Figure AppVIa, top square in the left column).

(b) *Interrelations* $w^{b,g}//M_p^{\,b}$ and $w^{b,g}//N_g^{\,p}$

These interrelations, (which are not statistically significant at 95% confidence level) reflect an analytical relation existing between the branch content, $w^{b,g}$ and the principal branching parameters ($w^{b,g} \sim M_p^{\,b} \cdot N_g^{\,p}$, cf. also equation 3-7), valid for comb-type molecules based on a common (identical MWD) backbone.

(c) *Interrelation* $w^{b,h}//M_p^{\,b}$

Strong, positive interrelation between $M_p^{\,b}$ and $w^{b,h}$ (t-Ratio=+7.75, Prob>|t|<0.0001) is a result of rapidly decreasing effectiveness of uncoupled BR removal with increasing branch prepolymer MW. This results in rapidly increasing $w^{b,h}$ content with increasing branch length. The relative strength of correlation between any rheological parameter and $w^{b,h}$ or $M_p^{\,b}$ may provides a clue whether a given rheological property is influenced primarily by branch length or rather by molecular weight and content of ungrafted BR.

(d) *Interrelation* $w^b // M_p^b$

Due to the extremely strong correlation between $w^b // w^{b,g}$, which reflects the simple fact that the majority of reactive, branch prepolymer molecules actually grafted onto CIIR. Separation of effects coming from branch length and graft chemical composition, w^b can be difficult.

Branching number, N_g^p, is free from statistically significant interrelations.

Other weak interrelations exist - Figure AppVIb, but they are either not statistically significant or not relevant to interpretation of rheological measurements in terms of the LCB structure.

Table AppVI. Interrelations between structural and compositional parameters: t-Ratio table.

t-Ratio values	M_p^b	N_g^p	$w^{b,g}$	$w^{b,h}$	w^b	PDI	vinyl
M_p^b							
N_g^p	-2.83						
$w^{b,g}$	+	+					
$w^{b,h}$	+7.75	-	+				
w^b	+3.04	0	+14.9	+3.96			
PDI	0	0	0	0	-		
vinyl	-	0	-	-	-2.58	+	

values of t-Ratio given for statistically significant correlations only

'-' - negative, non-significant correlation with |t-Ratio| values below 2.50 (95% conf. interval)

'+' - positive, non-significant correlation with |t-Ratio| values below 2.50 (95% conf. interval)

'0'- |t-Ratio| values below 1.00

Figure AppVIa. Prediction profiles for interrelations between structural and compositional parameters - I.

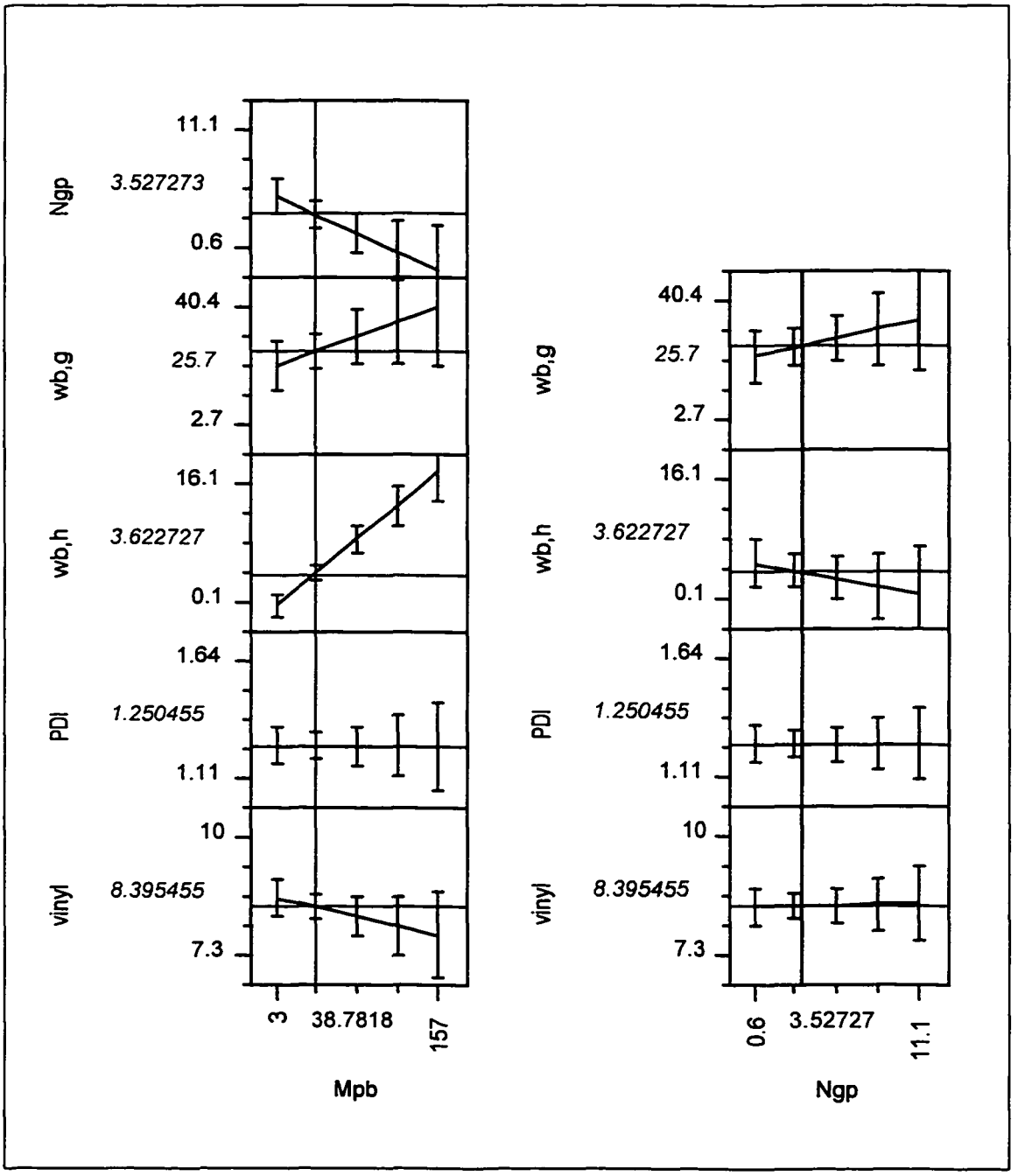


Figure AppVIb. **Prediction profiles for interrelations between structural and compositional parameters - II.**

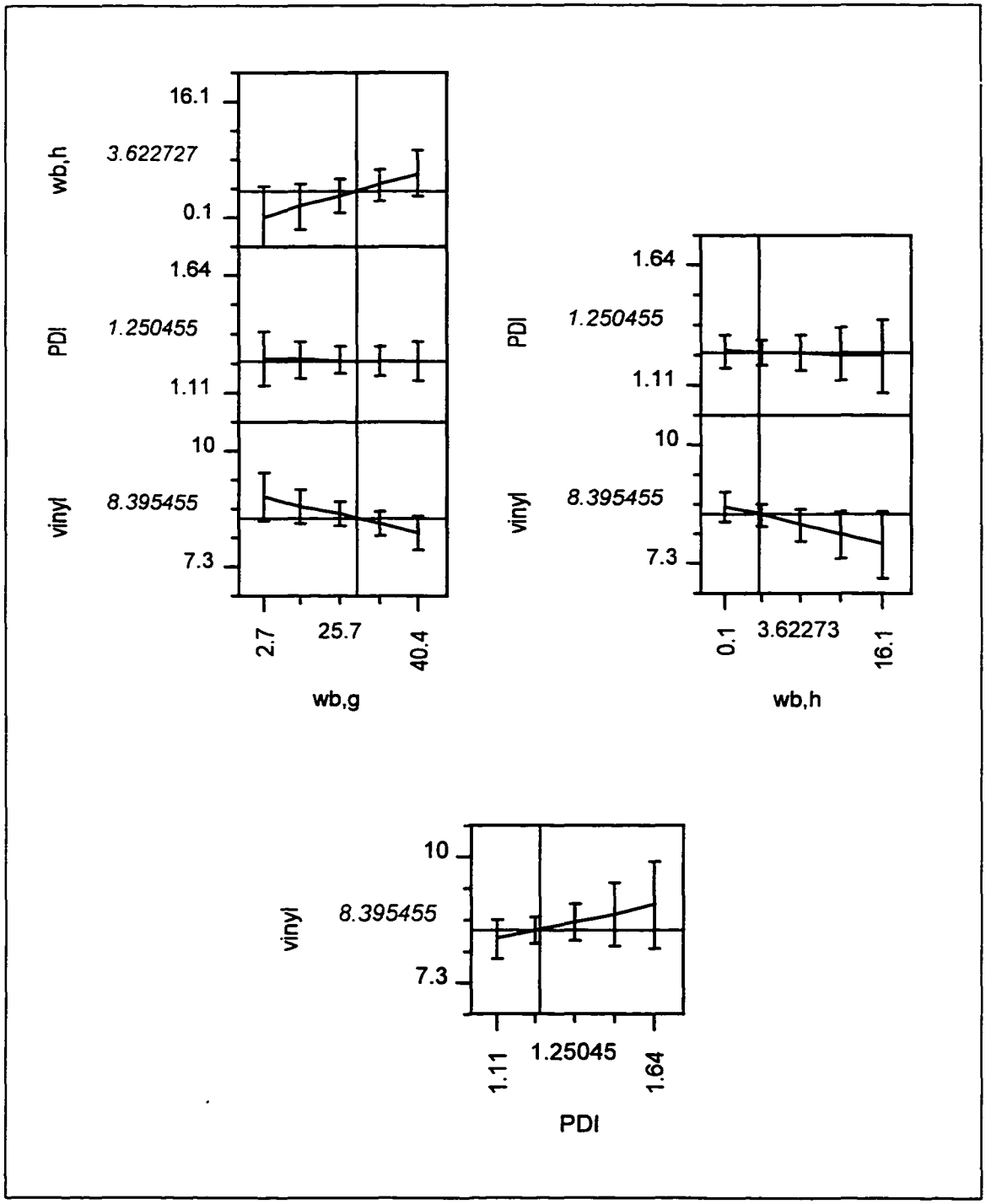
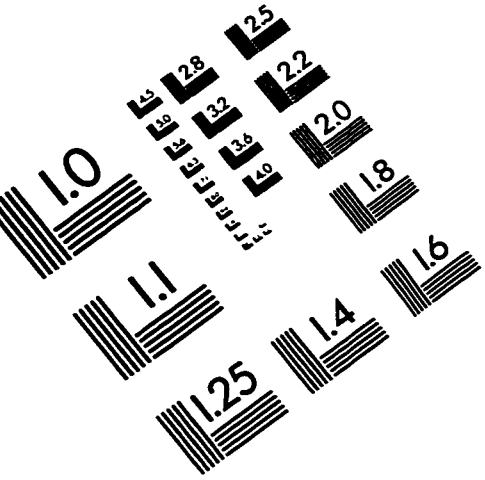
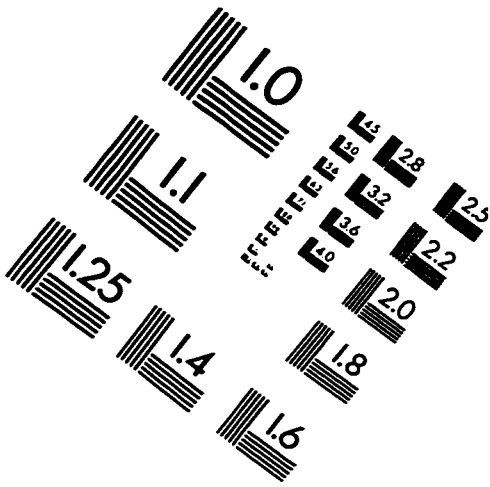
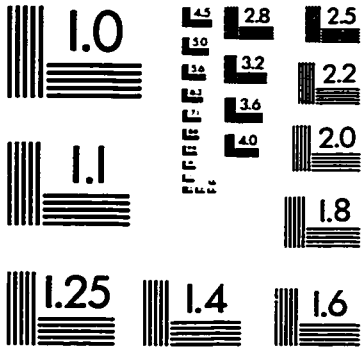
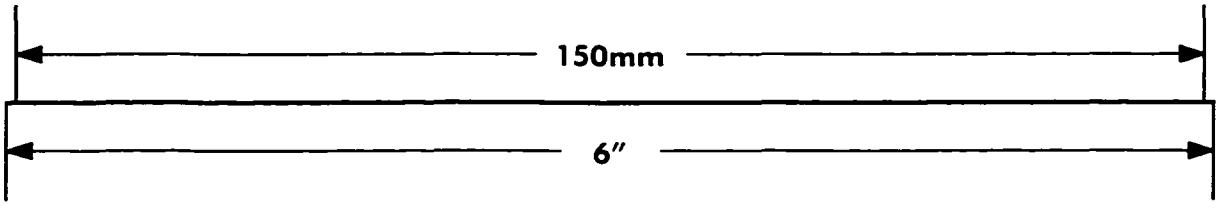


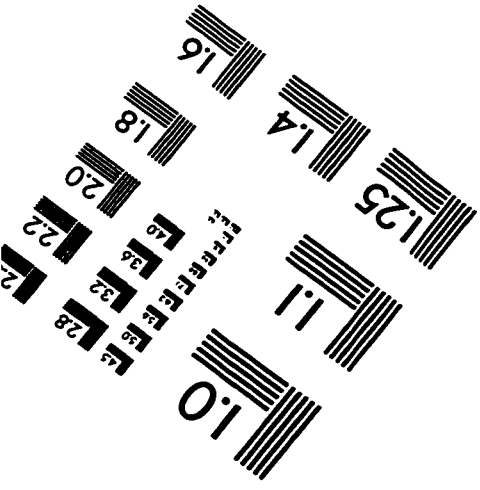
IMAGE EVALUATION
TEST TARGET (QA-3)

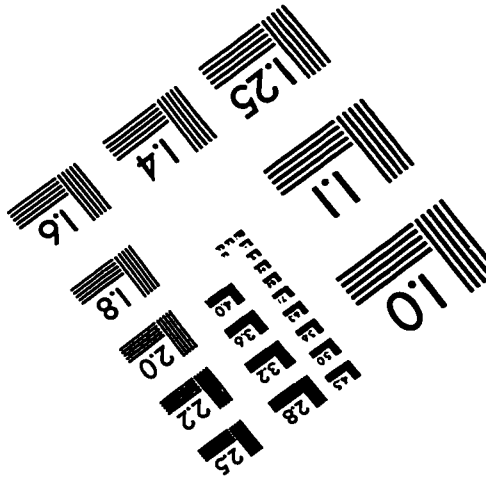












APPLIED IMAGE, Inc
1653 East Main Street
Rochester, NY 14609 USA
Phone: 716/482-0300
Fax: 716/288-5989

© 1993, Applied Image, Inc., All Rights Reserved